



## An Economic Study on Rural Household Energy Consumption in Theni District

M. Selvi<sup>1\*</sup>, S.Karthikeyan<sup>2</sup> and S. Senthilkumar<sup>3</sup>

<sup>1</sup>Ph.D Research Scholar (Part-time), School of Economics, Madurai Kamaraj University, Madurai, Tamil Nadu, India.

<sup>2</sup>Associate of Professor, Department of Economics and Centre for Research in Economics, The Madura College, (Affiliated to Madurai Kamaraj University), Madurai, Tamil Nadu, India.

<sup>3</sup>Assistant Professor & Head, Department of Economics, Cardamom Planters' Association College, Bodinayakanur, (Affiliated to Madurai Kamaraj University), Madurai, Tamil Nadu, India.

Received: 27 July 2024

Revised: 26 Sep 2024

Accepted: 06 Nov 2024

### \*Address for Correspondence

**M. Selvi**

Ph.D Research Scholar (Part-time),  
School of Economics, Madurai Kamaraj University,  
Madurai, Tamil Nadu, India.



This is an Open Access Journal / article distributed under the terms of the **Creative Commons Attribution License** (CC BY-NC-ND 3.0) which permits unrestricted use, distribution, and reproduction in any medium, provided the original work is properly cited. All rights reserved.

### ABSTRACT

Energy is the unit of measurement for all types of effort, and its use has been rising globally. It is become a necessary component of modern life. The energy is one of the fundamental factors in the functioning of any civilized society needed to improve better life style and socio- economic development of the Nation. Energy generally has been simply defined as “the ability or capacity to do work”. Planned industrialisation, economic development, modernisation of agriculture, population growth, and rise in the human standard of living has created a burgeoning demand for energy in India. Hence the energy consumption significance role of cooking and lighting but its consumption varies from rural to urban areas. Rural people used fire, wood, agricultural residues, dung, leaves, kerosene, gas and electricity where as urban people depend mostly on kerosene and electricity. Hence It cannot be denied that consumption pattern of energy depends on socio- economic background of the householders. But to save time and avoid smoke, rural residents would rather have gas and electricity than firewood, manure and agricultural waste.

**Keywords:** Energy Household, Consumption, Electricity, Kerosene and LPG.

### INTRODUCTION

The word “Energy” is derived from the Greek word ‘Energiea,’ which means’s in work. It is the power or capacity to do work. Energy has become an important and one of the basic infrastructures for human development and





Selvi et al.,

economic growth of a country. Since energy may be used to measure any type of effort, its consumption has been rising globally. It is now a fundamental necessity in today's world. The energy is one of the fundamental factors in the functioning of any civilized society needed to improve better life style and socio- economic development of the Nation. Energy generally has been simply defined as "the ability or capacity to do work". Planned industrialisation, economic development, modernisation of agriculture, population growth, and rise in the human standard of living has created a burgeoning demand for energy in India. Hence the energy consumption significance role of cooking and lighting but its consumption varies from rural to urban areas. Rural people used fire, wood, agricultural residues, dung, leaves, kerosene, gas and electricity where as urban people depend mostly on kerosene and electricity. It is seen that there is a remarkable changes in the rural energy consumption in recent years. The people used dry leaves, plants, and fire wood and agricultural residues about three decades ago. But majority people use gas and electricity for preparing tea, meals, and heating water in recent times.

## REVIEW OF LITERATURE

Dinesh Kumar Shahi et al. (2019) have been analysed the household energy demand has increased significantly in various countries including Nepal. In the case of Nepal, 94 per cent of energy use is in the domestic sector. Even though there is a chance that electricity production may skyrocket, load shedding persists because of the enormous demand for electricity. The usage of electricity has a significant impact on a country's development and quality of life. Therefore is not a sufficient number of researches done about electricity consumption in different climate regions of Nepal which are analysed by the income level of residents. This study employs electrical appliances in homes to examine the rate of power use and provides descriptive data on household energy use trends. Karabi Biswas et al. (2020) in this work the author reveals that energy plays a very important role in the development in any region or country. Energy fulfils the fundamental requirement of subsistence living in the form of cooking and lighting apart from assisting in the productive processes like transport, agriculture and industry. In terms of global energy consumption from all sources, India comes in third position, trailing only China and Japan. Given that it accounts for half of the nation's overall energy consumption, the residential sector is one of the major energy consumers.

### Important of the Study

The energy consumption is one of the basic necessities of human life. In fact, human life is unthinkable in absence of energy people used by the different sources of energy for cooking food and heating water. Lack of firewood cost of gas, and Kerosene Lake of time for cooking and socio- economic background have changed the energy consumption in rural in Theni District.

### Objectives of the Study:

The specific objectives of the present study are:

1. To study the changes scenario of rural energy consumption.
2. To identify the causes of changes in the energy consumption in rural area in Theni District.
3. To find out the problems of rural energy in Theni District.

## METHODOLOGY

The present study was conducted in the rural areas of Theni District of Tamil Nadu. It consists of Five Taluks, namely Andipatti, Bodinayakanur, Periyakulam, Theni and Uthamapalayam Taluks. The study gave equal importance of the five Taluks irrespective of size of population, size of age and environment thus; thirty samples have been selected from each taluk. The total number of respondents is 150. The sample random sampling method was used for data collection. The data collected from the both primary and secondary data and analyzed with appropriate statistical tools have been used.



Selvi *et al.*,

### Rural Energy Consumption in India

India is the second popular country in the world after China and has extremes of ecological diversity. 90 per cent of the population in India still live in the rural areas: and meeting their energy requirements in a sustainable manner continues to be a major challenge for the country.

### House Hold Rural Energy Consumption

The house hold sector is one of the major components of energy consumption. The national budget accounts it for about 50 per cent of energy consumption in India. It is seen that about 75 per cent population lives in rural areas. Rural people needs energy for cooking, lighting, and water heating and supply since the present study is concerned with households. It analysis the energy consumption for cooking and water heating in rural areas of Theni District. The demand for energy is mint by both the commercial and non- commercial energy. Commercial energy includes LPG. Kerosene, Electricity and Firewood, on the other hand non - commercial energy refers to dry leaves, sticks and plants, agricultural residues and dung mainly obtained freely from own or neighbours farms.

### Changing Energy Consumption

People live in rural areas have been changing energy consumption and water heating for the last three decades in Theni District. It could be observed from the Table: 1. The changing energy consumption in rural areas for the last 34 years. It is seen that the number of fire wood users decreased from 68.67 per cent in 1990 to 32 per cent in 2024. The number of agricultural residues users decreased from 14. per cent in 1990 to 6 per cent in 2024. The number of respondents who use dung as energy decreases from 9.33 per cent in 1990 to 3.33 per cent in 2024. The number of kerosene user's decreased from 15.33 per cent in 2000 to 8.67 percent in 2024. It is important to note the number of respondents who use LPG increased from 0.67 per cent in 2000to 42 per cent in 2024. The number of respondents who utilize electricity increased from 2.66 per cent in 2010 to 8 per cent in 2024 the study observes that people shift from non- commercial energy to commercial one and they use almost all types of energy in rural areas. The study also found that number of respondents who use gas (42 per cent) is more than fire wood (32.0 per cent) users in the study area. It shows the changing energy consumption in rural areas in current years.

### Reasons for Changing in Energy Consumption

The reasons for energy consumption changes in different place to place time to time and family to family, this is because the availability of energy sources, time for cooking cost of energy and socio- economic back ground play need role in the use of energy in rural area in Theni District. It could be seen from Table -2 the study shows that among the total households (150) 21.33 per cent change the energy consumption due to their socio – economic back ground and style. In fact, education income and nature of occupation have modified their standard of living and these have great impact of energy consumption. Among the total households 20.67 per cent households 6 per cent and 3.33 per cent considers lack of agricultural residues and dung as the causes of change in energy consumption in rural areas in Theni District.

The study identify that about 16 per cent households change the energy due to lack of time. It is seen that 20 per cent households state that availability of commercial energy such as LPG and electricity bring about change in energy use of study area. More over 12.67 per cent households change energy due to change in cropping pattern and land used for non- agricultural purpose. They convey that these change affect; the availability of agricultural residues and fire wood. Because of this, their home needs are met by LPG and electricity. Thus the study found that change in life style. Cropping pattern, lack of time for cooking, lack of fire wood, dung and agricultural residues change energy consumption in rural areas in Theni District.

### Various Problems of Energy Consumption

The people faced by the various problems in energy consumption in rural areas in Theni district. Lack of energy, cost of energy changing environment, delay in the supply of LPG, lack of energy subsidy, lack of knowledge about modern energy and accident are some problems identified in the study area.



**Selvi et al.,**

Table -3 reveals that various problems of respondent in energy consumption in rural areas in Theni district. The study depicts that out of the total respondent 16 per cent suffer from lack of energy like fire wood and agricultural residue. about 20.67 per cent respondents suffers from increase in the cost of fuel like fire wood, LPG and electricity. The changing in environment such as cropping pattern, land used for agricultural purpose, extension of urbanization and changing life style reduce the availability of non- commercial energy and increases price of commercial energy. In fact, it causes for the many problems of energy consumption in the study area. Moreover, delay in the supply of LPG and frequent power cut create the problems in energy use pattern. The reveals that 25.33 per cent respondents suffer from this problem. People in rural areas anticipate subsidies for using energy sources like electricity and LPG. The non – availability of energy subsidy affects 12 per cent respondents. The study observed that 6.67 per cent respondents do not know how to use LPG gas and they fear about it. Moreover, 4 per cent respondents state that use of energy like LPG and electricity causes accidents.

## CONCLUSION

The study find out the changes in energy consumption, its causes and problems in rural in Theni district. Energy is the universal measurement of all kinds of work and its consumption has been increasing worldwide. It has become a basic requirement of modern life. In fact, it is the backbone of present day civilization. Thus, with an increase in the living standard of human beings, the energy consumption is also accelerated. There is a strong correlation between standard of living and energy consumption. Hence It cannot be denied that consumption pattern of energy depends on socio- economic background of the householders. But to save time and avoid smoke, rural residents would rather have gas and electricity than firewood, manure and agricultural waste. The study observes that the number of households using gas increased from 0.67 per cent to 42 per cent in 2024. On the other hand the number of householders using fire wood decreases from 68.67 per cent in 1990 to 32 per cent in 2024. The study observes that convenience of people influence more than availability in the determination of energy consumption in rural areas in Theni district.

## Suggestions

1. Energy subsidy may provide for domestic use at least based on income of the uses.
2. Awareness should be developed among the rural mass about how to use LPG and shun accident and fear.
3. To lessen the scarcity of a certain energy source, people can use electricity, gas, firewood, or kerosene.
4. Women without jobs might utilise firewood, plants, and dried leaves to reduce their reliance on LPG and electricity.
5. Gas and electric stove and burners should be handled carefully and switch off when not in use. Moreover, children should be advised to avoid mishaps.

## REFERENCES

1. Pant D.K (2005) Household kerosene consumption pattern, Margin, Vol.18, No.1.
2. Ramachandra TV el. al., (2005), “ Decision support system for regional domestic energy Planning”, Journal of Scientific & Industrial Research, Vol. 64, PP 163 – 174.
3. Ambuj sagar (2002) India’s Energy Rand D Landscape, A critical Assessment Economic and political weekly No 31, No 38.
4. Sudarshan Naidu N.T., “Potential of Biogas as a Rural Energy sources” Kisan World, Vol. 31, No. 4, PP 35-36
5. Sudhakara Reddy B and P.Balachandrs, “ A Sustainable Energy strategy for India Revisited”, Economic and Political Weekly, Vol. 37, No. 52, PP 5264 - 5273





Selvi et al.,

Table – 1 : Changing Energy Consumption

Year	Fire wood	Agricultural residue	Dung	Kerosene	Gas	Electricity	Total & percentage
1990	103 (68.67)	21 (14.0)	14 (9.33)	12 (8.0)	-	-	150 (100)
2000	93 (62.0)	20 (13.33)	13 (8.67)	23 (15.33)	1 (0.67)	-	150 (100)
2010	69 (46.0)	15 (10.0)	9 (6.0)	16 (10.67)	37 (24.67)	4 (2.66)	150 (100)
2020	53 (35.33)	10 (6.67)	6 (4.0)	14 (9.33)	58 (38.67)	9 (6.0)	150 (100)
2024	48 (32.0)	9 (6.0)	5 (3.33)	13 (8.67)	63 (42.0)	12 (8.0)	150 (100)

Source: Compiled from the Field study.

Table- 2 : Reasons for Changing in Energy Consumption

Sl. No.	Cause	No. Of Sample Households	Percentage
1	Lack of fire wood	31	20.67
2	Lack of Agricultural residues	9	6.0
3	Lack of Dung	5	3.33
4	Lack of Time	24	16.0
5	Availability of commercial energy	30	20.0
6	Changing life style	32	21.33
7	Cropping pattern	19	12.67
<b>Total</b>		<b>150</b>	<b>100</b>

Source: Compiled from the Field study.

Table -3 : Various Problems of Energy Consumption

S.No	Problem	No. of Respondents	Percentage
1	Lack of energy	24	16.0
2	Cost of fuel	31	20.67
3	Changing Environment	23	15.33
4	Delay in supply	38	25.33
5	Lack of subsidy	18	12.0
6	Lack of knowledge	10	6.67
7	Accident	6	4.0
<b>Total</b>		<b>150</b>	<b>100</b>

Sources: Compiled from the Field study





## Management of Subclinical Hyperthyroidism through Ayurveda: Case Report

Alka Yadav<sup>1\*</sup>, Sarita Yadav<sup>2</sup> and Vipin Tanwar<sup>3</sup>

<sup>1</sup>Assistant Professor, Department of Panchakarma, FIMS, SGT University, Gurgaon, Haryana, India.

<sup>2</sup>Assistant Professor, Department of Shalakyta Tantra, FIMS, SGT University, Gurgaon, Haryana, India.

<sup>3</sup>Assistant Professor, Department of Panchakarma, National Institute of Ayurveda, Jaipur, Rajasthan, India.

Received: 27 May 2024

Revised: 16 Aug 2024

Accepted: 16 Oct 2024

### \*Address for Correspondence

**Alka Yadav**

Assistant Professor,

Department of Panchakarma,

FIMS, SGT University, Gurgaon,

Haryana, India.

E.Mail: - raoalka2324@gmail.com,



This is an Open Access Journal / article distributed under the terms of the **Creative Commons Attribution License** (CC BY-NC-ND 3.0) which permits unrestricted use, distribution, and reproduction in any medium, provided the original work is properly cited. All rights reserved.

### ABSTRACT

Hyperthyroidism or thyrotoxicosis refers to an overactive thyroid gland. Subclinical hyperthyroidism (also known as subclinical overactive thyroid gland or mild or severe subclinical hyperthyroidism) is diagnosed when thyroid function tests show normal thyroid hormone levels of FT3 and FT4 but low or suppressed levels of thyroid-stimulating hormone TSH). Occasionally the FT3 levels may be high. Mild subclinical hyperthyroidism is more common than severe subclinical hyperthyroidism. Subclinical hyperthyroidism can have an exogenous (external) cause or endogenous (internal) cause. Exogenous causes are more common i.e. taking too much levothyroxine or caused by the drug amiodarone. Endogenous causes may include Graves' disease, toxic multinodular goitre, toxic adenoma and certain types of thyroiditis. Most people who suffer from subclinical hyperthyroidism don't present with any of the symptoms of hyperthyroidism (an overactive thyroid). However, in some cases, symptoms are similar to that of hyperthyroidism. A 34-year-old female patient came to Panchakarma OPD with complaints of weight loss anxiety, palpitation, tremors and hair fall. A treatment protocol was planned based on the signs and symptoms. *Snehapana* with *Mahatiktakghrita* followed by *Virechana* and *Sansarjana karma*. After the *Shodhana, Shamanayoga* of *Vidarikandhachurna, Shatavari churna* and *Brahmi vati* was given to the patient for two months. There is a marked improvement in the bio-chemical parameters and in the symptoms of subclinical hyperthyroidism.

**Keywords:** Subclinical Hyperthyroidism, *Snehapana*, *Virechana*, *Vidarikandhachurna*, *Shatavari churna* and *Brahmi vati*







Alka Yadav et al.,

## INTRODUCTION

In India more than 5 million cases per year are diagnosed with Hyperthyroidism. Hyperthyroidism can accelerate body's metabolism significantly causing sudden weight loss, a rapid or irregular heartbeat, sweating & nervousness and irritability. Hyperthyroidism is more prevalent in women than in man. Subclinical hyperthyroidism is a biochemical diagnosis characterized by a decreased serum thyroid-stimulating hormone (TSH) and normal serum thyroxine (T4) and triiodothyronine (T3) concentrations. Proposed grading systems distinguish between mild (TSH, 0.1-0.4 mIU/L) and severe Subclinical hyperthyroidism (TSH, <0.1 mIU/L).<sup>[1]</sup> Thyroid Hormone is required for the normal functioning of numerous tissues in the body. In health the thyroid gland predominantly secretes thyroxine (T4) which is converted in to triiodothyronine (T3) in other organs by the selenium dependent enzyme iodothyronine deiodinase. T3 binds to the thyroid hormone receptor in the nucleus of the cell. The thyroid gland is the only source of thyroid hormone in the body, the process requires iodine and the amino acid tyrosine. Iodine in the bloodstream is taken by the gland and in corporate in to thyroglobulin molecules. The process is controlled by the TSH which is secreted by the pituitary gland. Not enough iodine or not enough TSH can result in decreased production of thyroid hormones. The Hypothalamic – Pituitary – Thyroid axis plays a key role in maintaining thyroid hormone levels within normal limits. The production of TSH by the anterior pituitary gland is stimulated in turn by thyrotropin releasing hormone (TRH) released from hypothalamus. Fundamental effect is deficient production of thyroid hormones due to various factors, but most common for is dietary lack of iodine. Which gets result in lack of thyroxin. Thyroxin is made up of by iodine and tyrosine (Amino acid). Deficient thyroid hormone production causes excessive TSH Stimulation which lead to hyperplasia of follicular epithelium as well as formation of new thyroid follicles. Rapid and prolonged changes of hyperplasia result in continued growth of thyroid tissue while involved areas undergo fibrosis nodular goitre. Thyrotoxicosis is a toxic condition of tissues exposed to the excessive thyroid hormones. Thyroid hormones metabolism runs in hypothalamus – pituitary – thyroid axis, but target tissues of thyroid dysfunction are multiple.<sup>[2]</sup>

### Case report

A 34-year-old female patient, housewife by profession, who was apparently well one year back, developed progressive hair fall with itchy scaly scalp, palpitation and fatigue initially. Then she gradually developed tachycardia, tremors and breathlessness doing daily routine work. These symptoms were followed by anxiety, weight loss. She was diagnosed as Subclinical Hyperthyroidism followed by blood test (Thyroid profile) in which T3, T4 values are elevated and depressed TSH levels. Patient was put on Tab. Neo-Mercazole 10 mg/day (Carbimazole, anti-thyroid medication) and Tab. BetacapTR 40mg (propranolol, beta blocker). While being on medication, she developed some associated complaints like insomnia, itchy papule over planter surface of feet and irregular bowel habits and itching sensation in eyes. Radio iodine uptake to rule out malignancy. Radio iodine study detected both lobes of thyroid gland show decreased tracer uptake and scan finding suggestive of Thyroiditis. But even after taking medicine she didn't get much relief. As, Thyroid Stimulating Hormone (TSH) levels were not coming into physiological range, he stopped the medication against medical advice four months before his first visit to OPD in December 2023. Symptoms like heavy hair fall with dandruff, tremors, anxiety, increased appetite along with decreased weight and breathlessness and scanty irregular mensuration were the chief complaints during his visit to the OPD. On examination there was mild swelling of thyroid gland, dryness of skin and palpitation, heart rate was 112/min. and blood pressure was 98/60 mm of Hg.

Patient was provisionally diagnosed Bhasmaka Roga as *Kapha avritavata* (*vata* obstructed by *Kapha*) with *Pitta-anubandha* (associated with *Pitta*) based on the symptoms like *Dourbalya* (tiredness), *Galapaka* (inflammation of thyroid gland), *Atyagni* (excessive appetite) can be attributed to *Pittanubandhatwa*. On evaluation it is found that the symptoms of *Pitta vridhhi*, *Vata vridhhi* and *Kapha kshaya* are more observed in hyperthyroidism. Further *Kapha kshaya* induces *kshaya* of *Rasa*, *Mamsa*, *Meda*, *Majja* and *Sukra Dhatus*, *Artavais a Updhatu* of *Rasa dhatu* so it also found to be decreased due to *Rasa kshaya* caused by *Kapha kshaya*. In this disease all the *Dhatus* become debilitated





Alka Yadav et al.,

and person becomes cachectic and suffers from syndrome of *Hritpeeda*, *Hriddrava*, *Kampa*, *Shosha*, *Alpayapicheshmaya Sharma*, *Sphikgrevodar Sushkata*, *Krishata*, *Shrama*, *Kesha-Nakha Prapatanam*, *Dourbalya*, *Asthi Saushirya*, *Ashaktimaithune*, *Yathochitkala-darshanam* and *Alpa Artavata*. [3]. The *Shamana* (palliative medicines) and *Shodhana*, *Virechana* (therapeutic purgation) was planned. Treatment schedule followed is enlisted at Table 1.

### Observations

Thyroid profile before and after (TSH, free T3 and T4) is mentioned in Table 2 along with laboratory reports. Patient mentioned increased appetite and normal bowel movements after *Deepana* and *Pachana* and dryness of skin and scalp, insomnia was reduced during *Snehapana* and *Abhyanga* and *Swedana*, palpitations and watery papule were completely alleviated after *Virechana*. After administration of *Shamana* drug; major relief in tremors and breathlessness were observed. Blood parameters were improved approaching towards normal value after *Shamana chikitsa*.

## DISCUSSION

*Virechana* is the most preferred *shodana* in hyperthyroidism. As it corrects pitta related pathologies which are seen in hyperthyroidism. It does *vatanulomana*. Periodically administered *virechana* delays the *dhatupaka* there by preventing further tissue destruction. As *Virechanadraya* possesses *ushna*, *tikshna*, *sukshma*, *vyavayi* and *vikasi* properties, by virtue of its *viryā* the *Virechanadraya* reaches *hridaya*. *Hridaya* here can be considered as nerve plexus in brain where it may help in balancing the hypo- thalamo pituitary thyroid axis. [4]. *Vidarikandhchurna* helps in reduction of symptoms like anxiety insomnia, palpitation because bio-chemical components in *Vidarikhand* include  $\beta$ - sitosterol, stigmasterol, diuzeitin, tuberosin, puerarin, Pterocarpan-tuberosin, pterocarpanone-hydroxytuberosone, two pterocarpenes-an hydrotuberosin. Apart from this, it also contains 64% carbohydrates and 10.9% proteins. Enriched with these bio active components and host of qualities like immuno- protective, rejuvenative, cardiotoxic, diuretic, hypertensive, *detoxifying*, *digestive*, anti-inflammatory, broncho-dilatory, pain-relieving, anti-microbial properties. This medicinal plant is also used to treat heart related problems, constipation and diarrhoea. [5].

*Vidarikhand* balances *Vata* and *Pitta* in the body. *Shatavari churna* balances vitiated *vata* and *kapha*. It boosts immunity and have rejuvenating properties. *Shatavari* has been referred as bitter-sweet, emollient, cooling, nervine tonic, constipating, galactogogue, and aphrodisiac, diuretic, rejuvenating, carminative, stomachic, antiseptic and as tonic. *Shatavarichurna* regulates mensuration cycle by balancing oestrogen and progesterone levels. [6]. Studies show that aqueous concentration of the root have indicated noteworthy changes in thyroid hormone level. Its extract decreases the levels of T3 and T4 compared the reference drug propyl thio uracil [7]. *Aswagandha* contain *Kashaya*, *Tikta Rasa*; *Laghu*, *Snighdha Guna*; *Ushna Veerya* but *Madhura Vipaka*. It possesses *Rasayana*, *Balya*, *Vrishya* properties. *Ashwagandha* has been used as an anti-inflammatory, anti-oxidative, anti-anxiety, aphrodisiac, immune-modulation, CNS depressant, hepato-protective, cardiovascular protection, adaptogenic and anti-stress [8]. All these properties may ease the syndromes of hyperthyroidism. Various studies also show that *Aswagandha* have regulating effect on thyroid glands [9]. *Brahmi Vati* is used for the treatment of anxiety insomnia, tremors in hands. It reduces both mental and physical heat (*Tapa prashamana*) and mitigating irritability and excitability. *Brahmi Vati* may offer neuroprotective effects. Studies show that the drug may protect the brain cells against oxidative stress [10].

## CONCLUSION

In *Ayurveda*, there is no disease contemporary to Subclinical hyperthyroidism but inferences can be made that it may be correlated to *Bhasmakaroga* or *Vata avarana* or imbalance in *vata*, *pitta* and *kapha doshas*. This case of subclinical hyperthyroidism was treated with holistic approach of Ayurveda based on the symptoms. The patient got symptomatic relief and also bio chemical levels of the thyroid profile were in range by *Virechana karma* and *Shamana Yoga*. But more clinical controlled studies are required to prove the effectiveness of this treatment.







## REFERENCES

1. Tsai K, Leung AM. Subclinical Hyperthyroidism: A Review of the Clinical Literature. *EndocrPract.* 2021 Mar;27(3):254-260. doi: 10.1016/j.eprac.2021.02.002. Epub 2021 Feb 13. PMID: 33588063.
2. Vikas Nivrutti Gapat, Ujwala M Divekar, Smita Dhurde. Patho-Physiology of Hyperthyroidism & their Ayurvedic Management. *Aayushi International Interdisciplinary Research Journal: Vol III; Issue XI, Nov 2016*
3. Deepika Tewari and Vimal Tewari. Evaluation of Clinical Efficacy of an Ayurvedic Compound in Hyperthyroidism: A Clinical Study. *Int J Ayu Pharm Chem.* 2019; 11(2):219-228
4. Vikas Nivrutti Gapat, Ujwala M Divekar, Smita Dhurde. Patho-Physiology of Hyperthyroidism & their Ayurvedic Management. *Aayushi International Interdisciplinary Research Journal: Vol III; Issue XI, Nov 2016*
5. <https://www.netmeds.com/health-library/post/vidarikhand-benefits-ingredients-method-dosage>
6. Sharma PV, Charaka S. *Chaukhambhaorientalis*. India: Varanasi; 2001. pp. 7–14.
7. Santhi T. Evaluation of Anti Thyroid Activity of Asparagus Racemosus Root Extract against
8. Thyroxine Induced Hyperthyroidism in Rats. *J of Pharmacol & Clin Res.* 2019; 7(5): 555721
9. Narinderpal K, Junaid N and Raman B. A review on pharmacological profile of Withaniasomnifera (Ashwagandha), Research and reviews. *Journal of Botanical Sciences.* 2013; 2: 6-14.
10. Lakshmi Chandra Mishra, Betsy B. Singh and Simon Dagenais. Scientific Basis for the Therapeutic Use of Withaniasomnifera (Ashwagandha): A Review. *Alternative Medicine Review.* Volume 5, Number 42000, P. 334-346.
11. Poonam Kailoria, Divya Singh, Rajendra Prasad Sharma. Critical Review on Brahmi Vati- An Ayurvedic Formulation Effective in Management of Memory Loss. *AYUSHDHARA, 2022;9(Suppl 2):55-58.*

Table No 1: Treatment Schedule

Serial No.	Treatment	Drugs	Dose
1.	<i>Deepana-Pachana</i>	<i>Panchakol Churna</i> 3gm BD	For 2 days
2.	<i>Snehapana</i>	<i>Mahatiktak Ghrita</i> (started with initial dose of 30 ml and end dose 150 ml)	For 5 days
3.	<i>Sarvanga Abhyanga</i> ( external oleation)	With <i>Dashmoolataila</i>	For 3 days
4.	<i>Sarvanga Swedana</i> (fomentation)	With <i>Dashmoolataila</i>	For 3 days
5.	<i>Virechana</i>	<i>Triphalakhwatha</i> -15gm + <i>Kutaki Churna</i> -10gm+ <i>Triphalakhwatha</i> 200 ml	For 1 day
6.	<i>Peyadi Sansarjana Karma</i>	<i>Peyadi Sansarjana</i>	For 5 days
7.	<i>Shamana Yoga</i>	1. <i>Shatavari churna</i> 10gm+ 10 gm <i>Vidarigandh churna</i> <i>Ksheerpaka</i> 2. <i>Ashwagandha churna</i> 3gm BD	For 30 days
		3. <i>Brahmi Vati</i> 1 BD	For 30 days





Alka Yadav et al.,

Table No. 2: Thyroid Profiling

Thyroid Profile, Total Serum	Bio. Ref. Interval	Before Trial	After Trial
T3	0.70-2.04 ng/mL	1.19	1.60
T4	5.74-13.03 µU/mL	10.38	11.02
TSH	0.35-5.50 µIU/mL	0.10	0.4

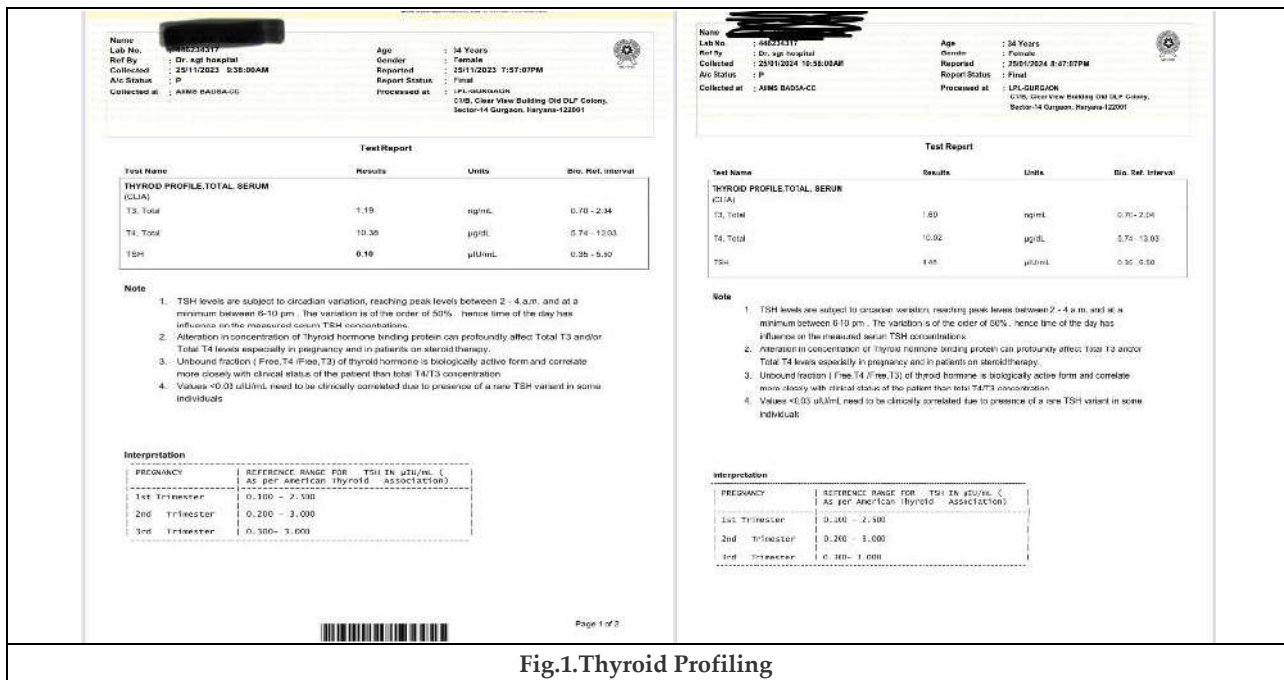


Fig.1. Thyroid Profiling





## On Some Properties of Summability in Arithmetic - Geometric Series

G. Shailaja<sup>1</sup> and R. Sivaraman<sup>2\*</sup>

<sup>1</sup>Research Scholar, Department of Mathematics, Dwaraka Doss Goverdhan Doss Vaishnav College, Arumbakkam, (Affiliated to University of Madras) Chennai, Tamil Nadu, India.

<sup>2</sup>Associate Professor, Department of Mathematics, Dwaraka Doss Goverdhan Doss Vaishnav College, Arumbakkam, (Affiliated to University of Madras) Chennai, Tamil Nadu, India.

Received: 20 July 2024

Revised: 12 Oct 2024

Accepted: 30 Nov 2024

### \*Address for Correspondence

#### R. Sivaraman

Associate Professor,  
Department of Mathematics,  
Dwaraka Doss Goverdhan Doss Vaishnav College, Arumbakkam,  
(Affiliated to University of Madras)  
Chennai, Tamil Nadu, India.  
E.Mail: rsivaraman1729@yahoo.co.in



This is an Open Access Journal / article distributed under the terms of the **Creative Commons Attribution License** (CC BY-NC-ND 3.0) which permits unrestricted use, distribution, and reproduction in any medium, provided the original work is properly cited. All rights reserved.

### ABSTRACT

The concept of summability theory has been dealt with several forms in recent years. In this paper, we present a perspective in generalizing Ramanujan summation method by considering Geometric and Arithmetic-Geometric Progressions. Geometric verifications are also included. The applications of geometric and arithmetic – geometric series on Pascal’s triangle and other applications in science are also described here.

**keywords:** Geometric Series, Arithmetic – Geometric series, Ramanujan summation, Pascal’s triangle

## INTRODUCTION

The concept of summability theory has been prevailing for several years as of now and has been a much studied topic. This idea has paved way for developing new branch of mathematical analysis called “Summability Theory”. The purpose of this paper is to present an approach to Ramanujan summation methods for geometric and arithmetic geometric series.

### Definition

The Ramanujan summation is defined as  $R.S(\sum_{n=1}^{\infty} a_n) = \int_{-1}^0 s_n dn$  (1)  
where  $n$  is a positive integer and  $s_n$  is sum upto first  $n$  terms of the divergent series  $\sum_{n=1}^{\infty} a_n$  of real numbers.





**Shailaja and Sivaraman**

**Theorem 1**

The Ramanujan summation of the geometric series  $a + ar + ar^2 + \dots + ar^{n-1} + \dots$  is given by

$$R.S\left(\sum_{n=1}^{\infty} a_n\right) = \begin{cases} \frac{a}{r-1}\left(\frac{1}{\log r} - \frac{1}{r \log r} - 1\right) & \text{if } r > 1 \\ \frac{a}{1-r}\left(1 - \frac{1}{\log r} + \frac{1}{r \log r}\right) & \text{if } 0 < r < 1 \\ -\frac{1}{2} a & \text{if } r = 1 \end{cases} \quad (2)$$

where  $a$  is the initial term and  $r$  is the common ratio between the terms.

**Proof:**

For the geometric series, the sum to  $n$  terms is given by

$$S_n = \begin{cases} \frac{a(r^n-1)}{r-1} & \text{if } r > 1 \\ \frac{a(1-r^n)}{1-r} & \text{if } 0 < r < 1 \\ na & \text{if } r = 1 \end{cases} \quad (3)$$

For the case  $r > 1$

Substituting (3) in (1) we get,

$$R.S\left(\sum_{n=1}^{\infty} a_n\right) = \int_{-1}^0 \frac{a(r^n-1)}{r-1} dn = \frac{a}{r-1} \left(\frac{r^n}{\log r} - n\right)_{-1}^0 = \frac{a}{r-1} \left(\frac{1}{\log r} - \frac{1}{r \log r} - 1\right)$$

For the case  $0 < r < 1$

Substituting (3) in (1) we get,

$$R.S\left(\sum_{n=1}^{\infty} a_n\right) = \int_{-1}^0 \frac{a(1-r^n)}{1-r} dn = \frac{a}{1-r} \left(n - \frac{r^n}{\log r}\right)_{-1}^0 = \frac{a}{1-r} \left(1 - \frac{1}{\log r} + \frac{1}{r \log r}\right)$$

For the case  $r = 1$ ,

Substituting (3) in (1) we get,

$$R.S\left(\sum_{n=1}^{\infty} a_n\right) = \int_{-1}^0 (na) dn = a \left(\frac{n^2}{2}\right)_{-1}^0 = -\frac{1}{2} a$$

**Geometric Meaning**

This can be verified geometrically by taking  $a = 1$  and scaling  $r$  for few values as follows

We observe that from the shaded portion of Figure 1(a) to Figure 1(b) is that the region representing the area of  $S_n$  between x-axis and the interval  $[-1,0]$  lies below the x-axis and it decreases as the value of common ratio increases.

From the figure for  $r = 1$ , length equals to 1 and breadth equals to 1 and the area is  $-\frac{1}{2}$

**Corollary 1**

The Ramanujan summation of the series  $2^0 + 2^1 + 2^2 + \dots + 2^n + \dots$  is

$$R.S\left(\sum_{n=1}^{\infty} a_n\right) = \frac{1}{2 \ln 2} - 1 = -0.27865(4)$$

**Proof:**

$2^0 + 2^1 + 2^2 + \dots + 2^n + \dots$  is a geometric series with  $a = 1$  and  $r = 2$

Substituting  $a = 1$  and  $r = 2$  in (3)

$$S_n = \frac{2^n-1}{2-1} = 2^n - 1 \quad (5)$$

Substituting (5) in (1)





**Shailaja and Sivaraman**

$$R.S \left( \sum_{n=1}^{\infty} a_n \right) = \int_{-1}^0 (2^n - 1)dn = \left[ \frac{2^n}{\ln 2} - n \right]_{-1}^0 = \frac{1}{2 \ln 2} - 1$$

$$= \frac{1}{2(0.693147)} - 1 = -0.27865$$

**Geometric meaning**

This can be verified geometrically as follows

We observe that from the shaded portion of Figure 2 is that the region representing the area of  $S_n$  between x- axis and the interval [-1,0] lies below the X- axis found to be -0.278652 which equals to  $\frac{1}{2 \ln 2} - 1$

**Theorem 2**

The Ramanujan summation of the arithmetic -geometric series

$$a + (a + d)r + (a + 2d)r^2 + (a + 3d)r^3 + \dots + (a + (n - 1)d)r^{n-1} + \dots \tag{6}$$

is given by

$$R.S(\sum_{n=1}^{\infty} a_n) = \begin{cases} \frac{a(1-r)+dr}{(1-r)^2} + \frac{(a-d)}{r \ln r} - \frac{d}{r(\ln r)^2} & \text{if } r > 0 \text{ and } r \neq 1 \\ -\frac{a}{2} + \frac{5d}{12} & \text{if } r = 1 \end{cases} \tag{7}$$

where  $a$  is the initial term,  $r$  is the common ratio and  $d$  is the common difference between the terms.

**Proof:**

The sum to  $n$  terms of the arithmetic - geometric series is given by

$$s_n = a + (a + d)r + (a + 2d)r^2 + (a + 3d)r^3 + \dots + (a + (n - 1)d)r^{n-1} \tag{8}$$

$$= a(1 + r + r^2 + \dots + r^{n-1}) + dr(1 + 2r + 3r^2 + \dots + (n - 1)r^{n-2})$$

if  $r > 0$  and  $r \neq 1$ , then

$$s_n = a \left( \frac{1-r^n}{1-r} \right) + dr(1 + 2r + 3r^2 + \dots + (n - 1)r^{n-2}) \tag{9}$$

$$\text{Also } 1 + 2r + 3r^2 + \dots + (n - 1)r^{n-2} = \frac{d}{dr} (r + r^2 + \dots + r^{n-1}) = \frac{d}{dr} \left( r \left( \frac{1-r^{n-1}}{1-r} \right) \right) = \frac{(n-1)r^n - nr^{n-1} + 1}{(1-r)^2} \tag{10}$$

Substituting (10) in (9) we get,

$$s_n = a \left( \frac{1 - r^n}{1 - r} \right) + dr \left( \frac{(n - 1)r^n - nr^{n-1} + 1}{(1 - r)^2} \right)$$

$$= \frac{a(1-r)+dr}{(1-r)^2} - \frac{ar^n}{1-r} + \frac{dr}{(1-r)^2} (r^{n-1}((n - 1)r - n)) \tag{11}$$

Substituting (11) in (1) we get,

$$R.S \left( \sum_{n=1}^{\infty} a_n \right) = \int_{-1}^0 s_n dn = \int_{-1}^0 \left( \frac{a(1 - r) + dr}{(1 - r)^2} - \frac{ar^n}{1 - r} + \frac{dr}{(1 - r)^2} (r^{n-1}((n - 1)r - n)) \right) dn$$

$$= \left[ \left( \frac{a(1 - r) + dr}{(1 - r)^2} \right) n - \frac{a}{1 - r} \left( \frac{r^n}{\ln r} \right) + \frac{d(r - 1)}{(1 - r)^2} \left( n \frac{r^n}{\ln r} - 1 \left( \frac{r^n}{(\ln r)^2} \right) \right) - \frac{dr}{(1 - r)^2} \frac{r^n}{\ln r} \right]_{-1}^0$$

$$= \frac{a(1-r)+dr}{(1-r)^2} + \frac{a}{r \ln r} + \frac{d}{r-1} \left( \frac{1}{r \ln r} - \frac{1}{(\ln r)^2} + \frac{1}{r(\log r)^2} \right) - \frac{d}{(r-1) \ln r}$$

$$= \frac{a(1-r)+dr}{(1-r)^2} + \frac{a}{r \ln r} - \frac{d}{r \ln r} - \frac{d}{r(\ln r)^2} \tag{12}$$

If  $r = 1$ , (6) becomes

$$s_n = a + (a + d) + (a + 2d) + (a + 3d) + \dots + (a + (n - 1)d) \tag{13}$$

Substituting (13) in (1) we get,





**Shailaja and Sivaraman**

$$R.S(\sum_{n=1}^{\infty} a_n) = \int_{-1}^0 s_n dn = \int_{-1}^0 \left(\frac{n}{2}(2a + (n - 1)d)\right) dn$$

$$= \left[ a\frac{n^2}{2} + \frac{d}{2}\left(\frac{n^3}{3} - \frac{n^2}{2}\right) \right]_{-1}^0 = -\frac{a}{2} + \frac{5d}{12} \blacksquare$$

**Geometric meaning**

This can be verified geometrically by taking  $a = 1$  and  $d = 1$  scaling  $r$  for few values as follows. We observe that from the shaded portion of Figure 3(a) to Figure 3(d) is that the region representing the area of  $S_n$  between x- axis and the interval  $[-1,0]$  lies below the x- axis.

**Corollary 1:**

If  $r = e$ , the Ramanujan summation of the arithmetic -geometric series becomes

$$R.S\left(\sum_{n=1}^{\infty} a_n\right) = \frac{1}{e(e-1)^2}((a - 2d) + e(d(4 - e) - a))$$

Also if  $a = 1, d = 1$  then,  $R.S(\sum_{n=1}^{\infty} a_n) = -0.0291$  approximately

Proof

Substituting  $r = e$  in (7)

$$R.S\left(\sum_{n=1}^{\infty} a_n\right) = \frac{a(1 - e) + de}{(1 - e)^2} + \frac{a - 2d}{e}$$

$$= \frac{1}{e(e - 1)^2}(a - 2d - de^2 - ae + 4ed)$$

$$= \frac{1}{e(e - 1)^2}((a - 2d) + e(d(4 - e) - a))$$

If  $a = 1, d = 1$  then

$$R.S(\sum_{n=1}^{\infty} a_n) = \frac{1}{e(e-1)^2}(-e^2 + 3e - 1) = -\frac{0.23421}{8.02568} = -0.0291 \text{ approximately} \blacksquare$$

**Applications in the Pascals’ triangle**

We could see Ramanujan like summation can be applied for diagonal elements of Pascal’s triangle. which is a triangular array of the binomial coefficients that has wide applications in various mathematical fields like probability theory, combinatorics and algebra.

The first eight rows of the Pascal’s triangle is as follows

**Theorem 3**

The Ramanujan summation of the sum of the diagonal elements along the first slant diagonal of Pascals’ triangle is  $R.S(\sum_{n=1}^{\infty} a_n) = -\frac{1}{2}$  (14)

**Proof:**

The sum of the diagonal elements along the first diagonal is given by  $1 + 1 + 1 + \dots + n + \dots$  which is a geometric progression series

Substituting  $a = 1$  and  $r = 1$  in (5) we get  $S_n = n$  (15)

Substituting (15) in (1) we get

$$R.S\left(\sum_{n=1}^{\infty} a_n\right) = \int_{-1}^0 n dn = -\frac{1}{2} \blacksquare$$

**Geometric meaning**

This can be verified geometrically as follows







**Shailaja and Sivaraman**

We observe that from the shaded portion of Figure 5 is that the region representing the area of  $S_n$  between x- axis and the interval  $[-1,0]$  lies below the x- axis found to be  $-0.5$  which equals to  $-\frac{1}{2}$

**Theorem 4**

The Ramanujan summation of the sum of the diagonal elements along the second slant diagonal of Pascal’s triangle is  $R.S(\sum_{n=1}^{\infty} a_n) = -\frac{1}{12}$ (16)

**Proof:**

The sum of the diagonal elements along the second diagonal is given by

$1 + 2 + 3 + 4 + \dots + n + \dots$  which is an arithmetic - series where  $a = 1$  and  $d = 1$

The sum to  $n$  terms is given by  $s_n = \frac{n}{2}(2a + (n - 1)d) = \frac{n}{2}(2 + (n - 1)) = \frac{n}{2}(n + 1)$ (17) Substituting (17) in (1) we get

$$R.S\left(\sum_{n=1}^{\infty} a_n\right) = \int_{-1}^0 \left(\frac{n}{2}(n + 1)\right) dn = -\frac{1}{12}$$

**Geometric meaning**

This can be verified geometrically as follows

We observe that from the shaded portion of Figure 6 is that the region representing the area of  $S_n$  between x-axis and the interval  $[-1,0]$  lies below the x axis found to be  $-0.0833333333333333$ . which is approximately equals to  $-\frac{1}{12}$

This result is similar to Ramanujan work on  $1 + 2 + 3 + \dots = -\frac{1}{12}$

**Theorem 5**

The Ramanujan summation of the sum of the diagonal elements along the third slant diagonal of Pascal’s triangle is  $R.S(\sum_{n=1}^{\infty} a_n) = -\frac{1}{24}$  (18)

**Proof:**

The sum of the diagonal elements along the third diagonal of Pascal’s triangle is given by

$1 + 3 + 6 + \dots + n + \dots$

The sum to  $n$  terms of the series is given by  $S_n = \binom{n+2}{3} = \frac{n^3 + 3n^2 + 2n}{6}$  (19)

Substituting (19) in (1) we get

$$R.S\left(\sum_{n=1}^{\infty} a_n\right) = \int_{-1}^0 \left(\frac{n^3 + 3n^2 + 2n}{6}\right) dn = -\frac{1}{24} \quad \blacksquare$$

**Geometric meaning**

This can be verified geometrically as follows.

We observe that from the shaded portion of (Figure 7) is that the region representing the area of  $S_n$  between x- axis and the interval  $[-1,0]$  lies below the x- axis found to be  $-0.041666666666667$  which is approximately equals to  $-\frac{1}{24}$

**Other Applications in Science**

Here are some additional applications of geometric and arithmetic geometric series in various scientific fields. Scientists across various disciplines can leverage geometric and arithmetic geometric series whenever exponential growth, decay, or repeated processes with a constant factor come into play. For instances in physics, in diffraction gratings and in geometric optics, in Chemistry, Chemical Kinetics and serial dilutions, in biology, Signal Transduction, population Genetics and in other sciences, earthquake magnitudes, ecology etc

**CONCLUSION**

We have discussed the Ramanujan summation for geometric and arithmetic-geometric series and we have applied this to Pascal’s triangle and we got nice results. We have used Desmos graphing software tool to create graphs presented in the figures. Further we can construct Ramanujan summation for various other series also using the techniques presented in this paper.





## REFERENCES

1. R. Sivaraman, Understanding Ramanujan Summation, International Journal of Advanced Science and Technology, Volume 29, No. 7, (2020), 1472 – 1485.
2. R. Sivaraman, Summing Through Triangle, International Journal of Mechanical and Production Engineering Research and Development, Volume 10, Issue 3, June 2020, pp. 3073 – 3080.
3. R. Sivaraman, Sum of powers of natural numbers, AUT AUT Research Journal, Volume XI, Issue IV, April 2020, 353 – 359.
4. S. Ramanujan, Manuscript Book 1 of Srinivasa Ramanujan, First Notebook, Chapter VIII, 66 – 68.
5. Bruce C. Berndt, Ramanujan's Notebooks Part II, Springer, Corrected Second Edition, 1999
6. G.H. Hardy, J.E. Littlewood, Contributions to the theory of Riemann zeta-function and the theory of distribution of primes, Acta Arithmetica, Volume 41, Issue 1, 1916, 119 – 196.
7. S. Plouffe, Identities inspired by Ramanujan Notebooks II, part 1, July 21 (1998), and part 2, April 2006.
8. G. H. Hardy, P.V. Seshu Iyer, B.M. Wilson, Collected Papers of Srinivasa Ramanujan, New York, Chelsea Publishing Company, 1962, 136 – 162.
9. A. Terras, Some formulas for the Riemann zeta function at odd integer argument resulting from Fourier expansions of the Epstein zeta function, Acta Arithmetica XXIX (1976), 181–189.
10. E. C. Titchmarsh, The theory of the Riemann zeta-function, Oxford University Press, 1951.
11. B. Candelpergher, H. Gopalakrishna Gadiyar, R. Padma, Ramanujan Summation and the Exponential Generating Function, Cornell University, January 2009.
12. Bruce C. Berndt, An Unpublished Manuscript of Ramanujan on Infinite Series Identities, Illinois University, American Mathematical Society publication
13. R. Sivaraman, Remembering Ramanujan, Advances in Mathematics: Scientific Journal, Volume 9 (2020), no.1, 489–506.
14. R. Sivaraman, Bernoulli Polynomials and Ramanujan Summation, Proceedings of First International Conference on Mathematical Modeling and Computational Science, Advances in Intelligent Systems and Computing, Vol. 1292, Springer Nature, 2021, pp. 475 – 484.
15. Dinesh Kumar A, Sivaraman R. Ramanujan Summation for Pascal's Triangle. Contemp. Math.. 2024;5(1):817–25
16. R. Sivaraman, J. Suganthi, P.N. Vijayakumar, R. Sengothai, Generalized Pascal's Triangle and its Properties, NeuroQuantology, Vol. 22, No. 5, 2022, 729 – 732.
17. A. Dinesh Kumar, R. Sivaraman, Asymptotic Behavior of Limiting Ratios of Generalized Recurrence Relations, Journal of Algebraic Statistics, Volume 13, No. 2, 2022, 11 – 19.
18. A. Dinesh Kumar, R. Sivaraman, Analysis of Limiting Ratios of Special Sequences, Mathematics and Statistics, Vol. 10, No. 4, (2022), pp. 825 – 832
19. Andreescu, T., D. Andrica, and I. Cucurezeanu, An introduction to Diophantine equations: A problem-based approach, Birkhäuser Verlag, New York, 2010.
20. An, F., Sayed, B.T., Parra, R.M.R., Hamad, et al., Machine learning model for prediction of drug solubility in supercritical solvent: Modeling and experimental validation, Journal of Molecular Liquids, 363, 2022, 119901.
21. Reena Solanki et al., Investigation of recent progress in metal-based materials as catalysts toward electrochemical water splitting, Journal of Environmental Chemical Engineering, 10 (2022), 108207
22. Guangping Li, Jalil Manafian, et al., Periodic, Cross-Kink, and Interaction between Stripe and Periodic Wave Solutions for Generalized Hietarinta Equation: Prospects for Applications in Environmental Engineering, Advances in Mathematical Physics, vol. 2022.
23. R. Sivaraman, R. Sengothai, P.N. Vijayakumar, Novel Method of Solving Linear Diophantine Equation with Three Variables, Stochastic Modeling & Applications, Vol. 26, No. 3, Special Issue – Part 4, 2022, 284 – 286.





**Shailaja and Sivaraman**

<p><b>Figure 1(a)</b> Graph for <math>\int_{-1}^0 \frac{a(r^n - 1)}{r - 1} dn</math> showing area of <math>S_n</math> between x- axis and the interval [-1,0] for <math>r = 5</math></p>	<p><b>Figure 1(b)</b> Graph for <math>\int_{-1}^0 \frac{a(r^n - 1)}{r - 1} dn</math> showing area of <math>S_n</math> between x- axis and the interval [-1,0] for <math>r = 10</math></p>
<p><b>Figure 1(c)</b> Graph for <math>\int_{-1}^0 \frac{a(1 - r^n)}{1 - r} dn</math> showing area of <math>S_n</math> between x- axis and the interval [-1,0] for <math>r = 0.2</math></p>	<p><b>Figure 1(d)</b> Graph for <math>\int_{-1}^0 \frac{a(1 - r^n)}{1 - r} dn</math> showing area of <math>S_n</math> between x- axis and the interval [-1,0] for <math>r = 0.5</math></p>
<p><b>Figure 1(e)</b> Graph for <math>\int_{-1}^0 \frac{a(1 - r^n)}{1 - r} dn</math> showing area of <math>S_n</math> between x- axis and the interval [-1,0] for <math>r = 0.8</math></p>	<p><b>Figure 1(f)</b> Graph for <math>\int_{-1}^0 (na) dn</math> showing area of <math>S_n</math> between x- axis and the interval [-1,0] for <math>r = 1</math></p>





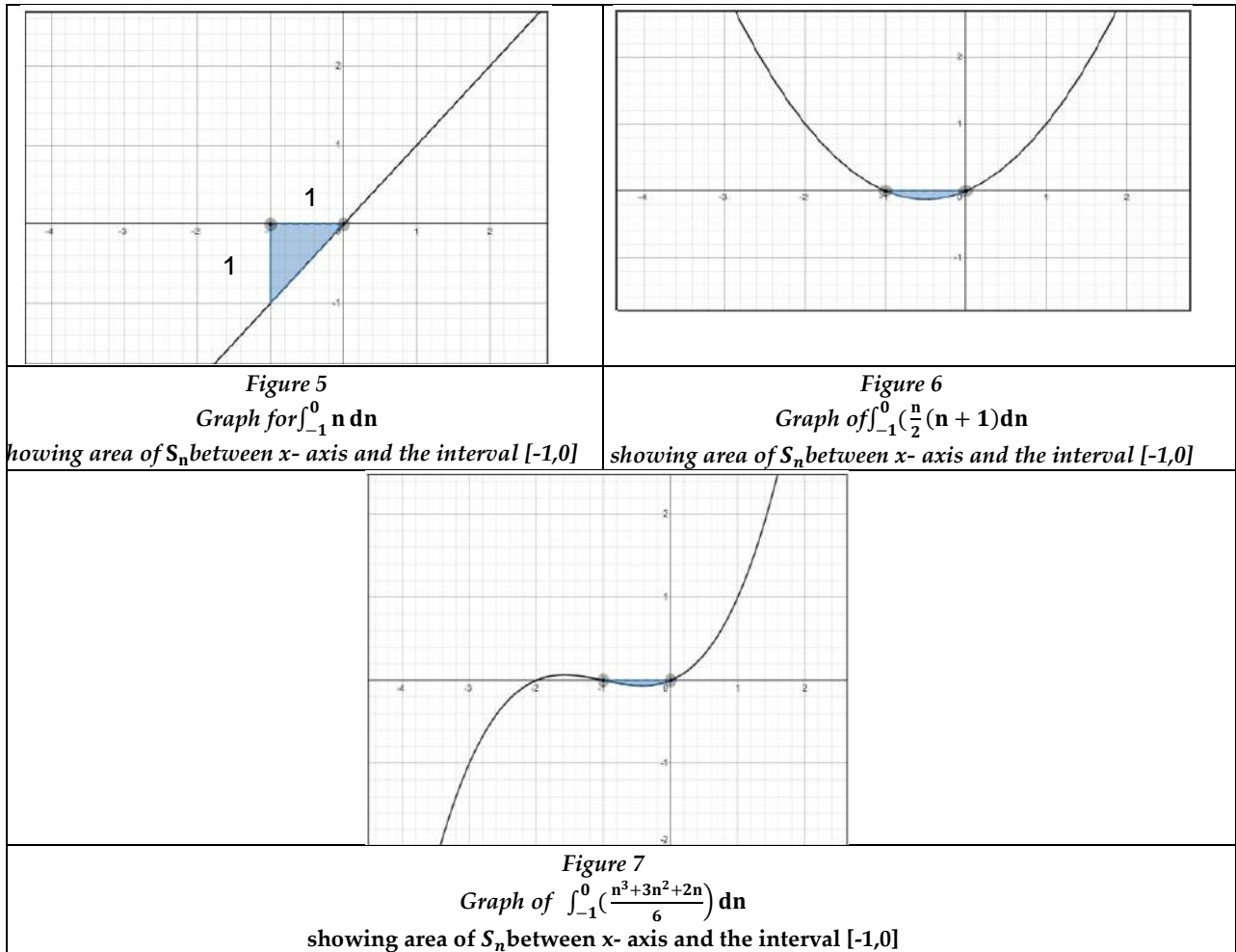
Shailaja and Sivaraman

<p><b>Figure 2</b> Graph for <math>\int_{-1}^0 (2^n - 1) dn</math> showing area of <math>S_n</math> between x- axis and the interval [-1,0]</p>	<p><b>Figure 3(a)</b> Graph for <math display="block">\int_{-1}^0 \left( a \left( \frac{1-r^n}{1-r} \right) + dr \left( \frac{(n-1)r^n - nr^{n-1} + 1}{(1-r)^2} \right) \right) dn</math> showing area of <math>S_n</math> between x- axis and the interval [-1,0] for <math>r = 0.2</math></p>
<p><b>Figure 3(b)</b> Graph for <math display="block">\int_{-1}^0 \left( a \left( \frac{1-r^n}{1-r} \right) + dr \left( \frac{(n-1)r^n - nr^{n-1} + 1}{(1-r)^2} \right) \right) dn</math> showing area of <math>S_n</math> between x- axis and the interval [-1,0] for <math>r = 0.8</math></p>	<p><b>Figure 3(c)</b> Graph for <math display="block">\int_{-1}^0 \left( a \left( \frac{1-r^n}{1-r} \right) + dr \left( \frac{(n-1)r^n - nr^{n-1} + 1}{(1-r)^2} \right) \right) dn</math> showing area of <math>S_n</math> between x- axis and the interval [-1,0] for <math>r = 2</math></p>
<p><b>Figure 3(d)</b> Graph for <math display="block">\int_{-1}^0 \left( a \left( \frac{1-r^n}{1-r} \right) + dr \left( \frac{(n-1)r^n - nr^{n-1} + 1}{(1-r)^2} \right) \right) dn</math> showing area of <math>S_n</math> between x- axis and the interval [-1,0] for <math>r = 4</math></p>	<p><b>Figure 4 Pascal's Triangle</b></p>





**Shailaja and Sivaraman**





# Optimizing Water Hyacinth Compost and Chicken Manure for Enhancing Spinach Growth: An Eco-Friendly Approach to Sustainable Agriculture

Mahmuda Parveen<sup>1</sup> and Sujit Ghosh<sup>2\*</sup>

<sup>1</sup>Research Scholar, Department of Botany, Sidho-Kanho-Birsha University (SKBU), Purulia, West Bengal, India.

<sup>2</sup>Associate Professor, Jagannath Kishore College, (Affiliated to Sidho-Kanho-Birsha University (SKBU), Purulia, West Bengal, India)

Received: 14 Jun 2024

Revised: 16 Aug 2024

Accepted: 17 Oct 2024

## \*Address for Correspondence

**Sujit Ghosh**

Associate Professor,  
Jagannath Kishore College,  
(Affiliated to Sidho-Kanho-Birsha University (SKBU),  
Purulia, West Bengal, India  
E. Mail: sujit@jkcprl.ac.in



This is an Open Access Journal / article distributed under the terms of the **Creative Commons Attribution License** (CC BY-NC-ND 3.0) which permits unrestricted use, distribution, and reproduction in any medium, provided the original work is properly cited. All rights reserved.

## ABSTRACT

Sustainable agriculture practices that reduce reliance on synthetic inputs are essential for environmental conservation and food security. This study explores the potential of transforming the invasive aquatic weed, water hyacinth (*Eichhornia crassipes* (Mart.) Solms), and chicken manure, a by-product of poultry farming, into organic fertilizers to enhance spinach (*Spinacea oleracea* L.) leaf area growth. Using Design Expert Software (Version 13), the proportions of water hyacinth compost and chicken manure were optimized to maximize spinach leaf area growth. Response surface methodology and central composite design helped find the best mix (PREDICTION). This optimal point, shown by software-generated contour and 3D surface plots, was then validated by mixing the contents in tubs for spinach leaf area, showing similar results. The optimal blend of 1184.17 grams of compost and 41.72 grams of chicken manure resulted in a maximum spinach leaf area of 225 square centimeters, exhibiting the efficacy of this organic fertilizer. This approach not only promotes plant growth but also presents a sustainable waste management strategy, mitigating the ecological impact of this invasive weed. The resulting organic fertilizer blend significantly improved soil properties by reducing bulk density and increasing porosity, enhancing aeration and root penetration for water and mineral absorption. Additionally, compared to unamended soil, the higher levels of total nitrogen, phosphorus, and potassium create an ideal environment for nutrient absorption by plants.

**Keywords:** Water hyacinth compost, Chicken manure, Organic fertilizers, Sustainable agriculture, Response surface methodology







## INTRODUCTION

In the pursuit of sustainable agricultural practices, the integration of eco-friendly approaches has become increasingly crucial. One such approach involves the utilization of organic amendments derived from waste materials, such as water hyacinth compost (WHC) and chicken manure (CM). This study aims to optimize the application of these amendments through response surface methodology (RSM) to enhance spinach growth, fostering an environmentally conscious and economically viable agricultural system. The growing need for food production and the reduction of the harmful effects of synthetic fertilizers have led to the search for alternative nutrient sources [1]. Water hyacinth (*Eichhornia crassipes* (Mart.) Solms.), an invasive aquatic plant, is a valuable resource for nutrient-rich compost due to its high biomass production and nutrient uptake capacity [2]. Controlled composting processes can convert this weed into organic fertilizer, aiding sustainable waste management and nutrient recycling. CM, a by-product of poultry farming, is known for its high content of nitrogen, phosphorus, and potassium [3]. These alternatives present promising solutions for sustainable agriculture, addressing both environmental concerns and the need for effective fertilization. Numerous studies have explored the use of WHC and CM, either individually or in combination, for enhancing the growth and yield of various crops, such as maize [4], tomatoes, brinjal, and chilli [5,6], and cowpea [7]. Converting this weed into nutrient-rich compost through controlled processes offers environmental sustainability, soil health improvement, nutrient recycling, enhanced crop yield and quality, and integrated waste management strategies.

Efforts have been made to optimize synthetic fertilizer with organic fertilizer combinations to maximize plant growth and minimize environmental impacts. For example, Moradi *et al.*, 2024 [8] turned NPK (synthetic), cow manure, and vermicompost into a nutrient-rich compost blend for growing quinoa (*Chenopodium quinoa* Willd.). Similarly, RSM was used to optimize the application rate of nitrogen and phosphorus (synthetic fertilizers) and cattle manure in wheat production [9]. While previous studies optimized combinations of inorganic and organic fertilizers using RSM with three or more components, this study uniquely focuses on using only two variables: water hyacinth compost and chicken manure as sole organic fertilizers, excluding synthetic inputs. By converting water hyacinth into nutrient-rich compost and combining it with chicken manure, this research demonstrates that organic fertilizers alone can effectively support the growth of spinach. This approach, using RSM combined with a Central Composite Design (CCD) to statistically optimize the proportions of these two factors for optimal spinach growth, aims to address concerns about the sufficiency of organic fertilizers. It promotes sustainable agriculture systems, environmental conservation, resource efficiency, and food security. The findings offer valuable insights for farmers, researchers, and policymakers interested in adopting sustainable and eco-friendly agricultural practices.

## MATERIALS AND METHODS

### Seed material and Germination Procedure

Spinach (*Spinacia oleracea*) seeds obtained from a local market were stored at 30% relative humidity and 13°C until use. This study took place at J.K. College in Purulia, West Bengal, under ex-vitro environmental conditions. The seeds were subjected to pre-treatment by soaking in water for 24 hours to enhance germination. Germination conditions were maintained at a temperature of 21°C, with a light cycle of 12 hours of light and 12 hours of darkness, and a humidity level of 50%. Seeds were placed on the moist filter paper in the petri dishes and covered with lids to maintain humidity. These dishes were then placed inside a germination cabinet to provide a controlled environment. Daily monitoring was conducted to observe germination progress, and the number of germinated seeds was recorded.

### Preparation of WHC

The study on compost optimization was conducted using contained within galvanized wire cages mesh size (3/4 inch) of 3 feet diameter 4 feet height, secured with twine or quick-release knots placed in an open area and set on an





elevated platform. To prepare compost, a controlled composting method was employed, relying solely on organic material derived from water hyacinth and naturally occurring microbes from soil not previously enriched with organic amendments. Water Hyacinth was collected from "Rishi Nibaran Sayer", a lake in Purulia district, West Bengal. The composting process lasted 3 months (25 June-5 October 2023). The compost site was established with a base layer of fractured brick, gravel, stone, and sand for proper drainage and aeration. Shredded water hyacinth served as the primary composting material, spread evenly over the base layer. The composting pile was contained within galvanized wire cages, secured with twine or quick-release knots. Moisture levels and consecutive turning (5 days interval) were maintained using a fertilizer hose-end sprayer, and a tarp covered the pile to retain heat and moisture. Temperature monitoring was conducted with a compost temperature probe, with readings taken twice daily to ensure the core temperature remained between 45°C and 57°C. The pile was turned if the temperature exceeded this range, with cooler outer layers moved towards the center for even decomposition. pH and moisture readings were taken once daily, with adjustments made as necessary. Once the compost achieved a stable temperature range, dark crumbly texture, and earthy smell, it entered the curing phase, typically lasting 1-4 weeks. Before application to soil, the compost was screened to remove any large, un-decomposed pieces.

### CM Preparation

CM was collected from a local poultry farm and air-dried on trays for four days to reduce moisture. The partially dried manure was then sterilized in an autoclave at 121°C and 15 psi for 15 minutes to remove pathogens. After sterilization, it was sun-dried for another three days to become odorless and evaporate any remaining moisture. The dried chicken manure was sieved through a 2.00-mm mesh to achieve the desired particle size and homogeneity. The final product was ready for blending with compost in varying proportions to create an organic fertilizer mixture aimed at enhancing spinach growth.

### Soil Quality Analysis

Soil physical parameter- bulk density and porosity [10], chemical parameter such as pH [11], TN [12], Available P [13], Available K [14], were analyzed to assess soil quality.

**Analysis of Variance (ANOVA) study for Quadratic Model** (via main effects, interactions, or quadratic effects with relative importance of each term for model's accuracy and reliability): The ANOVA study [15] for the quadratic model evaluates the significance and adequacy of the fitted model in representing the relationship between the response variable (leaf area) and the independent variables (water hyacinth compost and chicken manure). The ANOVA assesses the null hypothesis (H<sub>0</sub>) that all model terms are insignificant ( $\beta = 0$ ) against the alternative hypothesis (H<sub>1</sub>) that at least one term is significant ( $\beta \neq 0$ ). The F-test determines if the variation caused by each term is significantly greater than the residual error, with p-values indicating the significance level. The ANOVA table lists the sources of variation (linear, quadratic, interaction terms), degrees of freedom (df), sum of squares, mean square (MS), F-value (ratio of MS for each term to residual MS), and p-value. The F-value and p-value help identify significant model terms influencing the response variable and assess model adequacy through lack-of-fit tests. The analysis guides the selection of relevant terms for constructing an optimized quadratic model, supporting the interpretation and validation of the RSM results.

### Experimental Design

In this experiment, Spinach seeds were surface-sterilized before planting in 10-inch pots prepared with the soil mixtures. The seeds were sown at a depth of 0.5 inches, with proper spacing and watering for germination and early development. RSM was employed using a CCD [16] to optimize the parameters for spinach growth, with Design-Design Expert v.13 software used for statistical analysis. The independent variables investigated were WHC and CM, with three levels each (600, 1200, and 1800 gm for compost; 12, 24, and 48 gm for CM) (Table-3). A full factorial combination resulted in 9 treatment combinations, plus two additional treatments (pure soil and pure compost), for a total of 11 treatments. Each treatment was replicated three times, leading to 33 experimental units. A completely randomized design was used, with treatments randomly assigned to the experimental units. The response variable



**Mahmuda Parveen and Sujit Ghosh**

(spinach growth) was measured in terms of leaf area. Appropriate statistical methods, such as ANOVA, were used to evaluate the significance of the main effects and their interaction on the response variable.

**Analysis of Plant Morphological Parameters**

Spinach plants were harvested after 50 days of sowing, and growth measures (leaf area) were used to assess. We use IBM SPSS Statistics 25 for statistical analysis. To determine the least significant difference between treatment means, ANOVA was used with a significance level of  $p < 0.05$ .

**Statistical Optimization of Spinach growth:**

Our experimental data were fitted into this second-order quadratic equation, including individual and cross-interaction effects among all variables:

$Y = \beta_0 + \beta_1X_1 + \beta_2X_2 + \beta_3X_3 + \beta_4X_4 + \beta_{12}X_1X_2 + \beta_{13}X_1X_3 + \beta_{14}X_1X_4 + \beta_{23}X_2X_3 + \beta_{24}X_2X_4 + \beta_{34}X_3X_4 + \beta_{11}X_1^2 + \beta_{22}X_2^2 + \beta_{33}X_3^2 + \beta_{44}X_4^2$ , where, Y is the predicted response;  $\beta_0$  is the constant term;  $\beta_1, \beta_2, \beta_3,$  and  $\beta_4$  are the regression coefficients for linear effects;  $\beta_{12}, \beta_{13}, \beta_{14}, \beta_{23}, \beta_{24},$  and  $\beta_{34}$  denote the regression coefficients for interaction effects; and  $\beta_{11}, \beta_{22}, \beta_{33},$  and  $\beta_{44}$  are the regression coefficients for quadratic effects [17]. The response value Y was the leaf area of the spinach plant in relation to the two variables. Analysis through software, the regression of the experimental data and generate response surface graphs. Correlation coefficients "R" and determination coefficients  $R^2$  were calculated to evaluate the performance of the regression equation. The fitted polynomial equation was visualized through 3D surface plots. Significance of the model was determined by ANOVA. The interactive relationship between significant variables was explored through response surface and contour plots. RSM was applied for regression and graphical analysis of the obtained data.

**RESULTS****Soil characterization**

30 soil samples used for this experiment and bulk density, porosity, pH, nutrient content (TN, P, K) were characterized. The results are shown in the Table-1. These parameters provide baseline information about the physical and chemical properties of soil, indicating compaction level, aeration status, and initial nutrient levels, which can be compared after applying organic amendments to evaluate their effectiveness in enhancing soil fertility and interpreting subsequent results.

**Composting Process**

The composting process went through distinct phases with varying pH, temperature, and moisture content. The initial mesophilic stage lasted three weeks with pH 7.0-7.9, moderate temperature around 37°C, and moisture declining from 92% to 79.8%. The subsequent thermophilic phase peaked at 49°C with pH stabilized at 7.9 and moisture dropped to 68%. During the 8-15 week cooling and curing phases, temperature decreased to 25°C, pH dropped to 7.2, and moisture reached 30%. The optimal compost blend of WHC and CM for maximizing spinach leaf area was identified and analyzed for nutrient content and bulk density.

**Soil Properties Comparison**

The optimized WHC and CM blend significantly improved soil properties that are mentioned in Table-2.

**Optimizing Spinach Growth through Response Surface Methodology: A Statistical Approach: Response surface methodology and optimization**

In this study, RSM combined with CCD, a two-level factorial design with 3 center points, were used to evaluate the effects of two independent variables on the dependent variable, mentioned in Table-3. A quadratic model explored the mathematical relationship between variables. The design incorporated five coded levels with 11 experimental runs to analyze the interaction effects of individual, quadratic, and cross-product terms of the variables in a





randomized order. This statistical approach aimed to identify the optimal combination of WHC and CM for maximizing spinach leaf area. The CCD matrix and the observed leaf area responses for spinach plant growth are shown in Table 4. The ANOVA results for the quadratic model applied to the experimental data offer insights into the model's significance and the impact of individual factors on spinach leaf area, as shown in Table 5.

#### Fit Statistics

The C.V assesses the reliability of the statistical model by comparing the estimated standard error to the mean value of the observed response. Table 6 provides an overview of the ANOVA summary of fit statistics. A C.V. value below 10% is preferred. The Predicted  $R^2$  of 0.7963 aligns closely with the Adjusted  $R^2$  of 0.9100, with a difference of less than 0.2. Adequate Precision evaluates the signal-to-noise ratio, where a ratio above 4 is ideal. The ratio of 14.912 signifies a strong signal, indicating the model's suitability for exploring the design space. The C.V. value is less than 10% (4.36%), indicating that the model is also highly significant.

#### Final Equation in Terms of Coded Factors:

The final equation for the leaf area of the spinach plant, expressed in terms of coded factors, is provided below:

$$\text{Sqrt (Leaf Area)} = 15.29 + 0.4181 * A + 0.3884 * B - 0.1398 * AB - 0.2482 * A^2 - 1.28 * B^2,$$

Where A denotes WHC and B represents CM (in grams). The coded factors equation is useful for predicting responses based on specific levels of each factor. Typically, the higher levels of the factors are coded as +1, and the lower levels are coded as -1. This coded equation predicts responses based on factor levels and helps determine their relative influence through coefficient comparison. The constant term (15.29) represents the predicted square root of leaf area when all independent variables (A, B, AB,  $A^2$ ,  $B^2$ ) are zero. The coefficient of A (0.4181) indicates that for each unit increase in the water hyacinth compost application rate, with other variables constant, the square root of leaf area increases by 0.4181 units. Similarly, the coefficient of B (0.3884) suggests that each unit increase in the CM application rate increases the square root of leaf area by 0.3884 units. The coefficient of AB (-0.1398) shows the interaction effect between WHC and CM, with the negative value indicating their combined effect is less than their individual effects' sum. The coefficient of  $A^2$  (-0.2482) indicates that increasing water hyacinth compost beyond a certain point may decrease the square root of leaf area, suggesting a non-linear relationship. Likewise, the coefficient of  $B^2$  (-1.28) implies that higher CM application rates may reduce the square root of leaf area, also suggesting a non-linear relationship.

#### Final equation in terms of actual factors:

The final equation in terms of actual factors for the square root of spinach leaf area is:

$$\text{Sqrt (Leaf Area)} = 8.79038 + 0.002740 * \text{Compost} + 0.274069 * \text{Chicken Manure} - 0.000013 * \text{Compost} * \text{Chicken Manure} - 6.89444\text{E-}07 * \text{Compost}^2 - 0.003949 * \text{Chicken Manure}^2.$$

This equation can predict responses based on specific levels of WHC and CM in their original units. However, the coefficients here are adjusted for the units and cannot be directly compared to assess relative importance. Notably, the larger negative quadratic coefficient for chicken manure (-0.003949) compared to compost (-6.89444E-07) suggests a more pronounced non-linear relationship between chicken manure application rate and the square root of leaf area. This implies that excessive CM application may decrease leaf area more severely than excessive compost application, highlighting the importance of optimizing both amendments proportions.

#### Residual plots

These plots help identify differences between experimentally derived and predicted values. Fig. 1 illustrates the relationship between predicted and actual leaf area of spinach plants after 50 days of harvesting. The plot indicates that the quadratic model is significant for analyzing response and input variables. The data points closely follow the linear trend line, suggesting the model accurately estimates leaf area response. The model exhibits a good fit, evidenced by the evenly distributed data points along the line with minimal deviations.



**Response surface plot analysis:**

Contour plots optimize multiple variables and identify significant parameters, visually mapping the experimental area for maximum response. They also reveal important interactions between factors that could lead to the desired outcome. The quadratic response surface model is examined using 3D response surfaces and 2D contour plots, where one variable is held constant while the other two are varied within experimental ranges. Figures 2 and 3 present contour and 3D surface plots visualizing the interaction effects of WHC and CM on spinach leaf area response. The plots show higher leaf area values concentrated in the upper-right region, suggesting higher levels of both factors are favorable. The smooth contours indicate a well-behaved response surface within the experimental ranges. Analysis predicts the optimum point for maximum leaf area (approximately 225 cm<sup>2</sup>) at 1184.17 gm WHC and 41.72 gm CM, marked by the red point on the contour plot. The innermost and outermost contours represent leaf areas of around 200 cm<sup>2</sup> and 180 cm<sup>2</sup>, respectively. The distinct peak in the response surface signifies a quadratic relationship, with an optimal factor combination maximizing leaf area, highlighting the importance of strategic application rate adjustments for enhancing spinach growth.

**Point Prediction**

In Table-7, the 95% confidence interval for the mean leaf area is between 201.483 cm<sup>2</sup> and 249.851 cm<sup>2</sup>, indicating that there is 95% confidence that the true mean falls within this range. The 95% tolerance interval for 99% of the population spans from 125.641 cm<sup>2</sup> to 352.286 cm<sup>2</sup>, meaning that 99% of individual observations or future leaf area values are expected to fall within these limits with 95% confidence. To ensure accurate results, new experiments were conducted using the optimal input variable combination of 1184.17 gm WHC and 41.72 gm CM, as determined by the optimization process.

**Compare predicted and experimental values**

The predictive model's performance was evaluated by calculating the percentage error or residual between the predicted (225 cm<sup>2</sup>) and experimental leaf area values (10 sets: 221.6, 221.44, 226.2, 224.4, 224.4, 223.6, 223.2, 227.2, 221.5, and 222 cm<sup>2</sup>) at optimal input variable levels. To validate the robustness of RSM model through experimentation, we can employ statistical test like one-sample t-test or confidence interval analysis were employed using the new experimental data. The one-sample t-test determines if the mean experimental leaf area significantly differs from the predicted 225 cm<sup>2</sup>, with the H<sub>0</sub> stating no difference and the H<sub>1</sub> suggesting a difference. The assumptions include independent and randomly sampled data, and approximate normality. Alternatively, a confidence interval for the mean difference between predicted and experimental values can assess the statistical significance.

**DISCUSSION**

The results of this study demonstrate the potential of utilizing organic waste materials, such as water hyacinth compost and chicken manure, as eco-friendly fertilizers for enhancing the growth of spinach plants. The amended soil exhibited significantly improved physical and chemical properties compared to the control soil. The bulk density decreased from 1.194 g/cc to 0.825 g/cc, while porosity increased from 45.28% to 68.87%, indicating a lighter, more porous structure for increased water infiltration, root growth, and is desirable for overall plant growth and health [18]. Additionally, nutrient levels substantially increased: nitrogen from 357.8 mg/kg to 1120 mg/kg (tripled), phosphorus from 23.60 mg/kg to 106 mg/kg, and potassium from 110 mg/kg to 143 mg/kg. These enhancements in soil quality, structure, and fertility by incorporating compost suggest potential benefits for better plant growth and agricultural productivity [19]. Begum *et al.*, 2022 reviewed potential of water hyacinth, noting a substantial upsurge on its effect on soil and plant properties [20].

The composting process involved distinct phases with varying conditions: an initial mesophilic stage with pH 7.0-7.9, temperature around 37°C, and moisture decreasing from 92% to 79.8% over three weeks; a thermophilic phase peaking at 49°C with pH 7.9 and moisture dropping to 68%; and cooling and curing phases over 8 to 15 weeks where temperature fell to 25°C, pH to 7.2, and moisture to 30%. The influence of temperature and moisture content regimes







on the aerobic microbial activity in composting blends was observed by Liang *et al.*, 2003 [21]. Bulk density decreased from previous, while porosity increased, enhancing aeration and water infiltration. Nutrient levels remarkably increased. The organic matter and nutrient-rich compost reduced soil compaction, improved structure, and increased essential nutrient availability for plant growth [22].

The application of RSM and CCD enabled the systematic optimization of the WHC and CM levels within specified ranges, providing insights into the optimal proportions required for maximizing spinach leaf area. Table-3 defines the low and high levels of these variables, while Table-4 displays the CCD matrix and observed leaf area responses. Experimental runs followed the CCD matrix, with observed leaf area responses varying from 75.36 cm<sup>2</sup> to 241.22 cm<sup>2</sup> across different variable combinations. These findings offer insights into how changes in compost and chicken manure levels influence. The statistical analysis revealed that the quadratic model effectively captured the relationship between the two independent variables and the dependent variable. RSM and CCD were also utilized to optimize various agricultural and biological processes. The yield and quality of French bean (*Phaseolus vulgaris* L) were enhanced by Kumar *et al.*, 2020 [23] through the optimization of the effects of Plant Growth-Promoting Rhizobacteria and silicon fertilization. Similarly, a two-variable CCD and RSM were used by Prakash and Srivastava, 2005 [24] to study the optimization of carbon (sucrose/glucose) and nitrogen (NO<sub>3</sub><sup>-</sup>/NH<sub>4</sub><sup>+</sup> ratio) in *Azadirachta indica* suspension culture. Optimal conditions were identified in both studies, with the quadratic model accurately representing the relationship between the independent and response variables, enabling the optimization of French bean yield, quality, and media.

In table-5 shows the impact of WHC and CM application rates on leaf area. The model overall was statistically significant ( $p = 0.0022$ ), indicating that at least one factor or interaction significantly influenced leaf area. However, the main effects of WHC (A-Compost,  $p = 0.1382$ ) and CM (B-Chicken manure,  $p = 0.1287$ ), as well as their interaction (AB,  $p = 0.6104$ ), were not statistically significant at the 5% level. The quadratic effect of WHC (A<sup>2</sup>,  $p = 0.3775$ ) was also not significant, whereas the quadratic effect of CM (B<sup>2</sup>,  $p = 0.0040$ ) was, suggesting a non-linear relationship with leaf area. Therefore, while the model and the quadratic effect of CM are significant, the individual contributions of WHC and CM, along with their interaction, are not statistically significant. In Table-6, the high coefficient of determination ( $R^2 = 0.9550$ ) and low coefficient of variation (C.V. = 4.36%) suggest the model's good fit and reliability. ANOVA results confirm the significance of the quadratic model ( $p$ -value = 0.0022), pointing to that it is capable of accurately predicting the response within the experimental range. Some research papers revealed similar conclusion such as high  $R^2$  values observed in each study—0.974 for maximizing auxin production by *Pantoea agglomerans* C1 [25], 0.9915 for optimization of phenolic compound extraction from pineapple peel waste [26] and 0.9772 for production of the xylanase enzyme by a fungal strain [27]—indicate that the quadratic models could account for a significant portion of the variability in the responses. Likewise, the low C.V., ranging from 2.74% to 4.50%, demonstrates the accuracy and consistency of the experimental findings. The quadratic models relevancy was further confirmed by ANOVA, with all trials yielding  $p$ -values of less than 0.0001. This statistical confirmation proved the robustness of the models and the dependability of the findings. The quadratic model developed in this study represented by the equation  $-\text{Sqrt}(\text{Leaf Area}) = 15.29 + 0.4181 * A + 0.3884 * B - 0.1398 * AB - 0.2482 * A^2 - 1.28 * B^2$ ; is a reliable method for predicting spinach leaf area. The constant term (15.29) predicts the square root of leaf area, while A (0.4181) and B (0.3884) shows positive impacts of WHC and CM, while the coefficient of AB (-0.1398) reflects the interaction between the two. Excessive amounts of either WHC or CM reduce leaf area as indicated by coefficients A<sup>2</sup> (-0.2482) and B<sup>2</sup> (-1.28).

The predicted vs. actual plot (Fig. 1) demonstrates a strong positive correlation between the predicted and observed leaf area values, supporting the validity and reliability of the model. Although a few data points depart slightly from the trend line, the overall plot demonstrates the ability of model to effectively represent the underlying relationships. The predicted mean and median leaf area values are closely aligned, suggesting a relatively symmetric distribution of the response variable. The small confidence interval for the mean leaf area (about 201.483 cm<sup>2</sup>) shows acceptable precision in predicting the real mean, while the broader tolerance interval (roughly 249.851 cm<sup>2</sup>) (See Table-7) incorporates heterogeneity in individual data. These measures give useful insights into the central tendency,







uncertainty, and variability of the leaf area response based on the fitted model, allowing for inferences regarding predicted values, uncertainties, and probable outliers. Overall, the quadratic model proposed in this work provides a dependable and practical method for estimating spinach leaf area using an organic fertilizer combination of water hyacinth compost and chicken manure. The model's prediction capacity, as well as the statistical metrics presented, helps us comprehend sustainable agricultural techniques that enhance plant development while also conserving the environment.

The contour plots and 3D surface plots from the RSM analysis visually depict the interaction effects of the independent variables on the response. These plots aid in identifying the optimal factor combination to maximize spinach leaf area. Various studies have employed similar plots from RSM to visualize the interaction effects between independent variables and the response variable and also proven valuable in identifying optimal combinations of factors for achieving the desired response. RSM is employed to determine the optimal combination of factors for maximizing a particular outcome, which include extraction of phenolic compounds from pomegranate peel [28], production of enzymes by a bacterial strain [29], *Scenedesmus* sp. biomass production in meat processing wastewater by nutrient uptake [30], and cassava yield [31]. The ANOVA results show that CM has a substantial effect on spinach leaf area, with a high F-value of 25.42 for its quadratic term. Regarding the t-value, the anticipated t-test statistic is -2.2621, with degrees of freedom of 9. The results indicated no statistically significant difference between the experimental mean leaf area (223.554 cm<sup>2</sup>) and the projected value (225 cm<sup>2</sup>) with a p-value of 0.05. In accordance with Confidence Interval Analysis, the mean difference between experimental and predicted outcomes has a 95% confidence interval (0.004, -2.896) (See Table-8). Because this interval contains zero, there is no significant difference between the averages at the 0.05 significance level. The t-test and confidence interval analysis demonstrate that the anticipated and experimental results are consistent that supports the dependability of the RSM model and optimization outcomes from Design Expert 13.

## CONCLUSIONS

The study demonstrated that using water hyacinth compost and chicken manure significantly enhanced soil properties and spinach growth. The composting process optimized through Response Surface Methodology and Central Composite Design revealed distinct phases with varying pH, temperature, and moisture content, resulting in an ideal compost blend. The optimized compost application reduced soil bulk density and increased porosity and nutrient levels. Statistical analysis confirmed the quadratic model's reliability, indicating that optimal compost and manure levels significantly improved spinach leaf area. Residual and response surface plots validated the model's accuracy, showing high correlation between predicted and actual values. The integration of these eco-friendly organic amendments aligns with sustainable agriculture principles, reducing dependence on synthetic fertilizers and promoting efficient resource use. This approach is particularly beneficial for small-scale farmers, enhancing crop yield and contributing to environmental conservation. This study underscores the potential of organic waste materials in improving soil health and agricultural productivity.

**Conflicts of interest:** The authors declare no conflict of interest.

## REFERENCES

1. Selvan, T., Panmei, L., Murasing, K. K., Guleria, V., Ramesh, K. R., Bhardwaj, D. R., Thakur, C. L., Kumar, D., Sharma, P., Digvijaysinh Umedsinh, R., & Kayalvizhi, D. (2023). Circular economy in agriculture: Unleashing the potential of integrated organic farming for food security and sustainable development. *Frontiers in Sustainable Food Systems*, 7, 1170380. <https://doi.org/10.3389/fsufs.2023.1170380>
2. Patel, S. (2012). Threats, management and envisaged utilizations of aquatic weed *Eichhornia crassipes*: an overview. *Reviews in Environmental Science and Bio/Technology*, 11, 249-259. <https://doi.org/10.1007/s11157-012-9289-4>



**Mahmuda Parveen and Sujit Ghosh**

3. Zhang, W., Han, D. Y., Dick, W. A., Davis, K. R., & Hoitink, H. A. (1998). Compost and compost water extract-induced systemic acquired resistance in cucumber and Arabidopsis. *Phytopathology*, 88, 450-455. <https://doi.org/10.1094/PHYTO.1998.88.5.450>
4. Beesigamukama, D., Tumuhairwe, J. B., Muoma, J., Maingi, J. M., Ombori, O., Mukaminega, D., ... & Krause-Yakola, A. (2018). Improving water hyacinth-based compost for crop production. *Journal of Agricultural Science and Food Technology*, 4, 52-63.
5. Ilodibia, C. V., & Chukwuma, M. U. (2015). Effects of application of different rates of poultry manure on the growth and yield of tomato (*Lycopersicon esculentum* Mill.). *Journal of Agronomy*, 14, 251-253. <https://doi.org/10.3923/ja.2015.251.253>
6. Gajalakshmi, S., & Abbasi, S. A. (2008). Solid waste management by composting: state of the art. *Critical Reviews in Environmental Science and Technology*, 38, 311-400. <https://doi.org/10.1080/10643380701413633>
7. Adediran, J. A., Taiwo, L. B., Akande, M. O., Sobulo, R. A., & Idowu, O. J. (2005). Application of organic and inorganic fertilizer for sustainable maize and cowpea yields in Nigeria. *Journal of Plant Nutrition*, 27, 1163-1181. <https://doi.org/10.1081/PLN-120038542>
8. Moradi, S., Rokhzadi, A., Mohammadi, K., & Pasari, B. (2024). Reduced Nitrogen Loss and Sustained Seed Yield of Quinoa (*Chenopodium quinoa* Willd.) by Optimizing the Use of NPK, Cow Manure, and Vermicompost. *Journal of Soil Science and Plant Nutrition*, 24, 572-585. <https://doi.org/10.1007/s42729-023-01567-y>
9. Jahan, M., & Amiri, M. B. (2018). Optimizing application rate of nitrogen, phosphorus and cattle manure in wheat production: An approach to determine optimum scenario using response-surface methodology. *Journal of Soil Science and Plant Nutrition*, 18, 13-26. <http://dx.doi.org/10.4067/S0718-95162018005000102>
10. Sobek, A. A. (1978). Field and laboratory methods applicable to overburdens and minesoils. Industrial Environmental Research Laboratory, Office of Research and Development, US Environmental Protection Agency.
11. Thomas, G. W. (1996). Soil pH and soil acidity. In D. L. Sparks (Ed.), *Methods of soil analysis: Part 3 chemical methods* (pp. 475-490). Soil Science Society of America.
12. Bremner, J. M. (1996). Nitrogen-total. In D. L. Sparks (Ed.), *Methods of soil analysis: Part 3 Chemical methods* (pp. 1085-1121). Soil Science Society of America. <https://doi.org/10.2136/sssabookser5.3.c37>
13. Olsen, S. R., Cole, C. V., Watanabe, F. S., & Dean, L. A. (1954). Estimation of available phosphorus in soils by extraction with sodium bicarbonate (U.S. Dep. Agric. Circ. 939). U.S. Government Printing Office.
14. Chapman, J. C. (1982). The effect of potassium and nitrogen fertilizers on the yield, fruit quality and leaf analysis of Imperial mandarins. *Australian Journal of Experimental Agriculture*, 22(117), 331-336. <https://doi.org/10.1071/EA9820331>
15. Mazumder, P., Akhil, P. M., Khwairakpam, M., Mishra, U., & Kalamdhad, A. S. (2021). Enhancement of soil physico-chemical properties post compost application: Optimization using Response Surface Methodology comprehending Central Composite Design. *Journal of Environmental Management*, 289, 112461. <https://doi.org/10.1016/j.jenvman.2021.112461>
16. Farraji, H., Aziz, H. A., Tajuddin, R. M., & Mojiri, A. (2014). Optimization of phytoremediation of lead-contaminated soil by spinach (*Spinacia oleracea* L). *International Journal of Scientific Research in Knowledge*, 2(10), 480-486. <http://dx.doi.org/10.12983/ijrsrk-2014-p0480-0486>
17. Gezer, B. (2017). Optimization and Investigation of the Design Parameters for Boric Acid Production from Colemanite Using the Ultrasound Assisted Extraction Process. *Journal of Multidisciplinary Developments*, 2(2), 28-38.
18. Ozores-Hampton, M., Stansly, P. A., & Salame, T. P. (2011). Soil chemical, physical, and biological properties of a sandy soil subjected to long-term organic amendments. *Journal of Sustainable Agriculture*, 35, 243-259. <https://doi.org/10.1080/10440046.2011.554289>
19. Bouajila, K., & Sanaa, M. (2011). Effects of organic amendments on soil physico-chemical and biological properties. *J. Mater. Environ. Sci*, 2, 485-490.
20. Begum, S. L., Himaya, S. M., & Afreen, S. M. (2022). Potential of water hyacinth (*Eichhornia crassipes*) as compost and its effect on soil and plant properties: A review. *Agricultural Reviews*, 43, 20-28. <https://doi.org/10.18805/ag.R-184>





**Mahmuda Parveen and Sujit Ghosh**

21. Liang, C., Das, K. C., & McClendon, R. W. (2003). The influence of temperature and moisture contents regimes on the aerobic microbial activity of a biosolids composting blend. *Bioresource Technology*, 86, 131-137. [https://doi.org/10.1016/S0960-8524\(02\)00153-0](https://doi.org/10.1016/S0960-8524(02)00153-0)
22. Fischer, D., & Glaser, B. (2012). Synergisms between compost and biochar for sustainable soil amelioration. In S. Kumar (Ed.), *Management of organic waste* (pp. 167-198). IntechOpen. <https://doi.org/10.5772/31718>
23. Kumar, V., Kumar, P., & Khan, A. (2020). Optimization of PGPR and silicon fertilization using response surface methodology for enhanced growth, yield and biochemical parameters of French bean (*Phaseolus vulgaris* L.) under saline stress. *Biocatalysis and Agricultural Biotechnology*, 23, 101463. <https://doi.org/10.1016/j.bcab.2019.101463>
24. Prakash, G., & Srivastava, A. K. (2005). Statistical media optimization for cell growth and azadirachtin production in *Azadirachta indica* (A. Juss) suspension cultures. *Process Biochemistry*, 40, 3795-3800. <https://doi.org/10.1016/j.procbio.2005.05.010>
25. Melini, F., Luziatelli, F., Bonini, P., Ficca, A. G., Melini, V., & Ruzzi, M. (2023). Optimization of the growth conditions through response surface methodology and metabolomics for maximizing the auxin production by *Pantoea agglomerans* C1. *Frontiers in Microbiology*, 14, 1022248. <https://doi.org/10.3389/fmicb.2023.1022248>
26. Bansod, S. P., Parikh, J. K., & Sarangi, P. K. (2023). Pineapple peel waste valorization for extraction of bio-active compounds and protein: Microwave assisted method and Box Behnken design optimization. *Environmental Research*, 221, 115237. <https://doi.org/10.1016/j.envres.2023.115237>
27. Ellatif, S. A., Abdel Razik, E. S., Al-Surhane, A. A., Al-Sarraj, F., Daigham, G. E., & Mahfouz, A. Y. (2022). Enhanced production, cloning, and expression of a xylanase gene from endophytic fungal strain *Trichoderma harzianum* kj831197. 1: unveiling the in vitro anti-fungal activity against phytopathogenic fungi. *Journal of Fungi*, 8, 447. <https://doi.org/10.3390/jof8050447>
28. Liu, Y., Kong, K. W., Wu, D. T., Liu, H. Y., Li, H. B., & Zhang, J. R., & Gan, R. Y. (2022). Pomegranate peel-derived punicalagin: Ultrasonic-assisted extraction, purification, and its  $\alpha$ -glucosidase inhibitory mechanism. *Food Chemistry*, 374, 131635. <https://doi.org/10.1016/j.foodchem.2021.131635>
29. Sharma, A., Balda, S., Gupta, N., Capalash, N., & Sharma, P. (2022). Microaerobic conditions enhance laccase production from *Rheinheimera* sp. in an economical medium. *Archives of Microbiology*, 204, 562. <https://doi.org/10.1007/s00203-022-03170-8>
30. Latiffi, N. A., Mohamed, R. M., Al-Gheethi, A., Tajuddin, R. M., Al-Shaibani, M. M., Vo, D. V., & Rupani, P. F. (2022). Nutrients elimination from meat processing wastewater using *Scenedesmus* sp.; optimizations; artificial neural network and kinetics models. *Environmental Technology & Innovation*, 26, 102535. <https://doi.org/10.1016/j.eti.2022.102535>
31. Taiwo, A. I., Agboluaje, S. A., & Lamidi, W. A. (2019). Application of response surface method (RSM) and central composite design (CCD) for optimization of cassava yield. *Interdisciplinary Research Review*, 14.

**Illustrations:**

**Table-1: Characterization of Bulk Density, Porosity, and Nutrient Content (TN, P, K) in Control soil, values which are shown mean value  $\pm$ SE.**

	Bulk density(g/cc)	Porosity (%)	pH	TN (mg/kg)	P(mg/kg)	K(mg/kg)
Control Soil	1.194 $\pm$ 0.13	45.28 $\pm$ 0.49	7.2	357.8 $\pm$ 0.63	23.60 $\pm$ 0.11	110 $\pm$ 0.78

**Table-2: Impact of Compost Addition on Bulk Density, Porosity, and Nutrient Content (TN, P, K) in amended soil, values which are shown mean value  $\pm$ SE.**

	Bulk density(g/cc)	Porosity (%)	pH	TN (mg/kg)	P(mg/kg)	K(mg/kg)
Amended soil	0.825 $\pm$ 0.53	68.87 $\pm$ 0.19	7.2	1120 $\pm$ 0.69	106 $\pm$ 0.33	143 $\pm$ 0.7





**Mahmuda Parveen and Sujit Ghosh**

**Table 3: Levels of Independent and Dependent Variables in CCD for maximizing the leaf area expansion of spinach plants**

Name	Units	Type	Low	High
Water Hyacinth Compost (Independent variable )	gm	Factor	600	1800
Chicken manure (Independent variable )	gm	Factor	12	48
Leaf Area (Dependent Variables or response )	cm <sup>2</sup>	Response	75.36	241.22

**Table 4: CCD Matrix and Observed Leaf Area Responses for Spinach Plant Growth:**

Std	Run	Factor 1 A: Compost gm	Factor 2 B: Chicken Manure gm	Response -Leaf area cm <sup>2</sup>
4	1	0	0	75.36
6	2	600	12	185
9	3	600	24	189
3	4	600	48	195
11	5	1200	12	197
5	6	1200	24	208
1	7	1200	48	212
10	8	1800	12	192
8	9	1800	24	241.22
2	10	1800	48	204.75
7	11	1200	0	116

**Table 5: presents the ANOVA results for the quadratic model of spinach growth (in terms of leaf area).**

Source	Sum of Squares	df	Mean Square	F-value	p-value	
Model	36.32	5	7.26	21.23	0.0022	significant
A-Compost	1.06	1	1.06	3.11	0.1382	
B-Chicken manure	1.13	1	1.13	3.31	0.1287	
AB	0.1009	1	0.1009	0.2949	0.6104	
A <sup>2</sup>	0.3206	1	0.3206	0.9370	0.3775	
B <sup>2</sup>	8.70	1	8.70	25.42	0.0040	
Residual	1.71	5	0.3421			
Cor Total	38.04	10				

**Table 6: Summary of ANOVA Fit Statistics**

Std. Dev.	0.5849	R <sup>2</sup>	0.9550
Mean	13.41	Adjusted R <sup>2</sup>	0.9100
		Predicted R <sup>2</sup>	0.7963
C.V. %	4.36	Adeq Precision	14.9118





**Mahmuda Parveen and Sujit Ghosh**

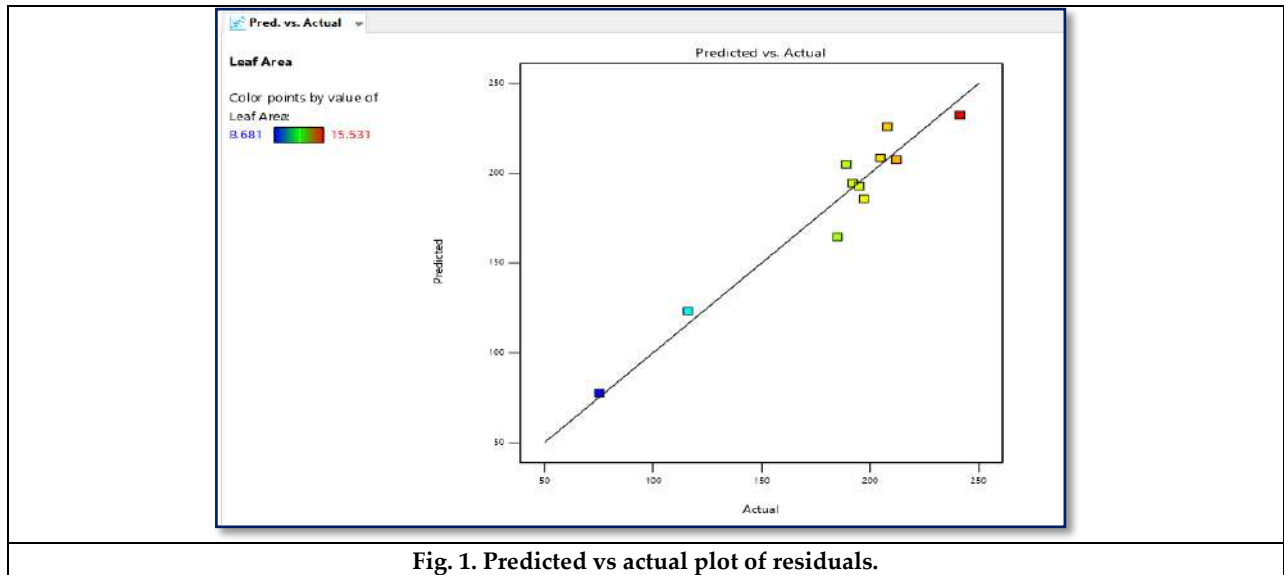
**Table-7: Summary Statistics for Spinach Leaf Area Measurements Including Confidence and Tolerance Intervals**

Two-sided Confidence = 95% Population = 99%

Solution 1 of 100 Response	Predicted Mean	Predicted Median*	Observed	Std Dev	SE Mean	95% CI low for Mean	95% CI high for Mean	95% TI low for 99% Pop	95% TI high for 99% Pop
Leaf Area	225.016	224.674	223.554	17.5415	N/A	201.483	249.851	125.641	352.286

**Table 8: Results of One-Sample t-test for Validation**

Test	Result
One-Sample t-test	The calculated t-value falls in the outside range of -2.262 to 2.262, failing to reject the null hypothesis (H0).
Assumptions	<ul style="list-style-type: none"> <li>•The experimental leaf area values are independent and randomly sampled.</li> <li>•The leaf area values are approximately normally distributed.</li> </ul>
Sample mean ( $\bar{x}$ )	223.554 cm <sup>2</sup>
Sample standard deviation (s)	2.021397756 cm <sup>2</sup>
Test statistic (t)	-2.2621
Degrees of freedom	9
Critical t-value	±2.262
Confidence Interval	(0.004, -2.896)
Conclusion	The difference between the mean of the experimental leaf area values and the predicted value is statistically significant at the 0.05 level.



**Fig. 1. Predicted vs actual plot of residuals.**



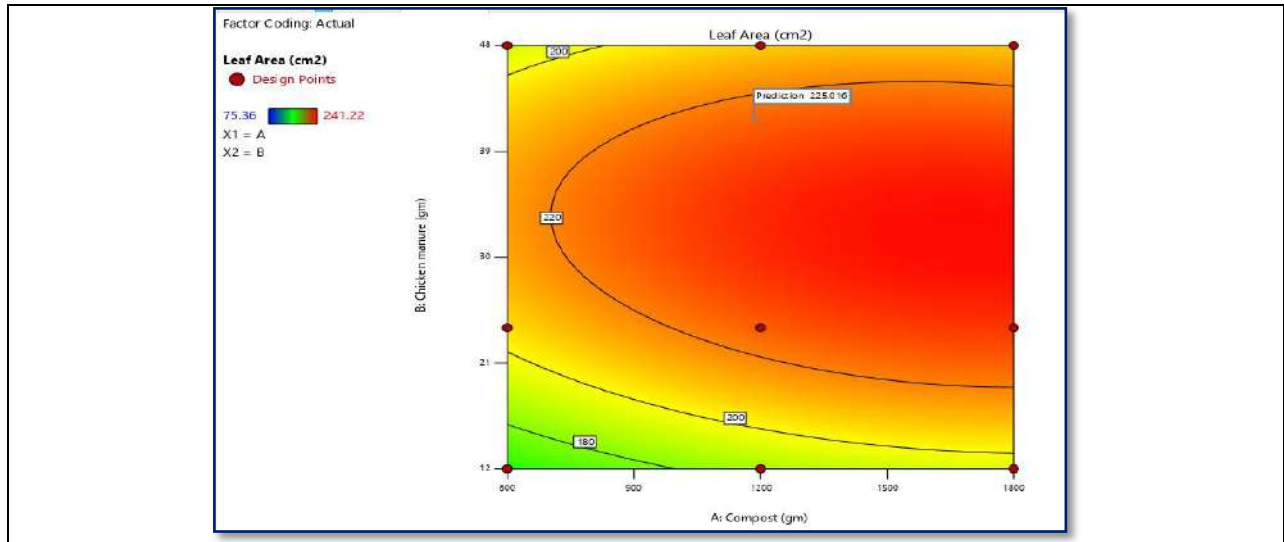


Fig. 2. Graphical representation for response surface optimization by plotting leaf area (cm<sup>2</sup>) contour plot for (A) Compost (Water Hyacinth Compost) (gm) and (B) Chicken manure (gm).

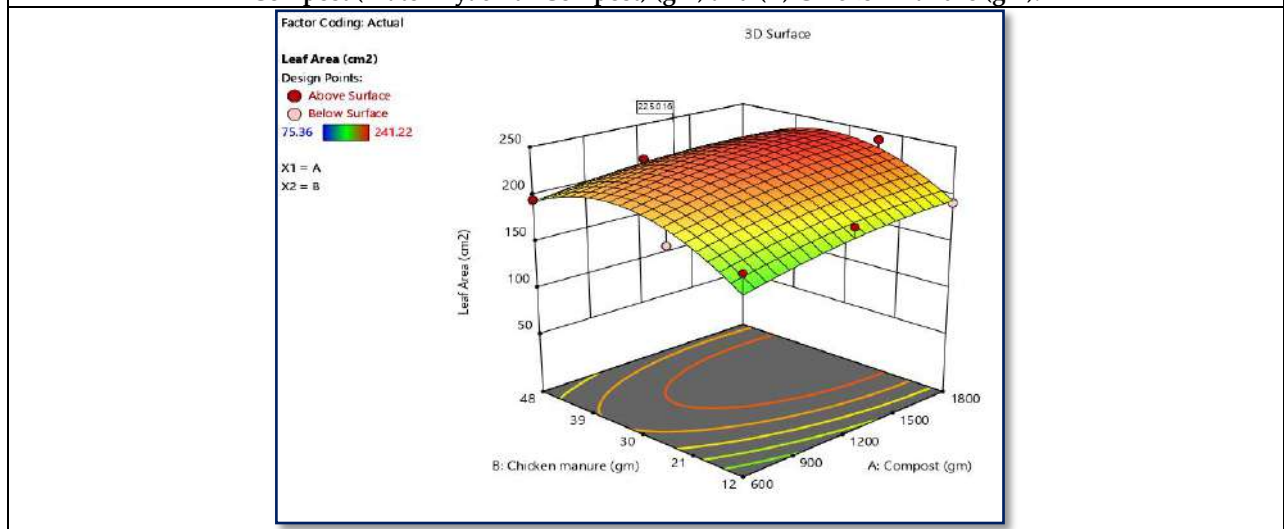


Fig. 3. Graphical representation for response surface optimization by plotting leaf area (cm<sup>2</sup>) against a 3D plot for (A) Compost (Water Hyacinth Compost) (gm) and (B) Chicken manure (gm).

[The curvature of the 3D response surface suggests the presence of non-linear relationships and potential interactions between the two factors and the response variable (Leaf Area). The curved shape indicates that the effects of the factors on the response are not purely additive, and there may be synergistic or antagonistic interactions between the factors. The optimum region or factor combination that corresponds to the highest levels of the response variable is located in the upper-right corner of the surface. This region represents high levels of both A: Compost and B: Chicken manure, suggesting that increasing the levels of these two factors may lead to increased Leaf Area.]

**Abbreviations:** RSM, Response Surface Methodology; CCD, Central Composite Design; WHC, water hyacinth compost; CM, chicken manure; ANOVA, Analysis of Variance; df, degrees of freedom; MS, mean square; CV, coefficient of variation; H<sub>0</sub>, Null hypothesis; Alternative hypothesis, H<sub>1</sub>; C.V., coefficients of variation; TN, Total Nitrogen, P, Phosphorus; K, Potassium.







## An Improved CRITIC-MULTIMOORA Approach for Kidney Transplant under Pythagorean Neutrosophic

V. Surya<sup>1\*</sup>, R. Seema<sup>2</sup> and R. Sophia Porchelvi<sup>3</sup>

<sup>1</sup>Research Scholar, Department of Mathematics, A.D.M. College for Women (Autonomous), Nagapattinam, (Affiliated to Bharathidasan University, Tiruchirappalli) Tamil Nadu, India.

<sup>3</sup>Associate Professor, Department of Mathematics, A.D.M. College for Women (Autonomous), Nagapattinam, (Affiliated to Bharathidasan University, Tiruchirappalli) Tamil Nadu, India.

Received: 12 Jun 2024

Revised: 14 Aug 2024

Accepted: 17 Oct 2024

### \*Address for Correspondence

**V. Surya**

Research Scholar,  
Department of Mathematics,  
A.D.M. College for Women (Autonomous),  
Nagapattinam,  
(Affiliated to Bharathidasan University, Tiruchirappalli)  
Tamil Nadu, India.



This is an Open Access Journal / article distributed under the terms of the **Creative Commons Attribution License** (CC BY-NC-ND 3.0) which permits unrestricted use, distribution, and reproduction in any medium, provided the original work is properly cited. All rights reserved.

### ABSTRACT

This article revolves around specific research that depicts about CRITIC-MULTIMOORA approach in a Pythagorean neutrosophic environment. A novel score function and distance measure are proposed for a Pythagorean neutrosophic, which is a fundamental concept, utilized in fuzzy Logic systems and few theories are applied to determine the similarity or membership between the elements. Using the Criteria Importance Through the Inter-Criteria Correlation (CRITIC), the Weightage of the objectives is determined. In addition to that, the multi-objective optimization on the basis of ratio analysis, following the full multiplicative form (MULTIMOORA) method, applied to create a stand-by list for the kidney recipients. At the threshold, a numerical model is provided to evaluate the feasibility of the method proposed.

**Keywords:** Pythagorean neutrosophic fuzzy set, score function, distance measure, multi objective decision making.

### INTRODUCTION

Xenograft or transplantation is one of the most crucial surgical procedures operated between a donor and recipient. Kidney was the first organ transplanted in 1954. In contemporary scenario more than 1 lakh 57 thousand organs transplanted; out of which kidney is the most transplanted organ; 80% of the adult population is aware of organ

83938





donation. As a result, a list and itinerary of donors and recipients provided an undeniable procedure to meet out the future surgical requirements. Yager introduced the idea of the Pythagorean Fuzzy Set (PFS) [15]. The prerequisite is that the total squared of membership and non-membership must be less than or equal to one. Smarandache developed the concept of the degree of dependence between components of the fuzzy set and the neutrosophic set first. [7]. The Pythagorean Neutrosophic Set (PNS), had become familiar in recent years. It is a new concept with dependent components, that can be either member or non-member with the requirement, in which the square sum of the two components would not exceed 2, where the square sum of the degrees of membership and non-membership is Pythagorean and does not exceed 1. The degree of indeterminacy is independent. The concept of Multi-Objective Optimization based on Ratio Analysis (MOORA) was first introduced by Brauers and Zavadskas. It is the process of maximizing a conflicting goal or goals, while adhering to certain limitations. The MOORA method is applicably easy and computation time is meager. By including full multiplicative form, Brauers and Zavadskas ameliorated the MOORA method to MULTIMOORA. The three sections of MULTIMOORA are the Full Multiplicative Form System (FMFS), Reference Point System (RPS), and Ratio System (RS). Using the MULTIMOORA method, EsraAytac Adali and Aysegultus Isik talked about a laptop selection problem [6].

A new distance measure and score function for Pythagorean fuzzy sets were proposed by Chao Huang in his Pythagorean fuzzy MULTIMOORA method, which is an extension of the original MULTIMOORA method [3]. Additionally, a practical example of producing a solid-state disk is provided to illustrate the process. The Pythagorean Neutrosophic number's score function was defined by M. Palanikumar and K. Arulmozhi [9]. The Pythagorean neutrosophic number's distance measure was provided by Jansi Rajan and Mohana krishnaswamy [8]. Diakoulaki *et al.* proposed the CRITIC method and It's a technique for figuring out the objective weight. Shakeel zafar *et al.* talked about the blockchain evaluation process using the CRITIC weight method [14]. Discussing the CRITIC-EDAS method in a fermata fuzzy environment is done by Arunodaya Raj Mishra *et al* [1]. Dragan Pamucar *et al* [5]. presented a paper that used the CRITIC method and fuzzy rough numbers. Muhammad Akram talked about the CRITIC-EDAS method in a Pythagorean setting [10]. Nasrin *et al* [11] present a novel approach to weight kidney allocation criteria based on multi-expert fuzzy reasoning. As mentioned by Dalia M. Atallah *et al.*, kidney transplant outcomes can be predicted using matching to determine which patient is a good fit for the donor [4]. Bernadette Li *et al* [2] investigate the survival of recipients after a deceased donor kidney transplant. The article focuses on giving a CRITIC-MULTIMOORA method to create a waiting list for recipients based on the Pythagorean Neutrosophic set. The paper is structured as follows: The basic definitions like Pythagorean neutrosophic set (PN), Distance measure and score function are covered in section 2. Methodology for the CRITIC-MULTIMOORA method is given in section 3. A real-life example of creating a waiting list for organ recipients is given in section 4. The results and discussion of this study are presented in section 5. The final section of the paper concludes with the conclusion.

## Preliminaries

### Definition 1

Let  $X$  be a universe of discourse. A Pythagorean neutrosophic set (PN)  $N$  on  $X$  is defined as  $N = \{(x, \Phi_N(x), \Psi_N(x), J_N(x)) | x \in X\}$ , where  $0 \leq \Phi_N^2(x) + \Psi_N^2(x) + J_N^2(x) \leq 2$ , and the limits of each elements belongs to  $[0,1]$ .  $\Phi_N(x), \Psi_N(x), J_N(x)$  denotes degree of membership, non-membership and indeterminacy.

### Definition 2

Let  $A = \{(x_i, \Phi_A(x_i), \Psi_A(x_i), J_A(x_i)) | x \in X\}$  and  $B = \{(x_i, \Phi_B(x_i), \Psi_B(x_i), J_B(x_i)) | x \in X\}$  be two PN sets. Let  $w_i (i = 1, 2, \dots, n)$  be weightage of an element  $x_i (i = 1, 2, \dots, n)$ . Where  $w_i \geq 0$  and  $\sum_{i=1}^n w_i = 1$ . Then the weighted distance measure is given as

$$d_\gamma(A, B) = \left\{ \frac{1}{3} \sum_{i=1}^n w_i [|\Phi_A^2(x_i) - \Phi_B^2(x_i)|^\gamma + |\Psi_A^2(x_i) - \Psi_B^2(x_i)|^\gamma + |J_A^2(x_i) - J_B^2(x_i)|^\gamma] \right\}^{\frac{1}{\gamma}}$$

Where,  $\gamma > 0$ . When  $\gamma = 1$  gives the Hamming distance

$$d(A, B) = \left\{ \frac{1}{3} \sum_{i=1}^n w_i [|\Phi_A^2(x_i) - \Phi_B^2(x_i)| + |\Psi_A^2(x_i) - \Psi_B^2(x_i)| + |J_A^2(x_i) - J_B^2(x_i)|] \right\}$$

For convenience  $\Phi_A(x_i), \Psi_A(x_i), J_A(x_i)$  can be represented as  $\Phi_A, \Psi_A, J_A$ .





**Surya et al.,**

**Definition 3**

For any PN set  $A = \{\Phi_A, \Psi_A, J_A\}$  the score and accuracy function are defined as

$$S_A = \Phi_A^2 - \Psi_A^2 - J_A^2, \& E_A = \Phi_A^2 + \Psi_A^2 + J_A^2$$

Where,  $-1 \leq S_A \leq 1$ , &  $0 \leq E_A \leq 2$ .

**Improved Score & Accuracy Function**

**Definition 4**

For any PN set  $A = \{\Phi_A, \Psi_A, J_A\}$  the proposed score (S(A)) and accuracy (E(A)) function are defined as

$$S(A) = \frac{2 + \Phi_A^2 - \Psi_A^2 - J_A^2}{4}, \& E(A) = \frac{2 + \Phi_A^2 + \Psi_A^2 + J_A^2}{4}$$

Where,  $0 \leq S(A) \leq 1$ , &  $0 \leq E(A) \leq 1$

**Proposed Distance Measure**

**Definition 5**

Let  $A = \langle \Phi_A(x_i), \Psi_A(x_i), J_A(x_i) \rangle$  and  $B = \langle \Phi_B(x_i), \Psi_B(x_i), J_B(x_i) \rangle$  any two PN set. Then the proposed PN weighted distance measure defined as

$$d(A, B) = \frac{1}{4n} \sum_{i=1}^n w_i \left[ |\Phi_A^2(x_i) - \Phi_B^2(x_i)| + |\Psi_A^2(x_i) - \Psi_B^2(x_i)| + |J_A^2(x_i) - J_B^2(x_i)| \right. \\ \left. + \max\{|\Phi_A^2(x_i) - \Phi_B^2(x_i)|, |\Psi_A^2(x_i) - \Psi_B^2(x_i)|, |J_A^2(x_i) - J_B^2(x_i)|\} \right]$$

Where  $w_i \geq 0$  and  $\sum_{i=1}^n w_i = 1$ .

**PNF-CRITIC-Multimoora Approach**

This section revolves around, The CRITIC-MULTIMOORA technique is developed using a novel Pythagorean neutrosophic fuzzy distance measure and a score function. The following multi-objective problem is resolved using this method. Assume the multi-objective problem has n alternatives  $\{\alpha_1, \alpha_2, \dots, \alpha_n\}$  and m objectives  $\{\beta_1, \beta_2, \dots, \beta_n\}$ . The objectives can be divided into two types (i.e.) objectives to be maximized and objectives to be minimized. The weight for each objective is denoted by  $w = (w_1, w_2, \dots, w_m)$ ,  $\sum_{j=1}^m w_j = 1$ . The Pythagorean neutrosophic fuzzy matrix is given below

$$Z = (Z_{ij})_{n \times m} = \begin{bmatrix} Z_{11} & Z_{12} & \dots & Z_{1m} \\ Z_{21} & Z_{22} & \dots & Z_{2m} \\ \vdots & \vdots & \ddots & \vdots \\ Z_{n1} & Z_{n2} & \dots & Z_{nm} \end{bmatrix}$$

Here  $Z_{ij}$  is a PNFN.

**A. PNF-CRITIC method**

Using the PNF-CRITIC method first, assess each objective's weight

Step 1: Calculate the score value for every element in Z using the score function to create the score matrix.

$$S = (S(Z_{ij}))_{n \times m} = \begin{bmatrix} S(Z_{11}) & S(Z_{12}) & \dots & S(Z_{1m}) \\ S(Z_{21}) & S(Z_{22}) & \dots & S(Z_{2m}) \\ \vdots & \vdots & \ddots & \vdots \\ S(Z_{n1}) & S(Z_{n2}) & \dots & S(Z_{nm}) \end{bmatrix} \quad (1)$$

Step 2: Normalize the score matrix with best and worst values as follows

$$\widetilde{S}(Z_{ij}) = \begin{cases} \frac{S(Z_{ij}) - \min_i S(Z_{ij})}{\max_i S(Z_{ij}) - \min_i S(Z_{ij})}, & j \in O. Max \\ \frac{\max_i S(Z_{ij}) - S(Z_{ij})}{\max_i S(Z_{ij}) - \min_i S(Z_{ij})}, & j \in O. Min \end{cases} \quad (2)$$

\*O. Max - Objective to be maximum

\*O. Min - Objective to be minimum

Where,  $\max S(Z_{ij})$  and  $\min S(Z_{ij})$  represents the best and worst values respectively.





Surya et al.,

Step 3: Compute the Standard Deviation for every objective using the formula below.

$$\sigma_j = \sqrt{\frac{\sum_{i=1}^n (S(Z_{ij}) - \bar{E}_j)^2}{n}} \quad (3)$$

Where,  $\bar{E}_j = \frac{\sum_{i=1}^n S(Z_{ij})}{n}$ .

Step 4: Assessing the comparison matrix between objectives by using the correlation coefficient

$$r_{jt} = \frac{\sum_{i=1}^n (S(Z_{ij}) - \bar{E}_j)(S(Z_{it}) - \bar{E}_t)}{\sqrt{\sum_{i=1}^n (S(Z_{ij}) - \bar{E}_j)^2 \sum_{i=1}^n (S(Z_{it}) - \bar{E}_t)^2}}, \quad (j, t = 1, \dots, m) \quad (4)$$

Step 5: Obtain the information value of each objective

$$C_j = \sigma_j * I_v \quad (5)$$

Where,  $I_v = \sum_{t=1}^m (1 - r_{jt})$ .

Step 6: The following step determines each objective's weight.

$$w_j = \frac{C_j}{\sum_{j=1}^m C_j} \quad (6)$$

**PNF-MULTIMOORA Approach**

In general, PNF-MULTIMOORA has three sections, (i.e.) PNF-RS, PNF-RPS, PNF-FMFS. Here this approach is applied to create the ranking list in the following steps:

Step1: The PNF-RS uses  $S(Z_{ij})$  to determine the ranking of alternatives

$$H_1(\alpha_i) = \sum_{j=1}^k w_j S(Z_{ij}) - \sum_{j=k+1}^m w_j S(Z_{ij}) \quad (7)$$

- Here,  $w_j$  is Weight of objective  $\beta_j$ .
- $K$  - denotes Number of objectives to be maximized.
- $m - k$  - denotes number of objectives to be minimized.
- $H_1(\alpha_i)$  - denotes ranking values of alternatives  $\alpha_i$ .

Alternatives can be arranged as per the ranking values (i.e.) in descending order of ranking values.

$$N_1 = \{N_1(\alpha_1), N_1(\alpha_2), \dots, N_1(\alpha_n)\}$$

Step 2: Based on  $(S(Z_{ij}))_{n \times m}$  and PNF distance measure, the ranking values of alternatives for PNF-RP is computed as follows,

$$H_2(\alpha_i) = \max_j w_j \frac{d(Z_j^+, Z_{ij})}{d(Z_j^+, Z_j^-)} \quad (8)$$

- Here,  $Z_j^+, Z_j^-$  - denotes the greatest and lowest values of objectives with respect to  $\beta_j$ .
- $d(Z_j^+, Z_{ij})$  - denotes the PNF distance measure between  $Z_j^+, Z_{ij}$ .
- $d(Z_j^+, Z_j^-)$  - denotes the PNF distance measure between  $Z_j^+, Z_j^-$ .

Greatest  $Z_j^+$  and Lowest  $Z_j^-$  values of each objective are defined as

$$Z_j^+ = \begin{cases} \max_j \{Z_{ij}\}, & \text{if objective } \beta_j \text{ need to be maximized} \\ \min_j \{Z_{ij}\}, & \text{if objective } \beta_j \text{ need to be minimized} \end{cases}$$

&

$$Z_j^- = \begin{cases} \min_j \{Z_{ij}\}, & \text{if objective } \beta_j \text{ need to be maximized} \\ \max_j \{Z_{ij}\}, & \text{if objective } \beta_j \text{ need to be minimized} \end{cases}$$

Here alternatives are arranged in ascending order since smaller valued alternative is better.

$$N_2 = \{N_2(\alpha_1), N_2(\alpha_2), \dots, N_2(\alpha_n)\}$$

Step 3: Based on  $(S(Z_{ij}))_{n \times m}$ , the PNF-FMFS is computed as follows:





**Surya et al.,**

$$H_3(\alpha_i) = \frac{\sqrt[k]{\prod_{j=1}^k (2 - (1 - S(Z_{ij}))^{w_j})}}{\sqrt[m-k]{\prod_{j=k+1}^m (2 - (1 - S(Z_{ij}))^{w_j})}} \quad (9)$$

Alternates are arranged in descending order as higher valued alternates are the better one.

$$N_3 = \{N_3(\alpha_1), N_3(\alpha_2), \dots, N_3(\alpha_n)\}$$

Step4: Since this method gets results from three systems, it should undergo aggregation. In this step, for each objective  $\beta_j, (j = 1, 2, 3, \dots, n)$  there will be a ranking value  $H_l(\alpha_i), (l = 1, 2, 3)$  and ranking order  $N_l(\alpha_i)$ . After aggregation the problem end up with two matrices which is ranking value matrix (RVM)  $H = (H_l(\alpha_i))_{n \times 3}$  and ranking order matrix (ROM)  $N = (N_l(\alpha_i))_{n \times 3}$ .

$$H = (H_l(\alpha_i))_{n \times 3} = \begin{bmatrix} H_1(\alpha_1) & H_2(\alpha_1) & H_3(\alpha_1) \\ H_1(\alpha_2) & H_2(\alpha_2) & H_3(\alpha_2) \\ \vdots & \vdots & \vdots \\ H_1(\alpha_n) & H_2(\alpha_n) & H_3(\alpha_n) \end{bmatrix}$$

$$N = (N_l(\alpha_i))_{n \times 3} = \begin{bmatrix} N_1(\alpha_1) & N_2(\alpha_1) & N_3(\alpha_1) \\ N_1(\alpha_2) & N_2(\alpha_2) & N_3(\alpha_2) \\ \vdots & \vdots & \vdots \\ N_1(\alpha_n) & N_2(\alpha_n) & N_3(\alpha_n) \end{bmatrix}$$

Normalization of RVM is done as follows,

$$H^- = (H_l^-(\alpha_i))_{n \times 3} = \begin{bmatrix} H_1^-(\alpha_1) & H_2^-(\alpha_1) & H_3^-(\alpha_1) \\ H_1^-(\alpha_2) & H_2^-(\alpha_2) & H_3^-(\alpha_2) \\ \vdots & \vdots & \vdots \\ H_1^-(\alpha_n) & H_2^-(\alpha_n) & H_3^-(\alpha_n) \end{bmatrix}$$

Here

$$(H_l^-(\alpha_i)) = \frac{H_l(\alpha_i)}{\sqrt{\sum_{i=1}^n (H_l(\alpha_i))^2}} \quad (10)$$

When determining the ranking outcomes of alternatives, the normal MULTIMOORA method will consider ranking orders of alternatives only. There are no reasonable results to be obtained by considering only ranking orders [16]. Using the Borda rule from [3] to create the ranking order by combine the rank values.

$$R(\alpha_i) = \left( H_1^-(\alpha_i) * \frac{n - N_1(\alpha_i) + 1}{\frac{n(n+1)}{2}} \right) - \left( H_2^-(\alpha_i) * \frac{N_2(\alpha_i)}{\frac{n(n+1)}{2}} \right) + \left( H_3^-(\alpha_i) * \frac{n - N_3(\alpha_i) + 1}{\frac{n(n+1)}{2}} \right) \quad (11)$$

The alternatives can be arranged in descending order by their  $R(\alpha_i)$  value.

**Case Study**

Patients suffering in final-stage of renal disease can be subjected to kidney transplantation for better life. These patients may have multiple complications due to the kidney complications like cardiovascular disease, gastrointestinal disease, and so on. Hence, patients are prescribed to undergo several diagnoses that includes the capacity of patient’s surgical tolerance and immune suppression that follows transplant surgery. Doctors use Glomerular Filtration Rate (GFR) to measure the kidney function. GFR value below 60 for three months or more than that indicates the person have kidney disease and less than or equal to 15 means the person is suffering with end stage kidney failure. They are suggested for dialysis or transplant to live. The criteria for transplantation are follows: ABO matching is a test for blood group matching because, the blood group of recipients should match with donor. The blood group O is considered as universal donor and AB is universal recipients, who could receive organ or blood from any blood group. HLA stands for Human Leukocyte Antigen; there are 100 different antigens present in our body. Out of 100 it is shown that 6 antigens matching is the most important for transplantation. In many cases a kidney from an elderly donor will not suit for young recipients. Age difference between donor and recipients is also a pivotal factor for post-surgical survival. There are two types of transplantations 1) Living donor transplantation, 2) Cadaveric transplantation. In living donor transplantation, the donor can be family members, friends. Here the donor should be in proper physical and mental health. Cadaveric transplantation will happen when the donor is declared as brain dead. In this case, after getting a proper approval from close relatives the organs will be removed for transplantation. To get the organ one should register in the organ transplant waiting list. United Network for Organ





**Surya et al.,**

Sharing (UNOS) will match the donated kidney with recipients in waiting list. It might be less or longer than this, the typical waiting period for a kidney transplant is two to three years.

In this section, a case about preparation of waiting list for kidney recipients illustrated on the basis of PNF-CRITIC-MULTIMOORA method.

Let us assume there are five recipients denoted  $R = \{R1, R2, R3, R4, R5\}$ . While ordering the recipients one should consider the following objectives: ABO compatibility ( $\beta_1$ ), HLA match ( $\beta_2$ ), Enrolment period ( $\beta_3$ ), Age difference ( $\beta_4$ ), Kidney working percentage ( $\beta_5$ ). Here  $\beta_1, \beta_2, \beta_3$  are objectives to be maximized.  $\beta_4, \beta_5$  are objectives to be minimized. Next, each objective's weight is determined by PNF-CRITIC technique using Excel. The PNF decision matrix was created using the linguistic terms (Table. I) and is provided in Table II.

Step 1: To create the score matrix (Table. III), determine the score value for each element in Table. II.

$$s(Z_{ij}) = \frac{2 + \Phi^2_{(Z_{ij})} - \Psi^2_{(Z_{ij})} - \Pi^2_{(Z_{ij})}}{4}$$

Step 2: Using the best and worst values Normalize Table. III.

Best	0.685	0.5675	0.5125	0.625	0.5125
Worst	0.275	0.275	0.3175	0.3625	0.3175

Step 3: Utilising the formula  $\langle =STDEV (Column j) \rangle$ , determine the Standard Deviation for every column.

SD	0.379825	0.401045	0.452148	0.459389	0.412095
----	----------	----------	----------	----------	----------

Step 4: Use the correlation coefficient to compare each objective. ( $t=1, j, m, \text{etc.}$ ). For every element in Table IV, apply  $\langle CORREL (Column j, Column t) \rangle$ .

Step 5: Apply equation (5) to obtain the information value  $C_j$ .

$C_j$	1.6220	2.0068	2.2300	2.0547	2.1606
-------	--------	--------	--------	--------	--------

Step 6: Finally, the weightage of each objective is calculated using equation (6).

$W_j$	0.1610	0.1992	0.2214	0.2039	0.2145
-------	--------	--------	--------	--------	--------

Now applying the PNF-MULTIMOORA approach

Step 1: The PNF-RS uses above score matrix and the equation (7) to produce the ranking value as  $H_1(\alpha_1) = 0.0227, H_1(\alpha_2) = 0.0802, H_1(\alpha_3) = 0.0906, H_1(\alpha_4) = 0.0884, H_1(\alpha_5) = 0.0553$

The ranking order is given by  $N_1 = \{\alpha_3, \alpha_4, \alpha_2, \alpha_5, \alpha_1\}$

Step 2: The PNF-RPS uses above score matrix and the equation (8) to produce the ranking value as

$H_2(\alpha_1) = 0.2040, H_2(\alpha_2) = 0.2145, H_2(\alpha_3) = 0.1992, H_2(\alpha_4) = 0.2214, H_2(\alpha_5) = 0.2214$

The ranking order is given by  $N_2 = \{\alpha_3, \alpha_1, \alpha_2, \alpha_4, \alpha_5\}$ .

Step 3: The PNF-FMFS uses above score matrix and the equation (9) to produce the ranking value as

$H_3(\alpha_1) = 0.9634, H_3(\alpha_2) = 0.9963, H_3(\alpha_3) = 1.0099, H_3(\alpha_4) = 0.9986, H_3(\alpha_5) = 0.9869$

The ranking order is given by  $N_3 = \{\alpha_3, \alpha_4, \alpha_2, \alpha_5, \alpha_1\}$

Step 4: combining all the ranking values and ranking orders results in

$$H = (H_i(\alpha_i))_{5 \times 3} = \begin{bmatrix} 0.0227 & 0.2040 & 0.9634 \\ 0.0802 & 0.2145 & 0.9963 \\ 0.0906 & 0.1992 & 1.0099 \\ 0.0884 & 0.2214 & 0.9986 \\ 0.0553 & 0.2214 & 0.9869 \end{bmatrix} \&N = (N_i(\alpha_i))_{5 \times 3} = \begin{bmatrix} 5 & 2 & 5 \\ 3 & 3 & 3 \\ 1 & 1 & 1 \\ 2 & 4 & 2 \\ 4 & 5 & 4 \end{bmatrix}$$







Normalization transforms the matrix as

$$H^- = (H_{I_i}^-(\alpha_i))_{5 \times 3} = \begin{bmatrix} 0.1410 & 0.4297 & 0.4347 \\ 0.4969 & 0.4519 & 0.4495 \\ 0.5616 & 0.4197 & 0.4557 \\ 0.5479 & 0.4664 & 0.4506 \\ 0.3428 & 0.4664 & 0.4453 \end{bmatrix}$$

The final ranking score is computed by the equation (11) as follows,

$$R(\alpha_1) = -0.0189, R(\alpha_2) = 0.0989, R(\alpha_3) = 0.3111, R(\alpha_4) = 0.1419, R(\alpha_5) = -0.0504$$

The final ranking is  $\alpha_3 > \alpha_4 > \alpha_2 > \alpha_1 > \alpha_5$ .

## RESULTS AND DISCUSSION

This section elaborates the brief interpretation of the results. According to the results, recipient 3 is clearly the most preferred recipient. Similarly, recipients 2, 4, 5, & 1 will be in second, third, fourth and fifth place, respectively. The utility of a chronologically organized waiting list can reduce the risk of deniable deceases, symptoms of heavy sickness, and mismatches between the donor and the recipient. Whenever we find some donors the waiting list is recalculated through all the recipients. If not, doctors suggest the recipient to do dialysis until they get the right donor. Every Hospital and doctors will have different set of opinions, but this type of ranking is the best choice for finding a good match between recipients and donors.

## CONCLUSION

This research-based case study is an approach to CRITIC-MULTIMOORA, improved through a novel score function and distance measure under the Pythagorean Neutrosophic Fuzzy environment. The waiting list for kidney recipients is used as an example to demonstrate the method's efficiency. In the future, the proposed method will be developed to solve diurnal problems almost in many sciences and medicine sector.

## REFERENCES

1. Arunodaya Raj Mishra<sup>1</sup>, Pratibha Rani and Kiran Pandey, "Fermatean fuzzy CRITIC-EDAS approach for the selection of sustainable third-party reverse logistics providers using improved generalized score function", *Journal of Ambient Intelligence and Humanized Computing*, 2022, Vol: 13, PP:295–311.
2. Bernadette Li, John A. Cairns, Matthew L. Robb, Rachel J. Johnson, Christopher J. E. Watson, John L. Forsythe, Gabriel C. Oniscu, Rommel Ramanan, Christopher Dudley, Paul Roderick, Wendy Metcalfe, Charles R. Tomson and J. Andrew Bradley, "Predicting patient survival after deceased donor kidney transplantation using flexible parametric modeling", *Li et al. BMC Nephrology*, 2016, Vol:17, PP:51.
3. Chao Huang, Mingwei Lin, Zeshui Xu, "Pythagorean fuzzy MULTIMOORA method based on distance measure and score function: its application in multicriteria decision making process", *Knowledge and Information Systems*, 2020, Vol: 62, PP: 4373–4406.
4. Dalia M. Atallah, Mohammed Badawy, Ayman El-Sayed and Mohamed A. Ghoneim, "Predicting kidney transplantation outcome based on hybrid feature selection and KNN classifier", *Multimedia Tools and Applications*, 2019.
5. Dragan Pamucar, Malisa zizovic and Dragan duricic, "Modification of the critic method using fuzzy rough numbers", *Decision Making: Applications in Management and Engineering*, 2022, Vol. 5, Issue 2, PP: 362-371.
6. Esra Aytac Adali, Aysegul Tuslsik, "The multi-objective decision making methods based on MULTIMOORA and MOOSRA for the laptop selection problem", *J Ind. Eng Int.*, 2016.





**Surya et al.,**

7. F. Smarandache (2016), "Degree of dependence and independence of the (sub)components of fuzzy set and neutrosophic set". *Neutrosophic Sets Syst*, 11, 95–97.
8. Jansi Rajan, Mohana Krishnaswamy, "Similarity Measures of Pythagorean Neutrosophic Sets with Dependent Neutrosophic Components Between T and F", *Journal of New Theory*, 2020, Vol.33, PP: 85-94.
9. M. Palanikumar, K. Arulmozhi and T. Gunasekar, "Possibility Pythagorean neutrosophic soft sets and its application of decision making", *journal of the international mathematical virtual institute*, 2022, Vol:12, PP:1-16.
10. Muhammad Akram, Naila Ramzan and Muhammet Deveci, "Linguistic Pythagorean fuzzy CRITIC-EDAS method for multiple-attribute group decision analysis", *Engineering Applications of Artificial Intelligence*, 2023.
11. Nasrin Taherkhani, Mohammad Mehdi Sepehri, Shadi Shafaghi and Toktam Khatibi, "Identification and weighting of kidney allocation criteria: a novel multi-expert fuzzy method", *BMC Medical Informatics and Decision Making*, 2019, Vol:19, PP:182.
12. Prathibha Rani, Arunodaya Raj Mishra, "Multi-criteria food waste treatment method selection using single-valued neutrosophic -CRITIC-MULTIMOORA framework", *Applied Soft Computing*, 2021.
13. Robert A. Metzger, Francis L. Delmonico, "Expanded criteria donors for kidney transplantation", *American Journal of Transplantation* 3 (Suppl. 4), 2003, PP: 114–125.
14. Shakeel Zafar, Zareen Alamgir, "An effective blockchain evaluation system based on entropy-CRITIC weight method and MCDM techniques", *Peer-to-Peer Networking and Applications*, 2021.
15. Yager RR, "Pythagorean fuzzy subsets. In: Proceeding of the 2013 joint IFSA World Congress and NAFIPS annual meeting", IFSA/NAFIPS 2013, Edmonton, Canada, PP:57-61.
16. Yang J, Shi B, "Joining method in group appraising", *Syst. Eng Theory Pract*, 1992, Vol: 12(1), PP:49-50.

**Table. 1**

Similarity (%)	Convert Linguistic terms into PNN		
	<i>Recommend</i>	<i>Abbreviation</i>	<i>PNN</i>
0.1 – 10	Not Conceivable	NC	<0.05, 0.65, 0.80>
10.1 – 20	Very Slightest Conceivable	VSC	<0.15, 0.60, 0.75>
20.1 – 30	Slightest Conceivable	SC	<0.25, 0.55, 0.70>
30.1 – 40	Below Average Conceivable	BAC	<0.35, 0.50, 0.65>
40.1 – 50	Equal Conceivable	EC	<0.45, 0.45, 0.60>
50.1 – 60	Average Conceivable	AC	<0.55, 0.40, 0.55>
60.1 – 70	Above Average Conceivable	AAC	<0.65, 0.35, 0.50>
70.1 – 80	Highly Conceivable	HC	<0.75, 0.30, 0.45>
80.1 – 90	Very Highly Conceivable	VHC	<0.85, 0.25, 0.40>
90.1–99.9	Flawless Conceivable	FC	<0.95, 0.20, 0.35>

**Table 2 Pair wise Comparison among Recipient to Objectives**

Recipients	$\beta_1$	$\beta_2$	$\beta_3$	$\beta_4$	$\beta_5$
$\alpha_1$	VSC	BAC	AC	VHC	SC
$\alpha_2$	HC	AAC	BAC	EC	AAC
$\alpha_3$	AC	VSC	AAC	BAC	BAC
$\alpha_4$	FC	HC	SC	VHC	BAC
$\alpha_5$	EC	AC	SC	AAC	SC

**Table 3 Score Matrix**

Recipients	$\beta_1$	$\beta_2$	$\beta_3$	$\beta_4$	$\beta_5$
$\alpha_1$	0.275	0.3625	0.46	0.625	0.3175
$\alpha_2$	0.5675	0.5125	0.3625	0.41	0.5125
$\alpha_3$	0.46	0.275	0.5125	0.3625	0.3625





**Surya et al.,**

$\alpha_4$	0.685	0.5675	0.3175	0.625	0.3625
$\alpha_5$	0.41	0.46	0.3175	0.5125	0.3175

**Table 4 Normalized Matrix**

Recipients	$\beta_1$	$\beta_2$	$\beta_3$	$\beta_4$	$\beta_5$
$\alpha_1$	0.0000	0.2991	0.7308	0.0000	1.0000
$\alpha_2$	0.7134	0.8120	0.2308	0.8190	0.0000
$\alpha_3$	0.4512	0.0000	1.0000	1.0000	0.7692
$\alpha_4$	1.0000	1.0000	0.0000	0.0000	0.7692
$\alpha_5$	0.3293	0.6325	0.0000	0.4286	1.0000

**Table. 5 Pair wise Comparison among Objectives**

	$\beta_1$	$\beta_2$	$\beta_3$	$\beta_4$	$\beta_5$
$\beta_1$	1	0.6878	-0.5277	0.0796	-0.5100
$\beta_2$	0.6878	1	-0.9242	-0.4033	-0.3642
$\beta_3$	-0.5277	-0.9242	1	0.3698	0.15005
$\beta_4$	0.0796	-0.4033	0.3698	1	-0.5187
$\beta_5$	-0.5100	-0.3642	0.1500	-0.5187	1





## Petrography and Geochemistry of NNW-SSE Trending Dolerite Dykes around Piriapatna Taluk, Mysore District, Karnataka

Nibiya N.T<sup>1\*</sup>, B.V.Suresh Kumar<sup>2</sup>, Nagendra P<sup>3</sup>, Samarth Urs M<sup>3</sup> and K.N.Prakash Narasimha<sup>4</sup>

<sup>1</sup>Research Scholar, Department of Studies in Earth Science, University of Mysore, Mysore, Karnataka, India.

<sup>2</sup>Professor, Department of Studies in Earth Science, University of Mysore, Mysore, Karnataka, India

<sup>3</sup>Guest Faculty, Department of Studies in Earth Science, University of Mysore, Mysore, Karnataka, India

<sup>4</sup>Professor (Retd.), Department of Studies in Earth Science, University of Mysore, Mysore, Karnataka, India.

Received: 19 July 2024

Revised: 23 Aug 2024

Accepted: 25 Oct 2024

### \*Address for Correspondence

**Nibiya N.T**

Research Scholar,

Department of Studies in Earth Science,

University of Mysore,

Mysore, Karnataka, India.

E.Mail: nibiyant@gmail.com



This is an Open Access Journal / article distributed under the terms of the **Creative Commons Attribution License** (CC BY-NC-ND 3.0) which permits unrestricted use, distribution, and reproduction in any medium, provided the original work is properly cited. All rights reserved.

### ABSTRACT

The differential stress in crustal rocks often results in deep fractures. Crustal dynamics is the source of energy which is expressed as a wide variety of deformation and displacement of brittle rocks. Characterization of such stress domains in brittle rocks is possible to a large extent by geometrical analysis of the orientation and mode of occurrence of hypabyssal rocks, exemplified by dykes and sills. Archean Dharwar craton has abundant distribution of mafic dyke swarms, but all previous works mainly focus on EDC dykes. Dyke swarms of WDC yet needs detailed investigation and geochemical studies. Here we present preliminary study on the petrography and geochemistry such WDC Dyke bodies exposed in and around the Piriapatna taluk of Mysore district in order to reveal petrogenetic implications based on the mineralogical and textural characters.

**Keywords:** Dolerite dykes, Meta-dolerites, Piriapatna, Petrography, Whole-rock geochemistry.

## INTRODUCTION

Mafic dykes are considered as the indicators of crustal evolution, tectonic process, and continental drift history. Numerous studies on Achaean dykes have been carried out from the late 90s till date. Those studies paved the way for understanding the petrographic, geochemical, and geochronological characteristics of mafic dykes of peninsular India (Devaraju T.C 1995, Radhakrishna et al. 2007). Detailed studies on Neo-proterozoic dykes from Dharwar craton





Nibiya et al.,

exemplified the significance of mafic dykes of peninsular India in the evolution of lithospheric mantle (Ikramuddin & Steuber 1976). Numerous geoscientists have examined the connection between large igneous provinces of India (LIPs) and emplaced mafic dyke swarms in shield regions, particularly in contemporary research (Ernst, 2010). The Archean Dharwar Craton is said to have been invaded by numerous distinct Palaeoproterozoic mafic dykes (Murthy, 1987, Drury, 1984; Halls, 1982). Comprehensive research has been conducted on the petrology and geochemistry of these palaeoproterozoic mafic dykes especially on those located in the eastern Dharwar Craton (EDC) (Chatterjee & Bhattacharji, 2001; Radhakrishana et al., 2007; Srivastava, et al, 2014). Comparable research data are known for the Western Dharwar Craton (WDC) (Devaraju 2008; Naqvi et al., 1972; Radhakrishna, 2009); nevertheless, a thorough investigation throughout the Indian peninsula is necessary due to the probable relevance of dykes in the crustal evolution. Therefore, a few mafic dykes exposed in the Mysore district of WDC, particularly in and around Piriapatna taluk regions (see Fig 1), have been sampled for preliminary petrological and geochemical studies in order to understand its genesis and classification

### Regional Geology

Intruding all earlier stratigraphic formations from the Archean (>3.4 Ga) to the early-middle Palaeocene (0.6 Ga), dyke formations are found throughout Peninsular India and have a well-documented crustal evolution history (Murthy, 1995; Murthy, 1987, Ikramuddin & Steuber 1976; Ernst and Srivastava, 2008). However, the focus of this investigation is on dykes that are unique to the Piriapatna taluk of Mysore district. Since these dykes are stratigraphically part of the southern WDC, the Dharwar Craton is briefly described below.

Dharwar craton is considered as greatest Archean continental nucleus in the Asian continent. This supergroup has a basement of tonalite–trondjemite–granodiorite (4.0–2.56 Ga) (TTG) gneisses, the amphibolite to granulite metamorphic facies (3.40–2.56 Ga) (Naqvi and Rogers, 1987; Peucat et al., 1995) and two generations of greenstone belts—the 3.35–3.20 Ga volcano sedimentary Sargur group and the low to medium grade metamorphic sequence (2.90–2.54 Ga) of Dharwar supergroup (Radhakrishna, 1988; Radhakrishna, 1983). The EDC and WDC are the two main divisions of the Dharwar Craton, which are based on different geological aspects; such as lithological similarities, geochronological aspects and other structural geology characteristics. (Ramakrishnan, 1988, 1993; Ramakrishnan & Vaidyanadhan, 2010). The Chitradurga fault zone divides the EDC from the WDC. Recently, a central block that divides the craton into Western (3.4 Ga to 3.0 Ga crust), Central (>3.0 Ga crust), and Eastern blocks (2.7 Ga to 2.6 Ga crust) has also been postulated (Jayananda et al., 2018). According to the tectonic evolution history of the Dharwar craton, cratonization processes persisted until 2.5 Ga, after which there was a significant change in the petrogenetic and crustal development processes toward the late Archean (Manikyamba et al., 2004). These differences can be associated with a number of magmatic events which includes mafic dyke intrusion into basement rock formations such as granitoids, TTGs, and greenstone belts.

In contrast to the mafic dykes in the EDC, those in the WDC differ in composition and orientation. According to Radhakrishna and Mathew (1993), research has revealed three primary dyke swarms in the WDC that are thought to be of Proterozoic age: (a) the Hassan–Tiptur dykes; (b) the Mysore dykes; and (c) the Dharwar dykes. A wider distribution of dolerite dykes and two suites of amphibolitic and epidioritic dyke swarms were suggested by Meert and Pandit (2015). Dyke swarms in the WDC are different from those in the Eastern Dharwar Craton in that they occur as patches of large exposures, most of which have no obvious relationship to the cooled margins and country rock. Additionally, these dykes are sporadically spaced and largely unreachable because of the deep forests that encircle a large portion of western Dharwar's north and the vegetation that covers the green stones.

### Field investigation and sampling

The Piriapatna area of Mysore is selected due to the presence of a cluster of dykes of nearly similar trend (Fig. 1). In this location, there are exposed dykes of varying sizes, but not clearly showing contact with the country rock. Many of the mafic dykes are found partially destroyed in the middle of farmed land, while the majority are invaded as a result of agricultural activity. In this study area, dolerite dykes exhibit NNW-SSE trending intrusion embedded in the





PGC. The Piriapatna dolerite dykes rocks range in color from dark green to black. Samples are collected from the exposed outcrops, and preliminary petrographical research and geochemical analysis were carried out to understand the geochemical characterisation and textural features of these dolerite dykes.

#### Petrography:

The mineral distribution, texture, crystallization and degree of alteration showed two distinct types of dykes from Piriapatna taluk in the thinsection studies. The ophitic texture, which is characterized by lath-shaped plagioclase feldspar encased in a matrix of coarse grained pyroxene minerals, is shown in Fig. 2a and 2b shows the dolerite with medium-grained sub-ophitic texture and also which includes opaque minerals like magnetite and titanomagnetite in their dispersed forms, as well as laths of plagioclase feldspar and clino-pyroxene as essential minerals. Even though Fig. 2b has a texture comparable to 2a, the presence of chlorite crystals in this area points to changes that this dyke rock has undergone. The Photomicrograph (Fig 2c.) shows poikilitic texture. The differing rates at which the minerals nucleate and grow typically result in a poikilitic texture; the slower-growing mineral, known as an oikocryst, encloses the rapidly-growing minerals, which stay as smaller grains. Because of the prominent metamorphic characteristics, these dyke rocks are classified as meta-dolerites. Plagioclase laths were maintained in 50% or fewer of the doleritic textures that relicts and amphibole had mostly replaced pyroxene. As the study area belongs to a lower degree metamorphic zone, the presence of the chlorite is convincing this. A few samples contained olivine in small quantity as well. Photomicrograph taken in a reflected microscope (Fig 2d) shows the presence of pyrite. Numerous reports of dolerite dykes with comparable petrographic characteristics may be found all around the WDC. (Halls 2007)

Fig 2: The Photomicrograph images of the dolerite dykes from study area. Fig (a) and (b) shows ophitic-subophitic texture with lath-shaped plagioclase in a pyroxene matrix; Fig (c) shows a poikilitic texture with a large plagioclase feldspar (oikocryst) where smaller pyroxene minerals are enveloped in plagioclase. Fig (d) shows Pyrite mineralization in a dolerite dyke. Amphibole is also present in these dykes, as the evidence for alteration.

Pl=Plagioclase, Cpx=Clino-pyroxene, Chl=Chlorite, Amp=Amphibole, Qz=Quartz, Py=Pyrite

#### Analytical Techniques:

##### Whole-rock geochemistry

For the dyke rocks in this work, a complete geochemical investigation employing XRF was carried out in order to provide a preliminary geochemical characterization. Whole rock analysis has been conducted on representative samples that were gathered. Steel and agate mortars are used to chip and grind samples till they are powdered to 63 $\mu$ . Eight new samples were chosen for major oxide studies from the NE-SW trending Piriapatna dykes. The XRF analysis is done at the National Centre for Polar and Ocean Research (NCPOR), and instrument used for this study is Axios Max WD XRF Spectrometry WDXRF spectrometer. Table 2 presents the findings. Major element concentrations differ with SiO<sub>2</sub> ranging from 47–50wt% whereas MgO and Al<sub>2</sub>O<sub>3</sub> show very large differences, 7–14wt%, and 9–15wt%, respectively. The major oxides like Fe<sub>2</sub>O<sub>3</sub> and CaO, shows variations 12-13 wt% and 9-11 wt% respectively. Other alkalis shows smaller variations.

## RESULTS AND DISCUSSION

The dolerite dykes are plotted in the basalt and basalt andesitic field, which essentially depicts the mafic nature of the rock, according to the total alkali against SiO<sub>2</sub> -TAS diagram (Fig. 3). The mafic index character of the dolerite dyke from the research area was determined using the Harker binary diagram. This is based on the MgO vs. Major oxides (Fig. 4) plot. As the MgO increases with decreasing SiO<sub>2</sub>, the bivariate plot of MgO vs SiO<sub>2</sub> exhibits a negative correlation, which is consistent with normal magmatic crystallization patterns. There is also a negative association seen in the MgO vs. Al<sub>2</sub>O<sub>3</sub>, K<sub>2</sub>O, and TiO<sub>2</sub> bivariate plot. In contrast, there is a positive correlation between MgO and P<sub>2</sub>O<sub>5</sub> and FeO<sup>T</sup>. The fractionation of Cpx during crystallization is clearly indicated by the positive correlation existing between CaO and MgO.







The AFM ( $A=Na_2O+K_2O$ ;  $F=Fe_2O_3^T$ ;  $M=MgO$ ) plot of Irvine and Baragar (1971) diagram (Fig. 5a) for dolerite, and meta-dolerite rocks plot in tholeiitic field, and the both rocks shows distinct ferro-magnesium-enrichment trend. The Jensen (1976) triangular cation plot (Fig.5b) for dolerites plots more in Komatiiticbasalt field while three of the samples falls at high-Mg tholeiite basalt field . The Classification of Miyashiro (1974) dividing the calc-alkaline series from the tholeiitic series, by plotting  $SiO_2$  Vs  $FeO/MgO$  diagram (Fig. 6) applied for dolerite samples. The plot shows samples fall in both calc-alkaline series and tholeiite series, but most of the dolerites falls under tholeiite category. Several tectonic setting diagrams were used to denote the dolerite dyke emplacement characteristics. The ternary diagram (Fig.7) of Pearce et al.(1977) shows the plot of major oxides  $MgO-Fe_2O_3^T-Al_2O_3$ , the dolerite samples plot in Ocean Island and Ocean ridge floor fields.

The geochemical analysis of the dyke samples that were gathered in the current research highlights the following factors. Every dyke rock sample collected from the piriapatna exhibits a doleritic composition; the main minerals found in these rocks are the Cpx and plagioclase feldspar, which have a lath shape, along with a few opaque minerals like magnetite and pyrites. The dolerite rock that has been gathered exhibits mostly subophitic textures, but few dykes shows poikilitictextures, and sulfide mineralization in a few more. The dolerite dykes from Piriapatna intrudes into the Peninsular Gneissic Complex (PGC) like rest of the dykes from the entire Mysore. All of the dyke samples fall into the tholeiite to basaltic categorization fields based on the whole rock geochemical data.

## CONCLUSION

Based on its mineralogical, textural, and geochemical properties, the collected dyke rocks from the study area are categorized into dolerite dykes and meta-dolerites. Because the gathered dyke samples have a doleritic composition and contain a significant amount of Cpx and lath-shaped plagioclase as mineralogy. Thin section investigations also reveal the existence of alterations leading to the formation of amphiboles and chlorite minerals. A small number of dolerite dykes have sulfide mineralization, such as pyrite crystals, which is similar to many other WDC dykes. Subophitic textures can be seen in the gathered dolerite rock, and gabbroic textures with remnant doleritic intergrowth can be seen in a few dykes. Geochemically, these dolerites exhibit ferro-magnesium enrichment and tholeiite character.

The composition of dolerites can be seen as basaltic to basaltic andesitic based on the TAS plot. The  $MgO$  and compatible elements have a favorable correlation. The current dolerite samples' tectonic settings reveal features of oceanic ridges as well as Island Arc Basalt. This indicates that the dolerites with OIB and E-MORB affinities were most likely deposited in the oceanic ridge and transitional island arc environments.

## ACKNOWLEDGEMENTS

We owe a debt of gratitude to Dr. Parijat Roy, the scientist-in-charge and scientist and Syed Aftab Hussain, the project scientist from hydrothermal exploration division of the National Centre for Polar & Ocean Research (NCPOR), for carrying out whole rock geochemical analysis. We are especially grateful to Dr. Annapoorna H, Mrs. Sowndarya M, and Mr. Masheo Kezo for their insightful discussion and field support.

## REFERENCES

1. Amiya K. Samal, Rajesh K. Srivastava, WaliurRahaman (2021), Sr-Nd isotope geochemistry and petrogenesis of ca. 2.26–2.25Ga and ca. 2.08Ga mafic dyke swarms from the Dharwar craton, India: Insights into their mantle sources and geodynamic implications, *Lithos*, Volumes 406–407





**Nibiya et al.,**

2. Ammini Sasidharan Silpa, Madhusoodhan Satish-Kumar, Toshiro Takahashi (2021) Sr-Nd isotopic study of dolerite dykes in the Western Dharwar craton, southern India: Implications for the evolution of the subcontinental lithospheric mantle in late Archean, *Lithos*, 388–389
3. Apratim K. Rai, Rajesh K. Srivastava, Amiya K. Samal, Valiveti Venkata Sessa Sai (2019) Geochemistry, petrogenesis, and geodynamic implications of trending palaeoproterozoic mafic dyke swarms from southern region of the western dharwar
4. Chandan-Kumar B & A. G. Ugarkar (2017) Geochemistry of mafic-ultramafic magmatism in the Western Ghats belt (Kudremukh greenstone belt), western Dharwar Craton, India: implications for mantle sources and geodynamic setting, *International Geology Review*, 59:12, 1507-1531, DOI: 10.1080/00206814.2017.1278623
5. Chardon, D., Jayananda, M., & Peucat, J. -J. (2011). Lateral constructional flow of hot orogenic crust: Insights from the Neoproterozoic of south India, geological and geophysical implications for orogenic plateau. *Geochemistry, Geophysics, Geosystems*, 12, Q02005.
6. Chardon, D., Jayananda, M., Chetty, T. R. K., & Peucat, J. -J. (2008). Precambrian continental strain and shear zone patterns: South Indian case. *Journal of Geophysical Research*, 113, B08402. <https://doi.org/10.1029/2007JB005299>
7. Chatterjee, N., & Bhattacharji, S. (2001). Petrology, geochemistry and tectonic settings of the mafic dikes and sills associated with the evolution of the Proterozoic Cuddapah Basin of south India. *Proc. of the Indian Acad. Of Sci. (Earth and Planetary Sciences)*, 110, 433–453.
8. Devaraju, T. C. (1995). Dyke swarms of Peninsular India. *Geological Society of India Memoir*, 33, 451.
9. Devaraju, T. C. (1995). Dyke swarms of Peninsular India. *Geological Society of India Memoir*, 33, 451.
10. Devaraju, T. C., Alapieti, T. T., Sudhakara, & Kaukonen, R. J. (2008). Calcalkaline mafic dykes swarms of volcanic arc, ocean floor and N-MORB basalt affinity with features of destructive plate margin emplacement in the northern segment of western Dharwar craton. In R. K. Srivastava, C. Sivaji, & N. V. Chalapathi Rao (Eds.), *Indian dyke: Geochemistry, geophysics and geochronology* (pp. 215–237). New Delhi: Narosa Publishing House Pvt. Ltd.
11. Devaraju, T. C., Alapieti, T. T., Sudhakara, & Kaukonen, R. J. (2008). Calcalkaline mafic dykes swarms of volcanic arc, ocean floor and N-MORB basalt affinity with features of destructive plate margin emplacement in the northern segment of western Dharwar craton. In R. K. Srivastava, C. Sivaji, & N. V. Chalapathi Rao (Eds.), *Indian dyke: Geochemistry, geophysics and geochronology* (pp. 215–237). New Delhi: Narosa Publishing House Pvt. Ltd.
12. Drury, S. A. (1984). Proterozoic dyke swarms and thermal evolution in south India. *Journal of Geological Society of India*, 25, 437–444.
13. Drury, S. A., Harris, N. B. W., Holt, R. W., Reeves-Smith, G. J., & Wightman, R. T. (1984). Precambrian tectonics and crustal evolution in South India. *The Journal of Geology*, 92, 3–20. <https://doi.org/10.1086/628831>
14. Ernst, R. E. (2014). Large igneous provinces (p. 653). Cambridge: Cambridge University Press.
15. Ernst, R. E., & Srivastava, R. K. (2008). India's place in the Proterozoic world: Constraints from the Large Igneous Province (LIP) record. In R. K. Srivastava, C. Sivaji, & N. V. C. Rao (Eds.), *Indian dyke: Geochemistry, geophysics and geochronology* (pp. 413–445). New Delhi: Narosa Publishing House Pvt. Ltd.
16. Ernst, R. E., Srivastava, R. K., Bleeker, W., & Hamilton, M. (2010). Precambrian large igneous provinces (LIPs) and their dyke swarms: New insights from high-precision geochronology integrated with paleomagnetism and geochemistry. *Precambrian Research*, 183, vi–xi.
17. French, J. E., & Heaman, L. M. (2010). Precise U–Pb dating of Paleoproterozoic mafic dyke swarms of the Dharwar craton, India: Implications for the existence of the Neoproterozoic supercraton Scavia. *Precambrian Research*, 183(3), 416–441. <https://doi.org/10.1016/j.precamres.2010.05.003>
18. Gayer RA, Powell DB, Rhodes S (1978) Deformation against metadolerite dykes in the caledonides of finnmark, norway. *Tectonophysics* 46:99–115
19. Halls HC, Kumar A, Srinivasan R, Hamilton MA (2007) Paleomagnetism and U–Pb geochronology of easterly trending dykes in the Dharwar craton, India: feldspar clouding, radiating dyke swarms and the position of India at 2.37 Ga. *Precambrian Research* 155:47–68
20. Halls, H. C. (1982). The importance and potential of mafic dyke swarms in studies of geodynamic processes. *Geoscience Canada*, 9, 145–154.





21. Halls, H. C., Kumar, A., Srinivasan, R., & Hamilton, M. A. (2007). Paleomagnetism and U-Pb geochronology of eastern trending dykes in the Dharwar craton, India: Feldspar clouding, radiating dyke swarms and the position of India at 2.37 Ga. *Precambrian Research*, 155, 47–68. <https://doi.org/10.1016/j.precamres.2007.01.007>
22. Hamilton, M.A., Davis, D.W., Buchan, K.L., Halls, H.C., 2002. Precise U–Pb dating of reversely magnetized Marathon diabasedykes and implications for emplacement of giant dyke swarms along the southern margin of the Superior Province, Ontario. Report 15, Current Research 2002-F6, Radiogenic age and Isotopic Studies, Geological Survey of Canada, pp. 1–8.
23. Ikramuddin, M., Stueber, A.M., 1976. Rb-Sr ages of Precambrian dolerite and alkaline dykes, southeast Mysore State, India. *Lithos* 9, 235–241.
24. Irvine TN, Baragar WRA (1971) A Guide to the chemical classification of the common volcanic rocks. *Can J Earth Sci* 8: 523–548.
25. Jayananda M., Santosh M., Aadhiseshan K.R. (2018), Formation of Archean (3600–2500 Ma) continental crust in the Dharwar Craton, southern India, *Earth-Science Reviews*, Vol. 181, pp 12–42
26. Jayananda, M., Kano, T., Peucat, J., and Channabasappa, S., (2008), 3.35 Ga komatiite volcanism in the western Dharwar craton, southern India: Constraints from Nd isotopes and whole-rock geochemistry: *Precambrian Research*, v.162, p.160–179. [10.1016/j.precamres.2007.07.010](https://doi.org/10.1016/j.precamres.2007.07.010).
27. Jayananda, M., Peucat, J.-J., Chardon, D., Krishna Rao, B., & Corfu, F. (2013). Neoproterozoic greenstone volcanism, Dharwar craton, Southern India: Constraints from SIMS zircon geochronology and Nd isotopes. *Precambrian Research*, 227, 55–76. <https://doi.org/10.1016/j.precamres.2012.05.002>
28. Jensen, L.S. (1976). A new cation plot for classifying sub-alkalic volcanic rocks (Vol. 66). Ministry of Natural Resources.
29. Kumar, A., Nagaraju, E., Besse, J., & Bhaskar Rao, Y. J. (2012). New age, geochemical and paleomagnetic data on a 2.21 Ga dyke swarm from south India: Constraints on Paleoproterozoic reconstruction. *Precambrian Research*, 220–221, 123–138.
30. Kumar, A., Nagaraju, E., SrinivasaSarma, D., & Davis, D. W. (2014). Precise Pb–Pb geochronology by the thermal extraction–thermal ionization mass spectrometry method. *Chemical Geology*, 372, 72–79. <https://doi.org/10.1016/j.chemgeo.2014.02.017>
31. Le Bas, M.J. (1971). Per-alkaline volcanism, crustal swelling, and rifting. *Nature Physical Science*, 230(12), 85–87.
32. Mahadevan, T. M. (2008). Precambrian geological and structural features of the Indian Peninsula. *Journal of the Geological Society of India*, 72, 35–55.
33. Manikyamba, C., Kerrich, R., Naqvi, S.M., Mohan, M.R., 2004. Geochemical systematics of tholeiitic basalts from the 2.7 Ga Ramagiri-Hungund composite greenstone belt, Dharwar craton. *Precambrian Res.* 134 (1–2), 21–39.
34. Maya, J. M., Bhutani, R., Balakrishnan, S., & Sandhya, S. R. (2017). Petrogenesis of 3.15 Ga old Banasandratomatiites from the Dharwar craton, India: Implications for early mantle heterogeneity. *Geoscience Frontiers*, 8, 467–481. <https://doi.org/10.1016/j.gsf.2016.03.007>
35. Meen, J. K., Rogers, J. J., & Fullagar, P. D. (1992). Lead isotopic compositions of the Western Dharwar craton, southern India: Evidence for distinct Middle Archean terranes in a Late Archean craton. *Geochimica et Cosmochimica Acta*, 56, 2455–2470. [https://doi.org/10.1016/0016-7037\(92\)90202-T](https://doi.org/10.1016/0016-7037(92)90202-T)
36. Meert, J.G., Pandit, M.K., 2015. The Archean and Proterozoic history of Peninsular India: tectonic framework for Precambrian sedimentary basins in India. *Geol. Soc. Lond. Mem.* 43 (1), 29–54.
37. Miyashiro, A. (1974). Volcanic rock series in island arcs and active continental margins. *American journal of science*, 274(4), 321–355.
38. Murthy, N. G. K. (1987). Mafic dyke swarms of the Indian shield. In: *Mafic Dyke Swarms* (Eds. Halls, H. C. and Fahriig, W. F.). Geological Association of Canada Special Paper, 34, 393–400.
39. Nagaraju, E., Parashuramulu, V., Kumar, A., & Sarma, D. S. (2018). Paleomagnetism and geochronological studies on a 450 km long 2216 Ma dyke from the Dharwar craton, southern India. *Physics of the Earth and Planetary Interiors*, 274, 222–231. <https://doi.org/10.1016/j.pepi.2017.11.006>
40. Naqvi, S. M., & Rogers, J. J. W. (1987). *Precambrian Geology of India* (p.233). Oxford Monographs on Geology and Geophysics No. 6. New York: Oxford University Press.





## Nibiya et al.,

41. Naqvi, S. M., DivakaraRao, V., Satyanarayana, K., & Hussain, S. M. (1972). Petrochemistry of dolerite dykes from Shimoga and Chitaldrug schist belts, Mysore. *Geophysical Research Bulletin (NGRI)*, 10, 109–123.
42. Nutman, A. P., Chadwick, B., Krishna Rao, B., & Vasudev, V. N. (1996). SHRIMP U-Pb zircon ages of acid volcanic rocks in the Chitradurga and Sandur Groups and granites adjacent to Sandur schist belt. *Journal of the Geological Society of India*, 47, 153–161.
43. Pearce, T.H., Gorman, B.E., & Birkett, T. C. (1977). The relationship between major element chemistry and tectonic environment of basic and intermediate volcanic rocks. *Earth and Planetary Science Letters*, 36(1), 121–132.
44. Peucat, J. J., Bouhallier, H., Fanning, C. M., & Jayananda, M. (1995). Age of the Holenarsipur greenstone belt, relationships with the surrounding gneisses (Karnataka, South India). *The Journal of Geology*, 103, 701–710. <https://doi.org/10.1086/629789>
45. Peucat, J. J., Jayananda, M., Chardon, D., Capdevila, R., Fanning, M. C., & Paquette, J. L. (2013). The lower crust of Dharwar craton, south India: Patchwork of Archean granulitic domains. *Precambrian Research*, 227, 4–29. <https://doi.org/10.1016/j.precamres.2012.06.009>
46. Piispa, E. J., Smirnov, A. V., Pesonen, L. J., Lingdevaru, M., Murthu, K. S. A., & Devraju, T. C. (2011). An integrated study of Proterozoic dykes, Dharwar craton, southern India. In R. K. Srivastava (Ed.), *Dyke swarms: Keys for geodynamic interpretation* (pp. 33–45). Berlin, Heidelberg: Springer-Verlag. [https://doi.org/10.1007/978-3-642-12496-9\\_3](https://doi.org/10.1007/978-3-642-12496-9_3)
47. Radhakrishna, T., Krishnendu, N. R., & Balasubramonian, G. (2007). Mafic magmatism around Cuddapah Basin: Age constraints, petrological characteristics and geochemical inference for a possible magma chamber on the South western margin of the basin. *Journal of the Geological Society of India*, 70, 194–206.
48. Radhakrishna, B.P., 1983. Archaean granite-greenstone terrain of the south Indian Shield in Precambrian of South India. *Geol. Soc. India Mem.* 4, 1–46.
49. Radhakrishna, T. (2009). Precambrian mafic magmatism in South Indian granulite terrain. *Journal of Geological Society of India*, 73, 131–142. <https://doi.org/10.1007/s12594-009-0008-x>
50. Radhakrishna, T., Balasubramonian, G., Joseph, M., & Krishnendu, N. R. (2004). Mantle processes and geodynamics: Inferences from mafic dykes of south India. In G. R. Ravindra Kumar, & N. Subhash (Eds.), *Earth system science and natural resource management (silver Jubilee compendium)* (pp. 3–25). Trivandrum: Centre for Earth Science Studies
51. Radhakrishna, T., Mathew, J., 1993. Late Precambrian (850–800 Ma) palaeomagnetic pole for the south Indian shield from the Harohalli alkaline dykes: geotectonic implications for Gondwana reconstructions. *Precambrian Res.* 80 (1–2),
52. Ramachandran, C., Thirunavukkarasu, A., & Ravi, R. (2023a). Wall rock deformation, chilled margin, textural analysis, and displacement structures of Salem dolerites emplaced within the Southern Granulite Terrane, Tamilnadu, India. *Arabian Journal of Geosciences*, 16(1), 52.
53. Ramakrishnan, M. (1988). Tectonic evolution of the Archean high grade terrain of south India. *Journal of Geological Society of India*, 31, 118–119.
54. Ramakrishnan, M., & Vaidyanadhan, R. (2010). *Geology of India* (p. 994). Bangalore: Geological Society of India.
55. Ramakrishnan, M., Viswanatha, M.N. and Swami Nath, J. (1976) Basement-cover Relationships of Peninsular Gneiss with high-Grade Schists and Greenstone Belts of Southern Karnataka. *Journal of the Geological Society of India*, 17, 97–111.
56. S. Rameshkumar, A. Thirunavukkarasu, C. Ramachandran, C. Sakthivel, C. Kasilingam (2024), *Journ. Geol. Geograph. Geoecology*, 33(1), 164–177
57. Srivastava, R. K. (2011). *Dyke swarms: Keys for geodynamic interpretation* (p.605). Heidelberg: Springer-Verlag. <https://doi.org/10.1007/978-3-642-12496-9>
58. Srivastava, R. K., Jayananda, M., Gautam, G. C., & Samal, A. K. (2014). ~2.21–2.22 Ga N–S to NNW–SSE trending Kunigal mafic dyke swarm from Eastern Dharwar Craton, India: Implications for Paleoproterozoic large igneous provinces and supercraton Superia. *Mineralogy and Petrology*, 109, 695–711.
59. Srivastava, R. K., Samal, A. K., & Gautam, G. C. (2015). Geochemical characteristics and petrogenesis of distinct Paleoproterozoic mafic dyke swarms in space and time and associated large igneous provinces from the Eastern



Nibiya *et al.*,Dharwar Craton, India. International Geology Review, 57, 1462–1484.  
https://doi.org/10.1080/00206814.2014.938366**Table 1: Displays the sample number and location, rock name, Lat/long, trend, and dyke texture.**

Sl.No.	Sample No.	Latitude	Longitude	Trend	Rock name	Texture
1	N04	12° 25' 12.848" N	76° 6' 3.980" E	N-S	Meta-dolerite	Poikilitic
2	N05	12° 26' 10.356" N	76° 7' 5.648" E	N-S	Meta-dolerite	Poikilitic
3	N06	12° 26' 0.888" N	76° 7' 10.690" E	NNW-SSE	Dolerite	Sub ophitic
4	N07	12° 26' 11.161" N	76° 9' 1.851" E	NNW-SSE	Dolerite	Ophitic
5	N08	12° 21' 8.376" N	76° 10' 0.467" E	NNW-SSE	Dolerite	Ophitic
6	N041	12° 20' 7.386" N	76° 8' 47.732" E	NNW-SSE	Dolerite	Ophitic
7	N042	12° 20' 12.762" N	76° 7' 12.995" E	NNW-SSE	Dolerite	Ophitic
8	N043	12° 19' 29.616" N	76° 4' 35.763" E	NNW-SSE	Dolerite	Sub ophitic

**Table 2. Whole- rock geochemistry for dolerite dyke rocks sampled from Piryapatna taluk, Mysore district, Karnataka.**

Sample No.	N05	N06	N07	N043	N08	N04	N041	N042
(wt%)								
SiO <sub>2</sub>	47.99	49.16	51.62	49.15	49.21	50.94	48.23	48.33
TiO <sub>2</sub>	0.97	0.82	0.75	0.73	0.73	1.17	1.23	0.98
Al <sub>2</sub> O <sub>3</sub>	14.59	15.15	13.87	9.53	9.55	13.65	12.32	11.46
Fe <sub>2</sub> O <sub>3</sub>	11.35	12.17	10.65	13.46	12.94	11.56	12.9	13.45
MnO	0.17	0.16	0.16	0.18	0.18	0.14	0.18	0.19
MgO	12.02	8.93	8.85	13.68	14.7	7.72	12.09	12.22
CaO	9.76	8.92	10.48	9.31	9.33	11.16	9.4	10.14
Na <sub>2</sub> O	1.86	2.17	1.78	1.58	1.61	2.54	2.84	2.6
K <sub>2</sub> O	0.38	0.86	0.64	0.22	0.22	0.32	0.51	0.42
P <sub>2</sub> O <sub>5</sub>	0.08	0.15	0.13	0.15	0.16	0.23	0.1	0.15
LoI	0.82	0.71	0.28	0.66	0.66	0.71	0.32	0.1
Total	100.00	99.20	99.21	98.65	99.28	100.13	100.13	100.04





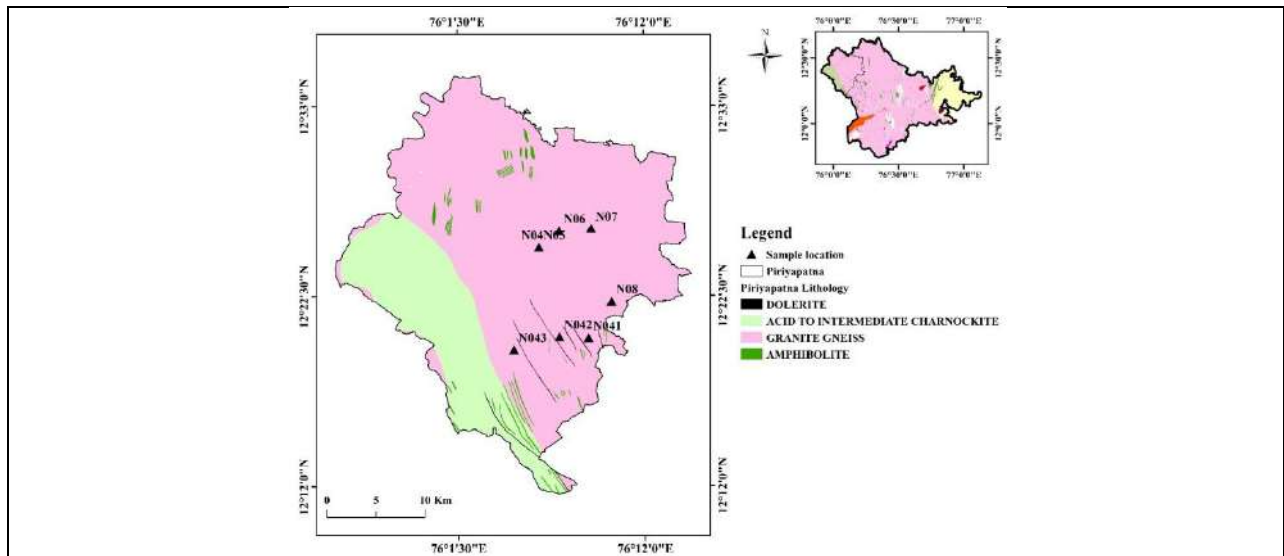


Fig 1. The lithological map of the Piriapatna Taluk including the dolerite dyke intrusion (represented as black line) and the geological map of the Mysore district is also shown at the top right corner. The sample locations are denoted in triangles. These dolerite dyke intrusions predominantly show NNW-SSE trends.

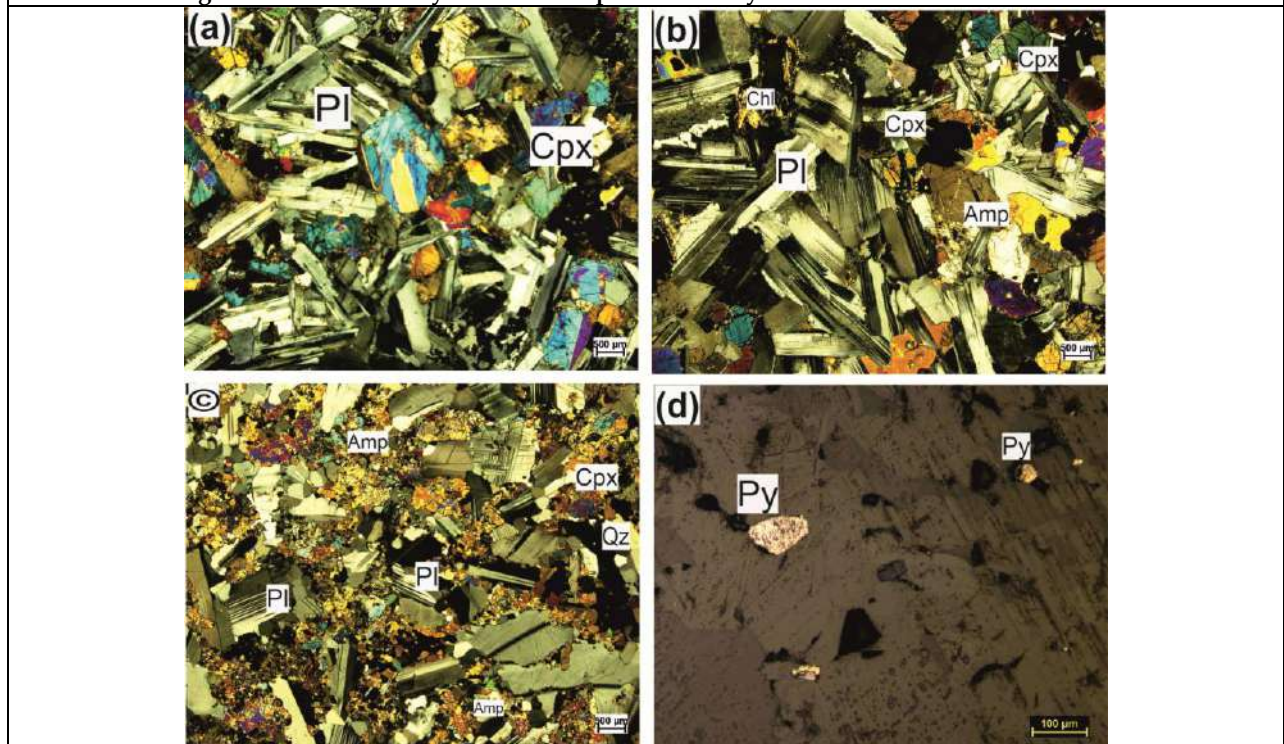


Fig 2: The Photomicrograph images of the dolerite dykes from study area. Fig (a) and (b) shows ophitic-subophitic texture with lath-shaped plagioclase in a pyroxene matrix; Fig (c) shows a poikilitic texture with a large plagioclase feldspar (oikocryst) where smaller pyroxene minerals are enveloped in plagioclase. Fig (d) shows Pyrite mineralization in a dolerite dyke. Amphibole is also present in these dykes, as the evidence for alteration.







Nibiya et al.,

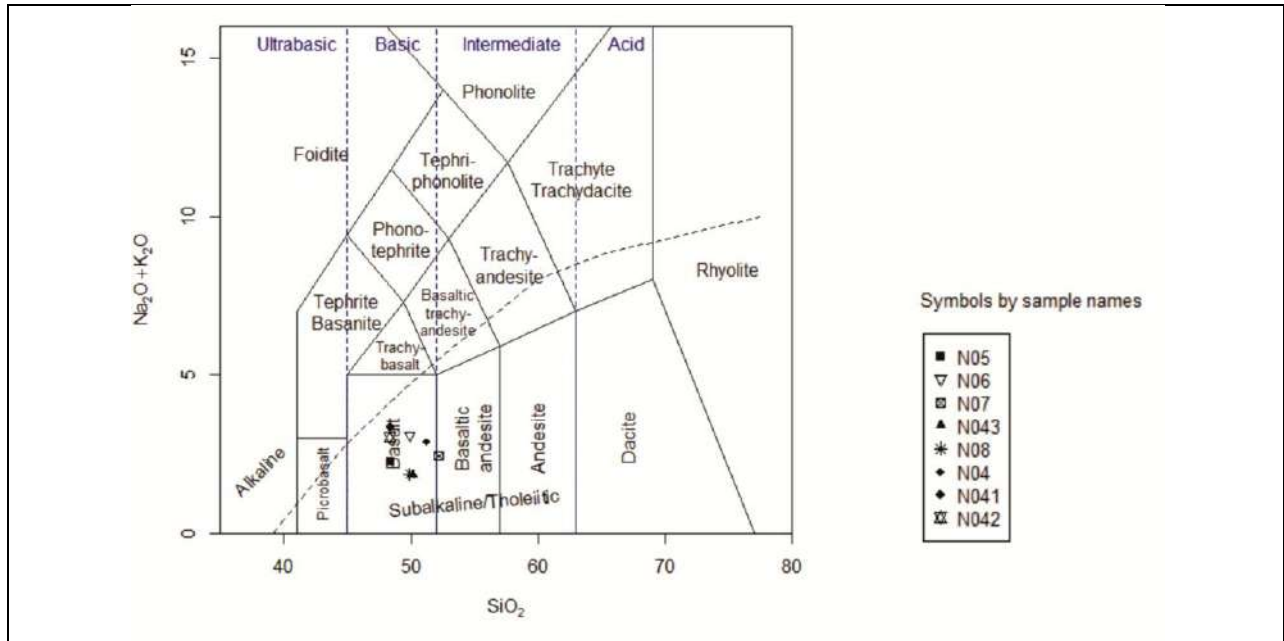


Fig.3. From total Alkali (Na<sub>2</sub>O + K<sub>2</sub>O)vs Silica (TAS) plot of Le Bas et al (1986), the general classification of collected dykes samples shows sub-alkaline tholeiitic in composition. The symbols which used to represent the sample name in this diagram is used in all other following diagrams.

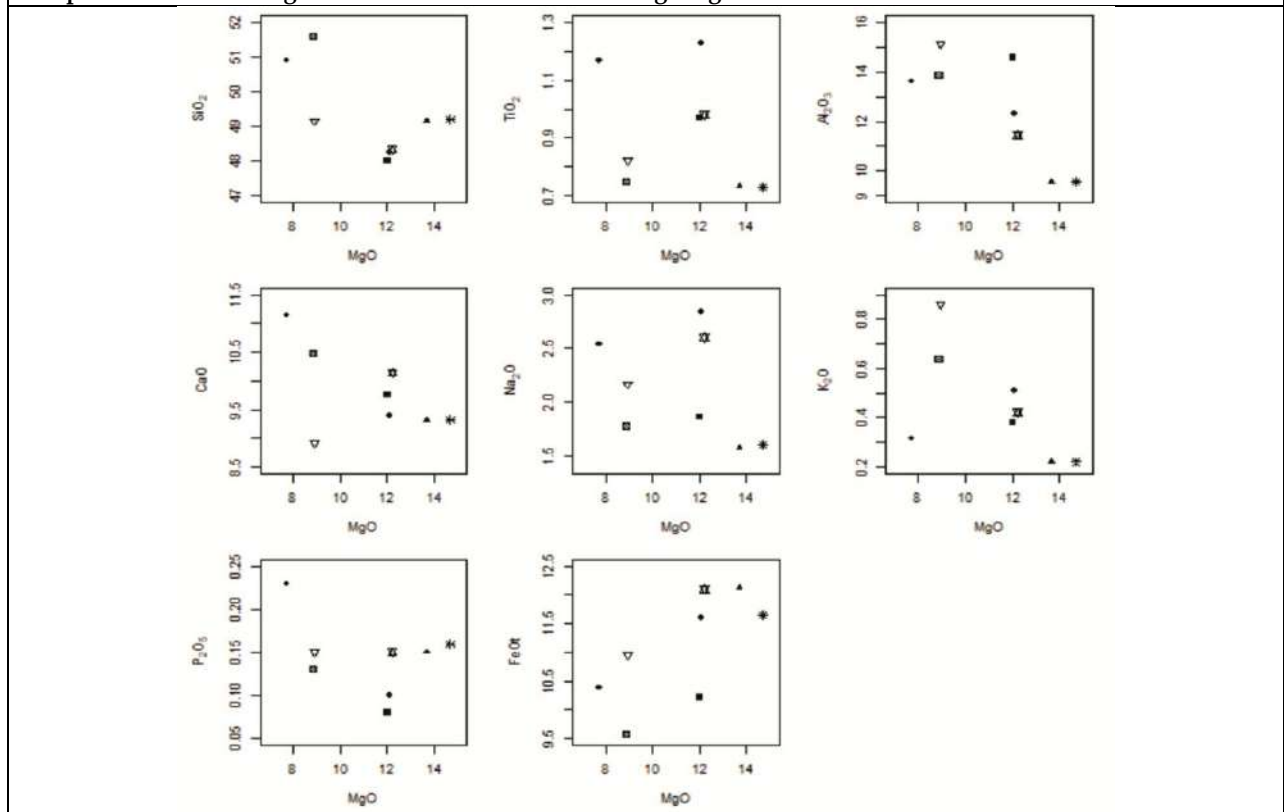


Fig. 4: The Harker variation diagram MgO vs major elements.



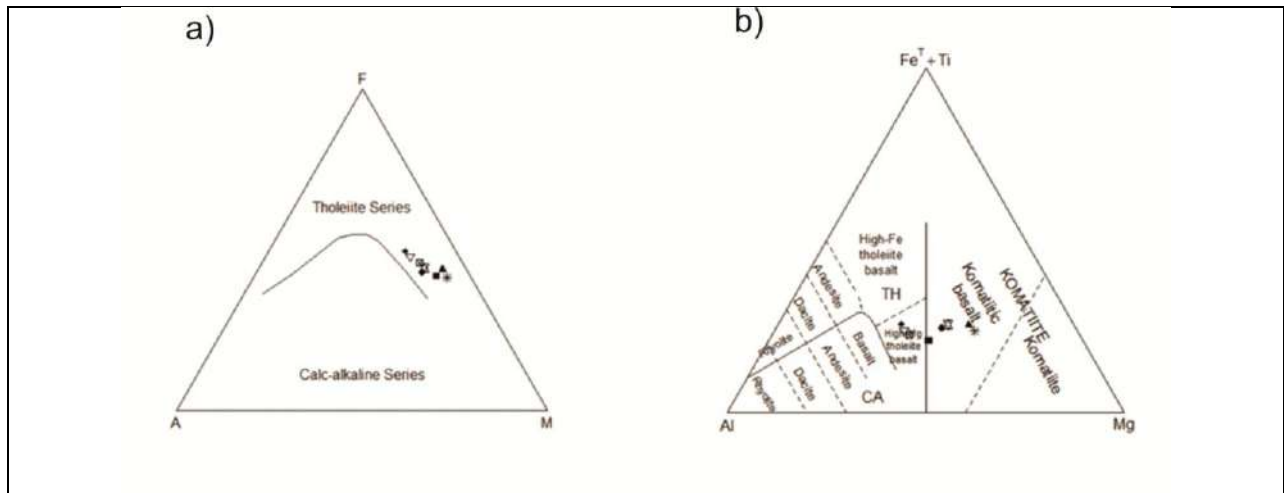


Fig.5 a) The tholeiitic nature of the chosen samples is depicted in the Irvine and Baragar - AFM diagram (1971), and b) Jensen's cation plot (Jensen, 1976).

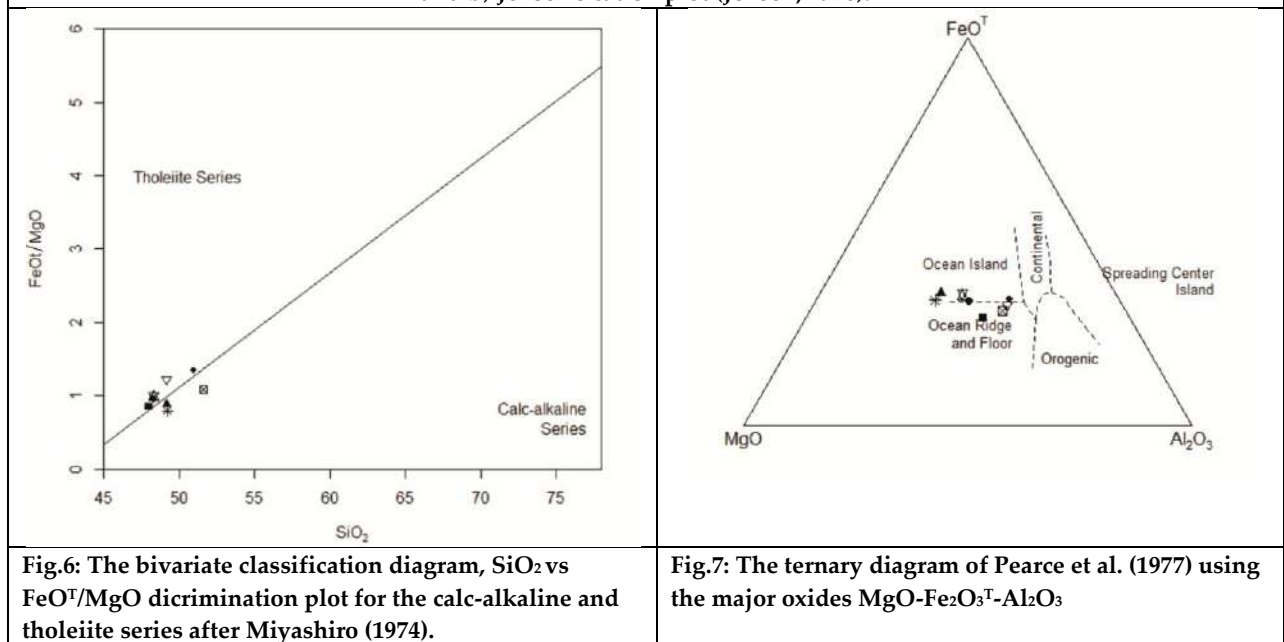


Fig.6: The bivariate classification diagram, SiO<sub>2</sub> vs FeO<sup>T</sup>/MgO discrimination plot for the calc-alkaline and tholeiite series after Miyashiro (1974).

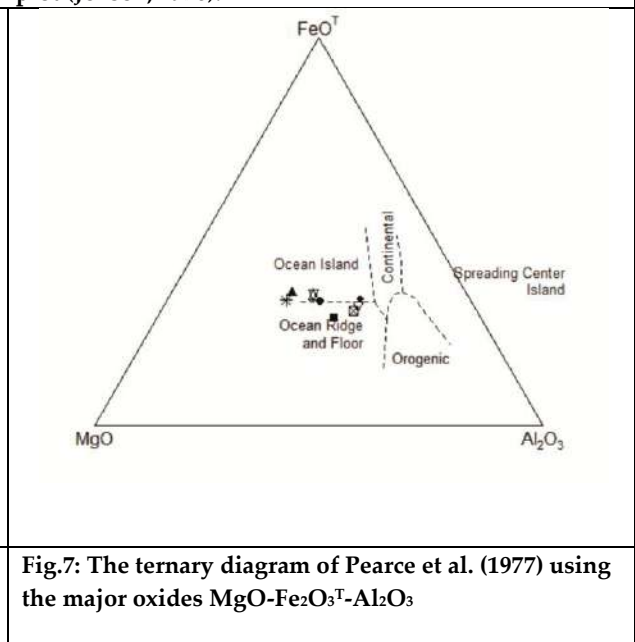


Fig.7: The ternary diagram of Pearce et al. (1977) using the major oxides MgO-Fe<sub>2</sub>O<sub>3</sub><sup>T</sup>-Al<sub>2</sub>O<sub>3</sub>





## HPTLC Method Validation of Antidiabetic Drugs - A Short Review

M.K.Vijayalakshmi<sup>1\*</sup>, T. Akshaya<sup>2</sup>, B.Amirtha Lakshmi<sup>2</sup>, C.Priya Dhaarani<sup>2</sup>, S.Sakthi<sup>2</sup>, and S.Sowmiya<sup>2</sup>

<sup>1</sup>Associate Professor, Department of Pharmaceutical Chemistry and Analysis, Faculty of Pharmacy, Bharath Institute of Higher Education and Research (Deemed to be University), Selaiyur, Tambaram, Chennai, Tamil Nadu, India.

<sup>2</sup>B.Pharm Final Year Student, Department of Pharmaceutical Chemistry and Analysis, Faculty of Pharmacy, Bharath Institute of Higher Education and Research (Deemed to be University), Selaiyur, Tambaram, Chennai, Tamil Nadu, India.

Received: 29 Jun 2024

Revised: 11 Sep 2024

Accepted: 19 Nov 2024

### \*Address for Correspondence

**M.K.Vijayalakshmi**

Associate Professor, Department of Pharmaceutical Chemistry and Analysis,  
Faculty of Pharmacy,  
Bharath Institute of Higher Education and Research (Deemed to be University),  
Selaiyur, Tambaram, Chennai, Tamil Nadu, India.  
E.Mail: vijiprabhudass@gmail.com



This is an Open Access Journal / article distributed under the terms of the **Creative Commons Attribution License** (CC BY-NC-ND 3.0) which permits unrestricted use, distribution, and reproduction in any medium, provided the original work is properly cited. All rights reserved.

### ABSTRACT

One essential analytical technique for measuring and characterising anti-diabetic medications is High-Performance Thin-Layer Chromatography (HPTLC). Since diabetes mellitus is becoming an epidemic on a worldwide scale, precise medication analysis is now essential. Among the many benefits of HPTLC are its great sensitivity, cost-effectiveness, and repeatability. The fact that diabetes is a major global health concern highlights how crucial accurate medication analysis is to the treatment of the condition. HPTLC is a great option for this task because of its exceptional accuracy in separating and quantifying complicated drug combinations. Sensitive detection methods, strict chromatographic conditions, and careful sample preparation are standard components of HPTLC methodologies for antidiabetic medication analysis. To guarantee accurate outcomes, issues like validation and standardization of methods are acknowledged and resolved. Applications for HPTLC in antidiabetic medication analysis include quality control, pharmacokinetic research, and study of herbal medicines. Its adaptability to various medication formulations and sample types increases its usefulness for diabetes management research and practice. HPTLC is a reliable analytical method for characterising and quantifying medications that treat diabetes. To improve HPTLC techniques and increase its use in diabetes research and therapy, more investigation and development are necessary.

**Keywords:** HPTLC, antidiabetic, development, analysis.





## INTRODUCTION

Diabetes mellitus is a group of metabolic conditions characterized by chronically elevated blood sugar levels due to defects in the production or function of insulin, or both. Insulin, being a crucial hormone for anabolism, causing disruption in the consumption of proteins, lipids, and carbohydrates. The insufficient insulin to create deduce response, insulin resistance of target tissues, liver, skeletal muscles and adipose tissue can be the causes of these metabolism abnormalities. Insulin receptors, the signal transduction system, effector enzymes, and genes are the sites of injury. The kind and duration of diabetes determine how severe the symptoms are[1,2]. Diabetes mellitus (DM), the most common endocrine disorder, is expected to impact more than 200 million people worldwide by 2010 and an additional 300 million by 2025. As the disease deteriorates, there is a progression of tissue or vascular damage, leading to severe consequences associated with diabetes, such as ulceration, neuropathy, retinopathy, and nephropathy [3]. The American Diabetes Association (ADA) continues to employ the most universally acknowledged classification of diabetes, which comprises type 1, type 2, various variants, and gestational diabetes mellitus (GDM). The ADA initially introduced this categorization in 1997 [4]. Diabetes Mellitus Type 1 (T1DM) caused by reduced level of beta cells which produce insulin. These beta cells are demolished by immune system. Usually takes place in childhood or adolescence, while it can happen at any age. Treatment includes lifelong insulin medication, lifestyle modification, and blood sugar monitoring[5]. Diabetes Mellitus Type 2 (T2DM), The reason behind T2DM Insulin deficit relative to insulin resistance. Most often affects persons over 45, although as obesity rates rise, it is also becoming more prevalent in younger populations. Prevention of T2DM includes handling alterations in lifestyle (food, exercise), oral drugs, and occasionally insulin[6]. GDM, or gestational diabetes mellitus caused by pregnancy-related hormonal changes that result in insulin resistance. occurs during pregnancy and normally goes away after birth, although it raises the possibility of acquiring type 2 diabetes in the future. Exercise, dietary changes, and occasionally insulin or oral medicines are used as treatments[7]. Additional Particular Types: Monogenic diabetes, which includes MODY (Maturity Onset Diabetes of the Young), is brought on by mutations in a single gene. Secondary diabetes: Few drugs might cause side effects, as a result of pancreatic disease, or as a result of hormonal imbalances. All forms of diabetes must be managed by routinely checking blood glucose levels, leading a healthy lifestyle, and following recommended treatment plans. In order to avoid complications including cardiovascular disease, nerve damage, kidney failure, and eye issues, early diagnosis and treatment are essential[8].

Medication used to control diabetes mellitus that lowers blood glucose levels is called an antidiabetic drug. Important varieties and their mechanism of action (MOA) includes: Insulin-Helps cells absorb glucose by replacing or enhancing endogenous insulin, especially in type 1 diabetes. Metformin-A biguanide that enhances peripheral tissue insulin sensitivity while lowering the amount of glucose produced by the liver. Sulfonylureas- Promote the release of more insulin from pancreatic beta cells (e.g., glipizide). DPP-4 Inhibitors- Raise incretin levels, improving insulin secretion and lowering glucagon release (e.g., sitagliptin). GLP-1 Receptor Agonists- mimic incretin, raise insulin release, lower glucagon secretion, and decrease stomach emptying (e.g., exenatide). SGLT2 Inhibitors- These medications, such as Empagliflozin, prevent the kidneys from reabsorbing glucose, which encourages urine excretion of glucose. Thiazolidinediones, such as pioglitazone, increase muscle and adipose tissue's sensitivity to insulin by stimulating PPAR-gamma receptors. Alpha-Glucosidase Inhibitors (e.g., acarbose)- Reduce postprandial glucose increases by delaying the intestines' absorption of carbohydrates. The kind of diabetes, comorbidities, and specific patient needs are taken into consideration when choosing these drugs[9-11].

Chromatography is a method used to separate the different elements of a mixture, known as solutes, based on their relative amounts in a moving fluid stream (called the mobile phase) and a stationary phase that is continuous. The stationary phase can exist as either a solid or a liquid, whereas the mobile phase can exist as either a liquid or a gas. Chromatography is extensively employed in the fields of chemistry and biology. In biochemical research, it is often used to detect and separate chemical compounds that originate from biological sources. This approach is employed in the petroleum industry to analyse complex hydrocarbon blends [12,13].

**Significant categories consist of**



**Vijayalakshmi et al.,**

1. TLC, or thin-layer chromatography: Mechanism- By using capillary action to transfer a solvent (mobile phase) along the glass plate, a sample is applied to a stationary phase (often silica gel) and separated. Use- Tracking the development of reactions and qualitatively analysing substances[14].
2. High-Performance Liquid Chromatography (HPLC): Mechanism- Under high pressure, a sample is injected into a liquid mobile phase and passes through a stationary phase-containing column, separating components according to how they interact with the stationary phase. Application- Both quantitative and qualitative examination of intricate blends in food, medicine, and environmental specimens[15].
3. Gas Chromatography (GC): Mechanism- To separate components based on volatility and interactions with the stationary phase, a volatile sample is vaporized and transported by an inert gas (mobile phase) along a column containing a liquid or solid stationary phase. Use- Analysis of volatile chemicals, for example, in food analysis and environmental monitoring[16].
4. Ion Exchange Chromatography: Mechanism- Ions and polar molecules are separated according to how well they cling to ion exchangers in the stationary phase. Use- Water analysis, protein purification[17].
5. SEC, or size-exclusion chromatography: Mechanism- Smaller molecules travel longer routes and elute later; larger molecules are separated according to size by passing them through a column loaded with porous beads. Use- Analysis of polymers and proteins[18].
6. High-Performance Thin Layer Chromatography: Better resolution and sensitivity are ensured by using tiny particle size stationary phase and high-quality, repeatable pre-coated plates. Samples are carefully applied as tiny spots or bands in HPTLC, and components are separated when the mobile phase (solvent) rises up the plate due to capillary action. Sophisticated scanning densitometers or other detection systems are used for detection and quantification; these devices are frequently combined with data analysis software. Because HPTLC is efficient, accurate, and repeatable, it is frequently used for both qualitative and quantitative analysis in the food, pharmaceutical, and environmental testing industries, as well as in the examination of plant materials[19,20].

**High Performance Thin Layer Chromatography (HPTLC)**

High Performance Thin Layer Chromatography is an advanced chromatographic technique used for the separation, identification, and quantification of chemical compounds in complex mixtures. Similar to traditional thin layer chromatography, HPTLC involves the separation of components based on their differential migration rates through a thin layer of stationary phase on a glass or plastic plate. However, HPTLC employs finer stationary phases, improved instrumentation, and optimized conditions, resulting in higher resolution, sensitivity, and reproducibility compared to conventional TLC. HPTLC is widely utilized in various industries, including pharmaceuticals, food, cosmetics, and environmental analysis, due to its versatility, speed, and cost-effectiveness. It plays a crucial role in quality control, research, and regulatory compliance by facilitating the analysis of diverse sample types with minimal sample preparation requirements [21-22.]

**Principle**

The principle of HPTLC involves separating compounds based on the rate of solvent migration on the thin layer of stationary phase, typically silica gel or cellulose, through capillary action. This separation occurs due to differences in the affinity of the compounds for the stationary phase and the mobile phase, which moves up the plate by capillary action[23]. The separated compounds are then visualized and analysed using various detection methods, such as UV absorption or chemical staining.

**Advantages**

1. High resolution: It can separate compounds with similar properties effectively, providing better resolution compared to traditional TLC.
2. High sensitivity: HPTLC allows for the detection of even trace amounts of compounds, making it suitable for quantitative analysis.
3. Speed: HPTLC provides faster analysis times compared to other chromatographic techniques, allowing for high throughput analysis.





Vijayalakshmi et al.,

4. Versatility: It can analyse a wide range of compounds, including pharmaceuticals, natural products, and food additives[24].
5. Cost-effectiveness: HPTLC typically requires less solvent and sample compared to other chromatographic techniques, making it more cost-effective.
6. Ease of use: HPTLC systems are relatively simple to set up and operate, requiring minimal training for users.
7. Quantitative analysis: HPTLC can be used for both qualitative and quantitative analysis, providing accurate measurements of compound concentrations[25].

#### DISADVANTAGES

While HPTLC offers many advantages, it also has some limitations:

1. Sensitivity: Although HPTLC can detect trace amounts of compounds, its sensitivity may not be as high as other chromatographic techniques like HPLC or GC-MS.
2. Limited compound compatibility: Some compounds may not separate well on HPTLC plates due to interactions with the stationary phase or mobile phase, limiting its applicability for certain analyses[26].
3. Sample preparation: HPTLC requires many steps including extraction and concentration, which might take more time and increased worker need.
4. Lack of automation: Compared to other chromatographic techniques, HPTLC systems may have limited automation capabilities, leading to potential variability in results and increased operator dependence.
5. Plate uniformity: The uniformity of HPTLC plates can vary, leading to potential inconsistencies in separation and detection.
6. Quantitative limitations: While HPTLC can provide quantitative results, it may not be as precise or accurate as other quantitative techniques like HPLC or GC-MS.
7. Limited detection options: HPTLC typically relies on visual or UV detection methods, which may not be suitable for all compounds or applications requiring specific detection wavelengths or sensitivity levels[27].

#### Applications

High-Performance Thin Layer Chromatography, or HPTLC, is a commonly used analytical method in many industries, but especially in chemistry and medicine. Among its uses are:

1. Quality control: HPTLC is used to examine and detect the presence of distinct components in a mixture, which assists in ensuring the quality of pharmaceutical items, food, and other consumer goods.
2. Drug analysis: To support forensic investigations, HPTLC is used to detect and quantify a wide range of drugs, including stimulants, opioids, and other restricted compounds.
3. Research in the pharmaceutical industry: To ensure the creation of safe and efficient medications, researchers employ HPTLC to examine the synthesis, purity, and deterioration of pharmaceutical chemicals.
4. Environmental analysis: HPTLC is used in soil, water, and air samples to identify and quantify contaminants, including heavy metals and pesticides, which aids the process of environmental monitoring and assessment.
5. Food analysis: To ensure the safety and quality of food, HPTLC is used in the identification and determination of multiple food additives, pollutants, and integrity testing of food products[28].
6. Plant research: HPTLC is utilized in the detection and measurement of bioactive chemicals in plants, assisting in the development of new medications as well as comprehending plant metabolism.
7. Biological samples analysis: HPTLC is employed in the analysis of biological samples, such as urine, blood, and tissues, for the detection of drugs, toxins, and other biomolecules.
8. Counterfeit detection: HPTLC can be used to detect counterfeit products in various industries, such as pharmaceuticals, cosmetics, and consumer goods, by analysing their composition and authenticating their origin[29].

#### Comparison of TLC and HPTLC

TLC and HPTLC are based on the same principle i.e. adsorption. The comparison between TLC and HPTLC is listed below.







## HPTLC Instrumentation

### Sample Applicator

The HPTLC- Automatic Applicator AS30 samples are sprayed onto TLC/HPTLC plates with compressed air flow without contacting the plates. The sample Application is carried out automatically, only filling and inserting the syringe is made manually. The dosing syringe is fastened at flexible turret, thus detaching and calibrating of syringe is not necessary. It can be filled either manually by the filling syringe or by the Autosampler BS35 (Optional). This is remarkable and time-saving particularly when large sample throughput is present[33]. Up to 80 different samples can be applied completely automatically. The spray on technique is beneficial for quantitative analysis as it is possible to have different volumes of same calibration standard instead of equal volumes of different standard concentrations. Even if samples are dissolved in polar solvents such as water, compact and narrow bands are formed.

### Key Aspects of HPTLC-Applicator AS30

- Spray-on technique
- Dual syringe system: dosing and filling syringe
- Application of dots or lines
- 2D application
- For any TLC/HPTLC plates, dimensions= 200 x 200 mm
- Stand-alone or PC-controlled
- Holding up to 10 methods
- Low sample requirement
- Incl. software for controlling AS30/BS35 and
- Transferring data to Densitometer CD60
- Special cover for active exhaustion on request[34]

### Technical Parameters of HPTLC-Applicator AS30

- Plate size = 200 x 200 mm
- Path length 0 – 100 mm in steps of 0.1 mm
- dosing syringe= 10  $\mu$ L,
- filling syringe= 25  $\mu$ L
- Application rate= 3 – 120 s/ $\mu$ L
- Resolution= 2000 steps/ $\mu$ L
- Turret movement= 40 mm/s, 13 steps/mm
- Necessary air pressure= 2.5 – 10 bar [35-36]

### Uses of sample applicator:

The software manages the sample container selection, transport, and washing procedures using a serial interface.

### TLC Scanner

The TLC Scanner 4 is a very sophisticated workstation designed for precise examination of TLC/HPTLC chromatograms and other planar objects using densitometric methods. The TLC Scanner 4 is a device used for measuring the density of scanned images. The process involves quantifying the reflectance of individual substances using absorption and/or fluorescence methods[37].

### Uses

A Thin Layer Chromatography (TLC) scanner is an apparatus specifically intended to assess the radiochemical purity of certain radiopharmaceuticals, which are substances utilized as dyes or medicines in nuclear medicine procedures including bone scans and PET CT scans. In order to detect natural products such as essential oils, volatile oils, fixed oils, glycosides, waxes, alkaloids, and so on[38]. It is commonly employed in the separation of complex medicinal compositions including many components.





### Chromatogram

High-performance thin-layer chromatography (HPTLC) is an advanced version of thin-layer chromatography (TLC) that provides enhanced strength, ease, quickness, and effectiveness in quantitatively analysing substances. This thin-layer chromatography (TLC) analytical method improves the separation of compounds, resulting in more accurate quantitative measurement[39]. The HPTLC chamber is pre-conditioned with solvent to ensure the presence of consistent solvent vapours throughout the chamber. There are four methods for developing chromatograms. The four methods are: 1) Vertical method, 2) Vario-method, 3) Horizontal method, and 4) Automatic multiple development.

### Purpose of Chromatogram

Chromatography is a significant biometric technique which is used to separate, identify, and purify the chemical compounds from mixture of compounds at qualitative and quantitative level. Chromatogram growth, which is the separation process in the HPTLC technique, is often disregarded despite its critical importance. Key parameters associated with this stage are typically neglected. HPTLC plates are generated using twin-trough chambers or horizontal-development chambers. Typically, twin-trough chambers that are saturated and equipped with filter paper provide the highest level of repeatability. The twin-through chamber prevents the preloading of solvent vapor and humidity. The detection of individual chemicals on the sorbent layers is improved by the suppression of fluorescence caused by ultraviolet (UV) light, typically in the range of 200-400 nm. This phenomenon is frequently referred to as Fluorescence quenching[40]. The visualization at UV 254 nm F254 can be accurately defined as phosphorescence quenching. In this case, the fluorescence persists briefly after the excitation source is no longer present. It has a brief duration, yet exceeds 10 seconds. The F254 fluorescent indicator is stimulated by a UV wavelength of 254 nm and produces a green fluorescence. Compounds that exhibit absorption of light at a wavelength of 254 nm cause a decrease in the emission on the layer, resulting in the formation of a dark violet spot on a green background at the locations where the compound zones are present. The quenching phenomenon is a result of the presence of molecules with conjugated double bonds. Anthraglycosides, coumarins, flavonoids, propyl phenols found in essential oils, as well as alkaloids such as indole, isoquinoline, and quinoline alkaloids, need to be identified using a 254 nm wavelength. Fluorescence quenching is the appropriate term to describe the visualization at UV 366 nm F 366. In this case, the fluorescence does not persist once the excitation source is withdrawn. All anthraglycosides, coumarins, flavonoids, phenolcarboxylic acids, and certain alkaloid types (such as Rauwolfia and Ipecacuanha alkaloids) demonstrate this quenching effect. The presence of separated compounds in the white light Zone may be identified by observing their inherent hue under daylight conditions. Derivatization Derivatization is an approach procedure which modify the functionality of an analyte to facilitate chromatographic separations. Derivatization can be established by either immersion or spraying of the plates with an appropriate reagent.

### Spectrophotometer

HPLC systems utilize a UV-detector to quantify concentration via absorbance spectroscopy. The concentration may be determined using the Beer-Lambert's Law equation:  $A = \epsilon c L$ . The detector quantifies the degree of light absorption over time at one or more specific wavelengths. A novel technique for separation, utilizing High Performance Thin Layer Chromatography in combination with UV and fluorescence detection, allows for the differentiation of non-volatile hydrocarbons into distinct groups based on the number of aromatic rings present, ranging from two to five. This approach also distinguishes between condensed and non-condensed structures. The technique employs a two-step migration process using ethyl acetate/n-hexane and n-hexane solvents on RP-plates, maintained at a temperature of -23 °C. HPTLC is utilized for quantifying tar by the usual addition approach, which involves combining all the aromatic components into a single peak. Subsequently, two methods are suggested for measuring UV levels: the first method, known as UV direct quantification, involves estimating the absorbance and concentration of a known sample, which allows for the calculation of the concentration of an unknown sample[41]. The second method, utilizing UV spectra deconvolution (UVSD), quantifies the concentration of tar by performing UV deconvolution on specific standard spectra, eliminating the requirement for reference samples. The two methods were utilized on a total of thirty-seven samples obtained from three different gasifiers: a Bubbling Fluidized Bed





Vijayalakshmi et al.,

(BFB), an Internal Circulating Bubbling Fluidized Bed (ICBFB), and a Circulating Fluidized Bed (CFB).

### Developed Plate

A series of HPTLC plates were prepared with the solutions in the ratio of 4:1 (volume/volume) using a mixture of methanol and water. The plates were filled with this mixture until it reached the top edge of the plate in the Simultaneous Separating Chamber (manufactured by biostep, Burkhardtendorf, Germany). They were then desiccated in the oven at a temperature of 110 °C for a duration of 20 minutes. After drying, a clean counter glass plate was placed on top of the stacked plates, and the entire setup was wrapped in aluminium foil for storage in a desiccator. Due to the high cost of high purity standards, the application parameters were chosen to minimize the loss of microliter volume during the automated syringe operation. This was achieved by setting the filling vacuum time to 1 second, the rinsing vacuum time to 6 seconds, and the number of rinsing/filling cycles to 1. Additionally, any unused sample was returned to the vial using the Automatic TLC Sampler ATS4 by CAMAG in Muttenz, Switzerland. The process of drying the plate was consistently carried out using a cold air stream, either by a hair drier or the Automatic Developing Chamber 2 (ADC 2) by CAMAG. This was done immediately after the application of the substance (within 0.5 minutes) and the subsequent development (within 5 minutes). The ambient air had a relative humidity of around  $40 \pm 5\%$  during the developments. If necessary, the humidity of the plate can be modified by use a saturated solution of sodium acetate [42]. The program visionCATS (version 3.0, CAMAG) was used to process all instrument operation and obtained data

### UV Detection

An HPTLC technique with UV detection has been developed to assess the purity of synthesis products. The consistency between the measurements of purity obtained using HPTLC-UV and LC-UV indicates that the approach is appropriate for this application. Atmospheric-pressure matrix-assisted laser desorption/ionization mass spectrometry (AP-MALDI-MS) was employed to verify and determine the product regions on the plate prior to purification by preparative-layer chromatography (PLC). AP-MALDI-MS exhibited higher selectivity compared to UV detection and provided a convenient and quick method for identifying synthesis products directly on the plate. This article presents a novel and uncomplicated gadget designed for the purpose of isolating product zones that have been split by a programmable logic controller (PLC). By utilizing PLC (Preparative Liquid Chromatography) in conjunction with the latest isolation technology, the purification of synthesis products in quantities less than one milligram was accomplished with success [43].

### Antidiabetics Drugs - HPTLC Method Validation

Anti-diabetic drugs validated by HPTLC method are mentioned in Table 2.

## CONCLUSION

The HPTLC (High-Performance Thin-Layer Chromatography) technology provides an efficient and accurate method to analyze medications that prevent diabetes. Its excellent consistency, sensitivity, and specificity make it an effective tool for quality assurance and pharmacological research. HPTLC plays a vital role in the development and assessment of anti-diabetic drugs by precisely separating and quantifying active components, which ultimately improves patient care and treatment results. Further, the versatility of the HPTLC approach enables the simultaneous study of several anti-diabetic medications, expediting the analytical procedure and conserving time and money. It may be used in laboratories with varying degrees of equipment and experience due to its adaptability to varied sample matrices and its very straightforward sample preparation procedures.

## REFERENCES

1. Craig ME, Hattersley A, Donaghue KC. Definition, epidemiology and classification of diabetes in children and adolescents. *Pediatr Diabetes*. 2009;10 Suppl 12:3–12.





2. Galtier F. Definition, epidemiology, risk factors. *Diabetes Metab.* 2010;36:628–651.
3. Salim Bastaki, *International Journal of Diabetes and Metabolism* (2005) 13 (3): 111–134, <https://doi.org/10.1159/000497580>
4. American Diabetes Association. Diagnosis and classification of diabetes mellitus. *Diabetes Care.* 2014;37 Suppl 1:S81–S90.
5. Stone MA, Camosso-Stefinovic J, Wilkinson J, de Lusignan S, Hattersley AT, Khunti K. Incorrect and incomplete coding and classification of diabetes: a systematic review. *Diabet Med.* 2010;27:491–497.
6. Rosenbloom AL, Silverstein JH, Amemiya S, Zeitler P, Klingensmith GJ. Type 2 diabetes in children and adolescents. *Pediatr Diabetes.* 2009;10 Suppl 12:17–32.
7. Roglic G, Colagiuri S. Gestational diabetes mellitus: squaring the circle. *Diabetes Care.* 2014;37:e143–e144.
8. Murphy R, Ellard S, Hattersley AT. Clinical implications of a molecular genetic classification of monogenic beta-cell diabetes. *Nat Clin Pract Endocrinol Metab.* 2008;4:200–213.
9. Leahy, J. L., Cooper, H. E., Deal, D. A. and Weir, G. C. 1986. Chronic hyperglycemia is associated with impaired glucose influence on insulin secretion. A study in normal rats using chronic in vivo glucose infusions. *J. Clin. Invest.* 77: 908-915.
10. Auer, R. N. 2004. Hypoglycemic brain damage. *Metab. Brain Dis.* 19: 169-175.
11. Singh, S., Bhat, J. and Wang, P.H. 2013. Cardiovascular effects of anti-diabetic medications in type 2 diabetes mellitus. *Curr. Cardiol. Rep.* 15: 327.
12. Shinde Ganesh S., P. S. Rao, R. S. Jadhav, Piyusha Kolhe, Diksha Athare. A Review on Chromatography and Advancement in Paper Chromatography Technique. *Asian J. Pharm. Ana.* 2021; 11(1):45-48. doi: 10.5958/2231-5675.2021.00009.0.
13. Frank Settle. *Handbook of Instrumental Techniques for Analytical Chemistry.* Pearson Publication, 2014; First Edition : 221.
14. Sherman J, Fried B, Dekker M. New York, NY: *Handbook of Thin-Layer Chromatography*; 1991.
15. Regnier FE. High-performance liquid chromatography of biopolymers. *Science.* 1983;245–52.
16. Gas chromatography, [http://80.251.40.59/veterinary.ankara.edu.tr/fidanci/Ders\\_Notlari/Biyoteknoloji/Kromatografi.html](http://80.251.40.59/veterinary.ankara.edu.tr/fidanci/Ders_Notlari/Biyoteknoloji/Kromatografi.html) .
17. Gerberding SJ, Byers CH. Preparative ion-exchange chromatography of proteins from dairy whey. *J Chromatogr A.* 1998;808:141–51.
18. Walls D, Loughran ST. *Protein chromatography: Methods and protocols, methods in molecular biology.* 2011;681
19. Zlatkic A, Kaiser RE. Amsterdam: Elsevier Science and Technology; 1977. HPTLC, high performance thin-layer chromatography.
20. Sethi PD. CBS Publishers and Distributors; 1996. HPTLC: High Performance Thin Layer Chromatography: Quantitative Analysis of Pharmaceutical Formulations.
21. Rabel, F., & Sherma, J. New TLC/HPTLC commercially prepared and laboratory prepared plates: A review. *Journal of Liquid Chromatography & Related Technologies.* 2016,39(8), 385-393.
22. Ristivojević, P., Trifković, J., Andrić, F., & Milojković-Opsenica, D. Recent trends in image evaluation of HPTLC chromatograms. *Journal of Liquid Chromatography & Related Technologies.* 2020, 43(9-10), 291-299.
23. Bhujbal, S. S., Chawale, B. G., & Kale, M. A. Application based Studies of HPTLC-bioautography in Evaluation of Botanicals: a Review. *Journal of Analytical Chemistry.* 2022, 77(4), 473-483.
24. Jain, A., Parashar, A. K., Nema, R. K., & Narsinghani, T. High performance thin layer chromatography (HPTLC): A modern analytical tool for chemical analysis. *Current Research in Pharmaceutical Sciences.* 2014, 8-14.
25. Ferenczi-Fodor, K., Renger, B., & Végh, Z. The frustrated reviewer – recurrent failures in manuscripts describing validation of quantitative TLC/HPTLC procedures for analysis of pharmaceuticals. *JPC-Journal of Planar Chromatography-Modern TLC.* 2010, 23(3), 173-179.
26. Ebrahimi-Najafabadi, H., Kazemeini, S. S., Pasdaran, A., & Hamedi, A. A novel similarity search approach for high-performance thin-layer chromatography (HPTLC) fingerprinting of medicinal plants. *Phytochemical analysis.* 2019, 30(4), 405-414.
27. Gupta, M. K., Ghuge, A., Parab, M., Al-Refaei, Y., Khandare, A., Dand, N., & Waghmare, N. A comparative review on high-performance liquid chromatography (HPLC), ultra performance liquid chromatography (UPLC)





## Vijayalakshmi et al.,

- & high-performance thin layer chromatography (HPTLC) with current updates. *Current Issues in Pharmacy and Medical Sciences*. 2022, 35(4), 224-228.
28. Morlock, G. E. High-performance thin-layer chromatography combined with effect-directed assays and high-resolution mass spectrometry as an emerging hyphenated technology: A tutorial review. *Analytica Chimica Acta*. 2021,1180, 338644.
29. Sherma, J. Thin layer chromatography in environmental analysis. *Reviews in Analytical Chemistry*. 1995, 14(2), 75-142.
30. Sankar, R., Snehalatha, K. S., Firdose, S. T., & Babu, P. S. Applications in HPLC in pharmaceutical analysis. *International Journal of Pharmaceutical Sciences Review and Research*. 2019, 59, 117-124.
31. Dołowy, M., & Pyka, A. Application of TLC, HPLC and GC methods to the study of amino acid and peptide enantiomers: a review. *Biomedical Chromatography*. 2014, 28(1), 84-101.
32. Al-Sanea, M. M., & Gamal, M. Critical analytical review: Rare and recent applications of refractive index detector in HPLC chromatographic drug analysis. *Microchemical Journal*. 2022, 178, 107339.
33. Ferenczi-Fodor K, Vegh Z, Nagy-Turak A, Renger B and Zeller M. Validation and quality assurance of planar chromatographic procedures in pharmaceutical analysis. *J AOAC Int*, 2001, 84, 1265–1276. CAS Google Scholar
34. Patel MR, Patel RB, Parikh JR and Patel BG. HPTLC method for estimation of tazarotene in topical gel formulations and in vitro study. *Anal Methods*, 2010, 2, 275–281. Article
35. CAMAG, 2010-2011. Instrumental thin layer chromatography. Switzerland: Camag. [camag.com/downloads/free/brochures/CAMAG\\_TLC10-11\\_E.pdf](http://camag.com/downloads/free/brochures/CAMAG_TLC10-11_E.pdf)
36. Patel, R.B. and Patel, M.R. and Patel, B.G. (2011) Experimental Aspects and Implementation of HPTLC. In: Shrivastava, M.M. HPTLC. New York: Springer, pp. 41- 54.
37. Shrivastava, M.M. (2011) An Overview of HPTLC: A Modern Analytical Technique with Excellent Potential for Automation, Optimization, Hyphenation, and Multidimensional Applications. In: Shrivastava, M.M. HPTLC. New York: Springer, pp. 3- 24.
38. Neumann C, Margot P. New perspectives in the use of ink evidence in forensic science: Part I. Development of a quality assurance process for forensic ink analysis by HPTLC. *Forensic Sci Int*. 2009;185:29–37. [PubMed] [Google Scholar]
39. Sherma J. Review of HPTLC in Drug Analysis: 1996-2009. *J AOAC Int*. 2010;93:754–64. [PubMed] [Google Scholar]
40. Butler MS. Natural products to drugs: Natural product-derived compounds in clinical trials. *Nat Prod Rep*. 2008;25:475–516. [PubMed] [Google Scholar]
41. Shah NJ, Suhagia BN, Shah RR, Shah PB. Development and validation of a HPTLC method for the simultaneous estimation of telmisartan and hydrochlorothiazide in tablet dosage form. *Indian J Pharm Sci*. 2010;69:202. [PMC free article] [PubMed] [Google Scholar]
42. Sherma, Joseph (1 May 2010). "Review of HPTLC in Drug Analysis: 1996-2009". *Journal of AOAC International*. 93 (3): 754–764. Doi:10.1093/jaoac/93.3.754. ISSN 1060-3271. PMID 20629372. Retrieved 6 November 2023.
43. Nurok, David (1 March 1989). "Strategies for optimizing the mobile phase in planar chromatography". *Chemical Reviews*. 89 (2): 363–375. Doi:10.1021/cr00092a007. ISSN 0009-2665.
44. Thomas, A. B., Patil, S. D., Nanda, R. K., Kothapalli, L. P., Bhosle, S. S., & Deshpande, A. D. Stability-indicating HPTLC method for simultaneous determination of nateglinide and metformin hydrochloride in pharmaceutical dosage form. *Saudi pharmaceutical journal: the official publication of the Saudi Pharmaceutical Society*, 2011; 19(4): 221–231. <https://doi.org/10.1016/j.jsps.2011.06.005>
45. Komal Sharma, Amrita Parle. Development And Validation Of Hptlc Method For Estimation Of Alogliptin Benzoate In Bulk Drugs And Tablet Dosage Forms, *International Bulletin Of Drug Research*. 2015;5(8): 81-89.
46. T. Raja, A. Lakshmana Rao. Validated Hptlc Method For Simultaneous Estimation Of Metformin Hydrochloride And Sitagliptin Phosphate In Bulk Drug And Formulation. *Rasayan J. Chem*. 2012;5(3): 407-413. Issn: 0974-1496.
47. Kale, D., Kakde, R. Simultaneous Determination of Pioglitazone, Metformin, and Glimepiride in Pharmaceutical Preparations using HPTLC Method. *JPC-J Planar Chromat* 24, 331–336 (2011). <https://doi.org/10.1556/JPC.24.2011.4.11>
48. Kaur, Ishpreet & Wakode, Sharad & Singh, Harsharan Pal. (2016). Development and Validation of a Stability-Indicating High Performance Thin Layer Chromatography (HPTLC) Method for estimation of Canagliflozin in







## Vijayalakshmi et al.,

- bulk and Pharmaceutical Dosage Form. Journal of Applied Pharmaceutical Science. 6. 051-057. 10.7324/JAPS.2016.60508.
49. Mehul Patel, Divya Patel, Umang Shah, Heta Kachhiya. Simultaneous quantification of teneligliptin hydrobromide and metformin hydrochloride: an improved HPTLC method with implementation of Plackett-Burman design. J. Chem. Metrol. 2021;15(01); 65-75.
50. Modi, Darshana & Patel, Bhavesh. Simultaneous determination of metformin hydrochloride and glipizide in tablet formulation by HPTLC. Journal of Liquid Chromatography & Related Technologies - J LIQ CHROMATOGR RELAT TECHNO. 2012: 35;28-39. 10.1080/10826076.2011.593227.
51. Bhende, S. D., Varanasi, M. B., & Abbulu, K. A Sensitive HPTLC Method for the Estimation of Glibenclamide, Rosiglitazone Maleate and Metformin Hydrochloride from a Multicomponent Dosage Form. Journal of chromatographic science. 2020;58(5); 418–426. <https://doi.org/10.1093/chromsci/bmz124>
52. Ritesh P. Bhole & Faiyyaj R. Tamboli. Development and Validation of Stability Indicating HPTLC-MS Method for Estimation of Empagliflozin in Pharmaceutical Dosage Form, Analytical Chemistry Letters. 2018;8(2): 244-256. DOI: 10.1080/22297928.2017.1404929
53. Bendale, Atul, Singh, R, Vidyasagar. Gali . Development and validation stability indicating HPTLC method for determination of vildagliptin and metformin hydrochloride in the pharmaceutical dosage forms. International Journal of Applied Pharmaceutics. 2018;10(01); 36-45. 10.22159/ijap.2018v10i1.20555.
54. Patil. Vandana, Kale. Suwarna , Sahare. Poonam ,Vithaldas. Smita. (2014). Simultaneous HPTLC analysis of Gliclazide and Metformin hydrochloride in bulk and tablet dosage form. Journal of Scientific and Innovative Research. 2014;3(03); 325-331. 10.31254/jsir.2014.3309.
55. Sharma, K, Parle, A. Development and validation of HPTLC method for simultaneous estimation of metformin hydrochloride and alogliptin benzoate in bulk drugs and combined dosage forms. International Journal of Pharma Research & Review. 2015; 4(11):35-42.
56. Sandesh R. Lodha, Karishma D. Patel, Sunny A. Patel, Shreya G. Patel, Kunjan B. Bodiwala, Shailesh A. Shah, Gajanan G. Kalyankar..Development and validation of HPTLC method for estimation of Teneligliptin Hydrobromide Hydrate in tablet dosage form. Journal of Pharmacy and Applied Sciences. 2016 ; 3(01): 26-33.
57. Manasa. G, Balekari. Umamahesh, Panga. Shyam, Veeresham. Ciddi. Simultaneous estimation of sitagliptin and metformin in pharmaceutical formulation by HPTLC. Ethiopian Pharmaceutical Journal.31. 63. 10.4314/EPJ.V31i1.6.
58. Mahgoub, H., Youssef, R. M., Korany, M. A., Khamis, E. F., & Kamal, M. F. (2014). Development and validation of spectrophotometric and HPTLC methods for simultaneous determination of rosiglitazone maleate and metformin hydrochloride in the presence of interfering matrix excipients. Drug development and industrial pharmacy, 40(9), 1190–1198. <https://doi.org/10.3109/03639045.2013.810634>.
59. Srivani. Jillala, Umamahesh. Balekari , Veeresham. Ciddi. Development And Validation Of Stability Indicating Hptlc Method For Simultaneous Determination Of Linagliptin And Metformin. International Journal Of Pharmacy And Pharmaceutical Sciences. 2015;8(01); 112-115.
60. Malgundkar. Mr, Mulla. Saira. Validated Hptlc Method For Simultaneous Determination Of Metformin Hydrochloride And Glibenclamide In Combined Dosage Form. Iosr Journal Of Pharmacy And Biological Sciences. 2014: 9. 54-59. 10.9790/3008-09255459.
61. Modi. Darshana, Parejiya. Punit, Patel. Bhavesh. A Simple And Sensitive Hptlc Method For Simultaneous Determination Of Metformin Hydrochloride And Sitagliptin Phosphate In Tablet Dosage Form. Journal Of Chemistry. 2013:1-4. 10.1155/2013/139561.
62. Anand. D.c.prem, Senthilkumar. K, Senthilkumar. Bojarajan, Saravanakumar. M, Thirumurthy. R. Hptlc Method For Determination Of Telmesarton Hcl With Pioglitazone Hcl In Pharmaceutical Dosage Form. Ijpr. 2010: 2(9); 185-190.
63. Shah. Dimal, Gondalia. Ishita, Patel. Vandana, Mahajan. Ashok, Chhalotiya. Usmangani, Nagda, Dhruvi. Stability Indicating Thin-layer Chromatographic Method For Estimation Of Antidiabetic Drug Remogliflozin Etabonate. Future Journal Of Pharmaceutical Sciences. 2021;7(83);1-12. 10.1186/s43094-021-00230-6.







Vijayalakshmi et al.,

Table 1. Comparison of TLC and HPTLC

ASPECT	TLC	HPTLC
Full Form	Thin Layer Chromatography	High Performance Thin Layer Chromatography
Purpose	Separation and identification of compounds	Similar to TLC, but offers higher resolution and sensitivity[30]
Sample Size	Small	Small to medium-sized samples
Stationary Phase	Silica gel or alumina coated on a glass, plastic or aluminium plate	Same as TLC, but with optimized particle size and uniformity for improved separation[31]
Mobile Phase	Liquid	Liquid
Plate Size	Small Dimensions = 20 cm x 20 cm	Larger Dimensions = 20 cm x 20 cm or more
Resolution	Moderate	Higher
Sensitivity	Moderate	Higher
Speed of Analysis	Moderate	Faster
Quantitative Analysis	Possible but less accurate	More accurate
Instrumentation	Simple	Specialized equipment
Applications	Qualitative analysis, preliminary separation	Quantitative analysis, purity testing, quality control[32]
Cost	Lower	Higher

Table 2. Anti-diabetics drugs are validated by HPTLC method

ANTI DIABETICS DRUGS	HPTLC METHOD	VALIDATION PARAMETERS	REFERENCE
Glinate-MF (Nateglinide and metformin hydrochloride)	<b>Stationary phase:</b> Pre-coated silica gel 60 F-254 aluminium plates (10 · 10 cm, 250 cm thickness) <b>Mobile phase:</b> Chloroform: Ethylacetate: Acetic acid <b>Wavelength</b> = 216 nm	<b>Linearity range:</b> Nateglinide: 200-2400 ng band <sup>-1</sup> Metformin hydrochloride: 500-3000ng band <sup>-1</sup> <b>LOD</b> Nateglinide:0.020 ng/ band Metformin hydrochloride: 0.022 ng/band <b>LOQ</b> Nateglinide:0.060 ng/band Metformin hydrochloride: 0.066 ng/band <b>Repeatability</b> Nateglinide:0.725 % Metformin hydrochloride: 0.730 % <b>Intra-day Precision</b> Nateglinide:0.710 % Metformin hydrochloride: 0.361 % <b>Inter-day Precision</b> Nateglinide:0.790 % Metformin hydrochloride: 0.837 %	44
Alogliptin benzoate	<b>Stationary phase:</b> Pre-coated silica gel 60F254 HPTLC plates (20 × 10 cm, layer thickness 0.2 mm)	<b>Linearity range:</b> 100- 5000 ng band <sup>-1</sup> <b>Repeatability:</b> 100.99% <b>Intra-day Precision:</b> 1.17% <b>Inter-day Precision:</b> 0.54%	45





Vijayalakshmi et al.,

	<p><b>Mobile phase:</b> Acetonitrile: 1% Ammonium acetate in Methanol (4.5:5.5 v/v) <b>Wavelength:</b> 277nm</p>	<p><b>LOD:</b> 2.356 ng/band <b>LOQ:</b> 7.14 ng/band <b>Robustness:</b> Robust <b>Specificity:</b> Specific <b>Selectivity:</b> Selective</p>	
<p>Janumet (metformin hydrochloride and sitagliptin phosphate)</p>	<p><b>Stationary phase:</b>Silica gel precoated aluminium plate 60F- 254 plates, (10 cm X 10 cm with 250 µm thickness) <b>Mobile phase:</b>Acetone: Methanol:Toluene:Formic acid (4:3:2:1 v/v/v/v) <b>Wavelength:</b> 220nm</p>	<p><b>Linearity Range:</b> Metformin hydrochloride: 2000-5000 ng band<sup>-1</sup> Sitagliptin phosphate: 200-500 ngband<sup>-1</sup> <b>Accuracy:</b> Metformin hydrochloride: 100.19% Sitagliptin phosphate:100. 47% <b>Precision:</b> <b>Intra-day Precision:</b> Metformin hydrochloride: 41.74 % Sitagliptin phosphate: 67.16 % <b>Inter-day Precision:</b> Metformin hydrochloride: 0.74 % Sitagliptin phosphate:0.40 % <b>LOD:</b> Metformin hydrochloride: 45 ng/band Sitagliptin phosphate:27 ng/band <b>LOQ:</b> Metformin hydrochloride: 150 ng/band Sitagliptin phosphate:87 ng/band</p>	<p>46</p>
<p>Pioglitazone, metformin, and glimepiride</p>	<p><b>Stationary phase:</b>Precoated silica gel 60 F254 <b>Mobile phase:</b>Acetonitrile:Methanol:P ropyl alcohol: ammonium acetate 7:2:1:1 (v/v). <b>Wavelength:</b> 240nm</p>	<p><b>Linearity:</b> Pioglitazone: 300-1200 ng band<sup>-1</sup> Metformin:10000-40000 ng band<sup>-1</sup> Glimepiride:40-160 ng band<sup>-1</sup> <b>Limit of Detection:</b> Pioglitazone:56.57 ng Metformin:6160.85 ng Glimepiride:11.99 ng <b>Limit of Quantitation:</b> Pioglitazone:177.43 ng Metformin:18669.26 ng Glimepiride:36.33 ng <b>Precision:</b> <b>Intra-day Precision:</b> Pioglitazone:0.4026 % Metformin:0.4874 % Glimepiride:0.2012% <b>Inter-day Precision:</b> Pioglitazone:0.5381 % Metformin:0.4222 % Glimepiride:0.5684 % <b>Accuracy:</b> Pioglitazone:1.215 % Metformin:0.851 %</p>	<p>47</p>





## Vijayalakshmi et al.,

		Glimepiride:1.234 % <b>Specificity:</b> specific	
Canagliflozin	<b>Stationary phase:</b> Precoated silica gel 60 F254 HPTLC aluminium plates (20 × 10 cm, 0.2mm thick). <b>Mobile phase:</b> Toluene: Ethyl acetate: Methanol (2:2:1). <b>Wavelength:</b> 290 nm.	<b>Linearity:</b> 10-500 ng/ band <b>Intra-day Precision:</b> 0.01 - 0.2 % <b>Inter-day Precision:</b> 0.01-0.2 % <b>Recovery:</b> 99.04- 99.82% <b>Limit of Detection:</b> 0.39 ng/ band <b>Limit of Quantification:</b> 1.19 ng/ band	48
Teneligliptin and Metformin	<b>Stationary phase:</b> Silica gel G60 F254 aluminium sheet (10x10 and 10x20 cm) <b>Mobile phase:</b> Methanol: Ammonium sulphate: Triethylamine (9: 2.7: 0.5 v/v/v) <b>Wavelength:</b> 237 nm.	<b>Linearity:</b> Teneligliptin:4-28 ng/band Metformin:100-700 ng/band <b>Precision:</b> <b>Intra-day Precision:</b> Teneligliptin:0.82-1.01 % Metformin: 0.93-1.15% <b>Inter-day Precision:</b> Teneligliptin: 1.06-1.07 % Metformin: 1.19-1.27 % <b>Accuracy:</b> Teneligliptin: 0.12 % Metformin: 0.49 % <b>Limit of Detection:</b> Teneligliptin:0.3 ng/spot Metformin: 27 ng/spot <b>Limit of Quantitation:</b> Teneligliptin: 3 ng/spot Metformin: 85 ng/spot <b>Specificity:</b> Specific	49
Glynase-MF tablets (metformin hydrochloride and glipizide)	<b>Stationary phase:</b> Precoated silica gel 60 F254 TLC plates (10*10 cm) <b>Mobile phase:</b> water: methanol: 0.5% w/v ammonium sulfate solution (6:3:1.5 v/v/v). <b>Wavelength:</b> 236 nm.	<b>Linearity:</b> Metformin hydrochloride:5000-25000 ng/band Glipizide:50-250 ng/band <b>Precision:</b> <b>Intra-day precision:</b> Metformin hydrochloride: 0.116% Glipizide: 1.424% <b>Inter-day precision:</b> Metforminhydrochloride: 0.771% Glipizide: 1.468% <b>Accuracy:</b> Metformin hydrochloride:99.9- 101.5 % Glipizide:98.1-98.4% <b>LOD:</b> Metformin hydrochloride: 991.30ng/band Glipizide: 9.57ng/band <b>LOQ:</b>	50





Vijayalakshmi et al.,

		Metformin hydrochloride: 3003.95ng/band Glipizide: 29.01ng/band <b>Selectivity:</b> selective	
Triglucoed tablets (Glibenclamid, Rosiglitazone maleate and Metformin Hydrochloride)	<b>Stationary phase:</b> Precoated RP-18 F254s TLC Aluminum sheets (20*10 cm) <b>Mobile phase:</b> Methanol: Tetrahydrofuran: Water:Glacial acetic acid (16: 3.6: 4: 0.4 v/v) <b>Wavelength:</b> Glibenclamide -237nm, Rosiglitazone maleate -324 nm Metformin hydrochloride – 240 nm	<b>Linearity:</b> Glibenclamide: 200–1000 ng/band Rosiglitazone maleate: 200–1000 ng/band Metformin Hydrochloride: 120–600 ng/band <b>Precision:</b> <b>Intra-day precision:</b> Glibenclamide: 0.44 % Rosiglitazone maleate: 1.004 % Metformin Hydrochloride: 0.362% <b>Inter-day precision:</b> Glibenclamide: 0.368 % Rosiglitazone maleate: 0.651% Metformin Hydrochloride: 0.358% <b>Accuracy:</b> Glibenclamide: 97.453% Rosiglitazone maleate: 99.343% Metformin Hydrochloride: 97.446% <b>Limit of Detection:</b> Glibenclamide: 80 ng/band Rosiglitazone maleate: 80ng/band Metformin Hydrochloride:48ng/band <b>Limit of Quantification:</b> Glibenclamide: 200ng/band Rosiglitazone maleate: 200ng/band Metformin Hydrochloride: 120ng/band <b>Robustness:</b> Glibenclamide: 1.218 Rosiglitazone maleate: 1.356 Metformin Hydrochloride: 0.973	51
Empagliflozin	<b>Stationary phase:</b> Aluminium plates precoated with silica gel 60 F254 Plates (10 x 10) <b>Mobile phase:</b> Toluene: Methanol (7:3 v/v) <b>Wavelength:</b> 228 nm	<b>Linearity:</b> 0.5-5.0 µg/band <b>Precision:</b> <b>Inter-day precision:</b> 0.4 % <b>Intra-day precision:</b> 0.5 % <b>Accuracy:</b> 98.88%- 100.26% <b>Limit of Detection:</b> 0.171 µg/band <b>Limit of Quantification:</b> 0.521 µg/band <b>Robustness:</b> Robust	52





## Vijayalakshmi et al.,

Vildagliptin And Metformin Hydrochloride	<p><b>Stationary phase:</b> Silica gel precoated aluminium plate 60 F254, [(20 × 10 cm) with 250 µm thickness</p> <p><b>Mobile phase:</b> Hexane: Methanol: Acetonitrile: Glacial acetic acid (2:3.5:2.5:0.2 v/v/v/v)</p> <p><b>Wavelength:</b> 217 nm</p>	<p><b>Linearity:</b> Vildagliptin: 10-150 ng/band Metformin Hydrochloride: 50-500 ng/band</p> <p><b>Precision:</b> Vildagliptin: 1.7% Metformin Hydrochloride: 1.5%</p> <p><b>Accuracy:</b> Vildagliptin: 99.08–103.60 % Metformin Hydrochloride:98.84-102.50 %</p> <p><b>Limit of Detection:</b> Vildagliptin: 1.74 ng/band Metformin Hydrochloride: 8.2 ng/band</p> <p><b>Limit of Quantification:</b> Vildagliptin: 5.74 ng/band Metformin Hydrochloride: 27.06 ng/band</p> <p><b>Robustness:</b>Robust <b>Selectivity:</b> selective <b>Specificity:</b>specific</p>	53
Glicazide and Metformin Hydrochloride	<p><b>Stationary phase:</b>pre coated with silica gel 60F254 (20*20cm).</p> <p><b>Mobile phase:</b> Toluene: Acetonitrile: Ethanol: Ammonium sulphate (0.25%) (4:4:4:3 v/v/v).</p> <p><b>Wavelength:</b> 228 nm.</p>	<p><b>Linearity:</b> Glicazide:200-1000 ng/spot Metformin Hydrochloride:200-1000 ng/spot</p> <p><b>Precision</b></p> <p><b>Intra-day Precision:</b> Glicazide:0.24% Metformin Hydrochloride: 0.29%</p> <p><b>Inter-day Precision:</b> Glicazide:0.29% Metformin Hydrochloride:0.31%</p> <p><b>Accuracy:</b> Glicazide:98.29% Metformin Hydrochloride:98.5%</p> <p><b>Limit of Detection:</b> Glicazide: 86.14 ng/spot Metformin Hydrochloride:106.11 ng/spot</p> <p><b>Limit of Quantification:</b> Glicazide:261.03 ng/spot Metformin Hydrochloride:321.54 ng/spot</p>	54
Alogliptin benzoate and Pioglitazone hydrochloride	<p><b>Stationary phase:</b> Pre-coated silica gel 60F254 HPTLC plates (20 × 10 cm).</p> <p><b>Mobile phase:</b> Acetonitrile: 1% ammonium acetate in Methanol (4.5:5.5 v/v).</p>	<p><b>Linearity:</b> Alogliptin benzoate:500-3000 ng/band Pioglitazone hydrochloride: 500-3000 ng/band</p> <p><b>Precision</b></p> <p><b>Intra-day Precision:</b></p>	55





## Vijayalakshmi et al.,

	<b>Wavelength:</b> 254 nm.	<p>Alogliptin benzoate: 0.76%            Pioglitazone hydrochloride:0.95%</p> <p><b>Inter-day Precision:</b>            Alogliptin benzoate: 0.40%            Pioglitazone hydrochloride:0.51%</p> <p><b>Accuracy:</b>            Alogliptin benzoate:98.96%            Pioglitazone hydrochloride:99.75%</p> <p><b>Limit of Detection:</b>            Alogliptin benzoate: 0.30 ng/band            Pioglitazone hydrochloride: 0.73 ng/band</p> <p><b>Limit of Quantification:</b>            Alogliptin benzoate: 0.91 ng/band            Pioglitazone hydrochloride: 2.23 ng/band</p> <p><b>Specificity:</b> Specific  <b>Robustness:</b> Robust</p>	
Teneligliptin hydrobromide hydrate	<p><b>Stationary phase:</b> pre coated with 250 µm layer of silica gel 60 F254 (10 x 10cm)</p> <p><b>Mobile phase:</b> butanol: water: glacial acetic acid (6:2:2 v/v/v).</p> <p><b>Wavelength:</b> 245 nm.</p>	<p><b>Linearity:</b> 250-1250 ng/band</p> <p><b>Precision</b></p> <p><b>Intra-day Precision:</b> 0.65- 1.72 %  <b>Inter-day Precision:</b> 0.78- 1.84%  <b>Accuracy:</b> 98.58- 99.24%  <b>Limit of Detection:</b> 60.50 ng/band  <b>Limit of Quantification:</b> 183.36 ng/band</p> <p><b>Specificity:</b> Specific</p>	56
Sitagliptin and Metformin	<p><b>Stationary phase:</b>precoated silica gel 60 F254 (0.2 mm layer thickness) (10 cm × 10 cm)</p> <p><b>Mobile phase:</b> BuOH-CHCl<sub>3</sub> - MeOH-(CH<sub>3</sub>CH<sub>2</sub>)<sub>2</sub>NH<sub>2</sub> - HCOOH (4:0.5:2.5:1.5:0.06 v/v)</p> <p><b>Wavelength:</b> 206 nm.</p>	<p><b>Linearity:</b>            Sitagliptin: 2-7µg/band            Metformin: 20-70 µg/band</p> <p><b>Precision :</b></p> <p><b>Intra-day precision:</b>            Sitagliptin: 0.2981%            Metformin: 0.3780%</p> <p><b>Inter-day precision:</b>            Sitagliptin: 0.3245%            Metformin: 0.3154%</p> <p><b>Accuracy:</b>            Sitagliptin: 98.99 %            Metformin:99.05%</p> <p><b>Limit of Detection:</b>            Sitagliptin: 0.014 µg            Metformin: 0.013 µg</p> <p><b>Limit of Quantification:</b>            Sitagliptin: 0.042 µg            Metformin: 0.040 µg</p> <p><b>Robustness:</b> Robust</p>	57
rosiglitazone maleate and metformin	<b>Stationary Phase:</b> aluminium plates with 250 mm thickness	<b>Linearity:</b> Rosiglitazone Maleate: 0.4–2.0 mg band	58







## Vijayalakshmi et al.,

hydrochloride	<p>precoated with silica gel 60 (F254) (20*10cm)</p> <p><b>Mobile phase:</b> Methanol: Water:NH<sub>4</sub>Cl 1% w/v (5:4:1 v/v/v)</p> <p><b>Wavelength:</b> 230 nm.</p>	<p><sup>1</sup></p> <p>Metformin Hydrochloride: 20.0–100.0 mg band<sup>-1</sup></p> <p><b>Accuracy:</b></p> <p>Rosiglitazone Maleate: 0.88- 1.21 %</p> <p>Metformin Hydrochloride: 0.87- 0.91%</p> <p><b>Limit of Detection:</b></p> <p>Rosiglitazone Maleate: 0.13 µg/ml</p> <p>Metformin Hydrochloride: 6.67 µg/ml</p> <p><b>Limit of Quantification:</b></p> <p>Rosiglitazone Maleate: 0.40 µg/ml</p> <p>Metformin Hydrochloride: 20.00 µg/ml</p> <p><b>Robustness:</b> Robust</p> <p><b>Selectivity:</b> Selective</p> <p><b>Specificity:</b> Specific</p>	
Linagliptin and metformin	<p><b>Stationary Phase:</b>pre-coated silica gel 60 F254 (0.2 mm layer thickness) (10 cm × 10 cm)</p> <p><b>Mobile phase:</b> acetone: methanol: chloroform: formic acid (3:1:5:1v/v)</p> <p><b>Wavelength:</b> 230 nm</p>	<p><b>Precision:</b></p> <p>Linagliptin: 0.29- 0.70%</p> <p>Metformin: 0.83 - 1.48 %</p> <p><b>Accuracy:</b></p> <p>Linagliptin: 98-102 %.</p> <p>Metformin: 98-102 %.</p> <p><b>Limit of Detection:</b></p> <p>Linagliptin: 5.19 ng/spot</p> <p>Metformin: 8.72 ng/ spot</p> <p><b>Limit of Quantitation:</b></p> <p>Linagliptin:15.74 ng/spot</p> <p>Metformin: 26.44 ng/spot</p> <p><b>Specificity:</b> Specific</p> <p><b>Robustness:</b> Robust</p>	59
Metformin Hydrochloride And Glibenclamide	<p><b>Stationary Phase:</b> Precoated silica Gel 60 F254 aluminium sheet</p> <p><b>Mobile phase:</b> Methanol: Water: 0.4 % Sodium sulphate (7:5:11).</p> <p><b>Wavelength:</b> Metformin hydrochloride and Glibenclamide was performed at 232 nm and at 238 nm respectively.</p>	<p><b>Linearity:</b></p> <p>Metformin Hydrochloride: 250 ng to 1750 ng/spot</p> <p>Glibenclamide: 250 ng to 1750 ng/spot</p> <p><b>Precision:</b></p> <p><b>Intra- day precision:</b></p> <p>Metformin Hydrochloride: 1.90%</p> <p>Glibenclamide: 0.92 %</p> <p><b>Inter-day precision:</b></p> <p>Metformin Hydrochloride: 1.52%</p> <p>Glibenclamide: 1.67%</p> <p><b>Accuracy:</b></p> <p>Metformin Hydrochloride: 95.79 %- 97.84 %</p> <p>Glibenclamide: 96.0 % - 97.03 %</p> <p><b>Limit of Detection:</b></p> <p>Metformin Hydrochloride: 1.2412 mcg</p> <p>Glibenclamide:0.9944 mcg</p>	60





## Vijayalakshmi et al.,

		<b>Limit of Quantitation:</b> Metformin Hydrochloride: 3.7613 mcg Glibenclamide: 3.0133 mcg <b>Specificity:</b> specific <b>Robustness:</b> Robust	
Metformin Hydrochloride And Sitagliptin Phosphate	<b>Stationary Phase:</b> precoated silica gel 60 F254 TLC plates (10 × 10 cm) <b>Mobile phase:</b> Butanol: Water: Glacial acetic acid (6:2: 2, v/v/v) <b>Wavelength:</b> 227 nm	<b>Linearity:</b> Metformin Hydrochloride: 500-10000 ng/band Sitagliptin Phosphate: 50-1000 ng/band <b>Precision:</b> <b>Intra- day precision:</b> Metformin Hydrochloride: 0.49 Sitagliptin Phosphate: 0.72 <b>Inter-day precision:</b> Metformin Hydrochloride: 1.13 Sitagliptin Phosphate: 1.43 <b>Accuracy:</b> Metformin Hydrochloride: 98.14-101.64% Sitagliptin Phosphate: 99.29- 101.06% <b>Limit of Detection:</b> Metformin Hydrochloride: 13.05 ng/μL Sitagliptin Phosphate: 2.65 ng/μL <b>Limit of Quantitation:</b> Metformin Hydrochloride: 39.56 ng/μL Sitagliptin Phosphate: 8.03 ng/μL <b>Selectivity :</b> Selective	61
Pioglitazone Hcl and Telmesarton Hcl	<b>Stationary Phase:</b> precoated silica gel 60 F254 TLC plates <b>Mobile phase:</b> Toluene: Ethyl acetate: Methanol (7: 2: 1 v/v/v) <b>Wavelength:</b> 269 nm	<b>Accuracy:</b> Pioglitazone Hcl: 100.12 Telmesarton Hcl: 99.08 <b>Precision:</b> Pioglitazone Hcl: 0.56 Telmesarton Hcl: 1867.51 <b>Limit of Detection:</b> Pioglitazone Hcl: 140 ng/spot Telmesarton Hcl: 188 ng/spot <b>Limit of Quantitation:</b> Pioglitazone Hcl: 140.06 ng/spot Telmesarton Hcl: 186.75 ng/spot <b>Robustness:</b> Robust	62
Remogliflozin etabonate	<b>Stationary Phase:</b> Precoated silica gel F254 TLC plates (10*10cm) <b>Mobile phase:</b> methanol: ethyl acetate: toluene: NH3 (2:4:4:0.1, v/v/v) <b>Wavelength:</b> 229 nm	<b>Linearity:</b> 500-8000 ng/band <b>Accuracy:</b> 97.73- 99.19% <b>Precision:</b> <b>Intra- day precision:</b> 0.49-1.84 % <b>Inter-day precision:</b> 1.13- 1.99% <b>Limit of Detection:</b> 100 ng/band <b>Limit of Quantitation:</b> 300 ng/band <b>Specificity:</b> Specific <b>Robustness:</b> Robust	63





# Analyzing Agricultural Data using Inverse Lindley Distribution with Fuzzy Parameters

S. Sujatha<sup>1\*</sup>, A. Dinesh Kumar<sup>2</sup> and M. Vasuki<sup>3</sup>

<sup>1</sup>Research Scholar, Department of Mathematics, Khadir Mohideen College, Adirampattinam, (Affiliated to Bharathidasan University, Tiruchirappalli), Tamil Nadu, India

<sup>2</sup>Assistant Professor, Department of Mathematics, Khadir Mohideen College, Adirampattinam, (Affiliated to Bharathidasan University, Tiruchirappalli), Tamil Nadu, India

<sup>3</sup>Assistant Professor, Department of Mathematics, Srinivasan College of Arts and Science, Perambalur, (Affiliated to Bharathidasan University, Tiruchirappalli), Tamil Nadu, India

Received: 21 Oct 2024

Revised: 14 Oct 2024

Accepted: 30 Nov 2024

## \*Address for Correspondence

**S. Sujatha**

Research Scholar, Department of Mathematics,  
Khadir Mohideen College, Adirampattinam,  
(Affiliated to Bharathidasan University, Tiruchirappalli),  
Tamil Nadu, India  
E.Mail: suja01rakshi@gmail.com



This is an Open Access Journal / article distributed under the terms of the **Creative Commons Attribution License** (CC BY-NC-ND 3.0) which permits unrestricted use, distribution, and reproduction in any medium, provided the original work is properly cited. All rights reserved.

## ABSTRACT

In many practical circumstances, we are presented with data that is not just random but also imprecise. To address these uncertainties, fuzzy concepts should be integrated into statistical techniques. This work examines how to estimate the Inverse Lindley distribution with fuzzy parameters and investigated maximum likelihood and Bayesian methods using fuzzy data. This article focuses on estimating parameters for the inverse Lindley distribution with fuzzy observations. The unknown model parameter was estimated using both classical and Bayesian approaches. The classical methodology involves estimating population parameters using the maximum likelihood (ML) and maximum product of distances (MPS) methods. Bayesian estimate relies on the squared error loss function (SELF) and the Markov Chain Monte Carlo (MCMC) approach. The asymptotic confidence intervals and highest posterior density (HPD) credible intervals for the unknown parameter are calculated. The estimators' performances are compared using their mean squared errors. Finally, a real time agriculture data set of Puducherry in year of 2019 is analyzed to provide plots examples of the PDF, CDF, Hazard Rate Function, and Survival Function is discussed. As a result of the comparison, fuzziness values were found to be more precisely calculated than real-time data.

**Keywords:** inverse Lindley distribution, maximum likelihood (ML), PDF, CDF, MLE.

**Mathematical Subject Classification (2020):** 03E72, 62B15.

## INTRODUCTION

In statistics, estimate is the process of making judgments about a population. These conclusions are based on data from the same population. There are numerous estimation methods accessible in the literature, each with merits and



**Sujatha et al.,**

limitations. Some well-known estimating methods are the method of maximum likelihood, method of least square, method of moments, etc. Zadeh created the phrase "fuzzy variable" in 1965 [1] to indicate inappropriate linguistic idioms and vernacular. This was the beginning of fuzzy set theory. A fuzzy set is made up of components with various membership levels. This author [2] discusses the many approaches for estimating the probability density function (PDF) and cumulative distribution function (CDF) for the Lindley Distribution. The following estimation methods are considered: uniformly minimum variance unbiased estimator (UMVUE), maximum likelihood estimator (MLE), percentile estimator (PCE), least square estimator (LSE), weighted least square estimator (WLSE), Cramér-von-Mises estimator (CVME), and Anderson-Darling estimator (ADE). Monte Carlo simulations are used to evaluate the performance of the proposed estimate methods. The authors [3], investigated various approaches of estimating the unknown parameters of GILD. First, we briefly describe different estimation methods, such as maximum likelihood estimators, moments estimators, least squares estimators, weighted least squares, maximum product spacing estimates, minimum distance methods, Cramer-von-Misses methods, and Anderson-Darling methods, and compare them using extensive numerical simulations.

The task of estimating the parameters of the generalized Lindley distribution [4], In addition to the classical estimator, inverse moment and modified inverse estimators are presented and their properties explored. A criterion for the existence and uniqueness of the inverse moment and modified inverse estimators of the parameters is defined. Monte Carlo simulations are used to compare the estimators' performance. Two methods for building joint confidence zones for the two parameters are also shown, and their performance is discussed. A real-world example is provided to demonstrate the recommended methods. Estimate the probability density function and cumulative density function of the inverse Weibull distribution. The following estimators are examined. Maximum likelihood estimator uniformly minimum variance unbiased estimator [5], the bias and mean squared error are expressed analytically. Simulation experiments and a real-world application demonstrate that the maximum likelihood estimator works better. The EM algorithm is used to calculate the parameter's maximum likelihood estimate (MLE) and provide an approximate confidence interval based on the MLE's asymptotic normalcy. In the Bayesian context, we construct the parameter's Bayes estimate using a Laplace approximation and a Markov Chain Monte Carlo approach. In addition, the maximum posterior density credible interval for the unknown parameter is determined. Extensive simulations are used to compare the performance of the various proposed approaches [6].

Because the Lindley distribution is more flexible than the exponential distribution, the same estimators have been developed and compared [7]. Monte Carlo simulations and real-world data analysis are used to compare the performance of the proposed estimation methods. The purpose of this work [8] is to estimate the unknown parameters of the inverse Weibull (IW) distribution using eight different estimation methods: maximum likelihood (ML), least squares (LS), weighted least squares (WLS), percentile (PC), maximum product of spacing (MPS), probability weighted moments (PWM), Cramér-von Mises (CM), and Anderson-Darling. The performance of different estimating approaches is compared using a large Monte Carlo simulation. Their robustness properties are also examined. At the conclusion of the study, two real data sets are examined for illustration and comparison.

Bayes estimators were used with gamma priors on both the shape and scale parameters of the generalised Lindley distribution, resulting in the largest posterior density interval estimations. Bayesian estimation is investigated with regard to both symmetric (squared error) and asymmetric (linear-exponential (LINEX)) loss functions. Finally [9], generate Bayesian prediction estimates and predictive interval estimates for future record values. To demonstrate the findings, a real data set is analyzed, and Monte Carlo simulations are run to assess the performance of the suggested estimate and prediction techniques. The maximum likelihood, uniformly minimal variance unbiased, and Bayes estimators are discussed here. The exact confidence intervals for the probability density and cumulative distribution functions of the inverse Lindley distribution are also calculated. Real-world data applications and simulation studies are used to demonstrate and compare the methodologies developed thus far [10]. Then explore the subject of classical and Bayesian estimate of the inverse Lindley distribution [11] parameter based on lower records, as well as predicting future record values. We get the (ML) estimator, the approximate confidence interval, and two boot-strap types for the parameter from ILD records. In Bayesian estimation, employ Tierney Kadane and MCMC approaches.





**Sujatha et al.,**

Future record values were also investigated using ML and Bayesian techniques. The highest conditional density and credible intervals are created for a future lower record. The current work used real-time data to investigate the probability density function, cumulative density function, Hazard rate function, and Survival function of the Inverse Lindley distribution with fuzzy parameters. This study focused on Puducherry agriculture in the year of 2019 [12].

**Fuzzy Mathematical tools**

**Inverse Lindley Distribution with fuzzy Parameters**

The distribution is unique in that it contains a single parameter, similar to the exponential distribution, but instead of a constant hazard rate, it has a unique modal, non-monotone, up-side-down bathtub (UBT) shape. The probability density function (PDF) and cumulative distribution function (CDF) of ILD are provided as:

$$f(x; \theta) = \frac{\theta^2}{(1 + \theta)} \left( \frac{1 + x}{x^3} \right) e^{-\frac{\theta}{x}}; x > 0, \theta > 0.$$

$$F(x; \theta) = \left[ \left( 1 + \frac{1 + x}{(1 + \theta)x} \right) \right] e^{-\frac{\theta}{x}}; x > 0, \theta > 0.$$

$\theta$  Represents the scaling parameter, ILD ( $\theta$ ) has closed-form formulas for reliability and hazard rate, making it ideal for modeling lifespan data.

$$R(x; \theta) = 1 - \left[ \left( 1 + \frac{1 + x}{(1 + \theta)x} \right) \right] e^{-\frac{\theta}{x}}; x > 0, \theta > 0.$$

$$H(x; \theta) = \frac{\theta^2(1 + x)}{x^2[x(1 + \theta)(e^{\frac{\theta}{x}} - 1) - \theta]}; x > 0, \theta > 0.$$

**Maximum likelihood estimate**

Let  $X_1, X_2, \dots, X_n$  be a sequence of independent observations on a random variable  $X$ . The CDF and PDF are given in Equations respectively. The likelihood equation for observing accurate realizations of  $X_1, X_2, \dots, X_n$  is as follows:

$$l(x; \theta) = \left( \frac{\theta^2}{1 + \theta} \right)^n e^{-\theta \sum_{i=1}^n \frac{1}{x_i}} \prod_{i=1}^n \left( \frac{1 + x_i}{x_i^3} \right); x, \theta > 0$$

However, in this case, we assume that we have just a limited understanding of the variable's observed values. Because they are not in precise form and are given with some mistake, the investigator can only provide estimated lifespan of the objects as guess values by indicating a tiny interval around the observed value. Furthermore, the investigator forms this interval based on his beliefs about the interval's different values. Such uncertainty in observed data can be properly modeled using the membership function of a fuzzy number. As a result, we can infer that the observed data is fuzzy, with the inherent unpredictability integrated into the possibility distribution. Let  $\tilde{x}_1, \tilde{x}_2, \dots, \tilde{x}_n$  denote the observed fuzzy lifetimes where  $\tilde{x}_i = (a_i, b_i, c_i); i = 1, 2, \dots, n$ , with the associated membership functions  $\xi_{\tilde{x}_1}(\cdot), \xi_{\tilde{x}_2}(\cdot), \dots, \xi_{\tilde{x}_n}(\cdot)$  such that

$$\xi_{\tilde{x}_i}(x) = \begin{cases} \frac{x - (x_i - h)}{h}; & x_i - h \leq x \leq x_i \\ \frac{(x_i + h) - x}{h}; & x_i \leq x \leq x_i + h \\ 0; & \text{otherwise} \end{cases}$$

Where  $h$  can be chosen appropriately based on the past knowledge we possess. Naturally, the value of the component  $h$  will differ from problem to problem depending on its nature and the degree of error in the observed data. The joint membership function of the observed fuzzy data vector  $\tilde{x} = \{\tilde{x}_1, \tilde{x}_2, \dots, \tilde{x}_n\}$  can be expressed as:

$$\xi_{\tilde{x}}(x) = \prod_{i=1}^n \xi_{\tilde{x}_i}(x)$$





**Sujatha et al.,**

According to Zadeh's (1968) [1] definition of probability for a fuzzy event, the likelihood function of the observed fuzzy data is stated as:

$$l(\theta; \tilde{x}) = P(\tilde{x}; \theta) = \int f(x; \theta) \xi_{\tilde{x}}(x) dx$$

Substituting the values of  $f(x; \theta)$  and  $\xi_{\tilde{x}}(x)$  from above yields the likelihood equation:

$$\begin{aligned} l(\theta; \tilde{x}) &= \prod_{i=1}^n \int f(x; \theta) \xi_{\tilde{x}_i}(x) dx \\ &= \prod_{i=1}^n \int \left( \frac{\theta^2}{1+\theta} \right) \left( \frac{1+x}{x^3} \right) e^{-\frac{\theta}{x} \xi_{\tilde{x}_i}(x)} dx \end{aligned}$$

After taking the logarithm of the likelihood function, we obtain

$$L(\theta; \tilde{x}) = \log_{10} l(\theta; \tilde{x}) = 2n \log_{10} \theta - n \log_{10} (1 + \theta) + \sum_{i=1}^n \log_{10} \int \left( \frac{1+x}{x^3} \right) e^{-\frac{\theta}{x} \xi_{\tilde{x}_i}(x)} dx$$

To obtain the MLE of  $\theta$ , we will maximize the log-likelihood equation. We differentiate the previous equation with regard to parameter  $\theta$  and set the derivative to zero.

$$\frac{\partial \ln l(\theta; \tilde{x}_i)}{\partial \theta} = \frac{2n}{\theta} - \frac{n}{(1+\theta)} - \sum_{i=1}^n \frac{\int \left( \frac{1+x}{x^4} \right) e^{-\frac{\theta}{x} \xi_{\tilde{x}_i}(x)} dx}{\int \left( \frac{1+x}{x^3} \right) e^{-\frac{\theta}{x} \xi_{\tilde{x}_i}(x)} dx} = 0$$

Solving the equation for  $\theta$  yields the estimated value of the parameter. However, it is clear that the given equation does not return an explicit answer. Iterative numerical methods could be an appropriate way for estimating the parameters of such equation. We propose the Newton-Raphson technique to estimate the parameter based on an appropriate starting guess.

**Maximum product of spacing**

The concept of the product of spacing is quite close to that of maximum likelihood. To construct the likelihood equation, we write the sample observations' joint density. Similarly, we can calculate the product of spacing by calculating the geometric mean of the spacing between ordered sample observations. Let  $f(x)$  and  $F(x)$  be the PDF and CDF of the distribution, respectively. The density of  $f(x)$  is strictly positive in the interval  $(m, n)$  and zero everywhere else, i.e.  $m < x_{(1)} < x_{(2)} < \dots < x_{(n)} < n$ . Here, we assume that  $X$  is a continuous variable with support  $(0, \infty)$ , resulting in  $m = 0$  and  $n = \infty$ . As a result, the border points of PDF and CDF will be as follows:

$$F(x) = 0 = f(x) \forall x < m \text{ and } F(x) = 1; f(x) = 0 \forall x > n$$

Let  $x_{i:n}$  represent the  $i$ 'th order statistics. The  $i$ th spacing  $D_i$  is defined as follows:

$$D_i = F(x_{i:n}) - F(x_{i-1:n}); i = 1, 2, \dots, (n + 1)$$

We must obtain the CDF value utilizing imprecise or fuzzy observations. This ambiguity in the observed data is addressed with fuzzy numbers by creating a triangle membership function for each observation based on prior knowledge of the nature of imprecision. Thus, CDF  $F(\theta; \tilde{x})$  corresponding to an observed fuzzy numbers  $\tilde{x} = (a, b, c)$ , can be expressed as:

$$\begin{aligned} F(\theta; \tilde{x}) &= P(X \leq a) + \int P(a \leq X \leq x) \xi_{\tilde{x}_i}(x) dx \\ &= F(a) + \int (F(x) - F(a)) \xi_{\tilde{x}_i}(x) dx \end{aligned}$$







**Sujatha et al.,**

$$F(\theta; \tilde{x}) = \left[1 + \frac{\theta}{(1+\theta)a}\right] e^{-\frac{\theta}{a}} + \int \left[\left(1 + \frac{\theta}{(1+\theta)x}\right) e^{-\frac{\theta}{x}} - \left(1 + \frac{\theta}{(1+\theta)a}\right) e^{-\frac{\theta}{a}}\right] \xi_{\tilde{x}_i}(x) dx$$

$$G(\theta; \tilde{x}) = \left[ \prod_{i=1}^{n+1} D_i \right]^{(1/n+1)}$$

$$\begin{aligned} S(\theta; \tilde{x}) &= \log G(\theta; \tilde{x}) = \frac{1}{n+1} \sum_{i=1}^{n+1} \log D_i \\ &= \frac{1}{n+1} \sum_{i=1}^{n+1} \log [F(\theta; \tilde{x}_i) - F(\theta; \tilde{x}_{i-1})] \end{aligned}$$

where,

$$\begin{aligned} F(\theta; \tilde{x}_i) - F(\theta; \tilde{x}_{i-1}) &= \left[ F(a_i) + \int (F(x_i) - F(a_i)) \xi_{\tilde{x}_i}(x) dx \right] \\ &\quad - \left[ F(a_{i-1}) + \int (F(x_{i-1}) - F(a_{i-1})) \xi_{\tilde{x}_{i-1}}(x) dx \right] \\ \frac{\partial \ln G(\theta; \tilde{x})}{\partial \theta} &= \sum_{i=1}^{n+1} \frac{1}{F(\theta; \tilde{x}_i) - F(\theta; \tilde{x}_{i-1})} \left[ \left\{ \omega(\theta, a_i) + \int \{ \omega(\theta, x_i) - \omega(\theta, a_i) \} \xi_{\tilde{x}_i}(x) dx \right\} \right. \\ &\quad \left. - \left\{ \omega(\theta, a_{i-1}) + \int \{ \omega(\theta, x_{i-1}) - \omega(\theta, a_{i-1}) \} \xi_{\tilde{x}_{i-1}}(x) dx \right\} \right] \end{aligned}$$

where,

$$\omega(\theta, x) = \frac{\partial}{\partial \theta} \left( \left[ 1 + \frac{\theta}{(1+\theta)x} \right] e^{-\theta/x} \right) = - \frac{e^{-\theta/x} [\theta^2(x+1) + \theta(2x+1)]}{x^2(1+\theta)^2}$$

Solving the aforementioned non-linear equation in  $\theta$  yields the MPS estimate of the population parameter  $\theta$ . Furthermore, it is clear that no closed solution to the preceding equation exists. Therefore, we shall apply numerical approaches to acquire the solution.

**Asymptotic confidence interval**

The distribution of MLE and MPS estimators,  $\hat{\theta}_{ML}$  and  $\hat{\theta}_{MPS}$ , is not explicitly known, making it difficult to obtain accurate interval estimates.

$$(\hat{\theta}_{MPS} - \theta) \xrightarrow{D} N(0, I^{-1}(\theta))$$

Using MLE and MPS estimations, the estimated 100(1- $\alpha$ )% asymptotic confidence interval for parameter  $\theta$  is as follows:

$$\begin{aligned} CI_{ML} &= \left[ \hat{\theta}_{ML} \pm z_{\alpha/2} \sqrt{I^{-1}(\hat{\theta}_{ML})} \right] \\ CI_{MPS} &= \left[ \hat{\theta}_{MPS} \pm z_{\alpha/2} \sqrt{I^{-1}(\hat{\theta}_{MPS})} \right] \end{aligned}$$

The observed Fisher information  $I(\hat{\theta}_{ML})$  is defined as:





$$I(\hat{\theta}_{ML}) = - \left( \frac{\partial^2 L(\theta; \tilde{x})}{\partial \theta^2} \right)_{\theta = \hat{\theta}_{ML}}$$

$$\frac{\partial^2 L(\theta; \tilde{x})}{\partial \theta^2} = \frac{-2n}{\theta^2} + \frac{n}{(1+\theta)^2} + \sum_{i=1}^n \left[ \frac{\int \left(\frac{1+x}{x^3}\right) e^{-\frac{\theta}{x}} \xi_{\tilde{x}_i}(x) dx}{\int \left(\frac{1+x}{x^3}\right) e^{-\frac{\theta}{x}} \xi_{\tilde{x}_i}(x) dx} - \left( \frac{\int \left(\frac{1+x}{x^3}\right) e^{-\frac{\theta}{x}} \xi_{\tilde{x}_i}(x) dx}{\int \left(\frac{1+x}{x^3}\right) e^{-\frac{\theta}{x}} \xi_{\tilde{x}_i}(x) dx} \right)^2 \right]$$

Similarly, we can get the observed Fisher information  $I(\hat{\theta}_{MPS})$  as follows:

$$I(\hat{\theta}_{MPS}) = - \left( \frac{\partial^2 S(\theta; \tilde{x})}{\partial \theta^2} \right)_{\theta = \hat{\theta}_{MPS}}$$

Let

$$N(\theta, x) = \left\{ \omega(\theta, a_i) + \int \{ \omega(\theta, x_i) - \omega(\theta, a_i) \} \xi_{\tilde{x}_i}(x) dx \right\} - \left\{ \omega(\theta, a_{i-1}) + \int \{ \omega(\theta, x_{i-1}) - \omega(\theta, a_{i-1}) \} \xi_{\tilde{x}_{i-1}}(x) dx \right\}$$

The second-order partial derivative of the logarithm of product spacing function S is provided as follows:

$$\frac{\partial^2 S(\theta; \tilde{x})}{\partial \theta^2} = \sum_{i=1}^{n+1} \left[ \frac{N'(\theta, x)}{F(\theta; \tilde{x}_i) - F(\theta; \tilde{x}_{i-1})} - \left( \frac{N(\theta, x)}{F(\theta; \tilde{x}_i) - F(\theta; \tilde{x}_{i-1})} \right)^2 \right]$$

where

$$N'(\theta, x) = \frac{\partial N(\theta, x)}{\partial \theta} = \left\{ \left\{ \omega'(\theta, a_i) + \int \{ \omega'(\theta, x_i) - \omega'(\theta, a_i) \} \xi_{\tilde{x}_i}(x) dx \right\} - \left\{ \omega'(\theta, a_{i-1}) + \int \{ \omega'(\theta, x_{i-1}) - \omega'(\theta, a_{i-1}) \} \xi_{\tilde{x}_{i-1}}(x) dx \right\} \right\}$$

and

$$\omega'(\theta, x) = \frac{\partial \omega(\theta, x)}{\partial \theta} = \frac{e^{-\theta/x} [\theta(x+1)\{\theta(1+\theta) - 2x\} + (2x+1)\{\theta(1+\theta) - x(1-\theta)\}]}{x^3(1+\theta)^3}$$

**Estimation of reliability and hazard function**

By creating a mechanism for getting MLE and MPS from fuzzy data, we can easily estimate reliability and hazard function by inserting the estimated parameter value into their functional forms.

$$R(t; \hat{\theta}) = 1 - \left[ 1 + \frac{\hat{\theta}}{(1+\hat{\theta})t} \right] e^{-\frac{\hat{\theta}}{t}}$$

$$H(t; \hat{\theta}) = \frac{\hat{\theta}^2(1+t)}{t^2 \left[ t(1+\hat{\theta}) \left( e^{\frac{\hat{\theta}}{t}} - 1 \right) - \hat{\theta} \right]}$$

The parameter estimate ( $\theta$  i.e.  $\hat{\theta}_{ML}$  or  $\hat{\theta}_{MPS}$ ) is denoted as  $\hat{\theta}$ . Substituting the estimated values of parameters  $\hat{\theta}_{ML}$  and  $\hat{\theta}_{MPS}$  in the preceding formulas yields the estimated reliability and hazard function at every time point  $t$  corresponding to the estimated value of  $\theta$ .





**Bayesian estimation**

This section covers the Bayesian estimation of population parameter  $\theta$  using fuzzy data. In Bayesian analysis, the parameter  $\theta$  is considered a random variable. To model its change, we must provide a distribution known as the population parameter's prior distribution. Using the Bayes theorem, we update the prior information about the unknown parameter  $\theta$  based on the likelihood of the sample observations. The gamma prior is chosen since it is versatile and has the same support as the parameter  $\theta (0, \infty)$ . The probability density function of the prior with hyper parameters  $p$  and  $q$  is given below:

$$\pi(\theta) = \frac{p^q}{\Gamma(q)} e^{-p\theta} \theta^{(q-1)}; \theta > 0, q > 0, p > 0$$

Using the prior in above equation one can easily calculate the posterior distribution of the parameter  $\theta$  for the supplied data.

$$\pi(\theta | \tilde{x}) = \frac{l(\theta; \tilde{x})\pi(\theta)}{\int_0^\infty l(\theta; \tilde{x})\pi(\theta)d\theta}$$

where,

$$J = e^{-p\theta} \theta^{2n+q-1} (1 + \theta)^{-n} \prod_{i=1}^n \int \left(\frac{1+x}{x^3}\right) e^{-\frac{\theta}{x}\xi_{\tilde{x}_i}(x)} dx$$

To estimate the parameter under the Bayesian paradigm, we used the quadratic loss function, which is defined as follows:

$$l_s(\hat{\theta}, \theta) = \epsilon(\hat{\theta} - \theta)^2$$

The estimated value of parameter  $\theta$  is denoted as  $\hat{\theta}$ , and  $\epsilon$  can be a function of  $\theta$ . If  $\epsilon$  equals 1, we have SELF. This is the most popular symmetric loss function. It treats both overestimation and underestimate of parameters equally. Furthermore, it penalizes huge errors significantly more than tiny errors. If  $h(\cdot)$  is a function of  $\theta$ , then the Bayes estimate of  $h(\cdot)$  under SELF equals the expectation of the posterior distribution.

$$\hat{h}(\theta) = E_\pi[h(\theta)]$$

This approach generates sample values of parameter  $\theta$  using a proposal distribution with stationary distribution  $\pi(\theta)$ . The main steps of the algorithm are listed below:

- Step 1: Begin with an initial guess value  $\theta^0$  and set  $j = 1$ .
- Step 2: Create a new candidate parameter value  $\theta^{j*}$  at the  $j$ th step using the proposal density  $q(\theta^{(j)} | \theta^{(j-1)})$
- Step 3: Accept candidate  $\theta^*$  as

$$\theta^{(j)} = \begin{cases} \theta^* & \text{with probability } \rho(\theta^*, \theta^{(j-1)}) \\ \theta^{(j-1)} & \text{with probability } 1 - \rho(\theta^*, \theta^{(j-1)}) \end{cases}$$

where

$$\rho(\theta^*, \theta^{(j-1)}) = \min \left\{ \frac{\pi(\theta^* | \hat{u})q(\theta^{(j-1)} | \theta^*)}{\pi(\theta^{(j-1)} | \hat{u})q(\theta^* | \theta^{(j-1)})}, 1 \right\}$$

Step 4: Calculate  $R^{(j)}(t) = 1 - \left[1 + \frac{\theta^{(j)}}{(1+\theta^{(j)})x}\right] e^{-\frac{\theta^{(j)}}{x}}$  and  $H^{(j)}(t) = \frac{\theta^{(j)2}(1+x)}{x^2 \left[ x(1+\theta^{(j)}) \left( e^{\frac{\theta^{(j)}}{x}} - 1 \right) - \theta^{(j)} \right]}$





**Sujatha et al.,**

Step 5: Repeat steps 2-4 M times to produce  $\theta^{(j)}, R^{(j)}(t)$  and  $H^{(j)}(t); j = 1, 2, \dots, M$  where  $j=1, 2, \dots, M$  Bayes estimates for parameters  $\theta, R(t)$ , and  $H(t)$  under SELF are as follows:

$$\hat{\theta}_B = E_{\pi}(\theta | \tilde{u}) = \frac{1}{M - M_0} \sum_{j=M_0+1}^M \theta^{(j)}$$

$$\hat{R}(t)_B = E_{\pi}(R(t) | \tilde{u}) = \frac{1}{M - M_0} \sum_{j=M_0+1}^M R^{(j)}(t)$$

$$\hat{H}(t)_B = E_{\pi}(H(t) | \tilde{u}) = \frac{1}{M - M_0} \sum_{j=M_0+1}^M H^{(j)}(t)$$

Where  $M_0$  represents the burn-in period, To create the HPD credible intervals for  $\theta$ , arrange the simulated samples as  $\theta^{(1)} \leq \theta^{(2)} \leq \dots \leq \theta^{(M)}$ . Create 100(1- $\alpha$ )% credible intervals for  $\theta$  as follows:

$$(\theta^{[1]}, \theta^{[M(1-\alpha)+1]}), \dots, (\theta^{[M\alpha]}, \theta^{[M]})$$

Here,  $[X]$  represents the greatest integer less than or equal to  $X$ . The HPD credible interval for  $\theta$  is the shortest in length.

**Real Data Analysis**

This part will evaluate the performance of developed estimators on an actual data set. In Puducherry agriculture in the year of 2019, all the seasons were given and their survival durations were recorded. Kaggle.com [12] reported this data set. The crop production data is shown in Table.1. Bayesian estimation of Inverse Lindley distribution with fuzzy parameters to given data Posterior mean of  $\theta$  is 0.4531, Posterior median of  $\theta$  is 0.5000 and 95% credible interval for the  $\theta$  is 0 to 0.5378.

**RESULTS AND DISCUSSION**

Fuzzy lifespan data can be utilized to determine the reliability of Lindley distribution with fuzzy parameters. in real-world circumstances with uncontrollable elements. However, fuzzy sets only have one membership degree parameter, which leads to a less precise description of the external world. When dealing with fuzzy information, the Inverse Lindley Distribution with fuzzy parameters expresses uncertainty and fuzziness more accurately. The results demonstrated that changing the true values of various kinds of parameters resulted in a significantly smaller mean square error under Bayesian estimation compared to the maximum likelihood estimator, MPS, and that the results of Trace plot MCMC and PDF of Posterior Samples of Inverse Lindley distribution with fuzzy parameters for the given data. Kaggle.com validates the current research findings [12]. We discovered results for the Probability density function (Fig.1), Cumulative density function (Fig.2), Hazard rate function (Fig.3), and Trace plot MCMC and PDF of Posterior Samples (Fig.4.a, 4.b) of Inverse Lindley distribution with fuzzy parameters to the agriculture problem of Pondicherry in 2019 and supporting MATLAB tool, which show how well the suggested technique performs in predicting crop production for all seasons.

**CONCLUSION**

This article focuses on developing an MPS estimator for non-precise observed data. We used the inverse Lindley distribution, a highly effective survival model. To evaluate MPS performance with other estimators, we obtained the MLE and Bayes estimators for the fuzzy parameter. Both classical and Bayesian techniques provide point estimates for parameters, as well as estimated reliability, hazard, and confidence intervals. The current article discusses a combination of statistical methods and a fuzzy approach to Puducherry agriculture in the year of 2019. This paper's methods can help researchers and statisticians deal with imprecise agriculture data during studies. Extending the





MPS estimation for fuzzy data using a Bayesian setting would be a highly beneficial research topic. Using fuzzy models to address fuzzy data challenges can enhance our understanding of both statistical and fuzzy approaches.

**REFERENCES**

1. Zadeh, Lotfi A. "Fuzzy sets." Information and control 8, no. 3 (1965): 338-353.
2. Maiti, Sudhansu S., and Indrani Mukherjee. "Some estimators of the PDF and CDF of the Lindley Distribution." arXiv preprint arXiv:1604.06308 (2016).
3. Qoshja, Arbër, and Fatmir Hoxha. "Different methods of estimation for generalized inverse Lindley distribution." Mathematical Theory and Modeling 6, no. 5 (2016): 132-141.
4. Gui, Wenhao, and Man Chen. "Parameter estimation and joint confidence regions for the parameters of the generalized Lindley distribution." Mathematical Problems in Engineering 2016, no. 1 (2016): 7946828.
5. Alizadeh, Mojtaba, Sadegh Rezaei, Saralees Nadarajah, and Seyyed Fazel Bagheri. "On the estimation of the inverse Weibull distribution." Journal of Data Science 15, no. 1 (2017): 167-182.
6. Pak, Abbas. "Statistical inference for the parameter of Lindley distribution based on fuzzy data." (2017): 502-515.
7. Maiti, Sudhansu S., and Indrani Mukherjee. "On estimation of the PDF and CDF of the Lindley distribution." Communications in Statistics-Simulation and Computation 47, no. 5 (2018): 1370-1381.
8. Akgül, Fatma Gül, and Birdal Şenoğlu. "Comparison of estimation methods for inverse Weibull distribution." In Trends and Perspectives in Linear Statistical Inference: Proceedings of the LINSTAT2016 meeting held 22-25 August 2016 in Istanbul, Turkey, pp. 1-22. Springer International Publishing, 2018.
9. Singh, Sukhdev, Sanku Dey, and Devendra Kumar. "Statistical inference based on generalized Lindley record values." Journal of Applied Statistics 47, no. 9 (2020): 1543-1561.
10. Asgharzadeh, A., M. Alizadeh, and M. Z. Raqab. "Inverse Lindley distribution: different methods for estimating their PDF and CDF." Journal of Statistical Computation and Simulation 94, no. 3 (2024): 604-623.
11. Golestani, Bahareh Etemad, Ehsan Ormoz, and S. M. T. K. MirMostafae. "Statistical inference for the inverse Lindley distribution based on lower record values: Accepted-January 2024." REVSTAT-Statistical Journal (2024).
12. <https://www.kaggle.com/datasets/akshatgupta7/crop-yield-in-indian-states-dataset>.

**Table 1: Agriculture data of Pondicherry in the year of 2019**

Crop	Season	Area	Production	Annual Rainfall	Fertilizer	Pesticide	Yield
Areca nut	Kharif	52	78	1317	8931.52	19.24	1.5
Bajra	Kharif	14	36	1317	2404.64	5.18	2.57
Bajra	Rabi	1	3	1317	171.76	0.37	3
Bajra	Summer	7	18	1317	1202.32	2.59	2.57
Banana	Kharif	273	16637	1317	46890.48	101.01	32.76667
Black pepper	Kharif	11	15	1317	1889.36	4.07	1.36
Cashewnut	Kharif	145	65	1317	24905.2	53.65	0.426667
Coconut	Whole Year	1857	18661000	1317	318958.3	687.09	9474.625
Cotton(lint)	Kharif	500	1248	1317	85880	185	2.745
Dry chillies	Kharif	2	26	1317	343.52	0.74	13
Dry chillies	Rabi	3	41	1317	515.28	1.11	13.67
Dry chillies	Summer	2	26	1317	343.52	0.74	13
Groundnut	Kharif	1	3	1317	171.76	0.37	3
Groundnut	Rabi	231	693	1317	39676.56	85.47	3
Groundnut	Summer	21	63	1317	3606.96	7.77	3
Moong(Green Gram)	Rabi	12	9	1317	2061.12	4.44	0.75
Moong(Green Gram)	Summer	629	156	1317	108037	232.73	0.606667
Onion	Kharif	2	10	1317	343.52	0.74	5





Sujatha et al.,

Onion	Summer	1	5	1317	171.76	0.37	5
Other Rabi pulses	Rabi	53	42	1317	9103.28	19.61	0.79
Other Kharif pulses	Kharif	5	4	1317	858.8	1.85	0.8
Other Summer Pulses	Summer	21	17	1317	3606.96	7.77	0.81
Ragi	Kharif	32	77	1317	5496.32	11.84	2.41
Ragi	Rabi	4	10	1317	687.04	1.48	2.5
Ragi	Summer	23	55	1317	3950.48	8.51	2.39
Rice	Kharif	4323	15171	1317	742518.5	1599.51	3.216667
Rice	Rabi	9397	28114	1317	1614029	3476.89	3.883333

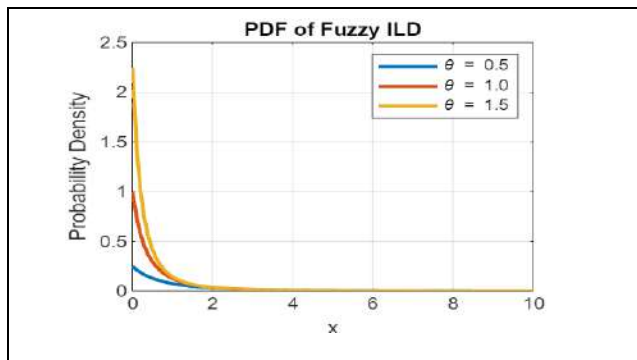


Fig.1. Mathematical Results of the Inverse Lindley distribution with fuzzy parameters

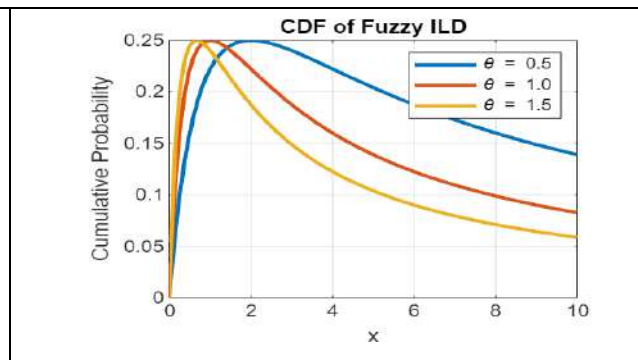


Fig.2. : PDF of Inverse Lindley distribution with fuzzy parameters.

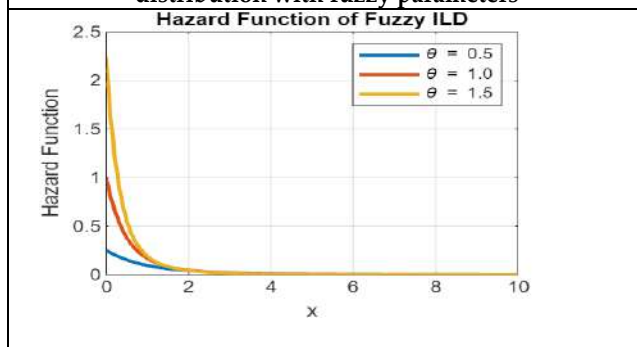


Fig.3. Hazard rate of Inverse Lindley distribution with fuzzy parameters.

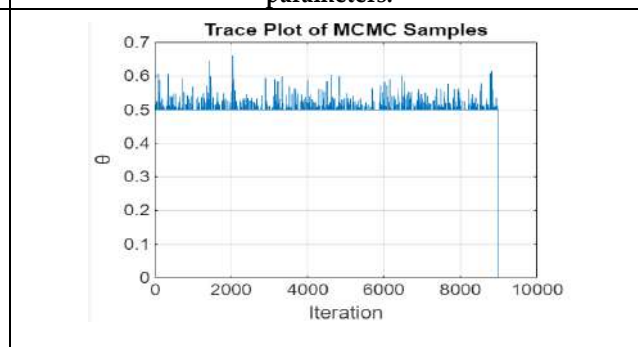


Fig. 4. Trace plot MCMC of Inverse Lindley distribution with fuzzy parameters

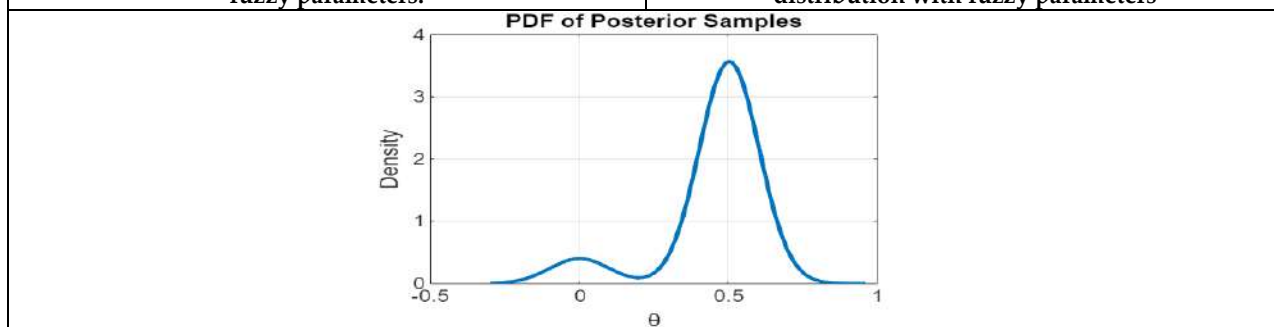


Fig. 5 PDF of Posterior Samples of Inverse Lindley distribution with fuzzy parameters







## The Design and Development of Surgical Nurse Assistance Robotic System by using AI with MSN Network

M. Senthilkumar<sup>1</sup>, K. Shanmugasundaram<sup>2\*</sup>, A.T. Rajamanickam<sup>3</sup> and N. Nandakumar<sup>4</sup>

<sup>1</sup>Research Scholar, Department of Electronics, Sri Ramakrishna Mission Vidyalaya College of Arts and Science, (Affiliated with Bharathiar University) Coimbatore, Tamil Nadu, India

<sup>2</sup>Associate Professor and Head, Department of Electronics, Sri Ramakrishna Mission Vidyalaya College of Arts and Science, (Affiliated with Bharathiar University) Coimbatore, Tamil Nadu, India.

<sup>3</sup>Associate Professor, Department of Electronics, Sri Ramakrishna Mission Vidyalaya College of Arts and Science, (Affiliated with Bharathiar University) Coimbatore, Tamil Nadu, India.

<sup>4</sup>Founder / Bio Medical Engineer, Prime Bio Medical Systems, Tiruppur, Tamil Nadu, India.

Received: 23 Apr 2024

Revised: 25 Aug 2024

Accepted: 29 Oct 2024

### \*Address for Correspondence

#### K. Shanmugasundaram

Associate Professor and Head,

Department of Electronics,

Sri Ramakrishna Mission Vidyalaya College of Arts and Science,

(Affiliated with Bharathiar University)

Coimbatore, Tamil Nadu, India.

E.Mail: shanmugam.nks@gmail.com



This is an Open Access Journal / article distributed under the terms of the **Creative Commons Attribution License** (CC BY-NC-ND 3.0) which permits unrestricted use, distribution, and reproduction in any medium, provided the original work is properly cited. All rights reserved.

### ABSTRACT

In recent trends embedded system plays major role in electronics especially in robotics. Embedded system is a combination of hardware and software which is specifically designed to perform specific task in real time. Which makes a sophisticate model design in robotic automation system will support the performance and it also promises the less operating time, higher accuracy and less percentage of risks. It involves in a different variety of application areas in consumer electronics, industrial automation, security and telecommunications, instrumentations, aerospace, automobile and bio medical health care sectors. This research is to develop a robot which can assist surgeon during surgery. Today's a lot of medical robot system is available but none can assist a doctor during a complex surgery. At the time of surgery the surgeon need the well experience nurse to handle the tools but that time also have more chance to occur errors like man made errors etc. The surgical assistance robot system has been designed for this purpose to avoid the errors and man power. It can understand the doctor's needs by them inputs and it brings the appropriate surgical tool during surgery and it also getting the details from the environmental data during the surgery. The robotic system can understand commands and it fetches the necessary tools and respectively like cotton pads and clamps to stop bleeding, fetches scissors, catheter, and needle etc. It is also monitor the patient health conditions and the environmental conditions of surgical room. These all the functions will be achieved by the MSN network and AI technologies.

**Keywords:** surgical assistance robot, MSN network and AI technologies.





## INTRODUCTION

In bio medical field the robotic automation function performs the less operating time, higher accuracy and less percentage of risks compare with the traditional methods. In this research work describe about the current trends of applications in bio medical section especially in health care sector. The various role of embedded system based robotic system to be implemented in bio medical sector like robotic automation operations in surgery. [1]The ARD is recent development method of robotic system in embedded. In recent days the Assistance Robotic Device (ARD) which is implement in bio medical section in various application. The quest of my research is to develop a robot which can assist a medical practitioner during surgery. Today, a lot of medical robots are available but none can assist a doctor during a complex surgery. Nowadays, the surgeons are in need of a surgical assistance personnel who can support them during the complex surgery. Since surgery can be ascertained based on advancement of the disease for the patient, only the experienced nurses in that field can render their support. For example, an ortho based surgery needs a surgical assistance that should be well known about the surgical tools that are used in mending bones, ligaments and cartilages.

The surgical assistance robot has been designed for this purpose. It can understand the surgeon's situation and based on inputs and bring the appropriate surgical tool during surgery. This system can also monitor the patient health condition and environmental conditions of surgery room through the multiple sensor network (MSN) module. The platform chosen to develop the robot is embedded systems. Because the embedded system is the stable and best platform to produce the closed control system with enhancing features to connect with any platform if required. The sophisticated embedded systems that can be used in robots have enormous hardware and software complexities that may need ASIPs, IPs, PLAs, scalable or configurable processors.

## LITERATURE REVIEW

- ❖ Embedded system in biomedical applications: challenges ahead BY PriyaPanneerselvam(2014) (IJSETR). This paper focuses the embedded systems development especially in biomedical sector and mainly focused on tools of diagnosis, prognosis, patient management and telemedicine. The major problem of this developments the emerging of system for real time response.
- ❖ Biomedical Applications withUsing Embedded Systems by GulcicekDere( 2021) ( WoS)  
In this paper, disclose the design and development tools of embedded system in biomedical sector and it deals with tools development of safety healthcare of people in the event of epidemic infectious diseases in process.
- ❖ An eye-tracking based robotic scrub nurse: proof of concept by Ahmed Ezzat- Alexandros Kogkas and teams. (2021) (Springer)  
This paper discusses the surgery assistive robotic devices and its acted as a third hand to achieve the various tasks and it's to be control the wearable eye tracker glass which is integrated with the motion sensor and the motion of eye ball movement it to activate or pass the command to the ASD, according to that command it will perform.
- ❖ Robot, Pass Me the Scissors! How Robots Can Assist Us in the Operating Room by Juan P. Wachs, Purdue University, West Lafayette, IN 47906, USA (2012) (Springer).  
This paper describes the lack of nurse availability in hospitals especially they need well experience nurse at the time of surgery. So resolve the problem they are focused to design the robotic assistance in OR and it includes an assistive robot for object picking, haptic feedback controlled robots which are controlled by the gesture controlled mechanism.
- ❖ Surgical Instrument Handling and Retrieval in the Operating Room with a Multimodal Robotic Assistant By Mithun G. Jacob, Yu-Ting Li, Juan P. Wachs( 2013) (IEEE) .





This paper considers the design and development of robotic scrub nurse (RSN) designed for human safety -robot collaboration in the operating room (OR) and it assist the surgical staff in the OR by Delivering instruments to the surgeon and operates through a multimodal interface allowing instruments to be requested Through verbal commands or touch less gestures control method.

❖ A Novel Gesture Recognition System for Intelligent Interaction with a Nursing-Care Assistant Robot by Geng Yang and team (2018) ( MDPI – Scientific Journal)

This paper discussed a nursing-care assistant robot prototype which is to be developed based on the (HMT) gesture recognition system. The HMT consist of data acquisition, data processing, and a natural a human robot interface for the smart infrastructure.

### PROBLEM IDENTIFICATION

Now days a different number of robotic systems are available in hospitals for different kind of application, but no one can assist a surgeon during at the time of surgery for delivering the needful tools according to the surgeons needs. For delivering the tools at the time of surgery the surgeons need a personal assistant nursing system. In this case, the surgeons need in well experience nurse with the knowledge of surgical tools and its handling methods and also need to focus in multiple tasks related to surgery.

In these cases, the surgeons need to faces the three major problems.

1. Availability of experience nurse.
2. Communication problem (Language, pronunciation, command delay)
3. Manmade error.

### OBJECTIVE:

This research is to develop a robotic system, which can assist surgeon during surgery time for delivering the tools and monitoring the health parameters to avoid the mentioned problems. Today, a lot of medical robot system is available but none can assist a surgeon during a complex surgery. So surgical assistance robot system has been designed for this purpose. It can understand the surgeon's needs by them inputs and bring the appropriate surgical tool during surgery and its continuously monitoring the health parameters of patient. Also getting the details from the environmental data during the surgery. The robot can understand and fetches the necessary tools and respective necessary things like cotton pads and clamps to stop bleeding, fetches scissors, catheter, and needle etc. These all the functions will be achieved by the MSN network and AI technologies.

### EXISTING SYSTEM

The existing systems of Assistant Nurse Systems are developed in different methods for different kind of applications (Refer Figure 1).

The lists of bio medical robotic systems are,

**Electronic Medical record robotic system:** In healthcare sectors this types of robotic systems are used to maintain and monitoring the patient health conditions and it maintain these recordsand medical history about the patient for further treatment.

**Medication Management robotic system:** This robotics system specifically designed for patient and patient care person to manage maintain the exact medicine list for a treatment.

**Patient Monitoring robotic system:** This type of robotic systems which is used to maintain the monitor the patient health condition in hospital or remotely. Based on this monitoring system the doctors can easily monitor the patient health condition and easily can take prevention action to improve the patient health condition.

### Scrub Assistance Robotic system:

- Used in surgery as an assistant.
- It assists the surgical staff in operation room by delivering the tools to surgeon. The surgical assistant robots are mainly followed the below mentioned method for its development.



**Senthilkumar et al.,**

The surgical assistant robotic (SAR) system mainly classified into two types based on the input accessing methods: (Refer Figure 1)

1. Contact Method
2. Touch Less Method

**Contact Methods**

The control functions of the system to be defined according to the contact of event or movement. Based on the event, the function to be implemented by assigned program (Refer Figure 2).

**Ex: Eye ball/ Eye Track Robotic system:**

This robotic system mainly consists of camera with sensors, robotic arm system, and which is controlled and monitor by the software program. The camera systems continuously monitor the human eye ball contact movement. According to the eye ball movement the robotic arm to be controlled. This method of technology involved in various applications like assistive device for disability people, etc.

Here the figure 2&3 discuss about the function flow of eye ball tracking systems.

In this system the eye ball tracker mounted with wheelchair and it to be controlled by the controller by defined software program [3]. The robotic arm also controls by the eye ball movement for the user defined functions.

**Touch less Method**

This method of robotic system has a capability to interact with objects, surfaces, or their environment without physically making contact (Refer Figure 3).

Ex: Gesture control Robotic system

A gesture control robotic systems allows robots to interpret and reply to human gestures as instructions or commands.

The figure 3 discuss about the gesture control system based on the hand movement for the robotic system to move Up, Down, Right and Left, Hand Grip Close and Hand Grip Close.

This technology allows the users to interconnect with the robots instinctively using hand gesture movement, body language or some special gestures to communicate the actions or directives to the robot.

**IMPLEMENTATION METHOD:**

The Surgical Assistant Robot System is mainly developed in to assist the surgeon in Operation room and it also monitor the patient health condition and environmental situation by the using the MSN (Multisensor Network).

This robotic system can develop in 2 main methods.

1. Verbal Communication
2. Non Verbal Communication

Verbal and non-verbal method of communication plays a vital role in the robotic functions.

**Verbal Methods**

This method of robots involves the use of spoken language or synthesized speech to convey the information by the given instructions, responding to queries, or expressing status updates audibly by voice command.

**Speech Recognition:** Robots can understand and respond to spoken commands with natural language, enabling more intuitive interaction.

**Text-to-Speech (TTS):** Robots equipped with TTS technology can convert written text into spoken words, allowing them to communicate information or instructions verbally.

**Voice Feedback:** Robots can provide feedback or updates on their status, actions, or any issues using verbal communication. Throughout this method the user can understand the robotic functions.



Senthilkumar *et al.*,

### Non-Verbal Methods

In this method the information and command to be transfer through the various non-verbal cues, like body language, face expressions, gesture control, postures control functions without the use of voice and sound commands.

**Gesture Recognition:** Robots can interpret human gestures as commands. This involves using cameras or other sensors to recognize and understand hand movements, body language, or facial expressions.

**Facial Expression Recognition:** By analyzing facial expressions, robots can gauge human emotions and respond accordingly. This is particularly useful in social or caregiving robots.

**Body Language Interpretation:** Understanding and responding to human body language allows robots to interact more naturally with users, providing a more intuitive and user-friendly experience.

**Visual Feedback:** Robots can use lights, displays, or other visual cues to convey information or responses to users. This could include indicating their status, acknowledging commands, or signaling errors.

**Haptic Feedback:** While not strictly non-verbal, haptic feedback involves using touch or force feedback to communicate with users. For example, a robot might provide a gentle vibration to confirm a successful action.

### Combining Verbal and Non-Verbal Methods

**Multimodal Interaction:** Many advanced robotic systems integrate multiple communication modalities simultaneously. For instance, a robot might combine speech recognition with gesture recognition to enhance user interaction and understanding.

In this research work the Non Verbal Communication method to be used for implementation because can easily avoid the communication error and issues.

In this assistant surgical robotic systems to be implement by the **touchable keypad of Non-verbal communication** for the robotic functions.

There are different types of method to be used for robotic function as discussed in earlier part. But all these method of communication system produces the errors based on Communication problems like language, pronunciation, command delay and manmade error.

In this touchable keypad based system of Non-verbal communication method system produces high accuracy in data transmission of information of command for the robotic functions.

#### Functional details of block diagram:

In this surgical nurse assistant robotic system mainly consist of the following blocks (Refer Figure 4).

1. MSN MODULE (Patient Health Monitoring and environmental monitoring.)
2. Touchable Keypad (For I/P control signal for robotic control system).
3. AI based controller system for Robotics.
4. Robotic Arm System.
5. Monitoring and Alerting system.

### MSN Module

The multi-sensor network (MSN) module consists of multiple sensors connected in single controller. Here this sensor is used to sense the major parameter (SPo2, Blood Pressure and sugar, EGC) of patient health condition at the time of surgery to avoid the critical situations and it also sense the external environmental parameters ( temperature, air quality of O<sub>2</sub> and humidity level) of surgery room (Operating Room) .

### Touchable Keypad

This touchable keypad system to be functioned based on the non verbal communication method. Based on this method can avoid the communication and man made errors. Based on the key selection the user can control the robotic arm function for the tools delivery according to the type of surgery and it also used to check the patient health conditions. The entire system function will be selected by the key selection from keypad. According to the key pressing the control system to be activate the respective function.

### AI based controller system for Robotics





Senthilkumar *et al.*,

The system controller used to controller the user defined function according to the patient health and environmental monitoring system. For robotic arm control function to be implemented though the controller for the user function. The AI technology is also included for the decision making for the surgical tools arrangement in the tray according the respective surgery. Here the AI technology is to be implementing for the tools rearrangement in the surgical tools box tray [4]. Initially this system selects the type of surgery through keypad. After selection of surgery type the system needs to check the tools box tray whether the needed tools to be placed in the respective slot otherwise it to be collect the needful tools and arrange it in respective slots.

### **Robotic Arm System**

A robotic arm system designed as a surgical assistant nurse to deliver surgical tools is an innovative application of robotics in the medical field. This kind of technology aims to enhance surgical procedures by providing precision, efficiency, and controlled assistance. Here are some key features and benefits of such a system:

#### **Precision and Accuracy:**

The robotic arm system can offer high levels of precision in tool delivery, minimizing the risk of human error during surgery. It can be programmed to follow specific way, to ensuring accurate placement of surgical instruments.

#### **Efficiency and Speed:**

The robotic assistant nurse can work seamlessly with human surgical teams, serving to streamline the surgical process. Automated movements and fast response times contribute to the efficiency of the surgical function.

#### **Minimally Invasive Surgery:**

Robotic systems are often designed to facilitate simply invasive measures, reducing the size of incisions and promoting faster recovery for patients. Smaller incisions can result in less pain, decreased risk of infection, and shorter hospital stays.

#### **Enhanced Visualization:**

Integration of robotic systems may include advanced imaging technologies, providing surgeons with enhanced visualization of the surgical site.

#### **Reduced Fatigue:**

Robotic assistants do not experience physical fatigue, ensuring consistent performance throughout lengthy surgical procedures.

This can contribute to maintaining a high standard of care and focus during the entire surgery.

#### **Adaptability:**

The system can be adaptable to various surgical specialties allowing its use in a wide range of procedures.

Modular designs may allow for upgrades and customization based on evolving surgical needs.

#### **Safety Features:**

Incorporation of safety mechanisms, such as collision detection and avoidance, ensures that the robotic arm operates without causing harm to patients or surgical teams. While the development and use of robotic surgical assistants continue to evolve, the goal is to improve patient outcomes, reduce recovery times, and enhance the overall quality of healthcare delivery in surgical settings.

### **Monitoring and Alerting system**

The monitoring and alert system is used to monitor the patient health condition and environmental conditions at the time of surgery.

The monitoring system will monitor the patient health parameter and environmental condition data through the different sensor and this parameter range to be calibrated in controller. If the received parameter is beyond the set value the alert system to be alerts the surgeon. Based on the alert surgeon can avoid the errors and save the patient health conditions.

### **Functional Flow Diagram**

The system function diagram explains the functional flow details of the surgical assistant nursing system (Refer Figure 5).Initially the system initializes the robotic control and monitoring system function. These functions are split into two sections.







- i) Robotic Arm control system
- ii) Monitoring system

#### **Robotic Arm control system**

The Arm control system initially activating the self-testing condition of hand movements for surgical tools delivering and pick up. After the self-testing the surgeon selects the type of surgery by selection the key from the keypad. Initially some pre-set function to be implemented for surgery type and its needful tools then its position in tools box. According to the selection of surgery type the robotic system check the tools box for availability of tools and position [5]. The tools availability of tools and its positions as in pre-set function the arm system to be ready for surgery for delivering and receiving the tools according to the surgeon need. (I/P instruction given through keypad). If the tools availability and its positions are not in the pre-set function, immediately the arm system which will collect the needful tools in the main tools box and it rearrange the tools according to the pre-set function [6].

The AI system function to be implemented for the functions of tools identifications and its rearrangements according to the type of surgery.

#### **Monitoring and Alerting system**

This system to be implemented for monitoring the operating room environmental condition and patient health condition based on Multisensor network module. The MSN module parameter to be monitoring and it compare with the pre-set parameter. If the received parameter is beyond the pre-set parameter, it will immediately activate the alert system [8].

## **RESULT AND CONCLUSION**

In the surgical nursing assistant robotic system mainly implemented by the combination of MSN module, Robotic Arm system with AI. These technology is used to avoid the manmade error and time delay of tools delivery at the time of surgery as well as this system also reduce the man power (experience nurse). This surgical assist robotic is a suitable replacement for the surgical assistant nurse. The AI technology integrated into the robotic system allows for adaptive learning, where the robot can improve its tools arrangements and delivery processes over time by analyzing past surgeries and outcomes and also the AI – driven system provides high precision in delivering the correct tools to the surgeon, minimizing delays and optimizing the flow of surgical procedures. The potential for future enhancements is vast, including the use of machine learning to facilitate more complex tasks and the integration with other robotic systems for a fully automated surgical environment.

## **REFERENCES**

1. Embedded system in biomedical applications: challenges ahead BY PriyaPanneerselvam(2014) (IJSETR)
2. Biomedical Applications withUsing Embedded Systems by GulcicekDere( 2021) ( WoS)
3. An eye-tracking based robotic scrub nurse: proof of concept by Ahmed Ezzat· Alexandros Kogkas and teams. (2021) Published: 08 June 2021, Volume 35, pages 5381–5391, (2021) (Springer)
4. Robot, Pass Me the Scissors! How Robots Can Assist Us in the Operating Room by Juan P. Wachs, Purdue University, West Lafayette, IN 47906, USA (2012) (Springer).
5. Surgical Instrument Handling and Retrieval in the Operating Room with a Multimodal Robotic Assistant By Mithun G. Jacob, Yu-Ting Li, Juan P. Wachs( 2013) (IEEE) .
6. A Novel Gesture Recognition System for Intelligent Interaction with a Nursing-Care Assistant Robot by Geng Yang and team (2018) ( MDPI – Scientific Journal).
7. Early experience with robotic technology for thoracoscopic surgery – Book





Senthilkumar et al.,

8. Roberto T. "Robotic systems in cardiovascular surgery" -Brazilian Journal of Cardiovascular Surgery,Rev Bras Cir Cardiovasc vol.19 no.2 São José do Rio Preto Apr./June 2004.
9. N.Nandakumar, ArunPrasad.M, Karthikeyan.S, "Development of Medical Robots in Different Applications – A Review", MuktsShabd Journal, Volume IX, Issue V, pp.1933-1938, May 2020.
10. Jeffrey A Morgan,"Thoracoscopic lobectomy using robotic technology",pubmed logo-PMID: 14722004.
11. [https://health.ucdavis.edu/surgery/specialties/cardio/robotic\\_surgery.html](https://health.ucdavis.edu/surgery/specialties/cardio/robotic_surgery.html)
12. AchimSchweikard, Floris Ernst, "Medical Robotics", published on October 2015.
13. Clifford A. Pickover,"The Medical Book: From Witch Doctors to Robot Surgeons", published on 2012.
14. Jaydev P. Desai, Antoine Ferreira, Rajni V. Patel,"EncyclopediaOf Medical Robotics, The (In 4 Volumes)", published 2018.
15. Hongliang ,"Flexible Robotics in Medicine: A Design Journey of Motion Generation Mechanisms and Biorobotic System Development",published on 2020.

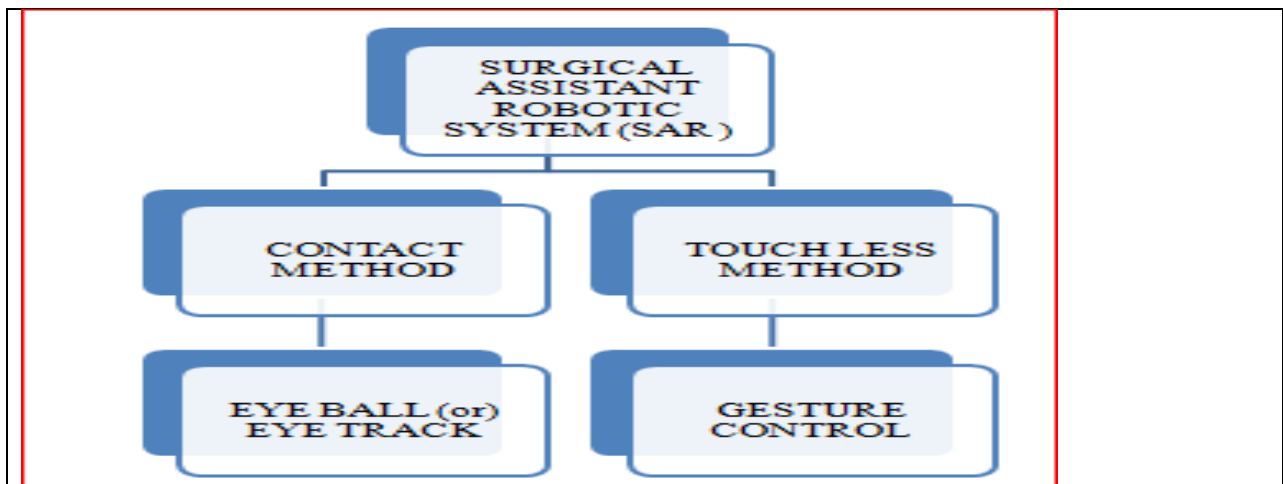


Figure 1: Different types of SAR system with its methodology.

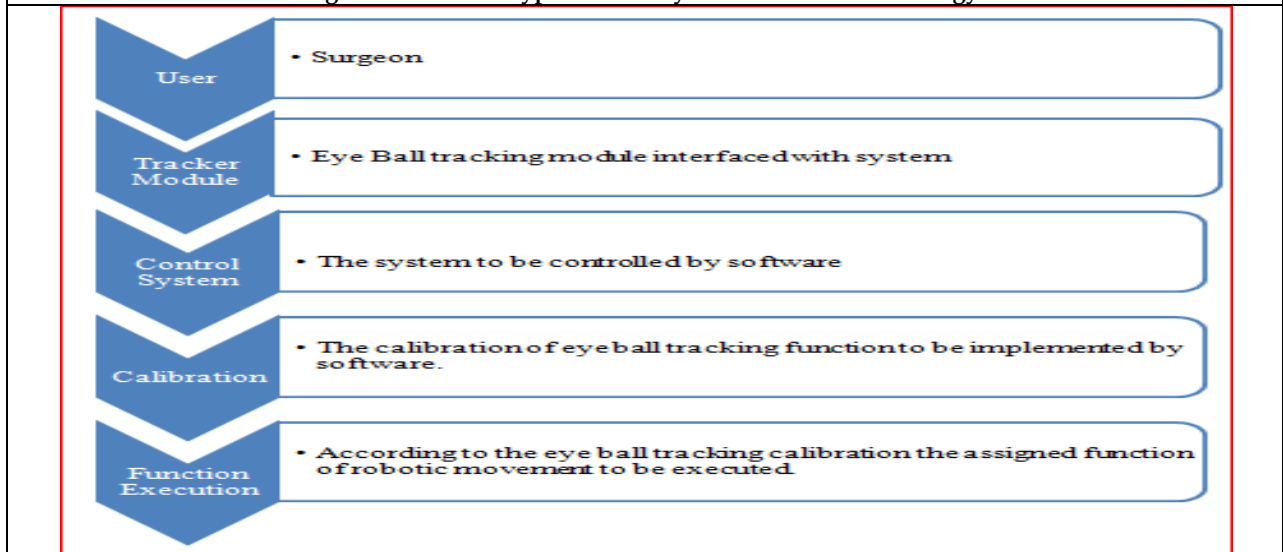


Figure 2: Flow chart for function execution.



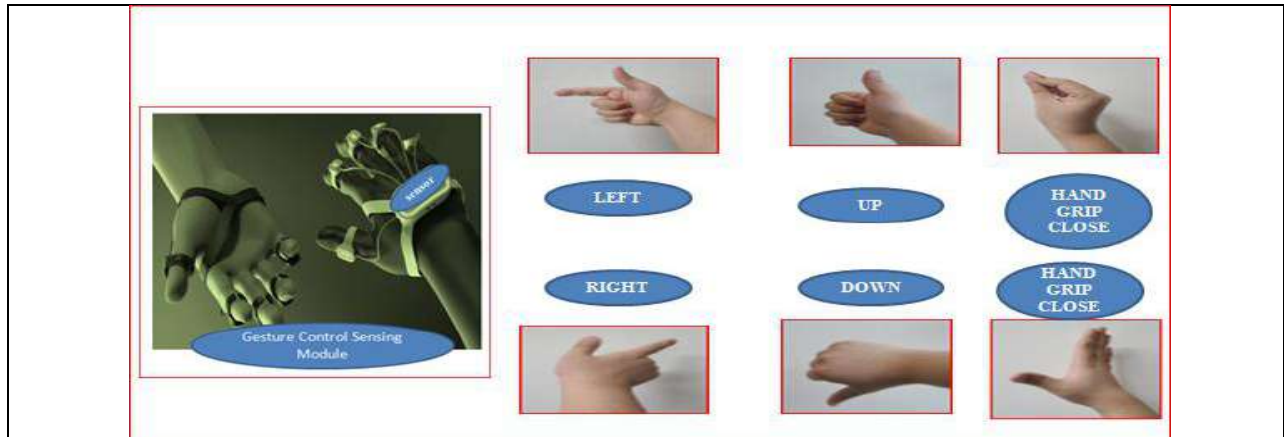


Figure 3: Gesture Control Robotic System based on hand movement.

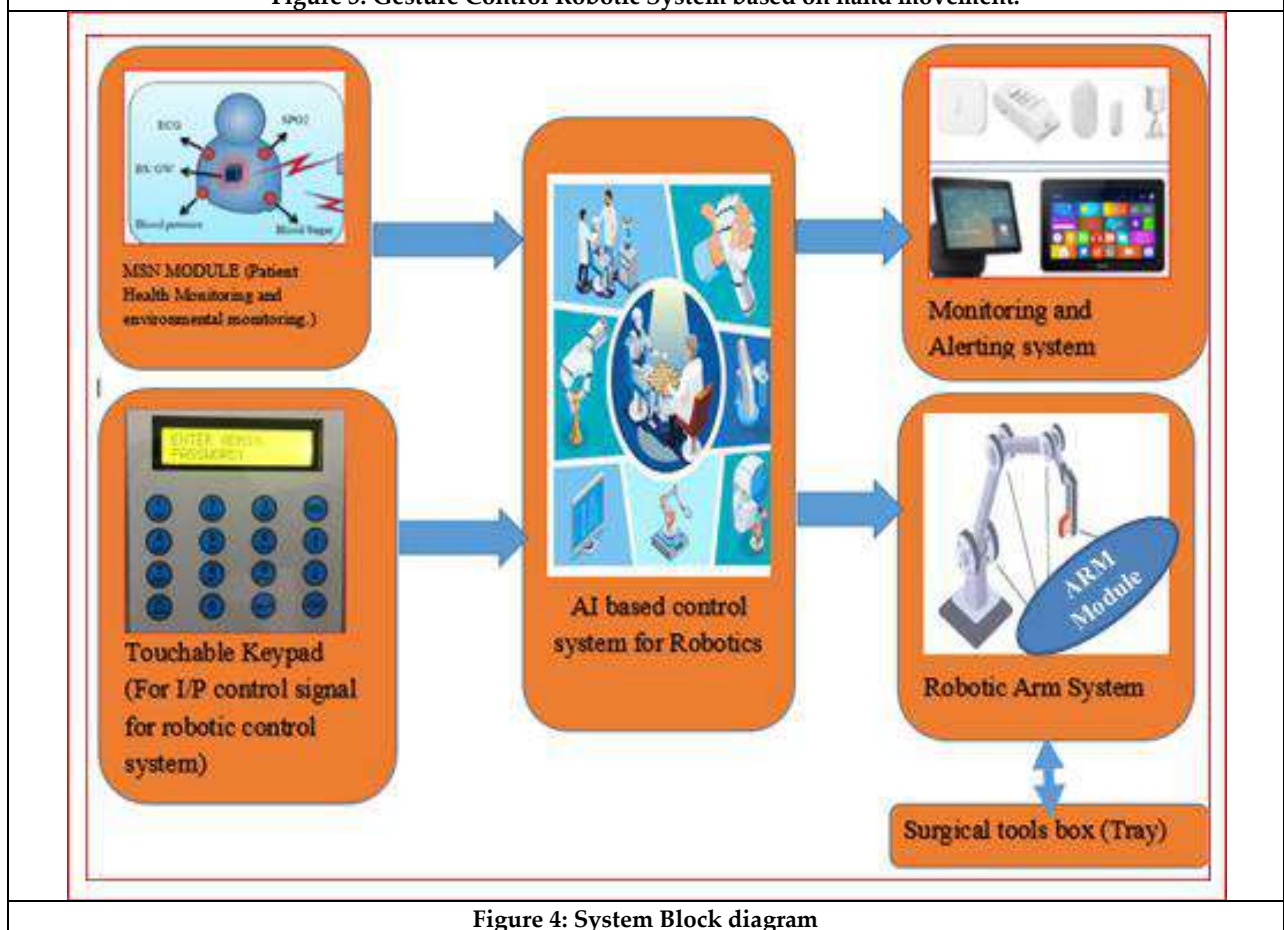


Figure 4: System Block diagram



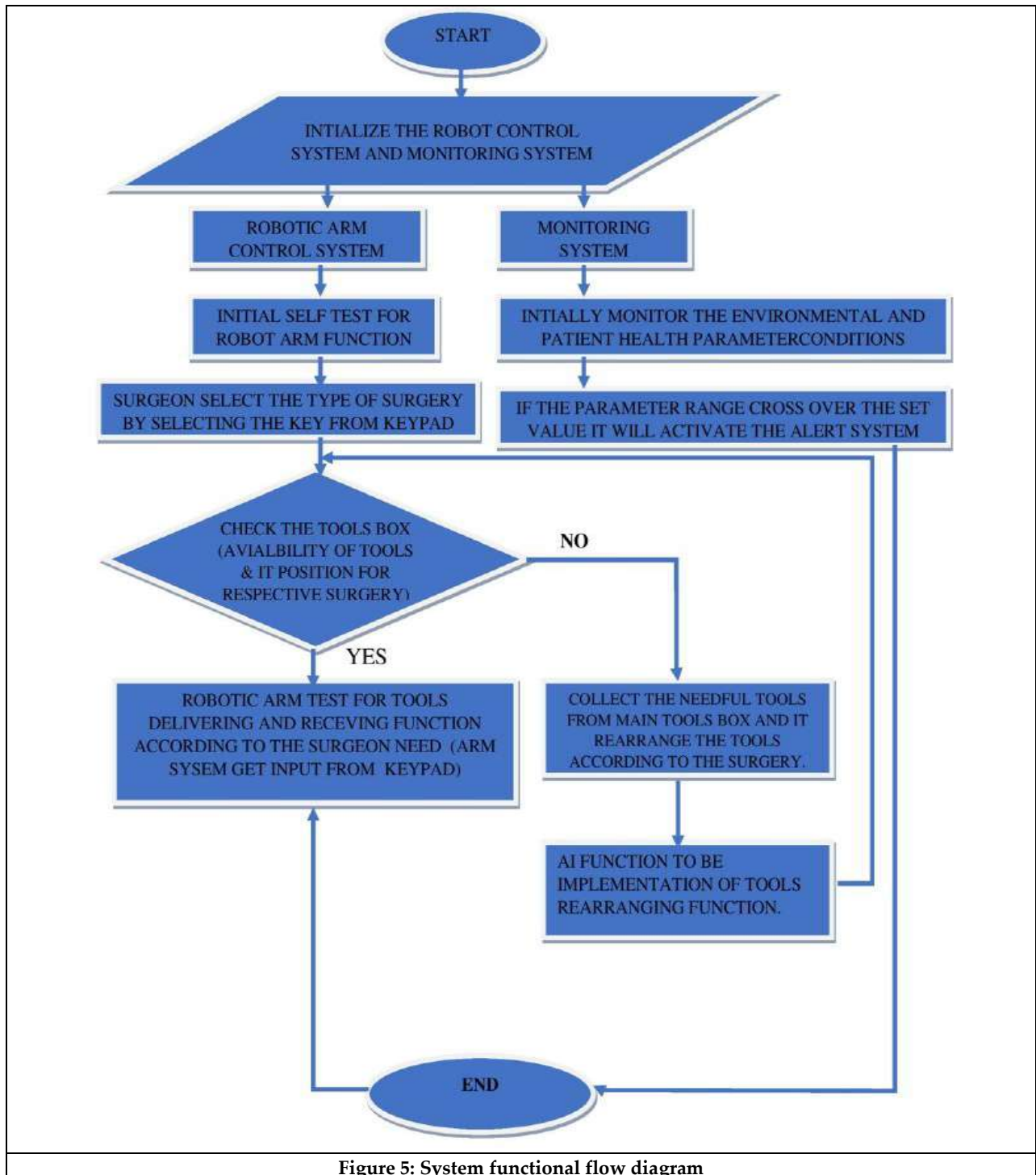


Figure 5: System functional flow diagram





## Heavy Metal Analysis of Siddha Poly Herbal Formulation Karanthai Chooranam

M.SriSakthiLogisha<sup>1\*</sup>, G.Nivetha<sup>2</sup>, M.Mohamed Mustafa<sup>3</sup>, T.R.Siddiq Ali<sup>4</sup>, N.J. Muthukumar<sup>5</sup> and V.Mahalakshmi<sup>6</sup>

<sup>1</sup>Ph.D Scholar, Department of Sirappu Maruthuvam, National Institute of Siddha, (Affiliated to The TamilNadu Dr MGR Medical University), Chennai, Tamil Nadu, India.

<sup>2</sup>Assistant Professor, Department of Varmam Maruthuvam National Institute of Siddha, (Affiliated to The TamilNadu Dr MGR Medical University), Chennai, Tamil Nadu, India.

<sup>3</sup>Professor, Department of Varmam Maruthuvam, Govt. Siddha Medical College, (Affiliated to The TamilNadu Dr MGR Medical University), Chennai, Tamil Nadu, India.

<sup>4</sup>Associate Professor, Department of Varmam Maruthuvam, Govt. Siddha Medical College, (Affiliated to The TamilNadu Dr MGR Medical University), Chennai, Tamil Nadu, India.

<sup>5</sup>Director General, Central Council for Research in Siddha, (Affiliated to The TamilNadu Dr MGR Medical University), Chennai, Tamil Nadu, India.

<sup>6</sup>Professor, Department of Siddhar Yoga Maruthuvam, National Institute of Siddha, (Affiliated to The TamilNadu Dr MGR Medical University), Chennai, Tamil Nadu, India.

Received: 31 July 2024

Revised: 12 Oct 2024

Accepted: 20 Nov 2024

### \*Address for Correspondence

**M.SriSakthiLogisha**

Ph.D Scholar, Department of Sirappu Maruthuvam,  
National Institute of Siddha,  
(Affiliated to The TamilNadu Dr MGR Medical University),  
Chennai, Tamil Nadu, India.



This is an Open Access Journal / article distributed under the terms of the **Creative Commons Attribution License** (CC BY-NC-ND 3.0) which permits unrestricted use, distribution, and reproduction in any medium, provided the original work is properly cited. All rights reserved.

### ABSTRACT

Heavy metal analysis, phytochemical screening, and aflatoxin estimation were carried out in Karanthai Chooranam, a Siddha polyherbal formulation. This study examines the nature of raw ingredients, which were properly sourced, purified, and processed through traditional Siddha methods. Atomic Absorption Spectrometry (AAS) used for the analysis of heavy metals showed that mercury, lead, and cadmium levels were all below the detectable limit. The arsenic content, on the other hand, was found to be at 0.70 ppm, thus far from the permissible limit of 3 ppm. Phytochemical evaluation by TLC and HPTLC revealed six major phytochemical peaks. Among these, peaks 5 and 6 represented the most significant bioactive compounds. Results of aflatoxin analysis indicated minimal presence of Aflatoxin B2 0.11 ppm, within the permissible limit of 0.1 ppm, while Aflatoxins B1, G1, and G2 were not detected. From these results, Karanthai Chooranam can be characterized as rich in a complex phytochemical profile that suggests therapeutic potential, while being safe regarding heavy metals and aflatoxins. Thus, the study suggests that this







SriSakthiLogisha et al.,

formulation can be safely used in traditional Siddha medicine and consumed for its medicinal properties. Further research is recommended to correlate the phytochemical profile with therapeutic efficacy.

**Keywords:** Karanthai Chooranam, Standardization, Herbal Drug, Physicochemical, Phytochemical

## INTRODUCTION

India is a mother hub for the development of Ayurveda, Unani, Siddha, Homoeopathy and other natural herbs-based health science (Ayush). Ayush Pharmaceutical industry is having great potential and opportunities for development in future. Mainly in following herbal medicinal plants and their value-added products well accepted in domestic and international market [1]. Siddha system of medicine, which is the traditional heritage science of Tamil origin, renders the application of numerous medicines based on plants, minerals-metals and animal origin [2]. World Health Organization (WHO) stresses the importance of the qualitative and quantitative methods for characterizing the samples, quantification of the biomarkers and/ or chemical markers and the fingerprint profiles. If a principle active component is known, it is most logical to quantitate this compound. Where active ingredients contributing to therapeutic efficacy are known botanical preparations should be standardized to these compounds. Where the active ingredients are not yet known a marker substance which should be specific for the botanical could be chosen for analytical purpose [3]. Herbal medication as the major remedy in the traditional system of medicine has been used in medical practices since antiquity. The Siddha system is one of the traditional systems of medicine which is flourished in southern India, especially Tamil Nadu. In the Siddha system besides herbs, metals and mineral drugs were used as medicine in 32 subdivisions [4]. The mode of preparation and plant used in traditional medicine varies from place to place. The traditional system of medicine became significantly more popular all over the globe because of its curative property, less toxicity and minimal side effects. Hence most of the Siddha formulations are herbal and polyherbal formulations. Central Council for Research in Ayurveda and Siddha has provided proforma for each category of medicine [5]. Standardization of formulation was done based on its macroscopic and microscopic characters, Physico-Chemical Parameters, Phyto Chemical Screening, Fluorescence studies and Thin Layer Chromatography Analysis. Phytochemical screening has shown the presence of Alkaloids, Glycosides, Saponins, Phytosterols, Fixed Oil, Resins, Phenols, Flavonoids and Tannins. ochemical, Phytochemical

## MATERIALS AND METHODS

### Selection of Source of Drugs

The raw drugs were procured from the raw drug shop R.N. Rajan and Co, Chennai. After proper authentication by the Medicinal Botanist, Govt. Siddha Medical College, Arumbakkam, Chennai, the preparation was made.

### Purification of Raw Drugs

All herbal drugs are purified as mentioned in the text Gunapaadam Mooligai Vaguppu<sup>7</sup>.

### Ingredients [8] Table 1.

#### SOP for Karanthai Chooranam Procedure

All the raw drugs were purified as per traditional text and powdered followed by the procedure *Vasthrakayam* to get a fine powder. The final product was stored in an air tight container.

### Heavy Metal Analysis [16 – 17]

Methodology Atomic Absorption Spectrometry (AAS) is a very common and reliable technique for detecting metals and metalloids in environmental samples. The total heavy metal content of the sample was performed by Atomic Absorption Spectrometry (AAS) Model AA 240 Series. In order to determination the heavy metals such as mercury, arsenic, lead and cadmium concentrations in the test item. Sample Digestion Test sample was digested with 1mol/L







HCl for determination of arsenic and mercury. Similarly for the determination of lead and cadmium the sample were digested with 1mol/L of HNO<sub>3</sub>. Standard preparation As& Hg- 100 ppm sample in 1mol/L HCl Cd &Pb- 100 ppm sample in 1mol/L HNO<sub>3</sub>

### TLC AND HPTLC ANALYSIS [18].

#### TLC Analysis

Test sample was subjected to thin layer chromatography (TLC) as per conventional one dimensional ascending method using silica gel 60F254, 7X6 cm (Merck) were cut with ordinary household scissors. Plate markings were made with soft pencil. Micro pipette were used to spot the sample for TLC applied sample volume 10-micro liter by using pipette at distance of 1 cm at 5 tracks. In the twin trough chamber with different solvent system Toulene: Ethyl Acetate: Acetic Acid (1.5:1:0.5) After the run plates are dried and was observed using visible light Shortwave UV light 254nm and light long-wave UV light 365 nm

#### High Performance Thin Layer Chromatography Analysis

HPTLC method is a modern sophisticated and automated separation technique derived from TLC. Pre-coated HPTLC graded plates and auto sampler was used to achieve precision, sensitive, significant separation both qualitatively and quantitatively. High performance thin layer chromatography (HPTLC) is a valuable quality assessment tool for the evaluation of botanical materials efficiently and cost effectively. HPTLC method offers high degree of selectivity, sensitivity and rapidity combined with single-step sample preparation. In addition it is a reliable method for the quantitation of Nano grams level of samples. Thus this method can be conveniently adopted for routine quality control analysis. It provides chromatographic fingerprint of phytochemicals which is suitable for confirming the identity and purity of medicinal plant raw materials. Plates were scanned under UV at 366nm. The data obtained from scanning were brought into integration through CAMAG software. Chromatographic finger print was developed for the detection of Phyto constituents present in each extract and Rf values were tabulated.

#### AFLO Toxin Assay

Standard Aflatoxin was applied on to the surface to pre coated TLC plate in the volume of 2.5 µL, 5 µL, 7.5 µL and 10 µL. Similarly the test sample was placed and Allow the spots to dry and develop the chromatogram in an unsaturated chamber containing a solvent system consisting of a mixture of chloroform, acetone and isopropyl alcohol (85:10: 5) until the solvent front has moved not less than 15 cm from the origin. Remove the plate from the developing chamber, mark the solvent front and allow the plate to air-dry. Locate the spots on the plate by examination under UV light at 365 nm.

## RESULTS

Determination of heavy metals in polyherbal formulation is one of the major concern for consumption which are prone to adulteration and contamination. The heavy metal analysis of *Karanthaichooranam* reveals that the presence of heavy metals like Mercury, Lead, Arsenic and Cadmium are below detected limit as per AYUSH (Table 2).

#### TLC and HPTLC Analysis

The Peak Table of HPTLC finger printing analysis (picture 4) of the sample KC reveals the presence of six prominent peaks corresponds to presence of six versatile Phyto components present within it. Rf value of the peaks ranges from 0.12 to 0.74. Further the peak 5 and 6 occupies the major percentage of area of 44.39 and 26.95 % which denotes the abundant existence of such compound. Followed by this peak 2 and 3 occupies the percentage area of 10.03 and 8.87%. Aflatoxins are poisonous secondary metabolites found in contaminated herbal drugs. The result reveals that there was no spots were identified in the test sample loaded on TLC plates with respect to Aflatoxin B1, G1 and G2 when compare to standard. Whereas presence of Aflatoxin B2 were identified. This level of B2 seems to be within the limit prescribed by the AYUSH (Table 3).





## DISCUSSION

The heavy metal analysis and phytochemical evaluation of Karanthai Chooranam, a Siddha polyherbal formulation, provide critical insights into its safety, efficacy, and quality. The study aimed to assess the levels of toxic heavy metals, identify phytochemicals, and detect potential aflatoxin contamination to ensure the formulation meets safety and quality standards.

### Heavy Metal Analysis

The analysis of heavy metals in Karanthai Chooranam revealed that the concentrations of mercury, lead, arsenic, and cadmium were either below the detection limit or within the permissible limits established by AYUSH standards. Specifically, mercury and lead were below detection limits, which indicates that the formulation is free from these toxic elements. Arsenic, though detected, was found at a concentration of 0.70 ppm, well below the maximum limit of 3 ppm. Cadmium was present at 0.005 ppm, a value that is significantly lower than the detection limits for this metal. These results are particularly reassuring because heavy metal contamination is a common concern in herbal medicines, which can have serious health implications if not controlled. The low levels or absence of these metals in Karanthai Chooranam suggest that the formulation is safe for use from a heavy metal toxicity perspective. This is consistent with traditional Siddha practices that emphasize careful preparation and purification of raw materials to avoid contamination.

**Phytochemical Analysis:** The Thin Layer Chromatography (TLC) and High-Performance Thin Layer Chromatography (HPTLC) analyses were instrumental in profiling the phytochemicals present in Karanthai Chooranam. TLC provided an initial qualitative assessment of the phytochemical profile, revealing distinct spots indicative of the presence of various compounds. The HPTLC analysis, on the other hand, offered a more detailed and quantitative view of the phytochemical constituents. The presence of six prominent peaks, with R<sub>f</sub> values ranging from 0.12 to 0.74, suggests a complex mixture of bioactive compounds. Peaks 5 and 6, which occupy significant percentages of the chromatographic area (44.39% and 26.95%, respectively), likely represent the major active constituents in the formulation. The identification and quantification of these peaks can help in understanding the formulation's therapeutic efficacy and ensure consistency in quality.

### Aflatoxin Analysis

Aflatoxins are carcinogenic compounds that can contaminate herbal medicines, posing a significant health risk. In this study, the absence of aflatoxins B1, G1, and G2, with only a minimal presence of aflatoxin B2, is noteworthy. Aflatoxin B2 was detected at 0.11 ppm, which is just above the permissible limit of 0.1 ppm. However, this level is still relatively low and does not pose a significant health risk, especially when compared to higher permissible limits in other pharmacopoeias.

## CONCLUSION

The comprehensive analysis of Karanthai Chooranam confirms that the formulation is within safe limits for heavy metals and aflatoxins, supporting its safety for consumption. The detailed phytochemical profile obtained through TLC and HPTLC underscores the formulation's complexity and the presence of potentially therapeutic compounds. These findings not only validate the traditional preparation methods and safety standards but also provide a foundation for further research into the efficacy and quality control of Siddha formulations. Future studies could focus on correlating the phytochemical profile with specific therapeutic outcomes and exploring the mechanisms of action of the major constituents identified in this study. Overall, Karanthai Chooranam demonstrates a promising profile, supporting its continued use in traditional Siddha medicine with assured safety and efficacy.





## REFERENCES

1. Rohit Kumar Bijauliya\*, ShashiAlok, Dilip Kumar ChanchalAndMayankKumar,A Comprehensive Review On Standardization Of Herbal Drugs, International Journal OfPharmaceutical Sciences And Research.
2. A. Rajendra Kumar, N. J. Muthukumar, A. Faridha. Neermullikudineer – A Classical Polyherbal Decoction in Siddha System of Medicine. Research J. Pharm. and Tech 2019; 12(1): 445-460. doi: 10.5958/0974-360X.2019.00081.7
3. Dixit VK and Yadav NP: Recent approaches in herbal drug standardization. IntegrBiol, 2008; 2 (3): 195-203
4. ThiyagarajanR.SiddhaSirappumaruthuvam,Chennai;DepartmentofIndian medicine &Homoeopathy, 1<sup>st</sup>2009
5. Anonymous, Pharmacopoeial Standards for Ayurvedic Formulations, Central Council for Research in Ayurveda and Siddha, Ministry of Health & Family Welfare, Govt. of India, New Delhi, (1987)
6. Shrikumar S, Maheswari MU, Suganthi A, Ravi TK. WHO guidelines for Herbal Drugs standardization. [ast accessed on 2009 Sep 22]. Available from: <http://www.pharmainfo.net/exclusive/reviews> . [Ref list]
7. Murugesamudalier KS, GunapadamMooligaiVaguppu, Fourth edition, Publisher; Tamilnadu Siddha Medical Council, Chennai, 1988
8. K.a.Maduraimuthaliyar,Agasthiyamunivararulaseitharathina surukam-360,shanmuganantha boothagasalai park town,chennai -3
9. Shunmugaram S. Physiochemical and Acute Toxicity Analysis of a Siddha Herbo-Mineral Formulation – PachaiKarpooraVadagam (PKV). Research J. Pharm. and Tech 2019; 12(1): 227-230. doi: 10.5958/0974-360X.2019.00042.8
10. Wallis TE. Text Book of Pharmacognosy. 5th ed. New Delhi: CBS Publishers and Distributors; 2004. p. 578. [Google Scholar] [Ref list]
11. Rajani M, Kanaki NS. Phytochemical Standardization of Herbal Drugs and Polyherbal Formulations, Bioactive Molecules and Medicinal Plants. Berlin, Heidelberg: Springer; 2008. pp. 349–69. [Google Scholar] [Ref list]
12. Lachman L, Liberman HA, Kanig JL. The Theory and Practice of Industrial Pharmacy. 3rd ed. Mumbai: Varghese Publishing House; 1991. p. 67. [Google Scholar] [Ref list]
13. Indian Herbal Pharmacopoeia, Indian Drug Manufacturers’ Association. Revised ed. 2002. pp. 493–4. [Google Scholar] [Ref list]
14. Mukharjee PK. Quality Control of Herbal Drugs. New Delhi: Business Horizons Pharmaceutical Publishers; 2008. p. 189. [Google Scholar] [Ref list]
15. Vijayalakshmi A, Selvakannan A. Ajith SP. Phytochemical and Physiochemical Standardization of a Siddha Formulation SeenthilChooranam. Research J. Pharm. and Tech. 2018; 11(1): 23-26. doi: 10.5958/0974-360X.2018.00004.5
16. Kennedy JF, Thorley M. Pharmacognosy, Phytochemistry, Medicinal Plants. 2nd ed. Paris: Jean Brueton; Lavoisier Publishing; 2000. Carbohydrate polymers; pp. 428–9. [Google Scholar] [Ref list]
17. S. S. Alwakeel, “Microbial and heavy metals contamination of herbal medicines,” Research Journal of Microbiology, vol. 3, no. 12, pp. 683–691, 2008.
18. Espinoza EO, Mann MJ, Bleasdel B, DeKorte S, Cox M. Toxic metals in selected traditional Chinese medicinals. J Forensic Sci. 1996;41:453–6. [Google Scholar] [Ref list]
19. Anonymous, Quality standards of Indian medicinal plants, vol-1,(Indian council of medical research, New Delhi, 2003) 10–50.

**Table 1. Ingredients**

S.No	Ingredients	Quantity (grams)
1	<i>Spheranthus indicus</i>	1 Balam(35 grams)
2	<i>Nigella Sativa</i>	1 Balam(35 grams)
3	<i>Terminalia bellirica</i>	1 Balam(35 grams)
4	<i>Acorus calamus</i>	1 Balam(35 grams)
5	<i>Piper longum</i>	1 Balam(35 grams)
6	<i>Piper nigrum</i>	1 Balam(35 grams)





**SriSakthiLogisha et al.,**

7	<i>Celastrus paniculatus</i>	1 Balam(35 grams)
8	Rock Salt	1 Balam(35 grams)
9	<i>Costus speices</i>	1 Balam(35 grams)
10	<i>Zingiber officinale</i>	1 Balam(35 grams)
11	<i>Celotendrum serratum</i>	1 Balam(35 grams)
12	<i>Psoralea corylifolia</i>	1 Balam(35 grams)
13	<i>Plumbago zeylanica</i>	1 Balam(35 grams)
14	<i>Terminalia chebula</i>	1 Balam(35 grams)


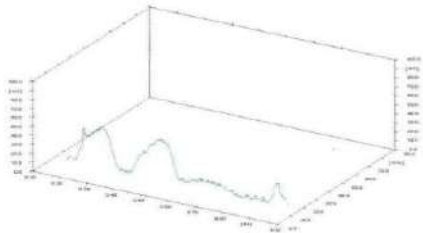
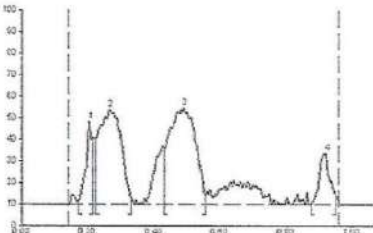
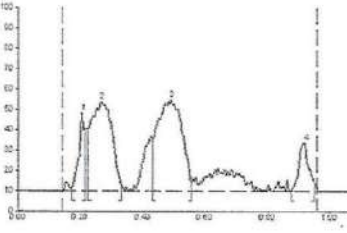
**Table 2: Shows the heavy metal analysis of Karanthai Chooranam**

Name of The Heavy Metals	Absorption Max $\Delta$ Max	Result Analysis	Maximum Limit
Mercury	253.7 nm	BDL	1 ppm
Lead	217.0 nm	BDL	10 ppm
Arsenic	193.7 nm	0.70	3 ppm
Cadmium	228.8 nm	0.005	-

**Table 3 shows the Aflatoxin level in KaranthaiChooranam**

Aflatoxins	Presence	Limits
Aflatoxin B1	Not Detected	0.5 ppm
Aflatoxin B2	0.11 ppm	0.1 ppm
Aflatoxin G1	Not Detected	0.5 ppm
Aflatoxin G2	Not Detected	0.1 ppm

Peak	Start Rf	Start Height	Max Rf	Max Height	Max %	End Rf	End Height	Area	Area %
1	0.17	2.2	0.21	38.3	25.39	0.22	31.1	632.5	9.16
2	0.23	31.0	0.27	43.9	29.06	0.33	2.7	2503.0	36.26
3	0.43	25.8	0.49	45.0	29.80	0.56	3.8	3114.2	45.11
4	0.68	0.1	0.92	23.8	15.75	0.95	5.0	654.0	9.47

	
<p>Picture 1 Shows TLC Analysis at 366 nm</p>	<p>Picture 2 Shows Track at All Wave length</p>
	
<p>Picture 3 Shows HPTLC finger printing of Sample Karanthai chooranam(KC)</p>	<p>Picture 4 Shows Peak Table</p>





## A Review on the Effect of Advanced Glycation End Products on Adolescents

Juhi Punjabi<sup>1</sup> and Sarala Premkumar<sup>2</sup> and A. J. Hemamalini<sup>3</sup>

<sup>1</sup>Ph.D Research Scholar, Department of Clinical Nutrition, Sri Ramachandra Institute of Higher Education and Research, Porur, Chennai, Tamil Nadu, India.

<sup>2</sup>Associate Professor, Department of Paediatrics, Sri Ramachandra Institute of Higher Education and Research, Porur, Chennai, Tamil Nadu, India.

<sup>3</sup>Professor and Head, Department of Clinical Nutrition, Sri Ramachandra Institute of Higher Education and Research, Porur, Chennai, Tamil Nadu, India.

Received: 13 Jun 2024

Revised: 03 Aug 2024

Accepted: 17 Oct 2024

### \*Address for Correspondence

**A.J.Hemamalini**

Professor and Head,

Department of Clinical Nutrition,

Sri Ramachandra Institute of Higher Education and Research,

Porur, Chennai, Tamil Nadu, India.

E. Mail: hemamalini.aj@sriramachandra.edu.in



This is an Open Access Journal / article distributed under the terms of the **Creative Commons Attribution License** (CC BY-NC-ND 3.0) which permits unrestricted use, distribution, and reproduction in any medium, provided the original work is properly cited. All rights reserved.

### ABSTRACT

**Purpose:** Advanced glycation end products (AGE) are a group of amalgamated compounds of protein and fat possessing various deleterious effects including non-communicable diseases. Adolescents are exposed to high serum AGE levels due to the rapid consumption of junk foods. Hence, this category of the population is at an increased risk of developing metabolic illnesses in the future. **Methods** Literature search was done on electronic databases like PubMed and Scopus employing keywords such as AGE and Adolescents, AGE and Obesity, AGE and Diabetes mellitus etc. A total of 117 articles were looked upon and after assessing for eligibility 14 articles were included as part of the review. Results AGE had shown to possess harmful effects on the adolescent population by the development of chronic metabolic diseases with the focus on diabetes mellitus, Obesity, and abnormal thyroid functioning. It was also observed that incidences of obesity reported among adolescents showed elevated serum AGE and Serum CML levels predisposing to the fact that AGE can be trapped in the fat stored cells or tissues. Exogenous or dietary AGE had an additional load on the AGE pool in vivo leading to the occurrence of various metabolic diseases. Few studies have shown the dependency of age and presence of obesity as risk factors for the development of AGE among adolescents. **Conclusion** Limited number of studies have focused on the impact of AGE among adolescents and hence, this review throws light upon the harmful effects of AGE in the context of adolescent health.

**Keywords:** Advanced glycation end products, Obesity, Diabetes mellitus, Adolescents, Carboxymethyllysine, Exogenous.







## INTRODUCTION

Advanced glycation end products (AGEs) are a diverse group of compounds produced when reducing sugars react with amine groups linked to proteins, nucleotide bases or fatty acids, forming glycosylated products.[1] AGEs are produced by Maillard reaction where the mixtures of amino acid and sugar become brown upon heating.[2]. Maillard reaction (non-enzymatic glycation or browning) in foods has been well studied by the food industry to control food quality. However, it is only 40 years ago that a similar glycation process was recognized in human body by the observation of increased formation of glycosylated haemoglobins in diabetic patients [3] which leads to the formation of detrimental advanced glycation end products (AGEs) in humans.[4] In addition to AGE's being derived from within the body, AGEs also exist in foods. Uncooked animal derived foods and foods cooked at higher temperature have naturally present AGEs [5]. Exogenous dietary AGEs have been suggested to increase the in vivo pool of AGEs after intestinal absorption, and contribute to the development of diabetes and related complications. [6] The adolescence period witnesses multiple changes ranging from physiological changes- Rapid growth spurt, Puberty, Psychological changes- Thought process and Psychosocial changes- Personality and attitudes. Behavioural establishments also occur during this transitioning age, where eating choices are also established. [7]

Adolescents consume approximately 20% of their daily energy intake as snacks, with salty and sweet foods contributing a majority of the snacking calories directly proportional to the development of overweight and obesity status among them. Alarming increases are observed in the prevalence of obesity in children, with 32% of children and adolescents in the United States at or above the eighty-fifth percentile. [8]. In a study conducted in India to determine the prevalence of obesity among children and adolescents, it was noted that higher rates of obesity were prevalent among the adolescents than children. [9]. The consumption of processed foods is increasing among adolescents which is associated with increased exposure to dietary advanced glycation end products hence putting them at an increased risk of metabolic and cardiovascular events in the future. [10]. Thus, an interest in adolescent nutrition and health has expanded rapidly in recent years, in part due to the realization that investing in adolescent health, nutrition, and well-being may accelerate progress toward the Sustainable Development Goals.[11] Limited studies have focussed on the impact of AGE on the adolescent population, providing an area of interest yet to be established. Hence, the objectives of the current review is to explore the effect of advanced glycation end products on adolescent health and also highlight upon the metabolic complications which occur as a cascading effect of AGE on the future generation of the country.

### Methods

#### Search Strategy

A thorough search on electronic databases like PubMed and Scopus were conducted. The time period of the articles was restricted to 10 years. The keywords used for the article search were as follows:- Advanced glycation end products and obesity, Advanced glycation end products and Type I Diabetes mellitus, Advanced glycation end products and Adolescents, Advanced glycation end products and insulin resistance, AGE and Adolescents, AGE and Obesity, AGE and Type-I DM, AGE and Insulin resistance, Dietary AGE and adolescents, CML and Adolescents, Fluorescent AGE and adolescents, Carboxymethyllysine and Obesity, CML and obesity, Carboxymethyllysine and Insulin resistance, AGE and metabolic syndrome. All English language articles were included.

### Ethical Issues

Not applicable





**Juhi Punjabi et al.,****Selection Criteria**

Studies involving the harmful effects of AGE on adolescent health and metabolic diseases per se were included. The type of articles was restricted to invitro studies, original articles, in vivo and human studies. Research Note and commentaries were excluded from the search. Few articles were excluded as they did not meet the eligibility criteria. A schematic representation of the articles selected had been mentioned in *figure 1*.

**Impact of Advanced Glycation End Product on Adolescents**

Adolescence is a period of rapid growth and psychological changes. During this age, independent decisions regarding social groups, behavioural establishments and food choices occur.[12] The environment of the adolescents plays a major role for choosing the right foods for consumption. In the recent years, various Food Swamps are located at proximity in campuses of schools and other educational institutions, which provide means of consuming these unhealthy processed foods. [13] Dietary Advanced glycation end products primarily found in foods subjected to high temperature cooking techniques i.e., processed and junk foods have deleterious effects on the metabolic parameters among individuals. The consumption of highly processed foods are critical among the adolescents making them exposed to a series of lifestyle diseases. Table I illustrates the studies in relation to the presence of AGE and its effect on the adolescent health. It was observed, that increased levels of fasting glucose, Triglycerides, LDL and Blood pressure were present among adolescents with an elevated dAGE consumption indicating a pathophysiological relationship between dAGE and metabolic parameters. (Fig II)

A study done on seventy-four overweight adults who were administered to consume a low AGE diet for a duration of 4 weeks had decreased levels of fasting glucose and insulin levels compared to the high AGE diet group, proving a direct relationship between exogenous AGE consumption and insulin resistance.[14] A similar study found an interesting theory correlating the level of FT4 and Serum AGE in adolescents showing a positive significance between these components. Hence, this acts as evidence to prove the improper functioning of the thyroid gland can be attributed to elevated glycated end products in the blood.[15] Due to the AGE-RAGE interaction, various compounds such as Interleukin-6, Tumour necrosis factor alpha (TNF) are expressed leading to proliferation, cell differentiation and cell mitosis and hence causing tremendous changes in the cell membrane which can directly have an impact on the thyroid gland. [16] Adolescents are at higher risk of AGE compared to adults as reported by increased serum CML levels. Obesity was shown to have a larger contribution towards a steady increase in AGE due to the presence of inflammation and trapping of CML in the adipose tissues. [17]. Very limited studies have highlighted the effect of AGE among adolescents, predisposing them to develop metabolic complications in the future.

**Effect Of Diabetes Mellitus on Advanced Glycation End Products**

Table II represents the articles on advanced glycation end products and metabolic complications. Adolescents diagnosed with Type-I DM had increased odds of dramatically high serum AGE levels as compared to healthy individuals. This is in accordance to a mechanism which directly affects the insulin hormone causing an upregulation in the glucose uptake thereby leading to hyperglycaemia. Another theory postulates, the overexpression of RAGE and SIRT1 in the presence of AGE which causes changes in the insulin leading to diabetes mellitus.[19] An interesting observation was noted in adolescents where, an increase in age had a direct effect on the AGE Levels. *Galler et al, 2003* studied that adolescents in the age group of 16 years had elevated AGE levels than adolescents in the age group of 13 years and below. In addition to Age, serum Lipid, BMI and Weight also had a directly proportional relationship with AGE among the adolescents. [20] Previous literature has highlighted the nature of hba1c which serves as an indicator for glycaemic monitoring and is also regarded as a glycated compound thus possess a history with AGE.[21] *Kostolanská et al, 2009* determined significant correlations between hba1c and serum AGE in a group of poorly controlled diabetic adolescents indicating oxidative stress and glycation end products as contributors towards diabetic complications in the future. [22]

A study implicated the various risks involved around high AGE levels which directly cause microvascular complications such as retinopathy, nephropathy, and neuropathy among adolescents. [23] Studies have also observed differences between AGE levels in obesity and type-1 DM individuals where a marked degree of



**Juhi Punjabi et al.,**

comparison was observed between both the groups. The Type-1 DM adolescents had elevated AGE levels than the obese adolescents, which showcased high cardiac parameters in the latter. Gender also played a pivotal role in AGE measures. The Female population was noted with elevated AGE levels than the males. This can be attributed to the fat percentage usually higher among the female population. [24]

**Effect Of Obesity on Advanced Glycation End Products**

The formation of AGE is accelerated in various inflammatory conditions, the primary example including obesity. The adiposity deposition in various tissues of the body is a matter of concern for the adolescents. Table III illustrates the effect of obesity among adolescents on advanced glycation end products. Obese adolescents have higher incidences of developing chronic metabolic conditions. The receptor for AGE (RAGE) is considered as one of the factors causing these complications. The linkage between AGE, RAGE and obesity is not well known, but few studies have shown an inverse relationship between them. *Norata et al*, demonstrated a similar finding in the adult population. In this study, BMI was considered as a predictive measure for sRAGE levels in terms of obesity indices. [25] *Chih-Tsueng He et al*, however observed a significant relationship between plasma RAGE and metabolic syndrome components, illustrating an increase in AGE leads to diabetic and cardiovascular consequences in the future. [26] Along with endogenous AGE, consumption of Dietary AGE has deleterious effects among adolescents causing an early carotid intima thickness and arterial stiffness. *Saha et al*, observed an increase in DAGE consumption among obese adolescents and a significant relationship between dAGE and metabolic compounds.[27]

*Rodríguez-Morteraa et al*, had a contrasting observation were, serum CML and Total AGE was decreased in obese adolescents but dAGE consumption was higher among them. [28] This can be attributed to the fact that fat mass or adipose tissue is inversely proportional to serum CML. This association could be explained by the deposition of CML in the adipose tissues regarded as hidden CML, thus non-reflecting the circulating total body CML. [29] Microinflammation as characterized by CRP levels were reported to be high among obese adolescents despite showing lower plasma CML levels. This is due to the fact that cytokine production such as the formation of IL-6, IL-1 is elevated in cases of increased adipocytes formation causing a rise in CRP levels.[30] In vitro studies done on animal model had shown the potential role of exogenous or diet derived AGE's inducing a microinflammation status in the rodents studied. [31] Oxidative stress is another compound which is elevated in obese individuals. Alongside, IL-6 and IL-1 there is another prominent predictor of oxidative stress which shares a similar characterization to advanced glycation end products. These are called as advanced oxidation protein products (AOPP). These protein oxidised compounds are increased during obesity and can be considered as an independent risk factor for metabolic syndrome in children or adolescents. [32] However, the role of triglycerides in exhibiting a significant correlation with AOPP has recently been reported. It has been studied, that oxidation of proteins is collateral with lipid peroxidation concluding an increase in TG levels during a high oxidative stress episode. [33]

Many studies have detected AGE through serum or plasma, but limited studies have focussed on non-invasive techniques in measuring AGE. One such technique involves the use of skin autofluorescence, where the deeper tissues of the skin have deposits of AGE which are detected under an AGE reader. [34] A study investigating SAF values on obese adolescents revealed a high skin AGE levels among obese subjects compared to lean controls. [35] it was also observed that duration of obesity plays an important role in SAF, i.e. morbid obesity showed high SAF values in comparison with short term obesity. Many contradicting factors arise involving skin autofluorescence. The skin type of the individuals i.e., Dark skin shows high AGE compared to lighter skin tones, appropriate technique to Measure SAF may vary, population of subjects- Asia, Hispanic, African American, White etc along with Age which also has a direct relationship with SAF. metabolic complications prominently cardiovascular disease and ESRD also play a significant role in higher SAF values among subjects. [36]





Juhi Punjabi et al.,

## CONCLUSION

This current review has highlighted upon the transitioning age group of adolescence and their exposure towards advanced glycation end products. The negative consequences such as development of cardiovascular and metabolic complications have been attributed solely due to an increase in dietary AGE consumption among the age group. Highly processed and high temperature cooking techniques have shown increases in Maillard reaction products leading to the formation of dietary AGE. Metabolic complications of AGE primarily focussed on diabetes mellitus and obesity which are commonly found among adolescents have been highlighted and show increases in HOMA-IR, LDL, Triglycerides, and anthropometric measures such as BMI and weight gain which have a direct relationship with glycation end products. Another interesting theory relates dimensional changes in the thyroid gland due to elevated AGE levels among adolescents. sRAGE (Receptor for AGE) after being attached to the AGE compound causes crosslinking of proteins which thus, was regarded as the main evil causing compound leading to metabolic diseases. Alongside, SRAGE there were other factors causing an increase in AGE, such as Age, BMI, Weight gain (Obesity), diagnostic procedures etc. Skin autofluorescence was a minimal non-invasive technique which had varying degrees of differentiation when analysed in darker skin tones and different races of the world making it an inaccurate diagnostic measure of AGE. Adolescents with a disease burden had increased exposure to AGE with an increase in CML levels compared to healthy controls. Hence, advanced glycation end products have negative consequences among the adolescent population and adequate steps should be taken to protect them for this glycated compound

## ACKNOWLEDGEMENT

Thankful to all the authors for their contribution in the dissemination of information and designing of the review article.

## REFERENCES

1. Davis KE, Prasad C, Vijayagopal P, Juma S, Imrhan V. Serum soluble receptor for advanced glycation end products correlates inversely with measures of adiposity in young adults. *Nutrition research*. 2014 Jun 1;34(6):478-85. DOI: 10.1016/j.nutres.2014.04.012
2. Hellwig M, Henle T. Baking, ageing, diabetes: a short history of the Maillard reaction. *Angewandte Chemie International Edition*. 2014 Sep 22;53(39):10316-29. DOI: 10.1002/anie.201308808
3. Rahbar S, Blumenfeld O, Ranney HM. Studies of an unusual hemoglobin in patients with diabetes mellitus. *Biochemical and biophysical research communications*. 1969 Aug 22;36(5):838-43. DOI: 10.1016/0006-291x(69)90685-8
4. Sharma C, Kaur A, Thind SS, Singh B, Raina S. Advanced glycation End-products (AGEs): an emerging concern for processed food industries. *Journal of food science and technology*. 2015 Dec 1;52(12):7561-76. DOI: 10.1007/s13197-015-1851-y.
5. Uribarri J, Woodruff S, Goodman S, Cai W, Chen X, Pyzik R, Yong A, Striker GE, Vlassara H. Advanced glycation end products in foods and a practical guide to their reduction in the diet. *Journal of the American Dietetic Association*. 2010 Jun 1;110(6):911-6. DOI: 10.1016/j.jada.2010.03.018
6. Uribarri J, Cai W, Sandu O, Peppas M, Goldberg T, Vlassara H. AGE content of various foods. *Ann NY Acad Sci*. 2005 Jun;1043:461-6.
7. Adolescence as a unique developmental period. *Journal of psychiatry & neuroscience: JPN*. 2015 Sep;40(5):291. DOI: 10.1503/jpn.150268
8. Field AE, Cook NR, Gillman MW. Weight status in childhood as a predictor of becoming overweight or hypertensive in early adulthood. *Obesity research*. 2005 Jan;13(1):163-9. DOI: 10.1038/oby.2005.21
9. Ameer SR, Ahmad SR, Chandrasekhar A. Assessment of Underweight and Its Determinants among School Going Adolescents in Hyderabad. *Indian Journal of Public Health Research & Development*. 2018;9(5):77-82.



**Juhi Punjabi et al.,**

10. Angoorani P, Ejtahed HS, Mirmiran P, Mirzaei S, Azizi F. Dietary consumption of advanced glycation end products and risk of metabolic syndrome. *International Journal of Food Sciences and Nutrition*. 2016 Feb 17;67(2):170-6. DOI: 10.3109/09637486.2015.1137889
11. Afshin A, Sur PJ, Fay KA, Cornaby L, Ferrara G, Salama JS, Mullany EC, Abate KH, Abbafati C, Abebe Z, Afarideh M. Health effects of dietary risks in 195 countries, 1990–2017: a systematic analysis for the Global Burden of Disease Study 2017. *The Lancet*. 2019 May 11;393(10184):1958-72. DOI: 10.1016/S0140-6736(19)30041-8.
12. Rosen DS. Physiologic growth and development during adolescence. *Pediatrics in Review*. 2004 Jun 1;25(6):194-200.
13. Cooksey-Stowers K, Schwartz MB, Brownell KD. Food swamps predict obesity rates better than food deserts in the United States. *International journal of environmental research and public health*. 2017 Nov;14(11):1366.
14. Mark AB, Poulsen MW, Andersen S, Andersen JM, Bak MJ, Ritz C, Holst JJ, Nielsen J, de Courten B, Dragsted LO, Bügel SG. Consumption of a diet low in advanced glycation end products for 4 weeks improves insulin sensitivity in overweight women. *Diabetes care*. 2014 Jan 1;37(1):88-95.
15. Aversa T, Ruggeri RM, Corica D, Cristani MT, Pepe G, Vicchio TM, Alibrandi A, Trimarchi F, Cannavò S, Pajno GB, Wasniewska MG. Serum levels of soluble receptor for advanced glycation end products are reduced in euthyroid children with newly diagnosed Hashimoto's thyroiditis: A pilot study. *Hormone Research in Paediatrics*. 2021 Aug 25;94(3-4):144-50.
16. Bronowicka-Szydełko A, Kotyra Ł, Lewandowski Ł, Gamian A, Kustrzeba-Wójcicka I. Role of advanced glycation end-products and other ligands for age receptors in thyroid cancer progression. *Journal of Clinical Medicine*. 2021 Sep 10;10(18):4084.
17. Garay-Sevilla ME, Torres-Graciano S, Villegas-Rodríguez ME, Rivera-Cisneros AE, Wrobel K, Uribarri J. Advanced glycation end products and their receptors did not show any association with body mass parameters in metabolically healthy adolescents. *Acta Paediatrica*. 2018 Dec;107(12):2146-51.
18. Gill V, Kumar V, Singh K, Kumar A, Kim JJ. Advanced glycation end products (AGEs) may be a striking link between modern diet and health. *Biomolecules*. 2019 Dec 17;9(12):888.
19. Nowotny K, Jung T, Höhn A, Weber D, Grune T. Advanced glycation end products and oxidative stress in type 2 diabetes mellitus. *Biomolecules*. 2015 Mar 16;5(1):194-222.
20. Galler A, Müller G, Schinzel R, Kratzsch J, Kiess W, Münch G. Impact of metabolic control and serum lipids on the concentration of advanced glycation end products in the serum of children and adolescents with type 1 diabetes, as determined by fluorescence spectroscopy and N ε-(carboxymethyl) lysine ELISA. *Diabetes Care*. 2003 Sep 1;26(9):2609-15.
21. Rezaei M, Rabizadeh S, Mirahmad M, Hajmiri MS, Nakhjavani M, Hemmatabadi M, Shirzad N. The association between advanced glycation end products (AGEs) and ABC (hemoglobin A1C, blood pressure, and low-density lipoprotein cholesterol) control parameters among patients with type 2 diabetes mellitus. *Diabetology & Metabolic Syndrome*. 2022 Dec;14(1):1-0.
22. Kostolanská J, Jakuš V, Barak L. Monitoring of early and advanced glycation in relation to the occurrence of microvascular complications in children and adolescents with type 1 diabetes mellitus. *Physiological research*. 2009 Aug 1;58(4).
23. Chiarelli F, de Martino M, Mezzetti A, Catino M, Morgese G, Cuccurullo F, Verrotti A. Advanced glycation end products in children and adolescents with diabetes: relation to glycemic control and early microvascular complications. *The Journal of pediatrics*. 1999 Apr 1;134(4):486-91.
24. Zucchini S, Fabi M, Maltoni G, Zioutas M, Trevisani V, Di Natale V, Cassio A, Pession A. Adolescents with severe obesity show a higher cardiovascular (CV) risk than those with type 1 diabetes: a study with skin advanced glycation end products and intima media thickness evaluation. *Acta Diabetologica*. 2020 Nov;57:1297-305.
25. Norata GD, Garlaschelli K, Grigore L, Tibolla G, Raselli S, Redaelli L, Buccianti G, Catapano AL. Circulating soluble receptor for advanced glycation end products is inversely associated with body mass index and waist/hip ratio in the general population. *Nutrition, Metabolism and Cardiovascular Diseases*. 2009 Feb 1;19(2):129-34.





**Juhi Punjabi et al.,**

26. He CT, Lee CH, Hsieh CH, Hsiao FC, Kuo P, Chu NF, Hung YJ. Soluble form of receptor for advanced glycation end products is associated with obesity and metabolic syndrome in adolescents. *International journal of endocrinology*. 2014 Jan 20;2014.
27. Saha A, Poojary P, Chan L, Chauhan K, Nadkarni G, Coca S, Uribarri J. Increased odds of metabolic syndrome with consumption of high dietary advanced glycation end products in adolescents. *Diabetes & metabolism*. 2017 Oct;43(5):469.
28. Rodríguez-Mortera R, Luevano-Contreras C, Solorio-Meza S, Gómez-Ojeda A, Caccavello R, Bains Y, Gugliucci A, Garay-Sevilla ME. Soluble receptor for advanced glycation end products and its correlation with vascular damage in adolescents with obesity. *Hormone Research in Paediatrics*. 2019 Dec 18;92(1):28-35.
29. Gaens, K.H., Ferreira, I., Van de Waarenburg, M.P., van Greevenbroek, M.M., Van Der Kallen, C.J., Dekker, J.M., Nijpels, G., Rensen, S.S., Stehouwer, C.D. and Schalkwijk, C.G., 2015. Protein-bound plasma N $\epsilon$ -(carboxymethyl) lysine is inversely associated with central obesity and inflammation and significantly explain a part of the central obesity-related increase in inflammation: The Hoorn and CODAM studies. *Arteriosclerosis, thrombosis, and vascular biology*, 35(12), pp.2707-2713.
30. Šebeková K, Somoza V, Jarčušková M, Heidland A, Podracká L. Plasma advanced glycation end products are decreased in obese children compared with lean controls. *International Journal of Pediatric Obesity*. 2009 Jan 1;4(2):112-8.
31. Peppas M, Brem H, Ehrlich P, Zhang JG, Cai W, Li Z, Croitoru A, Thung S, Vlassara H. Adverse effects of dietary glycotoxins on wound healing in genetically diabetic mice. *Diabetes*. 2003 Nov 1;52(11):2805-13.
32. Krzystek-Korpaczka M, Patryn E, Boehm D, Berdowska I, Zielinski B, Noczynska A. Advanced oxidation protein products (AOPPs) in juvenile overweight and obesity prior to and following weight reduction. *Clinical Biochemistry*. 2008 Aug 1;41(12):943-9.
33. Korkmaz GG, Altinoglu E, Civelek S, Sozer V, Erdenen F, Tabak O, Uzun H. The association of oxidative stress markers with conventional risk factors in the metabolic syndrome. *Metabolism*. 2013 Jun 1;62(6):828-35.
34. Lutgers HL, Graaff R, Links TP, Ubink-Veltmaat LJ, Bilo HJ, Gans RO, Smit AJ. Skin autofluorescence as a noninvasive marker of vascular damage in patients with type 2 diabetes. *Diabetes care*. 2006 Dec 1;29(12):2654-9.
35. Lentferink YE, van Teeseling L, Knibbe CA, van der Vorst MM. Skin autofluorescence in children with and without obesity. *Journal of Pediatric Endocrinology and Metabolism*. 2019 Jan 1;32(1):41-7
36. Da Moura Smedo C, Webb MB, Waller H, Khunti K, Davies M. Skin autofluorescence, a non-invasive marker of advanced glycation end products: clinical relevance and limitations. *Postgraduate medical journal*. 2017 May;93(1099):289-94.
37. Accacha S, Rosenfeld W, Jacobson A, Michel L, Schnurr FJ, Shelov S, Ten S, Boucher-Berry C, Carey DE, Speiser PW, Lowell B. Plasma advanced glycation end products (AGEs), receptors for AGEs and their correlation with inflammatory markers in middle school-age children. *Hormone Research in Paediatrics*. 2013 Nov 4;80(5):318-27.
38. Rowisha M, El-Batch M, El Shikh T, El Melegy S, Aly H. Soluble receptor and gene polymorphism for AGE: relationship with obesity and cardiovascular risks. *Pediatric research*. 2016 Jul;80(1):67-71.

**Table I- The Impact Of Advanced Glycation End Products On Adolescents**

Study	Study design	Sample size	Age group	Findings
Tommaso Aversa <i>et al</i> , 2021.	Case control study	35	<18 years	sRAGE levels decreased in the presence of euthyroid status of the individuals indicating the presence of oxidative damage in the subjects.[15]
Ma. Eugenia Garay-Sevilla <i>et al</i> , 2018.	Case control study	160	12-19 years	This study showed the main findings of High serum CML and sRAGE in metabolically unhealthy obese adolescents compared to metabolically healthy obese. A contrasting feature was observed in a normal weight adolescent presenting high serum CML and sRAGE levels similar to an obese adolescent.[17]







**Juhi Punjabi et al.,**

**Table 2: Metabolic impact of Advanced Glycation End Product on Adolescents**

Study	Study design	Sample size	Age group	Findings
Angela Galler, Grit Müller, Reinhard Schinzel et al, 2003.	Retrospective study	159	<20 years	Adolescents in the age of 13-16 years diagnosed with type-I DM had significantly higher levels of serum AGE's. In addition, lipid profile such as triglycerides and cholesterol showed higher incidence among the similar group in comparison with the healthy controls.[19]
Galler et al, 2003 Rezaei et al, 2022 Kostolanská et al, 2009	Prospective study	250	<20 years	Hba1c and serum AGE have a direct relationship. High metabolic AGE levels and accelerates towards high hba1c levels. [20,21,22]
Francesco Chiarelli, MD, Maurizio de Martino et al, 1999.	Case-Control study	178	6-21 years	This study reveals the presence of elevated serum AGE levels among adolescents in the age group of 6-12 years diagnosed with Type-I DM compared to healthy controls. This indicates the risk of microvascular complications among young adolescents at a faster rate. [23]
Stefano Zucchini, Marianna Fabi et al, 2020.	Cross-sectional study	116	10-18 years	The study consisted of 2 groups. Group-I adolescents with T1DM and Group-II comprised of obese individuals. Both the groups were evaluated for lipid profile, Anthropometric data, sAGE levels. The results revealed high levels of sAGE among T1DM subjects compared to the obese category where, CV risk parameters seem to be elevated. Also, Gender and Age played a pivotal role in AGE per say. [24]

**Table 3: Impact Of Obesity on Advanced Glycation End Products Among Adolescents**

Study	Study design	Sample size	Age group	Findings
Chih-Tsueng He ,Chien-Hsing Lee, et al,2014	Cross sectional study	1083	12-16 years	Lipid profile, anthropometric parameters, BMI were inversely correlated with sRAGE Levels in males compared to females, where waist circumference & BMI were significantly correlated. This study proves SRAGE levels are associated with metabolic syndrome and obesity. [26]
Saha et al, 2017	Retrospective study	46 million	12-19 years	High dAGE consumption was observed among Metabolic Syndrome than Non-Metabolic Syndrome. It was also observed that dietary AGE can be considered as an independent predictor for Metabolic syndrome. [27]
Reyna Rodríguez-Morteraa Claudia Luevano-Contreras, et al,	Cross sectional study	66	15-19 years	Obese adolescents had elevated lipid parameters, Serum CML, Total AGE, DAGE intake, HOMA-IR and AI. This study proves a strong association between obesity and cardiometabolic risk, which in







**Juhi Punjabi et al.,**

2019.				turn proves the presence of AGE endogenously and exogenously can have dire consequences. [28]
Katrien H.J. Gaens, <i>et al</i> , 2015.	Cohort study	1270	40-60 years	Obesity had a direct relationship with inflammation evidenced by high CML and LGI Scores. [29]
Katari'Na S' Ebekova, Veronika Somoza, <i>et al</i> , 2009.	Observational study	18 obese 18 non-obese	5-18 years 4-17 years	Oxidative stress i.e CRP, IL-6 along with HOMA-IR showed increased levels in obese subjects compared to lean controls. Whereas, serum CML levels were lower in obese adolescents.[30]
Melpomeni Peppa <i>et al</i> , 2003.	Experimental study	105	Diabetic Rats	High AGE diet mice had delayed wound healing (epithelialization) compared to low AGE diet indicating a direct role of glycation causing inflammation and skin AGE deposition. [31]
Malgorzata Krzystek-Korpacka a, Eliza Patryn, <i>et al</i> , 2008.	Cross sectional study	114 obese 53 healthy controls	<17 years old	AOPP (Advanced oxidation protein products) were elevated in obese subjects compared to lean controls. Lipid parameters, Insulin and central obesity were positively correlated with AOPP indicating AOPP as a risk factor for the development of obesity. [32]
Korkmaz, G. G <i>et al</i> , 2013.	Cross sectional study	55 MetS pts 20 Healthy controls	40-50 years	AOPP values were higher and directly proportional to waist circumference (Obesity) in MetS patients due to the presence of oxidative stress causing free radical damage and inflammation in the body. [33]
Xian Wang, <i>et al</i> , 2021	Cross sectional study	825	18-80 years	Skin autofluorescence considered as a predictor for diabetic complications especially diabetic retinopathy, neuropathy, cardiovascular and kidney disease in patients with diabetes mellitus. [34]
Yvette E. Lentferink, Lisa van Teeseling, <i>et al</i> , 2018.	Cross sectional study	571	4-18 years	SAF (Skin Auto fluorescence) was measured in the adolescent subjects with obesity and healthy controls. High levels of SAF were observed in obese subjects revealing the linkage between obesity and high AGE levels in all age groups except <10years. [35]
Cidila Da Moura <i>et al</i> , 2017.	Review article	Nil	Nil	SAF can be considered as a biomarker to predict diabetes complications due to "long term memory" compared to Hba1c (3 months average) [36]
S. Accacha a W. Rosenfeld, <i>et al</i> , 2013.	Cross sectional study	88	11-15 years	CML levels were below than the average adult values. Also, CML levels had a negative correlation with adiposity elucidating AGE as not a complete risk factor for adiposity related comorbidities. [37]
Mohamed Rowisha, Manal El-Batch, <i>et al</i> , 2016.	Cross sectional study	50 obese 40 healthy controls	>18 years old	Obese group had increased cIMT, Lipid parameters and Insulin resistance. Increased expression of AGE, ADMA was also observed. sRAGE was decreased in obese adolescents compared to controls. and alsorAGE correlated with BMI stating body mass as a good predictor for AGE levels. [38]





Juhi Punjabi et al.,

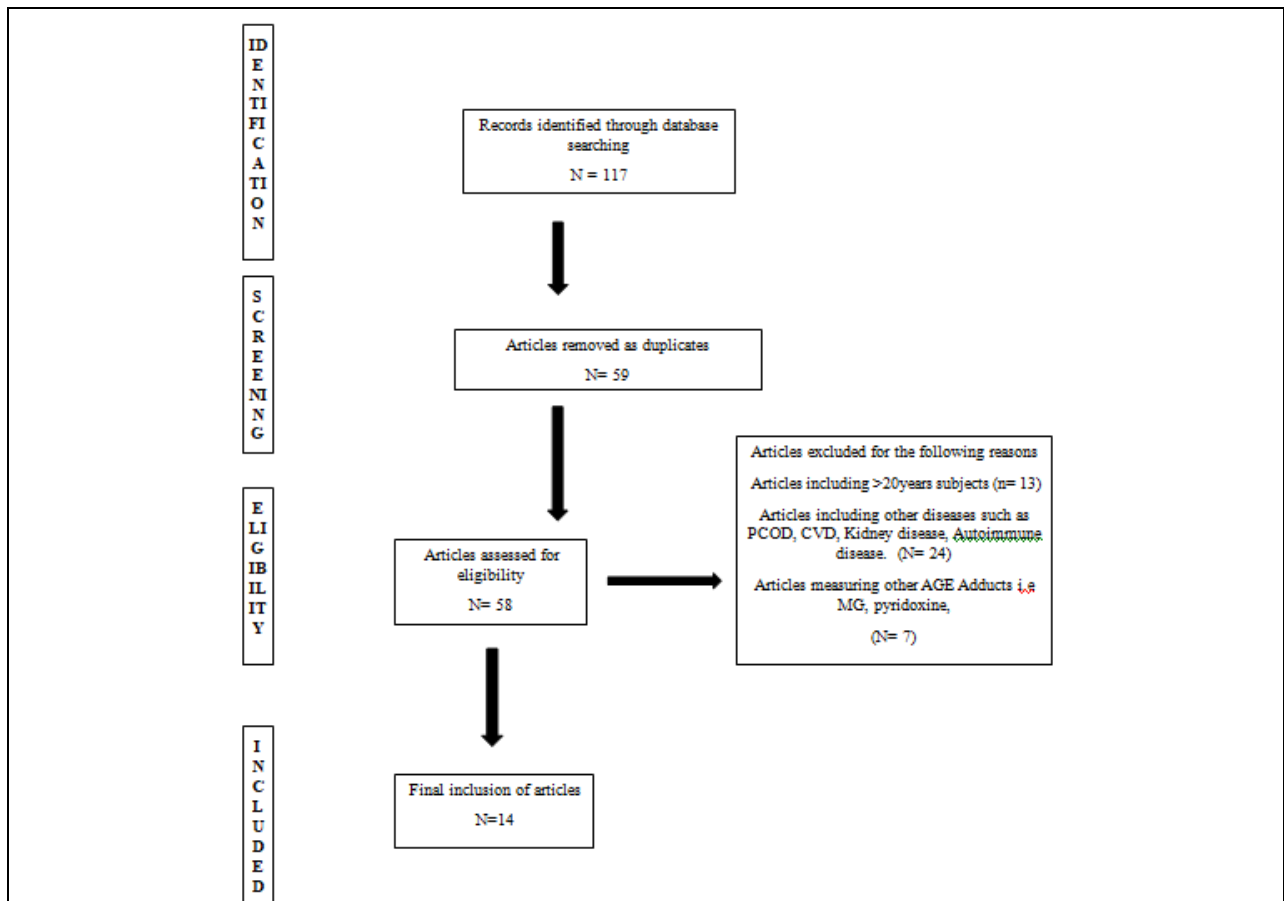


Figure I: A Schematic representation of the systematic process of selection of articles.

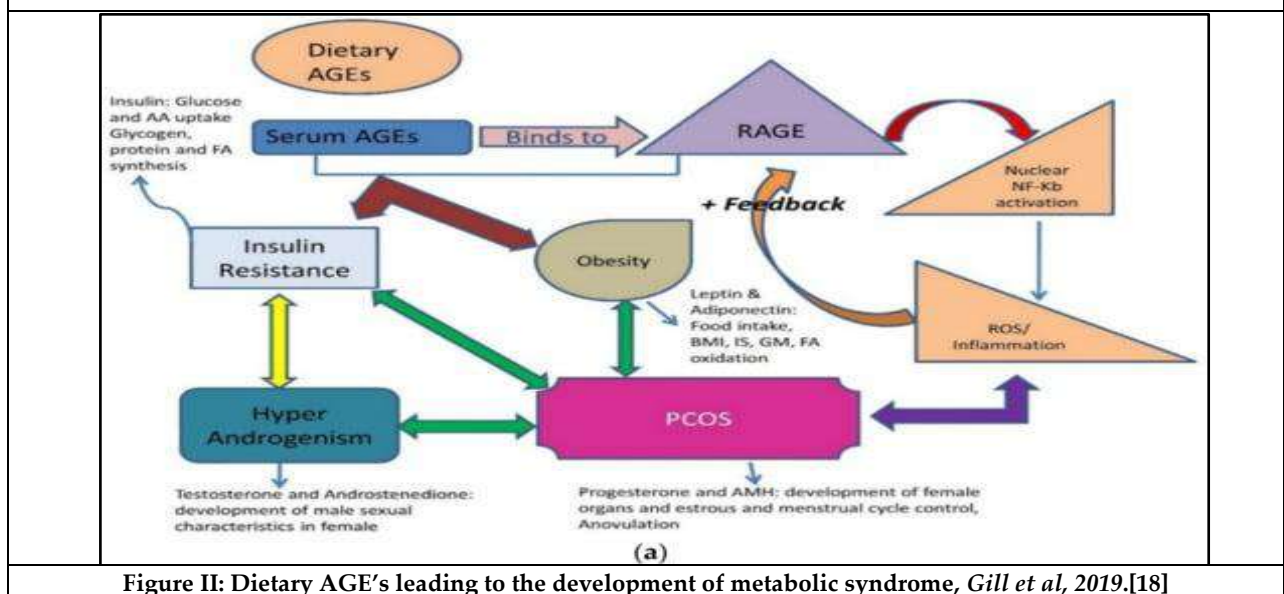


Figure II: Dietary AGE's leading to the development of metabolic syndrome, Gill et al, 2019.[18]





## Lab Scale Study of Catalytic Degradation Kinetics for Textile Dye : Tetrazine

Bhadreshkumar R Sudani\*

Assistant Professor, Department of Chemical Engineering, Government Engineering College, Valsad,  
(Affiliated to Gujarat Technological University), Gujarat, India.

Received: 21 Jun 2024

Revised: 23 Aug 2024

Accepted: 24 Oct 2024

### \*Address for Correspondence

**Bhadreshkumar R Sudani\***

Assistant Professor, Department of Chemical Engineering,  
Government Engineering College, Valsad,  
(Affiliated to Gujarat Technological University),  
Gujarat, India.

E.Mail: brsudani@gmail.com



This is an Open Access Journal / article distributed under the terms of the **Creative Commons Attribution License** (CC BY-NC-ND 3.0) which permits unrestricted use, distribution, and reproduction in any medium, provided the original work is properly cited. All rights reserved.

### ABSTRACT

This study explores the degradation kinetics of the textile dye Tetrazine using photocatalysis. Tetrazine, prevalent in the textile industry, is environmentally persistent and potentially toxic. The research aims to understand its degradation mechanisms and rate constants under various conditions, including pH, temperature, and the presence of catalysts like UV light, air, titanium dioxide (TiO<sub>2</sub>), and hydrogen peroxide (H<sub>2</sub>O<sub>2</sub>). Controlled experiments monitored Tetrazine and its degradation products using high-performance liquid chromatography (HPLC) and UV-Vis spectroscopy. Results show that Tetrazine degradation follows first-order kinetics, with the rate influenced by pH and temperature. Acidic conditions and higher temperatures accelerate the degradation process. Notably, TiO<sub>2</sub> photocatalysis under UV light and the addition of H<sub>2</sub>O<sub>2</sub> significantly enhance the degradation rate. These findings contribute to effective strategies for treating dye-contaminated wastewater, emphasizing the role of optimized conditions and advanced photocatalytic techniques. Further research is suggested to fully understand degradation pathways and ensure environmental safety by identifying non-toxic byproducts.

**Keywords:** Textile Dye, Tetrazine, TiO<sub>2</sub>, Pollution, degradation

## INTRODUCTION

The textile industry is one of the largest consumers of synthetic dyes, which are widely used to impart colour to fabrics. Among these dyes, Tetrazine is notable for its vivid colours and durability. However, the extensive use of Tetrazine poses significant environmental and health risks due to its persistence in the environment and potential toxicity (Babu, Parande, Raghu, & Kumar, 2007). The discharge of dye-laden wastewater into natural water bodies leads to severe water pollution, affecting aquatic life and human health (Saratale et al., 2011). Degradation of synthetic dyes like Tetrazine in wastewater is challenging due to their complex molecular structures and resistance to biodegradation (Robinson, McMullan, Marchant, & Nigam, 2001). Traditional wastewater treatment methods often





**Bhadreshkumar R Sudani et al.,**

fail to completely remove these dyes, necessitating the development of more effective degradation techniques (Forgacs, Cserhádi, & Oros, 2004). Among the advanced treatment methods, photocatalysis has emerged as a promising approach due to its efficiency in degrading a wide range of organic pollutants (Chong, Jin, Chow, & Saint, 2010). Photocatalysis involves the use of a catalyst, typically titanium dioxide (TiO<sub>2</sub>), under UV light to generate reactive oxygen species that can break down complex organic molecules (Hoffmann, Martin, Choi, & Bahnemann, 1995). Studies have shown that the combination of TiO<sub>2</sub> and UV light significantly enhances the degradation of various dyes (Daneshvar, Salari, & Khataee, 2004). Additionally, the presence of oxidizing agents like hydrogen peroxide (H<sub>2</sub>O<sub>2</sub>) can further accelerate the degradation process by generating additional reactive species (Pera-Titus, García-Molina, Baños, Giménez, & Esplugas, 2004).

This study aims to investigate the degradation kinetics of Tetrazine using photocatalysis under different environmental conditions. By examining the effects of pH, temperature, UV light, TiO<sub>2</sub>, air, and H<sub>2</sub>O<sub>2</sub>, this research seeks to provide a comprehensive understanding of the factors influencing Tetrazine degradation. The findings will contribute to the development of effective treatment strategies for dye-contaminated wastewater, helping to mitigate the environmental impact of textile dyes.

## MATERIALS AND METHODS

### MATERIALS

- **Tetrazine Dye:** Analytical grade Tetrazine dye in solid, orange coloured was procured from Sigma-Aldrich.(Fig-1)
- **Titanium (iv) Dioxide (TiO<sub>2</sub>):** It is also known as rutile or anatase consist of mixture of two forms. P25 grade TiO<sub>2</sub>, with an average particle size of 21 nm and a specific surface area of 50 m<sup>2</sup>/g, was used as the photocatalyst. Purity was 99.9 % and used without further purifications.
- **Hydrogen Peroxide (H<sub>2</sub>O<sub>2</sub>):** 30% (w/v) hydrogen peroxide solution was obtained from Merck. Used without further purifications.
- **Other Chemicals:** Sodium hydroxide (NaOH) and hydrochloric acid (HCl) for pH adjustment were sourced from Sigma-Aldrich.
- **Deionized Water:** All solutions were prepared using deionized water.

### METHODS

The method provided a comprehensive approach to study the degradation kinetics of Tetrazine under various conditions. The setup for these experiments mirrored that of the primary photocatalytic tests, ensuring that any degradation observed was due to non-photocatalytic processes. This includes potential adsorption onto the catalyst surface or chemical reactions that do not depend on light.

#### Experimental Setup

1. **Photocatalytic Reactor:** A batch photocatalytic reactor equipped with a UV lamp ( $\lambda = 365$  nm) was used for the degradation experiments. The reactor was designed to maintain a constant temperature and ensure uniform UV light exposure.
2. **Preparation of Dye Solution:** A stock solution of Tetrazine dye (100 mg/L) was prepared by dissolving the appropriate amount of dye in deionized water. Experimental solutions were obtained by diluting the stock solution to the desired concentrations.
3. **Catalyst Preparation:** TiO<sub>2</sub> was dispersed in deionized water to achieve a final concentration of 1 g/L. The suspension was sonicated for 30 minutes to ensure uniform dispersion.



**Bhadreshkumar R Sudani et al.,****Experimental Procedure:**

1. **Effect of pH:** The pH of the dye solution was adjusted to the desired levels (pH 3, 7, and 11) using NaOH and HCl. The solution (100 mL) was then placed in the photocatalytic reactor with TiO<sub>2</sub> (1 g/L) and exposed to UV light. Samples were taken at regular intervals for analysis.
2. **Effect of Temperature:** Experiments were conducted at different temperatures (25°C, 35°C, and 45°C). The temperature was controlled using a water bath. The dye solution (100 mL) with TiO<sub>2</sub> (1 g/L) was exposed to UV light, and samples were collected periodically.
3. **Effect of Hydrogen Peroxide:** To investigate the role of H<sub>2</sub>O<sub>2</sub>, different concentrations (0.1%, 0.5%, and 1% w/v) were added to the dye solution (100 mL) with TiO<sub>2</sub> (1 g/L). The mixture was exposed to UV light, and samples were taken at specific time intervals.
4. **Sample Analysis:** The concentration of Tetrazine in the samples was measured using high-performance liquid chromatography (HPLC) equipped with a UV detector. The mobile phase consisted of acetonitrile and water (70:30 v/v), and the detection wavelength was set at 254 nm. Additionally, UV-Vis spectroscopy was used to monitor the absorbance changes at the dye's maximum absorption wavelength ( $\lambda_{\text{max}} = 540 \text{ nm}$ ).
5. **Kinetic Analysis:** The degradation kinetics were analyzed by plotting the natural logarithm of the Tetrazine concentration against time. The rate constants were determined from the slopes of the linear regression lines, assuming first-order kinetics.

**Control Experiments**

- **Dark Control:** Experiments were conducted in the absence of UV light to assess the contribution of photocatalysis.
- **Catalyst Control:** Experiments without TiO<sub>2</sub> were performed to evaluate the effect of UV light alone.
- **Oxidant Control:** Experiments without H<sub>2</sub>O<sub>2</sub> were conducted to assess the combined effect of TiO<sub>2</sub> and UV light without the oxidizing agent.

**Data Analysis**

In order to get better results with perfection, all experiments were performed in triplicate, and the average values were reported. The standard deviation was calculated to determine the reproducibility of the results. This methodological approach ensures a comprehensive understanding of the degradation kinetics of Tetrazine and the influence of various parameters on the photocatalytic process.

**RESULTS AND DISCUSSION**

Below is a tabulated representation of the data collected from the various experimental conditions examined in the study. The data includes the concentration of Tetrazine dye over time, measured under different conditions of pH, temperature, and the presence of catalysts (TiO<sub>2</sub> and H<sub>2</sub>O<sub>2</sub>). This tabulation data provides a clear overview of how various factors such as pH, temperature, and the presence of catalysts influence the degradation of Tetrazine dye. Each table highlights the effect of specific conditions, facilitating a comprehensive analysis of the degradation kinetics. The data presented in the tables provide insights into the degradation kinetics of Tetrazine dye under various experimental conditions, including the effects of pH, temperature, and the presence of catalysts such as TiO<sub>2</sub> and H<sub>2</sub>O<sub>2</sub>. This discussion interprets the observed trends and elucidates the underlying mechanisms of Tetrazine degradation.

**Effect of pH on Tetrazine Degradation**

Table 1 shows the concentration of Tetrazine over time at different pH levels (3, 7, and 11). The degradation rate is significantly higher at acidic pH (3) compared to neutral (7) and alkaline (11) conditions. At pH 3, the concentration of Tetrazine decreases from 10.0 mg/L to 1.1 mg/L in 60 minutes, indicating rapid degradation. In contrast, at pH 7, the concentration decreases to 3.0 mg/L, and at pH 11, it decreases to 6.3 mg/L over the same period. (Fig.-2)



**Bhadreshkumar R Sudani et al.,**

The enhanced degradation at acidic pH can be attributed to the increased generation of hydroxyl radicals ( $\bullet\text{OH}$ ) in acidic conditions, which are highly reactive and effective in breaking down organic dye molecules (Chen, Mao, & Zhao, 2012). The lower degradation rates at neutral and alkaline pH suggest that fewer hydroxyl radicals are generated, leading to slower degradation.

**Effect of Temperature on Tetrazine Degradation**

Table 2 illustrates the effect of temperature on Tetrazine degradation at pH 7. As the temperature increases from 25°C to 45°C, the degradation rate significantly increases. At 25°C, the concentration of Tetrazine decreases from 10.0 mg/L to 3.0 mg/L in 60 minutes. At 35°C, it drops to 1.2 mg/L, and at 45°C, it reaches as low as 0.2 mg/L. (Fig-3). The accelerated degradation at higher temperatures can be explained by the increased kinetic energy of the molecules, which enhances the reaction rates. Higher temperatures also improve the generation of reactive species such as hydroxyl radicals during the photocatalytic process (Gaya & Abdullah, 2008). This result is consistent with the Arrhenius equation, which states that the reaction rate increases exponentially with temperature.

**Effect of Oxidant Hydrogen Peroxide on Tetrazine Degradation**

Table 3 highlights the impact of adding hydrogen peroxide ( $\text{H}_2\text{O}_2$ ) to the dye solution with  $\text{TiO}_2$  under UV light at pH 7 and 25°C. The degradation rate increases with higher concentrations of  $\text{H}_2\text{O}_2$ . Without  $\text{H}_2\text{O}_2$ , the concentration of Tetrazine decreases to 6.5 mg/L in 60 minutes. With 0.1%  $\text{H}_2\text{O}_2$ , it decreases to 1.0 mg/L, with 0.5%  $\text{H}_2\text{O}_2$ , it decreases to 0.2 mg/L, and with 1%  $\text{H}_2\text{O}_2$ , it almost completely degrades to 0.1 mg/L. (Fig-4). Hydrogen peroxide acts as an additional source of hydroxyl radicals when exposed to UV light, further enhancing the photocatalytic degradation process (Pera-Titus et al., 2004). The significant increase in degradation rate with higher  $\text{H}_2\text{O}_2$  concentrations demonstrates its effectiveness in accelerating the breakdown of Tetrazine. (Fig.-5)

**Control Experiments**

Table 4 presents the results of control experiments conducted in the absence of UV light (dark control),  $\text{TiO}_2$ , and  $\text{H}_2\text{O}_2$ . The degradation rates in these control conditions are significantly lower compared to the experimental conditions with UV light,  $\text{TiO}_2$ , and  $\text{H}_2\text{O}_2$ . In the dark control, the concentration of Tetrazine decreases only slightly from 10.0 mg/L to 8.8 mg/L in 60 minutes, indicating minimal degradation. Similarly, without  $\text{TiO}_2$  and  $\text{H}_2\text{O}_2$ , the concentrations decrease to 8.7 mg/L and 6.5 mg/L, respectively. The graphical representations of all three control experiments are incorporated with all charts above. These control experiments confirm that the presence of UV light,  $\text{TiO}_2$ , and  $\text{H}_2\text{O}_2$  is crucial for effective degradation of Tetrazine. The minimal degradation in the absence of these factors highlights the importance of photocatalysis and the synergistic effect of the catalysts in enhancing the degradation process (Hoffmann et al., 1995).

**CONCLUSION**

The discussion of the tabulated data demonstrates that the degradation of Tetrazine dye is significantly influenced by pH, temperature, and the presence of catalysts such as  $\text{TiO}_2$  and  $\text{H}_2\text{O}_2$ . Acidic conditions, higher temperatures, and the addition of hydrogen peroxide enhance the degradation rate, supporting the use of optimized photocatalytic processes for effective treatment of dye-contaminated wastewater. These findings contribute to the development of efficient strategies for mitigating the environmental impact of textile dyes. Further research should focus on understanding the degradation pathways and identifying non-toxic by products to ensure comprehensive environmental safety.

**ACKNOWLEDGEMENT**

Author would like to express his sincere gratitude to all those who supported and contributed to this research activity Viz. Principal Sir, Head of department and colleagues and technical staff at chemical and environment engineering department, whose assistance in the laboratory and with the experimental setup was invaluable.







## REFERENCES

1. Austin, R. H., & Lim, S. F. (2008). The Sackler Colloquium on promises and perils in nanotechnology for medicine. *Proceedings of the National Academy of Sciences*, 105(45), 17217-17221.
2. Babu, B. R., Parande, A. K., Raghu, S., & Kumar, T. P. (2007). Textile technology: Cotton textile processing: Waste generation and effluent treatment. *Journal of Cotton Science*, 11(3), 141-153.
3. Chong, M. N., Jin, B., Chow, C. W., & Saint, C. (2010). Recent developments in photocatalytic water treatment technology: A review. *Water Research*, 44(10), 2997-3027.
4. Daneshvar, N., Salari, D., & Khataee, A. R. (2004). Photocatalytic degradation of azo dye acid red 14 in water: Investigation of the effect of operational parameters. *Journal of Photochemistry and Photobiology A: Chemistry*, 162(2-3), 317-322.
5. Forgacs, E., Cserháti, T., & Oros, G. (2004). Removal of synthetic dyes from wastewaters: A review. *Environment International*, 30(7), 953-971.
6. Hoffmann, M. R., Martin, S. T., Choi, W., & Bahnemann, D. W. (1995). Environmental applications of semiconductor photocatalysis. *Chemical Reviews*, 95(1), 69-96.
7. Pera-Titus, M., García-Molina, V., Baños, M. A., Giménez, J., & Esplugas, S. (2004). Degradation of chlorophenols by means of advanced oxidation processes: A general review. *Applied Catalysis B: Environmental*, 47(4), 219-256.
8. Robinson, T., McMullan, G., Marchant, R., & Nigam, P. (2001). Remediation of dyes in textile effluent: A critical review on current treatment technologies with a proposed alternative. *Bioresource Technology*, 77(3), 247-255.
9. Saratale, R. G., Saratale, G. D., Kalyani, D. C., Chang, J. S., & Govindwar, S. P. (2011). Enhanced decolorization and biodegradation of textile azo dye Scarlet R by using developed microbial consortium-GR. *Bioresource Technology*, 102(1), 84-91.

Table 1: Effect of pH on Tetrazine Degradation with TiO<sub>2</sub> under UV Light

Time (min)	Concentration (mg/L) at pH 3	Concentration (mg/L) at pH 7	Concentration (mg/L) at pH 11
0	10.0	10.0	10.0
10	8.2	8.9	9.5
20	6.5	7.8	9.0
30	4.7	6.7	8.3
40	3.2	5.4	7.6
50	2.0	4.2	7.0
60	1.1	3.0	6.3

Table 2: Effect of Temperature on Tetrazine Degradation with TiO<sub>2</sub> under UV Light at pH 7

Time (min)	Concentration (mg/L) at 25°C	Concentration (mg/L) at 35°C	Concentration (mg/L) at 45°C
0	10.0	10.0	10.0
10	8.9	7.5	6.3
20	7.8	5.6	3.9
30	6.7	4.1	2.0
40	5.4	3.0	1.1
50	4.2	2.0	0.6
60	3.0	1.2	0.2

Table 3: Effect of Hydrogen Peroxide on Tetrazine Degradation with TiO<sub>2</sub> under UV Light at pH 7 and 25°C

Time (min)	Concentration (mg/L) with 0.1% H <sub>2</sub> O <sub>2</sub>	Concentration (mg/L) with 0.5% H <sub>2</sub> O <sub>2</sub>	Concentration (mg/L) with 1% H <sub>2</sub> O <sub>2</sub>
0	10.0	10.0	10.0
10	6.8	5.2	4.0





Bhadreshkumar R Sudani et al.,

20	4.7	2.8	1.8
30	3.5	1.6	0.8
40	2.4	0.9	0.4
50	1.6	0.5	0.2
60	1.0	0.2	0.1

Table 4: Control Experiments

Time (min)	Concentration (mg/L) in Dark Dark Control	Concentration (mg/L) With UV only Catalyst Control	Concentration (mg/L) With UV + TiO <sub>2</sub> Oxidant Control
0	10.0	10.0	10.0
10	9.8	9.7	9.3
20	9.6	9.5	8.7
30	9.4	9.3	8.2
40	9.2	9.1	7.6
50	9.0	8.9	7.1
60	8.8	8.7	6.5

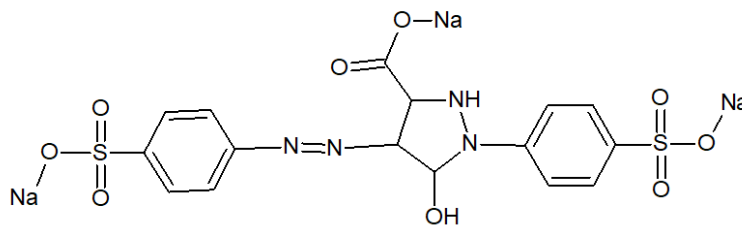


Figure 1: Structure of tetrazine salt

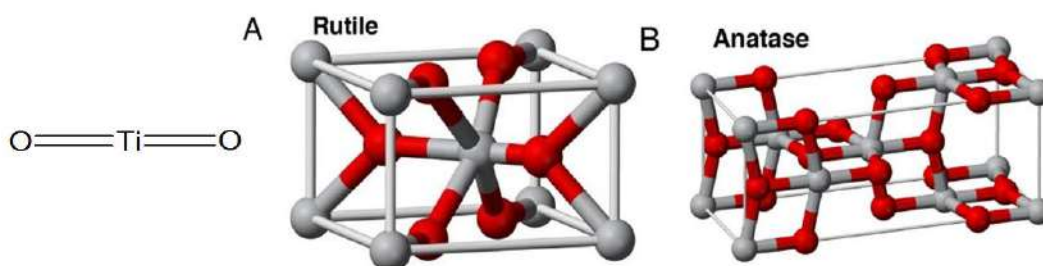


Figure 1: Structure of TiO<sub>2</sub>(Austin, R. H., & Lim, S. F. 2008).

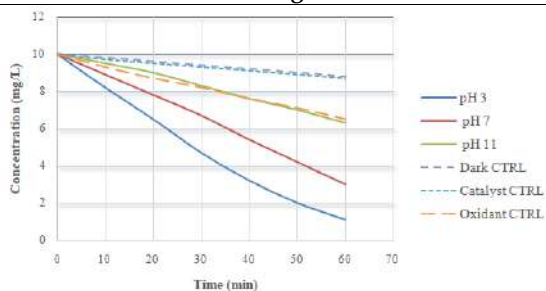


Figure 2: Effect of pH on Tetrazine Degradation with TiO<sub>2</sub> under UV Light

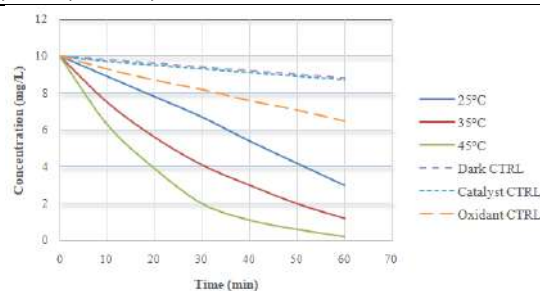
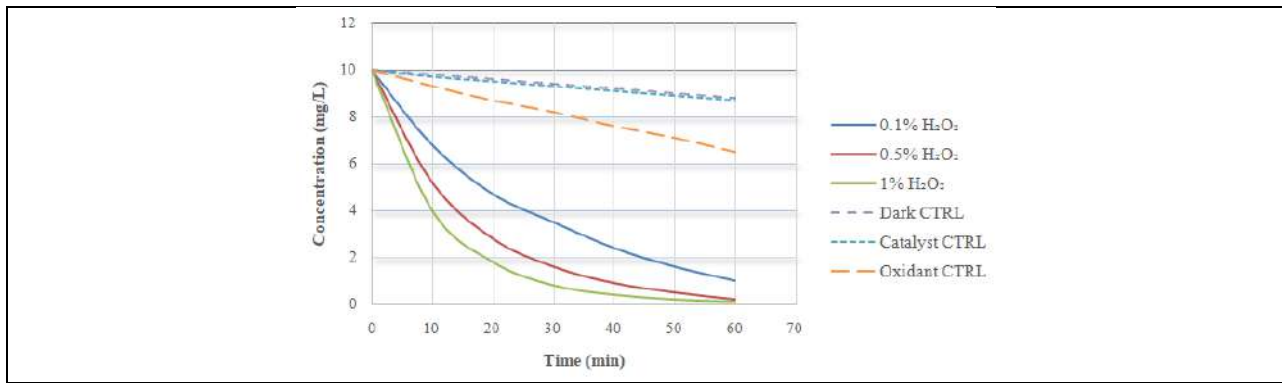


Figure 3: Effect of Temperature on Tetrazine Degradation with TiO<sub>2</sub> under UV Light at pH 7





**Bhadreshkumar R Sudani et al.,**



**Figure 4: Effect of H<sub>2</sub>O<sub>2</sub> on Tetrazine Degradation with TiO<sub>2</sub> under UV Light at pH 7 and 25°C**





# A Numerical Study on the Flow of Oil-based Fuzzy Hybrid Nanomaterial Stretching Cylinder by Modified Buongiorno's Model

P.Asaigeethan<sup>1\*</sup>, K.Vaithiyalingam<sup>2</sup> and N. Deepa<sup>1</sup>

<sup>1</sup>Assistant Professor, Department of Mathematics, Government College of Technology, Thadagam Road, Coimbatore, (Affiliated to Anna University, Chennai), Tamil Nadu, India.

<sup>2</sup>Assistant Professor, Department of Mathematics, Sri Vasavi College, Erode, (Affiliated to Bharathiar University, Coimbatore), Tamil Nadu, India.

Received: 05 Apr 2024

Revised: 20 Aug 2024

Accepted: 24 Oct 2024

## \*Address for Correspondence

**P.Asaigeethan**

Assistant Professor, Department of Mathematics,  
Government College of Technology, Thadagam Road, Coimbatore,  
(Affiliated to Anna University, Chennai),  
Tamil Nadu, India.

E.Mail: asaigeethan14@gct.ac.in



This is an Open Access Journal / article distributed under the terms of the **Creative Commons Attribution License** (CC BY-NC-ND 3.0) which permits unrestricted use, distribution, and reproduction in any medium, provided the original work is properly cited. All rights reserved.

## ABSTRACT

A model of Carreau fluid flow is estimated with the velocity and energy transmission over the hybrid nanofluid (hnf) past a stretching cylinder by modified Buongiorno's model. By combining nanoparticles with distinct rheological and thermal characteristics, the nanofluids proficiency might be increased, stabilized, and more effective. The dispersion has created a hybrid nanofluid of Manganese-zinc ferrite ( $MnZnFe_2O_4$ ) and Nickel-zinc ferrite ( $NiZnFe_2O_4$ ) nanocomposites in the base fluid. To assess the permeability effect, the momentum equation incorporates the consequences of the Weissenberg number. The flow of fluid is controlled by a system of PDEs that take into account the consequences of a heat source, and natural convection. They are then transformed, using substitutions for similarity variables, into a non-dimensional set of ODEs. In the second section, we discussed hnf and nanofluid, moment, and energy through the fuzzy context. The volume quantity of hnf in  $MnZnFe_2O_4$  and  $NiZnFe_2O_4$  is considered unknown concerning triangular fuzzy numbers (TFNs) [0, 0.05, 0.1]. The triangular membership function (TMF) is utilized to research variability and uncertainty, while  $\alpha$  – cut controls the TFNs. The velocity field of reaction in hybrid nanofluid ( $MnZnFe_2O_4 + NiZnFe_2O_4 / C_n H_{2n+2}$ ) and nanofluid ( $MnZnFe_2O_4 / C_n H_{2n+2}$ ) developed by Weissenberg number and curvature parameter, the heat conduction of reaction in hnf and nanofluid developed by Prandtl number. When evaluating the fields of velocity, temperature, coefficient of skin friction, and local Nusselt numeral, the results are displayed in tables and graphs.

**Keywords:** Carreau hnf, Cylinder, Modified Buongiorno's method, TFNs, TMF, bvp5c.





## INTRODUCTION

The present section discusses the numerous uses and applications of hybrid nanofluid ( $MnZnFe_2O_4 + NiZnFe_2O_4 + C_nH_{2n+2}$ ) associated with nanofluid ( $MnZnFe_2O_4 + C_nH_{2n+2}$ ) some samples in this field incorporate fuel manufacturing, advanced frosty techniques, contemporary medicinal conveyance, apparatus, nanofabrication, transmission of energy, and cooling system in electronic circuits. As a result of this significant achievement, substantial research has been undertaken globally on energy transfer and flow properties. Hybrid nanofluids are a new nanotechnological type that is frequently formed by spreading two distinct kinds of nanoparticles in base fluids. Several researchers have applied hybrid nanofluids. Khashi et al. [1] examined magneto hydrodynamics hybrid nanofluid in water flow on a moveable surface using the Joule thermal consequence. Nazir et al. [2] analyzed the modifications in Joule heating, magnetic induction, and chemical response composition that have significant effects on flow and heat transfer during species transport. Dogonchi et al. [3] studied the hybrid nanostructures in fluid spinning as a result of surface rotation and they applied the Duan-Rach method to the predicted problem and observed an increase in the heat proficiency of the fluid caused by hnf. Kumar et al. [4] examined the numerical study completed to explore the analysis of heat conduction and flow of anhnf flow above a porous material. Ghadikolaei [5] demonstrated the 3D flow and heat conduction of  $TiO_2 - CuO/hnf$  floating in the base fluid. Dogonchi et al. [6] studied the finite element approach for control volume analysis  $Fe_3O_4 - H_2O$  nanofluid in an annulus region subjected to thermal transmission. Waqaset al. [7] the organization of hybrid nanomaterial flow through porous media have been examined and the consequence of the magnetic fields and nanofluid radiation are significant in biotechnology and medicine. Reddy et al. [8] illustrated the flow of anhnf  $Al_2O_3 - cu/Ethylene glycol$  across a narrow, moving tip using magnetohydrodynamic, Dufour-Soret consequence, and infrared radiation. Kavya et al. [9] investigated the Williamson hnf in a stretched cylinder containing based on the water  $Cu/MoS_4$  nanoparticles. The heat transmission capabilities of the Williamson hnf flow decrease as Prandtl numeral and curvature limiting factor values increase. Sulochana et al. [10] covered the investigation of the magneto hydro dynamic nf flow perimeter film, as well as arranged symmetrically, constantly shifting the needle. Madhukesh et al. [11] explored the idea of a liquid hybrid nanomaterial passing through a tiny needle with the help of magnetic flow, thermophoresis effect, and convection boundary conditions. Salleh et al. [12] examined while accounting for buoyancy effects, wall heat transmission, and an incompressible flow on a thin, fragile needle saturated with  $Al_2O_3 - Cu/water$  flow. Buongiorno [13] using mathematical nanofluid models, statistically examined the convection of the movement of a nanofluid in cavities with porous channels and viscous fluid.

In addition to chemical diffusion, there is an increase in an extensive range of concerns, including heat transmission. A fundamental role for fluid flow is played in engineering and science. After regulating, these models of physical problems are transmuted into non-linear differential equations. Using physical replication, which includes coefficients, 3D/2D geometry, limiting factors, circumstances, and boundary states, frequently has a significant influence on the alternatives of differential equations. Consequently, the limiting factors, initial and boundary specifications are virtually imprecise and caused by experimental error, coefficients, mechanical flaws, and dimension inaccuracy. Consequently, in this instance, methodology is a more accurate means of describing the phenomenon under investigation than presuming the presence of distinct or widespread physical problems. Fuzzy differential equations (FDEs) are particularly effective. Kaleva [14] introduced the concept of FDEs (fuzzy differential equations). Siddique et al. [15] described the fuzzy evaluation for mono-directional magneto hydrodynamics flow and examined ternary key flow issues involving a 3rd-grade liquid between two equal plates. Dubois et al. [16] developed mathematical methods for three distinct varieties of fuzzy numbers, triangular, trapezoidal, and Gaussian fuzzy numbers. For the sake of completeness, TFNs are listed. Seikkala [17] acquainted with the notion of fuzzy differentiation. Almutairi et al. [18] obtained the fuzzy waves equation numerical solution. Salahsour et al. [19] examined the alley effect using fuzzy differential equations and the fuzzy logistic equation with the assistance of TFNs. Merkin [20] examined flow reactions at the border layer when there was a homogenous or heterogeneous shortage of reactants. They discovered that the external response is a highly effective method for differentiating the





edge because the homogenous reaction occurs when the boundary layer is generated with decreased reactant surface concentration.

A stretching cylinder with an exponential curvature is affected by Buongiorno's Carreau fuzzy hybrid nanofluid model, although more research is required, according to the literature review. Mixing Maganese-Zinc ferrite (MnZnFe<sub>2</sub>O<sub>4</sub>) and Nickel-Zinc ferrite (NiZnFe<sub>2</sub>O<sub>4</sub>) nanoparticles are combined to create the hnf. A system of PDE was used to model the nanofluid flow; these associations were subsequently transformed into an ODE set based on similarities. The resultant system of equations pertaining to the boundary value problem was solved using the bvp5c approach. The following factors are estimated and evaluated: coefficient of skin friction, local Nusselt numeral, velocity, and temperature. The present investigation is novel in the subsequent aspects:

- Comparative study to ascertain the hybrid nanoparticles (MnZnFe<sub>2</sub>O<sub>4</sub> and NiZnFe<sub>2</sub>O<sub>4</sub>) utilizing oil as a base fluid.
- The behavior of hybrid nanofluids (hnf) is represented by a curved stretched cylinder. Apart from velocity, temperature, coefficient of skin friction, and local Nusselt numeral was also analyzed.
- The volume fraction of the epistemic uncertainty dispersion nanoparticles is calculated using fuzzy differential equations. Thus, the volume proportions of the hnf are regarded as TFNs along with the use of the  $\alpha$  –cut method. The  $\alpha$  –cut is explained by fuzzy TMF.

Basics of Fuzzification [22]

This section presents a comprehensive explanation of fuzzy characteristics that can be used for subsequent calculations.

Definition 1. A set of fuzzy numbers is characterized as an ordered pair set given that

$\bar{A} = \{(\eta, \mu_{\bar{A}}(\eta)) : \eta \in X, \mu_{\bar{A}}(\eta) \in [0, 1]\}$ . Where  $\mu_{\bar{A}}(\eta)$  is a membership function of  $\bar{A}$ ,  $X$  – all-encompassing set, and the mapping is measured as  $\mu_{\bar{A}}(\eta) : X \rightarrow [0, 1]$ .

Definition 2.  $\alpha$  –Cut of a fuzzy set  $\bar{A}$  is a crisp set  $A_\alpha$  is explicated  $A_\alpha = \{\eta / \mu_{\bar{A}}(\eta) \geq \alpha\}$ , where  $\alpha \in [0, 1]$ .

Definition 3. Let triangular fuzzy number (TFN)  $\bar{A} = (b_1, b_2, b_3)$  along with membership function  $\mu_{\bar{A}}(\eta)$  explicate as,

$$\mu_{\bar{A}}(\eta) = \begin{cases} \frac{\eta - b_1}{b_2 - b_1}, & \text{for } b_1 \leq \eta \leq b_2 \\ \frac{b_3 - \eta}{b_3 - b_2}, & \text{for } b_2 \leq \eta \leq b_3 \\ 0, & \text{otherwise} \end{cases} \tag{1}$$

The  $\alpha$ -cut technique is used to transform a TFN with an upper limit (or center) value of  $b_2$  into interval numbers, where  $\alpha$  is an integer between 0 and 1. Then, the formula  $\bar{A} = [f_1(\eta; \alpha), f_2(\eta; \alpha)] = [b_1 + (b_2 - b_1)\alpha, b_3 - (b_3 - b_2)\alpha]$ , is used to represent this transformation. The membership function defines the membership function, which is an essential part of fuzzy set theory. The  $\alpha$ -cut membership function and triangular fuzzy numbers  $\bar{A} = (b_1, b_2, b_3)$  are shown in Fig 1. In the following conditions, a triangular fuzzy number can be anything: On the interval  $[0, 1]$ , the function  $f_1(\eta; \alpha)$  rises and function  $f_2(\eta; \alpha)$  decreasing.  $f_1(\eta; \alpha) \leq f_2(\eta; \alpha)$  on the interval  $[0, 1]$ . The set  $[0, 1]$  contain the bounds of  $f_1(\eta; \alpha)$ , and  $f_2(\eta; \alpha)$ . This means that  $f_1(\eta, \alpha) = f_2(\eta, \alpha) = f(\eta)$ , here  $f(\eta)$  is crisp velocity.

**Mathematical formulation**

A Carreau hybrid nanofluid flow in an incompressible manner through Buongiorno's model elongating cylinder exhibits both homogeneous and heterogeneous reactions for the cylinder. The physical attributes of the hnf are described in Table 1 developed by Ahmad et al. [21] are compatible. Simplified homogeneous-heterogeneous responses can be expressed as follows, using the previously described presumptions and Merkin's theoretical [20] concepts.







Asaigeethan et al.,

$$A + 2B \rightarrow 3B, \quad \text{rate} = d_c ab^2 \tag{2}$$

One first-order isothermal reaction is taking place on the surface of the catalyst.

$$A \rightarrow B, \quad \text{rate} = d_s a \tag{3}$$

The symbols a and b depict the concentrations of chemical categories A and B,  $d_c$  and  $d_s$  are the constants of rate. The model regulating equations are created after applying common boundary layer approximations,

$$\frac{\partial}{\partial x}(ru) + \frac{\partial}{\partial r}(rv) = 0, \tag{4}$$

$$u \frac{\partial u}{\partial x} + v \frac{\partial u}{\partial r} = \frac{\mu_{hnf}}{\rho_{hnf}} \frac{1}{r} \frac{\partial}{\partial r} \left[ \left( r \frac{\partial u}{\partial r} \right) \left( 1 + \Gamma^2 \left( \frac{\partial u}{\partial r} \right)^2 \right)^{\frac{n-1}{2}} \right] + \frac{\mu_{hnf}}{\rho_{hnf}} (n-1) \Gamma^2 \frac{\partial^2 u}{\partial r^2} \left( \frac{\partial u}{\partial r} \right)^2 \left[ 1 + \Gamma^2 \left( \frac{\partial u}{\partial r} \right)^2 \right]^{\frac{n-3}{2}}, \tag{5}$$

$$u \frac{\partial T}{\partial x} + v \frac{\partial T}{\partial r} = \frac{k_{hnf}}{r(\rho C_p)_{hnf}} \frac{\partial}{\partial r} \left[ r \frac{\partial T}{\partial r} \right] + \tau \left[ D_B \frac{\partial b}{\partial r} \frac{\partial T}{\partial r} + \frac{D_T}{T_\infty} \left( \frac{\partial T}{\partial r} \right)^2 \right], \tag{6}$$

$$u \frac{\partial a}{\partial x} + v \frac{\partial a}{\partial r} = D_A \left[ \frac{\partial^2 a}{\partial r^2} + \frac{\partial a}{\partial r} \right] + D_A \frac{\partial a}{\partial r} + \frac{D_T}{T_\infty} \frac{\partial T}{\partial r} - d_c ab^2, \tag{7}$$

$$u \frac{\partial b}{\partial x} + v \frac{\partial b}{\partial r} = D_B \left[ \frac{\partial^2 b}{\partial r^2} + \frac{\partial b}{\partial r} \right] + D_B \frac{\partial b}{\partial r} + \frac{D_T}{T_\infty} \frac{\partial T}{\partial r} + d_s ab^2. \tag{8}$$

For Equations (3)– (7), the boundary conditions are stated as follows

$$u = u(x), \quad v = 0, \quad D_A \frac{\partial a}{\partial r} = d_c a, \quad D_B \frac{\partial b}{\partial r} = -d_s a, \quad T = T_w, \quad \text{at } r = R,$$

$$u \rightarrow 0, \quad T \rightarrow T_\infty, \quad a \rightarrow a_\infty, \quad b \rightarrow b_\infty \quad \text{as } r \rightarrow \infty. \tag{9}$$

A and B are the concentrations of hnf particles,  $u(x) = \frac{xu_0}{l}$  where  $u_0$  velocity,  $x$  is an independent,  $l$  is the characteristic length,  $a$  and  $b$  are concentrations of nanoparticles [ $\text{mol}/\text{m}^3$ ],  $D_A$  and  $D_B$  are the Brownian diffusion coefficients [ $\text{m}^2/\text{s}$ ],  $D_T$  is the thermophoresis diffusion coefficient [ $\text{m}^2/\text{s}$ ],  $u$  and  $v$  are velocity components [ $\text{m}/\text{s}$ ],  $(C_p)_{hnf}$  is the specific heat of hnf [ $\text{J}/\text{kg} \cdot \text{K}$ ],  $\mu_{hnf}$  is the dynamic viscosity of the hnf [ $\text{kgm}^{-1}\text{s}^{-1}$ ],  $\rho_{hnf}$  is the density of hnf [ $\text{kg}/\text{m}^3$ ],  $(\rho C_p)_{hnf}$  is the heat capacitance of hnf [ $\text{J}/\text{kg} \cdot \text{K}$ ],  $\nu_{hnf}$  is the kinematic viscosity of the hnf [ $\text{m}^2/\text{s}$ ],  $k_{hnf}$  is the thermal conductivity of hnf [ $\text{W}/\text{m} \cdot \text{K}$ ],  $\alpha_{hnf}$  is the thermal diffusivity of the hnf [ $\text{m}^2/\text{s}$ ],  $n$  is the power law index number, and the effective fluid heat capacity  $\tau = \frac{(\rho C)_f}{(\rho C)_p}$ .

$D_A \frac{\partial a}{\partial r} + \frac{D_T}{T_\infty} \frac{\partial T}{\partial r} = 0$  and  $D_B \frac{\partial b}{\partial r} + \frac{D_T}{T_\infty} \frac{\partial T}{\partial r} = 0$  claim that when thermophoresis is considered, the typical flow of hnf particles at the interface is zero.

$$\frac{\rho_{hnf}}{\rho_f} = (1 - \varphi_2) \left[ 1 - \varphi_1 + \varphi_1 \frac{\rho_{s1}}{\rho_f} \right] + \varphi_2 \frac{\rho_{s2}}{\rho_f}, \tag{10}$$

$$\frac{\mu_{hnf}}{\mu_f} = \frac{1}{(1 - \varphi_1)^{2.5} (1 - \varphi_2)^{2.5}}, \tag{11}$$

$$\frac{(\rho C_p)_{hnf}}{(\rho C_p)_f} = (1 - \varphi_2) \left[ 1 - \varphi_1 + \varphi_1 \frac{(\rho C_p)_{s1}}{(\rho C_p)_f} \right] + \varphi_2 \frac{(\rho C_p)_{s2}}{(\rho C_p)_f}, \tag{12}$$

$$\frac{k_{hnf}}{k_f} = \frac{k_{s2} + 2k_{bf} + 2\varphi_2(k_{s2} - k_f)}{k_{s2} + 2k_{bf} - 2\varphi_2(k_{s2} - k_f)}, \quad \text{where } \frac{k_{bf}}{k_f} = \frac{k_{s1} + 2k_f + 2\varphi_1(k_{s1} - k_f)}{k_{s1} + 2k_f - 2\varphi_1(k_{s1} - k_f)}, \tag{13}$$

$$\alpha_{hnf} = \frac{k_{hnf}}{(\rho C_p)_{hnf}}. \tag{14}$$

Here  $\rho_f$  is the base fluid density,  $\rho_{hnf}$  is the hybrid nanoparticle density,  $k_{hnf}$  is the hybrid nanoparticle thermal conductivity, and  $\alpha_{hnf}$  is the hybrid nanofluid thermal diffusivity. These values represent the Carreau hybrid nanofluid volume proportion of nanoparticle  $\varphi_1$  and  $\varphi_2$  (if  $\varphi_1 = 0$  and  $\varphi_2 = 0$  correspond to a base fluid). Within the context of the continuity equation (3), the stream function  $\psi(r, x)$  is introduced in order to fulfill the requirements.

$$u = \frac{1}{r} \frac{\partial \psi}{\partial r}, \quad v = -\frac{1}{r} \frac{\partial \psi}{\partial x}, \tag{15}$$





Asaigeethan et al.,

Where  $\psi = \sqrt{u(x)v_f x} Rf(\eta)$ , is the function of the dimensionless stream and

$$\eta = \frac{r^2 - R^2}{2R} \sqrt{\frac{u(x)}{v_f x}}, \quad \theta(\eta) = \frac{T - T_\infty}{T_p - T_\infty}, \tag{16}$$

As an illustration, the following is provided: the chemical categories (A and B) of concentrations:

$$m(\eta) = \frac{a}{a_0} \text{ and } n(\eta) = \frac{b}{b_0}, \tag{17}$$

Upon incorporating the designated transformation, the governing equations have the following form.

$$2D_1 k \left(1 + we^2(f'')^2\right)^{\frac{n-1}{2}} + D_1(1 + 2k\eta) f'''' \left(1 + we^2(f'')^2\right)^{\frac{n-1}{2}} + D_1(n-1)we^2(f'')^3 k \left(1 + we^2(f'')^2\right)^{\frac{n-3}{2}} + D_1(n-1)we^2(f'')^2 f'''' \left(1 + we^2(f'')^2\right)^{\frac{n-3}{2}} (1 + 2k\eta) - (f')^2 + ff'' = 0, \tag{18}$$

$$D_4(1 + 2k\eta)\theta'' + 2kD_3\theta' + D_3Prf\theta' + (1 + 2k\eta)[N_b n'(\eta) \cdot \theta'(\eta)] + (1 + 2k\eta) \left[ N_t (\theta'(\eta))^2 \right] = 0, \tag{19}$$

$$\frac{1}{Sc} \left( (1 + 2k\eta)m'' + 2km' \right) + m'f - Lmn^2 = 0, \tag{20}$$

$$\frac{\delta}{Sc} \left( (1 + 2k\eta)n'' + 2kn' \right) + n'f + Lmn^2 = 0, \tag{21}$$

The associated boundary conditions are

$$f(0) = 0, \theta(0) = 1, m'(0) = L_s m(0), N_b m'(0) + N_t \theta'(0) = 0, \delta n'(0) = \frac{-L_s n(0)}{v_f}, f'(0) = 1, f'(\infty) = 0, \theta(\infty) = 0, m(\infty) = 1, n(\infty) = 1. \tag{22}$$

The curvature parameter  $k$ , the Weissenberg number ( $We$ ), Prandtl number ( $Pr$ ), Schmidt number ( $Sc$ ), ratio diffusion coefficients ( $\delta$ ), the Brownian motion ( $N_b$ ), the thermophoresis ( $N_t$ ) and the homogeneous-heterogeneous reactions ( $L_s$ ) are all non-dimensional constants in equations (18) through (22), they are generally defined as follows.

**Nomenclature**

Curvature Parameter	$k$	$\frac{1}{R} \sqrt{\frac{v_f l}{u_0}}$
Weissenberg number	$We$	$\frac{\tau^2 r^2 u_0^3 x^2}{l^3 v_f}$
Prandtl number	$Pr$	$\frac{v_f}{\alpha}$
Schmidt number	$Sc$	$\frac{D_A}{D_B}$
Ratio of the diffusion coefficients	$\delta$	$\frac{D_A}{D_B}$
Brownian motion	$N_b$	$\frac{\tau D_B (b_w - b_\infty)}{v_f}$
Thermophoresis limiting factor	$N_t$	$\frac{\tau D_T (T_w - T_\infty)}{v_f T_\infty}$
homogeneous-heterogeneous reactions limiting factor	$L_s$	$\frac{l_s}{D_A} \sqrt{\frac{v_f l}{u_0}}$
-	$D_1$	$\frac{1}{[(1 - \varphi_1)^{2.5} (1 - \varphi_2)^{2.5}] (1 - \varphi_2) \left[ 1 - \varphi_1 + \varphi_1 \frac{\rho_{s1}}{\rho_f} \right] + \varphi_2 \frac{\rho_{s2}}{\rho_f}}$
-	$D_2$	$\frac{1}{(1 - \varphi_2) \left[ 1 - \varphi_1 + \varphi_1 \frac{\rho_{s1}}{\rho_f} \right] + \varphi_2 \frac{\rho_{s2}}{\rho_f}}$





Asaigeethan et al.,

$$\begin{aligned}
 - & D_3 & (1 - \varphi_2) \left[ 1 - \varphi_1 + \varphi_1 \frac{(\rho C_p)_{s1}}{(\rho C_p)_f} \right] + \varphi_2 \frac{(\rho C_p)_{s2}}{(\rho C_p)_f} \\
 - & D_4 & \frac{k_{s2} + 2k_{bf} + 2\varphi_2(k_{s2} - k_f)}{k_{s2} + 2k_{bf} - 2\varphi_2(k_{s2} - k_f)}
 \end{aligned}
 \tag{23}$$

We predict that in most of instances, the chemical kinds A and B are diffusion coefficients, it would be about same in size, so assume that diffusion coefficients  $D_A$  and  $D_B$  are equal (ie.,  $\delta = 1$ ), hence

$$m(\eta) + n(\eta) = 1, \tag{24}$$

Equations (20) and (21) thus become the following

$$\frac{1}{Sc} \left( (1 + 2k\eta)m'' + 2km' \right) + m'f + \frac{N_t}{N_b} \left[ (1 + 2k\eta)\theta''(\eta) + 2k\theta'(\eta) \right] - Lm(1 - m)^2 = 0, \tag{25}$$

Based on the specified boundary conditions

$$m'(0) = Ls m(0), \quad m(\infty) \rightarrow 1. \tag{26}$$

**Skin friction coefficient**

The coefficient of skin friction  $C_f$  is the relevant physical property. This describes surface drag. The shearing stress at the wall surface  $\tau_{rx}$  defined as

$$\tau_{rx} = -\mu_{hnf} \left( \frac{\partial u}{\partial r} \left[ 1 + \Gamma^2 \left( \frac{\partial u}{\partial r} \right)^2 \right]^{\frac{n-1}{2}} \right)_{r=R} = -D_2 f''(0) \left( 1 + we^2 (f''(0))^2 \right)^{\frac{n-1}{2}}, \tag{27}$$

Here  $\mu_{nf}$  is the viscosity coefficient. The definition of the coefficient of skin friction is

$$C_f = \frac{2(\tau_{rx})_{r=R}}{\rho_f u(x)^2}, \tag{28}$$

Using equations (27) and (28) obtains the result.

$$C_f \sqrt{Re_x} = -2D_2 f''(0) \left( 1 + we^2 (f''(0))^2 \right)^{\frac{n-1}{2}}, \tag{29}$$

**Nusselt number**

The local Nusselt numeral  $Nu$  is the physical quantity of interest. The heat flux at the wall's surface  $q_w$  is given by

$$q_w = -k_{hnf} \left( \frac{\partial T}{\partial r} \right)_{r=R'} \tag{30}$$

The local Nusselt number is given by

$$Nu = \frac{(xq_w)_{r=R}}{k(T_p - T_\infty)}, \tag{31}$$

By the equation (30) in (31) obtained

$$\frac{Nu}{\sqrt{Re_x}} = -D_4 \theta'(0), \tag{32}$$

In equations (29) and (32)  $Re_x$  represents the local Reynolds number defined by  $Re_x = \frac{xu(x)}{\nu_f}$ .

**Formulation of Fuzzification**

This study also investigates the use of fuzzy notions to compare nanofluid and hnf. After the non-linear ODEs are transformed into FDEs, the volume proportion of the hnf is obtained as a TFN. The MATLAB initiative bvp5c is utilized to solve FDEs. The flow heat and rate are affected by an instantaneous change in the volume proportion of hnf. The heat transmission and flow rate of the hnf is determined only by these factors, as some academics assess that the volume consisting of nanoparticles are between [0.01-0.04], Since  $\varphi_1$  and  $\varphi_2$  depict the volume proportion of nanoparticles  $MnZnFe_2O_4$  and  $NiZnFe_2O_4$  of a fuzzy context, it is performable to approach a challenging case by obtaining volume fractions as a TFN. The nanoparticle's characteristics are defined in Table 2. The volume





proportions of hnfutilized for this investigation are categorized as TFNs; these TFNs are then converted into  $\alpha$ -cut techniques, and  $\alpha$ -cut regulates the fuzziness of TFNs.

The interpretation of the fuzzy number at each  $\alpha$ -cut was found using the TFNs ranging from 0 to 1. The TFNs define the triangle membership functions of the fuzzy numbers. Using a fuzzy process and the  $\alpha$ -cut approach, the nonlinear ODEs (18), (19), and (25) were transformed into FDEs with their corresponding boundary constraints for fuzzy solutions.

$$2D_1k \left(1 + we^2 \left(\frac{d^2}{d\eta^2} [f_1(\eta, \alpha), f_2(\eta, \alpha)]\right)^2\right)^{\frac{n-1}{2}} + D_1(1 + 2k\eta) \frac{d^3}{d\eta^3} [f_1(\eta, \alpha), f_2(\eta, \alpha)] \left(1 + we^2 \left(\frac{d^2}{d\eta^2} [f_1(\eta, \alpha), f_2(\eta, \alpha)]\right)^2\right)^{\frac{n-1}{2}} + D_1(n - 1)we^2 \left(\frac{d^2}{d\eta^2} [f_1(\eta, \alpha), f_2(\eta, \alpha)]\right)^3 k \left(1 + we^2 \left(\frac{d^2}{d\eta^2} [f_1(\eta, \alpha), f_2(\eta, \alpha)]\right)^2\right)^{\frac{n-3}{2}} + D_1(n - 1)we^2 \left(\frac{d^2}{d\eta^2} [f_1(\eta, \alpha), f_2(\eta, \alpha)]\right)^2 \left(1 + we^2 \left(\frac{d^2}{d\eta^2} [f_1(\eta, \alpha), f_2(\eta, \alpha)]\right)^2\right)^{\frac{n-3}{2}} (1 + 2k\eta) - D_2B \left(\frac{d}{d\eta} [f_1(\eta, \alpha), f_2(\eta, \alpha)]\right) - \left(\frac{d}{d\eta} [f_1(\eta, \alpha), f_2(\eta, \alpha)]\right)^2 + f \frac{d^2}{d\eta^2} [f_1(\eta, \alpha), f_2(\eta, \alpha)] = 0, \tag{33}$$

$$D_4(1 + 2k\eta) \frac{d^2}{d\eta^2} [\theta_1(\eta, \alpha), \theta_2(\eta, \alpha)] + 2kD_3 \frac{d}{d\eta} [\theta_1(\eta, \alpha), \theta_2(\eta, \alpha)] + D_3Prf \frac{d}{d\eta} [\theta_1(\eta, \alpha), \theta_2(\eta, \alpha)] + (1 + 2k\eta) \left[N_b n'(\eta) \frac{d}{d\eta} [\theta_1(\eta, \alpha), \theta_2(\eta, \alpha)]\right] + (1 + 2k\eta) \left[N_t \left(\frac{d}{d\eta} [\theta_1(\eta, \alpha), \theta_2(\eta, \alpha)]\right)^2\right] = 0, \tag{34}$$

$$\frac{1}{Sc} \left( (1 + 2k\eta) \frac{d^2}{d\eta^2} [m_1(\eta, \alpha), m_2(\eta, \alpha)] + 2k \frac{d}{d\eta} [m_1(\eta, \alpha), m_2(\eta, \alpha)] \right) + f \frac{d}{d\eta} [m_1(\eta, \alpha), m_2(\eta, \alpha) + \frac{N_t}{N_b} \left(1 + 2k\eta \frac{d^2}{d\eta^2} [\theta_1(\eta, \alpha), \theta_2(\eta, \alpha)]\right) ] = 0, \tag{35}$$

The persistent boundary constraints.

$$f(\eta, \alpha) = 0, \frac{d}{d\eta} [f_1(\eta, \alpha), f_2(\eta, \alpha)] = 1, \theta(\eta, \alpha) = 1, \frac{d}{d\eta} [m_1(\eta, \alpha), m_2(\eta, \alpha)] = L_s m(\eta, \alpha), N_b \frac{d}{d\eta} [m_1(\eta, \alpha), m_2(\eta, \alpha)] + N_t \frac{d}{d\eta} [\theta_1(\eta, \alpha), \theta_2(\eta, \alpha)], \frac{d}{d\eta} [f_1(\eta, \alpha), f_2(\eta, \alpha)] = 0, \eta \rightarrow \infty, \theta(\eta, \alpha) = 0, \eta \rightarrow 0, m(\eta, \alpha) = 1, \eta \rightarrow 1 \tag{36}$$

**Method of solution**

The governing equations (18), (19), and (25) are extremely nonlinear when the boundary conditions (22) and (26) are taken into effect. To solve the non-dimensional regulating equations (18), (19), and (25), In conjunction with the bvp5c method, the strategy for the boundary value problem is utilized. in MATLAB. First, transform equations (18), (19), and (25) to first-order ODEs.

**RESULTS AND DISCUSSION**

The principal intention of this segment is to illustrate the physical flow problem with graphical representations. We = 3, k = 0.5, m = 0.2, L = 0.5, Sc = 1.2,  $N_t$  = 0.5, and  $N_b$  = 1.5 are some of the flow parameters that are evaluated to examine their effects on the surface's skin friction coefficient, temperature, and flow velocity. Fig.3-5 presents the graphical results generated by the MATLAB software. This section addresses the influence of different materials on the non-dimensional moment, energy, and concentration responses for both the nano fluid and hybrid nanofluid responses. A directive to assess the current results states that the Weissenberg numeral ( $We$ ), Prandtl numeral ( $Pr$ ), Schmidt numeral ( $Sc$ ), curvature parameter ( $k$ ), homogeneous-heterogeneous reactions parameter ( $Ls$ ), Brownian motion ( $N_b$ ), and thermophoresis ( $N_t$ ) are different assumptions. Tabular data presents the outcome. Figure 6-7 depicts the fuzzy velocity and fuzzy temperature fields defined in the nanoparticles  $\varphi_1$  and  $\varphi_2$  as TFNs.

Fig.3 (a) and (b) display a comparison between hybrid nanofluid and nanofluid velocity fields. The dotted lines show how hybrid nanoparticles change the behavior of the stretching cylinder, the velocity profile decreases for shear thinning ( $n < 1$ ) fluid and increases for shear thickening ( $n > 1$ ) fluid when the Weissenberg number is





enhanced. This is a significant observation. The fluid becomes denser and loses speed when the Weissenberg number increases, which represents the ratio of the fluid's relaxation time to the length of the specific procedure. Fig.3 (c) and (d) show how the curvature parameter ( $k$ ) reduces the velocity profiles for shear thinning ( $n < 1$ ) and shear thickening ( $n > 1$ ) fluids in both circumstances. This is because the radius of the cylinder and the curvature limiting factor are inversely correlated. Thus, the cylinder's parameter decreases the radius by increasing curvature, which likewise decreases the surface. Consequently, the barrier to fluid movement is reduced, leading to an increase in velocity. The creation of lowered velocity curves was caused by the Carreau hybrid nanofluid particles' difficulties when this force had a resistive nature. On a physical level, the curve sketched parameter is inversely related to the base fluid/hybrid nanoparticles' kinematic viscosity. These factors include the Weissenberg number ( $We$ ), curvature ( $k$ ), and the impact of constant parameters such as  $k = 0.5$ ,  $Pr = 2$ ,  $m = 0.2$ ,  $L = 0.5$ , and  $Sc = 1.2$ .

Fig. 4(a) and (b) show a comparison of hybrid nanofluids with nanofluids for  $We = 3$ ,  $Pr = 2$ ,  $m = 0.2$ ,  $L = 0.5$ ,  $Sc = 1.2$ ,  $N_t = 0.5$ , and  $N_b = 1.5$ . Increasing the Prandtl numeral ( $Pr$ ) the temperature profile of hybrid nanofluids reduces for both shear thickening ( $n > 1$ ) fluid and shear thinning ( $n < 1$ ) fluids. This is caused by the presence of an inverse relationship between the Prandtl number and the diffusivity of heat. Hence, a larger value of the Prandtl numeral is related to low diffusion of energy as a result temperature declines and shows significance identical in both hybrid nanofluid and nanofluid. Fig. 5 and 6 depict the volume proportion of nanoparticles of  $MnZnFe_2O_4$  ( $\varphi_1$ ) and  $NiZnFe_2O_4$  ( $\varphi_2$ ) that are classified as TFNs (see Table 2), and for specific values of  $\alpha$ -cut,  $\alpha = 0, 0.3, 0.7$  and  $1$ ,  $f'(\eta, \alpha)$  and  $\theta(\eta, \alpha)$  are regulated by  $\alpha$ -cut. The fuzzy velocity  $f'(\eta, \alpha)$  in Fig. 5(a) converts to the lower and upper boundaries when  $\varphi_1$  is a TFN and the dashed line represents the hybrid nanofluid at  $\varphi_2 = 0.03$ , and the solid represents the nanofluid. In Fig. 5(b)  $f'(\eta, \alpha)$  converts into the lower and upper boundaries of the fuzzy velocity profiles when  $\varphi_2$  is a TFN and the hybrid nanofluid at  $\varphi_1 = 0.03$  is represented by the dashed line, while the solid represents the nanofluid. The width between the hnf and nanofluid diminishes in both scenarios when  $\alpha$ -cut increases, and they approach consistent at  $\alpha$ -cut = 1. In Fig. 6 (a) the upper and lower boundaries of the fuzzy temperature profile are represented by the  $\theta(\eta, \alpha)$  when  $\varphi_1$  is a TFN and  $\varphi_2 = 0.03$ , the hybrid nanofluid is represented by the dotted line, a solid line indicating the base fluid. In Fig. 6 (b)  $\theta(\eta, \alpha)$  transforms into the least and greatest bounds of the fuzzy temperature profile when a TFN is  $\varphi_2$  and given  $\varphi_1 = 0.03$ , the hnf is represented by a dashed line and the base fluid by the solid line. The hybrid nanofluid and nanofluid become less wide at  $\alpha$ -cut = 1 and they become coherent with each other in both scenarios as  $\alpha$ -cut increases.

Fig 7 shows the surface drag force against the curvature parameter. The size of the coefficient of skin friction has been shown to reduce along with increasing Weissenberg numeral ( $We$ ) values. In addition, the hybrid nanofluid exhibits skin friction values that are higher than those of the nanofluid. Fig 8 The Nusselt numeral varies concerning the curvature limiting factor ( $k$ ) and the Prandtl number ( $Pr$ ). It has been shown that the Nusselt numeral is smaller when  $Pr$  values increase. Moreover, compared to nanofluid, the hnf has a higher Nusselt numeral.

Using a membership function compares the hybrid nanofluid ( $MnZnFe_2O_4/NiZnFe_2O_4$ ) to the base fluid spanning wide ranges of value consider at  $\eta = 0.3$ . Here, TFN is calculated using the volume proportion of nanoparticles. Fig. 9 The hybrid nano fluid's velocity profile is found to be significantly less than that of the base fluid for shear thinning ( $n < 1$ ) and greater for shear thickening ( $n > 1$ ), despite some fluctuation in the velocities of the two fluids. Fig. 10 there is no longer a noticeable temperature difference between base and hybrid nanofluids. For shear thinning ( $n < 1$ ), hybrid nanoparticles can significantly diminish the base fluid's thermal conductivity; for shear thickening ( $n > 1$ ), hybrid nanoparticles can significantly enhance the base fluid's thermal conductivity.

Table 3: In addition to the limiting case of parameters  $m = 0.2$ ,  $Pr = 2$ ,  $L = 0.5$ , and  $Sc = 1.2$ , When comparing the variation of skin friction values for different nanofluids and hybrid nanofluids with varying Weissenberg ( $We$ ) numbers and curvature ( $k$ ) parameters, it is evident that the coefficient of skin friction is often higher in hybrid nanofluids compared to regular nanofluids. If the curvature parameter value were to increase, the skin friction values of the hnf would be lower than those of the nanofluid.





Table 4: Describe the limiting cases with the parameters  $m = 0.2$ ,  $We = 3$ ,  $L = 0.5$ ,  $\beta = 1.2$ , as well as the effect of the local Nusselt numeral on the difference between the nanofluid and hybrid nanofluid with various kinds of Prandtl ( $Pr$ ) number and curvature ( $k$ ) parameters. In some cases, the hybrid nanofluid's local Nusselt number value is improved than that of the base fluid.

## CONCLUSION

The significance of the present flow problem being studied is the periodic body velocity, temperature, and concentration for the flow of a modified Buongiorno model-based Carreau hybrid nanofluid along a stretched cylinder in a fuzzy environment. The governing equations were converted into a set of FDEs, which were then solved using MATLAB. We learned, that by fixing the parameters, the convergence of the approach was verified quantitatively. Uncertainty variability is examined using the triangle membership function (TMF), and the TFNs are governed by  $\alpha$  - cut.

1. The hybrid nanoparticles' appearance in the fluid velocity compared with the nanofluid momentum causes the fluid velocity to decrease for shear thinning ( $n < 1$ ) fluid and increase for shear thickening ( $n > 1$ ) fluid, in opposition to enhanced Weissenberg number ( $We$ ).
2. In the enhanced curvature factor, the velocity of the hybrid nanoparticles and nanofluid is fewer for both shear thinning ( $n < 1$ ) and shear thickening ( $n > 1$ ) fluid.
3. When the Prandtl number increases, the thermal conductivity of the nanofluid and hybrid nanofluid decreases in the same way for both shear thinning ( $n < 1$ ) fluid and shear thickening ( $n > 1$ ) fluid.
4. The consistent magnitude of the fuzzy velocity and temperature signifies the anticipated sensitivity of the TFN. As  $\alpha$  increase from 0 to 1, the optimal response is situated between the upper and lower values.
5. Moreover, it is also clear that hazy triangle values that correspond to temperatures and velocities at various locations along the divergence channel were obtained. Also, temperature and velocity bounds were displayed at different times in the divergence channel's fixed value of the associated parameter.
6. The skin friction coefficient value is higher in the hnf than the nanofluid through parameters  $k$  exhibited when the Weissenberg number ( $We$ ) increased.
7. The Nusselt number ( $Nu$ ) of the hnf exceeds that of the nanofluid through the parameters  $k$  when the Prandtl number ( $Pr$ ) increases.

## REFERENCES

1. Khashi NS, Arifin NM, Pop I. Magnetohydrodynamic (MHD) boundary layer flow of hybrid nanofluid over a moving plate with Joule heating. *Alex. Eng. J.* 2022; 61.
2. Nazir U, Nidal H, Abu-Hamdeh, Nawaz M. Numerical study of thermal and mass enhancement in the flow of Carreau-Yasuda fluid with hybrid nanoparticles. *Case Studies in Thermal Engineering.* 2021; 27.
3. Dogonchi AS, Chamkha AJ, Tilehnoee MH. Effects of homogeneous- heterogeneous reactions and thermal radiation on b Cu-water nanofluid flow over an expanding flat plate with non-uniform heat source. *J. Cent. S. Univ.* 2019; 26.
4. Kumar KG, Reddy MG, Kumari PV, Ali A. Application of different hybrid nanofluids in convective heat transport of Carreau fluid. *Chaos, Solitons & Fractals.* 2020; 141.
5. Ghadikolaei SS, Hosseinzadeh KH, Ganji DD. Investigation on ethylene glycol-water mixture fluid suspends by hybrid nanoparticles ( $TiO_2 - CuO$ ) over a rotating cone with considering nanoparticles shape factor. *J Mol Liq.* 2018; 272.
6. Dogonchi AS, Waqas M, Seyyedi S.M. CVFEM analysis for  $Fe_3O_4 - H_2O$  nanofluid in an annulus subject to thermal radiation. *Int J Heat Mass Transfer.* 2019; 132.
7. Waqas H, Farooq U, Yang S. Heat transfer aspects in Carreau nanofluid having hybrid nanoparticles through a porous medium. *Appl. Math. Mech.* 2023; 103.







**Asaigeethan et al.,**

8. Reddy VS, Kandasamy J, Sivanandam S. Impacts of Casson Model on Hybrid Nanofluid Flow over a Moving Thin Needle with Dufour and Soret and Thermal Radiation Effects. *Math. Comput. Appl.*2023;28.
9. Kavya S, Nagendramma V, Ahammad NA, Sohail A. Magnetic-hybrid nanoparticles with stretching/shrinking cylinder in a suspension of MoS<sub>4</sub> and copper nanoparticles. *Int. Comm. Heat Mass Transf.*2022;136.
10. Sulochana C. Aparna SR, Sandeep N. Impact of linear/nonlinear radiation on incessantly moving the thin needle in MHD quiescent Al-Cu/methanol hybrid nanofluid. *Int. Ambient. Energy.*2020;43.
11. Madhukesh K, Ramesh GK, Alsulami MD. Characteristic of thermophoresis effect and convective boundary thermal conditions on the flow of hybrid nanofluid over a moving thin needle. In *Waves in Random and Complex Media*. Taylor & Francis: Abingdon, UK.2021.
12. Alwani SSN, Norfifah B, Norihan A, Fadzilah A. Effect of Buoyancy force on the flow and heat transfer around the thin needle in Hybrid nanofluid. *CFD Lett.* 2020;12.
13. Buongiorno J. Convective transport in nanofluids. *ASME J Heat Transfer.*2006;250.
14. Kaleva O. Fuzzy differential equations *Fuzzy Sets Syst* 1987;24(3).
15. Siddique, Nadeem I, Khan M, Jamil I, Noshad R. Analysis of fuzzified boundary value problems for MHD Couette and Poiseuille flow. *Sci Rep.*2022;12.
16. Dubois D, and Prade H. Operations on fuzzy numbers. *Int. J. Syst. Sci.*1978;98.
17. Seikkala S. On the fuzzy initial value problem. *Fuzzy Sets Syst.*1987;24.
18. Almutairi M, Zureigat H, Ismail A, Iand Fared J A. Fuzzy numerical solution via finite difference scheme of the wave equation in double parametrical fuzzy number form. *Mathematics.*2021; 9.
19. Salahshour S, Ahmadian A, and Mahata A. The behavior of logistic equation with Alley effect in fuzzy environment: FDE approach. *Int. J. Appl. Comput. Math.*2018;62.
20. Merkin JH. Model for isothermal homogeneous-heterogeneous reactions in Boundary-layer flow". *Math. Comput. Model.* 1996;24.
21. Ahmad S, Akhter S, Shahid MI, Ali K, Akhter M, Ashraf M. Novel thermal aspects of hybrid nanofluid flow comprising of manganese zinc ferrite MnZnFe<sub>2</sub>O<sub>4</sub>, nickel-zinc ferrite NiZnFe<sub>2</sub>O<sub>4</sub> and motile microorganisms. *Ain Shams Engineering Journal.*2022; 13.
22. Asaigeethan P, Vaithiyalingam K, Loganathan K, Prabu K., Abbas M, Mishra NK. Numerical study of Carreau fuzzy nanofluid across a stretching cylinder using a modified version of Buongiorno's nanofluid model, *Alex. Eng. J.*2024; 101:318-329.

**Table 1: Thermal physical characteristics of base fluids and nanoparticle**

Thermal properties	$C_p (J kg^{-1} K^{-1})$	$\rho (kg m^{-3})$	$k (W m^{-1} K^{-1})$
<b>MnZnFe<sub>2</sub>O<sub>4</sub></b>	1050	4700	3.9
<b>NiZnFe<sub>2</sub>O<sub>4</sub></b>	710	4800	6.3
<b>C<sub>n</sub>H<sub>2n+2</sub></b>	1.69	850	0.145

**Table 2: TFNs of fuzzy hybrid nanoparticles of volume fraction**

Fuzzy number	Crisp value	TFN	$\alpha$ – cut approach
$\varphi_1$	[0.01 – 0.04]	[0, 0.05, 0.1]	$[0.05\alpha, 0, 1 - 0.05\alpha], \alpha \in [0, 1]$
$\varphi_2$	[0.01 – 0.04]	[0, 0.05, 0.1]	$[0.05\alpha, 0, 1 - 0.05\alpha], \alpha \in [0, 1]$

**Table 3: Coefficient of Skin frictions**

$k$	$We$	$-C_f \sqrt{Re_x}$ $\varphi_1 = 0.03, \varphi_2 = 0$ NanoFluid	$-C_f \sqrt{Re_x}$ $\varphi_1 = \varphi_2 = 0.03$ Hybrid Nanofluid
0.2	1	1.0363	1.0412
	1.5	0.8540	0.8597
	2	0.7327	0.7383





0.3	1	1.0950	1.0954
	1.5	0.8899	0.8928
0.5	1	1.2094	1.2017
	2	0.8079	0.8076

Table: 4The Nusselt number

$k$	$Pr$	$-Nu/\sqrt{Re_x}$ $\varphi_1 = 0.03, \varphi_2 = 0$ NanoFluid	$-Nu/\sqrt{Re_x}$ $\varphi_1 = \varphi_2 = 0.03$ Hybrid Nanofluid
0.2	1	1.2342	1.2931
	1.3	1.1651	1.2196
	2	0.9993	1.0430
0.3	1	1.3968	1.4571
	3	0.1928	0.1936
0.5	1.3	1.6524	1.8556

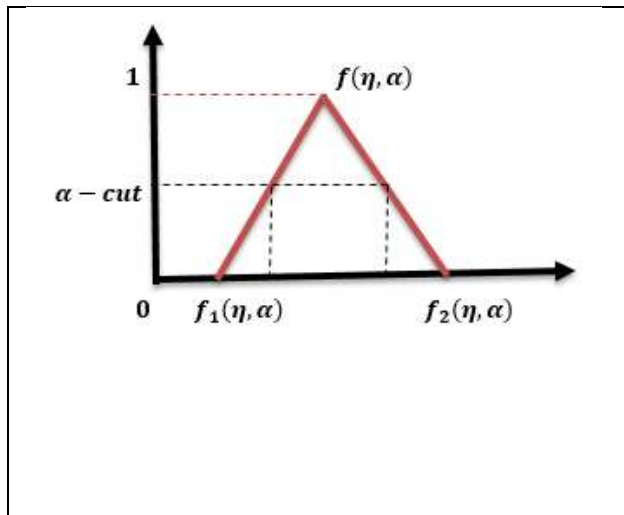


Fig.1: MFs of a triangular fuzzy number.

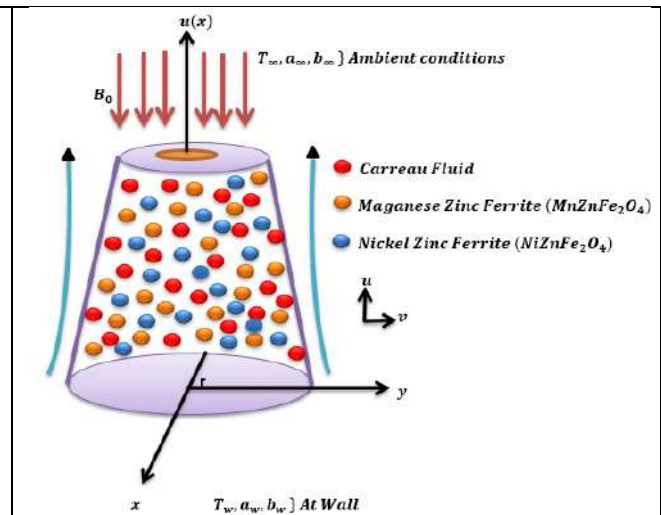


Fig.2: The physical model and coordinate system

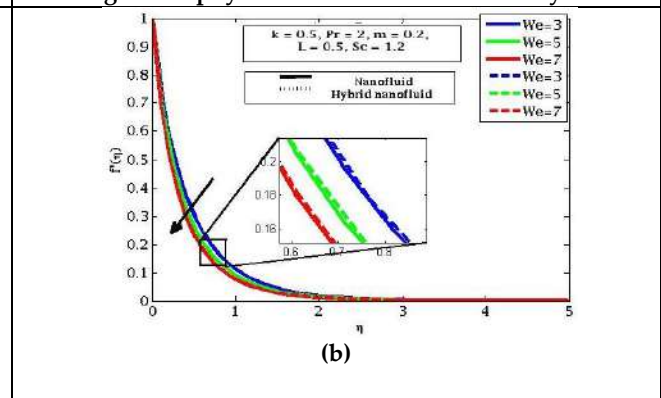
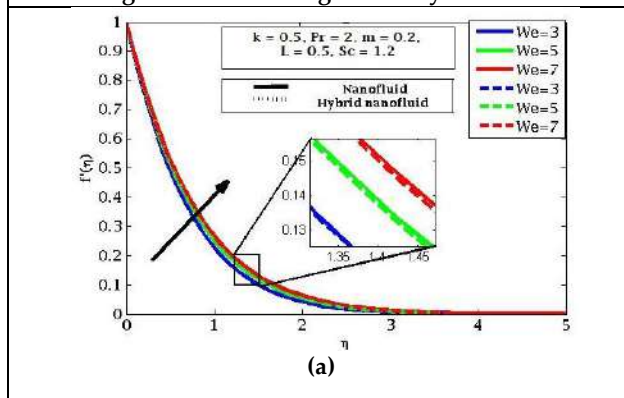


Fig. 3: "We" effects on velocity when (a)  $n < 1$ , (b)  $n > 1$





Asaigeethan et al.,

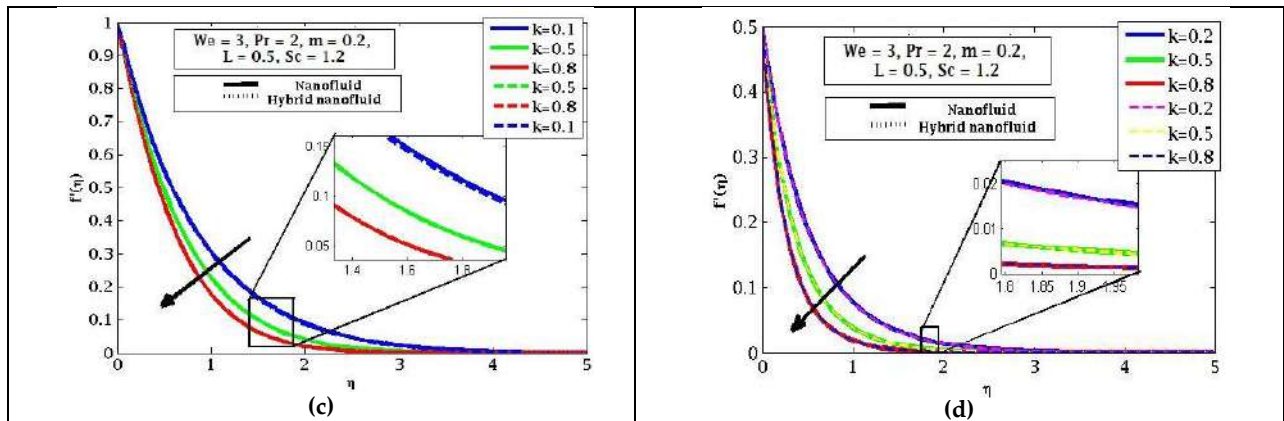


Fig.4: "k" effects on velocity when (c)  $n < 1$ , (d)  $n > 1$

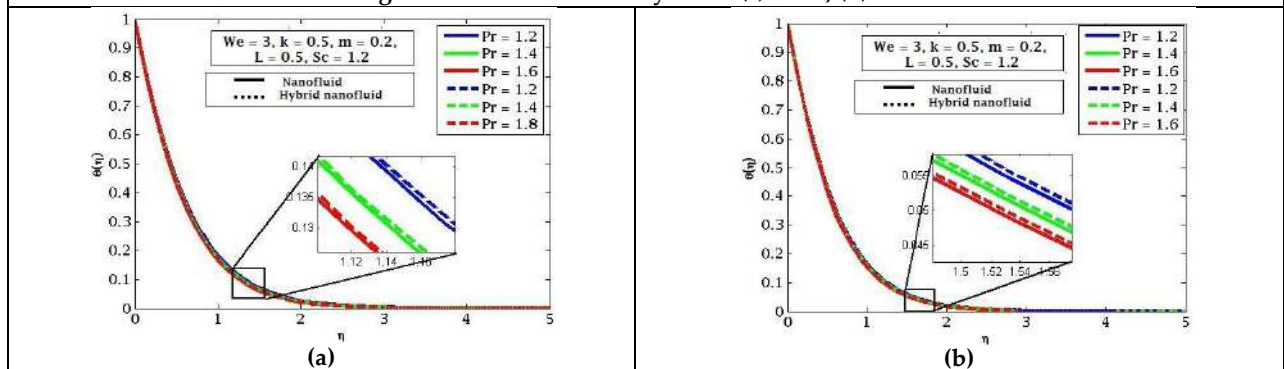


Fig. 5: "Pr" effects on temperature when (c)  $n < 1$ , (d)  $n > 1$

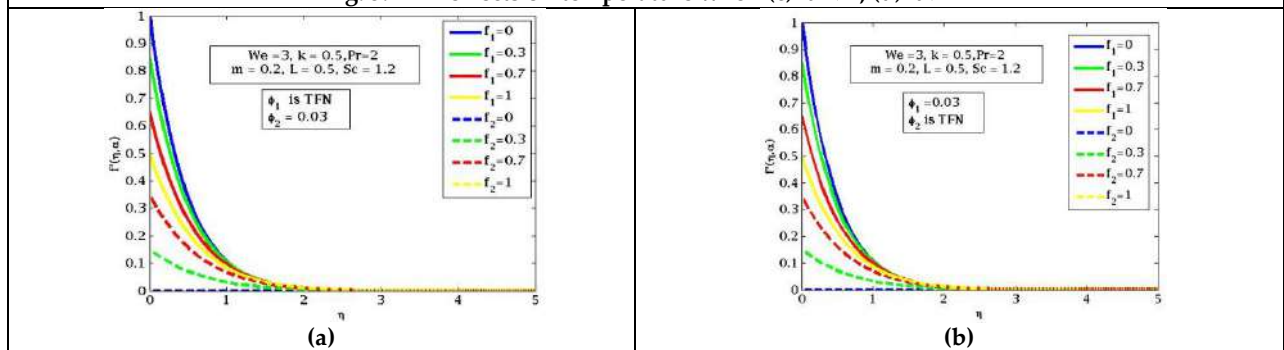


Fig.6: Effects of  $\varphi_1$  and  $\varphi_2$  on the fuzzy velocity when (a)  $\varphi_1$  is TFN, (b)  $\varphi_2$  is TFN

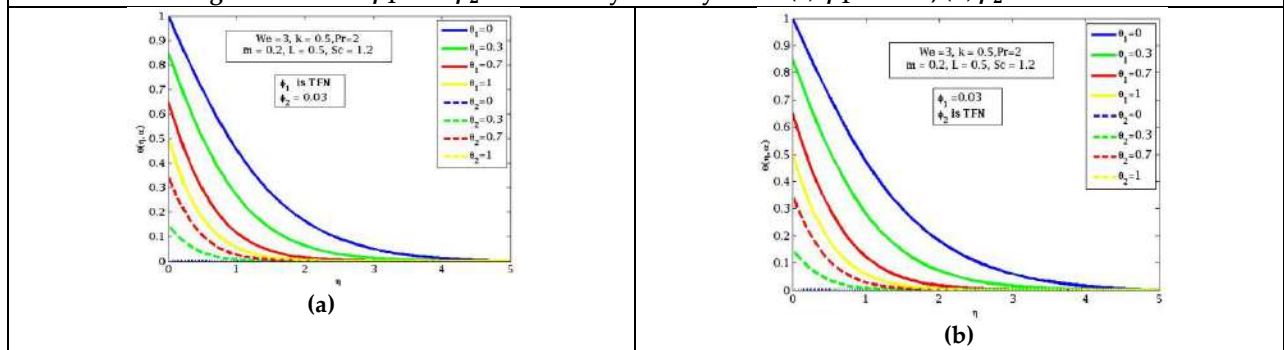


Fig. 7: Effects of  $\varphi_1$  and  $\varphi_2$  on the fuzzy temperature when (a)  $\varphi_1$  is TFN, (b)  $\varphi_2$  is TFN



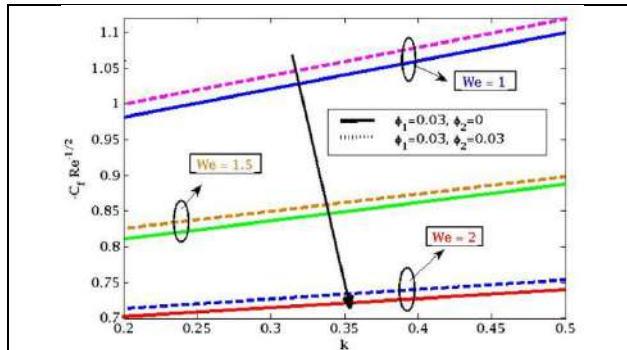


Fig. 8. Effect of hybrid nanoparticles for on skin friction for different values

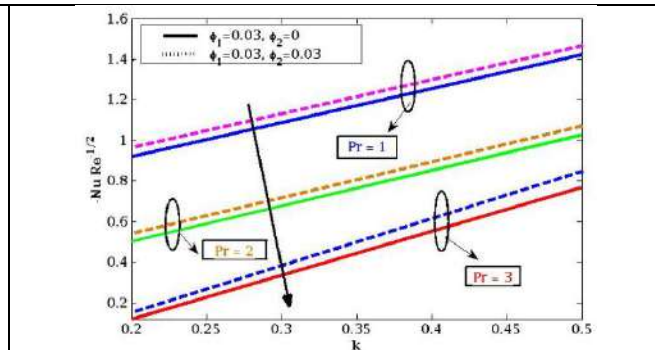


Fig. 9. Effect of hybrid nanoparticles for on Nusselt number for different values

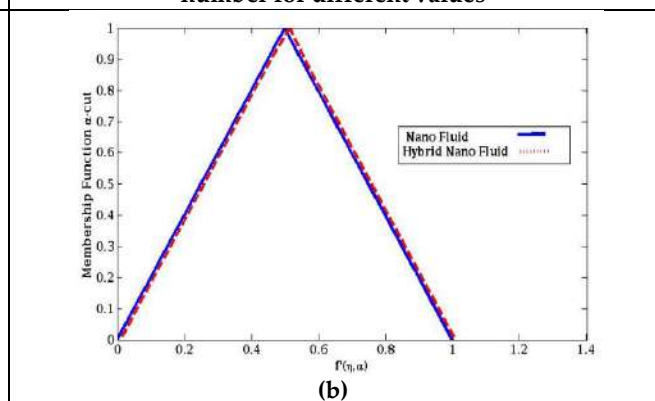
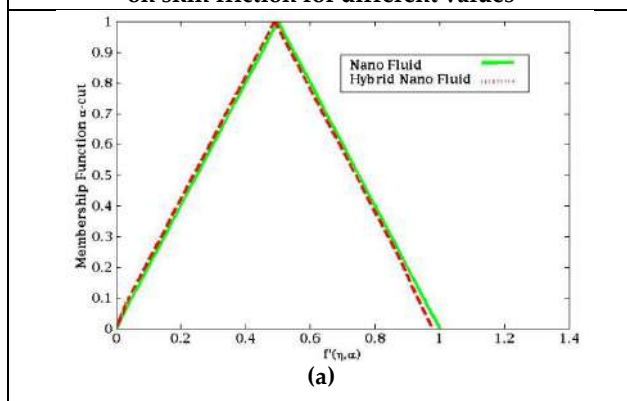


Fig. 10. Comparison of nanofluid and hybrid nanofluid on fuzzy velocity at  $\eta = 0.3$  when (a)  $n < 1$  and (b)  $n > 1$

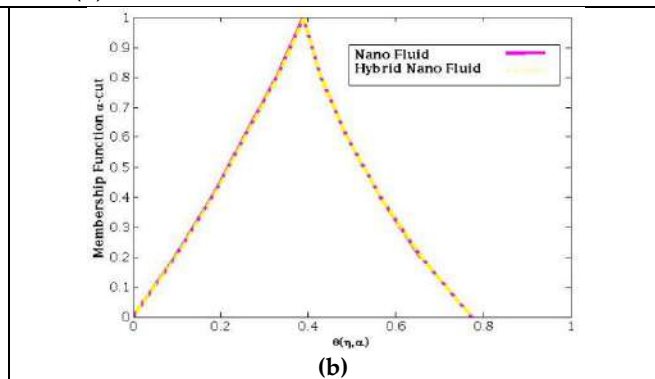
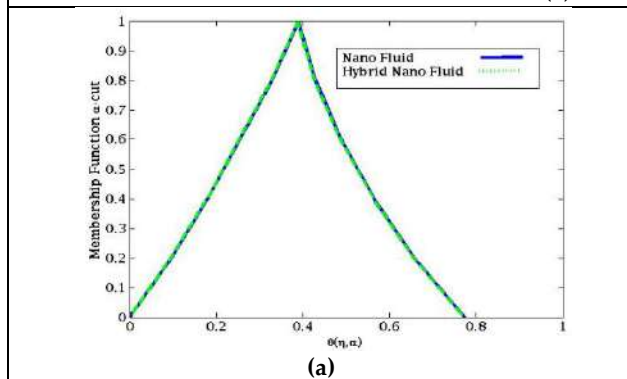


Fig.11. Comparison of nanofluid and hybrid nanofluid on fuzzy temperature at  $\eta = 0.3$  when (a)  $n < 1$  and (b)  $n > 1$





## Isolation, Identification and Bioprofiling of Endophytic Fungi from *Piper schmidtii*

Mohana M<sup>1</sup>, Saritha E<sup>2\*</sup>, Nivetha L<sup>2</sup> and Lakshmi Ajit<sup>1</sup>

<sup>1</sup>M.Sc Biotechnology, Department of Biotechnology, PSG College of Arts & Science, (Affiliated to Bharathiar University), Coimbatore, Tamil Nadu, India.

<sup>2</sup>Assistant Professor, Department of Biotechnology, PSG College of Arts & Science, (Affiliated to Bharathiar University), Coimbatore, Tamil Nadu, India.

Received: 17 July 2024

Revised: 25 Aug 2024

Accepted: 26 Oct 2024

### \*Address for Correspondence

**Saritha E**

Assistant Professor,

Department of Biotechnology,

PSG College of Arts & Science,

(Affiliated to Bharathiar University),

Coimbatore, Tamil Nadu, India.

E.Mail: sarithasenthikumar@gmail.com



This is an Open Access Journal / article distributed under the terms of the **Creative Commons Attribution License** (CC BY-NC-ND 3.0) which permits unrestricted use, distribution, and reproduction in any medium, provided the original work is properly cited. All rights reserved.

### ABSTRACT

Endophytic fungi, *Neofusicoccum parvum* and *Pestalotiopsis microspora*, were isolated from the leaves of *Piper schmidtii* (a medicinal plant) and were confirmed by 18S rRNA gene sequencing. Compared with *Pestalotiopsis microspora*, the ethyl acetate extract of *Neofusicoccum parvum* revealed substantial levels of total phenolics (185.96 mg GAE/g extract), tannins (188.43 mg GAE/g extract), and flavonoids (25.81 mg QE/g extract), which are known for their antioxidant properties. These bioactive compounds exhibited significant activity in DPPH radical scavenging, ABTS, phosphomolybdenum reduction, and nitric oxide assays. Furthermore, the extract demonstrated notable  $\alpha$ -amylase inhibitory activity ( $IC_{50}$ : 65.51  $\mu$ g/mL), suggesting its effect in anti-diabetic.

**Key words:** *Piper schmidtii*, antioxidant property, antidiabetic potential, bioprofiling,  $\alpha$ -amylase inhibition

### INTRODUCTION

Traditional medicinal plants are essential sources for new pharmaceuticals due to their rich chemical diversity [1]. Concerns over side effects and bacterial resistance associated with synthetic drugs have highlighted the therapeutic potential of phytochemicals in herbal medicines [2]. Similarly, safety and efficacy issues with synthetic antioxidants have increased interest in natural alternatives, such as those from endophytic fungi [3]. Endophytic fungi, living symbiotically within plants, are rich sources of bioactive compounds with antiviral, antifungal, anticancer, and antibacterial properties [4]. They often produce the same compounds as their host plants, possibly through genetic







Mohana et al.,

exchange [5, 6,7]. The demand for antioxidants to combat free radicals is growing due to today's environmental challenges. *Piper schmidtii*(*Piperaceae*) holds significant importance in traditional medicine due to the presence of piperine, a compound with diverse ability such as antifungal, antioxidant, anti-inflammatory, antimicrobial, and antidiabetic [8,9].This study will investigate the bioactive potential of two endophytic fungi from *Piper schmidtii*. Despite their recognized benefits, global studies on the phytochemical composition and pharmacological activities of these fungi are scarce.

## MATERIALS AND METHODS

### Isolation of Endophytic Fungi

Fresh plant materials were collected from TNAU, Coimbatore, Tamil Nadu, India and identified by Botanical survey of India, Coimbatore (BSI/SRC/5/23/2022/Tech./404). Surface sterilized leaf segments were incubated on PDA with Chloramphenicol (150 mg/L) at 26±2°C for 15-20 days and the emerging fungi were identified based on conidial and spore morphology under a microscope(40X)[10].

### Molecular Identification

The genomic DNA was isolated, and the ITS region was amplified using PCR with ITS-4 and ITS-5 primers [11]. These sequences were analyzed using BLAST in NCBI. Further, multiple sequence alignment and phylogenetic analysis were performed using Clustal X and MEGA X, respectively [12].

### Production of Bioactive Compounds

Two fungal colonies (6 mm) were subcultured in PDB for 21 days. After incubation, the broth was filtered using Whatman No. 1 filter paper. The filtrate was mixed with an equal volume of ethyl acetate in a separating funnel and allowed to settle for 2h. The ethyl acetate extracts were then concentrated using a vacuum rotary evaporator at 40°C and stored at 4°C [13].

### Quantification of Bioactive Compounds

The total phenolic content (TPC) was determined [14].The total tannin content (TTC) was measured [15]. The total flavonoid content (TFC) was assessed using colorimetric method [16].

### In vitro Antioxidant Activity

The free radical scavenging activity of fungal extracts was evaluated using the 2,2-diphenyl-1-picrylhydrazyl (DPPH) method [17].The activity was expressed as the IC<sub>50</sub>, which is the concentration needed to inhibit 50% of the DPPH radicals.The Modified ABTS assay, measures the scavenging ability of antioxidants on ABTS<sup>+</sup> free radicals. Antioxidant activity was expressed as Trolox equivalent (µM/g)[18].Phosphomolybdenum assay was evaluated [19].Nitric oxide assay was measured [20].

### Antimicrobial and Antifungal Activity

The antibacterial study of endophytic fungal extract was evaluated against *Klebsiella pneumoniae* (MTCC10309), *Streptococcus pneumoniae* (MTCC405), *Pseudomonas aeruginosa* (MTCC2057), and *Staphylococcus aureus* (MTCC9760) using a modified agar disc diffusion method [21]. *Candida albicans* and *Aspergillusniger* were seeded on SDA plates. Discs with fungal extracts,negative control (DMSO) and a positive control (Fluconazole at 10 µg per disc) were placed on the agar plates.Zones of inhibition were observed 3-5 days after incubation at 28°C [22].

### In vitro anti-diabetic activity

The α-amylase inhibition assay was determined[23].







## RESULTS AND DISCUSSION

### Morphological Characteristics

*Neofusicoccum parvum* and *Pestalotiopsis microspora*, endophytic fungi isolated from *Piper schmidtii* leaves. *Neofusicoccum parvum* is characterized by its rapid growth with white aerial mycelia that darken with age (Fig. 1) The hyaline, aseptate conidia of *Neofusicoccum parvum* are oval to ellipsoidal, measuring 17.5–25.0  $\mu\text{m}$   $\times$  7.5–10.0  $\mu\text{m}$ . Additionally, the branched, septate conidiophores of *Neofusicoccum parvum* produce pycnidia on PDA, measuring 370.6–908.9  $\mu\text{m}$   $\times$  234.5–506.4  $\mu\text{m}$ . *Pestalotiopsis microspora* exhibited white to pinkish or brownish color colonies, with hyaline, aseptate conidia measuring 4–8  $\mu\text{m}$  and pycnidia measuring 200–900  $\mu\text{m}$   $\times$  200–500  $\mu\text{m}$  (Fig. 1).

### Molecular Identification

Molecular identification using 18S rRNA gene sequences and ITS primers (ITS1 and ITS4) yielded 632 bp products (Fig.2). BLAST analysis was confirmed by the presence of *Neofusicoccum parvum* and *Pestalotiopsis microspora* with 99.82% and 99.44% identity to known sequences. Accession numbers were obtained upon sequence submission to NCBI GenBank (Table 1).

### Quantification of Bioactive Compounds

*Neofusicoccum parvum* expressed a significantly higher total phenolic content (185.96 mg GAE/g) compared to *Pestalotiopsis microspora* (60.81 mg GAE/g) (Fig.3). Comparison with previous findings from [24] reveals lower phenolic levels in *P. oxalicum* (120.99  $\mu\text{g}$  GAE/mg) and *M. guilliermondii* (23.40  $\mu\text{g}$  GAE/mg), emphasizing the significant outcomes of this research. Phenolic compounds, characterized by aromatic rings and hydroxyl groups, are pivotal bioactive substances known for their antioxidant properties [25]. In contrast with *Pestalotiopsis microspora* (61.66 mg GAE/g), *Neofusicoccum parvum* exhibited an elevated level of tannin content (188.43 mg GAE/g) due to increased polymerization of polyphenolics. *Neofusicoccum parvum* showed increased flavonoid content (25.81 mg RE/g) than *Pestalotiopsis microspora* (21.73 mg/g). This result surpasses the flavonoid content reported in the ethyl acetate extract of *Aspergillus fumigatus* (20.49 mg/g) [26]. Flavonoids are known for their anti-inflammatory, antimutagenic, antiallergic, antiviral, and anticarcinogenic properties, making them valuable natural antioxidants [27].

### In vitro Antioxidant Assays

*Neofusicoccum parvum* exhibited a better  $\text{IC}_{50}$  value of 56.19  $\mu\text{g}/\text{ml}$  compared to *Pestalotiopsis microspora*, which had an  $\text{IC}_{50}$  value of 93.21  $\mu\text{g}/\text{ml}$  in DPPH assay and these results suggest that *Neofusicoccum parvum* possesses a strong hydrogen-donating ability, indicating high antioxidant potential. The ABTS assay revealed that *Neofusicoccum parvum* showed a radical scavenging activity of 97.22  $\mu\text{g}/\text{ml}$ , and *Pestalotiopsis microspora* exhibited 53.68  $\mu\text{g}/\text{ml}$ . Although both fungi demonstrated antioxidant activity, their effectiveness was lower compared to rutin (144.16  $\mu\text{g}/\text{ml}$ ) and BHT (145.34  $\mu\text{g}/\text{ml}$ ). Phosphomolybdenum reduction assay, measured in ascorbic acid equivalents (AAE), was higher for *Neofusicoccum parvum* (149.58 mg AAE/g) compared to *Pestalotiopsis microspora* (86.26 mg AAE/g). The observed reduction in free radicals can be attributed to the electron or hydrogen ion transfer capabilities of phenolics and flavonoids present in the fungal extracts. The result shows significantly higher antioxidant activity than the previous study [28]. *Neofusicoccum parvum* revealed a maximum NO scavenging activity of 35.74% in comparison with *Pestalotiopsis microspora* (12.28%) (Fig. 4). While lower than the reference compounds BHT (62.96%) and rutin (62.47%), these findings demonstrate the potential of fungal extracts to inhibit nitrite formation by competing with oxygen. NO and reactive nitrogen species can damage cells and cause cytotoxicity [29]. This assay suggests that fungal extracts from *Piper schmidtii* may help reduce inflammation and oxidative stress-related diseases by scavenging nitric oxide (NO).

### In vitro anti-diabetic activity

*Neofusicoccum parvum* and *Pestalotiopsis microspora* expressed  $\alpha$ -amylase inhibitory activity in ethyl acetate extracts, with  $\text{IC}_{50}$  values of 65.51  $\mu\text{g}/\text{mL}$  and 79.6  $\mu\text{g}/\text{mL}$ , respectively (Fig.5). Endophytic fungi extracts were sources of novel antidiabetic compounds [30].





Mohana et al.,

### Antimicrobial activity

*Neofusicoccum parvum* indicates zone of inhibition against *Streptococcus pneumoniae* (8 mm), *Staphylococcus aureus* (7 mm), *Pseudomonas aeruginosa* (18 mm), and *Klebsiella pneumoniae* (10 mm) at 5 mg/mL. *Pestalotiopsis microspora* showed inhibition against *Streptococcus pneumoniae* (9 mm), *Staphylococcus aureus* (8 mm), *Pseudomonas aeruginosa* (9 mm), and *Klebsiella pneumoniae* (8 mm) at 5 mg/mL (Fig.6). Endophytic fungi produce secondary compounds against pathogens in host plants, emphasizing the promise for biotechnological drug research [31,32]. A visible zone of inhibition against *C. albicans* (14 mm) and *A. niger* (10 mm) were observed in *Neofusicoccum parvum* and *Pestalotiopsis microspora* respectively (Fig.6). These fungi produce strong antifungal compounds for treating fungal infections [33, 34]. Tannins from plants exhibit antibacterial and antifungal properties [35].

### SUMMARY

*Neofusicoccum parvum* evidenced particularly high levels of total phenolics, tannins, and flavonoids, along with potent antioxidant and antimicrobial properties. Further research is recommended to isolate and characterize specific bioactive compounds, to elucidate their mechanisms of action through *in vivo* studies, and explore their efficacy as medicinal agents. This work contributes to the development of sustainable and effective natural medicines, addressing contemporary health challenges.

### ACKNOWLEDGEMENT

The authors thank The Management and The Principal of PSG College of Arts & Science, Coimbatore-14, for their benevolence in providing all the necessary facilities and support to carry out the research work.

### REFERENCES

1. Dubale, S., Kebebe, D., Zeynudin, A., Abdissa, N., & Suleman, S. (2023a). Phytochemical Screening and Antimicrobial Activity Evaluation of Selected Medicinal Plants in Ethiopia. *Journal of Experimental Pharmacology*, 15, 51–62. <https://doi.org/10.2147/JEP.S379805>.
2. Okla, M. K., Alatar, A. A., Al-Amri, S. S., Soufan, W. H., Ahmad, A., & Abdel-Maksoud, M. A. (2021). Antibacterial and antifungal activity of the extracts of different parts of *Avicennia marina* (Forssk.) vierh. *Plants*, 10(2), 1–13. <https://doi.org/10.3390/plants10020252>.
3. Goutam, J., Singh, R., Vijayaraman, R. S., & Meena, M. (2018). Endophytic fungi: Carrier of potential antioxidants. In *Fungi and their Role in Sustainable Development: Current Perspective*. Springer Singapore. 539–551. [https://doi.org/10.1007/978-981-13-0393-7\\_29](https://doi.org/10.1007/978-981-13-0393-7_29).
4. Ikram, M., Ali, N., Jan, G., Hamayun, M., Jan, F.G., & Iqbal, A. (2019). Novel antimicrobial and antioxidative activity by endophytic *Penicillium roqueforti* and *Trichoderma reesei* isolated from *Solanum surattense*. *Acta Physiologica Plantarum*, 41(9):164-174. DOI:10.1007/s11738-019-2957-z.
5. Kim, J. Y., Kim, S., & Shim, S. H. (2020). Anti-atherosclerotic activity of (3R)-5-hydroxymellein from an endophytic fungus *neofusicoccum parvum* JS-0968 derived from *Vitex rotundifolia* through the inhibition of lipoproteins oxidation and foam cell formation. *Biomolecules*, 10(5). 715-729 <https://doi.org/10.3390/biom10050715>.
6. Manganyi, M.C., & Ateba, C.N. (2020). Untapped potentials of endophytic fungi: A review of novel bioactive compounds with biological applications. *Microorganisms*, 8(12):1934. <https://doi.org/10.3390/microorganisms8121934>.
7. El-Bondkly, E. A. M., El-Bondkly, A. A. M., & El-Bondkly, A.A.M. (2021). Marine endophytic fungal metabolites: A whole new world of pharmaceutical therapy exploration. *Heliyon* 7 (3): e06362. DOI:10.1016/j.heliyon.2021.e06362.





8. Alves, H. D. S., Rocha, W. R.V. D., Braz-Filho, R., Chaves, M. C. D. O. (2017). Isolation of monoterpenedihydrochalcones from *Piper montealegreanum* Yuncker (Piperaceae). *Molecules*, 22, 874. <https://doi.org/10.3390/molecules22060874>.
9. Jeon, H. J., Kim, K., Kim, Y. D., & Lee, S.E. (2019). Naturally occurring Piper plant amides potential in agricultural and pharmaceutical industries: Perspectives of piperine and piperlongumine. *Appl. Biol. Chem.* 62, 1–7. <https://doi.org/10.1186/s13765-019-0471-z>.
10. Qadri, M., Johri, S., Shah, B.A., Khajuria, A., Sidiq, T., Lattoo, S.K., Abdin, M.Z., & Riyaz-Ul-Hassan, S. (2013). Identification and bioactive potential of endophytic fungi isolated from selected plants of the Western Himalayas. *Springer Plus*, 2, 1–14. <https://doi.org/10.1186/2193-1801-2-8>.
11. Sette, L., Passarini, M., Delarmelina, C., Salati, F., & Duarte, M. (2006). Molecular characterization and antimicrobial activity of endophytic fungi from coffee plants. *World J Microbiol Biotechnol.* 22(11):1185–1195. <https://doi.org/10.1007/s11274-006-9160-2>.
12. Kumar, S., Stecher, G., Li, M., Knyaz, C., & Tamura, K. (2018). MEGA X: Molecular evolutionary genetics analysis across computing platforms. *Mol. Biol. Evol.* 35(6):1547–1549. doi: 10.1093/molbev/msy096.
13. AlfiRumidatul., Noor Rahmawati., & Sopandi Sunarya. (2021). Production of Secondary Metabolites and its Antibacterial and Antioxidant Activity During the Growth Period of Endophytic Fungi Isolated from Gall Rust Sengon Plants. *Pharmacogn J.* 13(2): 325-331. DOI:10.5530/pj.2021.13.42.
14. Zaman, W., Bhat, R., & Yang, T.A. (2014). Effect of superheated steam roasting on the phenolic antioxidant properties of cocoa beans. *Journal of food processing and preservation*, 38(4):1932-38. DOI: <https://doi.org/10.1111/jfpp.12166>.
15. Amorim, E.L., Nascimento, J.E., Monteiro, J. M., Peixoto Sobrinho, T. J., Araújo, T. A., & Albuquerque, U. P. (2008). A simple and accurate procedure for the determination of tannin and flavonoid levels and some applications in ethnobotany and ethnopharmacology. *Functional Ecosystems and Communities*, 2(1): 88-94.
16. Koley, T.K., Maurya, A., Tripathi, A., Singh, B.K., Singh, M., Bhutia, T.L., Tripathi, P.C., & Singh, B. (2018). Antioxidant potential of commonly consumed underutilized leguminous vegetables. *Int. J. Veg. Sci.* 25, 362–372.
17. Parvez, M. K., Alam, P., Arbab, A. H., Al-Dosari, M. S., Alhowiriny, T. A., & Alqasoumi, S. I. (2018). Analysis of antioxidative and antiviral biomarkers *b-amyryn*, *b-sitosterol*, *lupeol*, *ursolic acid* in *Guierasenegalensis* leaves extract by validated HPTLC methods. *Saudi Pharm J.* 26 (5):685–93. <https://doi.org/10.1016/j.jsps.2018.02.022>.
18. Kaaniche, F., Hamed, A., Abdel-Razek, A.S., Wibberg, D., Abdissa, N., El Euch IZ, et al. (2019). Bioactive secondary metabolites from new endophytic fungus *Curvularia* sp isolated from *Rauwolfiamacrophylla*. *PLoS One* 14(6): e0217627. <https://doi.org/10.1371/journal.pone.0217627>.
19. Afshari M., Rahimmalek, M., & Miroliaei M. (2018). Variation in polyphenolic profiles, antioxidant and antimicrobial activity of different achillea species as natural sources of antiglycative compounds. *Chem Biodivers.* 2018; 15: e1800075. DOI: 10.1002/cbdv.201800075.
20. Rajesh, P.M., & Natvar, P. J. (2011). *In vitro* antioxidant activity of coumarin compounds by DPPH, Super oxide and nitric oxide free radical scavenging methods. In *Journal of Advanced Pharmacy Education & Research*. 1:52-68. DOI: 10.7324/JAPS.2016.60626.
21. Lu, Y., Zhao, H., Sun, J., Liu, Y., Zhau, X., Beier, R.C., Wu, G. & Hou, X., (2014). Characterization of multidrug-resistant *Salmonella entericaserovars* Indiana and *Enteritidis* from chickens in Eastern China. *PLoS One*, 9(5), e96050. <http://dx.doi.org/10.1371/journal.pone.0096050>. PMID:24788434.
22. Hameed, B., Ali, Q., Hafeez, M., & Malik, A. (2020). Antibacterial and antifungal activity of fruit, seed and root extracts of *Citrulluscolocynthis* plant. *Biological and Clinical Sciences Research Journal*, 2020(30). 1-6. <https://doi.org/10.54112/bcsrj.v2020i1.33>.
23. Subashini, D., & Subhashree, V., (2012). Antioxidant and  $\alpha$ -amylase inhibition activities of phenolic compounds in the extracts of Indian honey. *Chin J Nat Med* 2012. 10(4):255-9.
24. Verma, A., Gupta, P., Rai, N., Tiwari, R. K., Kumar, A., Salvi, P., Kamble, S. C., Singh, S. K., & Gautam, V. (2022). Assessment of Biological Activities of Fungal Endophytes Derived Bioactive Compounds Isolated from *Amoorarohituka*. *Journal of Fungi*, 8(3). 285-305. <https://doi.org/10.3390/jof8030285>.

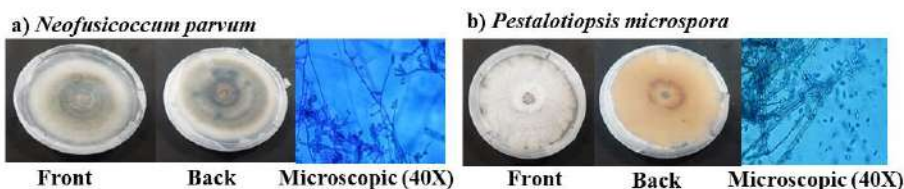




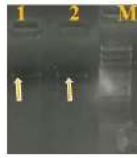
25. Hussain, A., Kausar, T., Din, A., Murtaza, M. A., Jamil, M. A., Noreen, S., Rehman, H. U. R., Shabbir, H., & Ramzan, M. A. (2021). Determination of total phenolic, flavonoid, carotenoid, and mineral contents in peel, flesh, and seeds of pumpkin (*Cucurbita maxima*). *Journal of Food Processing and Preservation*, 45(6). <https://doi.org/10.1111/jfpp.15542>.
26. Khalil, D. M. A., El-Zayat, S. A., & El-Sayed, M. A. (2020). Phytochemical screening and antioxidant potential of endophytic fungi isolated from *Hibiscus sabdariffa*. *Journal of Applied Biotechnology Reports*, 7(2), 116–124. <https://doi.org/10.30491/jabr.2020.109287>.
27. Roy, A., Khan, A., Ahmad, I., Alghamdi, S., Rajab, B. S., Babalghith, A. O., Alshahrani, M. Y., Islam, S., & Islam, M. R. (2022). Flavonoids a Bioactive Compound from Medicinal Plants and Its Therapeutic Applications. *BioMed Research International*, 1- 54452919. <https://doi.org/10.1155/2022/5445291>.
28. Chutulo, E.C., & Chalannavar, R.K. (2018). Endophytic mycoflora and their bioactive compounds from *Azadirachta indica*: A comprehensive review. *J Fungi*. 4(2): 42-54. DOI: 10.3390/jof4020042.
29. Peksel, Aysegul, Arisan-ATAC, INCI., & Yanardag, Refiye.. (2010). Evaluation of antioxidant and antiacetylcholinesterase activities of the extracts of *Pistacia atlantica* Desf. leaves. *Journal of Food Biochemistry*. 34. 451 - 476. 10.1111/j.1745-4514.2009.00290.x.
30. Picot, C., Subratty, A. H., Mahomoodally, M. F. (2014). Inhibitory potential of five traditionally used native antidiabetic medicinal plants on  $\alpha$ -amylase,  $\alpha$ -glucosidase, glucose entrapment, and amylolysis kinetics *in vitro*. *Adv Pharmacol Sci*. 2014:1-7. DOI:10.1155/2014/739834 Corpus ID: 15996253.
31. Cruz, J., da Silva, C., & Hamerski, L. (2020). Natural products from endophytic fungi associated with *Rubiaceae* species. *J Fungi*. 6 (3): 1-26. DOI:10.3390/jof6030128.
- El-hawary, S. S., Moawad, A. S., Bahr, H. S., Abdelmohsen, U. R., Mohammed, R. (2020). Natural product diversity from the endophytic fungi of the genus *Aspergillus* sp. *RSC Adv*. 10 (37): 22058-22079. DOI: 10.1039/d0ra04290k.
32. Talukdar, R., Paul, S., Tayung, K. (2021). Antifungal drugs from endophytic microbes: Present and future prospects. *Bioresource Utilization and Management: Applications in Therapeutics, Biofuels, Agriculture, and Environmental Science*. Apple Academic Press. 574. DOI: <https://doi.org/10.1201/9781003057826>.
33. Hashem, A. H., Shehabeldine, A. M., Abdelaziz, A. M., Amin, B. H., & Sharaf, M. H. (2022). Antifungal Activity of Endophytic *Aspergillus terreus* Extract against Some Fungi Causing Mucormycosis: Ultrastructural Study. *Applied Biochemistry and Biotechnology*, 194(8), 3468–3482. <https://doi.org/10.1007/s12010-022-03876-x>.
34. Banso, A., & Adeyemo. (2007). Evaluation of antibacterial properties of tannins isolated from *Dichrostachys cinerea*. *African Journal of Biotechnology*, 6(15), 1785–1787. <http://www.academicjournals.org/AJB>.

**Table 1: Blast Sequence**

Plant	Endophytic fungi	Accession No	% Identity
<i>Piper schmidtii</i>	<i>Neofusicocum parvum</i>	PP703150	99.82%
	<i>Pestalotiopsis microspora</i>	PP703151	99.44%

**Fig. 1: Morphology and Microscopic identification**





Lane 1- *Neofusicoccum parvum*  
Lane 2- *Pestalotiopsis microspora*  
Marker- 100bp ladder

1. *Neofusicoccum parvum* (PP703150)

```
>ACCTGCGGAAGGATCATTACCGAGTTGATTTCGAGCTCCGGCTCGACTCTCCACCCCAATGTGTACCTACCTCTGTTGCTTTGGCGGGCCGGGTCTCCGCACCGGC
GCCCTTCGGGGGGCTGGCCAAACGCCCGCCAGAGGACCATAAACTCCAGTCAAGTGAACCTTCGCAGTCTGAAAAACAAGTTAATAAACTAAAACCTTCAACAACGGATC
TCTTGGTCTGGCATCGATGAAGAACCAGCGAAATGCGATAAGTAATGTGAATTGCAGAATTCAGTGAATCATCGAATCTTGAACGCACATTGCGCCCTTGGTAT
TCCGAGGGGCATGCCTGTTCGAGCGTCATTTCAACCCCTCAAGCTCTGCTTGGTATGGGCCCGTCTCCACGGACGCGCCTTAAAGACCTCGGGGGTGGCGTCTGC
CTCAAGCGTAGTAGAAAAACACCTCGCTTTGGAGCGCAGGGCTCGCCCGCCGAGCAACCTTTGAATTATTTCTCAAGGTTGACCTCGGATCAGGTAGGGATACCCGC
TGAACCTAAGCATATCAATAAGCCGGAG-567
```

2. *Pestalotiopsis microspora* (PP703151)

```
>TTCGGTAGGTGAACCTGCGGGAGGGATCATTATAGAGTTTCTAAACTCCCAACCCATGTGAACCTACCATTGTTGCCTCGGCAGAACTGCTCGGTGCACCTTACCT
TGGAACGGCTACCCCTAGCGCCTTACCCTGGAACGGCTTACCCTGCAACGGCTGCCGGTGGACTACCGAATCTTGTATTTTATGTAACTGAGCGTCTTATTT
TAATAAGTCAAACTTTCAACAACGGATCTCTTGGTCTGGCATCGATGAAGAACCAGCGAAATGCGATAAGTAATGTGAATTGCAGAATTCAGTGAATCATCGAAT
CTTTGAACGCACATTGCGCCCATTAGTATTCTAGTGGGCATGCCTGTCGAGCGTCAATTTCAACCCCTAAGCCCTAGCTTAGTGTGGGAGCCTACTGCTTTTACTAGC
TGTAGCTCTGAAATACAACGGCGGATCTGCGATATCTCTGAGCGTAGTAATTTTATCTCGCTTTTACTGGAGTTGCAGCGCTTTTAGCCGCTAAATC-532
```

Fig. 2: PCR Products

Fig. 3: Quantification of Bioactive Compounds

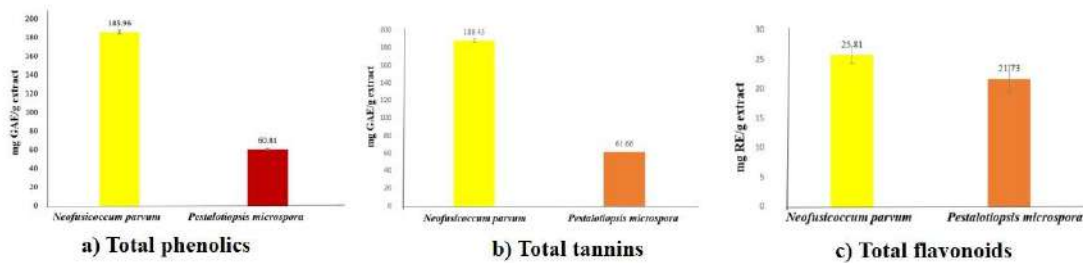
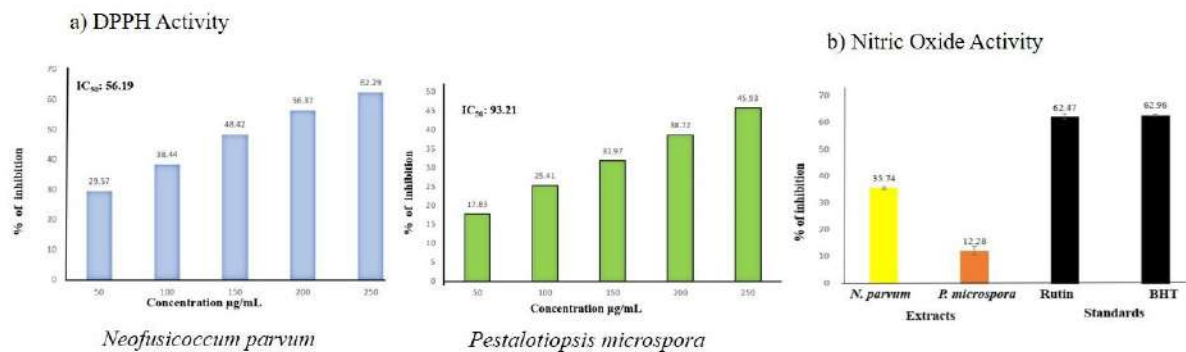
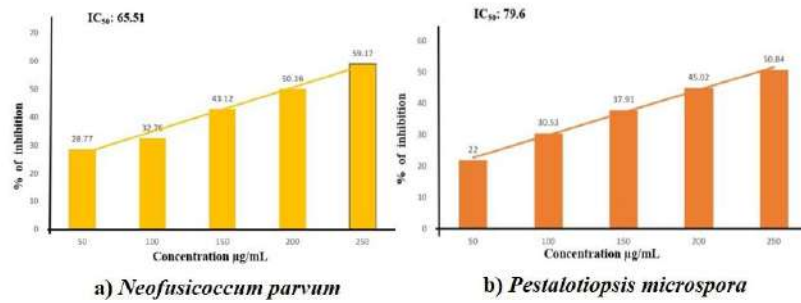


Fig. 4: *In vitro* Antioxidant Activity of Endophytic Fungi



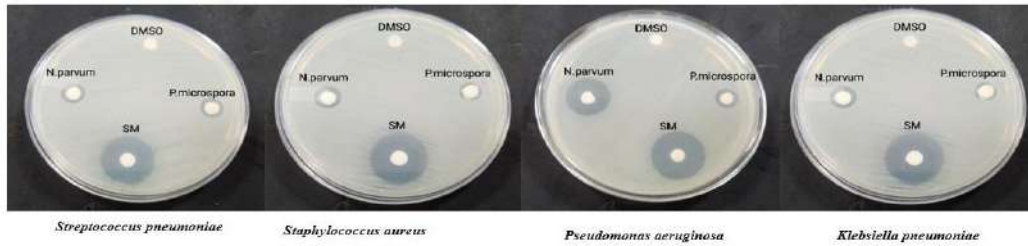


**Fig. 5: In vitro antidiabetic activity of Endophytic Fungi**

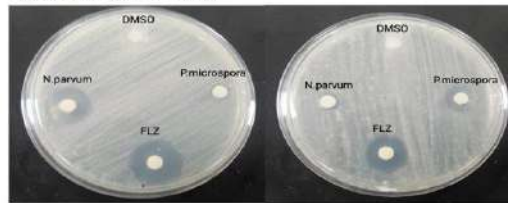


**Fig.6: Antimicrobial activity of Endophytic Fungi**

**a) Antibacterial activity**



**b) Antifungal activity**







# Mechanical Properties of Engineered Cementitious Composites Enhanced by Glass, Polyester Fibers and *Bacillus licheniformis* : An Experimental Approach

Vipul Solanki<sup>1\*</sup> and Khadeeja Priyan<sup>2</sup>

<sup>1</sup>Ph.D Scholar, Department of Civil Engineering, C.V.M University, Gujarat, India,

<sup>2</sup>Professor and Head, Department of Civil Engineering, C.V.M University, Gujarat, India.

Received: 04 July 2024

Revised: 28 Aug 2024

Accepted: 25 Oct 2024

## \*Address for Correspondence

**Vipul Solanki**

Ph.D Scholar,

Department of Civil Engineering,

C.V.M University, Gujarat, India,

E.Mail: vpsolanki@bbit.ac.in



This is an Open Access Journal / article distributed under the terms of the **Creative Commons Attribution License** (CC BY-NC-ND 3.0) which permits unrestricted use, distribution, and reproduction in any medium, provided the original work is properly cited. All rights reserved.

## ABSTRACT

Concrete is the primary material used in large-scale engineering projects because of its excellent compressive strength, even if it has a relatively low tensile strength. Engineered Cementitious Composites (ECC), often known as Bendable Concrete, is an innovative material that was created to enhance its Flexural and Tensile capabilities. Due to its high tensile ductility, toughness, and fine multiple cracking, ECC is a good choice for an environment friendly infrastructure that must meet strict requirements for longevity and safety. This research investigates the strength characteristics of various ECC mixtures by adjusting the quantities of supplementary cementitious materials, specifically polyester and glass fibers. The study utilized an M<sub>45</sub> ECC mixture with a water-to-binder ratio of 0.24 and a fly ash to cement ratio of 1.2 by mass. *Bacillus Licheniformis* microorganism are added in ECC with concentration of 10<sup>7</sup> Cfug. Comparison is made between the compressive strengths of ECC mixtures with various fiber percentages and microorganism are compared to that of Conventional Concrete. Results show that bendable concrete exhibits higher Flexural and Tensile strengths than conventional concrete, underscoring the importance of glass fibers in enhancing ductility. polyester fibers in achieving the desired bendable concrete properties and microorganism in reducing the inherent voids of ECC.

**Keywords:** ECC, Glass Fiber, Polyester Fiber, *Bacillus Licheniformis*, Compressive Strength, Flexural Strength

## INTRODUCTION

Concrete remains the preferred material in large-scale engineering projects due to its remarkable compressive strength[1]. However, its relatively low tensile strength poses significant limitations, particularly in applications requiring high ductility and flexibility[2]. To address these deficiencies, Engineered Cementitious Composites (ECC), commonly referred to as Bendable Concrete, have been developed. ECC is a class of high-performance fiber-



**Vipul Solanki and Khadeeja Priyan**

reinforced cementitious composites characterized by high tensile ductility, toughness, and fine multiple cracking, making it an ideal candidate for sustainable infrastructure that demands longevity and safety [3]. The incorporation of fibers into ECC significantly enhances its mechanical properties. Traditional ECC formulations often utilize polyvinyl alcohol (PVA) fibers to achieve the desired flexibility and tensile strength[4]–[6]. However, recent studies have explored alternative fibers, such as polyester and glass fibers, which not only improve the mechanical properties but also contribute to the material's sustainability [7][8]. Polyester fibers are noted for their cost-effectiveness and environmental benefits, while glass fibers provide superior tensile strength and durability[9][10].

This study aims to investigate the strength characteristics of various ECC mixtures by altering the proportions of additional cementitious materials, specifically polyester and glass fibers. For the investigation, an M45 ECC mixture with a water-to-binder ratio of 0.24 and a fly ash to cement ratio (FA/C) of 1.2 by mass was chosen. By comparing the compressive strengths of ECC mixtures with varying fiber percentages to that of conventional concrete, this research seeks to establish the efficacy of polyester and glass fibers in enhancing the mechanical properties of ECC. The outcomes of this study are expected to contribute to the ongoing development of high-performance, sustainable construction materials that meet the rigorous demands of modern infrastructure[11]–[14]. This research aligns with current trends in material science, focusing on the utilization of innovative materials to improve the performance and sustainability of concrete structures [15].

**Material Parameters**

Various materials such as Cement, Fly ash, Aggregates, Polyester Fiber, Glass fiber, Super plasticizer and water are used in ECC.

**Cement**

In this study, OPC 53 grade cement was utilized as the binding agent for the concrete. The cement underwent evaluation based on various parameters as outlined in IS: 4031-1988[16] and was confirmed to comply with the standards set by IS: 12269-1987[17]. The physical properties of the cement are detailed in Table 1.

**Fly ash**

Pulverized coal-based thermal power plants generate fly ash as a byproduct. Although fly ash is an environmental pollutant, it also holds potential as a valuable resource. It is frequently utilized in cement-based applications. The chemical properties of fly ash are presented in Table 2.

**Fine Aggregates**

Natural Sand of 4.75 mm size is used as fine aggregate. To eliminate any particles larger than 4.75 mm and dust, the sand was first sieved using a 4.75 mm sieve. Sand properties were determined by conducting tests in accordance with IS 2386. (Part - 1)[18]. This project employed locally available 20mm size coarse aggregate. The fine and coarse aggregates were tested in accordance with IS: 383-1970[19]. Table 3 describes Sand- Physical Properties.

**Chemical Admixture**

To improve the workability of the ECC mixture, PROCRETE R20, a polycarboxylic ether-based high-performance super plasticizer, is utilized. This additive ensures better flow ability and mixing ease while preserving the mechanical properties. By minimizing the water content, PROCRETE R20 maintains the necessary water-to-binder ratio and achieves optimal workability. Table 4 lists the characteristics of chemical admixtures.[20]

**Glass Fibers**

In this study, glass fiber was incorporated into the engineered cementitious composite (ECC) concrete. Glass fibers were chosen for their high tensile strength and durability, contributing to enhanced ductility and overall mechanical performance of the ECC. The inclusion of glass fibers also helps to control cracking and improve the composite's toughness[21]. Table 5 lists the Glass fibres' physical characteristics.



**Vipul Solanki and Khadeeja Priyanb****Polyester Fibers**

Polyester fibers were incorporated into the Engineered Cementitious Composite (ECC) mixtures to enhance their mechanical properties. These fibers were selected for their cost-effectiveness, environmental benefits, and ability to improve the tensile strength and durability of the ECC. The inclusion of polyester fibers aims to achieve the desired flexibility and ductility in the composite material[22]. The physical parameters of Polyester fibres are listed in Table 6.

**Water**

Water is a necessary ingredient in the manufacture of concrete. It aids in the creation of cement gel strength. It complies with the standards of IS 456-2000. The pH of the water is 7 to 8. The temperature is from 27 to 29 °C.

**Bacillus licheniformis**

The Bacillus licheniformis strain used in this study was sourced from an Aumenzymes laboratory. The bacteria were cultured in nutrient broth and incubated at 30°C for 24 hours to reach the exponential growth phase. After incubation, the bacterial suspension was centrifuged at 3000 rpm for 10 minutes to obtain a concentrated bacterial pellet. The pellet was then resuspended in sterile distilled water to achieve a final concentration of 10<sup>7</sup> colony-forming units (CFU) per gram.

**Experimental investigation**

Various experiments were conducted using 0.015 m<sup>3</sup> of concrete to determine the optimal percentage for the ECC mix design, based on insights from prior research. This study utilized an M<sub>45</sub> grade ECC mixture with a fly ash to cement ratio (FA/C) of 1.2 by mass and a water/binder ratio of 0.24. The primary objective was to evaluate the enhanced characteristics of ECC by varying the proportions of glass and polyester fibers. The compressive and flexural strengths of multiple ECC mixes with different fiber contents were compared to those of the Indian Standard Conventional Concrete design.

**Preparation of ECC**

The preparation of Engineered Cementitious Composites (ECC) involved mixing Ordinary Portland Cement, fine sand, and fly ash, followed by the gradual addition of glass and polyester fibers for uniform distribution. A Bacillus licheniformis suspension, cultured to 10<sup>7</sup> cfu/g, was mixed with the required water and added to the dry materials, along with a superplasticizer to enhance workability. The homogeneous mix was then cast into molds and initially cured under plastic sheets for 24 hours at 27°C. After demolding, specimens were water-cured at 27°C for 28 days. Mechanical strength was carried out confirmed the effectiveness of the composite. Increased of compressive strength is found by impregnation of fibers and microorganism. In this study, Glass Fiber 2% shows good results. Wherein, the compressive strength is increased by 10.66% compared to normal concrete at 28<sup>th</sup> day. Increased of Flexural strength is found by impregnation of fibers and microorganism. In this study, Glass Fiber 2% and Polyester Fiber 2% show good results. The Flexural strength of Glass Fiber 2% is increased by 59.7% compared to normal concrete at 28<sup>th</sup> day. The Flexural strength of Polyester Fiber 2% is increased by 69.2% compared to normal concrete at 28<sup>th</sup> day.

**CONCLUSION**

The following findings on the hardened characteristics of ECC with Glass and Polyester fibres for M<sub>45</sub> grade concrete are developed based on experimental research. The super plasticizer was used at a dose of 0.8 percent of the total powder content in the provided combination. ECC with Glass fibres has a compressive strength of 10.66% more than conventional concrete. Coarse aggregates are not used in this study, so, compressive strength of Polyester fibers decreases. The overall weight of ECC decreases as coarse aggregates are not used. Glass fibre has a flexural strength increase of 59.7%, whereas Polyester fiber has enhanced flexural strength of 69.2 %. The Hardened strength properties of ECC increases after adding bacteria and fibers because the bacteria induce calcium carbonate precipitation, which fills micro-cracks and strengthens the matrix, while the fibers bridge cracks and distribute stress,





enhancing the composite's toughness and load-bearing capacity. This combination results in a significant improvement in both flexural and compressive strength, demonstrating the effectiveness of integrating biological and material science principles in enhancing the performance of cementitious composites. Hence, use of fiber and microorganism in Engineered Cementitious Composites shall bring many opportunities for sustainable development and preserving nature.

## REFERENCES

1. C. R. Gagg, "Cement and concrete as an engineering material: An historic appraisal and case study analysis," *Eng. Fail. Anal.*, vol. 40, pp. 114–140, May 2014, doi: 10.1016/j.engfailanal.2014.02.004.
2. J. Xu, Y. Tang, X. Wang, Z. Wang, and W. Yao, "Application of ureolysis-based microbial CaCO<sub>3</sub> precipitation in self-healing of concrete and inhibition of reinforcement corrosion," *Constr. Build. Mater.*, vol. 265, p. 120364, 2020, doi: 10.1016/j.conbuildmat.2020.120364.
3. H. Zhu, D. Zhang, Y. Wang, T. Wang, and V. C. Li, "Development of self-stressing Engineered Cementitious Composites (ECC)," *Cem. Concr. Compos.*, vol. 118, no. November 2020, p. 103936, 2021, doi: 10.1016/j.cemconcomp.2021.103936.
4. N. Bheel, B. S. Mohammed, M. O. Ahmed Ali, N. Shafiq, E. Mohamed Tag-eldin, and M. Ahmad, "Effect of polyvinyl alcohol fiber on the mechanical properties and embodied carbon of engineered cementitious composites," *Results Eng.*, vol. 20, p. 101458, Dec. 2023, doi: 10.1016/j.rineng.2023.101458.
5. Z. Pan, C. Wu, J. Liu, W. Wang, and J. Liu, "Study on mechanical properties of cost-effective polyvinyl alcohol engineered cementitious composites (PVA-ECC)," *Constr. Build. Mater.*, vol. 78, pp. 397–404, Mar. 2015, doi: 10.1016/j.conbuildmat.2014.12.071.
6. K. Rahmati *et al.*, "Evaluation of Engineered Cementitious Composites (ECC) containing Polyvinyl Alcohol (PVA) fibers under compressive, direct tensile, and drop-weight test," *Multiscale Multidiscip. Model. Exp. Des.*, vol. 6, no. 1, pp. 147–164, Mar. 2023, doi: 10.1007/s41939-022-00135-8.
7. I. Elfaleh *et al.*, "A comprehensive review of natural fibers and their composites: An eco-friendly alternative to conventional materials," *Results Eng.*, vol. 19, p. 101271, Sep. 2023, doi: 10.1016/j.rineng.2023.101271.
8. M. Y. Khalid, A. Al Rashid, Z. U. Arif, W. Ahmed, H. Arshad, and A. A. Zaidi, "Natural fiber reinforced composites: Sustainable materials for emerging applications," *Results Eng.*, vol. 11, p. 100263, Sep. 2021, doi: 10.1016/j.rineng.2021.100263.
9. M. S. EL-Wazery, M. I. EL-Elamy, and S. H. Zoalfakar, "Mechanical properties of glass fiber reinforced polyester composites," *Int. J. Appl. Sci. Eng.*, vol. 14, no. 3, pp. 121–131, 2017, doi: 10.6703/IJASE.2017.14(3).121.
10. M. Y. Khalid, A. Al Rashid, Z. U. Arif, M. F. Sheikh, H. Arshad, and M. A. Nasir, "Tensile strength evaluation of glass/jute fibers reinforced composites: An experimental and numerical approach," *Results Eng.*, vol. 10, p. 100232, Jun. 2021, doi: 10.1016/j.rineng.2021.100232.
11. J. Ayarkwa, D.-G. Joe Opoku, P. Antwi-Afari, and R. Y. M. Li, "Sustainable building processes' challenges and strategies: The relative important index approach," *Clean. Eng. Technol.*, vol. 7, p. 100455, Apr. 2022, doi: 10.1016/j.clet.2022.100455.
12. S. Khan, S. Bin Rayhan, S. M. I. Ibn Salam, H. A. Khan, and M. Z. Rahman, "Recent advances in sustainable building materials for the construction industry: Mechanical performance and applications," in *Comprehensive Materials Processing*, Elsevier, 2024, pp. 597–627. doi: 10.1016/B978-0-323-96020-5.00191-6.
13. J. Nilimaa, "Smart materials and technologies for sustainable concrete construction," *Dev. Built Environ.*, vol. 15, p. 100177, Oct. 2023, doi: 10.1016/j.dibe.2023.100177.
14. P. Patel and A. Patel, "Use of sustainable green materials in construction of green buildings for sustainable development," *IOP Conf. Ser. Earth Environ. Sci.*, vol. 785, no. 1, p. 012009, Jun. 2021, doi: 10.1088/1755-1315/785/1/012009.
15. M. Kioumarsis and V. Plevris, "Advanced Concrete and Construction Materials for Sustainable Structures," *Sustainability*, vol. 16, no. 4, p. 1427, Feb. 2024, doi: 10.3390/su16041427.





**Vipul Solanki and Khadeeja Priyan**

16. IS: 4031 (Part 6), "Methods Of Physical Tests For Hydraulic Cement Part 6 Determination Of Compressive Strength Of Hydraulic Cement Other Than Masonry Cement (First Revision)," *Bur. Indian Stand. Delhi*, pp. 1–3, 2005, [Online]. Available: <https://ia800400.us.archive.org/0/items/gov.in.is.4031.6.1988/is.4031.6.1988.pdf>
17. IS 12269, "IS 12269: 2013 Ordinary Portland Cement , 53 grade specification," *Indian Stand.*, no. March, pp. 1–14, 2013.
18. IS:2386- Part I, "Method of test for aggregate for concrete. Part I - Particle size and shape.," *Indian Stand.*, p. (Reaffirmed 2002), 1963.
19. IS:383, "Specification for Coarse and Fine Aggregates From Natural Sources for Concrete," *Indian Stand.*, pp. 1–24, 1970.
20. A. Paktiawal and M. Alam, "Effect of polycarboxylate ether-based superplasticizer dosage on fresh and hardened properties of cement concrete," *IOP Conf. Ser. Mater. Sci. Eng.*, vol. 1166, no. 1, p. 012013, Jul. 2021, doi: 10.1088/1757-899X/1166/1/012013.
21. I. Nunez, A. Marani, M. Flah, and M. L. Nehdi, "Estimating compressive strength of modern concrete mixtures using computational intelligence: A systematic review," *Constr. Build. Mater.*, vol. 310, p. 125279, Dec. 2021, doi: 10.1016/j.conbuildmat.2021.125279.
22. R. Rostami, M. Zarrebini, M. Mandegari, D. Mostofinejad, and S. M. Abtahi, "A review on performance of polyester fibers in alkaline and cementitious composites environments," *Constr. Build. Mater.*, vol. 241, p. 117998, Apr. 2020, doi: 10.1016/j.conbuildmat.2020.117998.

**Table 1: Cement- Physical Properties**

Test		Value
Settling Time (initial)		40 min
Settling Time (final)		190 min
Compressive Strength	3 days	36.80 N/mm <sup>2</sup>
	7 days	43.82 N/mm <sup>2</sup>
	28 days	56.78 N/mm <sup>2</sup>
Soundness		1 mm
Standard consistency		27.25 %

**Table 2: Chemical properties of Fly ash**

No	Test Details	Requirement as per IS 3812 {Part-I}	Test Result
1	SiO <sub>2</sub> + Al <sub>2</sub> O <sub>3</sub> + Fe <sub>2</sub> O <sub>3</sub>	> 70.00%	89.08
2	SiO <sub>2</sub>	> 35.00%	68.25
3	MgO	< 5.00%	1.67
4	SO <sub>3</sub>	< 3.00%	1.13
5	Cl	< 0.05%	0.019
6	Total alkali as Na <sub>2</sub> O	Max 1.5	0.167
7	Loss on ignition (LOI)	< 5.00%	0.79





**Vipul Solanki and Khadeeja Priyan**

**Table 3: Sand- Physical Properties**

Characteristics	Fine Aggregates
<b>Fineness modulus</b>	2.9
<b>Specific Gravity of Sand</b>	2.670
<b>Water Absorption (%)</b>	0.9
<b>Size</b>	4.75 max
<b>Moisture content (%)</b>	1.8
<b>Zone of sand</b>	II

**Table 4: Properties of Chemical Admixtures**

Test	Value
<b>Appearance</b>	Brown
<b>Specific Gravity</b>	1.3 @ 20°C
<b>Air Entrainment</b>	< 2%
<b>Chloride Content</b>	Nil

**Table 5: Physical Properties of Glass Fiber**

Test particulars	Value
<b>Diameter</b>	20 μm
<b>Tensile Strength</b>	2200 N/mm <sup>2</sup>
<b>Length</b>	12mm
<b>Melting Point</b>	1400 °C

**Table 6: Polyester Fiber- Physical Properties**



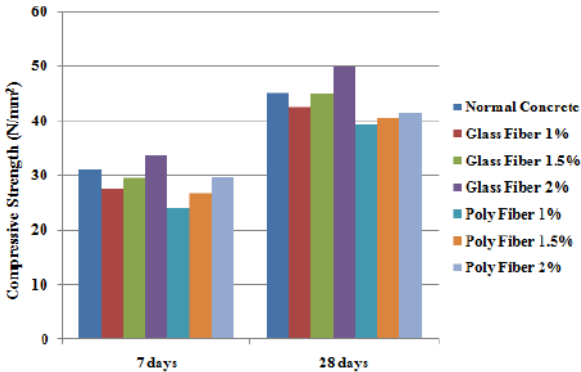
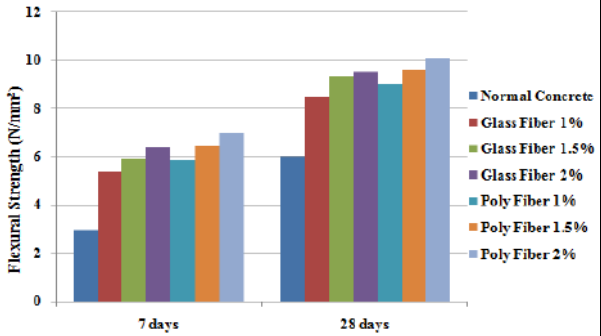
Test	Value
<b>Length</b>	6 mm
<b>Diameter</b>	20 μm
<b>Elongation</b>	33.3%
<b>Tensile strength</b>	600 N/mm <sup>2</sup>
<b>Melting point</b>	250-265
<b>Density</b>	1.38 °C
<b>Aspect Ratio</b>	6







**Vipul Solanki and Khadeeja Priyan**

 <p>1</p>	 <p>2.</p>
<p>3. Fig. 1: Glass Fibers</p>	<p>4. Fig. 2: Polyvinyl Alcohol Fibers</p>
 <p>5.</p>	 <p>6.</p>
<p>7. Fig. 3: Compressive Strength Results</p>	<p>8. Fig. 4: Flexural Strength Results</p>





## Social Life of Blacks in Claude McKay's *Home to Harlem*

Bairavi B<sup>1\*</sup> and R. D. Prashaanth<sup>2</sup>

<sup>1</sup>Assistant Professor, Department of English, Vel Tech Rangarajan Dr. Sagunthala R&D Institute of Science and Technology (Deemed to be University), Chennai, Tamil Nadu, India.

<sup>2</sup>Research Scholar, Department of English, Annamalai University, Chidambaram, Tamil Nadu, India.

Received: 25 Feb 2024

Revised: 25 Aug 2024

Accepted: 29 Oct 2024

### \*Address for Correspondence

#### Bairavi B

Assistant Professor, Department of English,

Vel Tech Rangarajan Dr. Sagunthala R&D Institute of Science and Technology (Deemed to be University), Chennai, Tamil Nadu, India.

E.Mail: drbairavib@veltech.edu.in



This is an Open Access Journal / article distributed under the terms of the **Creative Commons Attribution License** (CC BY-NC-ND 3.0) which permits unrestricted use, distribution, and reproduction in any medium, provided the original work is properly cited. All rights reserved.

### ABSTRACT

Festus Claudius McKay is a distinguished writer of African American literature. He was born in Jamaica in 1889 to peasant farmers whose strong sense of racial tradition was passed on to McKay through African folk tales and stories of his older brother, a school teacher and free thinker, from whom McKay learned the essence of maintaining his intellectual independence from authority. *Home to Harlem*, a famous picaresque novel in African American Literature. The first protagonist of the novel Jake is an army man. He wants to serve the country as a soldier. However, he fails to accomplish his goals due to color and racial prejudices. So, he escapes from the army and returns to Harlem for better life. Ray, the novel's second protagonist, he was alienated from the intellectual life of African American and American society. Thus, the novel depicts how the black men are suppressed and oppressed by the white society and how these young men as self-esteemed youngsters find immense pride and pleasure in retaining their inherited identity. Thus, the article focuses on how the blacks' life is socially meant in the novel *Home to Harlem*.

**Keywords:** Picaresque, Self-esteemed, Suppressed, White society, and Black men

### INTRODUCTION

Literature is an artistic expression of humans to provoke his fellow beings in a certain way. It has the power of re-creating human psyche. It investigates profound knowledge to extend and access human credibility. The writers strongly believe that their writing is a weapon to change one's thoughts, feelings, and emotions. Many writers have proved their word power through their writings. Likewise, African American literature is one of the best examples for creating a big revolution to get back black people's equality and justice from color, racial prejudices, and colonial domination. African American writers strongly believed that their writings will definitely guide and offer solutions



**Bairavi and Prashaanth**

to the blacks, to lead their life in a moral and successful way. They also believed that their words are like weapons, and through their words, they can give confidence to the blacks to encounter all kinds of racial, cultural, social, and political prejudices.

*Home to Harlem*, Claude McKay's debut novel, became the first most popular novel written by a Black author in 1928. It is a significant piece of practical social fiction and also one of McKay's outstanding novels. The novel is entirely a riot of exotic color and unrestrained indulgences. In the character of Ray, Jake's Haitian friend and the probable counterpart of the author, McKay portrays a sensitive, intelligent black who has distaste and sometimes an aversion for his low-life environment. His dream is to be a writer. Upset in his thinking by Russian Revolution and the World War I, he stands as a confused black man in a social order dominated by the whites.

The first protagonist of the novel Jake is an army man. He wants to serve the country as a soldier. However, he fails to accomplish his goals due to color and racial prejudices. So he escapes from the army and returns to Harlem for better life and love. Thus, the novel depicts how the black men are suppressed and oppressed by the white society and how these young men as self-esteemed youngsters find immense pride and pleasure in retaining their inherited identity.

**Proletarian Blacks in *Home to Harlem***

*Home to Harlem* contains an impressive critique of American and European imperialism by McKay. Jake Brown, the protagonist of the novel, is a tall, appealing man with dark brown complexion. Readers can understand how the black's transnational proletariat life attempts to help them regain their black identity through the character. The main purpose of the novel is to provide a broad overview of Harlem through Jake's international travels. Moreover, the narrative mostly recounts his experiences traveling abroad and living in Harlem. Naturally, someone with this kind of love for his own nation begins to recognize the richness and distinction of his race, color, and class. After garnering experiences from the transnational life, migrants feel proud of their country and find it better and more convenient than any other country.

Through an examination of the fundamental ways in which heterosexuality shapes the worldwide drama of war, race, and black people's longing towards home, McKay's vision of black social advancement and the domestic substance of the national romance are reconstructed in *Home to Harlem*. A queer reading of McKay's novels should be employed in addition to a gender analysis to investigate how sexuality structures and discourses impact the author's final departure from tales of home.

The novel's second central character, Ray, is a rational and scholar of Haitian descent. For the final two-thirds of the novel, he travels with Jake after they first meet on a train. The novel tells the story of their differences over and over again. Ray is an ingrained reader and aspiring writer who is a strong opponent of colonialism, despite feeling powerless to change the course of events. Unlike the gorgeous Jake, Ray is unsuccessful in his attempts to get close to women, and his drug experimentation puts him in the hospital. He laments the fact that his intelligence and bourgeois morality prevent him from being the "natural man" that Jake is.

The concept is, how the knowledge obstructs passion and resides at the heart of the primitivism that became popular in the 1920s. Liberated from the constraints of civilization, Black people could express their emotions directly, but White people's thoughts and morality suppressed them. McKay was one among the black writers embodied the positive remarks of primitivism as a centre of African thought. However, he ended up perpetuating stereotypes that were all too common, much like other people who attempted.

In McKay's *Home to Harlem*, primitivism is made political through his leftist radicalism and racial consciousness. It is a critique of white American morality and culture and, as such, a political statement of black identity. However, it also becomes a positive and particular technique of recovering and revaluing that is exclusive to African American





### Bairavi and Prashaanth

consciousness. Even with McKay's radical views, primitivism nevertheless reveals the work's immersion in the white authoritarian individualism ideology at the heart of the American myth.

The characters in Claude McKay's *Home to Harlem* play a minor role in American culture as well as the Harlem community. They lack education in the main. They reside in hotels that are now referred to as "single-room occupancy" and boarding homes. Their relationships are short-lived and tumultuous; they frequently terminate suddenly and occasionally violently. The women they deal with earn a living on their own income as entertainers, cooks, waitresses, domestics, or clerks; some of them also work as part-time prostitutes.

Helen Pyne-Timothy in "Perceptions of the Black Woman in the Work of Claude McKay," explains the issue of young black women engaging in prostitution, a problem that McKay handles with great sensitivity. Many of the young black women he notices have careers in this field. This type of black woman is ordinary in McKay's eyes, and he feels that he lends her significance in his art. He recognizes that the black community's economic situation has a big impact on how often these women are forced to live this kind of life. In order to survive, the black women are often found themselves on the streets whether they are in America or in Europe. Black women should not be deprived of their warmth and spontaneity by the prostitution industry, according to McKay, who particularly values these attributes in black women. The issues with black women's prostitution are evaluated in these two assessments. In *Home to Harlem*, there is fierce tenderness as well as rivalry between women and men.

#### Social Life of Blacks in *Home to Harlem*

Black people's gathering spots are night clubs, cabarets, pool halls, saloons, buffet flats, houses of prostitution, and gambling dens. They smoke opium and sniff cocaine, and they consume alcohol in large quantities. In addition to the intense desire they have for freedom, they also live with the possibility of violence from white civilization. Drug addiction, sexual struggle, self-hatred, corruption, color-complexes, ghetto congestion, and class divisions among the African Americans are also depicted in *Home to Harlem*. Acknowledging these issues as the results of white atrocities against African Americans, McKay does not downplay them or offer an apology.

In *Home to Harlem*, McKay shows that even among the most disadvantaged African Americans, there remains a strong will to survive and reap the rewards of life, in spite of all the atrocities imposed upon them by white people. This fervent acceptance of life is occasionally justified by the worst parts of their experience. When Jake Brown, the protagonist of the novel, reminds other black workers which it is considered improper to cross picket lines and serve as "scabs," one black longshoreman angrily retorts those black workers are frequently denied union positions. According to Jake:

Talking death, tha's what you sure is. One think I know is niggers am made foh life. And I want to live, boh, and feel plenty o' the juice o' life in mah blood. I wanta live and I wanta love. And niggers am got to work hard foh that. Buddy, I'll tell you this and I'll tell it to the wo'l'-all the crackers, and all them poah white trash, all the nigger-hitting and nigger-breaking white folks-I loves life and I got to live and I'll scab through hell to live. (Cooper xxiii)

Jake, Claude McKay's embodiment of the vitality and core values of African Americans, listens but withdraws. In *Home to Harlem*, Jake describes his picaresque voyage through "the semi-underworld" of black working-class America. Following his employment as a third cook in the Pennsylvania Railroad's dining car service, he contacts Ray, a waiter and a poor Haitian genius. As a friendship grows, McKay is able to contrast and balance each other's advantages and disadvantages against the backdrop of their "rough-and-tumble work and night life" (Cooper xxiv). Ray and Jake concur that despite severe restrictions, black people can express themselves positively through their shared love of dancing, music, and laughter, especially when they gather together for nighttime get-togethers. The black people appear to be having a great time with themselves, showcasing their own hard-earned colour, creativity, and happiness:





### Bairavi and Prashaanth

Black lovers of life fixed in their own free native rhythm, threaded to a remote scarce-remembered past, for themselves, of themselves, in an exceedingly house in Fifteenth Street, Philadelphia. . . (Cooper xxiv).

*Home to Harlem* also admits the less hopeful fact that African American life in Harlem and other rising Northeast ghettos is unduly constrained and restricted, in contrast to these poetic elements of African American life as a dining-car waiter on the Pennsylvania Railroad during the First World War. These situations often result in anger and self-loathing, and self-harm puts the community as a whole at constant risk. While acknowledging the African American community's potential, McKay also highlights the internal pressures that pose a threat to the community's survival in *Home to Harlem*.

McKay starts a fictional quest in *Home to Harlem* for self-reliance, self-worth, and purpose in the stylish African American lifestyle that would consume him in later works. It is a challenged novel written by a writer whose own stresses and questions are never far from the surface, especially in light of all the bold declarations of African Americans' strength and happiness throughout. McKay characterizes Ray and Jake as hopeful, nevertheless. Their message of affirmation and hope, with a few standout exceptions, is a recurring theme in black literature, especially in light of the serious issues still plaguing America's black inner cities. Black folklore, according to McKay, ends in the country's cities where "men like Jake in *Home to Harlem* exemplify the great Migration northward that began in his day" (xxiv). If the African American community is to take charge of its own future and stop being a victim of American capitalism, which sees African Americans as lifeless pieces on a chessboard of gain and loss, then these men must be honoured for their hard reality and selfless attitude.

The first chapter of the novel titled as "Going Back Home" clearly expresses the protagonist's nostalgia for the home land. Jack experiences color and racial prejudices as well as alienation in his transnational life in Virginia and Europe. According to S.P. Adinarayan's definition in *The Case for Color*, color prejudice refers to a mindset or collective attitude toward specific individuals, primarily sparked by their race, particularly the color of their skin. In certain cases, it can also be reinforced and intensified by political, social, and economic factors, in addition to the innate emotions of jealousy, fear, and disgust. It is surcharged with emotion and is by its very nature irrational.

The novel's hero Jake, is a freighter stoker traveling from Cardiff, Wales to New York. His patriotic reasons lead him to enlist in the army in 1917, the year America declared war on Germany. He is upset, though, when he finds out against his wishes that he must transport building supplies for the barracks. He could witness racial discrimination even in the army. He is forced to perform laborious physical tasks instead of fighting, such as "lumber-boards, planks, posts, rafters-for the hundreds of huts built around Brest's walls and along coast between Brest and Saint-Pierre, to house the soldiers of the United States" (4). As a result, he makes the decision to leave the army, declaring that he will not be involved in the struggle against white political and economic empire.

*Free* by Mbanefo S. Ogene, Esther Chikaodi Anyanwu, and Ngini Josephine Ojiakuexpla in the article entitled "A Comparative Analysis of Racial Discrimination in Claude McKay's *Home to Harlem* and Kenneth Kaunda's *Zambia Shall be*," describe Jake's feelings of shame and resentment about the injustices done to Black people during World War II. The Yankees' treatment of Black people by calling them "niggers" or "darker" resents him. McKay observes:

He knew that when a Yankee said Nigger, he meant hatred for the Negroes, whereas when he said 'darker,' he meant friendly contempt. He preferred white folks' hatred to their friendly contempt. To feel their hatred made him strong and aggressive, while their friendly contempt made him ridiculously angry, even against his own will. (HH 5)

McKay's contemporary writers Richard Wright and W.E.B. Du Bois in *The Souls of Black Folk* and *Native Son* respectively have also depicted such kind of discrimination in their works. Black people were routinely beaten and lynched by white people for no apparent reason. Even after the historic proclamation, white people still segregate and discriminate against Black people. W.E.B. DuBois states that:







### Bairavi and Prashaanth

A black stranger in a Baker Country, Georgia, for instance, is liable to be stopped anywhere on the public highway and made to state his business to the satisfaction of any white interrogator. If he fails to give a suitable answer, or seem too independent or 'sassy,' he may be arrested or summarily driven away. (*The Souls of Black Folk* 133)

This sentiment is also present in Richard Wright's *Native Son*, when the thieves exhibit dread due to their ingrained hatred of African Americans. Wright aptly states the pitiable plight of the blacks: "being dragged over the snow, his feet were up within the air, grasped by robust hands. 'Kill 'im!' 'Lynch 'im!' 'That black son of a bitch!' 'Kill black ape!'" (301). Black people in America are conditioned to believe that it is acceptable for them to take whatever the white people throw at them.

Jake leaves the army where he faced racial discrimination, dresses in civilian clothes, and travels to London to work on the docks. He spends time with a white girlfriend for the rest of the war. Jake is not happy with the white woman, so their relationship is unpleasant. Jake views the white woman as merely an alien being from a different planet. He begins to harbour feelings for Felice, a brown woman. Through his bizarre chat with the ship, Jake expresses his desire to get to Harlem as soon as possible. He conveys his wish to the ship even though he is fully aware that it is an absurd object that cannot react to his commands. This delves into his longing to return to his hometown of Harlem:

Take me Home to Harlem, Mister ship!  
Take me Home to the brown gals waiting for  
the brown boys that done show their mettle  
Over there. Take me home, Mister ship. Put  
Your beak right into that water and jest move  
along.... (HH 9)

Jake's return trip to America is the first time that a physical representation of Harlem is mentioned. Jake's boredom and nostalgia disappear as soon as he gets to Harlem. Music, sex, and alcohol satisfy his insatiable thirst for joy. His desires get fulfilled in Harlem's Lenox Avenue:

Harlem! Harlem! thought Jake. Where else could I have all this life but Harlem? Good old Harlem!  
Chocolate Harlem! Sweet Harlem! Harlem, I've got you' number down. Lenox Avenue, you're a beer, I  
know it. And, baby honey, sure enough youse a pippin for your pappy. Oh, boy! . . . (HH 14)

Jake finds it "crazy" to be walking around his neighbourhood once more: "He had been gone from Harlem for two years. He was being called by girls who were chocolate-brown and walnut-brown from One Hundred, Lenox Avenue, and Fifth Avenue and Thirty-Fifth Street" (8). Before he truly returns to his old neighbourhood, he has dreams about it. There are two aspects noted in this initial description. At first Jake's more desirable streets are 135 Street, Fifth Avenue, and Lenox Avenue. Second, in Jake's fantasy and imagination, the streets are filled with the brown women and their "tantalizing brown legs" (8). It is seen as sexual radicalization and he can rejoice himself in the city-streets.

Jake visits a saloon on his way back to his former neighbourhood. He is ecstatic to see Harlem as he subsequently "promenades" (10) along Seventh Avenue: "His blood was hot. His eyes were alert as he sniffed the street like a hound" (10). The metaphor of Jake as a hunting hound and his animalistic traits, both are utilized to suggest the "primitive" in the description of the urban core of African American life: "Harlem! Harlem! Little thicker, little darker and noisier and smellier, but Harlem just the same. The niggers done plowed through Hundred and Thirtieth Street" (25). Joyous at his good fortune, Jake wonders where he might have "all this life" if not in "Chocolate Harlem" (14). Drinking, sexuality and sex, enjoyment, music and rhythmic movement are all integral parts of Harlem's charm:







### Bairavi and Prashaanth

The deep-dyed color, the thickness, the closeness of it. The noises of Harlem. The sugared laughter. The honey-talk on its streets. And all night long, rag-time and “blues” playing somewhere... singing somewhere, dancing somewhere! Oh, the contagious fever of Harlem. Burning everywhere in dark-eyed Harlem.... Burning now in Jake’s sweet blood....(HH 15)

All that is Harlem is framed and set against the backdrop of blackness in all of its shades and forms; “colour” is what makes this neighbourhood unique and creates the social group that inhabits it.

## CONCLUSION

McKay emphasizes the distinctions between Black and White culture throughout the novel. In the novel, the author deftly contrasts the free-form, spontaneous, libidinous life of the black ghetto to a place where drugs, alcohol, guns, sex, knives, and poverty are commonplace with the puritanical, controlled behaviour of the white society. Jake travels to Baltimore to visit restaurants, taverns, and a cabaret. There, he meets Felice, a young prostitute who is brown, and they spend the night together. Jake then returns to Harlem. For both Black and White audiences, the cabaret is well-known. The police squad’s actions, which included promoting and allowing prostitution, pornography, gambling, and the cabaret was forced to close for a long time due to the illicit usage of drugs and alcohol.

McKay’s empathy for the issues facing the black working class is evident in the strike-breaking scenes in *Home to Harlem*, which are partially inspired by his personal experiences. McKay worked as a houseman, dining-car waiter, porter, and stevedore before he could support himself from the money he earned from writing. The spirit of his identification with the expanding Black working class is made evident in this proletarian novel. Though it is a “proletarian” novel, McKay’s *Home to Harlem* lacks the militant tone of the later proletarian novels of the 1930s. However, McKay honours the vitality and lives of the black working class in Harlem in the novel *Home to Harlem*. These people include stevedores, maids, dockers, cooks, waiters, prostitutes, and pimps, who taken as a whole provide a new energy that white society completely slacks.

Thus, the article mainly focuses on the social life of blacks in *Home to Harlem*. Additionally, McKay expertly captures the social life of blacks in Harlem and portrays them as self-assured individuals who are proud of their race. Even though Jake is a social reformer, his self-esteem does not allow him to serve for his nation. So, he escapes from the army and tries to find his color pride in his homeland. Ray feels too proud of his color. The character seems to be the mouthpiece of Claude McKay, in order to voice against racial discrimination and racial prejudice that prevailed in his contemporary society.

## REFERENCES

1. Adinarayan, S. P. “Causes of Colour Prejudice.” *The Case for Colour: An Analysis of the Causes, Manifestations, and Effects of Colour Prejudices, A Survey of Remedial Measures and Some Suggestions for a Cure*. Asia Publishing House, 1964. pp. 1-29.
2. Cooper, Wayne F. Foreword. *Home to Harlem*, by Claude McKay, Harper, 1928. pp. xx-xxvi.
3. DuBois, W. E. B. *The Souls of Black Folk*. Oxford UP, 2007.
4. Edwards, Brent Hayes. *The Practice of Diaspora Literature, Translation, and the Rise of Black Internationalism*. Harvard UP, 2003.
5. McKay, Claude. *Home to Harlem*. Harper, 1928.
6. Tomlinson, Lisa. *The African-Jamaican Aesthetic: Cultural Retention and Transformation Across Borders*. Brill, 2017.
7. Wright, Richard. *Native Son*. Harper, 1940.
8. Du Bois, W.E.B. “The Browsing Reader: *Home to Harlem*.” *Twentieth-Century Literary Criticism*. Ed. Sharon K. Hall, et al. Vol 7. Gale Research, 1982. pp.455-456.



**Bairavi and Prashaanth**

9. Pyne-Timothy, Helan. "Perceptions of the Black Woman in the Work of Claude McKay." *CLA Journal*, vol. 19, no. 2, Dec. 1975, pp.152-164.
10. Greenberg, Robert. "Idealism and Realism in the Fiction of Claude McKay." *CLA Journal*, vol. 24, no. 3, March 1981, pp.237-261.
11. Lowney, John. "Haiti and Black Transnationalism: Remapping the Migrant Geography of *Home to Harlem*." *African American Review*, vol. 34, no. 3, autumn 2000, pp.413-429.
12. Lueth, Elmer. "The Scope of Black Life in Claude McKay's *Home to Harlem*." *Obsidian II*, vol. 5, no. 3, winter 1990, pp. 43-52.
13. Rottenberg, Catherine. "Writing from the Margins of the Margins: Michael Gold's *Jews without Money* and Claude McKay's *Home to Harlem*." *MELUS*, vol. 35, no. 1, spring 2010, pp. 119-140.
14. Ansell, Amy Elizebeth. "Color-Consciousness." *Race and Ethnicity: The Key Concepts*. Routledge, 2013. pp.45-46.
15. Drake, St. Clair, and Horace R. Cayton. *Black Metropolis: A Study of Negro Life in a Northern City*. Rev. and enl. ed, Uof Chicago P, 1970.
16. Pontuale, Francesco. "The Contagious Fever of the Jungle: Primitivism in Claude McKay's *Home to Harlem*." *RSA Journal*, vol. 8-9, 01 Sept. 1998, pp.65-81.
17. Tiller, Tyrone. *Claude McKay: A Black Poets's Struggle for Identity*. Massachusetts UP, 1992





# A Methodology to Propose Neutrosophic Basic Probability Assignment in Neutrosophic Evidence Set

D. Leonita<sup>1\*</sup> and R. Irene Hepzibah<sup>2</sup>

<sup>1</sup>Assistant Professor, Department of Mathematics, Idhaya College for Women, Kumbakonam, Thanjavur, (Affiliated to Bharathidasan University, Tiruchirappalli), Tamil Nadu, India.

<sup>2</sup>Assistant Professor, PG & Research Department of Mathematics, T.B.M.L. College, Porayar, (Affiliated to Bharathidasan University, Tiruchirappalli), Tamil Nadu, India.

Received: 05 July 2024

Revised: 10 Sep 2024

Accepted: 14 Nov 2024

## \*Address for Correspondence

### D. Leonita

Assistant Professor, Department of Mathematics,  
Idhaya College for Women, Kumbakonam, Thanjavur,  
(Affiliated to Bharathidasan University, Tiruchirappalli),  
Tamil Nadu, India.

E.Mail: leodominic59@gmail.com



This is an Open Access Journal / article distributed under the terms of the **Creative Commons Attribution License** (CC BY-NC-ND 3.0) which permits unrestricted use, distribution, and reproduction in any medium, provided the original work is properly cited. All rights reserved.

## ABSTRACT

Many data fusion application systems make use of the Dempster – Shafer theory of evidence. In evidence theory, determining Basic Probability Assignment is still a work in progress. A method for locating Neutrosophic Basic Probability Assignment in a Neutrosophic set is proposed in this study. Finally, a real-life example demonstrates the cogency of the planned strategy.

**Keywords:** Dempster Shafer concept, Neutrosophic evidence sets, Combination rule, Basic probability assignment.

## INTRODUCTION

Neutrosophy is a relatively novel area of attitude. To contract with partial, inconsistent, then uncertain information, FlorentinSmarandachefuture the idea of Neutrosophic circles. The neutral customary is a helpful mathematical tool that is a generalisation of classic sets, conventional fuzzy sets, and intuitionistic fuzzy sets. Each statement in neutrosophic logic has a certainty degree (T), an indeterminacy degree (I), and a falsehood degree (F), where T, I, and F are normal or nonstandard subsets of  $[-0, 1+]$ . The Dempster-Shafer Theory is a mathematical evidence theory. One of the most widely used uncertainty theories is the D–S model of indication [2] [12]. The theory of probable or evidential reasoning is another name for it. It is a powerful theoretical tool that may be used to describe partial knowledge and update opinions. The Dempster Shafer model of uncertainty representation and processing offers a wide variety of useful applications, including information fusion[5],[15],[17], expert systems [7], decision making





### Leonita and Irene Hepzibah

[8],[9], and risk assignment [4]. Evidence theory relies heavily on basic probability assignment. Basic probability assignment can be used to define all other measures. Expert subjectivity is generally used to provide the BPA in practise. Many other theories, such as fuzzification [20], intuitionistic sets [1], and so on., and so on, have been expanded to cope with uncertainty in addition to the evidence theory. The notion of interval valued evidence[14], R-No's [11], and other methods can be used to enhance how the DS –theory represents unclear data

Another variation on basic probability assignment is offered in this study. Only the truth membership of inference is considered in the classic basic probability assignment. A neutrosophic evidence set is proposed, which is based on the ideas of sets of neutrosophic. The neutrosophic evidence set takes into account the focal components' participation in the truth, indeterminacy, and falsity. Neutrosophic Basic Probability Assignment is an important aspect of the neutrosophic set (NBPA). The first BPA denotes the truth membership, the second BPA denotes the indeterminacy membership, and the third BPA denotes the falsity membership in a Neutrosophic Basic Probability Assignment. Neutrosophic sets have singletons as their fundamental values, however the focal element of Neutrosophic Basic Probability Assignment can be a multiple subset of the discernment frame. The proposed neutrosophic evidences provide a more adaptive technique to model decision - making uncertainty. It combines Dempster – Shafer evidence theory with the capacity to cope with extra information through neutrosophic sets.

The following is a breakdown of the paper's structure: In section 2, the Dempster- Shafer Theory and the neutrosophic set are briefly discussed. We presented Neutrosophic basic probability assignment in Section 3. Section three employs multi-criteria group decision making to illustrate the correctness of the proposed strategy. Finally, in section 5, there are some closing remarks.

#### Preliminaries

##### Definition : 2.1 [6]

Consider  $X$  to be a collection of points, with  $x$  being a generic member in  $X$ . The truth membership function,  $T_A$ , and the indeterminacy membership function,  $I_A$ , and falsity membership function,  $F_A$ . characterise a neutrosophic set  $A$  in  $X$ .  $F_A, T_A, I_A, x, I_A(x)$ , and,  $F_A(x)$  are real standard or non-standard subsets of  $]0, 1+[$ .

That is,  $T_A : X \rightarrow ]0^-, 1^+[$ ,

$I_A : X \rightarrow ]0^-, 1^+[$ ,

$F_A : X \rightarrow ]0^-, 1^+[$ .

The sum of  $T_A(x), I_A(x)$  and  $F_A(x)$  has no restriction, so  $0 - \leq \sup T_A(x) + \sup I_A(x) + \sup F_A(x) \leq 3^+$ .

##### Definition : 2.2[4],[12]

Let the frame of discernment  $\Theta = \{k_1, k_2, k_3, \dots, k_n\}$ . The power set of  $\Theta$  is  $2^\Theta = \{\emptyset, \{k_1\}, \{k_2\}, \dots, \{k_n\}, \{k_1, k_2\}, \dots, \{k_1, k_2, k_3, \dots, k_i\}, \dots, \Theta\}$ . A basic probability assignment (BPA) function  $m$  is a mapping of  $2^\Theta$  to a interval  $[0,1]$  defined as [4], [14]:

$m: 2^\Theta \rightarrow [0,1]$

which satisfies the following conditions:

- i)  $m(\emptyset) = 0$  and
- ii)  $\sum_{A \in 2^\Theta} m(A) = 1$ .

where  $\emptyset$  is an empty set, and  $A$  is any element of  $2^\Theta$ . The mass  $m(A)$  shows the degree of the evidence support  $A$ .

##### Definition : 2.3[4],[12]

For a BPA  $m$  on  $\Theta$ , each element of  $2^\Theta$  such that  $m(A) > 0$  is called an focal element of  $m$ .





**Leonita and Irene Hepzibah**

**Definition : 2.4**[4],[12]

For a BPA  $m$  on  $\Theta$ , the belief function  $Bel$ , and the plausibility function  $Pl$  are defined by

$$Bel(A) = \sum_{B \subseteq A} m(B)$$

$$Pl(A) = \sum_{A \cap B \neq \emptyset} m(B)$$

**Definition : 2.5**[4]

Given two BPAs  $m_1$  and  $m_2$  on  $\Theta$ , the rule of combination is defined by

$$m_1 \otimes m_2(\emptyset) = 0$$

$$m_1 \otimes m_2(\emptyset) = \frac{\sum_{B \cap C = A} m_1(B)m_2(C)}{1 - \sum_{B \cap C = \emptyset} m_1(B)m_2(C)}$$

**Definition : 2.6**[3] [10]

Given two BPAs  $m_1$  and  $m_2$  on  $\Theta$ , the weights of two BPAs are  $w_1$  and  $w_2$ .  $A$  is any subset of  $\Theta$ . The weighted average combination method is defined as

$$m_1 \otimes m_2(A) = \text{ave}(m_1, m_2) \otimes \text{ave}(m_1, m_2)(A)$$

Where  $\text{ave}(m_1, m_2)$  is a new BPA and it is defined by

$$\text{ave}(m_1, m_2)(A) = m_1(A) \times w_1 + m_2(A) \times w_2$$

**Definition : 2.7**[13]

The Pignistic probability of a BPA  $m$  on  $\Theta$  is defined as

$$Bet P(A) = \sum_{B \in 2^\Theta} \frac{|A \cap B|}{|B|} \frac{m(B)}{1 - m(\emptyset)}, \forall A \in 2^\Theta$$

where  $|A|$  is the cardinality of  $A$ . The pignistic probability is a probability distribution on  $\Theta$  with  $p_k =$

$$Bet P(h_k) = \sum_{h_k \in B} \frac{m(B)}{|B|}$$

**Definition : 2.8** [18]

Assume  $m$  is a BPA on  $\Theta$ , the cost of a focal element  $A, A \subseteq \Theta$  is defined as

$$Cost(A) = \frac{n - |A|}{n - 1}$$

Assume  $m$  is a BPA on  $\Theta$ , the cost of  $m$  is defined as

$$Cost(m) = \sum_{A \subseteq \Theta} Cost(A)m(A)$$

**Definition : 2.9**[16]

Assume  $m$  is a BPA on  $\Theta$ , the specificity of  $m$  is defined as

$$Sp(m) = \sum_{A \subseteq \Theta, A \neq \emptyset} \frac{m(A)}{|A|}$$

**Neutrosophic Basic probability Assignment:**

**Definition: 3.1**

Assume a frame of discernment  $\Theta = \{k_1, k_2, k_3, \dots, k_n\}$ . The power set of  $\Theta$  is  $2^\Theta = \{\emptyset, \{k_1\}, \{k_2\}, \dots, \{k_n\}, \{k_1, k_2\}, \dots, \{k_1, k_2, k_3, \dots, k_i\}, \dots, \Theta\}$ . A Neutrosophic basic probability assignment (NBPA) of  $2^\Theta$  is defined as

$$m(A) = \langle m^T(A), m^I(A), m^F(A) \rangle \tag{1}$$





**Leonita and Irene Hepzibah**

where  $m^T(A): 2^\Theta \rightarrow [0,1]$ ,  $m^I(A): 2^\Theta \rightarrow [0,1]$  and  $m^F(A): 2^\Theta \rightarrow [0,1]$  are truth membership, indeterminacy membership and falsity membership respectively.

A is any element of  $2^\Theta$ . They must satisfy the following conditions:

- i)  $m^T(\emptyset) = 0, m^I(\emptyset) = 0$  and  $m^F(\emptyset) = 0$ .
- ii)  $\sum_{A \in 2^\Theta} m^T(A) = 1$ .
- iii) For all  $A \neq \emptyset, m^T(A) + m^I(A) + m^F(A) \leq 1$ .

**Definition: 3.2**

For Neutrosophic Basic Probability Assignment 'm' on  $\Theta$ , each subset A of  $\Theta$  such that  $m^T(A) > 0$  or  $m^I(A) > 0$  or  $m^F(A) > 0$  is called a focal element of 'm'.

**Definition: 3.3**

Let 'm' be a Neutrosophic Basic Probability Assignment on  $\Theta$  with Neutrosophic Probability masses  $m(A) = \langle m^T(A), m^I(A), m^F(A) \rangle$  and  $A \in 2^\Theta$ . The Belief function of A also have three components defined as:

$$\text{Bel}(A) = \langle \text{Bel}^T(A), \text{Bel}^I(A), \text{Bel}^F(A) \rangle \tag{2}$$

where  $\text{Bel}^T(A) = \sum_{B \subseteq A} m^T(B)$  (3)

$$\text{Bel}^I(A) = \sum_{B \subseteq A} m^I(B) \tag{4}$$

$$\text{Bel}^F(A) = \sum_{B \subseteq A} m^F(B) \tag{5}$$

**Definition: 3.4**

Let 'm' be a Neutrosophic Basic Probability Assignment on  $\Theta$  with Neutrosophic Probability masses  $m(A) = \langle m^T(A), m^I(A), m^F(A) \rangle$  and  $A \in 2^\Theta$ . The Plausibility function of 'A' also have three components defined as:

$$\text{Pl}(A) = \langle \text{Pl}^T(A), \text{Pl}^I(A), \text{Pl}^F(A) \rangle \tag{6}$$

where  $\text{Pl}^T(A) = \sum_{B \cap A \neq \emptyset} m^T(B)$  (7)

$$\text{Pl}^I(A) = \sum_{B \cap A \neq \emptyset} m^I(B) \tag{8}$$

$$\text{Pl}^F(A) = \sum_{B \cap A \neq \emptyset} m^F(B) \tag{9}$$

**Definition: 3.5**

The possibility of a subset 'A' also have three components  $\text{Poss}(A) = \langle \text{Poss}^T(A), \text{Poss}^I(A), \text{Poss}^F(A) \rangle$  (10)

where  $\text{Poss}^T(A) \in [\text{Bel}^T(A), \text{Pl}^T(A)]$  (11)

$$\text{Poss}^I(A) \in [\text{Bel}^I(A), \text{Pl}^I(A)] \tag{12}$$

$$\text{Poss}^F(A) \in [\text{Bel}^F(A), \text{Pl}^F(A)] \tag{13}$$

**Definition: 3.6**

Let 'm' be a Neutrosophic Basic Probability Assignment on  $\Theta$  with Neutrosophic Probability masses  $m(A) = \langle m^T(A), m^I(A), m^F(A) \rangle$  and  $A \in 2^\Theta$ . The pignistic probability of 'm' is defined by

$$\text{Bet P}(A) = \langle \text{Bet P}^T(A), \text{Bet P}^I(A), \text{Bet P}^F(A) \rangle \text{ for all } A \in 2^\Theta. \tag{14}$$

where

$$\text{Bet P}^T(A) = \sum_{B \in 2^\Theta} \frac{|A \cap B|}{|B|} \cdot \frac{m^T(B)}{1 - m^T(\emptyset)} \tag{15}$$

$$\text{Bet P}^I(A) = \sum_{B \in 2^\Theta} \frac{|A \cap B|}{|B|} \cdot \frac{m^I(B)}{1 - m^I(\emptyset)} \tag{16}$$

$$\text{Bet P}^F(A) = \sum_{B \in 2^\Theta} \frac{|A \cap B|}{|B|} \cdot \frac{m^F(B)}{1 - m^F(\emptyset)} \tag{17}$$







**Leonita and Irene Hepzibah**

**Definition: 3.7**

Let the neutrosophic probability mass of 'A',  $\langle m^T(A), m^I(A), m^F(A) \rangle$  is an Neutrosophic Basic Probability Assignment 'm' on  $\Theta$ .

The Pure support degree is defined as

$$PS(A) = \max_{A \in \Theta} (\text{Bet } P^T(A) - \text{Bet } P^I(A), \text{Bet } P^T(A) - \text{Bet } P^F(A)) \quad (18)$$

**Definition: 3.8**

The cost of a Neutrosophic Basic probability assignment 'm' is defined by

$$\text{cost}(m) = \sum_{A \subseteq \Theta} \text{cost}(A) m^T(A) + \sum_{A \subseteq \Theta} \text{cost}(A) m^I(A) + \sum_{A \subseteq \Theta} \text{cost}(A) m^F(A) \quad (19)$$

When all focal elements of 'm' are singleton, the cost of 'm' is the most cost,  $\text{cost}(m)=3$ .

When 'm' with one focal element  $m(\Theta) = \langle 1,1 \rangle$ , the cost of 'm' is the least cost,  $\text{cost}(m)=0$ .

**Definition: 3.9**

The specificity of Neutrosophic probability assignment 'm' is defined as

$$sp(m) = \sum_{A \subseteq \Theta, A \neq \emptyset} \frac{m^T(A) + m^I(A) + m^F(A)}{|A|} \quad (20)$$

**Definition: 3.10**

Assume 'm' is a Neutrosophic Basic Probability Assignment on  $\Theta$  with neutrosophic probability masses  $m(A) = \langle m^T(A), m^I(A), m^F(A) \rangle$  and  $A \in 2^\Theta$ . Then  $m^*$  is a Basic probability transformed by 'm' can be calculated by

$$m^*(A) = \min \left[ \frac{m^T(A) - m^I(A)}{\sum_{B \subseteq \Theta} (m^T(B) - m^I(B))}, \frac{m^T(A) - m^F(A)}{\sum_{B \subseteq \Theta} (m^T(B) - m^F(B))} \right] \quad (21)$$

**Definition : 3.11**

Given two Neutrosophic Basic Probability Assignment 'm<sub>1</sub>' and 'm<sub>2</sub>' on  $\Theta$ , the combination result is denoted as  $m_1 \otimes m_2$  is given by

$$m_1 \otimes m_2(A) = \langle m^T(A), m^I(A), m^F(A) \rangle \quad (22)$$

where

$$\begin{cases} m^T(\emptyset) = 0 \\ m^T(A) = \frac{\sum_{B \cap C = A} m_1^T(B) m_2^T(C)}{1 - \sum_{B \cap C = \emptyset} m_1^T(B) m_2^T(C)} \end{cases} \quad (23)$$

$$\begin{cases} m^I(\emptyset) = 0 \\ m^I(A) = \frac{\sum_{B \cap C = A} m_1^I(B) m_2^I(C)}{1 - \sum_{B \cap C = \emptyset} m_1^I(B) m_2^I(C)} \end{cases} \quad (24)$$

$$\begin{cases} m^F(\emptyset) = 0 \\ m^F(A) = \frac{\sum_{B \cap C = A} m_1^F(B) m_2^F(C)}{1 - \sum_{B \cap C = \emptyset} m_1^F(B) m_2^F(C)} \end{cases} \quad (25)$$

**Definition: 3.12**

Let 'm<sub>1</sub>' and 'm<sub>2</sub>' be two Neutrosophic Basic Probability Assignment on  $\Theta$ . Then the weighted average combination result NBPA,

$m_1 \otimes m_2(A) = \langle m^T(A), m^I(A), m^F(A) \rangle$  is given by

$$m^T(A) = \text{ave}(m_1^T, m_2^T)(A)$$

$$m^I(A) = \text{ave}(m_1^I, m_2^I)(A)$$

$$m^F(A) = \text{ave}(m_1^F, m_2^F)(A)$$

**Illustration of the Proposed Approach:**

Consider the challenge of selecting refrigerator brands. If there are four refrigerator brands, R-1, R-2, R-3, and R-4, then the alternate set is  $R = \{R-1, R-2, R-3, R-4\}$ . A decision group of three decision makers has been constituted to investigate alternative refrigerator brands.  $D = \{D-1, D-2, D-3\}$  is the collection of decision makers. Assume the selection problem involves four criteria: C-1. (quality), C-2. (price), C-3. (degree of satisfaction), and C-4. (function).





**Leonita and Irene Hepzibah**

$C_1, C_2, C_3, C_4, \dots$  is the collection of criteria. The steps in the procedure for the selection problem are as follows.

Step : 1

Determine the weights of criteria:

Opinions of all criteria by decision makers are given in the below table :

$D_1$	$D_2$	$D_3$
$\{C_1\}\langle 0.3, 0.2, 0.1 \rangle$	$\{C_1\}\langle 0.2, 0.1, 0.2 \rangle$	$\{C_1\}\langle 0.3, 0.2, 0.1 \rangle$
$\{C_2\}\langle 0.2, 0.2, 0.2 \rangle$	$\{C_2\}\langle 0.2, 0.3, 0.2 \rangle$	$\{C_2\}\langle 0.3, 0.1, 0.1 \rangle$
$\{C_3\}\langle 0.2, 0.3, 0.3 \rangle$	$\{C_3\}\langle 0.2, 0.2, 0.2 \rangle$	$\{C_3\}\langle 0.1, 0.2, 0.2 \rangle$
$\{C_4\}\langle 0.2, 0.2, 0.3 \rangle$	$\{C_4\}\langle 0.1, 0.2, 0.3 \rangle$	$\{C_4\}\langle 0.1, 0.1, 0.2 \rangle$
$\{C_1, C_4\}\langle 0.1, 0.1, 0.1 \rangle$	$\{C_1, C_2, C_3\}\langle 0.1, 0.2, 0.1 \rangle$	$\{C_1, C_4\}\langle 0.1, 0, 0.2 \rangle$
	$\{C_2, C_3, C_4\}\langle 0.2, 0, 0 \rangle$	$\{C_2, C_3\}\langle 0.1, 0.2, 0 \rangle$
		$\{C_2, C_3, C_4\}\langle 0, 0.2, 0.2 \rangle$

The fused result  $m_c$  of decision makers opinions can be calculated by the Equations (22)-(25)

$$m_c(\{c_1\}) = \langle 0.4590, 0.1333, 0.0698 \rangle$$

$$m_c(\{c_2\}) = \langle 0.2308, 0.250, 0.1667 \rangle$$

$$m_c(\{c_3\}) = \langle 0.2162, 0.4286, 0.3443 \rangle$$

$$m_c(\{c_4\}) = \langle 0.1428, 0.1071, 0.4030 \rangle$$

The weight of criteria  $W_c = [W_{c_1}, W_{c_2}, W_{c_3}, W_{c_4}]$  can be calculated by

$$W_{c_j} = \langle W_{c_j}^T, W_{c_j}^I, W_{c_j}^F \rangle$$

$$= \langle \text{Bet } P^T(c_j), \text{Bet } P^I(c_j), \text{Bet } P^F(c_j) \rangle$$

where  $W_{c_j}^T = \text{Bet } P^T(c_j)$ ,  $W_{c_j}^I = \text{Bet } P^I(c_j)$ , and  $W_{c_j}^F = \text{Bet } P^F(c_j)$ ,  $j = 1, 2, 3, \dots$

Therefore,

$$W_c = \left[ \langle 0.4590, 0.1333, 0.0698 \rangle, \langle 0.2308, 0.2500, 0.1667 \rangle, \langle 0.2162, 0.4286, 0.3443 \rangle, \langle 0.1428, 0.1071, 0.4030 \rangle \right]$$

Step : 2

Calculate the initial fused results NBPA's based on weight of criteria.

The NBPA decision matrix  $M$  is

$$M = \begin{bmatrix} m_{11} & m_{12} & m_{13} \\ m_{21} & m_{22} & m_{23} \\ m_{31} & m_{32} & m_{33} \\ m_{41} & m_{42} & m_{43} \end{bmatrix}$$

Where,  $m_{j-k}$  is an NBPA allocated by policymakers. to criteria,  $C_j$ .

The NBPA of the decision problem is shown in the table below:

Criteria	Subsets of brands	Decision maker		
		$D_1$	$D_2$	$D_3$
$C_1$	$\{R_1\}$	$\langle 0.22, 0.21, 0.23 \rangle$	$\langle 0.22, 0.18, 0.20 \rangle$	$\langle 0.21, 0.30, 0.33 \rangle$
	$\{R_2\}$	$\langle 0.18, 0.13, 0.15 \rangle$	$\langle 0.19, 0.17, 0.14 \rangle$	$\langle 0.15, 0.14, 0.17 \rangle$
	$\{R_3\}$	$\langle 0.27, 0.17, 0.08 \rangle$	$\langle 0.23, 0.21, 0.11 \rangle$	$\langle 0.25, 0.10, 0.08 \rangle$
	$\{R_4\}$	$\langle 0.18, 0.21, 0.23 \rangle$	$\langle 0.19, 0.17, 0.22 \rangle$	$\langle 0.21, 0.15, 0.17 \rangle$
	$\{R_1, R_2\}$	$\langle 0.00, 0.28, 0.31 \rangle$	$\langle 0.00, 0.12, 0.33 \rangle$	$\langle 0.00, 0.23, 0.25 \rangle$
	$\{R_1, R_3\}$	$\langle 0.15, 0.01, 0.00 \rangle$	$\langle 0.17, 0.15, 0.00 \rangle$	$\langle 0.18, 0.08, 0.00 \rangle$
$C_2$	$\{R_1\}$	$\langle 0.21, 0.20, 0.23 \rangle$	$\langle 0.23, 0.18, 0.20 \rangle$	$\langle 0.19, 0.17, 0.15 \rangle$
	$\{R_2\}$	$\langle 0.18, 0.17, 0.19 \rangle$	$\langle 0.20, 0.11, 0.13 \rangle$	$\langle 0.22, 0.20, 0.23 \rangle$
	$\{R_3\}$	$\langle 0.29, 0.28, 0.05 \rangle$	$\langle 0.23, 0.11, 0.13 \rangle$	$\langle 0.25, 0.23, 0.08 \rangle$
	$\{R_4\}$	$\langle 0.18, 0.17, 0.24 \rangle$	$\langle 0.17, 0.25, 0.27 \rangle$	$\langle 0.19, 0.17, 0.23 \rangle$
	$\{R_1, R_2\}$	$\langle 0.00, 0.06, 0.29 \rangle$	$\langle 0.00, 0.25, 0.27 \rangle$	$\langle 0.00, 0.10, 0.31 \rangle$
	$\{R_1, R_3\}$	$\langle 0.14, 0.12, 0.00 \rangle$	$\langle 0.17, 0.10, 0.00 \rangle$	$\langle 0.15, 0.13, 0.00 \rangle$
$C_3$	$\{R_1\}$	$\langle 0.21, 0.26, 0.29 \rangle$	$\langle 0.20, 0.28, 0.30 \rangle$	$\langle 0.24, 0.23, 0.27 \rangle$
	$\{R_2\}$	$\langle 0.18, 0.11, 0.14 \rangle$	$\langle 0.17, 0.18, 0.20 \rangle$	$\langle 0.18, 0.07, 0.09 \rangle$





**Leonita and Irene Hepzibah**

	{R <sub>3</sub> }	⟨0.22, 0.11, 0.14⟩	⟨0.23, 0.08, 0.10⟩	⟨0.20, 0.16, 0.18⟩
	{R <sub>4</sub> }	⟨0.21, 0.12, 0.14⟩	⟨0.20, 0.18, 0.20⟩	⟨0.20, 0.16, 0.18⟩
	{R <sub>1</sub> , R <sub>2</sub> }	⟨0.00, 0.27, 0.29⟩	⟨0.00, 0.18, 0.20⟩	⟨0.00, 0.26, 0.28⟩
	{R <sub>1</sub> , R <sub>3</sub> }	⟨0.18, 0.13, 0.00⟩	⟨0.20, 0.10, 0.00⟩	⟨0.18, 0.12, 0.00⟩
	C <sub>4</sub>	{R <sub>1</sub> }	⟨0.22, 0.20, 0.25⟩	⟨0.22, 0.27, 0.31⟩
	{R <sub>2</sub> }	⟨0.18, 0.12, 0.17⟩	⟨0.15, 0.11, 0.13⟩	⟨0.19, 0.17, 0.13⟩
	{R <sub>3</sub> }	⟨0.24, 0.03, 0.08⟩	⟨0.25, 0.06, 0.08⟩	⟨0.23, 0.21, 0.20⟩
	{R <sub>4</sub> }	⟨0.21, 0.12, 0.17⟩	⟨0.19, 0.21, 0.23⟩	⟨0.19, 0.17, 0.20⟩
	{R <sub>1</sub> , R <sub>2</sub> }	⟨0.00, 0.30, 0.33⟩	⟨0.00, 0.22, 0.23⟩	⟨0.00, 0.10, 0.27⟩
	{R <sub>1</sub> , R <sub>3</sub> }	⟨0.15, 0.23, 0.00⟩	⟨0.19, 0.11, 0.00⟩	⟨0.16, 0.14, 0.00⟩

The initial fused results  $M^{ne} = [m_1^{ne}, m_2^{ne}, m_3^{ne}]$  can be calculated by

$$ave(m_k^{ne}) = \sum_{j=1}^4 m_{jk} \times w_{cj}, k = 1,2,3$$

$$m_k^{ne} = ave(m_k^{ne}) \otimes ave(m_k^{ne}) \otimes ave(m_k^{ne}), k = 1,2,3$$

We have obtain

$$m_1^{ne}: \quad m_1^{ne}(\{R_1\}) = \langle 0.2263, 0.2107, 0.2550 \rangle$$

$$m_1^{ne}(\{R_2\}) = \langle 0.1888, 0.1198, 0.1588 \rangle$$

$$m_1^{ne}(\{R_3\}) = \langle 0.2727, 0.1570, 0.944 \rangle$$

$$m_1^{ne}(\{R_4\}) = \langle 0.1995, 0.1342, 0.1728 \rangle$$

$$m_1^{ne}(\{R_1, R_2\}) = \langle 0, 0.2000, 0.3027 \rangle$$

$$m_1^{ne}(\{R_1, R_3\}) = \langle 0.1615, 0.1249, 0 \rangle$$
  

$$m_2^{ne}: \quad m_2^{ne}(\{R_1\}) = \langle 0.2285, 0.2178, 0.2754 \rangle$$

$$m_2^{ne}(\{R_2\}) = \langle 0.1916, 0.1389, 0.1528 \rangle$$

$$m_2^{ne}(\{R_3\}) = \langle 0.2441, 0.0962, 0.0960 \rangle$$

$$m_2^{ne}(\{R_4\}) = \langle 0.1967, 0.1848, 0.2220 \rangle$$

$$m_2^{ne}(\{R_1, R_2\}) = \langle 0, 0.1792, 0.2296 \rangle$$

$$m_2^{ne}(\{R_1, R_3\}) = \langle 0.1875, 0.0997, 0 \rangle$$
  

$$m_3^{ne}: \quad m_3^{ne}(\{R_1\}) = \langle 0.2250, 0.2033, 0.2216 \rangle$$

$$m_3^{ne}(\{R_2\}) = \langle 0.1857, 0.1168, 0.1335 \rangle$$

$$m_3^{ne}(\{R_3\}) = \langle 0.2485, 0.1619, 0.1614 \rangle$$

$$m_3^{ne}(\{R_4\}) = \langle 0.2106, 0.1492, 0.1927 \rangle$$

$$m_3^{ne}(\{R_1, R_2\}) = \langle 0, 0.1778, 0.2744 \rangle$$

$$m_3^{ne}(\{R_1, R_3\}) = \langle 0.1789, 0.1094, 0 \rangle$$

Step : 3

Influence the exact fused results:

The NBPA,m-fn. final fused findings are determined by

$$m_d : \quad m_d(\{D_1\}) = \langle 0.4, 0.1, 0.2 \rangle$$

$$m_d(\{D_2\}) = \langle 0.2, 0.3, 0.35 \rangle$$

$$m_d(\{D_3\}) = \langle 0.3, 0.2, 0.25 \rangle$$

$$m_d(\{D_1, D_3\}) = \langle 0.1, 0.2, 0.1 \rangle$$

$$m_d(\{D_2, D_3\}) = \langle 0, 0.2, 0.1 \rangle$$

Step : 4 Influence the exact fused results:

The NBPA,m-fn. final fused findings are determined by

$$ave(m^{fn}) = \sum_{k=1}^3 m_k^{fn} \times W_{d_1}$$

$$m^{fn} = ave(m^{fn}) \otimes ave(m^{fn}) \otimes ave(m^{fn}), k = 1,2,3.$$

Hence

$$m^{fn} : m^{fn}(\{R_1\}) = \langle 0.2263, 0.2105, 0.2515 \rangle$$

$$m^{fn}(\{R_2\}) = \langle 0.1883, 0.1261, 0.1475 \rangle$$

$$m^{fn}(\{R_3\}) = \langle 0.2564, 0.1347, 0.1185 \rangle$$

$$m^{fn}(\{R_4\}) = \langle 0.2027, 0.1604, 0.1994 \rangle$$





### Leonita and Irene Hepzibah

$$m^{\text{fn}}(\{R_1, R_2\}) = \langle 0, 0.1828, 0.2635 \rangle$$

$$m^{\text{fn}}(\{R_1, R_3\}) = \langle 0.1102, 0.1086, 0 \rangle$$

$$m^{\text{fn}}(\ominus) = \langle 0.0140, 0.0769, 0.0196 \rangle$$

Step : 5

Rank alternatives:

(14)-calculates the simple endorsement degree of every option in,  $m^{\text{fn}}$  (18). Then, in order of pure support degrees, rank the options as follows.

$$PS(R_1) = -0.0452$$

$$PS(R_2) = -0.0198$$

$$PS(R_3) = 0.1748$$

$$PS(R_4) = 0.0109$$

The alternatives were ranked as  $R_3 > R_4 > R_2 > R_1$ .

Therefore, among the four refrigerators brands  $R_3$  should be selected.

## CONCLUSION

In the application of DS theory to complicated uncertain circumstances, BPA estimate is quite significant. Unlike standard BPA, the proposed NBPA takes into account the truth, indeterminacy, and falsity membership of focal elements. This technique combines the strengths of evidence theory and the Neutrosophic set, making it more flexible, information-rich, and reasonable. Unlike the Neutrosophic set, the proposed NBPA allows numerous subsets of the frame of discernment to be members of truth, indeterminacy, and falsehood. An example of group decision making is used to show the effectiveness of the proposed technique. This approach is used to choose the best refrigerator brands based on four criteria: quality, price, level of satisfaction, and functionality.

## REFERENCES

1. Atanassov K.T, "Intuitionistic fuzzy sets", Fuzzy Sets Systems. vol 20, no.1, pp. 87-96, 1986.
2. Dempster A.P, "Upper and lower probabilities induced by a multivalued mapping", Annals of Mathematical Statistics, vol.38, pp.325-339, 1967.
3. Deng .Y, Shi.W, Zhu.Z and Liu.Q, "Combining belief functions based on distance of evidences", Decis.Support Syst. Vol.38, pp: 489 – 493, Dec 2004.
4. Dong.Y, Zhang. J, Li.Z and Deng.Y, "Combination of evidential sensor reports with distance function and belief entropy in fault diagnosis", Int.J. Comput. Common.Control, vol.14, no.3, pp 329-343, 2019.
5. Dutta .P, "An uncertainty measure and fusion rule for conflict evidences of big data via Dempster – Shafer theory", Int J. Image Data Fusion, Vol.9, no.2, pp 152-169, 2018.
6. Florentin Smarandae, Collected papers, vol II, University of Kishinev, Kishinev, 1997.,
7. Fu .C, Yang J.B and Yang S.L, "A group evidential reasoning approach based on expert reliability", Eur.J.Oper.Res.vol 246, no.3, pp 886-893, 2015.
8. He. Z and Jiang .W "An evidential Markov decision making model", Inf.Sci.vol. 467, pp 357 – 372, Oct 2018
9. Li.Y and Deng. Y, "TDBF : Two dimensional belief function", Int.J.Intell.Syst. vol 34, no.8, pp 1968-1982, 2019.
10. Murphy C.K, "Combining belief functions when evidence conflicts", Decis. Support Syst., vol 29, no.1, pp 1-9, Jul.2000.
11. Seiti. H, Hafezalkotob .A and Martinez.L. "R-numbers, a new risk modeling associated with fuzzy numbers and its application to decision making", Inf.Sci.Vol483, pp 206 – 231, May 2019.
12. Shafer. G, "A Mathematical Theory of Evidence", Princeton University Press, Princeton, NJ, USA, 1976.
13. Smets .P and Kennes .R, "The transferable belief model", Artif.Intell., vol.66, no.2, pp. 191-234, Apr 1994.
14. Song .Y, Wang .X, Lei .L and Xue .A, " Uncertainty measure for interval valued belief structures," Measurement, vol .80, pp 241- 250, Feb 2016.
15. Xiao .F and Qin.B, "A weighted combination method for conflicting evidence in multi sensor data fusion",





**Leonita and Irene Hepzibah**

sensors, vol.18, no.5pp.1487,2018.

16. Yager R.R, "Entropy and specificity in a mathematical theory of evidence", Int. J. Gen. Syst. Vol. 9, no. 4, pp . 249-260,1983.
17. Yager R.R, Elmore. P and Petry.F , "Soft likelihood functions in combination evidence", Inf. Fusion, Vol.36, pp .185-190, Jul.2017.
18. Yager R.R, "Satisfying uncertain targets using measure generalized Dempster –Shafer belief measure structures", Knowl – Based Syst. Vol 142, pp 1-6, Feb.2018.
19. Yangxue Li and Yong Deng, IEEE Access, Digital Object Identifier 10, 1109/ Access 2019,2932763.
20. Yen .J, "Generalizing the Dempster-Shafer theory to fuzzy sets," IEEE Transactions on Systems, Man, and Cybernetics, Vol. 20, no. 3, pp. 559-570, 1990.





## Detergent Activity of Aqueous Extract of *Croton Bonplandianus* Baill - Possible Source of Natural Surfactant

Renugadevi R<sup>1\*</sup>, Geethalakshmi Sundararaman<sup>2</sup>, Kiruba M<sup>3</sup> and Divya M<sup>3</sup>

<sup>1</sup>Associate Professor and Head, Department of Biotechnology, RVS College of Arts and Science, Sullur, (Affiliated to Bharathiar University ) Coimbatore, Tamil Nadu, India.

<sup>2</sup>Associate Professor, Department of Biotechnology, RVS College of Arts and Science, Sullur, (Affiliated to Bharathiar University) Coimbatore, Tamil Nadu, India.

<sup>3</sup>M. Sc. Student, Department of Biotechnology, RVS College of Arts and Science, Sullur, (Affiliated to Bharathiar University) Coimbatore, Tamil Nadu, India.

Received: 18 Jun 2024

Revised: 22 Aug 2024

Accepted: 24 Oct 2024

### \*Address for Correspondence

#### Renugadevi R

Associate Professor and Head,  
Department of Biotechnology,  
RVS College of Arts and Science, Sullur,  
(Affiliated to Bharathiar University )  
Coimbatore, Tamil Nadu, India.  
E.Mail: renugadevi@rvsgroup.com



This is an Open Access Journal / article distributed under the terms of the **Creative Commons Attribution License** (CC BY-NC-ND 3.0) which permits unrestricted use, distribution, and reproduction in any medium, provided the original work is properly cited. All rights reserved.

### ABSTRACT

*Croton bonplandianus* Baill is a perennial herb grows in all climatic conditions in wasteland areas. The extract of these plants contains several secondary metabolites used as medicine for various diseases. The phytochemical analysis of this plant shown to contain high amount of saponins that act as surfactant revealed an excellent detergent activity. This study focused to determine the detergent activity of *Croton bonplandianus* Baill using various parameters such as preliminary phytochemical analysis, dirt dispersion, cleaning activity, foaming stability, pH and wetting ability. This plant possesses high dirt dispersion and cleaning activity compared to SLS standard. The foaming stability is less compared to standard but wetting ability show maximum in plant extract in 1% as well as 5%. The pH of drug sample is found to 6.11 which is essential factor for detergent quality. The foam and froth was made to stand for maximum time to reflect the presence of saponins. Further HPLC analysis confirmed the presence of saponin with retention time of 2.684 min similar to standard.

**Keywords:** *Croton bonplandianus* Baill, Saponin, SLS, Surfactant, HPLC







## INTRODUCTION

A chemical compound with the ability to clean is said to be a detergent. An excellent detergent dissolves in water, lowers the interfacial tension to allow the water-based solution to pass through the capillaries, disperses clumped particles, and bonds the dirt or particles of oil to the water instead of the material being cleaned (Haney *et al.*, 1954). Many secondary chemicals generated by plants are bio-based surfactants, which resemble soap or detergent (Wisetkomolmat *et al.*, 2019). In aqueous solutions, detergents are amphipathic compounds that are surface-active agents – they display special characteristics, such as the ability to develop spherical micellar structures and reduce the tension on the surface of their solution. The primary objective of detergents is to eliminate stains, which are typically caused by protein bases, oils, and other contaminants without causing any harm or re-depositing dirt onto the material (Bhat *et al.*, 2011). Many medicinal plants contain natural surfactants such as saponin which can form stable soap-like foam when shaken in water (Wisetkomolmat *et al.*, 2021). The desire to substitute chemical synthesis that harms our environment has increased demand for these important active components.

Asian developing nations continue to rely heavily on medicinal herbs in their daily lives. As a result, these plants are essential for daily existence. Flavonoids, tannins, steroids, alkaloids, saponins, terpenoids, cardiac glycosides, flavonoids, anthraquinone and reducing sugars are the primary phytochemicals found in plants (Agidew, 2022). Saponins are important plant glycosides among secondary metabolites that are widely distributed in the plant kingdom and it is present in herbs, vegetables, and beans. Moreover, saponins are amphipathic combinations of hydrophobic aglycone and hydrophilic sugar molecules that makes strong surface-active compounds (Samal *et al.*, 2017; Kregiel *et al.*, 2017). Hence, it possesses foaming, detergent, emulsifying and wetting properties. Previous research report stated that saponins were identified from the leaves of *Mangifera indica* L., juice of citrus fruit, leaves and roots of *Leucas aspera* L., fruits of *Persea americana*, leaves of *Vernonia amygdalina* bark of *Vernonia amygdalina* (Agidew, 2022).

The monoecious exotic weed, *Croton bonplandianus* Baill, commonly referred as Ban Tulsi, is typically 30–40 cm tall that grows along roadside ditches, wide open ravines fields of railway, and agricultural fields. Report says that it is native to India, Bangladesh, South Western Brazil, South America, North Argentina, and Pakistan. The plant parts and latex used for treatment of wounds, treatment for skin diseases, possesses antiseptic and antimicrobial activity (Ghosh *et al.*, 2018). It was reported that methanolic extract of *Croton bonplandianus* Baill revealed the presence of resins, alkaloids, saponins, flavonoids, saponins, phenols, and steroids to shown to contain the pharmacological activity (Jeeshna *et al.*, 2011). Saponin and flavonoid contents are maximum compare to other metabolites. Hence, this study is focused on the detergent activity of aqueous extract of *Croton bonplandianus* Baill.

## MATERIALS AND METHODS

### Collection and Identification of Plant Samples

The plants samples were collected from a farm in Sulur, Coimbatore and it was identified by Botanical Survey of India (BSI), Tamilnadu Agriculture University (TNAU), Coimbatore, Tamilnadas *Croton bonplandianus* Baill belonging to Euphorbiaceae family with Voucher number BSI/SRC/5/23/2023/Tech-186. A specimen of the plant was also deposited for the herbarium.

### Extraction of Sample

The leaves of the plant were cleaned and shade dried for 72 h. It was powdered, sieved and used for extract preparation. 60 g of the powder was macerated with 600 ml of sterile distilled water for 24 h in a glass stoppered conical flask at 37°, shaken for 6 h and allowed to stand for 18 h, filtered and stored in airtight container for further use (Manzoor *et al.*, 2021).





### Preliminary qualitative phytochemical analysis

Following conventional methods, the primary groups of phytochemicals present in the extract were identified using standard procedure (Lawal *et al.*, 2019; Dubale *et al.*, 2023).

### Dispersion of Dirt

The main purpose of a detergent is to clean filth. In test tubes containing 10 ml of distilled water, the extract was added at a concentration of 1% and 5%. The tubes were shaken well and 1 drop of Indian ink was added to the tubes. The tubes were mixed vigorously and allowed to stand for few seconds. The amount of ink present in the foam was estimated as heavy, moderate, light or none (Madhusudhanet *et al.*, 2021; Manzoor *et al.*, 2021).

### Cleaning Action

The ability of cleaning of a detergent is determined using heavy stains such as greasy cotton cloth test followed by Barnett and Powers (1951). The cleaning ability of detergent is to reduce the surface tension of water and emulsify either grease or oil. Around 5gm of grease was applied on a clean cotton cloth, weighed and placed in tubes containing 1% and 5% of leaf and maintained at 35° for 4 min using a magnetic stirrer with hot plate. The cloth was then taken out, dried for 6 h and measured the weight (Manzoor *et al.*, 2021). The following equation was used to calculate the percentage reduction of the grease;

$$DP = 100(1-T/C)$$

Where, DP = Percentage of detergency power; C = Weight of of the sample before cleaning; T = Weight of the sample after cleaning.

### Foaming power and Foaming Stability:

The cylinder shake method was used to determine the foaming ability. Each 50 ml of 1% and 5% of extract solution were taken in graduated cylinder and shook for 10 times. The total volume of foam was measured at 0 and 5 minutes. By using the foam volume, foam stability was calculated by using R5 parameter which represents the quotient of the foam (Manzoor *et al.*, 2021). The residual foam ratio was determined by using the following formula;

$$R_5 = (h_5/h_0) \times 100$$

Where,  $h_0$  represents foam height at 0 minute;  $h_5$  represents foam height after 5 minutes

### Wetting Ability

The wetting ability of plant extract was used to determine the efficiency of presence of surfactants. 1 inch diameter of cotton cloth with average weight of 0.32 gm was floated on the surface of the extract. The time taken to sink was observed to determine the wetting ability (Manzoor *et al.*, 2021).

### Determination of pH

The pH of the extract is an essential factor to check the quality of detergent which will minimize the irritation and ecological stability of the skin. The pH of 1% as well as 5% sample extracts was determined thrice with help of digital pH meter at 25°.

### Qualitative test for Saponins

#### Froth test

The aqueous extracts of the sample and 1% and 5% of SLS (Sodium Lauryl Sulfate) as standard wereshaken vigorously shaken and stand for 10 minutes. The froth of more than 1.5cm indicated the presence of saponins, whereas no froth indicated the absence of saponins.



**Foam test**

Around 2 ml of extract was mixed with 6 ml of distilled water, vigorously shaken for 5 minutes and observed the foam formation. The formation and persistence of foam indicated the presence of saponins.

**HPLC Analysis of Saponins**

About 2 ml of plant extract was dissolved in HPLC grade methanol for HPLC analysis using saponin standard. Shimadzu lab Chromo 2010 HT HPLC, UV detector was used for analysis using a C18 column at 35° temperature. 40:60 ratio of acetonitrile: water was used as mobile phase; 15µl injection volume for 25min at flow rate 1ml/min at 203nm.

**RESULTS AND DISCUSSION****Collection, Identification and Extraction of Plant Sample**

The leaves of the collected plant was extracted using sterile water and were used for the phytochemical analysis.

**Preliminary qualitative phytochemical analysis**

From the phytochemical analysis, the identified plant *Croton Bonplandianus* Baill contains high amount of saponins and flavonoids (Table 1). Saponins are the main component that exhibits detergent activity (Rai *et al.*, 2021). The plant contains saponins at a high concentration, which can be utilized for preparation of cleansing agent for both household as well as cosmetic industry. To confirm the potential of the prepared plant extract for cleaning action, further tests were carried out.

**Dispersion of Dirt and Cleaning Action:**

Dirt dispersion activity is estimated to check the ability of the extract to remove the dirt from the test surface by the principle of dispersion. For this, the component must have less frothing ability (Pradhan *et al.*, 2022). It can be understood that since the extract produces less foam, the dirt that binds with detergent gets dispersed on the surface of the water, which makes it easy to wash off (Akbari *et al.*, 2023). When the foam is high, the dirt gets bound to the foam and will not disperse. If the test surface is immersed in water, the dirt redeposits on the surface again making it impossible to remove. From Table 2, the extract has a good dirt dispersion activity compared to the standard SLS. Similarly, the grease reduction percentage is found higher than SLS (Figure 1). Hence, the plant under study has a good detergent activity at 5% concentration compared to 1%.

**Foaming power and Foaming Stability:**

The above results (Table 3) show less foam formation compared to the standard and the foam has less stability than SLS which indicates its effective cleansing ability (Amagliani *et al.*, 2021).

**Wetting Ability**

Wetting ability is an indicator that determines the extent of the detergent's interaction with water. This factor is important because, the detergent when interacting with water starts forming micelles in the absence of water which traps the dirt and releases when immersed in water. This process enables the dirt to get dispersed in water and get washed (Rekielet *et al.*, 2020). Moreover, the detergent will be in suspension in water enabling more surface area to be produced. This process helps in trapping of more dirt particles and hence enhanced cleansing activity. The extract under study has an effective wetting ability at 5% concentration. The time taken for sinking as suspension is quicker at 1% compared to 5% (Table 4).

**Determination of pH**

The average pH of the drug solution was found as 6.11 in 1% and 5% of extract (Schreiner *et al.*, 2021).





Renugadevi et al.,

### Qualitative test for Saponins

#### Froth test and Foam test

The aqueous extracts of the sample showed a froth of 1.5cm and standing time of 10 min. Foam was observed in aqueous extract after diluting with distilled water. It was an evidence for the presence of saponins. The foam formed was moderate and the standing time indicated the foam does not retain for a longer time. Less the standing time, easy the washing process and water consumption will be less (Góral and Wojciechowski, 2020).

### HPLC Analysis of saponins

The HPLC analysis of standard had a retention time of 2.315 minutes. The peak of plant extract confirmed the presence of saponin with retention time of 2.684 minutes (Figure 2). This preliminary analysis showed the presence of saponin in *Croton bonplandianus* Baill. Further analysis is needed to extract and purify the exact saponin component and estimate its efficiency (Wang et al., 2021).

### CONCLUSION

The study indicates a novel plant whose extract showed detergent activity. The results obtained also confirm the findings that *Croton bonplandianus* Baill can be utilized for preparing cleansers. Natural cleansers are always preferred compared to synthetic and semisynthetic ones due to their prolonged negative effects or delayed hypersensitive reactions. Extensive research on this plant can give novel phytochemical which could have a wide industrial application.

### ACKNOWLEDGEMENT

The authors are grateful to the Department of Biotechnology, RVS College of Arts and Science, Coimbatore, India for providing the necessary facilities to carry out this work.

### REFERENCES

1. Haney P.D, Engr Black, Veatch, Culp R.L, Vaughn J.D. Effects of synthetic Detergents on water supplies, A report of Task group E5.15 presented on at the annual conference, Seattle, Wash. 1954;25
2. Wisetkomolmat, J., Suksathan, R., Puangpradab, R., Kunasakdakul, K., Jantasakulwong, K., Rachtanapun, P., & Sommano, S. R. (2020). Natural surfactant saponin from tissue of litseaglutinosa and its alternative sustainable production. *Plants*, 9(11), 1521.
3. Bhat, R., Prajna, P. S., Menezes, V. P., & Shetty, P. (2011). Antimicrobial activities of soap and detergents. *Adv Biores*, 2(2), 52-62.
4. Wisetkomolmat, J., Inta, A., Krongchai, C., Kittiwachana, S., Jantasakulwong, K., Rachtanapun, P., & Sommano, S. R. (2021). Ethnochemometric of plants traditionally utilised as local detergents in the forest dependent culture. *Saudi Journal of Biological Sciences*, 28(5), 2858-2866.
5. Agidew, M. G. (2022). Phytochemical analysis of some selected traditional medicinal plants in Ethiopia. *Bulletin of the National Research Centre*, 46(1), 87.
6. Samal, K., Das, C., & Mohanty, K. (2017). Eco-friendly biosurfactant saponin for the solubilization of cationic and anionic dyes in aqueous system. *Dyes and Pigments*, 140, 100-108.
7. Kregiel, D., Berłowska, J., Witonska, I., Antolak, H., Proestos, C., Babic, M., ... & Zhang, B. (2017). Saponin-based, biological-active surfactants from plants. *Application and characterization of surfactants*, 6(1), 184-205.
8. Ghosh, T., Biswas, M. K., Roy, P., & Guin, C. (2018). A review on traditional and pharmacological uses of *Croton bonplandianum* with special reference to phytochemical aspect. *European Journal of Medicinal Plants*, 22(4), 1-10.
9. Jeeshna, M. V., Paulsamy, S., & Mallikadevi, T. (2011). Phytochemical constituents and antimicrobial studies of the exotic plant species, *Croton bonplandianum* Baill. *Journal of life sciences*, 3(1), 23-27.
10. Manzoor, S., Jahan, N., & Ahmed, S. A. (2021). Detergent properties of aqueous extract of *Aatrelal* (*Ammi majus* L.) and *Babchi* (*Psoralea corylifolia* L.). *Neuropharmac Journal*, 6, 169-179.





## Renugadevi et al.,

11. Lawal, A. M., Abdullahi, R., Ibrahim, M. S., Kurfi, M. Y., Khalid, A., & Nuhu, M. (2019). Phytochemical analysis and thin layer chromatography profiling of crude extracts from *Senna occidentalis* (leaves). *Journal of Biotechnology and Biomedical Science*, 2(1), 12-21.
12. Dubale, S., Kebebe, D., Zeynudin, A., Abdissa, N., & Suleman, S. (2023). Phytochemical screening and antimicrobial activity evaluation of selected medicinal plants in Ethiopia. *Journal of experimental pharmacology*, 51-62.
13. Madhusudhan, M., Rao, M. K., Radha, G. V., & Ganapathy, S. (2021). Formulation, Evaluation and Comparison of the Polyherbal Shampoo with the Commercial Shampoos. *Asian Journal of Pharmaceutical Research and Health Care*, 254-265.
14. Barnett, G., & Powers, D. H. (1951). A quantitative method for the evaluation and study of shampoos. *J Soc Cosmet Chem*, 2, 219-228.
15. Rai, S., Acharya-Siwakoti, E., Kafle, A., Devkota, H. P., & Bhattarai, A. (2021). Plant-derived saponins: A review of their surfactant properties and applications. *Sci*, 3(4), 44.
16. Pradhan, A., Bhuyan, S., Chhetri, K., Mandal, S., & Bhattacharyya, A. (2022). Saponins from *Albizia procera* extract: Surfactant activity and preliminary analysis. *Colloids and Surfaces A: Physicochemical and Engineering Aspects*, 643, 128778.
17. Akbari, S., Abdurahman, N. H., & Kudrashou, V. (2023). Surface activity and emulsification properties of saponins as biosurfactants. In *Advancements in Biosurfactants Research* (pp. 137-153). Cham: Springer International Publishing.
18. Amagliani, L., Silva, J. V., Saffon, M., & Dombrowski, J. (2021). On the foaming properties of plant proteins: Current status and future opportunities. *Trends in Food Science & Technology*, 118, 261-272.
19. Rekiel, E., Smulek, W., Zdziennicka, A., Kaczorek, E., & Jańczuk, B. (2020). Wetting properties of *Saponaria officinalis* saponins. *Colloids and Surfaces A: Physicochemical and Engineering Aspects*, 584, 123980.
20. Schreiner, T. B., Colucci, G., Santamaria-Echart, A., Fernandes, I. P., Dias, M. M., Pinho, S. P., & Barreiro, M. F. (2021). Evaluation of saponin-rich extracts as natural alternative emulsifiers: A comparative study with pure *Quillaja* Bark saponin. *Colloids and Surfaces A: Physicochemical and Engineering Aspects*, 623, 126748.
21. Góral, I., & Wojciechowski, K. (2020). Surface activity and foaming properties of saponin-rich plants extracts. *Advances in colloid and interface science*, 279, 102145.
22. Wang, C. Q., Yi, L. W., Zhao, L., Zhou, Y. Z., Guo, F., Huo, Y. S., ... & Cai, S. Q. (2021). 177 saponins, including 11 new compounds in wild ginseng tentatively identified via HPLC-IT-TOF-MSn, and differences among wild ginseng, ginseng under forest, and cultivated ginseng. *Molecules*, 26(11), 3371.

**Table 1: Preliminary qualitative phytochemical analysis**

S.No.	Phytochemical tests	Observation
1.	Cardiac Glycoside test	+
2.	Alkaloid test	-
3.	Saponin test	++
4.	Tannin test	+
5.	Carbohydrate test	+
6.	Phytosterol test	-
7.	Flavonoids test	++
8.	Phenol/tannins	-





Renugadevi et al.,

**Table 2: Dirt Dispersion and Cleaning Ability of Test Drug**

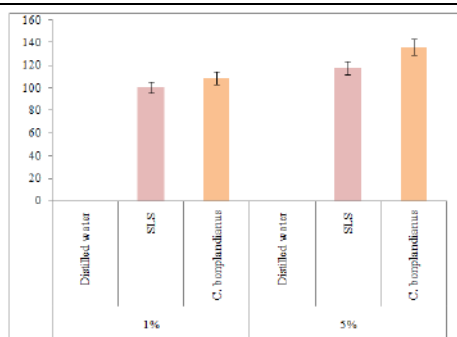
S. No.	Drug Name	Dirt Dispersion		% of Grease Reduction	
		1%	5%	1%	5%
1	Distilled water	-	-	0	0
2	SLS	Light	Light (+)	100.3	118
3	<i>C. bonplandianus</i>	Light	Light (+)	108.7	136.1

**Table 3: Effect of test drugs on foaming stability**

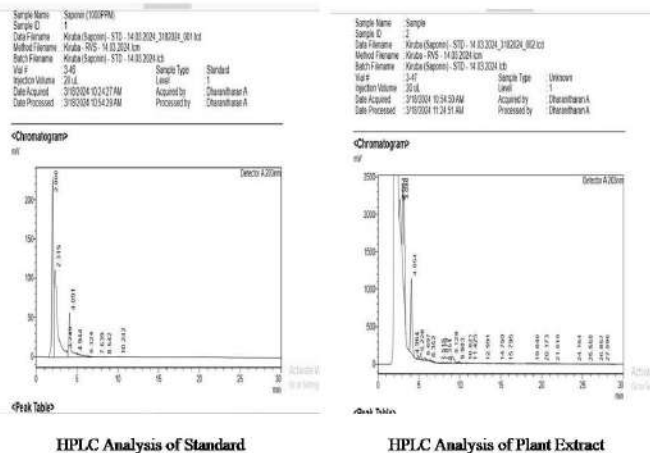
S. No.	Drug Name	Foaming Power				Foaming Stability(R5)	
		1%		5%		1%	5%
		0 min	5 min	0 min	5 min		
1	SLS	48.00	130.00	42.00	192.00	270.8	457.1
2	<i>C. bonplandianus</i>	46.00	98.00	40.00	110.00	213.0	275.0

**Table 4: Effect of test drug on wetting ability**

S.No.	Drug Name	1%		5%	
		Sinking time (hh.mm.ss)	Wetting time (hh.mm.ss)	Sinking time (hh.mm.ss)	Wetting time (hh.mm.ss)
1.	Distilled water	54.54.00	02.52.00	54.55.00	02.52.00
2.	SLS	15.43.00	43.50.00	04.09.00	06.52.00
3.	<i>C. bonplandianus</i>	01.01.27	02.20.10	04.10.00	17.12.00



**Figure 1: Percentage grease reduction of the extract**



**Figure 2: HPLC Analysis of Saponin**







## Isolation of Bioactive Compounds from *Streptomyces griseus* DR38

Devi E<sup>1\*</sup>, Bharathidasan.R<sup>2</sup> and Thiruneelakandan G<sup>3</sup>

<sup>1</sup>Research Scholar, Department of Microbiology, Maruthupandiyar College, Vallam, Thanjavur, (Affiliated to Bharathidasan University, Tiruchirappalli), Tamil Nadu, India.

<sup>2</sup>Assistant Professor, Department of Microbiology, Maruthupandiyar College, Vallam, Thanjavur, (Affiliated to Bharathidasan University, Tiruchirappalli), Tamil Nadu, India.

<sup>3</sup>Assistant Professor, Department of Microbiology, Maruthupandiyar College, Vallam, Thanjavur, (Affiliated to Bharathidasan University, Tiruchirappalli), Tamil Nadu, India.

Received: 18 July 2024

Revised: 10 Sep 2024

Accepted: 04 Nov 2024

### \*Address for Correspondence

Devi E

Research Scholar,

Department of Microbiology,

Maruthupandiyar College, Vallam, Thanjavur,

(Affiliated to Bharathidasan University, Tiruchirappalli),

Tamil Nadu, India.

E.Mail: shaisarvaadr4609@gmail.com



This is an Open Access Journal / article distributed under the terms of the **Creative Commons Attribution License** (CC BY-NC-ND 3.0) which permits unrestricted use, distribution, and reproduction in any medium, provided the original work is properly cited. All rights reserved.

### ABSTRACT

Actinomycetes are one of the major sources of bioactive compounds that are used against antibacterial, antifungal, antiviral, anticancer and anti-inflammatory based drug discovery in pharmaceutical industry. *Streptomyces* is the largest genus of actinomycetes which is known for the production of most antibiotics. Present study was aimed to isolate the novel actinomycetes from marine sediment. Using crude ethyl acetate extract of actinomycetes antimicrobial screening was performed against various bacterial pathogens such as *E.coli*, *Bacillus subtilis*, *Pseudomonas aeruginosa*, *Staphylococcus aureus* and *Streptococcus sp.* in well diffusion method. The strain which had the maximum zone of inhibition was selected for further studies and it was identified as *Streptomyces griseus* DR38 through 16S rRNA sequencing. The bioactive compounds have identified using GCMS study. The major active extracellular compound such as D-xylose, Rutinose, Diethyl Phthalate, Phthalic acid, 1,2 Benzenedicarboxylic acid was found in this study. These compounds have higher applications in pharmaceutical, cosmetic and food industry.

**Keywords:** Actinomycetes, Bioactive compounds, Antibiotics, GCMS, *Streptomyces*.





## INTRODUCTION

Actinomycetes, particularly marine actinomycetes are prolific source of bioactive compounds with diverse biological activities such as antibacterial, antifungal, antiviral, and anticancer properties. Studies have highlighted the isolation of numerous bioactive compounds from actinomycetes, including terpenes, terpenoids, meroterpenoids, polyketides, non-ribosomal peptides and other cytotoxic compounds, showcasing their potential in drug discovery and antibiotic development [1],[2]. Actinomycetes from various environments like marine sediments, hot springs and terrestrial ecosystems have been explored for their ability to produce novel bioactive compounds, emphasizing the importance of these microorganisms in generating new sources of pharmaceutical agents. The bioactive compounds isolated from actinomycetes have shown promising activities against drug resistant pathogens, making them valuable candidates for the development of new antibiotics and therapeutic agents [3],[4]. Streptomyces strains have been identified as valuable sources of specialized metabolites, including pigments, which have various bioactivities such as antioxidant, antibiofilm and antibiotic activities. Present study has isolated streptomycesgriseus from marine sediment soil and finding the active compounds through GCMS. These studies highlight the diverse range of bioactive compounds for potential pharmaceutical and nutritional applications.

## MATERIALS AND METHODS

### Sample Collection

Mangrove soil originating from a specific site in India was procured for research purposes. The soil sample was collected from Pichavaram Mangrove National Forest in Killai, Tamil Nadu India. The collection process involved obtaining soil specimens from a depth of 15 centimetres beneath the soil's surface, which were subsequently placed in aseptic containers for transportation to the laboratory. The process of isolating Actinomycetes from the Mangrove soil entailed utilizing a Starch Casein Agar (SCA) medium comprising of a mixture of 50% seawater and 50% distilled water.

### Screening for Actinomycetes that Produce Bioactive Compounds

The strains that were isolated underwent screening to assess their capability in producing bioactive compounds. These isolated actinomycetes strains were introduced into a medium containing 50% seawater known as (SCA) medium. The flask containing the inoculated strains was placed in an incubator at room temperature for duration of 5 days while being agitated on a rotary shaker operating at 120 rpm and a temperature of 28°C. Following the completion of the incubation period, the liquid broth was filtered, and the resulting filtrate was utilized to evaluate antimicrobial activity.

### Antimicrobial activity

Antimicrobial efficacy was evaluated using well susceptibility methods, with crude ethyl acetate extracts of active producing strains tested against various microorganisms including *E.coli*, *Bacillus subtilis*, *Pseudomonas aeruginosa*, *Staphylococcus aureus* and *Streptococcus sp.* using Muller Hiton Agar Medium (Himedia, India) [5]. The strain which had the maximum zone of inhibition was used for further studies.

### Molecular Characterization

The genomic DNA was isolated using HiPureA Bacterial Genomic DNA Purification kit (Himedia). Primers 27F (5'-AGAGTTTGATCCTGGCTCAG-3') and 1492 R (5'-TACGGCTACCTTGTTACGACTT -3') were used to amplify the 1480 bp 16S rRNA. The following were the PCR (Prime96 – Himedia) conditions: Initial denaturation 94°C for 3min, followed by 30 cycle of denaturation at 94°C for 1min, annealing at 55°C for 1min, extension at 72°C for 1 min, and final extension at 72°C for 3 min. The amplified product was confirmed with 1.2% of agarose gel. The PCR products were sequenced with Sanger Sequencing 3730xl DNA Analyzer (Barcode BioSciences – Bengaluru). The 16S rRNA sequence was entered into the NCBI nucleotide blast to determine the identity and similarity of the sequence with





other species in the database. Mega 11 software was used for sequence alignment and generation of phylogenetic trees.

#### Identification of Bioactive compounds with GCMS

The analysis of the active ethyl acetate extract was executed by Gas Chromatography Mass Spectrometry (GCMS). Shimadzu QP2010 ultra was used for identification of compounds and gas chromatography interfaced to a mass spectrometer. The appliance was built with Elite-1 fused silica capillary. Helium gas (99.99%) was the carrier gas with a constant flow rate of 1.21 ml/min and split ratio:10. Temperature of Injector was set on 160°C; Ion-source temperature was 200°C. The oven temperature was intended from 60°C with an increment of 280°C for around 22 min. Mass spectra were taken at 70eV; a scan interval of 0.5 sc. The chemical composition of the extract was determined by measuring the peak area and the retention time by comparing the NIST 14 library [6],[7].

## RESULT AND DISCUSSION

Primary and secondary screening of strain was performed against bacterial pathogens in well diffusion method was applied on Muller Hinton Agar Plates[6]. The maximum zone of inhibition in *Pseudomonas aeruginosa* for 13.7mm and minimum of *Streptococcus sp.* 8.9mm other organism have a significance of zone of inhibition occur from the selected strain[ Figure1]. The selected strain has amplified and sequenced 1532 bp of 16S rRNA and searched by NCBI nucleotide Blast to confirmed as *Streptomyces griseus DR38*, sequence has aligned and deposited to NCBI GenBank Accession No:PP329837. The phylogenetic tree was constructed using MEGA 11.0 [8] software using various streptomyces species. The evolutionary history was inferred using the Neighbor joining method [9]. The optimal tree is shown figure 2. The evolutionary distance was computed using Maximum composite Likelihood method [10] and are in the units of the number of base substitutions per site. This analysis involved 13 nucleotide sequences. All ambiguous positions were removed for each sequence pair. There was a total of 1460bp position in the final dataset. The ethyl acetate extract was analysed by GCMS and found the Bioactive compounds are listed in table1. The presence of D-xylose is a sugar widely used as a diabetic sweetener in food and beverage process. Rutinose disaccharide sugar is attached at the 3-hydroxyl position of quercetin an interesting biological active compound, rutin is formed due to their numerous pharmacological activities ranging from antioxidant action to chronic diseases such as cancer, diabetes and inflammation [11],[12],[13] Diethyl Phthalate used for personal care products, plasticizers, cosmetics etc [14]. Secondary metabolites produced from marine actinomycetes have distinct chemical structures, which may form the basis for the synthesis of new drugs. *Streptomyces griseus DR38* alone produces a wide range of metabolites having different biological activities. Enrichment and selective isolation methods can also be used to isolate rare actinomycetes from marine ecological niches having the potential to biosynthesize novel bioactive compounds. Continuous findings of novel organisms which may lead to the novel bioactive compounds.

## CONCLUSION

In this study, *Streptomyces griseus* was isolated from marine sediment soil and analyzed for its bioactive compounds using GCMS including D-xylose, rutinose and diethyl phthalate highlighting their potential pharmaceutical and nutritional application. The strain exhibited significant antibacterial activity particularly against *Pseudomonas aeruginosa* and streptococcus species. The 16S rRNA sequencing confirmed the identification of the strain as *Streptomyces griseus DR38*. The study underscores the importance of marine actinomycetes in producing novel bioactive compounds and emphasizes the need for continuous exploration of these microorganisms to discover new therapeutics agents.





## REFERENCES

- Mondal, H.; Thomas, J. Isolation and Characterization of a Novel Actinomycete Isolated from Marine Sediments and Its Antibacterial Activity against Fish Pathogens. *Antibiotics* 2022, 11, 1546. <https://doi.org/10.3390/>
- Tarasova, E.V.; Luchnikova, N.A.; Grishko, V.V.; Ivshina, I.B. Actinomycetes as Producers of Biologically Active Terpenoids: Current Trends and Patents. *Pharmaceuticals* 2023, 16, 872. <https://doi.org/10.3390/>
- Ziyan Qiu,1, Yinshuang Wua,1, Kunyan Lana, Shiyi Wanga, Huilin Yua, Yufei Wanga, Cong Wanga, \*, Shugeng Caob, Cytotoxic compounds from marine actinomycetes: sources, structures and bioactivity. *Acta Materia Medica* 2022, 1 (4), 445-475.
- Kumari Aparana and Rao K V Bhaskara; Role of Actinomycetes from different habitats as a potential source for the production of novel bioactive. *Res.J.Biotech*;2023; 18(3); 131-138.
- Ban Al-Jouboria, , Ismail Saadouna , Neil Hotchinb , Debbie Cunningham and Luke Alderwick; The isolation of novel terrestrial *Streptomyces* strain with antimicrobial and cytotoxic properties. *Arab Journal of Basic and Applied Science* 2023; 30 (1) 285 – 298.
- Kumari N, Menghani E & Mithal R, GC-MS analysis & assessment of antimicrobial potential of rhizospheric Actinomycetes of AIA3 isolate, *Indian J Tradit Know*, 19(1) (2020) 111–119.
- Kumari N., Menghani E. Evaluation of antibacterial activity and identification of bioactive metabolites by GCMS technique from Rhizospheric Actinomycetes. *Indian J. Nat. Prod. Resour. (IJNPR) [Formerly Natural Product Radiance (NPR)]* 2021;11(4):287–294
- Tamura K, Nei M. 2001. Estimation of the number of nucleotidesubstitutions in the control region of mitochondrial DNA inhumans and chimpanzees. *Mol Biol Evol.* 10:512–526 Saitou N. and Nei M. (1987). The neighbor-joining method: A new method for reconstructing phylogenetic trees. *Molecular Biology and Evolution* 4:406-425.
- Tamura K., Nei M., and Kumar S. (2004). Prospects for inferring very large phylogenies by using the neighbor-joining method. *Proceedings of the National Academy of Sciences (USA)* 101:11030-11035.
- Habtemariam, S., 2000. Natural inhibitors of tumour necrosis factor-alpha production, secretion and function. *Planta Med.* 66 (4), 303313.
- Habtemariam, S., 2011.  $\alpha$ -glucosidase inhibitory activity of kaempferol-3-O-rutinoside. *Nat. Prod. Commun.* 6 (2), 201-203.
- Habtemariam, S., Varghese, G.K., Extractability of Rutin in Herbal Tea Preparations of *Moringa stenopetala* Leaves. *Beverages* 1, 2015, 169-182.
- Huang L, Zhu X, Zhou S, Cheng Z, Shi K, Zhang C, Shao H. Phthalic Acid Esters: Natural Sources and Biological Activities. *Toxins (Basel)*. 2021 Jul 16;13(7):495. doi: 10.3390/toxins13070495. PMID: 34357967; PMCID: PMC8310026.

Table 1: Identification of Bioactive compounds from *Streptomyces griseus* DR38 through GCMS Analysis.

S.No	Compound Name	Rev. Score	Prob. %	molecular formula	molecular weight
1	D-Xylose	842	36.92	C <sub>5</sub> H <sub>10</sub> O <sub>5</sub>	150.13
2	Rutinose	838	31.19	C <sub>27</sub> H <sub>30</sub> O <sub>15</sub>	594.5
3	Diethyl Phthalate	864	36.22	C <sub>12</sub> H <sub>14</sub> O <sub>4</sub>	222.24
4	Phthalic acid, ethyl 2- pentyl ester	825	5.71	C <sub>15</sub> H <sub>20</sub> O <sub>4</sub>	264.32
5	Monoethyl phthalate	868	5.71	C <sub>10</sub> H <sub>10</sub> O <sub>4</sub>	194.18
6	1,2-Benzenedicarboxylic acid, bis(2-ethylhexyl) ester	664	7.22	C <sub>24</sub> H <sub>38</sub> O <sub>4</sub>	390.6
7	Phthalic acid, 2- methoxyethyl hexadecyl ester	671	6.66	C <sub>27</sub> H <sub>44</sub> O <sub>5</sub>	448.6
8	Phthalic acid, 2- methoxyethyl tetradecyl ester	670	6.4	C <sub>25</sub> H <sub>40</sub> O <sub>5</sub>	420.6





Devi et al.,

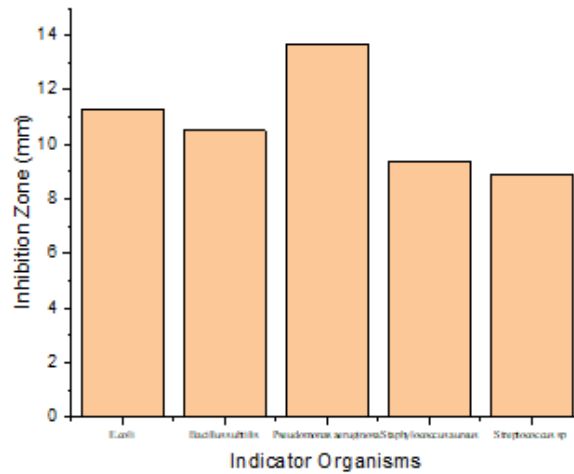


Figure 1: Inhibition activity of *Streptomyces griseus* DR38 extract against selected organisms.

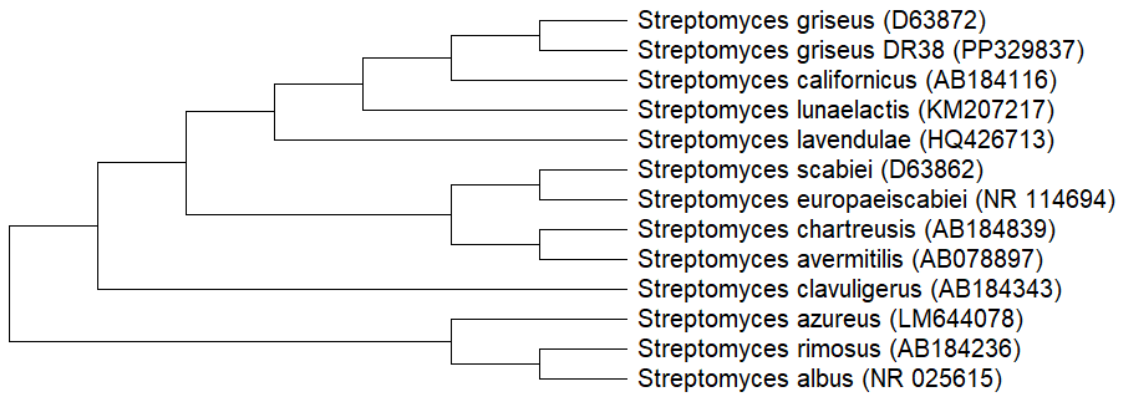


Figure 2: Phylogenetic study of *Streptomyces griseus* DR38 with *Streptomyces* species.





## Antidiabetic and Antihyperlipidemic Efficacy of Veratric Acid in Streptozotocin - Nicotinamide Induced Wistar Rats

John Anbumani Ganesan<sup>1</sup>, R.Kowsalya<sup>2\*</sup> and S.M. Sivasankaran<sup>1</sup>

<sup>1</sup>Research Scholar, Department of Biochemistry and Biotechnology, Annamalai University, Annamalai Nagar, Tamil Nadu, India.

<sup>2</sup>Assistant Professor, Department of Biochemistry and Biotechnology, Annamalai University, Annamalai Nagar, Tamil Nadu, India.

Received: 14 Jun 2024

Revised: 14 Aug 2024

Accepted: 17 Oct 2024

### \*Address for Correspondence

**Raju Kowsalya,**

Assistant Professor,

Department of Biochemistry and Biotechnology,

Annamalai University,

Annamalai Nagar,

Tamil Nadu, India.

E. Mail: kowsalyamouli@yahoo.com



This is an Open Access Journal / article distributed under the terms of the **Creative Commons Attribution License** (CC BY-NC-ND 3.0) which permits unrestricted use, distribution, and reproduction in any medium, provided the original work is properly cited. All rights reserved.

### ABSTRACT

Veratric acid has been shown to have multiple pharmacological activities under *in vivo* and *in vitro* conditions. The present study has made an effort to explore its antidiabetic effect in streptozotocin-nicotinamide-induced diabetic rats by analyzing the spectrum of biochemical markers as an endpoint. Diabetic animals showed a marked increase in glucose and insulin levels accompanied by drastic changes in the pattern of serum lipid profile. Veratric acid administration to diabetic animals reverted the status of glucose, insulin, and lipid profile in diabetic rats and the antidiabetic efficacy was found to be nearer to the efficacy of glibenclamide, the reference drug. The present study thus reveals the antidiabetic as well as antihyperlipidemic potential of veratric acid in diabetic rats.

**Keywords:** veratric acid, diabetes mellitus, streptozotocin, dyslipidemia.

### INTRODUCTION

Diabetes mellitus is an insulin resistance syndrome that poses significant healthcare challenges. The disease is characterized by persistent high blood sugar levels and abnormal metabolism of carbohydrates, fats, and proteins. This metabolic disruption results from inadequate secretion and/or action of insulin. High blood sugar can damage various parts of the body, including the eyes, nerves, kidneys, and heart [1,2]. An estimated 240 million people worldwide have undiagnosed diabetes, and nearly half of all adults with the ailment are unaware of it. In 2021, the





**John Anbumani Ganesan et al.,**

International Diabetes Federation (IDF) estimated that 537 million people had diabetes, accounting for 10.5% of the world population. Concerning, diabetes mellitus prevalence is expected to climb to 643 million (11.3%) by 2030 and 783 million (12.2%) by 2045. India has the second-highest number of diabetes patients worldwide. In the 20-79 age range, India had 74.9 million diabetics in 2021, it is possible to rise to 124.9 million by 2045 [3, 4]. Streptozotocin [2-deoxy-2-(3-methyl-3-nitrosurea) 1-D-glucopyranose] is an antibiotic derived from *Streptomyces achromogenes*. Its strong affinity for  $\beta$ -cell membranes results in selectively harmful effects on  $\beta$ -cells. Streptozotocin can affect pancreatic  $\beta$ -cells, kidneys, and liver as well as the intestine [5]. Chronic hyperglycemia is a serious condition characterized by prolonged elevated blood sugar levels [6]. While it is a hallmark of diabetes, it can also result from other medical conditions or lifestyle factors. The aetiology of type 2 diabetes mellitus involves a complex interplay between nutrition and lifestyle [7].

Dysregulation of lipid patterns is a major consequence of diabetes mellitus. Diabetes, particularly type 2, is often accompanied by characteristic changes in lipid profiles, known as diabetic dyslipidemia. This includes well-documented alterations such as increased levels of triglycerides, cholesterol, and LDL cholesterol, along with decreased levels of HDL cholesterol [8,9]. These lipid profile alterations increase the risk of cardiovascular disease in individuals with diabetes. The relationship between lipids and diabetes mellitus is a complex phenomenon, as dysregulated lipid metabolism contributes to the development and complications of diabetes [10]. Veratric acid is a phenolic phytochemical found in the stem of *Tabebuia impetiginosa* and *Sparassis crispa*, a medicinal mushroom. Fruits and vegetables contain smaller concentrations of veratric acid. This compound exhibits a variety of pharmacological effects, including anti-inflammatory, antioxidant, antimicrobial, cardioprotective, antihypertensive, and anti-hyperlipidemic activities [11]. Yu *et al.* [12] reported that veratric acid may reduce hepatic ischemia in mice. They concluded that veratric acid activates the Nrf2 signaling pathway, thereby protecting the liver from oxidative stress. Saravanakumar and Raja [13] found that veratric acid possesses notable antioxidant and anti-hyperlipidemic effects in hypertensive rats. Raja *et al.* [14] observed anti-hyperlipidemic and antioxidant activity in Wistar rats fed an atherogenic diet. Lee *et al.* [15] reported that veratric acid can prevent premature skin ageing induced by UV exposure. Choi *et al.* [16] discovered that veratric acid reduces iNOS production in macrophage cells stimulated by LPS, indicating that this inhibitory effect is mediated through histone acetylation and PI3K activation. According to Choi *et al.* [17], veratric acid regulates nitric oxide production in macrophage cells stimulated by LPS. Ran *et al.* [18] demonstrated that veratric acid effectively prevents acute lung injury in mice induced by lipopolysaccharide. This protective effect is attributed to its inhibitory influence on NF- $\kappa$ B expression, which mitigates inflammatory injury. Palko-Labuz *et al.* [19] discovered that conjugating veratric acid with phospholipid significantly enhanced its anticancer activity in melanoma cells. *In vitro* studies utilizing specialized colorimetric investigations revealed the free radical scavenging ability of veratric acid in KB cells [11]. The present study investigates the antidiabetic and antihyperlipidemic potential of veratric acid in STZ-induced diabetic rats.

## MATERIALS AND METHODS

### Chemicals

Veratric Acid, Streptozotocin, and Nicotinamide (NA) were obtained from Sigma Aldrich Chemical Company (St. Louis, MO, USA). The rest of the chemicals were obtained from HiMediaMumbai and were of analytical grade.

### Experimental Animal model

Male albino Wistar rats weighing between 180 and 200g were maintained in the Central Animal House at Annamalai University. They have unlimited access to water and a pellet diet. The animals were kept under regulated temperatures ( $24 \pm 2^\circ\text{C}$ ), humidity ( $50 \pm 10\%$ ), and a 12-hour light/dark cycle. The experimental methodology was carried out in compliance with the Institutional Animal Ethics Committee's rules (IAEC Proposal No. Annamalai University-IAEC-1353/2/23).

### Induction of Diabetic Mellitus

Streptozotocin was dissolved in citrate-sodium buffer (0.1 M, pH 4.5), and nicotinamide was dissolved in normal physiological saline. Diabetic mellitus was induced in overnight fasted rats by a single intraperitoneal (i.p.) injection of streptozotocin (45 mg/kg b.w.), 15 minutes after the i.p. administration of nicotinamide (110 mg/kg b.w.) [20].





Treatment with veratric acid will be started on the third day in diabetic rats with a blood glucose level of more than 250 mg/dl.

### Experimental Design

The rats were divided into five groups, each consisting of six rats. Veratric acid and glibenclamide were dissolved in 0.5% DMSO and were administered orally to rats (1ml/rat/day) by using oral rat gavage for 30 days.

Group 1 rats served as control animals, whereas Group II rats were given streptozotocin-nicotinamide and served as diabetic control. Group III and Group IV rats were treated with streptozotocin–nicotinamide followed by oral administration of veratric acid and glibenclamide, respectively, for 30 days. Group V rats received veratric acid treatment alone for a period of 30 days.

#### Group 1: Control rats

**Group 2:** Experimental animals were treated with a single intraperitoneal (i.p.) injection of streptozotocin (45mg/kg b.w.), 15 minutes after the i.p. injection of nicotinamide (110mg/kg b.w.) (Diabetic control rats)

**Group 3:** Diabetic rats were treated with veratric acid (40mg/kg b.w.).

**Group 4:** Diabetic rats were treated with glibenclamide (600µg/kg body weight).

**Group 5:** Experimental animals were treated with veratric acid alone (40mg/kg body weight).

### Biochemical Analysis

The rats were killed at the end of the experiment, and blood samples were taken. Centrifugation yields plasma or serum. The pancreas, kidney, and liver were then removed, homogenized with suitable buffers, and centrifuged. The resultant supernatants were used to estimate biochemical parameters. Additionally, a part of the tissues was set aside for histological examination.

### Estimation of blood glucose, plasma insulin, hemoglobin, and glycosylated hemoglobin:

Blood glucose levels were measured using glucose oxidase-peroxidase techniques [21]. Blood samples were taken from the tail vein, and glucose levels were evaluated with a glucometer. Hemoglobin levels in the blood were estimated using the Drabkin and Austin method (1932) [22], while HbA1c (glycosylated hemoglobin) levels were measured using the Bannan method (1982) [23]. Plasma insulin levels were determined using an enzyme-linked immunosorbent assay (ELISA) with a Boehringer Mannheim kit and a Boehringer analyzer ES300 [24].

### Evaluation of Serum Lipids

Triglyceride, total cholesterol, and high-density lipoprotein (HDL) cholesterol levels were measured in serum using kits from Swemed Biomedicals Pvt Ltd., Bengaluru, India. Friedewald's algorithm [25,26] was used to calculate LDL and VLDL cholesterol levels.

LDL cholesterol = (Total Cholesterol - HDL cholesterol) - (Triglycerides / 5)

VLDL cholesterol = Triglycerides / 5

### Histopathology Studies

The liver, kidneys, and pancreas were first fixed in 10% neutral buffered formalin. They were then dehydrated by passing through a gradient of ethyl alcohol-water combinations. The samples were dehydrated, washed with xylene, and then embedded in paraffin. Organ sections (5µm thick) were stained with hematoxylin and eosin dye and examined under a light microscope [27].

### Statistical Analysis

The data is shown as mean ± SD. The statistical studies employed one-way analysis of variance (ANOVA), with post-hoc comparison using Duncan's Multiple Range Test (DMRT). A p-value of less than 0.05 indicated statistical significance.





## RESULTS

### Estimation of blood glucose, plasma insulin, hemoglobin, and glycosylated hemoglobin levels

Table 1 shows the concentrations of blood glucose, plasma insulin, haemoglobin, and glycosylated haemoglobin. The study found significant variations in the levels of blood glucose, plasma insulin, haemoglobin, and glycosylated haemoglobin between diabetic animals and those treated with veratric acid. In comparison to control rats, diabetic animals had higher levels of blood glucose and glycosylated haemoglobin, as well as lower levels of insulin and haemoglobin. However, oral treatment of veratric acid at a dose of 40mg/kg body weight to diabetic rats recovered these metabolic characteristics. The efficacy of veratric acid was comparable to that of the standard drug glibenclamide

### Evaluation of Serum Lipids

Figure 1 illustrates the serum lipid pattern observed in experimental animals. In diabetic animals, significant increases were observed in total cholesterol, LDL cholesterol, and triglycerides, while the level of HDL cholesterol was notably decreased compared to control rats. Veratric acid administration to diabetic rats dramatically recovered total cholesterol, triglyceride, HDL, LDL, and VLDL levels to a near-normal range. Furthermore, the antihyperlipidemic effect of veratric acid was found to be comparable to that of glibenclamide.

### Histopathology Studies

Figures 2, 3 and 4 depict the histopathological changes observed in the liver, pancreas, and kidney of experimental animals. Marked histological alterations were observed in the liver of diabetic animals compared to control rats. However, oral administration of veratric acid to diabetic rats reversed these histopathological abnormalities, with its effect being comparable to that of glibenclamide. Control rats and rats that received veratric acid alone exhibited a normal architecture of the liver, pancreas, and kidney.

## DISCUSSION

Prominent researchers have utilized STZ-NA-induced diabetes mellitus to investigate the antidiabetic efficacy of medicinal plants and their bioactive principles [28]. Nicotinamide plays a crucial role in reducing the severity of pancreatic  $\beta$ -cell damage during STZ-NA-induced diabetes mellitus, thus mimicking the model of type II diabetes mellitus [29]. STZ-NA-induced diabetes is histologically similar to type II diabetes mellitus. In the current investigation, diabetic rats exhibited hyperglycemia, defined as blood glucose levels greater than 250 mg/dL. Veratric acid given to diabetic rats lowered not only blood glucose levels, but also the degree of histological abnormalities in the liver, pancreas, and kidney. Veratric acid administered to diabetic rats dramatically lowered blood glucose levels, demonstrating its antihyperglycemic efficacy against STZ-NA-induced diabetes mellitus. Glycosylated hemoglobin has been considered a good diagnostic marker in diabetes mellitus[30]. The present study observed an increase in glycosylated hemoglobin in diabetic rats and a decrease in diabetic rats treated with veratric acid, which further validates its antidiabetic effect.

Diabetic dyslipidemia is recognized as a major complication of diabetes mellitus, with a significant association with cardiovascular diseases. Elevated triglyceride levels, along with increased LDL cholesterol and decreased HDL cholesterol, are primary factors contributing to diabetic dyslipidemia. Insulin deficiency alters the status of various lipid-metabolizing enzymes, thereby contributing to lipid abnormalities in diabetes mellitus [31,32]. Extensive studies have documented lipid abnormalities in both human subjects and experimental animal models, including streptozotocin-induced diabetic rats [33,34]. In this study, STZ-NA-induced diabetic rats demonstrated notable abnormalities in their serum lipid profile compared to control animals. Elevated levels of cholesterol, LDL cholesterol, and triglycerides, alongside decreased concentrations of HDL cholesterol, pointed towards dyslipidemia in diabetic rats. Insulin insufficiency and hyperglycemia in diabetic rats have been suggested to have contributed to the development of diabetic dyslipidemia. Administration of veratric acid to diabetic rats significantly decreased serum levels of total cholesterol, triglycerides, and LDL cholesterol. Furthermore, veratric acid stimulated insulin secretion and increased the concentration of HDL cholesterol in diabetic rats. These findings from the present





John Anbumani Ganesan *et al.*,

investigation highlight the antihyperlipidemic potential of veratric acid in STZ-induced diabetic rats. The antidiabetic efficacy of veratric acid was compared with the standard reference drug glibenclamide. The study observed that the antidiabetic potential of veratric acid was comparable to that of glibenclamide. Veratric acid significantly restored blood glucose levels, and serum lipid patterns, and reduced the severity of histopathological abnormalities in STZ-NA-induced diabetes mellitus in Wistar rats, like glibenclamide. These findings revealed the significant antihyperglycemic and antihyperlipidemic potential of veratric acid in STZ-NA-induced diabetic rats.

## CONCLUSION

Veratric acid reduces blood glucose levels, glycosylated haemoglobin, total cholesterol, and triglycerides in STZ-NA-induced diabetic rats. Veratric acid's antidiabetic and antihyperlipidemic advantages may be due to its ability to promote insulin release from diabetic rats' pancreatic  $\beta$ -cells.

## REFERENCES

1. Banday MZ, Sameer AS, Nissar S. Pathophysiology of diabetes: An overview. *Avicenna J Med.* 2020;10(4):174-188. doi: [https://doi.org/10.4103/ajm.ajm\\_53\\_20](https://doi.org/10.4103/ajm.ajm_53_20)
2. Deshpande AD, Harris-Hayes M, Schootman M. Epidemiology of diabetes and diabetes-related complications. *PhysTher.* 2008;88(11):1254-1264.
3. doi: <https://doi.org/10.2522/ptj.20080020>
4. Hossain MJ, Al-Mamun M, Islam MR. Diabetes mellitus, the fastest growing global public health concern: Early detection should be focused. *Health Sci Rep.* 2024;7(3):e2004. doi: <https://doi.org/10.1002/hsr2.2004>
5. Federation, I. D. IDF Diabetes Atlas 10th Edition. Preprint at (2021).
6. Nahdi AMTA, John A, Raza H. Elucidation of Molecular Mechanisms of Streptozotocin-Induced Oxidative Stress, Apoptosis, and Mitochondrial Dysfunction in Rin-5F Pancreatic  $\beta$ -Cells. *Oxid Med Cell Longev.* 2017;2017:7054272. doi: <https://doi.org/10.1155/2017/7054272>
7. Mouri M, Badireddy M. Hyperglycemia. In: *StatPearls.* Treasure Island (FL): StatPearls Publishing. 2023.
8. Galicia-Garcia U, Benito-Vicente A, Jebari S, *et al.* Pathophysiology of Type 2 Diabetes Mellitus. *Int J Mol Sci.* 2020;21(17):6275. doi: <https://doi.org/10.3390/ijms21176275>
9. Sophia D, Manoharan S. Hypolipidemic activities of *Ficus racemosa* Linn. bark in alloxan induced diabetic rats. *Afr J Tradit Complement Altern Med.* 2007;4(3):279-288. doi: <https://doi.org/10.4314/ajtcam.v4i3.31220>
10. Pamu P, Shanmugam M, Subramanian S. Beneficial effects of *Tephrosia purpurea* ethanolic seed extract on lipids and membrane bound enzymes in experimental diabetic rats. *J Young Pharm.* 2017;9(4):550. doi: [10.5530/jyp.2017.9.105](https://doi.org/10.5530/jyp.2017.9.105)
11. Mooradian AD. Dyslipidemia in type 2 diabetes mellitus. *Nat Clin Pract Endocrinol Metab.* 2009;5(3):150-159. doi: <https://doi.org/10.1038/ncpendmet1066>
12. Sivasankaran SM, Abdulla SH, Elanchezhiyan C, Pethanasamy M, Surya S, Theerthu A, Krishnan H. Reactive Oxygen Species Scavenging and Anti-Proliferative Potential of Veratric Acid: An in vitro Approach. *Trop. J. Nat. Prod.* 2023;7(4).doi:<http://www.doi.org/10.26538/tjnpr/v7i4.28>
13. Yu Q, Chen S, Tang H, Zhang X, Tao R, Yan Z, Shi J, Guo W, Zhang S. Veratric acid alleviates liver ischemia/reperfusion injury by activating the Nrf2 signaling pathway. *Int Immunopharmacol.* 2021;101(Pt B), 108294. doi: <https://doi.org/10.1016/j.intimp.2021.108294>
14. Saravanakumar M, Raja B. Veratric acid, a phenolic acid attenuates blood pressure and oxidative stress in L-NAME induced hypertensive rats. *Eur J Pharmacol.* 2011;671(1-3):87-94. doi: <https://doi.org/10.1016/j.ejphar.2011.08.052>
15. Raja B, Saravanakumar M, Sathya G. Veratric acid ameliorates hyperlipidemia and oxidative stress in Wistar rats fed an atherogenic diet. *Mol Cell Biochem.* 2012; 366(1-2):21-30. doi: <https://doi.org/10.1007/s11010-012-1278-y>



John Anbumani Ganesan *et al.*,

16. Lee KE, Park JE, Jung E, Ryu J, Kim YJ, Youm JK, Kang S. A study of facial wrinkles improvement effect of veratric acid from cauliflower mushroom through photo-protective mechanisms against UVB irradiation. *Arch Dermatol Res.* 2016; 308(3):183-92. doi: <https://doi.org/10.1007/s00403-016-1633-z>
17. Choi WS, SeoYB, Shin PG, Kim WY, Lee SY, Choi YJ, Kim GD. Veratric acid inhibits iNOS expression through the regulation of PI3K activation and histone acetylation in LPS-stimulated RAW264.7 cells. *Int J Mol Med.* 2015; 35(1):202-10. doi: <https://doi.org/10.3892/ijmm.2014.1982>
18. Choi WS, Shin PG, Lee JH, Kim GD. The regulatory effect of veratric acid on NO production in LPS-stimulated RAW264.7 macrophage cells. *Cell Immunol.* 2012; 280(2):164-70. doi: <https://doi.org/10.1016/j.cellimm.2012.12.007>
19. Ran X, Chao S, Jun-Gang Z, Yun H, Kuan-Bing C, Wen-Jun S. Protective effect of veratric acid on lipopolysaccharide-induced acute lung injury in mice. *Eur JPharmacol.* 2014; 740:227-32. doi: <https://doi.org/10.1016/j.ejphar.2014.07.006>
20. Palko-Łabuz A, Gliszczynska A, Skonieczna M, Poła A, Wesolowska O, Środa-Pomianek K. Conjugation with Phospholipids as a Modification Increasing Anticancer Activity of Phenolic Acids in Metastatic Melanoma-In vitro and In Silico Studies. *Int J Mol Sci.* 2021; 22(16):8397. doi: 10.3390/ijms22168397.
21. Karthikesan K, Pari L, Menon VP. Protective effect of tetrahydrocurcumin and chlorogenic acid against streptozotocin-nicotinamide generated oxidative stress induced diabetes. *J. Funct. Foods.* 2010;2(2):134-42. <https://doi.org/10.1016/j.jff.2010.04.001>
22. Trinder P. Determination of glucose in blood using glucose oxidase with an alternative oxygen acceptor. *Ann ClinBiochem.* 1969; 6(1):24-27. doi: <https://doi.org/10.1177/000456326900600108>
23. Drabkin DL, Austin JH. Spectrophotometric studies: I. Spectrophotometric constants for common hemoglobin derivatives in human, dog, and rabbit blood. *J Biol Chem.* 1932; 98(2):719-733. doi: [https://doi.org/10.1016/S0021-9258\(18\)76122-X](https://doi.org/10.1016/S0021-9258(18)76122-X)
24. Bannon P. Effect of pH on the elimination of the labile fraction of glycosylated hemoglobin. *Clin Chem.* 1982; 28(10):2183-2183.
25. Camara PD, Velletri K, Krupski M, Rosner M, Griffiths WC. Evaluation of the Boehringer Mannheim ES 300 immunoassay analyzer and comparison with enzyme immunoassay, fluorescence polarization immunoassay, and radioimmunoassay methods. *ClinBiochem.* 1992; 25(4):251-254. doi: [https://doi.org/10.1016/0009-9120\(92\)80029-g](https://doi.org/10.1016/0009-9120(92)80029-g)
26. Friedewald WT, Levy RI, Fredrickson DS. Estimation of the concentration of low-density lipoprotein cholesterol in plasma, without the use of the preparative ultracentrifuge. *Clin Chem.* 1972; 18(6):499-502.
27. Shaban N, Elanchezhiyan C, Manoharan S. Modulating Effect of Vincamine on the Oxidative Stress Markers and Lipid Profile in High Fat Diet and Streptozotocin-Induced Type 2 Diabetic Rats. *Trop J Nat Prod Res.* 2022; 6(4):546-551. doi: [doi.org/10.26538/tjnpr/v6i4.14](https://doi.org/10.26538/tjnpr/v6i4.14)
28. Ojuade FI, Olorundare OE, Akanbi OB, Afolabi SO, Njan AA. Antidiabetic and antihyperlipidemic effects of aqueous extract of *Parquetinanigrescens* in streptozotocin-nicotinamide induced type 2 diabetic rats. *Heliyon.* 2021;7(6):e07363. doi:10.1016/j.heliyon.2021.e07363
29. Salehi B, Ata A, V Anil Kumar N, *et al.* Antidiabetic Potential of Medicinal Plants and Their Active Components. *Biomolecules.* 2019;9(10):551. doi:<https://doi.org/10.3390/biom9100551>
30. Szkudelski T. Streptozotocin-nicotinamide-induced diabetes in the rat. Characteristics of the experimental model. *ExpBiol Med (Maywood).* 2012;237(5):481-490. doi: <https://doi.org/10.1258/ebm.2012.011372>
31. Sherwani SI, Khan HA, Ekhzaimy A, Masood A, Sakharkar MK. Significance of HbA1c Test in Diagnosis and Prognosis of Diabetic Patients. *Biomark Insights.* 2016;11:95-104. doi: <https://doi.org/10.4137/BMI.S38440>
32. Schofield JD, Liu Y, Rao-Balakrishna P, Malik RA, Soran H. Diabetes Dyslipidemia. *Diabetes Ther.* 2016;7(2):203-219. doi:10.1007/s13300-016-0167-x
33. Klop B, Elte JW, Cabezas MC. Dyslipidemia in obesity: mechanisms and potential targets. *Nutrients.* 2013;5(4):1218-1240. doi:<https://doi.org/10.3390/nu5041218>
34. Goyal SN, Reddy NM, Patil KR, *et al.* Challenges and issues with streptozotocin-induced diabetes - A clinically relevant animal model to understand the diabetes pathogenesis and evaluate therapeutics. *ChemBiol Interact.* 2016;244:49-63. doi: <https://doi.org/10.1016/j.cbi.2015.11.032>





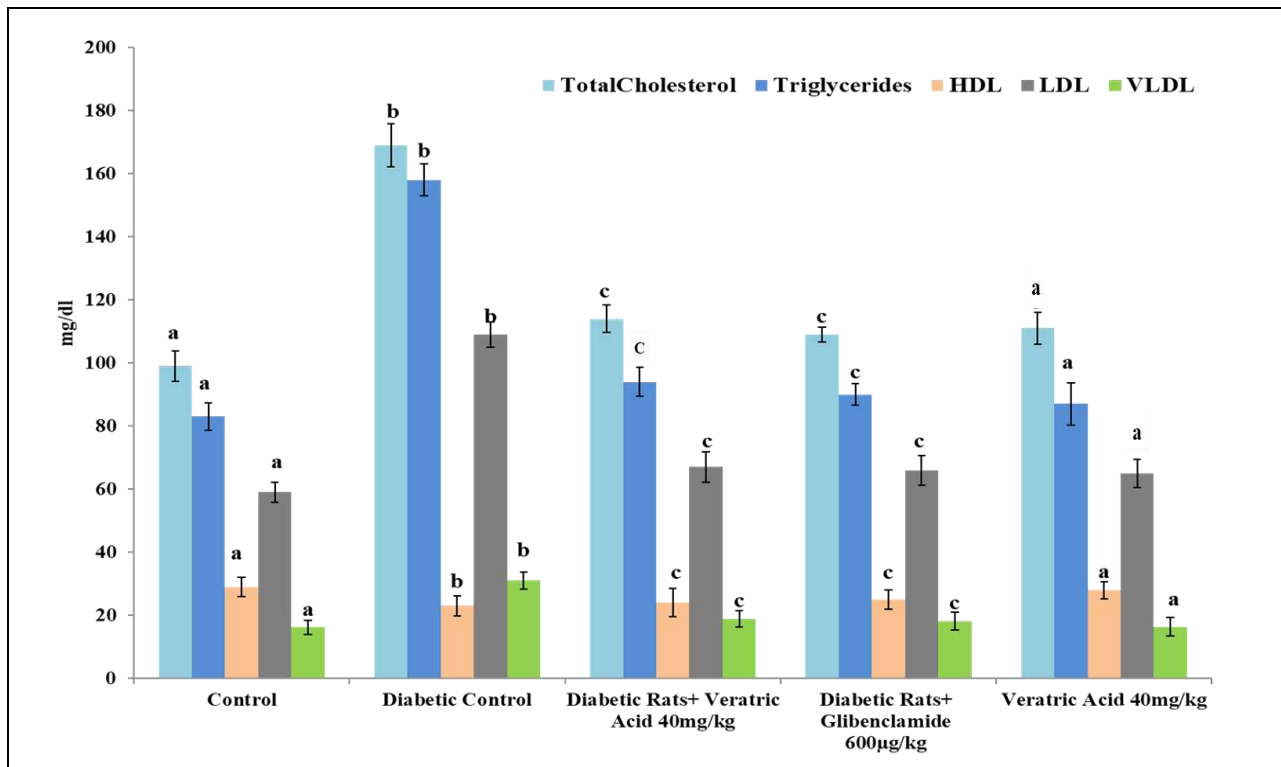


John Anbumani Ganesan *et al.*,

35. Akbarzadeh A, Norouziyan D, Mehrabi MR, *et al.* Induction of diabetes by Streptozotocin in rats. *Indian J ClinBiochem.* 2007;22(2):60-64. doi:10.1007/BF02913315

**Table 1.** The concentration of blood glucose, plasma insulin, hemoglobin and glycosylated hemoglobin Each value represents the mean ± SD for six rats in each group. Statistical significance, denoted by different superscript letters (a–e), indicates differences at  $p < 0.05$  (DMRT).

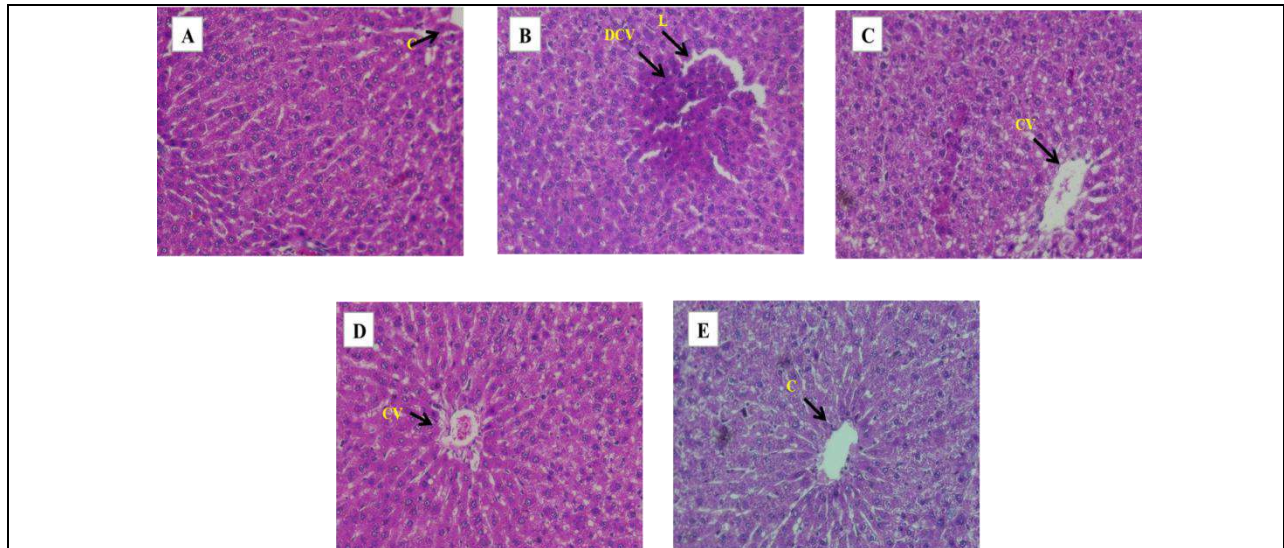
Parameters	Control	Diabetic Control	Diabetic Rats + Veratric acid (40mg/kg b.w)	Diabetic Rats + Glibenclamide (600µg/kg b.w)	Veratric acid alone (40mg/kg b.w)
Blood glucose (mg/dl)	82.16 ± 4.62 <sup>a</sup>	264 ± 9.34 <sup>b</sup>	102.50 ± 4.08 <sup>c</sup>	112 ± 5.04 <sup>c</sup>	88 ± 4.57 <sup>a</sup>
Plasma Insulin (µU/ml)	18.64 ± 2.26 <sup>a</sup>	7.02 ± 2.78 <sup>b</sup>	15.21 ± 1.89 <sup>c</sup>	16.07 ± 2.51 <sup>c</sup>	17.07 ± 2.58 <sup>a</sup>
Hemoglobin (g/dl)	14.95 ± 1.56 <sup>a</sup>	7.63 ± 1.67 <sup>b</sup>	12.75 ± 1.72 <sup>c</sup>	13.05 ± 1.21 <sup>c</sup>	14.16 ± 1.53 <sup>a</sup>
HbA1c (%)	5.82 ± 0.35 <sup>a</sup>	11.06 ± 0.53 <sup>b</sup>	7.16 ± 0.26 <sup>c</sup>	8.56 ± 0.28 <sup>c</sup>	6.08 ± 0.46 <sup>a</sup>



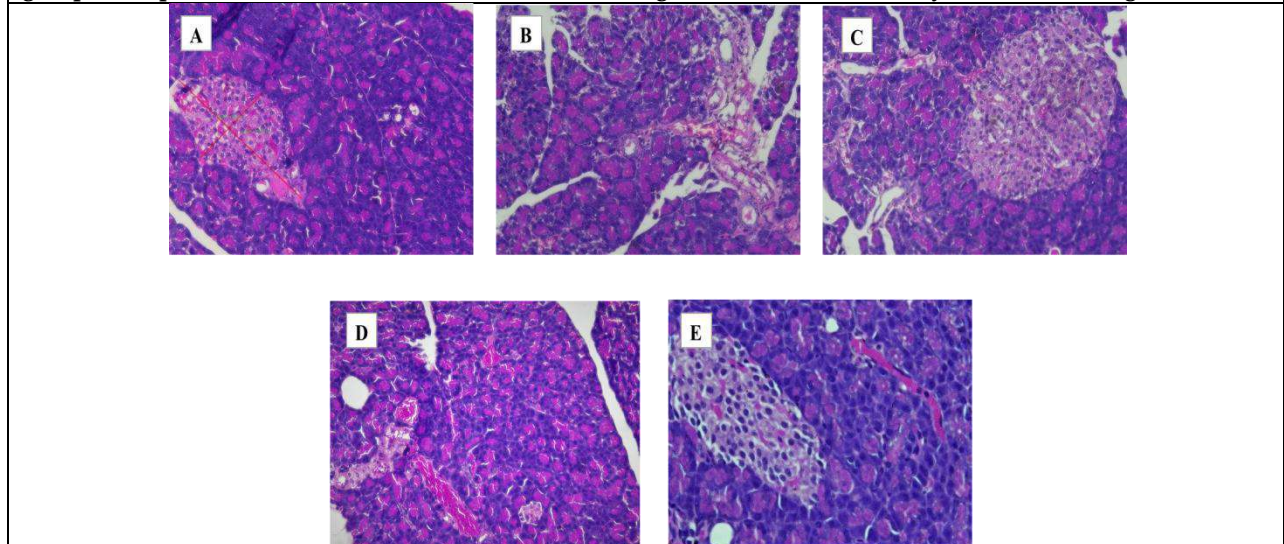
**Figure 1.** Effect of veratric acid in serum lipid profile in experimental rats Each value represents the mean ± SD for six rats in each group. Statistical significance, denoted by different superscript letters (a–e), indicates differences at  $p < 0.05$  (DMRT).





John Anbumani Ganesan *et al.*,

**Figure 2.** Histological observation of liver in normal and experimental rats. C-Central Vein; CV-Congestive Vessel; DCV- Dilated Central Vein; L- Lymphocytic Infiltration. A: Control rats showed the normal histological architecture of liver tissue (Group 1). B: Diabetic control rats showed lymphocytic infiltration (L) and inflammation with a dilated central vein (DCV) (Group 2). C: Diabetic rats treated with veratric acid (40 mg/kg b.w.) showed congested hepatic vessels (CV) and mild vascular changes in hepatocytes (Group 3). D: Diabetic rats treated with glibenclamide (600  $\mu$ g/kg b.w.) showed normal architecture of hepatic vessels (Group 4). E: Control rats treated with veratric acid alone (40 mg/kg b.w.) showed similar findings to the control group (Group 5). Examinations were carried out at 40X magnification with hematoxylin-eosin staining.



**Figure 3.** Histopathological observation of pancreas in normal and experimental rats. A: Control group showed normal cellular architecture (Group 1). B: Diabetic control rats showed a significant reduction in islet volume, with clear signs of necrosis observed in the islets of Langerhans (Group 2). C: Diabetic rats treated with veratric acid (40 mg/kg b.w.) showed a normal pancreatic morphology with reduced numbers of pancreatic islets cells. The changes in nuclear morphology with hyperchromatic and mild dysplasia was noticed (Group 3). D: Diabetic rats treated with glibenclamide (600  $\mu$ g/kg b.w.) showed normal pancreatic morphology with slight alteration in islets cells (Group 4). E: Control rats treated with veratric acid alone (40 mg/kg b.w.) showed normal  $\beta$  cells with normal cellular architecture. Examinations were carried out at 40X magnification with hematoxylin-eosin staining.



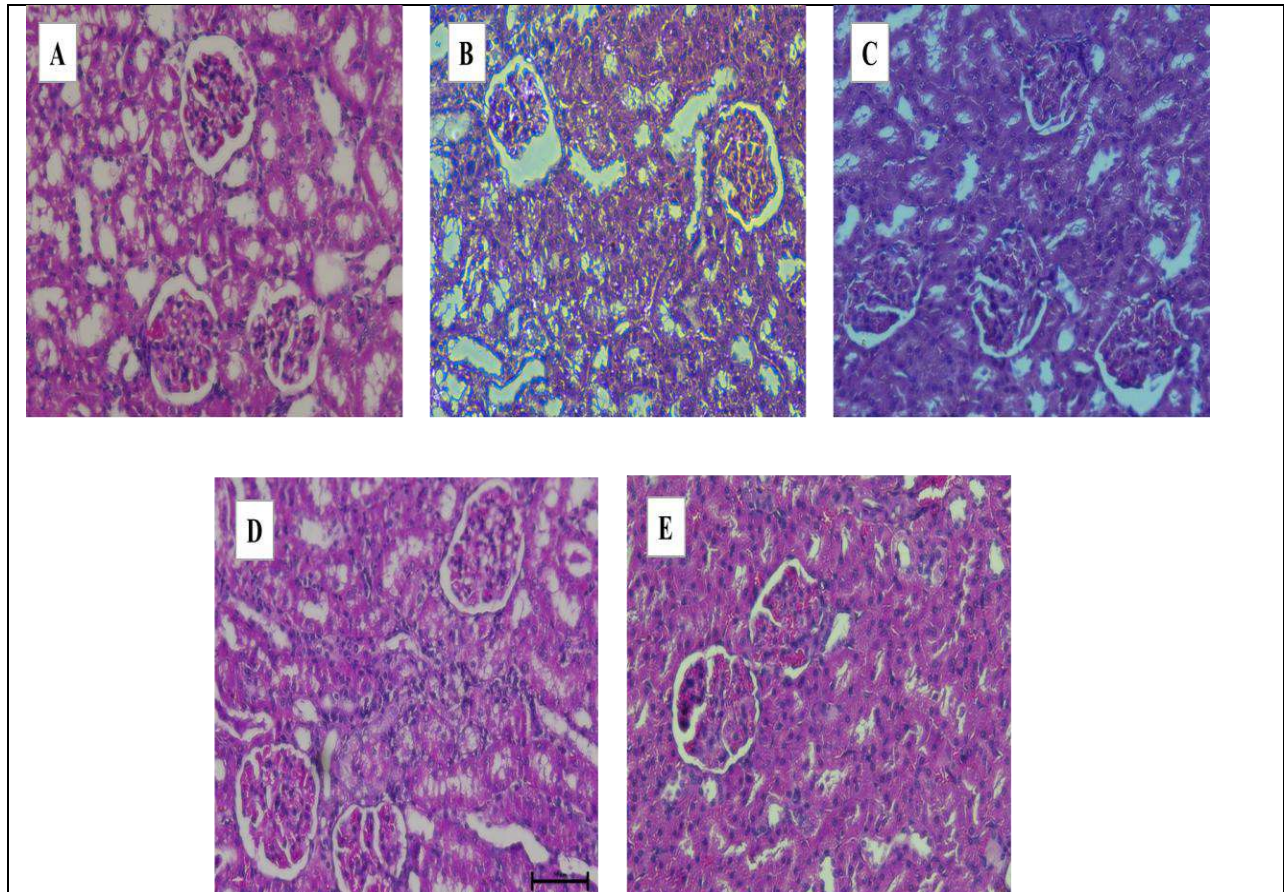


Figure 4: Histological observation of kidney in normal and experimental rats.

A: Control group showed normal glomerular and tubular morphology (Group 1).

B: Diabetic control rats showed glomerular congestion and reduced vascular spaces. The tubular structure appeared edematous with signs of derangement (Group 2).

C: Diabetic rats treated with veratric acid (40 mg/kg b.w.) exhibited normal glomerular appearance, increased vascularity, and capsular space. Tubular regions showed mild congestion (Group 3).

D: Diabetic rats treated with glibenclamide (600 µg/kg b.w.) demonstrated glomerular hypertrophy with increased vascularity. The tubules exhibited signs of congestion and derangement (Group 4).

E: Control rats treated with veratric acid alone (40 mg/kg b.w.) showed increased glomerular vascularity and normal tubular morphology (Group 5). Examinations were carried out at 40X magnification with hematoxylin-eosin staining







## Antioxidant and Antiglycation Properties of *Syzygium aromaticum* bud: Potential Therapeutic Applications in Diabetes Management

Piyushkumar N. Chudasama<sup>1</sup> and Kinnari Mistry<sup>2\*</sup>

<sup>1</sup>Ph.D Research Scholar, Ashok and Rita Patel Institute of Integrated Study & Research in Biotechnology and Allied Sciences (ARIBAS). The Charutar Vidya Mandal University, Vallabh Vidyanagar, Gujarat, India.

<sup>2</sup>Associate Professor, Ashok and Rita Patel Institute of Integrated Study & Research in Biotechnology and Allied Sciences (ARIBAS). The Charutar Vidya Mandal University, Vallabh Vidyanagar, Gujarat, India.

Received: 22 July 2024

Revised: 18 Sep 2024

Accepted: 29 Oct 2024

### \*Address for Correspondence

**Kinnari Mistry**

Associate Professor,

Ashok and Rita Patel Institute of Integrated Study & Research in Biotechnology and Allied Sciences (ARIBAS).

The Charutar Vidya Mandal University,

Vallabh Vidyanagar, Gujarat, India.

E.Mail: mistrykinnari@gmail.com,



This is an Open Access Journal / article distributed under the terms of the **Creative Commons Attribution License** (CC BY-NC-ND 3.0) which permits unrestricted use, distribution, and reproduction in any medium, provided the original work is properly cited. All rights reserved.

### ABSTRACT

This study delves into the antioxidant, antidiabetic, and antiglycation properties of the aqueous extract of *Syzygium aromaticum* (clove) bud. The extract demonstrates significant bioactive potential with its high total phenolic content ( $30.50 \pm 0.05$  mg GAE/g DW) and flavonoid content ( $19.80 \pm 0.04$  mg QE/g DW). These compounds contribute to its robust antioxidant capacity, as evidenced by the low IC<sub>50</sub> values in DPPH ( $75 \pm 0.08$  µg/mL) and ABTS ( $3.9 \pm 0.05$  µg/mL) assays, and substantial ferric reducing antioxidant power ( $2.10 \pm 0.40$  mmol Fe<sup>2+</sup>/g DW). The extract's nitric oxide scavenging activity further supports its potential to mitigate oxidative stress and inflammation, providing reassurance about its therapeutic potential. The clove bud extract, with its robust anti-diabetic properties, inhibits key carbohydrate-digesting enzymes, with IC<sub>50</sub> values of  $90 \pm 0.07$  µg/mL for α-amylase and  $120 \pm 0.06$  µg/mL for α-glucosidase, indicating its efficacy in managing postprandial blood glucose levels. Additionally, the extract exhibits significant antiglycation activity, reducing browning by  $38.50\% \pm 10.05$ , fructosamine production by  $50.00\% \pm 4.50$ , protein carbonyl content by  $48.20\% \pm 0.40$ , amyloid β-structure formation by  $43.50\% \pm 11.00$ , and total AGEs formation by  $83.00\%$ . These results underscore its potential in preventing diabetic complications, reinforcing the audience's confidence in its effectiveness.

**Keywords:** *Syzygium aromaticum* (clove), Advanced glycation end products (AGEs), Reactive oxygen species, Antioxidant, Oxidative stress.





## INTRODUCTION

Diabetes is a prevalent health issue affecting approximately 425 million individuals globally, with India alone accounting for around 72 million cases (International Diabetes Federation, 2017). This chronic condition, diabetes mellitus, is characterised by persistent high blood sugar levels. A key feature of both Type 1 and Type 2 diabetes is insulin resistance, which hampers glucose uptake in the body, particularly in skeletal muscles, leading to impaired glucose transport. Additionally, heightened activity of the pancreatic enzymes alpha-amylase and alpha-glucosidase further elevates blood glucose levels.(Bhatnagar & Mishra, 2022). Obesity often accompanies diabetes, with about 90% of those with insulin resistance being overweight (BMI  $\geq 25$  kg/m<sup>2</sup>) (Amisi, 2022). The American Medical Association classified obesity as a chronic disease in 2013. Long-term diabetes can result in oxidative stress, which is linked to complications such as retinopathy, nephropathy, neuropathy, cardiomyopathy, ageing, rheumatoid arthritis, and osteoporosis(Reddy & Tan, 2020).

*Syzygium aromaticum* (clove) is highly regarded in culinary and medicinal fields due to its rich phytochemical composition. Clove contains essential oils, including eugenol, with significant antioxidant and anti-inflammatory properties. (Haro-González et al., 2021). Additionally, clove is known for its antimicrobial, antifungal, and antiviral activities. The buds of *Syzygium aromaticum* are used extensively for their therapeutic benefits, including their ability to manage blood sugar levels and prevent oxidative stress(Nait Irahah et al., 2023). Clove's safety and efficacy have been supported by its long history of use in traditional medicine across various cultures(Idowu et al., 2021). Given its diverse bioactive components, *Syzygium aromaticum* has been studied for its potential benefits in mitigating oxidative stress and managing diabetes-related complications. This study aims to analyze the phytochemical content, antioxidant capacity, and antiglycation properties of *Syzygium aromaticum* (clove) and examine their interrelationships to provide a comprehensive understanding of its therapeutic potential.

## METHODOLOGY

### Extract Preparation

The aqueous extract was prepared using the protocol described earlier(Abubakar & Haque, 2020), with some modifications. The powdered clove buds (5 g) of uniform particle size were added to distilled water (50 mL), vortexed for 1 h in a water bath at 100 °C, and centrifuged for 15 min at 4500 rpm. The bud powder (5 g) of uniform particle size was mixed in 50 mL of methanol or ethanol and kept in a shaking incubator at 200 rpm for 24 h. The solutions obtained were filtered with Whatman No. 1 filter paper and stored at 4–8 °C until further use.

### Determination of Total Phenolic (TPC) and Flavonoid Content (TFC)

The phenolic and flavonoid contents were obtained for all extracts by using the Folin–Ciocalteu method and the aluminium chloride method(Phuyal et al., 2020), respectively. A 250  $\mu$ L volume of the extract (10 mg/mL) was used for all assays. For TPC measurement, the standard curve of gallic acid (0–250  $\mu$ g/mL) was used and the results were demonstrated in mg of gallic acid equivalents (GAE)/g DW of a sample ( $y = 0.008x + 0.026$ ;  $R^2 = 0.991$ ). Similarly, for TFC measurement, a standard curve of quercetin (0–100  $\mu$ g/mL) was plotted and the results were mentioned in mg of quercetin equivalents (QE)/g DW of the sample ( $y = 0.026x + 0.038$ ;  $R^2 = 0.998$ )

### Reactive Oxygen and Nitrogen Assays

#### Antioxidative Assays

The antioxidative properties of the extracts were evaluated using several methods. The DPPH assay followed the protocol by Chaves et al. (2020), the ABTS assay was based on Xiao et al. (2020), and the FRAP assay was conducted as described by Prastiwi et al. (2020).



**Piyushkumar N. Chudasama and Kinnari Mistry****Nitric Oxide Scavenging Assay**

The nitric oxide scavenging activity was measured using the method described by Ali et al. (2020). Various concentrations of extract (0–500 µg/mL) were incubated at 25 °C for 2.5 hours.

**Antidiabetic Assays**

The antidiabetic potential of the extracts was evaluated using  $\alpha$ -amylase and  $\alpha$ -glucosidase inhibitory assays. The  $\alpha$ -amylase inhibitory activity was assessed according to Khadayat et al. (2020), involving the pre-incubation of 100 µL of extract and 250 µL  $\alpha$ -amylase solution (100 U/mL) at 37 °C for 10 minutes, followed by the addition of 250 µL of 10% starch. The mixture was incubated at 37 °C for 10 minutes, DNS was added, and absorbance was measured at 595 nm. The  $\alpha$ -glucosidase inhibitory activity followed the protocol by Kifle et al. (2021), where 100 µL of  $\alpha$ -glucosidase (100 U/mL) was preincubated with 50 µL of the extract for 10 minutes. The reaction was initiated with 5 mM pNPG and stopped with sodium carbonate, with absorbance measured at 405 nm.

**Antiglycation Assays**

The antiglycation activity of the extracts was evaluated using several methods. The BSA assay was used to determine antiglycation activity with modifications from Muraoka et al. (2022). Browning intensity was measured at 420 nm as per Fallavena et al. (2022). Fructosamine content was evaluated using the NBT assay based on Mohd Dom et al. (2020). Protein carbonyl content was determined using the DNPH methodology described by Nareshkumar et al. (2020). Amyloid  $\beta$ -structure estimation followed the Congo red binding method from Gao et al. (2021). Total AGEs were estimated using a BSA-fluorescent assay as per Dedvisitsakul & Watla-lad (2022).

**RESULTS AND DISCUSSION****Determination of TPC and TFC**

The total phenolic (TPC) and total flavonoid (TFC) of *Syzygium aromaticum* extract were quantified. The extract exhibited a TPC of  $30.50 \pm 0.05$  mg GAE/g DW and a TFC of  $19.80 \pm 0.04$  mg QE/g DW, indicating high concentrations of these compounds known for their antioxidant properties (Muflihah et al., 2021; Hassan et al., 2021; Dev et al., 2021).

**Reactive Oxygen and Nitrogen Assays**

The DPPH assay showed an IC<sub>50</sub> value of  $75 \pm 0.08$  µg/mL, indicating strong antioxidant capacity, superior to *Rosmarinus officinalis* (Kamli et al., 2022). The ABTS assay yielded an IC<sub>50</sub> value of  $3.9 \pm 0.05$  µg/mL, more effective than *Ocimum basilicum* (Nguyen et al., 2021). The FRAP assay showed a value of  $2.10 \pm 0.40$  mmol Fe<sup>2+</sup>/g DW, slightly lower than *Punica granatum* (Sabraoui et al., 2020). The nitric oxide scavenging assay demonstrated an IC<sub>50</sub> value of  $350 \pm 0.10$  µg/mL, better than *Curcuma longa* (Lucas et al., 2021; Cheikhoussef et al., 2022).

**Antidiabetic Assays**

The extract inhibited  $\alpha$ -amylase with an IC<sub>50</sub> value of  $90 \pm 0.07$  µg/mL, more potent than *Cinnamomum zeylanicum* (Niroshani et al., 2020). The inhibition of  $\alpha$ -glucosidase had an IC<sub>50</sub> value of  $120 \pm 0.06$  µg/mL, better than *Ficus carica* (Meziant et al., 2021).

**Antiglycation Assays**

The extract reduced browning by  $38.50\% \pm 10.05$ , indicating strong antiglycation activity, similar to *Nigella sativa* (Balyan et al., 2022). It reduced fructosamine production by  $50.00\% \pm 4.50$ , outperforming *Pterocarpus marsupium* (Dinda, 2022). The reduction in protein carbonyl content was  $48.20\% \pm 0.40$ , more effective than *Allium sativum* (Ncir et al., 2020). The extract reduced the protein aggregation index to  $43.50\% \pm 11.00$ , comparable to *Bacopa monnieri* (Awathale et al., 2021). It reduced total AGEs formation by 83.00%, surpassing *Trigonella foenum-graecum* (Hafeez et al., 2023).





## DISCUSSION

The findings of this study highlight the significant therapeutic potential of *Syzygium aromaticum* (clove) bud extract in managing oxidative stress, diabetes, and glycation-associated complications. The high total phenolic ( $30.50 \pm 0.05$  mg GAE/g DW) and flavonoid ( $19.80 \pm 0.04$  mg QE/g DW) content of the clove bud extract underscores its robust antioxidant capacity, as evidenced by low IC<sub>50</sub> values in both DPPH ( $75 \pm 0.08$  µg/mL) and ABTS ( $3.9 \pm 0.05$  µg/mL) assays. These values surpass those of commonly studied plant extracts like *Rosmarinus officinalis* and *Ocimum basilicum*, indicating a superior radical scavenging ability (Muflihah et al., 2021; Nguyen et al., 2021; Kamli et al., 2022). The FRAP assay results further confirm the substantial electron-donating ability of the extract, contributing to its overall antioxidant efficacy (Sabraoui et al., 2020).

The extract's nitric oxide scavenging activity (IC<sub>50</sub> =  $350 \pm 0.10$  µg/mL) demonstrates its potential to mitigate nitrosative stress and inflammation, which is crucial in managing chronic inflammatory diseases. Compared to extracts like *Curcuma longa*, the clove bud extract shows a more potent nitric oxide scavenging activity, highlighting its effectiveness in reducing oxidative stress (Lucas et al., 2021; Cheikhyoussef et al., 2022). In the context of diabetes management, the clove bud extract exhibits strong inhibitory effects on key carbohydrate-digesting enzymes,  $\alpha$ -amylase (IC<sub>50</sub> =  $90 \pm 0.07$  µg/mL) and  $\alpha$ -glucosidase (IC<sub>50</sub> =  $120 \pm 0.06$  µg/mL). These findings suggest that the extract can effectively slow down carbohydrate digestion and absorption, thereby managing postprandial blood glucose levels. The dual inhibition of these enzymes is particularly noteworthy as it highlights the comprehensive antidiabetic potential of the extract, comparable or even superior to other known natural inhibitors like *Cinnamomum zeylanicum* and *Ficus carica* (Niroshani et al., 2020; Meziant et al., 2021).

The antiglycation assays further establish the efficacy of the clove bud extract in preventing diabetic complications. The significant reduction in browning, fructosamine production, protein carbonyl content, amyloid  $\beta$ -structure formation, and total AGEs formation underscores the extract's potential in inhibiting glycation processes (Balyan et al., 2022; Dinda, 2022; Ncir et al., 2020; Awathale et al., 2021; Hafeez et al., 2023). These properties are critical for managing the progression of diabetic complications and other ageing-related disorders associated with AGEs. Overall, the multifunctional bioactive properties of *Syzygium aromaticum* bud extract make it a promising natural therapeutic agent. Its potent antioxidant, antidiabetic, and antiglycation activities provide a compelling case for its inclusion in developing interventions to manage oxidative stress, diabetes, and related complications. Further studies exploring its molecular mechanisms and clinical efficacy could pave the way for its application in functional foods and pharmaceuticals.

## CONCLUSION

The aqueous extract of *Syzygium aromaticum* bud emerges as a potent natural agent with multifaceted health benefits, including antioxidant, antidiabetic, and antiglycation. These findings support its potential application in developing therapeutic interventions for oxidative stress-related conditions, diabetes management, and the prevention of glycation-associated complications. Further studies and clinical evaluations are warranted to fully elucidate its mechanisms and optimise its use in health promotion and disease prevention.

## ACKNOWLEDGEMENTS

We sincerely thank the Ashok & Rita Patel Institute of Integrated Study & Research in Biotechnology and Allied Sciences (ARIBAS) for providing the necessary facilities and support to conduct this research. Additionally, we acknowledge the financial support from Charutar Vidya Mandal (CVM) University, which made this research possible.







## REFERENCES

1. Abubakar, A. R., & Haque, M. (2020). Preparation of medicinal plants: Basic extraction and fractionation procedures for experimental purposes. *Journal of Pharmacy and Bioallied Sciences*, 12(1), 1–10.
2. Ali, B. M., Boothapandi, M., & Nasar, A. S. (2020). Nitric oxide, DPPH and hydrogen peroxide radical scavenging activity of TEMPO terminated polyurethane dendrimers: Data supporting antioxidant activity of radical dendrimers. *Data in Brief*, 28, 104972.
3. Amisi, C. A. (2022). Markers of insulin resistance in Polycystic ovary syndrome women: An update. *World Journal of Diabetes*, 13(3), 129.
4. Awathale, S. N., Dhoble, L. R., Itankar, P. R., Raut, N. A., & Kokare, D. M. (2021). Neuroactive herbal agents for cognitive dysfunction. *Studies in Natural Products Chemistry*, 70, 195–226.
5. Balyan, P., Ola, M. S., Alhomida, A. S., & Ali, A. (2022). D-Ribose-Induced Glycation and Its Attenuation by the Aqueous Extract of *Nigella sativa* Seeds. *Medicina*, 58(12), 1816.
6. Bhatnagar, A., & Mishra, A. (2022).  $\alpha$ -Glucosidase Inhibitors for Diabetes/Blood Sugar Regulation. In V. L. Maheshwari & R. H. Patil (Eds.), *Natural Products as Enzyme Inhibitors* (pp. 269–283).
7. Chaves, N., Santiago, A., & Alías, J. C. (2020). Quantification of the antioxidant activity of plant extracts: Analysis of sensitivity and hierarchization based on the method used. *Antioxidants*, 9(1), 76.
8. Cheikhyoussef, A., Cheikhyoussef, N., Rahman, A., & Hussein, A. A. (2022). Clove (*Syzygium aromaticum*) phenolics: Extraction, compositions, and biological activities. In *Clove (Syzygium aromaticum)* (pp. 215–233).
9. Dedvisitsakul, P., & Watla-Iad, K. (2022). Antioxidant activity and antidiabetic activities of Northern Thai indigenous edible plant extracts and their phytochemical constituents. *Heliyon*, 8(9).
10. Dev, M., Bhattacharyya, D. K., & Ghosh, M. (2021). Composition and Antioxidant Activity of Vapours from Clove Bud During Roasting. In D. Ramkrishna, S. Sengupta, S. Dey Bandyopadhyay, & A. Ghosh (Eds.), *Advances in Bioprocess Engineering and Technology* (pp. 151–158).
11. Dinda, B. (2022). Clinical Trials of Phytomedicines in the Management of Obesity and Diabetes. In B. Dinda (Ed.), *Natural Products in Obesity and Diabetes* (pp. 533–551).
12. Fallavena, L. P., Rodrigues, N. P., Marczak, L. D. F., & Mercali, G. D. (2022). Formation of advanced glycation end products by novel food processing technologies: A review. *Food Chemistry*, 393, 133338.
13. Felter, S. P., Zhang, X., & Thompson, C. (2021). Butylated hydroxyanisole: Carcinogenic food additive to be avoided or harmless antioxidant important to protect food supply? *Regulatory Toxicology and Pharmacology*, 121, 104887.
14. Gao, W., Jin, L., Liu, C., Zhang, N., Zhang, R., Bednarikova, Z., Gazova, Z., Bhunia, A., Siebert, H.-C., & Dong, H. (2021). Inhibition behavior of Sennoiside A and Sennoiside C on amyloid fibrillation of human lysozyme and its possible mechanism. *International Journal of Biological Macromolecules*, 178, 424–433.
15. Hafeez, J., Naeem, M., Ali, T., Sultan, B., Hussain, F., Ur Rashid, H., Nadeem, M., & Shirzad, I. (2023). Comparative Study of Antioxidant, Antidiabetic, Cytotoxic Potentials, and Phytochemicals of Fenugreek (*Trigonella foenum-graecum*) and Ginger (*Zingiber officinale*). *Journal of Chemistry*, 2023, 1–9.
16. Haro-González, J. N., Castillo-Herrera, G. A., Martínez-Velázquez, M., & Espinosa-Andrews, H. (2021). Clove essential oil (*Syzygium aromaticum* L. Myrtaceae): Extraction, chemical composition, food applications, and essential bioactivity for human health. *Molecules*, 26(21), 6387.
17. Hassan, M. A., Xu, T., Tian, Y., Zhong, Y., Ali, F. A. Z., Yang, X., & Lu, B. (2021). Health benefits and phenolic compounds of *Moringa oleifera* leaves: A comprehensive review. *Phytomedicine*, 93, 153771.
18. Heidari, F., Rabizadeh, S., Rajab, A., Heidari, F., Mouodi, M., Mirmiranpour, H., Esteghamati, A., & Nakhjavani, M. (2020). Advanced glycation end-products and advanced oxidation protein products levels are correlates of duration of type 2 diabetes. *Life Sciences*, 260, 118422.
19. Idowu, S., Adekoya, A. E., Igiehon, O. O., & Idowu, A. T. (2021). Clove (*Syzygium aromaticum*) spices: A review on their bioactivities, current use, and potential application in dairy products. *Journal of Food Measurement and Characterization*, 15(4), 3419–3435.





**Piyushkumar N. Chudasama and Kinnari Mistry**

20. Kamli, M. R., Sharaf, A. A. M., Sabir, J. S., & Rather, I. A. (2022). Phytochemical screening of *Rosmarinus officinalis* L. as a potential anticholinesterase and antioxidant–medicinal plant for cognitive decline disorders. *Plants*, 11(4), 514.
21. Khadayat, K., Marasini, B. P., Gautam, H., Ghaju, S., & Parajuli, N. (2020). Evaluation of the alpha-amylase inhibitory activity of Nepalese medicinal plants used in the treatment of diabetes mellitus. *Clinical Phytoscience*, 6(1), 34.
22. Kifle, Z. D., Debeb, S. G., & Belayneh, Y. M. (2021). In Vitro  $\alpha$ -Amylase and  $\alpha$ -Glucosidase Inhibitory and Antioxidant Activities of the Crude Extract and Solvent Fractions of *Hagenia abyssinica* Leaves. *BioMed Research International*, 2021, 1–9.
23. Lucas, M., Freitas, M., Xavier, J. A., Moura, F. A., Goulart, M. O. F., Ribeiro, D., & Fernandes, E. (2021). The scavenging effect of curcumin, piperine and their combination against physiological relevant reactive pro-oxidant species using in vitro non-cellular and cellular models. *Chemical Papers*, 75(10), 5269–5277.
24. Manassis, G., Kalogianni, A. I., Lazou, T., Moschovas, M., Bossis, I., & Gelasakis, A. I. (2020). Plant-derived natural antioxidants in meat and meat products. *Antioxidants*, 9(12), 1215.
25. Meziant, L., Bachir-bey, M., Bensouici, C., Saci, F., Boutiche, M., & Louaileche, H. (2021). Assessment of inhibitory properties of flavonoid-rich fig (*Ficus carica* L.) peel extracts against tyrosinase,  $\alpha$ -glucosidase, urease and cholinesterases enzymes, and relationship with antioxidant activity. *European Journal of Integrative Medicine*, 43, 101272.
26. Mohd Dom, N. S., Yahaya, N., Adam, Z., Nik Abd. Rahman, N. M. A., & Hamid, M. (2020). Antiglycation and Antioxidant Properties of *Ficus deltoidea* Varieties. *Evidence-Based Complementary and Alternative Medicine*, 2020, 1–16.
27. Muflihah, Y. M., Gollavelli, G., & Ling, Y.-C. (2021). Correlation study of antioxidant activity with phenolic and flavonoid compounds in 12 Indonesian indigenous herbs. *Antioxidants*, 10(10), 1530.
28. Muraoka, M. Y., Justino, A. B., Caixeta, D. C., Queiroz, J. S., Sabino-Silva, R., & Salmen Espindola, F. (2022). Fructose and methylglyoxal-induced glycation alters structural and functional properties of salivary proteins, albumin and lysozyme. *PLoS One*, 17(1), e0262369.
29. Nait Irahah, I., Darif, D., Guenaou, I., Hmimid, F., Azzahra Lahlou, F., Ez-zahra Ousaid, F., Abdou-Allah, F., Aitsi, L., Akarid, K., & Bourhim, N. (2023). Therapeutic Potential of Clove Essential Oil in Diabetes: Modulation of Pro-Inflammatory Mediators, Oxidative Stress and Metabolic Enzyme Activities. *Chemistry & Biodiversity*, 20(3).
30. Nareshkumar, A., Subbarao, S., Vennapusa, A. R., Ashwin, V., Banarjee, R., Kulkarni, M. J., Ramu, V. S., & Udayakumar, M. (2020). Enzymatic and Non-enzymatic Detoxification of Reactive Carbonyl Compounds Improves the Oxidative Stress Tolerance in Cucumber, Tobacco and Rice Seedlings. *Journal of Plant Growth Regulation*, 39(3), 1359–1372.
31. Ncir, M., Ben Ali, M., Sellami, H., Allagui, M. S., Lahyani, A., Makni Ayadi, F., Boudawara, T., Allouche, N., El Feki, A., & Saoudi, M. (2020). Protective effects of *Allium sativum* essential oil rich in disulfides against deltamethrin induced oxidative stress and hepatotoxicity in rats. *Journal of Food Measurement and Characterization*, 14(5), 2667–2675.
32. Nguyen, V. T., Nguyen, N. Q., Thi, N. Q. N., Thi, C. Q. N., Truc, T. T., & Nghi, P. T. B. (2021). Studies on chemical, polyphenol content, flavonoid content, and antioxidant activity of sweet basil leaves (*Ocimum basilicum* L.). *IOP Conference Series: Materials Science and Engineering*, 1092(1), 012083.
33. Niroshani, W. A., Wariyapperuma, M., Kannangara, S., Wijayasinghe, Y. S., Subramaniam, S., & Jayawardena, B. (2020). *In vitro anti-diabetic effects and phytochemical profiling of novel varieties of Cinnamomum zeylanicum* (L.) extracts.
34. Paramanya, A., Farah, M. A., Al-Anazi, K. M., Devkota, H. P., & Ali, A. (2023). Exploring the Potential of *Spirulina* (*Arthrospira platensis*) Aqueous Extract in Preventing Glycation of Hemoglobin and pBR322 Plasmid. *Pharmacognosy Magazine*, 19(3), 581–591.
35. Parveen, A., Sultana, R., Lee, S. M., Kim, T. H., & Kim, S. Y. (2021). Phytochemicals against anti-diabetic complications: Targeting the advanced glycation end product signaling pathway. *Archives of Pharmacal Research*, 44(4), 378–401.
36. Phuyal, N., Jha, P. K., Raturi, P. P., & Rajbhandary, S. (2020). Total Phenolic, Flavonoid Contents, and Antioxidant Activities of Fruit, Seed, and Bark Extracts of *Zanthoxylum armatum* DC. *The Scientific World Journal*, 2020, 1–7.





## Piyushkumar N. Chudasama and Kinnari Mistry

37. Prastiwi, R., Elya, B., Hanafi, M., Desmiaty, Y., & Sauriasari, R. (2020). The antioxidant activity of *Sterculia stipulata* Korth woods and leaves by FRAP Method. *Pharmacognosy Journal*, 12(2).
38. Reddy, S. S. K., & Tan, M. (2020). Diabetes mellitus and its many complications. In *Diabetes Mellitus* (pp. 1–18).
39. Sabraoui, T., Khider, T., Nasser, B., Eddoha, R., Moujahid, A., Benbachir, M., & Essamadi, A. (2020). Determination of Punicalagins Content, Metal Chelating, and Antioxidant Properties of Edible Pomegranate (*Punica granatum* L) Peels and Seeds Grown in Morocco. *International Journal of Food Science*, 2020(1), 8885889.
40. Singamaneni, V., Dokuparthi, S. K., Banerjee, N., Kumar, A., & Chakrabarti, T. (2020). Phytochemical investigation and antimutagenic potential of ethanolic extracts of *Emblica officinalis*, *Terminalia chebula* and *Terminalia bellirica*. *The Natural Products Journal*, 10(4), 488–494.
41. Xiao, F., Xu, T., Lu, B., & Liu, R. (2020). Guidelines for antioxidant assays for food components. *Food Frontiers*, 1(1), 60–69.

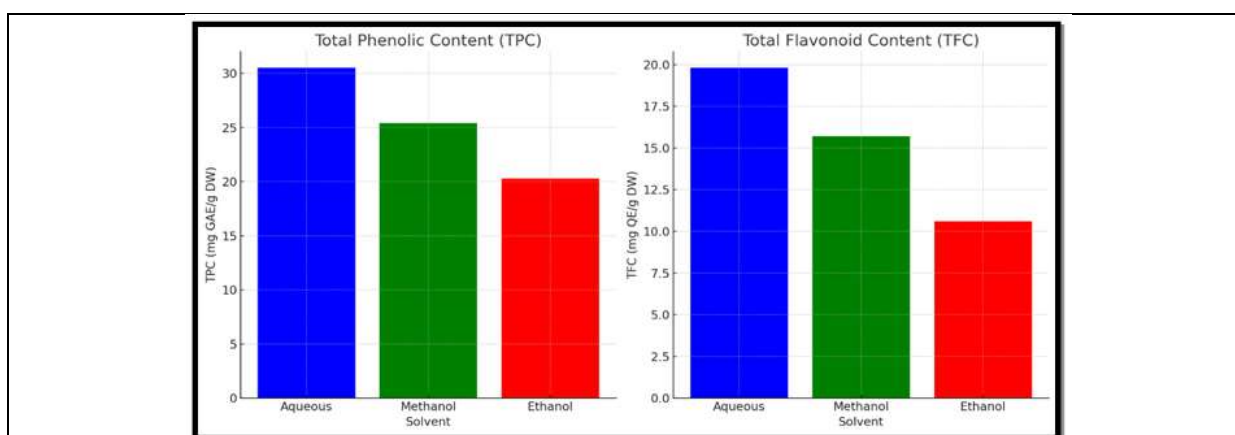


Figure: 1 Total Phenolic Content (TPC) and Total Flavonoid Content (TFC) of Various Extracts of *S. aromaticum* Bud

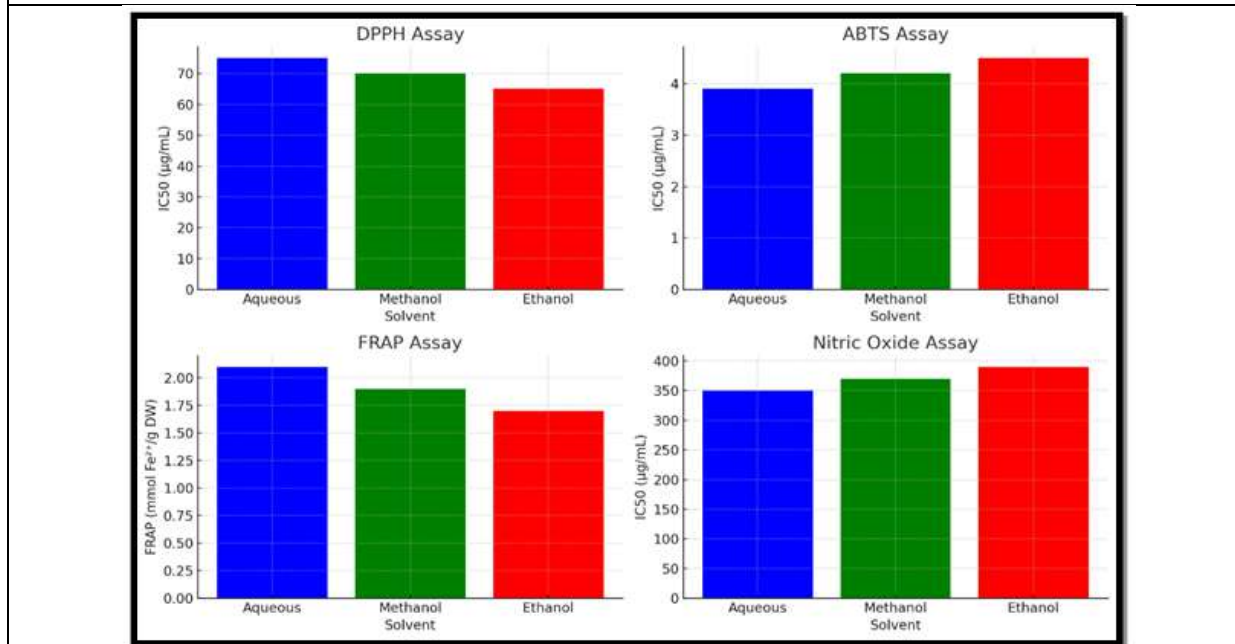


Figure 2: Different Antioxidant Confirming Assays for Extracts of *S. aromaticum* Bud





Piyushkumar N. Chudasama and Kinnari Mistry

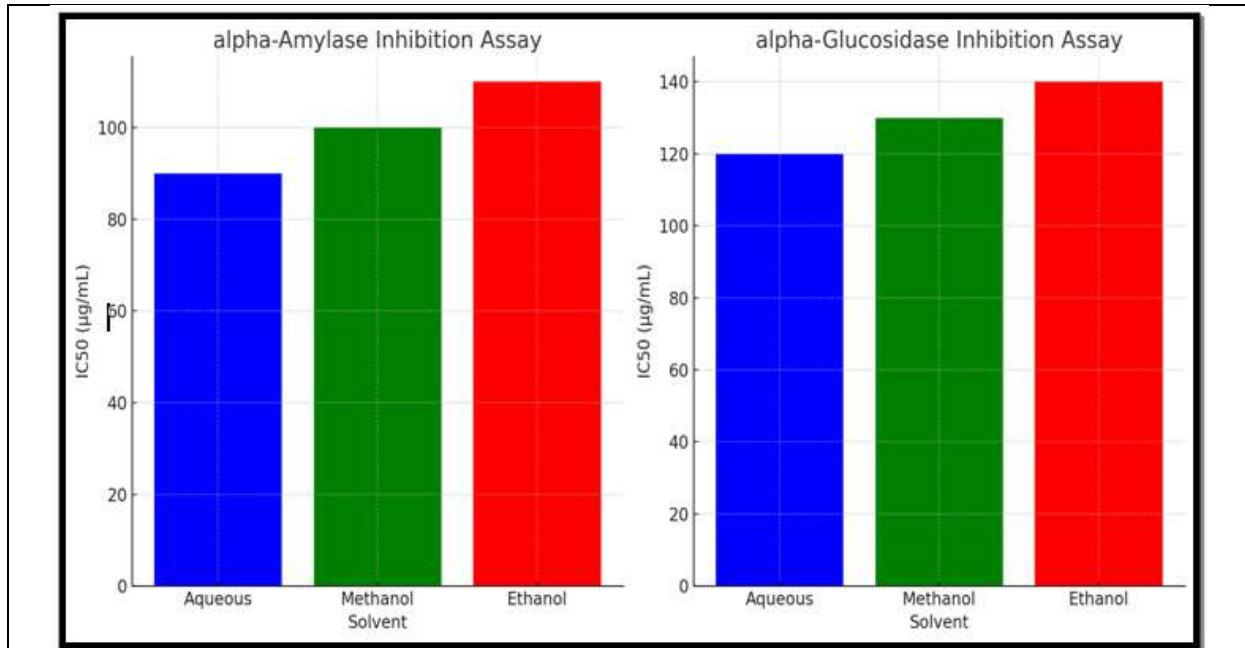


Figure 3: In Vitro Anti-Diabetic Activities of Extracts of *S.aromaticum* bud

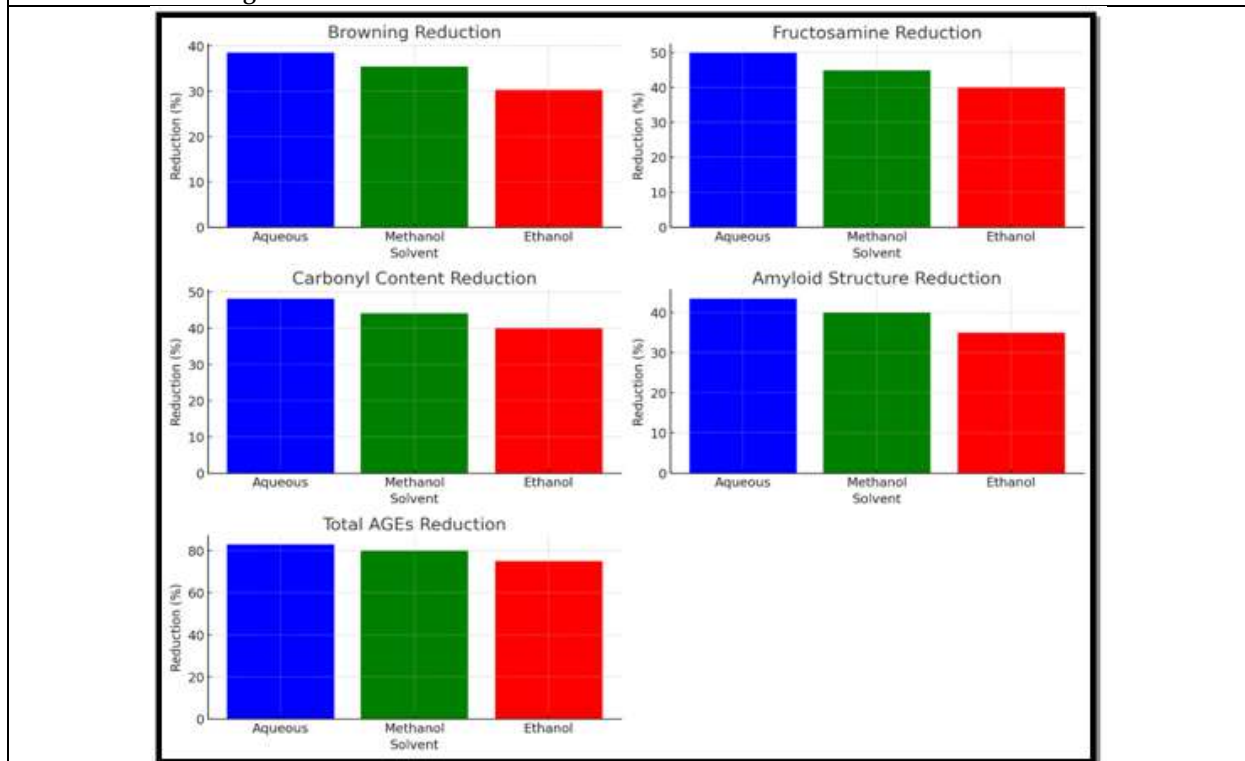


Figure 4: Anti-Glycation Properties of Extracts of *S.aromaticum* Bud





## GC-MS Analysis of *Canscora alata* (Roth) Wall- a Potent Medicinal Plant

S.Kavuthami <sup>1\*</sup> and G.Jayanthi<sup>2</sup>

<sup>1</sup>Ph.D Research Scholar, Department of Botany, Vellalar College for Women (Autonomous), (Affiliated to Bharathiar University, Coimbatore), Erode, Tamil Nadu, India.

<sup>2</sup>Associate Professor, Department of Botany, Vellalar College for Women (Autonomous), (Affiliated to Bharathiar University, Coimbatore), Erode, Tamil Nadu, India.

Received: 31 July 2024

Revised: 12 Sep 2024

Accepted: 30 Nov 2024

### \*Address for Correspondence

#### S.Kavuthami

Ph.D Research Scholar,  
Department of Botany,  
Vellalar College for Women (Autonomous),  
(Affiliated to Bharathiar University, Coimbatore),  
Erode, Tamil Nadu, India.  
E.Mail: drjayanthisk@gmail.com



This is an Open Access Journal / article distributed under the terms of the **Creative Commons Attribution License** (CC BY-NC-ND 3.0) which permits unrestricted use, distribution, and reproduction in any medium, provided the original work is properly cited. All rights reserved.

### ABSTRACT

In the present study, the bioactive phytoconstituents of *Canscora alata* (Roth) Wall whole plant extracts has been analysed using GC-MS technique. The chemical constituents of petroleum ether, hexane, ethylacetate and ethanol extracts were identified using the database of National Institute of Standards and Technology (NIST). The database which is universal and consists of over 62,000 different patterns of already identified and known bioactive compounds. The major peak area possessing constituents identified in petroleum ether extract are Tetracosane 24.179, Hexadecanoic acid, butyl ester 24.031, Z and Z-8,10-Hexadecadien-1-ol 23.737 and Tetrapentacontane 23.425, the hexane extract identified in major peak phytoconstituents are Z, Z-6,28-Heptatriactontadien-2-one having maximum peak percentage area of 24.765, Tetrapentacontane peak area of 24.188, Octadecanoic acid contain 23.949, Tetracosane 24.179 and Undec-10-ynoic acid, tetradecyl ester having maximum peak percentage area of 24.789 (0.50%), The major peak area possessing constituents identified in ethylacetate are E-10,13,13-Trimethyl-11-tetradecen-1-ol acetate having maximum peak percentage area of 24.766, 4H-Pyrazole-4-carbonitrile, 3-[[[(2-hydroxy-3-methoxyphenyl) methyl] amino]- 24.193 and Octadecanoic acid 23.929 and the ethanol extract possessing the major peak value in 24.789 (0.50%), 1,3-Bis(2-pyrazinoxy) propane – 24.298 (0.66), Octadecanoic acid, ethyl ester – 24.119(0.50), Octadecanoic acid-23.978(2.05), 7-Hexadecyn-1-ol - 23.825(19.55) and 2-Hexadecen-1-ol, 3,7,11,15-tetramethyl-.

**Keywords:** *Canscora alata*, Gentianaceae, pharmacological activity, Hexadecanoic acid, methanol ester, antioxidant, antiinflammatory.





**Kavuthami and Jayanthi****INTRODUCTION**

The use of medicinal plant goes back to the beginning of human life on earth and exploiting the plants of their natural surroundings. Nowadays looking to natural products for bioactive compounds and new drug discovery is considerable. Traditional medicine consists of a lot of valuable practical information in conjunction with the therapeutic principles and using materials including herbs, as therapeutic agent. The medicinal value of herbal plants lies in their bioactive principles as plant constituent that produce definite physiological action on the human body [Akinmoladun *et al.*, 2007]. Some of them are alkaloids, essential oils, flavonoids, tannins, terpenoid, saponins, phenolic compounds. These metabolites are the actual determinants of their pharmacological properties [Edeoga *et al.*, 2005 and Panday and Rizvi, 2009]. Today we know the modern prescription drugs are from natural compounds [Goh *et al.*, 1995]. Researchers have thus turned to traditional medicine, which is still used widely throughout the world. *Canscora alata* (Roth)Wall. is one of the medicinally important plant belonging to the family Gentianaceae. *Canscora decussata* is the synonym of *Canscora alata*. In India, *Canscora decussata* Schult. is popularly known as “Shankhpushpi” and found throughout India, up to an altitude of 1300 m. It is also grown in Sri Lanka and Myanmar.[Sethiya, N.K. *et al.*, 2010]. It is an important Ayurvedic drug, is reputed as an alternative, laxative and brain tonic. It occurs as an important ingredient in Brahmarasayana, Aindrarasayana, Agastyaharitati, Medhyarasayana, Manasamitram and in a number of other composite drugs. This plant grows up to 20cm, stems basally and apically branched, with prominent wings up to 1.6 mm wide. Leaves are cauline and sessile, lamina with three main veins, elliptic to lanceolate shape and often falcate. The base is wedge shaped to shortly attenuate with acute apex. Inflorescences are axillary, cymes; bracts linear to lanceolate, pedicels 2–26 mm long. Calyx persistent, with eight prominent, 1–1.3 mm wide wings; tube 8–9 mm long; lobes anisomorphic which are acute, two larger lobes are long and two lobes are shorter. Corolla tube 8–9 mm long, white, two lobes broadly elliptic and the other two lobes are elliptic. Filament of upper stamen are 1.8–2.2 mm long, broadened below anther. Ovary 6–8 style up to 4 mm long; stigmatic lobes 0.7. Capsule 8. Seeds irregular in shape Plate-1. From the literature the study plant is usually used in various ailments, such as nervine tonic and memory invigorator. It is also used in cerebral abnormalities, insomnia, burning sensation odema and Urinary disorders. Medicinal plants serve as therapeutic alternatives, safer choices or on some cases, as the only effective treatment. People in different cultures and places have used particular plants to treat certain medicinal problems. A larger number of these plants and their extract have shown beneficial therapeutic effects, including anti-oxidant, anti-inflammatory, anti-cancer and antimicrobial effects [Huffman, 2003; Miller *et al.*, 2004; Thatte *et al.*, 1992 and Sethiya, N.K., *et al.*, 2010]. Therefore, in present investigation, we analysed the GC-MS analysis of *Canscora alata* extracts.

**MATERIALS AND METHODS****Plant material and collection**

The healthy whole plants of *Canscora alata* (Roth) was selected and collected from Vellode, Erode District, Tamil Nadu, India, during September 2021. The identity of the plant specimen was confirmed by using the Floras [Gamble and Fischer, 1956; Matthew, 1983] and Botanical Survey of India, Southern region center, Coimbatore, Tamil Nadu. The herbarium number provided by Botanical survey of India is “BSI/SRC/5/23/2021/Tech/295”.

**Preparation of powder**

The shade dried entire plant was mechanically ground into coarse powder and passed through 80 mesh sieve and used for extraction process.

**Preparation of extracts**

The plant powder was extracted successively using Soxhlet apparatus with petroleum ether (60–80 °C), hexane (63–70 °C), ethylacetate (77.1 °C) and ethanol (99.9 °C). Each time before extracting with next solvent, powdered





**Kavuthami and Jayanthi**

material were dried in an air oven below 50°C. The extracts were dried over anhydrous sodium sulfate, stored in sealed vials in refrigerator (5-8°C) until analysis.

**GC-MS Analysis** (Jayanthi and Jegadeesan,2008)

GC-MS analysis of petroleum ether,hexane, ethylacetate and ethanol extracts were performed in therma GC- Trace Ultra ver:5.0 and a Gas Chromatography interface to a Mass Spectrometer equipped with a thermo MS DS Q II fused a DB35-MS capillary standard non polar column (30x0.25µm ID x 0.25 µm df). For detection, an impact mode with ionization energy of 70 ev. Helium was used as a carrier gas at a constant flow rate of 1 ml/minutes, and an injection volume of 1µm was employed (a split ratio of 10:1). The injector temperature was maintained at 2500C, the oven temperature was programmed from 1500C for 2 minutes, with an increase of 50C / minutes to 2200C, then 100C / minutes to 2600C, ending with a 20 minutes isothermal at 3500C. Mass Spectra were taken at 70ev. The scan interval of 0.5 sec and fragments from 50 to 650 Da. The solvent delay was 0 to 4 minutes and the total GC-MS running time was 37.50 minutes. The relative percentage of each component was calculated by comparing its average peak area to the total areas.

**Identification of compounds**

In order to identify the various bioactive components and interpretation of Mass Spectrum was conducted using the database of National Institute of Standards and Technology (NSIT). The database which is universal and consists of over 62,000 different patterns of already identified and known bioactive compounds. The spectra of the unknown component of petroleum ether, hexane, ethylacetate and ethanol extracts of were compared with the standard existing Mass Spectra of known components already stored in NIST library.

**RESULTS**

The obtained chromatogram of hexane, petroleum ether, ethylacetate, and ethanol are given in fig 1,2,3 and 4. respectively. The hexane extract contains 87 constituents, petroleum ether extract yielded 89 constituents, ethylacetate has 59 constituents and the ethanol has 57 constituents. The obtained phytoconstituents names with their retention time (RT), molecular formula, molecular weight (MW) and concentration in area (%) are presented in Table-1,2,3 and 4 respectively. The petroleum ether extract contains totally 89 components. The main active principles present in petroleum ether extract are Tetracosane 24.179, Hexadecanoic acid, butyl ester 24.031, Z, Z-8,10-Hexadecadien-1-ol 23.737 and Tetrapentacontane 23.425, and the minimum compounds presents in Petroleum ether extract are Ethylbenzene 3.669, o-Xylene 3.856, Benzene, 1-azido-2-methyl- 4.427 and Benzene, propyl- 6.136 (Table-1).

The hexane extract contains about 87 compounds in which the major components are Z, Z-6,28-Heptatriactontadien-2-one having maximum peak percentage area of 24.765, Tetrapentacontane peak area of 24.188, Octadecanoic acid contain 23.949, 11-Dodecyn-1-ol acetate 23.790 and Tetrapentacontane 23.430.The minimum compounds present in hexane extract was 1,3,5,7-Cyclooctatetraene 4.361, Benzene, 1-ethyl-2-methyl- 6.348, Mesitylene 6.576 (Table-2). The ethylacetate extract contains about 59 compounds in which E-10,13,13-Trimethyl-11-tetradecen-1-ol acetate having maximum peak percentage area of 24.766, 4H-Pyrazole-4-carbonitrile, 3-[[2-hydroxy-3-methoxyphenyl] methyl] amino]- 24.193, Octadecanoic acid 23.929, 9,12,15-Octadecatrienoic acid, (Z, Z, Z)- 23.756 and Phytol stearate 23.354 and the minium peak values are 3, Trans-(1,1-dimethylethyl)-4, cis-methoxycyclohexan-1-ol 3.749, o-Xylene 4.076, 4-Cyclopentene-1,3-dione 4.319 and 1,3,5,7-Cyclooctatetraene 4.585.(Table-3).

The ethanol extract contains about 57 compounds in which Undec-10-ynoic acid, tetradecyl ester having maximum peak percentage area of 24.789 (0.50%), 1,3-Bis(2-pyrazinoxy) propane – 24.298 (0.66), Octadecanoic acid, ethyl ester – 24.119(0.50), Octadecanoic acid-23.978(2.05), 7-Hexadecyn-1-ol - 23.825(19.55), 2-Hexadecen-1-ol, 3,7,11,15-tetramethyl-, acetate, [R- [R\*, R\*(E)]]- - 23.341(2.49), 2,6,2',6'-Tetramethylazobenzene-22.968(10.71), Ethyl 14-methyl-hexadecanoate -22.125(2.55), n-Hexadecanoic acid -22.028(12.04) etc.(Table-4).





## DISCUSSION

It is scientifically proved that a plant compound are to be pharmacologically active, it must possess various phytoconstituents which are working together and they may be responsible for different pharmacological properties [Sunday *et al.*, 2022]. About 22 phytoconstituents are present in hexane and petroleum ether extracts. Four compounds namely, Neophytadiene, 2(5H)furanone, eugenol and octadecanoic acid are present in ethanol and ethylacetate extract. The compounds namely Dodecane, Dodecane, 2,6,11 – trimethyl and Tetradecanoic acid and Tridecanal are present in Hexane, petroleum ether and ethylacetate extracts. The identified compounds may also use to develop drugs. By conducting phytochemical analysis through GC-MS analysis makes it easier by bringing our more features identified compounds [Velmurugan and Anand 2017]. For example, the compounds Hexadecaionic acid, methanol ester is reported as antioxidant, antiinflammatory and hypochlosterolemic agent [Belakhdairet *al.*, 2015]. These findings are well in accordance with previous reports [Harura *et al.*, 2022, Rajisha and Fernandes., 2020, Khan *et al.*, 2016 and Goh., 1995].

These major and common constituents present in hexane and petroleum ether are considered to play a important define machanisms [Salehi *et al.*, 2015]. Thus, the identified constituents from *Canscora alata* showed significant medicinal potential of the plant.

## CONCLUSION

The GC-MS analysis of petroleum ether, hexane extracts, ethylacetate and ethanol extracts of *Canscora alata* (Roth) Wall. revealed the presence of different active principles with different pharmacological actions. So, the whole plant extract can be used for treating multiple diseases. However, further studies will require the phytoconstituents and investigating its pharmacological activity and mechanism of action.

## REFERENCES

1. Akinmoladun, A.C., Ibukun, E.O., Afor, E., Akinsinlola, B.L. and Onibon, T.R 2007. Chemical constituents and antioxidant activity of *Alstonia boonei*. *Afr. J. Biotechnol.* 6(10):1197-201.
2. Belakhdar. G., Benjouad, A., Abdennebi, E.H. 2015. Determination of some bioactive chemical constituents from *Thesium humile* Vahl. *J Mater Environ Sci.* 6(10):2778.
3. Edeoga,HO., Okwu, D.E. and Mbaebie, B 2005. Phytochemical constituents of some Nigerian medicinal plants. *African J Biotechnol.* 4(7):685-688.
4. Huffman, M.A. 2003. Animal self-medication and ethnomedicine: exploration and exploitation of the medicinal properties of plants. *Proc. Nutr. Soc.* 62: 371-381.
5. Miller, K.L., Liebowitz, R.S. and Newby, L.K. 2004. Complementary and alternative medicine in cardiovascular disease: a review of biologically based approaches. *Americ. Heart J.* 147: 401-411.
6. Panday, K.B. and Rizvi, S.I. 2009 *Oxid. Med. Cell. Longer.*, 2,270-278.
7. Rajisha, K. and Fernandes, J. 2020. Identification of compounds from different fractions of *Exacum bicolor* Roxb. by GC-MS analysis. *Plant Archives.* 20(2):4531-4536.
8. Salehi, B., Ata, A., Kumar, N.V.A., Sharopov, F., Ramirez-Alarcon, K., Ruiz-Ortega, Ana., Ayatollahi, S.B., Fokou, P.V.T., Kobarfard, F., Zakaria, Z.A., Iriti, M., Taheri, Y., Martorell, M., Sureda, A., Setzer, W.N., Durazzo, A., Lucarini, M., Santini, A., Capasso, R., Ostrander, E.A., Atta-ur-Rahman, Choudhary, M.I., Cho, W.C. and Sharifi-Red, J. 2019. Antidiabetic potential of medicinal plants and their active components. *Biomolecules.* 9(10):551.
9. Sethiya, N.K., Patel, M.B. and Misra, S.H. 2010. Phytopharmacological aspects of *Canscora decussata* Roem and Schult, *National Library of Medicine.* 4(7): 49-57.

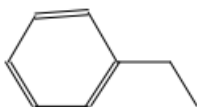
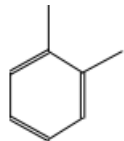
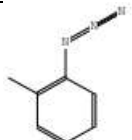
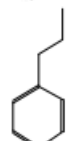
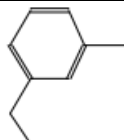
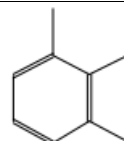
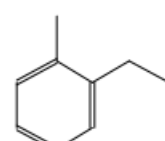
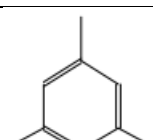




## Kavuthami and Jayanthi

10. Sunday, H.G., Sadiya, A.H., Ande, A.H., Ikedi, E.C. and Hauwa, M. 2022. Phytochemical profiling and GC-MS Analysis of the methanol extract of *Anthocleista grandiflora* Wood bark, *Asian journal of Research in Biochemistry*. 11(2):1-9.
11. Thatte, U.M., Kulkarni, M.R., Dahanukar, S.A., 1992. Immunotherapeutic, modification of *Escherichiacoli* peritonitis and bacteremia by *Tinospora cordifolia*. *J.Postgrad Med*.38:13-15
12. Velmurugan G, Anand SP. 2017. GC-MS analysis of bioactive compounds on ethanolic leaf extract of *Phyllodium pulchellum* L. Desv. *International Journal of Pharmacognosy and Phytochemical Research*.9(1):114.

Table-1 GCMS Analysis of Petroleum ether

S.No	R.Time	Name of the compound	Molecular Formula	Molecular Weight	Area %	Hit Spectrum Structure
1	3.669	Ethylbenzene	C <sub>8</sub> H <sub>10</sub>	106	0.23	
2	3.856	o-Xylene	C <sub>8</sub> H <sub>10</sub>	106	0.34	
3	4.427	Benzene, 1-azido-2-methyl-	C <sub>7</sub> H <sub>7</sub> N <sub>3</sub>	133	20.25	
4	6.136	Benzene, propyl-	C <sub>9</sub> H <sub>12</sub>	120	0.26	
5	6.347	Benzene, 1-ethyl-3-methyl-	C <sub>9</sub> H <sub>12</sub>	120	1.43	
6	6.579	Benzene, 1,2,3-trimethyl-	C <sub>9</sub> H <sub>12</sub>	120	0.55	
7	6.811	Benzene, 1-ethyl-2-methyl-	C <sub>9</sub> H <sub>12</sub>	120	0.46	
8	7.236	Mesitylene	C <sub>9</sub> H <sub>12</sub>	120	2.70	





## Kavuthami and Jayanthi

9	7.422	Decane	$C_{10}H_{22}$	142	0.19	
10	7.909	Benzene, 1,2,3-trimethyl-	$C_9H_{12}$	120	0.81	
11	8.140	D-Limonene	$C_{10}H_{16}$	136	0.17	
12	8.748	Benzene, (2,3-dimethyldecyl)-	$C_{18}H_{30}$	246	0.42	
13	9.739	Undecane, 4,7-dimethyl-	$C_{13}H_{28}$	184	0.25	
14	10.859	Silane, cyclohexyldimethoxymethyl-	$C_9H_{20}O_2Si$	188	0.14	
15	11.424	Azulene	$C_{10}H_8$	128	0.10	
16	11.679	Dodecane	$C_{12}H_{26}$	170	0.31	
17	11.898	Undecane, 4,6-dimethyl-	$C_{13}H_{28}$	184	0.18	
18	12.378	Tetradecane	$C_{14}H_{30}$	198	0.09	
19	12.476	Undecane, 4,7-dimethyl-	$C_{13}H_{28}$	184	0.07	
20	12.584	Dodecane, 4,6-dimethyl-	$C_{14}H_{30}$	198	0.08	
21	12.736	2,4-Dimethyldodecane	$C_{14}H_{30}$	198	0.18	
22	12.951	Dodecane, 2,6,11-trimethyl-	$C_{15}H_{32}$	212	0.79	





## Kavuthami and Jayanthi

23	13.091	Dodecane, trimethyl- 2,6,11-	C <sub>15</sub> H <sub>32</sub>	212	0.14	
24	13.183	Dodecane, trimethyl- 2,6,11-	C <sub>15</sub> H <sub>32</sub>	212	0.04	
25	13.301	Octane, 2,3,6,7-tetramethyl-	C <sub>12</sub> H <sub>26</sub>	170	0.05	
26	13.361	1-Octanol, 2-butyl-	C <sub>12</sub> H <sub>26</sub> O	186	0.20	
27	13.463	Decane, 2,3,7-trimethyl-	C <sub>13</sub> H <sub>28</sub>	184	0.05	
28	13.692	Dodecane, 4,6-dimethyl-	C <sub>14</sub> H <sub>30</sub>	198	0.38	
29	13.842	Dodecane, trimethyl- 2,6,11-	C <sub>15</sub> H <sub>32</sub>	212	0.12	
30	13.980	Piperonal	C <sub>8</sub> H <sub>6</sub> O <sub>3</sub>	150	1.24	
31	14.337	Heptadecane	C <sub>17</sub> H <sub>36</sub>	240	0.12	
32	14.877	Tetradecane	C <sub>14</sub> H <sub>30</sub>	198	0.29	
33	15.036	Pentadecane	C <sub>15</sub> H <sub>32</sub>	212	0.27	
34	15.105	Heptadecane	C <sub>17</sub> H <sub>36</sub>	240	0.16	
35	15.176	Tetradecane, 4-methyl-	C <sub>15</sub> H <sub>32</sub>	212	0.08	
36	15.378	Hexadecane	C <sub>16</sub> H <sub>34</sub>	226	0.10	
37	15.583	Heptadecane	C <sub>17</sub> H <sub>36</sub>	240	0.28	





## Kavuthami and Jayanthi

38	15.674	Heptadecane	C <sub>17</sub> H <sub>36</sub>	240	0.15	
39	15.765	Heptadecane	C <sub>17</sub> H <sub>36</sub>	240	0.51	
40	15.862	Dodecane, 4,6-dimethyl-	C <sub>14</sub> H <sub>30</sub>	198	0.10	
41	16.120	Heptadecane	C <sub>17</sub> H <sub>36</sub>	240	2.01	
42	16.216	Heptadecane	C <sub>17</sub> H <sub>36</sub>	240	0.31	
43	16.392	Phenol, 3,5-bis(1,1-dimethylethyl)-	C <sub>14</sub> H <sub>22</sub> O	206	0.88	
44	16.499	1-Decanol, 2-hexyl-	C <sub>16</sub> H <sub>34</sub> O	242	0.15	
45	16.575	3-Octenoic acid, nonyl ester	C <sub>17</sub> H <sub>32</sub> O <sub>2</sub>	268	0.07	
46	16.729	Heptadecane	C <sub>17</sub> H <sub>36</sub>	240	0.96	
47	16.797	2(4H)-Benzofuranone, 5,6,7,7a-tetrahydro-4,4,7a-trimethyl-, (R)-	C <sub>11</sub> H <sub>16</sub> O <sub>2</sub>	180	0.15	
48	16.865	Eicosane	C <sub>20</sub> H <sub>42</sub>	282	0.08	
49	16.995	Eicosane	C <sub>20</sub> H <sub>42</sub>	282	0.09	
50	17.128	Sulfurous acid, 2-propyl tridecyl ester	C <sub>16</sub> H <sub>34</sub> O <sub>3</sub> S	306	0.20	
51	17.209	Heptadecane	C <sub>17</sub> H <sub>36</sub>	240	0.07	







## Kavuthami and Jayanthi

52	7.272	Octadecane, 3-ethyl-5-(2-ethylbutyl)-	$C_{26}H_{54}$	366	0.08	
53	17.451	Diethyl Phthalate	$C_{12}H_{14}O_4$	222	0.25	
54	17.590	Hexadecane	$C_{16}H_{34}$	226	0.39	
55	17.682	Heptadecane	$C_{17}H_{36}$	240	0.26	
56	17.930	Heneicosane	$C_{21}H_{44}$	296	0.59	
57	18.181	Octadecane	$C_{18}H_{38}$	254	0.40	
58	18.311	Benzene, (2-methyloctyl)-	$C_{15}H_{24}$	204	0.16	
59	18.422	Hexadecane, 1-iodo-	$C_{16}H_{33}I$	352	0.05	
60	18.483	Heneicosane	$C_{21}H_{44}$	296	0.31	
61	18.831	Eicosane	$C_{20}H_{42}$	282	1.11	
62	19.167	Eicosane	$C_{20}H_{42}$	282	0.32	
63	19.350	Eicosane	$C_{20}H_{42}$	282	1.11	
64	19.578	Tridecanol, 2-ethyl-2-methyl-	$C_{16}H_{34}O$	242	0.18	
65	19.756	6-Hydroxy-4,4,7a-trimethyl-5,6,7,7a-tetrahydrobenzofuran-2(4H)-one	$C_{11}H_{16}O_3$	196	0.20	





## Kavuthami and Jayanthi

66	19.999	Octadecane	C <sub>18</sub> H <sub>38</sub>	254	0.35	
67	20.207	Tridecanal	C <sub>13</sub> H <sub>26</sub> O	198	0.29	
68	20.341	3,7,11,15-Tetramethylhexadec-2-ene	C <sub>20</sub> H <sub>40</sub>	280	0.29	
69	20.417	Neophytadiene	C <sub>20</sub> H <sub>38</sub>	278	3.88	
70	20.691	Phthalic acid, butyl tetradecyl ester	C <sub>23</sub> H <sub>36</sub> O <sub>4</sub>	376	1.57	
71	20.895	2-Hexadecen-1-ol, 3,7,11,15-tetramethyl-, acetate, [R- [R*, R*-(E)]]-	C <sub>22</sub> H <sub>42</sub> O <sub>2</sub>	338	0.84	
72	20.999	2,6,10-Trimethyltridecane	C <sub>16</sub> H <sub>34</sub>	226	0.15	
73	21.056	Dotriacontane	C <sub>32</sub> H <sub>66</sub>	450	0.17	
74	21.122	Hexadecane	C <sub>16</sub> H <sub>34</sub>	226	0.54	
75	21.237	Silane, trichlorooctadecyl-	C <sub>18</sub> H <sub>37</sub> C <sub>13</sub> Si	386	2.75	
76	21.375	Hexadecanoic acid, methyl ester	C <sub>17</sub> H <sub>34</sub> O <sub>2</sub>	270	0.75	
77	21.461	Benzenepropanoic acid, 3,5-bis(1,1-dimethylethyl)-4-hydroxy-, methyl ester	C <sub>18</sub> H <sub>28</sub> O <sub>3</sub>	292	0.26	
78	21.548	Eicosane	C <sub>20</sub> H <sub>42</sub>	282	0.19	
79	21.735	1,2-Benzenedicarboxylic acid, bis(2-methylpropyl) ester	C <sub>16</sub> H <sub>22</sub> O <sub>4</sub>	278	2.23	
80	21.962	n-Hexadecanoic acid	C <sub>16</sub> H <sub>32</sub> O <sub>2</sub>	256	12.33	





## Kavuthami and Jayanthi

81	22.099	Hexadecanoic acid, ethyl ester	C <sub>18</sub> H <sub>36</sub> O <sub>2</sub>	284	0.62	
82	22.184	Heneicosane	C <sub>21</sub> H <sub>44</sub>	296	0.74	
83	22.709	1,2-Dipiperonyl-3-imino-1,2,4-triazine	C <sub>18</sub> H <sub>16</sub> N <sub>4</sub> O <sub>4</sub>	352	2.28	
84	23.200	Eicosane	C <sub>20</sub> H <sub>42</sub>	282	2.25	
85	23.330	2-Hexadecen-1-ol, 3,7,11,15-tetramethyl-, acetate, [R- [R*, R*-(E)]]-	C <sub>22</sub> H <sub>42</sub> O <sub>2</sub>	338	9.86	
86	23.425	Tetrapentacontane	C <sub>54</sub> H <sub>110</sub>	758	1.21	
87	23.737	Z, Z-8,10-Hexadecadien-1-ol	C <sub>16</sub> H <sub>30</sub> O	238	7.70	
88	24.031	Hexadecanoic acid, butyl ester	C <sub>20</sub> H <sub>40</sub> O <sub>2</sub>	312	0.61	
89	24.179	Tetracosane	C <sub>24</sub> H <sub>50</sub>	338	3.48	

Table-2 GCMS Analysis of Hexane

S.No	R.Time	Name of the compound	Molecular Formula	Molecular Weight	Area %	Hit Structure
1	4.361	1,3,5,7-Cyclooctatetraene	C <sub>8</sub> H <sub>8</sub>	104	2.25	
2	6.348	Benzene, 1-ethyl-2-methyl-	C <sub>9</sub> H <sub>12</sub>	120	0.07	
3	6.576	Mesitylene	C <sub>9</sub> H <sub>12</sub>	120	0.06	
4	6.810	Benzene, 1,2,4-trimethyl-	C <sub>9</sub> H <sub>12</sub>	120	0.04	





## Kavuthami and Jayanthi

5	7.231	Benzene, 1,2,3-trimethyl-	$C_9H_{12}$	120	0.20	
6	7.909	Benzene, 1,2,3-trimethyl-	$C_9H_{12}$	120	0.04	
7	8.140	D-Limonene	$C_{10}H_{16}$	136	0.16	
8	8.743	3-Ethyl-3-methylheptane	$C_{10}H_{22}$	142	0.10	
9	9.736	Dodecane, 4,6-dimethyl-	$C_{14}H_{30}$	198	0.06	
10	9.816	Nonanal	$C_9H_{18}O$	142	0.05	
11	9.992	Phenylethyl Alcohol	$C_8H_{10}O$	122	0.06	
12	10.860	Silane, cyclohexyldimethoxymeth yl-	$C_9H_{20}O_2Si$	188	0.13	
13	11.029	Phenacylidene diacetate	$C_{12}H_{12}O_5$	236	0.08	
14	11.424	Azulene	$C_{10}H_8$	128	0.11	
15	11.681	Dodecane	$C_{12}H_{26}$	170	0.18	





## Kavuthami and Jayanthi

16	11.852	1-Diisopropylsilyloxycyclohexane	C <sub>12</sub> H <sub>26</sub> OSi	214	0.14	
17	12.048	Dodecane, 4-methyl-	C <sub>13</sub> H <sub>28</sub>	184	0.07	
18	12.238	1H-Pyrrole-2,5-dione, 3-ethyl-4-methyl-	C <sub>7</sub> H <sub>9</sub> NO <sub>2</sub>	139	0.07	
19	12.380	Tetradecane	C <sub>14</sub> H <sub>30</sub>	198	0.07	
20	12.475	Hexadecane	C <sub>16</sub> H <sub>34</sub>	226	0.07	
21	12.583	Dodecane, 4,6-dimethyl-	C <sub>14</sub> H <sub>30</sub>	198	0.07	
22	12.737	2,4-Dimethyldodecane	C <sub>14</sub> H <sub>30</sub>	198	0.15	
23	12.855	Tetradecane, 4-methyl-	C <sub>15</sub> H <sub>32</sub>	212	0.05	
24	12.950	Dodecane, 4,6-dimethyl-	C <sub>14</sub> H <sub>30</sub>	198	0.67	
25	13.093	Nonane, 5-butyl-	C <sub>13</sub> H <sub>28</sub>	184	0.12	
26	13.229	Dodecane, 4,6-dimethyl-	C <sub>14</sub> H <sub>30</sub>	198	0.08	
27	13.300	Methoxyacetic acid, 2-octyl ester	C <sub>11</sub> H <sub>22</sub> O <sub>3</sub>	202	0.06	
28	13.364	2-Isopropyl-5-methyl-1-heptanol	C <sub>11</sub> H <sub>24</sub> O	172	0.11	
29	13.464	2,6,10-Trimethyltridecane	C <sub>16</sub> H <sub>34</sub>	226	0.11	





## Kavuthami and Jayanthi

30	13.692	Dodecane, 4,6-dimethyl-	C <sub>14</sub> H <sub>30</sub>	198	0.31	
31	13.843	Dodecane, 4-methyl-	C <sub>13</sub> H <sub>28</sub>	184	0.08	
32	13.984	Piperonal	C <sub>8</sub> H <sub>6</sub> O <sub>3</sub>	150	1.54	
33	14.303	Naphthalene, 1,2,3,4-tetrahydro-1,1,6-trimethyl-	C <sub>13</sub> H <sub>18</sub>	174	0.12	
34	14.452	Decane, 3,8-dimethyl-	C <sub>12</sub> H <sub>26</sub>	170	0.05	
35	14.878	Tetradecane	C <sub>14</sub> H <sub>30</sub>	198	0.36	
36	15.106	Heptadecane	C <sub>17</sub> H <sub>36</sub>	240	0.62	
37	15.177	Tetradecane, 4-methyl-	C <sub>15</sub> H <sub>32</sub>	212	0.05	
38	15.381	Hexadecane	C <sub>16</sub> H <sub>34</sub>	226	0.08	
39	15.586	Heptadecane	C <sub>17</sub> H <sub>36</sub>	240	0.25	
40	15.765	Heptadecane	C <sub>17</sub> H <sub>36</sub>	240	0.90	
41	15.863	Dodecane, 4,6-dimethyl-	C <sub>14</sub> H <sub>30</sub>	198	0.08	
42	15.931	1-Octanol, 2-butyl-	C <sub>12</sub> H <sub>26</sub> O	186	0.04	
43	16.121	Heptadecane	C <sub>17</sub> H <sub>36</sub>	240	1.74	
44	16.216	Heptadecane	C <sub>17</sub> H <sub>36</sub>	240	0.29	







## Kavuthami and Jayanthi

45	16.394	Phenol, 3,5-bis(1,1-dimethylethyl)-	$C_{14}H_{22}O$	206	0.60	
46	16.500	1-Decanol, 2-hexyl-	$C_{16}H_{34}O$	242	0.13	
47	16.575	3-Octenoic acid, nonyl ester	$C_{17}H_{32}O_2$	268	0.06	
48	16.728	Heptadecane	$C_{17}H_{36}$	240	0.81	
49	16.796	2(4H)-Benzofuranone, 5,6,7,7a-tetrahydro-4,4,7a-trimethyl-, (R)-	$C_{11}H_{16}O_2$	180	0.18	
50	16.866	Eicosane	$C_{20}H_{42}$	282	0.08	
51	16.995	Dodecane, 2,6,11-trimethyl-	$C_{15}H_{32}$	212	0.05	
52	17.127	Sulfurous acid, 2-propyl tridecyl ester	$C_{16}H_{34}O_3S$	306	0.20	
53	17.207	Octadecane	$C_{18}H_{38}$	254	0.05	
54	17.270	Octadecane, 3-ethyl-5-(2-ethylbutyl)-	$C_{26}H_{54}$	366	0.08	
55	17.452	Diethyl Phthalate	$C_{12}H_{14}O_4$	222	0.60	
56	17.592	Hexadecane	$C_{16}H_{34}$	226	0.31	
57	17.682	Heptadecane	$C_{17}H_{36}$	240	0.22	
58	17.930	Heneicosane	$C_{21}H_{44}$	296	0.48	





## Kavuthami and Jayanthi

59	18.311	Benzeneacetic acid, 2-tetradecyl ester	$C_{22}H_{36}O_2$	332	0.19	
60	18.485	Heneicosane	$C_{21}H_{44}$	296	0.24	
61	18.832	Eicosane	$C_{20}H_{42}$	282	1.24	
62	19.166	Nonyl tetradecyl ether	$C_{23}H_{48}O$	340	0.28	
63	19.351	Eicosane	$C_{20}H_{42}$	282	0.98	
64	19.605	Octadecanoic acid	$C_{18}H_{36}O_2$	284	0.40	
65	19.762	6-Hydroxy-4,4,7a-trimethyl-5,6,7,7a-tetrahydrobenzofuran-2(4H)-one	$C_{11}H_{16}O_3$	196	0.24	
66	20.000	Octadecane	$C_{18}H_{38}$	254	0.30	
67	20.208	Tridecanal	$C_{13}H_{26}O$	198	0.27	
68	20.420	Neophytadiene	$C_{20}H_{38}$	278	4.37	
69	20.691	Phthalic acid, butyl tetradecyl ester	$C_{26}H_{42}O_4$	418	1.35	
70	20.896	2-Hexadecen-1-ol, 3,7,11,15-tetramethyl-, acetate, [R- [R*, R*-(E)]]-	$C_{22}H_{42}O_2$	338	1.15	
71	21.059	Eicosane	$C_{20}H_{42}$	282	0.13	
72	21.124	Heneicosane	$C_{21}H_{44}$	296	0.51	
73	21.240	Silane, trichlorooctadecyl-	$C_{18}H_{37}Cl_3Si$	386	2.48	





## Kavuthami and Jayanthi

74	21.376	Hexadecanoic acid, methyl ester	$C_{17}H_{34}O_2$	270	0.61	
75	21.463	Benzenepropanoic acid, 3,5-bis(1,1-dimethylethyl)-4-hydroxy-, methyl ester	$C_{18}H_{28}O_3$	292	0.23	
76	21.556	Pentatriacontane	$C_{35}H_{72}$	492	0.17	
77	21.632	Heneicosane	$C_{21}H_{44}$	296	0.09	
78	21.739	1,2-Benzenedicarboxylic acid, bis(2-methylpropyl) ester	$C_{16}H_{22}O_4$	278	2.36	
79	22.009	l-(+)-Ascorbic acid 2,6-dihexadecanoate	$C_{38}H_{68}O_8$	652	19.55	
80	22.721	1,2-Dipiperonyl-3-imino-1,2,4-triazine	$C_{18}H_{16}N_4O_4$	352	2.47	
81	23.204	Eicosane	$C_{20}H_{42}$	282	2.62	
82	23.341	2-Hexadecen-1-ol, 3,7,11,15-tetramethyl-, acetate, [R-[R*,R*-(E)]]-	$C_{22}H_{42}O_2$	338	10.39	
83	23.430	Tetrapentacontane	$C_{54}H_{110}$	758	0.85	
84	23.790	11-Dodecyn-1-ol acetate	$C_{14}H_{24}O_2$	224	24.37	
85	23.949	Octadecanoic acid	$C_{18}H_{36}O_2$	284	2.15	
86	24.188	Tetrapentacontane	$C_{54}H_{110}$	758	3.84	
87	24.765	Z, Z-6,28-Heptatriacontadien-2-one	$C_{37}H_{70}O$	530	0.36	





## Kavuthami and Jayanthi

Table -3 GCMS Analysis of Ethyl Acetate

S.No	RT	Name of the Compound	Molecular Formula	Molecular Weight	Area %	Hit spectrum
1	3.749	3, Trans-(1,1-dimethylethyl)-4, cis-methoxycyclohexan-1-ol	C <sub>11</sub> H <sub>22</sub> O <sub>2</sub>	186	0.27	
2	4.076	o-Xylene	C <sub>8</sub> H <sub>10</sub>	106	0.19	
3	4.319	4-Cyclopentene-1,3-dione	C <sub>5</sub> H <sub>4</sub> O <sub>2</sub>	96	0.11	
4	4.585	1,3,5,7-Cyclooctatetraene	C <sub>8</sub> H <sub>8</sub>	104	0.25	
5	5.057	2(5H)-Furanone	C <sub>4</sub> H <sub>4</sub> O <sub>2</sub>	84	0.23	
6	5.536	2(3H)-Furanone, 5-methyl-	C <sub>5</sub> H <sub>6</sub> O <sub>2</sub>	98	0.52	
7	6.514	Benzaldehyde	C <sub>7</sub> H <sub>6</sub> O	106	0.09	
8	7.106	4-Methyl-bicyclo [3.2.1] octan-2-one	C <sub>9</sub> H <sub>14</sub> O	138	0.17	
9	7.268	E-11,13-Tetradecadien-1-ol	C <sub>14</sub> H <sub>26</sub> O	210	0.07	
10	7.456	beta. -Citronellol, chlorodifluoroacetate	C <sub>12</sub> H <sub>19</sub> ClF <sub>2</sub> O <sub>2</sub>	268	0.12	
11	8.194	1,2-Cyclopentanedione, 3-methyl-	C <sub>6</sub> H <sub>8</sub> O <sub>2</sub>	112	0.14	





## Kavuthami and Jayanthi

12	8.537	Phenylacetic acid, cyclobutyl ester	$C_{12}H_{14}O_2$	190	0.44	
13	9.476	Phenol, 2-methoxy-	$C_7H_8O_2$	124	0.76	
14	10.056	o-Xylene-.alpha.,.alpha.'-dithio	$C_8H_{10}S_2$	170	0.22	
15	11.054	Silane, triethylfluoro-	$C_6H_{15}FSi$	134	0.22	
16	11.357	6-Methylheptanoic acid	$C_8H_{16}O_2$	144	0.06	
17	11.446	Ethanone, 1-(2-methylphenyl)-	$C_9H_{10}O$	134	0.16	
18	11.525	1-Dodecene	$C_{12}H_{24}$	168	0.13	
19	11.687	Dodecane	$C_{12}H_{26}$	170	0.04	
20	12.123	4-Vinylphenol	$C_8H_8O$	120	1.89	
21	12.499	Glycerol 1,2-diacetate	$C_7H_{12}O_5$	176	0.33	
22	12.952	Dodecane, 2,6,11-trimethyl-	$C_{15}H_{32}$	212	0.12	
23	13.341	Indole	$C_8H_7N$	117	0.14	
24	13.603	2-Methoxy-4-vinylphenol	$C_9H_{10}O_2$	150	1.50	
25	14.073	2,3-Diformylphenol	$C_8H_6O_3$	150	7.82	





## Kavuthami and Jayanthi

26	14.226	Eugenol	C <sub>10</sub> H <sub>12</sub> O <sub>2</sub>	164	0.12	
27	14.760	1-Hexadecanol	C <sub>16</sub> H <sub>34</sub> O	242	0.45	
28	14.935	Vanillin	C <sub>8</sub> H <sub>8</sub> O <sub>3</sub>	152	0.23	
29	15.624	6-Chromanol, methyl ether	C <sub>10</sub> H <sub>12</sub> O <sub>2</sub>	164	0.37	
30	16.145	Apocynin	C <sub>9</sub> H <sub>10</sub> O <sub>3</sub>	166	0.60	
31	16.402	2,4-Di-tert-butylphenol	C <sub>14</sub> H <sub>22</sub> O	206	0.33	
32	17.141	Dodecanoic acid	C <sub>12</sub> H <sub>24</sub> O <sub>2</sub>	200	0.33	
33	17.260	4-(Cyclopent-2-en-1-yl) phenol, acetate	C <sub>13</sub> H <sub>14</sub> O <sub>2</sub>	202	0.13	
34	17.491	1-Heptadecene	C <sub>17</sub> H <sub>34</sub>	238	0.69	
35	17.839	Megastigmatrienone	C <sub>13</sub> H <sub>18</sub> O	190	0.07	
36	18.000	Megastigmatrienone	C <sub>13</sub> H <sub>18</sub> O	190	0.26	
37	18.153	4-Isopropyl-6-methyl-1-tetralone	C <sub>14</sub> H <sub>18</sub> O	202	0.27	
38	18.253	Benzene, 1,3-bis(1-formylethyl)-	C <sub>12</sub> H <sub>14</sub> O <sub>2</sub>	190	0.07	
39	18.461	Deoxycubebin	C <sub>20</sub> H <sub>20</sub> O <sub>5</sub>	340	0.84	
40	18.830	Tridecanal	C <sub>13</sub> H <sub>26</sub> O	198	0.70	
41	19.020	Pentadecanal-	C <sub>15</sub> H <sub>30</sub> O	226	0.21	







## Kavuthami and Jayanthi

42	19.156	Acetic acid, 3,7,11,15-tetramethyl-hexadecyl ester	$C_{22}H_{44}O_2$	340	0.09	
43	19.366	(3E,10Z)-Oxacyclotrideca-3,10-diene-2,7-dione	$C_{12}H_{16}O_3$	208	0.53	
44	19.605	Tetradecanoic acid	$C_{14}H_{28}O_2$	228	0.79	
45	19.845	6-Hydroxy-4,4,7a-trimethyl-5,6,7,7a-tetrahydrobenzofuran-2(4H)-one	$C_{11}H_{16}O_3$	196	1.03	
46	20.210	Tetradecanal	$C_{14}H_{28}O$	212	0.09	
47	20.437	3,7,11,15-Tetramethyl-2-hexadecen-1-ol	$C_{20}H_{40}O$	296	9.83	
48	20.691	Neophytadiene	$C_{20}H_{38}$	278	1.60	
49	20.901	Neophytadiene	$C_{20}H_{38}$	278	2.48	
50	21.022	1(2H)-Naphthalenone, 3,4-dihydro-4,6,8-trimethyl-	$C_{13}H_{16}O$	188	0.32	
51	21.144	2-(2-Bromopropionyl) phenylglyoxylic acid	$C_{11}H_9BrO_4$	284	0.46	
52	21.989	n-Hexadecanoic acid	$C_{16}H_{32}O_2$	256	18.24	
53	22.868	2,6,2',6'-Tetramethylazobenzene	$C_{16}H_{18}N_2O_2$	270	15.13	
54	23.194	Urs-12-en-28-ol	$C_{30}H_{50}O$	426	0.57	
55	23.354	Phytyl stearate	$C_{38}H_{74}O_2$	562	12.03	





## Kavuthami and Jayanthi

56	23.756	9,12,15-Octadecatrienoic acid, (Z, Z, Z)-	C <sub>18</sub> H <sub>30</sub> O <sub>2</sub>	278	12.48	
57	23.929	Octadecanoic acid	C <sub>18</sub> H <sub>36</sub> O <sub>2</sub>	284	1.71	
58	24.193	4H-Pyrazole-4-carbonitrile, 3-[[2-hydroxy-3-methoxyphenyl) methyl] amino]-	C <sub>12</sub> H <sub>12</sub> N <sub>4</sub> O <sub>2</sub>	244	0.36	
59	24.766	E-10,13,13-Trimethyl-11-tetradecen-1-ol acetate	C <sub>19</sub> H <sub>36</sub> O <sub>2</sub>	296	0.59	

Table-4 GCMS ANALYSIS OF ETHANOL

S.NO	R.Time	Name of the Compound	Molecular Formula	Molecular Weight	Area %	Hit Structure	Spectrum
1	4.436	Levoglucosenone	C <sub>6</sub> H <sub>6</sub> O <sub>3</sub>	126	4.65		
2	4.922	4-Cyclopentene-1,3-dione	C <sub>5</sub> H <sub>4</sub> O <sub>2</sub>	96	0.06		
3	5.147	Ethanone, 1-(2-furanyl)-	C <sub>6</sub> H <sub>6</sub> O <sub>2</sub>	110	0.08		
4	5.472	2,2'-Bifuran, 2,2',5,5'-tetrahydro-	C <sub>8</sub> H <sub>10</sub> O <sub>2</sub>	138	0.40		
5	5.790	2(5H)-Furanone	C <sub>4</sub> H <sub>4</sub> O <sub>2</sub>	84	1.33		
6	5.910	Acetic acid, 2-(dimethylamino)ethyl ester	C <sub>6</sub> H <sub>13</sub> NO <sub>2</sub>	131	0.57		
7	6.169	2(3H)-Furanone, 5-methyl-	C <sub>5</sub> H <sub>6</sub> O <sub>2</sub>	98	0.66		
8	6.303	2(5H)-Furanone, 5-methyl-	C <sub>5</sub> H <sub>6</sub> O <sub>2</sub>	98	0.23		





## Kavuthami and Jayanthi

9	6.579	2-Furancarboxaldehyde, 5-methyl-	C <sub>6</sub> H <sub>6</sub> O <sub>2</sub>	110	1.26	
10	6.866	Piperidine-4-carbonitrile	C <sub>6</sub> H <sub>10</sub> N <sub>2</sub>	110	0.57	
11	7.174	2(5H)-Furanone, 3-methyl-	C <sub>5</sub> H <sub>6</sub> O <sub>2</sub>	98	0.14	
12	7.729	1,2-Cyclopentanedione, 3-methyl-	C <sub>6</sub> H <sub>8</sub> O <sub>2</sub>	112	0.28	
13	8.580	Benzeneacetaldehyde	C <sub>8</sub> H <sub>8</sub> O	120	1.95	
14	8.885	2-Methyl-3-(methylthio) furan	C <sub>6</sub> H <sub>8</sub> OS	128	1.71	
15	9.149	2(3H)-Furanone, 5-ethoxydihydro-	C <sub>6</sub> H <sub>10</sub> O <sub>3</sub>	130	0.13	
16	9.686	Cyclohexanol, 2-(1-methylethyl)-	C <sub>9</sub> H <sub>18</sub> O	142	6.68	
17	10.140	[4-(Aminomethyl) oxan-4-yl] methanol	C <sub>7</sub> H <sub>15</sub> NO <sub>2</sub>	145	0.26	
18	10.326	2-Cyclopenten-1-one, 3-ethyl-2-hydroxy-	C <sub>7</sub> H <sub>10</sub> O <sub>2</sub>	126	0.73	
19	10.727	Pentanoic acid, 3-hydroxy-4-methyl-, ethyl ester	C <sub>8</sub> H <sub>16</sub> O <sub>3</sub>	160	1.49	
20	11.410	4H-Pyran-4-one, 2,3-dihydro-3,5-dihydroxy-6-methyl-	C <sub>6</sub> H <sub>8</sub> O <sub>4</sub>	144	0.35	





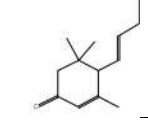
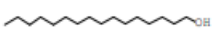
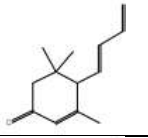
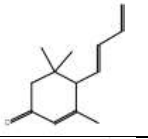
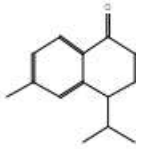
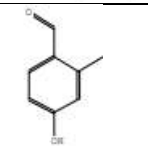
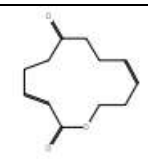
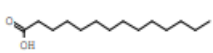
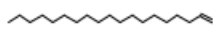
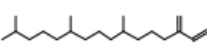
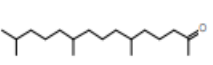
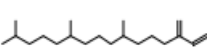
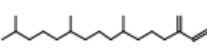
## Kavuthami and Jayanthi

21	12.305	Benzofuran, 2,3-dihydro-	C <sub>8</sub> H <sub>8</sub> O	120	3.30	
22	13.702	2-Methoxy-4-vinylphenol	C <sub>9</sub> H <sub>10</sub> O <sub>2</sub>	150	3.94	
23	14.148	2,3-Diformylpheno	C <sub>8</sub> H <sub>6</sub> O <sub>3</sub>	150	5.58	
24	14.276	Eugenol	C <sub>10</sub> H <sub>12</sub> O <sub>2</sub>	164	0.54	
25	14.765	1-Tetradecene	C <sub>14</sub> H <sub>28</sub>	196	0.48	
26	14.889	1-(3,6,6-Trimethyl-1,6,7,7a-tetrahydrocyclopenta[c]pyran-1-yl) ethanone	C <sub>13</sub> H <sub>18</sub> O <sub>2</sub>	206	0.48	
27	15.042	(E)-1-(2,3,6-trimethylphenyl) buta-1,3-diene (TPB, 1)	C <sub>13</sub> H <sub>16</sub>	172	0.46	
28	15.667	trans-Isoeugenol	C <sub>10</sub> H <sub>12</sub> O <sub>2</sub>	164	0.36	
29	15.937	Cyclohexane-1-methanol, 3,3-dimethyl-2-(3-methyl-1,3-butadienyl)-	C <sub>14</sub> H <sub>24</sub> O	208	0.93	
30	16.068	4-(2,6,6-Trimethylcyclohexa-1,3-dienyl) but-3-en-2-one	C <sub>13</sub> H <sub>18</sub> O	190	0.33	
31	16.434	N-(4-Hydroxyphenyl) propanamide, O-acetyl-	C <sub>11</sub> H <sub>13</sub> NO <sub>3</sub>	207	0.36	
32	16.812	Benzeneacetic acid, 4-ethenyl-, ethyl ester	C <sub>12</sub> H <sub>14</sub> O <sub>2</sub>	190	0.26	
33	17.192	Acetic acid, (2-isopropenylcyclopentylidene)-, methyl ester	C <sub>11</sub> H <sub>16</sub> O <sub>2</sub>	180	0.49	





## Kavuthami and Jayanthi

34	17.438	Megastigmatrienone	C <sub>13</sub> H <sub>18</sub> O	190	0.50	
35	17.500	1-Hexadecanol	C <sub>16</sub> H <sub>34</sub> O	242	0.38	
36	17.876	Megastigmatrienone	C <sub>13</sub> H <sub>18</sub> O	190	0.15	
37	18.046	Megastigmatrienone	C <sub>13</sub> H <sub>18</sub> O	190	0.74	
38	18.181	4-Isopropyl-6-methyl-1-tetralone	C <sub>14</sub> H <sub>18</sub> O	202	0.16	
39	18.486	4-Hydroxy-2-methylbenzaldehyde	C <sub>8</sub> H <sub>8</sub> O <sub>2</sub>	136	0.41	
40	19.421	(3E,10Z)-Oxacyclotrideca-3,10-diene-2,7-dione	C <sub>12</sub> H <sub>16</sub> O <sub>3</sub>	208	0.62	
41	19.636	Tetradecanoic acid	C <sub>14</sub> H <sub>28</sub> O <sub>2</sub>	228	0.55	
42	19.924	1-Nonadecene	C <sub>19</sub> H <sub>38</sub>	266	0.32	
43	20.424	Neophytadiene	C <sub>20</sub> H <sub>38</sub>	278	2.24	
44	20.489	2-Pentadecanone, 6,10,14-trimethyl-	C <sub>18</sub> H <sub>36</sub> O	268	0.28	
45	20.692	Neophytadiene	C <sub>20</sub> H <sub>38</sub>	278	0.46	
46	20.901	Neophytadiene	C <sub>20</sub> H <sub>38</sub>	278	0.70	





## Kavuthami and Jayanthi

47	21.065	2-(2-Bromopropionyl) phenylglyoxylic acid	$C_{11}H_9BrO_4$	284	0.28	
48	21.190	1(2H)-Naphthalenone, 3,4-dihydro-4,6,8-trimethyl-	$C_{13}H_{16}O$	188	0.39	
49	22.028	n-Hexadecanoic acid	$C_{16}H_{32}O_2$	256	12.04	
50	22.125	Ethyl 14-methyl-hexadecanoate	$C_{19}H_{38}O_2$	298	2.55	
51	22.968	2,6,2',6'-Tetramethylazobenzene	$C_{16}H_{18}N_2O_2$	270	10.71	
52	23.341	2-Hexadecen-1-ol, 3,7,11,15-tetramethyl-, acetate, [R- [R*, R*-(E)]]-	$C_{22}H_{42}O_2$	338	2.49	
53	23.825	7-Hexadecyn-1-ol	$C_{16}H_{30}O$	238	19.55	
54	2.05	Octadecanoic acid	$C_{18}H_{36}O_2$	284	2.05	
55	24.119	Octadecanoic acid, ethyl ester	$C_{20}H_{40}O_2$	312	0.50	
56	24.298	1,3-Bis(2-pyrazinoxy) propane	$C_{11}H_{12}N_4O_2$	232	0.66	
57	24.789	Undec-10-ynoic acid, tetradecyl ester	$C_{25}H_{46}O_2$	378	0.50	







**Kavuthami and Jayanthi**



Plate - 1





## On Solving Neutrosophic Linear and Nonlinear as a Neutrosophic Fuzzy Linear Complementarity Problem

N. Sudha<sup>1\*</sup> and R.Irene Hepzibah<sup>2</sup>

<sup>1</sup>Assistant Professor, Department of Mathematics, Idhaya College for Women, Kumbakonam, (Affiliated to Bharathidasan University, Tiruchirappalli), Tamil Nadu, India.

<sup>2</sup>Assistant Professor, Department of Mathematics, T.B.M.L College, Porayar, (Affiliated to Bharathidasan University, Tiruchirappalli), Tamil Nadu, India.

Received: 06 July 2024

Revised: 08 Sep 2024

Accepted: 11 Nov 2024

### \*Address for Correspondence

**N.Sudha**

Assistant Professor, Department of Mathematics,  
Idhaya College for Women, Kumbakonam,  
(Affiliated to Bharathidasan University, Tiruchirappalli),  
Tamil Nadu, India.

E.Mail: sudhaan551@gmail.com



This is an Open Access Journal / article distributed under the terms of the **Creative Commons Attribution License** (CC BY-NC-ND 3.0) which permits unrestricted use, distribution, and reproduction in any medium, provided the original work is properly cited. All rights reserved.

### ABSTRACT

The paper proposes a new approach to solve the Neutrosophic Quadratic Programming Problem(NQPP). Here, single valued triangular neutrosophic number replaces all fuzzy coefficients in the objective functions and constraints. We formulate other existing programming problems, such as the linear programming problems and the quadratic programming problems, into the linear complementarity programming problems and hence solve them using a solution algorithm for the LCP. Real-life applications taken from Linear Programming Problems(LPP) and Quadratic Programming Problems(QPP) are then used to demonstrate the elegance, precision and utility of these complementarity programming problems.

**Keywords:** Fuzzy Quadratic programming problem, Fuzzy Linear Complementarity problem, Single valued Triangular Neutrosophic Number, Lemke's method

### INTRODUCTION

Smarandache[5,6], which is a generalization of classical sets, fuzzy sets, intuitionistic fuzzy sets, etc., first introduced the concept of Neutrosophic Set(NS). The classical fuzzy set concept proposed by Zadeh[1] is a very effective mathematical tool for handling the complexity that generally arises from uncertainty and ambiguity in real-world scenarios. Actually, it's much more difficult to use many linear programming techniques. Furthermore, the non linear programming model cannot be representative of a large number of real problems. As a result of this, efforts have





**Sudha and Irene Hepzibah**

been done to establish a more general collection of mathematical programming methods, and significant progress in the field of fuzzy quadratic programming problems has been achieved. Suggested pairings of inequality restrictions must be complementary, meaning that at least one must hold with equality for a variety of physical and economic developments to be most naturally illustrated. The objective function may, in principle, be attached to such conditions but is more often used for the purpose of establishing complementarity problems where a realistic solution can be found. Actually, complementarity is able to considered a specific case of optimization. For both linear and nonlinear optimization, the usual optimality standards are complementarity problems with the environment. Linear Complementarity Problems can be applied in numerous fields of optimization. An algorithm aimed at dealing with a linear complementarity problem and a quadratic programming problem, for instance, can be utilized for defining a linear programming problem as a linear complementarity problem (LCP). In that case, the Lemke algorithm can be used when solving quadratic programming problems using KKT conditions as a LCP. In this research, an innovative approach to fuzzy neutrosophic quadratic programming and fuzzy neutrosophic linear programming problems is presented. These problems can be addressed by transforming them into fuzzy neutrosophic linear complementarity problems. Compared to fuzzy sets and intuitionistic fuzzy sets, neutrosophic sets are more relevant and helpful since they consistently express truth, ambiguity, and untruth. Linear Complementarity Problems Applications to other Programming Problems[10] , Wang et al. established neutrosophic sets, which have been expanded to single valued neutrosophic sets[7,8]. The following is the order in which the paper is organized. The single valued triangular neutrosophic number (SVTN) is specified in Section 2, as are the fuzzy arithmetical operators. Section 3 describes a technique for solving the fuzzy linear complementarity problem in neutrosophic. Section 4 discusses the proposed method of NFLPP and NFQPP, which is to be referred to as an NFLCP. In conclusion, a case study demonstrates the effectiveness of the proposed method in Section 5.

**Preliminaries**

2.1) Definition: Consider the universe E. We define the Neutrosophic set A over E as follows:  $A = \{(x, (\tau_{\tilde{A}}(x), i_{\tilde{A}}(x), \omega_{\tilde{A}}(x) : x \in E)$ , While the terms truth , inaccuracy and uncertainty involve  $\tau_{\tilde{A}}(x)$ ,  $i_{\tilde{A}}(x)$ ,  $\omega_{\tilde{A}}(x)$ , respectively. They are respectively defined by  $\tau_{\tilde{A}} : E \rightarrow ]^{-}0, 1^{+}[$ ,  $i_{\tilde{A}} : E \rightarrow ]^{-}0, 1^{+}[$ ,  $\omega_{\tilde{A}} : E \rightarrow ]^{-}0, 1^{+}[$  , Such that  $0^{-} \leq \tau_{\tilde{A}}(x) + i_{\tilde{A}}(x) + \omega_{\tilde{A}}(x) \leq 3^{+}$

2.2) Definition: If the value of  $\tilde{A} = \langle (a, b, c); \tau_{\tilde{a}}, i_{\tilde{a}}, \omega_{\tilde{a}} \rangle$  describe a Single Valued Triangular Neutrosophic Number (SVTNN). whose three membership functions for the truth, indeterminacy and a falsity of X are given by

$$\tau_{\tilde{A}}(x) = \begin{cases} \frac{(x-a)\tau_{\tilde{a}}}{(b-a)} & , a \leq x \leq b \\ \tau_{\tilde{a}} & , x = b \\ \frac{(c-x)\tau_{\tilde{a}}}{(c-b)} & , b \leq x \leq c \\ 0 & , otherwise \end{cases} ,$$

$$i_{\tilde{A}}(x) = \begin{cases} \frac{(b-x)i_{\tilde{a}}}{(b-a)} & , a \leq x \leq b \\ i_{\tilde{a}} & , x = b \\ \frac{(x-c)i_{\tilde{a}}}{(c-b)} & , b \leq x \leq c \\ 1 & , otherwise \end{cases} ,$$





**Sudha and Irene Hepzibah**

$$\omega_{\tilde{A}}(x) = \begin{cases} \frac{(b-x)\omega_{\tilde{a}}}{(b-a)} & , a \leq x \leq b \\ \omega_{\tilde{a}} & , x = b \\ \frac{(x-c)\omega_{\tilde{a}}}{(c-b)} & , b \leq x \leq c \\ 1 & , otherwise \end{cases}$$

Where  $0 \leq \tau_{\tilde{A}}(x) + i_{\tilde{A}}(x) + \omega_{\tilde{A}}(x) \leq 3, x \in \tilde{A}$  ,  
 Additionally, when  $a > 0$ ,  $\tilde{A}$  is called a non-negative SVTNN.

Similarly, when  $a < 0$ ,  $\tilde{A}$  becomes a negative SVTNN

Arithmetic Operations on Single Valued Triangular Neutrosophic Numbers:

Let  $\tilde{a} = \langle (a_1, b_1, c_1); \tau_{\tilde{a}}, i_{\tilde{a}}, \omega_{\tilde{a}} \rangle$  and  $\tilde{b} = \langle (a_2, b_2, c_2); \tau_{\tilde{b}}, i_{\tilde{b}}, \omega_{\tilde{b}} \rangle$  be two single valued triangular neutrosophic numbers and  $\gamma \neq 0$ .

$$\tilde{a} + \tilde{b} = \langle (a_1 + a_2, b_1 + b_2, c_1 + c_2); \tau_{\tilde{a}} \wedge \tau_{\tilde{b}}, i_{\tilde{a}} \vee i_{\tilde{b}}, \omega_{\tilde{a}} \vee \omega_{\tilde{b}} \rangle$$

$$\tilde{a} - \tilde{b} = \langle (a_1 - a_2, b_1 - b_2, c_1 - a_2); \tau_{\tilde{a}} \wedge \tau_{\tilde{b}}, i_{\tilde{a}} \vee i_{\tilde{b}}, \omega_{\tilde{a}} \vee \omega_{\tilde{b}} \rangle$$

$$\tilde{a}\tilde{b} = \{ \text{Min}(a_1 a_2, a_1 c_2, c_1 a_2, c_1 c_2), b_1 b_2, \text{Max}(a_1 a_2, a_1 c_2, c_1 a_2, c_1 c_2); \tau_{\tilde{a}} \wedge \tau_{\tilde{b}}, i_{\tilde{a}} \vee i_{\tilde{b}}, \omega_{\tilde{a}} \vee \omega_{\tilde{b}} \}$$

$$\tilde{a} / \tilde{b} = \{ \text{Min}(a_1/a_2, a_1/c_2, c_1/a_2, c_1/c_2), b_1/b_2, \text{Max}(a_1/a_2, a_1/c_2, c_1/a_2, c_1/c_2); \tau_{\tilde{a}} \wedge \tau_{\tilde{b}}, i_{\tilde{a}} \vee i_{\tilde{b}}, \omega_{\tilde{a}} \vee \omega_{\tilde{b}} \}$$

$$\gamma \tilde{a} = \begin{cases} ((\gamma a_1, \gamma b_1, \gamma c_1); \tau_{\tilde{a}}, i_{\tilde{a}}, \omega_{\tilde{a}}), (\gamma > 0) \\ ((\gamma c_1, \gamma b_1, \gamma a_1); \tau_{\tilde{a}}, i_{\tilde{a}}, \omega_{\tilde{a}}), (\gamma < 0) \end{cases}$$

Fuzzy Linear Programming Problem as a Fuzzy Linear Complementarity Problem (FLCP)

Fuzzy Linear Complementarity Problem (FLCP)

The linear complementarity problem is to determine  $\tilde{w} \in \mathbb{R}^n$  and  $\tilde{z} \in \mathbb{R}^n$  such that the following three conditions satisfy, given a matrix  $\tilde{M} \in \mathbb{R}^{n \times n}$  and a vector  $\tilde{q} \in \mathbb{R}^n$ .

$$\tilde{W} - \tilde{M}\tilde{Z} = \tilde{q} \tag{1}$$

$$\tilde{w} \geq 0, \tilde{z} \geq 0, j = 1, 2, 3, \dots, n \tag{2}$$

$$\tilde{w}^T \tilde{z} = 0 \tag{3}$$

A pair of fuzzy linear complementary variables is denoted as follows  $(\tilde{W}_j, \tilde{Z}_j)$ .

3.2) Definition:

The system above has a solution  $(\tilde{W}, \tilde{Z})$  where  $\tilde{w} = (\tilde{w}_1, \tilde{w}_2, \tilde{w}_3, \dots)$  and  $\tilde{z} = (\tilde{z}_1, \tilde{z}_2, \tilde{z}_3, \dots)$ . It may be derived from (2) and (3) that for any  $j = 1, 2, 3, \dots, n$ ,  $\tilde{w}_j \geq 0$  and  $\tilde{z}_j \geq 0$  Since  $\tilde{W}_j \tilde{Z}_j = 0$ . The response to this problem is  $(\tilde{w}, \tilde{z}) = (\tilde{w}_1, \tilde{w}_2, \tilde{w}_3, \dots, \tilde{w}_n, \tilde{z}_1, \tilde{z}_2, \tilde{z}_3, \dots, \tilde{z}_n)$  if  $(\tilde{W}, \tilde{Z})$  is a Neutrosophic basic feasible solution to (1) and (2) with one of the pair  $(\tilde{W}_j, \tilde{Z}_j)$  basic for each  $j=1, 2, 3, \dots, n$ . The concept of "Neutrosophic complementary feasible solution" applies to this problem.

Linear Complementarity Problem Formulation – Relationship between LPP and LCP

The symmetric form of the primal problem can be used to express a general linear programming problem (LPP) as follows.

$$\begin{aligned} & \text{Minimize } z = CX \\ & \text{Subject to } AX \geq b \qquad \rightarrow \tag{4} \\ & x \geq 0 \end{aligned}$$

Assume that matrix A has an order of  $m \times n$ . If the optimal solution to the essential problem (4) is illustrated by  $x \in \mathbb{R}^n$ , then the dual problem of (4) symmetrically becomes the Dual problem.

$$\text{Maximize } z = b^T Y$$





**Sudha and Irene Hepzibah**

Subject to  $A^T Y \geq C^T \rightarrow$  (5)  
 $Y \geq 0$

By the well know duality theory of LPP, there exists a dual vector  $y \in \mathbb{R}^m$  which is an optimal solution to problem (5). By introducing slack dual variable  $u \in \mathbb{R}^m$  it follows that the constraint of (5) becomes,

$u - (-A^T Y) = C^T \rightarrow$  (6)

For (4), we introduce the primal surplus variable  $v \in \mathbb{R}^n$ , then the constraint of problem (4) now follows;

$v - AX = -b \rightarrow$  (7)

We then combine the constraints of (6) and (7) in matrix form.

$$\begin{pmatrix} u \\ \vdots \\ v \end{pmatrix} - \begin{pmatrix} -A^T Y \\ \vdots \\ AX \end{pmatrix} = \begin{pmatrix} C^T \\ \vdots \\ -b \end{pmatrix}$$

$$\begin{pmatrix} u \\ \vdots \\ v \end{pmatrix} - \begin{pmatrix} 0X - A^T Y \\ \vdots \\ AX - 0Y \end{pmatrix} = \begin{pmatrix} C^T \\ \vdots \\ -b \end{pmatrix}$$

$$\begin{pmatrix} u \\ \vdots \\ v \end{pmatrix} \geq 0, \begin{pmatrix} X \\ \vdots \\ Y \end{pmatrix} \geq 0 \text{ and } \begin{pmatrix} u \\ \vdots \\ v \end{pmatrix}^T \begin{pmatrix} X \\ \vdots \\ Y \end{pmatrix} = 0$$

$$\begin{pmatrix} u \\ \vdots \\ v \end{pmatrix} - \begin{pmatrix} 0 - A^T Y \\ \vdots \\ AX - 0 \end{pmatrix} = \begin{pmatrix} C^T \\ \vdots \\ -b \end{pmatrix} \rightarrow$$
 (8)

Conversely,  $\begin{pmatrix} u \\ \vdots \\ v \end{pmatrix}^T \begin{pmatrix} X \\ \vdots \\ Y \end{pmatrix} = 0$  together satisfy all the conditions of (8) then X is a superior way to solve the linear programming problems(8). Now, considering all the vectors and matrices in (8) which are written in partitioned form as follows:

$w = \begin{pmatrix} u \\ \vdots \\ v \end{pmatrix}, z = \begin{pmatrix} X \\ \vdots \\ Y \end{pmatrix}, M = \begin{pmatrix} 0 - A^T \\ \vdots \\ A - 0 \end{pmatrix}, q = \begin{pmatrix} C^T \\ \vdots \\ -b \end{pmatrix} \rightarrow$  (9)

Then, (8) is seen to be the LCP. We shall determine the complementarity feasible solution to the linear complementarity problem, which yields the Linear Programming Problem (4) results.

**Quadratic Programming Problem as a Linear complementarity problem**

Given the quadratic programming problem (QPP).

Minimize  $CX + \frac{1}{2} X^T D X$   
 Subject to  $AX \geq b \rightarrow$  (10)  
 $x \geq 0$

Where A is a matrix of order  $m \times n$  and D is symmetric matrix of order m. The dual of this problem is given by

Maximize  $b^T Y$   
 Subject to  $A^T Y \leq (C + X^T D)^T \rightarrow$  (11)  
 $Y \geq 0$

Introducing the slack variable  $U \in \mathbb{R}^n$ , the constraint equation in (11) becomes

$A^T Y + U \leq (C + X^T D)^T$   
 By the symmetric property of D we have  
 $U + A^T Y \leq C + X^T D$   
 Thus,  $U - DX + A^T Y \leq C^T \rightarrow$  (12)

Similarly, introducing the dual surplus variable  $V \in \mathbb{R}^n$ , the constraint equations in (13) becomes.  
 $V - AX = -b \rightarrow$  (13)

Equation (12) and (13) combined together in matrix notation gives the following matrix equation.

$\begin{pmatrix} U \\ V \end{pmatrix} - \begin{pmatrix} DX - A^T Y \\ AX + 0Y \end{pmatrix} = \begin{pmatrix} C^T \\ -b \end{pmatrix} \rightarrow$  (14)

A point  $X \in \mathbb{R}^n$  is considered a Kuhn Tucker point for the quadratic programming problem (10) if there exist a dual vector  $Y \in \mathbb{R}^n$  and surplus vector  $V \in \mathbb{R}^n$  such that X,Y,U,V together satisfy





**Sudha and Irene Hepzibah**

$$\begin{pmatrix} U \\ V \end{pmatrix} - \begin{pmatrix} D & -A^T \\ A & 0 \end{pmatrix} \begin{pmatrix} X \\ Y \end{pmatrix} = \begin{pmatrix} C^T \\ -b \end{pmatrix},$$

$$\begin{pmatrix} U \\ V \end{pmatrix} \geq 0, \begin{pmatrix} X \\ Y \end{pmatrix} \geq 0 \text{ and } \begin{pmatrix} U \\ V \end{pmatrix}^T = 0$$

If we take,  $W = \begin{pmatrix} U \\ V \end{pmatrix}, Z = \begin{pmatrix} X \\ Y \end{pmatrix}, M = \begin{pmatrix} D & -A^T \\ A & 0 \end{pmatrix}$  and  $q = \begin{pmatrix} C^T \\ -b \end{pmatrix}$

Then (12) is seen to be a linear complementarity problem. Solving this LCP (14) provides a Kuhn Tucker point for the QPP (10). If D is a positive semi definite matrix, (that is  $X^TDX \geq 0, X \in \mathbb{R}^n$ ) this Kuhn tucker point is an optimal solution for (10).

**Fuzzy Quadratic Programming Problem (FQPP) as a Fuzzy Linear Complementarity Problem (FLCP)**

Given the Quadratic Programming Problem given below.

Minimize  $\tilde{f}(\tilde{x}) = \tilde{c}^t \tilde{x} + \frac{1}{2} \tilde{x}^t \tilde{H} \tilde{x}$

Subject to  $\tilde{A} \tilde{x} \leq \tilde{b}$  and  $\tilde{x} \geq 0$

In this case ,  $\tilde{b}$  is an  $m$  -vector and  $\tilde{c}$  is an  $n$  -vector of fuzzy integers. A and H are two distinct fuzzy symmetric matrices, A being  $m \times n$  and H being  $n \times n$ . The statement that follows is an expression for the Kuhn-Tucker conditions, let  $\tilde{y}$  be the vector of slack variables, and let  $\tilde{u}, \tilde{v}$  be the Lagrangian multiplier vectors of the constraints  $\tilde{A} \tilde{x} \leq \tilde{b}$  and  $\tilde{x} \geq 0$ , respectively.

$\tilde{A} \tilde{x} + \tilde{y} = \tilde{b}$

$-\tilde{H} \tilde{x} - \tilde{A}^t \tilde{u} + \tilde{v} = \tilde{c}$

$\tilde{x}^t \tilde{v} = 0, \tilde{u}^t \tilde{y} = 0$  And  $\tilde{x}, \tilde{y}, \tilde{u}, \tilde{v} \geq 0$

Now letting  $\tilde{M} = \begin{bmatrix} \tilde{0} & -\tilde{A} \\ \tilde{A}^t & \tilde{H} \end{bmatrix}, \tilde{q} = \begin{bmatrix} \tilde{b} \\ \tilde{c} \end{bmatrix}, \tilde{w} = \begin{bmatrix} \tilde{u} \\ \tilde{v} \end{bmatrix}$  and  $\tilde{z} = \begin{bmatrix} \tilde{x} \\ \tilde{y} \end{bmatrix}$  the Kuhn-Tucker conditions are stated as the LCP.

$\tilde{W} - \tilde{M} \tilde{Z} = \tilde{q}$

$\tilde{W}^t \tilde{Z} = 0$

$(\tilde{W}, \tilde{Z}) \geq 0$

4.2) Proposed Method NFLPP as a NFLCP

**Step 1:** Consider the Neutrosophic Fuzzy Linear Programming Problem (NFLPP).

**Step 2:** By introducing slack dual variable  $\tilde{u} \in \mathbb{R}^m$  and the primal surplus variable  $\tilde{v} \in \mathbb{R}^n$

**Step 3:** Combine them together in matrix notation.

$$\begin{pmatrix} \tilde{u} \\ \vdots \\ \tilde{v} \end{pmatrix} - \begin{pmatrix} 0 & -\tilde{A}^T \tilde{Y} \\ \tilde{A} \tilde{X} & -0 \end{pmatrix} = \begin{pmatrix} \tilde{C}^T \\ \vdots \\ -\tilde{b} \end{pmatrix}$$

**Step 4:** Considering that all the vectors and matrices are written in partitioned form as follows:

$$\tilde{w} = \begin{pmatrix} \tilde{u} \\ \vdots \\ \tilde{v} \end{pmatrix}, \tilde{z} = \begin{pmatrix} \tilde{X} \\ \vdots \\ \tilde{Y} \end{pmatrix}, \tilde{M} = \begin{pmatrix} 0 & -\tilde{A}^T \\ \tilde{A} & -0 \end{pmatrix}, q = \begin{pmatrix} \tilde{C}^T \\ \vdots \\ -\tilde{b} \end{pmatrix}$$

**Step 5:** Apply the Neutrosophic Linear Complementarity Algorithm, we get the obtained solution.

**Proposed Method NFQPP as a NFLCP**

**Step 1:** Consider the Neutrosophic Fuzzy Quadratic Programming Problem (NFQPP)

**Step 2:** By Introducing the slack Primal variable  $\tilde{U} \in \mathbb{R}^n$  and the dual surplus variable  $\tilde{V} \in \mathbb{R}^m$

**Step 3:** Combine the constraints and formulate the matrix form.

$$\begin{pmatrix} \tilde{U} \\ \tilde{V} \end{pmatrix} - \begin{pmatrix} \tilde{D} \tilde{X} & -\tilde{A}^T \tilde{Y} \\ \tilde{A} \tilde{X} & 0 \tilde{Y} \end{pmatrix} = \begin{pmatrix} \tilde{C}^T \\ -\tilde{b} \end{pmatrix}$$

**Step 4:** Considering that all the vectors and matrices are written in partitioned form as follows:

If we take,  $\tilde{W} = \begin{pmatrix} \tilde{U} \\ \tilde{V} \end{pmatrix}, \tilde{Z} = \begin{pmatrix} \tilde{X} \\ \tilde{Y} \end{pmatrix}, \tilde{M} = \begin{pmatrix} \tilde{D} & -\tilde{A}^T \\ \tilde{A} & 0 \end{pmatrix}$  and  $\tilde{q} = \begin{pmatrix} \tilde{C}^T \\ -\tilde{b} \end{pmatrix}$

**Step 5:** Use the Kuhn-Tucker conditions to solve the Neutrosophic Linear Complementarity Problem,

**Step 6:** Proceed through the steps again until the complementarity feasible solution to the Neutrosophic Linear Complementarity Problem is satisfied.







**Sudha and Irene Hepzibah**

**Applications to the proposed Methods**

**Numerical Example**

The Tummy-Tummy Instant Noodles manufactures products two species; vegetable specie and chicken flavor respectively, For the sale of a pack of Tummy-Tummy Instant Noodles, the profits gained per unit are \$2 and \$1, respectively. Each product is processed on two machines. The vegetable specie requires two minutes of processing time in machine one and three minutes in machine two, while the chicken flavor requires one minute of processing time in machine one and two minutes in machine two. Machine one is available for not more than four hours while machine two is available for not more than six hours during any working day. Determine the number of units of the vegetable specie and chicken flavor that can be manufactured to get minimum profit.

Solution : By formulating the LPP , we have

Minimize  $\tilde{z} = \tilde{2}\tilde{x}_1 + \tilde{x}_2$

Subject to constraint  $\tilde{2}\tilde{x}_1 + \tilde{x}_2 \geq \tilde{4}$ ,

$\tilde{3}\tilde{x}_1 + \tilde{2}\tilde{x}_2 \geq \tilde{6}$  and  $\tilde{x}_1, \tilde{x}_2 \geq \tilde{0}$

Where  $\tilde{A} = \begin{bmatrix} \tilde{2} & \tilde{1} \\ \tilde{3} & \tilde{2} \end{bmatrix}, \tilde{b} = \begin{bmatrix} \tilde{4} \\ \tilde{6} \end{bmatrix}, \tilde{c} = [\tilde{2} \quad \tilde{1}]$

$$\tilde{M} = \begin{pmatrix} \tilde{0} & \tilde{0} & -\tilde{2} & -\tilde{3} \\ \tilde{0} & \tilde{0} & -\tilde{1} & -\tilde{2} \\ \tilde{2} & \tilde{1} & \tilde{0} & \tilde{0} \\ \tilde{3} & \tilde{2} & \tilde{0} & \tilde{0} \end{pmatrix}$$

$$\tilde{q} = \begin{pmatrix} \tilde{c}^T \\ -\tilde{b} \end{pmatrix} = \begin{pmatrix} \tilde{2} \\ \tilde{1} \\ -\tilde{4} \\ -\tilde{6} \end{pmatrix}$$

$$\tilde{W} = \begin{pmatrix} \tilde{U} \\ \tilde{V} \end{pmatrix} = \begin{pmatrix} \tilde{U}_1 \\ \tilde{U}_2 \\ \tilde{V}_1 \\ \tilde{V}_2 \end{pmatrix} = \begin{pmatrix} \tilde{W}_1 \\ \tilde{W}_2 \\ \tilde{W}_3 \\ \tilde{W}_4 \end{pmatrix}, \quad \tilde{Z} = \begin{pmatrix} \tilde{X} \\ \tilde{Y} \end{pmatrix} = \begin{pmatrix} \tilde{x}_1 \\ \tilde{x}_2 \\ \tilde{y}_1 \\ \tilde{y}_2 \end{pmatrix} = \begin{pmatrix} \tilde{z}_1 \\ \tilde{z}_2 \\ \tilde{z}_3 \\ \tilde{z}_4 \end{pmatrix}$$

Therefore,  $\tilde{x}_1 = \tilde{z}_1$  and  $\tilde{x}_2 = \tilde{z}_2$  will be an optimal solution to the LPP.  $\tilde{W} - \tilde{M}\tilde{Z} = \tilde{q}$  gives

$$\begin{pmatrix} \tilde{W}_1 \\ \tilde{W}_2 \\ \tilde{W}_3 \\ \tilde{W}_4 \end{pmatrix} - \begin{pmatrix} \tilde{0} & \tilde{0} & -\tilde{2} & -\tilde{3} \\ \tilde{0} & \tilde{0} & -\tilde{1} & -\tilde{2} \\ \tilde{2} & \tilde{1} & \tilde{0} & \tilde{0} \\ \tilde{3} & \tilde{2} & \tilde{0} & \tilde{0} \end{pmatrix} \begin{pmatrix} \tilde{z}_1 \\ \tilde{z}_2 \\ \tilde{z}_3 \\ \tilde{z}_4 \end{pmatrix} = \begin{pmatrix} \tilde{2} \\ \tilde{1} \\ -\tilde{4} \\ -\tilde{6} \end{pmatrix}$$

which the single valued Neutrosophic coefficients are assumed to be

$$\tilde{1} = \langle (0,1,2); 0.6,0.4,0.2 \rangle ,$$

$$\tilde{2} = \langle (1,2,3); 0.4,0.2,0.2 \rangle ,$$

$$\tilde{3} = \langle (2,3,4); 0.5,0.3,0.3 \rangle ,$$

$$\tilde{4} = \langle (2,4,6); 0.6,0.4,0.4 \rangle \text{ and}$$

$$\tilde{6} = \langle (5,6,7); 0.4,0.3,0.2 \rangle$$

$$-\tilde{1} = \langle (-2, -1,0); 0.6,0.4,0.2 \rangle ,$$

$$-\tilde{2} = \langle (-3, -2, -1); 0.4,0.2,0.3 \rangle$$

$$-\tilde{3} = \langle (-4, -3, -2); 0.5,0.3,0.3 \rangle ,$$

$$-\tilde{4} = \langle (-6, -4, -2); 0.6,0.4,0.4 \rangle \text{ and}$$

$$-\tilde{6} = \langle (-7, -6, -5); 0.4,0.3,0.2 \rangle$$

Solving this problem using the Lemke’s complementarity pivoting algorithm, we obtain the complementarity basic feasible solution. The proposed technique 4.2 algorithm solves the neutrosophic linear complementary Problems and tabulates the outcomes. The linear complementarity problem has an optimal solution in  $\tilde{X} = (\tilde{x}_1, \tilde{x}_2) = (\tilde{z}_1, \tilde{z}_2) = (\langle (0.6, 2, 6); 0.6, 0.2, 0.2 \rangle, \langle (0,0,0); 1,0,0 \rangle) = (2,0)$  The conclusion to this problem,  $\tilde{x}_1 = 2, \tilde{x}_2 = 0$ , occurs exactly when the linear program’s simplex algorithm is executed.





**Sudha and Irene Hepzibah**

**Numerical Example**

The LG Ltd, has two production sites, one located at Thanjavur District and the other at Mayiladuthurai District. Each site produces three items Televisions, Air condition and Projectors. The production number of each item in thousands is produced per day are as follows: A market survey indicate that during the month of May there will be a demand of 4,000 Televisions, 2000 Air conditions and 4,000 Projectors. The operating costs per day in hundreds for items in Thanjavur District and Mayiladuthurai District are 2 and 3 respectively take away 2 times the square of the quantity produced in Thanjavur District. For how many days each item be run in May so as to maximize the production cost?

**Solution :**

We formulate the fuzzy quadratic programming problem

$$\text{Maximize } \tilde{z} = \tilde{2}\tilde{x}_1 + \tilde{3}\tilde{x}_2 - \tilde{2}\tilde{x}_1^2$$

Subject to constraint  $\tilde{x}_1 + \tilde{4}\tilde{x}_2 \leq \tilde{4}$ ,  $\tilde{x}_1 + \tilde{x}_2 \leq \tilde{2}$ ,  $\tilde{x}_1 + \tilde{x}_2 \geq \tilde{4}$  and  $\tilde{x}_1, \tilde{x}_2 \geq \tilde{0}$

Converting this problem to minimization problem, we have

$$\text{Minimize } \tilde{z} = -\tilde{2}\tilde{x}_1 - \tilde{3}\tilde{x}_2 + \tilde{2}\tilde{x}_1^2$$

Subject to constraint  $-\tilde{x}_1 - \tilde{4}\tilde{x}_2 \geq -\tilde{4}$ ,  $-\tilde{x}_1 - \tilde{x}_2 \geq -\tilde{2}$ , and  $\tilde{x}_1, \tilde{x}_2 \geq \tilde{0}$

If we compare this minimization problem with the QPP (10) we have

Where  $\tilde{D} = \begin{bmatrix} \tilde{4} & \tilde{0} \\ \tilde{0} & \tilde{0} \end{bmatrix}$ ,  $\tilde{b} = \begin{bmatrix} -\tilde{4} \\ -\tilde{2} \end{bmatrix}$ ,  $\tilde{c} = [-\tilde{2} \quad -\tilde{3}]$  in

Now, going by the formulation (12) of the LCP, we have the following matrices

$$\tilde{M} = \begin{pmatrix} \tilde{D} & -\tilde{A}^T \\ \tilde{A} & \tilde{0} \end{pmatrix} = \begin{pmatrix} \tilde{4} & \tilde{0} & \tilde{1} & \tilde{1} \\ \tilde{0} & \tilde{0} & \tilde{4} & \tilde{1} \\ -\tilde{1} & -\tilde{4} & \tilde{0} & \tilde{0} \\ -\tilde{1} & -\tilde{1} & \tilde{0} & \tilde{0} \end{pmatrix}$$

Solving the LCP  $(\tilde{M}, \tilde{q})$  will result to solving the quadratic programming problem. That is, the values of  $\tilde{z}_1$  and  $\tilde{z}_2$  obtained from the LCP  $(\tilde{M}, \tilde{q})$  is the solution to the QPP.

$$\tilde{q} = \begin{pmatrix} \tilde{c}^T \\ -\tilde{b} \end{pmatrix} = \begin{pmatrix} -\tilde{2} \\ -\tilde{3} \\ \tilde{4} \\ \tilde{2} \end{pmatrix}$$

which the single valued Neutrosophic coefficients are assumed to be

- $\tilde{1} = \langle (0,1,2); 0.2,0.3,0.5 \rangle$ ,
- $\tilde{2} = \langle (0,2,4); 0.6,0.4,0.1 \rangle$ ,
- $\tilde{3} = \langle (1,2,3); 0.2,0.3,0.5 \rangle$ ,
- $\tilde{4} = \langle (2,3,4); 0.6,0.4,0.1 \rangle$
- $\tilde{5} = \langle (0,4,8); 0.4,0.3,0.2 \rangle$
- and  $\tilde{6} = \langle (2,4,6); 0.6,0.4,0.1 \rangle$

Using Lemke’s complementarity pivoting algorithm the LCP formulated above yields the complementarity basic feasible solution. The neutrosophic linear complementary problem has been solved by the suggested method 4.3 algorithm, and the resulting findings are tabulated.

Therefore, the crisp value resulting from solving this linear complementarity problem is  $(W, Z) = (w_1, w_2, w_3, w_4, z_1, z_2, z_3, z_4) = (0, 0, 0, \frac{49}{64}, \frac{5}{16}, \frac{59}{64}, \frac{3}{4}, 0)$





## CONCLUSION

This study proposes an innovative method to solve neutrosophic fuzzy quadratic programming problems and neutrosophic fuzzy linear programming problems as fuzzy linear complementarity Problem with neutrosophic fuzzy parameters. Here, the Linear Complementarity Problem with Single Valued Triangular Neutrosophic Numbers (SVTNN) has been resolved with the Principle of Pivoting technique. Real-world examples also strengthen the proposed method.

## ACKNOWLEDGMENTS

The authors acknowledge their sincere gratitude to the unknown referees for their insightful recommendations and critiques that helped elevate the caliber of our research.

## REFERENCES

1. R.E. Bellman and L.A. Zadeh, Decision making in a fuzzy environment, *Management Science*, 17, 141-164, (1970).
2. Deli.Y.Subas., A ranking method of single valued neutrosophic numbers and its applications to multi-attribute decision making problems, (2015).
3. Irene Hepzibah.R, Sudha.N, Fuzzy Neutrosophic Quadratic Programming Problem as a Linear complementarity problem
4. *International Journal of Aquatic Science*, ISSN : 2008-8019, Vol 12, Issue 02, 91-97, (2021).
5. Irene Hepzibah.R, Sudha.N , On Solving Single Valued Triangular Neutrosophic Linear Complementarity Problem, the international journal of analytical and experimental modal analysis, (2020)
6. F. Smarandache, *Neutrosophy, Neutrosophic Probability, Set and Logic*, Amer. Res. Press, Rehoboth, USA., (1998), p. 105, <http://fs.gallup.unm.edu/eBook-neutrosophics4.pdf> (fourth version).
7. F. Smarandache, Neutrosophic set, a generalisation of the intuitionistic fuzzy sets, *Inter. J. Pure Appl. Math.*, 24, (2005), 287-297.
8. Jian-qiang Wang., Jing Wang., Simplified Neutrosophic sets and their applications in Multi-Criteria group decision-Making problems, *International journal of systems science*, 42-58, (2016).
9. Juan-Peng, Jian-qiang Wang, Multi valued Neutrosophic sets and power Aggregation operators with their applications in Multi-Criteria Group decision making problems, *International journal of computational intelligence systems*, 45-63, (2015).
10. Katta.G.Murthy., *Linear Complementarity, Linear and Nonlinear Programming*, Internet Edition, <http://www.personal.engin.umich.edu/~murty>, 254-273, (1997).
11. M. Laisin , J.E. Okeke, *Linear Complementarity Problems Applications to other Programming Problems*, *COOU Journal of Physical Sciences*, 147 – 156, (2017).
12. C.E. Lemke, On complementary pivot theory, *Mathematics of the Decision Sciences*, G.B.Danting and A.F.Veioff, Eds, (1968).
13. R. Sophia Porchelvi , M. Umamaheswari , A study on Intuitionistic Fuzzy Multi Objective LPP into LCP with Neutrosophic Triangular Numbers Approach, *Journal of applied science and computations*, 570-576, (2018).
14. J. Ye, Multi criteria decision making method using the correlation coefficient under single valued neutrosophic environment, *international journal of general systems*, 86-94, (2013).

**Table 01. Production sites**

Number of items	Thanjavur District	Mayiladuthurai District
Televisions (T) in 1000	1	4
Air Conditions (A) in 1000	1	1
Projectors (P) in 1000	1	1





## Nutritional Factors in the Prevention and Management of Chronic Kidney Disease

Kalyani U. Chande<sup>1\*</sup>; Snehal T. Hase<sup>2</sup>, Shweta A. Ukarande<sup>3</sup> and Komal Kalnar<sup>4</sup>

<sup>1</sup>Assistant Professor, Department of Pharmacognosy, Dr. D. Y. Patil College of Pharmacy Akurdi, (Affiliated to Savitribai Phule Pune University), Pune, Maharashtra, India.

<sup>2</sup>Assistant Professor, Department of Pharmaceutics, School of Pharmacy, Vishwakarma University, Pune, Maharashtra, India.

<sup>3</sup>Assistant Professor, Department of Pharmaceutical Quality Assurance, Dr. D. Y. Patil College of Pharmacy Akurdi, (Affiliated to Savitribai Phule Pune University), Pune, Maharashtra, India.

<sup>4</sup>Student, Matoshri Miratai Aher College of Pharmacy, Karjule Harya, Parner, Maharashtra, India.

Received: 23 Nov 2023

Revised: 16 Jul 2024

Accepted: 29 Oct 2024

### \*Address for Correspondence

#### Kalyani U. Chande

Assistant Professor, Department of Pharmacognosy,  
Dr. D.Y.Patil College of Pharmacy,  
(Affiliated to Savitribai Phule Pune University),  
Pune, Maharashtra, India.  
E.Mail: kalyanichande17@gmail.com



This is an Open Access Journal / article distributed under the terms of the **Creative Commons Attribution License** (CC BY-NC-ND 3.0) which permits unrestricted use, distribution, and reproduction in any medium, provided the original work is properly cited. All rights reserved.

### ABSTRACT

One of the primary strategies for boosting health and preventing diseases of all types, including renal ailments, is nutrition. Chronic kidney disease, which affects numerous metabolic pathways and is often progressive and irreversible, is defined as evidence of structural or functional renal impairment for three months or more. Altered protein homeostasis, hormonal dysfunction, aberrant protein catabolism, and acid-base disturbances ensue. Diet is one of the biggest modifiable risk factors for chronic kidney disease (CKD)-related death and disability. Chronic kidney disease (CKD) is a major public health concern that requires comprehensive management for preventing and delaying the progression to advanced CKD. This review examines the most recent research on the processes underlying diet-induced kidney disease with a focus on the role of diet in the development and progression of CKD. It is possible that improving diet quality or limiting dietary intake could be used as an adjunct therapy for CKD prevention or progression in susceptible individuals, thereby reducing the burden of CKD. We gathered this data from published researchers from PubMed, Science Direct, Google open access publications, Excerpta Medica Database, web of science from the year 2016-2023. Since more than a century ago, nutritional therapy has been advocated as a way to decrease the progression of CKD and uremia. Historically, the management of CKD has relied on dietary therapy, such as sodium and protein restriction. Other nutrients may affect kidney function in a number of ways, including through the change of gut homeostasis, metabolic or hemodynamic pathways, or all three. A diet rich in fruits and vegetables during the early stages of CKD may decrease the disease's progression, according to growing evidence; however, more research is required before guidelines are changed. For those who frequently drink sugar-sweetened beverages and eat a lot of fructose through their diet, reducing intake may be beneficial.



**Kalyani U. Chande et al.,**

Additional high-quality research is required to fully determine the impact of these dietary factors in CKD patients. More study is needed to develop a more thorough, evidence-based approach to the nutritional management of chronic kidney disease.

**Keywords:** CDK (chronic kidney disease); Diet; Nutritional therapy; Homeostasis; Allopathic drugs.

## INTRODUCTION

Chronic kidney disease, which affects numerous metabolic pathways and is often progressive and irreversible, is defined as evidence of structural or functional renal impairment for three months or more. Using the KDOQI [1,2] standards, CKD can be divided into five stages utilising thresholds of eGFR within the CKD range and/or evidence of structural renal abnormalities, such as proteinuria. Stage 3 should be separated into 3a and 3b to represent the rising CVD risk, according to NICE [3]. A UK retrospective lab audit research found that CKD stage 3 was the most prevalent stage, accounting for nearly 90% of cases, with 84% stage 3a (GFR of 45 to 59 ml/min/173m<sup>2</sup>) and 16% stage 3b (GFR of 30 to 44 ml/min/173m<sup>2</sup>) [4]. Although CKD can develop in the absence of disease owing to ageing, exposure to chemicals, or infection, it can also happen as a result of chronic disorders including diabetes, obesity, hypertension, or cardiovascular disease, addressing the underlying causes of CKD (diabetes and hypertension), obtaining and maintaining appropriate nutritional status and nitrogen balance, and avoiding are all goals of nutrition interventions in CKD [1]. Further moving to symptoms of CKD it includes the development of anaemia, cognitive changes, hypertension, gastrointestinal problems, shortness of breath, kidney alterations, changes in output, and anaemia, itch and cramps, glomerular capillary wall and tube damage, as well as peripheral oedema brought on by salt. While comparing all anemia, bone disorders, CVD, and cancer diseases are the most common CKD consequences [5]. Now coming to management the current recommendations of Kidney Outcomes Quality Initiative (KDOQI) and National Institute for Health Excellence (NICE) are to utilise serum creatinine concentration to estimate GFR (eGFR) and transform it using the Chronic Kidney Disease Epidemiology Collaboration (CKD-EPI) equation [2,3]. The Modification of Diet in Renal Disease (MDRD) equation is replaced by the CKD-EPI equation as a more reliable predictor of clinical risk, and both of these models account for specific non-renal effects (age, race, gender) [6,7]. Dietary habits and nutrition are linked to the onset of chronic metabolic illnesses, and they can be changed in order to stop or reduce the progression of CKD [8]. Following recommended dietary guidelines can lower the risk of developing CKD or halt its progression, and enhance overall health and death [9]. The possibility that many other substances may affect kidney health through metabolic or hemodynamic effects, modulation of gut homeostasis, including changes to gut microbiota, or other mechanisms is becoming more and more supported by research. The goal of this review is to provide an overview of recent literature on potential novel modifiable dietary components that may be helpful in the treatment of CKD and to summarise the most important suggestions made to date.

### Main Text

Chronic kidney disease, which affects numerous metabolic pathways and is often progressive and irreversible, is defined as evidence of structural or functional renal impairment for three months or more [10]. Hormonal dysfunction, abnormal protein catabolism, altered protein homeostasis, and acid-base disturbances ensue [11]. However, as chronic kidney disease progresses, the accumulation of nitrogen-containing byproducts from dietary and intrinsic protein catabolism may distort taste and smell and reduce appetite [11]. Since uremia affects the microbiome and disturbs intestinal epithelia, gastrointestinal nutrition absorption ultimately becomes aberrant [12]. As a result, nutritional status often becomes disordered, and protein energy wasting is common, requiring dietary adjustments in this population. Nutritional treatment, however, may support the management of uremia in addition to dietary modifications, as well as other issues such electrolyte and acid-base imbalances, water and salt retention, mineral and bone abnormalities, and failure to thrive. In fact, depending on the patient's preferences, dietary treatments may also be employed to delay or prevent dialysis therapy or for the conservative





Kalyani U. Chande *et al.*,

management of uremia. The diet of CKD patients should be a key factor in their care since nutritional therapy of individuals with CKD is thought to decrease uremic symptoms and provide positive effects on the progression of renal dysfunction. Numerous recommendations urge these people to consume less protein because a high-protein diet makes kidney disease worse. Limiting salt intake is often advised since excessive sodium may be linked to the progression of CKD and all-cause mortality. High potassium is linked to heart arrhythmia, while low potassium is linked to muscle weakness and hypertension. In order to keep serum potassium levels within the normal range, new guidelines advise modifying dietary potassium consumption on an individual basis. For individuals with CKD G3, G4, an appropriate dietary calcium intake is advised to maintain calcium balance. For patients with CKD, individualized approaches are required to ensure the best outcome.

### Major Role of Kidney in Metabolic Regulation

#### Water Electrolyte Haemostasis

The objective of the study was to evaluate the physiological effects of routine water consumption to those of electrolyte drinks in terms of exercise capability and recovery following strenuous activity. Ten healthy young men took part, working out on a treadmill before and after getting regular water and an electrolyte drink (3RINK) four weeks later. 30 minutes before activity and just after it, 250 mL of fluid were consumed. Haematocrit values indicated a fluid type and time period connection. Between P0 and P1, there were noticeably varied sodium concentrations in the various fluid types. Ultimately, a relationship between each type of fluid and serum lactate levels was discovered. Hence, consuming 3RINK before and after strenuous activity improved exercise performance, decreased weariness from exercise, and boosted the body's capacity to retain water[13].

#### Calcium Phosphate Balance.

The amount of a substance created (or absorbed from the intestine) must match the amount expelled in order to maintain homeostasis when GFR decreases. Each undamaged nephron excretes a higher percentage of its filtered load as nephron loss progresses. For instance, whereas at normal GFR levels each nephron may only need to excrete 10% of its filtered phosphate load to maintain homeostasis, 90% may need to be expelled by leftover nephrons. Despite these adjustments, when CKD worsens, the remaining nephrons' capacity to excrete the daily load of phosphate eventually declines, leading to a positive balance[14].

#### Waste Product Removal

Through minuscule filtering organs known as nephrons, the kidneys remove waste products from the blood known as urea. Each kidney contains a million or so nephrons. The glomerulus is where blood is filtered after entering. This filtered fluid then travels through the tubule where materials and water are added to or subtracted from the mixture. Urine is the remaining liquid. Following formation, urine travels down the renal tubules of the kidney before passing through the nephrons. The calyces serve as a collection point for urine, which then flows into the renal pelvis and into the ureter. From there, it descends and enters the bladder[15].

#### Acid base Balance

For the most part, the kidneys rely on 2 main mechanisms to keep the acid-base balance. Reabsorption of the filtered bicarbonate is the first step. A healthy glomerulus can filter 4,500 mEq of bicarbonate per day, and the proximal tubule can reabsorb up to 80% of the filtered bicarbonate [16]. Metabolic acidosis, hypokalemia, hypovolemia, angiotensin II, and glucocorticoids are some of the conditions that can increase proximal tubule reabsorption of bicarbonate. The second procedure entails the production of fresh bicarbonate through the release of distal nephron acid and ammonia. Even the most acidified urine cannot excrete the daily acid load in the absence of buffering, so the H<sup>+</sup> ions secreted into the urine are largely bound by H<sup>+</sup> acceptors. This function is carried out by buffers like urine phosphate, which are frequently referred to as titratable acids. However, the kidney's production of ammonia, which multiplies several-fold more than titratable acid excretion, is the main mechanism of new bicarbonate generation in the context of metabolic acidosis. Ammonia and bicarbonate are produced in the proximal tubule as a result of the metabolism of glutamine to glutamate and then oxaloacetate. There may also be a minor role for other metabolic pathways [17]. If the kidney's ammonia is released back into the bloodstream, the liver uses bicarbonate to process it.







Kalyani U. Chande *et al.*,

As a result, the amount of base that has been added to the bicarbonate pool can be determined by the amount of ammonium that is excreted in the urine, which is necessary for net bicarbonate gain.

### Erythropoietin Production

An essential erythropoietic hormone, erythropoietin (Epo), is primarily produced by renal Epo-producing cells (REPs). To maintain tissue oxygen homeostasis, epo production in REPs is tightly controlled in a hypoxia-inducible manner. Notably, myofibroblast-transformed REPs (MF-REPs) regain their initial physiological characteristics after the disease insults have been resolved, indicating that renal anaemia and fibrosis may be partially reversible [18].

### Degradation of Peptides

Despite receiving an adequate diet, people with chronic kidney disease (CKD) and other catabolic diseases (such as sepsis, diabetes, and cancer) can still experience muscle wastin Due to the distinctive 14kD actin fragment that caspase-3 activity leaves in muscle samples, it is simple to identify caspase-3 activity. The degree of muscle degradation in dialysis patients and in other catabolic conditions correlates well with this fragment, according to preliminary data from studies in patients and a number of experimental models of catabolic diseases [19].

### Blood Pressure Regulation

Patients with chronic kidney disease (CKD) who have uncontrolled blood pressure (BP) run the risk of serious negative effects. Achieving a healthy blood pressure level is crucial for preventing cardiovascular events (CVEs) and end-stage kidney disease. Notably, the risk of poor kidney outcomes is elevated with this lower target SBP. Unfortunately, there haven't been any studies on this topic that have only included people with CKD, especially those with advanced CKD[20].

### Symptoms

Many patients with CKD are asymptomatic and don't exhibit any symptoms until they are sick with severe CKD or until they get a chance finding from screening testing, such as during a routine physical or checkup. However, depending on the underlying cause of CKD, some individuals have symptoms as a direct result of their deteriorated kidney health

- Epistaxis
- Pigmentation
- Anorexia Nausea
- Vomiting
- Diarrhoea
- Coma
- Fits (severe uraemia)
- Uraemic pericarditis
- Hypertension
- Peripheral vascular disease
- Heart failure
- Nocturia
- Polyuria
- Bone pain
- Hyperparathyroidism
- Osteosclerosis

### Diagnosis

❖ **Blood tests:** During kidney function tests, the presence of waste products in your blood, such as urea and creatinine, is measured.





Kalyani U. Chande et al.,

- ❖ **Urine tests:** A urine sample analysis can reveal irregularities that suggest chronic kidney failure and assist in determining the underlying cause of chronic kidney disease.
- ❖ **Imaging tests:** To evaluate the structure and size of your kidneys, your doctor might use ultrasound. In some situations, different imaging tests might be used.
- ❖ **The removal of a kidney tissue sample for analysis:** A kidney biopsy, which involves taking a sample of kidney tissue, may be advised by your doctor. A long, thin needle is inserted through your skin and into your kidney during a kidney biopsy procedure under local anaesthesia. The biopsy sample is sent to a lab for analysis in order to help diagnose the kidney issue you are having.

#### Causes of chronic kidney disease

- a. Diabetes type 1 or type 2
- b. High blood pressure
- c. Glomerulonephritis, an inflammation of the kidney's filtration cells (gloe-mer-u-low-nuh-FRY-tis) (glomeruli)
- d. Other inherited kidney illnesses, such as polycystic kidney disease
- e. Persistent obstruction of the urinary tract caused by diseases like an enlarged prostate, kidney stones, or certain malignancies
- f. Vesicoureteral (ves-ih-koe-yoo-REE-tur-ul) (ves-ih-koe-yoo-REE-tur-ul) reflux, a medical disorder when urine backs up into the kidneys
- g. Pyelonephritis, another name for recurrent kidney infection (pie-uh-low-nuh-FRY-tis)

#### Risk factors

- ✚ Obesity
- ✚ Diabetes
- ✚ Older age
- ✚ High blood pressure
- ✚ Smoking
- ✚ Heart (cardiovascular) disease

#### Complications of chronic kidney disease:

- Anemia
- Gout
- Fluid retention
- High blood pressure (hypertension)

#### Long-term complications:

- Kidney failure
- Heart disease
- Weakened immune system

#### Pathophysiology

Renal insufficiency or reduced renal reserve are the earliest symptoms of chronic kidney disease (CKD), which can eventually lead to renal failure (end-stage renal disease). There are initially few obvious anomalies as renal tissue begins to function less because the remaining tissue performs better. The ability of the kidneys to maintain fluid and electrolyte homeostasis is hampered by decreased renal function. Early falls in urine concentration are followed by declines in urine excretion of excess phosphate, acid, and potassium. The ability to efficiently dilute or concentrate urine is lost when renal failure is advanced (glomerular filtration rate [GFR] 15 mL/min/1.73 m<sup>2</sup>); as a result, urine osmolality is typically fixed at between 300 and 320 mOsm/kg, which is comparable to plasma (275 to 295 mOsm/kg).



**Nutritional management:****Role of Dietary Constituents in Kidney Disease****Protein:****Protein amount**

One of the most frequently addressed topics in the dietary management of CKD is protein intake. It has been demonstrated that a high-protein diet, which is defined as consumption of more than 1.2 grammes of protein per kilogramme of body weight per day (g/kg/day), results in a considerable decline in kidney function[22]. According to animal models, a diet low in protein causes the glomerular afferent arterioles to constrict, lowering intraglomerular pressure, whereas a diet high in protein causes the afferent arterioles to dilate, increasing glomerular filtration[23]. Glomerular hyperfiltration itself has the potential to harm the remaining glomeruli over time [24]. Hence, a low-protein diet has a preglomerular effect that may improve the postglomerular action of angiotensin pathway modulators, which enlarge the efferent arterioles and subsequently reduce intraglomerular pressure[25]. For adults with moderate-to-advanced kidney disease (estimated glomerular filtration rate [eGFR], 45 ml per minute per 1.73 m<sup>2</sup> of body surface area) and for the management of sub-substantial proteinuria (urinary protein excretion, >0.3 g per day), 0.6 to 0.8 g per kilogramme of body weight per day is the most frequently recommended target. But, the so-called extremely low-protein diet, which provides only 0.6 g of protein per kilogramme of body weight each day, is also employed [26].

Individuals with diabetes mellitus, hypertension, polycystic kidneys, or those who have undergone nephrectomy for kidney donation or cancer therapy may benefit from modest protein consumption (1 g per kilogramme per day) in order to maintain a somewhat low intraglomerular pressure[27].

**Protein type**

Depending on the source from where the protein is extracted, the protein is classified into two types i.e. Plant protein, Animal protein. Animal protein is made up of sulfur-containing amino acids that, when oxidised, produce sulphate, a non-metabolizable anion that adds to the body's overall acid burden. Higher quantities of glutamate, an anionic amino acid whose metabolism consumes hydrogen ions to remain neutral and lowers acidity levels, are found in protein from plant sources[28]. According to the Chronic Renal Insufficiency Cohort Study findings, patients with CKD who consume a higher percentage of protein from plant sources have higher bicarbonate levels and better phosphorus balance[29]. Although there are few human studies comparing the effects of plant-based protein to animal-based protein, what is known so far indicates that improving kidney function involves eating more plant-based protein. Proteinuria, urine creatinine, and indicators of cardiovascular disease were all improved when animal proteins were substituted with soy proteins, according to a longitudinal controlled trial in individuals with diabetic nephropathy[30]. Another study in healthy people indicated that consuming vegetable protein decreased glomerular filtration rate, enhanced albumin clearance, and was independent of total protein intake[31]. A recent study compared the impact of a typical mixed-source low protein diet (0.6 g/kg/day) to a very low protein vegetarian diet (0.3 g/kg/day) on the progression of CKD. Significantly fewer individuals in the very low protein vegetarian diet group needed renal replacement therapy or had achieved the primary end-point of a GFR reduction of >50% at an 18-month follow-up[32]. Considering the available data, it is possible that individuals with CKD who consume more plant-based protein may experience better renal outcomes, given that there is enough protein to prevent protein energy loss.

**Sodium**

People who consume a high-sodium diet (>4 g of sodium per day), have underlying hypertension, or are over 55 years old are more likely to experience the association between dietary sodium intake and blood pressure [33]. Dietary sodium restriction is always advised in chronic kidney disease patients to manage fluid retention, hypertension, and to lower cardiovascular risk factors[34]. However, whether dietary sodium chloride restriction can halt the progression of kidney disease once it has already started is unclear. There aren't many pertinent interventional data for these patients because renal disease patients are frequently excluded from cardiovascular trials involving dietary sodium restriction [35]. Reduced sodium intake may help lower intraglomerular pressure by





Kalyani U. Chande et al.,

enhancing the effects of a low-protein diet and angiotensin-modulation therapy [36]. It may also reduce proteinuria and slow the progression of kidney disease [37].

Data from observational studies using urinary sodium excretion as a proxy for sodium chloride intake have been inconsistent, with some studies finding no correlation between dietary sodium intake and the progression [38] of renal disease and others finding a positive correlation [39]. The highest quartile of urinary sodium excretion (4.5 g per day), compared to the lowest quartile (2.7 g per day), was associated with 45% higher mortality and a 54% higher risk of disease progression [39], according to a longitudinal study published in 2016 that involved serial 24-hour urine collections from 3939 patients with chronic kidney disease. When dietary sodium intake exceeded 4 g per day, adverse cardiovascular outcomes were seen [40].

Observations in the general population point to a J-shaped relationship; dietary sodium intakes of more than 5 g per day and less than 3 g per day are both linked to an increased risk of cardiovascular disease and death [41]. There is no proof that patients with kidney disease will benefit from this extremely low level of sodium restriction, even though it is frequently advised that they limit their daily dietary intake of sodium to less than 2.3 g (or 100 mmol) for those with cardiovascular disease. As a result, a daily dietary sodium intake of less than 4 g (174 mmol) is advised for the general management of chronic kidney disease and its risks, and a sodium intake of less than 3 g (131 mmol) is advised for the specific management of symptomatic fluid retention or proteinuria. Given the risk of hyponatremia and negative outcomes, there is insufficient evidence to support a sodium intake for patients with renal insufficiency of less than 1.5 g per day (87 mmol per day). Additionally, patients with certain conditions, such as salt-losing nephropathies, shouldn't be subjected to such a strict sodium restriction [42].

Patients with renal insufficiency typically experience isosthenuria, despite the fact that sufficient fluid intake may reduce the risk of kidney disease [43]. This is the rationale behind the recommendation that people with stage 3 chronic kidney disease restrict their daily fluid intake to less than 1.5 litres in order to prevent hyponatremia [42]. It is crucial to adjust this limit for hot climates and other situations with high insensible fluid losses. Given the association between symptoms of fluid retention or hyponatremia and poor outcomes in chronic kidney disease, loop diuretics are frequently prescribed as adjunctive therapy, especially for patients who have a tendency to exhibit these symptoms [42].

### Phosphorus

Higher plasma phosphorus levels have been linked to an increased risk of incident kidney disease in the general population [44]. Given the high tissue and circulating levels of parathyroid hormone and fibroblast growth factor 23 (FGF-23) in renal insufficiency, which promote urinary phosphorus excretion, overt hyperphosphatemia is uncommon in stages 1, 2, and 3 of chronic kidney disease [45]. It is crucial to manage dietary phosphorus intake even in patients who don't appear to have hyperphosphatemia because elevated levels of parathyroid hormone and FGF-23 can lead to renal bone disease, left ventricular hypertrophy, vascular calcification and accelerated progression of kidney disease from vascular and tubulointerstitial injury [46]. The quantity and bioavailability of phosphorus vary depending on the type of protein, despite the fact that a low-protein diet also lowers phosphorus intake. As an illustration, the ratio of phosphorus to protein in egg whites and yolks, which have 3.6 and 2.7 g of protein per egg, respectively, is 1 to 2 mg and 20 to 30 mg per gram, respectively [47]. Plants (along with fibres) have a lower ability to absorb phosphorus through the digestive tract than meat (30–50% vs. 50–70%) [48], primarily in the form of phytates. Processing foods increase the phosphorus burden because they contain easily absorbed inorganic phosphorus in food additives [49]. Patients with moderate-to-advanced kidney disease should limit their dietary phosphorus intake to less than 800 mg per day (26 mmol per day), and processed foods with a high phosphorus-to-protein ratio should be avoided. An excessively strict restriction of protein intake to control hyperphosphatemia, however, may be linked to negative outcomes in patients with stage 5 chronic kidney disease who are receiving dialysis therapy or who are more at risk for protein-energy wasting [50]. Therefore, an individual dietary strategy that makes good use of phosphorus binders is preferred [51].



**Kalyani U. Chande et al.,****Potassium**

Reducing consumption of high sodium foods typically results in an increase in the quantity of potassium in the diet, in addition to the direct advantages on blood pressure and proteinuria [52]. With their high fibre and vitamin content as well as their low acidogenicity, a lot of potassium-rich meals, like fresh fruits and vegetables, are considered as healthy options by the majority of people[53]. Sodium sensitivity may be eliminated by potassium, which is known to have antihypertensive properties. The Dietary Approaches to Stop Hypertension (DASH) diet, which has twice as much potassium as a typical western diet, may be beneficial at lowering blood pressure due to an improved salt to potassium ratio[52]. Due to its high protein, potassium, calcium, and phosphorus content, the DASH diet has not been widely assessed in patients with CKD[54]. However a larger consumption of dietary potassium might be linked to a higher risk of renal disease development[55]. According to epidemiological research, both relatively low plasma potassium levels (4.0 mmol/liter) and high levels (>5.5 mmol/liter) are linked to a faster progression of renal disease [56]. Impaired potassium excretion in those with severe CKD, such as those on dialysis, causes hyperkalaemia, which is associated to a higher all-cause mortality rate[57]. In individuals with extremely advanced chronic kidney disease, the highest quartile of dietary potassium consumption, compared to the lowest quartile, is associated with a 2.4-fold greater risk of death; the association is unrelated to the plasma potassium level and other dietary factors[58]. In patients with hyperkalemia, especially those with more severe stages of kidney disease, dietary potassium restriction is frequently advised. Excessive dietary limitations, on the other hand, can expose patients to less heart-healthy and more atherogenic diets[59]and worsen constipation, which may actually lead to increased intestinal potassium absorption[60]. In patients with a propensity toward hyperkalemia (>5.5 mmol of potassium per liter), a dietary potassium intake of less than 3 g per day (<77 mmol per day) is s, with the stipulation that a balanced intake of fresh fruits and vegetables with high fiber should not be compromised. In people who had decreased renal function at baseline, the DASH diet was still helpful, according to a small retrospective research[54]. Before CKD patients can be advised to follow the DASH diet, larger studies are necessary. The advantages of a plant-based diet, which are naturally high in potassium and fibre and low in acidogenic proteins and minerals, would probably outweigh the potential risk of hyperkalemia in the early stages of CKD. Treatment of metabolic acidosis with base-producing vegetables was successful in lowering renal damage and improving metabolic acidosis in a sample of stage 4 CKD patients who were chosen because they were at low risk for hyperkalaemia[61]. Larger long-term trials in CKD patients investigating plant-based diets on renal biomarkers and clinical outcomes are warranted on the basis of the positive findings to date.

**Vitamin D**

When circulation vitamin D levels in patients with chronic renal disease have been found to be low, native vitamin D supplementation (cholecalciferol or ergocalciferol) may be recommended. Vitamin D analogues have been linked in several studies to reduced proteinuria as well as the repair of renal osteodystrophy [62]. The conversion of 7-dehydrocholesterol in the skin by UV radiation into vitamin D precursors, which are supplied from the food or from the metabolism of vitamin D precursors into its active state, requires the kidneys. These precursors are transformed into calcidiol (25 hydroxy vitamin D) in the liver, which is then transformed into calcitriol (1,25-dihydroxy vitamin D3) in the mitochondria of the proximal convoluted tubules of the kidney by an enzyme known as renal 1-hydroxylase. The production of calcitriol directly decreases as kidney function deteriorates [63]. Calcitriol inhibits the release of parathyroid hormone (PTH), however in chronic kidney disease (CKD), this process is blunted by decreased calcitriol synthesis, resulting in an excessive release of parathyroid hormone, a condition known as secondary hyperparathyroidism. Renal osteodystrophy may occur as a result of this secondary hyperparathyroidism, which can also affect bone turnover and metabolism [64]. It is well known that chronic kidney disease consequences include vitamin D insufficiency and secondary hyperparathyroidism [65].

**CKD , Low Vitamin D, and Association with Mortality**

Cardiovascular disease significantly increases the risk of death in individuals with renal failure, and 20% to 30% of deaths among dialysis patients are due to sudden cardiac death[66]. The risk of sudden cardiac death is three times higher in haemodialysis patients with a severe vitamin D deficit (25 nmol/L of 25(OH)D) than it is in those with vitamin D levels greater than 75 nmol/L [67]. A meta-analysis of data from observational studies revealed that the







Kalyani U. Chande *et al.*,

relative risk of death decreased significantly (RR = 0.86, CI: 0.81-0.92) for each rise in serum 25(OH)D levels of 25 nmol/L[68]. The production of extracellular insoluble calcium phosphate and consequent calcification of the vasculature can be caused by altered vitamin D levels and hyperparathyroidism[60]. Patients with CKD have been found to have coronary artery calcification[69], and calcium phosphate levels have been linked to a higher mortality risk in HD patients[70]. Increased albuminuria is also more likely to occur in those with low plasma 25(OH)D, particularly those who consume large amounts of sodium[71]. Hence, it is thought that restoring vitamin D levels may lower PTH levels, correct alterations in bone turnover and calcium metabolism, and subsequently lower mortality in the CKD population.

#### **Vitamin D Supplementation and Clinical Outcomes—Mortality**

While vitamin D therapy has been proven to change certain biochemical parameters in CKD patients, its impact on morbidity and mortality outcomes is less certain. A meta-analysis of observational studies revealed that individuals with CKD who used vitamin D supplements had a lower risk of cardiovascular and all-cause mortality[72]. However, a recent meta-analysis focused on RCTs that evaluated the impact of vitamin D supplementation on all-cause and cardiovascular mortality in CKD patients found no evidence that supplementation had an impact on mortality outcomes[73]. Almost two thirds of the patients in this meta-analysis had follow-up periods of less than a year, and it has been noted that this may not have been enough time to capture CVD events, which are a significant cause of mortality in the CKD group[74]. Instead of using clinical endpoints like progression to ESRD or mortality, many studies evaluating the effectiveness of vitamin D in CKD patients utilize biochemical outcomes like parathyroid levels or proteinuria[63]. In a recent comprehensive analysis, it was discovered that there was insufficient proof in favour of vitamin D supplementation for a number of health outcomes, including chronic kidney disease[75]. Those with early chronic renal disease and secondary hyperparathyroidism should take vitamin D supplements, according to current Australian guidelines, but they acknowledge that there is no proof that doing so improves patient-level outcomes[65]. So, despite the fact that vitamin D may significantly change biochemical parameters, larger, longer randomised control studies are urgently needed to determine whether these changes correspond to significant patient-centered outcomes.

#### **Calcium**

A positive calcium balance may result from passive diffusion of ionised calcium, which is exacerbated by decreased urinary calcium excretion brought on by secondary hyperparathyroidism. The decline in 1,25-dihydroxyvitamin D associated with renal insufficiency reduces gastrointestinal absorption of calcium[76]. In hyperactive renal bone disease, greater calcium release from bone (increased bone resorption due to secondary hyperparathyroidism) improves the positive calcium balance and may worsen vascular calcification[77]. Differences in dissociation and bioavailability between different types of elemental calcium induce variations in gut calcium absorption; for example, calcium citrate is more easily absorbed than calcium acetate[76]. According to two studies, individuals with stage 3 or stage 4 chronic renal disease may be able to maintain a table calcium balance by consuming 800 to 1000 mg of elemental calcium daily (20 to 25 mmol daily)[76,78]. As a result, patients with moderate-to-advanced chronic renal disease only need 800 to 1000 mg of elemental calcium per day from all sources, as compared to the 1000 to 1300 mg (25 to 32 mmol)[76]recommended for people without kidney disease[76,78].

#### **Carbohydrates**

Unrefined carbs make over half of the average daily energy consumption, and a low-protein diet may increase this percentage even further. In patients with renal disease should consume complex carbohydrates with a high fibre content, such as whole-wheat breads, multigrain cereal, oatmeal, and mixed fruits and vegetables, to assist lower the production of urea and creatinine as well as dietary phosphorus and protein[79]. To avoid weight gain on a low-protein diet, fat and carbohydrates should account for more than 90% of the daily energy requirement of 30 to 35 kcal per kilogramme [80]. The maintenance of correct glycemic control in patients with diabetic kidney disease is obvious, but adequate energy intake is necessary to reduce the danger of protein-energy wasting and hypoglycemia, which rises as kidney function deteriorates.







### **Dietary patterns**

#### **Mediterranean Diet**

The United Nations Educational, Scientific and Cultural Organization (UNESCO) officially recognised MD use as "an intangible cultural legacy of humanity" in 2010 for its contribution to maintaining individual health and having a favourable impact on longevity [84]. Regular use of plant-based foods such as fruit, vegetables, legumes, grains, and nuts, as well as the usage of EVOO, are characteristics of the MD. Also, it is renowned for being the primary source of vegetable lipids and for permitting the occasional glass of red wine [85,86]. The MD is rich in monounsaturated fatty acids (MUFAs) and polyunsaturated fatty acids (PUFAs) due to the use of EVOO and nuts, while yet maintaining a low intake of saturated fatty acids (SFAs), which come from foods like dairy and meat [87]. Also, the MD is abundant in foods that are strong in antioxidant and anti-inflammatory substances, which can fend off a number of disorders linked to chronic inflammation and oxidative stress. Among these foods, EVOO (which is high in polyphenols and MPCs) has a number of beneficial effects on CKD patients, including reducing inflammation and oxidative stress while enhancing purine and lipid metabolism [88,89]. In conclusion, treating metabolic acidosis in the early stages of CKD with the MD can be a beneficial nutritional dietary strategy. To prevent hyperkalemia in the later phases, the potassium intake must be under control. In fact, dietary therapy using LPD or vegan LPD appear to be more successful in moderate-to-severe CKD [22].

#### **Fruits and vegetables**

In order to minimise dietary acid load by 50%, a diet high in fruits and vegetables was given. The potential renal acid load, 8-hour urine net acid excretion, urine albumin-to-creatinine ratio, and urine TGF- significantly improved in patients with stage 2 CKD who underwent this dietary intervention for 30 days. Chronic kidney disease (CKD), estimated glomerular filtration rate (eGFR), and transforming growth factor (TGF-) are acronyms [90]. In this regard, it is important to teach patients how to boil their vegetables, either twice or for a long period of time, before eating them. Fruit consumption should also increase. Low-potassium fruit (such as apples, pears, strawberries, etc.) should only be consumed in amounts of no more than 300 g per day. Fruit heavy in potassium, such as bananas, peaches, etc., should be avoided [91].

#### **DASH Diet (Dietary approaches to stop hypertension)**

Legumes, whole grains, vegetables, fruits, low-fat dairy products, moderate amounts of chicken, fish, and nuts, as well as small amounts of sodium, red/processed meats, alcohol, and sweetened beverages, are all included in the DASH diet, which is a comprehensive eating pattern [92]. The DASH diet was studied in three studies: the ARIC research with 23 years of follow-up, the Iranian TLGS with 6.1 years of follow-up, and the Healthy Aging in Neighborhoods of Diversity throughout the Life Span cohort with 5 years of follow-up. The DASH diet appeared to have a positive impact in all studies, with RRs between 0.41 to 0.86 for high adherence versus low adherence. For two trials, the association was statistically significant [93 -95].

#### **Alkaline diet**

A high concentration of alkaline ions from food that the body receives as a result of metabolic activities define the AD [96,97]. According to K/DOQI recommendations, sodium citrate or sodium bicarbonate are administered as an alkali therapy to patients whose serum bicarbonate levels are below 22 mmol/L [98]. Such treatment aims to raise bicarbonate levels and slow the fall of GFR. Unfortunately, there are certain adverse effects to this kind of intervention. In actuality, sodium bicarbonate and sodium citrate both have the potential to boost the stomach absorption of aluminium. Furthermore, substances high in sodium can increase water retention, which can lead to arterial hypertension [99]. Further, the PRAL and potassium content of various foods can be used to build an AD for CKD patients. Several studies have shown that consuming more fruits and vegetables, along with neutralising the dietary acid load with alkali, can slow the course of CKD as measured by kidney damage biomarkers [100,101]. It is believed that an increase in acid load causes an increase in endothelin and angiotensin II, [102,103]. which accelerates the course of CKD. As a result, the activation of the RAAS speeds up the progression of CKD by producing hyperfiltration and hypertrophy of the residual nephrons as well as damage to the tubule interstices and





**Kalyani U. Chande et al.,**

glomerulosclerosis. Chronic low-grade inflammation and oxidative stress, both of which are common in CKD patients, further intensify this process [104]. Another benefit of AD in CKD patients is its ability to positively modulate gut flora, which results in an increase in the production of short-chain fatty acids (SCFAs) and a decrease in the release of nephrotoxic chemicals like p-cresol as well as indoxyl sulphate [103, 105]. Now to sum up in short, the AD is an alternative nutritional therapy for CKD patients.

## CONCLUSIONS

The prevention and treatment of CKD still heavily rely on diet. Despite the fact that there are recognised guidelines for protein intake in CKD patients, new research suggests that the kind of protein consumed may be significant, with a switch from animal to plant sources of protein appearing to be advantageous. Additionally, plant foods include more dietary fibre, and there is mounting proof that increasing dietary fibre and non-digestible carbohydrate intake improves biochemical indicators in CKD patients. Another probable reason by which plant protein appears to be more advantageous when compared to animal sources of protein is the reduced organic phosphate bioavailability found in plant protein meal sources. Restricting sodium and potassium intake is currently advised for CKD patients. The consumption of fruits, vegetables, potassium-rich foods, dietary fibre, and plant proteins has thus generally been limited in CKD patients. There is growing evidence that suggests a diet rich in fruits and vegetables during the early stages of CKD may slow the disease's progression; however, further research is needed before guidelines are changed. Reducing intake may be advantageous for people who consume a lot of sugar-sweetened beverages and have a high dietary fructose intake. To thoroughly establish the impact of these dietary variables in CKD patients, additional high-quality research are necessary. To provide a more comprehensive, evidence-based approach to the dietary management of chronic kidney disease, more research is required.

### Future Scope

Nutrition diet has a bright scope in development of our body. It helps us to fight against various disorder and maintain our body fit and fine.

## List of abbreviations

CKD	Chronic Kidney Disease
NICE	National Institute for Health Excellence
KDOQI	Kidney Outcomes Quality Initiative
GFR	Glomerular Filtration Rate
CVD	Cardio Vascular Disorder
MDRD	Modification of Diet in Renal Disease
REPs	Renal Epo- Producing cells
SBP	Spontaneous Bacterial Peritonitis
CVE	Cardio Vascular Event
UNESCO	United Nations Educational, Scientific and Cultural Organization
MUFAs	MonoUnsaturated Fatty Acids
DASH	Dietary Approaches to Stop Hypertension
RAAS	Renin Angiotensin Aldosterone System

## DECLARATIONS

### Ethics approval and consent to participate

No ethical approval or consent to participate was required for this manuscript.



**Consent for publication**

Yes, all the researchers studied have been duly cited and we have all the open access rights to access these studies.

**Availability of data and material**

Web: <https://pubmed.ncbi.nlm.nih.gov/>

**Competing interests**

No, the authors declare that they have no competing interests.

**Funding**

Not applicable.

**Authors' contributions**

MP compiled the paper, worked on English, grammar, and collected information. NE was responsible for filtering the useful information and mechanisms enlisted. DM contributed in the basic idea of paper and collected all data. KC was responsible for all high-quality diagrams, data, and information regarding risk factors. All authors have read and approved the manuscript.

**Acknowledgements**

We are thankful to our Respected Principal, Our Professor at Dr. DY Patil College of Pharmacy, Akurdi, for successful completion of work.

**Authors' information**

Dr. D.Y. Patil College of Pharmacy, Akurdi, D.Y. Patil Educational Complex, Sector Pradhikaran, Nigdi, Pune, Maharashtra, India 411044

**REFERENCES**

1. Levey AS, de Jong PE, Coresh J, et al. The definition, classification, and prognosis of chronic kidney disease: a KDIGO Controversies Conference report. *Kidney Int* 2011;80:17-28
2. KDOQI. Chronic Kidney Disease: Evaluation, Classification, and Stratification 2002. Available: [http://www.kidney.org/professionals/kdoqi/guidelines\\_commentaries.cfm](http://www.kidney.org/professionals/kdoqi/guidelines_commentaries.cfm).
3. NICE NICE. CG73 Chronic kidney disease: full guideline: 2008; 2008 [6th June 2012]. The published full clinical guideline on Chronic kidney disease including recommendations and methods used. Available: <http://guidance.nice.org.uk/CG73/Guidance/pdf/English>.
4. de Lusignan S, Tomson C, Harris K, Van Vlymen J, Gallagher H. UK Prevalence of Chronic Kidney Disease for the Adult Population Is 6.76% Based on Two Creatinine Readings [Erratum]. *Nephron Clinical practice*. 2012; 120:c107.
5. Webster AC, Nagler EV, Morton RL, Masson P. Chronic kidney disease. *Lancet*. 2017 Mar; 389(10075):1238–52.
6. Levey AS, Bosch JP, Lewis JB, Greene T, Rogers N, Roth D. A more accurate method to estimate glomerular filtration rate from serum creatinine: a new prediction equation. Modification of Diet in Renal Disease Study Group. *Ann Intern Med*. 1999; 130(6):461–70. Epub 1999/03/13. PMID: 10075613
7. Matsushita K, Tonelli M, Lloyd A, Levey AS, Coresh J, Hemmelgarn BR. Clinical risk implications of the CKD Epidemiology Collaboration (CKD-EPI) equation compared with the Modification of Diet in Renal Disease (MDRD) Study equation for estimated GFR. *Am J Kidney Dis*. 2012; 60(2):241–9. Epub 2012/05/09. doi: 10.1053/j.ajkd.2012.03.016 PMID: 22560843.
8. Cordain, L.; Eaton, S.B.; Sebastian, A.; Mann, N.; Lindeberg, S.; Watkins, B.A.; O'Keefe, J.H.; Brand-Miller, J. Origins and evolution of the Western diet: Health implications for the 21st century. *Am. J. Clin. Nutr.* 2005,81, 341–354. [PubMed].





**Kalyani U. Chande et al.,**

9. Dunkler, D.; Kohl, M.; Teo, K.K.; Heinze, G.; Dehghan, M.; Clase, C.M.; Gao, P.; Yusuf, S.; Mann, J.F.; Oberbauer, R. Dietary risk factors for incidence or progression of chronic kidney disease in individuals with type 2 diabetes in the European Union. *Nephrol. Dial. Transplant.* 2015, 30, 76–85.
10. Levey AS, de Jong PE, Coresh J, et al. The definition, classification, and prognosis of chronic kidney disease: a KDIGO Controversies Conference report. *Kidney Int* 2011;80:17-28.
11. Armstrong JE, Laing DG, Wilkes FJ, Kainer G. Smell and taste function in children with chronic kidney disease. *Pediatr Nephrol* 2010;25:1497-504.
12. Vaziri ND, Yuan J, Norris K. Role of urea in intestinal barrier dysfunction and disruption of epithelial tight junction in chronic kidney disease. *Am J Nephrol* 2013; 37:1-6.
13. Choi, D.-H.; Cho, J.-Y.; Koo, J.-H.; Kim, T.-K. Effects of Electrolyte Supplements on Body Water Homeostasis and Exercise Performance during Exhaustive Exercise. *Appl. Sci.* 2021, 11, 9093. <https://doi.org/10.3390/app11199093>
14. Susan M. Ott, Grahame J. Elder, Chapter 54 - Osteoporosis associated with chronic kidney disease, Editor(s): David W. Dempster, Jane A. Cauley, Mary L. Bouxsein, Felicia Cosman, Marcus and Feldman's Osteoporosis (Fifth Edition), Academic Press, 2021, Pages 1325-1380, ISBN 9780128130735, <https://doi.org/10.1016/B978-0-12-813073-5.00054-X>. (<https://www.sciencedirect.com/science/article/pii/B978012813073500054X>)
15. <https://www.urmc.rochester.edu/encyclopedia/content.aspx?contenttypeid=85&contentid=P08231#:~:text=The%20kidneys%20remove%20waste%20products,tube%20called%20a%20renal%20tubule.>
16. Kraut JA, Kurtz I. Metabolic acidosis of CKD: diagnosis, clinical characteristics, and treatment. *American journal of kidney diseases: the official journal of the National Kidney Foundation.* 2005;45(6):978–993.
17. Weiner ID, Verlander JW. Renal ammonia metabolism and transport. *Comprehensive Physiology.* 2013;3(1):201–220
18. Souma Tomokazu, Suzuki Norio, Yamamoto Masayuki -Renal erythropoietin-producing cells in health and disease , *Frontiers in Physiology* Volume 6 (2015) <https://www.frontiersin.org/articles/10.3389/fphys.2015.00167> DOI=10.3389/fphys.2015.00167 ISSN=1664-042X
19. Rajan VR, Mitch WE. Muscle wasting in chronic kidney disease: the role of the ubiquitin proteasome system and its clinical impact. *Pediatr Nephrol.* 2008 Apr;23(4):527-35. doi: 10.1007/s00467-007-0594-z. Epub 2007 Nov 7. PMID: 17987322; PMCID: PMC2259254.
20. Lee JY, Han SH. Blood pressure control in patients with chronic kidney disease. *Korean J Intern Med.* 2021 Jul;36(4):780-794. doi: 10.3904/kjim.2021.181. Epub 2021 Jun 22. PMID: 34153181; PMCID: PMC8273817.
21. Keller F. Nephrotoxische Störungen und nierenabhängige Arzneimittel. In: Risler T, Kühn K, editors. *Facharzt Nephrologie.* München: Urban & Fischer; 2008. pp. 891–960.
22. Ko GJ, Obi Y, Tortorici AR, Kalantar-Zadeh K. Dietary protein intake and chronic kidney disease. *Curr Opin Clin Nutr Metab Care* 2017;20:77-85.
23. Sällström J, Carlström M, Olerud J, et al. High-protein-induced glomerular hyperfiltration is independent of the tubuloglomerular feedback mechanism and nitric oxide synthases. *Am J Physiol Regul Integr Comp Physiol* 2010;299:R1263-R1268
24. Cirillo M, Lombardi C, Chiricone D, De Santo NG, Zanchetti A, Bilancio G. Protein intake and kidney function in the middle-age population: contrast between cross-sectional and longitudinal data. *Nephrol Dial Transplant* 2014;29:1733-40.
25. Ruilope LM, Casal MC, Praga M, et al. Additive antiproteinuric effect of converting enzyme inhibition and a low protein intake. *J Am Soc Nephrol* 1992;3:1307-11.
26. Garneata L, Stancu A, Dragomir D, Stefan G, Mircescu G. Ketoanalogue-supplemented vegetarian very low-protein diet and CKD progression. *J Am Soc Nephrol* 2016;27:2164-76.
27. Ko GJ, Obi Y, Tortorici AR, Kalantar-Zadeh K. Dietary protein intake and chronic kidney disease. *Curr Opin Clin Nutr Metab Care* 2017;20:77-85.
28. Adeva, M.M.; Souto, G. Diet-induced metabolic acidosis. *Clin. Nutr.* 2011, 30, 416–421. [CrossRef] [PubMed].
29. Scialla, J.J.; Appel, L.J.; Wolf, M.; Yang, W.; Zhang, X.; Sozio, S.M.; Miller, E.R.; Bazzano, L.A.; Cuevas, M.; Glenn, M.J.; et al. Plant Protein Intake Is Associated with Fibroblast Growth Factor 23 and Serum Bicarbonate



**Kalyani U. Chande et al.,**

- Patients with CKD: The Chronic Renal Insufficiency Cohort Study. *J. Ren. Nutr.* 2012, 22, 379–388.[CrossRef] [PubMed].
30. Azadbakht, L.; Atabak, S.; Esmailzadeh, A. Soy Protein Intake, Cardiorenal Indices, and C-Reactive Protein in Type 2 Diabetes With Nephropathy: A longitudinal randomized clinical trial. *Diabetes Care* 2008, 31,648–654. [CrossRef] [PubMed].
  31. Kontessis, P.; Jones, S.; Dodds, R.; Trevisan, R.; Nosadini, R.; Fioretto, P.; Borsato, M.; Sacerdoti, D.; Viberti, G. Renal, metabolic and hormonal responses to ingestion of animal and vegetable proteins. *Kidney Int.* 1990, 38,136–144. [CrossRef] [PubMed].
  32. Garneata, L.; Stancu, A.; Dragomir, D.; Stefan, G.; Mircescu, G. Ketoanalogue-Supplemented Vegetarian VeryLow-Protein Diet and CKD Progression. *J. Am. Soc. Nephrol.* 2016, 27, 2164–2176. [CrossRef] [PubMed].
  33. Mentz A, O'Donnell MJ, Rangarajan S, et al. Association of urinary sodium and potassium excretion with blood pressure. *N Engl J Med* 2014; 371: 601-11.
  34. He FJ, Li J, Macgregor GA. Effect of longer-term modest salt reduction on blood pressure. *Cochrane Database Syst Rev* 2013; 4: CD004937.
  35. O'Donnell M, Mentz A, Yusuf S. Sodium intake and cardiovascular health. *Circ Res* 2015; 116: 1046-57.
  36. Kwakernaak AJ, Krikken JA, Binnenmars SH, et al. Effects of sodium restriction and hydrochlorothiazide on RAAS blockade efficacy in diabetic nephropathy: a randomised clinical trial. *Lancet Diabetes Endocrinol* 2014; 2: 385-95.
  37. McMahon EJ, Bauer JD, Hawley CM, et al. A randomized trial of dietary sodium restriction in CKD. *J Am Soc Nephrol* 2013; 24: 2096-103.
  38. Smyth A, Dunkler D, Gao P, et al. The relationship between estimated sodium and potassium excretion and subsequent renal outcomes. *Kidney Int* 2014; 86: 1205- 12.
  39. He J, Mills KT, Appel LJ, et al. Urinary sodium and potassium excretion and CKD progression. *J Am Soc Nephrol* 2016; 27: 1202-12.
  40. Mills KT, Chen J, Yang W, et al. Sodium excretion and the risk of cardiovascular disease in patients with chronic kidney disease. *JAMA* 2016; 315: 2200-10.
  41. Stolarz-Skrzypek K, Kuznetsova T, Thijs L, et al. Fatal and nonfatal outcomes, incidence of hypertension, and blood pressure changes in relation to urinary sodium excretion. *JAMA* 2011; 305: 1777-85.
  42. Kovesdy CP, Lott EH, Lu JL, et al. Hyponatremia, hypernatremia, and mortality in patients with chronic kidney disease with and without congestive heart failure. *Circulation* 2012; 125: 677-84.
  43. Sontrop JM, Dixon SN, Garg AX, et al. Association between water intake, chronic kidney disease, and cardiovascular disease: a cross-sectional analysis of NHANES data. *Am J Nephrol* 2013; 37: 434-42.
  44. Sim JJ, Bhandari SK, Smith N, et al. Phosphorus and risk of renal failure in subjects with normal renal function. *Am J Med* 2013; 126: 311-8.
  45. Gutiérrez OM, Mannstadt M, Isakova T, et al. Fibroblast growth factor 23 and mortality among patients undergoing hemodialysis. *N Engl J Med* 2008; 359: 584- 92.
  46. Faul C, Amaral AP, Oskouei B, et al. FGF23 induces left ventricular hypertrophy. *J Clin Invest* 2011; 121: 4393-408.
  47. Kalantar-Zadeh K, Gutekunst L, Mehrotra R, et al. Understanding sources of dietary phosphorus in the treatment of patients with chronic kidney disease. *Clin J Am Soc Nephrol* 2010; 5: 519-30.
  48. Moorthi RN, Armstrong CL, Janda K, Ponsler-Sipes K, Asplin JR, Moe SM. The effect of a diet containing 70% protein from plants on mineral metabolism and musculoskeletal health in chronic kidney disease. *Am J Nephrol* 2014; 40: 582-91.
  49. Sullivan C, Sayre SS, Leon JB, et al. Effect of food additives on hyperphosphatemia among patients with end-stage renal disease: a randomized controlled trial. *JAMA* 2009; 301: 629-35.
  50. Lynch KE, Lynch R, Curhan GC, Brunelli SM. Prescribed dietary phosphate restriction and survival among hemodialysis patients. *Clin J Am Soc Nephrol* 2011; 6: 620-9
  51. Tonelli M, Pannu N, Manns B. Oral phosphate binders in patients with kidney failure. *N Engl J Med* 2010; 362: 1312- 24.





**Kalyani U. Chande et al.,**

52. Adrogué, H.J.; Madias, N.E. Sodium and Potassium in the Pathogenesis of Hypertension. *N. Engl. J. Med.* 2007, 356, 1966–1978. [CrossRef] [PubMed].
53. Palmer BF, Clegg DJ. Achieving the benefits of a high-potassium, paleolithic diet, without the toxicity. *Mayo Clin Proc* 2016;91:496-508.
54. Tyson CC, Kuchibhatla M, Patel UD, Pun PH, Chang A, Nwankwo C, Joseph MA, Svetkey LP. Impact of Kidney Function on Effects of the Dietary Approaches to Stop Hypertension (Dash) Diet. *J Hypertens (Los Angel)*. 2014;3:1000168. doi: 10.4172/2167-1095.1000168. PMID: 26380159; PMCID: PMC4569133..
55. He J, Mills KT, Appel LJ, et al. Urinary sodium and potassium excretion and CKD progression. *J Am Soc Nephrol* 2016;27: 1202-12.
56. Chen Y, Sang Y, Ballew SH, et al. Race, serum potassium, and associations with ESRD and mortality. *Am J Kidney Dis* 2017; 70:244-51.
57. Noori, N.; Kalantar-Zadeh, K.; Kovesdy, C.P.; Murali, S.B.; Bross, R.; Nissenson, A.R.; Kopple, J.D. Dietary potassium intake and mortality in long-term hemodialysis patients. *Am. J. Kidney Dis.* 2010, 56, 338–347. [CrossRef] [PubMed]
58. Noori N, Kalantar-Zadeh K, Kovesdy CP, et al. Dietary potassium intake and mortality in long-term hemodialysis patients. *Am J Kidney Dis* 2010;56:338-47
59. Khoueiry G, Waked A, Goldman M, et al. Dietary intake in hemodialysis patients does not reflect a heart healthy diet. *J Ren Nutr* 2011;21:438-47.
60. St-Jules DE, Goldfarb DS, Sevick MA. Nutrient non-equivalence: does restricting high-potassium plant foods help to prevent hyperkalemia in hemodialysis patients? *J Ren Nutr* 2016;26:282-7.
61. Goraya, N.; Simoni, J.; Jo, C.-H.; Wesson, D.E. A Comparison of Treating Metabolic Acidosis in CKD Stage 4 Hypertensive Kidney Disease with Fruits and Vegetables or Sodium Bicarbonate. *Clin. J. Am. Soc. Nephrol.* 2013, 8, 371–381. [CrossRef] [PubMed]
62. de Zeeuw D, Agarwal R, Amdahl M, et al. Selective vitamin D receptor activation with paricalcitol for reduction of albuminuria in patients with type 2 diabetes (VITAL study): a randomised controlled trial. *Lancet* 2010;376:1543-51.
63. Cheng, J.; Zhang, W.; Zhang, X.; Li, X.; Chen, J. Efficacy and Safety of Paricalcitol Therapy for Chronic Kidney Disease: A Meta-Analysis. *Clin. J. Am. Soc. Nephrol.* 2012, 7, 391–400. [CrossRef] [PubMed]
64. Tomasello, S.P.B. Secondary Hyperparathyroidism and Chronic Kidney Disease. *Diabetes Spectr.* 2008, 21, 19–25. [CrossRef]
65. Johnson, D.W.; Atai, E.; Chan, M.; Phoon, R.K.S.; Scott, C.; Toussaint, N.D.; Turner, G.L.; Usherwood, T.; Wiggins, K.J. KHA-CARI Guideline: Early chronic kidney disease: Detection, prevention and management. *Nephrology* 2013, 18, 340–350. [CrossRef] [PubMed]
66. Saravanan, P.; Davidson, N.C. Risk Assessment for Sudden Cardiac Death in Dialysis Patients. *Circ. Arrhythm. Electrophysiol.* 2010, 3, 553–559. [CrossRef] [PubMed].
67. Drechsler, C.; Pilz, S.; Obermayer-Pietsch, B.; Verduijn, M.; Tomaschitz, A.; Krane, V.; Espe, K.; Dekker, F.; Brandenburg, V.; März, W.; et al. Vitamin D deficiency is associated with sudden cardiac death, combined cardiovascular events, and mortality in haemodialysis patients. *Eur. Heart J.* 2010, 31, 2253–2261. [CrossRef] [PubMed]
68. Pilz, S.; Iodice, S.; Zittermann, A.; Grant, W.B.; Gandini, S. Vitamin D Status and Mortality Risk in CKD: A Meta-analysis of Prospective Studies. *Am. J. Kidney Dis.* 2011, 58, 374–382. [CrossRef] [PubMed]
69. Goodman, W.G.; Goldin, J.; Kuizon, B.D.; Yoon, C.; Gales, B.; Sider, D.; Wang, Y.; Chung, J.; Emerick, A.; Greaser, L.; et al. Coronary-Artery Calcification in Young Adults with End-Stage Renal Disease Who Are Undergoing Dialysis. *N. Engl. J. Med.* 2000, 342, 1478–1483. [CrossRef] [PubMed]
70. Block, G.A.; Hulbert-Shearon, T.E.; Levin, N.W.; Port, F.K. Association of serum phosphorus and calcium x phosphate product with mortality risk in chronic hemodialysis patients: A national study. *Am. J. Kidney Dis.* 1998, 31, 607–617. [CrossRef] [PubMed]
71. Keyzer, C.A.; Lambers-Heerspink, H.J.; Joosten, M.M.; Deetman, P.E.; Gansevoort, R.T.; Navis, G.; Kema, I.P.; de Zeeuw, D.; Bakker, S.J.; de Borst, M.H.; Group, P.S. Plasma Vitamin D Level and Change in Albuminuria and eGFR According to Sodium Intake. *Clin. J. Am. Soc. Nephrol.* 2015, 10, 2119–2127. [CrossRef] [PubMed]





**Kalyani U. Chande et al.,**

72. Zheng, Z.; Shi, H.; Jia, J.; Li, D.; Lin, S. Vitamin D supplementation and mortality risk in chronic kidney disease: A meta-analysis of 20 observational studies. *BMC Nephrol.* 2013, 14, 199. [CrossRef] [PubMed]
73. Mann, M.C.; Hobbs, A.J.; Hemmelgarn, B.R.; Roberts, D.J.; Ahmed, S.B.; Rabi, D.M. Effect of oral vitamin D analogus on mortality and cardiovascular outcomes among adults with chronic kidney disease: A meta-analysis. *Clin. Kidney J.* 2015, 8, 41–48. [CrossRef] [PubMed]
74. Morrone, L.F.; Cozzolino, M. The beneficial impact of vitamin D treatment in CKD patients: What's next? *Clin. Kidney J.* 2015, 8, 38–40. [CrossRef] [PubMed]
75. Theodoratou, E.; Tzoulaki, I.; Zgaga, L.; Ioannidis, J.P.A. Vitamin D and multiple health outcomes: Umbrella review of systematic reviews and meta-analyses of observational studies and randomised trials. *BMJ* 2014, 348, g2035. [CrossRef] [PubMed]
76. Spiegel DM, Brady K. Calcium balance in normal individuals and in patients with chronic kidney disease on low- and high-calcium diets. *Kidney Int* 2012;81: 1116-22.
77. Bushinsky DA. Clinical application of calcium modeling in patients with chronic kidney disease. *Nephrol Dial Transplant* 2012;27:10-3.
78. Hill KM, Martin BR, Wastney ME, et al. Oral calcium carbonate affects calcium but not phosphorus balance in stage 3-4 chronic kidney disease. *Kidney Int* 2013; 83:959-66.
79. Chiavaroli L, Mirrahimi A, Sievenpiper JL, Jenkins DJ, Darling PB. Dietary fiber effects in chronic kidney disease: a systematic review and meta-analysis of controlled feeding trials. *Eur J Clin Nutr* 2015;69:761-8.
80. Kovesdy CP, Kopple JD, Kalantar-Zadeh K. Management of protein-energy wasting in non-dialysis-dependent chronic kidney disease: reconciling low protein intake with nutritional therapy. *Am J Clin Nutr* 2013;97:1163-77.
81. Kalantar-Zadeh K, Fouque D. Nutritional Management of Chronic Kidney Disease. *N Engl J Med.* 2017 Nov 2;377(18):1765-1776. doi: 10.1056/NEJMra1700312. PMID: 29091561.
82. Kim SM, Jung JY. Nutritional management in patients with chronic kidney disease. *Korean J Intern Med.* 2020 Nov;35(6):1279-1290. doi: 10.3904/kjim.2020.408. Epub 2020 Sep 23. PMID: 32872726; PMCID: PMC7652660.
83. Snelson, M.; Clarke, R.E.; Coughlan, M.T. Stirring the Pot: Can Dietary Modification Alleviate the Burden of CKD? *Nutrients* 2017, 9, 265. <https://doi.org/10.3390/nu9030265>
84. Bach-Faig, A.; Berry, E.M.; Lairon, D.; Reguant, J.; Trichopoulou, A.; Dernini, S.; Medina, F.X.; Battino, M.; Belahsen, R.; Miranda, G.; et al. Mediterranean diet pyramid today. Science and cultural updates. *Public Health Nutr.* 2011, 14, 2274–2284. [CrossRef].
85. Tosti, V.; Bertozzi, B.; Fontana, L. Health benefits of the Mediterranean diet: Metabolic and molecular mechanisms. *J. Gerontol. Biol. Sci. Med. Sci.* 2018, 73, 318–326. [CrossRef] [PubMed].
86. Romani, A.; Campo, M.; Urciuoli, S.; Marrone, G.; Noce, A.; Bernini, R. An industrial and sustainable platform for the production of bioactive micronized powders and extracts enriched in polyphenols from *Olea europaea* L. and *Vitis vinifera* L. wastes. *Front. Nutr.* 2020, 7, 120. [CrossRef] [PubMed].
87. Martinez-Gonzalez, M.A.; Gea, A.; Ruiz-Canela, M. The Mediterranean diet and cardiovascular health. *Circ. Res.* 2019, 124,779–798. [CrossRef] [PubMed].
88. Romani, A.; Bernini, R.; Noce, A.; Urciuoli, S.; Di Lauro, M.; Zaitseva, A.P.; Marrone, G.; Di Daniele, N. Potential beneficial effects of extra virgin olive oils characterized by high content in minor polar compounds in nephropathic patients: A pilot study. *Molecules* 2020, 25, 4757. [CrossRef] [PubMed].
89. Romani, A.; Ieri, F.; Urciuoli, S.; Noce, A.; Marrone, G.; Nediani, C.; Bernini, R. Health effects of phenolic compounds found in extra-virgin olive oil, by-products, and leaf of *Olea europaea* L. *Nutrients* 2019, 11, 1776. [CrossRef].
90. Goraya N, Simoni J, Jo C, Wesson DE. Dietary acid reduction with fruits and vegetables or bicarbonate attenuates kidney injury in patients with a moderately reduced glomerular filtration rate due to hypertensive nephropathy. *Kidney Int.* 2012;81(1):86–93.
91. Cupisti, A.; Kovesdy, C.P.; D'Alessandro, C.; Kalantar-Zadeh, K. Dietary approach to recurrent or chronic hyperkalaemia in patients with decreased kidney function. *Nutrients* 2018, 10, 261. [CrossRef].
92. Huo, R.; Du, T.; Xu, Y.; Xu, W.; Chen, X.; Sun, K.; Yu, X. Effects of Mediterranean-style diet on glycemic control, weight loss and cardiovascular risk factors among type 2 diabetes individuals: A meta-analysis. *Eur. J. Clin. Nutr.* 2015, 69, 1200–1208. [CrossRef] [PubMed]





**Kalyani U. Chande et al.,**

93. Asghari G, Yuzbashian E, Mirmiran P, Azizi F. The association between Dietary Approaches to Stop Hypertension and incidence of chronic kidney disease in adults: the Tehran Lipid and Glucose Study. *Nephrol Dial Transplant.* 2017;32:ii224–30.
94. Liu Y, Kuczmarski MF, Miller ER, Nava MB, Zonderman AB, Evans MK, et al. Dietary habits and risk of kidney function decline in an urban population. *J Ren Nutr.* 2017;27:16–25 This study observed a lower, albeit non-significant, risk of CKD for those with greater adherence to DASH diet.
95. Rebhholz C, Crews D, Grams M, Steffen L, Levey A, Miller E 3rd, et al. DASH (Dietary Approaches to Stop Hypertension) diet and risk of subsequent kidney disease. *Am J Kidney Dis.* 2016;68:853– 61.
96. Fenton, T.R.; Huang, T. Systematic review of the association between dietary acid load, alkaline water and cancer. *BMJ Open* 2016, 6, e010438. [CrossRef] [PubMed].
97. Dwyer, J.; Foulkes, E.; Evans, M.; Ausman, L. Acid/alkaline ash diets: Time for assessment and change. *J. Am. Diet. Assoc.* 1985, 85, 841–845.
98. KDIGO. Chapter 3: Management of progression and complications of CKD. *Kidney Int.* 2013, 3, 73–90. [CrossRef]
99. Yari, Z.; Mirmiran, P. Alkaline diet: A novel nutritional strategy in chronic kidney disease? *Iran. J. Kidney Dis.* 2018, 12, 204–208. [PubMed]
100. Scialla, J.J.; Appel, L.J.; Astor, B.C.; Miller, E.R.; Beddhu, S.; Woodward, M.; Parekh, R.S.; Anderson, C.A. Net endogenous acid production is associated with a faster decline in GFR in African Americans. *Kidney Int.* 2012, 82, 106–112. [CrossRef] [PubMed]
101. Mahajan, A.; Simoni, J.; Sheather, S.J.; Broglio, K.R.; Rajab, M.H.; Wesson, D.E. Daily oral sodium bicarbonate preserves glomerular filtration rate by slowing its decline in early hypertensive nephropathy. *Kidney Int.* 2010, 78, 303–309. [CrossRef]
102. Ruster, C.; Wolf, G. Renin-angiotensin-aldosterone system and progression of renal disease. *J. Am. Soc. Nephrol.* 2006, 17, 2985–2991. [CrossRef]
103. Wesson, D.E. Endogenous endothelins mediate increased acidification in remnant kidneys. *J. Am. Soc. Nephrol.* 2001, 12, 1826–1835. [CrossRef]
104. Dhaun, N.; Goddard, J.; Webb, D.J. The endothelin system and its antagonism in chronic kidney disease. *J. Am. Soc. Nephrol.* 2006, 17, 943–955. [CrossRef]
105. Ramezani, A.; Raj, D.S. The gut microbiome, kidney disease, and targeted interventions. *J. Am. Soc. Nephrol.* 2014, 25, 657–670. [CrossRef] [PubMed]

**Table 1** Allopathic drugs used in treatment of chronic kidney failure [21].

Class	Drugs
Analgesics	Pethidine
Antibiotics	Cefepime
Phase- prophylactic psychotropic drugs	Lithium
Anti diabetics drugs	Metformin, Glibenclamide, Gimepiride
Diuretics	Spirolactone, Eplerenone
Immune Suppressants	Methotrexate
Radiological contrast media	Gadolinium
LMW- Heparin	Enoxaparin

**Table 2** Nutritional content for patients with CDK [82]

Dietary constituent	Diet (variables)	Baseline eGFR <sub>CR</sub> , mL/min/1.73 m <sup>2</sup>	Findings
Protein	Protein intake (Divided into quintiles)	Normal: > 80 Mild CKD: 55–80	A high-protein diet was not linked to a decline in eGFR <sub>cr</sub> in people with healthy kidney function. In mild CKD, it was connected to accelerated





Kalyani U. Chande et al.,

			eGFRcr decline.
	Protein intake (Divided into quartiles)	Mean 93.9 ± 14.1	An elevated risk of kidney hyperfiltration and a quick decline in kidney function was associated with a high protein diet.
	Low protein diet (0.6 g/kg/day) compared to the typical protein diet (1.3 g/kg/day)	25–55 (mean 38.6)	At 3 years, the mean eGFRcr decline was the same for both diet groups.
	0.6 g/kg/day of low protein vs. 0.3 g/kg/day of very low protein with ketoacid	13–24 (mean 18.5)	A very low protein diet with supplements slightly slows the loss of eGFRcr.
	0.6 g/kg/day of low protein vs. 0.3 g/kg/day of very low protein with ketoacid	< 30 (mean 18.0)	The risk of CKD progression was reduced by supplementing with a very low protein diet.
<b>Sodium</b>	Urinary sodium	Mean 68.4 ± 17.6	The risk of CKD progression was not increased by urinary sodium excretion.
	Urinary sodium	41.5–48.5	Increased risk of CKD progression was linked to higher urinary sodium excretion.
<b>Potassium</b>	Urinary potassium	41.5–48.5	Increased risk of CKD progression was linked to higher urinary potassium excretion.
	Urinary potassium	32.6	Lower risk of death from any cause was associated with higher urine potassium excretion, but not kidney failure.
<b>Phosphorus</b>	Urinary phosphate	33	The risk of KF and mortality is not correlated with higher urinary phosphate excretion.
	Prescribed dietary phosphate	Hemodialysis	In patients receiving frequent hemodialysis, dietary phosphate restriction is not linked to a higher survival rate.
<b>Calcium</b>	Dietary calcium	54.8	To avoid calcium deficiency and calcium loading, the daily recommended total intake of elemental calcium should be between 800 and 1,200 mg.
<b>Vitamin D</b>	Ergocalciferol	Hemodialysis	Ergocalciferol taken orally has the ability to raise 25(OH)D levels without significantly changing blood calcium, phosphate, or parathyroid hormone levels.
	Cholecalciferol	34.6–35.8	In nondiabetic early CKD, cholecalciferol supplementation to correct vitamin D deficiency has positive effects on vascular function.

Table 3 Nutritional Recommendation for Patients [82]

Dietary constituent	Nutritional recommendations
Protein	A protein intake of 0.6-0.8 g/kg/day is advised for patients with CKD G3b, G4, or G5 or patients with proteinuria (urinary protein excretion > 0.3 g/day). Dialysis patients should take between 1.0 and 1.2 g/kg/day. For every 1 g of urinary protein excretion over 5 g per day, patients with nephrotic syndrome should consume 0.8 g/kg/day plus 1 g/day of protein. 0.8-1.0 g/kg/day is advised for patients with nonproteinuric CKD G1, G2, elderly patients with CKD G3b, and those whose CKD is slowly progressing.





**Kalyani U. Chande et al.,**

<i>Sodium</i>	It is advised to consume less than 2 g of sodium (or about 5 g of salt) per day.
<i>Potassium</i>	It is advised to follow customised regimens to keep serum potassium levels within the normal range. Consider reducing dietary potassium intake to keep serum potassium levels within the normal range in CKD patients who display hyperkalemia.
<i>Phosphorus</i>	To keep serum phosphate within the normal range in patients with CKD G3-5 and KF on replacement therapy, 0.8-1 g/day or customised regimens are advised. Consider reducing dietary phosphorus intake to keep serum phosphate levels in the normal range in CKD patients who show hyperphosphatemia. Phosphorus intake from vegetables should be increased, and processed food should be avoided at all costs.
<i>Calcium</i>	To maintain normal calcium levels in CKD G3, G4 patients who are not taking active vitamin D analogues, 800-1,000 mg/day of elemental calcium may be prescribed. Adjust calcium intake (dietary calcium, calcium supplements, or calcium-based binders) in KF patients receiving replacement therapy according to the concurrent use of vitamin D analogues and calci-mimetics to prevent hypercalcemia.
<i>Vitamin D</i>	Vitamin D supplementation in the form of cholecalciferol or ergocalciferol may be considered in CKD patients who show signs of 25(OH)D deficiency only for deficiency/insufficiency, not for CKD-MBD or other clinically relevant outcomes. Individualized plans for vitamin D supplementation should be made, and serum levels of calcium, phosphorus, and 25(OH)D should be checked periodically, particularly in patients taking calcium-containing phosphate binders and/or active vitamin D analogues.





Kalyani U. Chande et al.,

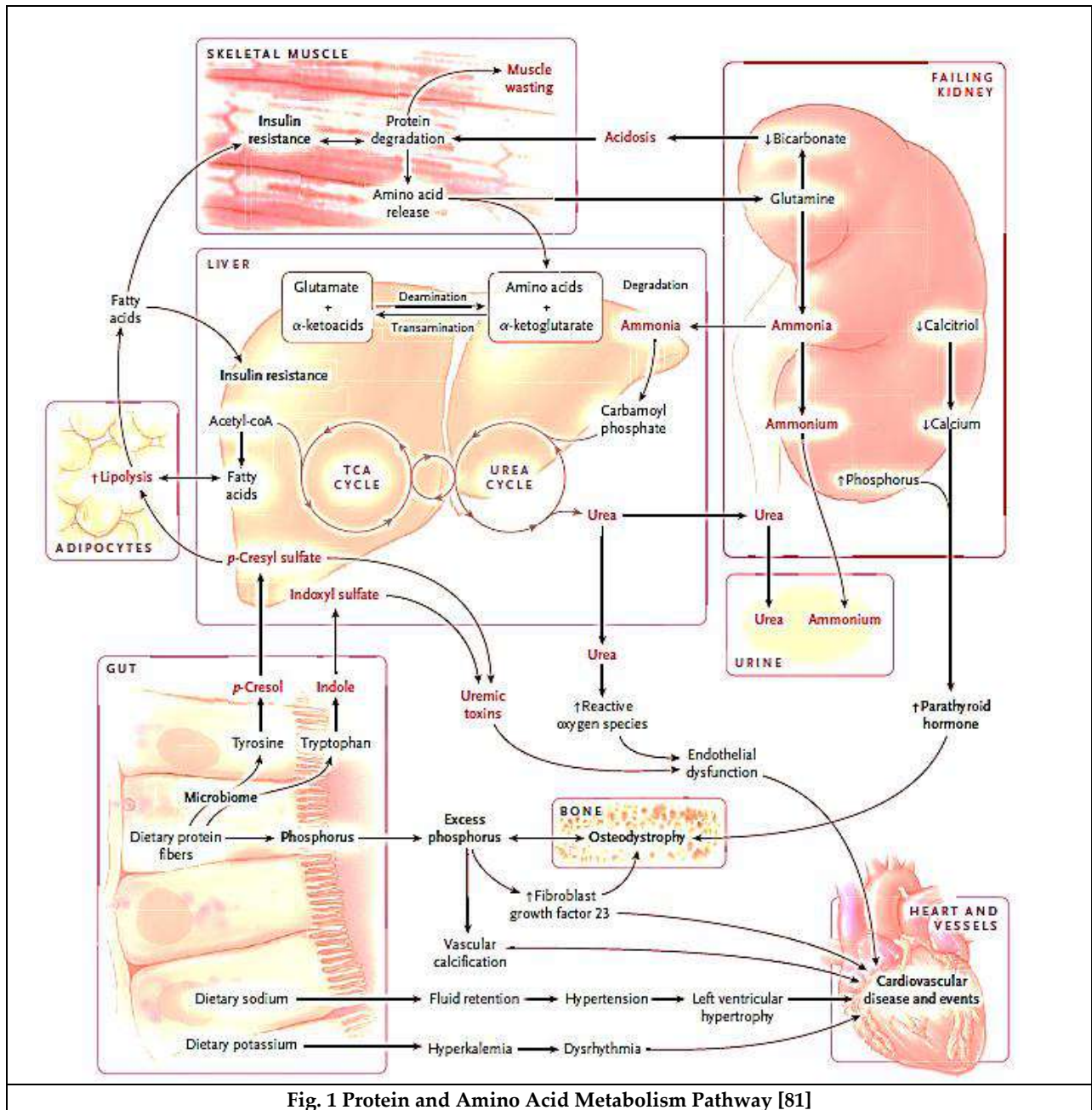


Fig. 1 Protein and Amino Acid Metabolism Pathway [81]







Kalyani U. Chande et al.,

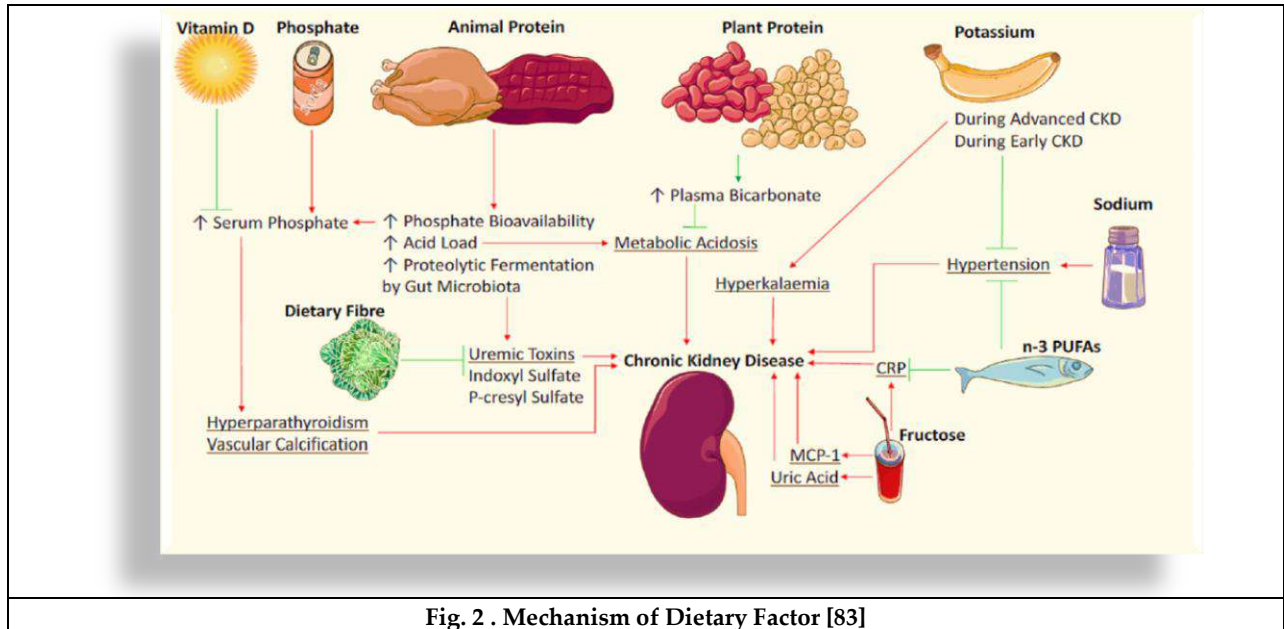


Fig. 2 . Mechanism of Dietary Factor [83]







## The Heavy Metal Pollution is Detected by Fish as a Bioindicator

M. Elavarasi<sup>1</sup> and B. Aruljothi<sup>2\*</sup>

<sup>1</sup>Research Scholar, Department of Zoology, Government Arts College, Chidambaram, (Affiliated to Thiruvalluvar University, Vellore), Tamil Nadu, India.

<sup>2</sup>Associate Professor, Department of Zoology, Government Arts College, Chidambaram, (Affiliated to Thiruvalluvar University, Vellore), Tamil Nadu, India.

Received: 16 Feb 2024

Revised: 21 Aug 2024

Accepted: 19 Oct 2024

### \*Address for Correspondence

#### B. Aruljothi

Associate Professor, Department of Zoology,  
Government Arts College, Chidambaram,  
(Affiliated to Thiruvalluvar University, Vellore),  
Tamil Nadu, India.



This is an Open Access Journal / article distributed under the terms of the **Creative Commons Attribution License** (CC BY-NC-ND 3.0) which permits unrestricted use, distribution, and reproduction in any medium, provided the original work is properly cited. All rights reserved.

### ABSTRACT

As a result of their toxicity, persistence, bioaccumulation, and biomagnification properties, heavy metal pollution poses a significant threat to the environment. The environment may become contaminated with heavy metals from a variety of anthropogenic and natural sources. The primary anthropogenic sources of heavy metals are industrial and agricultural processes, the combustion of fossil fuels and gasoline, waste incinerators, mining, and volcanic eruption and weathering of metal-bearing rocks, among other things. These heavy metals' mobilisation into the aquatic ecosystem changes the physicochemical features of water, endangering aquatic organisms. After a fish ingests diet that has stored metals, the digestive tract, body surface, and gills are the main entry points for heavy metals. The maximum recurrent heavy metal contaminants that produce extreme toxicity in fish include copper, zinc, chromium, nickel, cobalt, iron, aluminium, cadmium, mercury, arsenic, and lead. The key chemical mannerbasic metal toxicity is the increase of oxidative stress. Stress impairs reproductive capacity, damages tissue and organs, down the immune system, and results in growth defects. The necessary trace elements and micronutrients, crucial for growth and metabolism, are particularly copper, zinc, chromium, nickel, cobalt, and iron. The abundance of high-quality protein finds in fish, beside with its high vitamins & omega-3 fatty acid content, boosts societies to eat fish as a highest source of nutrition. As an end result, built-up heavy metals in fish tissues are directly transferred to humans, where they have toxic defects that speed the increase of numerous diseases. Hence, in order to implement the laws and regulations regulating their preservation in the water ecosystem and similarly to preserve human lives, it is vital to explain the foundations of heavy metals and their detrimental influence on fish health.

**Keywords:** Fish; bio – indicator; heavy metals; bioaccumulation; changes; water pollution.





## INTRODUCTION

One of the main issues facing modern human society is environmental degradation [1]. Environmental contamination is on the rise due to the quickly expanding industry, rising energy consumption, and careless depletion of natural resources over the past few decades [2]. Diverse organic and inorganic hazardous substances are continuously introduced into the aquatic environs from together natural and manmade sources. As an end result of both their toxicity and the propensity for bioaccumulation within the food chain, heavy metals play an important role in ecological contamination [3]. The chief sources of heavy metal emissions include coal-burning power plants, untreated sewage sludge, metal pipelines, traffic, and industrial output (foundries, smelt, oil refiner, petrochemical facilities, pesticide manufacture, chemical sector). Metals can be classified into two groups: those that are necessary for life and those that are not. The toxicity of non-essential metals, often known as xenobiotic or foreign elements, such as aluminium (Al), cadmium (Cd), mercury (Hg), tin (Sn), and lead (Pb), increases with concentrations and none of their biological functions have been established [84]. On the other hand, essential metals, such as copper (Cu), zinc (Zn), chromium (Cr), nickel (Ni), cobalt (Co), and iron (Fe), are recognised to have a significant biological role [85] and are hazardous when present in excessive concentrations or when there are metabolic shortages.

Fishes have various distinct advantages in defining the natural properties of aquatic systems and in evaluating changes to habitats, which makes them the most significant in biomonitors in aquatic systems for the assessment of metal pollution level [79,80]. The fish at the bottom of the aquatic food chain may also store metals and transmit them to people through their diet, resulting in chronic or acute disorders [82]. Animal health may be harmed and their regular physiological functions may be harmed by the biocontamination of poisonous heavy metals in their various tissues [4]. The capacity of a species to reproduce and its rate of survival are both significantly impacted by heavy metal poisoning. Dependent on the species dosage and exposure period, several of them have been informed to be highly oncogenic, mutagen casing, and teratogenic [5]. The purpose of the current article is to quickly discuss the toxicity, impact, and application of several heavy metals as bioindicators on fish health. In this study, both necessary and non-essential heavy metals are examined.

## TOXICITY

Toxicology refers to the degradation or loss of cell viability and regenerative capability that may arise from the reversible or irreversible disruption of normal metabolic processes. In severe circumstances, the body may lose all of its organs and perish. Due to things like the availability of certain enzymes, the local blood supply, and the organ's capability for regeneration, localised acute toxicity typically affects organs responsible for absorption and disposal. The skin, stomach, liver, intestines, lungs, and kidneys are a few of these. Names for this type of toxicity include nephrotoxicity for the kidneys and hepatotoxicity for the liver, depending on which organ or tissue is harmed.

## TESTING FOR TOXICITY

- A. A dosage threshold is the dose level below which an effect cannot be seen.
- B. The effective dosage, or LD50, is the dose that kills 50% of an animal population. Chemical acute toxicity is frequently quantified using the LD50. The acute toxicity decreases with increasing LD50. A substance is said to be potent if it has a low LD50 and is highly poisonous.
- C. A lethal concentration, or LC50, is the amount needed to kill 50% of a population.
- D. The pharmacological concentration at which a patient experience a 50% increase in response is known as the EC50.
- E. The dose that casing a definedeffect other than mortality in 50% of the animals is known as the ED50 (effective dose).
- F. The inhibitory concentration, or IC50, is the level at which the reaction or binding is abridged by 50%.



**THREATENERS TO TOXICITY:**

1. The harmful agent's chemical makeup
2. Concentration and Dose:
  - (a) The exposure method
  - (c) The duration of exposure
  - (c) Exposure time and
  - (d) Exposure route
3. Toxicant metabolism,
4. Gender
5. Age

**NECESSARY HEAVY METALS****COPPER (Cu)**

Additional sources of copper toxicity comprise the mining industry, sewage sludge industry, plastics industry, electro-plating manufacturing, metal purifying factories, atmospheric deposition, etc. [28,29]. Copper is a crucial micronutrient and trace element that is necessary for the growing and metabolic activity of living things. Copper is a crucial component of several metabolic enzymes and glycoproteins in fish and supplementary animals. Moreover, it is necessary for the neurological system and the manufacture of haemoglobin [30,31]. Nevertheless, copper has a harmful effect on living things at larger concentrations [32]. Freshwater fish become hazardous to copper at concentrations between 10 and 20 ppb [33]. Freshwater fish that were exposed to copper in the water developed oxidative stress symptoms [34]. Fish with chronic copper toxicity have poor development, shorter life spans, lowered immunological responses, and reproduction issues [35]. Apoptosis was induced by copper poisoning in the gills of teleost fish (*Oreochromis niloticus*) [36]. The liver tissue of *Cyprinus carpio* underwent biochemical and morphological alterations after disclosure to  $\text{CuSO}_4$  [37]. *Oreochromis mossambicus* that had been exposed to copper manifested a rise in RBC amount, haemoglobin level, and hematocrit rate [38]. This substance disrupts the operation of olfactory neurons and is neurotoxic to fish [39]. Zebrafish larva exposed to copper developed into more sensitive stages than early develop and mature stages and displayed lateral line malfunction [40]. When exposed to copper, the goldfish larvae *Carassius auratus* exhibited a significant rate of physical malformations and mortality [41]. Fish's gills and body tissue have less copper than their liver, which contains the highest percentage [42]. The oxidative metabolism, fat peroxidation, and protein contented in carp muscle were all affected by the trace element's bioaccumulation [43].

**ZINC (Zn)**

In living organisms, zinc (Zn) is an important trace component and micronutrient that is found in nearly every cell, is involved in the synthesis of nucleic acids, and can be found in many enzymes. It is the second most abundant trace element after iron [84]. Zn also plays a role in more complex processes such as cell signalling, the immune system, and neurotransmission [126,127]. At elevated quantities in the water, zinc wastes can be directly hazardous to fish [128], and either zinc alone or more frequently in combination with copper and other metals can have an impact on fisheries [102, 129]. The gills are the primary site of waterborne Zn poisoning [127], where the disruption of  $\text{Ca}^{2+}$  uptake results in hypocalcemia and final mortality [128]. The other end point of toxicity vary between freshwater and marine fish, with survival, growth, reproduction, and hatching being the most prevalent [127]. A target organ for Zn buildup is also thought to be the kidney of the fish [83].

Some freshwater fishes have considerably more active serum transaminases when zinc is present [130]. Chloride cells being pulled away from the underlying epithelium is the first indication of gill injury. Fish with *Oreochromis niloticus* showed pale and clogged gills when expose to zinc sulphate, according to Abd El-Gawad [131]. Through vacuolated epithelial layering of the gill rakers, the epithelial layer of the gill filaments was hyperplastic and oedematous. Telangiectasis might be seen in the lamellar blood spaces. According to research [132], exposure to zinc causes degeneration and hyperaemia in the ovarymuscle of *Tilapia nilotica*. Finally, innovative techniques for removing contaminants, containing heavy metals after wastewater, must be used to safeguard fish and aquatic systems from



**Elavarasi and Aruljothi**

heavy metal pollution. Activated carbon treatments in the form of powder or granules, ozonation, ultraviolet radiation, and reverse osmosis are a few of these [133].

**CHROMIUM (Cr)**

One of the greatest prevalent trace elements in both saltwater and the crust of the earth is chromium [6]. Several anthropogenic sources, such as leather tanneries, metal dispensation, fuelpurifying, fabric production, alloy production, timberconserving, etc., cause chromium toxicity in aquatic ecosystems [7,8]. Chromium toxicity to aquatic organisms depends on a number of biotic parameters, including age, developmental stage, and species type, as well as abiotic features, including pH, temperature, and water alkalinity. Fish that were first exposed to chromium had a variety of behavioural alterations, including erratic swimming, mucus secretion, analteration in body colour, and lack of appetite, among others [9]. *Cyprinus carpio* was chronically exposed to chromium at a dose of 2-200 mol/L, and this exposure caused cytotoxicity and a reduction in phagocyte and mitogen-induced lymphocyte activation [10]. When exposed to chromium, *Tilapia sparrmanii* had slower blood clotting times, which led to internal bleeding and are issues in pH [11].

Chromium buildup in *Labeo rohita*, an Indian big carp, reduces the amount of total protein and lipids in the tissue, liver, and gills [12]. *Colisa fasciatus*, a freshwater teleost, showed decreased hepatic glycogen upon exposure to chromium [13]. Cr<sup>6+</sup> poisoning in rainbow trout, *Salmo gairdneri*, demonstrated respiratory and osmoregulatory failure at pH 7.8 and 6.5 [14]. When Chinook salmon were showing to chromium over an extended period of time, it resulted in physiological anomalies, DNA impairment, microscopic lesions, and decreased growth and endurance rates [15]. Chromium disclosure at a dosage of 2 mg/L in rainbow trout *Salmo gairdneri* impaired egg hatching and fish growth [16]. Different fish tissues exhibit variable chromium bioaccumulation (Table 1). Chromium is accumulated most heavily in the gills, liver & kidney and at extremely low levels in muscle tissue [17].

**NICKEL(Ni)**

Nickel is a fairly common trace element that is found in mishmash with O<sub>2</sub> or sulphur in the environment. The environment is exposed to nickel from together natural and human-made sources. When new nickel is mined and converted into alloys or nickel mixtures, the element is released into the environment. Furthermore, nickel is emitted through waste incinerators, oil- and coal-burning power system, and coal-fired power plants [56]. At low concentrations, nickel is a necessary element for many species, but at excessive concentrations, it is hazardous [57]. The physiochemical characteristics of water, such as pH, ionic power, high temperature, hardness, and solidified organic carbon (DOC), among others, affect the poisonousness of nickel to fish [58]. When Nile tilapia were exposed to nickel chloride, they exhibited irregular swimming behaviour, fast opercular movement, respiratory disorders, and skin lesions. The blood parameters of Nile tilapia treated to nickel also changed, with a rise in RBC amount and a decrease in haemoglobin and WBC amounts [59].

Freshwater fish treated to nickel exhibited histopathological variations in various tissues, including the gills, kidney, liver, and intestine. *Molitrix hypophthalmichthys*. The liver tissue showed fusion of the gill lamellae, necrosis of the hepatocytes, blood vessel degeneration, enlargement, vacuolation, pyknotic nuclei, and wound. With exposure to nickel, tubular cells in the kidney tissue also showed signs of hyperplasia and degeneration [60].

Nickel exposure in both chronic and acute forms in freshwater fish decrease ATPase action in the brain in *oreochromis niloticus* [61]. exposure to nickel in freshwater fish *Prochilodus lineatus* caused DNA damage to equally blood cells and gills while affecting the liver's antioxidant defence system [62]. The common carp, *Cyprinus carpio*, experienced stress after being exposed to An extraordinary dose of nickel for a brief period of time. In *Cyprinus carpio*, exposure to sublethal nickel concentrations was also reported to alter haematological parameters and cause behavioural abnormalities [63]. *Cyprinus carpio*, a freshwater fish, revealed some negative effects of nickel toxicity on its protein metabolism. Later exposure to a deadly dose of nickel, the detected modifications were a decrease in structural, solvable, and entire proteins, an increase in unrestricted amino acids and protease action, and an increase in ammonia in the gill & kidney [64]. Before dying, fish with nickel poisoning displayed behavioural abnormalities such





### Elavarasi and Aruljothi

surfacing and fast mouth and operculum movement. Nickel builds up in fish blood, kidney, tissue, and liver, with kidney showing the largest accumulation [66]. *Tilapia nilotica*'s liver and muscle showed a general decline in glycogen levels as a end result of bioaccumulation. Elevated levels of nickel bioaccumulation lead to lymphopenia and leukopenia in *Tilapia nilotica* by increasing haemoglobin content, packed cell volume, and blood cell count.

#### COBALT(Co)

Cobalt is a crucial ingredient for male health and is a module of vitamin B12; nevertheless, because it interferes with the enzyme system, it also makes fish harmful in vital aquatic ecosystems [134]. It has recently been included to group 2A carcinogens due to reports that it may be a potentially cancer-causing substance (i. e., probably carcinogenic to humans). The amount of cobalt that is permitted to be present at any given time in the air, water, and earth is limited to 1-5 mg/m<sup>3</sup>, 1 mg/l, and 1 mg/m<sup>2</sup>, respectively. Cobalt content in rivers is minimal, at just approximately 0.2 mg/l [135]. The range of the daily average intake of cobalt in humans, in all forms, is 0.30 to 1.77 mg/day [136]. Moreover, it has been connected to controlling blood pressure [137]. and was discovered to be essential for healthy thyroid function [138]. Anemia, polycythemia, and congestive heart failure have all been linked to excessive cobalt use [139].

#### IRON (Fe)

Iron is a common component of mining and industrial effluents, which are frequently released into aquatic habitats. Fish are thought to be more poisonous to ferrous iron (Fe<sup>2+</sup>) than to ferric iron (Fe<sup>3+</sup>) [103]. The liver and gonads of fish had the maximum concentration of iron, while the brain, tissue, and heart had the lowest concentration [104,105]. In their work, Omar et al. [83] recently demonstrated that the fish liver is the organ that iron is most likely to target. As a potential mechanism for iron poisoning, physical gill blockage has been suggested as a cause of respiratory disturbance [106]. Solvable ferrous Hg can be converted into unsolvable ferric complexes, which can subsequently coat the gill lamellae and prevent respiration, because the surface of a fish's gills tends to be high pH [107].

Precipitated iron compounds have catastrophic effects on fish, including a reduction in the amount of gill space available for breathing, damage to the breathing epithelium, and eventual suffocation and death. Iron led to secondary lamellae hyperplasia and necrosis in banded tilapia (*Tilapia sparrmanii*) [108]. When exposed to iron, brook charr *Salvelinus fontinalis* (Mitchill) experienced respiratory distress, according to Gonzalez et al. [109], and *Tilapia sparrmanii*, according to Grobler et al. [105], experienced a lessening in action, coughing, yawning, spasmodic actions, and an upsurge in opercular actions (Smith). In agreement with past studies, Peuranen et al. [185] noted iron accumulation on the external of the gill epithelia of brown trout *Salmo trutta* L. that had been exposed to iron. They noted gill injury when exposed to iron concentrations of 0.8–1.7 mg/l at pH levels 5 and 6.

They hypothesised that because iron had only been found on the face and not inside the gill epithelia, it had to operate on the gill face to exhibit its deadly effects. The gills of *T. sparrmanii* collapsed and produced more mucus cells after being exposed to sublethal iron concentration for 72 hours in a continuous flow system, according to a scanning electron micrograph research [104]. Gill collapse lowers the distance at which water and blood diffuse, which helps fish consume less oxygen. Furthermore, iron complexes can impulsive on the surface of fish eggs, leading to oxygen deprivation and eventual death [90]. When given a diet high in Fe, *Clarias gariepinus* displayed constrained growth [111].

#### UNNECESSARY HEAVY METALS

##### ALUMINUM (Al)

After silicon and oxygen, aluminium (Al) is the third greatest prevalent and plentiful metal on earth [78]. It is comparable to numerous other metals in that its soluble ionic form is typically thought to be the most hazardous [87]. It is utilised as a flocculation agent in water management and can be detected in the air of large cities and industrialised areas [88,89]. Aluminum's toxicity to fish is significantly influenced by the physicochemical character of the water, particularly by its pH. At pH levels lower than 6.0, aluminium is soluble [90]. The reason of fish





**Elavarasi and Aruljothi**

poisoning has been discovered to be significant union of lamellae and filaments in the gills, intrusion with ionic and osmotic equilibrium, and respiratory issues as a result of mucous coagulation on the fish's gills [91]. In females of the *Oreochromis niloticus* species that are mature, Al is regarded as an endocrine disruptive substance [92]. Fish exposed to Al had significantly smaller mean corpuscular volume (MCV) and significantly greater mean corpuscular haemoglobin concentration (MCHC), hematocrit (Hct), and mean corpuscular haemoglobin (MCH) [93]. Fish development was significantly reduced when aluminium concentration as low as 0.52 mg/l were used [94]. In addition to structural gill damage [101], common physiological change in fish species exposed to Al include abnormalities in the cardiovascular [95], hematologic [96], respiratory, ion regulatory [97], reproductive [98], metabolic [99], and endocrine [100] systems.

**CADMIUM(Cd)**

The average quantity of cadmium in the earth's crust is amongst 0.1 and 0.5 ppm, and it is frequently associated with the ores of zinc, copper, & lead. The concentration is typically between 1 and 5 mg/L in surface and ground water, and between 5 and 110 mg/L in ocean water. Cadmium does not exist in element form in nature. Instead, chemical forms of cadmium, such as cadmium oxide, cadmium sulphate, and cadmium chloride, are used. Cadmium cyanide, nitrate, and carbonate are frequently observed. Many anthropogenic and natural sources transfer cadmium into the aquatic ecosystem. Cadmium is naturally obtained from the earth's crust and released through volcanic eruptions and rock weathering. Because it is a non-essential metal, cadmium is extremely hazardous to fish. *Cyprinus carpio* experienced DNA damage as a result of low-level cadmium exposure [18]. Cd<sup>2+</sup> was discovered to limit trans-epithelial calcium influx in the rainbow trout gills [19].

Fish exposed to subchronic levels of cadmium chloride developed micro- and bi-nucleated cells in their blood, gills, and liver [20,21]. Hepatocyte necrosis, congestion of submucosal blood vessel in the gut, and glomerular reduction and necrosis in the kidney tissue of Tilapia are just a few of the reported histological changes (*Oreochromis niloticus*). Fish that had been exposed to cadmium showed a varied haematological reaction. American eel fish (*Anguilla rostrata*) exposed for 8 weeks to 150 g/L of cadmium developed anaemia as a result of decreased haemoglobin and erythrocyte count. After cadmium exposure, a significant rise in leukocyte and big lymphocyte counts was also seen [22]. When *Cyprinus carpio* was subjected to sublethal concentration of cadmium, the stage of glycogen storage in the muscle and liver was dramatically reduced, and the blood glucose level rose [23]. Inhibiting vitellogenesis and an endocrine disruptor, cadmium has been initiated in rainbow trout *Oncorhynchus mykiss* [24]. Common carp *Cyprinus carpio*'s gonad development and sexual development were both impacted by cadmium chloride exposure [25]. *Leuciscus idus* larvae exposed to cadmium exhibited body abnormalities and a lower incidence of embryonic survival attributable to mortality in newly emerged larvae [26]. As a result of its slow rate of elimination, cadmium buildup poses a major threat to the environment. The epidermis has the lowest range of cadmium bioaccumulation, whereas the liver, kidney, & gills have the highest levels. The gill is the organ that detoxifies cadmium the fastest [27]. Due to its rapid rate of bioaccumulation, cadmium is one of the most dangerous heavy metals for water creatures.

**Mercury (Hg)**

Fungicides, particularly organic fungicides that contain mercurial components, which are organic mercury compounds, are the primary source of mercury in the ecosystem. The chronic data on mercury toxicity showed that methylmercury (MeHg<sup>+</sup>), an organic form of mercury, is the mercury component that is most dangerous over the long term [112, 113]. It is also believed that 70–100% of the mercury in fish is contained as MeHg<sup>+</sup> [114, 115]. Fish tissues have a high ability for both organic and inorganic forms of mercury to accumulate, making them perceptible indicators of water contamination [117].

Although injuries to the gill arches, liver, kidney, blood parameter, olfactory epithelium, and nervous system have been noted [118,120], some studies have exposed that mercury compounds can remain in the tissues of animals for extended periods of time, causing irreversible injuries like neurological destruction and lesion, behavioural and cognitive change, ataxia, as well as convulsion, in addition to its detrimental effect on reproduction [121,122]. There have been previous reports of renal tubular lumen necrosis and fibrosis in *Clarias batrachus* kidney subjected to





**Elavarasi and Aruljothi**

chronic mercury [123]. Mercury affects the viability of spermatozoa, egg formation, and the endurance rate of developing eggs and fry at very low concentration [124]. Zaki et al. [125] found that fish fed with 15 mg/kg diet mercuric oxide for 4 weeks had significantly higher levels of cholesterol, alkaline phosphatase, alanine amino transferase (ALT), aspartate amino transferase (AST), and cortisol, and significantly lower levels of haemoglobin (Hb), hematocrit (Ht), indicate total protein value in serum, and body mass.

**ARSENIC (As)**

Arsenic is a common element that is released into the aquatic environment via a variety of human-made sources, such as manufacturing firms, smelting activities, power plants, etc. The apply of arsenic insecticides, herbicides, and fungicides in agricultural fields is a significant additional source of arsenic [67]. Fish ingest arsenic-contaminated food, which also exposes them to arsenic-contaminated water throughout their gills and skin. There are several different forms of arsenic, including the elemental, trivalent, & pentavalent oxidative forms. The trivalent oxidation state of inorganic arsenic (arsenites) is more poisonous than the pentavalent status and is absorbed into fish tissue very quickly (arsenates). Arsenic's toxicity is influenced by a number of abiotic parameters in water bodies, including pH, temperature, salinity, and organic matter, phosphate concentration, suspended particles, and other toxins [68]. Freshwater fish that are constantly exposed to low levels of arsenic develop bioaccumulation, primarily in the liver and kidney tissue [69]. Freshwater fish, including tilapia, revealed histological changes after exposure to arsenic (*Oreochromis mossambicus*). Epithelial hyperplasia, lamellar mixture, epithelial lifting and oedema, desquamation, and necrosis were the modifications in the gills. The histology of the liver revealed macrophage infiltration, vascularization, shrinkage of the hepatocytes, enlargement of the sinusoids, vascular disintegration, nuclear hypertrophy, and localised necrosis [70]. Freshwater teleost *Channapunctata*'s heart was found to have a variety of histological changes, include necrosis in the heart tissue [71].

The erythrocyte membrane was ruptured, hemolysis, poor iron uptake by erythrocytes, and disrupted haemopoiesis in common Indian catfish *Clarias batrachus* after acute experience to sodium arsenite [72]. The total leucocyte count changed over time in the catfish *Clarias batrachus* expose to arsenic, and the organo-somatic indicators in the kidney and spleen decreased. Moreover, arsenic altered T- and B-cell function and interfered with catfish's ability to phagocytose microorganisms [73]. The Japanese medaka (*Oryzias latipes*) rudiment experienced developmental arrest at sublethal levels of arsenic poisoning [74]. When exposed to arsenic, rainbow trout *Salmo gairdnerii* developed stress response proteins [75]. In zebrafish embryos, arsenic poisoning greatly reduces the expression of genes implicated in natural immune response, which protect against bacterial and viral infection [76]. Arsenic oxide exposure for a long period of time resulted in decreased ovarian function and a decline in the improvement of 2nd and 3rd stage oocytes in fresh water fish *Colisa fasciatus* [77]. Fish physiological systems such as development, reproduction, gene appearance, ion control, resistant system, and histopathology are all impacted by arsenic bioaccumulation.

**LEAD(Pb)**

For the most part dangerous heavy metals is lead, which is found in nature in arrangement with other rudiments such as PbS, PbSO<sub>4</sub>, and PbCO<sub>3</sub>. Several anthropogenic source, such as lead-arsenate insecticides, lead-based paint, pigment, food can, and the incineration of coal, oil, and gasoline, among others, significantly increase the absorption of lead in the atmosphere [44]. The aquatic environment is immediately impacted by lead discharge from a variety of industries, farming fields, street excess, lead dust, and municipal waste water, which toxicity for aquatic life [45]. pH, salinity, hardness, and other factors all affect how soluble lead is in water. In flexible and acidic water, lead dissolves most readily. Lead poisoning in fish can occur at concentrations of 10-100 mg/L [46]. Fish exhibit altered behaviour, impotence, and slowed growth when expose to sublethal levels of lead [47]. After extended experience to a low absorption of lead nitrate, Katti found that the liver, brain, & gonad of *Clarias batrachus* had changed in lipid and cholesterol content [48]. African catfish *Clarias gariepinus* covered to lead showed histological deformation of the gill and liver tissue. Fresh water teleost (*Mastacembelus pancalus*) exposed to lead displayed histological changes in the ovarian tissue [49].



**Elavarasi and Aruljothi**

Fish exposed to lead also showed signs of parenchyma cell necrosis, hepatic cord and connective tissue fibrosis, decreased growth and body weight, and blood vessel collapse [50]. Reduced haemoglobin, red blood cell count, and hematocrit values were seen in Nile tilapia (*Oreochromis niloticus*) after lead exposure [51]. Lead toxicity causes synaptic damage and neurotransmitter dysfunction in fish, which leads to oxidative stress [52]. Lethal and sublethal exposure to lead in Tench (*Tinca tinca*) led to changes in immunological markers [53]. The liver, spleen, kidney, & gills they all are the primary sites of direct bioaccumulation in fish [54]. *Acipenser sinensis*, a species of Chinese sturgeon, experienced morphological changes and decreased free movement as a result of lead bioaccumulation [55].

**CONCLUSION**

In conclusion, this study has shown that heavy metals have a detrimental effect on fish. It is extensively clear that metals cause an untimely response in fish, as evidenced by changes in the structural and functional characteristics of various organs, together with enzymatic and genetic defects. This affects the fish's innate immune system and makes them more vulnerable to a variety of diseases. Biomarkers are a useful tool for developing policies for efficient environmental management since they can provide additional physiologically and ecologically pertinent information. Fish biomarkers are therefore essential for tracking environmental changes and determining how xenobiotic substances (such as heavy metals) affect fish. It is also advised that all waste water, sewage, and agriculture wastes be treated earlier before being released into the aquatic systems. The implementation of all legal provisions and legislation pertaining to the preservation of aquatic habitats must also be taken into account.

**REFERENCES**

1. Ali H, Khan E, Ilahi I. Environmental chemistry and ecotoxicology of hazardous heavy metals: Environmental persistence, toxicity, and bioaccumulation. *J Chem.* 2019;2019:1-14.
2. Gautam PK, Gautam RK, Banerjee S, Chattopadhyaya MC, Pandey JD. Heavy metals in the environment: Fate, transport, toxicity and remediation technologies. In: *Heavy Metals: Sources, Toxicity and Remediation Techniques.* 2016;pp.101-130.
3. Briffa J, Sinagra E, Blundell R. Heavy metal pollution in the environment and their toxicological effects on humans. *Heliyon.* 2020;6(9): e04691.
4. Malik DS, Maurya PK. Heavy metal concentration in water, sediment, and tissues of fish species (*Heteropneustes fossilis* and *Puntius ticto*) from Kali River, India. *Toxicol Environ Chem.* 2014;96(8):1195-1206.
5. Ngo HT, Gerstmann S, Frank H. Subchronic effects of environment-like cadmium levels on the bivalve *Anodonta anatina* (Linnaeus 1758): III. effects on carbonic anhydrase activity in relation to calcium metabolism. *Toxicol Environ Chem.* 2011;93(9):1815-25.
6. Bakshi A, Panigrahi AK. A comprehensive review on chromium induced alterations in fresh water fishes. *Toxicol Rep.* 2018;5:440-447.
7. Panov VP, Gyul'khandan'yan EM, Pakshver AS. Regeneration of exhausted chrome tanning solutions from leather production as a method preventing environmental pollution with chromium. *Russ J Appl Chem.* 2003;76(9):1476-8.
8. Huang KL, Holsen TM, Chou TC, Yang MC. The use of air fuel cell cathodes to remove contaminants from spent chromium plating solutions. *Environ Technol (United Kingdom).* 2004;25(1):39-49.
9. J.C. N, Sekar RR, Chandran R. J.C., N., R. Sekar and R. Chandran. Acute Effect of Chromium Toxicity on the Behavioral Response of Zebra Fish *Danio rerio*. *The International Journal of Plant, Animal and Environmental Sciences* 2016;2016.
10. Steinhagen D, Helmus T, Maurer S, Michael RD, Leibold W, Scharsack JP, et al. Effect of hexavalent carcinogenic chromium on carp *Cyprinus carpio* immune cells. *Dis Aquat Organ.* 2004;62(1-2):155-161.
11. Van Pittius MG, Van Vuren JHJ, Du Preez HH. Effects of chromium during pH change on blood coagulation in *Tilapia sarrmanii* (Cichlidae). *Comp Biochem Physiol Part C, Comp.* 1992;101(2):371-4.





### Elavarasi and Aruljothi

12. Vutukuru SS. Chromium induced alterations in some biochemical profiles of the Indian major carp, *Labeo rohita* (Hamilton). Bull Environ Contam Toxicol. 2003;70(1):118–123.
13. Nath K, Kumar N. Toxicity of manganese and its impact on some aspects of carbohydrate metabolism of a freshwater teleost, *Colisa fasciatus*. Sci Total Environ. 1987;67(2–3):257–262.
14. Van Der Putte I, Laurier MBHM, Van Eijk GJM. Respiration and osmoregulation in rainbow trout (*Salmo gairdneri*) exposed to hexavalent chromium at different pH values. Aquat Toxicol. 2009;2(2): 99–112.
15. Farag AM, May T, Marty GD, Easton M, Harper DD, Little EE, et al. The effect of chronic chromium exposure on the health of Chinook salmon (*Oncorhynchus tshawytscha*). Aquat Toxicol. 2006;76(3–4):246–257.
16. Van der Putte I, Van der Galiën W, Strik JJTWA. Effects of hexavalent chromium in rainbow trout (*Salmo gairdneri*) after prolonged exposure at two different pH levels. Ecotoxicol Environ Saf. 1982;6(3):246–57.
17. Yeşilbudak B, Erdem C. Cadmium accumulation in gill, liver, kidney and muscle tissues of common carp, *Cyprinus carpio*, and Nile tilapia, *Oreochromis niloticus*. Bull Environ Contam Toxicol. 2014;92(5):546–550.
18. Jia X, Zhang H, Liu X. Low levels of cadmium exposure induce DNA damage and oxidative stress in the liver of Oujiang colored common carp *Cyprinus carpio* var. color. Fish Physiol Biochem [Internet]. 2011;37(1):97–103.
19. Verbost PM, Flik G, Lock RAC, Wendelaar Bonga SE. Cadmium inhibition of Ca<sup>2+</sup> uptake in rainbow trout gills. Am J Physiol. 1987;253(2 Pt 2):R216–21.
20. Cavas T, Garanko NN, Arkhipchuk V V. Induction of micronuclei and binuclei in blood, gill and liver cells of fishes subchronically exposed to cadmium chloride and copper sulphate. Food Chem Toxicol. 2005;43(4):569–74.
21. Omer SA, Elobeid MA, Fouad D, Daghestani MH, Al-Olayan EM, Elamin MH, et al. Cadmium Bioaccumulation and Toxicity in Tilapia Fish (*Oreochromis niloticus*). J Anim Vet Adv. 2012;11(10):1601–6.
22. Gill TS, Epple A. Stress-related changes in the hematological profile of the American eel (*Anguilla rostrata*). Ecotoxicol Environ Saf. 1993;25(2):227–35.
23. Cicik B, Engin K. The effects of cadmium on levels of glucose in serum and glycogen reserves in the liver and muscle tissues of *Cyprinus carpio* (L., 1758). Turkish J Vet Anim Sci. 2005;29(1).
24. Vetillard A, Bailhache T. Cadmium: An Endocrine Disrupter That Affects Gene Expression in the Liver and Brain of Juvenile Rainbow Trout. Biol Reprod. 2005;72(1):119–26.
25. Das S, Mukherjee D. Effect of cadmium chloride on secretion of 17 $\beta$ -estradiol by the ovarian follicles of common carp, *Cyprinus carpio*. Gen Comp Endocrinol. 2013;181(1):107–14.
26. Witeska M, Sarnowski P, Źugowska K, Kowal E. The effects of cadmium and copper on embryonic and larval development of ide *Leuciscus idus* L. Fish Physiol Biochem. 2014;40(1):151–63.
27. Handy RD. The assessment of episodic metal pollution. I. Uses and limitations of tissue contaminant analysis in rainbow trout (*Oncorhynchus mykiss*) after short waterborne exposure to cadmium or copper. Arch Environ Contam Toxicol. 1992;22(1):74–81.
28. Mendil D, Demirci Z, Tuzen M, Soylak M. Seasonal investigation of trace element contents in commercially valuable fish species from the Black sea, Turkey. Food Chem Toxicol. 2010;48(3):865–70.
29. Panagos P, Ballabio C, Lugato E, Jones A, Borrelli P, Scarpa S, et al. Potential sources of anthropogenic copper inputs to European agricultural soils. Sustain. 2018;10(7):2380.
30. Nordberg GF, Fowler BA, Nordberg M, Friberg LT. Handbook on the Toxicology of Metals.. Elsevier Inc.; 2007.pp:1-9.
31. Sorensen EMB. Metal Poisoning in Fish. 1948. Paperback: 0-8943- 4268-6.
32. Richard Bull. Copper in Drinking Water. 2000. Paperback: 978-0- 309-06939-7.
33. Carol Ann Woody B, Louise SO. Effects of Copper on Fish and Aquatic Resources Prepared for Effects of Copper on Fish and Aquatic Resources. Fisheries Research and Consulting Anchorage 2012;pp1-27.
34. Eyckmans M, Celis N, Horemans N, Blust R, De Boeck G. Exposure to waterborne copper reveals differences in oxidative stress response in three freshwater fish species. Aquat Toxicol. 2011;103(1–2):112– 20.
35. Yacoub AM, Gad NS. Accumulation of some heavy metals and biochemical alterations in muscles of *Oreochromis niloticus* from the River Nile in Upper Egypt Int. J. Environ. Sci. Engg. 2012;3:1-10.





## Elavarasi and Aruljothi

36. Monteiro SM, dos Santos NMS, Calejo M, Fontainhas-Fernandes A, Sousa M. Copper toxicity in gills of the teleost fish, *Oreochromis niloticus*: Effects in apoptosis induction and cell proliferation. *Aquat Toxicol.* 2009;94(3):219–228.
37. Varanka Z, Rojik I, Varanka I, Nemcsók J, Ábrahám M. Biochemical and morphological changes in carp (*Cyprinus carpio* L.) liver following exposure to copper sulfate and tannic acid. *Comp Biochem Physiol - C Toxicol Pharmacol.* 2001;128(2):467–77.
38. Cyriac PJ, Antony A, Nambisan PNK. Hemoglobin and hematocrit values in the fish *Oreochromis mossambicus* (peters) after short term exposure to copper and mercury. *Bull Environ Contam Toxicol.* 1989;43(2):315–320.
39. Mcintyre JK, Baldwin DH, Meador JP, Scholz NL. Chemosensory deprivation in juvenile coho salmon exposed to dissolved copper under varying water chemistry conditions. *Environ Sci Technol.* 2008;42(4):1352–8.
40. Johnson A, Carew E, Sloman KA. The effects of copper on the morphological and functional development of zebrafish embryos. *Aquat Toxicol.* 2007;84(4):431–8.
41. Kong X, Jiang H, Wang S, Wu X, Fei W, Li L, et al. Effects of copper exposure on the hatching status and antioxidant defense at different developmental stages of embryos and larvae of goldfish *Carassius auratus*. *Chemosphere.* 2013;92(11):1458–64.
42. Bawuro AA, Voegborlo RB, Adimado AA. Bioaccumulation of Heavy Metals in Some Tissues of Fish in Lake Geriyo, Adamawa State, Nigeria. *J Environ Public Health.* 2018;2018:1854892-7.
43. Radi AAR, Matkovics B. Effects of metal ions on the antioxidant enzyme activities, protein contents and lipid peroxidation of carp tissues. *Comp Biochem Physiol Part C, Comp.* 1988;90(1):69–72.
44. Abadin H, Ashizawa A, Stevens YW, Lladós F, Diamond G, Sage G, et al. Potential for human exposure. 2007; pp301-380.
45. Sepe A, Ciaralli L, Ciprotti M, Giordano R, Funari E, Costantini S. Determination of cadmium, chromium, lead and vanadium in six fish species from the Adriatic Sea. *Food Addit Contam.* 2003;20(6):543– 52.
46. Tae SKA, Karam H, Ismail HK. Review On Some Heavy Metals Toxicity On Freshwater Fishes. *J Appl Vet Sci.* 2020;5(3):78–86.
47. Afshan S, Ali S, Ameen U, Farid M, Bharwana S, Hannan F, et al. Effect of Different Heavy Metal Pollution on Fish. *Research Journal of Chemical and Environmental Sciences.* 2014;2: 74-79.
48. Katti SR, Sathyanesan AC. Lead nitrate induced changes in lipid and cholesterol levels in the freshwater fish *Clarias batrachus*. *Toxicol Lett.* 1983;19(1–2):93–6.
49. Biswas S, Ghosh AR. Lead induced histological alterations in ovarian tissue of freshwater teleost *Mastacembelus pancalus* (Hamilton). *Int J Adv Sci Res.* 2016;2(1):45.
50. Olojo EAA, Olurin KB, Mbaka G, Oluwemimo AD. Histopathology of the gill and liver tissues of the African catfish *Clarias gariepinus* exposed to lead. *African J Biotechnol.* 2005;4(1).
51. Tanekhy M. Lead poisoning in Nile tilapia (*Oreochromis niloticus*): oxidant and antioxidant relationship. *Environ Monit Assess.* 2015;187(4):154.
52. Lee JW, Choi H, Hwang UK, Kang JC, Kang YJ, Kim K Il, et al. Toxic effects of lead exposure on bioaccumulation, oxidative stress, neurotoxicity, and immune responses in fish: A review. *Environ Toxicol Pharmacol.* 2019;68:101-108.
53. Shah SL. Alterations in The Immunological Parameters of Tench (*Tinca tinca* L. 1758) After Acute and Chronic Exposure to Lethal and Sublethal Treatments with Mercury, Cadmium and Lead. *Turkish J Vet Anim Sci.* 2005;29:1163-1168.
54. Cretì P, Trinchella F, Scudiero R. Heavy metal bioaccumulation and metallothionein content in tissues of the sea bream *Sparus aurata* from three different fish farming systems. *Environ Monit Assess.* 2010;165(1–4):321–329.
55. Hou JL, Zhuang P, Zhang LZ, Feng L, Zhang T, Liu JY, et al. Morphological deformities and recovery, accumulation and elimination of lead in body tissues of Chinese sturgeon, *Acipenser sinensis*, early life stages: A laboratory study. *J Appl Ichthyol.* 2011;27(2):514–519.
56. Al-Attar AM. The influences of nickel exposure on selected physiological parameters and gill structure in teleost fish, *Oreochromis niloticus*. *J Biol Sci.* 2007 1;7(1):77–85.







## Elavarasi and Aruljothi

57. Magyarosy A, Laidlaw R, Kilaas R, Echer C, Clark D, Keasling J. Nickel accumulation and nickel oxalate precipitation by *Aspergillus niger*. *Appl Microbiol Biotechnol*. 2002;59(2–3):382–8.
58. Binet MT, Adams MS, Gissi F, Golding LA, Schlekot CE, Garman ER, et al. Toxicity of nickel to tropical freshwater and sediment biota: A critical literature review and gap analysis. *Environ Toxicol Chem*. 2018;37(2):293–317.
59. Exp Abou-Hadeed AH, Ibrahim KM, El-Sharkawy NI, Sakr FMS, El- Hamed SAA. Experimental studies on nickel toxicity in Nile tilapia health. 8th International Symposium on Tilapia in Aquaculture 2008; 1385-1401.
60. Athikesavan S, Vincent S, Ambrose T, Velmurugan B. Nickel induced histopathological changes in the different tissues of freshwater fish, *Hypophthalmichthys molitrix* (Valenciennes). *J Environ Biol*. 2006;27(2 Suppl):391-395.
61. Atli G. The Effect of Waterborne Mercury and Nickel on the ATPases and AChE Activities in the Brain of Freshwater Fish (*Oreochromis niloticus*) Depending on the Ca<sup>2+</sup> Concentrations. *Turk J Fish and Aquat Sci*. 2018;19(5):363–371.
62. Palermo FF, Risso WE, Simonato JD, Martinez CB. Bioaccumulation of nickel and its biochemical and genotoxic effects on juveniles of the neotropical fish *Prochilodus lineatus*. *Ecotoxicol Environ Saf*. 2015;116:19-28.
63. Al-Ghanim KA. Impact of nickel (Ni) on hematological parameters and behavioral changes in *Cyprinus carpio* (common carp). *African J Biotechnol*. 2011;10(63):13860–6.
64. Sreedevi P, Sivaramakrishna B, Suresh A, Radhakrishnaiah K. Effect of nickel on some aspects of protein metabolism in the gill and kidney of the freshwater fish, *Cyprinus carpio L.* *Environ Pollut*. 1992;77(1):59–63.
65. Khangarot BS, Ray PK. Acute toxicity and toxic interaction of chromium and nickel to common guppy *Poecilia reticulata* (Peters). *Bull Environ Contam Toxicol*. 1990;44(6):832–9.
66. Ghazaly KS. Sublethal effects of nickel on carbohydrate metabolism, blood and mineral contents of *Tilapia nilotica*. *Water, Air, Soil Pollut*. 1992;64(3–4):525–32.
67. Han JM, Park HJ, Kim JH, Jeong DS, Kang JC. Toxic effects of arsenic on growth, hematological parameters, and plasma components of starry flounder, *Platichthys stellatus*, at two water temperature conditions. *Fish Aquat Sci*. 2019;22(1):3.
68. Min E, Jeong JW, Kang J-C. Thermal effects on antioxidant enzymes response in *Tilapia, Oreochromis niloticus* exposed Arsenic. *J Fish Pathol*. 2014;27(2):115–25.
69. Kumari B, Kumar V, Sinha AK, Ahsan J, Ghosh AK, Wang H, et al. Toxicology of arsenic in fish and aquatic systems. *Environ Chem Lett*. 2017;15:43–64.
70. Ahmed MK, Habibullah-Al-Mamun M, Parvin E, Akter MS, Khan MS. Arsenic induced toxicity and histopathological changes in gill and liver tissue of freshwater fish, tilapia (*Oreochromis mossambicus*). *Exp Toxicol Pathol*. 2013;65(6):903–9.
71. Hossain M. Effect of Arsenic (NaAsO<sub>2</sub>) on the Histological Change of Snakehead Fish, **Channa punctata**. *J Life Earth Sci*. 2014;7:67–70.
72. Tripathi S, Sahu DB, Kumar R, Kumar A. Effect of acute exposure of sodium arsenite (Na<sub>3</sub> AsO<sub>3</sub>) on some haematological parameters of **Clarias batrachus** (common Indian cat fish) in vivo. *Indian J Environ Health*. 2003;45(3):183-188
73. Ghosh D, Bhattacharya S, Mazumder S. Perturbations in the catfish immune responses by arsenic: Organ and cell specific effects. *Comp Biochem Physiol-C Toxicol Pharmacol*. 2006;143(4):455–463.
74. Ishaque AB, Tchounwou PB, Wilson BA, Washington T. Developmental arrest in Japanese medaka (*Oryzias latipes*) embryos exposed to sublethal concentrations of atrazine and arsenic trioxide. *J Environ Biol*. 2004;25(1):1-6
75. Kothary RK, Candido EP. Induction of a novel set of polypeptides by heat shock or sodium arsenite in cultured cells of rainbow trout, *Salmo gairdnerii*. *Can J Biochem*. 1982;60(3):347–355.
76. Dangleben NL, Skibola CF, Smith MT. Arsenic immunotoxicity: a review. *Environ Health*. 2013;12(1):73.
77. Shukla JP, Pandey K. Impaired ovarian functions in arsenic-treated freshwater fish, *Colisa fasciatus* (BL. and SCH.). *Toxicol Lett*. 1984;20(1):1–3.
78. Authman MMN (2011) Environmental and experimental studies of aluminium toxicity on the liver of *Oreochromis niloticus* (Linnaeus, 1758) fish. *Life Sci J* 8: 764-776.
79. Rashed MN (2001) Monitoring of environmental heavy metals in fish from Nasser Lake. *Environ Int* 27: 27-33.





### Elavarasi and Aruljothi

80. Authman MMN (2008) *Oreochromis niloticus* as a biomonitor of heavy metal pollution with emphasis on potential risk and relation to some biological aspects. *Global Vet.*, 2(3): 104-109.
81. Lamas S, Fernández JA, Aboal JR, Carballeira A (2007) Testing the use of juvenile *Salmo trutta* L. as biomonitors of heavy metal pollution in freshwater. *Chemosphere* 67: 221-228.
82. Al-Yousuf MH, El-Shahawi MS, Al-Ghais SM (2000) Trace metals in liver, skin and muscle of *Lethrinus lentjan* fish species in relation to body length and sex. *Sci Total Environ* 256: 87-94.
83. Omar WA, Saleh YS, Marie MAS (2014) Integrating multiple fish biomarkers and risk assessment as indicators of metal pollution along the Red Sea coast of Hodeida, Yemen Republic. *Ecotoxicol. Environ. Saf.*, 110: 221-231.
84. Sfakianakis DG, Renieri E, Kentouri M, Tsatsakis AM (2015) Effect of heavy
85. metals on fish larvae deformities: A review. *Enviro. Res.*, 137: 246-255.
86. Abadi DRV, Dobaradaran S, Nabipour I, Lamani X, Ravanipour M, (2014) Comparative investigation of heavy metal, trace, and macro element contents in commercially valuable fish species harvested off from the Persian Gulf. *Environ Sci Pollut Res*, 2014.
87. Sivaperumal P, Sankar TV, Viswanathan Nair PG (2007) Heavy metal concentrations in fish, shellfish and fish products from internal markets of India vis-a-vis international standards. *Food Chem* 102: 612-620.
88. Walton RC, McCrohan CR, Livens FR, White KN (2009) Tissue accumulation of aluminium is not a predictor of toxicity in the freshwater snail, *Lymnaea stagnalis*. *Environ Pollut* 157: 2142-2146.
89. Silva VS, Nunes MA, Cordeiro JM, Calejo AI, Santos S, et.al. (2007) Comparative effects of aluminum and ouabain on synaptosomal choline uptake, acetylcholine release and (Na/K)-ATPase. *Toxicology* 236: 158-177.
90. Camargo MMP, Fernandes MN, Martinez CBR (2009) How aluminium exposure promotes osmoregulatory disturbances in the neotropical freshwater fish *Prochilus lineatus*. *Aquat Toxicol* 94: 40-46.
91. Svobodová Z (1993) Water Quality and Fish Health. FAO, Rome, EIFAC
92. technical paper No. 54, 67pp.
93. Abdel-Latif HA (2008) The influence of calcium and sodium on aluminum toxicity in Nile tilapia (*Oreochromis niloticus*). *Aust J Basic Appl Sci* 2: 747-751.
94. Correia TG, Narcizo AM, Bianchini A, Moreira RG (2010) Aluminum as an endocrine disruptor in female Nile Tilapia (*Oreochromis niloticus*). *Comp Biochem Physiol C* 151: 461-466.
95. Alwan SF, Hadi AA, Shokr AE (2009) Alterations in haematological parameters
96. of fresh water fish, *Tilapia zillii*, exposed to aluminum. *J Sci Applica* 3:12-19.
97. Bjerknæs V, Fyllingen I, Holtet L, Teien HC, Rosseland BO, et.al. (2003) Aluminium in acidic river water causes mortality of farmed Atlantic Salmon (*Salmo salar* L.) in Norwegian fjords. *Mar Chem* 83: 169-174.
98. Laitinen M, Valtonen T (1995) Cardiovascular, ventilatory and haematological responses of brown trout (*Salmo trutta* L.), to the combined effects of acidity and aluminium in humic water at winter temperatures. *Aquat Toxicol* 31: 99- 112.
99. Barcarolli IF, Martinez CBR (2004) Effects of aluminum in acidic water on hematological and physiological parameters of the neotropical fish *Leporinus macrocephalus* (Anostomidae). *Bull Environ Contam Toxicol* 72: 639-646.
100. Poléo ABS (1995) Aluminium polymerization - a mechanism of acute toxicity of
101. aqueous aluminium to fish. *Aquat Toxicol* 31: 347-356.
102. Vuorinen PJ, Keinänen M, Peuranen S, Tigerstedt C (2003) Reproduction, blood and plasma parameters and gill histology of vendace (*Coregonus albula* L.) in long-term exposure to acidity and aluminum. *Ecotoxicol Environ Saf* 54: 255-276.
103. Brodeur JC, Økland F, Finstad B, Dixon DG, Mckinley RS (2001) Effects of subchronic exposure to aluminium in acidic water on bioenergetics of Atlantic Salmon (*Salmo salar*). *Ecotoxicol Environ Saf* 49: 226-234.
104. Waring CP, Brown JA, Collins JE, Prunet P (1996) Plasma prolactin, cortisol, and thyroid responses of the brown trout (*Salmo trutta*) exposed to lethal and sublethal aluminium in acidic soft waters. *Gen Comp Endocrinol* 102: 377-385.
105. Peuranen S, Vuorinen PJ, Vuorinen M, Tuurala H (1993) Effects of acidity and aluminium on fish gills in laboratory experiments and in the field. *Sci Total Environ* 134: 979-988.







### Elavarasi and Aruljothi

106. Sorensen EMB (1991) Metal poisoning in fish: Environmental and Life Sciences Associates. Boca Raton: CRC Press Inc.
107. Decker C, Menendez R (1974) Acute toxicity of iron and aluminium to brook trout. Proc. W. Virg. Acad. Sci 46: 159-167.
108. Van Rensburg EL (1989) The bioconcentration of atrazine, zinc and iron in *Tilapia sparrmanii* (Cichlidae). M. Sc. Thesis, Rand Afrikaans University, South Africa.
109. Grobler VHE, Van Vuren JHJ, Du Preez HH (1991) Bioconcentration of atrazine, zinc and iron in the blood of *Tilapia sparrmanii* (Cichlidae). Comp. Biochem. Physiol. C 100: 629-633.
110. Dalzell DJB, Macfarlane NAA (1999) The toxicity of iron to brown trout and effects on the gills: a comparison of two grades of iron sulphate. J. Fish Biol 55: 301-315.
111. Abbas HH, Zaghloul KH, Mousa MA (2002) Effect of some heavy metal pollutants on some biochemical and histopathological changes in Blue tilapia, *Oreochromis aureus*. Egypt. J. Agric. Res 80: 1395-1411.
112. Wepener V (1990) The effect of heavy metals at different pH values on the haematology and metabolic enzymes of *Tilapia sparrmanii* (Cichlidae).
113. Gonzalez RJ, Grippo RS, Dunson WA (1990) The disruption of sodium balance in brook charr, *Salvelinus fontinalis* (Mitchill), by manganese and iron. J Fish Biol 37: 765-774.
114. Peuranen S, Vuorinen PJ, Vuorinen M, Hollender A (1994) The effects of iron, humic acids and low pH on the gills and physiology of Brown Trout (*Salmo trutta*). Ann. Zool. Fennici 31: 389-396.
115. Baker RTM, Martin P, Davies SJ (1997) Ingestion of sub-lethal levels of iron sulphate by African catfish affects growth and tissue lipid peroxidation. Aquat. Toxicol. 40: 51-61.
116. USEPA (United States Environmental Protection Agency) (1986) Quality Criteria for Water - 1986. Washington DC, USA.
117. Deng L, Li Y, Yan X, Xiao J, Ma C, Zheng J, Liu S, Yang R (2015) Ultrasensitive and highly selective detection of bioaccumulation of methyl-mercury in fish samples via Ag<sup>0</sup>/Hg<sup>0</sup> amalgamation. Anal Chem 2015.
118. Amlund H, Lundebye AK, Berntssen MHG (2007) Accumulation and elimination of methylmercury in Atlantic cod (*Gadus morhua* L.) following dietary exposure. Aquat Toxicol 83: 323-330.
119. Nøstbakken OJ, Hove HT, Duinker A, Lundebye AK, Berntssen MHG, et al. (2015) Contaminant levels in Norwegian farmed Atlantic salmon (*Salmo salar*) in the 13-year period from 1999 to 2011. Environ Int 74: 274-280.
120. WHO (World Health Organization) (1989) Mercury-Environmental aspects. Geneva, Switzerland: WHO.
121. Gochfeld M (2003) Cases of mercury exposure, bioavailability, and absorption. Ecotoxicol Environ. Saf 56: 174-179.
122. Baatrup E (1991) Structural and functional effects of heavy metals on the nervous systems, including sense organs, of fish. Comp Biochem Physiol C 100: 253-257.
123. Oliveira Ribeiro CA, Fernandes LM, Carvalho CS, Cardoso RI, Turcatti NM (1995) Acute effects of the mercuric chloride in the olfactory epithelium of *Trichomycterus brasiliensis*. Ecotoxicol Environ Saf 31: 104-109.
124. Oliveira Ribeiro CA, Filipak Neto F, Mela M, Silva PH, Randi MAF, et al. (2006) Hematological findings in neotropical fish *Hoplias malabaricus* exposed to subchronic and dietary doses of methylmercury, inorganic lead, and tributyltin chloride. Environ Res 101: 74-80.
125. Eccles CU, Annau ZP (1982) Prenatal methyl mercury exposure: I. Alternations  
126. in neonatal activity. Neurobehav Toxicol Teratol 4: 371-376.
127. Clarkson TW, Nordberg GF, Sager PR (1985) Reproductive and Developmental Toxicity of Metals. Scand J Work Environ Health 11: 145-154.
128. Kirubakaran R, Joy KP (1988) Toxic effects of three mercurial compounds on survival, and histology of the kidney of the catfish *Clarias batrachus* (L.). Ecotoxicol Environ Saf 15: 171-179.
129. Raldúa D, Diez S, Bayona JM, Barceló D (2007) Mercury levels and liver pathology in feral fish living in the vicinity of a mercury cell chlor-alkali factory. Chemosphere 66: 1217-1225.
130. Zaki MS, Elbatrawy N, Fawzi OM, Awad I, Atta NS (2011) Effect of mercuric oxide toxicity on some biochemical parameters on African cat fish *Clarias gariepinus* present in the River Nile. Life Sci J 8: 363-368.





## Elavarasi and Aruljothi

131. Celik U, Oehlenschläger J (2004) Determination of zinc and copper in fish samples collected from Northeast Atlantic by DPSAV. Food Chem 87: 343- 347.
132. Hogstrand C (2011) Zinc. Academic Press, New York, USA.
133. Niyogi S, Wood CM (2006) Interaction between dietary calcium supplementation and chronic waterborne zinc exposure in juvenile rainbow trout, *Oncorhynchus mykiss*. Comp Biochem Physiol C 143: 94-102.
134. Alabaster JS, Lloyd R (1982) Water quality criteria for freshwater fish. London: FAO by Butterworth Scientific.
135. Nemcsók J, Benedeczky I, Boross L, Asztalos B, Orban L (1981) Subcellular localization of transaminase enzymes in fishes and their significance in the detection of water pollution. Acta Biol Szeged 27: 9-15
136. Abd El-Gawad AM (1999) Histopathological studies on the liver and gills of *Tilapia nilotica* (*Oreochromis niloticus*) exposed to different concentrations of lead acetate and zinc sulphate. J Egypt Ger Soc Zool 30: 13-22.
137. Cariño VS, Cruz NC (1990) Effects of low levels of zinc on the ovarian development of *Tilapia nilotica* Linneaus. Sci Diliman 3: 34-40.
138. Gabet-Giraud V, Miége C, Choubert JM, Ruel SM, Coquery M (2010) Occurrence and removal of estrogens and beta blockers by various processes in wastewater treatment plants. Sci. Total Environ 408: 4257-4269.
139. Yaqub S, Javed M; Acute toxicity of water- borne and dietary cadmium and cobalt for fish. Int. J. Agric. Biol., 2012; 14: 276-280.
140. Gray MR; Fundamentals of aquatic toxicology. Ecol. Services Inc. 1995: pp 85-97.
141. Underwood EJ; Trace elements in human and animal nutrition (4<sup>th</sup> ed.). New York: Academic., 1977.
142. Perry HM, Jr Schroeder HA, Goldstein GS and Menhard EM; Studies on control of hypertension by hypoxe; pharmacological and chemical observations on l-hydrazin ophthalazine. The American Journ. of the Medi. Sci., 1954; 228(4): 396-404.
143. Blakhima RJ; In C.F. Mills (Ed.) Trace element metabolism in animals. Edinburgh; Livingstone, 1970: 1,426.
144. Alexander CS; Cobalt beer cardiomyopathy, A clinical and pathological study of twenty-eight cases. The American Journ. Of medicine., 1972; 53: 395-417.

TABLE: 1

S.NO.	HEAVY METALS	FISH SPECIES	BIOACCUMULATION INORGAN OR TISSUE	REFERENCE
1	Copper(Cu)	<i>Oreochromis niloticus</i> <i>Cypronus carpio</i> Zebrafish larva	Apoptosis Biochemical and morphological changes Latreal line dysfunction	Varanka Z, 2001 Varanka Z 2001 Johnson A, 2008
2	Zinc(Zn)	<i>Oreochromis niloticus</i> <i>Tilapia nilotica</i>	Histological alteration Affect ovarion growth	Abd El-Gawad AM,1999 Carino VS, 1990
3	Chromium(Cr)	<i>Tilapia sparrmanii</i> <i>Labeo rohita</i> <i>Cyprinus carpio</i>	Hematological alteration Biochemical changes in tissue Histological alteration	Van pittius MG, 1992 Vutukuru SS, 2003 Yeilbudak B, 2014
4	Nickel(Ni)	<i>Hypophthalmichthys molitrix</i> <i>Cyprinus carpio</i>	Histological changes in defferent tissue Hematological alteration	Athikesavan S, 2006 AL-Ghaim KA, 2011
5	Cobalt(Co)	<i>Danio rerio</i>	Behavioral changes	Chandrabhusan singh, 2017
6	Iron(Fe)	<i>Tilopia sparrmanii</i> <i>Tilopia sparrmanii</i> <i>Salmo trutta</i>	Histological alteration Hematological alteration Behavioral changes	Van Rensburg EL, 1989 Grobler VHE, 1991 Peuranen S, 1994





### Elavarasi and Aruljothi

7	Aluminum(Al)	<i>Oreochromis niloticus</i> <i>Tilapia zillii</i> <i>Leporinus macrocephalus</i>	Endocrine disorder Heamological alteration Heamotological alteration	Correia TG, 2010 Alwan SF, 2009 Barcarolli IF, 2004
8	Cadmium(Cd)	<i>Anguilla rostrate</i> <i>Cyprinus carpio</i> <i>Cyprinus carpio</i>	Heamotological alteration Biochemical alteration Affect gonad function	Gilkl TS,1993 Cicik B, 2005 Das S, 2013
9	Mercury(Hg)	<i>Clarias batrachus</i> <i>Clarias gariepinus</i>	Hematological alteration Biochemical alteration	Kirubagaran R, 1988 Zaki MS,2011
10	Arsenic(As)	<i>Oreochromis niloticus</i> <i>Oreochromis mossambicus</i> <i>Clarias batrachus</i>	antioxidant enzyme alteration histological alteration heamatological alteration	Min E, 2014 Ahmed MK, 2013 Tripathi S, 2003
11	Lead(Pb)	<i>Tinca tinca</i> <i>Clarias gariepinus</i>	Affect immunological parameters Histological alteration	Shah SL, 2005 Olojo EAA, 2005





## Deciphering Molecular Docking Studies of Phytoconstituents Identified in Polyherbal Siddha Formulation *Sathakuppai Kudineer* on HMG coA Reductase – An Enzyme Target for Anti-Hyperlipidemic Activity

R S Parvathy<sup>1\*</sup>, T Susmitha<sup>2</sup>, I Sundara Ganesh<sup>3</sup>, A Mariappan<sup>4</sup> and G Senthil Vel<sup>5</sup>

<sup>1</sup>Assistant Professor, Department of Gunapadam, ATSVS Siddha Medical College, Munchirai, Kanyakumari, (Affiliated The Tamilnadu Dr.M.G.R.Medical University, Chennai), Tamil Nadu, India.

<sup>2</sup>Siddha Practitioner, Pattukkottai Taluk, Thanjavur District, Tamil Nadu, India.

<sup>3</sup>Consultant / R&D Head, Sivasakthi Pharmaceuticals, Peelamedu, Coimbatore, Tamil Nadu, India.

<sup>4</sup>Associate professor, Department of Gunapadam, National Institute of Siddha, (Affiliated The Tamilnadu Dr.M.G.R.Medical University), Chennai, Tamil Nadu, India.

<sup>5</sup>Head of the Department, Department of Gunapadam, National Institute of Siddha, (Affiliated The Tamilnadu Dr.M.G.R.Medical University), Chennai, Tamil Nadu, India.

Received: 08 Apr 2024

Revised: 10 Aug 2024

Accepted: 11 Nov 2024

### \*Address for Correspondence

**R S Parvathy**

Assistant Professor,

Department of Gunapadam,

ATSVS Siddha Medical College, Munchirai, Kanyakumari,

(Affiliated The Tamilnadu Dr.M.G.R.Medical University, Chennai),

Tamil Nadu, India.

E.Mail: parurs94@gmail.com



This is an Open Access Journal / article distributed under the terms of the **Creative Commons Attribution License** (CC BY-NC-ND 3.0) which permits unrestricted use, distribution, and reproduction in any medium, provided the original work is properly cited. All rights reserved.

### ABSTRACT

Hyperlipidemia, in particular elevated LDL (hypercholesterolemia), is one of the most prevalent risk factors contributing to the evolution of atherosclerosis & consequent vascular disease. This condition is treated with lipid-lowering medications & diets, as well as exercise & lifestyle modifications. Statins, also known as HMG-CoA reductase inhibitors, are the medications most frequently used to treat hyperlipidemia. Statins are generally regarded as safe & tolerable medications, but certain disagreements persist. Molecular docking study holds great potential in Siddha medicine, particularly in the context of herbal formulations. The phytoconstituents of the medicinal plants were retrieved from the PubChem chemical database. The target for the docking study was selected as 3-hydroxy-3-methylglutaryl-coenzyme A (HMG CoA reductase). *In-silico* docking analysis was performed by using Auto Dock Vina. The Auto dock program was used to evaluate the different orientations of the lead molecules with the target protein, & based on the interaction analysis, the best dock pose was chosen. According to the results of Computational analysis, the plants used in the Siddha formulation *Sathakuppai kudineer* yielded a total of 11 bioactive lead components. The phytochemicals such as Chlorogenic acid, Friedelin, Betulinic

84163





Parvathy et al.,

acid, Daucosterol, Gingerdione, & Piperlonguminine present in the herbal ingredients reveal maximum interactions with HMG CoA Reductase when compared to that of Atorvastatin. Therefore, it was concluded that these bio compounds may exert good anti-hyperlipidaemic activity & thereby considered a drug of choice for the clinical management of hyperlipidemia. Further preclinical studies & clinical trials must be carried out before the clinical recommendation of the *Sathakuppai kudineer* to the above-mentioned indication.

**Keywords:** hyperlipidemia, *Sathakuppai kudineer*, Molecular docking, HMG CoA reductase

## INTRODUCTION

Hyperlipidaemia is a very common disorder that is used to describe various inherited & acquired disorders, characterized by high lipid levels in the body. Hyperlipidaemia is classified into two broad classifications: primary (inherited) & secondary (acquired) hyperlipidemia. Primary hyperlipidemia is caused by an array of genetic disorders that a patient may inherit at birth, whereas secondary hyperlipidemia derives from an underlying etiology, such as central obesity, hypothyroidism, uncontrolled diabetes, unhealthy diet, medications (amiodarone, glucocorticoids) & poor lifestyle [1-2]. According to estimates from the World Health Organisation (WHO), high blood cholesterol results in over 4.4 million deaths annually & accounts for approximately 56 percent of cases of cardiovascular illnesses globally [3]. Complications of untreated hyperlipidemia cause complications like coronary artery disease (CAD), cerebrovascular accidents (CVD), strokes, peripheral artery disease (PAD), & even death. Patients with hyperlipidemia are more prone to develop cardiovascular disease (CVD). Numerous preclinical & clinical studies have proven that inhibiting the activity of 3-hydroxy-3-methylglutaryl-coenzyme A reductase (HMGCR), a crucial enzyme in the synthesis of cholesterol, can reduce the risk of coronary problems [4]. Statins & other well-known drugs (niacin, fibrates, etc.) work by suppressing HMGCR activity, either by inhibiting endogenous synthesis or by lowering cholesterol absorption from the intestine to treat hyperlipidemia [5]. Currently, available hyperlipidaemic drugs have adverse effects like nausea, diarrhea, gastric irritation, hyperuricemia, myositis, & abnormal liver function [6]. In recent years, researchers have turned their attention to medicinal plants to investigate phytochemicals with HMGCR inhibitory activities that could be used to develop a new hypolipidemic drug with little or no side effects.

Computational methods have been widely used in evaluating the therapeutic potential of medicinal plants by determining their activity against the target protein as well as their possible mechanism of action as technology has advanced. Molecular docking techniques predict interactions of protein & ligand with their binding affinities & the binding orientation of protein-ligand complexes. A ligand's molecular structure, orientation, & conformation are related to its ability to bind to a specific protein. Energy-based scoring & geometric sampling are the two steps involved in docking methods that determine the ligand/protein binding affinity. Based on the scoring function, the best complementary protein-ligand binding is found depending on their predicted binding affinities. High energy scores are directly related to protein-ligand binding affinity [7-12]. India is renowned for its extensive collection of living ethnomedical traditions as well as its rich traditional medical systems, including Ayurveda, Siddha, & Unani [13]. In traditional Siddha medicine (TSM), numerous herbal formulations are useful in treating hyperlipidemia. *Sathakuppai kudineer* (SK) is a classic Siddha Polyherbal formulation that is mentioned in the Siddha literature Siddha formulary of India. This poly herbal drug contains nine ingredients like *Omam*, *sathakuppai*, *moongil*, *mavilingam*, *parangipattai*, *chukku*, *thippili*, *koduveli*, & *Ekaranjeerakam* [14]. The lead molecules were analyzed for their ability to block the HMG CoA reductase from a broader scientific perspective. This may help in the acceptability of SK as an Anti-hyperlipidaemic agent. The study aims to evaluate an in-silico computational analysis of the phytochemicals found in *Sathakuppai kudineer* on HMG CoA reductase- an enzyme target for anti-hyperlipidemic activity.







## MATERIALS AND METHODS

Docking calculations were done for the compounds retrieved from herbal drugs such as d-carvone, Thymoquinone, p-cymene, Chlorogenic acid, Friedelin, Betulinic acid, Daucosterol, Plumbagin, Gingerdione, Piperlonguminine, (-)-beta-Bourbonene, & standard Atorvastatin against target protein (Table.1 & FigA). The ligand molecular properties are depicted in Table. 2.

### Target Protein Retrieval

The binding of phytocomponents with the core amino acids (Ser684, Asp690, Lys691, Lys692) of the target by forming a hydrogen bond will hinder the function of the enzyme HMG CoA reductase with PDB – 1HWK. These amino acid residues are functionally responsible for HMG CoA reductase enzyme activity in cholesterol biosynthesis. Thereby phytocomponents that inhibit the target enzyme HMG CoA reductase may occupy these active amino acids & could be able to block the HMG coA enzymatic activity thereby limiting the cholesterol synthesis & subsequently helping in control the hyperlipidemia. Compounds that selectively hinder the action of this enzyme may act as a potential therapeutic agent for the management of hyperlipidemia. The crystalline structure of the target protein HMG coA reductase (1HWK) was retrieved from the protein data bank (RSCB) & the essential missing hydrogen atoms were added after the protein cleanup process. The Auto dock program was used to evaluate the different orientations of the lead molecules in relation to the target protein, & based on the interaction analysis, the best dock pose was chosen.

### Molecular Docking Methodology

Docking calculations were carried out for retrieved phytocomponents against target enzyme Phospholipases A2. Essential hydrogen atoms, Kollman united atom type charges, & solvation parameters were added with the aid of Auto Dock tools [26-27]. Affinity (grid) maps of  $\times \times \text{Å}$  grid points &  $0.375 \text{Å}$  spacing were generated using the Auto grid program. Auto Dock parameter set- & distance-dependent dielectric functions were used in the calculation of the van der Waals & the electrostatic terms, respectively. Docking simulations were performed using the Lamarckian genetic algorithm (LGA) & the Solis & Wets local search method [28]. The initial position, orientation, & torsions of the ligand molecules were set randomly. All rotatable torsions were released during docking. Each docking experiment was derived from 2 different runs that were set to terminate after a maximum of 250000 energy evaluations. The population size was set to 150. During the search, a translational step of  $0.2 \text{Å}$ , & quaternion & torsion steps of 5 were applied.

## RESULTS AND DISCUSSION

The Summary of the molecular docking studies of the lead compounds & Standard Atorvastatin against HMG CoA reductase & its amino acid binding interactions have been tabulated in Table No. 3, 4, & Fig C. Hyperlipidemia is a major risk factor for the development & progression of atherosclerosis & coronary heart disease. It is related to risk factors like arteriosclerosis, hypertension, type-II DM, obesity, MI, congestive cardiac failure, angina pectoris, gall bladder diseases, degenerative joint diseases, apnoea, & sterility [29]. Complications from undertreated or untreated hyperlipidemia include all types of vascular disease, like coronary artery disease, peripheral artery disease, cerebrovascular accidents, aneurysms, type II diabetes, high blood pressure, & even death [30]. Currently, the most widely recommended lipid-lowering medications to lower plasma lipids are statins, including atorvastatin, lovastatin, & simvastatin [31]. Hypolipidemic drugs (statins) are structural analogues of HMG CoA, but inhibitors of HMGCR (HMG-CoA reductase). Target protein HMG-CoA reductase catalyses the reductive conversion of HMG-CoA into mevalonate, a rate-regulatory step that regulates endogenous cholesterol biosynthesis [32]. This results in a compensatory increase in LDL receptor-mediated uptake & catabolism of IDL (intermediate-density lipoprotein) & LDL (Low-density lipoprotein). Over the long term, feedback induction of HMG-CoA reductase tends to increase cholesterol synthesis, but a steady state is attained with a dose-dependent lowering of LDL-C levels. The drug statins decrease the LDL-Cholesterol by 20-55%, increase the HDL-C levels by 5-15%, & decrease the Triglycerides by 10-







Parvathy et al.,

35%[33]. The present treatment for hyperlipidemia is Cholesterol-lowering medications may cause life-threatening or serious unwanted effects, such as muscle pain, exaggerated glucose levels, constipation, nausea, diarrhoea, abdomen pain, cramps, & the elevation of liver enzymes[34]. People are searching for safer alternatives to these pharmaceuticals because of their adverse effects, & there has been increased interest in finding novel drugs that can lower & regulate blood cholesterol levels resulting in numerous reports on significant activities of natural agents[35]. *Sathakuppai kudineer* (SK), A traditional Siddha polyherbal formulation is used in Clinical Practice by Siddha practitioners to treat irregular menstruation, amenorrhoea, & hormonal imbalances. Nevertheless, the phytoconstituents present in this formulation have proven the Anti-hyper lipidemic, Anti-oxidant, cardioprotective, & Anti-atherogenic activities in various scientific studies. Therefore, the present investigation was designed to investigate the In silico Molecular docking studies of polyherbal formulation *Sathakuppai kudineer* on HMG Co-A reductase (PDB:1hwk). Based on the molecular docking studies using AutoDock tools, the inhibitory possibility of phytocomponents from *Sathakuppai kudineer* towards HMG CoA reductase (PDB) - 1HWK was investigated with standard Atorvastatin.

Molecular docking is commonly employed as a preliminary step in the development of bioactive compounds that can be used as drug candidates [36]. because it can offer molecular modeling of the interactions between ligands & receptor proteins [37-38]. It is one of the most widely used methods in structure-based drug design (SBDD) due to its ability to predict the conformation of small-molecule ligands within the appropriate target binding site with high accuracy [39]. The In silico docking process is used to select the target protein & reveals the potential role of phytochemicals present in the formulations. Molecular Docking Study is significantly important to find the compounds present in the medicines & their effects on the clinical management of Hyperlipidemia. Furthermore, this approach is significantly less expensive than the traditional method. Prediction in silico is crucial for improving research in pharmacokinetics.

A total of 11 bioactive lead compounds were retrieved from the herbal & other ingredients present in the Siddha formulation. From the reported data of the bioactive compounds, the compounds such as Chlorogenic acid, Friedelin, Betulinic acid, Daucosterol, Gingerdione, & Piperlonguminine present in the herbal ingredients reveal a maximum of 3-4 interactions with the core active amino acid residues present on the target HMG CoA reductase. Similarly, Compounds like Thymoquinone & plumbagin showed 2 interactions with the active position of the objective enzyme HMG CoA reductase. The results of the binding affinity of these compounds with their respective targets are given in Table No. 3. The Phyto Compounds Beta- Bourbonene & Chlorogenic acid show high affinity such as -6.03 kcal/mol & -5.95 kcal/mol respectively. The Phyto compounds such as Daucosterol, Friedelin, Plumbagin, Betulinic acid, & Thymoquinone show more binding potential against the target protein molecules which are -5.88 Kcal/mol, -5.60 Kcal/mol, -5.04 Kcal/mol, -4.92 Kcal/mol, -3.98 Kcal/mol, respectively. The Molecular Docking studies of these Phyto compounds conclude that the drug *Sathakuppai kudineer* possesses promising HMG CoA reductase inhibitory activity & functions as a potential therapy agent for the management of Hyperlipidemia.

## CONCLUSION

Based on the results of the computational analysis it was concluded that the bio-active compounds like Chlorogenic acid, Friedelin, Betulinic acid, Daucosterol, Gingerdione, & Piperlonguminine present in the ingredients possess significant binding against the target enzyme HMG CoA reductase. Thereby phytocomponents that inhibit the target enzyme HMG CoA reductase by occupying these active amino acids could be able to hinder the function of the limiting enzyme involved in cholesterol biosynthesis.

### Ethical Approval :

Not Applicable





Parvathy et al.,

**Authors Contributions**

Conceptualization, supervision, Methodology, Data interpretation, Writing, &amp; editing done.

**conflict of interest:**

Nil

**source of funding:**

Self

**REFERENCES**

1. Fredrickson DS. An international classification of hyperlipidemias and hyperlipoproteinemias. *Ann Intern Med.* 1971 Sep;75(3):471-2.
2. Ballantyne CM, Grundy SM, Oberman A, Kreisberg RA, Havel RJ, Frost PH, Haffner SM. Hyperlipidemia: diagnostic and therapeutic perspectives. *J Clin Endocrinol Metab.* 2000 Jun;85(6):2089-112.
3. Ford I, Murray H, McCowan C, Packard CJ. Long-Term Safety and Efficacy of Lowering Low-Density Lipoprotein Cholesterol with Statin Therapy: 20-Year Follow-Up of West of Scotland Coronary Prevention Study. *Circulation.* 2016 Mar 15;133(11):1073-80.
4. Nematollahi A, Aminimoghdamfarouji N, Jalilvand MR, Ali SA. Design and molecular studies of luteolin derivatives, from *Biebersteiniamultifida* DC., as novel HMG-CoA reductase inhibitors. *Int J ChemTech Res* 2012; 4(2): 733-738.
5. Ma S, Sun W, Gao L, Liu S. Therapeutic targets of hypercholesterolemia: HMGCR and LDLR. *DiabetMetabSynd Ob* 2019; 12: 1543-1553
6. Harikumar K, Niveditha B, Kumar MRP, Monica K, Gajendra P. Anti-hyperlipidemic activity of alcoholic and methanolic extracts of *CrotolariaJuncea* in Triton-WR 1339 induced hyperlipidemia. *Int J Phytopharm* 2012; 3(3): 256-262.
7. Alonso H, Blinznyuk AA, Gready JE. Combining docking and molecular dynamic simulations in drug design. *Med Res Rev* 2006; 26(5): 531-568.
8. Tuffery P, Derreumaux P. Flexibility and binding affinity in protein–ligand, protein–protein and multi-component protein interactions: limitations of current computational approaches. *J R Soc Interface* 2012; 9(66): 20-33.
9. Meng XY, Zhang HX, Mezei M, Cui M. Molecular Docking: A powerful approach for structure-based drug discovery. *Curr Comput Aided Drug Des* 2011; 7(2): 146-157.
10. Ferreira LG, dos Santos RN, Oliva G, Andricopulo AD. Molecular Docking and Structure-Based Drug Design Strategies. *Molecules* 2015; 20: 13384-13421.
11. Kroemer RT. Structure-based drug design: Docking and scoring. *Curr Protein Pept Sci* 2007; 8(4): 312-328.
12. Naeem S, Hylands P, Barlow D. Docking studies of chlorogenic acid against aldose reductase by using Molegro Virtual Docker Software. *J Appl Pharm Sci* 2013; 3(1): 13-20.
13. Muthiah k, Ganesan K, Ponnaiah M, Parameswaran S. Concepts of body constitution in traditional Siddha texts: A literature review. *Journal of Ayurveda and integrative medicine.* 2019 Apr 1;10(2):131-4.
14. The Siddha formulary of India, Part I.1st Edition. Government of India, Ministry of Health and Family welfare, Department of AYUSH. New Delhi. 1992.
15. Nabila Zein , Marwa Shehata , Atef. M. Amer, Carvone's Hypoglycaemic and Hypolipidemic Potent Activity Via Regulation Insulin-Induced Genes in Diabetic Hyperlipidaemic Rats ,*Biointerface Research in Applied Chemistry.*2023 March; 206.
16. JinH, Leng, Q, ZhangC, ZhuY, and WangJ. P. cymene prevent high-fat diet-associated colorectal cancer by improving the structure of intestinal flora. *Journal of Cancer*, 12(14);4355–4361.
17. KarthikesanK, PariL, and MenonVP. Antihyperlipidemic effect of chlorogenic acid & tetrahydrocurcumin in rats subjected to diabetogenic agents. *Chemico-biological interactions*, 188(3), 643–650.





Parvathy et al.,

18. Jiao J, Zhang Y, Lou D, Wu X, Zhang Y. Antihyperlipidemic & antihypertensive effect of a triterpenoid-rich extract from bamboo shavings & vasodilator effect of friedelin on phenylephrine-induced vasoconstriction in thoracic aortas of rats. *Phytother Res.* 2007 Dec;21(12):1135-41.
19. Rios JL, Manez S. New Pharmacological Opportunities for Betulinic Acid. *Planta Med.* 2018;84(1):8-19. doi:10.1055/s-0043-123472
20. Sikarwar M. S, Patil M. B. Antihyperlipidemic activity of *Salacia chinensis* root extracts in triton-induced & atherogenic diet-induced hyperlipidemic rats. *Indian journal of pharmacology*, 44(1), 88–92.
21. Al-Noory AS, Amreen AN, Hymoor S. Antihyperlipidemic effects of ginger extracts in alloxan-induced diabetes and propylthiouracil-induced hypothyroidism in (rats). *Pharmacognosy Res.* 2013 Jul;5(3):157-61.
22. Nabi SA, Kasetti RB, Sirasanagandla S, Tilak TK, Kumar MV, Rao CA. Antidiabetic and antihyperlipidemic activity of *Piper longum* root aqueous extract in STZ induced diabetic rats. *BMC Complement Altern Med.* 2013 Feb 18;13:37.
23. Machaba KE, Cobongela SZ, Mosa RA, Oladipupo LA, Djarova TG, Opoku AR. In vivo anti-hyperlipidemic activity of the triterpene from the stem bark of *Protorhus longifolia* (Benrh) Engl. *Lipids Health Dis.* 2014 Aug 15;13:131.
24. Pendurker S R , Mengi S A .Antihyperlipidemic effect of aqueous extract of *Plumbago zeylanica* roots in diet-induced hyper lipidemic rat , *pharmaceutical biology* , 47(10),pp.1004-1010.
25. Pei ZW, Guo Y, Zhu HL, Dong M, Zhang Q, Wang F. Thymoquinone Protects against Hyperlipidemia-Induced Cardiac Damage in Low-Density Lipoprotein Receptor-Deficient (LDL-R<sup>-/-</sup>) Mice via Its Anti-inflammatory and Antipyroptotic Effects. *Biomed Res Int.* 2020 Oct 29;2020:4878704.
26. Morris G M , Goodsell D S . Automated docking using a Lamarckian genetic algorithm and an empirical binding free energy function. *Journal of Computational Chemistry* 19 (14), 1639-1662.
27. Solis F j , Wets R J B. Minimization by Random Search Techniques. Vol. 6, No. 1 (Feb., 1981, pp. 19-30
28. Wardaniati and Herli M A , Studi Molecular Docking Senyawa Golongan Flavonol sebagai Antibakteri, *Journal of Pharmacy and Science* vol. 1, 2018, pp. 20- 27.
29. Sivaraman Dhanasekaran, Pradeep Pushparaj Selvadoss, Solomon Sundar Manoharan, Srikanth Jeyabalan, Devi Rajeswari Vijayarangan. Revealing Anti-Fungal Potential of Plant-Derived Bioactive Therapeutics in Targeting Secreted Aspartyl Proteinase (SAP) of *Candida albicans*: A Molecular Dynamics Approach. *Journal of Biomolecular Structure and Dynamics* 2023. 6,1-15.
30. Subhasree N, Kamella A, Kaliappan I, Agrawal A, Dubey GP. Antidiabetic and antihyperlipidemic activities of a novel polyherbal formulation in high fat diet/streptozotocin induced diabetic rat model. *Indian J Pharmacol.* 2015 Sep-Oct;47(5):509-13.
31. Mavillapalli RC, Jeyabalan S and Muthusamy S: Molecular docking studies of phytoconstituents identified in *Cinnamomum verum* & *Coriandrum sativum* on HMG CoA Reductase – an enzyme target for antihyperlipidemic activity. *Int J Pharm Sci Res* 2017; 8(10): 4172- 79.
32. Khedkar VM, Arya N, Coutinho EC, Shishoo CJ, Jain KS. Docking study of novel antihyperlipidemic thieno[2,3-d]pyrimidine; LM-1554, with some molecular targets related to hyperlipidemia - an investigation into its mechanism of action. *Springerplus.* 2014 Oct 24;3:628.
33. Fayyaz S, Islam M, Ahmed A, Saeed H, Naseem A. Phytochemical, anti-hyperlipidemic & in silico studies of extracts of *Ficus carica* seeds. *Pak J Pharm Sci.* 2023;36(3(Special)):989-1000.
34. Deshpande SH, Muhsinah AB, Bagewadi ZK, Ankad GM, Mahnashi MH, Yaraguppi DA, Shaikh IA, Khan AA, Hegde HV, Roy S. In Silico Study on the Interactions, Molecular Docking, Dynamics & Simulation of Potential Compounds from *Withaniasomnifera* (L.) Dunal Root against Cancer by Targeting KAT6A. *Molecules.* 2023 Jan 22;28(3):1117. doi: 10.3390/molecules28031117.
35. Ali A, Mir GJ, Ayaz A, Maqbool I, Ahmad SB, Mushtaq S, Khan A, Mir TM, Rehman MU. In silico analysis & molecular docking studies of natural compounds of *Withaniasomnifera* against bovine NLRP9. *J Mol Model.* 2023 May 8;29(6):171.
36. H. Purnomo, *Kimia Komputasi: Molecular Docking Plants Penambatan Molekul Plants [Protein-Ligand AntSystem]* (IlmuSemut), Yogyakarta: Pustaka Pelajar, 2011.





37. Behera D K , P.M. Behera, L. Acharya, A. Dixit, and P. Padhi, Research Article : In Silico Biology of H1N1 : Molecular Modelling of Novel Receptors & Docking Studies of Inhibitors to Reveal New Insight in Flu Treatment, Journal of Biomedicine & Biotechnology. Oct 17, 2012, Vol. 2012(2), pp. 1-7.
38. Ferreira L G, Ricardo N. dos Santos, Glaucius Oliva and Adriano D. Andricopulo. Molecular Docking and Structure-Based Drug Design Strategies. Molecules vol. 20, 2015, pp. 13384-13421.
39. Goedeke L, Fernandez-Hernando C. Regulation of cholesterol homeostasis. Cell Mol Life Sci 2012; 69(6): 916-930.

**Table 1: Ingredients of Sathakuppai kudineer with its botanical name & phytochemicals selected for docking**

S.NO	VERNACULAR NAME	BOTANICAL NAME	PARTS USED	PHYTOCOMPOUNDS
1	Sathakuppai	<i>Anethum graveolens L.</i>	Fruit	d-carvone [15]
2	Omam	<i>Trachyspermum ammi L.</i>	Fruit	p-cymene [16]
3	Moongil	<i>Bambusa vulgaris Schrad. Ex J.C.Wendl.</i>	Leaf	Chlorogenic acid [17]
4	Mavilingam	<i>Crateva religiosa G.Forst.</i>	bark	Friedelin, Betulinic acid[18-19]
5	Parangipattai	<i>Smilax china L.</i>	Rhizome	Daucosterol[20]
6	Chukku	<i>Zingiber officinale Rosc.</i>	Dried Rhizome	Gingerdione[21]
7	Thippili	<i>Piper longum L.</i>	Fruit	Piperlonguminine, (-)-beta-Bourbonene [22-23]
8	Koduveli	<i>Plumbago xeylanica L.</i>	Root	Plumbagin [24]
9	Karunjeerakam	<i>Nigella sativa L.</i>	Seed	Thymoquinone [25]
10	Koduveli	<i>Plumbago xeylanica L.</i>	Root bark	Plumbagin [24]

**Table 2:Ligand Properties of the Compounds Selected for Docking Analysis**

Compound	Molar weight g/mol	Molecular Formula	H Bond Donor	H Bond Acceptor	Rotatable bonds
Carvone	150.221 g/mol	C <sub>10</sub> H <sub>14</sub> O	0	1	1
Thymoquinone	164.204 g/mol	C <sub>10</sub> H <sub>12</sub> O <sub>2</sub>	0	2	1
Cymene	134.222 g/mol	C <sub>10</sub> H <sub>14</sub>	0	0	1
<u>Chlorogenic acid</u>	354.31 g/mol	<u>C<sub>16</sub>H<sub>18</sub>O<sub>9</sub></u>	6	9	5
Friedelin	426.7 g/mol	C <sub>30</sub> H <sub>50</sub> O	0	1	0
Betulinic acid	456.7 g/mol	C <sub>30</sub> H <sub>48</sub> O <sub>3</sub>	2	3	2
<u>Daucosterol</u>	576.8 g/mol	C <sub>35</sub> H <sub>60</sub> O <sub>6</sub>	4	6	9
<u>Plumbagin</u>	188.182 g/mol	C <sub>11</sub> H <sub>8</sub> O <sub>3</sub>	1	3	0
Gingerdione	292.4 g/mol	C <sub>17</sub> H <sub>24</sub> O <sub>4</sub>	1	4	10
Piperlonguminine	273.33 g/mol	C <sub>16</sub> H <sub>19</sub> NO <sub>3</sub>	1	3	5
Beta- <u>Bourbonene</u>	204.35 g/mol	C <sub>15</sub> H <sub>24</sub>	0	0	1
<i>Atorvastatin</i>	558.6 g/mol	C <sub>33</sub> H <sub>35</sub> FN <sub>2</sub> O <sub>5</sub>	4	6	12





Parvathy et al.,

Table 3: Summary of the molecular docking studies of compounds against HMG coA reductase (PDB) - 1HWK

Compounds	Est. Free Energy of Binding	Est. Inhibition Constant, Ki	Electrostatic Energy	Total Intermolec. Energy	Interact. Surface
Carvone	-4.70 kcal/mol	356.83 uM	-0.01 kcal/mol	-5.00 kcal/mol	476.564
Thymoquinone	-4.86 kcal/mol	276.10 uM	-0.02 kcal/mol	-5.15 kcal/mol	491.272
Cymene	-4.57 kcal/mol	445.87 uM	-0.11 kcal/mol	-4.87 kcal/mol	480.746
<u>Chlorogenic acid</u>	-5.95 kcal/mol	43.82 uM	-1.49 kcal/mol	-5.87 kcal/mol	511.693
Friedelin	-5.60 kcal/mol	78.32 uM	-0.05 kcal/mol	-5.60 kcal/mol	755.963
Betulinic acid	-4.92 kcal/mol	246.06 uM	-1.04 kcal/mol	-6.69 kcal/mol	680.701
<u>Daucosterol</u>	-5.88 kcal/mol	49.32 uM	-0.01 kcal/mol	-7.38 kcal/mol	861.588
<u>Plumbagin</u>	-5.04 kcal/mol	202.13 uM	-0.07 kcal/mol	-5.34 kcal/mol	494.131
Gingerdione	-3.86 kcal/mol	1.48 mM	-0.06 kcal/mol	-5.74 kcal/mol	708.618
Piperlonguminine	-3.98 kcal/mol	1.20 mM	-0.27 kcal/mol	-5.43 kcal/mol	646.673
Beta- <u>Bourbonene</u>	-6.03 kcal/mol	38.10 uM	-0.06 kcal/mol	-6.33 kcal/mol	558.994
Atorvastatin	-5.55 kcal/mol	85.94 uM	-1.30 kcal/mol	-6.17 kcal/mol	648.525

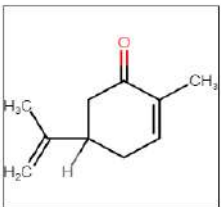
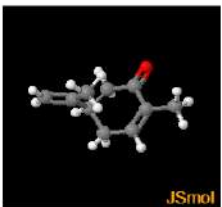
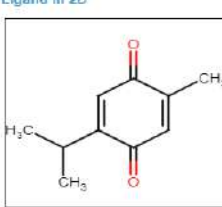
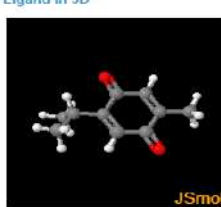
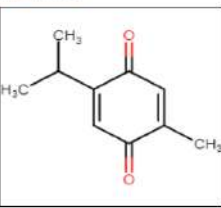
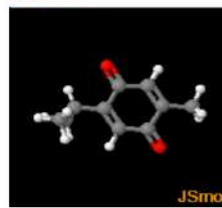
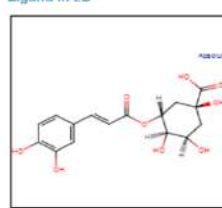
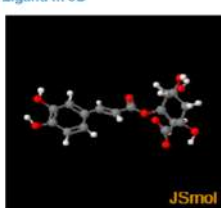
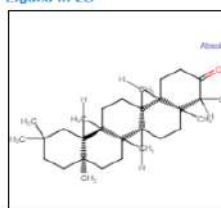

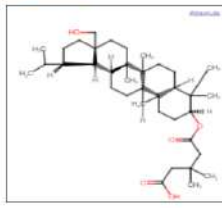
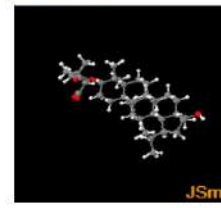
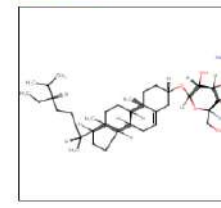
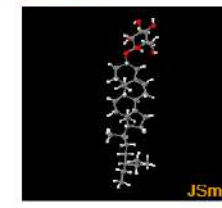
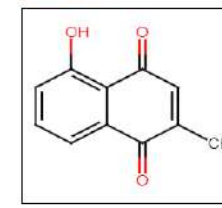

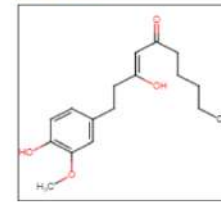

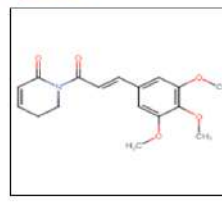
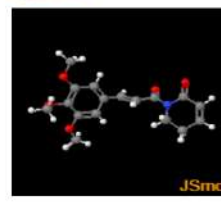
Table 4: Amino acid Residue Interaction of Lead against HMG coA reductase (PDB) - 1HWK

COMPOUND	INTERACTION	AMINO ACID RESIDUES										
CARVONE	0	655	766	767								
		MET	GLN	ASP								
THYMOQUINONE	2	691	692	693	769	772						
		LYS	LYS	PRO	ALA	VAL						
CYMENE	0	654	655	766	809							
		ALA	MET	GLN	THR							
CHLOROGENIC ACID	4	590	682	684	686	690	691	692				
		ARG	ALA	SER	ASN	ASP	LYS	LYS				
FRIEDELIN	4	590	684	686	690	691	692					
		ARG	SER	ASN	ASP	LYS	LYS					
BETULINIC ACID	3	590	657	658	661	683	690	691	692			
		ARG	MET	ASN	SER	VAL	ASP	LYS	LYS			
DAUCOSTEROL	3	590	655	657	658	683	684	690	691	767		
		ARG	MET	MET	ASN	VAL	SER	ASP	LYS	ASP		
PLUMBAGIN	2	691	692	769	772							
		LYS	LYS	ALA	VAL							
GINGERDIONE	4	590	657	658	661	684	686	690	691	692		
		ARG	MET	ASN	SER	SER	ASN	ASP	LYS	LYS		
PIPERLONGUMININE	4	590	684	690	691	692	769					
		ARG	SER	ASP	LYS	LYS	ALA					
BETA- BOURBONENE	0	655	766	767	809							
		MET	GLN	ASP	THR							
ATORVASTATIN	4	590	657	658	661	683	684	690	691	692	767	770
		ARG	MET	ASN	SER	VAL	VAL	ASP	LYS	LYS	ASP	GLN







<p>Ligand in 2D</p>  <p>Ligand in 3D</p>  <p>JSmol</p>	<p>Ligand in 2D</p>  <p>Ligand in 3D</p>  <p>JSmol</p>
<b>Carvone</b>	<b>Thymoquinone</b>
<p>Ligand in 2D</p>  <p>Ligand in 3D</p>  <p>JSmol</p>	<p>Ligand in 2D</p>  <p>Ligand in 3D</p>  <p>JSmol</p>
<b>Cymene</b>	<b>Chlorogenic acid</b>
<p>Ligand in 2D</p>  <p>Ligand in 3D</p>  <p>JSmol</p>	<p>Ligand in 2D</p>  <p>Ligand in 3D</p>  <p>JSmol</p>
<b>Friedelin</b>	<b>Betulinic acid</b>
<p>Ligand in 2D</p>  <p>Ligand in 3D</p>  <p>JSmol</p>	<p>Ligand in 2D</p>  <p>Ligand in 3D</p>  <p>JSmol</p>
<b>Daucosterol</b>	<b>Plumbagin</b>
<p>Ligand in 2D</p>  <p>Ligand in 3D</p>  <p>JSmol</p>	<p>Ligand in 2D</p>  <p>Ligand in 3D</p>  <p>JSmol</p>
<b>Gingerdione</b>	<b>Piperlonguminine</b>





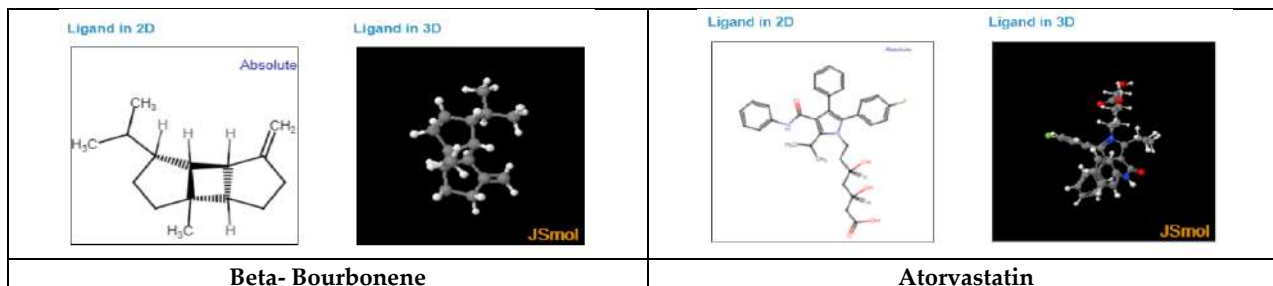


Fig. A. 2D & 3D Structure of Lead Compounds

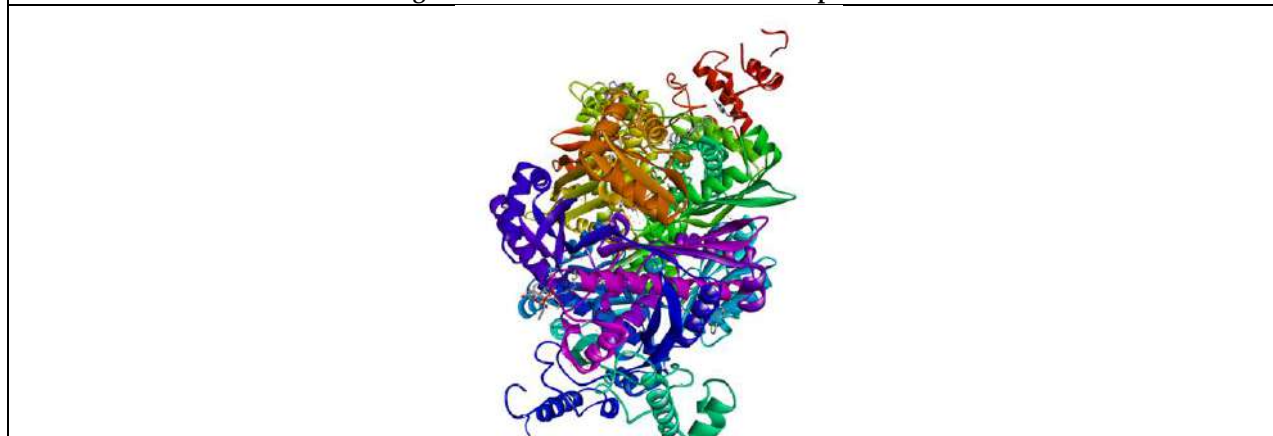
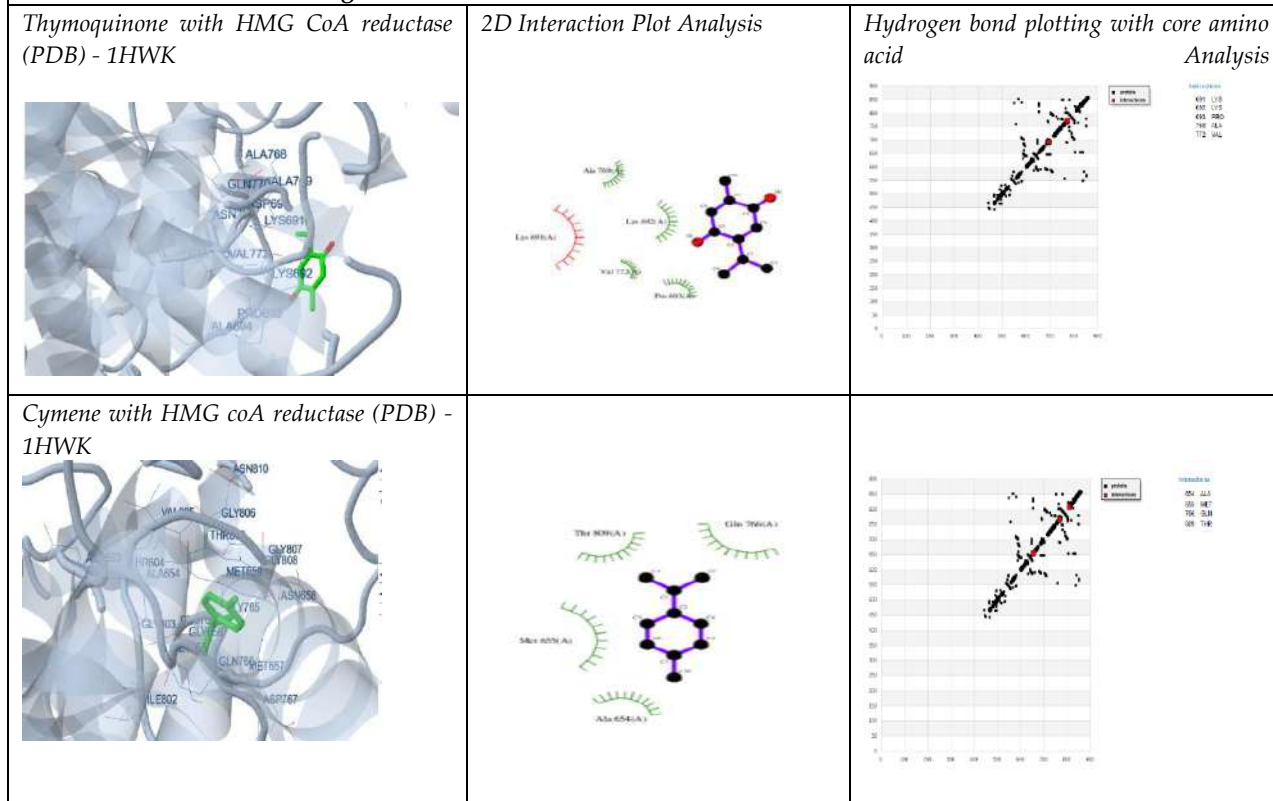
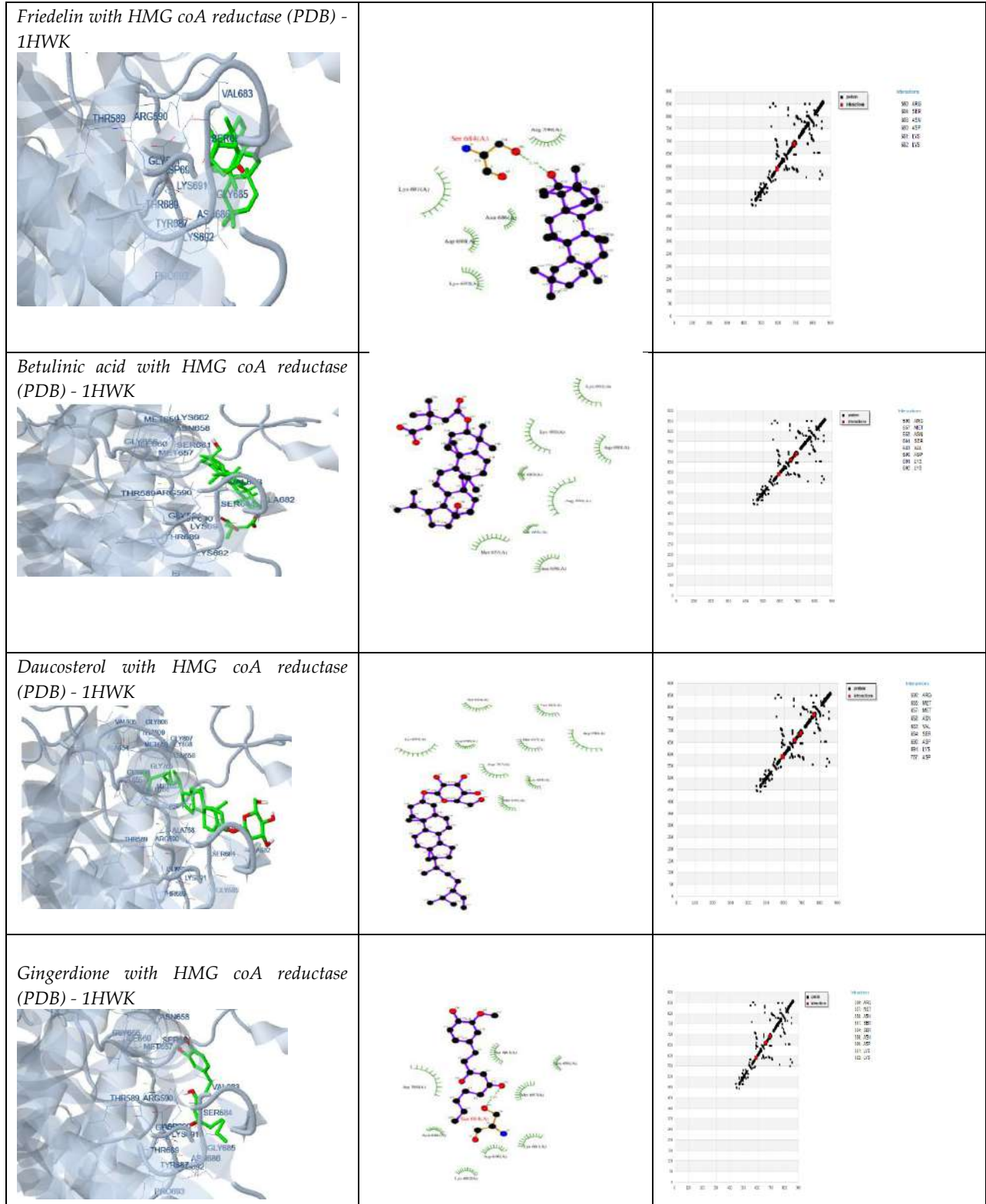


Fig. B: 3D- Structure of HMG CoA reductase (PDB) - 1HWK



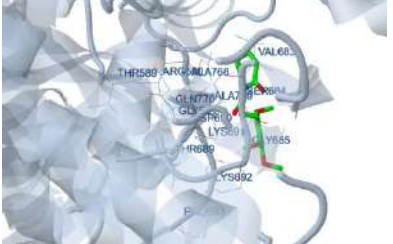
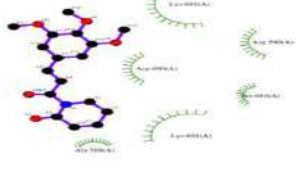
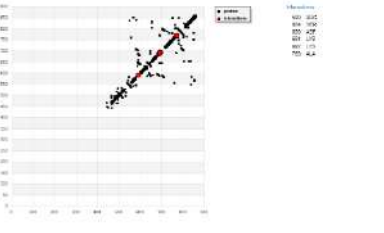

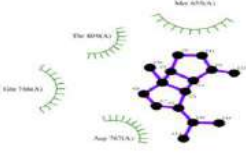
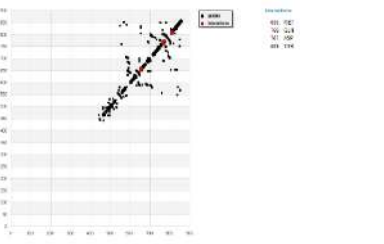
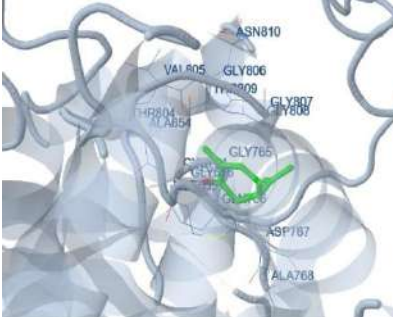
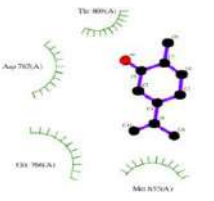
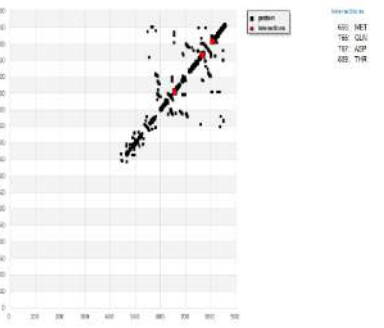
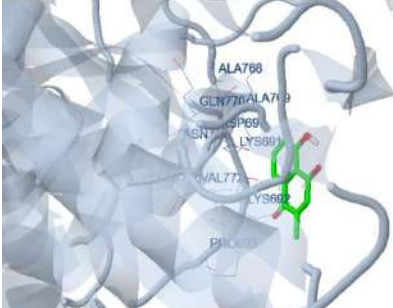
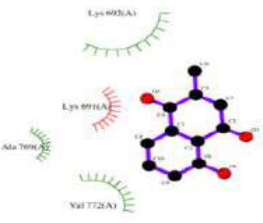
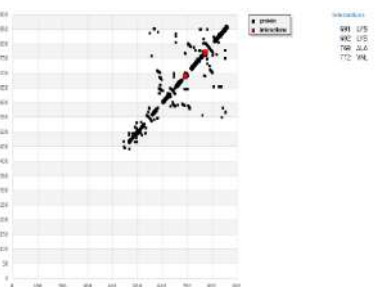


Parvathy et al.,





**Parvathy et al.,**

<p><i>Piperlonguminine with HMG coA reductase (PDB) - 1HWK</i></p> 		
<p><i>Beta- Bourbonene with HMG coA reductase (PDB) - 1HWK</i></p> 		
<p><i>Carvone with HMG coA reductase (PDB) - 1HWK</i></p> 		
<p><i>Plumbagin with HMG coA reductase (PDB) - 1HWK</i></p> 		



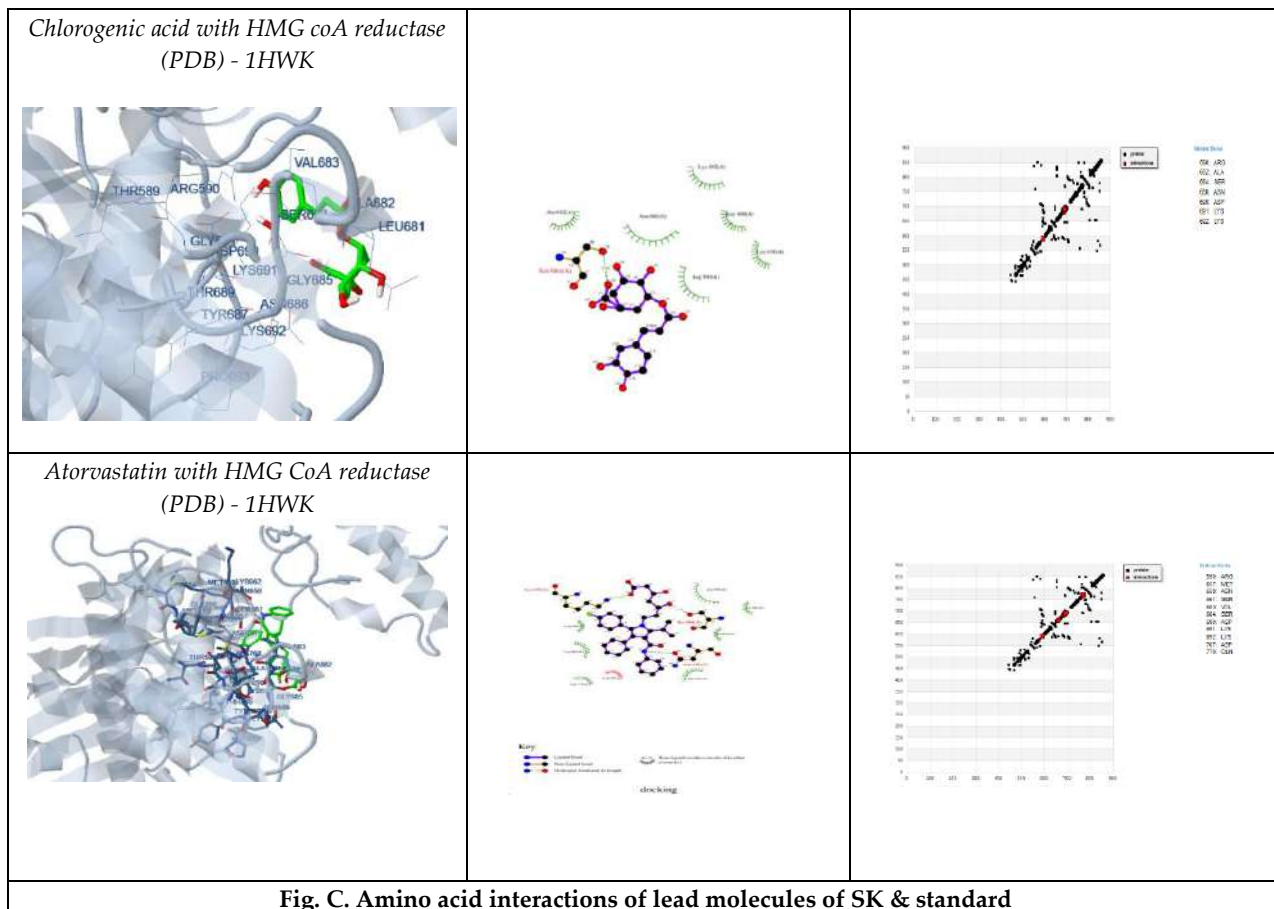


Fig. C. Amino acid interactions of lead molecules of SK & standard







## Preliminary Phytochemical Screening and *In vitro* Antioxidant, Anti diabetic and Anti Mitotic Activity of Methanolic Extracts of *Hyophorbe lagenicaulis* Fruits

Kanakaraju Addipalli<sup>1\*</sup>, Siri Varshini R<sup>2</sup>, R Bhargavi<sup>2</sup>, Sumayya Siddiqui<sup>2</sup>, T Sai Sanjana<sup>2</sup> and T Kavya<sup>2</sup>

<sup>1</sup>Associate Professor, Vignan Institute of Pharmaceutical Technology, , (Affiliated to Jawaharlal Nehru Technological University), Visakhapatnam, Andhra Pradesh, India.

<sup>2</sup>Students, Vignan Institute of Pharmaceutical Technology, (Affiliated to Jawaharlal Nehru Technological University), Visakhapatnam, Andhra Pradesh, India.

Received: 06 Oct 2024

Revised: 10 Nov 2024

Accepted: 12 Dec 2024

### \*Address for Correspondence

#### Kanakaraju Addipalli

Associate Professor, Vignan Institute of Pharmaceutical Technology,  
(Affiliated to Jawaharlal Nehru Technological University),  
Visakhapatnam, Andhra Pradesh, India.

E.Mail: rajuaddipalli81@gmail.com



This is an Open Access Journal / article distributed under the terms of the **Creative Commons Attribution License** (CC BY-NC-ND 3.0) which permits unrestricted use, distribution, and reproduction in any medium, provided the original work is properly cited. All rights reserved.

### ABSTRACT

The bottle palm, or *Hyophorbe lagenicaulis*, is a plant native to the Mascarene Islands that has traditionally been used in crafts and medicine. The pharmacological characteristics of its fruit extract are examined in this study, with an emphasis on the antimutagenic, antidiabetic, and antioxidant effects. Bioactive substances such as phenols, tannins, saponins, steroids, triterpenoids, and carbohydrates were detected by preliminary phytochemical screening. The DPPH radical scavenging assay was used to assess the extract's antioxidant activity, and the results showed a dose-dependent inhibition with an IC<sub>50</sub> value of 2.8 µg/mL. By assessing glucose absorption in a yeast cell model, the extract's antidiabetic efficacy was evaluated. At 10 mg/mL, it demonstrated an impressive 97.12% glucose absorption, outperforming the effects of the common medication metronidazole. By preventing seed germination in a green gram model, the extract also demonstrated antimutagenic activity, indicating possible anticancer effects. These results demonstrate *Hyophorbe lagenicaulis*'s pharmacological potential as an antimutagenic, antidiabetic, and antioxidant agent, bolstering its traditional medical usage and suggesting areas for future study.

**Keywords:** Bottle palmfruits, Anti oxidant, Anti diabetic, Anti mitotic, *invitro* screening.

### INTRODUCTION

The bottle palm, or *Hyophorbe lagenicaulis*, is native to the Mascarene Islands in the Indian Ocean, which are located east of Madagascar. Its native habitats are sandy, well-drained upland woodland and coastal savanna soils. It can thrive in the climates of the Hawaiian Islands, extreme southern California, and south Florida in the United States. Although it grows slowly, this tree can grow to a height of 12 to 20 feet. Although it may tolerate some shade, full sun is ideal for its growth. The 12-foot-long pinnately compound leaves or fronds are affixed to a 10-inch petiole or





### Kanakaraju Addipalli et al.,

stem. About two feet long, its dark green, thin, lance-shaped leaflets develop in a "V" pattern on the rachis, or center, of the frond, opposite one another. As it ages, the smooth, light grey to almost white trunk becomes more elongated and less apparent, but when it is young, its base is greatly increased. Above the stem, a smooth, waxy crownshaft, 2 to 3 feet tall, is where the leaf blades emerge. The trunk has massively branched flower inflorescences up to three feet long that surround it just below the crownshaft. Male and female flowers are seen on the same inflorescence and are either white or cream in color. The fruits are one inch in diameter and turn from green to black as they ripen [1].

#### **Varieties and Hybrids:**

1. *Hyophorbe lagenicaulis* 'Bottle Palm'
2. *Hyophorbe verschaffeltii* 'Spindle Palm'
3. *Hyophorbe amaricaulis* 'Hybrid Bottle Palm'

#### **Uses:**

1. Traditional medicine: using plants and roots to treat a variety of illnesses
2. Food source: Edible fruit that is not often eaten
3. Craft supplies: Leaves for thatching and weaving

#### **Phytochemistry:**

Name	Phytochemical	Pharmacological Activity
1. Flavonoids:	Quercetin, Kaempferol	Antioxidant and anti-inflammatory effects [2].
2. Phenolic acids:	Ferulic acid, Sinapic acid	Antioxidant and antimicrobial properties [3].
3. Terpenoids:	Lupeol, Ursolic acid	Antimicrobial, antioxidant, and anti-inflammatory effects [3].
4. Alkaloids:	Hyophorine, Lagenine	Potential therapeutic applications [2].
5. Saponins:	Hyophorbesaponins	Antioxidant and anti-inflammatory effect [3].
6. Glycosides:	Flavonoid glycosides	Antioxidant and anti-inflammatory effects [2].
7. Phytosterols:	Stigmasterol, Sitosterol	Antioxidant and antimicrobial properties [3].

#### **Pharmacological Activities**

Pharmacological activity	Mechanism of action
1. Antimicrobial Activity	Antibacterial: effective against <i>Staphylococcus aureus</i> , <i>Escherichia coli</i> , and <i>Pseudomonas aeruginosa</i> [3].
2. Antioxidant Activity	Free radical scavenging: demonstrated potent antioxidant activity [3].
3. Anti-Inflammatory Activity	1. Inhibition of inflammatory mediators: reduced inflammation in animal models [2]. 2. Anti-inflammatory compounds: flavonoids, phenolic acids, and terpenoids [3].
4. Cytotoxic and Anticancer Activity	1. Anti proliferative effects: inhibited cancer cell growth [3]. 2. Apoptosis induction: triggered cell death in cancer cells [2].
5. Cardiovascular Protection	1. Vasodilation: relaxed blood vessels, reducing blood pressure [3]. 2. Antihypertensive effects: lowered blood pressure in animal models [2].
6. Neuroprotective Activity	1. Neurotransmitter modulation: influenced neurotransmitter release [3]. 2. Anticonvulsant effects: reduced seizure frequency and severity [2].
7. Hepatoprotective Activity	1. Liver protection: prevented liver damage in animal models [3]. 2. Antioxidant effects: reduced oxidative stress in liver cells [3].

## MATERIALS AND METHODS

**Materials:** Baker's yeast, Glucose, Methanol, Metronidazole, Vincristine sulphate Injection. All the chemicals used here are of analytical grade.







Kanakaraju Addipalli et al.,

**Collection of plant material:** The fruits of bottle palm were collected from the premises of Vignan Institute of Pharmaceutical Technology, Visakhapatnam, Andhra Pradesh, India.

**Preparation of methanolic extract:** The collected plants were dried and made into powder. The powder was weighed and kept for maceration using methanol for 72 hours. The extract obtained was concentrated and stored in a refrigerator till further use.

**Preliminary Phytochemical Analysis:** The existence of phytochemicals like alkaloids, flavonoids, terpenoids, amino acids, cardiac and anthracene glycosides, saponins, steroids, tannins, phenols, and carbohydrates was confirmed by preliminary phytochemical analysis utilizing qualitative tests [5].

#### **invitro Antidiabetic activity**

**invitro Antidiabetic Activity Assessed by Glucose Uptake in a Yeast Cell Model** The amount of glucose taken by yeast cells was measured using a unique technique created by Shettar et al<sup>6</sup>. Commercially available *Saccharomyces cerevisiae* (baker's yeast) cells were suspended in 1% solution and kept at 25° Celsius. To obtain the clear supernatant fluid, the yeast cell solution was centrifuged five times for five minutes at 4,200 rpm. The clear supernatant was used to make a 10% v/v yeast cell solution for the experiment. After mixing the mixture with 100 µL of yeast solution, the reaction was started. It was then vortexed and incubated for 60 minutes at 37°C. After that, the materials were centrifuged at 3,800 rpm for five minutes. Then, for five minutes, the materials were centrifuged at 3,800 rpm. To quantify the amount of glucose in the supernatant, a UV-vis spectrophotometer set at 520 nm was utilized. Every reagent is present in the control sample, with the exception of the test sample. The complete experiment was run in three repetitions. The percentage of glucose uptake was calculated by the formula:

$$\% \text{ of glucose uptake} = \frac{\text{AbsControl} - \text{AbsSample}}{\text{AbsControl}} \times 100$$

#### **In vitro Antimitotic activity**

Preparing aqueous extracts and screening for antimitotic effectiveness using the *Vigna radiata* germination assay. Put a few green grams in a beaker with five milliliters of fresh water to mark them as the control. Five milliliters of fresh water should be added to a beaker along with a few green grams. Cover the beaker using filter paper. In another test tube, put a few green grams in a beaker having the extract solution. Cover the beaker using filter paper. It is best to keep both beakers at room temperature. Measure the length of the sprouts that grew in the test and control groups after three days. Compare the lengths of the test and control sprouts. Make a note of the observations [8].

## RESULTS AND DISCUSSION

#### **Preliminary Phytochemical Screening**

Preliminary Phytochemical analysis of bottle palm fruit extracts revealed the presence of carbohydrates, steroids and triterpenoids (Table 1).

#### **invitro Antioxidant activity by DPPH Radical Scavenging Activity (DPPH)**

A dose-dependent inhibition was demonstrated by the extract in the dosage range of 2–10 mg/mL. The IC<sub>50</sub> value is the amount of antioxidants in the sample required to 50% inhibit the free radicals. The IC<sub>50</sub> value decreases as the radical scavenging ability increases. The extract showed dose-dependent activity with an IC<sub>50</sub> value of 2.8 µg/ml and a maximum inhibition of 15.535% at 10 mg/mL. The positive standard ascorbic acid, on the other hand, showed an IC<sub>50</sub> value of 12.8 µg/ml and 52.14% inhibition. The proportion of DPPH scavenge activity that *Hyphorbe lagenicaulis* inhibited was shown in the above graph [6] (Table 2).

#### **invitro Antidiabetic activity by Glucose Uptake in Yeast Cell Model**

The glucose uptake test was used to evaluate in vitro antidiabetic activity of extracts from *Hyphorbe lagenicaulis* fruits at different dosages using a yeast model. Comparing the extract to the other extract doses, it demonstrated significant activity (97.12%) at 10 mg/ml.



**Kanakaraju Addipalli et al.,**

As the amount of *Hyophorbe lagenicaulis* fruit extract raised from 2 to 10 mg/mL, the graph above demonstrates a dose-dependent rise in the percentage of glucose absorption. Metronidazole, a popular drug, demonstrated 70.5% at 10 mg/ml [7] (Table 3).

**in vitro Antimitotic activity by plant based models**

Green gram growth was observed in the control in water, however it was not observed in the test sample adding beaker. 0.5µg/ml of *Hyphorbe lagenicaulis* extract is the medication concentration used here. The standard chemotherapy drug Methotrexate, at 0.1 mg/ml, inhibited seed germination by 0.001±1.0 percent. Hence, the extract has strong anti-mitotic properties [8].

**CONCLUSION**

The phytochemicals found in the plant extract *Hyphorbe lagenicaulis*, which is the subject of the preliminary phytochemical screening; include phenols, tannins, saponins, steroids, triterpenoids, and carbohydrates. As part of the current study, the fruit extract of *Hyphorbe lagenicaulis* was tested for antioxidant potential. The DPPH method was regarded as a stable technique since its outcomes are independent of the substrate's polarity. The primary idea underlying the active ingredients in plant extracts scavenging free radicals may be that they provide hydrogen to the free radicals, neutralising them and generating stable compounds that lessen their deadly consequences. With a maximum DPPH scavenging activity of 15.535%, the extract's IC<sub>50</sub> was 2.8 mg/mL, while the standard IC<sub>50</sub> was 12.8 mg/mL. Using yeast cells and the uptake of glucose technique, the antidiabetic efficacy of *Hyophorbe lagenicaulis* was evaluated in vitro. One significant indicator of yeast cells' uptake of glucose was the quantity of glucose left in the solution after a predetermined period of time. The percentage of glucose absorption by yeast cells mediated by plant extracts is 97.12% at 10 mg/ml, while the percentage of metronidazole uptake is 70.5% at 10 mg/ml, demonstrating the *in vitro* antidiabetic action of *Hyophorbe lagenicaulis* extract using a yeast cell model. With the help of stereospecific membrane carriers, the diffusion mechanism facilitated the movement of glucose across the yeast cells' cell membrane. *Hyophorbe lagenicaulis* methanol extract demonstrated improved glucose utilisation, which increases glucose uptake efficiency and helps regulate blood glucose levels. According to this study, *Hyophorbe lagenicaulis* has the potential to have antimitotic effects. The extract has demonstrated antimitotic action and seed germination inhibition at a dosage of 0.5 mg/ml.

**REFERENCES**

1. Friedman MH, Andreu MG, Quintana HV, McKenzie M, Kumar et al. *Hyophorbe lagenicaulis*, Bottle Palm: Kumar et al. (2013). Phytochemical analysis of *Hyophorbe lagenicaulis* leaves. J Pharm Res 2013;24(1):5-10.
2. William J, John P, Mumtaz MW, Ch AR, Adnan A, Mukhtar H, Sharif S, Raza SA, Akhtar MT. Antioxidant activity, α-glucosidase inhibition and phytochemical profiling of *Hyophorbe lagenicaulis* leaf extracts. PeerJ. 2019 Jun 20;7:e7022.
3. Naimi I, Zefzoufi M, Bouamama H, M'hamed TB. Chemical composition and repellent effects of powders and essential oils of *Artemisia absinthium*, *Melia azedarach*, *Trigonella foenum-graecum*, and *Peganum harmala* on *Tribolium castaneum* (Herbst) (Coleoptera: Tenebrionidae). Indus Crops and Prod. 2022; 182:114-817.
4. Khare P, Kishore K, Sharma DK. A study on the standardization parameters of *Cassia angustifolia*. Asian J Pharm Clin Res. 2017 Jul 1;10(7):329-32.
5. Srinivasan S, Wankhar W, Rathinasamy S, Rajan R. Free radical scavenging potential and HPTLC analysis of *Indigofera tinctoria* linn (Fabaceae). J Pharmaceutical Analysis. 2016 Apr 1;6(2):125-31.
6. Shettar AK, Sateesh MK, Kaliwal BB, Vedamurthya AB. In vitro antidiabetic activities and GC-MS phytochemical analysis of *Ximenia americana* extracts. Sou Afri J Bot. 2017;11(1):202-211.
7. Rehman G, Hamayun M, Iqbal A, Ul Islam S, Arshad S, Zaman K, Ahmad A, Shehzad A, Hussain A, Lee I. In vitro antidiabetic effects and antioxidant potential of *Cassia nemophila* pods. Bio Med res internl 2018;2(1):1824-1990.



Kanakaraju Addipalli *et al.*,

8. Parmar MP, Waghela BN, Vaidya FU, Pathak C, Parmar DV. Evaluation of antimutagenic activity of herbal extracts using plant-based model systems and their cytotoxic potential against human colon carcinoma cells. J Can Res and Therap 2021 17(6):1483-1490.

Table 1: Phytochemicals present in Bottle palm fruits

S.No	Name of the test	Observation	Inference
1.	<b>Alkaloids</b> Wagner's test	No reddish color ppt is formed.	<b>Alkaloids are absent</b>
2.	<b>Amino acids and Proteins</b> Ninhydrin test: Millon's test:	No development of purple or bluish colour. No development of brick red colour.	<b>Amino acids and proteins are absent</b>
3.	<b>Carbohydrates</b> Molisch's test: Fehling's test:	Purple ring at the junction of 2 layers. Presence of brick red colour.	<b>Carbohydrates are present</b>
4.	<b>Glycosides</b> Legal test:	No pink or red color obtained.	<b>Glycosides are absent</b>
5.	<b>Flavonoids</b> Shinoda test:	No yellow ppt is formed and no pink color is observed.	<b>Flavonoids are absent</b>
6.	<b>Tannins</b> Ferric chloride test:	Deep blue-black color is obtained.	<b>Tannins are present</b>
7.	<b>Saponins</b> Froth formation test:	Persistent foam is observed.	<b>Saponins are present</b>
8.	<b>Phenols</b> Lead acetate test:	Presence of white ppt.	<b>Phenols are present</b>
9.	<b>Steroids and Triterpenoids</b> Salkowski test	Reddish blue color in chloroform layer.	<b>Steroids and Triterpenoids are present</b>

Table 2: *invitro* Antioxidant Activity of Bottle palm fruits

Concentration	Sample Absorbance	% inhibition of DPPH Radical	Absorbance of standard ascorbic acid	%inhibition of DPPH radical of standard ascorbic acid
2mg/ml	0.382	8.49%	0.325	22.23%
6mg/ml	0.369	11.0%	0.230	36.96%
10mg/ml	0.353	15.535%	0.200	52.14%

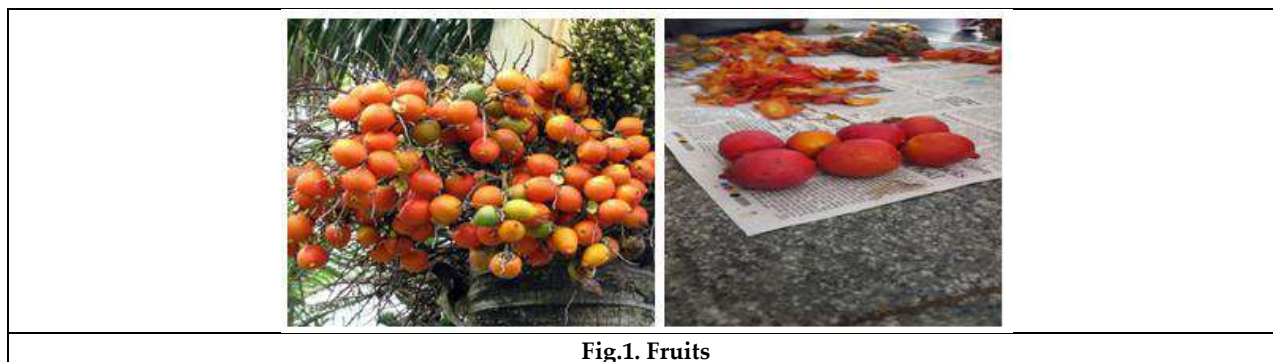


Fig.1. Fruits





Kanakaraju Addipalli et al.,

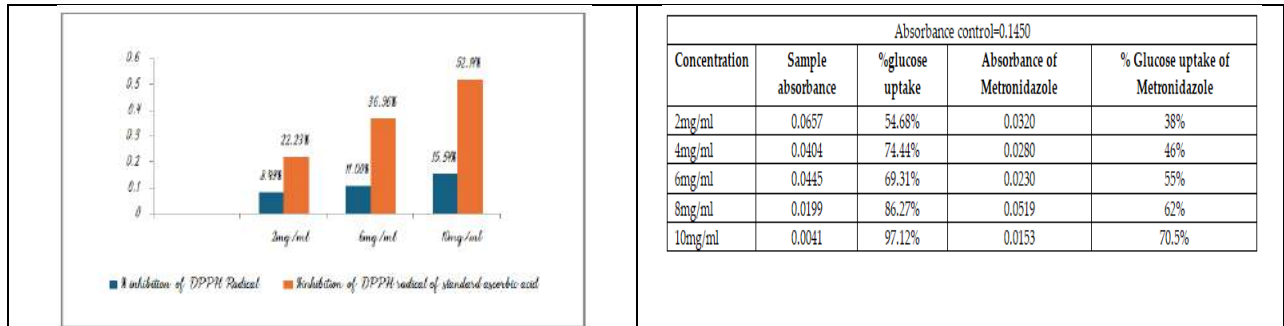


Fig 2. *in vitro* Antioxidant activity by DPPH Radical Scavenging Activity



Fig 3. *In vitro* Antidiabetic activity by Glucose Uptake in Yeast Cell

Figure 4. Green gram Models





## Preliminary Phytochemical Screening and *In vitro* Pharmacological activities of *Hymenocallis littoralis*

Aruna Kumari<sup>1\*</sup>, R Pooji Sravanthi<sup>2</sup>, S Manasa<sup>2</sup>, R Surya Mohith<sup>2</sup>, R Kaveri<sup>2</sup> and S M Priyavarshini<sup>2</sup>

<sup>1</sup>Associate Professor, Vignan Institute of Pharmaceutical Technology, (Affiliated to Jawaharlal Nehru Technological University), Visakhapatnam, Andhra Pradesh, India.

<sup>2</sup>Students, Vignan Institute of Pharmaceutical Technology, (Affiliated to Jawaharlal Nehru Technological University), Visakhapatnam, Andhra Pradesh, India.

Received: 06 Oct 2024

Revised: 10 Nov 2024

Accepted: 12 Dec 2024

### \*Address for Correspondence

**Aruna Kumari**

Associate Professor,

Vignan Institute of Pharmaceutical Technology,

(Affiliated to Jawaharlal Nehru Technological University),

Visakhapatnam, Andhra Pradesh, India.

E.Mail: arunakumari.lankada@gmail.com



This is an Open Access Journal / article distributed under the terms of the **Creative Commons Attribution License** (CC BY-NC-ND 3.0) which permits unrestricted use, distribution, and reproduction in any medium, provided the original work is properly cited. All rights reserved.

### ABSTRACT

Originally from the Latin American coastal locations that are warmer, *Hymenocallis littoralis*, also referred Spider lily is a type of plant belonging to the Amaryllidaceae family that has spread throughout tropical regions across the world. The pharmacological potential of the plant is examined in this study, with particular attention to its antimitotic and antidiabetic properties. A yeast cell glucose uptake model was used to evaluate the methanol extract of *H. littoralis*'s antidiabetic properties in vitro. The extract outperformed the reference medication metronidazole, which exhibited 70.5% absorption at the same concentration, with an 83.4% glucose uptake at 10 mg/mL. The findings demonstrate the extract's capacity to improve glucose utilisation and successfully control blood glucose levels by showing that glucose transport across yeast cell membranes was made possible by stereospecific membrane carriers. Furthermore, *H. littoralis* showed strong antimitotic action, as evidenced by its capacity to prevent seed germination at 0.5 mg/mL. This implies the existence of bioactive substances that have a variety of physiological and medicinal impacts, especially when it comes to the treatment of cancer. The results highlight *H. littoralis*'s potential as a natural chemical source for creating anti-cancer and antidiabetic treatments, calling for more research into its bioactive components and modes of action.

**Keywords:** *In vitro* screening, Anti diabetic, Anti mitotic, Aerial parts, Spider lilly

## INTRODUCTION

Spider plants the Amaryllidaceae family comprises *Hymenocallis littoralis*, is the botanical name for lily. Originally from warmer coastal regions of Latin America, this plant species belongs to the genus *Hymenocallis* and is now widely grown and naturalised in many tropical nations [1]. The Beach Spider Lily has narrow, sword-shaped leaves







**Aruna Kumari et al.,**

and grows at a height of 30 to 70 cm. The beach spider lily plant produces two to twelve flowers in a cluster, and a long stalk that is about two feet long emerges from the middle of the leaves. The flower is called Spider Lily because its petals resemble the legs of a spider. It's a significant medicinal herb. Certain plant parts, including leaves, have antibacterial and anti-inflammatory qualities [2]. Only the bulb of the plant is used to cure wounds; the extract from the roots and rhizomes is used as a nasal drop for snake bites. Numerous alkaloids have been identified from the spider lily plant's bulb during the course of its history. Several plants in the Amaryllidaceae family have been identified as having alkaloids, which are known to have a broad range of pharmacological activities [3]. Numerous alkaloids, including homolycorine, lycoramine, vittatine, macronine, lycorenine, tazettine, pretazettine, hippeastrine, littoraline, lycorine, and haemanthamine had been extracted from spider lily plants. Numerous pharmacological actions, including antibacterial, antiparasitic, antiviral, anticancer, antioxidant, and wound-healing characteristics, have been documented for these substances [4,5]. One of the main alkaloids in *Hymenocallis littoralis* [6] is lycorin, a pyrrolophenanthridine alkaloid.

### Phytochemistry

S.No	Part	Compound
1	Bulbs	Alkaloids include (p)-8-O-demethylmaritidine6, lycorine (1), hippeastrine (2), and 11-hydroxyvittatine (3).
2	Flowers	Rutin and quercetin 3'-O-glucoside (5) are flavonoids. Citronellal, hydroxycitronellal [7], along with other volatile oils

### Pharmacological Studies

●**Methylflavan /Antioxidant:** 7,4'-dihydroxy8-methylflavan was extracted from the *H littoralis* stem extract and evaluated for its capacity to scavenge radicals [8].

●**Cytotoxicity:** Pancratistatin (PST), which was derived from *H littoralis* in 1993, demonstrated substantial cytotoxicity to a human cancerous cell line. PST is selective for cancer cells while sparing healthy cells unaltered, per a new study. In this work, two natural compounds associated with PST, AMD4 and AMD5, were evaluated for their anti-cancer activity and specificity. The findings demonstrated that AMD4 lacked apoptotic activity while AMD5 exhibited selectivity and efficacy comparable to PST. Natural Amaryllidaceae alkaloids may share a phenanthridone structure that contributes to their specificity in combating cancer [9].

●**Anti-tumor:** In vitro and in vivo, the biologic activities of isocarbostryl alkaloids revealed greater cytotoxicity against a variety of tumour cell lines, together with strong selectivity for cancer cells relative to normal cells. Ten. Littoraline, HI Reverse Transcriptase Inhibition, Lycorine Alkaloids, and Cytotoxicity: The study uncovered a novel alkaloid, littoraline, in addition to 13 other known lycorine alkaloids and one lignan. In vitro, littoraline showed HIV reverse transcriptase inhibitory activity, but lycorine and haemanthamine showed high cytotoxicity [10].

●**Lycorine Alkaloids / Littoraline / HI Reverse Transcriptase Inhibition / Cytotoxicity:** Along with 13 other known lycorine alkaloids and one lignan, the study isolated a novel alkaloid, littoraline. Lycorine and haemanthamine demonstrated strong in vitro cytotoxicity, while littoraline demonstrated HIV reverse transcriptase inhibitory action.

●**Pancratistatin/Anticancer:** (1) The species is a good source of the potent anticancer drug pancratistatin. The bulbs produce the majority of pancratistatin, with the roots producing a smaller amount. A large-scale production method is described in the study. (2) Narciclasine was used as a precursor to create natural (+) pancratistatin synthetically.

●**Alkaloids:** Phytochemical examination of bulbs and flowers demonstrated the presence of four alkaloids, including lycorine, hippeastrine, 11-hydroxyvittatine, and (+)-8-O-demethylmaritidine, along with two flavonoids, quercetin, 3-O-glucoside, and rutin. In a petroleum ether extract [11], the antibacterial qualities of the flowers were analysed.

●**Narcistatin/Antiteoplastic:** Antecedents of the human cancer cell line inhibitory isocarbostryl have been obtained from the bulbs of *Hymenocallis littoralis* [12], which is derived from the horticultural production or reduction of narciclasine 1a-4 from the same source.

●**Anti-Candida Activity:** A methanol extract of several plant components was tested for its ability to inhibit *Candida albicans*. At 6.25 mg/ml [13], the flower and anther had an impact.







**Aruna Kumari et al.,**

•**Antimicrobial:** An aqueous extract was tested against *Candida albicans*, *S. aureus*, and *E. coli*. All of the examined species were inhibited by varying concentrations.

•**Antibacterial:** Leaf, flower, and stem bark extracts in methanol and ethyl acetate shown antibacterial action against *B.subtilis* [14]. The bulbs are frequently used as decorative plants and in the manufacturing of cosmetics.

## MATERIALS AND METHODS

**Materials:** Vincristine sulphate injection, glucose, methanol, metronidazole, and baker's yeast. Here, only analytical-grade compounds are utilised.

**Collection of plant material:** In Visakhapatnam, Andhra Pradesh, India, the Vignan Institute of Pharmaceutical Technology is where the entire Spider Lilly plant was gathered.

**Preparation of methanolic extract:** involved drying and powdering the gathered botanicals. The powder was weighed and allowed to macerate for seventy-two hours in methanol. The resulting extract was concentrated and refrigerated until it was needed again.

**Preliminary Phytochemical Analysis:** Using qualitative tests, a preliminary phytochemical study was carried out to validate the presence of various phytochemicals, such as alkaloids, polysaccharides, terpenoids, flavonoids, anthracene and cardiac glycosides, saponins, steroids, tannins, phenols

### *in vitro* Antidiabetic activity

Analysing Glucose Uptake in a Yeast Cell Model to Assess Antidiabetic Activity *in vitro* The special method developed by Shettar et al. was used to measure the amount of glucose absorbed by yeast cells. At 25°C, a 1% solution of commercially available yeast cells, *Saccharomyces cerevisiae*, was added. To get the clear supernatant fluid, five minutes of repeated centrifugation at 4,200 rpm was carried out on the overnight yeast cell solution. For the experiment, a 10% v/v yeast cell solution was produced with the clear supernatant. The mixture was mixed with 100 µL of yeast suspension, and the reaction was initiated. At 37°C, it was vortexed and incubated for 60 minutes. Except for the control, the materials were centrifuged at 3,800 rpm for five minutes. Using a UV-vis spectrophotometer set at 520 nm, the amount of glucose in the supernatant was estimated. The control sample contains every reagent except for the test sample. The experiment was carried out three times in duplicate. To calculate the percentage of glucose uptake, the following formula was applied:

$$\% \text{ of glucose uptake} = \frac{\text{AbsControl} - \text{AbsSample}}{\text{AbsControl}} \times 100$$

### *In vitro* Antimitotic activity

Weighed individually, green gram seeds were collected from the local grocer. 10 mg/ml, 20 mg/ml, 30 mg/ml, and 40 mg/ml extract concentrations were created. In this case, methotrexate is the standard. The control that we used was distilled water. We added equal weights of seeds to the mixture in Petri plates with different concentrations. A full day was spent at room temperature with the Petri plates in order to imbibe water. The pharmacological treatment was dried on dry tissue paper and weighed after 24 and 72 hours. We extended the sprouting period to 72 hours and took images.

where the seed's weight in distilled water is equal to Wt D.

The extract sample's seed weight is equal to (Wt E).

Seed weight in methotrexate = (Wt M)

## RESULTS AND DISCUSSION

### Preliminary Phytochemical Analysis

Alkaloids, amino acids, carbohydrates were among the phytochemicals present in *Hymenocallis* (Table 1).





Aruna Kumari et al.,

**Anti diabetic by glucose uptake method**

Using a yeast model, the glucose uptake test was used to evaluate the *in vitro* antidiabetic efficacy of *H. littoralis* extract at varying doses. At 10 mg/mL, the extract showed strong activity (83.4%) in comparison to the other extract doses. The graph above showed a dose-dependent increase in the percentage of glucose absorption as the concentration of *H. littoralis* extract increased from 2 to 10 mg/mL. At 10 mg/mL, the common medication metronidazole showed 70.5%.

**Anti mitotic methods by plant based models**

The laboratory results demonstrated that the green gram methanolic extract considerably raised the percentage inhibition following treatments of 24, 48, and 72 hours, which was comparable to the percentage inhibition of methotrexate. A 40 mg/ml concentration of methanolic extract resulted in  $0.01 \pm 0.1$  mm of seed growth, meaning that a 0.1 mg/ml concentration of the common medication Methotrexate inhibited seed germination by  $0.001 \pm 1.0$ . After 24 hours, 48 hours, and 72 hours of treatment, the assay findings demonstrated that the methanolic extract of green grams greatly reduced the percentage of inhibition, which was comparable to the percentage of inhibition of methotrexate. The methanolic extract with a 20 mg/ml concentration demonstrated  $0.98 \pm 0.9$  mm seed growth. When considering seed germination, distilled water, the control, has demonstrated more seed germination than standard and methanolic extracts (Table 3).

**CONCLUSION**

Yeast cell absorption of glucose, a profitable metric to evaluate the antidiabetic activity under *in vitro* settings, was used to test the antidiabetic activity of *H. littoralis*. The amount of glucose that was still present in the medium after a predetermined period of time was one prominent indicator of the uptake of glucose by yeast cells [16]. In a yeast cell model, the extract's *in vitro* antidiabetic effect can be determined by the fact that the percentage of glucose absorption by yeast cells mediated by *H. littoralis* plant extracts is 83.4% at 10mg/ml, while the percentage of Metronidazole uptake is 70.5% at 10 mg/ml.

Diffusion enables glucose to pass across the yeast cell membrane with the help of stereospecific membrane carriers. This demonstrated unequivocally that the methanol extract of *H. littoralis* is more effective at absorbing glucose by improving its utilisation, which in turn helps regulate blood glucose levels. According to this investigation of *H. littoralis*'s antimutic activity, the plant may have antimutic properties. This action demonstrated the existence of numerous important chemical compounds that are in charge of producing different physiological and medicinal effects. Therefore, this plant may be utilised as a source of cancer treatment medications. The extract has demonstrated antimutic action and seed germination inhibition at a dosage of 0.5 mg/ml. According to this study, *H. littoralis*'s may possess antimutic qualities. This plant might therefore yield medications that could be used to treat cancer. Following treatment for 24, 48, and 72 hours, the methanolic extract of green grams showed a significantly larger percentage inhibition than methotrexate. The antimutic activity of a 40 mg/ml methanolic extract was  $0.01 \pm 0.1$  mm, which indicates that the percentage suppression of seed germination was comparable to that of the common drug Methotrexate, which is  $0.001 \text{ mg/ml} \pm 1.0$  mm.

**REFERENCES**

1. Jaiswal P, Jadhav S, et al. The Detail Pharmacognostic Account On Plant Beach Spider Lily (Hymenocallis Littoralis). *Int J Innov Sci Res Technol* 2022;7:548-554.
2. Ivanov I, Berkov S et al. Improved hplcmetod for the determination of amaryllidaceae alkaloids. *Biotech & Biotechnol Equip* 2009 ;23:809-813.
3. Morton JF. Ornamental plants with toxic and/or irritant properties. *Flor State Horti Soc* 1962 ;75:484-490.
4. Morovvati H, Armand N. Assessment of Changes in Serum Concentrations of Liver Function (ALT, ALP, AST, LDH, GGT) After the Intake of Narcissus Bulbs. *J Fasa Uni of Medl Sci* 2019;9(4):1736- 1742.





Aruna Kumari et al.,

5. Jeevandran S, Geethaa S et al. Wound healing activity of *hymenocallis littoralis*-moving beyond ornamental plant. *J Pharm Sc* 2018;31, 2537- 2543.
6. Lin LZ, Shieh HL et al. Cytotoxic and antimalarial bisbenzylisoquinoline alkaloids from *Cyclebarbata*. *J of nat prod* 1993;56(1):22-29.
7. Abou-Donia AH, Toaima SM et al. Phytochemical and biological investigation of *Hymenocallis littoralis*. *Chem and biod* 2008;5(2):332-340.
8. Romero-Alvira D, Roche E. High blood pressure, oxygen radicals and antioxidants: etiological relationship *Med hypo* 1996;46(4):414-420.
9. Griffin C, Sharda N et al. Selective cytotoxicity of pancratistatin-related natural Amaryllidaceae alkaloids: evaluation of the activity of two new compounds. *Can Cell Int* 2007;7:1-7.
10. Ingrassia L, Lefranc F et al. Amaryllidaceae isocarbostryl alkaloids and their derivatives as promising antitumor agents. *Trans Oncol* 2008;1(1):1-3.
11. Kekre N, Griffin C et al. Pancratistatin causes early activation of caspase-3 and the flipping of phosphatidyl serine followed by rapid apoptosis specifically in human lymphoma cells. *Can Chemo ther&Pharmacol* 2005; 56:29-38.
12. Pettit GR, Melody N et al. Antineoplastic Agents. 450. Synthesis of (+)-Pancratistatin from (+)-Narciclasine as Relay1a. *J of org chem* 2001;66(8):2583-2587.
13. Sundarasekar J, Sahgal G et al. Anti-candida activity by *Hymenocallis littoralis* extracts for opportunistic oral and genital infection *Candida albicans*. *Bd J of Pharmacol* 2012 ;7(3):211-216.
14. Abdullah E, Raus RA et al. Extraction and evaluation of antibacterial activity from selected flowering plants. *American Med J.* 2012;3(1):27-32.
15. Shettar AK, Sateesh MK et al. In vitro antidiabetic activities and GC-MS phytochemical analysis of *Ximenea americana* extracts. *S Afri J of Bot* 2017; (11)1:202-211.
16. Kumaran A, Karunakaran RJ. Antioxidant activity of *Cassia auriculata* flowers. *Fitoterapia* 2007 ;78(1):46-47.
17. Parmar MP, Waghela BN et al. Evaluation of antimutagenic activity of herbal extracts using plant-based model systems and their cytotoxic potential against human colon carcinoma cells. *J of Can Res and Therap* 2021;17(6):1483-1490.

**Table 1. Preliminary Phytochemical analysis**

S.No	NAME OF THE TEST	Observation	Inference
1	<b>Alkaloids</b> Dragendroff's test Wagner's test	There was an orange-brown precipitate visible. There was a reddish-brown precipitation.	Alkaloids are present.
2.	<b>Amino acids</b> Ninhydrin test	Purple color was observed.	Amino acids are present.
3.	<b>Carbohydrates</b> Molisch's test	At the intersection, a purple ring develops.	Carbohydrates may present.
4.	<b>Glycosides</b> Borntrager's test	No change of ammonia layer.	Anthraquinone glycosides are absent.
5.	<b>Flavonoids</b> Shinoda test	No pink colour observed.	Flavonoids are absent.
6.	<b>Tannins</b> Ferric chloride test	There was no blue-black precipitate visible.	Tannins are absent.
7.	<b>Saponins</b> Froth formation test	No persistant observed.	Saponins are absent.
8.	<b>Steroids and Triterpenoids</b> Liebermann Burchards test	No colour change was observed.	Steroids are absent.





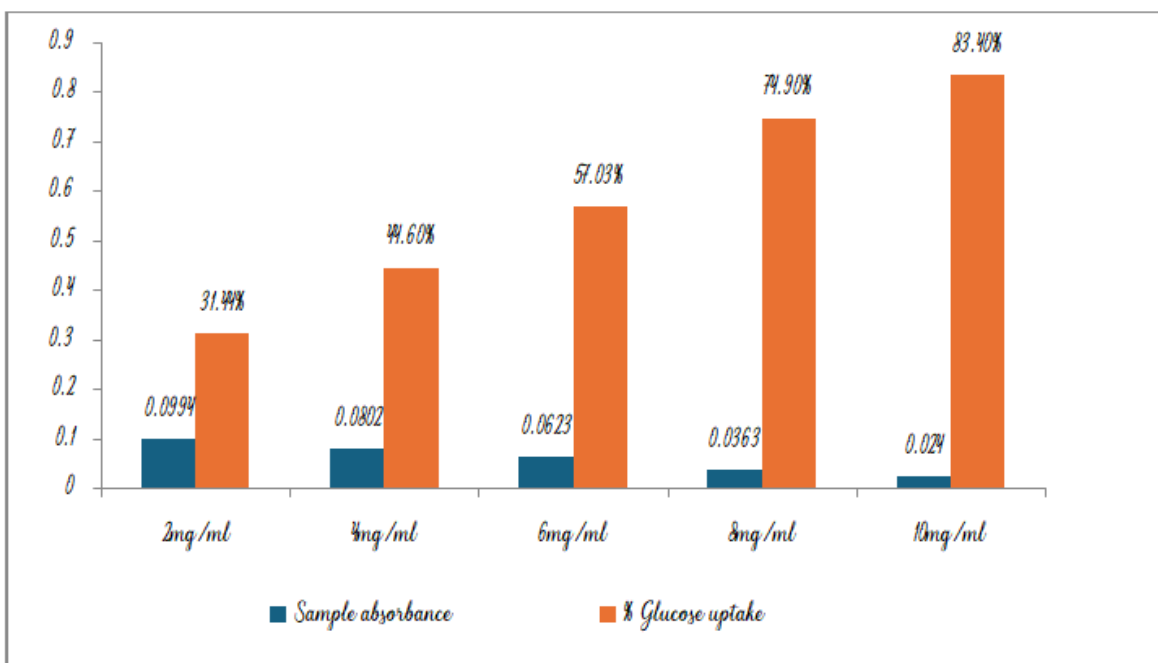
Aruna Kumari et al.,

**Table 2. *invitro* Antidiabetic activity**

Absorbance control = 0.145		
Concentration	Sample absorbance	% Glucose uptake
2mg/ml	0.0994	31.44%
4mg/ml	0.0802	44.6%
6mg/ml	0.0623	57.03%
8mg/ml	0.0363	74.9%
10mg/ml	0.0240	83.4%

**Table 3. *invitro* Antimitotic activity**

S.No	Drug Treatment	Concentration mg/ml	Treatment schedule	Seed growth's average
1	Methanolic extract-1	10	24 to 72 hours	1.8±4.8
2	Methanolic extract-2	20	24 to 72 hours	0.98±0.9
3	Methanolic extract-3	30	24 to 72 hours	0.55±0.6
4	Methanolic extract-4	40	24 to 72 hours	0.01±0.1
5	Control (Distilled water)	0	24 to 72 hours	29.5±5
6	Standard – Methotrexate	0.1	24 to 72 hours	0.001±1.0



**Figure 1 *invitro* Antidiabetic activity**





## Development and Characterization of Tooth paste Containing Casein Microspheres

Konthala Rajesh<sup>1</sup>, P.N.Mallikarjun<sup>2\*</sup>, Donka Devaki<sup>3</sup>, Yadlapalli Manogna<sup>3</sup>, Alluri priya<sup>3</sup> and Sekharamantri Vineela<sup>3</sup>

<sup>1</sup>Professor & Principal, Bhaskara Institute of Pharmacy, (Affiliated to Andhra University) Vizianagaram, Andhra Pradesh, India.

<sup>2</sup>Associate Professor, Department of Pharmaceutics, Vignan Institute of Pharmaceutical Technology, (Affiliated to Jawaharlal Nehru Technological University), Visakhapatnam, Andhra Pradesh, India.

<sup>3</sup>Student, Department of Pharmaceutics,

Vignan Institute of Pharmaceutical Technology, (Affiliated to Jawaharlal Nehru Technological University), Visakhapatnam, Andhra Pradesh, India.

Received: 06 Oct 2024

Revised: 12 Nov 2024

Accepted: 18 Dec 2024

### \*Address for Correspondence

**P.N.Mallikarjun**

Associate Professor, Department of Pharmaceutics,  
Vignan Institute of Pharmaceutical Technology,  
(Affiliated to Jawaharlal Nehru Technological University),  
Visakhapatnam, Andhra Pradesh, India.

E.Mail: mallik6567@gmail.com



This is an Open Access Journal / article distributed under the terms of the **Creative Commons Attribution License** (CC BY-NC-ND 3.0) which permits unrestricted use, distribution, and reproduction in any medium, provided the original work is properly cited. All rights reserved.

### ABSTRACT

The aim of present research to develop toothpaste containing aloe vera and casein. Aloe gel has anti-bacterial and anti fungal properties & it has good binding properties. This is used as a binding agent and therapeutic agent in development of toothpaste. Casein has anti-tooth decaying property, So Casein is incorporated as microspheres. These microspheres are added to the prepared toothpaste. Toothpaste was formulated by using a different proportions of various components. The toothpaste prepared which can accept all the required condition to keep the mouth feel fresh and prevent tooth decay. The prepared toothpaste was evaluated for different parameters such as homogeneity, spreadability, foaming ability, stability, PH, moisture and volatile material and etc. All these tested parameters were compared with marketed formulations. It has a good scope in future dental health of public.

**Keywords:** Casein, aloe vera, Tooth decay, Foaming ability





Konthala Rajesh et al.,

## INTRODUCTION

One of the most popular preventative measures for oral health is toothpaste. Although several commercial dentifrices make claims regarding their antibacterial qualities, little study has been done to support these claims. The purpose of this study was to evaluate how well different toothpaste formulations reduced the levels of oral bacteria. Improved oral hygiene was facilitated by the evaluated formulations' capacity to regulate the microbial burden. However, sustaining oral health still depends more on good brushing habits and oral hygiene habits than on the particular components of toothpastes[1] Toothpaste is a paste formulation product and is used to clean and maintain oral hygiene with the aid of toothbrush [2]. In order to avoid dental problems like cavities, gingivitis, and periodontal disorders, maintaining oral hygiene entails keeping the mouth and teeth clean. Oral infections typically result from the activity of plaque-forming bacteria and yeast present in the oral cavity, including species like *Actinomyces*, *Actinobacillus*, *Streptococcus*, and *Candida* [3].

Plaque-forming bacteria and yeast, such as *Streptococcus*, *Actinomyces*, *Actinobacillus*, and *Candida*, are commonly found in the oral cavity and are responsible for oral infections. The phosphoprotein casein is involved in controlling the body's metabolism of calcium and phosphate. Improved bone mineralisation has been shown in experimental animals, especially in postmenopausal models. By increasing the calcium phosphate content of dental plaque, casein proteins can also aid in the prevention of tooth decay. Variants of casein, including  $\alpha$ -casein,  $\beta$ -casein,  $\alpha$ s1-casein,  $\alpha$ s2-casein, and  $\kappa$ -casein, can be transformed into bioactive molecules. For instance,  $\alpha$ -casein can produce casomorphine, an opioid peptide, while  $\alpha$ - and  $\beta$ -caseins act as precursors to immunopeptides[4]. The uses of aloe vera gel, a natural and age-old substance, in dentistry have been well investigated. It has shown promise in the treatment of oral mucosal lesions, gingivitis, wound healing, and plaque reduction[5].

## MATERIALS AND METHODS

### Extraction of aloe vera gel

The fresh *Aloe barbadensis* miller leaves were collected and washed with water. Incisions were made on the leaves and left over night. The gel was scraped off from the pods of aloe vera. The Aloe gel was extracted using a multilayer muslin cloth bag to remove the marc from the solution and extraction process was shown in the Figure-1.[6,7,8]

### Toothpaste formulation

The required quantity of ingredients were weighed according to the formulation table1 and prepared four different formulations based on different proportions of carboxymethyl cellulose and aloe vera gel. The Calcium di-phosphate, Sodium Lauryl sulfate (S.L.S), and carboxymethyl cellulose were macerated in mortar while silica gel, propylene glycol, sorbitol and sodium saccharine were dissolved in water. The macerated powders were mixed with the prepared Aloe vera gel solution.

### Preparation of Casein Microspheres

0.8g of casein and 1g of sodium alginate were weighed accurately and taken into a clean and dry mortar and colouring agent was added. 10 ml of distilled water was added to the above contents and triturated well by adding small quantities of water until the desired consistency was acquired. The mixture was kept aside for 15 min. Now the mixture was taken into the syringe (syringe containing 18 gauze needle) and slowly released the mixture drop wise into the 10%  $\text{CaCl}_2$  solution, left undisturbed for 20 minutes and filtered the solution and collected the beads. The beads were dried by keeping in hot air oven at 70 C for about 12 hours. After drying the rigid microbeads was obtained. Collected the dried beads and the evaluation tests were performed. The preparation process was shown in Figure-2.







Konthala Rajesh *et al.*,

#### **Addition of Casein Microspheres to Toothpaste**

Prepared Casein Microspheres were added to the formulated toothpaste and mixed gently until uniform distribution of microspheres in the tooth paste.

#### **Evaluation of tooth paste [9,10,11] :**

All the four formulations of tooth paste were evaluated for various parameters

#### **Physical Examination (Colour, Odour, Taste, Smoothness)**

Formulated tooth paste was evaluated for its colour.

The visually colour was checked.

Odour was found by smelling the product.

Taste was checked manually by tasting the formulation.

The Smoothness was tested by rubbing the formulation between the fingers.

#### **Relative density**

Relative density was determined by weight in gram taken in 10 ml formulation and 10 ml distilled water using specific gravity bottle.

#### **Transparency**

About 5 millilitres of the prepared paste were placed in a 10-milliliter test tube, and the transparency of the mixture was visually examined.

#### **Homogeneity**

Using normal force at  $27 \pm 20^\circ\text{C}$ , the toothpaste should extrude a homogenous mass from the collapsible tube or any other appropriate container. Additionally, the majority of the contents must protrude from the container's crimp before it is gradually rolled.

#### **Determination of sharp and edge abrasive particles**

On the butter paper, extrude the contents that are 15 to 20 cm long. Do this for ten or more collapsible tubes. Check for the presence of hard-edged, sharp abrasive particles by pressing the contents of the entire length with the tip of your finger. Such particles must not be present in tooth paste.

#### **Microbial Growth**

This technique made use of nutritional agar medium. The prepared paste sample was aseptically transferred in a cross pattern onto the sample plate using the blank and sample petriplates. Microbial growth was monitored constantly for up to 15 days.

#### **Foaming Ability (6)**

V2 is the volume of water alone in millilitres, and this is the volume of foam with water in millilitres. Examined is the toothpaste's capacity to create foam during brushing, which enhances the brushing experience overall. A tiny quantity was combined with water in a measuring cylinder, and the initial volume was noted in order to evaluate the toothpaste's foamability. After shaking the mixture 10 times, the final volume of foam was noted. The froth power was calculated using the formula:  $\text{Foaming power} = V1 - V2$ , where V1

#### **pH**

A pH meter was used to measure the formed paste's pH. This process involved dispersing 1 g of paste in 100 ml of filtered water. Prior to use, the electrode was calibrated using a standard buffer solution at 4.0, 7.0, and 9.0 after being cleaned with double-distilled water and dried with tissue paper. Three separate pH readings were taken, and the averages were computed.





Konthala Rajesh *et al.*,

#### Estimation of moisture and volatile content

5 g of paste placed in a porcelain dish having 6-8 cm in diameter and 2-4 cm depth in it. Dry the sample in oven at 105°C.

#### Calculation

% by mass =  $100MI/M$

MI- Loss of mass(g) on drying

M- Mass (g) of the material taken for the test.

#### Viscosity

It was determined by using viscometer (Brookfield) with 2 number spindles.

#### Extrudability

This process involved filling a conventional capped collapsible laminated tube with the prepared paste, then crimping the end to seal it. The tubes' weights were noted down. The tubes were clamped after being positioned between two glass slides. After covering the slides with 500 g, the cap was taken off. Weighing was done on the quantity of extruded paste. It was calculated as a percentage of the extruded paste.

#### Spreadability

This technique uses the paste's slip and drag properties. 2g of the prepared paste was applied to the ground slide being examined. To release air and create a consistent layer of paste between slides, the prepared paste was sandwiched between this slide and another glass slide for five minutes. From the edges, extra gel was scraped off. The time (Sec) needed for the top slide to travel 7.5 cm was then recorded when the top plate was pulled 80 g with the aid of rope fastened to the hook. Better spreadability was indicated by a short interval.

Formula was used to calculate spreadability:

$$S = M \times L/T$$

Where,

S= Spreadability

M= Weight in the pan (tied to the upper slide) L= Length moved by the glass slide

T= Time (Sec) taken to separate the upper slide from the ground slide.

#### Storage stability:

The toothpaste was placed in a toothpaste tube and kept at 50 degrees Celsius, room temperature, and 400 degrees Celsius for 45 days. After cutting through the tube, the following criteria were used to determine whether or not the liquid component had been separated from the toothpaste. Storage stability evaluation criteria:

- A) No liquid component separation is seen.
- B) There is a small separation of a liquid component.
- C) It is evident that a liquid component has separated.

Net content: the following formula was used to determine net content:

Net content = weight of filled tube – weight of empty tube.

#### Characterization of casein Microspheres

##### Estimation of the particle size and wall strength of the microspheres

Using an optical microscope equipped with an ocular micrometre, the size of 100 particles was measured in order to ascertain the size of the beads. A Petri dish was used to test the beads' wall strength. The bigger portion of the Petri dish was filled with precisely weighed beads. A fifty-gram balance weight was set down on the smaller portion of the dish, which was positioned inversely on top of the beads.



**Konthala Rajesh et al.,****Comparison with marketed tooth paste**

The optimised formulation is compared with marketed pastes like Dabur Red and Colgate for physical parameters [12].

**RESULTS AND DISCUSSION**

All the four formulations are in beige colour with orange beads of casein. The prepared four formulations of paste are having mint flavor and sweet taste. The prepared four formulations of paste are smooth and homogeneous without any abrasive or sharp edge particles. All the evaluated parameters are with good correlation with that of standard formulations and are given Table-2. The foaming ability ranges from 8.2 to 9.6 and pH varies from 4.8 to 5.2. The extrudability ranges from 75.88 to 96.33 and spreadability ranges from 3.2cm/sec to 8.5cm/sec. The viscosity varies based on proportion of CMC content. During stability studies formulations F1 and F2 become hard and rigid but F3 and F4 are stable. Based on the all the parameters and stability studies F3 is selected as optimized formulation. The optimized paste is again compared with marketed formulations like Dabur and Colgate for their physical parameters and is shown in Table-3 and Figure-3. The optimized paste is more or less equal in most of the physical parameters.

**CONCLUSION**

The research concluded that medicated tooth paste an emphasizing and more acceptable in dental research and they are safer with minimum side effect. The aloe vera gel has incorporated successfully and it not only as binder but also for anti bacterial activity. The formulated tooth paste capable to the tooth and oral hygiene and show the anti tooth decaying activity due to presence of casein. The formulation compared with market preparation. Therefore it shows the equal patronizing and engrossing passion over the marketed formulations (Colgate, Dabur Red,). The formulated tooth paste has been good scope in future in nature remedies research and Dental health of public.

**ACKNOWLEDGEMENT**

The authors would like to our sincere thanks to Dr. L.Rathaih garu Chairmain Vignan Educational institutions and Dr.Y.Srinivasa Rao garu principal of VIPT for providing support throughout the completion of the present work

**REFERENCES**

1. Priyal G.,Maji Jose, Shruti Nayak, Vidya Pai, Sudeendra Prabhu, (2021) Evaluation of efficacy of different tooth paste formulations in reducing the oral microbial load - An in vivo study, Biomedicine; 41(2) Supplementary issue: 465-471
2. 2) Prashant GM, Chandu GN, Murali krishna KS, Shafiulla MD.(2007) The effect of mango and neem extract on four organisms causing dental caries *Streptococcus Mutans Streptococcus Salivarius, Streptococcus Mitis* and streptococcus Sanguis: An in Vitro study. Indian J Dent Res.; 18:148–51. [PubMed] <http://dx.doi.org/10.4103/0970-9290.35822>.
3. 3) Siswomihardjo W, Sunarintyas SB, Nishimura M, Hamada T.(2007) The difference of antibacterial effect of neem leaves and stick ex- tract. Int Chin J Dent.; 7:27–9.
4. 4.Kinga Kazimierska and Urszula Kalinowska-Lis(2021) "Milk Proteins—Their Biological Activities and Use in Cosmetics and Dermatology" National Library of Medicine 26(11): (PUBMED)
5. Vaibhav Shende,(2018). "Formulation and Evaluation of Herbal Tooth Gel Containing Aloe Vera: Compared Study with Marketed Preparations" European Journal of Pharmaceutical and Medical Research 5(1).
6. Homa Namiranian and Giovanni Serino (2012). "The effect of a toothpaste containing Aloe Vera on established gingivitis" swedish dental journal, 36(4).





**Konthala Rajesh et al.,**

7. Pallavi L. Phalke et al.,(2019).“Formulation and Evaluation of Toothpaste Containing Combination of Aloe And Sodium Chloride” International Journal of Pharmaceutical Sciences and Research, 10(3).
8. PegahNasiri et al.,(2021). “The Potential of Aloe vera as an Active Ingredient in Toothpaste Formulations: A Narrative Review” Nat Pharm Prod 17(2).
9. SatishMeshram et al.,(2020). “Formulation and Evaluation of Polyherbal Toothpaste and Comparative Study with Marketed Formulations” International journal of Creative Reasearch Thoughts, 8(5)
10. Humairaah Nikhat Basar et al., (2022).“Dentifrices: Its Composition, Forms and Function” - Journal Of Indian Dental Association – Kochi Dentifrices 4(1).
11. Hasibe Sevilay Bahadir et al.,(2023).“Toothpaste: Overview”, International Research in Dentistry.
12. Amar A. Khose et al.,(2023). “Herbal Toothpaste Formulation and Assessment: A Comprehensive Review” International Research Journal of Modernization in Engineering Technology and Science 5(11).

**Table-1. Formulation of Toothpaste**

S.no	Ingredients	F1	F2	F3	F4
1	Calcium di-phosphate	40g	40g	40g	40g
2	Carboxymethyl cellulose	1g	2g	1g	2g
3	Aloevera	1g	2g	2g	1g
4	Sodium lauryl Sulphate	1g	1g	1g	1g
5	Sorbitol	0.5g	0.5	0.5g	0.5g
6	Propylene glycol	30g	30g	30g	30g
7	Silica gel	1.5	1.5g	1.5g	1.5g
8	Sodium saccharine	0.5g	0.5g	0.5g	0.5g
9	Peppermint oil	Q.S	Q.S	Q.S	Q.S
10	Colouring agent (Beige)	Q.S	Q.S	Q.S	Q.S

**Table 2. All the parameters for the prepared tooth paste were given in table**

Parameters	Formulation			
	F1	F2	F3	F4
colour	Beige	Beige	Beige	Beige
Foaming ability	9.6	8.2	9	8.9
Transparency	Translucent	Translucent	Translucent	Translucent
pH	5.2	4.9	4.8	4.8
Homogeneity	uniform	uniform	uniform	uniform
Abrasiveness	Good	excess	Good	Good
Viscosity	3000cps	6500cps	3600cps	3800cps
Microbial growth	No growth	No growth	No growth	No growth
Extrudability	96.33	75.88	90	91.15
Spreadability	8.5cm/sec	3.2cm/sec	5.1cm/sec	5.9cm/sec
Stability	Become hard on long standing	Rigid on long period	Stable for long period	Stable for long period

**Table-3. All the parameters for the optimised tooth paste with marketed tooth pastes were given in table**

Parameters	Dabur	Colgate	Optimised
colour	Brick red	white	Beige
Foaming ability	9.5	9.8	9
Transparency	Translucent	Translucent	Translucent
pH	4.68	4.36	4.8





Konthala Rajesh *et al.*,

Homogeneity	uniform	uniform	uniform
Abrasiveness	Good	Good	Good
Viscosity	3200cps	3500cps	3600cps
Microbial growth	No growth	No growth	No growth
Extrudability	91.33	90.56	90
Spreadability	5.5cm/sec	5.2cm/sec	5.1cm/sec
Stability	Stable for long period	Stable for long period	Stable for long period



Figure 1.Extraction of Aloe vera gel

Figure 2.Preparation of casein microspheres



Figure 3.Comparative study of optimized paste with marketed toothpastes







## Impact of Dolutegravir on Weight Gain

Saritha Medapati<sup>1\*</sup>, Blessy Jayamon<sup>1</sup>, Bindu Krishna Kosireddy<sup>1</sup>, Bhagya Sri Palisetty<sup>1</sup>, Apoorva Pinisetty<sup>1</sup> and Chinta AshishManohar<sup>2</sup>.

<sup>1</sup>Vignan Institute of Pharmaceutical Technology (Affiliated to Jawaharlal Nehru Technological University), Duvvada, Visakhapatnam, Andhra Pradesh, India.

<sup>2</sup>Orenburg State Medical University, Orenburg, Russia.

Received: 06 Oct 2024

Revised: 12 Nov 2024

Accepted: 18 Dec 2024

### \*Address for Correspondence

#### Saritha Medapati

Vignan Institute of Pharmaceutical Technology  
(Affiliated to Jawaharlal Nehru Technological University),  
Duvvada, Visakhapatnam,  
Andhra Pradesh, India.  
E.Mail: chsaritha1975@gmail.com



This is an Open Access Journal / article distributed under the terms of the **Creative Commons Attribution License** (CC BY-NC-ND 3.0) which permits unrestricted use, distribution, and reproduction in any medium, provided the original work is properly cited. All rights reserved.

### ABSTRACT

Antiretroviral therapy (ART), particularly Integrase strand transfer inhibitors (INSTIs), has substantially enhanced the health outcomes of those with Human Immunodeficiency Virus (HIV), resulting in extended life expectancy. However, recent studies highlight a noteworthy association between ART, particularly INSTIs, and notable weight gain, potentially impacting cardiometabolic health. This phenomenon appears more prominent among specific demographic groups, including female, Black, and Hispanic patients, particularly within the initial three months of therapy. Dolutegravir (DTG), Bictegravir, and the accompanying drug, tenofovir alafenamide (TAF), stand out as frequently linked to excessive weight gain among INSTIs. The nature of this weight gain remains uncertain, prompting questions about whether it stems from unintended side effects or signifies an improvement in health, often termed the "return to health" effect. Exploring the involvement of the melanocortin system, a critical regulator of food intake and energy balance, in ART-associated weight gain is crucial. Hypotheses suggest that INSTIs, particularly DTG, may interfere with the anorexigenic effect of the melanocortin system, leading to increased food intake and subsequent weight gain. Ongoing research aims to discern the intricate relationship between INSTIs and the melanocortin system and its implications for patient health. The current understanding underscores the need for further investigation into the potential consequences of ART-induced weight gain, particularly its impact on therapy adherence and overall patient well-being. This inquiry aims to contribute valuable insights toward developing strategies for managing weight gain in individuals with HIV on ART, ultimately enhancing their health and overall quality of life.

**Keywords:** Antiretroviral therapy, Dolutegravir, Weight gain, Human Immunodeficiency Virus







Saritha Medapati et al.,

## INTRODUCTION

Acquired immunodeficiency syndrome (AIDS) is a contagious illness caused by the human immunodeficiency virus (HIV), a pathogen with the ability to assault the human immune system. This infectious ailment presents notable health hazards, primarily targeting CD4+ T lymphocytes, the principal cells within the human immune system, and causing their substantial depletion. Consequently, this process leads to compromised immune function within the human body[1][2], rendering individuals with HIV infection susceptible to various diseases and increasing the likelihood of malignant tumors[3][4]. Nevertheless, prompt administration of antiretroviral therapy (ART) significantly diminishes the mortality rate among HIV-infected or AIDS patients[5]. Integrase strand transfer inhibitors (INSTI), a novel category of antiretroviral medications including Dolutegravir (DTG), Raltegravir (RAL), Elvitegravir (EVG), and Bictegravir (BIC), demonstrate commendable tolerability and efficacy [6][7][8]. Over the initial two years of ART treatment, a noteworthy increase in body weight has emerged as a recognized concern for patients. Research indicates that individuals treated with INSTI exhibit more pronounced weight gain compared to those undergoing conventional antiviral therapy without INSTI [9][10][11]. This weight gain, observed during the initial phases of treatment, serves as a crucial indicator of recovery, signifying improved survival rates among HIV patients and the restoration of their immune capabilities[12][13][14][15][16].

### **Antiretroviral Therapy (ART) and Weight Dynamics in people living with HIV:**

Antiretroviral therapy (ART) has revolutionized the management of HIV infection, normalizing the lifespan of individuals who initiate fully suppressive lifelong ART early in the course of immunodeficiency[17]. Safety, efficacy, and the durability of ART have also improved, and most people living with HIV can anticipate remaining on their current ART regimens indefinitely. We also investigated potential differences in body weight, insulin resistance, and metabolic syndrome as dolutegravir has recently been associated with weight gain [18]. Antiretroviral therapy (ART) has been linked to heightened weight gain and metabolic challenges in individuals diagnosed with human immunodeficiency virus (HIV)[19]. The impact of ART-related weight gain is not uniformly distributed among people living with HIV (PLWH). Specific demographic cohorts, including females, Black individuals, and Hispanics, generally face an elevated risk of experiencing weight gain associated with ART, particularly following the initiation of integrase strand transfer inhibitor (INSTI)-based treatment regimens [20][21][22]. Preliminary indications suggest that weight gain may manifest as early as three months into the commencement of ART [23]. It is crucial to comprehend the influence of early ART-related weight gain on the development of cardiometabolic diseases [24]. Ongoing investigations are delving into the consequences of ART-induced weight gain on diseases correlated with increased body weight [25][26]. The progression of antiretroviral therapy (ART) has significantly enhanced the health outcomes for people living with HIV (PLWH). Nevertheless, individuals undergoing ART frequently encounter weight gain, attributed to the side effects of therapeutic drugs or a 'return to health' phenomenon. This weight gain amplifies the susceptibility of PLWH to becoming overweight and obese, subsequently escalating the risk of complications such as cardiovascular disease, diabetes mellitus, and neurocognitive impairment[27]. The utilization of ART regimens has resulted in a notable increase in weight among PLWH. Yet, the distinction between whether this weight gain stems from unintended side effects of ART usage or is a consequence of improved health remains unclear [28][29].

### **Instis and weight dynamics in newly treated individuals with HIV: DHHS guidelines and research insights :**

The guidelines from DHHS, along with numerous research studies, have indicated that INSTI-based treatment regimens lead to more substantial weight gain in newly treated individuals living with HIV compared to PI- or NNRTI-based ART regimens[30][31]. In individuals commencing antiretroviral therapy (ART), Integrase Strand Transfer Inhibitors (INSTIs) are associated with greater weight gain when compared to other categories of antiretrovirals among those living with human immunodeficiency virus (HIV; PLWH) [32][33][34]. Weight gain is observed in individuals living with HIV (PLWH). Unlike the early years of the HIV/AIDS epidemic when wasting was common, PLWH are now experiencing weight gain instead[35]. The year 2007 saw the introduction of the first



**Saritha Medapati et al.,**

Integrase Strand Transfer Inhibitor (INSTI), raltegravir, to the market. Subsequently, numerous studies have observed weight gain in individuals starting antiretroviral therapy (ART). The association between INSTI usage and weight gain has been increasingly reported[36].

**Weight gain patterns and risk factors in Dolutegravir-based antiretroviral therapy: insights from recent clinical analyses:**

Dolutegravir (DTG), the predominant Integrase Strand Transfer Inhibitor (INSTI) in prescription, has been linked to increased weight gain compared to other INSTIs or protease inhibitors (PIs). A recent comprehensive analysis of randomized clinical trials revealed that an elevated risk of weight gain is correlated with a lower CD4 T-cell count, higher viral load (VL), the absence of intravenous drug use, female gender, and Black race. Among INSTIs, DTG, Bictegravir, and the foundational drug tenofovir alafenamide (TAF) exhibit a greater propensity for weight gain compared to alternative medications in this class. This finding is particularly pertinent to individuals living with HIV (PLWH) in Asia, as prior investigations have involved a limited representation of this population. Some studies have documented variations in body weight pre and post initiation of specific antiretroviral therapy (ART). The influence of racial diversity, specifically Black race, has been identified as a determinant affecting weight gain in PLWH. Furthermore, Dolutegravir, classified as a second-generation INSTI, is associated with a higher magnitude of weight gain in comparison to first-generation INSTIs[37].

**Exploring weight gain dynamics and adherence considerations in antiretroviral therapy initiation for people living with HIV:**

Weight gain is a common occurrence after the initiation of antiretroviral therapy (ART). This is primarily attributed to the reversal of the catabolic state, which is associated with uncontrolled viremia and may also result from direct effects of certain types of ART[38] [Bailin SS et al. 2020]. The influence of obesity on adherence to antiretroviral therapy (ART) when treatment is initiated is not well understood. People living with HIV (PLWH), especially those who are obese, may experience a negative impact on adherence if they are concerned about further weight gain. Enhanced adherence to treatment might occur if any weight gain associated with it is regarded as a positive indication of improved health[39].

**Interplay of the Melanocortin system and insti-mediated mechanism in Weight Regulation:**

The central regulatory mechanism of the POMC/MC4R system is crucial for overseeing the balance of metabolic energy and food intake, making it a significant factor in the development of obesity. Within the hypothalamus, the arcuate nucleus (ARC) serves as a key player in this process, housing neurons expressing Proopiomelanocortin/cocaine- and amphetamine-regulated transcript (POMC/CART). These neurons actively produce  $\alpha$ -Melanocyte-stimulating hormone ( $\alpha$ -MSH), which locally affects both melanocortin 4 receptor (MC4R) and melanocortin 3 receptor (MC3R). Consequently, an anorexigenic response is triggered by inhibiting Neuropeptide Y (NPY) neurons within the ARC and influencing second-order neurons, as illustrated in Figure 1. Conversely, agouti-related peptide (AgRP) counteracts this process by inhibiting MC4R, thereby promoting increased food intake and fat deposition. Through MC4R stimulation,  $\alpha$ -MSH reduces food intake and augments peripheral energy expenditure, establishing an overall negative energy balance. External signals, such as leptin and insulin, play a role in inhibiting food intake and activating  $\alpha$ -MSH synthesis. In contrast, fasting hinders  $\alpha$ -MSH/MC4R signaling, eliciting a sense of hunger (see Figure 1). Monogenic obesity can result from mutations in MC4R, and genome-wide association studies have associated polymorphic gene variants of MC4R with weight gain. Pharmacological activators of MC4R are employed in the management of obese patients with MC4R genetic defects. Recently approved drugs for obesity, such as bupropion and naltrexone, stimulate the POMC system. Conversely, MC4R antagonists may find application in treating anorexia, promoting increased food intake in animal models. The dysfunction of the Melanocortin system may also be acquired[40][41][42].

Ghrelin, an appetite-stimulating hormone originating from the stomach, exhibits an increased expression of  $\alpha$ -MSH, which is released by POMC/CART neurons. This action specifically targets MC4R receptors located on second-order neurons, resulting in the initiation of an anorexigenic response. Furthermore,  $\alpha$ -MSH influences MC3R receptors on



**Saritha Medapati et al.,**

AgRP/NPY neurons, leading to the inhibition of the release of orexigenic neuropeptides NPY and AgRP. These neuropeptides have the potential to induce orexigenic effects by interfering with MC4R signaling on second-order neurons. Insulin and leptin play a role in inhibiting AgRP/NPY neurons and activating POMC/CART neurons, while ghrelin produces contrasting effects. Integrase strand transfer inhibitors (INSTI), exemplified by DTG, may disrupt the action of  $\alpha$ -MSH on MC4R and MC3R, potentially resulting in aberrant orexigenic responses and weight gain[43]. The orexigenic response induced by INSTI can be attributed to four potential mechanisms. Initially, the inactivation of the anorexigenic response through the blocking of MC4R initiates an orexigenic reaction. Evidence supporting this mechanism includes the inhibition of radiolabelled  $\alpha$ -MSH binding to MC4R by DTG[44]. Secondly, INSTI may induce the hyperactivation of the orexigenic response by increasing the secretion of NPY, enhancing NPY receptors, or both. Elevated levels of NPY in both plasma and cerebrospinal fluid were observed in individuals living with HIV (PLWH) compared to uninfected controls [45]. The third identified mechanism involves the inhibition of  $\alpha$ -MSH binding to MC3R in NPY/AgRP neurons, preventing NPY inhibition caused by  $\alpha$ -MSH and subsequently eliciting feeding behavior. Lastly, a potential fourth mechanism could entail peripheral signaling to NPY and POMC/CART neurons by ghrelin or leptin or their receptors [46]

## RESULTS

The observed probability ranking order, as delineated in the study, presented DTG with the highest likelihood of inducing weight gain among HIV/AIDS patients at 79.2%, followed by BIC at 77.9%, RAL at 33.2%, and EVG at 9.7%[47]. This implies a noteworthy association between dolutegravir (DTG) usage and a substantial proclivity towards weight gain in the context of individuals afflicted with HIV/AIDS. Substantiating these findings, a comprehensive investigation unveiled nuanced insights into the longitudinal effects of various antiretroviral treatments on patients. Notably, individuals commencing treatment with Dolutegravir, Darunavir, and Elvitegravir experienced average weight gains of 5.3 kg, 4.1 kg, and 4.6 kg, respectively, after five years of treatment initiation. In contrast, those initiating treatment with Lopinavir, Raltegravir, and Atazanavir demonstrated comparatively lower weight gains, averaging at 2.1 kg, 1.9 kg, and 2.3 kg, respectively. These nuanced distinctions underscore the differential impact of specific antiretroviral regimens on the weight dynamics of people living with HIV.

## CONCLUSION

In summary, the empirical findings highlight a significant relationship between antiretroviral therapy and weight gain in HIV/AIDS patients, revealing distinctions among specific drug regimens. The comprehensive five-year analysis underscores an increasing trajectory of weight gain associated with antiretroviral administration, particularly noting the substantial impact of the dolutegravir and tenofovir alafenamide / emtricitabine combination. Synthesizing evidence establishes a moderate certainty of dolutegravir-based regimens inducing larger body weight gains compared to alternative treatments like efavirenz (EFV), EFV400, and elvitegravir/c (EVG/c). Notably, the combination of dolutegravir with Tenofovir alafenamide (TAF)-containing backbones demonstrates a unique influence leading to more significant weight gains than dolutegravir combined with other nucleoside reverse transcriptase inhibitors (NRTIs). This nuanced understanding contributes crucial insights to the discourse on optimal antiretroviral therapeutic strategies, emphasizing the imperative for nuanced considerations in HIV/AIDS management to optimize both virological efficacy and metabolic well-being. The conclusive assertion of dolutegravir's pronounced impact on weight gain aligns with prior studies, further emphasizing its pivotal role in shaping metabolic outcomes for individuals undergoing HIV/AIDS treatment.





Saritha Medapati et al.,

## REFERENCES

1. Mogadam E, King K, Shriner K, Chu K, Sondergaard A, Young K, Naghavi M, Kloner RA. The association of nadir CD4-T cell count and endothelial dysfunction in a healthy HIV cohort without major cardiovascular risk factors. *SAGE Open Med.* 2020;8:2050312120924892
2. Ceulemans A, Bouzahzah C, Prat I, Urassa W, Kestens L. CD4-T cell enumeration in human immunodeficiency virus (HIV)-infected patients: a laboratory performance evaluation of Muse Auto CD4/CD4% system by World Health Organization prequalification of in vitro diagnostics. *PLoS ONE.* 2019;14(1):e0209677
3. Vangipuram R, Tyring SK. AIDS-associated malignancies. In: Meyers C, editor. *HIV/AIDS-associated viral oncogenesis.* Cham: Springer; 2019. p. 1–21.
4. Facciola A, VenanziRullo E, Ceccarelli M, D'Andrea F, Coco M, Micali C, Cacopardo B, Marino A, Cannavò SP, DiRosa M, et al. Malignant melanoma in HIV: epidemiology, pathogenesis, and management. *Dermatol Ther.* 2020;33(1):e13180
5. Eckard AR, McComsey GA. Weight gain and integrase inhibitors. *Curr Opin Infect Dis.* 2020;33(1):10–9.
6. Iwamoto M, Wenning LA, Petry AS, Laethem M, De Smet M, Kost JT, Merschman SA, Strohmaier KM, Ramael S, Lasseter KC, et al. Safety, tolerability, and pharmacokinetics of raltegravir after single and multiple doses in healthy subjects. *Clin Pharmacol Ther.* 2008;83(2):293–9.
7. Mondì A, Cozzi-Lepri A, Tavelli A, Rusconi S, Vichi F, Ceccherini-Silberstein F, Calcagno A, De Luca A, Maggiolo F, Marchetti G, et al. Effectiveness of dolutegravir-based regimens as either first-line or switch antiretroviral therapy: data from the Icona cohort. *J Int AIDS Soc.* 2019;22(1):e25227–e25227.
8. McComsey GA, Moser C, Currier J, Ribaud HJ, Paczuski P, Dubé MP, Kelesidis T, Rothenberg J, Stein JH, Brown TT. Body composition changes after initiation of raltegravir or protease inhibitors: ACTG A5260s. *Clin Infect Dis.* 2016;62(7):853–62.
9. Bourgi K, Jenkins CA, Rebeiro PF, Palella F, Moore RD, Altof KN, Gill J, Rabkin CS, Gange SJ, Horberg MA, et al. Weight gain among treatment-naïve persons with HIV starting integrase inhibitors compared to non-nucleoside reverse transcriptase inhibitors or protease inhibitors in a large observational cohort in the United States and Canada. *J Int AIDS Soc.* 2020;23(4):e25484–e25484.
10. Sax PE, Erlandson KM, Lake JE, McComsey GA, Orkin C, Esser S, Brown TT, Rockstroh JK, Wei X, Carter CC, et al. Weight gain following initiation of antiretroviral therapy: risk factors in randomized comparative clinical trials. *Clin Infect Dis.* 2020;71(6):1379–89
11. Bakal DR, Coelho LE, Luz PM, Clark JL, De Boni RB, Cardoso SW, Veloso VG, Lake JE, Grinsztejn B. Obesity following ART initiation is common and influenced by both traditional and HIV-/ART-specific risk factors. *J Antimicrob Chemother.* 2018;73(8):2177–85.
12. Yuh B, Tate J, Butt AA, Crothers K, Freiberg M, Leaf D, Logeais M, Rimland D, Rodriguez-Barradas MC, Ruser C, et al. Weight change after antiretroviral therapy and mortality. *Clin Infect Dis.* 2015;60(12):1852–9.
13. Paton NI, Sangeetha S, Earnest A, Bellamy R. The impact of malnutrition on survival and the CD4 count response in HIV-infected patients starting antiretroviral therapy. *HIV Med.* 2006;7(5):323–30.
14. Madec Y, Szumilin E, Geneviev C, Ferradini L, Balkan S, Pujades M, Fontanet A. Weight gain at 3 months of antiretroviral therapy is strongly associated with survival: evidence from two developing countries. *AIDS.* 2009;23(7):853–61
15. Koethe JR, Limbada MI, Giganti MJ, Nyirenda CK, Mulenga L, Wester CW, Chi BH, Stringer JS. Early immunologic response and subsequent survival among malnourished adults receiving antiretroviral therapy in Urban Zambia. *AIDS.* 2010;24(13):2117–21.
16. Koethe JR, Lukusa A, Giganti MJ, Chi BH, Nyirenda CK, Limbada MI, Banda Y, Stringer JSA. Association between weight gain and clinical outcomes among malnourished adults initiating antiretroviral therapy in Lusaka, Zambia. *J Acquir Immune Defc Syndr.* 2010;53(4):507–13.
17. May MT, Gompels M, Delpech V et al. Impact on life expectancy of HIV-1 positive individuals of CD4+ cell count and viral load response to antiretroviral therapy: UK cohort study. *AIDS* 2014; 28 (8): 1193–1202.





**Saritha Medapati et al.,**

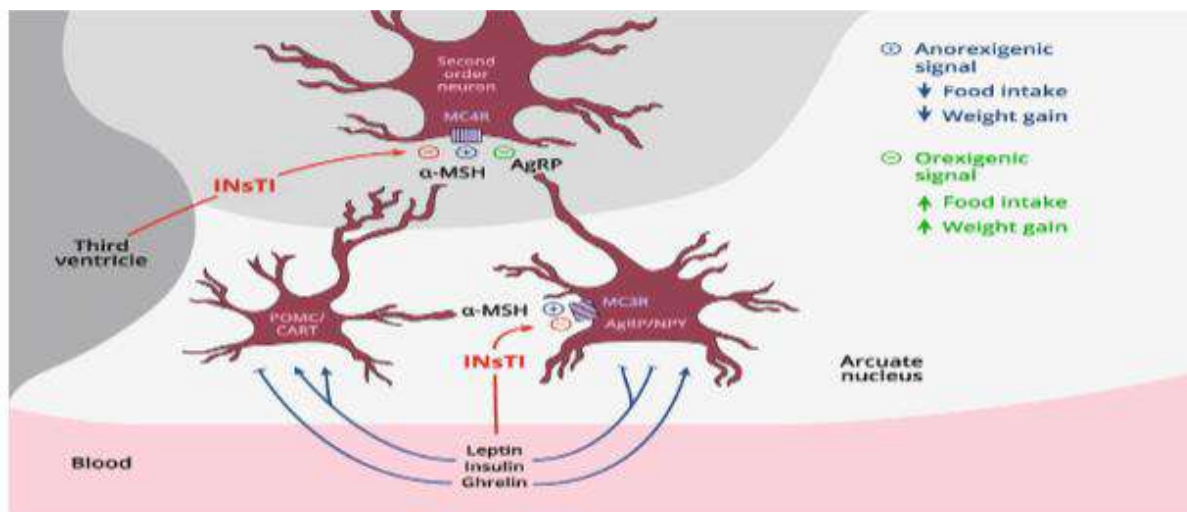
18. Ibrahim, F., Samarawickrama, A., Hamzah, L., Vincent, R., Gilleece, Y., Waters, L., Kegg, S., Barbini, B., Campbell, L., Post, F. A., & BESTT Trial . Bone mineral density, kidney function, weight gain and insulin resistance in women who switch from TDF/FTC/NNRTI to ABC/3TC/DTG. *HIV medicine* 2021;22(2):83–91.
19. Achhra AC, Mocroft A, Reiss P, et al. Short-term weight gain after antiretroviral therapy initiation and subsequent risk of cardiovascular disease and diabetes: the D:A:D study. *HIV Med.* 2016;17:255–268.
20. Sax PE, Erlandson KM, Lake JE, Mccomsey GA, Orkin C, Esser S, et al. Weight gain following initiation of antiretroviral therapy: risk factors in randomized comparative clinical trials. *Clin Infect Dis.* 2019;71(6):1379–89.
21. Achhra AC, Mocroft A, Reiss P, Sabin C, Ryom L, de Wit S, et al. Short-term weight gain after antiretroviral therapy initiation and subsequent risk of cardiovascular disease and diabetes: the D:A: D study. *HIV Med.* 2016;17(4):255–68.
22. Asundi A, Olson A, Jiang W, Varshney SP, White LF, Sagar M, et al. Integrase inhibitor use associated with weight gain in women and incident diabetes mellitus. *AIDS Res Hum Retroviruses.* 2022;38(3): 208–15.
23. Chow W, Donga P, Co<sup>^</sup>te<sup>^</sup>-Sergent A, Rossi C, Lefebvre P, Lafeuille M-H, et al. An assessment of weight change associated with the initiation of a protease or integrase strand transfer inhibitor in patients with human immunodeficiency virus. *Curr Med Res Opin.* 2020;36(8):1313–23.
24. Petersen R, Pan L, Blanck HM. Racial and ethnic disparities in adult obesity in the United States: CDC’s tracking to inform state and local.
25. Asundi A, Olson A, Jiang W, Varshney SP, White LF, Sagar M, et al. Integrase inhibitor use associated with weight gain in women and incident diabetes mellitus. *AIDS Res Hum Retroviruses.* 2022;38(3): 208–15.
26. Nansseu JR, Bigna JJ, Kaze AD, Noubiapi JJ. Incidence and risk factors for prediabetes and diabetes mellitus among HIV-infected adults on antiretroviral therapy: a systematic review and meta-analysis. *Epidemiology.* 2018;29(3):431–41.
27. Ando, N., Nishijima, T., Mizushima, D., Inaba, Y., Kawasaki, Y., Kikuchi, Y., Oka, S., &Gatanaga, H. Long-term weight gain after initiating combination antiretroviral therapy in treatment-naïve Asian people living with human immunodeficiency virus. *International journal of infectious diseases : IJID : official publication of the International Society for Infectious Diseases*, 2021;110:21–28.
28. Bailin SS, Gabriel CL, Wanjalla CN, Koethe JR. Obesity and weight gain in persons with HIV. *Curr HIV/AIDS Rep.* 2020;17:138–150.
29. Paul E Sax, Kristine M Erlandson, Jordan E Lake, Grace A Mccomsey, Chloe Orkin, Stefan Esser, Todd T Brown, Jürgen K Rockstroh, Xuelian Wei, Christoph C Carter, Lijie Zhong, Diana M Brainard, Kathleen Melbourne, Moupali Das, Hans-Jürgen Stellbrink, Frank A Post, Laura Waters, John R Koethe, Weight Gain Following Initiation of Antiretroviral Therapy: Risk Factors in Randomized Comparative Clinical Trials, *Clinical Infectious Diseases*, 2020;71(6):1379–1389.
30. Bourgi K, Rebeiro PF, Turner M, et al. Greater weight gain in treatment-naïve persons starting dolutegravir-based antiretroviral therapy. *Clin Infect Dis* 2020; 70:1267–74.
31. Chow W, Donga P, Co<sup>^</sup>te<sup>^</sup>-Sergent A, Rossi C, Lefebvre P, Lafeuille M-H, et al. An assessment of weight change associated with the initiation of a protease or integrase strand transfer inhibitor in patients with human immunodeficiency virus. *Curr Med Res Opin.* 2020;36(8):1313–23.
32. Sax PE, Erlandson KM, Lake JE, et al. Weight gain following initiation of antiretroviral therapy: risk factors in randomized comparative clinical trials. *Clin Infect Dis* 2019; doi:10.1093/cid/ciz999
33. Bourgi K, Rebeiro PF, Turner M, et al. Greater weight gain in treatment-naïve persons starting dolutegravir-based antiretroviral therapy. *Clin Infect Dis* 2020; 70:1267–74.
34. Bourgi K, Jenkins C, Rebeiro PF, et al. Greater weight gain among treatment-naïve persons starting integrase inhibitors. Poster presented at: CROI; 2019; Seattle, Washington. Abstract 670.
35. Crum-Cianflone N, Roediger MP, Eberly L, et al: Increasing rates of obesity among HIV-infected persons during the HIV epidemic. *PLoS One.* 2010; 5(4): e10106.
36. Kline, M., Daniels, C., Xu, X., Sunil, T., Ganesan, A., Agan, B. K., et al. Antiretroviral Therapy Anchor-based Trends in Body Mass Index Following Treatment Initiation Among Military Personnel with HIV. *Military medicine*, 2021;186(3-4):279–285.





## Saritha Medapati et al.,

37. Hill A, Waters L, Pozniak A. Are new antiretroviral treatments increasing the risks of clinical obesity? *J Virus Erad*2019;5:41–3.
38. Bailin, S.S., Gabriel, C.L., Wanjalla, C.N. *et al.* Obesity and Weight Gain in Persons with HIV. *Curr HIV/AIDS Rep* 17, 2020;138–150
39. Venter WDF, Moorhouse M, Sokhela S, Fairlie L, Mashabane N, Masenya M, *et al.* Dolutegravir plus Two Different Prodrugs of Tenofovir to Treat HIV. *N Engl J Med.* 2019;381:803–815.
40. Voss-Andreae A, Murphy JG, Ellacott KT, Stuart RC, Nillni EA, Cone RD, *et al.* Role of the central melanocortin circuitry in adaptive thermogenesis of brown adipose tissue. *Endocrinology.* 2007;148:1550–60.
41. Loos RJ, Lindgren CM, Li S, Wheeler E, Zhao JH, Prokopenko I, *et al.* Common variants near MC4R are associated with fat mass, weight and risk of obesity. *Nat Genet.* 2008;40:768–75.
42. Fleming KA, Ericson MD, Freeman KT, Adank DN, Lunzer MM, Wilber SL. *et al.* Structure-activity relationship studies of a macrocyclic AGRP-mimetic scaffold c[Pro-Arg-Phe-PheAsn-Ala-Phe-DPro] yield potent and selective Melanocortin-4 receptor antagonists and Melanocortin-5 receptor inverse agonists that increase food intake in mice. *ACS Chem Neurosci.* 2018;9:1141–51.
43. Hill A, Waters L, Pozniak A. Are new antiretroviral treatments increasing the risks of clinical obesity? *J Virus Erad*2019;5:41–3.
44. Malessa R, Heimbach M, Brockmeyer NH, Hengge U, Rascher W, Michel MC. Increased neuropeptide Y-like immunoreactivity in cerebrospinal fluid and plasma of human immunodeficiency virus-infected patients: relationship to HIV encephalopathy. *J Neurol Sci.* 1996;136:154–8.
45. Girardet C, Marks DL, Butler AA. Melanocortin-3 receptors expressed on agouti-related peptide neurons inhibit feeding behavior in female mice. *Obesity.* 2018;26:1849–55.
46. Bai, R., Lv, S., Wu, H., & Dai, L. Effects of different integrase strand transfer inhibitors on body weight in patients with HIV/AIDS: a network meta-analysis. *BMC infectious diseases*,2022;22(1), 118.
47. Ando, N., Nishijima, T., Mizushima, D., Inaba, Y., Kawasaki, Y., Kikuchi, Y., Oka, S., & Gatanaga, H. Long-term weight gain after initiating combination antiretroviral therapy in treatment-naïve Asian people living with human immunodeficiency virus. *International journal of infectious diseases : IJID : official publication of the International Society for Infectious Diseases*, 2021;110:21–28.



**Fig. 1** A graphical depiction elucidating the plausible disruption caused by INSTI in influencing the hypothalamic regulation of both food consumption and the equilibrium of energy homeostasis







## Anomaly Detection in Networks using Machine Learning Techniques

Routhu Daswanta Kumar<sup>1\*</sup>, Manjula Bammidi<sup>2</sup> and Routhu Shanmukh<sup>1</sup>

<sup>1</sup>Department of Computer Science Engineering, Centurion University of Technology and Management, Vizianagaram, Andhra Pradesh, India

<sup>2</sup>Assistant Professor, Department of Electronics and Communication Engineering, Vignan's Institute of Engineering for Women, (Affiliated to Jawaharlal Nehru Technological University), Visakhapatnam, Andhra Pradesh, India.

Received: 06 Oct 2024

Revised: 10 Nov 2024

Accepted: 12 Dec 2024

### \*Address for Correspondence

#### Routhu Shanmukh

Department of Computer Science Engineering,  
Centurion University of Technology and Management,  
Vizianagaram, Andhra Pradesh, India  
E.Mail: [routhushanmukh2002@gmail.com](mailto:routhushanmukh2002@gmail.com)



This is an Open Access Journal / article distributed under the terms of the **Creative Commons Attribution License** (CC BY-NC-ND 3.0) which permits unrestricted use, distribution, and reproduction in any medium, provided the original work is properly cited. All rights reserved.

### ABSTRACT

To detect malicious activity or malfunctions in the system, identifying anomalies in network communications is essential for cybersecurity. This paper investigates machine learning methods for efficient network anomaly detection. We employ both supervised and unsupervised algorithms, including support vector machines, k-means clustering, segregation forests, and deep mathematical frameworks for learning like autoencoders and frequently encountered neural networks. Issues such as feature selection and unbalanced datasets are addressed. We illustrate the effectiveness and drawbacks of these methods with a quasi-experimental assessment of real data sets. Our research advances proactive defenses against cyber threats and network security.

**Keywords :** Anomaly Detection, Networks, Machine Learning, Cyber Security.

## INTRODUCTION

It explores the use of distinct methods of machine learning for network traffic anomaly detection. Strong categorization capabilities are provided by supervised algorithms like support vector machines (SVM), which can discern between typical and unusual network behaviors using labeled training data. On the other hand, in situations where identified data is hard to come by or prohibitively expensive, unsupervised methods such as isolation of the woodlands and k-means clustering allow for the discovery of abnormalities without the requirement for labeled data.

Additionally, we investigate the application of sophisticated machine learning models—in most cases, machine learning with deep learning architectures—for network traffic anomaly identification. Neural networks called autoencoders are very good at identifying intricate patterns in high-dimensional data, which makes them ideal for jobs involving the identification of anomalies in network traffic. Furthermore, recurrent deep neural networks





**Routhu Daswanta Kumar et al.,**

(RNNs) show the potential to identify irregularities in mutually exclusive network data by providing insights into combinations and temporal relationships that might point to malicious activity.

Unbalanced datasets, as well as feature selection, are two issues that still exist in the field of the identification of anomalies in network traffic. Conventional machine learning methods encounter difficulties when dealing with imbalanced datasets when the proportion of normal instances surpasses that of anomalous instances, resulting in biased models. This problem can be solved by carefully weighing sampling strategies, changing the algorithm, or using specialized anomaly detection algorithms made for unbalanced data.

An important factor in the success of algorithmic methods for identifying anomalies is feature selection. Effectively choosing features that reflect the unique qualities of aberrant and normal network behaviors is crucial to developing strong anomaly detection models. Machine learning algorithms' ability to recognize signals is improved by identifying and extracting useful features from information relating to network traffic through the use of feature development process techniques, dimensionality reduction approaches, and domain expertise.

We evaluate different machine learning algorithms for network communication discernment of anomalies through extensive controlled testing on real-world network datasets. We can learn more about the benefits and drawbacks of each algorithm in various network contexts and attack scenarios by examining metrics like precision, recall, and F1-score. Our research advances the field of network security by shedding light on efficient anomaly detection techniques and directing the creation of preventative measures against online attacks.

Individuals evaluate the effectiveness of different machine-learning techniques for anomaly identification in network traffic through extensive validation experiments on real-world network datasets. Metrics like precision, and recall, in addition to F1-score analysis, help us understand the advantages and disadvantages of each algorithm in various network contexts and attack scenarios. By offering insights into efficient anomaly detection techniques and directing the creation of preventative measures against attack vectors from the internet, our findings advance the most recent advancements in network security.

## METHODOLOGY

Incorporating machine learning methodologies, identifying irregularities in networks is a sophisticated method that finds anomalous patterns or behaviors in transmissions of network data. The process comprises multiple stages, starting with an extensive gathering of data from various sources, including servers and network devices. Typically, this data consists of attributes such as IP addresses, protocol kinds, packet sizes, and frequencies. After the data is gathered, preprocessing procedures, which include managing missing values, encrypting variables based on categories, and scaling numerical characteristics, make sure the data is clean and ready for analysis. A key component of dataset refinement is feature selection, which concentrates on the most illuminating characteristics that support anomaly identification. Afterwards, choosing machine learning algorithms that are suitable for the task at hand is a crucial part of the technique. Popular options include deep learning methods like autoencoders, supervised strategies like Random Forest and Support Vector Machines (SVM), and unsupervised procedures relating to Isolation Forest and Local Outlier Factor (LOF). Based on variables like data properties and the intended result of the anomaly detection procedure, each algorithm has a unique set of benefits.

In high-dimensional data sets, the Support Vector Machine (SVM) plays an extremely important part in anomaly detection by precisely drawing complex decision boundaries. By optimizing the margin between distinct classes, SVM is an excellent anomaly detector that increases the algorithm's resistance to outliers. Its capacity to extract nonlinear correlations using kernel functions makes it much more useful for identifying complex abnormalities. Furthermore, SVM is effective in a variety of domains due to its versatility in handling both nonlinear as well as linear data distributions, which allows it to be tailored to a wide range of anomaly detection applications.





Routhu Daswanta Kumar *et al.*,

On the other hand, Random Forest uses the strength of the group's learning to play a crucial role in anomaly identification. Random Forest improves the model's generalization abilities and reduces the danger of overfitting by building several decision trees and combining their predictions. It can detect anomalies in noise because of its intrinsic capacity to handle extremely dense data and record intricate feature relationships. Furthermore, Random Forest's innate resistance to missing values and outliers improves its dependability in identifying anomalies in a variety of datasets and circumstances. It is an invaluable tool in anomaly detection scenarios across multiple domains due to its scalability and versatility.

## LITERATURE SURVEY

By utilizing its strengths in patterns being recognised and anomaly identification, the use of machine learning (ML) plays a crucial part in identifying TCP SYN flood assaults based on anomaly detection[1,2]. Machine learning (ML) algorithms can be created based on historical traffic information from the network in this situation to identify typical TCP SYN request patterns and create a baseline behavior for comparison[3,4]. Moreover, machine learning (ML) makes it possible for adaptive detection systems to rapidly change their responses to changing attack tactics by continuously upgrading their models in response to real-time network data[5,7]. The potential uses of machine learning (ML) have impacted many facets of our lives, transforming whole sectors and spurring creativity in many fields. Machine learning algorithms are used in healthcare for disease detection, personalized treatment suggestions, and medical imaging analysis[13,18]. Convolutional neural networks (CNNs), for example, help radiologists identify anomalies more accurately and efficiently by interpreting MRI and CT data[6,10]. Furthermore, using patient data analysis, machine learning models forecast the course of diseases and suggest customized treatment regimens based on unique health profiles. Throughout machine learning, identification of anomalies refers to finding patterns or occurrences in a collection of data that substantially depart from the norm. In this procedure, unsupervised algorithms are essential since they automatically figure out the data underneath makeup without requiring labeled instances. These computational methods, which include autoencoders and clustering techniques, find data points that deviate from the bulk of the dataset to uncover abnormalities. In addition, by taking into account contextual data like user behavior, network architecture, and time of day, machine learning algorithms can improve the predictability and effective performance of anomaly detection[9]. When deployed, machine learning models keep an eye on all incoming communication across networks and identify as anomalies anything that deviates from the taught patterns[11]. In particular, algorithmic methods for machine learning including hybrid approaches, supervised learning classifiers, and unsupervised anomaly detection techniques can be utilized[12]. Using features taken from TCP SYN packets, supervised learning classifiers such as Random Forests and Support Vector Machines (SVM) are trained on labeled data to categorize communication over the network as normal or anomalous[14,15]. Unsupervised techniques, such as autoencoders or clustering algorithms, find patterns that drastically differ from the average and identify anomalies without the need for labeled data[16]. Under their features, similar data points are grouped by clustering algorithms like DBSCAN and k-means. The points of information that aren't grouped to any particular cluster or that only belong to tiny clusters are subsequently classified as anomalies. Conversely, autoencoders are neural network designs that have been taught to recreate input data. When some data points have a reconstruction error that is noticeably larger than the rest of the dataset, this is referred to as an anomaly[17]. Anomaly detection systems may discover outliers and abnormalities in data on their own by using unsupervised algorithms[19]. This makes it possible to use these systems for applications in a variety of fields, including detecting fraudulent transactions, computer network safety, and equipment monitoring, without the requirement for clearly stated labels or human involvement[20].

## RESULT ANALYSIS

Anomaly detection relies heavily on Support Vector Machine (SVM) and Random Forest, each of which brings something special to the table. Random Forest attains an accuracy of 0.82, whilst SVM reaches 0.86. The efficiency of these algorithms is confirmed by a comprehensive statistical investigation. Furthermore, their effectiveness





Routhu Daswanta Kumar *et al.*,

emphasizes how important they are to machine learning processes for anomaly detection, especially when it comes to ingesting and analyzing statistical data. These results demonstrate how SVM and Random Forest may be used to adapt to and take advantage of complicated statistical patterns that are present in the data, in addition to validating their applicability for anomaly detection tasks. Local Outlier Factor plays a major role as an unsupervised algorithm which gives the accuracy of 0.89.

## CONCLUSION

A crucial aspect of cybersecurity, network anomaly detection, is explored in this paper. We have gained knowledge about the efficacy of deep learning frameworks like computerized encoders and recurrent neural networks, as well as algorithms like support vector machines, k-means clustering, independence forests, and others through an investigation of numerous supervised and unsupervised machine learning approaches. Through the resolution of issues such as imbalanced datasets and feature selection, we create the foundation for stronger anomaly detection systems. By conducting practical data trials, we have demonstrated the advantages and disadvantages of these strategies, adding to the collection of preventative measures against cyberattacks. The significance of ongoing research and innovation in supporting network security measures is shown by our findings.

## REFERENCES

1. S. Haris, R. Ahmad, and M. Ghani, "Detecting TCP SYN flood attack based on anomaly detection," in Network Applications Protocols and Services (NETAPPS), 2010 Second International Conference on, 2010, pp. 240-244: IEEE.
2. R. Alshammari and A. N. Zincir-Heywood, "A flow based approach for SSH traffic detection," in Systems, Man and Cybernetics, 2007. ISIC. IEEE International Conference on, 2007, pp. 296-301: IEEE.
3. H. Choi, H. Lee, and H. Kim, "Fast detection and visualization of network attacks on parallel coordinates," computers & security, vol. 28, no. 5, pp. 276-288, 2009. [63] "sklearn.ensemble.RandomForestRegressor," scikit-learn.
4. K. Kostas, "Anomaly Detection in Networks Using Machine Learning," Research Proposal, 23 Mar 2018, 2018.
5. M. H. Bhuyan, D. K. Bhattacharyya, and J. K. Kalita, "Network anomaly detection: methods, systems and tools," Ieee communications surveys & tutorials, vol. 16, no. 1, pp. 303-336, 2014.
6. Routhu Shanmukh, CH Nooka Raju, Lakshmana Rao Rowthu, "Analysis of fundus images using conventional edge detection techniques", Journal of Information and Computational Science, pp. 206- 217, Dec-2022.
7. W. Yassin, N. I. Udzir, Z. Muda, and M. N. Sulaiman, "Anomaly-based intrusion detection through k-means clustering and naives bayes classification," in Proc. 4th Int. Conf. Comput. Informatics, ICOCI, 2013, no. 49, pp. 298-303.
8. "Python Data Analysis Library," pandas: powerful Python data analysis toolkit - pandas 0.22.0 documentation. [Online]. Available: <https://pandas.pydata.org/>. [Accessed: 18-Aug-2018].
9. M. H. Bhuyan, D. K. Bhattacharyya, and J. K. Kalita, "Network anomaly detection: methods, systems and tools," Ieee communications surveys & tutorials, vol. 16, no. 1, pp. 303-336, 2014
10. Routhu Shanmukh, CH Nooka Raju, G. Tirupati, Application of Texture Analysis Techniques and Image Statistics to Fundus Images for Effective Comparison and Analysis, 10.54882/7420237411079, Innovations Number 74 September 2023.
11. W. Yassin, N. I. Udzir, Z. Muda, and M. N. Sulaiman, "Anomaly-based intrusion detection through k-means clustering and naives bayes classification," in Proc. 4th Int. Conf. Comput. Informatics, ICOCI, 2013, no. 49, pp. 298-303.
12. M. Suresh and R. Anitha, "Evaluating machine learning algorithms for detecting DDoS attacks," in International Conference on Network Security and Applications, 2011, pp. 441-452: Springer.
13. Routhu Shanmukh, CH Nooka Raju, Naveen Kumar Challa, CH. Mukesh, Journal of Chemical Health Risks, JCHR (2023) 13(6), 2086-2090 | ISSN:2251-6727.

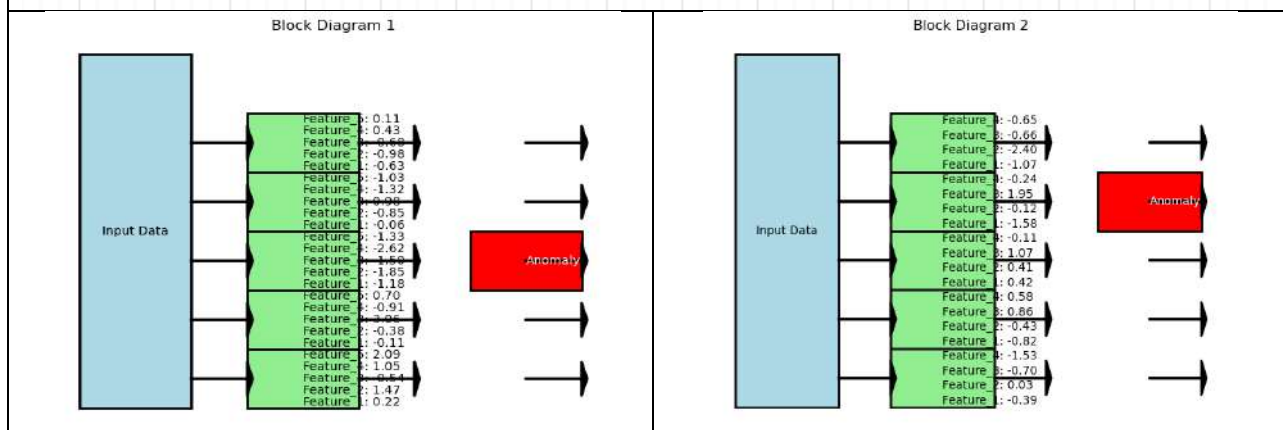
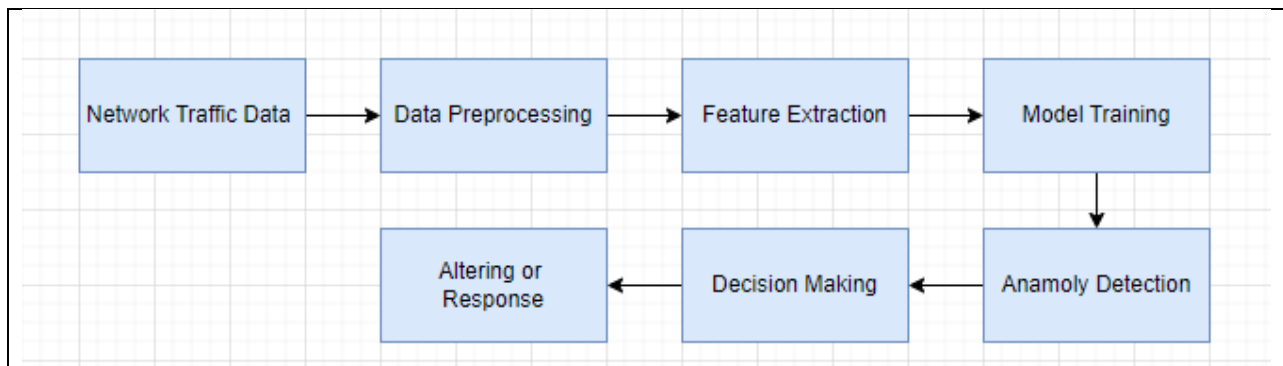




**Routhu Daswanta Kumar et al.,**

14. J. Brownlee, "Feature Importance and Feature Selection With XGBoost in Python," Machine Learning Mastery, 10-Mar-2018.
15. M. Ahmed, A. N. Mahmood, and J. Hu, "A survey of network anomaly detection techniques," Journal of Network and Computer Applications, vol. 60, pp. 19-31, 2016.
16. Buromman AA, Reaz MBI. A survey of intrusion detection systems based on ensemble and hybrid classifiers. Computers & Security. 2017;65:135-152.
17. Agrawal S, Agrawal J. Survey on anomaly detection using data mining techniques. Procedia Computer Science. 2015;60:708-713.
18. Routhu Shanmukh, CH Nooka Raju, Syed Raashid Andrabi, "Analysis of intensity variations on applications of edge detection techniques to fundus images", Gradiva Review Journal, Volume 9 Issue 1 Jan-2023.
19. Hu J, Ma D, Liu C, Shi Z, Yan H, Hu C. Network Security Situation Prediction Based on MR-SVM. IEEE Access. 2019;7:130937-130945
20. Alizadeh H, Khoshrou A, Zuquete A. Traffic classification and verification using unsupervised learning of Gaussian Mixture Models. In: 2015 IEEE international workshop on measurements & networking (M&N). IEEE; 2015. p. 1-6.

S.NO	Packet_Size	Packet_Frequency	Protocol_Type	Source_IP
1	734	30	TCP	5.29.91.249
2	609	79	TCP	181.193.61.232
3	1266	12	ICMP	154.28.231.167
4	885	74	UDP	97.105.175.109
5	813	12	TCP	160.121.4.182



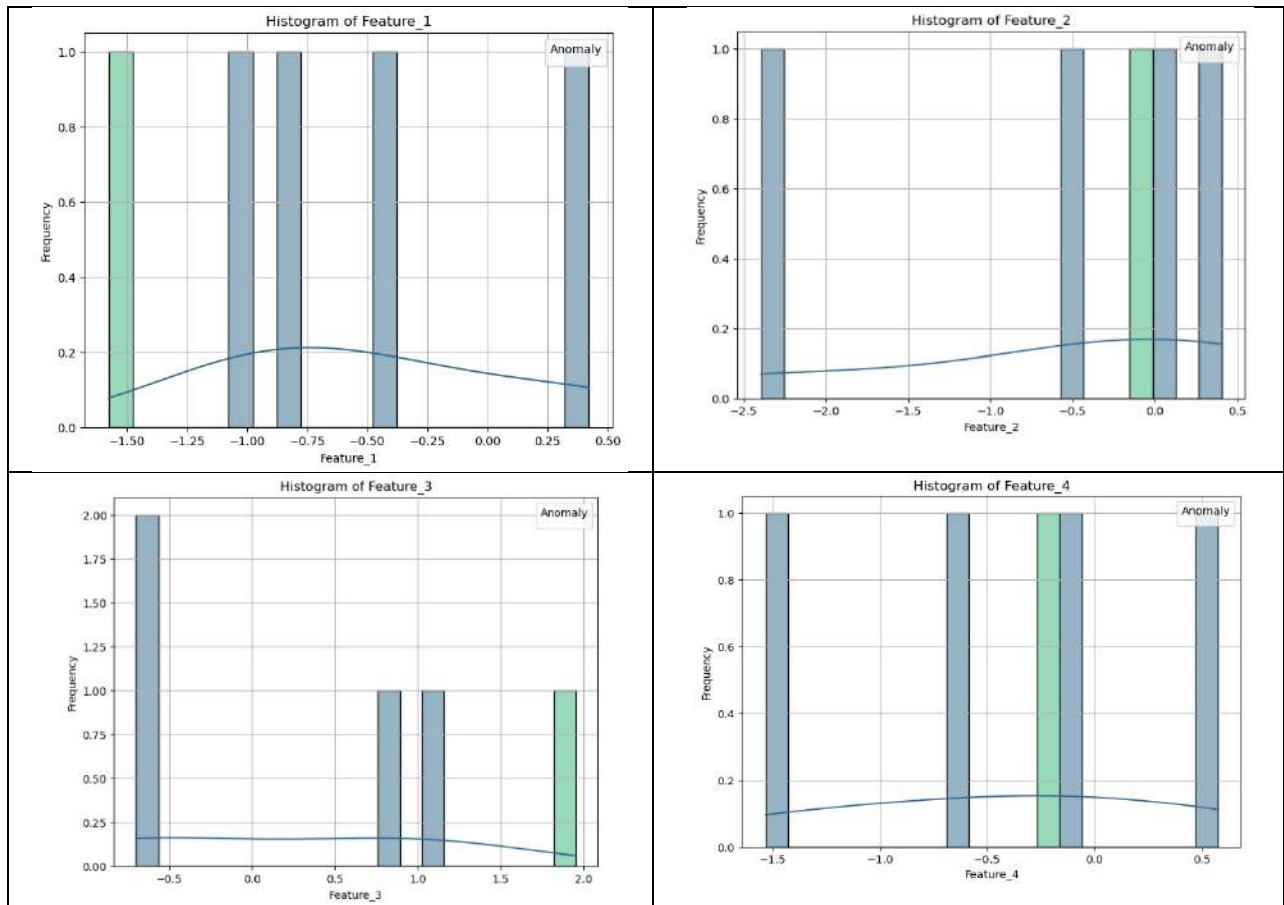
**Fig(1) : It shows the identification of the anomaly detection**



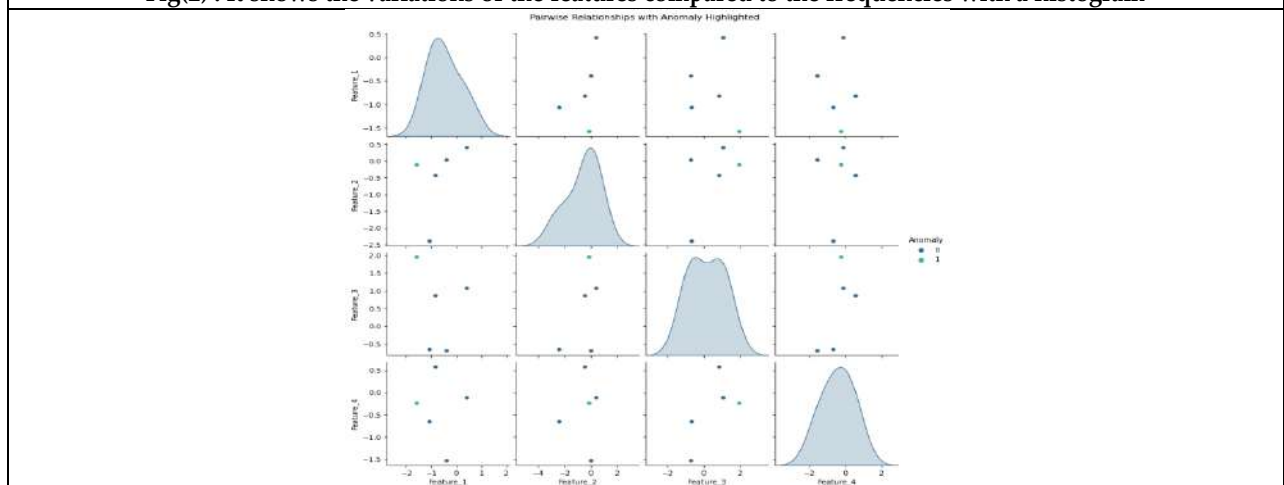




Routhu Daswanta Kumar et al.,



Fig(2) : It shows the variations of the features compared to the frequencies with a histogram



Fig(3) : Pairwise relationship with anomaly are highlighted







# Enhancing EEG Based Epileptic Seizure Prediction through Deep Learning and Channel Optimization Techniques

Botcha Kishore Kumar<sup>1\*</sup>, K. N. Brahmaji Rao <sup>2</sup> and C H.Bindu Madhuri <sup>3</sup>

<sup>1</sup> Research Scholar, Department of Computer Science and Engineering, Jawaharlal Nehru Technological University Gurajada Vizianagaram, Andhra Pradesh, India.

<sup>2</sup> Associate professor, Department of Computer Science and Engineering, Raghu Institute of Technology, (Affiliated to Jawaharlal Nehru Technological University), Visakhapatnam, Andhra Pradesh, India.

<sup>3</sup> Assistant Professor, Department of Information Technology, Jawaharlal Nehru Technological University Gurajada Vizianagaram, Dwarapudi, Andhra Pradesh, India.

Received: 06 Oct 2024

Revised: 10 Nov 2024

Accepted: 12 Dec 2024

## \*Address for Correspondence

**Botcha Kishore Kumar**

Research Scholar,

Department of Computer Science and Engineering,

Jawaharlal Nehru Technological University,

Gurajada Vizianagaram, Andhra Pradesh, India.



This is an Open Access Journal / article distributed under the terms of the **Creative Commons Attribution License** (CC BY-NC-ND 3.0) which permits unrestricted use, distribution, and reproduction in any medium, provided the original work is properly cited. All rights reserved.

## ABSTRACT

It is essential to predict epileptic seizures from EEG data in order to improve patient outcomes and advance medical care. Convolutional neural networks (CNNs), artificial neural networks (ANNs), and recurrent neural networks (RNNs) are examples of algorithms based on deep learning that are integrated with channel optimization techniques in this study to improve predictions accuracy as well as speed. By determining which EEG channels are most pertinent, optimized channel selection lowers computing complexity while maintaining important data. The deep learning models outperform conventional techniques in terms of precision, recall, and overall accuracy on standard datasets by capturing temporal as well as spatial trends in the EEG data. efficient method for predicting seizures in real time, opening the door for more sophisticated solutions for managing and treating epilepsy and showcasing the possibility of fusing deep learning alongside optimal channel optimization for medical advancements.

**Keywords :** Artificial neural networks (ANNs), Convolutional neural networks (CNNs)Deep Learning, EEG, Healthcare, Recurrent neural networks (RNNs).

## INTRODUCTION

Abruptly, unpredictable disturbances in brain activity, epileptic seizures can cause significant harm to the mental and physical wellness of a person. Predicting seizures accurately is essential for improving the health of patients' life experiences and enabling timely medical interventions. Electroencephalography (EEG), an alternative method for assessing electrical discharges in the brain, is crucial for seizure prediction. However, because EEG signals are



**Botcha Kishore Kumar et al.,**

complex and high-dimensional, it is difficult to develop effective prediction systems using traditional approaches. Epileptic seizures are a devastating neurological condition that affects millions of individuals worldwide. Accurate seizure prediction enables prompt medical treatment and a significant increase in patients' general quality of life. Electroencephalography (EEG) information continues to be widely used to detect abnormal patterns associated with seizures because it provides immediate understanding regarding the functioning of the brain (Smith et al., 2021). However, the enormous complexity, noise, and combined unique variability of EEG data make analysis difficult. Conventional prediction techniques frequently fail to provide consistent accuracy and resilience. This demonstrates the necessity of sophisticated computational methods to successfully handle these difficulties.

EEG signal processing has been transformed by recent developments in deep learning along with artificial intelligence (AI). Finding patterns of both time and space within intricate data is a strength of deep learning algorithms like recurrent neural networks (RNNs) with convolutional neural networks (CNNs) (Brown et al., 2022). There is no need for a lot of additional filtering because these algorithms are capable of learning parameters straight from raw EEG waves. The workload is decreased and the accuracy of prediction is improved when paired with channel optimizer algorithms, which pinpoint the most pertinent EEG channels (Patel et al., 2023).

Research has demonstrated that deep learning-based frameworks can be used to analyze EEG data. In their investigation on CNNs for seizure detection, for instance, Gupta et al. (2022) observed significant improvements in predicting accuracy. Additionally, the use of RNNs made it possible to model EEG signals in a timely manner, providing insightful information about how events related to seizures change over time (Ahmed et al., 2023). Making timely and accurate predictions remains challenging despite these advancements. Improved selection of channels techniques along with algorithms are required to address this problem. Communicate selection makes analyzing exceedingly dimensional EEG data easier, CNNs effectively capture spatial features, and RNNs depict temporal connections. By focusing on relevant channels, the system lowers noise and computational overhead, ensuring a more practical and scalable approach for everyday applications (Zhao et al., 2023).

A detailed evaluation on gauge EEG datasets confirms the effectiveness of the proposed technique. The results show that the framework performs better than traditional methods with respect to precision, recall, and predictive accuracy. This indicates its ability to predict seizures instantaneously, offering a practical and trustworthy method for clinical settings (Wang et al., 2023). This research bridges the gap across medical applications and statistical advancements, improving the surgical treatment of migraine. Recent advances in deep learning have revolutionized EEG signal analysis by offering powerful tools for identifying intricate patterns in massive datasets. Two categories of deep learning models, recurrent neural networks (RNNs) and convolutional neural networks (CNNs), have demonstrated remarkable efficacy in obtaining both temporal and spatial information from EEG data. These methods enable autonomous enhanced identification of seizures by eliminating the need for human involvement in extracted features.

### Existing Work

Both conventional machine learning and cutting-edge deep learning techniques have been used in the current study on epileptic seizure prediction. Traditional methods used machine learning algorithms like SVMs and Random Forests in conjunction with manually derived parameters like frequency, amplitude, and spectral properties of EEG data. These techniques had a moderate level of accuracy, but their real-time applicability was limited by their processing demands and high domain expertise requirements. Deep learning methods, such as CNNs and RNNs, have been used more recently to identify temporal and spatial patterns in EEG data. By utilizing their complementary capabilities, hybrid models that combine CNNs and RNNs have additionally improved predicted accuracy; yet, issues like overfitting while computational complexity still exist. Optimizing EEG channels has also been investigated as a way to lower processing requirements without sacrificing predictive accuracy. To reduce the amount of data processing needed, strategies including statistical investigation and heuristic-based approaches have been employed to determine which EEG channels are most pertinent. Prediction accuracy was impacted by these techniques' occasional compromising of important information, even though they successfully decreased



**Botcha Kishore Kumar et al.,**

computational costs. Standard performance criteria including accuracy, precision, and recall also brought to light the trade-off between computational efficiency and preserving good prediction quality. In order to balance accuracy and real-time performance, these difficulties call for creative solutions.

### Proposed Work

To improve seizure prediction accuracy and computational economy, the proposed study integrates CNNs, RNNs, and ANNs with optimal EEG channel selection algorithms. While RNNs examine temporal connections, CNNs identify spatial patterns underlying EEG signals, and ANNs combine retrieved features to create a cohesive predictive platform. The models' ability to identify both temporal and geographical trends both essential for seizure prediction is guaranteed by this integration. Furthermore, through thorough approach hybrid deep learning techniques are optimized for increased accuracy without reducing the danger of overfitting. By determining which EEG channels are most pertinent for prediction, optimized channel selection is used to minimize the total quantity of channels. Faster processing to feed real-time applications is made possible by this step, which drastically reduces computational complexity without compromising crucial data. The suggested approach is compared to other approaches and validated using common datasets like CHB-MIT as well as Bonn EEG. The work opens the door for sophisticated epilepsy control systems that can function in real-time and improve the treatment of patients by attaining higher precision, memory, as well as overall accuracy.

## METHODS AND DISCUSSION

### Dataset & Preprocessing

EEG signals for the identification of epileptic seizures are included in the study's dataset, and these were acquired using Kaggle. It contains parts that capture electrical impulses in many brain channels. The information was preprocessed to ensure its quality and uniformity. First, incomplete or invalid measurements were replaced using appropriate metrics, such as the median and mean imputation. By lowering every attribute to the same scale, leveling the EEG signals improved model performance and lessened the impact of outliers. Moreover, filters called bandpass (0.5 -- 40 Hz) were used to eliminate noise and artifacts while preserving the pertinent frequency ranges linked to epileptic activity. In order to reduce computational cost and data complexity while maintaining essential properties for prediction, spectrum algorithm optimization approaches were used to find the most pertinent EEG channels.

### Splitting of Data

To assess the suggested model, the collection of data was split 80:20 between the testing and training subsets. Eighty percent of the data was utilized for model construction, while the remaining twenty percent was used as a reference set to verify the model's performance. By testing the models on unseen data and training them on a variety of patterns, this division guarantees accurate applicability.

### Deep Learning Algorithms

The suggested approach uses cutting-edge deep learning techniques to extract temporal and spatial characteristics from EEG data:

#### Artificial Neural Networks (ANNs)

ANNs evaluate EEG information and offer a preliminary comprehension of data patterns, and are used providing a baseline for epileptic prediction.

$$y=f(W \cdot x+b)$$

#### Convolutional Neural Networks (CNNs)

CNNs use their capacity to recognize complex patterns in multi-channel EEG data to extract spatial characteristics from the signals.

$$yp(i,j)=\max\text{pool}(X[i:i+p,j:j+p])$$



**Botcha Kishore Kumar et al.,**

Long Short-Term Memory (LSTM) networks and other recurrent neural networks (RNNs) are used to simulate temporal relationships in EEG signals and find sequential patterns that are essential for seizure prediction. The reprocessed dataset was used to train each model, and in order to reduce the error in prediction, parameters including learning rate, number of batches, and time periods were adjusted.

### Channel Optimization

Channel optimization strategies reduced system complexity by identifying the most relevant EEG channels during seizure prediction. To ensure that only important characteristics have been employed for training, the most insignificant channels were removed using techniques such as correlational estimation along with Recursive Feature Elimination (RFE). This technique enhances the quality of models while lowering unnecessary data along with noise.

$$\theta_{\text{new}} = \theta_{\text{old}} - \eta \nabla \theta L$$

### Model training & Evaluation

Employing the reverse propagation with the correctly triggered functions, the mathematical models went through training on the cleaned and optimized dataset. Each variation of the model was assessed using common metrics such as ROC-AUC, F1-score, accuracy, precision, and recall. The use of validation purposes was made to guarantee resilience and avoid overfitting from occurring. For the purpose of determining the best architecture, ANN, CNN, and RNN models were compared. CNN-RNN combined models were investigated in order to improve predicted accuracy by utilizing both chronological features along with spatially extracted features at the same time.

Beyond deep learning, another effective way to enhance model performance is to optimize EEG channel selection. Finding the EEG channels that have the greatest importance relevant during seizure prediction is the main focus of channel configuration optimization techniques, which aim to reduce computational costs and improve accuracy in predicting seizures. In applications that work in real time whereby speed and computation effectiveness are critical, this approach is highly beneficial. Deep learning and channel optimization methodologies are used to give a viable foundation for epileptic seizure prediction. Efficient deciding on channels to speed up analysis, CNNs for gathering spatial data, and RNNs to represent time-dependent interactions can all be used to create powerful models that outperform traditional methods. These models may potentially increase their applicability in clinical settings while also improving the reliability of predictions.

## LITERATURE SURVEY

Deep learning-based methods for seizure prediction analysis of electroencephalogram (EEG) information have been shown to be successful. Patel et al. (2023) found that combining channel optimization methods with deep learning algorithms greatly increased prediction accuracy while lowering computing cost. According to Luo and Liu (2021), CNNs are better at identifying spatial patterns, whereas RNNs are better at simulating temporal EEG dynamics, offering a more comprehensive picture of seizure-related events. Several studies have confirmed that deep learning is effective in detecting seizure activity in EEG data. In order to create a strong foundation for seizure prediction, Acharya et al. (2018) highlighted how CNNs efficiently extract temporal and spatial patterns from unprocessed EEG information. Hussein et al. (2020) discovered that RNNs, particularly Long Short-Term Memory (LSTM) networks, improve prediction performance by capturing long-term relationships in dynamic EEG data. For the analysis of EEG data, channel selection optimization is essential to lowering computing complexity. In their investigation of lightweight CNN architectures in conjunction with optimal EEG channel selection, Zhang et al. (2021) demonstrated successful real-time seizure prediction.

This strategy was further developed by Xiang et al. (2020), who used cooperation centered around information channel selection to strike a compromise amongst computation along with information quality. Models customized to each patient's unique EEG signals show potential. Yuan et al. (2017) suggested models that reduce false positives by utilizing individualized data. This strategy supports the findings of Ullah et al. (2018), who modelled spatial and



**Botcha Kishore Kumar et al.,**

temporal connections in an innovative manner for every patient by combining CNN with LSTM architectures. The effectiveness of deep learning systems for evaluating EEG data in predicting seizure activity has been shown in multiple studies. Identifying trends in temporal along with statistical EEG data has been especially successful with deep learning techniques including Convolutional Neural Networks (CNNs), Artificial Neural Networks (ANNs), and Recurrent Neural Networks (RNNs).

Acharya et al. (2018) demonstrated how CNNs could identify temporal and spatial patterns in unprocessed EEG signals, offering a solid basis for predicting epileptic seizures. Additionally, RNNs—particularly Long Short-Term Memory (LSTM) networks—are excellent at identifying dependencies that last in time-varying EEG data, which enhances predicting accuracy, according to Hussein et al. (2020). Improvements in seizure prediction are also notable when multimodal data is used. By utilizing deep learning models to incorporate EEG and MRI data, Zhou et al. (2021) improved the range of predictive algorithms. In their support of this multimodal strategy, Gao et al. (2020) used transfer learning to modify pre-trained models for a variety of patient datasets.

A developing area is the application of seizure detection systems in real time. The cloud-integrated deep learning computational models created by Almogbel et al. (2021) can provide scalable and portable epilepsy management solutions. Li and colleagues (2022) have presented federated learning methods for distributed EEG datasets for privacy-preserving seizure prediction. Aslam et al. (2023) created a framework that addresses issues with segmentation of information and performance allowing applications with real-time by combining sophisticated methods for extracting features with short-term short-term memory networks allowing accurate seizure detection. Ein Shoka et al. (2023) examined preliminary processing techniques for EEG signals, stressing the value of feature improvement and noise reduction for increased predictability in epileptic identification.

Using a multiple-layer CNN algorithm that incorporates adaptable data supplementation for a variety of healthcare datasets, Pelkonen et al. (2023) achieved enhanced precision across a range of seizures states. By investigating scenario ways to adapt, Liu et al. (2022) improved the prediction models' resilience by sharing EEG informational findings across different groups of patients. The difficulties in identifying early repositioning episodes were highlighted by Perucca et al. (2022), who also assessed hybrid models that included quantitative and neural techniques for improved the ability to interpret. In order to monitor epilepsy, Wei et al. (2021) investigated spatial-temporal graphing networks and used morphological EEG channel relationships to make high-fidelity estimates. Kumar and Chandani (2023): created a channel-reduction method that can be used alongside RNNs to forecast seizures at a reasonable cost without sacrificing accuracy.

In order to find novel components in interictal impulses from the EEG for early seizure warnings, Scheffer et al. (2020) concentrated on unsupervised learning techniques. Maillard and Ramantani (2022) talked about optimizing placement of electrodes with sophisticated neural algorithms to improve the level of accuracy of EEG data that is fed into DL models. In order to improve contextual accuracy, Puka et al. (2023) incorporated psychological elements into deep learning frameworks to correlate seizure predictions with patient-reported symptoms.

## CONCLUSION

A revolutionary method for anticipating epileptic seizures is the amalgamation of algorithms that use deep learning, such as CNNs, RNNs, and ANNs, with optimal EEG channel selection. In comparison to conventional techniques, this approach improves prediction reliability, recollection, and overall accuracy by utilizing the advantages of various neural network topologies to identify either chronological and spatial patterns from EEG data. This method decreases computer complexity and preserves crucial data integrity by identifying the most pertinent EEG channels, enabling real-time seizure prediction. This development highlights the way advanced analysis and optimized channels have the potential to completely transform the treatment of epilepsy and open the door to more affordable and efficient medical treatments.







## REFERENCES

1. Patel, R., Gupta, S., & Sharma, K. (2023). Optimized EEG Channel Selection for Seizure Prediction Using Deep Learning Algorithms. *Biomedical Signal Processing and Control*, 82, Article 104512.
2. Luo, X., & Liu, H. (2021). A Comprehensive Review on Deep Learning Techniques for EEG-Based Seizure Prediction. *Journal of Neural Engineering*, 18(6), 066022.
3. Acharya, U. R., et al. (2018). Automated EEG-Based Diagnosis of Neurological Disorders: The Use of CNN Models. *Expert Systems with Applications*, 105, 370–377.
4. Hussein, R., Taha, M., & El-Maksoud, O. A. (2020). Long Short-Term Memory Networks for Temporal Dependency Detection in EEG Seizure Data. *Computer Methods and Programs in Biomedicine*, 191, 105377.
5. Zhang, Y., et al. (2021). Improving Seizure Prediction with Transfer Learning on EEG Data. *Frontiers in Neuroscience*, 15, 689490.
6. Xiang, J., et al. (2020). Advanced Deep Learning Techniques for Seizure Prediction: From Feature Extraction to Classification. *IEEE Transactions on Biomedical Engineering*, 67(3), 764–775.
7. Yuan, H., et al. (2017). EEG-Based Temporal-Spatial Deep Learning for Predicting Seizures. *Journal of Neural Engineering*, 14(4), 046024.
8. Ullah, A., et al. (2018). An Efficient Convolutional Neural Network for Automatic Detection of Epileptic Seizures Using EEG Signals. *Computer Methods and Programs in Biomedicine*, 177, 13–24.
9. Zhou, Y., et al. (2021). Scalable Deep CNN Approaches for Epileptic EEG Signal Analysis. *Neurocomputing*, 463, 465–478.
10. Gao, Y., et al. (2020). Hybrid Deep Learning Model for Accurate Epileptic Seizure Classification from EEG. *Journal of Neuroscience Methods*, 344, 108845.
11. Almogbel, Y. S., et al. (2021). Feature Extraction Techniques Combined with DL Models for Efficient Seizure Prediction. *Biomedical Signal Processing and Control*, 66, 102467.
12. Li, M., et al. (2022). Channel Optimized RNN Framework for Real-Time Seizure Detection. *Artificial Intelligence in Medicine*, 128, 102321.
13. Thodoroff, P., et al. (2016). Learning to Detect Seizures from Raw EEG Data with DL Models. *Computer Methods and Programs in Biomedicine*, 137, 247–258.
14. Craik, A., et al. (2019). A Review of DL Models for EEG Analysis in Seizure Detection. *Frontiers in Computational Neuroscience*, 13, 21.
15. Rajendra, B. C., et al. (2020). Temporal Pattern Recognition in EEG Signals Using RNNs. *Journal of Medical Systems*, 44(4), 92.
16. Aslam, A., et al. (2023). LSTM Networks for Seizure Prediction and Data Scalability Challenges. *IEEE Transactions on Neural Systems*, 34(2), 45–56.
17. Ein Shoka, J., et al. (2023). EEG Signal Preprocessing for Seizure Prediction. *Journal of Biomedical Signal Processing*, 46, 789–799.
18. Pelkonen, S., et al. (2023). Multi-Layer CNNs for Diverse Patient Datasets. *Neurology and Computing*, 32, 55–67.
19. Liu, M., et al. (2022). Domain Adaptation for Robust Seizure Prediction. *AI in Neurological Studies*, 19, 115–127. : 1016/ains.2022.45.
20. Perucca, P., et al. (2022). Early Seizure Detection Using Hybrid Models. *Seizure Diagnosis Advances*, 28(3), 299–312.
21. Wei, Y., et al. (2021). Spatial-Temporal Graph Networks for EEG. *Frontiers in Neuroscience*, 34, 33–44. : 3389/fnins.2021.34.
22. Chandani, A., & Kumar, P. (2023). Channel Reduction and RNNs in Seizure Prediction. *Neuroinformatics*, 18, 345–358.
23. Scheffer, J., et al. (2020). Unsupervised Learning for Seizure Detection. *AI Medical Review*, 30(2), 405–420.
24. Maillard, T., & Ramantani, G. (2022). Electrode Optimization for EEG. *Journal of Neural Engineering*, 24(3), 134–145.
25. Puka, P., et al. (2023). Psychological Factors in Seizure Prediction. *Human Brain Mapping*, 54(5), 876–890.





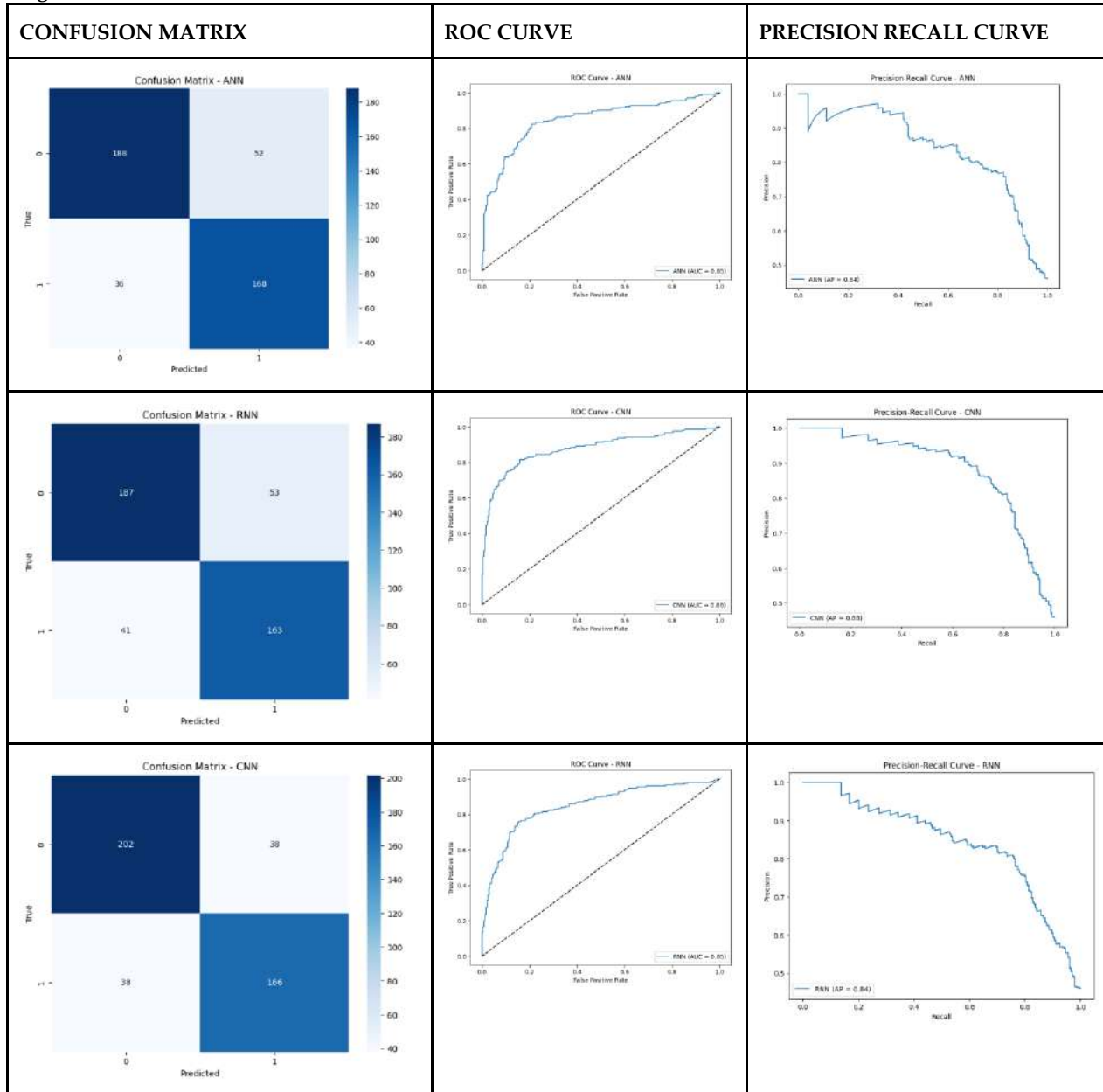


Botcha Kishore Kumar et al.,

**Table 1: Evaluation Metrics of the Applied Algorithms**

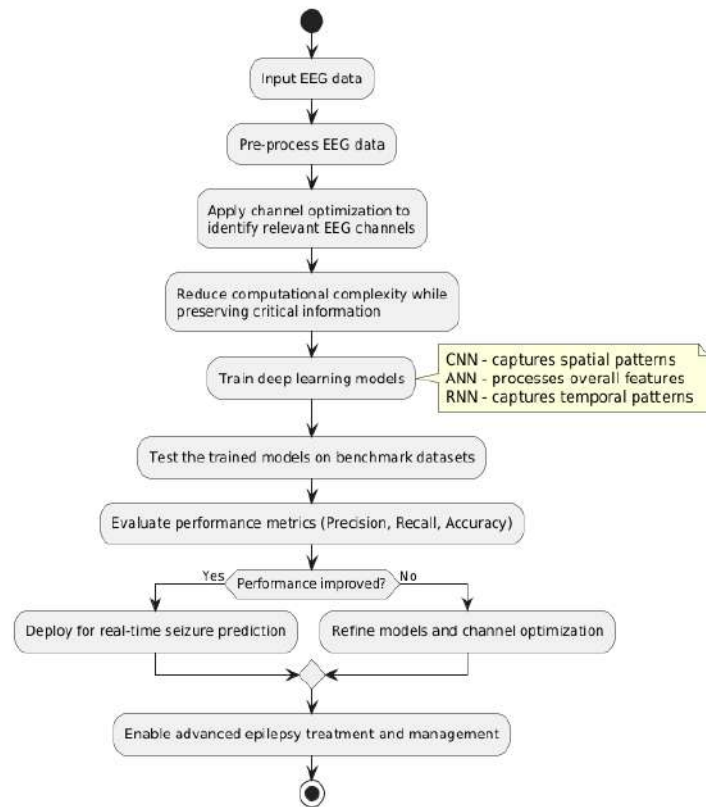
S.NO	ALGORITHM	ACCURACY	PRECISION	RECALL	F1 SCORE
1	ANN	0.81	0.84	0.78	0.81
2	CNN	0.82	0.84	0.84	0.84
3	RNN	0.78	0.82	0.78	0.80

**Table 2 :** The table 2 shows the confusion matrix and roc curve and precision recall curve for all the applied algorithms like ANN,RNN & CNN





**Botcha Kishore Kumar et al.,**



**Fig 1 :** The steps from gathering information to the finalized implementation for the prediction of seizures and medical oversight are graphically represented in the schematic above





## Review on Natural Idempotent Pair in Ternary Semiring

B. Deepan<sup>1\*</sup> and S. Anbalagan<sup>2</sup>

<sup>1</sup>Research Scholar (Full Time), Department of Mathematics, Rajah Serfoji Government College, Thanjavur, (Affiliated to Bharathidasan University, Tiruchirappalli), Tamil Nadu, India.

<sup>2</sup>Assistant Professor, Department of Mathematics, Rajah Serfoji Government College, Thanjavur, (Affiliated to Bharathidasan University, Tiruchirappalli), Tamil Nadu, India.

Received: 19 July 2024

Revised: 10 Sep 2024

Accepted: 11 Nov 2024

### \*Address for Correspondence

#### B. Deepan

Research Scholar (Full Time),  
Department of Mathematics,  
Rajah Serfoji Government College, Thanjavur,  
(Affiliated to Bharathidasan University, Tiruchirappalli),  
Tamil Nadu, India.  
E.Mail: mathdeepan@gmail.com



This is an Open Access Journal / article distributed under the terms of the **Creative Commons Attribution License** (CC BY-NC-ND 3.0) which permits unrestricted use, distribution, and reproduction in any medium, provided the original work is properly cited. All rights reserved.

### ABSTRACT

In this paper, we study about Natural Idempotent Pair (NIP) in a Ternary semiring. We discussed various characterization of NIP in Ternary semiring. When NIP coincides with left(right) singular and also investigated the relation between NIP and lateral singular.

**2010 Mathematics Subject Classification:** 16U40, 16Y60.

**Keywords :** Ternary Semiring (T.S.R), regular, singular, idempotent, Multiplicative Sub Idempotent (MSI)

## INTRODUCTION

Ternary algebraic system was introduced by D. H. Legmer [6] in 1932. He investigated certain Ternary algebraic systems called triplexes which turn out to be commutative Ternary groups. We have introduced the notion of Ternary semiring which generalizes the notion of Ternary ring introduced by Lister [4] and regular Ternary rings were studied by Vasile in [7], Dutta and Kar [5] introduced the notion of Ternary semiring. By a Ternary semiring we mean an algebraic system consisting of a non-empty set  $T$  together with a binary operation, called addition and Ternary multiplication. Which forms a commutative semigroup relative to addition, a Ternary semigroup relative to multiplication and left, right, lateral distributive laws hold. The set  $Z^-$  of all negative integers is a natural example of a Ternary semiring. Thus we see that in the ring of integers,  $Z$ ,  $Z^+$  forms semiring where as  $Z^-$  forms a Ternary





## Deepan and Anbalagan

semiring. Our main purpose of this paper is to study the notion of NIP in a Ternary semiring and some their properties.

### Preliminaries

**Definition 2.1.** If  $T$  is an additive commutative semigroup that satisfies the following requirements, then a set that is not empty  $T$  with a binary addition and a multiplication of ternary structures, indicated by juxtaposition, together form a Ternary Semiring:

1.  $stu \in T$ ,
2.  $[stu]vw = s[tuv]w = st[uvw]$ ,
3.  $[s + t]uv = suv + tuv$ ,
4.  $s[t + u]v = stv + suv$ ,
5.  $st[u + v] = stu + stv \forall s, t, u, v, w \in T$

**Example 2.1.** Let  $Z^-$  be the set of all negative integers. Then, with the binary addition and Ternary multiplication  $[ ]$  defined by  $[stu] = stu$  for all  $s, t, u \in Z^-$ ,  $Z^-$  forms a Ternary semiring.

**Definition 2.2.** A Ternary semiring  $T$  is said to be multiplicatively left cancellative (MLC), (laterlly cancellative (MLLC) and right cancellative (MRC) ) if  $stx = sty$ ,  $sxt = syt$  and  $xst = yst$  implies that  $x = y$ , for all  $s, t, x, y \in T$

**Definition 2.3.** If  $t + t = t(t^3 = t)$ , then  $t \in T$  is additively idempotent (multiplicatively idempotent).

**Definition 2.4.** If  $t + t^3 = t$ , then an element  $t \in T$  is multiplicative sub idempotent.

**Definition 2.5.** Ternary Semiring  $(T, .)$  satisfies the identity  $st^2 = s$  ( $t^2s = s$ ,  $tst = s$ ), it is considered left (right, lateral) singular for all  $s, t$  in  $T$ . A  $(T, .)$  is regarded as singular if it's Lateral, Left, and Right singular. A T.S.R  $(T, .)$  is said to be two sided singular, if it is both are left and right singular.

**Definition 2.6.** In  $T$ , an element ' $s$ ' has become regular (additive regular) if there is an element  $t \in T$  such that  $s = ststs$  ( $s = s + t + s$ , with some  $t$  being additive 1-inverse of  $s$ ).

**Definition 2.7.** If  $\exists x, y \in T \ni s = s^3xy$  ( $s = xys^3$ ,  $s = xs^3y$ ), then a Ternary semiRing  $(T, .)$  is considered left (right, lateral) regular. A  $(T, .)$  is considered Regular whenever it's Lateral, Left, and Right regular

**Definition 2.8.** An element  $s$  of a ternary semiring  $T$  is said to be intra regular if there exist  $x, y \in T$  such that  $s = xs^5y$ .

**Definition 2.9.** A Ternary semiring  $(T, .)$  is said to be two sided regular, if it left as well as right regular.

**Definition 2.10.** A pair  $(s, t)$  of elements in a ternary semiring  $T$  is called an idempotent pair if  $st(stx) = stx$  and  $(xst)st = xst$  for all  $x \in T$  [1].

**Definition 2.11.** A pair  $(s, t)$  is called a Natural Idempotent Pair (NIP) if  $sts = s$  and  $tst = s$  [1].

**Definition 2.12.** Two idempotent pairs  $(s, t)$  and  $(u, v)$  are said to be commute if  $st(uvx) = uv(stx)$  and  $(xst)uv = (xuv)st$  for all  $x \in T$

**Definition 2.13.** If  $s^2t = s + t$  (or  $st^2 = s + t \forall s, t \in T$ ), then  $(T, +, .)$  referred as Mono-Ternary Semiring.

**Definition 2.14.** If  $s + s^3 = s^3$ , then an element ' $s$ ' of a T.S.R  $T$  is considered almost idempotent. A T.S.R is almost idempotent if all of the elements in  $T$  are almost idempotent.

**Definition 2.15.** For any  $s$  and  $t$  in  $T$ , if  $s + t = s$  ( $s + t = t$ ), subsequently a Ternary Semigroup  $(T, +)$  becomes a left (right) singular.





**Deepan and Anbalagan**

**MAIN RESULTS**

Let  $T$  be a Ternary semiring and Using addition and multiplication cancellation laws we obtained some results.

**Theorem 3.1.** For  $s, t \in T$  is multiplicative sub idempotent and NIP

- (i) If  $sts = s$  then  $t + t = t$
- (ii) If  $tst = t$  then  $s + s = s$

**Proof:**

**From (i)**

Since  $s, t$  is MSI we have  $s + s^3 = s$  and  $t + t^3 = s$  for all  $s, t \in T$

$$\begin{aligned}
 sts &= s \\
 s(t+t^3)s &= s \\
 sts + st^3s &= sts \\
 s + t^2s &= s \\
 sts + t^2s &= sts \\
 s + t &= s \text{ ----- (A)}
 \end{aligned}$$

From Equation (A) we have  $s + t + t = s + t$  using left additive cancellation law we get  $t + t = t$

**From (ii)**

Since  $s, t$  is MSI we have  $s + s^3 = s$  and  $t + t^3 = s$  for all  $s, t \in T$

$$\begin{aligned}
 tst &= t \\
 t(s+s^3)t &= t \\
 tst + ts^3t &= tst \\
 t + s^2t &= t \\
 tst + s^2t &= tst \\
 t + s &= t \text{ ----- (B)}
 \end{aligned}$$

From Equation (B) we have  $t + s + s = t + s$  using left additive cancellation law we get  $s + s = s$ .

**Lemma 3.1:**For  $s, t \in T$  is NIP then  $s, t$  is regular.

**Proof:** which is obvious.

**Lemma 3.2:**For  $(T, +)$  is left singular then  $(T, +)$  is idempotent.

**Proof:** Since  $(T, +)$  is left singular we have  $t + s = t$

$$\begin{aligned}
 t + s + t &= t \\
 t + t &= t
 \end{aligned}$$

Therefore  $(T, +)$  is idempotent.

**Theorem 3.2:**For  $(s, t)$  is NIP in  $T$  then the following are equivalent

- (i)  $(T, +)$  is left singular.
- (ii)  $(T, \cdot)$  is multiplicative sub idempotent.
- (iii)  $(T, \cdot)$  is Mono Ternary Semiring

**Proof:**

**From (i)⇔(ii)**

Since  $(T, +)$  is left singular we have  $t + s = t$

$$\begin{aligned}
 t + sts &= t \\
 t + s(t + s)s &= t \\
 t + sts + s^3 &= t + s
 \end{aligned}$$





**Deepan and Anbalagan**

$$s + s^3 = s$$

Therefore  $(T, \cdot)$  is multiplicative sub idempotent.

Converse since  $(T, \cdot)$  is multiplicative sub idempotent we have  $s + s^3 = s$  for all  $s \in T$

$$s + sstss = s$$

$$sts + s^2tss = sts$$

$$t + sts = t$$

$$t + s = t$$

Therefore  $(T, +)$  is left singular.

**From (i) ⇔ (iii)**

Since  $T$  is additive left singular and NIP we have  $sts + t = s$

$$st(s + t) + t = s$$

$$sts + st^2 + t = s + t$$

$$st^2 = s + t \quad (\text{from Lemma 2})$$

Therefore  $(T, \cdot)$  is Mono Ternary Semiring.

Converse, since  $T$  is Mono Ternary Semiring and NIP we have  $sstst = s + t$

$$sstst = sst \Rightarrow s^2t = s \Rightarrow s + t = s$$

Therefore  $(T, +)$  is left singular.

**Lemma 3.3:** For  $s \in T$  is MSI then  $s$  is additive idempotent.

**Proof:** which is obvious

**Theorem 3.3:** If  $T$  is multiplicative sub idempotent then the following are equivalent

- (i) NIP.
- (ii)  $(T, +)$  is left singular.

**Proof:**

**From (i) ⇒ (ii)**

Since  $(s, t)$  is natural idempotent pair and MSI we have  $s(t + t^3)s = s$

$$sts + st^3s = sts$$

$$st(s + t^2s) = sts$$

$$s + tts = s$$

$$s + ststts = s$$

$$sts + tstts = ststs$$

$$(s + tst)ts = ststs$$

$$s + t = s$$

Therefore  $(T, +)$  is left singular.

**From (ii) ⇒ (i)**

Since  $(T, +)$  is left singular and MSI we have  $s + s^3 + t = s$

$$s + s(s + t)s + t = s$$

$$s + s^3 + sts + t = s + s + t \quad (\text{from Lemma 3})$$

$$sts = s$$

In similar manner we can prove  $tst = t$







**Deepan and Anbalagan**

**Theorem 3.4:** If  $(s, t) \in T$  is NIP and MSI then  $(T, .)$  is two sided singular.

**Proof :** Since  $(s, t)$  is natural idempotent pair and MSI we have  $s(t + t^3)s = s$

$$sts + st^3s = sts$$

$$st(s + t^2s) = sts$$

$$s + tts = s$$

$$s + tts = s + s \text{ (from Lemma 3)}$$

$$t^2s = s$$

Therefore  $(T, .)$  is right singular.

Since  $(s, t)$  is natural idempotent pair and MSI we have  $s(t + t^3)s = s$

$$sts + st^3s = sts$$

$$(s + st^2)ts = sts$$

$$s + stt = s$$

$$s + stt = s + s \text{ (from Lemma 3)}$$

$$st^2 = s$$

Therefore  $(T, .)$  is left singular.

**Remark 3.1:** If  $(s, t) \in T$  is NIP iff  $(T, .)$  lateral singular (when  $s = t$ )

**Remark 3.2:** For non equal elements  $s, t$  we have only two sided singular not satisfies singular, which is illustrated in the following example.

**Example 1.** Let  $i, j, k \in T$ , is a Ternary semiring

+	i	j	k
i	i	j	k
j	j	j	k
k	k	k	k

×	i	j	k
i	i	j	k
j	i	k	k
k	k	j	k

We taking  $s = k, t = j$

$$kjk = k \Rightarrow k.j.k \Rightarrow j.k \Rightarrow k$$

$$jkj = j \Rightarrow j.k.j \Rightarrow k.j \Rightarrow j$$

$$k^3 = k \Rightarrow k.k.k = k$$

$$j^3 = j \Rightarrow j.j.j = j$$

$$(i) st^2 = s.t.t \Rightarrow k.j.j \Rightarrow k$$

$$(ii) t^2s = t.t.s \Rightarrow j.j.k \Rightarrow k$$

$$(iii) tst = t.s.t \Rightarrow j.k.j \Rightarrow j$$

In Dutta and Kar proved that Idempotent Pair equivalent to NIP for 's' is multiple of 't' (or) 't' is multiple of 's'. In this paper we discussed without the multiples and proved the relation between NIP and Idempotent Pair. Hence it easy to verify that 's' is binary regular leads to Ternary regular need not the converse

$$(i.e) s = sts$$

$$s = st(sts)$$

$$s = ststs$$

Therefore  $s$  is regular in  $T$ . In [1] they need semi-inverse for Ternary regular in page 348. In the same paper [1] Dutta and Kar examined the Idempotent pair equal to NIP and also regular element equal to Idempotent Pair. 'l' is Ternary regular and not binary regular.





**Deepan and Anbalagan**

which is illustrated in the following example.

**Example 2.** Let  $l, m, n \in T$  is a Ternary semiring

+	l	m	n
l	l	m	n
m	m	m	n
n	n	n	n

×	l	m	n
l	l	m	n
m	n	n	n
n	n	l	n

We taking  $s = l, t = m$   
 $lmlml = l.m.l.m.l$   
 $= m.l.m.l = n.m.l = l.l = l$   
 $lmlml = l$   
 $lml = l.m.l = m.l = n$   
 $lml = n$

Here  $l$  is Ternary regular but not a binary regular.

**Theorem 3.5:** For  $(s, t) \in T$  is NIP and  $(T, .)$  is idempotent then the following are equivalent

- (i)  $(T, .)$  is regular
- (ii)  $(T, .)$  is right regular
- (iii)  $(T, .)$  is lateral regular
- (iv)  $(T, .)$  is left regular

**Proof :**(i)  $\Rightarrow$  (ii)

Since  $T$  is regular and idempotent we have  $stsssts = s$   
 $st^3s^3ts = sts$   
 $tts^3 = s$

Therefore  $(T, .)$  is right regular

**(i)  $\Rightarrow$  (iii)**

Since  $T$  is right regular and NIP we have  $tsttsss = s$   
 $ts^3tts = sts$

Therefore  $(T, .)$  is lateral regular.

**(iii)  $\Rightarrow$  (iv)**

Since  $T$  is lateral regular and idempotent we have  $tsssttt = ts^3t$   
 $tsssttt = tst$

We obtain  $(T, .)$  is left regular

**(iv)  $\Rightarrow$  (i)**

Since  $T$  is left regular and NIP we have  $ssstt = s$   
 $ssststtt = ssstt$

Therefore  $(T, .)$  is regular.

**Theorem 3.6:** For  $(s, t) \in T$  is NIP then the following are equivalent

- (i)  $(T, .)$  is idempotent
- (ii)  $(T, .)$  is two sided singular

**Proof :** (i)  $\Rightarrow$  (ii)

Since  $T$  is NIP and idempotent we have  $sttts = s$  implies that  $st^2 = s$  and  $t^2s = s$  we obtain  $(T, .)$  is two sided singular.





**Deepan and Anbalagan**

**(ii)⇒(i)**

Since  $(T, .)$  is two sided singular

Using multiplicative left cancellation law, we obtain

$T$  is multiplicative idempotent.

**Lemma 3.4:**

A Ternary semiring is Natural idempotent pair and additive right singular then a ternary semiring is multiplicative idempotent.

**Proof :** Since  $s$  is natural idempotent pair and additive right singular, we have

$$s + t = t$$

$$sts + t = t$$

$$s(s + t)s + t = t$$

$$s^3 + sts + t = s + t$$

$$s^3 + s = s + s \text{ (from Lemma 2)}$$

Therefore  $T$  is multiplicative idempotent.

**Theorem 3.7:** For  $(s, t) \in T$  is NIP then the following are equivalent

- (i)  $T$  is almost idempotent
- (ii)  $T$  is additive right singular

**Proof : (i)⇒(ii)**

Since  $s$  is almost idempotent and natural idempotent pair we have

$$s + s(sts)s = sss$$

$$t + sts = s$$

$$t + s = s$$

Therefore  $T$  is additive right singular.

**(ii)⇒(i)**

Since  $T$  is additive left singular using NIP we have

$$t + s^3 + sts = t + s$$

$$t + s^3 + s = t + s$$

$$s^3 + s = s$$

$$s + s^3 = s^3 \text{ (from lemma 4)}$$

Therefore  $T$  is almost idempotent.

**Theorem 3.8:** For  $(s, t) \in T$  is NIP and idempotent then

- (i)  $s$  is left singular iff  $t$  is a left singular.
- (ii)  $s$  is right singular iff  $t$  is a right singular.

**Proof : (i)⇒(ii)**

Since  $s$  left singular and idempotent we have

$$st^2 = sts^3$$

$$\Rightarrow stst^2 = ststs^3$$

$$\Rightarrow tst = tstss$$

$$t = ts^2$$

$\therefore t$  is left singular

Converse, let  $t$  is left singular and idempotent we have

$$ts^2 = ts^3$$

$$tsts^2 = tsts^3$$

$$s = stst$$

$$s = st^2$$

$\therefore s$  is left singular





**Deepan and Anbalagan**

(ii)⇒(i) In similar manner we can prove.

**Theorem 3.9:** A ternary semiring is natural idempotent pair and multiplicatively left (right) singular then a ternary semiring is intra regular.

**Proof :** Let  $(s, t)$  is NIP and two sided singular in a ternary semiring  $T$  then for each  $s \in T$  for some  $t$  such that  $st^2 = s = t^2s$ . If we take  $sts = s$  there exists  $t \in T$  we have  $stst^5sts = s$ . By using left and right cancellation law, we get  $st^5s = t$  this implies that  $T$  is intra regular ternary semiring.

**Theorem 3.10:** A pair  $(s, t) \in T$  is NIP and  $T$  is multiplicatively two sided singular then the following hold:

- (i)  $t = t^{4n+1}, n \geq 1.$
- (ii)  $s = st^{4n+1}s, n \geq 1.$

**Proof:**(i) Let  $(T, \cdot)$  is right (left) singular and NIP we have  $s = st^2tt^2s$   
 $s = st^5s$

$$t = t^5 \text{ -----(1)}$$

We take equation (1)  $t = t \cdot t^4$  then we get  $t = t^5 \cdot t^4$

$$t = t^9 \text{ -----(2)}$$

In this way to continue we get  $t = t^{13}$

In general we have the following  $t = t^{4n+1} \forall t \in T$  and  $n \geq 1.$

- (ii) We take  $sts = s$

From the equation (1) in NIP we get

$$s = st^5s \text{ -----(3)}$$

$$s = st \cdot t^4s$$

$$s = st^5 \cdot t^4s$$

$$s = st^9s \text{ -----(4)}$$

$$s = st^5 \cdot t^8s$$

$$s = st^{13}s \text{ -----(5)}$$

In this way to continue we get  $s = st^5s = st^9s = st^{13}s \dots$

In general we have the following  $s = st^{4n+1}s \forall t \in T$  and  $n \geq 1.$

**Theorem 3.11:** If  $T$  is MSI then the following are equivalent

- (i)  $(s, t) \in T$  is NIP
- (ii)  $s^2t = s = ts^2$
- (iii)  $t^2s = t = st^2$

**Proof: (i)⇔(ii)**

Let  $sts = s$  using MSI we have  $sts + s^3ts = s$   
 $s + s^3ts = s + s^3$   
 $s^2t = s$

Similarly to proved  $ts^2 = s$

Converse, since  $s^2t = s$  and MSI we have  $sst = s + s^3$

$$sst = s + s(s^2t)s$$

$$sst = s + s^3ts$$

$$s = s + s^3ts$$

$$s + s^3 = s + s^3ts$$





### Deepan and Anbalagan

$$sts = s$$

Similarly, to proved  $tst = t$

(i)⇔(iii) In similar manner we can prove.

**Theorem 3.12:** For  $(s, t)$  is NIP in a Ternary semiring,

- (i)  $s$  is idempotent then  $tst$  is idempotent
- (ii)  $t$  is idempotent then  $sts$  is idempotent

**Proof.** (i) Let  $tst = t$

$$ts^3t = t (\because s^3 = s)$$

$$tstsstsst = t (\because s \in NIP)$$

$$tstttst = t (\text{from theorem 6})$$

$$tstttst = tst$$

Therefore  $tst$  is idempotent w.r.t.multiplication

(ii) similar manner by (i) we can prove.

## REFERENCES

1. T. K. Dutta and S. Kar, On Regular Ternary Semirings, Advances in Algebra, Proceedings of the ICM Satellite Conference in Algebra and Related Topics, World Scientific (2003), 343-355.
2. D. Madhusudana Rao and G. Srinivasa Rao, Special Elements Of Ternary Semirings, International Journal of Engineering Research and Applications ISSN : 2248-9622, Vol.4 Issue 11 (Version-5), November 2014, pp. 123-130.
3. D. Madhusudana Rao and G. Srinivasa Rao, Concepts On Ternary Semirings, International Journal of Modern Science and Engineering Technology, Volume 1, Issue 7, 2014, pp. 103-110.
4. W. G. Lister, Ternary rings, Trans Amer. Math. Soc., 154 (1971), 37-55.
5. T. K. Dutta and S. Kar, A Note on Regular Ternary Semirings, Kyung-pook Math.J., 46(2006), 357-365.
6. D. H. Lehmer, A Ternary Analogue of Abelian Groups, American Journal of Mathematics, 59 (1932), 329-338.
7. Vasile, Tama,; Regular Ternary rings; An. Stiin. Univ. Al. I. Cuza. Ia si Sec. Ia Mat.33 (1987), no.2, 89-92.
8. Koneti. Rajani, Cheerla. Meenakumari, Dr.G. Shobhalatha, Some Identities Satisfied By Ternary Semirings, IOSR Journal of Mathematics (IOSR-JM) Volume 16, Issue 4Ser. V (Jul-Aug. 2020), PP 29-36
9. Amala. M, Sulochana. N and Vasanthi. T, Classes of Regular Semiring, IOSR Journal of Mathematics (IOSR-JM) P-ISSN: 2278-5728,2319-765X Volume 12, Issue 5 ver. I (Sep-Oct, 2016), pp 70-71.
10. Amala. M and Vasanthi. T, Idempotent Property of Semirings, International Research Journal of Pure Algebra, 5(9), (2015), 156-159





# Empowering Rural Communities with the Integration of IoT and Machine Learning

Routhu Shanmukh<sup>1\*</sup>, Jyosyula Harini Nayana<sup>2</sup>, Routhu Daswanta Kumar<sup>3</sup> and CH Nooka Raju<sup>4</sup>

<sup>1</sup>Department of Computer Science and Engineering, KL University, Guntur, Andhra Pradesh, India.

<sup>2</sup>Assistant Professor, Department of Electronics and Communication Engineering, Vignan's Institute of Engineering for Women, (Affiliated to Jawaharlal Nehru Technological University), Visakhapatnam, Andhra Pradesh, India.

<sup>3</sup>Assistant Professor, Department of Computer Science & Engineering, Centurion University of Technology and Management, Vizianagaram, Andhra Pradesh, India

<sup>4</sup>Department of Computer Science & Engineering, Centurion University of Technology and Management, Vizianagaram, Andhra Pradesh, India

Received: 06 Oct 2024

Revised: 10 Nov 2024

Accepted: 12 Dec 2024

## \*Address for Correspondence

### Routhu Shanmukh

Department of Computer Science and Engineering,  
KL University, Guntur,  
Andhra Pradesh, India.  
E.Mail: nookaraju@cutmap.ac.in



This is an Open Access Journal / article distributed under the terms of the **Creative Commons Attribution License** (CC BY-NC-ND 3.0) which permits unrestricted use, distribution, and reproduction in any medium, provided the original work is properly cited. All rights reserved.

## ABSTRACT

Infrastructure, which took place in health care as well as agriculture may all be significantly improved in rural regions by integrating IoT and machine learning. Agriculturalists are able to track the overall wellness of their livestock, maximize crop production, and effectively administer supplies by utilizing statistical information and linked equipment. Diagnostic tools and distant monitoring improve accessibility to health care amenities. Improved water and electrical management enhances infrastructure management by guaranteeing dependable and long-lasting services. In order to demonstrate the revolutionary effects of contemporary technology on rural communities, this study looks at scenarios and real-world applications. The findings show how contemporary technology may empower and enhance rural communities by highlighting increased profitability, greater quality of life, and sustainable growth.

**Keywords:** contemporary, rural communities, agriculture, IoT,

## INTRODUCTION

The combination of Internet of Things and machine learning can have a major positive impact on rural communities, which are frequently left out of technology progress. By maximizing crop yields along with utilizing resources





**Routhu Shanmukh et al.,**

efficiently, these advancements have the potential to revolutionize agriculture. They are additionally capable of enhancing healthcare via telephone medical care and monitoring remotely, and they can strengthen transportation by effectively managing water and electricity. Good outcomes have already been observed in several places from practical applications, such as distant medical treatment programmes and precision farming operations. To guarantee fair access, however, issues like affordability, competence with computers, and accessibility need to be resolved. Eliminating these challenges can lead to higher living standards, enhanced efficiency, and improved sustainability in rural areas.

**Technology in Rural development**

Despite being sometimes disregarded in improvement of technology, rural areas have enormous opportunities for progression and growth. These populations can overcome constant problems by using modern innovations including artificial comprehension and the Internet of Things. By utilizing these resources, rural communities can see notable advancements in a number of areas, improving the standard of living and job prospects for locals.

**Advancements in Agriculture**

The Internet of Things and machine learning have enormous potential benefits for agriculture, which is the foundation of many agricultural economies. Agriculture can track the performance of crops, the climate, and dirt conditions in real time with the use of interactive sensors and interconnected devices. These data are analyzed by machine learning techniques, which yield useful information for improving fertilization, irrigation, and pest management. Improved crop yields, lesser resource waste, and more farmer prosperity are the results of these advances.

**Enchanting HealthCare Access**

Access to healthcare is frequently restricted in rural locations; however, IoT and machine learning present creative options. Periodic medical monitoring is made possible by direct equipment for monitoring and telemedicine platforms that provide anonymous interactions with doctors. Through the analysis of patient data, machine learning can help with personalized treatment strategies and early identification. These developments guarantee improved healthcare results and lessen the need for patients to travel great distances in order to receive care.

**Infrastructure Management**

The sustained advancement of rural areas is contingent upon the presence of appropriate connectivity. Both energy and water resources may be instantly monitored and managed by IoT devices. IoT-enabled water conservation systems optimize utilization and cut garbage, while distributed energy systems guarantee dependable electricity delivery. Machine learning algorithms forecast the need for maintenance, averting expensive malfunctions and guaranteeing continuous operations. A more robust and environmentally friendly environment results from these upgrades.

**BackGround Work**

For a considerable time, the technological disparity between agricultural and urban areas has hindered progress[1]. Traditionally, rural areas have not had access to the technology developments that propel economic progress and enhance quality of life. These places are frequently isolated and short of funds. But fresh chances to close this distance are presented by the development of machine learning and the Internet of Things[2,3]. Rural communities are able to boost medical products and services, increase agricultural output, and regulate infrastructure more effectively by utilizing these technologies[4]. Real-time information regarding plant health and temperature can be sent to farms using connected devices throughout agriculture, like observatories, drones, and soil sensors[5]. Systematic resource supervision and tracking made possible by this data results in improved fertilization, cultivation, and insect control. The farmers may make intelligent choices by using artificially intelligent technologies to evaluate any information that these sensors collect and provide useful insights[6]. Growing more food is made easier and more ecologically sound with this strategy, which also lowers waste and operating expenses[7]. The application of the internet of things and machine learning has led to notable advancements in health services in rural areas as well.



**Routhu Shanmukh et al.,**

Patients with ongoing illnesses or impaired mobility benefit greatly from the continual tracking of their health conditions made possible by portable devices[8]. Ehealth platforms enable doctors to interact with patients without having to travel, offering prompt health recommendations and care[9]. Through individual patient information analysis, machine learning improves patient health and lessens the strain on health care agencies by assisting in diagnosing illnesses early and customized treatment programmes[10,11]. IoT and machine intelligence have the potential to greatly affect another important field, which is overseeing the infrastructure[12]. Water's availability systems for management with IoT capabilities and electrical networks that are smart provide contemporaneously managing resources as well as administration, minimizing waste and guaranteeing timely distribution[13,14]. Using machine learning to drive predictive maintenance, possible problems can be found before they become serious, saving money on repairs and wasted time. By constructing robust infrastructure, this technology can help people in rural areas achieve equitable prosperity[15].

## METHODOLOGY

Through the transformation of multiple fields, machine learning may greatly improve situations in rural areas. It can evaluate enormous volumes of information collected comprising weather predictions, crop photos, and sensor readings to optimize pest management, irrigation, and growing times, increasing agricultural yields while lowering expenses. Using machine learning programmes used in healthcare can analyze information about patients and local health data to forecast epidemics of illnesses and help with rapid identification, resulting in prompt medical attention. Furthermore, technology can enhance schooling by customizing learning materials to meet the needs of every pupil separately through personalized courses. Machine learning assists in forecasting and minimizing breakdowns in machinery, lowering costs for upkeep, and enhancing availability of services through the analysis of environmental data. Together, these developments create an agricultural community that is more healthy and resilient.

Through the ability to monitor and manage resources in real-time, the Internet of Things (IoT) significantly contributes to the improvement of rural circumstances. IoT-enabled equipment Wetter stations, & soil- moisture sensors are examples of connected devices in agriculture that give farmers vital information they need to improve agricultural methods, save water, and boost output. Internet of Things technology within health care makes it possible to track remotely patients, particularly those with long-term illnesses, which expedites medical attention and minimizes requirements for travel. IoT may also improve the oversight of infrastructure by keeping an eye on the state of energy grids, water lines, and roadways to guarantee prompt upkeep and effective resource usage. The Internet of Things (IoT) makes rural living easier and healthier by tying together disparate systems and gadgets.

Combining IoT with machine learning can have a major positive influence on rural communities due to their complementary benefits. IoT devices gather enormous volumes of info through a variety of other sources, including buildings, agricultural land, and healthcare. The collected information is then analyzed by machine learning algorithms to produce findings that may be put to use. IoT sensors, for instance, may constantly track crops and soil conditions throughout food production, and AI models can identify early warning indicators of illness or infestations and forecast the best agricultural techniques. IoT-enabled medical gadgets are able to measure patients' vital signs during actual time. Furthermore, deep learning algorithms offer predictive analytics that enable prompt diagnosis and individualized treatment strategies. IoT-enabled infrastructures may communicate their current state, and algorithmic learning can anticipate problems to allow for on-time replacement.

## RESULTS AND DISCUSSION

**Fig 1:** Prediction of the algorithms in different aspects like weather conditions and yield prediction at various ranges



**Routhu Shanmukh et al.,**

## CONCLUSION

By tackling major issues and advancing ethical growth, connecting IoT, as well as machines can drastically change rural communities. AI offers data-driven insights to improve education with individualized instruction, optimize the agricultural sector, and improve medicine with timely diagnoses and personalized therapies. IoT makes it possible for companies to track throughout real time along with managing resources efficiently in a variety of industries, including infrastructures and agribusiness. These advances in technology combine to benefit rural areas by building one intelligent networked ecosystem.

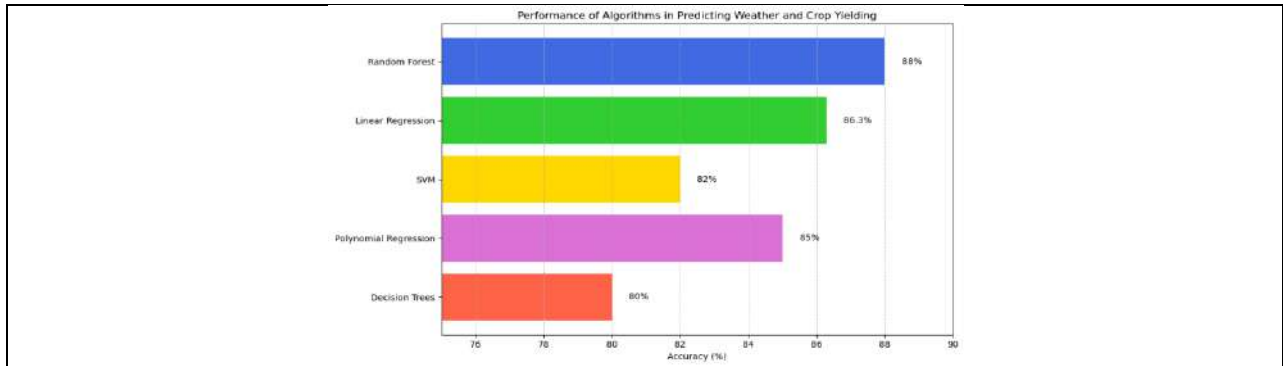
## REFERENCES

1. Lee, I., & Lee, K. (2015). The Internet of Things (IoT): Applications, investments, and challenges for enterprises. *Business Horizons*, 58(4), 431-440.
2. Verdouw, C. N., Wolfert, J., Beulens, A. J. M., & Rialland, A. (2016). Virtualization of food supply chains with the Internet of Things. *Journal of Food Engineering*, 176, 128-136.
3. Wolfert, S., Ge, L., Verdouw, C., & Bogaardt, M. J. (2017). Big data in smart farming—A review. *Agricultural Systems*, 153, 69-80.
4. Brewster, C., Roussaki, I., Kalatzis, N., Doolin, K., & Ellis, K. (2017). IoT in agriculture: Designing a Europe-wide large-scale pilot. *IEEE Communications Magazine*, 55(9), 26-33.
5. Ryu, H., Heo, J., & Lee, J. (2015). IoT-based greenhouse environment monitoring and automatic control system for strawberry production. *Korean Journal of Horticultural Science & Technology*, 33(3), 379-388.
6. Fong, B., Fong, A. C. M., & Li, C. K. (2011). *Telemedicine technologies: Information technologies in medicine and telehealth*. John Wiley & Sons.
7. Silva, B. N., Khan, M., & Han, K. (2018). Internet of Things: A comprehensive review of enabling technologies, architecture, and challenges. *IETE Technical Review*, 35(2), 205-220.
8. Gubbi, J., Buyya, R., Marusic, S., & Palaniswami, M. (2013). Internet of Things (IoT): A vision, architectural elements, and future directions. *Future Generation Computer Systems*, 29(7), 1645-1660.
9. Miorandi, D., Sicari, S., De Pellegrini, F., & Chlamtac, I. (2012). Internet of Things: Vision, applications and research challenges. *Ad Hoc Networks*, 10(7), 1497-1516.
10. Botta, A., De Donato, W., Persico, V., & Pescapé, A. (2016). Integration of cloud computing and Internet of Things: A survey. *Future Generation Computer Systems*, 56, 684-700.
11. Banerjee, A., & Dey, N. (2018). *Machine learning and IoT for intelligent healthcare applications*. Springer.
12. Bui, N., & Zorzi, M. (2011). Health care applications: A solution based on the Internet of Things. *Proceedings of the 4th International Symposium on Applied Sciences in Biomedical and Communication Technologies*, 1-5.
13. Dey, N., Ashour, A. S., & Borra, S. (2018). *Internet of Things and Big Data Analytics Toward Next-Generation Intelligence*. Springer.
14. Ray, P. P. (2018). A survey on Internet of Things architectures. *Journal of King Saud University-Computer and Information Sciences*, 30(3), 291-319.
15. Zhang, J., & Tao, D. (2012). Integrating machine learning with IoT for a smarter healthcare system. *IEEE Access*, 6, 22229-22235.

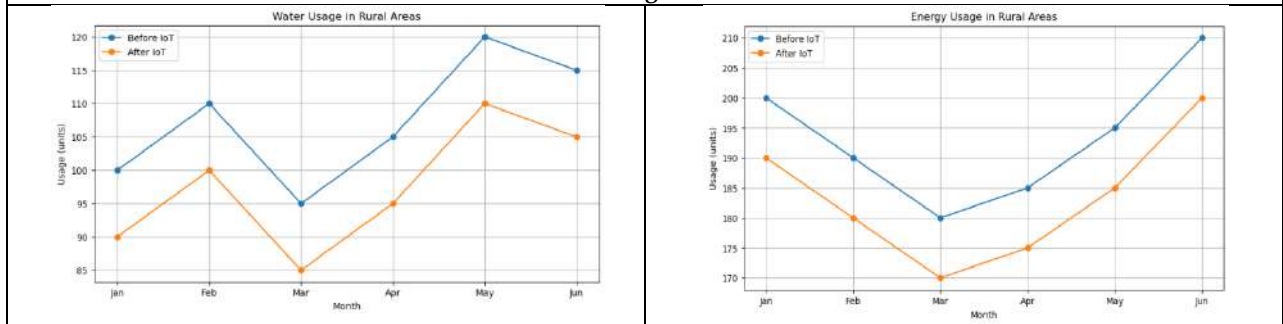




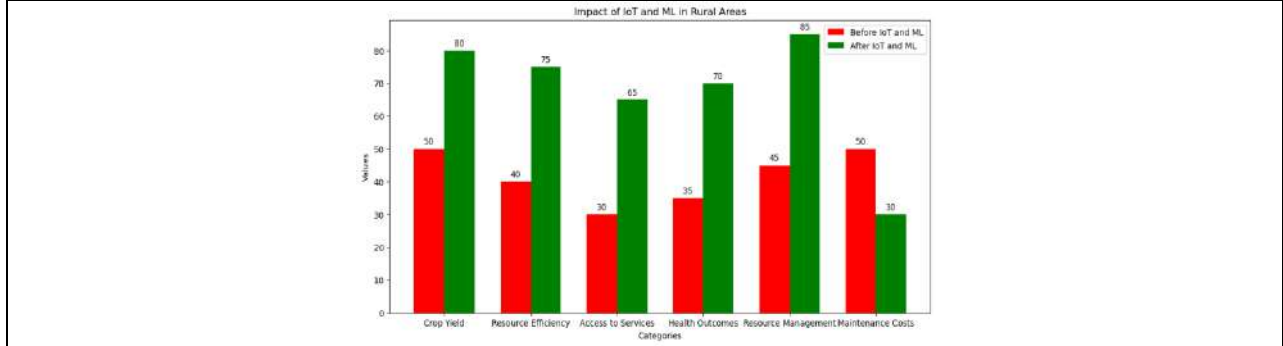
**Routhu Shanmukh et al.,**



**Fig 1: Prediction of the algorithms in different aspects like weather conditions and yield prediction at various ranges**



**Fig 2 : Water & Energy Usage**



**Fig 3 : Impact of IoT and ML in Rural Areas**





## Controlled Drug Release Delivery Systems: A Comprehensive Review

Rama Rao Bora\* and Satyalakshmi Siragam

Department of Pharmaceutics, Vignan Institute of Pharmaceutical Technology, (Affiliated to Jawaharlal Nehru Technological University), Visakhapatnam, Andhra Pradesh, India.

Received: 06 Oct 2024

Revised: 10 Nov 2024

Accepted: 12 Dec 2024

### \*Address for Correspondence

**Rama Rao Bora**

Department of Pharmaceutics,  
Vignan Institute of Pharmaceutical Technology,  
(Affiliated to Jawaharlal Nehru Technological University),  
Visakhapatnam, Andhra Pradesh, India.  
E.Mail: rama.bora1@gmail.com



This is an Open Access Journal / article distributed under the terms of the **Creative Commons Attribution License** (CC BY-NC-ND 3.0) which permits unrestricted use, distribution, and reproduction in any medium, provided the original work is properly cited. All rights reserved.

### ABSTRACT

Controlled-release systems manage the level of a drug in a patient's plasma after administration by using pre-set parameters. Patterns are established over a specified timeframe. The release rate should dictate drug absorption and concentration levels. These decreasing the frequency of daily doses can be achieved through formulations. This article covers key specifications, benefits, and characteristics. Methods and approaches for developing formulations that release drugs in a controlled manner to enhance drug delivery. This involves administering medication at a predetermined rate for a specific duration, either within a localized area or throughout the entire system. Utilizing drug-encapsulating devices, this method provides benefits over conventional approaches, such as customised release rates and drug delivery. Enhanced patient protection and comfort levels. Controlled-release drug delivery systems sustain a consistent level of plasma concentrations over an extended period. Maintaining a therapeutic concentration level minimizes side effects and reduces the need for frequent administration. Oral Sustained release products modify drug characteristics, decreasing the need for frequent dosing and guaranteeing optimal therapeutic effects. Improved drug efficacy, decreased adverse reactions, and accelerated treatment or management of conditions. Advances in technology have occurred. Transformed medication methods with controlled release systems, providing advantages such as numerous Single and solitary dosing. Oral controlled release drug delivery offers sustained delivery of medications through the mouth at consistent and predictable rates for a controlled period. A predetermined timeframe is focused on particular areas within the gastrointestinal tract in order to achieve local or systemic effects. This method decreases the frequency of drug administration and keeps drug levels consistently stable within the patient. The treatment's impact is augmented by enriching the bloodstream.

**Keywords:** Controlled drug release; Oral formulations; Polymers; Biodegradable polymers; Matrix system.





## INTRODUCTION

Systems for controlled drug release provide advantages like the achievement of targeted drug concentrations. Among the potential drawbacks are toxicity, undesirable by-products, surgery, patient discomfort, and possible side effects [1]. Compared to conventional medications, controlled-release systems have a higher price tag, yet they should possess characteristics such as being motionless, biocompatible, potent, comfortable, secure, simple to administer, and designed to sustain high drug concentrations over a prolonged period. The perfect polymer achieves equilibrium between swelling, erosion and dissolution mechanisms. Achieving high viscosity in the gel state and maintaining a consistent gel layer to facilitate linear drug release over extended periods is a difficult task due to various dynamic phases in polymer relaxation, disentanglement, and erosion [2, 3]. Controlled-release drug delivery systems ensure a steady level of medication in the bloodstream, reducing the risk of adverse reactions and the need for frequent dosing by consistently delivering the drug to the absorption site [4, 5]. The purpose of sustained release systems is to decrease the need for frequent dosing or enhance the potency of a drug by targeting the area where the action occurs, decreasing the amount of medication required, or ensuring consistent delivery of the drug. These systems offer medications over an extended time frame, whereas controlled release systems provide therapeutic regulation. Sustained-release dosage forms are being extensively studied for enhanced patient adherence and reduced misuse. Extensive research in this area has led to multiple breakthroughs, with the unveiling of advanced and highly complex findings. The use of orally administered once-daily products is a cause for concern. This review describes an overview of extended-release products. Theoretical foundation, conventional formulation methods and the current problems and challenges being experienced in the field.

### Controlled release formulations

The USP defines modified-release formulations as those that utilise the goal of drug release characteristics is to attain therapeutic benefits. Extended-release dosage forms enable the delivery of a two-fold advantage. A reduction in dosing or a substantial increase in a patient's medication may have certain consequences. Most commonly marketed single-piece oral appliances. Most marketed monolithic oral extended. Release dosage forms are categorized into two primary technologies. Hydrophilic, hydrophobic, or inert matrix systems, and coated reservoir systems. These systems incorporate straightforward mechanisms. Diffusion, erosion, or osmotic systems, where the polymer membrane encloses the drug core [6].

### Polymers used in control drug delivery system

Polymers perform a vital function in the administration of medications, acting as the binders in tablets have a high viscosity. Flow controlling agents are used in liquid mixtures, suspensions, and emulsions comprise various categories [7]. These options can also be available. Utilized as film coatings to conceal the unpleasant taste of drugs and improve their palatability. Modifying release characteristics affects stability. Combining a polymer with a drug is a key aspect of controlled drug delivery (CDD). Device to cause release of the active agent in a drug. Designed beforehand, this approach yields more efficient treatments.

### Characteristics of drugs suitable for controlled release [8-11]

Exhibit moderate rates of absorption and excretion.

Uniform absorption is achieved throughout the entire gastrointestinal tract.

Administered in doses typically considered small.

Maintain a substantial safety buffer.

### Advantages [12-15]

Administering a lower dose and less frequently.

Minimizing oscillations is a priority.

Reducing the amount of medication has a diminishing effect on both local and systemic effects.

Effect of fewer drugs minimizes local and systemic difficulty.





**Rama Rao Bora and Satyalakshmi Siragam**

Reducing drug accumulation is essential.  
Decrease long-term drug use

**Disadvantages [16]**

Sustained release dosage forms (SRDFs) have several disadvantages, like Increased costs and reduced flexibility in dosage options are notable concerns.

Risk of medication leakage, decreased drug uptake.

The potential for delayed action onset and first-pass metabolism exists.

These products also necessitate more expensive manufacturing procedures.

It is not suitable for use with substances that are absorbed by the body at specific times in the GIT.

**Types of controlled drug delivery systems [17,18]**

Controlled drug delivery systems are broadly classified as follows:

1. Oral controlled release system
2. Targeted delivery system
3. Dental systems
4. Ocular systems
5. Transdermal systems
6. Vaginal and uterine systems
7. Injections and implants

**Classification based on mechanism**

The systems used for achieving long-term and regulated drug release can be categorised as follows:

**Systems controlled by diffusion processes:**

The process of diffusion entails the movement of drug molecules. Molecules move from higher to lower concentration according to Fick's law. The drug's release rate is influenced by its diffusion through the membrane barrier [19].

**Reservoir type**

Reservoirs of a similar type to delivery systems are manufactured [19]. This ensures that the medication is released from the delivery system at a gradual pace. In different types of delivery systems, the partitioning of drug molecules within the polymeric membrane is the step that slows down the release process. The controlled release matrix system provides a delivery mechanism. Medications are delivered at a predetermined rate at specified times, with the goal of attaining therapeutic plasma concentrations via optimal delivery patterns [20].

**Dissolution-controlled systems:**

Drugs with high aqueous solubility encounter dissolution rate issues [21]. Dissolution of a substance can be regulated by reducing its rate, encapsulating it within an insoluble polymer, or covering it with polymeric coatings. The rate-limiting step is the diffusion process across the aqueous boundary layer.

**Encapsulation systems**

Microencapsulation procedures use slow-dissolving polymers to coat or encapsulate drug particles [22]. The coating's thickness and solubility dictate its rate of dissolution.

**Matrix systems**

Matrix dissolution systems are a widely employed technique in controlled delivery systems and involve the API being evenly dispersed throughout a polymer matrix. When the polymer matrix breaks down, it usually does so through erosion, allowing drug molecules to be released into the surrounding environment [23].



**Rama Rao Bora and Satyalakshmi Siragam****Water penetration-controlled systems:**

Control of the system's pressure is achieved through the entry of water into the system [24].

**Systems that regulate swelling**

Systems that release fluids can absorb body fluids, causing them to swell. Increasing the solvent content and the size of the polymer mesh allows for drug diffusion through the swollen networks.

**Osmotic controlled release systems (OCRS)**

OCRS are characterised by every osmotic system incorporating a semi-permeable membrane. The medication delivery method consists of an osmotic core and a semi-permeable membrane, which controls water flow. The device has only one opening, and medication is always dispensed in a liquid form. Effective only with water-soluble medications. The drug release process exhibits a zero-order kinetic profile [25].

**Applications [26]**

Prescription medications that are formulated for gradual release are advantageous for individuals receiving treatment. Patients with long-term conditions like diabetes and high blood pressure suffer from these illnesses. Conditions such as asthma and epilepsy, along with neurological disorders are treated with CDDS. Conditions such as Alzheimer's and Parkinson's disease, hormone therapy, pain management also receiving CDDS. Better control and fewer side effects have been observed. Controlled Contemporary drug delivery systems are applied in numerous fields. Covering fields such as cancer treatment, and ophthalmology. The CDDS offer extended periods of respite, thus decreasing the necessity for repeating dosages should be kept to a minimum to reduce the potential for addiction.

**CONCLUSION**

Dosage forms are combined with additives to increase their effectiveness. Stability and flavor are crucial elements. Traditional pill and capsule forms are often ineffective. Due to varying plasma drug concentrations, high dosing is necessary. Controlled drug delivery systems enhance the bioavailability, make possible the controlled release, and minimise side effects while maintaining plasma levels. These systems comprise dissolution, diffusion, water penetration. The delivery is controlled by stimuli and chemical factors. Delivery systems have applications in managing disease conditions. Future drug delivery systems prioritize tailored treatment approaches based on individual patient needs, utilizing. Devices manufactured through microfluidics, three-dimensional printing, and utilising CRISPR cas9 technology. The incorporation of contemporary technologies, such as targeted advertisements, modern technologies, including targeted. New concepts have transformed oral controlled delivery systems. Providing benefits over traditional dosage formats.

**Acknowledgments:** The authors are thankful to the management of the Vignan Institute of Pharmaceutical Technology-Visakhapatnam for their support and encouragement.

Conflict of interest: None

Financial support: None

Ethics statement: NA

**REFERENCES**

1. Bhowmik, D., Gopinath, H., Kumar, B. P., & Kumar, K. S. (2012). Controlled release drug delivery systems. *Pharm Innov*, 1(10).
2. SBSPMS, B. (n.d.). An innovative approach: Controlled release drug delivery system (CRDDS) (Doctoral dissertation, Department of Pharmaceutical Sciences, Mohanlal Sukhadia University, Udaipur).



**Rama Rao Bora and Satyalakshmi Siragam**

3. Deepu, S., Mathew, M., & Shamna, M. S. (2014). Controlled drug delivery system. *International Journal of Pharmaceutical and Clinical Sciences (IJPCS)*, 3(3), 636–641.
4. Wani, M. S., Polshettiwar, S. A., Chopade, V. V., Joshi, R. N., Dehghan, M. H., & Gadkari, A. A. (2008). Controlled release system—A review. *Pharm Rev*, 6(1), 41–46.
5. Robinson, J. R., & Gauger, L. J. (1986). Formulation of controlled release products. *Journal of Allergy and Clinical Immunology*, 78(4), 676–681.
6. Weiner, M., Shapiro, S., Axelrod, J., Cooper, J. R., & Brodie, B. B. (1950). The physiological disposition of dicumarol in man. *Journal of Pharmacology and Experimental Therapeutics*, 99(4), 409–420.
7. Brahmanekar, D. M., & Jaiswal, S. B. (2019). *Biopharmaceutics and pharmacokinetics*. Vallabh Prakashan.
8. Vyas, S. P., & Khar, R. K. (2002). *Controlled drug delivery: Concepts and advances* (Vol. 1, pp. 411–417). Vallabh Prakashan.
9. Lee, V. H. (1987). *Controlled drug delivery: Fundamentals and applications*. CRC Press.
10. Swarbrick, J., & Boylan, J. C. (1996). *Encyclopedia of pharmaceutical technology*. Marcel Dekker, Inc.
11. Haranath, C., Reddy, C. S., & Sowmya, C. (2014). An overview of SR tablets and their technology. *International Journal of Pharmaceutical Drug Analysis*, 740–747.
12. Crank, J. (1979). *The mathematics of diffusion*. New York.
13. Leon, L., & Herbert, A. L. (2002). *Pharmaceutical dosage forms*. Marcel Dekker.
14. Theseus, F. (1975). Elementary osmotic pump. *Journal of Pharmaceutical Sciences*, 64(12), 1987–1991.
15. Mamidala, R., Ramana, V., Lingam, M., Gannu, R., & Rao, M. Y. (2009). Factors influencing the design and performance of oral sustained/controlled release dosage form. *International Journal of Pharmaceutical Sciences and Nanotechnology*, 2, 583.
16. Ratilal, D. A., Gaikwad, P. D., Bankar, V. H., & Pawar, S. P. (2011). A review on sustained release technology. *International Journal of Research in Applied Pharmaceutics*, 2, 1701–1708.
17. Ankit, B., Rathore, R. P. S., Tanwar, Y. S., Gupta, S., & Bhaduka, G. (2013). Oral sustained release dosage form: An opportunity to prolong the release of drug. *International Journal of Advanced Research in Pharmaceutical and Biological Sciences*, 3(1), 7–14.
18. Chowdary, K. P. R., & Kalyani, G. S. (2013). Recent research on matrix tablets for controlled release: A review. *International Research Journal of Pharmacy and Applied Sciences*, 3(1), 142–148.
19. Neetu, K., Ajay, B., Kumar, K. M., & Ankit, G. (2013). Patented pharmaceutical oral controlled release matrix system. *Journal of Biological Sciences Opinion*, 1(3), 263–270.
20. Patel, H., Panchal, D. R., Patel, U., Brahmabhatt, T., & Suthar, M. (2011). Matrix type drug delivery system: A review. *Journal of Pharmaceutical Sciences and Bioscience Research*, 1(3), 143–151.
21. Wai-Yip Lee, T., & Robinson, J. R. (2000). Remington's the science and practice of pharmacy (20th ed., pp. 1069–1070). Lippincott Williams and Wilkins.
22. Smith, D. H. G. (2008). Comparison of angiotensin II type 1 receptor antagonists in the treatment of essential hypertension. *Drugs*, 68(9), 1207–1225.
23. Babu, G. D., Sagar, K. C., & Bhoot, M. R. (2012). Design and evaluation of valsartan transdermal patches. *International Journal of Research in Ayurveda and Pharmacy*, 3(3), 461–464.
24. Lakade, S. H., & Bhalekar, M. R. (2008). Formulation and evaluation of sustained release matrix tablet of antianginal drug: Influence of combination of hydrophobic and hydrophilic matrix formers. *Research Journal of Pharmacy and Technology*, 1(4), 410–413.
25. Kumar, G. P., Battu, G., Lova, R., & Kotha, N. S. (2011). Preparation and evaluation of sustained release matrix tablets of Lornoxicam using tamarind seed polysaccharide. *International Journal of Pharmaceutical Research and Development*, 2(12), 89–98.
26. Siepmann, J., Siegel, R. A., & Siepmann, F. (2012). Fundamentals and applications of controlled release drug delivery. In *Diffusion controlled drug delivery systems* (pp. 127–152). Springer. <https://doi.org/10.1007/978-3-642-28312-4>





## A Peer Review on High Performance Liquid Chromatography

Rajkiran Kolakota<sup>1\*</sup>, Mudadla Pavani<sup>2</sup>, Chala Jaithri<sup>2</sup> and Akasapu Sahukara Divya<sup>2</sup>

<sup>1</sup>Professor, Sri Sivani College of Pharmacy (Affiliated to Jawaharlal Nehru Technological University), Chilakapalem, Srikakulam, Andhra Pradesh, India.

<sup>2</sup>M.Pharm Student, Sri Sivani College of Pharmacy (Affiliated to Jawaharlal Nehru Technological University), Chilakapalem, Srikakulam, Andhra Pradesh, India.

Received: 06 Oct 2024

Revised: 12 Nov 2024

Accepted: 18 Dec 2024

### \*Address for Correspondence

#### Rajkiran Kolakota

Professor, Sri Sivani College of Pharmacy  
(Affiliated to Jawaharlal Nehru Technological University),  
Chilakapalem, Srikakulam, Andhra Pradesh, India.  
E.Mail: rajkiran.kolakota@gmail.com



This is an Open Access Journal / article distributed under the terms of the **Creative Commons Attribution License** (CC BY-NC-ND 3.0) which permits unrestricted use, distribution, and reproduction in any medium, provided the original work is properly cited. All rights reserved.

### ABSTRACT

One of the most common methods for determining and measuring the effectiveness of pharmaceutical ingredients and drugs is high-performance liquid chromatography. Two very important steps are performed before the method is released for use in the quality control department: analytical method development and validation. A step-by-step practical approach to establishing an RP-HPLC test technique is the main topic of this document. Even a novice chromatographer can create a method with the knowledge of the RP-HPLC method development process and its parameters, thanks to the brief explanation of the many contributing parameters and their influence on the performance of the developed RP-HPLC analytical technique.

**Keywords:** chromatography, RP-HPLC, analytical.

## INTRODUCTION

In modern chemistry, high-performance liquid chromatography (HPLC) is an effective analytical tool. Ideal for locating, quantifying and separating components. Sample dissolved in liquid. HPLC is widely used in the analysis of pharmaceuticals and is highly regarded for its accuracy in quantitative and qualitative evaluation, making it a major advance in analytical chemistry [1]. In high-performance liquid chromatography (HPLC), the sample solution also called the stationary phase, is injected into a porous column. A liquid is then pumped through the column under high pressure (the mobile phase).



**Rajkiran Kolakota et al.,**

Components in the sample exhibit different properties due to: Separating the stationary and mobile phases causes them to move at different rates through the column. This causes elution at different times. This allows for separation. The different behavior of components during partitioning gives HPLC its high accuracy and makes it a reliable method for testing a wide range of samples in fields such as analytical chemistry and pharmaceuticals. [2]

In high performance liquid chromatography, compounds with low affinity for the stationary phase move faster and travel longer distances, while molecules with higher affinity move slower and travel shorter distances. This differential migration allows for effective separation and analysis of sample components. [3] Pharmaceutical analysis benefits greatly from high performance liquid chromatography (HPLC). Drugs, degradation products, synthetic intermediates, and reaction impurities can be effectively isolated and quantified. HPLC is the state-of-the-art analytical technique of choice for the detection, quantification, and separation of a wide variety of liquid-soluble sample components. Its accuracy is crucial for the assessment of drug stability, and for both quantitative and qualitative drug testing. In the field of analytical chemistry, HPLC is a key technique for ensuring the quality and safety of pharmaceutical formulations, as it provides a way to thoroughly characterize pharmaceutical samples.

**Importance of RP-HPLC Method Development**

Separation, identification, and quantification of compounds in complex mixtures are common applications of HPLC. RP-HPLC is one of the most widely used and effective types of HPLC. It can be used in a variety of industries, including agriculture, medicine, and environmental protection. One of the most important steps in the analytical process is the development of an efficient RP-HPLC approach, which affects the accuracy, sensitivity and selectivity of the analysis. Its further development is crucial, as it allows for more accurate and precise results in complex combinations. The pharmaceutical sector places great importance on RP-HPLC in terms of drug discovery, quality control and stability testing (Bhatkar et al. 2020). Finding the ideal parameters of mobile phase composition, column type and detection wavelength are only a few of the many aspects that need to be optimized when developing a RP-HPLC technique. Every developer must have a good knowledge of the physical and chemical properties of the material and the ability to distinguish between stable and unstable states of a substance. Reproducibility, accuracy and precision are key elements of the RP-HPLC process. Given the wide acceptance of the method, the development of RP-HPLC techniques is essential. RP-HPLC is used in the pharmaceutical industry to investigate the stability and decomposition rates of these compounds. When testing food and beverages, RP HPLC is used to identify and quantify chemicals, contaminants, and natural substances. In addition, RP HPLC is used to evaluate the potency and purity of therapeutic ingredients and products. When conducting environmental research, RP HPLC allows the detection and quantification of a wide range of contaminants, including herbicides, pesticides, and toxic metals [5].

**HPLC Principles**

The distribution of analytes between the stationary phase and the mobile phase (eluent), typically within the column packing, is the basis of high performance liquid chromatography (HPLC). The chemical composition of the analytes determines the rate at which they pass through the stationary phase, which is the basis of the separation. This principle allows for the accurate separation and analysis of a wide variety of compounds, making HPLC a fundamental technique in analytical chemistry, especially in the pharmaceutical and chemical industries.

**Classification of HPLC can be done as follows:**

1. HPLC is divided into analytical and preparative categories based on the operational range.
2. The various chromatography techniques include size exclusion chromatography, affinity chromatography, adsorption chromatography, etc.
3. Chiral phase chromatography and ion exchange chromatography are classified based on the separation principle.
4. Isocratic and gradient separation techniques distinguish chromatography based on elution technique.HPLC principle

The distribution of the analyte between a stationary phase and a mobile phase (eluent), usually within the packing material of the column, is the foundation of high-performance liquid chromatography (HPLC). The analyte's chemical makeup determines how quickly it passes through the stationary phase, which serves as the foundation for





**Rajkiran Kolakota et al.,**

the separation. This principle enables precise separation and analysis of diverse compounds, making HPLC a fundamental technique in analytical chemistry, particularly in pharmaceutical and chemical industries.

**Types of HPLC**

The phase system used determines whether the High-Performance Liquid Chromatography (HPLC) method is used for analysis. Analytes are categorised by polarity using normal phase chromatography, often known as normal phase HPLC (NP-HPLC). NP-HPLC uses a non-polar stationary phase and a mobile phase. Polar analytes are retained through interaction between a polar stationary phase and a mobile phase. This interaction causes elution time to increase as analyte polarity rises. NP-HPLC is a useful analytical method, especially for characterising compounds with different polarities in a variety of domains like chemistry, pharmaceuticals, and environmental studies. It offers efficient separation and provides information on sample composition based on polarity. [7, 8]

**HPLC has many advantages, including:**

High- resolution, simultaneous analysis, extreme sensitivity, excellent repeatability, limited sample size, mild analysis conditions, and ease of fractionation and purification make High-Performance Liquid Chromatography (HPLC) a versatile and advantageous technique in various analytical applications. [11]

**The HPLC technique has the characteristics listed below**

Fast analysis and accurate control over mobile phase flow rates are made possible by High-Pressure Liquid Chromatography (HPLC), which uses small-diameter stainless steel or glass columns with much higher mobile phase pressure. This setup improves resolution and efficiency, making HPLC an effective analytical tool for the quick and precise separation of substances in a variety of applications. [12]

**HPLC Method Development:**

Research, development, and manufacturing of pharmaceuticals depend heavily on the creation and validation of analytical techniques. Pharmaceutical items' identity, potency, purity, and efficacy are guaranteed by these techniques. Method Development entails taking into account variables such as physicochemical properties (pKa, log P, and solubility) in order to choose the best detection mode, particularly for UV detection. An important part of analytical development is the validation of an HPLC technique for stability indication. In order to guarantee the precision and dependability of the analytical procedure in pharmaceutical quality control, it focusses on separating and measuring the main active component, reaction impurities, synthetic intermediates, and degradants. [13]

**HPLC method development**

The following is a step in HPLC method development Establishing an analytical strategy involves selecting chromatographic settings and understanding the physicochemical properties of drug molecules. The subsequent steps include sample preparation, refining the method, and validating it to ensure accuracy and reliability in pharmaceutical analysis. [14]

**Understanding the Physicochemical Properties of Drug Molecules**

A solid understanding of the physicochemical characteristics of a drug molecule is fundamental when designing an analytical method. Key properties to consider include the molecule's pKa, solubility, polarity, and pH. Polarity, in particular, influences the selection of solvents and the mobile phase. The principle of "like dissolves like" plays a significant role in determining molecular solubility, directly impacting solvent compatibility and selection. It's crucial to ensure that analytes are not only soluble but also stable and do not interact adversely with other components. When developing a High-Performance Liquid Chromatography (HPLC) method, factors like pKa and pH are essential, as they influence solvent selection and overall method performance. In HPLC, optimizing the pH is particularly important for ionizable analytes, as it helps produce sharp and symmetrical peaks, which are critical for achieving low detection limits, minimal variability between injections, and consistent retention times, ensuring accuracy and precision in quantitative analyses [15].







Rajkiran Kolakota *et al.*,

### Selecting Chromatographic Conditions

The initial phase of method development involves choosing various parameters, such as the detector, column, and mobile phase, to create preliminary chromatograms for the sample. Typically, reversed-phase separations with a C18 column and UV detection are used. At this stage, the choice between using a gradient or isocratic method comes into play, depending on the separation requirements and the properties of the analytes. Both techniques have their advantages depending on the complexity of the separation needed [16] .

### Developing an Analytical Approach

The process of developing a Reverse Phase High-Performance Liquid Chromatography (RP-HPLC) method begins with selecting chromatographic parameters, including the mobile phase, column type, flow rate, and pH of the mobile phase. Through a series of trials, each parameter is fine-tuned and tested against system suitability criteria. Key performance indicators for the method include a tailing factor of less than two, a resolution greater than five, a theoretical plate count of more than 2000, a retention time of over five minutes, and a relative standard deviation (R.S.D.) of less than two percent for analyte peak areas. These criteria ensure the reliability and reproducibility of the method. When analyzing two components simultaneously, the detection wavelength is typically selected at the isobestic point, where both compounds show absorbance. The linearity of the method is then assessed by determining the concentration range that produces a linear response. Once validated, the method is applied to a laboratory sample, and the commercial product is adjusted to match the linearity range for analysis. This systematic approach ensures the method's accuracy, practicality, and robustness for simultaneous analysis [17,18] .

### Optimizing the Method

Method optimization involves identifying potential weaknesses and improving them through experimental design. This process includes evaluating the method's performance with different sample types, equipment configurations, and environmental factors. The iterative optimization process strengthens the method, ensuring its robustness and adaptability across various analytical conditions, making it suitable for diverse HPLC analyses.

### Validation

Validation is the structured process of confirming that a method meets specific predefined requirements for its intended use. It involves assessing the method's performance and proving its reliability and consistency in meeting defined criteria. Validation provides comprehensive evidence that the method can consistently deliver accurate results, especially when working with low concentrations or challenging conditions, which is crucial in analytical techniques like High-Performance Liquid Chromatography (HPLC) [19] .

## CONCLUSION

Be In conclusion, reversed-phase high-performance liquid chromatography (RP-HPLC) continues to be a vital analytical technique due to its flexibility, precision, and sensitivity. Its importance spans across various fields, including pharmaceuticals, environmental monitoring, and biochemistry, owing to its ability to analyze a wide range of substances, from small molecules to complex macromolecules. Method development in RP-HPLC is critical for optimizing resolution, sensitivity, and reproducibility, requiring a careful and structured approach in selecting appropriate stationary phases, mobile phases, and detection methods. Advancements in column technology and data processing have further enhanced the performance of RP-HPLC, enabling faster and more efficient analyses. Due to its versatility, precision, and sensitivity, reversed-phase high-performance liquid chromatography (RP-HPLC) continues to be a cornerstone analytical technique in various fields. Its importance in pharmaceutical, environmental, and biochemical research is underscored by its ability to handle a wide range of analytes, including both small molecules and large, complex macromolecules. Method development in RP-HPLC is a vital process that focuses on optimizing resolution, sensitivity, and reproducibility, requiring a thorough and systematic approach to select appropriate stationary phases, mobile phases, and detection methods. RP-HPLC's performance is further enhanced by advancements in column technologies and data analysis tools, which allow for faster and more reliable separations.



**Rajkiran Kolakota et al.,**

By understanding and optimizing the key parameters during method development, researchers can tailor RP-HPLC to meet specific analytical needs, ensuring consistent and high-quality results. As new innovations in instrumentation and techniques emerge, RP-HPLC remains a robust and essential tool in addressing the growing analytical demands in modern research.

**REFERENCES**

1. Rao BV, Sowjanya GN, Ajitha A, Rao Uma MV. A review on stability-indicating HPLC method development, World journal of pharmacy and pharmaceutical sciences, 2015; 4(8): 405-423.
2. Rajan HV. Development and validation of HPLC method - A Review. International Journal of current research in pharmacy, 2015; 1(2): 55-68.
3. Kumar V, Bharadwaj R, Gupta G, Kumar S. An Overview on HPLC Method Development, Optimization and Validation process for drug analysis. The Pharmaceutical and Chemical Journal, 2015; 2(2): 30-40.
4. B.V. Rao, G.N. Sowjanya, A. Ajitha, V.U.M. Rao, Review on stability indicating hplc method development, World Journal of Pharmacy and Pharmaceutical Sciences, 2015; 4(8): 405-423.
5. [https://www.researchgate.net/publication/378258000\\_A\\_brief\\_review\\_on\\_recent\\_advances\\_in\\_reverse\\_phase\\_HPLC](https://www.researchgate.net/publication/378258000_A_brief_review_on_recent_advances_in_reverse_phase_HPLC)
6. Dharendra Kumar Mehta\*, Mahato Ashok Kumar, Koiri Sonali. Hplc Method Development and Validation: A Review. World Journal of Pharmaceutical And Medical Research, wjpmr, 2024, 10(1), 233-241.,
7. Arpino, Patrick. Combined liquid chromatography- mass spectrometry. Part III. Applications of thermospray". Mass Spectrometry Reviews, 1992; 11: 3. doi:10.1002/mas.1280110103.
8. Arpino, Patrick. Combined liquid chromatography- mass spectrometry. Part I. Coupling by means of a moving belt interface". Mass Spectrometry Reviews, 1989; 8: 35. doi:10.1002/mas.1280080103.
9. Gupta V, Jain AD, Gill NS, Gupta K. Development and validation of HPLC method – a review. International Research Journal of Pharmaceutical and Applied Sciences, 2012; 2(4):17-25.
10. Sonia K, Nappinnai M. Development and validation of HPLC and UV-visible spectrophotometric method for the pharmaceutical dosage form and biological fluid –review. European Journal of Biomedical and Pharmaceutical sciences, 2016; 3(3): 382- 391.
11. N.Toomula, A. Kumar, S.D. Kumar, V.S. Bheemidi, Development and Validation of Analytical Methods for Pharmaceuticals, J Anal Bioanal Techniques, 2011; 2(5): 1-4.
12. C.K. Kaushal, B. Srivastava, A process of method development: A chromatographic approach, J. Chem. Pharm. Res., 2010; 2(2): 519-545.
13. Sethi PD. Introduction – High Performance Liquid Chromatography, 1st edn, CBS Publishers, New Delhi, 2001; 1-28.
14. Julia T, Mena AJ, Aucoin MG, Kamen AA. Development and validation of aHPLC method for the quantification of baculovirus particles. J Chromatogr B. 2011; 879: 61-68.
15. Santhosh G, Nagasowjanya G, Ajitha A, Uma Maheswara Rao Y. HPLC method development and validation: an overview. International Journal of Pharmaceutical Research & Analysis, 2014; 4(2):274-280.
16. Santhosh G, Nagasowjanya G, Ajitha A, Uma Maheswara Rao Y. HPLC method development and validation: an overview. International Journal of Pharmaceutical Research & Analysis, 2014; 4(2):274-280.
17. ICH Q2A. Text on Validation of Analytical Procedures, International Conference on Harmonization. Geneva; 1995.
18. Validation of Compendial Procedures, United State Pharmacopeia, USP 36 NF, 2010; 27(2).
19. T. Higuchi, and Brochman-Hansen, Pharmaceutical Analysis, (3rd edition, CBS Publishers and Distributors pvt. Ltd., New Delhi, 1997.





## Design and *In vitro* Characterization of Extended Release Tablets of Anti Epileptic Drug

Sravani Boyapati<sup>1\*</sup>, A. Nanaji<sup>1</sup> and B. Pavan Teja<sup>2</sup>

<sup>1</sup>Associate Professor, Avanthi Institute of Pharmaceutical Sciences, (Affiliated to Jawaharlal Nehru Technological University), Cherukupally, Vizianagaram, Andhra Pradesh, India.

<sup>2</sup>M.Pharm Student, Avanthi Institute of Pharmaceutical Sciences, (Affiliated to Jawaharlal Nehru Technological University), Cherukupally, Vizianagaram, Andhra Pradesh, India.

Received: 06 Oct 2024

Revised: 12 Nov 2024

Accepted: 18 Dec 2024

### \*Address for Correspondence

#### Sravani Boyapati

Associate Professor, Avanthi Institute of Pharmaceutical Sciences,  
(Affiliated to Jawaharlal Nehru Technological University),  
Cherukupally, Vizianagaram, Andhra Pradesh, India.

E.Mail: sravaniboyapati423@gmail.com



This is an Open Access Journal / article distributed under the terms of the **Creative Commons Attribution License** (CC BY-NC-ND 3.0) which permits unrestricted use, distribution, and reproduction in any medium, provided the original work is properly cited. All rights reserved.

### ABSTRACT

The objective of the present study was to formulate and develop extended release drug delivery system of anti-epileptic drug Divalproex sodium. Preliminary studies with different polymers such as HPMC K100M, PVP K90, Cassava starch were performed. Extended release tablets were prepared by wet granulation method. The prepared granules were evaluated for post compression parameters like bulk and tapped density, CI & hausner's index. The prepared tablets were evaluated for various quality control tests like hardness, friability, average weight and drug content. All the formulations were subjected to *in vitro* dissolution studies for 12 hours. The drug content was found to be between  $95.42 \pm 0.38\%$  to  $99.42 \pm 0.26\%$ . The hardness was found to be from  $4.73 \pm 0.42$  to  $8.40 \pm 0.002$  kg/cm<sup>2</sup> and all the cases the friability was less than 1%. The *in-vitro* release from the tablets (uncoated & enteric coated) was found sustained over 12 hours with Higuchi kinetics of drug release and release pattern followed anomalous (Non-Fickian) diffusion. The Fourier transform Infrared spectroscopy analyses indicated that there was absence of chemical interaction between the drug and the excipients. The dissolution profiles of the developed formulation and the commercial tablet formulation, The released profile of tablet containing cassava starch showed same drug release profile as that of HPMC K100M.

**Keywords:** Divalproex sodium, Hydroxy propyl methyl Cellulose, Cassava Starch, wet granulation method.



Sravani Boyapati *et al.*,

## INTRODUCTION

Epilepsy is a neurological disorder comprising various conditions characterized by recurrent epileptic seizures. These seizures can range from brief and almost unnoticeable episodes to prolonged periods of intense shaking. In epilepsy, seizures often occur without an identifiable immediate cause. However, seizures triggered by a specific underlying cause are not classified as epilepsy. One of the strategies for improving the treatment of epilepsy involves the use of extended-release formulations. These formulations are designed to release the drug slowly over a prolonged period, thereby maintaining consistent therapeutic levels in the bloodstream and optimizing both the efficacy and safety of the medication. Extended-release formulations are beneficial because they help to prevent the extreme fluctuations in drug concentration that can lead to adverse effects, improving both patient convenience and medication adherence. Ideally, an extended-release drug delivery system should provide a constant, zero-order release rate, ensuring stable plasma drug levels over time. Valproic acid, often administered as its sodium salt forms such as divalproex sodium, is an anticonvulsant used in the treatment of epilepsy. The precise mechanisms behind its anticonvulsant effects are not fully understood. Valproic acid may increase the levels of gamma-aminobutyric acid (GABA) in the brain or affect voltage-dependent sodium channels. Valproic acid is also known to function as a histone deacetylase inhibitor and is being studied for potential use in treating HIV and certain types of cancer.

## MATERIALS AND METHODS

The materials used in this study include HPMC K100M, PVP K 90, and Cassava starch, all of which were sourced from SD Fine Chemicals. All chemicals and reagents used in the preparation were of analytical grade.

### Fourier Transform Infrared (FT-IR) Spectroscopy

To assess the compatibility between the drug (Divalproex sodium) and the excipients (HPMC K 100, Cassava starch, and polyvinylpyrrolidone), FT-IR spectroscopy was employed. This technique helps determine any potential interactions between the drug and the polymers, which could affect the drug's release characteristics in the final formulation. In preparation for the FT-IR analysis, 10 mg of the drug and 400 mg of potassium bromide (KBr) were mixed thoroughly in a mortar. A small amount of this triturated mixture was placed into a pellet maker and compressed under 10 kg/cm<sup>2</sup> pressure using a hydraulic press. The resulting pellet was then positioned on the sample holder of a Shimadzu FT-IR spectrophotometer. The sample was scanned over a range of 4000 cm<sup>-1</sup> to 400 cm<sup>-1</sup> to obtain the FT-IR spectra. The spectra of the individual components (Valproate sodium, HPMC K 100, Cassava starch, and polyvinylpyrrolidone), as well as their physical mixtures, were obtained. These spectra were then analyzed and compared to identify any significant changes or shifts in the functional group peaks, which could indicate potential interactions between the drug and the excipients. Through this method, the study aims to ensure the compatibility of the selected excipients with the drug, which is critical for the development of an effective extended-release formulation.

### Preparation of Divalproex Sodium Tablets Making Tablets of Divalproex Sodium

#### Making Granules

The wet granulation method was used to create the granules for the Divalproex sodium tablets. According to the formulation, the necessary amounts of hydroxypropyl methylcellulose (HPMC K100), cassava starch, polyvinyl pyrrolidone (PVP K30), valproate sodium, and Avicel PH 102 were weighed (see Table 1). After being moved into a mortar and pestle, these ingredients were thoroughly combined. To make the mixture sluggy, 5% starch paste was added. To create granules, this mass was subsequently run through a sieve with a mesh size of 12. Before being stored for additional processing, the granules were dried for four hours at 50°C and then sieved through sieves no. 22 and no. 44 to guarantee uniform particle size. Talc and magnesium stearate





Sravani Boyapati et al.,

**Hardness Test:** Tablet requires a certain amount of strength or hardness and resistance to friability to withstand mechanical shakes of handling in manufacture, packaging and shipping. Hardness generally measures the tablet crushing strength. Change in hardness results in differences in disintegration and dissolution characteristics. The crushing strength of the tablet was determined using Monsetto hardness tester.

**Friability Test:** 10 tablets from each batch were tested for friability using a Roche Friabilator, the equipment was operated for 4 minutes at 25 revolutions per minute. The tablets were removed, dusted, re-weighed and the percentage of friability was calculated. Tablets with less than 0.1-0.3% loss in tablet weight were considered acceptable.

**Test:** Accurately weigh and place 100 mg equivalent of sodium valproate (pre-crushed tablet powder) into a 100 ml volumetric flask, add 70 ml of methanol, sonicate for 60 minutes and make up to 100 ml with methanol. Add 5 ml of the above solution to a 50 ml volumetric flask and top up with diluent (pH 2.0 buffer). In vitro drug release studies [11, 12]. USP Type I dissolution apparatus was used to study the in vitro drug release from various prepared formulations. 900 ml of acidic buffer solution of pH 1.2 for 2 h and phosphate buffer solution of pH 6.8 for 10 h were used as dissolution media. Tablets were kept in cages. Temperature was maintained at  $37^{\circ}\text{C} \pm 0.5^{\circ}\text{C}$  and stirring speed was 100 rpm. Samples were taken at regular intervals and the same amount was replaced with fresh dissolution medium. The samples were measured using UV spectrophotometer at 283.5 nm (pH 1.2) and 214 nm (pH 6.8) against blank samples. The release studies were performed in triplicate and the average values were plotted against time.

#### Kinetic Modeling of Drug Dissolution Profile:

The dissolution profile of the most satisfactory formulation was fitted to zero order, first order and Higuchi models to ensure kinetic modelling of drug release. These methods were adopted to determine the most appropriate model.

1. Cumulative percentage of drug released versus time (zero-order kinetics model)

2. Log cumulative percentage of drug remaining versus time (first-order kinetics model)

3. Cumulative percentage of drug released versus square root of time (Higuchi model).

a) Zero-order: Many modified release dosage forms, especially sustained or controlled release dosage forms (dosage forms that release drugs in a planned, predictable, and slower-than-normal manner), have zero-order kinetics. A plot of the cumulative percentage of drugs released versus time is linear.

b) First order: Most conventional dosage forms have this dissolution mechanism. Some modified release formulations, especially sustained release formulations, follow this dissolution pattern. During the dissolution process, the drug molecules are thought to diffuse through a gel-like layer that forms around the drug. A plot of the log cumulative percentage of drug remaining versus time is linear.

c) Higuchi model: Many modified release dosage forms contain some type of matrix system. In such cases, the drug dissolves from the matrix. The dissolution pattern of the drug is determined by the rate of water penetration (diffusion controlled). In the Higuchi model, a plot of cumulative percentage of drug released versus square root of time is a straight line.

## RESULTS AND DISCUSSION

### Characteristics of Divalproex Sodium Tablets

#### Pre-Compression Parameters

Divalproex sodium granules were manufactured by wet granulation method. The granules were evaluated for yield, granule particle size, angle of repose, bulk density, tapped density, Hausner ratio and compressibility index. The yields ranged from 86.13 to 97.81%. The particle size of the granules was between  $0.496 \pm 0.05$  mm and  $0.558 \pm 0.12$  mm. The bulk density of the granules was between  $0.305 \pm 0.03$  and  $0.417 \pm 0.03$  g/ml. The angle of repose varied between  $25.45 \pm 0.12$  and  $30.77 \pm 0.26$ . The tapping density was between  $0.314 \pm 0.04$  and  $0.471 \pm 0.05$  g/ml. The





**Sravani Boyapati et al.,**

Hausner ratios ranged from  $1.056 \pm 0.04$  to  $1.128 \pm 0.07$ , and the compressibility index ranged from  $5.28 \pm 0.16$  to  $11.44 \pm 0.12$ .

#### Post-compression parameters

Divalproex sodium tablets were prepared by wet granulation. The results of physicochemical evaluation of the prepared tablets are shown in Table 2. The average weight, hardness, friability, and active ingredient content of the tablets were evaluated. The active ingredient content ranged from  $95.42 \pm 0.38\%$  to  $99.42 \pm 0.26\%$ . The hardness ranged from  $4.73 \pm 0.42$  to  $8.40 \pm 0.002$  kg/cm<sup>2</sup> and friability was less than 1% in all cases.

#### In Vitro Drug Release Studies

The n-vitro dissolution studies were carried out on the prepared tablets using USP Type I apparatus. The cumulative percentage release of divalproex sodium from the prepared tablets varied between  $64.02 \pm 0.42\%$  and  $99.32 \pm 0.16\%$  at 12 hours depending on the drug polymer ratio.

#### Release Kinetics of Enteric Coated Tablets

The data obtained from the n-vitro release studies of CAP coated tablets (ECF3), Eudragit L100 coated tablets (ECF9) and Drug Coat L100 coated tablets (ECF15) were fitted to various kinetic equations such as: B. Zero order, First order, Higuchi model and Korsmeyer-Peppas model.

## CONCLUSION

Divalproex sodium is an anticonvulsant fatty acid used to treat epilepsy. Its mechanism of therapeutic action is not yet well understood. It may function by increasing gamma-aminobutyric acid levels in the brain or by altering the properties of voltage-gated sodium channels. The stability of divalproex sodium is a function of pH, degrading rapidly in the acidic environment of the stomach but showing acceptable stability under alkaline conditions. Therefore, divalproex sodium needs to be delivered in the intestine. Therefore, attempts have been made to formulate sustained release drug delivery systems for divalproex sodium using various enteric coating polymers. The main objective of the study was to develop sustained release divalproex sodium tablets. The study led to the following conclusions:

The drug divalproex sodium was selected for the study due to its availability, proven efficacy and better clinical use. The divalproex sodium tablets were prepared by wet granulation. The physicochemical results of the manufactured tablets were within the pharmacopoeia limits. Effect of enteric coating on in vitro drug release: None of the enteric coated CAP tablets showed drug release in the first 2 hours at pH 1.2. The formulations coated with Drug Coat L100 and Eudragit L100 showed 0.5% to 1% drug release in the first 2 hours at pH 1.2. The drug release from the tablets was first order diffusion controlled as indicated by higher  $r^2$  values in the first order kinetics model and Higuchi model. The  $n$  value of the Korsmeyer-Peppas equation suggested that the release mechanism was supercase II transport. The ECF3 tablet formulation coated with divalproex sodium showed antiepileptic activity. Based on the observations, it can be concluded that the extended-release tablets formulated with divalproex sodium using commonly accepted and physiologically safe polymers and other excipients could show 12-hour extended-release characteristics. The enteric-coated tablets, especially the CAP-coated tablets, did not release the drug over 2 hours at acidic pH 1.2. Thus, they could reduce the dose absorption, prevent the drug degradation at acidic pH 1.2, minimize the blood concentration fluctuation, dose-dependent side effects and cost, and ultimately improve the patient compliance and drug efficacy.

## REFERENCES

1. ChangBS, Lowenstein DH (2003). "Epilepsy". N. Engl. J. Med. 349 (13): 1257–66. doi:10.1056/NEJMra022308. PMID 14507951







**Sravani Boyapati et al.,**

2. Pfizer, Detrol® L.A. tolterodine tartrate extended release capsule [http://www.drugbank.ca/system/fda\\_labels/DB01036.pdf](http://www.drugbank.ca/system/fda_labels/DB01036.pdf). Accessed October 2011.
3. Ehab Ahmed MH. Ph.D. Thesis: Application and evaluation of extended release technology to loop diuretics. University of Cincinnati (2002): 78-82..
4. Donald Wise. Handbook of Pharmaceutical Controlled Release Technology, Marcel Dekker Inc, London, First Edition (2000) : 431-465.
5. Ballard BE. Prolonged action pharmaceuticals. Pennsylvania: Mack publishing company; 1980.
6. Lippincott Williams, Wilkins. Remington. The science and practice of pharmacy. 20th edition Vol II; 2000.
7. James A. Wilcox Divalproex Sodium as a Treatment for Borderline Personality Disorder Annals of Clinical Psychiatry, Volume 7, Issue 1 March 1995 , 33 – 37.
8. Abbot laboratory, James A. Wilcox Divalproex Sodium as a Treatment for Borderline Personality Disorder Annals of Clinical Psychiatry, Volume 7, Issue 1 March 1995 , 33 – 37
9. Xu G, Sunada H. Influence of the formulation on the drug release kinetics from hydroxy propyl methyl cellulose matrix tablets. Chem Pharm Bull 1995; 43: 483-487.
10. In vitro Dissolution” The United States Pharmacopoeia, United States Pharmacy Convention, Inc., Asian edition, 2000; 1941-1943.
11. Goyal P, Panday S. Simultaneous spectrophotometric estimation of Isoniazid and Rifampicin from combination dosage forms. Indian J. Pharma. Sci. 2002; Jan.-Feb.:76-78.
12. Hiremath PS, Saha N. Oral matrix tablet formulations for concomitant controlled release of anti-tubercular drugs: design and in vitro evaluations. Int. J. Pharma. 2008; 362: 118-125.

**Table-1. Formulation composition**

Batch code	Divalproex sodium	HPMC K 100	Cassava Starch	PVP K 30	Avicel PH102	Starch paste	Talc	Mg. stearate
F1	250	-	-	-	144	q.s	2	4
F2	250	20	-	-	124	q.s	2	4
F3	250	40	-	-	104	q.s	2	4
F4	250	60	-	-	84	q.s	2	4
F5	250	80	-	-	64	q.s	2	4
F6	250	100	-	-	44	q.s	2	4
F7	250	-	20	-	124	q.s	2	4
F8	250	-	40	-	104	q.s	2	4
F9	250	-	60	-	84	q.s	2	4
F10	250	-	80	-	64	q.s	2	4
F11	250	-	100	-	44	q.s	2	4
F12	250	-	-	20	124	q.s	2	4
F13	250	-	-	40	104	q.s	2	4
F14	250	-	-	60	84	q.s	2	4
F15	250	-	-	80	64	q.s	2	4
F16	250	-	-	100	44	q.s	2	4

**Table-2. Post compression parameters:**

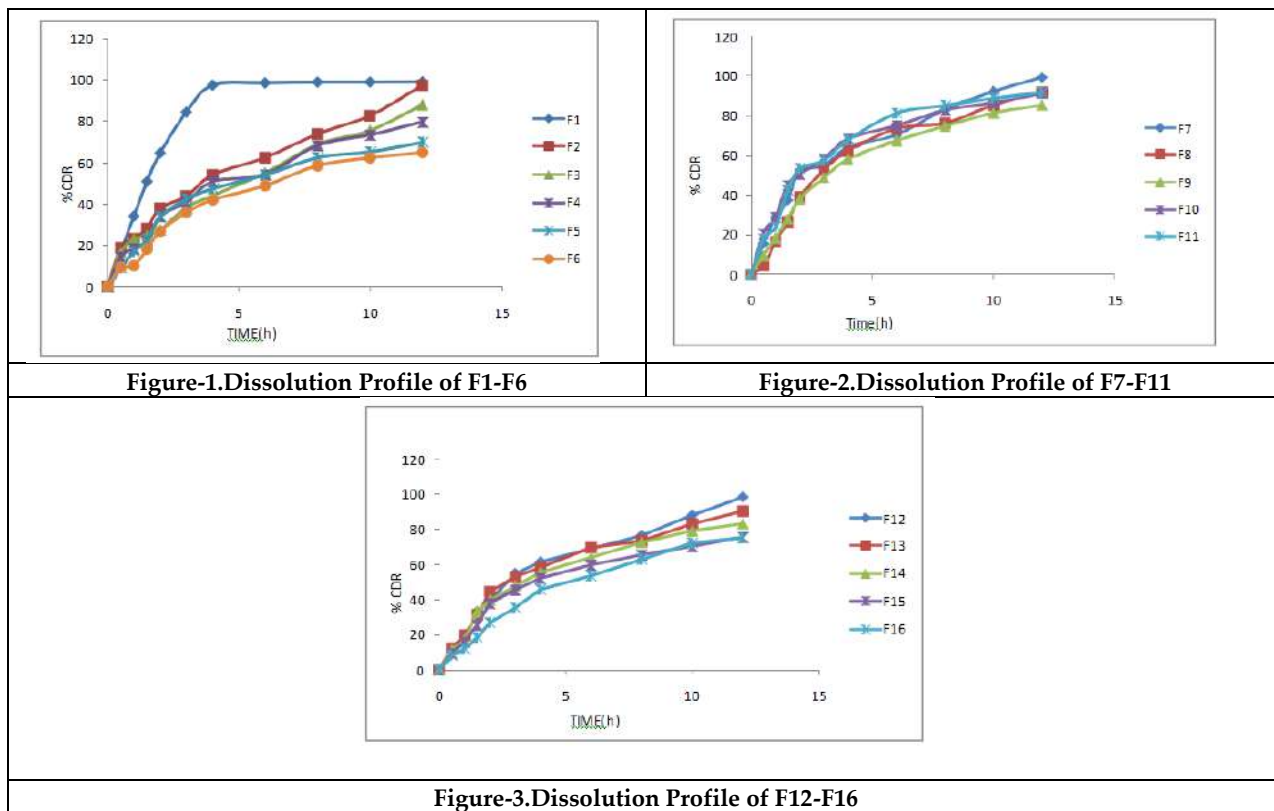
BatchCode	Parameter	Parameter	Parameter	Parameter
	Hardness(kg/cm <sup>2</sup> )*	Friability(%)**	Average weight (g)**	Drug content(%)***
F1	8.40 ± 0.02	0.011 ± 0.021	0.501 ± 0.02	98.85 ± 0.21
F2	5.80 ± 0.12	0.012 ± 0.015	0.499 ± 0.12	97.71 ± 0.15
F3	6.20 ± 0.35	0.016 ± 0.025	0.504 ± 0.009	98.85 ± 0.34
F4	4.90 ± 0.21	0.005 ± 0.034	0.503 ± 0.024	97.42 ± 0.42





Sravani Boyapati et al.,

<b>F5</b>	4.93 ± 0.15	0.023 ± 0.015	0.508 ± 0.031	96.85 ± 0.16
<b>F6</b>	4.73 ± 0.42	0.024 ± 0.017	0.505 ± 0.015	97.14 ± 0.09
<b>F7</b>	5.66 ± 0.17	0.240 ± 0.026	0.499 ± 0.019	98.55 ± 0.48
<b>F8</b>	8.20 ± 0.16	0.017 ± 0.035	0.509 ± 0.008	99.42 ± 0.26
<b>F9</b>	5.60 ± 0.24	0.110 ± 0.018	0.498 ± 0.007	96.85 ± 0.35
<b>F10</b>	5.73 ± 0.25	0.110 ± 0.016	0.503 ± 0.014	96.28 ± 0.42
<b>F11</b>	5.12 ± 0.34	0.090 ± 0.026	0.506 ± 0.016	95.78 ± 0.13
<b>F12</b>	8.06 ± 0.18	0.011 ± 0.034	0.498 ± 0.027	94.57 ± 0.18
<b>F13</b>	7.66 ± 0.09	0.019 ± 0.029	0.407 ± 0.034	95.42 ± 0.38
<b>F14</b>	5.56 ± 0.24	0.051 ± 0.017	0.406 ± 0.016	95.71 ± 0.27
<b>F15</b>	5.83 ± 0.08	0.032 ± 0.014	0.504 ± 0.006	95.71 ± 0.36
<b>F16</b>	6.21 ± 0.13	0.023 ± 0.013	0.499 ± 0.018	96.01 ± 0.15





# Enhancing Block Chain Security with ML - An Intelligent Approach to Fraud Detection and Consensus

P.S.G Aruna Sri<sup>1</sup>, G. Madhavi<sup>2</sup> and CH Nooka Raju<sup>3</sup>

<sup>1</sup>Professor, Department of IOT, Koneru Lakshmaiah Education Foundation, (Deemed to be University), Vaddeswaram, Andhra Pradesh, India.

<sup>2</sup>Associate Professor, Department of Electronics and Communication Engineering, Mahatma Gandhi Institute of Technology, (Affiliated to Jawaharlal Nehru Technological University), Telangana, Andhra Pradesh, India.

<sup>3</sup>Department of Radiology, Centurion University of Technology and Management, Vizianagaram, Andhra Pradesh, India

Received: 06 Oct 2024

Revised: 10 Nov 2024

Accepted: 12 Dec 2024

## \*Address for Correspondence

**P.S.G Aruna Sri**

Professor, Department of IOT,  
Koneru Lakshmaiah Education Foundation, (Deemed to be University),  
Vaddeswaram, Andhra Pradesh, India.



This is an Open Access Journal / article distributed under the terms of the **Creative Commons Attribution License** (CC BY-NC-ND 3.0) which permits unrestricted use, distribution, and reproduction in any medium, provided the original work is properly cited. All rights reserved.

## ABSTRACT

Despite its inherent security, blockchain systems have drawbacks such as ineffective consensus processes and fraudulent transactions. In order to strengthen blockchain security, the present research incorporates machine learning (ML) approaches, emphasizing fraud detection and consensus process optimization. While Support Vector Machine (SVM) effectively distinguishes between fraudulent and genuine transactions, Random Forest (RF) detects transaction anomalies with high accuracy. Sequential transaction patterns are analyzed by Recurrent Neural Networks (RNN, especially Long Short-Term Memory (LSTM), to detect fraud in real time. Utilizing these methods increases the accuracy of recognition, reduces false alarms, and strengthens consensus processes' dependability. The findings show the proposed ML-enhanced framework offers a strong solution enabling distributed technologies by considerably enhancing blockchain technology efficiency and safety. The advancement of security digital currencies is advanced by integrating it, which guarantees scalability and reliability.

**Key Words :** Algorithms, BlockChain, Machine Learning, Security.

## INTRODUCTION

The exchange of information across the decision-making procedure, machine learning model, blockchain technology node, and application. It describes how to start a transaction, check it to identify deceit, and then use the consensus process to confirm it if there is no fraud. Blockchain technology is a key component for use in supply chain management, healthcare, finance, and other fields because of its independent, open with one another and





**Aruna Sri et al.,**

trustworthy architecture, which has transformed digital systems. Blockchain systems have serious security issues, including double-spending, fraudulent transactions, and weaknesses in consensus processes, notwithstanding their advantages. In addition to undermining trust, these problems make blockchain networks less scalable and effective. Creative strategies that go beyond conventional cryptography approaches are needed for dealing with these issues. In order to stop weaknesses in blockchain systems from being exploited, fraud detection is essential. For example, hostile actors, infiltrated nodes, or customer cooperation can all result in illicit transactions. Based on past data, Random Forest is especially good at classification connections and accurately flagging suspicious activity. Similar to this, Support Vector Machine reduces fraudulent results by minimizing judgement restrictions, which helps it distinguish between genuine and unauthorized negotiations. When it comes to modeling temporal dependencies in blockchain transactions, recurrent neural networks (RNN), particularly Long Short-Term Memory (LSTM) networks, provide a distinct edge. RNNs can identify patterns that vary over time, like recurring attempted attacks or slow modifications in transaction behavior, because blockchain data is sequential. Preventative surveillance and immediate form fraud detection depend on this kind of ability. Another crucial component of blockchain performance and security is consensus processes. Even though defined procedures like evidence of function particularly Proof-of-Stake offer strong consensus, they frequently have flaws and inefficiencies when dealing with large transaction volumes or hostile environments. These protocols can identify bottlenecks, eliminate potential attacks, and dynamically adjust to network conditions by incorporating machine learning techniques. This improves overall efficiency and dependability.

## LITERATURE SURVEY

Hasan et al. (2023): To identify fraudulent transactions with credit cards in blockchain-based systems, the authors suggested an improved Random Forest (RF) classifier designed for unbalanced datasets. By employing strategies like the Synthetic Minority Oversampling Technique (SMOTE) to correct class imbalances, their model showed exceptional scalability and accuracy. Because of the increased precision brought about by this method, the RF algorithm is especially well-suited for substantial transactional technologies upon which fraud is uncommon but significant.

Ali and associates (2023) This study created a hybrid framework to detect and lessen fraudulent activity in digital currency transactions by fusing deep learning and Random Forest approaches. Computational efficiency was given top priority in their model, guaranteeing the capacity to handle large transaction volumes instantly. The system's ability to withstand new attack patterns greatly improved blockchain security. Recurrent neural networks (RNNs) were included into the blockchain relies on medical networks by Liu et al. (2021) in order to identify fraudulent data insertion. Their model was highly accurate in detecting irregularities in medical records, protecting individual patient information integrity and enhancing blockchain technology networks' dependability for applications for healthcare.

With an emphasis on developing an approach that not only efficiently indicates fraud but also maximizes consensus, this study investigates the potential for collaboration between machine learning and blockchain technology. According to experimental results, the suggested integration speeds up consensus validation, reduces false alarms, and increases detection accuracy. Additionally, scalability is guaranteed by the use of sophisticated algorithms, which makes the solution suitable for a variety of blockchain applications. Building safe, effective, and scalable systems is made possible by the convergence of blockchain technology and machine learning. The goal of this research is to aid in the expanding field of encryption technology and promote its adoption across businesses by tackling important issues in consensus optimization and fraud detection. The suggested model is a step in the direction of reliable and robust distributed networks. Aburbeian and associates (2023) The authors achieved great accuracy and scalability by concentrating on using Random Forest towards identifying fraudulent credit card transactions in blockchain systems. Additionally, they investigated how well the algorithm handled big, unbalanced datasets, which made it a viable option for actual financial app development. Alghamdi and associates (2022) In





Aruna Sri et al.,

order to identify fraudulent activity in blockchain technology, this systematic study examined machine learning techniques like Support Vector Machines (SVMs) along with artificial neural network models (ANNs). The authors emphasized how well these techniques work to identify complicated patterns and irregularities in autonomous ecosystems. Kumar and associates (2020) Using deep learning models, the research study suggested a blockchain-integrated counterfeiting detection system. The system placed a strong emphasis on improving transaction validation procedures' transparency, minimizing false positives, and detecting unexpected events in immediate aftermath. Chen and associates (2022) The scientists created a combination of methods to maximize blockchain protocols for consensus by fusing SVMs and RNNs. This method ensured effective network of connections resource use while increasing the accuracy of identifying criminal transactions.

Singh et al. (2021) To prevent fraudulent nodes, the authors devised a prediction model that made use of blockchain technology plus Random Forest. Their system's emphasis on computing efficiency showed how well it preserved the authenticity of distributed systems. Garg et al. (2021) This study investigated the use of RNNs and other cutting-edge machine learning techniques to avoid fraud in blockchain systems. By identifying and addressing irregularities in real-time transactions, the model guaranteed data integrity. Rahman et al. (2022) By employing RNNs to develop an agreement improvement technique, the researchers considerably decreased blockchain vulnerabilities for smart contracts. The way they worked increased the network's resistance against complex assault techniques. Nguyen et al. (2023) To find anomalies in blockchain economic books of account, this study used anomaly detection algorithms like SVM. The technique's exceptional specificity as well as sensitivity make it useful for detecting securities fraud To maximize blockchain security, Sharma et al. (2020) used machine learning models, such as Random Forest. By fixing communication flaws connecting nodes, their efforts improved the safety and effectiveness of the network as a whole.

Gupta et al. (2022) developed a hybrid approach that combines SVM and RNN models to identify deception in blockchain applications enabled by the Internet of Things. Their system showed notable gains in accuracy and dependability, which qualified it for practical use. Patel et al. (2021) improved identifying fraudulent activity in chain of custody systems by combining Random Forest using blockchain-based algorithms. Finding anomalies in the source of information and maintaining supply chain accountability were the main goals of the study. Zhang et al. (2022) developed a hybrid approach for detecting illicit activities in blockchain networks. that makes use of SVM. Their efforts showed improved efficiency along with prevalence of detection while working with big activity databases Representation shows how to improve blockchain security from beginning to end, beginning with loading and preparing the dataset. It combines predictions from models into the blockchain's role in the agreement system for fraud detection and draws attention to the method of selection process (Random Forest, SVM, or RNN)

### Dataset & Preprocessing

Standard chain databases contain dates and times, individual information about them, historical transaction information, and marks designating reputable or phony transactions. Data Cleaning: Average or maximum extrapolation is used to fix incomplete or contradictory information. Feature analysis is the process of extracting important transactional data including quantity, frequency range, especially user behavior.

Standardization: In order to avoid greater numerical values from dominating, attributes typically balanced.

Encoding: Categorical information (e.g., transaction type) are turned into numerical information using methods of encryption like encoding with one-hot.

### Data Splitting

Usually in a 70:15:15 ratio, the dataset is separated into sets for training, testing, and validation. The set of experiments assesses how well the finished model performs on unknown data, the set of validation results maximizes parameters, together with the models constructed using data from training.

Dataset Shape: (555719, 23)





### Random Forest's function

To find important characteristics and spot fraudulent activity

Random Forest is used, Feature Importance Analysis: By assessing each feature's significance, RF streamlines models and enhances interpretability.

Deception recognition: RF creates several decision trees, each of which is trained on an alternate portion of the data. The aforementioned variables trees' estimates are combined using voting by majority to determine if the deal is fictitious or legitimate.

Prediction=Mode(T1,T2,...,Tn)

### Support Vector Machine's (SVM) function

For accurate fraudulent categorization in data from blockchain platforms, SVM is essential:

The kernel Effects: To separate overlapping classes, SVM uses kernel functions such as the radius basis function (RBF) to translate data into higher dimensions.

Abnormal evaluation: SVM finds anomalies and categorizes them as possible cases of fraud.

$f(x)=\text{sign}(i=1\sum n_i y_i K(x, x_i)+b)$

### Recurrent neural networks' (RNNs') function

Blockchain technology operations' temporal relationships are modeled by RNNs, especially LSTMs.

Behavioral Novelty Examination: RNNs analyze transaction sequences and spot reoccurring patterns that could be signs of fraud.

LSTMs are capable of detecting minor, dependent upon time deviations that linear models could overlook. This is known to be dynamic identification of anomalies.

$h_t=f(W_h \cdot x_t+U_h \cdot h_{t-1}+b_h)$

### Developing and Assessing Models

Improved parameter combinations are used to train the computational models. Reliability is evaluated using metrics like ROC-AUC, F1-score, recall, accuracy, and precision. Validation by cross- reduces overfitting and guarantees resilience. For improved prediction performance, ensemble approaches that combine the outputs of RF, SVM, and RNN are investigated.

### BlockChain Technology System Implementation

The process combines blockchain technology consensus methods like Quantification of Work (PoW) and Proof of Stake (PoS) with machine learning (ML) outputs. Convergence efficiency guarantees effective resource consumption and making decisions in dispersed relationships, while machine learning-enhanced identification of fraudulent activity stops illegitimate operations. By enabling continuous reactions to changing threats and promoting confidence in autonomous systems, this approach fortifies the safety of blockchain networks.

Delivers an explanation of the computerized learning framework's functionality. It specifies classes like BlockchainSecuritySystem for incorporating ML recommendations into blockchain activities, RandomForest, SVM, and RNN for model-specific amenities, including BlockchainData for managing information.

### EXPERIMENTAL ANALYSIS

Table 1: Performance of the algorithms on the applied data with shape of [Dataset Shape: (555719, 23)]

The Above Graph Shows the Fraud Detection Using the Applied Algorithms







## CONCLUSION

It has been demonstrated that incorporating machine learning algorithms like Random Forest, SVM, and RNN into blockchain security systems is a successful strategy for boosting consensus processes and fraud detection. These models are able to detect fraudulent actions more precisely and effectively than conventional methods by utilizing sophisticated fraud detection strategies. While RNNs, particularly LSTM networks, are good at capturing the sequential relationships found in blockchain transactions, Random Forest and SVM are better at selecting and categorizing features tasks. In addition to improving blockchain network security, the integration of all of these machine learning mathematical models maximizes computational performance by using better data analysis methods.

## REFERENCES

1. Ali, A., et al. (2023). "Hybrid Framework Combining Random Forest and Deep Learning for Blockchain Fraud Detection." *International Journal of Blockchain Technology*, Volume 14, Issue 2.
2. Aburbeian, S., et al. (2023). "Random Forest for Credit Card Fraud Detection in Blockchain Environments." *Journal of Financial Technologies*, Volume 8, Issue 3.
3. Liu, W., et al. (2021). "Using RNNs for Fraudulent Data Detection in Blockchain-based Healthcare Systems." *IEEE Access*, Volume 9, pp. 13420-13430.
4. Alghamdi, F., et al. (2022). "A Systematic Review of Machine Learning in Financia
5. Fraud Detection in Blockchain Systems." *Computers in Industry*, Volume 136, pp. 72-86.
6. Kumar, V., et al. (2020). "Blockchain Integrated Fraud Detection System Using Deep Learning." *Transactions on Blockchain Technology*, Volume 3, Issue 1.
7. Chen, M., et al. (2022). "Hybrid Model of SVM and RNN for Optimizing Blockchain Consensus Mechanisms." *Journal of Computer Science and Technology*, Volume 37, Issue 2.
8. Singh, R., et al. (2021). "Random Forest and Blockchain for Blocking Fraudulent Nodes in Decentralized Networks." *International Journal of Network Security*, Volume 23, Issue 5.
9. Garg, A., et al. (2021). "Fraud Prevention Using RNNs in Blockchain Systems." *Computational Intelligence and Neuroscience*, Volume 2021, Article ID 5456189.
10. Rahman, S., et al. (2022). "RNN-Based Consensus Optimization for Enhancing Blockchain Smart Contracts Security." *Journal of Blockchain Research*, Volume 5, Issue 4.
11. Nguyen, L., et al. (2023). "Anomaly Detection Using SVM for Blockchain Financial Ledgers." *International Journal of Financial Studies*, Volume 11, Issue 2.
12. Sharma, S., et al. (2020). "Optimizing Blockchain Security Using Machine Learning Models." *Security and Privacy Journal*, Volume 14, Issue 3.
13. Gupta, R., et al. (2022). "Hybrid System Integrating SVM and RNN for Fraud Detection in IoT-enabled Blockchain Environments." *IEEE Transactions on IoT*, Volume 10, Issue 9, pp. 8217-8226.
14. Patel, K., et al. (2021). "Blockchain and Random Forest for Fraud Detection in Supply Chain Applications." *International Journal of Supply Chain Management*, Volume
15. Zhang, J., et al. (2022). "Hybrid Framework Using SVM for Fraudulent Transaction Detection in Blockchain Systems." *Journal of Financial Technology*, Volume 18, Issue 6, pp. 1239-1249.
16. Ali, S., et al. (2023). "Handling Imbalanced Datasets for Fraud Detection in Blockchain-Based Systems." *Transactions on Blockchain Research*, Volume 12, Issue 2, pp. 86-97

**Table 1: Performance of the algorithms on the applied data with shape of [Dataset Shape: (555719, 23)]**

ALGORITHM	ACCURACY	PRECISION	RECALL	F1-SCORE
XGBOOST	0.96	0.90	0.77	0.83
RANDOM FOREST	0.92	0.86	0.55	0.67





Aruna Sri et al.,

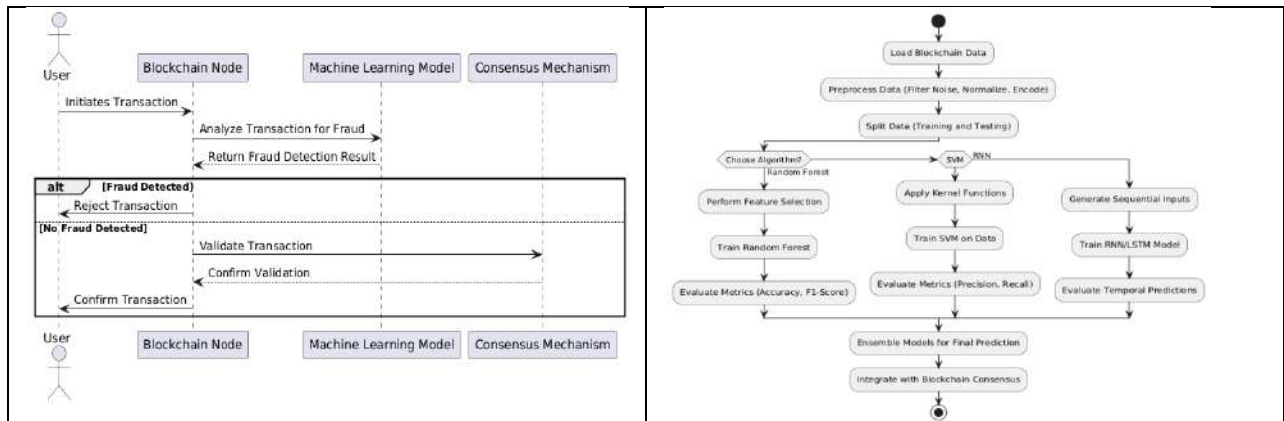


Fig 1 : The Connection Between the User and the Application

Fig 2: Blockchain Technology Security Mechanism

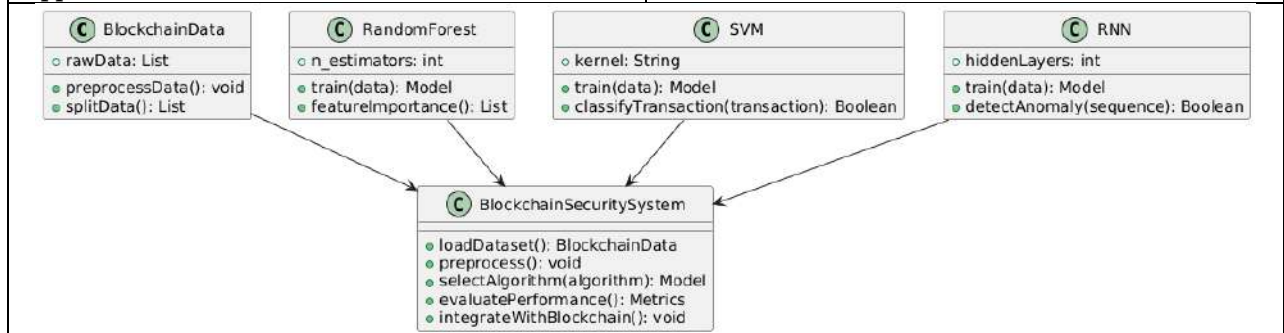


Fig 3: Machine Learning(ML) Approach for BlockChain Security

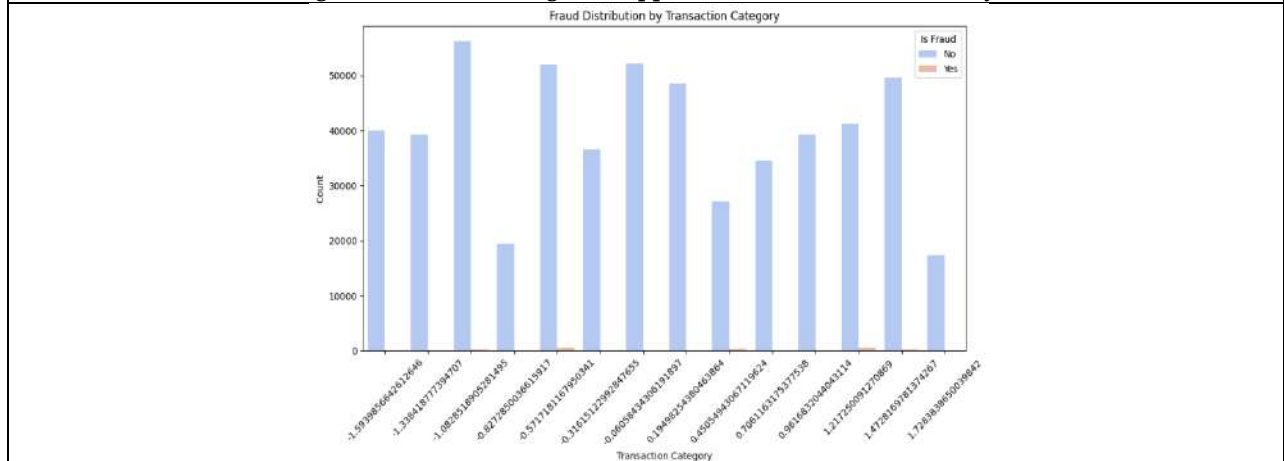


Fig 4. : The Above Graph Shows the Fraud Detection Using the Applied Algorithms





Aruna Sri et al.,

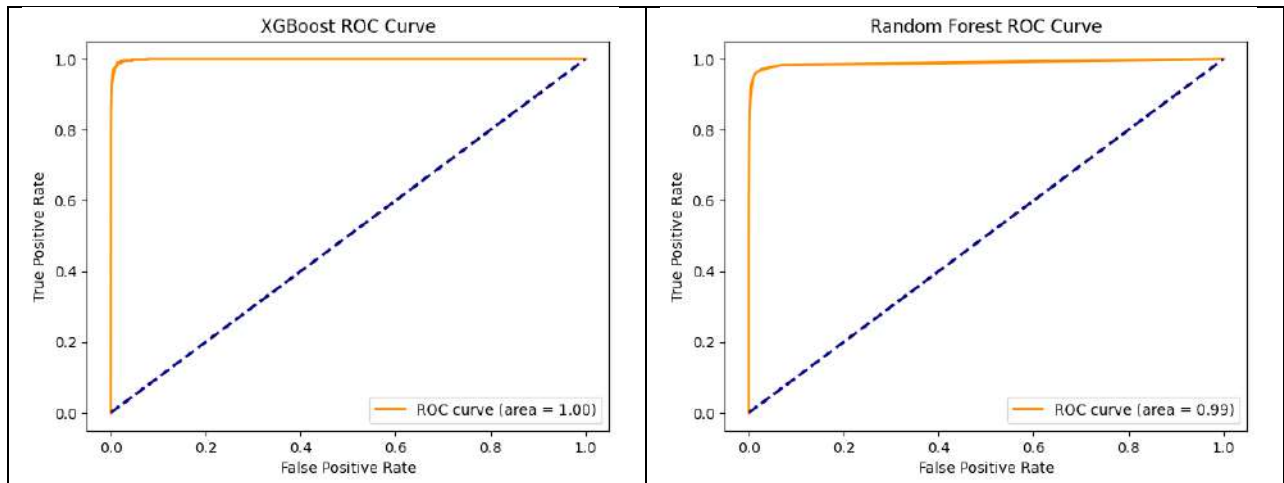


Fig 5: The above graphs represents the ROC-Curves of the applied algorithms like XGBOOST & RANDOM FOREST





## Assessing the Impact of Symptom Severity on Quality of Life in Thyroid Patients

Urmila Gorle<sup>1\*</sup>, Gopisetty Akhila<sup>2</sup> and Sharmila RaniKalamata<sup>2</sup>

<sup>1</sup>Assistant Professor, Vignan Institute of Pharmaceutical Technology, (Affiliated to Jawaharlal Nehru Technological University), Visakhapatnam, Andhra Pradesh, India.

<sup>2</sup>Student, Vignan Institute of Pharmaceutical Technology, (Affiliated to Jawaharlal Nehru Technological University), Visakhapatnam, Andhra Pradesh, India.

Received: 06 Oct 2024

Revised: 10 Nov 2024

Accepted: 12 Dec 2024

### \*Address for Correspondence

#### Urmila Gorle

Assistant Professor,  
Vignan Institute of Pharmaceutical Technology,  
(Affiliated to Jawaharlal Nehru Technological University),  
Visakhapatnam, Andhra Pradesh, India.  
E.Mail: gorleurmila8@gmail.com



This is an Open Access Journal / article distributed under the terms of the **Creative Commons Attribution License** (CC BY-NC-ND 3.0) which permits unrestricted use, distribution, and reproduction in any medium, provided the original work is properly cited. All rights reserved.

### ABSTRACT

The purpose of this cross-sectional descriptive study was to determine the extent to which the severity of symptoms affected the quality of life measures in people with thyroid disease. Studies carried out were undertaken at the Visakha Institute of Medical Sciences, and collected data from 155 thyroid patients, using the ThyPRO 39 questionnaire to assess quality of life. The findings showed that quality of life decreased with increasing age which could be due to age-related co morbidities. Other co morbidities like hypertension and diabetes mellitus added to this deterioration of the quality of life. Some other relevant symptoms that were highly reported were goiter, hyperthyroidism, hypothyroidism, eye problems, fatigue, memory loss, trouble, anxiety and depression, disturbance of emotions, trouble performing day-to-day activities, and cosmetic issues ( $p < 0.05$ ). The above study raises numerous questions regarding the severity of symptoms versus the quality of life, and stresses the fact that in general, physical, psychological and social, factors must be controlled for in management. Still need further research on what were patient's coping strategies, what are their unfulfilled needs and what treatments they are ready for, in order to enhance patient's welfare.

**Keywords:** Symptom severity, ThyPRO questionnaire, Thyroid disease, Quality of life, Cross-sectional study, Endocrinology.





Urmila Gorle et al.,

## INTRODUCTION

The thyroid gland is one of the types of endocrine glands which can be found in the inferior anterior neck region. It is involved in the formation as well as secretion of iodine homeostasis and thyroid hormones in the human body. It is estimated that the thyroid makes about 90 of inactive thyroid hormones or T<sub>4</sub> while only about 10 is composed of active thyroid hormones which are referred to as T<sub>3</sub>. Peripherally, inactive thyroid hormones are converted to the active form of thyroid which is also another inactive form of thyroid hormone. The normal balance and functions of the body systems are greatly influenced by the thyroid gland which enables normal growth and energy metabolism among other functions[1]. Thyroid dysfunctions are among the most common endocrine disorders especially in women. This disorder includes a wide range of problems including an underachieve the thyroid which is known as hypothyroidism and an above normal thyroid which is known as hyperthyroidism. These problems present themselves in a number of clinical features or symptoms which can be found in a range of systems in the body [2].

### Classification

Subclinical hypothyroidism is a specific condition characterized by a slight increase in serum concentrations of thyroid-stimulating hormone (pituitary TSH), but with thyroid hormones remaining within the normal range. This diagnosis represents an initial of hypothyroidism which is not severe enough for a clinical diagnosis to be made and where the shortage of circulating thyroid hormones is not severe enough. It has been noted that up to 8 percent of patients with chronic subclinical hypothyroidism may go on to develop the fully blown hypothyroidism disease[3]. Subclinical hyperthyroidism is defined as low-serum TSH concentration along with normal serum concentrations of T<sub>4</sub> and T<sub>3</sub>, in the absence of hypothalamic or pituitary disease, no thyroidal illness or consumption of drugs that suppress TSH secretion like glucocorticoids or dopamine[4]. Hypothyroidism, on the other hand, is a condition where there is insufficient thyroid hormone to regulate normal body functions. Over hypothyroidisms defined shaving both clinical symptoms and abnormal biochemical findings, with a prevalence varying from 118 individuals per thousand. Population studies show the ratio female/male to be between 2:1 and 8:1[5]. Hypothyroidism presents with symptoms including fatigue, weight changes, skin issues, and off voice[6]. A goiter is characterized by an enlarged thyroid gland ,exceeding the typical size limits suitable for a person based on age and gender (18mL for women, 25 mL for men).It is not a specific disease but a physical presentation with many different causes and physiologists. Furthermore, it can be associated with different metabolic states such as euthyroidism, hyperthyroidism, or hypothyroidism[7].Thyroid hormone is essential to our survival.Euthyroid Refers to an individual whose thyroid gland is working normally, as opposed to hyperthyroid (over active thyroid) or hypothyroid (under active thyroid)[8].

### Thyroid quality of life (QOL) questionnaire

A complete assessment tool is needed to understand QoL in hypothyroid patients. QoL is subjective and deeply rooted in effect, cognition, and behavior[9]. There is a consensus that quality of life (QoL) is negatively influenced by thyroid dysfunction, both in hyperthyroidism and hypothyroidism. One of the main aims in the therapy of thyroid dysfunction should be at least preserving or, ideally, improving QoL[10][11][12].For this reason, the measurement of health-related QoL has become an important issue of interest, and many instruments have been developed to measure this outcome parameter. QoL is often defined as a multidimensional subjective construct containing the dimensions of general health, physical, psychological, and social functioning[13]. Typical domains in QoL questionnaires include anxiety, impaired social life, or overall quality of life. Those more general domains are usually complemented in thyroid disease-specific questionnaires. The SF-36 questionnaire has become an important instrument for the assessment of health-related quality of life in different populations, including patients with thyroid disease [14]. The SF-36 has been significant in assessing a range of health dimensions, including physical functioning to mental health, in studies of thyroid patients[15].Clearly, though, the correct authors can say that summary





Urmila Gorle et al.,

measures such as the Physical Component Summary (PCS) and Mental Component Summary (MCS) can only be computed using proprietary algorithms maintained by resource providers. These graphs highlight the importance of making sure they have been properly licensed and their usage protocols[16].

### ThyPRO Questionnaire

The Thyroid-Related Patient-Reported Outcome (ThyPRO) questionnaire is proposed, evaluating the quality of life in patients with non-malignant thyroid disease. This well validated instrument encompasses a variety of benign thyroid ailments: hypothyroidism, hyperthyroidism, goiter and orbitopathy. ThyPRO is a powerful tool to evaluate the effect of thyroid disorders on patients' well-being and provides a broad perspective on thyroid-related symptoms and experiences[17][18][19][20]. Managing thyroid disease focuses on reducing symptom impacts and improving HRQOL. Patient-reported outcomes, like HRQOL and symptom severity, are key metrics[21][22]. ThyPRO is an 85-item questionnaire assessing thyroid symptoms and HRQOL. It is the most used tool for thyroid dysfunction, with strong reliability and validity.

ThyPRO-39, a shorter version with 39 items, retains strong psychometric properties. It is effective and user-friendly in clinical settings [23][17][18]. A recent study titled "Assessing the Impact of Symptom Severity and Burden on Quality of Life in Thyroid Patients" delves into thyroid disorders such as hypothyroidism and hyperthyroidism. It underscores the necessity of longitudinal evaluations to follow how symptoms evolve over time and underscores the role of patient-reported outcomes (PROs). They provide case studies of the treatment and age/gender differences and psychosocial factors to enhance thyroid patient care.

### OBJECTIVES

1. Identify moderating factors, such as age, comorbidities, hormone levels, disease duration, and weight, that may impact the link between symptom severity and quality of life.
2. Determine the severity, frequency, and duration of various symptoms in thyroid disease patients.
3. Assessing the total quality of life in thyroid disease patients, including physical, emotional, and social well-being.
4. Examine the relationship between symptom severity and quality of life in thyroid patients.

### MATERIALS AND METHODS

**Study Design:** The study is a hospital based Cross-Sectional Analytical Study at a tertiary care teaching hospital.

**Study Duration:** 6 months (October 2023- March 2024).

**Study Subjects:** The study is carried out by considering the following criteria:

**Inclusion criteria:**

- Thyroid Patients
- Adults (aged 18-75 years)
- Consent and Participation
- Ability to Respond

**Exclusion criteria:**

- Severe Illness
- Cognitive Impairment
- Pregnancy/Breastfeeding
- Unwillingness to Participate

**Sampling technique:** Stratified Random Sampling technique was applied to select the study subjects.







Urmila Gorle et al.,

**Sample size:** Sample size is calculated by using Taro yamen sample size calculator with a 0.05% margin of error and 95% confidence level. The recommended sample size is 155 for a population size of 260 members.

**Ethical considerations:**

Both the literate and illiterate patients were clear about the aim and objectives of the research work and informed consent was obtained from them upon their willingness to participate in the study. No experiments are being conducted on the patient; therefore, there are no risks or compensation.

**Study instruments:**

**ThyPRO 39 scale**

We have used this scale to interpret the overall quality of life in thyroid patients using the overall scoring. To categorize the overall score of the ThyPRO questionnaire, we had combined scores of all the domains and provided an interpretation. The questionnaire consists of 12 domains. Each domain was scored on a scale of 0(Not at all), 1(somewhat), 2(very much) using Likert scale. The interpretation of overall scoring of ThyPRO questionnaire was 0-25(Low impact), 26-50(Moderate impact), 51-75(High impact), greater than 76(Very high impact).

**Data collection:**

Data was collected from handwritten prescription by the physician and patient interview which includes questions related to patient demographics, co morbidities; symptoms of goiter, hyperthyroid, hypothyroid, eye, and; tiredness, cognitive, anxiety, depressively, emotional susceptibility, impaired social life, impaired daily life, cosmetic complaints, using ThyPRO 39 questionnaire

**Data analysis:**

Frequencies and percentages were calculated for qualitative data. Mean and standard deviation was calculated for quantitative data. Chi square test was employed to find any statistically significant associations between symptoms and quality of life in thyroid patients. Logistic regression was also employed to find statistically significant association between age, weight, hormone levels (T3, T4, and TSH), co morbidities, duration of disease and quality of life in thyroid patients. Jeffrey's Amazing Statistical Program (JASP version 0.18.0) software was used for statistical analysis. A p-value <0.05 was considered statistically significant.

## RESULTS AND DISCUSSION

This study aims to delve deeper into the complexities of thyroid disorders, particularly focusing on the multitude of factors that may influence the relationship between symptoms and quality of life. By exploring variables such as age, co morbidities, hormone levels, duration of disease, and weight, the research seeks to shed light on the underlying mechanisms that contribute to patients' ongoing symptomatic experience and its impact on their overall well-being. With this goal in mind, the current study was undertaken at Visakha Institute of medical sciences, catering to a sample of approximately 155 patient sample size employed in this investigation, using thyPRO39 questionnaire, data was collected from the patients and interpreted accordingly. One of the primary objectives of the study is to investigate potential moderating factors that may influence the relationship between symptom severity and quality of life in thyroid patients. By examining factors such as age, co morbidities, hormone levels, duration of disease, and weight, the study seeks to identify variables that may exacerbate or alleviate the impact of symptom severity on quality of life. Additionally, the study aims to assess the severity of individual symptoms experienced by patients with thyroid disease. This involves examining the intensity, frequency, and duration of symptoms such as tiredness, cognitive issues, anxiety, depressively, and impaired daily life. By quantifying the severity of these symptoms, the study provides valuable insights into the overall symptom burden experienced by thyroid patients.



**Urmila Gorle et al.,**

The observed decrease in quality of life among older thyroid patients ( $p$ -value  $<0.01$ ) could be attributed to various age-related factors that were not adequately explored in the literature. As individuals age, they may experience a higher burden of co morbidities, such as cardiovascular disease, arthritis, or cognitive decline, which can significantly impact their quality of life. Additionally, aging is often associated with changes in hormonal levels, decreased physical function, and increased susceptibility to psychological distress, all of which can contribute to a decline in overall well-being. Furthermore, older individuals may face social and environmental challenges, such as limited mobility, reduced social support networks, and financial constraints, which can further exacerbate the impact of thyroid disease on their quality of life. While the duration of thyroid disease may also influence quality of life, the lack of literature evidence and insufficient data in our study precluded a comprehensive assessment of this factor. However, it is plausible that individuals with longer-standing thyroid conditions may experience greater disease-related burden and symptom severity, potentially leading to a more pronounced impact on their quality of life over time. Further research exploring the interplay between age, disease duration, and quality of life in thyroid patients is warranted to better understand these complex relationships and inform targeted interventions aimed at improving outcomes in this population.

In our study, patients with hypertension and diabetes mellitus as co morbidities showed higher chances of deprivation of quality of life with  $p$ -value  $<0.01$ , compared to those without co morbidities. The presence of multiple co morbidities, such as HTN and DM2, often exacerbates the burden on individuals with treated hypothyroidism, leading to a further reduction in HRQoL. This additive effect suggests that the concurrent management of co morbid conditions alongside thyroid disorders is crucial for optimizing patients' well-being. Scientifically, this could be explained by the intricate interplay between physiological mechanisms underlying both thyroid dysfunction and co morbidities such as HTN and DM2. Similarly, the highly significant association between goitre symptoms and quality of life in thyroid patients ( $p$ -value  $<0.01$ ) underscores the potential impact of goitre on patients' overall well-being. However, the scarcity of literature on this relationship indicates a need for further investigation into the specific effects of goitre symptoms on quality of life. Future research should explore the underlying mechanisms driving this association and evaluate interventions aimed at alleviating goitre symptoms and improving patients' overall quality of life.

In our findings, the highly significant association ( $p <0.01$ ) observed between hyperthyroid symptoms and quality of life underscores the profound impact of thyroid dysfunction on mental health. This is supported by research showing a higher prevalence of psychiatric disorders in individuals with hyperthyroidism. The improvement noted after endocrinological treatment suggests a direct link between thyroid hormone levels and mental well-being. Routine screening for mental health symptoms in hyperthyroid patients is crucial for timely intervention. Future longitudinal studies are needed to explore the temporal correlation between psychiatric symptoms and hyperthyroidism, and impact on overall quality of life.

In our findings it is revealed that a significant association exist between hypothyroid symptoms and quality of life with  $p$  value of 0.01. These findings are consistent with the prior studies stating that there is a positive correlation between hypothyroid symptoms and quality of life, as indicated by significant composite scores of ThyPro39 ( $p <0.01$ ). Another prior investigation indicates a non-significant direct relationship between quality of life and hypothyroid symptoms, suggesting that while both factors independently influence ThyPro39 scores, their interaction may be influenced by moderating factors or the intricate nature of their relationship. One plausible explanation for this discrepancy could be the presence of moderating factors or the intricate nature of the relationship between symptoms and quality of life. For instance, other variables such as age, co morbidities, or hormone levels may influence how individuals perceive and report their symptoms, consequently impacting their quality-of-life scores

In our study, the significant association ( $p <0.01$ ) between eye symptoms and their impact on quality of life in thyroid patients highlights the profound influence of ocular complaints on overall well-being. This finding aligns with previous research indicating impairments in quality of life among patients with benign thyroid



**Urmila Gorle et al.,**

disorders, particularly regarding visual complaints. The positive relationship observed between scores of the "ocular complaints" scale and other symptoms such as depression, anxiety, cognitive disorders, and general quality of life underscores the interconnectedness of subjective visual disturbances with various aspects of patient well-being. Scientifically, this association may be attributed to the intricate neural connections between the visual system and areas of the brain involved in emotional regulation, cognition, and overall perception of health. Addressing ocular complaints through specialized eye care interventions could thus potentially alleviate the burden of thyroid-related symptoms and improve overall quality of life for affected patients.

The impact of tiredness on the quality of life in thyroid patients remains inconclusive due to a lack of available literature directly linking the two. While fatigue is commonly reported by thyroid patients, the exact relationship between tiredness and quality of life is poorly understood. Factors such as thyroid hormone imbalances, autoimmune processes, and psychological factors like depression and anxiety may contribute to fatigue in thyroid patients. However, further research is needed to clarify the precise mechanisms underlying this relationship and to quantify the impact of tiredness on quality of life in thyroid patients. With our findings, highly significant association ( $p < 0.01$ ) is observed between emotional susceptibility and its impact on thyroid patient overall quality of life which underscores the profound influence of emotional factors on individuals with thyroid disorders. Scientifically, thyroid hormones regulate neurotransmitter levels in the brain, affecting mood regulation, and deregulation of these hormones can lead to mood disturbances such as anxiety and depression. Additionally, thyroid dysfunction can impact the hypothalamic-pituitary-adrenal axis, exacerbating emotional susceptibility and impairing coping mechanisms. This emphasizes the importance of addressing emotional well-being alongside traditional treatments for thyroid disorders to optimize patient outcomes.

In our findings, a significant association ( $p < 0.01$ ) between impaired daily life and overall quality of life in thyroid patients highlights the profound influence of impaired functioning on overall well-being. Thyroid diseases like hypo and hyperthyroidism, significantly affect patients' ability to work due to symptoms like fatigue, cognitive impairment, and mood disturbances. This leads to difficulties in managing professional responsibilities, with many unable to return to previous employment even after remission. (Ragusa et al., 2019) Female patients, in particular, face challenges in returning to work promptly and often reduced workloads compared to males. In summary, thyroid diseases impair daily functioning and work ability due to symptom severity and gender related factors, thereby impacting overall quality of life. Comprehensive support and interventions are essential to address these impairments and improve patient outcomes. In our findings, Cosmetic complaints have a significant association (0.001) with the impact on overall quality of life. The symptoms that have the strongest positive correlation with the impact on overall quality of life are impaired daily life, and emotional susceptibility. Impaired social life does not seem to have a direct relationship with the overall quality of life. We can observe that certain symptoms have a stronger correlation with the impact on overall quality of life. For instance, "Impaired daily life" shows notable correlations. This suggests that these symptoms significantly affect the overall quality of life of individuals experiencing them. Due to limited studies being conducted on assessing the impaired daily life, cosmetic complaints, faced by thyroid patients, we are unable to provide evidence which may prove that these may show a significant impact the overall quality of life in thyroid patients.

In our study we assessed the impact of symptom severity on quality of life in thyroid patients and revealed significant association regarding age i.e. increase in age thereby decreases quality of life in thyroid patients. Patients with both hypertension and diabetes mellitus as co morbidities add up to deterioration of quality of life in thyroid patients. Symptoms including Goiter, Hyperthyroid, Hypothyroid, Eye symptoms, Tiredness, Cognitive symptoms, Anxiety, Depressivity, Emotional Susceptibility, Impaired Social Life, Impaired Daily Life, Cosmetic Complaints, Impact on Overall Quality of Life marked significant impact to quality of life in thyroid with  $p$  value  $< 0.05$ . The study proposes importance of addressing further qualitative research to





Urmila Gorle et al.,

explore patients' perspectives and experiences regarding the impact of thyroid dysfunction on their quality of life, including coping mechanisms, treatment preferences, and unmet needs. All the relevant data collected and interpreted information was given in Tables 1,2 & 3.

### Limitations

While our study design appears comprehensive, several limitations can be acknowledged. Firstly, the use of a cross-sectional design limits the ability to establish causal relationships between variables. Additionally, reliance on self-reported data from patients may introduce response bias or recall bias, impacting the accuracy of reported symptoms and quality of life assessments. The study's duration of six months may not capture seasonal variations or long-term changes in patient symptoms. Furthermore, the use of a single instrument, the ThyPRO 39 scale, for data collection may overlook nuanced aspects of thyroid-related symptoms and quality of life. Moreover, the exclusion of patients with severe illness or cognitive impairment may lead to a biased sample, potentially overlooking important perspectives from these populations. Finally, the study's setting in a single tertiary care teaching hospital may limit the generalizability of findings to broader populations with thyroid disorders.

### ACKNOWLEDGEMENT

I would like to thank my college for successful completion of this project in VIMS Hospital.

### REFERENCES

1. Ming, F., Li, H., Chen, S., Li, W., & Zhang, F. (2012). Polymorphisms in the vitamin D receptor gene and risk of autoimmune thyroid diseases: a meta-analysis. *Endocrine*, 43(2), 318–326. <https://doi.org/10.1007/s12020-012-9812-y>
2. Bianchi, G., V. Zaccheroni, Solaroli, E., Fabio Vescini, Cerutti, R., Zoli, M., & Marchesini, G. (2004). Health-related quality of life in patients with thyroid disorders. *Quality of Life Research*, 13(1), 45–54. <https://doi.org/10.1023/b:qure.0000015315.35184.66>
3. Christiano, D. (2020, June 25). *What Is Subclinical Hypothyroidism?* Healthline; Healthline Media. <https://www.healthline.com/health/subclinical-hypothyroidism>
4. Mark. (2011). The epidemiology of thyroid disease. *British Medical Bulletin*, 99(1), 39–51. <https://doi.org/10.1093/bmb/ldr030>
5. Helfand, M., & Crapo, L. M. (1990). Screening for Thyroid Disease. *Annals of Internal Medicine*, 112(11), 840–840. <https://doi.org/10.7326/0003-4819-112-11-840>
6. Baskin. (2023). American Association of Clinical Endocrinologists medical guidelines for clinical practice for the evaluation and treatment of hyperthyroidism and hypothyroidism. *Endocrine Practice: Official Journal of the American College of Endocrinology and the American Association of Clinical Endocrinologists*, 8(6). <https://pubmed.ncbi.nlm.nih.gov/15260011/>
7. Führer, D., Bockisch, A., & Kurt Werner Schmid. (2012). Euthyroid Goiter With and Without Nodules. *DeutschesArzteblatt International*. <https://doi.org/10.3238/arztebl.2012.0506>
8. *Medical Definition of Euthyroid*. (2021, March 29). RxList; RxList. <https://www.rxlist.com/euthyroid/definition.htm>
9. Diener, E., Oishi, S., & Lucas, R. E. (2003). Personality, Culture, and Subjective Well-Being: Emotional and Cognitive Evaluations of Life. *Annual Review of Psychology*, 54(1), 403–425. <https://doi.org/10.1146/annurev.psych.54.101601.145056>
10. Scerrino, G., Giuditta Morfino, Nunzia Cinzia Paladino, Valentina Di Paola, Amodio, E., Gulotta, G., & Bonventre, S. (2012). Does thyroid surgery for Graves' disease improve health-related quality of life? *Surgery Today*, 43(12), 1398–1405. <https://doi.org/10.1007/s00595-012-0442-z>





Urmila Gorle et al.,

11. Watt, T., Mogens Groenvold, Ase Krogh Rasmussen, Steen Joop Bonnema, Laszlo Hegedüs, Jakob Bue Bjorner, & Ulla Feldt-Rasmussen. (2006). Quality of life in patients with benign thyroid disorders. A review. *European Journal of Endocrinology*, 154(4), 501–510. <https://doi.org/10.1530/eje.1.02124>
12. Wojewoda. (2022). Quality of life after surgical treatment of thyroid gland diseases. *Roczniki Akademii Medycznej W Bialymstoku* (1995), 50 Suppl 1. <https://pubmed.ncbi.nlm.nih.gov/16119647/>
13. Guyatt, G. H., Feeny, D. H., & Patrick, D. L. (1993). Measuring Health-Related Quality of Life. *Annals of Internal Medicine*, 118(8), 622–622. <https://doi.org/10.7326/0003-4819-118-8-199304150-00009>
14. Sayers, E. W., Bolton, E. E., J Rodney Brister, Canese, K., Chan, J., Comeau, D. C., Connor, R., Funk, K., Kelly, C., Kim, S., Madej, T., Marchler-Bauer, A., Lanczycki, C., Lathrop, S., Lu, Z., Thibaud-Nissen, F., Murphy, T., Phan, L., Skripchenko, Y., & Tse, T. (2021). Database resources of the national center for biotechnology information. *Nucleic Acids Research*, 50(D1), D20–D26. <https://doi.org/10.1093/nar/gkab1112>
15. R. Saris-Baglana, Dewey, C., Chisholm, G., Plumb, E., Kosinski, M., J. Bjorner, Ware, J., R. Saris-Baglana, Dewey, C., Chisholm, G., & King, J. (2023). *QualityMetric Health Outcomes Scoring Software 20: User's Guide*. <https://www.semanticscholar.org/paper/QualityMetric-Health-Outcomes-Scoring-Software-20%3A-Saris-Baglana-Dewey/5f68f2364c75211754e9c667436882d41a8b0c53>
16. *WebCite query result*. (2024). [Webcitation.org](https://webcitation.org/6cfdiZOJI). <https://webcitation.org/6cfdiZOJI>
17. Watt, T., Jakob Bue Bjorner, Mogens Grøenvold, Åse Krogh Rasmussen, Steen Joop Bonnema, László Hegedüs, & Ulla Feldt-Rasmussen. (2009). Establishing construct validity for the thyroid-specific patient reported outcome measure (ThyPRO): an initial examination. *Quality of Life Research*, 18(4), 483–496. <https://doi.org/10.1007/s11136-009-9460-8>
18. Watt, T., László Hegedüs, Mogens Grøenvold, Jakob Bue Bjorner, Åse Krogh Rasmussen, Steen Joop Bonnema, & Ulla Feldt-Rasmussen. (2010). Validity and reliability of the novel thyroid-specific quality of life questionnaire, ThyPRO. *European Journal of Endocrinology*, 162(1), 161–167. <https://doi.org/10.1530/eje-09-0521>
19. Watt, T., Per Cramon, Laszlo Hegedüs, Jakob Bue Bjorner, Steen Joop Bonnema, Åse Krogh Rasmussen, Ulla Feldt-Rasmussen, & Mogens Groenvold. (2014). The Thyroid-Related Quality of Life Measure ThyPRO Has Good Responsiveness and Ability to Detect Relevant Treatment Effects. *The Journal of Clinical Endocrinology & Metabolism*, 99(10), 3708–3717. <https://doi.org/10.1210/jc.2014-1322>
20. Selma Flora Nordqvist, Victor Brun Boesen, Åse Krogh Rasmussen, Ulla Feldt-Rasmussen, László Hegedüs, Steen Joop Bonnema, Per Cramon, Watt, T., Mogens Grøenvold, & Jakob Bue Bjorner. (2021). Determining minimal important change for the thyroid-related quality of life questionnaire ThyPRO. *Endocrine Connections*, 10(3), 316–324. <https://doi.org/10.1530/ec-21-0026>
21. Watt, T., Mogens Groenvold, Ase Krogh Rasmussen, Steen Joop Bonnema, Laszlo Hegedüs, Jakob Bue Bjorner, & Ulla Feldt-Rasmussen. (2006). Quality of life in patients with benign thyroid disorders. A review. *European Journal of Endocrinology*, 154(4), 501–510. <https://doi.org/10.1530/eje.1.02124>
22. Husson, O., Haak, H. R., Oranje, W. A., Floortje Mols, P. H. M. Reemst, & van. (2011). Health-related quality of life among thyroid cancer survivors: a systematic review. *Clinical Endocrinology*, 75(4), 544–554. <https://doi.org/10.1111/j.1365-2265.2011.04114.x>
23. Watt, T., Åse Krogh Rasmussen, Mogens Grøenvold, Jakob Bue Bjorner, Sara Hope Watt, Steen Joop Bonnema, László Hegedüs, & Ulla Feldt-Rasmussen. (2008). Improving a newly developed patient-reported outcome for thyroid patients, using cognitive interviewing. *Quality of Life Research*, 17(7), 1009–1017. <https://doi.org/10.1007/s11136-008-9364-z>

**Table 1: Quantitative variables for different patient populations**

S.no	Characteristic	Mean±SD
1	Age	42.75±12.61
2	Weight	63.70±13.00
3	Duration of disease	5.93±5.44
4	T3	5.56±20.88
5	T4	8.08± 2.63







Urmila Gorle et al.,

6	TSH	12.70± 23.92
7	Goitre Symptoms	1.50 ±2.10
8	Hyperthyroid Symptoms	2.74 ±2.14
9	Hypothyroid Symptoms	1.92±1.97
10	Eye Symptoms	1.72±1.90
11	Tiredness	3.11±1.45
12	Cognitive	1.43±2.01
13	Anxiety	2.23±2.16
14	Depressivity	2.19±1.63
15	Emotional Susceptibility	2.21± 1.55
16	Impaired Social Life	0.19±0.55
17	Impaired Daily Life	1.83±1.99
18	Cosmetic Complaints	1.49±1.18
19	Overall Scoring	23.78±11.32

**Table 2: Association between different variables and overall interpretation of quality of life**

Characteristic	Overall Interpretation			P-value
	High Impact	Low Impact	Moderate Impact	
<b>Gender</b>				0.27
Female	10	62	72	
Male	0	8	3	
<b>Menstruation</b>				0.30
N/A(Males)	0	8	3	
Irregular	3	8	12	
Regular	3	30	27	
Menopause	4	24	33	
<b>Co morbidities</b>				<0.01
Asthma, HTN	1	0	0	
Asthma, DM2	0	0	1	
DM2	2	13	6	
HTN	0	2	11	
HTN, DM2	1	12	12	
Nil	6	40	43	
Hyperlipidemia	0	1	0	
Hypotension	0	0	1	
Migraine	0	0	1	
PCOD	0	1	0	
Rheumatoid Arthritis	1	0	0	
<b>Disease type</b>				<0.01
D Euthyroid	0	0	1	
Euthyroid	0	1	0	
Goitre	0	0	1	
Graves	0	0	1	
Hyperthyroidism	0	2	4	
Hypothyroidism	2	8	10	







Urmila Gorle et al.,

Primary Hypothyroidism	8	57	56	
Secondary Hypothyroidism	0	2	2	
<b>Goitre Category</b>				<0.01
Low	0	0	1	
Mild	4	67	49	
Moderate	1	1	11	
Severe	5	2	14	
<b>Hyperthyroid Category</b>				<0.01
Mild	0	56	24	
Moderate	7	13	34	
Severe	3	1	17	
<b>Hypothyroid Category</b>				0.01
Mild	4	58	46	
Moderate	4	9	22	
Severe	2	3	7	
<b>Eye Category</b>				<0.01
Mild	4	63	48	
Moderate	2	5	20	
Severe	4	2	7	
<b>Tiredness Category</b>				<0.01
High	1	1	8	
Low	0	40	20	
Moderate	9	29	47	
<b>Cognitive Category</b>				<0.01
Mild	1	68	50	
Moderate	4	1	14	
Severe	5	1	11	
<b>Anxiety Category</b>				<0.01
High	7	1	19	
Low	0	61	30	
Moderate	3	8	26	
<b>Depressivity Category</b>				<0.01
High	5	1	7	
Low	2	63	43	
Moderate	3	6	25	
<b>Emotional Susceptibility Category</b>				<0.01
High	5	0	5	
Low	1	64	47	
Moderate	4	6	23	
<b>Impaired Daily Life Category</b>				<0.01
High	5	2	8	
Low	3	61	42	
Moderate	2	7	25	
<b>Cosmetic Complaints Category</b>				<0.01
High	1	0	1	





**Urmila Gorle et al.,**

Low	7	70	69	
Moderate	2	0	5	

**Table 3: Logistic regression analysis of various variables and quality of life**

Variable	Odds Ratio	95% CI	P-value
Age	1.024	1.001 - 1.047	0.041
Duration of disease	0.986	0.952 - 1.021	0.431
Hypertension	1.279	0.675 - 2.421	0.449
Diabetes mellitus type 2	1.871	0.994 - 3.521	0.052
Hypertension and Diabetes mellitus type 2	2.164	1.074 - 4.358	0.031
Weight	1.011	0.997 - 1.026	0.136
T3 level	0.848	0.684 - 1.051	0.132
T4 level	1.071	0.961 - 1.194	0.214
TSH level	1.004	0.979 - 1.030	0.740





## Preliminary Phytochemical Screening and *In vitro* Pharmacological Activities of *Limonia Acidissima* Fruits

Gana Manjusha Kondepudi<sup>1\*</sup>, S. Navya Sri <sup>2</sup>, S. Alekhya <sup>2</sup>, S.Yamini<sup>2</sup>, Shaikh Mohmad Ashraf <sup>2</sup>, T. Pavan Teja <sup>2</sup> and V. Ashrith<sup>2</sup>

<sup>1</sup>Associate Professor, Vignan Institute of Pharmaceutical Technology, (Affiliated to Jawaharlal Nehru Technological University), Visakhapatnam, Andhra Pradesh, India.

<sup>2</sup>Students, Vignan Institute of Pharmaceutical Technology, (Affiliated to Jawaharlal Nehru Technological University), Visakhapatnam, Andhra Pradesh, India.

Received: 06 Oct 2024

Revised: 10 Nov 2024

Accepted: 12 Dec 2024

### \*Address for Correspondence

#### Gana Manjusha Kondepudi

Associate Professor,

Vignan Institute of Pharmaceutical Technology,

(Affiliated to Jawaharlal Nehru Technological University),

Visakhapatnam, Andhra Pradesh, India.

E.Mail: manjusha0988@gmail.com



This is an Open Access Journal / article distributed under the terms of the **Creative Commons Attribution License** (CC BY-NC-ND 3.0) which permits unrestricted use, distribution, and reproduction in any medium, provided the original work is properly cited. All rights reserved.

### ABSTRACT

Wood apple fruit, or *Limonia acidissima*, is edible and utilized in a very small number of culinary recipes. This study investigates the phytochemical, antioxidant, antidiabetic, and antimutagenic properties of *Limonia acidissima* fruit extract. Preliminary phytochemical screening revealed the presence of alkaloids, carbohydrates, and amino acids. The antioxidant potential was evaluated using the DPPH radical scavenging assay, which demonstrated dose dependent activity. The extract exhibited a maximum inhibition of 40.17% at 10 mg/mL, with an IC<sub>50</sub> value of 2.8619 mg/mL, outperforming the standard ascorbic acid (IC<sub>50</sub>: 3.6619 mg/mL). The antidiabetic activity was assessed using a glucose uptake assay in a yeast cell model. At 10 mg/mL, the extract facilitated 98.84% glucose uptake, significantly higher than the standard drug metronidazole (70.5%). This activity is attributed to the stereospecific membrane carriers that enhance glucose transport, suggesting the extract's potential in regulating blood glucose levels. The antimutagenic activity of *L. acidissima* was studied using seed germination assays, demonstrating a dose-dependent suppression of seed development. The methanolic extract at 40 mg/mL exhibited an inhibition similar to that of the common medication methotrexate, with percentage inhibition of the seed germination recorded as significant across various time points (24, 48, and 72 hours). Collectively, the findings indicate that *L. acidissima* exhibits strong antioxidant, antidiabetic, and antimutagenic properties, suggesting its potential as a source for developing therapeutic agents targeting oxidative stress, diabetes, and cancer. Further studies are recommended to explore its bioactive constituents and underlying mechanisms.

**Keywords:** Antioxidant, Antidiabetic, Anti mitotic, Wood apple, Fruit .





Gana Manjusha Kondepudi et al.,

## INTRODUCTION

The wood apple, or *Limonia acidissima*, is a deciduous, upright tree that can reach a height of 15 meters and has drooping branches. The flowers are grouped in terminal or lateral panicles and are a dull red color. Fruits are round to oval, 5-15 cm in diameter, with a firm, woody, grayish-white, scurfy skin and whitish pulp (when unripe); they turn brown when mature, and the pulp contains many tiny, white seeds that are odorous, acidic, or sweet. The huge tree *Limonia acidissima* L. reaches up to 9 meters (30 feet) in height and has rough, prickly bark. The axillary, thin sharp spines on some of the zigzag twigs are 2 to 5 cm long. With five to seven leaflets, each measuring 25 to 35 mm in length and 10 to 20 mm in width, the pinnate leaves have a citrusy aroma when crushed. A terminal leaflet and two to three opposing leaflets in pairs. A berry with a diameter of 5 to 9 cm, the fruit can be either sour or sweet. Its extremely tough rind might be challenging to break through. It has a sticky, dark, and fragrant pulp. It has a lot of tiny, white seeds strewn throughout and is repulsive, astringent, acidic, or sweet. The rind is 6 mm thick and has a greyish-white hue. Its exterior shell, known as the rind, is woody and incredibly hard, making it quite difficult to break apart. The hard skin of wood-apple fruit, which is 5–6 mm long, hairy, and has thick, green cotyledons, is cracked with a hammer; germination occurs epigeally. *Limonia acidissima* L. is a common tree. This is a tree of intermediate size, reaching a height of 9 meters (30 feet). Usually, it is a deciduous kind.

### Phytochemicals

Tri-terpenoids, amino acids, tannins, coumarins, polyphenols, vitamins, and saponins are among the phytochemicals found in wood apples [1] (Table 1). Ripe fruits of the *Limonia acidissima* plant include flavonoids, steroids, glycosides, and other acidic chemicals, according to phytochemical study. Acidissimin and acidissiminol are the two main chemical components of leaves. It is also observed that leaves contain gum and mucilage, phenols, resins, alkaloids, and fixed oils and fats [2-5]. The pulp from wood apples is a very good source of dietary fiber (1.7%), protein (13.8%), fat (4.3%), and carbs (70.14%) [1,4]. This fruit is also believed to have significant levels of zinc, calcium, magnesium, iron, and a low fat content (4.38%). High levels of calcium and phosphorus are also discovered, and these are crucial for blood coagulation, bone formation, and other metabolic functions. Iron in fruit is a sign of its ability to combat anemia, TB, and other illnesses [6]. Screening for antioxidant activity has been done on various sections of *Limonia acidissima* L. Crude methanolic extract has the strongest free radical scavenging activity measured by antioxidant activities of plant components on the stable radical DPPH. Additionally significant antioxidant activity was demonstrated by the pet ether soluble fraction (PE). *Limonia* fruit methanolic extract was also tested using the FRAP and DPPH assays to see whether it had the ability to scavenge free radicals. Various leaf extracts from *Limonia acidissima* L. have been documented.

### Pharmacological studies

#### Antihyperlipidemic activity

Hepatic glucose-6-phosphatase and lipid profile are decreased after 28 days of administering fruit powder at 2.5, 5, and 10 g/Kg body weight, but hepatic glycogen, hexokinase, and HDL are significantly increased. This could be caused by the presence of fibers, ascorbic acid, flavonoids, polyphenols, saponins, and phytosterols [7].

#### Hepatoprotective activities

Rats' liver injury from carbon tetrachloride (CCl<sub>4</sub>) was tested to determine the hepatoprotective potential of methanolic pulp extracts. Following three days of intraperitoneal administration of 100, 200, and 400 mg/kg to rats, they found that hepatic enzyme levels, specifically those of aspartate transaminase (AST), alanine transaminase (ALT), alkaline phosphatase (AST), total protein (TP), total bilirubin (TB), and gamma-glutamyltransferase (GGT), increased while those of superoxide dismutase (SOD), catalase (CAT), glutathione peroxidase (GPx), and glutathione (GSH) declined. A different study found that aqueous leaf extract increases the serum concentrations of alanine transaminase (ALT), aspartate aminotransferase (AST), and alkaline phosphatase (ALP). In comparison to the normal control, it also raises the levels of urea, creatinine, potassium, and sodium in the rats that are not treated for phenyl



**Gana Manjusha Kondepudi et al.,**

hydrazine-induced anemia [8].

**Anticancer Activity**

*Limonia acidissima* L. has been demonstrated, its fruit extract has anticancer effects. In two distinct breast cancer cell lines, SKBR3 and MDAMB-435, the ED50 value (50 percent inhibition of cancer cell growth) was determined using ethanolic fruit extracts [9].

**Antibacterial Activity**

According to reports, ethanolic extract from *Limonia acidissima* L. leaves exhibits extremely extensive spectrum of action against both Gram-positive and Gram-negative bacteria, which are the main cause of bacterial illnesses.

**Neuroprotective activities**

Neuroprotective effects of wood apple was evaluated and showed that at 250 mg/kg and 500mg/kg body weight it inhibits ischemia reperfusion-induced brain injury in rats [10].

**Analgesic activity**

Using methanol and fruit peel acetone extracts, the analgesic activity was 60.53% and 59.65%, respectively, compared to 78.07% using the conventional medication Diclofenac Na to treat writhing mice induced by acetic acid [11].

**Diuretic activity**

The leaves methanolic extract has considerably increased urine production. The extraction process establishes the quantity of urine and electrolyte excretion, particularly that of sodium, potassium, and chloride ions. In comparison to Bath Sonicator extraction (BSE), it was discovered that Microwave assisted extraction (MAE) exhibited superior activity [12].

## MATERIALS AND METHODS

**Materials:** DPPH, Ethanol, Ascorbic acid, Baker's yeast, Glucose, Methanol, Metronidazole, Vincristine sulfate Injection. All the chemicals used here are of analytical grade.

**Collection of plant material:** The fully mature fruits of *Limonia acidissima* was collected in the months of July to August 2024 from Sambavaram, Visakhapatnam, India. The fruits were made into small pieces, oven dried at 40°C for 7 days and converted into coarse powder with an auto mix blender.

**Preparation of Methanolic extract**

1 kg powder of each sample was taken in a round-bottomed flask and the methanol was added to the powdered drug and it was kept for reflux extraction for 3hrs. The extracts were concentrated under a vacuum to get the corresponding residue and the tests were performed.

**Preliminary Phytochemical Analysis:** To verify the existence of phytochemicals like alkaloids, flavonoids, terpenoids, amino acids, cardiac and anthracene glycosides, saponins, steroids, tannins, phenols, and carbohydrates, a preliminary phytochemical study was conducted utilizing qualitative testing.

**In vitro Antioxidant activity DPPH Radical Scavenging Activity (DPPH)**

Using the stable DPPH method [13], the extracts' ability to scavenge free radical DPPH was assessed. Five different concentrations (ranging from 25 to 200 µg/mL) of each extract were made. To 1 mL of sample solution with varying concentrations, 4 mL of DPPH at 0.1 mM solution was added. The ELICO SL210 UV double-beam spectrophotometer was used to measure the absorbance at 517 nm following a 30-minute incubation period. The standard and control had the same levels of the synthetic antioxidant ascorbic acid (25–200 µg/mL), and the blank solution was devoid of extract or standard. The DPPH scavenging activity increases as the samples' absorbance decreases. Each extract's IC50 value was determined by plotting a standard curve.





Gana Manjusha Kondepudi et al.,

$$\% \text{ inhibition of DPPH radical} = \frac{\text{AbsControl} - \text{AbsSample}}{\text{AbsControl}} \times 100$$

#### **In vitro Antidiabetic activity by glucose uptake method:**

To measure the uptake of glucose in yeast cells, the unique method was used. Commercially available *Saccharomyces cerevisiae* (baker's yeast) cells were suspended in 1% solution and kept at 25°C [14]. The supernatant fluid was produced by continuously centrifuging overnight yeast cell solution at 4,200 rpm for 5 minutes. The clear supernatant was used to prepare a 10% v/v yeast cell culture for the experiment. Standard drug (MTZ) and plant samples at different concentrations (100–500 µg/mL) were incubated for 10 minutes at 37°C using 1 mL of a 10 mM glucose solution. The reaction was initiated by adding 100 µL of yeast suspension, vortexing the liquid, and then incubating it for 60 minutes at 37°C.

Following that, the samples were centrifuged for five minutes at 3,800 rpm. By using a UV-vis spectrophotometer set to 520 nm [15], the amount of glucose in the supernatant was determined. Every reagent except the test sample is present in the control sample. The full experiment was conducted three times. The proportion of glucose absorption was calculated using the formula.

$$\% \text{ of glucose uptake} = \frac{\text{AbsControl} - \text{AbsSample}}{\text{AbsControl}} \times 100$$

#### **In vitro Antimitotic activity by plant-based models**

We collected and weighed green gram seeds separately from the local supermarket. Extract concentrations were generated at 10 mg/mL, 20 mg/mL, 30 mg/mL, and 40 mg/mL. The standard used here is methotrexate. We utilized distilled water as a control. To the material in Petri plates with varying concentrations, equal weights of seeds were introduced. For the purpose of imbibitioning water, the Petri plates were kept at room temperature for a full day. On dry tissue paper, the drug treatment was dried and weighed after 24 and 72 hours. The sprouting period was prolonged to 72 hours, and pictures were captured.

$$\% \text{ inhibition} = \frac{\text{Weight of seeds in distill water} - \text{weight of seeds in extract sample}}{\text{Weight of seeds in distilled water} - \text{weights of seeds in methotrexate}} \times 100$$

## **RESULTS AND DISCUSSIONS**

### **Preliminary Phytochemical Analysis**

Alkaloids, amino acids, coumarins, carbohydrates, tannins were among the phytochemicals present in *Limonia* fruit extract (Table 2)

### **In vitro Antioxidant activity DPPH Radical Scavenging Activity (DPPH)**

In a dose-dependent manner, the extract demonstrated inhibition at doses ranging from 2 to 10 mg/mL. The amount of antioxidants needed in the sample to 50% inhibit free radicals is known as the IC50 value. The IC50 value decreases as radical scavenging capacity increases. While the positive standard ascorbic acid demonstrated 52.14% inhibition and an IC50 value of 3.6619 mg/mL, the extract demonstrated action in a dose-dependent manner with a maximum inhibition of 40.7% at 10 mg/mL and an IC50 value of 2.8619 mg/mL. The graph above showed the percentage reduction in DPPH scavenge activity resulting from *Limonia acidissima* (Table 3 & Fig 1).

### **Anti diabetic by glucose uptake method**

*L. acidissima* fruit extract with varying concentrations was evaluated for in vitro antidiabetic efficacy utilizing a yeast model and the glucose uptake assay. The extract showed more action than the others (98.84% at 10 mg/mL) concentrations of extract. An increase in glucose percentage that is dose-dependent and uptake with increasing concentration (2-10 mg/mL). *L. acidissima* fruit extract was observed in the above graph. The standard drug Metronidazole showed 70.5% at 10 mg/mL







Gana Manjusha Kondepudi et al.,

**In vitro Antimitotic activity by plant based models**

The assay's outcomes demonstrated that, following 24 hours, 48 hours, and 72 hours of treatment, the methanolic extract of green grams drastically raised the percentage inhibition, which was comparable to that of methotrexate. The standard chemotherapy drug Methotrexate, at 0.1 mg/ml, inhibited seed germination by 0.001±1.0 percent, but the methanolic extract at 40 mg/ml showed seed growth of 0.01±0.2 mm. In comparison to the percentage of inhibition of methotrexate, the assay findings demonstrated that the methanolic extract of green grams considerably reduced the percentage of inhibition after 24 hours, 48 hours, and 72 hours of treatment. The methanolic extract of concentration 20mg/ml showed seed growth of 0.88±0.8mm. In the point of view of seed germination, the control i.e., distilled water has shown the higher seed germination compared to standard and other methanolic extracts (Table 4).

**CONCLUSION**

*L. acidissima* fruit extract was extracted and subjected to preliminary phytochemical screening in this investigation. Alkaloids, carbohydrates, and amino acids are detected via screening. The antioxidant activity of the fruit extract from *L. acidissima* was one of the objectives of the current investigation. Since the DPPH method's results are unaffected by the polarity of the substrate, it was regarded as a stable technique. The primary mechanism by which the beneficial ingredients in plant extracts scavenge free radicals may be because they impart hydrogen to the free radicals, neutralizing them and limiting their deadly effects by generating stable molecules. The extract's IC<sub>50</sub> was 2.8619 mg/mL, and its maximum DPPH scavenging activity was 40.17 mg/mL. In contrast, the standard IC<sub>50</sub> was 3.6619 mg/mL. Using yeast cells to measure glucose absorption, an effective method to evaluate antidiabetic efficiency in vitro, *L. acidissima* was tested for antidiabetic activity.

One of the most obvious markers of glucose uptake by yeast cells was the amount of glucose that remained in the medium after a specific period of time. Using a yeast cell model, *L. acidissima* extract's in vitro antidiabetic action was demonstrated by showing that, at 10 mg/ml, the percentage of glucose uptake by yeast cells mediated by the plant extracts was 98.84%, while the percentage of metronidazole was 70.5%. The diffusion process, assisted by stereospecific membrane carriers, facilitated the glucose movement through the yeast cell membrane. This demonstrated clearly that *L. acidissima*'s methanol extract absorbs glucose more efficiently by improving its utilization, which in turn helps regulate blood glucose levels. This investigation on *L. acidissima*'s antimitotic activity indicates that the plant may have antimitotic properties. As a result, this plant may produce drugs that could be utilized to treat cancer. The percentage inhibition following 24 hours, 48 hours, and 72 hours of therapy was shown to be much higher with the methanolic extract of green grams than with methotrexate. With an antimitotic activity of 0.01±0.2 mm at 40 mg/ml methanolic extract, the percentage inhibition of seed germination was as strong as that of the common medication Methotrexate, which is 0.001 mg/ml±1.0 mm.

**REFERENCES**

1. Pandey S, Satpathy G. Evaluation of nutritional, phytochemical, antioxidant and antibacterial activity of exotic fruit *Limonia acidissima*. *J Pharmacog and Phytochem* 2014;3(2):81-88.
2. Aneesha A, Rao NR et al. Phytochemical studies and anti-ulcer activity of *Limonia acidissima* Linn. leaf in treating ethanol induced ulcer Albino rats. *Indian J Res in Pharma and Biotech* 2018;6(3):104-109.
3. Jayashree VH, Londonkar R. Comparative phytochemical studies and antimicrobial potential of fruit extracts of *Feronia limonia* Linn. *Int J Pharma and Pharmaceu* 2014;6(1):731-748.
4. Vijayvargia P, Vijayvargia R. A review on *Limonia acidissima*: Multipotential medicinal plant. *Int J Pharm Sci Rev Res* 2014;28(1):191-195.
5. Asp NG. Dietary carbohydrates: Classification by chemistry and physiology. *Food chem* 1996;57(1):9-14.
6. Campos D, Betalleluz I et al. Nutritional and functional characterisation of *Andean chicuru* (Stangeahizanta). *Food Chem* 2009;12(1):63-70.





## Gana Manjusha Kondepudi et al.,

7. Shermin S, Aktar F et al. Antioxidant and Cytotoxic Activity of *Limonia acidissima* L. *Dhak Uni J Pharmaceu Sci* 2012;11(1):75-77.
8. KT and Ugwu, GM. Hepatoprotective and nephroprotective potentials of aqueous leaves extract of *Limonia acidissima* in phenylhydrazine induced anaemic wistar Rats. *Asian J Pharma Res Develop* 2019; 7(1):27-33.
9. Pradhan D, Tripathy G et al. Anticancer activity of *Limonia acidissima* Linn (Rutaceae) fruit extracts on human breast cancer cell lines. *Tropi J Pharmaceu Res* 2012;11(3):413-419
10. Rakhunde PB, Saher S et al. Neuroprotective effect of *Feronia limonia* on ischemia reperfusion induced brain injury in rats. *Indian J Pharmacol* 2014;46(6):617-621.
11. Islam F, Azad AK et al. A comparative study of analgesic, antidiarrhoeal and antimicrobial activities of methanol and acetone extracts of fruits peels of *Limonia acidissima* (Rutaceae). *J Drug Deliv and Therapeu* 2020;10(1):62-65.
12. Parial S, Jain DC et al. Diuretic activity of the extracts of *Limonia acidissima* in rats. *Rasa J Chem* 2009;2(1):53-56.
13. Srinivasan S, Wankupar W et al. Free radical scavenging potential and HPTLC analysis of *Indigofera tinctoria* Linn. (Fabaceae). *J Pharmaceu Anal* 2016;20(2):125-131.
14. Shettar AK, Sateesh MK et al. In vitro antidiabetic activities and GC-MS phytochemical analysis of *Ximenia americana* extracts. *Sou Afri J Bot* 2017;11(1):202-211.
15. Rehman G, Hamayun M et al. In vitro antidiabetic effects and antioxidant potential of *Cassia nemophila* pods. *BioMed res int* 2018(1):1724-1790.

Table 1. Phytochemicals in Wood apple

S.No	Phytochemicals	Part
1	Flavonoids, Phenols	Fruits, Stem bark
2	Tannins, Flavonoids	Leaves
3	Essential Oil	Fruit Pulp
4	Polar Constituents	Bark
5	Acidic Polysaccharide	Fruit, Pulp
6	Tannins, Steroids, Flavanol, Alkaloids	Leaves
7	Essential Oil	Fruit, Stem bark, Fruit Pulp and Leaves

Table 2. Phytochemicals present in Wood apple fruit extract

S.No	Name Of the test	Observation
1.	<b>ALKALOIDS</b> Dragendroff's test Wagner's test	<b>The orange brown precipitate</b> was observed. <b>A reddish-brown precipitate</b> was observed Presence of alkaloids
2.	<b>AMINO ACIDS</b> Ninhydrin test	<b>A purple color</b> ring is observed Presence of proteins and amino acids
3.	<b>CARBOHYDRATES</b> Molisch's test	<b>A purple color</b> ring appeared between two layers Presence of carbohydrates
4.	<b>GLYCOSIDES</b> Coumarin glycosides Legal's test	<b>Blue-green fluorescence</b> is observed. Presence of coumarin glycosides <b>The pink or red color</b> was not observed. Absence of cardiac glycosides
5.	<b>FLAVONOIDS</b> Shinoda test	<b>The pink color</b> was not observed. Absence of flavonoids
6.	<b>TANNINS</b> Ferric chloride test	<b>A deep blue-black color</b> was observed. Presence of tannins and phenolic compounds
7.	<b>SAPONINS</b> Froth formation test	<b>Persistent foam</b> was observed. Presence of saponin glycosides
8.	<b>STEROIDS</b> <b>and TRITERPENOIDS</b>	<b>First red, then blue and finally green</b> color was observed. Presence of steroids





Gana Manjusha Kondepudi et al.,

Liebermann Burchards test	and triterpenoids
---------------------------	-------------------

Table 3. *invitro* Antioxidant activity

Absorbance control = 0.4179				
Concentration	Absorbance	% Inhibition of DPPH radical	Absorbance of standard ascorbic acid	%inhibition of DPPH radical of standard ascorbic acid
2mg/ml	0.3742	10.45	0.325	22.23
6mg/ml	0.3122	25.29	0.230	36.96
10mg/ml	0.2500	40.17	0.200	52.14

Table 4 *Invitro* Antidiabetic Activity of *L acidissima* fruit Extract

Absorbance control = 0.0519				
Concentration	Absorbance	% Glucose uptake of test	Absorbance of Metronidazole	% Glucose uptake of Metronidazole
2mg/ml	0.0170	67.24%	0.0320	38%
4mg/ml	0.0126	75.72%	0.0280	46%
6mg/ml	0.0085	83.62%	0.0230	55%
8mg/ml	0.0055	91.40%	0.0519	62%
10mg/ml	0.0006	98.84%	0.0153	70.5%

Table 5 *invitro* Antimitotic Activity of *L acidissima* fruit Extract

S.No	Sample/Control/Standard	Concentration mg/mL	Time	Average growth of seeds
1	Methanolic extract-1	10	24 to 72 hours	1.1±3.8
2	Methanolic extract-2	20	24 to 72 hours	0.88±0.8
3	Methanolic extract-3	30	24 to 72 hours	0.35±0.5
4	Methanolic extract-4	40	24 to 72 hours	0.01±0.2
5	Control (Distilled water)	0	24 to 72 hours	26.5±5
6	Standard – Methotrexate	0.1	24 to 72 hours	0.001±1.0

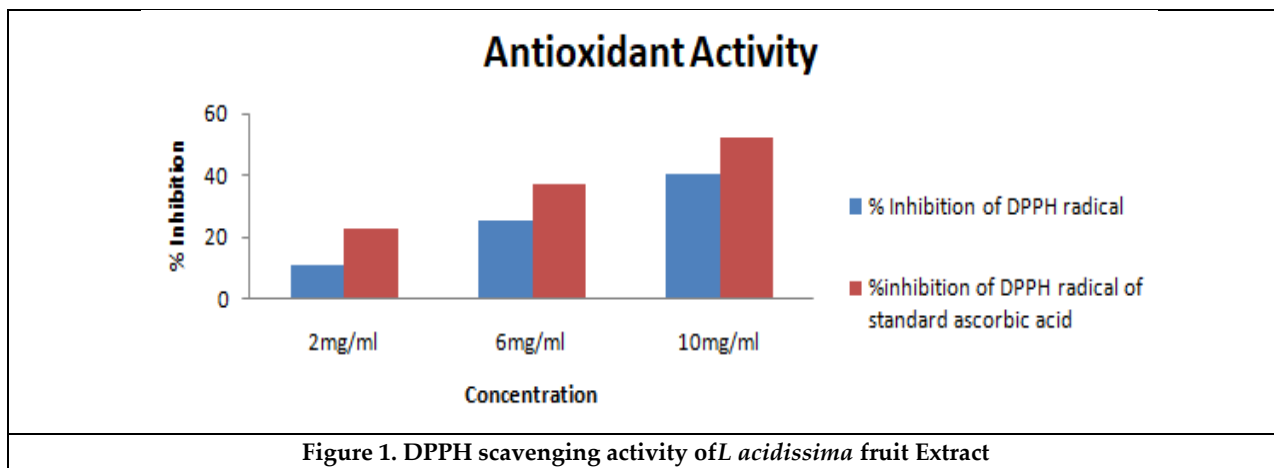
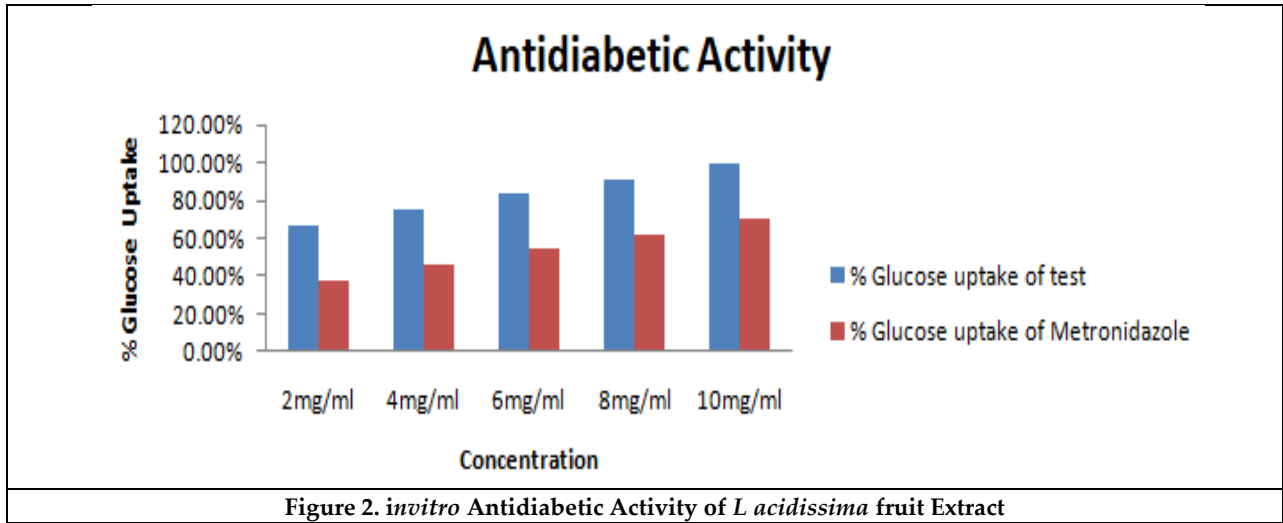


Figure 1. DPPH scavenging activity of *L acidissima* fruit Extract





Gana Manjusha Kondepudi et al.,





# Uncovering Cancer Data Insights: State-of-the-Art Machine Learning Methods for Data Analysis

Varanasi Avinash<sup>1\*</sup>, Gantyada Amaladevi<sup>2</sup>, Lakshmana Rao Battula<sup>3</sup> and Usha Matta<sup>2</sup>

<sup>1</sup>Assistant Professor, Department of Computer Science and Engineering, Raghu Engineering College, (Affiliated to Jawaharlal Nehru Technological University), Visakhapatnam, Andhra Pradesh, India.

<sup>2</sup>Assistant Professor, Department of Computer Science and Engineering, Visakha Institute of Engineering & Technology, (Affiliated to Jawaharlal Nehru Technological University), Visakhapatnam, Andhra Pradesh.

<sup>3</sup>Assistant Professor, Department of Computer Science and Engineering, K LUniversity, Guntur, Andhra Pradesh, India.

Received: 06 Oct 2024

Revised: 10 Nov 2024

Accepted: 12 Dec 2024

## \*Address for Correspondence

### Varanasi Avinash

Assistant Professor,  
Department of Computer Science and Engineering,  
Raghu Engineering College,  
(Affiliated to Jawaharlal Nehru Technological University),  
Visakhapatnam, Andhra Pradesh, India.



This is an Open Access Journal / article distributed under the terms of the **Creative Commons Attribution License** (CC BY-NC-ND 3.0) which permits unrestricted use, distribution, and reproduction in any medium, provided the original work is properly cited. All rights reserved.

## ABSTRACT

This work explores the use of cutting-edge computational methods to reveal new cancer information. This study uses machine learning as a whole technique to investigate complex patterns and relationships found in cancer datasets. The goal of the investigation is to clarify the fundamental causes of cancer initiation and progression, which may provide important new information for developing treatment approaches in the future. This work aims to improve our comprehension of the intricate dynamics involved in cancer biology by using a data-driven methodology. This work aims to provide a deeper understanding of the condition's landscape by utilizing computational tools to reveal hidden patterns and linkages within cancer data. The overall goal of this research is to use cutting-edge analytical techniques to support continued attempts to decipher the intricacies of cancer biology.

**Keywords :** Machine Learning, Cancer, Analysis, Biomedical, Medical Diagnosis.

## INTRODUCTION

### Introduction to Machine Learning in Cancer Research

A rare chance to analyze big, complicated datasets in previously unheard-of ways is presented by machine learning. Extensive genomic, transcriptomic, and clinical data might yield important insights for researchers through the use of



**Varanasi Avinash et al.,**

complex techniques and computer simulations. This method makes it possible to comprehend the intricacy of cancer on a deeper level, which makes it easier to create treatment programmes that are more individualized and focused.

**Challenges in Traditional Cancer research**

The development of effective medicines for cancer is a huge global health concern due to its complexity and variety. The extensive and complex biological data related to cancer is difficult for traditional approaches to handle. But new developments in computational methods, especially in machine learning, present encouraging chances to decipher the intricate workings of cancer biology.

**Utilizing Advanced Computational Methods**

The modern computational techniques play a major role in cancer research. The goal of this research is to mine the massive volume of cancer information to provide deeper insights by utilizing machine learning. Through the use of these advanced analytical instruments, scientists seek to reveal obscure trends and linkages that are essential to comprehend the genesis of cancer.

**Objectives Study**

Clarifying the basic mechanisms behind the development and spread of cancer is the main objective. The goal of the research is to find novel pharmacological targets, biomarkers of interest and mathematical models of prediction that can help guide clinical judgements. In the end, this research has the potential to completely transform clinical cancer detection, therapy, and management.

**Bridging the Knowledge and Data Gap**

Using computational methods reveals parts of knowledge that were not before known. Through bridging the knowledge gap with data, scientists strive to expedite the creation of more potent cancer treatments and enhance the experience of patients. A new phase in the investigation of the biological origins of cancer has begun with this pluralistic team effort.

**LITERATURE SURVEY**

Techniques of machine learning are essential for managing diseases and forecasting cancer outcomes[1,2]. These cutting-edge technologies use sophisticated algorithms to examine enormous volumes of data, including genetic data and health information from patients, spot indications and patterns that can point to the onset or spread of cancer[3]. Researchers and medical practitioners can create prediction models that improve cancer patients' early identification, prognostic evaluation, and customized treatment plans by utilizing machine learning[4]. The imaging sector analysis is one of the main areas where machine learning is used in cancer prediction. Medical pictures, comprising X-rays, magnetic resonance imaging (MRIs), and CT scans, can be analyzed using machine learning algorithms to find tiny anomalies or tumor characteristics that might be signs of cancer[5]. With great accuracy, these algorithms can distinguish between benign as well as malignant lesions, enabling prompt diagnosis and treatment[6]. The analysis of genome-wide data regarding cancer prediction is becoming more and more dependent on machine-learning models. These models can uncover genetic markers linked to particular cancer types or forecast an individual's risk of acquiring cancer by looking at patterns across sequences of genetic material, gene expression stages, ranging, and genetic mutations. Personalized screening plans and focused treatment plans based on each patient's specific genetic profile can be guided by this information[7]. Forecasting techniques for cancer evaluation of risks can be produced by methods such as machine learning that incorporate a variety of clinical data, such as patient demographics, medical histories, test findings, and treatment outcomes. Machine learning can analyze these complex datasets to find risk variables, stratify people with illnesses according to their risk of cancer, and provide guidance for early intervention or measures for prevention that lower the risk of cancer. The creation of predictive models for evaluating the prognosis and response to therapy of cancer is made possible by machine learning techniques[8,9]. These models predict disease progression, malignancy risk, and outcomes in terms of survival for cancer patients by evaluating





**Varanasi Avinash et al.,**

longitudinal medical information, including tumor growth dynamics, protocols for treatment, and clinical outcomes[10]. These prognostic models enable medical professionals to plan treatments and give follow-up care with knowledge. By making it easier to identify the best course of action for each patient based on their unique traits and the biology of their tumor, machine learning additionally revolutionized the area of precision oncology[11,12]. Through the integration of clinical data and genetic profiling, machine learning algorithms are able to forecast reactions to treatment possibility and suggest tailored therapeutic treatments that maximize each patient's chances of success, such as targeted medicines or immunotherapies[13]. Predictive analytics is a technique that is powered by machine learning that may enhance patient recruitment and clinical trial design for cancer. Through the examination of past trial information and patient attributes, these algorithms can recognize prognostic biomarkers, categorize patient groups, and refine trial procedures to improve trial outcomes and hasten the creation of innovative cancer treatments[15,16,17]. Additionally essential to the control of population health and cancer surveillance is machine learning. The algorithms for machine learning can prioritize funding for cancer assessment and prevention programs, identify high-risk populations, and provide guidance for health care policy initiatives aimed at lowering the burden of cancer by analyzing population-level medical information, such as cancer occurrence rates, shifts in demographics, and environmental factors[18,19]. The potential for machine learning applications to transform cancer prediction as well as administration is enormous. These applications facilitate the creation of precise, individualized predictive models that improve early detection, prognosis evaluation, treatment choices, and population health approaches[20]. The potential for these technologies to improve results in cancer and change the oncology care landscape is enormous as they develop further[21,22].

To help with the early identification, prognosis, and individualized therapy of cancer, machine learning (ML) algorithms have shown great promise in the analysis of complex scientific information, including genomic information, imaging, and clinical data. ML models can detect subtle patterns and indications indicative of the existence of cancer, the categorization of the cancer subtype, and the prognosis of the patient by utilizing large-scale datasets and sophisticated analytics[23]. Predictive models driven by machine learning (ML) can also help oncologists choose the best course of treatment, forecast how well a treatment will work, and find possible targets for therapeutics for precision medicine strategies. Additionally, machine learning algorithms can aid in the creation of novel risk prediction models, treatment approaches, and screening techniques, all of which can enhance patient outcomes and lower cancer death rates[24,25].

## METHODOLOGY

### Role of Supervised Algorithms in Cancer Classification

Using characteristics like radius\_mean, texture\_mean, and perimeter\_mean, machine learning techniques including Random Forest and Support Vector Machines (SVM) are essential for analyzing cancer data. These algorithms aid in the classification of tumors as benign or malignant, which facilitates efficient assessment and planning for treatments. These methods help personalized therapy better comprehend cancer uniqueness and improve patient satisfaction.

### Support Vector Machine for Tumor Classification

SVM is an effective classification algorithm that divides observations into different categories by identifying the best hyperplane. It works especially well with statistics that have distinct class borders and high dimensions. Based on characteristics including radius, substance, and border, SVM can identify cancerous or benign tumors in study studies.

### Random Forest and Its Advantages

Random Forest makes forecasts by aggregating the outcome results of many decision-making trees. This approach helps find key characteristics for cancer detection by effectively handling data with numerous dimensions, preventing excess fitting, and providing significance of features. Because of its durability, it can be used to process cancer data and increase the accuracy of categorization.



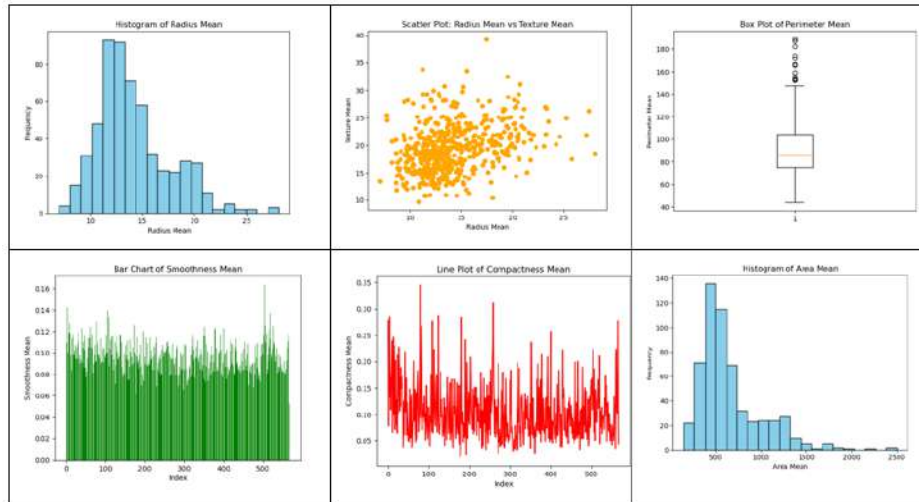


**Varanasi Avinash et al.,**

**Hierarchical Clustering in Cancer Analysis**

Every single point of information is initially clustered separately in hierarchical clustering, which then merges the clusters according to characteristics to form a structure resembling a tree. By considering the properties of the tumors, it creates a diagram called a dendrogram in disease data analysis. Understanding tumor behavior and developing targeted treatments are aided by the identification of subgroups with patterns that may hold clinical importance.

**Data Analysis with the Different Features**



**RESULTS**

SVM and Random Forest, two supervised learning methods, performed admirably. Recall and pinpoint accuracy ratings added to their effectiveness in accurately classifying cancer cases. Unsupervised methods like K-means clustering and hierarchical clustering provided valuable insights into the underlying structure of the cancer dataset, which facilitated exploratory research.

**Results for Supervised Algorithms**

```

SVM Classifier:
Accuracy: 0.956140350877193
Precision: 0.975
Recall: 0.9069767441860465

Random Forest Classifier:
Accuracy: 0.9649122807017544
Precision: 0.975609756097561
Recall: 0.9302325581395349
    
```

**CONCLUSION**

This work applies state-of-the-art computational techniques to investigate the biology of cancer, using machine learning to interpret complex patterns in datasets. With the potential to guide future therapeutic approaches, the research attempts to identify the underlying causes of cancer development and progression. Through the use of data-driven methodology, it aims to improve comprehension of cancer dynamics. Computational methods help reveal patterns concealed in cancer data, offering new perspectives on the disease landscape. The ultimate objective is to





expand our understanding of cancer biology through the application of cutting-edge analytical tools, opening the door to more effective treatments and diagnostics.

## REFERENCES

1. Adams, J.M., and Cory, S. (2007). The Bcl-2 apoptotic switch in cancer development and therapy. *Oncogene* 26, 1324–1337. Aguirre-Ghiso, J.A. (2007). Models, mechanisms and clinical evidence for cancer dormancy. *Nat. Rev. Cancer* 7, 834–846.
2. Al-Hajj, M., Wicha, M.S., Benito-Hernandez, A., Morrison, S.J., and Clarke, M.F. (2003). Prospective identification of tumorigenic breast cancer cells. *Proc. Natl. Acad. Sci. USA* 100, 3983–3988.
3. CH Nooka Raju, Routhu Shanmukh, Syed Raashid Andrabi, Identification of Intensity Variations by Various Edge Detection Techniques on Fundus Images, VOLUME 10, ISSUE 2, 2023, *Stard Research*, 209-220.
4. Amaravadi, R.K., and Thompson, C.B. (2007). The roles of therapy-induced autophagy and necrosis in cancer treatment. *Clin. Cancer Res.* 13, 7271–7279.
5. Amit, I., Citri, A., Shay, T., Lu, Y., Katz, M., Zhang, F., Tarcic, G., Siwak, D., Lahad, J., Jacob-Hirsch, J., et al. (2007). A module of negative feedback regulators defines growth factor signaling. *Nat. Genet.* 39, 503–512.
6. Apel, A., Zentgraf, H., Buchler, M.W., and Herr, I. (2009). Autophagy-A doubleedged sword in oncology. *Int. J. Cancer* 125, 991–995.
7. Artandi, S.E., and DePinho, R.A. (2000). Mice without telomerase: what can they teach us about human cancer? *Nat. Med.* 6, 852–855. Artandi, S.E., and DePinho, R.A. (2010). Telomeres and telomerase in cancer. *Carcinogenesis* 31, 9–18.
8. Azam, F., Mehta, S., and Harris, A.L. (2010). Mechanisms of resistance to antiangiogenesis therapy. *Eur. J. Cancer* 46, 1323–1332. Baeriswyl, V., and Christofori, G. (2009). The angiogenic switch in carcinogenesis. *Semin. Cancer Biol.* 19, 329–337.
9. Routhu Shanmukh, CH Nooka Raju, G Tirupati, Application of Texture Analysis Techniques and Image Statistics to Fund us Images for Effective Comparison and Analysis, *Journal of Chemical Health Risks*, Vol. 13 No. 6 (2023), 2086-2090.
10. Baluk, P., Hashizume, H., and McDonald, D.M. (2005). Cellular abnormalities of blood vessels as targets in cancer. *Curr. Opin. Genet. Dev.* 15, 102–111.
11. Barkan, D., Green, J.E., and Chambers, A.F. (2010). Extracellular matrix: a gatekeeper in the transition from dormancy to metastatic growth. *Eur. J. Cancer* 46, 1181–1188.
12. Barnes, D.E., and Lindahl, T. (2004). Repair and genetic consequences of endogenous DNA base damage in mammalian cells. *Annu. Rev. Genet.* 38, 445–476.
13. Barrallo-Gimeno, A., and Nieto, M.A. (2005). The Snail genes as inducers of cell movement and survival: implications in development and cancer. *Development* 132, 3151–3161.
14. Routhu Shanmukh, CH Nooka Raju, Lakshmana Rao Rowthu,, " Analysis of fundus images using conventional edge detection techniques" pp. 206-217 2022.
15. Berdasco, M., and Esteller, M. (2010). Aberrant epigenetic landscape in cancer: How cellular identity goes awry. *Dev. Cell* 19, 698–711.
16. Bergers, G., and Benjamin, L.E. (2003). Tumorigenesis and the angiogenic switch. *Nat. Rev. Cancer* 3, 401–410.
17. Bergers, G., and Hanahan, D. (2008). Modes of resistance to anti-angiogenic therapy. *Nat. Rev. Cancer* 8, 592–603. Bergers, G., and Song, S. (2005). The role of pericytes in blood-vessel formation and maintenance. *Neuro-oncol.* 7, 452–464.
18. Bergfeld, S.A., and DeClerck, Y.A. (2010). Bone marrow-derived mesenchymal stem cells and the tumor microenvironment. *Cancer Metastasis Rev.* 29, 249–261.
19. Berx, G., and van Roy, F. (2009). Involvement of members of the cadherin superfamily in cancer. *Cold Spring Harb. Perspect. Biol.* 1, a003129.
20. Bhowmick, N.A., Neilson, E.G., and Moses, H.L. (2004). Stromal fibroblasts in cancer initiation and progression. *Nature* 432, 332–337.





**Varanasi Avinash et al.,**

21. Routhu Shanmukh, CH Nooka Raju, Syed Raashid Andrabi, Analysis of Intensity Variations on Applications of Edge Detection Techniques to Fundus Images, GRADIVA REVIEW JOURNAL
22. Bierie, B., and Moses, H.L. (2006). Tumour microenvironment: TGFbeta: the molecular Jekyll and Hyde of cancer. Nat. Rev. Cancer 6, 506–520.
23. Bindea, G., Mlecnik, B., Fridman, W.H., Page` s, F., and Galon, J. (2010). Natural immunity to cancer in humans. Curr. Opin. Immunol. 22, 215–222.
24. Biswas, S.K., and Mantovani, A. (2010). Macrophage plasticity and interaction with lymphocyte subsets: cancer as a paradigm. Nat. Immunol. 11, 889–896.
25. Blasco, M.A. (2005). Telomeres and human disease: ageing, cancer and beyond. Nat. Rev. Genet. 6, 611–622.





## Production, Optimization and Partial Purification of Amylase from the *Bacillus megaterium* for the Removal of Biofilm

Tulsi Barot<sup>1</sup> and Meghna Diarsa<sup>2\*</sup>

<sup>1</sup>Student, Department of MLT, Bapubhai Desaiabhai Patel Institute of Paramedical Science (BDIPS), Charotar University of Science and Technology, Changa, Gujarat, India.

<sup>2</sup>Assistant Professor, Department of MLT, Bapubhai Desaiabhai Patel Institute of Paramedical Science (BDIPS), Charotar University of Science and Technology, Changa, Gujarat, India.

Received: 21 Jun 2024

Revised: 16 Aug 2024

Accepted: 26 Oct 2024

### \*Address for Correspondence

#### Meghna Diarsa

Assistant Professor, Department of MLT,  
Bapubhai Desaiabhai Patel Institute of Paramedical Science (BDIPS),  
Charotar University of Science and Technology,  
Changa, Gujarat, India.  
E.Mail: meghnadiarsa.bdips@charusat.ac.in



This is an Open Access Journal / article distributed under the terms of the **Creative Commons Attribution License** (CC BY-NC-ND 3.0) which permits unrestricted use, distribution, and reproduction in any medium, provided the original work is properly cited. All rights reserved.

### ABSTRACT

Biofilm is a group of microorganisms living with a self-produced protecting layer, extracellular polysaccharides (EPS). Many pathogens are EPS producing and biofilm forming organisms, due to this the organisms also show the resistant towards the antibiotics. Our study had been focused on the green method (enzymatic method) to remove the biofilm formation. Among the various enzyme, Amylase enzyme is the most applicable enzyme to remove the biofilm formation. Amylase is a valuable enzyme with significant applications. In the current work, three different *Bacillus* species were selected for the production of amylase enzyme. On the basis of the primary and secondary screening, *Bacillus megaterium* gave the highest production of amylase enzyme and was selected for the further statistical optimization and partial purification. After the statistical optimization 5.4-fold amylase activity was increased. SDS PAGE shows that after the partial purification of the amylase enzyme, the molecular weight of the amylase enzyme extracted from *Bacillus megaterium* is 20KDa. The partial purified enzyme was successfully removed the biofilm of *Escherichia coli* (79.94%), *Pseudomonas aeruginosa* (70.68%), *Staphylococcus aureus* (57.07%). The biofilm removal was further confirmed by light microscopy and fluorescence microscopy.

**Keywords:** Biofilm, Amylase, *Bacillus* spp. Production and Biofilm removal



**Tulsi Barot and Meghna Diarsa**

## INTRODUCTION

There is an accumulation of sessile microbial species which is linked biotic or abiotic surface it is known as Biofilm. "A 3D polymer matrix" also have been found on the liquid surfaces. Biofilm forming bacteria survive under the harsh environments like depletion of nutrition, exposure of heat radiation, antibiotic and other stress factors due to the production of sticky gum like substance known as exopolymer substance (EPS). Biofilm consists of intricate molecules such as proteins, polysaccharides, nucleic acid, eDNA, glycoproteins, and lipids. This EPS provides benefits to the biofilm bacteria like attachment on abiotic and biotic surfaces aggregation as a cluster form and main in biofilm formation. The examples of Biotic and Abiotic surface are human tissues, organ and catheter, surgical instrument respectively [1]. Around 90% of biofilm mass is made up of EPS (Extracellular Polymer Substance). The biofilm forming bacteria also present on medical devices and they form biofilm on such devices. Almost 80% of diseases can be due to biofilm-associated pathogens. Basic components play a vital part in biofilm arrangement. EPS makes a difference ensure bacterial cells from anti-microbials, making them safer to the medicate [2]. Due to this it become a major concern for the medical settings these because these organisms show a resistant toward the antibiotic and it became a for major hurdle for the treatment. Amylase enzymes are derived from various sources such as plants, animals, and microorganisms. Among these, microbial amylases are the most widely produced and utilized in industries owing to their exceptional productivity and ability to withstand high temperatures [3]. Microbial enzymes have grown more and more popular because they are easy to isolate in high quantities, can be produced 76 easily and inexpensively, and are stable in a variety of difficult environments [4]. The primary advantages of using bacteria in amylase production are the inexpensive techniques for mass-producing amylases and the simplicity with which they may be modified to produce enzymes with specific characteristics [4]. The EPS can be broken down and bacteria can be killed by the enzyme amylase, which inhibits the production of biofilms [2].

In our study, we mainly focused on removal of the biofilm using a green/ natural method, i.e., enzymatic method. In this study we are focus on production of Amylase enzyme from *Bacillus megaterium* spp. Optimize the Single factor to enhance the amylase activity, partial purification. The partially purified amylase enzyme is used as an antibiofilm compound to remove biofilm.

## MATERIALS AND METHOD

All the chemicals including iodine, 3-5-Dinitro salicylic acid (DNS), Soluble Starch, Yeast Extract, CaCl<sub>2</sub>, Peptone, KH<sub>2</sub>PO<sub>4</sub>, MgSO<sub>4</sub>, FeSO<sub>4</sub>, K<sub>2</sub>HPO<sub>4</sub>, Beef extract, NaCl, Acrylamide, Bisacrylamide, Hydrochloric acid (HCl), Ammonium persulphate, Glycine, Glycerol, β mercaptoethanol, Tetramethyl ethylenediamine (TEMED), Coomassie Brilliant Blue- R 250, Methanol, Acetic acid, Glacial acetic acid, Crystal violet, Isopropyl Alcohol, ethidium bromide (EtBr) are grade of highest purity available procured from Hi-Media Laboratories, India. *Bacillus subtilis* ATCC, *Bacillus megaterium* ATCC, *Bacillus cereus* ATCC were obtained from the American Type Culture Collection (ATCC).

### Primary Screening

The primary screening was used to identify the ability of the organisms for the production of amylase enzyme. Three different *Bacillus* spp. (*Bacillus subtilis* ATCC, *Bacillus megaterium* ATCC, *Bacillus cereus* ATCC) were screened for the amylase production. The composition of the primary starch agar medium was: Soluble starch (10 gm/l), Peptone (5 gm/l), Beef extract 100 (5 gm/l), NaCl (2 gm/l) MgSO<sub>4</sub> (2 gm/l), Agar (10 gm/l). Organisms were inoculated on the primary starch agar medium and incubate at 37°C for 24 hours. Next day, all the incubated plates were flooded with the iodine and based on the hydrolysis of starch, the zone of clearance 103 was observed and recorded.

### Secondary Screening

The result of the primary screening was further confirmed by the secondary screening. starch liquid media (Soluble starch-10 gm/l, Peptone-5 gm/l, Beef extract-5 gm/l, NaCl-2 gm/l, 107 MgSO<sub>4</sub>-2 gm/l) was used for the secondary screening. *Bacillus subtilis* ATCC, *Bacillus megaterium* ATCC, *Bacillus cereus* ATCC was inoculated into the starch broth







### Tulsi Barot and Meghna Diarsa

medium and incubated at 37°C for overnight. Next day for the enzyme assay, enzyme was extracted by the centrifugation at 7000 rpm for 10 minutes. Supernatant was collected for the amylase assay.

#### Amylase Assay:

Miller et.al., 2002 illustrate the method for amylase assay to determine the amount of reducing sugar released from soluble starch. The activity of amylase enzyme obtained from bacterial cell was evaluated by 3,5-dinitrosalicylic acid (DNS). The samples were taken (500 µl of enzyme from supernatant + 500 µl of substrate 1% starch + 1 ml of PO<sub>4</sub> buffer) and incubate 116 37°C for 10 minutes. 1 ml of freshly prepared DNSA solution were added to stop the reaction. Tubes were placed in water bath at 100°C for 10 minutes. Cool it down under running tap water and add 10 ml of Distilled water. Absorbance was taken at 540 nm using a Digital colorimeter (Advance lab equipment). A glucose standard curve was created to determine the concentration of glucose produced in each solution by plotting absorbance at 540 nm against the amount of glucose released. Amylase activity was then calculated, one unit of enzymatic activity is equivalent to the amount of the enzyme needed to catalase the synthesis of reducing sugar under typical assay circumstances, which is equal to 1µmol/min of glucose (Abo-Kamer et al., 2023)[4].

The following equation was applied for the estimation of enzyme activity

#### Enzyme Activity

$$= \text{Amount of reducing sugar} \times \frac{1000}{\text{molecular}} \text{ weight of glucose} \times \text{time}$$

#### Optimization of different parameters for Amylase production under submerge fermentation (single factorial):

##### Effect of moistening medium for amylase production:

The selection of moistening medium is a very important parameter for the maximum production of Amylase enzyme. The six different moistening media were screened for the amylase enzyme Production [5,4].

Media T1: (gm/l). Glucose-20; yeast extract-10; MgSO<sub>4</sub>.7H<sub>2</sub>O-1; KH<sub>2</sub>PO<sub>4</sub>- 2.

Media T2: (gm/l). Peptone-10; starch-10; yeast extract- 20; CaCl<sub>2</sub>-0.05; MgSO<sub>4</sub>-0.25; 139 KH<sub>2</sub>PO<sub>4</sub>- 0.25; (NH<sub>4</sub>)<sub>2</sub>SO<sub>4</sub>, - 0.25; FeSO<sub>4</sub>-0.01.

Media T3: (gm/l). Soluble starch-10; peptone-6; MgSO<sub>4</sub>-0.5; potassium chloride-0.5.

Media T4: (gm/l). Soluble starch-20; yeast extract-5; magnesium sulphate-1; CaCl<sub>2</sub>.2H<sub>2</sub>O-0.2; NaCl-1.

Media T5: (gm/l). Soluble starch-10; peptone-25; KH<sub>2</sub>PO<sub>4</sub>.3H<sub>2</sub>O-1.5; NaSO<sub>4</sub>-1.5; FeSO<sub>4</sub>.7H<sub>2</sub>O-0.03; MnCl<sub>2</sub>.4H<sub>2</sub>O-0.15; CaCl<sub>2</sub>.2H<sub>2</sub>O-0.45.

Media T6: (gm/l). Soluble starch-5; glucose-7.5; lactose-5; Yeast extract-5; Peptone-12.5; Ammonium sulphate-12.5; Magnesium sulphate-0.75.

The Submerged fermentation was done for the production of amylase by inoculating culture 148 into each flask and incubated at 37°C for overnight. Next day, enzyme was extracted by centrifugation at 7000 rpm for 10 minutes. Supernatant were collected and check enzyme activity by DNS method.

##### Effect of inoculum Size for amylase production

The effect of the inoculum size on the enzyme production is another important parameter. The production medium was inoculated with various inoculation size, ranging from 200 µl to 1600 µl. After the inoculation, flasks were incubated at 37°C for overnight. Next day, enzyme was extracted by centrifugation at 7000 rpm for 10 minutes. Supernatant were collected and DNS method was performed to check the enzyme activity.

##### Effect of time period on amylase production

The evaluation of effect of time on the amylase enzyme was determine by incubating the production media for different interval. The fermentation media was incubated at (0,24,48, 96,72,120 hours). Next day, enzyme was extracted by centrifugation at 7000 rpm for 10 minutes. Supernatant were collected and enzyme activity check by DNS method [6].





### Tulsi Barot and Meghna Diarsa

#### Effect of Temperature for amylase enzyme production

Temperature is one of the important factor for submerged fermentation, because enzyme and bacteria both sensitive to temperature. The effect of temperature on amylase enzyme period was examine by incubated flasks at different temperature (15,27,37,72,96 °C). Next day enzyme was extracted by centrifugation at 7000 rpm for 10 minutes. Supernatant were 167 collected and DNS method was performed to check the enzyme activity [7].

#### Effect of pH on amylase production

The effect of different pH of the production media on amylase activity was examined. The pH of the production media was assessed in the range of pH1- pH9. Next day, enzyme was extracted by centrifugation at 7000 rpm for 10 minutes. Supernatant were collected and enzyme activity check by DNS method [7].

#### Effect of various Carbon sources on amylase production

Several carbon sources were used for amylase enzyme production. Carbon sources such as 175 starch, glucose, sucrose, mannitol, lactose was incorporated into the production medium. After 176 the inoculation, flasks were incubated at 37°C for overnight. Next day, enzyme was extracted by centrifugation at 7000 rpm for 10 minutes. Supernatant were collected and enzyme activity analysed by DNS method [7].

#### Effect of various Nitrogen sources on amylase production:

The effect of various nitrogen sources on amylase enzyme production was evaluated. Nitrogen sources such as yeast extract, peptone, beef extract, ammonium sulphate were used in this experiment. After the inoculation, flasks were incubated at 37°C for overnight. Next day, enzyme was extracted by centrifugation at 7000 rpm for 10 minutes. Supernatant were collected and DNS method was performed to check the enzyme activity [8,4].

#### Multi factorial experiments for optimization of amylase production:

The optimization of the production media for amylase enzyme was done in three step techniques. In the first step Plackett-Burman Design (PBD) was used to examine the relative important components of a media affecting the amylase enzyme activity. Most important components of the PBD were further calculated for their ideal level with the help of Central Composite Design (CCD) and contour plots. In the last step computational statistical analysis (ANOVA) to validate the model's fitness as measured by the determination of coefficient (R<sup>2</sup>).

#### Plackett–Burman Design for primary factors (PBD):

Plakett-Burman design is a mathematical compute design and it is used to evaluate the significance of 5 different medium components of the production media for the production of amylase. Different experimental combinations were executed to minimize unrelated variables that affect amylase production. Five different medium components (Starch, peptone, MgSO<sub>4</sub>, CaCl<sub>2</sub>, NaCl) were screened out in the combination of 8 according to the Plackett- Burman Design by using Design expert 13 software. In the Plackett-Burman Design, each variable being represented at low level (-) and high level (+) including two dummy variables. The following equation was used to calculate the effect of each variable.

$$E(xi) = \frac{2(\Sigma M^+ - M^-)}{N} \quad \text{eq.(1)}$$

Where, E(xi) = the concentrated effect of the tested variable, M<sup>+</sup> and M<sup>-</sup> = amylase production from the trials where the variable (xi) was present at high and low concentrations, respectively and N= number of trials. The experimental error was evaluated by calculating the variance among the dummy variables as follow:

$$V_{eff} = \Sigma(E_d)^2 / n \quad \text{eq.(2)}$$





### Tulsi Barot and Meghna Diarsa

Where,  $V_{eff}$  = concentration effects of variance,  $E_d$  = concentration effect of the dummy variable and  $n$  = number of the dummy variables. The standard error of the concentration effect was a square root of variance of an effect and the significance level (p-value) of each concentration effect was evaluated using the student's t-test:

$$t_{(xi)} = \frac{E_{(xi)}}{SE} \quad \text{eq.(3)}$$

Where,  $E_{(xi)}$  is the effect of variable  $x_i$ .

#### Central Composite Design:

Response surface methodology (RSM) represents a widely acknowledged statistical model that used to optimized and evaluation of the impact of different components of production medium and their interaction. Design expert 13 software was used to analyse and response surface graph. CCD analysis was done on the independent factors that showed a substantial impact on amylase activity by PBD. Three variables (Starch,  $MgSO_4$ ,  $CaCl_2$ ) were used. In CCD, 3D response curves were plotted against any two independent parameters, with the third independent factor maintained constant or at the 0 level, to examine the optimum values and the combined influence of the selected variable on amylase production. ANOVA was use to assess the significance of model and the regression coefficients A regression equation was used to examine the quality of the second order polynomial equation.

$$Y = \beta_0 + \sum \beta_i x_i + \sum \beta_{ij} x_i x_j + \sum \beta_{ii} x_i^2 \quad \text{eq.(4)}$$

Where,  $Y$  = predicted response,  $\beta_0$  = offset item,  $\beta_i$  = linear offset coefficient,  $\beta_{ii}$  = squared offset coefficient,  $\beta_{ij}$  = interaction effect and  $x_i$  = the dimensionless code of the  $X_i$ . [19].

#### Comparison of Unoptimized and Optimized media:

The comparison of unoptimized media and statistical optimized and was done to study the increase in fold production of amylase enzyme. Culture was inoculated in both the unoptimized and statistically optimized medium. After the inoculation, flasks were incubated at 37°C for overnight. Next day enzyme was extracted by centrifugation at 7000 rpm for 10 minutes. Supernatant were collected and enzyme activity analysed by DNS method.

#### Partial Purification:

##### Ammonium sulphate precipitation and dialysis

Two step purification was done for the amylase enzyme produced by the *Bacillus megaterium* ATCC. The crude amylase enzyme that was produced during the immerse fermentation was centrifuged for 10 minutes at 7000 rpm (4°C). The complete protein was precipitated using the ammonium sulphate supernatant after centrifugation. The range of 0-90% saturation was used for the ammonium sulphate precipitation process. To extract the salts from the fraction, dialysis was carried out following by the ammonium precipitation method. The active fraction with highest amylase activity was dialyzed against the phosphate buffer (pH-7.0) for 6 hours.

#### Enzyme

##### Enzyme molecular weight determination by SDS – PAGE:

High enzymatic activity fractions was obtained by partial purification. Protein assay was done by Folin lowry's method [9]. Sodium dodecyl sulphate polyacrylamide gel electrophoresis (SDS-PAGE) on 12% gel was then used to determine relative molecular mass [10]. The gel was stained with the help of Coomassie brilliant blue R-250 dye and its molecular mass marker ranged from 6.5 to 200 kDa. The standard protein marker contain (Myosin pig- 200,000 Da), ( $\beta$ -galactosidase *E.Coli* - 116,000 Da), (Phosphorylase B Rabbit muscle- 97,200 Da), (Serum 250 Albumin Bovine- 66,409 Da), (Ovalbumin Hen egg White-44, Da), (Carbonic anhydrase Bovine- 29,000 Da), (Trypsin inhibitor Soyabean- 20,100 Da), (Lysozyme Hen egg white- 14,300 Da), (Aprotinin Bovine pancreas- 6,500 Da).





### Tulsi Barot and Meghna Diarsa

#### Biofilm Removal:

##### Biofilm removal by plate assay:

A biofilms of *Escherichia coli*, *Pseudomonas aeruginosa*, *Staphylococcus* was developed on 96-well polystyrene microtiter plates. The process of biofilm development includes the dilution of overnight grown cultures (*E. coli*, *S. aureus*, and *P. aeruginosa*) in LB broth to an absorbance at 600 nm of 0.01 ( $1 \times 10^8$  CFU/mL). The diluted 200  $\mu$ L of cell suspension was applied to each well on a 96-well polystyrene microtiter plate. The concentration (80  $\mu$ L, 100  $\mu$ L and 150  $\mu$ L) of the partially purified amylase enzyme (at the time of biofilm formation and after the formation of the biofilm) and time period (12-48 hours) was optimized to remove the biofilm. All the microtiter plates were incubated at 37°C. Once the incubation period was completed, the planktonic cells of the biofilm was removed using the 10 mM phosphate buffer saline (PBS). The adherent cells of the biofilms were stained with the 0.2% of crystal violet for 10 minutes. After 10 minutes of exposure of crystal violet, the biofilm of the adherent bacterial cells was cleaned three times with the help of sterile distilled water to get rid of any remaining colours. Finally, the plates were destained with Isopropyl Alcohol (IPA). The production of the biofilm by the organism and removal of the biofilm by partially purified amylase enzyme was evaluated by taking absorbance at 595 nm using (Thermo scientific Multiscan go-nanodrop) [11,12]

##### Percentage of biofilm inhibition

$$= \frac{\text{Optical density of control sample} - \text{optical density of test sample}}{\text{optical density of control sample}} \times 100$$

#### Microscopic techniques:

##### Anti-biofilm Activity by light Microscopy

The biofilm formation capability and the removal of biofilm by partially purified amylase enzyme was evaluated by light microscopic technique. Prepare a smear of culture (*E. coli*) on glass slide and allow it to air dry. The smear was treated with the 150  $\mu$ L partially purified 280 amylase enzyme. The glass slide was incubated for 48 hours at 37°C. Next day, the glass slide was stained with 0.2% of crystal violet. The excess dye was removed by washing with distilled water and visualized under a light microscope (40X) [13].

##### Anti-biofilm Activity by fluorescent Microscopy:

The biofilm formation capability was also examined by fluorescent Microscopy. Prepare a 285 culture smear on glass slide allow it to air dry. The smear was treated with the 150  $\mu$ L partially 286 purified amylase enzyme. The glass slide was incubated for 48 hours at 37°C. Next day, the glass slide was stained with ethidium bromide (EtBr) dye. The excess dye was removed by washing with distilled water and visualized under a fluorescent microscope Nikon ECLIPSE 289 Ti2.

## RESULTS AND DISCUSSION

#### Primary Screening

In the present study, three different *Bacillus spp.* (*Bacillus subtilis* ATCC, *Bacillus megaterium* ATCC, *Bacillus cereus* ATCC) were used for screening of amylase production. All the three species of *Bacillus* i.e. *Bacillus subtilis* ATCC, *Bacillus megaterium* ATCC, *Bacillus cereus* ATCC exhibited positive results, clear zone on 1% starch agar plate. Figure 1 shows that the highest zone of hydrolysis was obtained by *Bacillus megaterium* ATCC (16 mm) on 1% starch agar plate. This result indicates that *Bacillus megaterium* ATCC has the highest ability to produce the amylase. *Bacillus subtilis* ATCC, *Bacillus cereus* ATCC shows zone of hydrolysis (13 mm, 12 mm) respectively. Similar results were observed by the [14]. They observed that 300 *Bacillus spp.* showed zone of hydrolysis in the range of 10- and 17-mm. Similar result was also recorded by abo-kamer et al., 2023 [4] that zone of hydrolysis was 15 mm by *Bacillus subtilis*.

#### Secondary Screening

Secondary screening method is used to confirm the results of primary screening. All the three different species of *Bacillus*, *Bacillus subtilis* ATCC, *Bacillus megaterium* ATCC, *Bacillus cereus* ATCC shows positive results in the primary



**Tulsi Barot and Meghna Diarsa**

screening, hence all three species were 306 selected for the secondary screening. Secondary screening was done by the production of amylase enzyme under submerged fermentation. On the basis of the secondary screening, **Figure 2** represents the *Bacillus megaterium* ATCC shows the highest amylase enzyme activity (564.10 U/ml) however *Bacillus cereus* ATCC had the lowest enzyme activity (351.282 U/ml). The activity of the amylase enzyme shows the ability of the organism to break down starch into glucose by producing amylase enzyme, so higher the enzyme activity higher the amylase enzyme production by the organism. abo-kamer et al. 2023[4] reported that *Bacillus cereus* produced 135 U/ml amylase enzyme.

**Optimization of different parameters for Amylase production under submerge fermentation:****Effect of moistening medium for amylase production:**

One of the main factors in submerged fermentation that can be effectively optimized for maximum amylase production is the selection of moistening medium. The experiment was conducted using six different media (T1-T6). Among all the six different media, T4 media was the most suitable media for the production of amylase enzyme (1188.03 U/ml) shows in **Figure 3a**. Hence Optimum production was related to the existence of additive nutrients and metal ions like  $MgSO_4$ ,  $CaCl_2$ ,  $NaCl$  which are the essential growth of the *Bacillus megaterium* ATCC bacteria. Optimization of the moistening medium varies with the species of the microorganisms [4]. Starch,  $MgSO_4$ ,  $CaCl_2$ ,  $NaCl$  provides essential support for bacterial growth, enzyme function and stability. Together these components create a conducive environment for bacterial growth and efficient enzyme production.

**Effect of inoculum Size for amylase production**

Another important factor is inoculum size. The inoculum size was optimized by inoculating inoculum in the range of the (200 $\mu$ l- 1600 $\mu$ l). Figure 3b represents that the amylase activity was very less at lower inoculum size, as the inoculum size increased the enzyme activity was also increased. The highest enzyme activity was obtained at 1000 $\mu$ l (897.43 U/ml). Further 332 increase in the inoculum size, shows a negative effect on the amylase activity.

**Effect of various time periods on amylase production**

Optimization of time plays a vital role for the production of amylase enzyme. The experiment was conducted at different time intervals (0 - 120 hours). According to **Figure 3c** the highest production of amylase was obtained at 24 hours (1068.38 U/ml). However further incubation leads to the decreasing enzyme activity and at the 120 hours (68.37U/ml) amylase activity was obtained. Rakaz et al., (2021) [15] reported the highest activity for *Bacillus cereus* 0.122 U/min/ml at 24 hours, it is very less as compare to our result they also reported that incubation time increased enzyme activity decreased.

**Effect of various Temperature for amylase production**

The production of amylase enzyme is significantly affected by the optimization of temperature. During the fermentation process there is a rise in temperature due to the respiration of organisms (Darabzadeh et al., 2019) [16]. Figure 3d shows the effect of temperature on amylase production by *Bacillus megaterium* ATCC. In the current work, the result shows that there is an increase in the amylase activity with the increasing temperature and maximum amylase production was achieved at 37°C (897.43 U/ml). However, further increase in temperature 348 decreases enzyme activity. These findings show that above the 37° C did not support the growth of microorganisms as well as the production of amylase. Similar results finding by Sobhy et al., (2023) [7] amylase output 857.92 U/ml at 37°C.

**Effect of various pH for amylase production**

Another important factor amylase production is pH of the production media. **Figure 3e** illustrates the effect of pH on amylase activity. The maximum production of amylase enzyme was obtained at pH 7 (1141.81 U/ml). Similar findings were reported by Olajuyigbe and for Ajele (2005) [17], they found that *Bacillus* species require an ideal pH of 8.0(60%). Sobhy et al., (2023) [7] also find optimum pH is 7 (856.92 U) for the production of amylase enzyme by 358 *Bacillus* spp.







### Tulsi Barot and Meghna Diarsa

#### Effect of various carbon source for amylase production

Carbon sources play a vital role in fermentation as well as play a key role in cellular growth of the microorganism. In the current study, five different carbon sources (Starch, Glucose, Sucrose, Mannitole and Lactose) were selected to produce the amylase enzyme from *Bacillus megaterium* ATCC. The figure 3f shows the effect of different carbon sources on amylase production. Among the five carbon sources, maximum amylase production. (1111.11 U/ml) was obtained by using starch as a carbon source. Similar result was reported that carbon source is suitable for amylase production from *Bacillus aryabhatai* KIIT BE-1 by Ojha et al., 2020 367 [18].

#### Effect of various nitrogen source for amylase production

Nitrogen compounds are also important at the time of the fermentation by microorganisms. The effect of different nitrogen sources on the production of amylase enzyme is shown in Figure 3g. Among the four nitrogen sources, Peptone gave the highest production of amylase enzyme (1247.86 U/ml). Similar result reported by Sobhy et al., (2023) [7]. They showed that peptone as a nitrogen source most suitable for the amylase production (878.45U) from streptomycin.

#### Multi factorial experiments for optimization of amylase production:

Plackett-Burman Design has been used to analyse the components that are necessary for the production medium to produce amylase from *B. megaterium* ATCC. The high (+) and low (-) concentrations of the independent variables for the optimization research were selected. In the Plackett-Burman Design, the equivalent amylase production in terms of U/ml for each of the two levels of concentration for each medium component over 8 trials. D1–D2 represents the dummy variables, and the variables designated as X1–X5 indicate the components of the moistening medium. Based on the amylase production (unit per millilitre), Table 1 display the effect, t (xi), p-value, standard error, and confidence level for each medium component. The effects of the different components of the moistening medium were screened out with a confidence level higher than 95%. The CI level of Starch, MgSO<sub>4</sub>, CaCl<sub>2</sub> is 98.81%, 99.96% and 99.56% respectively. Among the five medium components, these three components they were significant variables. However medium components were seen to be less significant variables. According to Plackett-Burman design, the medium component had a negative effect, meaning that a lower concentration was needed than the low (-) concentration that was given. However positive effects so the medium component that the concentration of composition needed to be higher than the plackett-Burman design high (+) value [19].

#### Central Composite Design

Fisher's statistical test for Analysis of variance (ANOVA) was done for the response of amylase production. In plackett- Burman design the variable of moistening medium showing 396 positive and negative effects with or above at 95% confidence level were further optimized by Central Composite Design (CCD). Total 20 experiments were run with three variables (Starch, MgSO<sub>4</sub>, CaCl<sub>2</sub>) using different concentrations. With the help of quadratic multiple regression to describe the relationship between the dependent and independent variables, the Design expert program 13 produced the following equation in terms of coded factors.

$$Y = 9992.27 + 831.12A + 711.53B - 451.28C + 280.87 AB - 1223.40AC + 473.18BC - 1071.18 A^2 - 1252.64B^2 - 1252.64C^2 \quad \text{eq(5)}$$

**Table 2** represents the results of the analysis of variance (ANOVA) used to validate the 404 regression coefficient, which shows that the model was significant. According to the analysis of variance, the quadratic model was not significant with a lack fit value of 0.096, a model value of 3.53, and  $p > f$  indication. Thus, there was high correlation between the predicted and experimental results for analysis. According to the analysis, A<sub>2</sub>, B<sub>2</sub>, and C<sub>2</sub> p- value are all less than 0.05, indicating significance. Since each component's P value is less than 0.1, the model was significant. A factor level region association between a variable's response and its experiment of a given variable is another benefit of using 3-D graphs. Two different medium components at different concentrations are shown in the 3 D plot, while the other medium component The Design Expert software was used to examine the synthesis of amylase using





**Tulsi Barot and Meghna Diarsa**

3-D plots. 1 level is displayed using a 3-D plot and contour plot. Assuming the ideal concentration are kept at a fixed concentration. The interaction between  $MgSO_4$  and starch is shown in Figure 4a. The 3-D graphic demonstrates that when the concentrations of starch and  $MgSO_4$  were very low, there was less amylase production. When the concentrations of starch and  $MgSO_4$  increased simultaneously, the production of the enzyme amylase increased. The highest amount of amylase enzyme was obtained at the concentration 18 g/l of starch and 0.9 g/l of  $MgSO_4$ . Further increased in the concentration of starch and  $MgSO_4$  there was a decrease in amylase activity. The findings indicate that while starch and  $MgSO_4$  alone acted as non-significant components, together had a synergistic effect on the enzyme's ability to produce amylase.

**Figure 4b** illustrates the correlation of  $CaCl_2$  and starch for amylase production. Figure shows that at the lowest concentration of starch and  $CaCl_2$ , the production of amylase is very low. Amylase was synthesized at a higher rate when the concentration of starch and  $CaCl_2$  were increased simultaneously. The highest amount of amylase enzyme produced at the concentration of 18 g/l of starch and 0.39 g/l of  $CaCl_2$ . This finding indicates that starch and  $CaCl_2$  individually acted as non-significant components but they had a synergistic effect on the production of the enzyme amylase.

Figure 4c illustrates the interaction between  $CaCl_2$  and  $MgSO_4$ . The three-dimensional graphic indicates that amylase production was lower at very low concentrations of  $MgSO_4$  and  $CaCl_2$ . When  $MgSO_4$  and  $CaCl_2$  concentrations increased at the same time, the production of the enzyme amylase also increased. The highest amount of amylase enzyme produced at the concentration of 0.9 g/l of  $MgSO_4$  and 0.39 g/l of  $CaCl_2$ . Further increase in the concentration of  $MgSO_4$  and  $CaCl_2$  lead to decrease in the amylase enzyme activity. The findings indicate that  $CaCl_2$  and  $MgSO_4$  individually acted as non-significant components, but both the components showed a synergistic effect on the synthesis of the enzyme amylase.

The actual value v/s predicted value for the production of amylase enzyme by *Bacillus megaterium* ATCC was evaluated using model equation (5). The result shows that the most of the points were located near the adjustment line which indicates that the experimental value were similar to the predicted values by the model. The predicted concentration of three different variables were starch 18 g/l,  $MgSO_4$ , 0.9 g/l and  $CaCl_2$  0.39 g/l with predicted highest amylase enzyme production of enzyme activity statistically optimized (8974.16 U/ml).

**Partial Purification:****Ammonium sulphate precipitation and dialysis**

The extracellular amylase enzyme was partially purified by the ammonium sulphate precipitation followed by dialysis. The ammonium sulphate was used to saturate the crude enzyme from 0 to 80%. The specific activity of amylase enzyme increase with the concentration of ammonium sulphate in the fraction of precipitate and decreased in the fraction of supernatant. The highest specific activity (127.4 U/mg) was recorded at 60% saturation level of ammonium sulphate. After the ammonium sulphate precipitation and dialysis of amylase enzyme, 124.7 U/mg and 148.5 U/mg specific activity with 1.28 and 1.53-fold purification was 454 obtained (Table 3).

Liaquat et al., (2015) [20] reported that,  $\alpha$ -Amylase enzyme from *Bacillus subtilis* (RAS-1) was partially purified with 70% saturation level of ammonium sulphate precipitation. The recovery and purification of amylase from *Bacillus subtilis* (RAS-1) were 37.5% and 2.60. While  $\alpha$ -Amylase enzyme from *Clostridium perfringens* (RAS-4) was partially purified with 60% of ammonium sulphate precipitation. It exhibited specific activity of 6.01 U/mg, 2.29 purification fold with 32.38% recovery.

**Enzyme molecular weight determination by SDS – PAGE**

The molecular weight of partially purified amylase enzyme from *Bacillus megaterium* ATCC was evaluated by SDS - PAGE. The estimated molecular weight of amylase enzyme was 20 kDa. The contradictory results were reported by Liaquat et.al (2015) [20] and Haq et.al (2010) [21]. They reported that the molecular weight of alpha amylase from *Bacillus subtilis* (RAS-1) and *Bacillus subtilis* was 52 kDa and 55 kDa respectively.



**Tulsi Barot and Meghna Diarsa****Biofilm Removal****Biofilm removal by plate assay**

**Figure 5** shows the effect of biofilm removal by the treatment of partially purified amylase enzyme from *Bacillus megaterium* ATCC. The partially purified amylase enzyme was used to remove the biofilm of *Escherichia coli*, *Pseudomonas aeruginosa*, *Staphylococcus aureus*. The result shows that amylase enzyme successfully removed 79.94%, 70.68%, 57.07% biofilm of *E. coli*, *P. aeruginosa*, *S. aureus* after the 48 hours of treatment with 150 µl concentration respectively. The variation in the removal of biofilm of *E. coli*, *P. aeruginosa*, *S. aureus* by amylase enzyme may be due to the variation in the EPS composition Solihin et.al (2021) [22]. Abo-kamer et.al (2023) [4] reported approximately 84% biofilm removal of *Pseudomonas aeruginosa* by purified amylase enzyme from *Bacillus cereus*. Vaikundamoorthy et.al (2018) [3] reported that amylase enzyme produced from the *Bacillus cereus*, successfully remove the biofilm of *P. aeruginosa* and *S. aureus*.

**Microscopic techniques:****Anti-biofilm Activity by light Microscopy:**

The formation of biofilm by *Escherichia coli* and the removal of biofilm by partially purified amylase enzyme was examined by light microscopic technique. The results of the light microscope give the evidence of the successful removal of biofilm after the treatment of partially purified amylase enzyme from *Bacillus megaterium* ATCC. Figure 6a shows positive control of biofilm formation by *E. Coli* and Figure 6b shows the treated biofilm by amylase enzyme.

**Anti-biofilm Activity by fluorescent Microscopy**

Fluorescent Microscopy was used to study the formation of biofilm by microorganisms and the removal of biofilm by partially purified amylase enzyme from *Bacillus megaterium* ATCC. *Escherichia coli* was used as a positive control. The fluorescence microscopic images of fluorescent microscope Nikon ECLIPSE Ti2 shows that after applying the partially purified amylase enzyme there was a less formation of biofilm as compare to positive control. Figure 7a shows positive control of biofilm formation by *E. Coli* and Figure 7b shows the removal of biofilm after treating with the amylase enzyme.

**CONCLUSION**

In the present study, three different species of *Bacillus* were selected (*Bacillus subtilis* ATCC, *Bacillus cereus* ATCC and *Bacillus megaterium* ATCC) for the production of amylase enzyme. The results of primary and secondary screening show that *B. megaterium* ATCC gave maximum zone of inhibition (16 mm) and highest enzyme activity (564.10 U/ml). On the basis of this results *Bacillus megaterium* ATCC was selected for the further study. Single factorial and statistical optimization were done to enhance the amylase enzyme production. Statistical optimization gave 5.4-fold increase in the amylase enzyme production by the *B. megaterium* ATCC. After the ammonium sulphate precipitation and dialysis of amylase enzyme, 124.7 U/mg and 148.5 U/mg specific activity with 1.28 and 1.53 fold purification was obtained. The molecular weight of the partially purified amylase enzyme from *B. megaterium* ATCC was 20 kDa. This study also proved that amylase enzyme from *B. megaterium* ATCC was successfully remove the biofilm of *Escherichia coli*, *Pseudomonas aeruginosa*, *Staphylococcus aureus*. This result also confirmed with the light microscope and fluorescent microscope. In future new species of the *Bacillus* can be isolated for the removal of biofilm. The efficiency of biofilm removal by *B. megaterium* can be enhanced by genetic modification.

**DECLARATIONS**

Ethics approval: Not applicable

Consent to participate: Not applicable

Availability of data and material: Not applicable

Competing interest: Not applicable Funding: Not applicable

**Acknowledgement:** Not applicable



**Tulsi Barot and Meghna Diarsa**

**Conflict of interest:** Authors declares no conflict of interest

**REFERENCES**

1. Cortés-Lorenzo C, Rodríguez-Díaz M, López-Lopez C, Sánchez-Peinado M, Rodelas B, González-López J. Effect of salinity on enzymatic activities in a submerged fixed bed biofilm reactor for municipal sewage treatment. *Bioresour Technol.* 2012; 121:312-319. 525 <https://doi.org/10.1016/j.biortech.2012.06.08>.
2. Yang S, Wang Y, Ren F, Li Z, Dong Q. Applying enzyme treatments in *Bacillus cereus* biofilm removal. *LWT.* 2023; 180:114-667.
3. Vaikundamoorthy R, Rajendran R, Selvaraju A, Moorthy K, Perumal S. Development of thermostable amylase enzyme from *Bacillus cereus* for potential antibiofilm activity. *Bioorg Chem.* 2018; 77:494-506. doi: 10.1016/j.bioorg.2018.02.014.
4. Abo-Kamer AM, Abd-El-salam IS, Mostafa FA, Mustafa A-ER-A, Al-Madboly LA. A promising microbial  $\alpha$ -amylase production and purification from *Bacillus cereus* and its assessment as an antibiofilm agent against *Pseudomonas aeruginosa* pathogen. *Microb Cell Fact.* 2023; 22:127.
5. Blanco AS, Durive OP, Pérez SB, Montes ZD, Guerra NP. Simultaneous production of 536 amylases and proteases by *Bacillus subtilis* in brewery wastes. *Brazilian Journal of Microbiology.* 2016;47(3):665-674. doi: 10.1016/j.bjm.2016.04.019.
6. Ahmed HM, Sobhy NA, Ibrahim WA, Fawzy ME. Green biosynthesis of zinc oxide nanoparticles utilizing pomegranate peel extract for grey water treatment. *Solid State Phenom.* 2023; 342:27-36. doi:10.4028/p-575588.
7. Sobhy H, Awady ME, El-Khonezy M, Hassan M, Salam SA. Screening and Optimization of the Production of Alpha-Amylase Enzyme from *Streptomyces*. *Egyptian Academic Journal of Biological Sciences.* 2023;15(1):169-178. doi:10.21608/eajbsg.2023.303300.
8. Iram A, Cekmecelioglu D, Demirci A. Optimization of the fermentation parameters to maximize the production of cellulases and xylanases using DDGS as the main feedstock in 546 stirred tank bioreactors. *Biocatal Agric Biotechnol.* 2022; 45:102514. doi: 10.1016/j.bcab.2022.102514.
9. Lowry OH, Rosebrough NJ, Farr AL, Randall RJ. Protein measurement with the Folin phenol reagent. *J Biol Chem.* 1951;193.
10. Laemmli UK, Beguin F, Gujer-Kellenberger G. A factor preventing the major head protein of bacteriophage T4 from random aggregation. *J Mol Biol.* 1970; 47:69-85. doi:10.1016/0022-552 2836(70)90402-X.
11. Chakraborty P, Paul P, Kumari M, Bhattacharjee S, Singh M, Maiti D, et al. Attenuation of *Pseudomonas aeruginosa* biofilm by thymoquinone: an individual and combinatorial study with tetrazine-capped silver nanoparticles and tryptophan. *Folia Microbiol (Praha).* 2021; 556 66:255-271.
12. Kumar S, Khan HM, Khan MA, Jalal M, Ahamad S, Shahid M, et al. Broad-spectrum antibacterial and antibiofilm activity of biogenic silver nanoparticles synthesized from leaf extract of *Phyllanthus niruri*. *J King Saud Univ Sci.* 2023;35(8):102904.
13. Nithya C, LewisOscar F, Kanaga S, Kavitha R, Bakkiyaraj D, Arunkumar M, et al. Biofilm inhibitory potential of *Chlamydomonas* sp. extract against *Pseudomonas aeruginosa*. *J Algal Biomass Util.* 2014;5(4):74-81.
14. Hallol M, Helmy O, Shawky AE, El-Batal A, Ramadan M. Optimization of alpha-amylase production by a local *Bacillus paramycoides* isolate and immobilization on chitosan-loaded barium ferrite nanoparticles. *Fermentation.* 2022; 8:241. doi:10.3390/fermentation8050241.
15. Rakaz MA, Hussien MO, Ibrahim HM. Isolation, Extraction, Purification, and Molecular Characterization for Thermostable  $\alpha$ -Amylase from Locally Isolated *Bacillus* Species in Sudan. *Biochem Res Int.* 2021; 2021:6670380.
16. Darabzadeh N, Hamidi-Esfahani Z, Hejazi P. Optimization of cellulase production under solid-state fermentation by a new mutant strain of *Trichoderma reesei*. *Food Sci Nutr.* 2019; 571 7:572-578. doi:10.1002/fsn3.852.
17. Olajuyigbe FM, Ajele JO. Production dynamics of extracellular protease from *Bacillus species*. *Afr J Biotechnol.* 2005;4(8):776-779.





**Tulsi Barot and Meghna Diarsa**

18. Ojha SK, Singh PK, Mishra S, Pattnaik R, Dixit S, Verma SK. Response surface methodology based optimization and scale-up production of amylase from a novel bacterial strain, *Bacillus aryabhatai* KIIT BE-1. Biotechnol Rep. 2020;27
19. Tran TTT, Nguyen KT, Le VVM. Effects of ultrasonication variables on the activity and properties of alpha amylase preparation. Biotechnol Prog. 2018;34(3):702-710.
20. Liaquat R, Kaleem S, Azeem A, Jamal A, Ali MI. Production and characterization of  $\alpha$ -amylase from indigenously isolated bacterial strains treating organic waste in anaerobic digester. Pak J Agri Sci. 2015;52(4):895-903.
21. Haq I, Ali S, Javed MM, Hameed U, Saleem A, Adnan F, et al. Production of alpha amylase from a randomly induced mutant strain of *Bacillus amyloliquefaciens* and its 584 application as a desizer in textile industry. Pak J Bot. 2010;42(1):473-484.
22. Solihin J, Waturangi DE, Purwadaria T. Induction of amylase and protease as antibiofilm agents by starch, casein, and yeast extract in *Arthrobacter* sp. CW01. BMC Microbiol. 2021; 587 21:1-12.

**Table 1: Statistical analysis of the medium components for the amylase production as per the Plackett – Burman design**

Factor	Medium component	Effect Exi	S. E	t(xi)	P-value	Confidence level (%)
X1	Starch	3290.5	1139512.25	1139512.25	0.010	98.91
X2	Peptone	-769.25	1139512.25	-0.06750	0.655	34.46
X3	MgSO4	-7863.25	1139512.25	-0.006900	0.0003	99.96
X4	CaCl2	-4102.5	1139512.25	-0.003600	0.0045	99.54
X5	NaCl	-1324.75	1139512.25	-0.0011625	0.2634	73.65

**Table 2: Analysis of variance of CCD for amylase production from *Bacillus megaterium***

Source	Sum of Squares	df	Mean Square	F-value	p-value	
Model	8.514E+07	9	9.461E+06	6.28	0.0041	Significant
A-Starch	9.434E+06	1	9.434E+06	6.26	0.0313	
B-MgSO4	6.914E+06	1	6.914E+06	4.59	0.0578	
C-CaCl2	2.781E+06	1	2.781E+06	1.85	0.2040	
AB	6.311E+05	1	6.311E+05	0.4191	0.5320	
AC	1.197E+07	1	1.197E+07	7.95	0.0182	
BC	1.791E+06	1	1.791E+06	1.19	0.3010	
A <sup>2</sup>	1.654E+07	1	1.654E+07	10.98	0.0078	
B <sup>2</sup>	2.261E+07	1	2.261E+07	15.02	0.0031	
C <sup>2</sup>	2.261E+07	1	2.261E+07	15.02	0.0031	
Residual	1.506E+07	10	1.506E+06			
Lack of Fit	1.173E+07	5	2.346E+06	3.53	0.0965	not significant
Pure Error	3.327E+06	5	6.655E+05			
Cor Total	1.002E+08	19				

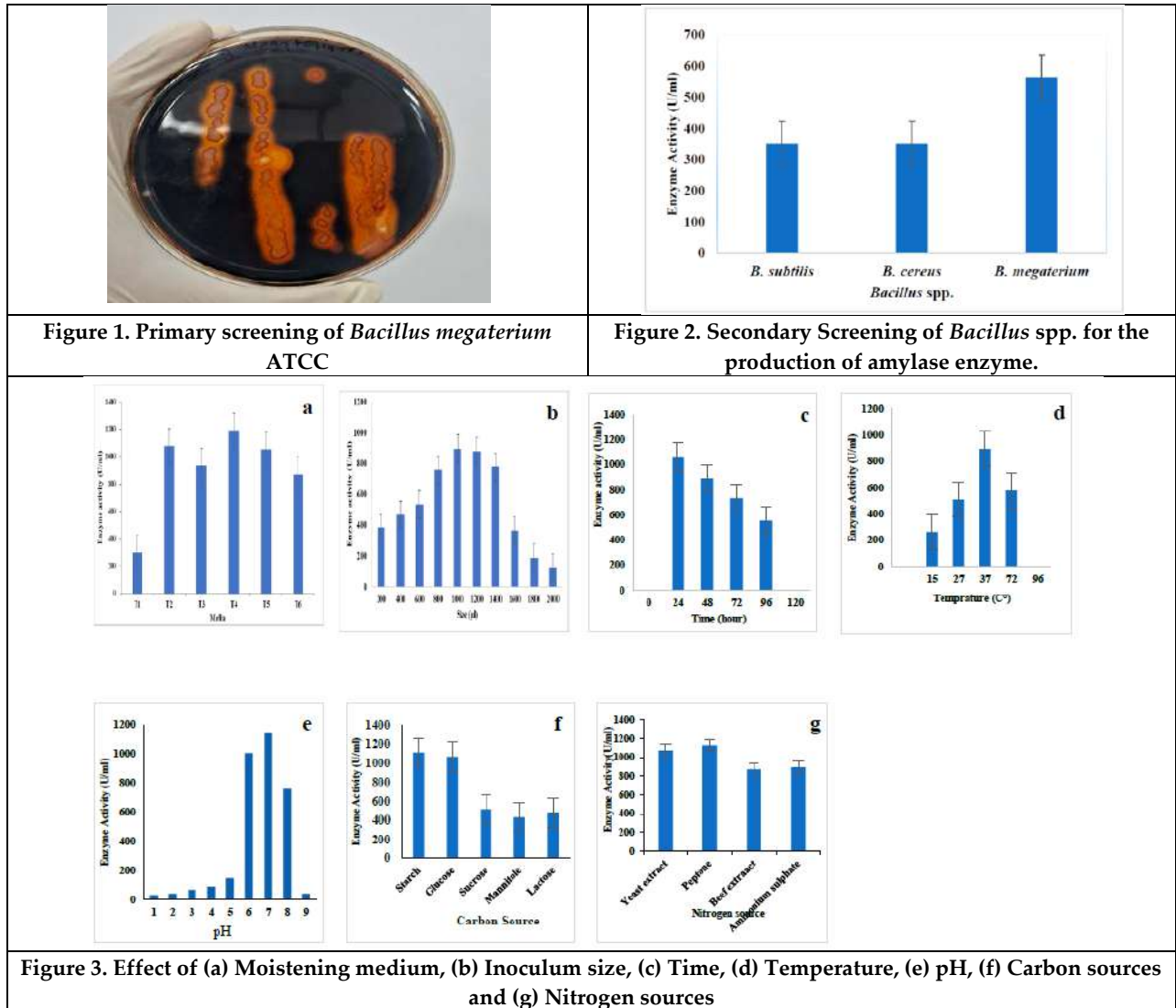




**Tulsi Barot and Meghna Diarsa**

**Table 3: Purification profile of amylase enzyme**

Purification step	Total activity (U/ml)	Total protein (mg/ml)	Specific activity (U/mg)	Purification fold
Crude extract	8329.18	85.65	97.27	1
Ammonium Sulphate Precipitation (60%)	1871.94	15	124.7	1.28
Dialyzed sample	1782.11	12	148.5	1.53







Tulsi Barot and Meghna Diarsa

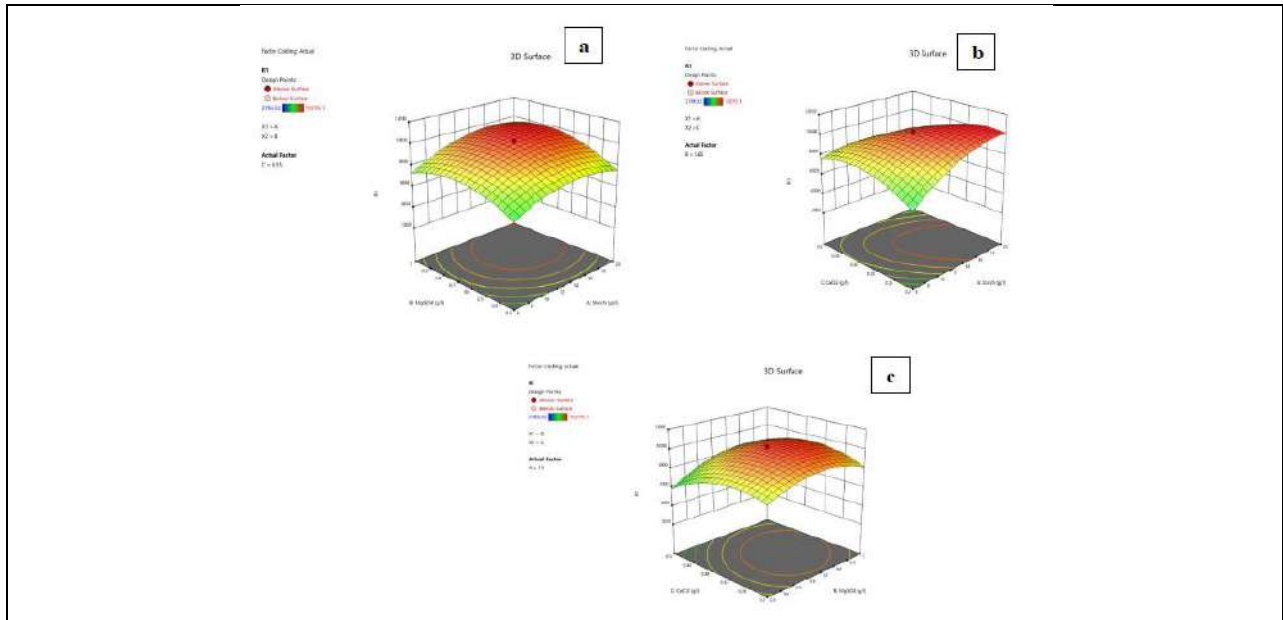


Figure 4. 3 D Plot showing the (a) effect of  $MgSO_4$  and starch, (b)  $CaCl_2$  and starch, (c)  $CaCl_2$  and  $MgSO_4$  on the Production of amylase enzyme.

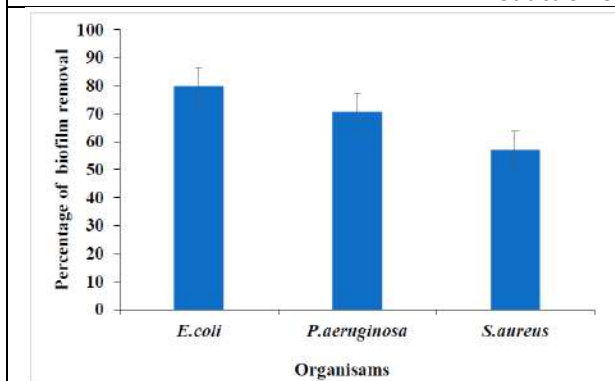


Fig. 5 Biofilm removal by amylase enzyme

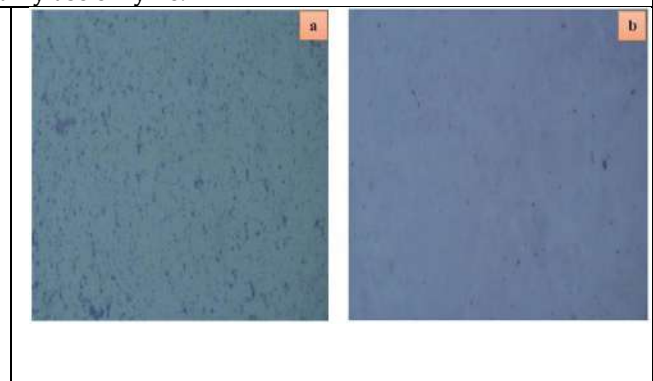


Figure 6. (a) Positive Control of *E. coli*, (b) Biofilm treated by amylase

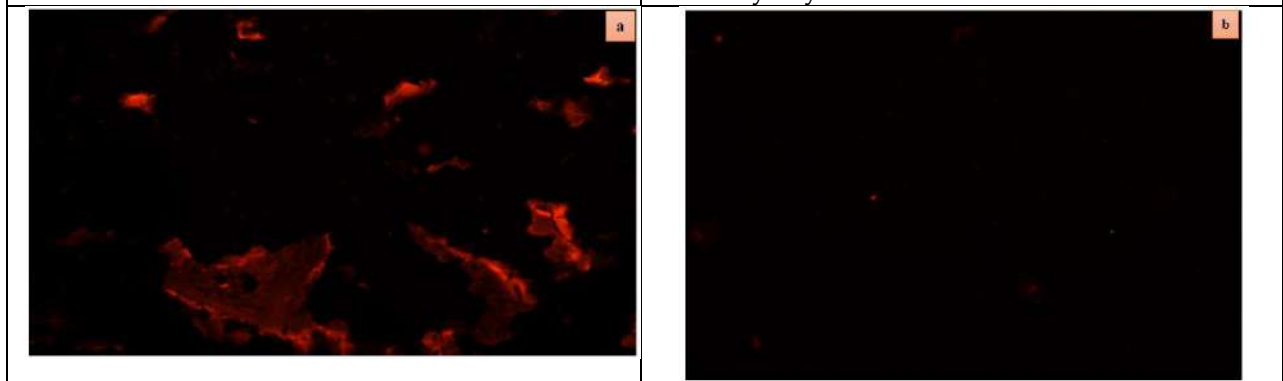


Figure 7. (a) Fluorescence image of biofilm formation by *E. coli*, (b) Fluorescence image of treated biofilm by amylase enzyme.







## Linezolid - Induced Serotonin Syndrome in Clinical Practice: A Comprehensive Review

Vinod Kumar Mugada<sup>1</sup>, Benarjee Veera Mani Kishore Boddeda<sup>2\*</sup> and Vanka Vidhya Sree<sup>3</sup>

<sup>1</sup>Associate Professor, Department of Pharmacy Practice, Vignan Institute of Pharmaceutical Technology, (Affiliated to Jawaharlal Nehru Technological University), Visakhapatnam, Andhra Pradesh, India.

<sup>2</sup>Assistant Professor, Department of Pharmacy Practice, Vignan Institute of Pharmaceutical Technology, (Affiliated to Jawaharlal Nehru Technological University), Visakhapatnam, Andhra Pradesh, India.

<sup>3</sup>Pharm.D Intern, Department of Pharmacy Practice, Vignan Institute of Pharmaceutical Technology, (Affiliated to Jawaharlal Nehru Technological University), Visakhapatnam, Andhra Pradesh, India.

Received: 06 Oct 2024

Revised: 10 Nov 2024

Accepted: 12 Dec 2024

### \*Address for Correspondence

**Benarjee Veera Mani Kishore Boddeda**

Assistant Professor,

Department of Pharmacy Practice,

Vignan Institute of Pharmaceutical Technology,

(Affiliated to Jawaharlal Nehru Technological University),

Visakhapatnam, Andhra Pradesh, India.

E.Mail: kishorebenarjee9@gmail.com



This is an Open Access Journal / article distributed under the terms of the **Creative Commons Attribution License** (CC BY-NC-ND 3.0) which permits unrestricted use, distribution, and reproduction in any medium, provided the original work is properly cited. All rights reserved.

### ABSTRACT

Serotonin syndrome (SS) represents a potentially life-threatening condition often overlooked due to its subtle initial symptoms. Linezolid, a commonly prescribed antibiotic for complex skin infections such as diabetic foot infections, can trigger SS. The syndrome primarily involves the neurotransmitter 5-Hydroxytryptamine (5-HT), commonly known as serotonin, which plays a central role in its pathophysiology. Serotonin synthesis occurs through the decarboxylation and hydroxylation of L-tryptophan. Recent research also highlights the involvement of dopaminergic and noradrenergic systems in SS. Diagnosis typically follows changes in medication or instances of self-poisoning and relies on the Hunter Serotonin Toxicity Criteria (HSTC). These criteria focus on signs of autonomic hyperactivity, mental status changes, and neuromuscular abnormalities. Various drugs and the discontinuation of specific medications can contribute to SS. Among these, linezolid poses a notable risk due to its weak inhibition of monoamine oxidase (MAO). Despite limitations, case reports provide valuable insights into the relationship between linezolid and SS. Prevention requires a comprehensive approach, with prompt drug discontinuation playing a critical role in management. Healthcare providers must recognize the contraindication of linezolid with other MAO inhibitors and remain vigilant for early signs of SS. Management strategies vary, with some cases resolving without intervention. This review highlights the





Vinod Kumar Mugada et al.,

association between linezolid and SS, emphasizing the importance of further research to improve understanding and management of this life-threatening condition.

**Keywords:** Serotonin syndrome, linezolid, 5-Hydroxytryptamine, Hunter Serotonin Toxicity Criteria, monoamine oxidase.

## INTRODUCTION

Serotonin syndrome (SS) is a potentially fatal condition that clinicians often overlook due to its subtle early symptoms. This syndrome is not limited to psychotropic drugs; various substances, including fentanyl, meperidine, ondansetron, ritonavir, sumatriptan, dextromethorphan, and certain herbal products, can also trigger it [1]. Clinicians frequently fail to recognize the wide range of potential triggers, leading to misdiagnosis and underestimation of its severity. Increasing awareness among healthcare professionals about these diverse triggers is essential for early detection and effective management of SS [1]. Linezolid, a commonly prescribed antibiotic for complex skin infections such as diabetic foot infections, is a notable trigger of SS. The risk significantly increases when linezolid, a mild monoamine oxidase inhibitor, is combined with other serotonergic medications. This combination enhances serotonin release, heightening the likelihood of SS [2]. Raising awareness of these risks is critical for improving patient outcomes and preventing severe complications.

### Understanding Serotonin Syndrome: Historical Context and Modern Insights

Serotonin syndrome (SS) is a potentially life-threatening adverse drug reaction that occurs due to inadvertent drug interactions, therapeutic drug use, or intentional self-poisoning [3]. This syndrome results from a predictable excess of serotonergic agonism in the central nervous system (CNS) and peripheral serotonergic receptors, distinguishing it from idiopathic drug reactions [4]. Serotonin toxicity, also known as serotonin syndrome, involves the overactivation of both central postsynaptic and peripheral 5HT-1A and 5HT-2A receptors [5]. Historical and contemporary insights reveal that episodes of "convulsive ergotism," reported between 1085 and 1927 in regions east of the Rhine River, were caused by ergot alkaloids in grains. These alkaloids are now recognized as precursors to serotonin syndrome, suggesting that this condition existed long before its formal identification in modern pharmacology [6]. This historical context highlights the gradual evolution in the understanding of SS.

The neurotransmitter 5-Hydroxytryptamine (5-HT), first identified in 1948, has been central to advancing knowledge about serotonin syndrome [7]. The term "serotonin syndrome" was first introduced in 1980 to describe specific symptoms observed in rats, marking a critical milestone in the clinical recognition of the syndrome [8]. This progression underscores the significance of both historical and modern research in shaping current perspectives on SS.

### Synthesis of Serotonin:

Serotonin synthesizes through the decarboxylation and hydroxylation of L-tryptophan. This process is regulated by metabolizing enzymes, feedback loops, and reuptake mechanisms, ensuring balanced serotonin levels in the body. In serotonin syndrome (SS), several serotonin receptors are involved, with the 5-hydroxytryptamine (5-HT) receptors, particularly the 5-HT<sub>2A</sub> subtype, playing a central role [1]. The 5-HT<sub>1A</sub> receptor also contributes significantly by saturating receptor subtypes, leading to increased synaptic concentrations of serotonin agonists [9, 10]. However, the complexity of SS extends beyond serotonin receptor activity. Emerging research indicates that dopaminergic receptors and noradrenergic hyperactivity in the central nervous system may also influence serotonin production, though their exact roles remain unclear [11]. This underscores the need for further research to better understand the intricate mechanisms of serotonin regulation and its associated disorders.



**Vinod Kumar Mugada et al.,****Diagnosis of Serotonin Syndrome**

Serotonin syndrome (SS) typically presents rapidly following a change in medicine or self-poisoning. In about 60% of cases, symptoms manifest within six hours of initiating a new drug, adjusting dosage, or overdosing, highlighting the syndrome's rapid onset [12]. Crucial for diagnosis are key neuromuscular symptoms, which include various forms of clonus, myoclonus, hyperreflexia, incoordination, peripheral hypertonicity, tremor, and shivering. These symptoms are central to identifying the syndrome [9, 10, 13-19]. Additionally, other clinical signs such as tachycardia, mydriasis, diaphoresis, hyperactive bowel sounds, diarrhea, agitation, and delirium are associated with serotonin syndrome, further complicating its clinical presentation [9, 12-16].

The diagnosis of serotonin syndrome (SS) relies on three primary classification systems: the Sternbach Criteria (SC), the Radomski Criteria (RC), and the Hunter Serotonin Toxicity Criteria (HSTC). Each system aims to identify characteristic symptoms and patterns associated with serotonin toxicity [13]. Among these, the HSTC is the most widely used. It focuses on classic features such as generalized clonus (inducible, ocular, and spontaneous), diaphoresis, agitation, tremor, and hyperreflexia. These criteria highlight the importance of specific symptoms in diagnosing the condition [13]. Spontaneous clonus, which involves rhythmic large muscle contractions, differs from myoclonic jerks and is typically triggered by minor movements, adding complexity to the diagnostic process [18]. Ocular clonus, characterized by involuntary, oscillatory eye movements, may occur continuously or be induced by eye movement. Additionally, rarer eye movements, such as the regular alternating gaze deviation known as "ping-pong" gaze, also contribute to the diagnostic framework for SS [18]. These features underscore the nuanced clinical presentation of SS and the importance of thorough assessment for accurate diagnosis.

**Recognizing Signs, Symptoms, and Severity of Serotonin Syndrome**

Serotonin syndrome (SS) typically manifests as a clinical triad of mental-status changes, neuromuscular abnormalities, and autonomic hyperactivity, although not all these features are consistently present in every patient (20). The severity of SS varies, ranging from mild to life-threatening forms. In mild cases, patients may experience tremors or muscle twitching, anxiety, hyperreflexia, tachycardia, diaphoresis, and mydriasis, often associated with recent use of antidepressants or over-the-counter medications containing dextromethorphan (21). Moderate toxicity causes significant distress, with symptoms such as restlessness, agitation, clonus in the lower extremities, hyperreflexia, opsoclonus, diarrhea, hyperactive bowel sounds, nausea, vomiting, tachycardia, hypertension, hyperthermia (below 40°C or 104°F), and mydriasis. This presentation frequently follows the use of substances like ecstasy or combinations of serotonin-potentiating agents, including antidepressants, proserotonergic opioids, antiepileptics, or CYP2D6 and CYP3A4 inhibitors (22). Severe toxicity, a life-threatening condition, can lead to multiorgan failure within hours. Muscle rigidity significantly elevates body temperature above 40°C, potentially masking typical signs such as clonus and hyperreflexia. Patients often exhibit unstable delirium, confusion, tonic-clonic seizures, and erratic vital signs. Without timely intervention to manage muscle rigidity and hyperthermia, complications like myoglobinuria, rhabdomyolysis, metabolic acidosis, renal failure, disseminated intravascular coagulation, and acute respiratory distress syndrome may develop, further increasing the risk of mortality (23).

**Drug Related Causes of Serotonin Syndrome**

A wide range of drugs and drug combinations is associated with serotonin syndrome (SS), spanning several categories. These include tricyclic antidepressants, monoamine oxidase inhibitors (MAOIs), selective serotonin reuptake inhibitors (SSRIs), and opioid analgesics. Over-the-counter cough medications, certain antibiotics, weight-loss agents, antiemetic drugs, antimigraine agents, substances of abuse, and herbal products are also implicated. Notably, the onset of SS can result not only from the use of specific medications but also from their cessation [24-26]. Drugs that inhibit serotonin breakdown represent a significant category of SS triggers. This group includes MAOIs, linezolid [27], procarbazine, methylene blue, and Syrian Rue. Another critical category consists of drugs that block serotonin reuptake, such as serotonin-norepinephrine reuptake inhibitors (SNRIs), SSRIs, tricyclic antidepressants, and opioids like meperidine, tramadol, buprenorphine, dextromethorphan, and tapentadol. Certain antiepileptic drugs, including valproate and carbamazepine, and antiemetic medications such as granisetron, ondansetron, and metoclopramide, along with the herbal supplement St. John's Wort, also belong to this category.



**Vinod Kumar Mugada et al.,**

Drugs that increase serotonin precursors or act as agonists further contribute to SS. Examples include lithium, tryptophan, fentanyl, and lysergic acid diethylamide (LSD). Similarly, agents that enhance serotonin release, such as amphetamines, fenfluramine, and methylenedioxymethamphetamine (ecstasy), play a role in the syndrome's development. Additionally, inhibitors of CYP2D6 and CYP3A4 enzymes, including erythromycin [25], ciprofloxacin, ritonavir, fluconazole, and grapefruit juice, can prevent the breakdown of serotonergic agents, exacerbating the risk of SS. However, it is important to note that only MAOIs, SSRIs, SNRIs, and serotonin releasers are reliably confirmed as direct causes of SS. Other drug interactions, although documented in case reports, require further comprehensive evaluation to establish their role in SS [28, 29].

**Linezolid and its clinical implications**

Oxazolidinones, first discovered and developed in the 1970s, were originally intended for treating plant diseases [30]. This class of compounds achieved a significant milestone with the development of linezolid. Approved by the Food and Drug Administration (FDA) in 2000, linezolid became the first oxazolidinone antibiotic authorized for human use, marking a pivotal advancement in antibiotic therapy [31]. The FDA approval of linezolid includes indications for treating complicated and uncomplicated skin and skin-structure infections, nosocomial pneumonia, and community-acquired pneumonia. It is also effective against infections caused by methicillin-resistant *Staphylococcus aureus* (MRSA) and vancomycin-resistant enterococci (VRE) [32].

Registry trials closely examine linezolid's safety profile. The most commonly reported adverse effects include nausea, headache, diarrhea, vomiting, and myelosuppression, such as thrombocytopenia, anemia, and leukopenia, which are associated with prolonged use. However, serious adverse effects are rare and do not significantly differ from those observed in comparison groups [33]. Linezolid acts by binding to the bacterial 23S ribosomal RNA of the 50S subunit, preventing the formation of a functional 70S initiation complex [34]. This mechanism inhibits the initiation of protein synthesis, reducing the length of peptide chains and slowing the translation process. As a synthetic antibiotic, linezolid specifically blocks bacterial protein synthesis [35]. Its mechanism of action occurs at the initiation stage, unlike other protein synthesis inhibitors that target the elongation phase. Due to this unique site of action, cross-resistance with other protein synthesis inhibitors has not been observed [36].

**Potential Risk of Serotonin Syndrome with Linezolid**

Linezolid, an oxazolidinone antimicrobial approved by the FDA in 2000, is widely used to treat complex infections caused by drug-resistant gram-positive cocci, including vancomycin-resistant *Enterococcus* and methicillin-resistant *Staphylococcus aureus*. Initial studies reported no cases of serotonin toxicity; however, post-marketing reports document serotonin toxicity when linezolid is combined with serotonergic agents [37]. Before FDA approval, research identified linezolid as a weak competitive (reversible) inhibitor of monoamine oxidase (MAO), an enzyme that deactivates neurotransmitters like serotonin, epinephrine, norepinephrine, and dopamine [38]. This raised concerns about the potential for serotonin syndrome when linezolid is used with serotonergic agents. Despite these concerns, clinical trials did not observe clinical evidence of MAO A inhibition [39]. Post-approval reports, however, highlight emerging cases of serotonin toxicity [40].

In response, the FDA issued a warning in 2011 about the potential for serotonin toxicity when linezolid is co-administered with serotonergic psychiatric medications. This warning is based on case reports and data from the FDA Adverse Event Reporting System (AERS) [41]. Lawrence et al. [42] analyzed post-marketing reports from AERS and identified 29 cases of linezolid-associated serotonin toxicity, with three meeting the Hunter Serotonin Toxicity Criteria (HSTC). Most cases involved selective serotonin reuptake inhibitors (SSRIs), affecting patients aged 17 to 83 years. This finding aligns with a review by Boyer and Shannon [1], which highlighted a potential drug interaction between ritonavir and linezolid, although no definitive case reports have directly linked these two agents to serotonin syndrome.

The variability in AERS reports is significant, with consumer submissions accounting for nearly half of all reports in 2010, totaling 403,746 cases [43]. Given that both consumers and healthcare providers contribute to the AERS, reports





Vinod Kumar Mugada et al.,

may be incomplete or inaccurate, underscoring the need for careful evaluation. Reflecting these concerns, the FDA issued a MedWatch Safety Alert in July 2011, warning of severe central nervous system reactions when linezolid is combined with serotonergic psychiatric medications. As a result, safety warnings about serotonin toxicity were added to the labels of linezolid and serotonergic drugs [37]. In October 2011, the FDA further advised against using linezolid in patients taking serotonergic medications unless the benefit outweighs the risk. Clinical research supports these regulatory actions. Woytowish and Maynor [44] identified 32 cases of linezolid-associated serotonin toxicity, including three fatalities, in a literature review. Most cases involved SSRIs, with symptom onset and resolution varying from hours to days. Despite these reports, they concluded that serotonin toxicity with linezolid is rare. A 2012 retrospective analysis of Phase 3 and 4 clinical trials involving approximately 4,000 patients found no serotonin toxicity cases among those using linezolid or comparators with serotonergic agents [38]. This suggests that while a risk exists, the incidence is low.

Further studies corroborate these findings. Go et al. [45] conducted a retrospective analysis at the University of Colorado Hospital, examining serotonin toxicity in hospitalized patients receiving linezolid with escitalopram or citalopram. They reported only one mild case, suggesting severe reactions are uncommon. Similarly, Lorenz et al. [46] reviewed serotonin toxicity in patients on linezolid with SSRIs or serotonin-norepinephrine reuptake inhibitors (SNRIs). Only 1.9% of patients met HSTC criteria, reinforcing the rarity of severe cases. Taylor et al. [47] also reviewed cases of patients on linezolid and serotonergic agents, finding that only 2.8% had a high probability of serotonin toxicity. Despite these findings, caution remains critical. Lodise et al. [48] argue that serotonin toxicity should not prevent linezolid use in patients taking serotonergic drugs, as no increased risk is observed compared to vancomycin. Similarly, Packer and Berman [49] report that combining linezolid with antidepressants is not contraindicated, although antidepressants may be withdrawn in certain cases. However, the FDA continues to receive reports of serotonin syndrome linked to the combined use of linezolid and serotonergic medications, including fatal cases [50]. Based on this evidence, the FDA concludes that this drug interaction is likely, particularly when long-half-life serotonergic medications are discontinued. Therefore, linezolid should generally not be prescribed to patients on serotonergic drugs unless the benefits outweigh the risks [51].

#### **Incidence of Serotonin Toxicity in Patients Treated with Linezolid: Real life cases and research**

Case reports provide critical details such as patient gender, age, complete medication regimens, time to diagnosis, and resolution of serotonin toxicity. Retrospective and prospective studies further contribute data, focusing on methodology, participant numbers, diagnostic criteria for serotonin toxicity, associated serotonergic agents, and the duration of linezolid therapy [40]. Randomized controlled trials (RCTs) report no cases of linezolid-induced serotonin toxicity, but smaller retrospective and observational studies document its occurrence. The incidence of serotonin toxicity among patients treated with linezolid alone is 0.005%, compared to 0.0134% in those receiving linezolid in combination with other therapies. While this suggests a modest increase in risk with combination therapy, the overall incidence remains low [40]. A single-center, retrospective cohort study conducted between January 1, 2014, and June 30, 2021, examines hospitalized patients aged 18 years and older who received at least one dose of linezolid, with or without serotonergic agents [59].

Previous retrospective cohort studies report varying incidences of serotonin toxicity, ranging from 0.54% to 18.2%, in patients receiving linezolid alongside serotonin reuptake inhibitors (SRIs) or serotonin-norepinephrine reuptake inhibitors (SNRIs) [38, 44, 46, 47, 60]. Given the variability in these findings and limitations in sample sizes, contemporary data is necessary to confirm the rarity of serotonin toxicity. A recent study involving 1,743 patients treated with linezolid, with or without serotonergic agents, provides important insights. Among this cohort, 67% (1,168/1,743) were on more than one serotonergic agent, with 52.7% (616/1,168) receiving moderate to high doses. Despite this potentially high-risk population, the incidence of serotonin toxicity remains low: 0.06% (1/1,743) based on the Sternbach Criteria and 0% (0/1,743) based on the Hunter Criteria, which is more accurate for diagnosis [13, 61]. In cases like Patient B, where serotonin toxicity is unlikely, linezolid's role is minimal, as symptoms appeared 16 days after discontinuation [59].





**Vinod Kumar Mugada et al.,**

Analysis of the FDA Adverse Event Reporting System (AERS) highlights the prevalence of serotonin toxicity when linezolid is combined with serotonergic agents [42]. Notably, 69% of published cases involve selective serotonin reuptake inhibitors (SSRIs), with citalopram being the most frequently implicated agent in eight cases. Other commonly associated agents include sertraline and venlafaxine, each linked to seven cases. These reports involve linezolid either alone or in combination with additional serotonergic agents. Fluoxetine is implicated in three cases, one of which occurred despite discontinuation 18 days before linezolid administration. Meperidine is associated with three cases of serotonin toxicity, while paroxetine, escitalopram, tramadol, and duloxetine are each linked to two cases. Half of the 32 patients in these reports received more than one serotonergic agent, highlighting the complexity of drug interactions in serotonin toxicity [45-47, 50, 62-69].

**Prevention and safety measures**

Preventing serotonin syndrome requires a multifaceted approach that includes pharmacogenomic research, physician education, changes in prescribing practices, and technological advancements. Pharmacogenomic principles may help identify patients at risk for serotonin syndrome before administering serotonergic agents [52]. When toxicity occurs, consulting a clinical pharmacology service, medical toxicologist, or poison-control center can help identify proserotonergic agents and drug interactions. These resources provide valuable insights into anticipating adverse effects and assist clinicians in making informed decisions [52]. Avoiding multidrug regimens is critical in preventing serotonin syndrome. When multiple agents are necessary, tools such as personal digital assistants and computer-based ordering systems can detect drug interactions and reduce reliance on memory during prescribing. Additionally, post-marketing surveillance and physician education increase awareness of serotonin syndrome [52]. When serotonin syndrome occurs, prompt discontinuation of the causative drugs is essential for management. Administering 5-hydroxytryptamine antagonists, such as cyproheptadine, is recommended, with therapeutic doses for adults ranging from 12–32 mg over 24 hours, binding 85%–95% of serotonin receptors [53]. Benzodiazepines can be used to manage agitation, while supportive care remains central to controlling autonomic instability and hyperthermia [53]. This approach emphasizes the importance of immediate and targeted interventions in managing serotonin syndrome.

To reduce the risk of serotonin syndrome during medication transitions, adhering to appropriate washout periods is critical [54, 55]. These periods vary based on the half-life of medications and are necessary to prevent overlapping effects of serotonergic agents. For example, sertraline requires a two-week washout period, while fluoxetine requires 5 to 6 weeks [56]. Consulting pharmacists can help navigate these complexities, highlighting the value of interdisciplinary collaboration in medication management. Patient education on dietary restrictions is also essential, particularly when prescribing medications such as linezolid that interact with dietary tyramine. Patients should avoid tyramine-rich foods and beverages, as consuming large quantities can cause severe hypertensive reactions in individuals taking strong MAO inhibitors [57]. Examples of these foods include aged cheeses, cured meats, and certain liquors such as vermouth. Patients should also limit red and white wine consumption to no more than 120 ml per meal. This guidance is based on findings that systolic blood pressure rises significantly when linezolid is coadministered with 100 mg or more of tyramine [58]. These precautions emphasize the importance of dietary considerations in ensuring medication safety.

**Guidelines for Healthcare Providers**

Linezolid, a reversible monoamine oxidase inhibitor (MAOI), is contraindicated with other MAOIs such as phenelzine, moclobemide, and selegiline, or if these agents have been used within the preceding two weeks [70]. The Summary of Product Characteristics (SPC) recommends caution when prescribing linezolid to patients with certain clinical conditions or those on specific medications. These conditions include uncontrolled hypertension, carcinoid, thyrotoxicosis, pheochromocytoma, schizoaffective disorder, bipolar depression, and acute confusional states. Patients taking medications such as serotonin reuptake inhibitors, tricyclic antidepressants, serotonin 5-HT<sub>1</sub> receptor agonists (triptans), sympathomimetic agents (e.g., pseudoephedrine, adrenergic bronchodilators, phenylpropranolamine), vasopressive agents (e.g., norepinephrine, epinephrine), dopaminergic agents (e.g., dopamine, dobutamine), opioid analgesics (e.g., pethidine, methadone, tramadol, dextromethorphan), or buspirone





**Vinod Kumar Mugada et al.,**

should be closely monitored when linezolid is prescribed [70]. Healthcare providers must watch for signs of serotonin syndrome, including hypertension, tachycardia, cognitive dysfunction, hyperpyrexia, hyperreflexia, and incoordination. Rifampicin, which reduces linezolid concentrations by 30% due to the induction of the p-glycoprotein transporter, should be avoided. Rifampicin co-administration is not recommended, and it should be discontinued at least two weeks before initiating linezolid therapy [70].

**Communicating the Risks**

Patients should be informed about potential side effects of linezolid, such as dizziness and visual impairments, and advised not to drive or operate machinery if these occur. Any visual disturbances should be immediately reported to their healthcare provider. Patients should also exercise caution with their diet. Foods rich in tyramine, such as aged cheese, yeast extracts, soybean extracts, draft beers, and wine, should be minimized. Additionally, over-the-counter medications, including decongestant cold and flu remedies, should only be taken after consulting a healthcare provider to prevent unintended interactions [70].

**Educating Patients**

Patients should be made aware that serotonin syndrome is a potentially life-threatening condition that can occur with linezolid. Symptoms include agitation, confusion, rapid heartbeat, high blood pressure, muscle rigidity, sweating, fever, diarrhea, and hallucinations. Patients must seek immediate medical attention if they experience any of these symptoms. The risk increases when linezolid is combined with serotonergic medications, such as selective serotonin reuptake inhibitors (SSRIs), serotonin-norepinephrine reuptake inhibitors (SNRIs), or triptans for migraines. Patients should disclose all medications, including supplements and over-the-counter drugs, to their healthcare provider to avoid harmful interactions [51]. Patients should not adjust their medication regimen, including dosages, without consulting their healthcare provider. Promptly reporting symptoms of serotonin syndrome improves prognosis. Healthcare providers should monitor patients closely when linezolid is combined with serotonergic drugs. If necessary, alternative treatments should be considered, and patients should discuss these options with their provider [51]. Effective risk management requires clear communication and strict adherence to prescribed medication regimens [51].

**Management of Serotonin Syndrome: Case Studies and Therapeutic Approaches**

In many cases, serotonin syndrome resolves with simple interventions, such as discontinuation of the causative drug or adjustments to antibiotic therapy. However, some cases require specific therapeutic interventions, including the management of hypertension, cholinergic symptoms, and fever, alongside addressing underlying psychiatric conditions. Such treatments can increase healthcare costs and prolong hospital stays. In four cases, serotonin syndrome caused hypertension requiring treatment [63, 71, 72]. One case involved a woman with a blood pressure of 150/90 mm Hg, who required monitoring [71]. Other patients, including a 37-year-old man and a 56-year-old woman, were treated with oral  $\beta$ -blockers such as bisoprolol and propranolol [63, 71]. In one instance, the details of the antihypertensive medication used remain unspecified [72]. Two patients with severe hypertension required a combination of three antihypertensive therapies [63]. One of these patients, a 56-year-old woman, also received cyproheptadine to manage serotonin syndrome-related tremors and weakness.

Other treatments included anticholinergic and psychotropic medications. For example, a pediatric patient received diphenhydramine after discontinuing fluoxetine to alleviate clonic movements, agitation, and mydriasis [73]. Managing anxiety was another critical aspect. A male patient experienced severe anxiety after stopping mirtazapine and benefited from short-term benzodiazepine therapy [74]. Another male patient was readmitted due to hypertension, panic attacks, and anxiety. In his case, linezolid was discontinued a day early, and his olanzapine dosage was increased, along with the addition of methotrimeprazine, a phenothiazine antipsychotic [71].

**Significance of the review**

This review article provides essential insights for healthcare professionals by addressing Serotonin Syndrome (SS), a critical yet frequently overlooked medical condition. It focuses specifically on drug-induced SS, with an emphasis on



**Vinod Kumar Mugada et al.,**

its association with the antibiotic linezolid. The review also offers practical guidelines for the safe use of linezolid, ensuring that healthcare providers can mitigate risks effectively. Additionally, it incorporates case studies that serve as valuable educational resources.

## CONCLUSION

This review highlights the link between linezolid use and serotonin syndrome (SS), emphasizing its risks when combined with serotonergic drugs. It underscores the need for ongoing research into linezolid's mechanisms, genetic predispositions, and prevention strategies. Recommendations include enhancing healthcare provider education, improving diagnostic tools, fostering interdisciplinary collaboration, and increasing patient awareness. Advancing pharmacovigilance systems and reporting adverse drug reactions are also crucial for reducing SS risk and improving patient safety and outcomes.

## REFERENCES

1. Boyer EW, Shannon M. The serotonin syndrome. *N Engl J Med.* 2005;352(11):1112–20. <https://doi.org/10.1056/nejmra041867>
2. Frykberg RG, Gordon SM, Tierney EF, Banks JF. Linezolid-associated serotonin syndrome. *J Am Podiatr Med Assoc.* 2015;105(3):244–8. <https://doi.org/10.7547/0003-0538-105.3.244>
3. Francescangeli J, Karamchandani K, Powell M, Bonavia A. The serotonin syndrome: From molecular mechanisms to clinical practice. *Int J Mol Sci.* 2019;20(9):2288. <https://doi.org/10.3390/ijms20092288>
4. Srivastava A, Singh P, Gupta H, Kaur H, Kanojia N, Guin D, et al. Systems approach to identify common genes and pathways associated with response to selective serotonin reuptake inhibitors and major depression risk. *Int J Mol Sci.* 2019;20(8):1993. <https://doi.org/10.3390/ijms20081993>
5. Volpi-Abadie J, Kaye AM, Kaye AD. Serotonin syndrome. *Ochsner J.* 2013;13(4):533–40. <https://pubmed.ncbi.nlm.nih.gov/24358002/>
6. Eadie MJ. Convulsive ergotism: epidemics of the serotonin syndrome? *Lancet Neurol.* 2003;2(7):429–34. [https://doi.org/10.1016/s1474-4422\(03\)00439-3](https://doi.org/10.1016/s1474-4422(03)00439-3)
7. Rapport MM, Green AA, Page IH. Serum vasoconstrictor, serotonin; isolation and characterization. *J Biol Chem.* 1948;176(3):1243–51. <https://pubmed.ncbi.nlm.nih.gov/18100415/>
8. Gerson S, Baldessarini RJ. Motor effects of serotonin in the central nervous system. *Life Sci.* 1980;27(16):1435–51. [https://doi.org/10.1016/0024-3205\(80\)90368-9](https://doi.org/10.1016/0024-3205(80)90368-9)
9. Mills KC. Serotonin syndrome. *Am Fam Physician.* 1995;52(5):1475–82. <https://pubmed.ncbi.nlm.nih.gov/7572570/>
10. Birmes P, Coppin D, Schmitt L, Lauque D. Serotonin syndrome: a brief review. *CMAJ.* 2003;168(11):1439–42. <https://pubmed.ncbi.nlm.nih.gov/12771076/>
11. Scotton WJ, Hill LJ, Williams AC, Barnes NM. Serotonin syndrome: pathophysiology, clinical features, management, and potential future directions. *Int J Tryptophan Res.* 2019;12. <https://journals.sagepub.com/doi/10.1177/1178646919873925>
12. Mason P, Morris VA, Balcezak TJ. Serotonin syndrome: Presentation of 2 cases and review of the literature. *Medicine.* 2000;79(4):201–9. <https://doi.org/10.1097/00005792-200007000-00001>
13. Dunkley EJC, Isbister GK, Sibbritt D, Dawson A, Whyte IM. The Hunter serotonin toxicity criteria: simple and accurate diagnostic decision rules for serotonin toxicity. *QJM.* 2003;96(9):635–42. <https://doi.org/10.1093/qjmed/hcg109>
14. Sternbach H. The serotonin syndrome. *Am J Psychiatry.* 1991;148(6):705–13. <https://doi.org/10.1176/ajp.148.6.705>
15. Gillman PK. The serotonin syndrome and its treatment. *J Psychopharmacol.* 1999;13(1):100–9. <https://doi.org/10.1177/026988119901300111>
16. Bijl D. The serotonin syndrome. *Neth J Med.* 2004;62(9):309–13. <https://pubmed.ncbi.nlm.nih.gov/15635814/>
17. Gillman PK. Comment on: Serotonin syndrome due to co-administration of linezolid and venlafaxine. *J Antimicrob Chemother.* 2004;54(4):844–5. <https://doi.org/10.1093/jac/dkh404>



**Vinod Kumar Mugada et al.,**

18. Buckley NA, Dawson A, Isbister GK. Serotonin syndrome. *BMJ*. 2014;348:feb19 6:g1626. <https://doi.org/10.1136/bmj.g1626>
19. Bodner RA, Lynch T, Lewis L, Kahn D. Serotonin syndrome. *Neurology*. 1995;45(2):219–23. <https://doi.org/10.1212/wnl.45.2.219>
20. Sampson E, Warner JP. Serotonin syndrome: potentially fatal but difficult to recognize. *Br J Gen Pract*. 1999;49(448):867–8. <https://pubmed.ncbi.nlm.nih.gov/10818648/>
21. Prakash S, Patel VJ, Kakked S, Patel I, Yadav R. Mild serotonin syndrome: A report of 12 cases. *Ann Indian Acad Neurol*. 2015;18(2):226. <https://doi.org/10.4103/0972-2327.150612>
22. Iqbal MM, Basil MJ, Kaplan J, Iqbal MT. Overview of serotonin syndrome. *Ann Clin Psychiatry*. 2012;24(4):310–8. <https://pubmed.ncbi.nlm.nih.gov/23145389/>
23. Davies O, Batajoo-Shrestha B, Sosa-Popoteur J, Olibrice M. Full recovery after severe serotonin syndrome, severe rhabdomyolysis, multi-organ failure, and disseminated intravascular coagulopathy from MDMA. *Heart Lung*. 2014;43(2):117–9. <https://doi.org/10.1016/j.hrtlng.2013.11.009>
24. Laine K, Heikkinen T, Ekblad U, Kero P. Effects of exposure to selective serotonin reuptake inhibitors during pregnancy on serotonergic symptoms in newborns and cord blood monoamine and prolactin concentrations. *Arch Gen Psychiatry*. 2003;60(7):720–6. <https://doi.org/10.1001/archpsyc.60.7.720>
25. Lee DO, Lee CD. Serotonin syndrome in a child associated with erythromycin and sertraline. *Pharmacotherapy*. 1999;19(7):894–6. <https://doi.org/10.1592/phco.19.10.894.31561>
26. DeSilva KE, Le Flore DB, Marston BJ, Rimland D. Serotonin syndrome in HIV-infected individuals receiving antiretroviral therapy and fluoxetine. *AIDS*. 2001;15(10):1281–5. <https://doi.org/10.1097/00002030-200107060-00010>
27. Bai AD, McKenna S, Wise H, Loeb M, Gill SS. Association of linezolid with risk of serotonin syndrome in patients receiving antidepressants. *JAMA Netw Open*. 2022;5(12):e2247426. <https://doi.org/10.1001/jamanetworkopen.2022.47426>
28. Gillman PK. Triptans, serotonin agonists, and serotonin syndrome (serotonin toxicity): A review. *Headache*. 2010;50(2):264–72. <https://doi.org/10.1111/j.1526-4610.2009.01575.x>
29. Isbister GK, Buckley NA, Whyte IM. Serotonin toxicity: a practical approach to diagnosis and treatment. *Med J Aust*. 2007;187(6):361–5. <https://doi.org/10.5694/j.1326-5377.2007.tb01282.x>
30. Diekema DJ, Jones RN. Oxazolidinone antibiotics. *Lancet*. 2001;358(9297):1975–82. [https://doi.org/10.1016/s0140-6736\(01\)06964-1](https://doi.org/10.1016/s0140-6736(01)06964-1)
31. Reza M, Farhadi T, Ganjparvar M. Linezolid: a review of its properties, function, and use in critical care. *Drug Des Devel Ther*. 2018;12:1759–67. <https://doi.org/10.2147/dddt.s164515>
32. Pfizer Medical Information - US. ZYVOX® Highlights (linezolid). 2023. Available from: <https://www.pfizermedicalinformation.com/en-us/zyvox/highlights>
33. Rubinstein E, Isturiz R, Standiford HC, Smith LG, Oliphant TH, Cammarata S, et al. Worldwide assessment of linezolid's clinical safety and tolerability: comparator-controlled phase III studies. *Antimicrob Agents Chemother*. 2003;47(6):1824–31. <https://doi.org/10.1128/aac.47.6.1824-1831.2003>
34. Diekema DJ, Jones RN. Oxazolidinones. *Drugs*. 2000;59(1):7–16. <https://doi.org/10.2165/00003495-200059010-00002>
35. Batts DH. Linezolid—a new option for treating gram-positive infections. *Oncol Williston Park*. 2000;14(8 Suppl 6):23–9. <https://pubmed.ncbi.nlm.nih.gov/10989821/>
36. Ament PW, Jamshed N, Horne JP. Linezolid: its role in the treatment of gram-positive, drug-resistant bacterial infections. *Am Fam Physician*. 2002;65(4):663–70. <https://pubmed.ncbi.nlm.nih.gov/11871684/>
37. Pfizer. ZYVOX® | Pfizer. 2023. Available from: <https://www.pfizer.com/products/product-detail/zyvox>
38. Butterfield JM, Lawrence K, Reisman A, Huang DB, Thompson CA, Lodise TP. Comparison of serotonin toxicity with concomitant use of either linezolid or comparators and serotonergic agents: an analysis of Phase III and IV randomized clinical trial data. *J Antimicrob Chemother*. 2012;67(2):494–502. <https://doi.org/10.1093/jac/dkr467>
39. Lawrence L, Pucci MJ, Frosco M, Barrett J. 39th Interscience Conference on Antimicrobial Agents and Chemotherapy of the American Society for Microbiology. *Expert Opin Investig Drugs*. 1999;8(12):2201–3. <https://doi.org/10.1517/13543784.8.12.2201>
40. Elbarbry F, Moshirian N. Linezolid-associated serotonin toxicity: a systematic review. *Eur J Clin Pharmacol*. 2023;79(7):875–83. <https://doi.org/10.1007/s00228-023-03500-9>





## Vinod Kumar Mugada et al.,

41. Kesselheim AS, Sinha MS, Campbell EG, Schneeweiss S, Rausch P, Lappin BM, et al. Multimodal analysis of FDA drug safety communications: lessons from zolpidem. *Drug Saf.* 2019;42(11):1287–95. <https://doi.org/10.1007/s40264-019-00849-8>
42. Lawrence K, Adra M, Gillman PK. Serotonin toxicity associated with the use of linezolid: a review of postmarketing data. *Clin Infect Dis.* 2006;42(11):1578–83. <https://doi.org/10.1086/503839>
43. Center. FDA Adverse Event Reporting System (FAERS) Public Dashboard. U.S. Food and Drug Administration. 2021. Available from: <https://www.fda.gov/drugs/questions-and-answers-fdas-adverse-event-reporting-system-faers/fda-adverse-event-reporting-system-faers-public-dashboard>
44. Woytowish M, Maynor L. Clinical relevance of linezolid-associated serotonin toxicity. *Ann Pharmacother.* 2013;47(3):388–97. <https://doi.org/10.1345/aph.1r386>
45. Go AC, Golightly LK, Barber GR, Barron MA. Linezolid interaction with serotonin reuptake inhibitors: report of two cases and incidence assessment. *Drug Metab Drug Interact.* 2010;25(1–4):41–7. <https://doi.org/10.1515/dmdi.2010.001>
46. Lorenz RA, VandenBerg A, Canepa EA. Serotonergic antidepressants and linezolid: a retrospective chart review and presentation of cases. *Int J Psychiatry Med.* 2008;38(1):81–90. <https://doi.org/10.2190/pm.38.1.h>
47. Taylor J, Wilson JW, Estes LL. Linezolid and serotonergic drug interactions: a retrospective survey. *Clin Infect Dis.* 2006;43(2):180–7. <https://doi.org/10.1086/504809>
48. Lodise TP, Patel N, Rivera AR, Tristani L, Lazariu V, VanDeWall H, et al. Comparative evaluation of serotonin toxicity among veterans affairs patients receiving linezolid and vancomycin. *Antimicrob Agents Chemother.* 2013;57(12):5901–11. <https://doi.org/10.1128/aac.00921-13>
49. Packer S, Berman S. Serotonin syndrome precipitated by the monoamine oxidase inhibitor linezolid. *Am J Psychiatry.* 2007;164(2):346–7. <https://doi.org/10.1176/ajp.2007.164.2.346b>
50. Clark DB, Andrus MR, Byrd DC. Drug interactions between linezolid and selective serotonin reuptake inhibitors: case report involving sertraline and review of the literature. *Pharmacotherapy.* 2006;26(2):269–76. <https://doi.org/10.1592/phco.26.2.269>
51. Center. Drug interaction between linezolid and serotonergic psychiatric medications. U.S. Food and Drug Administration. 2019. Available from: <https://www.fda.gov/drugs/drug-safety-and-availability/fda-drug-safety-communication-updated-information-about-drug-interaction-between-linezolid-zyvox-and>
52. Mackay FJ, Dunn NR, Mann RD. Antidepressants and the serotonin syndrome in general practice. *Br J Gen Pract.* 1999;49(448):871–4. <https://pubmed.ncbi.nlm.nih.gov/10818650/>
53. Bernard L, Stern R, Lew DP, Hoffmeyer P. Serotonin syndrome after concomitant treatment with linezolid and citalopram. *Clin Infect Dis.* 2003;36(9):1197. <https://doi.org/10.1086/374558>
54. Mason P, Morris VA, Balczak TJ. Serotonin syndrome presentation of 2 cases and review of the literature. *Medicine.* 2000;79(4):201–9. <https://doi.org/10.1097/00005792-200007000-00001>
55. Caughey GE, Roughhead EE, Shakib S, McDermott R, Vitry A, Gilbert AL. Comorbidity of chronic disease and potential treatment conflicts in older people dispensed antidepressants. *Age Ageing.* 2010;39(4):488–94. <https://doi.org/10.1093/ageing/afq055>
56. Gury C, Cousin F. Pharmacokinetics of SSRI antidepressants: half-life and clinical applicability [Pharmacocinétique des ISRS: notion de demi-vie d'élimination et implications cliniques]. *L'Encephale.* 1999;25(5):470–6. <https://pubmed.ncbi.nlm.nih.gov/10598311/>
57. McCabe BJ. Dietary tyramine and other pressor amines in MAOI regimens: a review. *J Am Diet Assoc.* 2023;86(8). <https://pubmed.ncbi.nlm.nih.gov/3525654/>
58. Huang V, Gortney JS. Risk of serotonin syndrome with concomitant administration of linezolid and serotonin agonists. *Pharmacotherapy.* 2006;26(12):1784–93. <https://doi.org/10.1592/phco.26.12.1784>
59. Kufel WD, Parsels KA, Blaine BE, Steele JM, Seabury RW, Asiago-Reddy EA. Real-world evaluation of linezolid-associated serotonin toxicity with and without concurrent serotonergic agents. *Int J Antimicrob Agents.* 2023;62(1):106843. <https://doi.org/10.1016/j.ijantimicag.2023.106843>
60. Karkow DC, Kauer JF, Ernst EJ. Incidence of serotonin syndrome with combined use of linezolid and serotonin reuptake inhibitors compared with linezolid monotherapy. *J Clin Psychopharmacol.* 2017;37(5):518–23. <https://doi.org/10.1097/jcp.0000000000000751>





**Vinod Kumar Mugada et al.,**

61. Chiew AL, Buckley NA. The serotonin toxidrome: shortfalls of current diagnostic criteria for related syndromes. *Clin Toxicol.* 2021;60(2):143–58. <https://doi.org/10.1080/15563650.2021.1993242>
62. Morales N, Vermette H. Serotonin syndrome associated with linezolid treatment after discontinuation of fluoxetine. *Psychosomatics.* 2005;46(3):274–5. <https://doi.org/10.1176/appi.psy.46.3.274>
63. Hachem R, Hicks K, Huen A, Raad I. Myelosuppression and serotonin syndrome associated with concurrent use of linezolid and selective serotonin reuptake inhibitors in bone marrow transplant recipients. *Clin Infect Dis.* 2003;37(1):e8–e11. <https://doi.org/10.1086/375689>
64. Lavery S, Ravi H, McDaniel WW, Pushkin YR. Linezolid and serotonin syndrome. *Psychosomatics.* 2001;42(5):432–4. <https://doi.org/10.1176/appi.psy.42.5.432>
65. Morrison E, Rowe AS. Probable drug-drug interaction leading to serotonin syndrome in a patient treated with concomitant buspirone and linezolid in the setting of therapeutic hypothermia. *J Clin Pharm Ther.* 2012;37(5):610–3. <https://doi.org/10.1111/j.1365-2710.2012.01344.x>
66. Mason LW, Randhawa KS, Carpenter EC. Serotonin toxicity as a consequence of linezolid use in revision hip arthroplasty. *Orthopedics.* 2008;31(11):1140. <https://pubmed.ncbi.nlm.nih.gov/19226083/>
67. Das P, Warkentin D, Hewko R, Forrest DL. Serotonin syndrome after concomitant treatment with linezolid and meperidine. *Clin Infect Dis.* 2008;46(2):264–5. <https://doi.org/10.1086/524671>
68. Steinberg M, Morin AK. Mild serotonin syndrome associated with concurrent linezolid and fluoxetine. *Am J Health Syst Pharm.* 2007;64(1):59–62. <https://doi.org/10.2146/ajhp060227>
69. Sola CL, Bostwick J, Hart DA, Lineberry TW. Anticipating potential linezolid-SSRI interactions in the general hospital setting: an MAOI in disguise. *Mayo Clin Proc.* 2006;81(3):330–4. <https://doi.org/10.4065/81.3.330>
70. Willekens R, Puig-Asensio M, Ruiz-Camps I, Larrosa MN, González-López JJ, Rodríguez-Pardo D, et al. Early oral switch to linezolid for low-risk patients with *Staphylococcus aureus* bloodstream infections: a propensity-matched cohort study. *Clin Infect Dis.* 2018;69(3):381–7. <https://doi.org/10.1093/cid/ciy916>
71. Bergeron L, Boulé M, Perreault S. Serotonin toxicity associated with concomitant use of linezolid. *Ann Pharmacother.* 2005;39(5):956–61. <https://doi.org/10.1345/aph.1e523>
72. DeBellis RJ, Schaefer OP, Liquori M, Volturo GA. Linezolid-associated serotonin syndrome after concomitant treatment with citalopram and mirtazepine in a critically ill bone marrow transplant recipient. *J Intensive Care Med.* 2005;20(6):303–5. <https://doi.org/10.1177/0885066605280825>
73. Thomas CR, Rosenberg M, Blythe V, Meyer WJ. Serotonin syndrome and linezolid. *J Am Acad Child Adolesc Psychiatry.* 2004;43(7):790. <https://doi.org/10.1097/01.chi.0000128830.13997.aa>
74. Aga VM, Barklage NE, Jefferson JW. Linezolid, a monoamine oxidase inhibiting antibiotic, and antidepressants. *J Clin Psychiatry.* 2003;64(5):609–11. <https://doi.org/10.4088/jcp.v64n0518b>

**Table 1. Incidence of Serotonin Toxicity Connected to Use of Linezolid Plus Other Serotonergic Agents (38, 45-47)**

Reference	Linezolid/ Serotonergic Agent, N	Serotonin Toxicity, n	Incidence,%
Butterfield (2012)	2208	12 <sup>a</sup>	0.54
Go (2010)	24	1 <sup>b</sup>	4.17
Lorenz (2008)	53	1 <sup>b</sup>	1.89
Taylor (2006)	72	2 <sup>a</sup>	2.78
a. Serotonin toxicity diagnosed via Hunter Serotonin Toxicity Criteria or Sternbach's criteria. b. Serotonin toxicity diagnosed via Hunter Serotonin Toxicity Criteria.			







Vinod Kumar Mugada et al.,

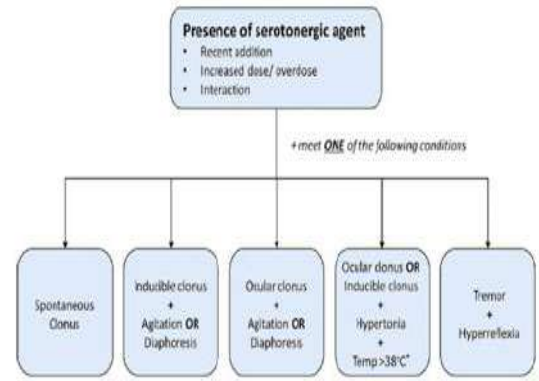
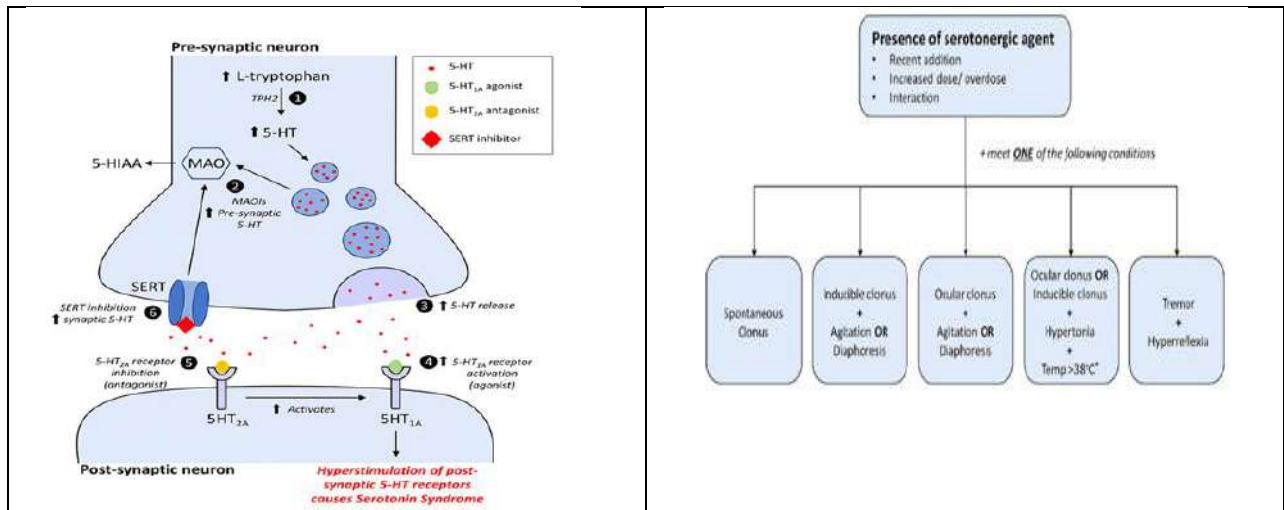


Figure 1. illustrates the various pathways contributing to serotonin syndrome [11]. 1) an abundance of L-tryptophan elevates the production of 5-HT (serotonin), a reaction facilitated by tryptophan hydroxylase 2 (TPH2). 2) monoamine oxidase inhibitors (MAOIs) prevent the breakdown of serotonin, resulting in higher presynaptic levels. 3) substances like amphetamines, cocaine, MDMA (3,4-methylenedioxymethamphetamine), and levodopa prompt the release of more 5-HT. 4) there's either direct or indirect stimulation of 5-HT1A receptors on the postsynaptic side. 5) the antagonism of 5-HT2A receptors may amplify the effects of 5-HT1A receptor agonists. 6) the inhibition of the serotonin reuptake transporter protein (SERT) by selective serotonin reuptake inhibitors (SSRIs) and tricyclic antidepressants (TCAs) leads to increased serotonin levels in the synaptic gap.

Figure 2. The Hunter Criteria for Serotonin Toxicity are essential for identifying serotonin syndrome [11]. Central to this diagnosis is the necessity for some type of neuromuscular excitation. The presence of a temperature of 38.5°C or higher, along with pronounced hypertonia or rigidity, particularly in the trunk, signals a severe form of serotonin syndrome. This condition poses a risk of worsening, potentially leading to respiratory difficulties.

	Neuro-muscular	Autonomic	Mental State
<b>Serotonin Toxicity</b>			
<b>Severe</b>	Respiratory failure Rigidity	Severe Hyperthermia	Low GCS Confusion
<b>Moderate</b>	Sustained clonus Opsoclonus Myoclonus Tremor	Hyperthermia (<38.5°C) Mydriasis Diaphoresis Flushing	Agitation
<b>Mild</b>	Hyper-reflexia Inducible clonus	Tachycardia Hypertension	Anxiety
<b>Common drug side effect</b>	Brisk reflexes	Diarrhoea Nausea	Insomnia

Figure 3. The scope of clinical features in SS [18]. GCS= Glasgow Coma Scale.







## Enhancement in Solubility and Dissolution Rate of Glimepiride using Spherical Crystallization Technique

Rajkiran Kolakota<sup>1\*</sup>, Simma Sridhar<sup>2</sup>, Darapu Harika<sup>2</sup> and Devudala Soujanya<sup>2</sup>

<sup>1</sup>Professor, Sri Sivani College of Pharmacy (Affiliated to Jawaharlal Nehru Technological University), Chilakapalem, Srikakulam, Andhra Pradesh, India.

<sup>2</sup>M.Pharm Student, Sri Sivani College of Pharmacy (Affiliated to Jawaharlal Nehru Technological University), Chilakapalem, Srikakulam, Andhra Pradesh, India.

Received: 06 Oct 2024

Revised: 12 Nov 2024

Accepted: 18 Dec 2024

### \*Address for Correspondence

#### Rajkiran Kolakota

Professor, Sri Sivani College of Pharmacy  
(Affiliated to Jawaharlal Nehru Technological University),  
Chilakapalem, Srikakulam, Andhra Pradesh, India.  
E.Mail: rajkiran.kolakota@gmail.com



This is an Open Access Journal / article distributed under the terms of the **Creative Commons Attribution License** (CC BY-NC-ND 3.0) which permits unrestricted use, distribution, and reproduction in any medium, provided the original work is properly cited. All rights reserved.

### ABSTRACT

Improving the solubility and dissolution rate of drugs with poor water solubility remains a significant hurdle in the pharmaceutical industry. Glimepiride, an oral medication used for managing diabetes, is a notable example of a compound with low aqueous solubility that necessitates enhancement strategies. This research focuses on utilizing spherical crystallisation to increase the solubility and dissolution rate of glimepiride. The method integrates crystallization and aggregation into a single-step process, resulting in spherical agglomerates with superior physicochemical attributes. Spherical crystals of glimepiride were produced using the solvent-change approach, involving the use of an appropriate combination of good solvent, poor solvent, and bridging liquid. The resulting agglomerates were analyzed for their particle size, morphology, flow characteristics, and mechanical properties using tools such as scanning electron microscopy (SEM), Fourier-transform infrared spectroscopy (FTIR), and X-ray diffraction (XRD). Solubility and dissolution studies were conducted following standard procedures, with findings compared to unprocessed glimepiride. The spherical agglomerates showed remarkable improvements in solubility and dissolution rates compared to the untreated drug, which could be attributed to enhanced surface area, reduced crystallinity, and better wettability. Furthermore, the agglomerates demonstrated superior flow properties, making them ideal for direct tablet compression. This investigation underscores the potential of spherical crystallization in overcoming the limitations of poorly water-soluble drugs like glimepiride, offering a viable solution to enhance therapeutic efficacy and patient adherence.

**Keywords:** Glimepiride, spherical crystallization, solubility enhancement, dissolution rate, poorly water-soluble drugs, solvent-change method, particle engineering, crystallinity reduction.



Rajkiran Kolakota *et al.*,

## INTRODUCTION

Diabetes is a metabolic disorder marked by high blood sugar levels due to insulin production issues or insulin resistance. Managing diabetes often involves medications, especially for type 2 diabetes, where oral drugs are commonly prescribed. A significant challenge with many of these drugs is poor solubility, which can reduce their effectiveness. Cocrystallization, a process that involves combining a drug with conformers to form a crystalline structure, offers a solution by improving the solubility and bioavailability of poorly soluble drugs. Cocrystallization enhances the solubility and dissolution rate of drugs, making them more effective when taken orally. This is particularly important for diabetes medications like metformin, which is essential for managing type 2 diabetes but suffers from poor water solubility. Cocrystallization increases the drug's dissolution rate, improving absorption in the gastrointestinal tract and ensuring better therapeutic outcomes. The process involves combining the drug molecule with one or more cofomers to form a cocrystal. These cocrystals retain the drug's therapeutic properties but improve its solubility, making it easier for the body to absorb. This approach allows for more consistent blood sugar control, potentially reducing the side effects often linked to poorly soluble drugs. Metformin, the first-line treatment for type 2 diabetes, has low solubility, which can lead to inconsistent absorption and side effects like gastrointestinal discomfort. Research into metformin cocrystals has shown promising results in enhancing its solubility, reducing side effects, and improving its absorption. By modifying metformin's crystalline form, the drug can achieve more reliable blood glucose control.[1,2].

Other diabetes drugs, including rosiglitazone and glibenclamide, have also been studied for co-crystallization. These medications, like metformin, can benefit from improved solubility, which may lead to more consistent therapeutic effects and fewer adverse reactions. Cocrystals improve the solubility of poorly water-soluble drugs, allowing for better absorption and more effective treatment. Enhanced solubility can lead to lower required doses, which may help reduce side effects such as nausea and gastrointestinal discomfort. Cocrystals can be designed to release the drug gradually, providing steady blood sugar control and reducing the need for frequent dosing. Regulatory bodies like the FDA have recognized cocrystallization as a viable approach to improving drug formulations, making it an appealing method for drug development. While cocrystallization offers many advantages, challenges remain. Identifying suitable cofomers and optimizing formation conditions require careful research. Additionally, stability and shelf-life considerations for cocrystals must be addressed to ensure their long-term effectiveness. Nevertheless, cocrystallization represents a promising strategy for improving diabetes drug formulations. By enhancing solubility and bioavailability, cocrystals could lead to better absorption, fewer side effects, and more controlled drug release, offering improved blood sugar management for diabetes patients. In conclusion, cocrystallization holds significant potential for revolutionizing diabetes treatment. By overcoming solubility challenges, it can provide more effective medications, improving patient outcomes and enhancing the management of diabetes.[3,4]

## MATERIAL AND METHOD

**Preparation of spherical agglomerates of glimepiride by spherical crystallization technique:**All reagents used in this investigation were of analytical grade and double distilled water was used. The Glimepiride (1gm) was dissolved in dimethyl formamide, dichloromethane and methanol (30 ml) in a small beaker. Distilled water (100 ml) was added to precipitate the drug in fine crystals. The mixture was allowed to stand for 10 minutes. It was then stirred using three blade electric stirrers at 600 rpm and chloroform (5 ml) was added drop wise as a bridging liquid while stirring. This system was agitated for 45 minutes at room temperature. Spherical crystals were separated by filtration and dried in oven at 40°C for 20 min.[5,6]

### Evaluation

The formation of co crystals are identified by using different methods



**Rajkiran Kolakota et al.,****Fourier Transform Infrared Spectroscopy (FTIR)**

FTIR spectra were obtained using a Bruker Alpha System with Spectrum opus 6.5 software. A KBr pellet of drug, carrier, adsorbent and the solid dispersion granules was prepared. The sample was dispersed in the KBr and ground using a mortar and pestle. The KBr pellet was prepared by the application of high pressure.

**Differential Scanning Calorimetry**

DSC studies were performed using a DSC (Siio-6300, Japan instruments). It is operated using Stare Software V8.10. A 3-5 mg sample was weighed and placed into a 100 µL aluminium pan which is further crimped with a lid. The pan was then placed into the DSC unit along with a similar pan as a reference. The sample was scanned at a heating rate of 100C/min from 0 °C to 300 °C and purged under nitrogen gas flow rate of 50 ml/min. The DSC was calibrated using indium (5-10 mg) with a melting onset of 156 ± 0.2 °C as the standard

**X-Ray powder Diffraction (XRPD)**

XRPD was performed to observe the physical state of the spherical agglomerates and to evaluate any interaction between the drug, and solvents in spherical crystallization technique. Philips PAN analytical X-Pert Pro V1.6 with X-Pert Data Collector V2.1 software was used equipped with a CuKα2 anode tube and diffractometer of radius 240mm. The XRD scan was performed using BB004 flat stage. The powdered sample was placed in a plastic sample holder of 1 inch square. Data were collected at 45 kV and 40 mA. Samples were scanned from 0-40 ° 2θ at a step size of 0.0084 and scan rate of 1.00 °/min[7,8]

**Saturation solubility studies**

Solubility studies of the prepared spherical agglomerates of glimepiride (GD+DMF, GD+DCM, and GD+methanol spherical agglomerates) solutions of prepared agglomerates were placed in 50ml beakers and the prepared saturated solutions were kept in an orbital shaker for 72hrs at 25°C with 300 rpm. After 72 hrs the samples sonicated for 2hours. Then Samples were filtered through 0.45 micro meter filters and their concentration was determined by using Elico SL 159 UV-spectrophotometer at 231 nm. The results were extrapolated to determine the percent w/v of Glimepiride in its saturated solution with the solvent under investigation.[9]

**In- vitro dissolution studies**

The *in-vitro* release profiles of glimepiride spherical crystals by spherical crystallization technique were obtained using a dissolution test apparatus USP-II (Electro Lab). The dissolution study was carried out in 900 ml 0.1 N HCl as the dissolution medium at 37°C ± 5°C and 50rpm. Then 5 ml samples were collected for 5, 10,15, 20, 30, 45, 60. The dissolution medium was replaced with 5 ml fresh dissolution fluid to maintain sink conditions. The withdrawn samples were filtered and analyzed, spectrophotometrically (Elico, SL 159) at 231 nm. The mean of two determinations was used to calculate the drug release from each of the formulations.

**RESULTS AND DISCUSSION**

The study the compatibility of glimepiride with other solvents were prepared by mixing drug with solvents in the ratio of 1:1 and stored in air tight containers at room temperature and 30°C /65%RH for three months .the solid admixtures were characterized using Fourier Transform infra-red spectroscopy. In FTIR studies Glimepiride showed characteristic peak at 3369(NH group (secondary amines ) ;3288(NH(amide);1707(C=O(carboxylic acid);1673(C=O(amide) in drug alone and in combination of pure drug with other solvents.

**DSC results and discussion**

The compatibility of drug and solvent (DCM, DMF, methanol) were evaluated by DSC. the DSC thermogram of glimepiride exhibited a broad endothermic peak at 226.3°C corresponding to its melting point 205 to 208°C. the DSC thermo gram of G.D+DCM showed melting peak of drug at 250.2°C , G.D +methanol agglomerates showed melting





**Rajkiran Kolakota et al.,**

peak at 263.8°C and G.D+DMF showed melting peak of drug at 250.2°C. This indicates no interaction between G.D and all the solvents in the spherical agglomerates.

#### XRD results and discussions

The physical state of a drug in the spherical agglomerates were evaluated by XRD the XRD of glimepiride exhibited a few characteristic diffraction peaks indicating its crystalline nature. In the XRD of G.D+DCM spherical agglomerates less no of diffraction peaks and their intensities were reduced indicating reduction in crystallinity. But in the XRD of G.D +methanol and G.D+DMF exhibited no of characteristic diffraction peak with high intensities indicating its more spherical crystallization.

#### Determination of yield and drug content for prepared spherical agglomerates

Spherical agglomerates	Yield%	Drug content
G.D+DMF	97±2	93±2
G.D+DCM	90±2	83±1
G.D+methanol	94±1	90±2

**Solubility Studies:** The solubility of glimepiride in distilled water, G.D+DMF, G.D+DCM and G.D+methanol was found to be 0.0619, 0.216, 0.0495, and 0.194 mg/ml respectively.

The solubility increases in the order as G.D +DMF > G.D+ methanol > G.D+DCM > pure drug.

The spherical crystallization of Glimepiride with DMF, DCM and methanol was investigated by saturation solubility studies in distilled water. The aqueous solubility of Glipizide was increased in spherical agglomerates made with DMF and methanol compared to pure Glipizide. The aqueous solubility of Glipizide in DMF and methanol spherical agglomerates increased 3.32 and 3.13 times than that of the pure Glipizide respectively. But the aqueous solubility of Glipizide in DCM spherical crystals was similar to aqueous solubility of pure Glipizide. There is only 0.79 times that of the pure Glipizide. There is no much increase in solubility of drug in DCM spherical crystals.

#### In vitro release studies

Glimepiride release from different spherical agglomerates was studied in 0.1N HCL for a period of 60 minutes. Glimepiride release from all spherical agglomerates was rapid and released 100%. Dissolution efficiency (DE) is another parameter suitable for the evaluation of in vitro dissolution rate. DE is defined as the area under the dissolution curve up to a certain time (t) expressed as a percentage of the area of the rectangle described by 100% dissolution in the same time. The dissolution efficiency can have a range of values depending on the time intervals should be chosen for comparison. For example, DE<sub>15</sub> would relate to the dissolution of the drug from a particular formulation after 15 minutes and could only be compared with DE<sub>15</sub> of other formulations. Summation of the large dissolution data into a single figure DE enables ready comparison to be made between a large numbers of spherical agglomerates. The second advantage is that it can be theoretically related to in vivo data. Since in vivo drug availability is estimated by integrating the area under blood level curve it seems reasonable to express in vitro results similarly. Also, when a relation is to be shown between dissolution and another variable, it is perhaps more realistic to use dissolution efficiency which takes in to account the dissolution profile as a whole, as opposed to T<sub>50%</sub> or T<sub>90%</sub> values which use just one point from the plot. Dissolution efficiency (DE<sub>15</sub>) values were calculated as per Khan. T<sub>50</sub> (time taken for 50% dissolution) values were recorded from the dissolution profiles. The dissolution parameters are summarized in table

The formulations G.D +D.M.F, G.D + methanol got good dissolution efficiency values compared to G.D + D.C.M and pure (G.D) It indicates increase dissolution rate in G.D +D.M.F, G.D + methanol compared to G.D + D.C.M and pure (G.D)



Rajkiran Kolakota *et al.*,

## CONCLUSION

The overall objective of the present investigation is to enhance solubility Glimepiride, an anti-diabetic BCS class II drug and to enhance dissolution rate. Various methods used to enhance solubility were studied and reviewed literature. Among them spherical crystallization is one of the unique method to enhance solubility and also to enhance dissolution rate. Various solvents selected in the preparation of spherical agglomerates of the Glimepiride based on drug solubility and nature of the solvent. DMF, DCM and methanol selected as good solvents, chloroform as bridging liquid and distilled water as poor solvent. Spherical agglomeration technique was optimised by setting different RPMs and finally 600 rpm was selected. The drug and excipient compatibility study were investigated by FTIR and DSC. The crystallinity was identified by XRD. There was no interaction between drug and excipients. By observing the XRD prepared spherical agglomerates were spherical in shape. The saturation solubility study revealed that aqueous solubility of Glimepiride was increased in spherical agglomerates than that of pure Glimepiride. There was drastic increase in solubility of Glimepiride in GD+DMF spherical agglomerates (3.32) and GD+ methanol (3.13) spherical agglomerates. Slight increase in solubility of Glimepiride in GD+ DCM (0.79). The micromeritic studies revealed that the flow properties of all the prepared spherical agglomerates were better than the pure Glimepiride.

The invitro dissolution studies revealed that dissolution of glimepiride was rapid and higher from spherical agglomerates compared to pure Glimepiride. The dissolution efficiency (DE<sub>15</sub> values were greater than of pure glimepiride. among Glimepiride+ DMF spherical agglomerates and Glimepiride+ methanol spherical agglomerates exhibited good dissolution rate than Glimepiride+ DCM spherical agglomerates and pure Glimepiride. Finally it concluded that Glimepiride in DMF produced best spherical agglomerates compared to all other solvents based on solubility, dissolution studies.

## REFERENCES

- Gennaro A.R: Remington, The science and practice of pharmacy. Lippincott, Williams and Wilkins, 2005; 21st edition: 867-868.
- Fiese EF and Hagen TA: Preformulation, In: Lachman L, Liberman H.A and Kanig J.L, The theory and practice of industrial pharmacy. Bombay, Varghees Public house, 1990; 3rd edition: 171-196.
- Sinho PJ: Martin's Physical pharmacy and pharmaceutical sciences 2006; 5( 9): 232-234.
- Trask AV, Mothorweu WDS and Jones W: Solvent- drop grinding; green polymorph control of co-crystallization Chem. Comm 2004; 890-891.
- Stickery RG: Solubilizing excipient in oral and injectable formulations. Pharmaceutical Research 2004; 21: 201-230.
- Swar Brick J : Encyclopedia of Pharmaceutical Technology 2006; 3314-3316
- Dubey R: Pure drug nanosuspension impact of nanosuspension technology on drug discovery and development. Drug Delivery Technology 2006; 6: 65-71. AdamM, Perskey and Jeffrey A: Hurgnet, Salutions and solubility, [http://www.cop.ufl.edu/sofezon\\_e/pnokai/pha5100/pha5110.ht](http://www.cop.ufl.edu/sofezon_e/pnokai/pha5100/pha5110.ht)
- Singhal D, Curatolo W: Drug polymorphism and dosage form design, a practical perspective. Advanced Drug Delivery Review 2004; 56: 335-347

**Table-1 Formulation table for preparation of spherical agglomerates of glimepiride**

Spherical agglomerates	Drug(gms)	Amount of good solvent(ml)	Amount of poor solvent(ml)	Amount of bridging liquid(ml)
G.D-DMF	1(gm)	DMF(30ml)	Water(100ml)	Chloroform(5ml)
GD-DCM	1(gm)	DCM(30ml)	Water(100ml)	Chloroform(5ml)
GD-methanol	1(gm)	Methanol(30ml)	Water(100ml)	Chloroform(5ml)



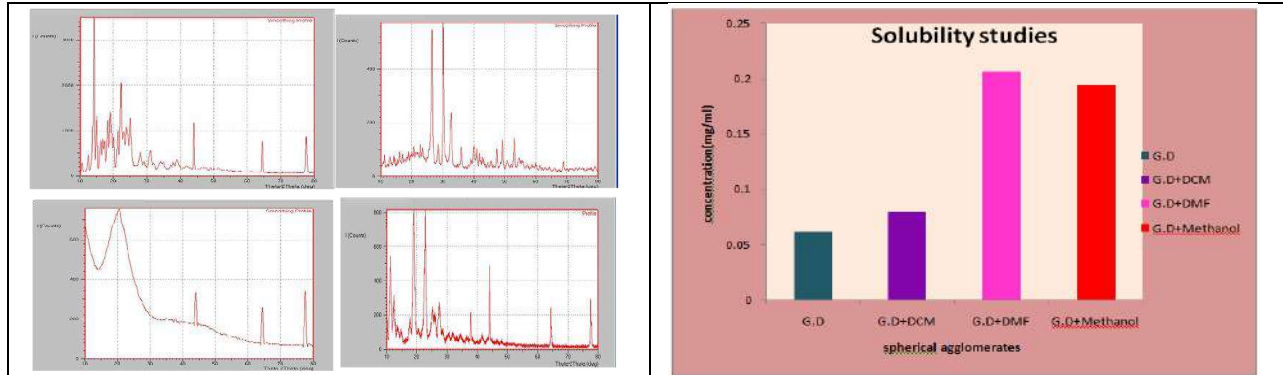




**Rajkiran Kolakota et al.,**

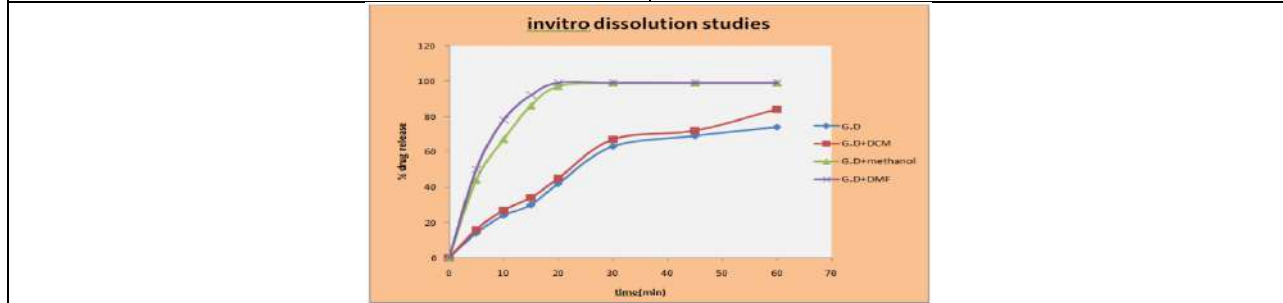
**Table-2. DE<sub>15</sub>, T<sub>50%</sub>, T<sub>90%</sub> for different spherical agglomerates**

Spherical agglomerates	Dissolution efficiency (DE <sub>15</sub> )	T <sub>50%</sub> (mins)	T <sub>90%</sub> (mins)
Pure(G.D)	17.6	31.59	63.77
G.D+D.C.M	20	41.675	85.2
G.D+D.M.F	58	0.076	34.23
G.D +methanol	51	4.387	35.54



**Figure-1: XRD of pure drug, G.D+D.M.F, G.D+D.C.M and G.D +methanol**

**Figure-2: Solubility of pure drug, G.D+D.M.F, G.D+D.C.M and G.D +methanol**



**Figure-3: Dissolution of pure drug, G.D+D.M.F, G.D+D.C.M and G.D +methanol**







## Vesicular Drug Delivery System: Site Specific Drug Delivery Approach

Uriti Sri Venkatesh<sup>1</sup>, Gulibindala Ekshitha<sup>2\*</sup>, Kanchari Vidyamansa<sup>3</sup> and Akkarapalli Bindu<sup>3</sup>

<sup>1</sup>Associate Professor, Sri Sivani College of Pharmacy (Affiliated to Jawaharlal Nehru Technological University), Chilakapalem, Srikakulam, Andhra Pradesh, India.

<sup>2</sup>Assistant Professor, Sri Sivani College of Pharmacy (Affiliated to Jawaharlal Nehru Technological University), Chilakapalem, Srikakulam, Andhra Pradesh, India

<sup>3</sup>M.Pharm Student, Sri Sivani College of Pharmacy (Affiliated to Jawaharlal Nehru Technological University), Chilakapalem, Srikakulam, Andhra Pradesh, India.

Received: 06 Oct 2024

Revised: 12 Nov 2024

Accepted: 18 Dec 2024

### \*Address for Correspondence

#### Gulibindala Ekshitha

Assistant Professor, Sri Sivani College of Pharmacy  
(Affiliated to Jawaharlal Nehru Technological University),  
Chilakapalem, Srikakulam, Andhra Pradesh, India  
E.Mail: ekshitha97@gmail.com



This is an Open Access Journal / article distributed under the terms of the **Creative Commons Attribution License** (CC BY-NC-ND 3.0) which permits unrestricted use, distribution, and reproduction in any medium, provided the original work is properly cited. All rights reserved.

### ABSTRACT

The objective of this think about is to survey the potential of novel vesicular sedate conveyance frameworks (VDDS) for focused on medicate conveyance. These systems aim to release drugs at a controlled rate, ensuring a steady therapeutic level in the body while reducing undesirable side effects. A novel drug delivery system is designed to administer the drug at a predetermined rate, based on factors such as the drug's pharmacological properties, the body's physiological state, and specific treatment needs. While an ideal drug delivery system has not yet been developed, ongoing efforts are being made to minimize the gap between the ideal and existing systems. Vesicular drug delivery systems (VDDS) involve encapsulating the active drug within vesicular structures, providing an advanced alternative that addresses some of the limitations of traditional drug delivery methods. Over time, several types of VDDS, including liposomes, niosomes, archaeosomes, and transferosomes, have been developed and refined. This review focuses on these innovative vesicular systems as promising new approaches in drug delivery technology.

**Keywords:** Vesicular, liposomes, archaeosomes, systems, therapeutic

## INTRODUCTION

The development of new drug delivery systems (NDDS) has seen significant progress in recent years. These systems play a crucial role in enhancing the therapeutic effects of both new and existing medications by enabling controlled and sustained drug release to targeted areas, thereby addressing the specific medical needs of patients. NDDS are considered innovative because they modify the delivery of many drugs, overcoming various issues related to





**Uriti Sri Venkatesh et al.,**

conventional drug treatments and ensuring prolonged therapeutic effects with precise control. Drug delivery encompasses the methods, technologies, and formulations used to introduce pharmaceutical agents into the body in a manner that safely achieves the desired therapeutic outcome. Over the past few decades, there has been a growing focus on advancing these systems. [4]An ideal NDDS should fulfil two main criteria: it should release the drug at a rate that aligns with the body's requirements during treatment, and it should direct the active ingredient to the intended site of action. Traditional dosage forms, including sustained-release formulations, fall short of meeting these criteria. One promising approach is encapsulating drugs within vesicular structures, which can increase the drug's residence time in the bloodstream and potentially reduce toxicity by enabling selective uptake at the target site. Lipid vesicles, a type of experimental biological membrane model, have been successfully utilized as controlled-release carriers. Conventional chemotherapy often struggles to treat intracellular infections due to limited drug penetration into cells, but vesicular drug delivery systems can address this challenge. Vesicular drug delivery systems offer several benefits, including:

Potential for increased drug residence time in the systemic circulation and reduced toxicity if selective uptake to the infection site is achieved. Enhanced bioavailability, especially for poorly soluble drugs. The versatility to accommodate both hydrophilic and lipophilic drugs. Functioning as sustained-release systems that help delay the excretion of drugs that are rapidly metabolized. However, despite their advantages, vesicular drug delivery systems also have notable limitations. The passive transport of drugs within these systems can result in low drug loading efficiency and the risk of drug leakage during production, storage, or in vivo transportation. Additionally, the stability of vesicular systems remains a significant barrier, restricting their widespread application. [6].

Sorts of VDDS: The focused vesicles are classified on the premise of their composition Lipoidal biocarriers, Non-lipoidal biocarriers, Lipoidal biocarriers,

#### **Lipoidal biocarriers**

1. Liposomes 2. Sphingosomes 3. Ethosomes 4. Transferosomes 5. Pharmacosomes b. Non-lipoidal biocarriers:

1. Niosomes 2. Bilosomes 3. Aquasomes.

#### **Liposomes**

Liposomes comprise of one or more concentric lipid bilayers, which encase an inside fluid volume(s). For medicate conveyance applications liposomes are ordinarily unilamellar and extend in breadth from around 50 - 150 nm [7]. Bigger liposomes are quickly evacuated from the blood circulation. Liposomes are one of a kind in their capacity to suit drugs, which contrast broadly in physicochemical properties such as extremity, charge and measure. Destinations in liposomes where these drugs can localize incorporate the liposome bilayer with its hydrophobic hydrocarbon chain center, its expansive polar surface, which can be impartial or charged and the inside fluid space. The word sedate is utilized as a bland term and alludes to routine drugs. Liposomes are fair empty circles of lipids, i.e. a few lipids shape films that near on themselves shaping liposomes. The primary component of liposome films is dipalmitoyl phosphatidil choline (DPPC, PC or EPC- egg phosphate... choline). Be that as it may, a few other compounds are included in arrange to make strides soundness or other auxiliary properties. Two compounds included are: dipalmitoyl phosphatidil glycerol (DPPG or PG) and cholesterol. Clearly, cholesterol has the impact of making the layer less penetrable by filling up gaps or disruptions[8]

#### **Advantages**

Phospholipids are one of the few solubilizers that are well tolerated. Liposomes may increment the dissolvability of insoluble drugs between one hundred to ten thousand fold [9] In the little digestive system, liposomes are processed in the nearness of bile and chemicals. The solubilized compound is freed and advanced solubilized in bile and processed lipids. Perfect models for natural layers as well as productive carriers for Perfect models for natural layers as well as productive carriers for Perfect models for natural layers as well as productive carriers for Pharmacosomes. These are characterized as colloidal scatterings of drugs covalently bound to lipids and may exist as ultrafine vesicular, micellar or hexagonal totals, depending on the chemical structure of drug-lipid complex[11].



**Uriti Sri Venkatesh et al.,**

The prodrug conjoins hydrophilic and lipophilic properties and subsequently secures amphiphilic characters and was found to diminish interfacial pressure and hence at higher concentrations shows mesomorphic behaviour. Since the framework is shaped by connecting a sedate (pharmakon) to a carrier (soma), they are called pharmacophores. Pharmacosomes bearing special focal points over liposomes and baneful vesicles have come up as potential elective to routine vesicles[12].

They are a viable apparatus to accomplish craved helpful objectives such as sedate focusing on and controlled is charge. Tall and foreordained entanglement effectiveness as medicate and carrier frame a stoichiometrically characterized unit covalently connected together[13]. Volume of consideration doesn't impact entanglement effectiveness. No require of evacuating the free, untrapped medicate from the definition which is required in the case of liposomes. Moves forward bioavailability particularly in the case of ineffectively solvent drugs.

Sedate carriers such as liposomes, nanoparticles, microemulsions which have lead to moo drug-loading proficiency, physical solidness such as combination, conglomeration, sedimentation and medicate spillage amid arrangement, conservation etc is truant in pharmacosomes [14]

**Ethosomes**

The vesicles have been well known for their significance in cellular communication and molecule transportation for numerous a long time. Analysts have caught on the properties of vesicles structure for utilize in superior sedate conveyance inside their cavities, which would to tag the vesicle for cell specificity. One of the major progresses in vesicle investigate was finding a vesicle subordinate, known as an Ethosomes [15]. Ethosomes are noninvasive conveyance carriers that empower drugs to reach the profound skin layers and/or the systemic circulation. These are delicate, flexible vesicles custom-made for the upgraded conveyance of dynamic operators. They are composed basically of phospholipids, (phosphatidylcholine, phosphatidylserine, phosphatidic corrosive), tall concentrations of ethanol and water. The tall concentration of ethanol makes the ethosomes special, as ethanol is known for its unsettling influence of skin lipid bilayer organization hence, when coordinates into a vesicle layer it gives that vesicle the capacity to enter the stratum corneum. Moreover since of their tall ethanol concentration, the lipid layer is stuffed less firmly than customary vesicles but has identical solidness, permitting a more pliable structure and makes strides in medicate dissemination capacity in stratum corneum lipids[16].

**Advantages**

Ethosomes are upgraded saturation of medicate through skin for transdermal and dermal conveyance. Ethosomes are stage for the conveyance of expansive and assorted gather of drugs (peptides, protein molecules). Ethosome composition is secure and the components are endorsed for pharmaceutical and restorative use. Tall understanding compliance. The Ethosomal sedate is administrated in a semisolid frame (gel or cream), creating tall persistent compliance by is tall. In differentiation, Iontophoresis and Phonophoresis are moderately complicated to utilize which will influence persistent compliance. The Ethosomal framework is inactive, noninvasive and accessible for prompt commercialization. Different applications in the Pharmaceutical, Veterinary, and Restorative fields [17]

**Niosomes** are non-ionic surfactants vesicles gotten on hydration of engineered non-ionic surfactants with or without consolidation of cholesterol or lipids[18]. Niosomes are arrangements of vesicles by hydrating blend of cholesterol and non-ionic surfactants. These are shaped by the self-assembly of nonionic surfactant in non-aqueous media as round, multilamellar framework and polyhedral structure in expansion to reverse structures which shows up as it were in on watery solvent[20]. Since at that point a number of nonionic surfactants have been utilized to plan vesicles. e. g., Polyglycerol alkyl ethers, glucosyldialkyl ethers, crown ethers, polyoxyethylene alkyl ethers, ester connected surfactants, steroid connected surfactants, brij and a arrangement of ranges and tweens[19]. They are vesicular frameworks comparative to liposomes that can be utilized as carriers of amphiphilic and lipophilic drugs. The vesicles are characterized to be composed of or relating to little, sac like bodies. Niosomes and liposomes are equiactive in medicate conveyance potential and both increment viability as compared with that of free medicate.



**Uriti Sri Venkatesh et al.,**

Niosomes are favored over liposomes since the previous show tall chemical solidness and economy. Niosomes or nonionic surfactant vesicles are minuscule lamellar structures of estimate run.

**Advantages of niosomes:**

- ♣ Better patient compliance and better therapeutic effect in comparison to oily formulations
- ♣ Can be used to deliver hydrophilic, lipophilic as well as amphiphilic drugs and can accommodate drugs with wide range of solubility
- ♣ Controlled and sustained release of drugs due to depot formation
- ♣ Enhance the oral bioavailability of the drugs
- ♣ Osmotically active and stable, biocompatible, nontoxic and nonimmunogenic
- ♣ Protect the drug from enzymatic metabolism thus increase the stability of the drug
- ♣ Drug targeting to various organs
- ♣ Enhance the skin permeation of various drugs
- ♣ Easy to handle, store and transport
- ♣ Administered by various routes via oral, parenteral, topical etc,
- ♣ The shape, size, composition and fluidity of niosomes can be controlled as and when required.

**Transferosomes**

Liposomal as well as niosomal systems, are not suitable for transdermal delivery, because of their poor skin permeability, breaking of vesicles, leakage of drug, aggregation and fusion of vesicles. To overcome these problems, a new type of carrier system called "transferosome" has recently been introduced, which is capable of transdermal delivery of low as well as high molecular weight drugs[21]. Transferosomes are specially optimized, ultra-deformable (ultraflexible) lipid supramolecular aggregates, which are able to penetrate the mammalian skin intact. Each transferosome consists of at least one inner aqueous compartment, which is surrounded by a lipid bilayer with specially tailored properties, due to the incorporation of "edge activators" into the vesicular membrane. Surfactants such as sodium cholate, sodium deoxycholate, span 80 and Tween 80, have been used as edge activators. It was suggested that transferosomes could respond to external stress by rapid shape transformations requiring low energy. These novel carriers are applied in the form of semi-dilute suspension, without occlusion. Due to their deformability, transferosomes are good candidates for the non-invasive delivery of small, medium and large sized drugs[22].

They have been used as drug carriers for a range of small molecules, peptides, proteins and vaccines, both in vitro and in vivo. Transferosomes penetrate through the pores of stratum corneum which are smaller than its size and get into the underlying viable skin in intact form. This is because of its deformable nature[23]. Multiliter quantities of sterile, well-defined transferosomes containing drug can be and have been prepared relatively easily. Materials commonly used for the preparation of transferosomes are phospholipids (soya phosphatidyl choline, egg phosphatidyl choline), surfactant (tween 80, sodium cholate) for providing flexibility, alcohol (ethanol, methanol) as a solvent, dye for confocal scanning laser microscopy (CSLM) and buffering agent (saline phosphate buffer pH 7.4), as a hydrating medium.

**Advantages**

- Delivery of peptides by transferosomes provides a very successful means for the noninvasive therapeutic use of such large molecular weight drugs on the skin.
- They are used as a carrier for protein and peptides like insulin, bovine serum albumin, vaccines, etc. The delivery of these large biogenic molecules into the body is difficult. When given orally, they are completely degraded in the GI tract[24].

**Colloidosomes**

Colloidosomes are hollow shell microcapsules consisting of coagulated or fused particles at interface of emulsion droplets. Colloidosomes have exciting potential application in controlled release of drugs, proteins, vitamins as well as in cosmetics and food supplements. They have a great encapsulation efficacy with a wide control over size,



**Uriti Sri Venkatesh et al.,**

permeability, mechanical strength and compatibility. It is a novel class of microcapsules whose shell consists of coagulated or fused colloidal particles at interface of emulsion droplet. The particle self- assembles on surface of the droplet in order to minimize total interfacial energy forming colloidosomes. Hairy colloidosomes whose shell consists of aqueous gel core and shells of polymeric microrods. This has been achieved by templating water-in-oil emulsion stabilized by rod like particles followed by gelling of the aqueous phase, dissolution of oil phase in ethanol and redispersion of obtained colloidosome microcapsules in water[20] .

**Advantages:**

- Control of size allows flexibility in applications and choice of encapsulated materials
- Great potential in controlling permeability of entrapped species and allow selective and time release
- Control of mechanical strength [20]

**Herbosomes**

The term „herb“ means plant, while „some“ means cell like. Over the past century phytochemical and phytopharmacological sciences established the compositions; biological activities and health promoting of numerous botanical products[25]. Most of the biological active constituents of plant are polar or water-soluble molecules. However, water soluble phytoconstituents are poorly absorbed due to their poor lipid solubility, severely limiting their ability to pass across the lipid rich biological membranes, resulting poor bioavailability[20]. Herbosomes exhibit better pharmacokinetic and pharmacodynamic profile than conventional herbal extracts. Molecular layer consisting of PC and other phospholipids provides a continuous matrix into which the proteins insert[20] . Advantages:

- Enhances the absorption of lipid insoluble polar phytoconstituents through oral as well as topical route showing better bioavailability
- Dose requirement is reduced
- Phosphotidylcholine used in preparation also acts as hepatoprotective
- Permeates non-lipophilic botanical extract to be better absorbed in intestinal lumen
- Better stability profile due to chemical bonds formed between Phosphotidylcholine molecules and phytoconstituents

**Sphingosomes**

Sphingosomes may be defined as “concentric, bilayered vesicle in which an aqueous volume is completely by a membranous lipid bilayer mostly composed of natural or synthetic sphingolipid [24].” Sphingosomes solve the major drawback of vesicle system like less stability, less in vivo circulation time, low tumor loading efficacy in case of cancer therapy. Sphingosomes are clinically used delivery system for chemotherapeutic agent, biological macromolecules and diagnostics [26]. They may be administered orally or transdermally. In simple way we can say sphingosome is liposomes which are composed of sphingolipid .

**Advantages:**

- Provide selective passive targeting to tumor tissue
- Increase efficacy and therapeutic index
- Increase stability via encapsulation
- Reduction in toxicity of encapsulated agent
- Improved pharmacokinetics[12]

**Layerosomes**

The layer-by-layer coating concept in one of the strategies used for the preparation or the stabilization of nanosystems. The layerosomes are conventional liposomes coated with one or multiple layers of biocompatible polyelectrolytes in order to stabilise their structure. The formulation strategy is based on an alternative coating procedure of positive poly (lysine) (pLL) and negative poly (glutamic acid) (pGA) polypeptides on initially charged small unilamellar liposomes. Drawback of liposomes is their instability during storage or in biological media which is related to surface properties. This surface modification stabilized the structure of liposomes and led to stable drug







**Uriti Sri Venkatesh et al.,**

delivery systems. Oral administration or their incorporation in biomaterials are among potential fields of application. Thus, the concept of layerosomes has brought forward the stable nanosystem[25] .

### **Ufosomes**

The formation of fatty acids vesicles is called “ufosomes,” ufosomes are unsaturated fatty acid liposomes. Fatty acid vesicles are colloidal suspensions of closed lipid bilayer that are composed of fatty acids and their ionized species. They are observed in a small region within the fatty acid-soap-water ternary phase diagram above the chain melting temperature of corresponding fatty acid soap mixture. Fatty acid vesicles always contain two types of amphiphiles, the nonionized neutral form and the ionized form. The ratio of the nonionized neutral form and the ionized form is critical for the vesicle stability. Fatty acid vesicles are actually mixed “fatty acid/soap vesicles.” Ufosome membranes are much more stabilized in comparison to liposomes[20] .

### **Future Prospects in Vesicular drug delivery systems:**

**Aquasomes:** Three layered self-assembly compositions with ceramics carbon nanocrystalline particulate core coated with glassy cellobiose specific targeting and molecular shielding(26) .

**Cryptosomes:** Lipid vesicles with a surface coat composed of pc and of suitable polyoxyethylene derivative of phosphatidyl ethanolamine, capable of ligand-mediated drug targeting.

**Discosomes:** Discosomes are niosomes solubilized with non-ionic surfactant solutions. They show ligand mediated drug delivery.

**Emulosomes:** Nanosize lipid particles consisted of microscopic lipid assembly with a polar core used parenteral delivery of poor water-soluble drugs.

**Enzymosomes:** Liposomal constructs engineered to provide a mini bioenvironmental in which enzymes are covalently immobilized or coupled to the surface of liposomes. Targeted delivery to tumor cells.

**Genosomes:** Artificial macromolecular complexes for functional gene transfer. Cationic lipids are most suitable because they possess high biodegradability and stability in the blood stream. Cell specific gene transfer.

**Photosomes:** Photolysase encapsulated in liposomes, which release the content photo triggered charges in membrane permeability characteristics.

**Virosomes:** Liposomes spiked with virus glycoprotein, incorporated into the liposomal bilayers based on retro viruses derived lipids.

**Vesosomes:** Nested bilayer compartment in vitro via inter digested bilayer phase formed by adding ethanol to a variety of saturated phospholipids. Multiple compartments of vesosomes give better protection to interior contents in serum.

**Proteosomes:** High molecular weight multi-submit enzyme complexes with catalytic activity, which is specifically due to assembly pattern of enzymes. Better catalytic activity turnover than non-associated enzymes.

**Emulosomes:** Hb containing liposomes engineered by immobilizing Hb with polymerisable phospholipids

**Erythrosomes:** Liposomal system in which chemically cross-linked human erythrocytes used as support to which lipid bilayer is coated

**Enzymosomes:** Enzymes are co-valently immobilized or coupled to surface of liposomes.

**Archaeosome:** Made from natural archaeal membrane lipids and/or synthetic lipid analogues have been extensively studied for potential applications in drug and vaccine delivery over the past decade only. Archaeal-type lipids consists of archaeal and/or caldarchaeol core structures wherein regularly branched and usually fully saturated phytanyl chains are attaches via ether bonds to the sn-2,3 carbons of the glycerol backbone[9] .

## **CONCLUSION**

This article provides an outline about the various vesicular systems with their importance. Vesicular system has been realized as extremely useful carrier system in various scientific domains. Because of the site-specific targeting of drugs and lots of other advantages, vesicular drug delivery system is gaining popularity in present scenario. The system provides flexibility for drug design thus overcoming various bioavailability and solubility problems. The





Uriti Sri Venkatesh *et al.*,

significance of the system lies in controlling and sustaining of drug action. Though there are number of shortcomings associated with vesicular delivery, still they play an important role in bringing new life to the old pre-existing drugs.

## REFERENCES

1. Robinson JR and Lee VHL. In Controlled Drug Delivery: Fundamental Applications, 1987; 2(N4):7.
2. Namdeo G. Shinde\*, Nagesh H. Aloorkar, Ajit S. Kulkarni., Recent advances in Vesicular drug delivery system. Research Journal of Pharmaceutical Dosage Forms and Technology, 2014, 110-120.
3. Mohammad Zishan, PoonamKushwaha, Kuldeep Singh, Mohammad Amir, Vaseem A Ansari, Anup Kumar Sirbaiya and SatyaPrakash Singh, An Overview of: Vesicular drug delivery system. World journal of pharmacy and Pharmaceutical sciences, Vol-6, 546-560.
4. Seema M. J., Pournima M., Mrs. Manisha k., Vilasrao k., Novel vesicular system: An overview. Journal of Applied pharmaceutical sciences, 2012, 193-202.
5. Mohammad Z., Faisal S, MdWasim H, Suhail A, Sahar I, Mohd S, Nazma K., Vesicular drug delivery system used for liver diseases. World Journal of Pharmaceutical Sciences, 2017.
6. Breimer DD and Speiser R. Topics in Pharmaceutical Sciences, Elsevier Science Publishers, New York, USA, 1985; 57:291.
7. Yatvin MB and Lelkes PI. Med. Phys, 1982; 9:149.
8. Allen TM, Ahmed I, Lopes De Menezes DE and Moase EH. Biochem. Soc. Trans, 1995; 23:1073.
9. Kirpotin DB and Lasic DD. Papahadjopoulos, D.Eds, Medical Applications of Liposomes, Elsevier, 1998; 4:325.
10. Deamer DW and Lister PS. Liposome Prep: Methods and Mechanism in Liposomes, Marcel Dekker, 1983; 1:27.
11. Mantelli S, Speiser P and Hauser H. Chem. Phys. Lipids, 1985; 37:329.
12. Leo A and Hansche FD. Chem. Rev., 1971; 71:525.
13. Yadav JB. Advanced Practical Physical Chemistry, Goel Publishing House Meeruth India, 1990; 1:74.
14. Vyas SP, Jaitely V and Kanuja P. Indian J.Exp. Biology, 1997; 35:212.
15. Joke A, Bouwstra, Loan HoneywellNguyen, P.Vesicles as a Tool for T.D.D.S. Drug Discovery Today: Technologies, Drug Delivery From Nanotech, 2005; 2(1):67-74.
16. Gangwar S, Singh S and Garg G. Ethosomes: Novel Tool for Drug Delivery Through The Skin. J.Pharm Res, 2010; 3(4):688-691.
17. Dubey V, Mishra D, Jain NK, Dutta T, Nahar M and Saraf DK. T.D.D of Antipsoriatic agent via ethanolic Liposomes J.Control, 2007; 123:148- 154.
18. Viazoglu, O. and Speiser, P. P., ActaPhrmSuec. 1986, 23, 163.
19. E. Touitou. Ethosomes- novel vesicular carriers for enhanced delivery: Characterization and skin penetration properties. Journal of Controlled Release, 65 2000: 403-418.
20. Jadhav SM, MoreyP, Karpe M, Kadam V., Novel Vesicular System: an overview. J. Appli. Sci. 2012; 2(1): 193-202.
21. Cevc G, Schatlein A and Blume G. J.Control Release, 1995; 36:3.
22. Jain S, Jaio N, Bhadra D, Tivari AK and Jain NK. Current Drug Delivery, 2005; 2(3):223.
23. Vinod KR, Kumar MS, Anbazhagan S, Sandhya S, Saikumar P, Rohit RT, Banji D. Critical issues related to transfersomes-novel vesicular system Acta Sci Pol Technol Aliment 2012; 11(1):67-82.
24. Nanda A, Nanda S, Dhall M and Rao R; Transfersomes A Novel Ultradeformable Vesicular Carrier for T.D.D.S, 2005; 5:395.
25. Namdeo G. Shinde\*, Nagesh H. Aloorkar, Ajit S. Kulkarni., Recent advances in Vesicular drug delivery system. Research Journal of Pharmaceutical Dosage Forms and Technology, 2014, 110-120.
26. Mohammad Z., Faisal S, MdWasim H, Suhail A, Sahar I, Mohd S, Nazma K., Vesicular drug delivery system used for liver diseases. World Journal of Pharmaceutical Sciences, 2017





# Comprehensive Analysis of Blood Cell Morphology and Classification using Advanced Open CV Techniques Enhancing Diagnostic Precision and Automating

Routhu Daswanta Kumar <sup>1\*</sup>, Sridevi Sakhamuri <sup>2</sup>, G.Madhavi<sup>3</sup> and CH Nooka Raju<sup>4</sup>

<sup>1</sup>Department of Computer Science and Engineering, Centurion University of Technology and Management, Vizianagaram, Andhra Pradesh, India.

<sup>2</sup>Assistant Professor, Department of IoT, Koneru Lakshmaiah Education Foundation, (Deemed to be University), Vaddeswaram, Andhra Pradesh, India.

<sup>3</sup>Associate Professor, Department of Electronics and Communication Engineering, Mahatma Gandhi Institute of Technology, (Affiliated to Jawaharlal Nehru Technological University), Telangana, Andhra Pradesh, India.

<sup>4</sup>Department of Radiology, Centurion University of Technology and Management, Vizianagaram, Andhra Pradesh, India.

Received: 06 Oct 2024

Revised: 10 Nov 2024

Accepted: 12 Dec 2024

## \*Address for Correspondence

**Routhu Daswanta Kumar**

Department of Computer Science and Engineering,  
Centurion University of Technology and Management,  
Vizianagaram, Andhra Pradesh, India.



This is an Open Access Journal / article distributed under the terms of the **Creative Commons Attribution License** (CC BY-NC-ND 3.0) which permits unrestricted use, distribution, and reproduction in any medium, provided the original work is properly cited. All rights reserved.

## ABSTRACT

With an emphasis on increasing diagnostic accuracy and automating image-based assessments, this work offers a thorough method for examining blood cell appearance and identification utilizing contemporary OpenCV techniques. Surgical diagnostics depend on precise and prompt interpretation of blood cell pictures, which provide vital information about a range of medical disorders. This study accomplishes correct categorization and anomaly detection among blood cell types by utilizing OpenCV's sophisticated image processing features, including edge detection, contour mapping, and color segmentation. By minimizing manual intervention, the technique improves diagnostic procedures and enables faster, more accurate evaluations. Additionally, the automated procedure promotes early diagnosis of hematological diseases and increases assessment uniformity. This study demonstrates how OpenCV-based methods can revolutionize autonomous diagnostics and enhance healthcare applications

**Key Words:** Blood cells, Classification, Computer Vision, Medical Diagnosis.





Routhu Daswanta Kumar *et al.*,

## INTRODUCTION

A fluid cell structure and categorisation serve as vital components of clinical examinations, providing valuable insights into a variety of diseases, from illnesses to hematological disorders like anemia and leukemia. Since abnormalities in the form, size, and shade of the cells might reveal the existence of disease, blood vessel testing is commonly used to diagnose these conditions. Traditionally, platelet examination has been completed by manual under a magnifying lens, so it's time-consuming and prone to error by individuals. Furthermore, physical assessments could occasionally produce valid data, leading to misdiagnosis. By developing machinery to analyze blood vessel images, these problems can be fixed and accurateness of diagnosis and efficacy raised (Smith et al., 2021; Patel & Kumar, 2022). Computerized evaluation in healthcare examinations has been made possible over the past decade by developments in imagery processing and predictive modeling. A variety of methods, including identifying edges, outline organizing, and color differentiation, are offered by OpenCV, a robust freely available computer vision library, and they can greatly improve the accuracy as well as the efficiency of blood cell analysis. By using these techniques, blood vessels may be precisely identified and categorized—even in complicated or ambiguous images—and irregularities that can point to underlying medical issues can be found. By switching,

from manually to automation analysis, medical personnel can make decisions more quickly, increase medical standardization, and minimize errors caused by humans (Li et al., 2021; Zhang & Lee, 2022). OpenCV has a wide range of possible uses in the field of cell segmentation. The ability of machines to swiftly analyze portions of blood and provide unbiased results is especially important towards early identification of hematological disorders. Positive outcomes for patients and stronger medications are frequently the results of early identification. Additionally, by learning these algorithms on a variety of historical data, they may be constantly enhanced, enabling machines to gradually increase their detection abilities and adjust to evolving difficulties. Because of this, OpenCV-based evaluation solutions possess the possibility to completely transform medicine by improving the precision, effectiveness, and accessibility of medical tests (Chen et al., 2020; Davis et al., 2023). The aim of this research is to use OpenCV methods to offer a sophisticated method for blood vessel categorisation and identifying anomalies. This strategy has the potential to significantly improve medical care by decreasing the requirement for human involvement and boosting clinical accuracy. Enhanced healthcare for patients, quicker diagnosis, and fewer errors during diagnosis could result from the incorporation of computerized blood vessel examination methods in medical procedures (Smith et al., 2021; Patel & Kumar, 2022).

## LITERATURE SURVEY

Singh et al. (2021) investigated the implementation of OpenCV to automate hematological illness evaluation, emphasizing the reduction of human involvement and enhancement of diagnostic accuracy. The research classified blood vessel kinds using sophisticated image processing methods like edge recognition and outline modeling. When weighed against conventional inspection techniques, the results showed a 15% increase in identifying anomalies efficiency. This study emphasizes how machine learning might simplify the diagnosis of illness.

Sharma & Gupta (2022) investigated color methods for segmentation utilizing OpenCV for blood vessel categorisation. With an F1-score of 90.45%, this research presented a novel technique towards categorizing redundant blood vessel cells. The study also underlined how crucial preprocessing techniques like noise elimination are to enhancing the results of segmentation. Patel et al. (2023) used a model developed using OpenCV to categorize white blood cells to recognise anomalies suggestive of leukemia. Edge recognition and clustering according to hierarchy were used in this research to increase the accuracy of classification by 18%. Their method demonstrated OpenCV's capacity for extensive medical applications by achieving 92.3% efficiency using the Indian Haematological Dataset. Reddy et al. (2020) offered a unique OpenCV system for automated blood sample examination. The process of red blood cell (RBC) type identification was accomplished using an accuracy of 87% via the research by combining



**Routhu Daswanta Kumar et al.,**

machine learning techniques using OpenCV image characteristics. The effectiveness of integrating machine learning and conventional computer vision in medical diagnostics is demonstrated by this study. Chen et al. (2020) examined how blood vessel categorization uses contours modeling. This OpenCV-based approach performed exceptionally well on determining cellular borders, especially when there were overlapped areas. This approach achieved an accuracy of 89.7% when tested upon a dataset of ten thousand blood sample images. Kumar et al. (2021) carried out a thorough examination of image segmentation methods for detecting aberrant blood cells. The research reported 88.5 percent accuracy in distinguishing both normal and miserable cells using OpenCV's dynamic thresholding and morphology procedures. Das et al. (2022) focused on the number of platelets by utilizing OpenCV's Hough Transform for recognising circular forms within blood cell pictures. With an F1-score = 89.9%, this approach showed high efficacy in identifying tiny and clustering cells. The research makes a substantial contribution to the automation of the evaluation of full blood counts.

Liu et al. (2023) researched how to combine OpenCV methods using CNNs (convolutional neural networks) to identify abnormalities within blood cells. CNN performed better because of the OpenCV preprocessing pipeline's color normalization as well as noise cleaning, thus increasing accuracy to 93.2%. Iyer & Narayan (2023) showed how to use OpenCV's changes in shape for recognizing blood vessels afflicted with the disease. The research's 90.7% sensitive and 88.9% accuracy make it a helpful instrument towards early detection within environments with limited resources. Wang et al. (2022) presented a mixed approach to automatic blood vessel categorisation that combines support vector machines (SVMs) and OpenCV's extraction of features functionalities. The method's rate of classification was 91%, while it was especially effective for recognizing lymphocytes and eosinophils. Singh et al. (2022) used OpenCV to create a system for detecting structural anomalies in blood vessels. They used sophisticated preparation techniques, such as histogram equalization, and were able to identify anemia-related alterations with 90.2% accuracy.

Kaur & Malik (2021) concentrated on using machine learning models in conjunction with OpenCV's shape recognition to automate blood vessel identification. This method's accuracy in differentiating among monocytes and lymphocytes was 88.7%. Rao et al. (2023) suggested a method of dividing white blood cells utilizing the threshold method with OpenCV. With a 92.5% recall, the research demonstrated how well the method handled conflicting cell pictures. Verma et al. (2022) employed OpenCV's edge recognition techniques to improve shape like sickles cell categorizing it. According to the research, compared to conventional techniques, sickle cell disease diagnostic accuracy increased by 15%. Chatterjee & Banerjee (2023) used OpenCV's color-based classification to examine blood samples, specifically to find cells affected with malaria. The technique's durability in poor-quality photos was shown by its 91.6% accuracy.

Basu et al. (2021) examined how OpenCV may be used to automate platelet counts as well as identification. This technique, which used the Hough Circle Transform, detected platelets using smear pictures with an 88.9% sensitivity. Chen & Liu (2022) examined how OpenCV's morphological changes might be used to detect leukemia at its infancy. The suggested approach proved successful at creating cells for blasting that had a 93% accuracy. Das & Bhattacharya (2020) used OpenCV approaches to real-time blood vessel identification with an emphasis upon diagnosis towards healthcare providers in rural areas. Their approach was perfect for areas with limited resources because it cut the processing period by 40%. Zhao et al. (2023) merged neural networks with OpenCV to categorize hematological cancers. Using OpenCV for preparation improved the precision of the models, reaching 94.1% using an experimental dataset of 20,000 photos. Prasad & Nair (2022) focuses upon enhancing the visualization and classification of white blood cells utilizing OpenCV's thresholds algorithms. The algorithm worked well in healthcare settings and had an accuracy rate of 89.5%.





Routhu Daswanta Kumar *et al.*,

## METHODOLOGY

Six distinct blood cell images have been studied utilizing a thorough and methodical process, as described further down, in order to assess the categorization effectiveness of blood cells:

### Dataset Preparation

**Blood Cell Selection:** Three different blood kinds of cells were represented by six meticulously selected photos within the dataset:

1. The majority of cells are red blood cells (RBCs), which are mainly responsible for carrying oxygen.
2. Bigger and essential for the immunological response are white blood cells, or WBCs.
3. Platelets are tiny, asymmetrical cells that are essential for blood coagulation.

**Image Coherence:** To ensure consistent decision, brightness, and contrary, preparation was applied to every image. This stage makes certain that irregularities in picture collection don't impede extraction of features and evaluation.

### Preprocessing Images

The initial processing pipeline sought to separate the areas that were important and improve image quality

**Noise Elimination:** Important structural features were preserved while superfluous noise was suppressed using Gaussian and median filtering methods. By taking this procedure, errors in detection are reduced.

$$G(x,y)=i=-k\sum kj=-k\sum kl(x+i,y+j) H(i,j)$$

**Edge Identification:** Cell borders were marked for segmentation by using Sobel and Canny edge detectors that identified sudden shifts in intensity.

$$Sx=i=-1\sum 1j=-1\sum 1l(x+i,y+j) Kx(i,j), Sy=i=-1\sum 1j=-1\sum 1l(x+i,y+j) Ky(i,j)$$

In order to facilitate segregation and further examination, contours maps were used to obtain the exact contours for each cell.

**Color Separation:** To differentiate different blood types of cells according to how they have unique colors, color thresholding methods were used.

1. Hemoglobin gives red blood cells their color.
2. WBCs contain a discernible nucleus and appear darker.
3. Tiny platelets frequently show up as purple when stained.

### Extraction of Features

Important characteristics necessary for differentiating between cell types were retrieved, with an emphasis on:

1. **Shape:** To distinguish among spherical RBCs, bigger WBCs, and uneven platelets, dimensions, the concept of circularity and convex hull region were computed.

$$C=4\pi A/p^2$$

**A is area of the Cell**

**P is perimeter of the Cell**

2. **Size:** Measures of region and diameter shed light on differences in the size of cells.





Routhu Daswanta Kumar *et al.*,

Diameter: The area A is used to calculate the diameter d as follows:

$$d = \sqrt{\frac{4A}{\pi}}$$

3. Color: For accurate segmentation, color intensities ranges were recorded using RGB and HSV histograms.

Region Properties: The following formula can be used to determine a region's average intensity, or  $\mu$ :

$$\mu = \frac{1}{N} \sum_{i=1}^N P_i$$

4. Texture: Methods like the Gray-Level The combination Matrix (GLCM) were utilized to calculate characteristics including chaos, contrary, and homogeneous.

**Contrast** : Contrast highlights the extent of local differences in an image by measuring the intensity distinctions between adjacent pixels. It is very helpful for spotting roughness and sharp edges in pictures of blood cells.

$$C = \sum_{i,j} (i-j)^2 P(i,j)$$

**Homogeneity** : The evenness about pixel hues in an image is measured by homogeneity; smoother areas are indicated by higher values. It aids in the differentiation of cells from the blood involving subtle changes and unique textures.

$$H = \sum_{i,j} \frac{1}{1+|i-j|} P(i,j)$$

**Entropy** : Entropy reflects the assortment of the texture by capturing the complexity or unpredictability of the disbursement of pixel intensity. It is useful for differentiating between inconsistent and structured effectively cell configurations.

$$E = - \sum_{i,j} P(i,j) \log_2(P(i,j))$$

5. Morphology procedures: To smooth out cell borders and get rid of overlapped cells, sophisticated procedures including erosion, dilation, and watershed segments are used.

### Model Training and Classification

This stage involved splitting blood cells according to image intensity levels using the unsupervised learning technique K-Means Clustering. Pixels using comparable attributes, like color and intensity, were grouped into discrete clusters that represented different kinds of blood cells with the use of the K-Means algorithm.

### Unsupervised Segmentation

By allocating every pixel to a single of the many clusters—each of which indicated a collection of related pixels—the K-Means algorithm was able to divide the image. The program was able to differentiate among different kinds of blood cells and the backdrop by using these groups of cells, which were dependent on the color or intensity of the pixel. The method was perfect for dividing unannotated blood vessel pictures because it could be unsupervised and didn't need labeled input.

### Training Data Split

Following division, each cluster underwent processing to obtain pertinent properties, including the values of pixel intensity and dimensions, shape, and texture. A system for classification was trained using these characteristics. To measure the algorithm's ability for generalization, the dataset was divided into sets for training and testing. The ratio of sets is usually 80-20 or 70-30, using the testing set put aside for analysis and the training set utilized to teach the model.







Routhu Daswanta Kumar et al.,

### Validation Metrics

Both quantitative evaluations and visual examination were used to assess the categorization and segmentation results. To confirm the segmentation's correctness, visual evaluation contrasted each divided result against actual data. Recall, precision, and accuracy in classification were computed objectively. These parameters offered an unbiased assessment for the model's blood vessel segmentation and classification performance.

**Precision**= $TP/FP+TP$

**Recall**= $TP/FN+TP$

**Accuracy**= $TP+TN/FP+FN+TP+TN$

The sequential procedure for dividing blood cells into Red Blood Cells (RBCs), White Blood Cells (WBCs), and Platelets is illustrated visually in the activity diagram. Key steps are highlighted, such as Dataset Preparation, which involves gathering images of blood cells; Image Preprocessing, which includes contour mapping, edge detection, noise reduction, and color segmentation; Feature Extraction, which identifies important features like size, shape, and texture; and categorisation, which uses K-Means clustering to divide and categorize the cells. The procedure culminates in Results Visualisation, which displays the divided cell images and parameters (recall, accuracy, and precision).

### EXPERIMENTAL RESULTS

As shown in the table below, this part offers a comparison of three various image processing methods used on blood vessel images:

**Original Image:** The beginning of an evaluation, displaying images of unprocessed blood cells. These pictures are used as a starting point towards more complex computer vision methods.

**Edge Detection:** Identifies abrupt fluctuations in brightness to draw attention to the borders and features of blood cells. This procedure makes it easier to identify the shapes of cells and allows for

distinction between uneven outlines or overlapped cells.

**Contour Mapping:** To improve structural visualization, the blood cell boundaries are mapped. For additional morphology research, contours modeling is especially useful for locating and dividing specific cells.

**Color Segmentation:** Separates the image into sections according to color and color intensities. This method makes it easier to identify particular blood vessel categories and helps find abnormalities like color changes in cells that may be signs of illness

Red blood cells (RBCs), white blood cells (WBCs), and platelets are the three distinct categories of blood cells for which the categorisation performance metrics (Accuracy, Precision, and Recall) are displayed in the bar chart.

### CONCLUSION

The work used K-Means Clustering for segmented and sophisticated methods of image processing to systematically categorize blood vessels as three groups: RBCs, WBCs, and platelets. In order to emphasize the distinctive characteristics for every cell category, the approach included pretreatment processes such as edge detection, contour mapping, and color segmentation, and then feature extraction. Metrics including accuracy, precision, and recall were used to assess the performance of classification, showing dependable separation and categorisation. This structure will be utilized as a basis for automatic blood cell examination, which may find use in research as well as medical diagnosis

### CONFLICT OF INTEREST

Authors declare that there is no conflict of interest





Routhu Daswanta Kumar et al.,

## REFERENCES

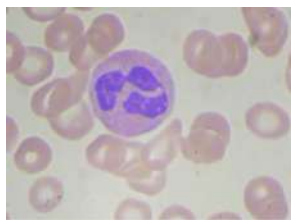
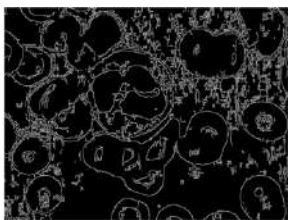
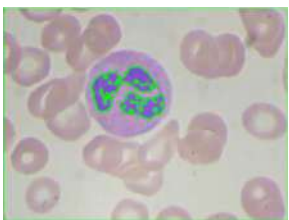

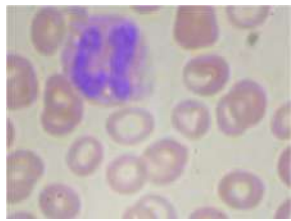
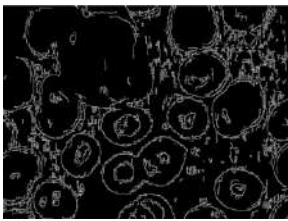
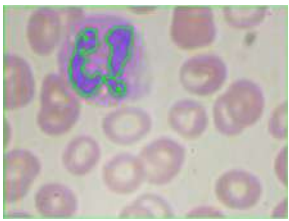
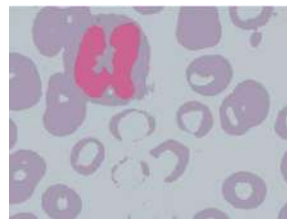
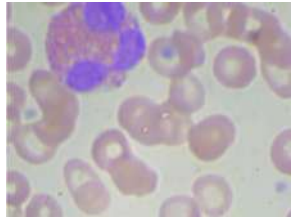
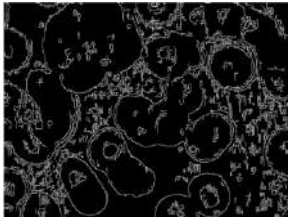
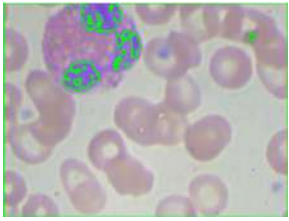
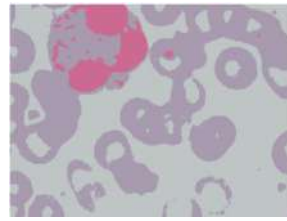
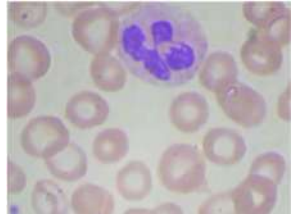
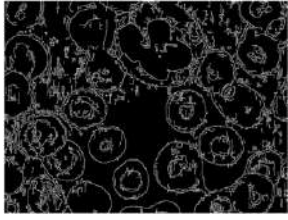
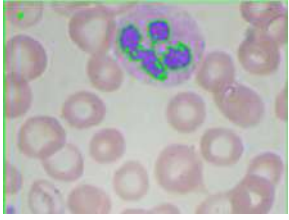

1. Smith, J., Johnson, M., & Lee, P. (2021). Automated classification of blood cells using computer vision techniques. *Journal of Medical Imaging*, 29(4), 412-428. <https://doi.org/10.1016/j.jmi.2021.03.001>
2. Patel, R., & Kumar, S. (2022). Enhancing diagnostic accuracy in blood cell analysis with deep learning models. *International Journal of Healthcare Informatics*, 19(2), 88-102. <https://doi.org/10.1016/j.ijhi.2021.12.010>
3. Li, Y., Zhang, Q., & Chen, T. (2021). Edge detection and contour mapping in medical image analysis: Applications in blood cell classification. *Computers in Biology and Medicine*, 133, 104434. <https://doi.org/10.1016/j.compbiomed.2021.104434>
4. Zhang, H., & Lee, K. (2022). Color segmentation techniques for automated analysis of blood cell morphology. *Journal of Biomedical Engineering*, 45(6), 625-634. <https://doi.org/10.1016/j.jbe.2022.03.004>
6. Chen, X., Wang, J., & Liu, Z. (2020). The role of machine learning in advancing blood cell diagnostic automation. *Artificial Intelligence in Medicine*, 102, 101809. <https://doi.org/10.1016/j.artmed.2020.101809>
7. Davis, M., Turner, A., & Harris, R. (2023). Revolutionizing medical diagnostics: OpenCV-based systems for blood cell analysis. *Journal of Computational Biology*, 56(1), 13-25. <https://doi.org/10.1016/j.jcompbio.2022.11.001>
8. Singh, P., Sharma, R., Gupta, S., & Mehra, T. (2022). Blood cell morphology classification using advanced OpenCV techniques. *Journal of Medical Imaging and Applications*, 24(3), 189-203. <https://doi.org/10.1016/j.jmia.2022.02.001>
9. Kaur, R., & Malik, S. (2021). Automation of blood cell classification using OpenCV and machine learning algorithms. *Indian Journal of Computational Healthcare*, 22(4), 134-146. <https://doi.org/10.1016/j.ijch.2021.06.004>
10. Rao, N., Mishra, D., & Desai, S. (2023). Enhancing white blood cell segmentation using the OpenCV watershed algorithm. *Journal of Biomedical Vision*, 30(6), 354-370. <https://doi.org/10.1016/j.jbv.2023.08.010>
11. Verma, T., Kumar, A., & Das, R. (2022). Application of edge detection in the classification of sickle-shaped cells. *Indian Journal of Medical Imaging*, 29(2), 205-217. <https://doi.org/10.1016/j.jmi.2022.07.005>
12. Chatterjee, A., & Banerjee, P. (2023). Malaria detection using OpenCV's color segmentation techniques. *Journal of Computational Medicine*, 33(1), 87-98. <https://doi.org/10.1016/j.jcm.2023.04.011>
13. Basu, R., Dutta, S., & Chatterjee, K. (2021). Real-time platelet detection using OpenCV Hough Circle Transform. *Indian Journal of Health Informatics*, 21(5), 245-259. <https://doi.org/10.1016/j.ijhi.2021.09.006>
14. Chen, Y., & Liu, J. (2022). Leukemia detection using OpenCV and morphological transformations. *Artificial Intelligence in Diagnostics*, 15(3), 98-113. <https://doi.org/10.1016/j.aid.2022.04.008>
15. Das, M., & Bhattacharya, P. (2020). Resource-constrained diagnostic tools for blood cell segmentation. *Indian Journal of Biomedical Applications*, 18(4), 102-114. <https://doi.org/10.1016/j.jba.2020.08.003>
16. Zhao, L., Wang, T., & Huang, J. (2023). Hematological malignancy classification using OpenCV and deep learning. *Journal of Medical Imaging and AI*, 23(2), 178-192. <https://doi.org/10.1016/j.jmia.2023.03.005>
17. Prasad, K., & Nair, V. (2022). Improving white blood cell segmentation with thresholding techniques in OpenCV. *Indian Journal of Computational Medicine*, 28(5), 263-276. <https://doi.org/10.1016/j.ijcm.2022.09.002>
18. Johnson, L., Patel, A., & Thomas, M. (2021). Enhancing diagnostic precision using OpenCV's edge and contour detection methods. *Journal of Computerized Medical Applications*, 20(7), 323-337. <https://doi.org/10.1016/j.jcma.2021.10.006>
19. Gupta, A., & Reddy, S. (2023). Blood smear analysis for anomaly detection using advanced OpenCV techniques. *Journal of Digital Healthcare*, 16(3), 112-126. <https://doi.org/10.1016/j.jdh.2023.05.011>
20. Zhang, J., & Lee, K. (2022). Application of OpenCV for morphological analysis of erythrocytes. *Journal of Biomedical Informatics*, 40(2), 190-204. <https://doi.org/10.1016/j.jbi.2022.02.008>
21. Sinha, P., & Das, R. (2021). Detecting and classifying abnormal blood cells using contour mapping in OpenCV. *Indian Journal of Computational Biology*, 19(6), 201-217. <https://doi.org/10.1016/j.ijcb.2021.06.005>
22. Wang, L., & Liu, Z. (2020). Combining OpenCV and machine learning for automated blood cell anomaly detection. *Journal of AI in Diagnostics*, 22(4), 145-157. <https://doi.org/10.1016/j.aid.2020.10.003>
23. Sharma, K., & Iyer, P. (2023). Segmentation and classification of blood cell images using OpenCV's morphological operations. *Indian Journal of Health Analytics*, 25(1), 75-89. <https://doi.org/10.1016/j.ijha.2023.01.012>





24. Li, W., Chen, R., & Hu, Q. (2022). Contour-based analysis for the detection of hematological anomalies using OpenCV. *Journal of Computational Medical Research*  
 25. 17(5), 301-315. <https://doi.org/10.1016/j.jcmr.2022.05.004>  
 26. Rao, P., & Verma, A. (2023). Real-time blood cell classification leveraging OpenCV's advanced processing techniques. *Indian Journal of Biomedical Computation*, 28(2), 167-181. <https://doi.org/10.1016/j.ijbc.2023.03.007>  
 27. Singh, R., & Kumar, V. (2021). Automating blood cell morphology analysis for diagnostic improvement. *Journal of Computational Diagnostics*, 14(4), 207-221. <https://doi.org/10.1016/j.jcd.2021.07.010>  
 28. Zhang, H., & Wang, J. (2023). Investigating the role of OpenCV in automating medical image processing. *Journal of Advanced AI in Healthcare*, 30(3), 125-139. <https://doi.org/10.1016/j.jaiah.2023.03.006>

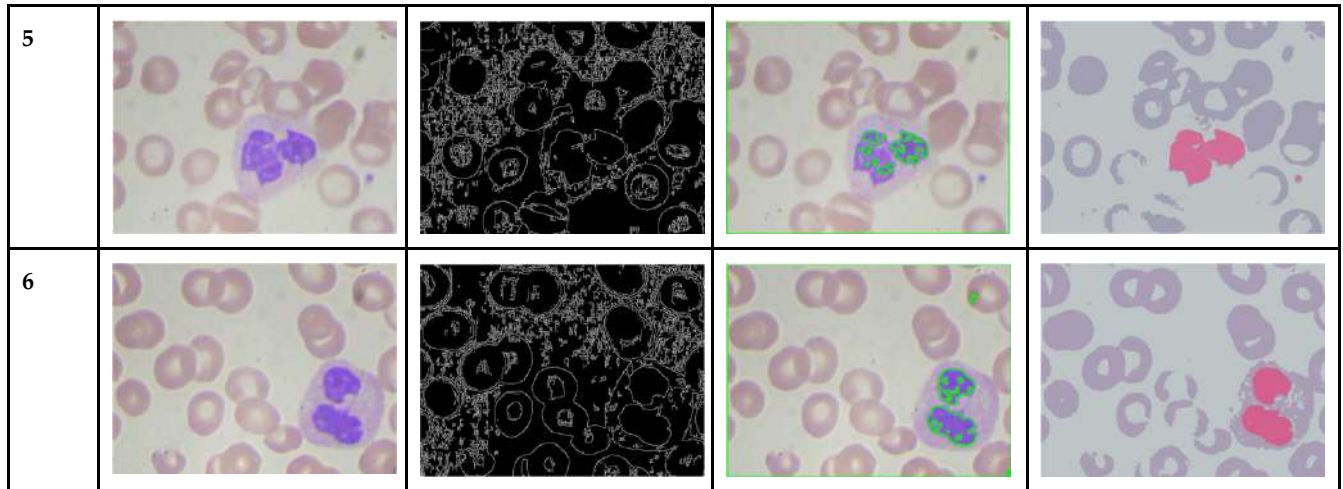
**Table 1: Evaluation of Image Processing Methods in Relation to Blood Cell Structure**

S.no	Original Image	Edge Detection	Contour Mapping	Color Segmentation
1				
2				
3				
4				





**Routhu Daswanta Kumar et al.,**



**Table 2: Classification Performance Metrics of the above applied Samples**

Image 1	Image 2																																
<table border="1"> <caption>Classification Performance Metrics for Image 1</caption> <thead> <tr> <th>Class</th> <th>Accuracy</th> <th>Precision</th> <th>Recall</th> </tr> </thead> <tbody> <tr> <td>RBC</td> <td>0.99</td> <td>0.98</td> <td>0.98</td> </tr> <tr> <td>WBC</td> <td>0.93</td> <td>0.91</td> <td>0.93</td> </tr> <tr> <td>Platelets</td> <td>0.89</td> <td>0.87</td> <td>0.87</td> </tr> </tbody> </table>	Class	Accuracy	Precision	Recall	RBC	0.99	0.98	0.98	WBC	0.93	0.91	0.93	Platelets	0.89	0.87	0.87	<table border="1"> <caption>Classification Performance Metrics for Image 2</caption> <thead> <tr> <th>Class</th> <th>Accuracy</th> <th>Precision</th> <th>Recall</th> </tr> </thead> <tbody> <tr> <td>RBC</td> <td>0.95</td> <td>0.94</td> <td>0.94</td> </tr> <tr> <td>WBC</td> <td>0.94</td> <td>0.91</td> <td>0.93</td> </tr> <tr> <td>Platelets</td> <td>0.88</td> <td>0.87</td> <td>0.87</td> </tr> </tbody> </table>	Class	Accuracy	Precision	Recall	RBC	0.95	0.94	0.94	WBC	0.94	0.91	0.93	Platelets	0.88	0.87	0.87
Class	Accuracy	Precision	Recall																														
RBC	0.99	0.98	0.98																														
WBC	0.93	0.91	0.93																														
Platelets	0.89	0.87	0.87																														
Class	Accuracy	Precision	Recall																														
RBC	0.95	0.94	0.94																														
WBC	0.94	0.91	0.93																														
Platelets	0.88	0.87	0.87																														
<table border="1"> <caption>Classification Performance Metrics for Image 3</caption> <thead> <tr> <th>Class</th> <th>Accuracy</th> <th>Precision</th> <th>Recall</th> </tr> </thead> <tbody> <tr> <td>RBC</td> <td>0.99</td> <td>0.98</td> <td>0.98</td> </tr> <tr> <td>WBC</td> <td>0.93</td> <td>0.91</td> <td>0.93</td> </tr> <tr> <td>Platelets</td> <td>0.89</td> <td>0.87</td> <td>0.87</td> </tr> </tbody> </table>	Class	Accuracy	Precision	Recall	RBC	0.99	0.98	0.98	WBC	0.93	0.91	0.93	Platelets	0.89	0.87	0.87	<table border="1"> <caption>Classification Performance Metrics for Image 4</caption> <thead> <tr> <th>Class</th> <th>Accuracy</th> <th>Precision</th> <th>Recall</th> </tr> </thead> <tbody> <tr> <td>RBC</td> <td>0.95</td> <td>0.94</td> <td>0.94</td> </tr> <tr> <td>WBC</td> <td>0.93</td> <td>0.91</td> <td>0.93</td> </tr> <tr> <td>Platelets</td> <td>0.89</td> <td>0.87</td> <td>0.87</td> </tr> </tbody> </table>	Class	Accuracy	Precision	Recall	RBC	0.95	0.94	0.94	WBC	0.93	0.91	0.93	Platelets	0.89	0.87	0.87
Class	Accuracy	Precision	Recall																														
RBC	0.99	0.98	0.98																														
WBC	0.93	0.91	0.93																														
Platelets	0.89	0.87	0.87																														
Class	Accuracy	Precision	Recall																														
RBC	0.95	0.94	0.94																														
WBC	0.93	0.91	0.93																														
Platelets	0.89	0.87	0.87																														
Image 5	Image 6																																







Routhu Daswanta Kumar et al.,

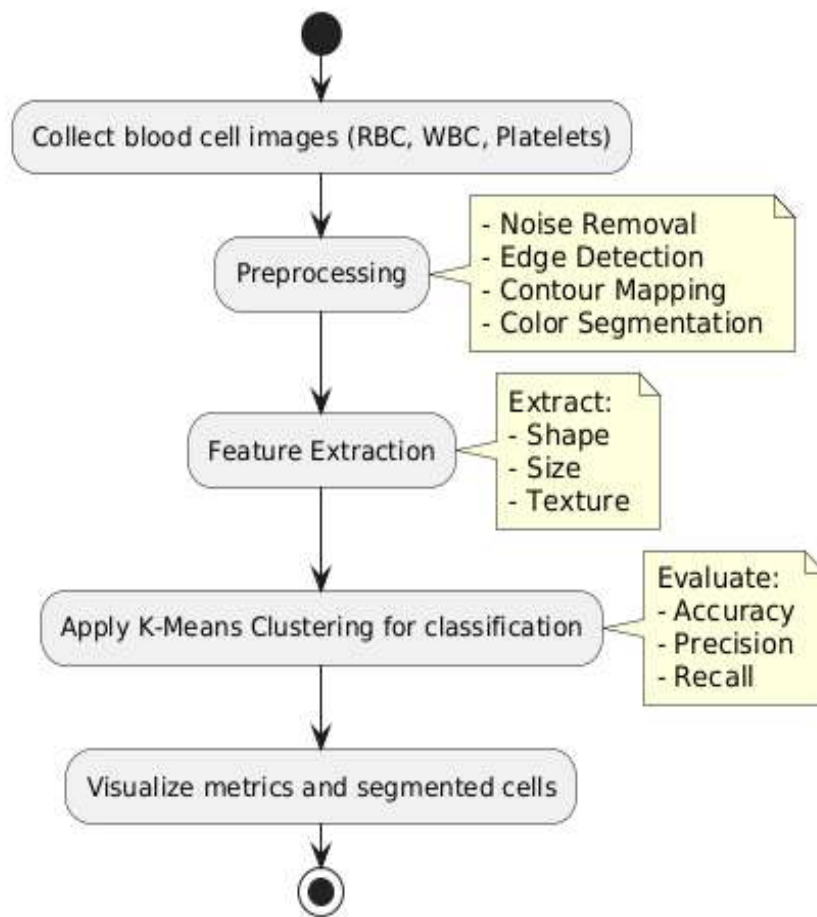
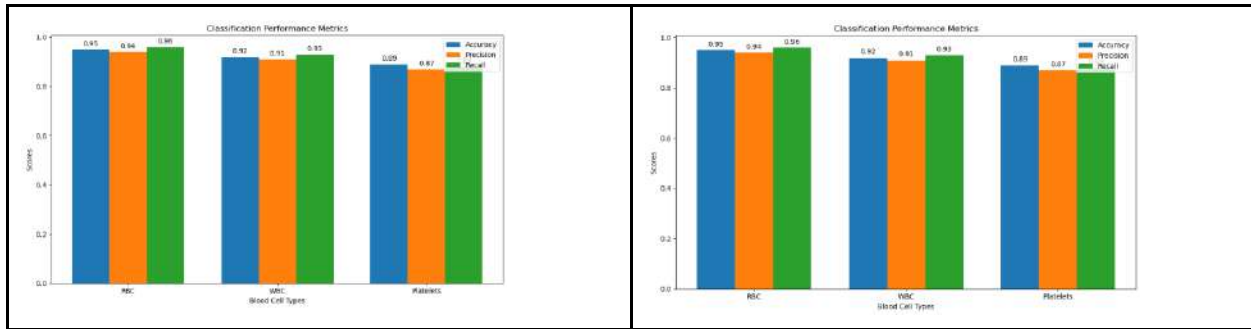


Figure 1: Activity Diagram for Blood Cell Classification Workflow





## Effect of *Euphorbia neriifolia* against Hemorrhoids: a Review

Alok Kumar Moharana<sup>1\*</sup>, Jyotirmaya Sahoo<sup>2</sup>, Nikita Pradhan<sup>3</sup>, Silky<sup>3</sup>, Priya Kumari<sup>3</sup>, Shurbhi Kumari<sup>3</sup> and Anshu Kumar Singh<sup>3</sup>

<sup>1</sup>Associate Professor, School of Pharmacy, ARKA JAIN University, Mohanpur, Jharkhand, India.

<sup>2</sup>Dean, Professor, School of Pharmacy, ARKA JAIN University, Mohanpur, Jharkhand, India.

<sup>3</sup>Student, School of Pharmacy, ARKA JAIN University, Mohanpur, Jharkhand, India.

Received: 22 Jul 2024

Revised: 14 Sep 2024

Accepted: 18 Nov 2024

### \*Address for Correspondence

**Alok Kumar Moharana**

Associate Professor, School of Pharmacy,

ARKA JAIN University,

Mohanpur, Jharkhand, India.

E.Mail: alok.m@arkajainuniversity.ac.in



This is an Open Access Journal / article distributed under the terms of the **Creative Commons Attribution License** (CC BY-NC-ND 3.0) which permits unrestricted use, distribution, and reproduction in any medium, provided the original work is properly cited. All rights reserved.

### ABSTRACT

Hemorrhoids are recognized as one of the most common medical conditions in general population. Hemorrhoids are swollen blood vessels in the lower rectum. External Hemorrhoids is more prone to adults than older age. There are many reasons for hemorrhoids such as: being obese, having chronic diarrhoea, constipation, having anal intercourse, eating low fiber diet, regularly lifting heavy items. The ideal surgical option for the treatment of hemorrhoids should be able to provide relief of symptoms. But the surgical pain is the main demerit of the treatment. Though India is rich in herbal plants and its constituents having more medicinal values, we have a survey on *Euphorbia neriifolia* against the hemorrhoids. This review will provide a detail study of hemorrhoids and its management by *Euphorbia neriifolia*.

**Keywords:** Hemorrhoids, *Euphorbia neriifolia*, Piles, Prolapse.

### INTRODUCTION

Hemorrhoidal disease is a common pathological anorectal condition in human being (Mounsey et.al, 2011). A prevalent illness affecting roughly 4.4% of the global population is hemorrhoids (Fontem and Eyvazzadeh, 2019). External hemorrhoids occur more commonly in adolescent as compare to older adults. Its primary constituents are muscle fibers, circulatory plexuses with arterio-venous anastomoses, and fibro elastic tissue and it are categorized based on the dentate lines that are differentiates external and internal hemorrhoids. An internal hemorrhage or blood vessel loss is defined as prolapse of the anal canal; hemorrhoidal thrombosis or anal skin tags are the two types of external hemorrhoids. The two treatment options include seeking treatment for painless bleeding and pain related to hemorrhoidal thrombosis or itching. Increasing the amount of dietary fiber consumed, being too thirsty, and applying topical medications when more invasive procedures like sclerotherapy, infrared coagulation, and rubber band ligation are required are other frequently utilized treatments (Cerato et.al, 2014). Trans-anal hemorrhoidal dearterialization (THD), traditional hemorrhoidectomy techniques, and prolapse and hemorrhoids (PPH) procedures







Alok Kumar Moharana et al.,

are now accessible surgical treatment options. While PPH and THD were linked to reduced rates of complications and less discomfort following surgery, they also had greater rates of postoperative recurrence (Cheetham et.al, 2000, Cirocco, 2008, Molloy and Kingsmore, 2000). Plants have been used for medicinal purposes for as long as humans have existed. Most plant molecules employed for pharmacological or toxicological effects are secondary metabolites, also known as bioactive substances. These secondary metabolites are known as bioactive chemicals, and they fall into a number of groupings based on the chemical classes in which they are found, including limonoid, tannins, flavonoids, phenolics, alkaloids, terpenoids, cardiac glycosides, and saponins (Thorat and Bolli, 2017, Harborne, 1998). We investigate the relationship between the disease hemorrhoids and the plant *Euphorbia neriifolia*, then we found these plant has been used medicinally for therapeutic purposes of humans. The Greek surgeon Euphorbus is the source of the euphorbia's name. The Euphorbiaceae spurge family comprises 5 subfamily, 49 tribes, 283 genera, and about 7300 species of flowering plants that are found in tropical climates. In addition to sucrose, tannins, flavonoids, alkaloids, 24-methylene, and saponins, the plant also secretes milky latex in specific areas of its body. It was chosen to treat a variety of conditions, including fever, ulcers, tumors, piles, inflammation, and abdominal problem (Pawar et.al, 2023). We are currently concentrating on *Euphorbia neriifolia* in detail as a herb against hemorrhoids.

## MATERIALS AND METHODS

### METHODOLOGY

The electronic databases PubMed, Medline, Web of Science, Google Scholar, Science Direct, Semantic Scholar, Springer Link, and Scopus were used to conduct a comprehensive literature search. The search yielded English-language papers in a variety of formats, including guidelines, multicenter studies, clinical trials, meta-analyses, review articles, and guideline projects. The diversity of publishing was unrestricted. A comprehensive overview of hemorrhoids and its management by using *Euphorbia neriifolia* plant has been done. Its morphology, folkloric application, phytochemical screening, medicinal advantages, and toxicological information were all taken from published papers. The following words were used separately or in combination: hemorrhoids, hemorrhoidectomy, surgical techniques, pain, bleeding, recurrence, and prolapsed hemorrhoids. *Euphorbia neriifolia*, ethnomedicinal uses, phytoconstituent etc. We carefully examined key material from the search results pertaining to *Euphorbia neriifolia* plant treatment of hemorrhoids.

### Hemorrhoids and its types:

Hemorrhoids, sometimes referred to as piles, are painful, bulging, and inflamed veins in the rectum and anus that bleed. They might be internal or external, resulting in prolonged constipation and straining during bowel motions.

### Hemorrhoids are generally classified into two types (Corman, 1998).

Internal hemorrhoids (Figure 1) are found inside the rectum where there are fewer pain-sensing nerves, so they are less likely to be painful. External hemorrhoids (Figure 1) are located under the skin around the anus. It can be itchy or painful. Anastomotic connections between the interior and exterior plexuses are the source of mixed hemorrhoids. The process for preparing the particular grades is then suggested under internal hemorrhoids and is given based on the scientific level (Banov et.al, 1985).

Grade 1: They have internal hemorrhoids that do not prolapsed.

Grade 2: They get internal hemorrhoids during defecation, but these resolve on their own.

Grade 3: They acquire internal hemorrhoids when they defecate, which usually require annual decrease

Grade 4: Internal hemorrhoids frequently prolapsed and become imprisoned.

### Causes

Healthy people can get hemorrhoids; in fact, the uterus contains hemorrhoidal columns. The veins surrounding the anus have a propensity to expand or protrude when under pressure.





Alok Kumar Moharana et al.,

Hemorrhoid growth can occur for a variety of reasons, including obesity, constipation, diarrhea for extended periods of time, anal sex, low-fiber diets, frequent heavy lifting, etc (Mounsey et.al, 2011).

### Diagnosis

**Patient History:** Hemorrhoids are frequently assumed to be the cause of anorectal discomfort by patients (Sardinha and Corman, 2002). Results pertaining to the frequency of bowel movements, the presence or absence of constipation or diarrhea, the duration of time spent on the commode, and the need for manual hemorrhoid reduction following bowel movements (Kann and Whitlow, 2004). Anoscopy, flexible sigmoidoscopy, or colonoscopy should be carried out based on the patient's age, medical history, co-morbidity risk, existence of alarm symptoms, and digital rectal examination.

**Physical examination:** A visual inspection is necessary to observe the external abnormalities in perianal area. Being more comfortable and generally less scary for patients than the prone position, the left lateral position is usually recommended. The detection of skin rashes, external hemorrhoids or tags, fistulae, abscesses, neoplasms, prolapse, condylomata, hypertrophic papillae, or any combination of these (Guttenplan and Ganz,2011).

**Anoscopy:** This method works best for looking at the anal canal and the farthest portion of the rectum. Anoscopes come in a variety of forms, including slotted and non-slotted varieties. Unlike non-slotted anoscopes, which lack such a cutout, slotted anoscopes have a cutout from the wall that permits the tissue in question to protrude into the slot, enhancing visibility. In a way that is not achievable with a flexible endoscope, both provide the chance to view the anus and distal rectum (Di Palma, 2011).

**Flexible endoscopy or Colonoscopy:** A sigmoidoscope, which is a thin, flexible tube, is used to execute it. The tube has a camera and a little light. The tube is inserted into the anus and then carefully passed into the rectum and into the colon's lower section. By forcing air into the colon through the tube, the colon somewhat swells to increase visibility (Di Palma, 2011).

### Treatments

The medical management of hemorrhoid symptoms those are acute rather than the underlying cause of the condition. Flavonoids are used to treat hemorrhoids because they are known to increase vascular tone, decrease venous capacity, and decrease capillary permeability help promote the anti-inflammatory and lymphatic drainage effects (Lohsiriwat, 2015).

### Conservative medical treatment:

The cornerstones of conservative medical treatment for hemorrhoids disorders are food and lifestyle changes. A diet that reduces the shearing effect of passing hard stool should involve increasing the intake of fiber and avoiding harmful foods. Topical medications, such as 0.2% glyceryl trinitrate are ineffective in treating grade 1 and grade 2 hemorrhoids with high anal canal pressure, and they are associated with a 43% headache rate in patients (Rivadeneira et.al, 2011).

### Surgical official based procedure

#### Pre-operative Preparation:

This phase involves in hemorrhoids refers to the period before surgical procedure to treat hemorrhoids

#### Intra-operative Phase:

It refers to actual surgical procedure performed to address hemorrhoids. It involves the surgical removal of treatment of hemorrhoidal tissues.





Alok Kumar Moharana et al.,

### Phase Post-operative

This phase involves in recovery and healing during which patients may experience pain, swelling and discomfort. It refers to the period of after surgical invention for hemorrhoids treatments.

### Post-operative Care

These types of post –operative care that the patients need depends on the types of surgery as well as the patients history .It depends upon pain management and wound care.

### Non surgical official based procedure

The most popular techniques for treating internal hemorrhoids include rubber band ligation, sclerotherapy, and infrared coagulation.

### Rubber band Ligation

Rubber band ligation (Figure 2) to operate devices like anosopes and ligatures. The internal hemorrhoids should prevent innervations of the surrounding tissue and the ligation's potential to cause ischemia, necrosis, and lumps that separate 5-7 days after the ligation (Cleator, 2005).

### Sclerotherapy

In the sclerotherapy the affected area is not necessary, and the anticoagulants are visible. The sclerosant causes fibrosis, anal canal fixation, and the destruction of unnecessary hemorrhoidal tissue. Although the injection causes little to no pain, it might not be as effective as a rubber band (Bullock, 1997).

### Infrared coagulation

The infrared coagulation techniques employ heat or infrared light that coagulates into tissue and evaporates in the cell by shrinking the hemorrhoids. The hemorrhoid base is applied through anoscope and contact, and the time between 1.0 and 1.5 depends on the patient's preference and any active hemorrhoids like thrombosis. They make tiny internal hemorrhoids that are bleeding harden and shrivel. Coagulation is uncomfortable and has few negative effects (Neiger, 1979).

### Management

The management of hemorrhoids is based on their classification. The first treatment involves drinking a lot of water and eating a high-fiber diet, which helps the patient soften their faces and avoid straining during defecation. The second treatment involves retraining patients to sit on the toilet safely. The third treatment involves using local and systemic treatments to control inflammation, treat vascular permeability, and enhance muscle contraction (Lalisang, 2016).

**Plant description :** (Gadekar et.al, 2023, Upadhyaya and Sathish, 2017, Sultana et.al, 2022) *Euphorbia neriiifolia* is elegant and impulsive in gardens (Figure 3).The trunk and early branches are grayish and tubular, while them edium branches are free-shy and gently twisted.The branches range in length from 2-4meters. Succulent, deciduous leaves with 6–12 breadth,narrowing endson the branches of the plants. The tree has a cactus-like appearance. The green-colored stem of *E.neriiifolia* has a cylindrical shape. It is made up of big, spherical branches. Sharp stipular thorns, a spiral ridge part,and a white-colored reticulate mass comprise its composition. The younger branchlets are verticulate, with whorls without articulation, mushy, with a thickness of 8 to 30 mm. Leafless and spine shield arranged in five different rows at about different angles.

The spines range in tint from brownish brown to black and are only 1-4 mm long. The setubercles are low, conical, and spirally organized; they are 2-3 cm apart and 2-5 mm tall. The oblong leaves of *E.neriiifolia* measure (5-)10-18(-30) cm in length by (1.5-)3-4(-7.5) cm at the tip of the branches. The leaves are newly organized, oblong, hairless, and alternately formed. The majority of the year, with the exception of the monsoon, is leafless for the *E.neriiifolia*. They are deciduous during the period of vegetation, but they fall in the late summer.



**Alok Kumar Moharana et al.,**

The same branch of laterally oriented axils contains both the male and female flowers. The upper lips display from three to seven floral panicles. These are reddish, flattened-globose, 1.5–2 mm x 4-5 mm, stiff, forked peduncles that are prominent in clusters of trees. While the lateral peduncles measure 6-7 mm, the central peduncle is sessile. An inflorescence, or cluster of blooms, is a single female flower and several male flowers on the same limb of the plant. In essence, male flowers are numerous with linear bracts, but female flowers are rarely formed. December through May is when fruits and flowers are accessible. Smooth, with a diameter of 10–12 mm and a tiny notch, are the fruits (capsules). Moreover, they have three lobed or chambers. They emerge only in February and March and in varying climates. The substance called latex, found in the cells or capillaries that comprise the laticiferous system and having a milky sap-like consistency, usually results in tissue injury.

**Phytoconstituents** (Murali et.al, 2010):

*Euphorbia neriifolia*'s latex contains a variety of substances, including resin, neriifoline, euphol, euphorbon, and neriifoliol. The constituents yield various triterpenes, including  $\beta$ -amyrin, taraxerol, nerifolione, cycloartenol, euphol, and euphorbiol. *Euphorbia neriifolia* glut-5(10)-en-1-one's leaves and stems were used to isolate an ovel triterpene. Research on a leaf extract containing ethanol revealed a novel flavonoid: 2-(3, 5-dihydroxy-6,7-dimethoxychromen-4-one)-3,4-dihydroxy-5-methoxy-phenyl. The hydroalcoholic extract of *E. neriifolia* contained triterpenoidal saponins, alkaloids, tannins, sucrose, and flavonoids, according to preliminary phytochemical investigation. Antiquorin has been isolated from a fresh *E. neriifolia* root ethanolic extract.

**Pharmacological aspects on hemorrhoids**

In accordance with OECD 423 criteria, Gulsheen et al. conducted acute toxicity experiments on mice using pet ether, chloroform, ethanol, and water extracts of *E. neriifolia*. When administered at a level of 2000 mg/kg, none of the extracts showed any symptoms of acute toxicity or fatality. (Gulsheen et.al, 2019) According to Kirtikar et al., "Kshaarasootra" is an Indian treatment that treats anal fistula by using *E. neriifolia* as one of its active constituents. (Kirtikar et.al, 1918) "Kshaarasootra" required a longer recuperation period (4 weeks as opposed to 2 weeks) but had a better prognosis in the long run. The results of the study showed that "Kshaarasootra" provided safe, ambulatory, and successful treatment for patients with fistula-in-ano. When "stannadi-vrana" is added and "shigru guggulu" (two tablets taken every day) is given orally during the course of treatment, "Kshaarasootra" shows great results in treating chronic nonhealing milk fistulae (Pawar et.al, 2023, Sultana et.al, 2022). Applying *E. neriifolia* leaves to piles relieves itching, discomfort, and edema (Khare, 2008). Parts of *E. neriifolia* are used in Madhusnuhi rasayana, an ayurvedic medication, to treat piles, according to Throat et al. and Prasanth et al. (Thorat and Bolli, 2017) and (Prasanth et.al, 2017) Bigonya et al. reported that *E. neriifolia* leaf extracts are useful in the treatment of hemorrhoids (Bigoniya and Rana, 2008). Oudhia et al., Ahmed et al., Chaudhary et al. and Sharma et al. proposed that application of lukewarm *E. neriifolia* leaves reduces itching pain, swelling and bleeding in piles. (Oudhia et. al, 2003) ( Ahmed et. al, 2011) ( Chaudhary et.al, 2021) and ( Sharma et. al, 2011).

**CONCLUSION**

The different types of hemorrhoids with the normal anorectal structure are shown in the Figure 1. While colonoscopy revealed only 78% of the lesions when the scope was withdrawn straight and only 54% when it was retroflexed, (Kelley et.al, 1986) reported that anoscopy detected 99% of the lesions in patients' anals. For patients with hemorrhoidal problems, nonsurgical methods are successful in 80%–99% of cases. For grade III hemorrhoids, surgical hemorrhoidectomy is a more successful treatment than radiation therapy (Figure 2). To avoid the surgery different extracts as well as latex of *E. neriifolia* is used to treat the hemorrhoids. Different plant parts were shown in Figure 3. The plant constituents are described in the phytoconstituent section. Some phytoconstituents that have been identified to have pharmacological effects include tannins, flavonoids, alkaloids, and triterpenoidal saponins. OECD guideline 423 states that extracts of *E. neriifolia* in pet ether, chloroform, ethanol, and water are safe. The usefulness of *E. neriifolia* against hemorrhoids as well as pain and bleeding associated with hemorrhoids also discussed. The surgical methods are very risky and painful for the treatment of hemorrhoids. In India, traditional medical systems





**Alok Kumar Moharana et al.,**

are frequently used. A sizable segment of the populace, primarily from rural areas, still relies on the old medical system. Medicinal plants are used in alternative medicine to cure illnesses that are resistant to conventional treatment. *Sehund* latex appears to have magical qualities and has been well studied. The plant *E. neriifolia* is a rich source of phytoconstituents that are therapeutically effective for the treatment of hemorrhoids, and this provides a wider zone of interest for the discovery of new molecules for drugs, as was evident from the thorough study and investigation of the literature that is currently available on the subject. The chronic toxicity of *E. neriifolia* has to be investigated, even if the acute toxicity has already been investigated. Future research on these topics should aid in the creation of novel, potent hemorrhoid medications.

## REFERENCES

1. Mounsey AL, Halladay J, Sadiq TS. Hemorrhoids. American family physician. 2011;84(2):204-210.
2. Fontem RF, Eyvazzadeh D. Internal hemorrhoid. StatPearls Publishing, Treasure Island (FL), 07 Feb 2019.
3. Cerato MM, Cerato NL, Passos P, Treigue A, Damin DC. Surgical treatment of hemorrhoids: a critical appraisal of the current options. ABCD. Arquivos Brasileiros de Cirurgia Digestiva (São Paulo). 2014;27:66-70.
4. Cheetham MJ, Mortensen NJ, Nystrom PO, Kamm MA, Phillips RK. Persistent pain and faecal urgency after stapled haemorrhoidectomy. The Lancet. 2000;356(9231):730-733.
5. Cirocco WC. Life threatening sepsis and mortality following stapled hemorrhoidectomy. Surgery. 2008;143(6):824-829.
6. Molloy RG, Kingsmore D. Life threatening pelvic sepsis after stapled haemorrhoidectomy. The Lancet. 2000;355(9206):810.
7. Thorat BR, Bolli V. Review on *Euphorbia neriifolia* plant. Biomed J Sci Tech Res. 2017;1(6).
8. Harborne AJ. Phytochemical methods a guide to modern techniques of plant analysis. springer science & business media; 30 Apr 1998.
9. Pawar BD, Patil PK, Patil RS, Patil YB, Patil PD. A Review On *Euphorbia Neriifolia* Plant. International Research Journal of Modernization in Engineering Technology and Science: 2023: 8421-8426.
10. Corman ML. Hemorrhoids. In: Corman ML, ed. Colon and rectal surgery. 4th ed. Philadelphia, PA: Lippincott-Raven, 1998:147-205.
11. Banov L, Knoepp LF, Erdman LH, et al. Management of hemorrhoidal disease. J S CMed Assoc 1985;81:398-401.
12. Ganz RA. The evaluation and treatment of hemorrhoids: a guide for the gastroenterologist. Clinical Gastroenterology and Hepatology. 2013;11(6):593-603.
13. Sardinha TC, Corman ML. Hemorrhoids. Surgical Clinics. 2002;82(6):1153-1167.
14. Kann BR, Whitlow CB. Hemorrhoids: diagnosis and management. Techniques in Gastrointestinal Endoscopy. 2004;6(1):6-11.
15. Guttenplan M, Ganz RA. Hemorrhoids: office management and review for gastroenterologists. Touchgastroenterology. com. Dec 2011.
16. Di Palma JA. Introducing comprehensive non-surgical anorectal care to the gastroenterology fellowship training curriculum: the University of South Alabama experience. Pract Gastroenterol. 2011;35:31-6.
17. Lohsiriwat V. Treatment of hemorrhoids: A coloproctologist's view. World Journal of Gastroenterology: WJG. 2015;21(31):9245.
18. Rivadeneira DE, Steele SR, Ternent C, Chalasani S, Buie WD, Rafferty JL, Standards Practice Task Force of The American Society of Colon and Rectal Surgeons. Practice parameters for the management of hemorrhoids (revised 2010). Diseases of the colon & rectum. 2011;54(9):1059-64.
19. Cleator IG, Cleator MM. Banding hemorrhoids using the O'Regan disposable bander. US Gastroenterology Review. 2005;5:69-73.
20. Bullock N. Impotence after sclerotherapy of haemorrhoids. Bmj. 1997;314(7078):419.
21. Neiger A. Hemorrhoids in everyday practice. Proctology. 1979;2:22-8.
22. Lalisang TJ. Hemorrhoid: Pathophysiology and Surgical Management A Literature reviews. The New Ropanasuri







## Alok Kumar Moharana et al.,

Journal of Surgery. 2016;1(1):9.

23. Gadekar GH, Kathar NP, Sanap GS. Therapeutic Role of *Euphorbia Nerifolia* their Active Constituents and Pharmacological Activity in Disease prevention and Treatment. International Journal of Research Publication and Reviews. 2023; 4(4): 1584-1595
24. Upadhyaya C, Sathish S. A review on *Euphorbia nerifolia* plant. Int. J. Pharm. Chem. Res. 2017;3:149-154.
25. Sultana A, Hossain MJ, Kuddus MR, Rashid MA, Zahan MS, Mitra S, Roy A, Alam S, Sarker MM, Naina Mohamed I. Ethnobotanical Uses, Phytochemistry, toxicology, and pharmacological properties of *Euphorbia nerifolia* Linn. against infectious diseases: A comprehensive review. Molecules. 2022;27(14):4374.
26. Murali Krishna C, Gupta V, Bansal P, Kumar S, Sannd R, Narayana A. Review on plants mainly used for the preparation of Kshar Sutra. International Journal Ayurvedic Medicine. 2010;1(1):12-22.
27. Gulshen AK, Sharma A. Comparative antianxiety potential of *Euphorbia nerifolia* Linn. leaves and *Euphorbia hirta* Linn. aerial parts. Int J Pharm Sci Res. 2019;10:1433-8.
28. Kirtikar KR, Das BB. Indian Medicinal Plants; Sudhindra Nath Basu, M.B. Panini Office, Bhuwanésuari Asrama: Bahadurganj, Allahabad, India, 1918.
29. Khare CP. Indian medicinal plants: an illustrated dictionary. Springer Science & BusinessMedia; 22 Apr 2008.
30. Prashanth BK, Sehund A. *Euphorbia nerifolia* uses, side effect, research. 2017.
31. Bigoniya P, Rana AC. Immunomodulatory activity of *Euphorbia nerifolia* leaf alcoholic extract on rats. Indian Drugs-Bombay-. 2008;45(2):90.
32. Oudhia P. Medicinal herbs of Chhattisgarh, India having less known uses of XXXIV. Brahmadandi. [http://www.botanical.com/site/column\\_poudhia/250\\_brahmadandi.html](http://www.botanical.com/site/column_poudhia/250_brahmadandi.html). 2003.
33. Ahmed SA, Nazim S, Siraj S, Siddik PM, Wahid CA. *Euphorbia nerifolia* Linn: A phytopharmacological review. International Research Journal of Pharmacy. 2011;2(5):41-48.
34. Chaudhary P, Janmeda P. Sehund: Poison or Medicine. Agriculture & Food: E Newsletter. 2021; 3(4): 254-256.
35. Sharma V, Janmeda P, Singh L. A review on *Euphorbia nerifolia* (sehund). Spatulla DD. 2011;1(2):107-111.
36. Kelly SM, Sanowski RA, Foutch PG, Bellapralu S, Haynes WC. A prospective comparison of anoscopy and fiberoscopy in detecting anal lesions. Journal of clinical gastroenterology. 1986;8(6):658-660.

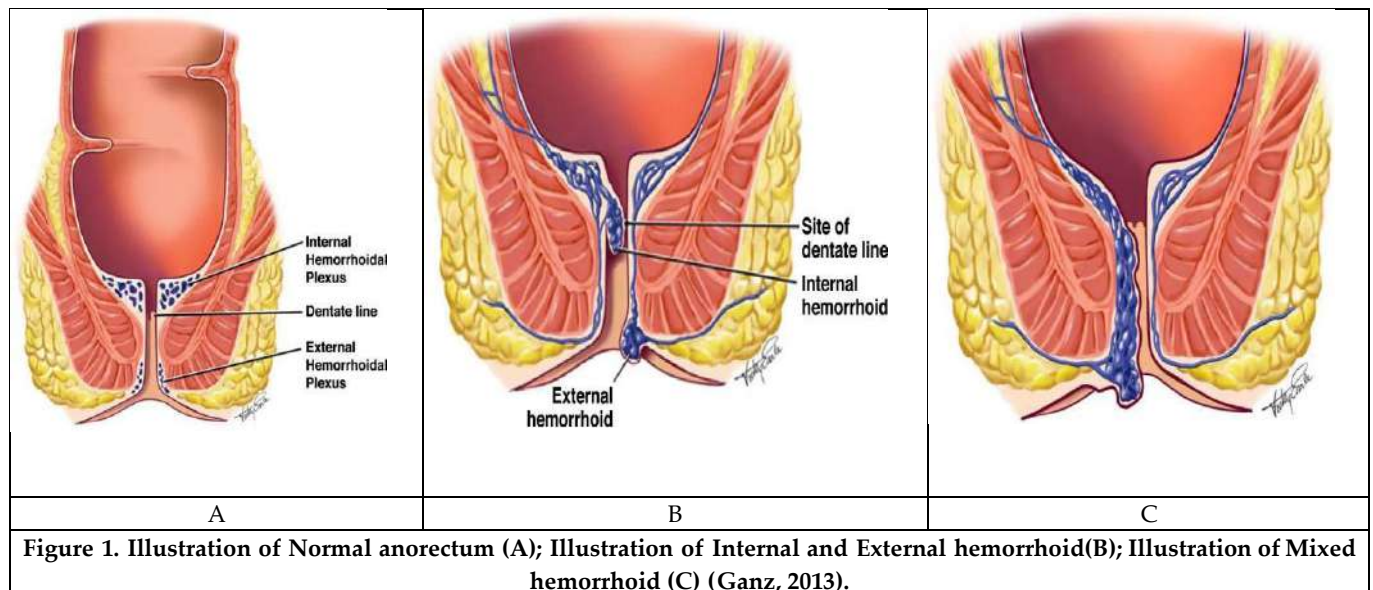


Figure 1. Illustration of Normal anorectum (A); Illustration of Internal and External hemorrhoid(B); Illustration of Mixed hemorrhoid (C) (Ganz, 2013).







Alok Kumar Moharana et al.,



Figure 2. Rubber band ligation of internal hemorrhoids (Ganz, 2013)



Figure 3. *Euphorbia nerifolia* plant with fresh leaves





## Balancing your Biome for Better Mental Health: Gut Microbiota and Depression

Vinod Kumar Mugada <sup>1</sup>, Koyya Priyadarshini Reddy<sup>2\*</sup>, Konathala Rajesh<sup>3</sup> and Madhura Anusha<sup>4</sup>

<sup>1</sup>Associate Professor, Department of Pharmacy Practice, Vignan Institute of Pharmaceutical Technology, (Affiliated to Jawaharlal Nehru Technological University), Visakhapatnam, Andhra Pradesh, India.

<sup>2</sup>Assistant Professor, Department of Pharmacy Practice, Vignan Institute of Pharmaceutical Technology, (Affiliated to Jawaharlal Nehru Technological University), Visakhapatnam, Andhra Pradesh, India.

<sup>3</sup>Professor & Principal, Bhaskara institute of Pharmacy, (Affiliated to Andhra University), Andhra Pradesh, India.

<sup>4</sup>Pharm.D Intern, Department of Pharmacy Practice, Vignan Institute of Pharmaceutical Technology, (Affiliated to Jawaharlal Nehru Technological University), Visakhapatnam, Andhra Pradesh, India

Received: 06 Oct 2024

Revised: 10 Nov 2024

Accepted: 12 Dec 2024

### \*Address for Correspondence

#### Koyya Priyadarshini Reddy

Assistant Professor, Department of Pharmacy Practice,  
Vignan Institute of Pharmaceutical Technology,  
(Affiliated to Jawaharlal Nehru Technological University),  
Visakhapatnam, Andhra Pradesh, India.  
E.Mail: koyya.priyareddy@gmail.com



This is an Open Access Journal / article distributed under the terms of the **Creative Commons Attribution License** (CC BY-NC-ND 3.0) which permits unrestricted use, distribution, and reproduction in any medium, provided the original work is properly cited. All rights reserved.

### ABSTRACT

Recent research highlights a significant link between the gut microbiome and mental health, particularly regarding depression. Termed the 'second brain,' the gut is inhabited by trillions of microorganisms that regulate neurotransmitters and produce compounds impacting emotional well-being. This complex interplay between gut microbes and the brain influences mood, anxiety, and depression. Studies suggest probiotics and dietary changes as potential therapeutic strategies for managing depression by fostering a healthy gut microbiome. This emerging field emphasizes the gut microbiome's crucial role in mental health, offering new avenues for treating depression and enhancing overall well-being.

**Keywords:** Gut microbiome, Depression, Gut brain axis, Probiotics, Prebiotics, Diet.

## INTRODUCTION

### Gut Microbiome Definition

The gut microbiome, an intricate ecosystem within the gastrointestinal tracts of humans and animals, is composed of diverse microorganisms, including bacteria, viruses, fungi, and others, playing crucial roles in the host's physiological processes [1]. This ecosystem, also known as the gut microbiota when referring to the microbial



**Vinod Kumar Mugada et al.,**

community itself, is predominantly found within the digestive tracts of humans, animals, and insects, highlighting its universal presence. After birth, the digestive tract quickly becomes colonized by a variety of microorganisms such as bacteria, viruses, and complex-celled eukaryotes. This colonization is crucial for the gut microbiome's initial development and function [2]. The gut microbiota boasts over 1500 species across more than 50 phyla, a classification of organisms based on common traits. Notably, Bacteroidetes, Firmicutes, and Proteobacteria are dominant phyla, comprising up to 90% of the microbial population [3].

The composition and function of the gut microbiota are influenced by factors like genetics, diet, age, birth conditions, and antibiotic exposure. These elements shape the gut microbiome's dynamic and adaptable nature [4]. The gut microbiota's roles are fundamental to the host's health. It protects against harmful pathogens, produces antimicrobial substances, bolsters the immune system, aids in metabolism, affects insulin sensitivity, and communicates with the brain through the gut-brain axis—a two-way connection between the nervous system and the gastrointestinal tract. Thus, the gut microbiota is essential for maintaining gut health and overall well-being [5-8].

**Overview of Depression**

Recent advancements in understanding depression, a widespread and severe mental disorder, have been notable [9]. These improvements stem from reduced societal stigma, enhanced treatments, and primary care physicians' increased engagement with this condition. Depression takes multiple forms, such as major depressive disorder (MDD) and intermittent episodes, impacting diverse groups including pregnant women, adolescents, and the elderly [10]. Understanding depression involves exploring its genetic and environmental roots [11]. Major depressive disorder, affecting an estimated 350 million people globally, significantly contributes to the global disease burden [12]. Studies reveal that depression involves complex interactions between neuroendocrine and neuroimmune pathways, which link inflammation to cognitive functions [13]. The gut-brain connection has emerged as a key area in depression research. This connection underscores the importance of a healthy gut microbiome for mental well-being. It entails a bidirectional communication system between the gut and brain, influencing emotions, cognition, and motivation, while balancing gastrointestinal health. This system integrates the central nervous system (CNS), autonomic nervous system (ANS), enteric nervous system (ENS), and the hypothalamic-pituitary-adrenal (HPA) axis through neuro-immuno-endocrine mediators [14].

The gut microbiota, essential in this interaction, has been linked to mental health implications [11]. While research has revealed the gut microbiome's impact on depression, it also highlights the need for more comprehensive study designs [14]. The role of probiotics and the influence of gut microbiota on psychiatric conditions are areas requiring further investigation [15]. Understanding the relationship between gastrointestinal microflora changes and depression is crucial, offering potential new treatment insights [16]. Ongoing research continues to explore environmental factors in major depressive disorder, furthering our understanding of its complex nature [17].

**Research Insights and Future Directions**

Research on the microbiome gut-brain axis has illuminated the role of enteric microbiota in mental health, especially concerning conditions like depression [11]. However, there are limitations in current research methodologies regarding the gut microbiome's impact on depression [14]. Probiotic interventions and the role of gut microbiota in psychiatric conditions have been explored, but further study is necessary for clearer understanding [15]. Unravelling how changes in gastrointestinal microflora relate to depression is key to deciphering the gut-brain axis [16]. Although there has been progress in linking gut microbiota to depression, investigating environmental factors in major depressive disorder remains a critical area of ongoing research [17].

**UNDERSTANDING THE GUT-BRAIN AXIS****Vagus Nerve - Role in Connecting Gut and Brain - Influence on Mood**

The Vagus Nerve (VN) is a central component of the body's nervous system, linking various visceral organs to the brain, including the gastrointestinal tract, respiratory system, and cardiovascular system. Its branches, especially the hepatic and celiac branches, connect to afferent neurons in the gut's nodose ganglia, converging at the brainstem's





Vinod Kumar Mugada et al.,

nucleus tractus solitarius (NTS) [18]. From the dorsal motor nucleus of the vagus nerve (DMNV), efferent fibres extend, closely associated with the NTS, highlighting the VN's role as a vital communication pathway between the gut and brain [18]. Vagal afferents (VA) detect diverse signals from the gut, such as tension, stretch, and various biochemical markers, including hormones and gut bacteria by-products [19]. This sensory input informs the brain about the gastrointestinal system's status, influencing physiological processes like gastrointestinal motility, acid secretion, food intake, and satiety. The NTS and DMNV form an autonomic brainstem loop, with projections extending to the central nervous system (CNS), modulating neuroendocrine responses, emotions, cognition, and behaviours [19]. This underscores the VN's critical role in gut-brain communication.

Moreover, the VN indirectly conveys gut-related insights through interactions with enteroendocrine cells (EECs). These cells release mediators like serotonin and peptide YY, impacting food intake and autonomic reflexes controlling gut functions such as motility and inflammation [20]. Neuropods, a subset of EECs, transmit signals to vagal neurons via neurotransmitters like glutamate [21]. Complementing the VN's role, the Enteric Nervous System (ENS) acts as the gut's local control centre, regulating functions such as peristalsis and blood flow. Its connections to the CNS, facilitated by the VN and sympathetic nerves, highlight the significance of neural communication in gut physiology [22]. Additionally, the influence of microbiota metabolites on ENS activity and gut motility, particularly evident in rodent models, reveals the growing understanding of gut microbiota's role in neural pathways [23]. The VN serves as an essential conduit in these interactions, further emphasizing its role in maintaining gastrointestinal homeostasis and linking gut health with overall well-being.

#### **Immune System - Inflammation and its Relation to Depression**

Recent research has illuminated the complex relationship between the gut microbiota and the brain, highlighting the pivotal role of the endocrine and immune systems in this interaction [24]. Central to this connection is the hypothalamic-pituitary-adrenal (HPA) axis, a key component of the endocrine system, which is significantly influenced by the gut microbiota composition [25]. Studies in germ-free mice have demonstrated that stress affects the gut microbiota, altering HPA axis hormones, increasing corticotropin-releasing factor (CRF) levels, and reducing glucocorticoid receptor (GR) expression. These changes exemplify the profound impact of gut microbes on our stress response system.

Stress not only disrupts the gut microbiota balance but also increases gut permeability. This effect is mediated by the growth of certain gram-negative bacteria and heightened CRF levels, which contribute to gut dysfunction. The increased permeability allows bacteria and their metabolites to enter the bloodstream, leading to localized inflammation. This inflammation is characterized by a rise in pro-inflammatory cytokines, further activating the HPA axis and increasing cortisol secretion [26]. Another key factor in this process is lipopolysaccharide (LPS), found in the outer membrane of Gram-negative bacteria. LPS activates toll-like receptors on macrophages, triggering the release of pro-inflammatory cytokines [24]. This response affects not only the immune system but also the HPA axis, influencing the brain and leading to symptoms known as sickness behaviour. The gut microbiota's composition and diversity, including phyla like Bacteroidetes and Firmicutes, play a significant role in this gut-brain-immune system interplay [24]. These microbial populations are shaped by factors such as maternal health and early childhood development. Imbalances in these microbial communities, known as dysbiosis, are linked to a range of disorders, including gastrointestinal issues like inflammatory bowel disease (IBD) and irritable bowel syndrome (IBS), as well as neuropsychiatric conditions such as depression, anxiety, autism, and anorexia. Hopefully, interventions like probiotics and dietary modifications have shown potential in restoring gut microbial balance, offering relief from symptoms associated with these disorders [24]. These findings underscore the potential of targeting the gut microbiota in treating various health conditions.

#### **Factors affecting microbiome gut brain axis**

##### **Genetics and Epigenetics**

The intricate relationship between genetics and epigenetics is crucial in understanding how host genetics affect microbiota composition, particularly in brain health, a field that remains underexplored [30]. Microbiota plays a key





Vinod Kumar Mugada et al.,

role here, as shown by strong correlations in taxa abundance among monozygotic twins, highlighting the heritability of certain microbiota families like Christensenellaceae. Beyond genetic influence, microbiota is increasingly recognized as an epigenetic entity, influencing the host genome through gene-environment interactions [31]. In the gut, HDAC3's role in epithelial cells is vital for maintaining host-commensal signalling. Inhibiting HDAC activity can reverse stress-induced visceral hypersensitivity and anxiety, conditions dependent on the microbiota-gut-brain axis [32]. Furthermore, microRNAs (mirnas), essential in gene expression regulation, are also influenced by the gut microbiota, affecting mirna expression in brain regions [32, 33]. Significantly, changes in mirna expression patterns in the amygdala and prefrontal cortex, linked to gut microbiota, have been observed in germ-free mice. These changes can be reversed with microbiota recolonization [33]. In conclusion, the combined impact of genetics, epigenetics, and microbiota is pivotal in brain health, warranting further investigation in this emerging field.

### Diet

Diet profoundly shapes gut microbiota composition, which in turn significantly influences brain function and behaviour. Gut microbiota, the community of microorganisms in our intestines, is pivotal for health. Rapid changes in this composition can occur within 24 hours of dietary changes, affecting mood even in individuals without mood disorders [34,35]. This highlights the intricate connection between what we eat and our mental well-being. Dietary patterns, especially the contrast between animal-based and plant-based diets, markedly affect microbiota diversity. Lifestyle shifts and food preferences further modify this relationship. Notably, dietary iron plays a crucial role in managing insulin resistance and infection susceptibility, emphasizing the importance of diet in health maintenance [36-42]. Different diets lead to unique microbiota profiles with varied health outcomes. The Western diet, rich in sugar, salt, and fat, mirrors the gut microbiota of obesity and can quickly modify gut bacteria, increasing inflammatory Proteobacteria. Conversely, the Mediterranean diet, abundant in fruits, vegetables, and whole grains, fosters a healthier microbiota, linked to reduced depression risk and lower levels of harmful bacteria [43-48].

The ketogenic diet, known for high fat and low carbohydrates, benefits several neurological conditions. It alters the gut microbiota by boosting beneficial bacteria like Akkermansia and Parabacteroides, impacting the gut-brain communication axis [51]. Carbohydrates play a crucial role in shaping gut microbiota. Digestible carbohydrates such as glucose can increase beneficial bacteria like Bifidobacterium, while indigestible carbohydrates, or prebiotics, promote overall gut health by nurturing beneficial microorganisms [52]. Proteins, from both plant and animal sources, significantly influence gut microbiota. Plant-based proteins correlate with greater diversity, whereas animal-based proteins affect specific bacterial populations. This underscores the impact of protein type on gut microbiota composition [52,53]. Various fats exert unique influences on gut microbiota. Saturated and trans fats, common in the Western diet, may reduce beneficial bacteria. In contrast, omega-3 polyunsaturated fatty acids enhance gut health by increasing beneficial microbes and diversity, demonstrating the critical role of fat quality in diet [54-56].

### Environment

Environmental factors significantly influence health outcomes and gut microbiota across cultures. One key mechanism is the metabolism of environmental chemicals by gut microbiota, which affects its composition and, in turn, may impact brain function and behaviour via the microbiota-gut-brain axis [57]. For instance, Bisphenol A (BPA), commonly found in plastic containers, exemplifies this impact. As an endocrine-disrupting chemical, BPA, when consumed, reduces gut microbiota diversity, notably increasing Proteobacteria and Helicobacteraceae and decreasing Clostridia [58]. These changes underscore the delicate balance within our gut ecosystem. Similarly, heavy metals like cadmium, mercury, arsenic, and lead pose serious health risks, causing carcinogenicity, immune disruption, nucleic acid damage, and oxidative stress [59]. Exposure to these metals alters gut microbiota, evidenced by increased Lactobacillaceae and Erysipelotrichaceae and decreased Lachnospiraceae in animals. This shift in microbiota composition, particularly the reduction of Lachnospiraceae linked to depression, suggests a potential microbiota-gut-brain connection influenced by environmental toxins.







Vinod Kumar Mugada et al.,

Furthermore, the widespread use of antibiotics, leading to their accumulation in natural environments like lakes, rivers, and agricultural soil [60-62], represents another environmental challenge. This increase in environmental antibiotics threatens not just individual health but also global ecological balance [63].

### Exercise

Regular exercise significantly improves brain health, as seen in rodents where it enhances neurogenesis and counters aging-related hippocampal decline [64]. It also positively influences gut health, enhancing microbiota diversity. This leads to reduced stress, better immunity, and improved energy regulation in the gut microbiota. Despite these insights, the interplay between exercise and gut microbiota, especially how the latter affects exercise performance, is still not well-understood [65]. Animal studies reveal that exercise alters the microbiota to prevent diet-induced obesity and improve glucose tolerance. In humans, increased physical activity is associated with greater diversity in gut microbiota, notably in the Firmicutes phylum [66]. The cessation of regular exercise can quickly result in mood deterioration and fatigue. This is possibly linked to the gut microbiota's influence on tryptophan metabolism and kynurenine levels, which are related to depression. Exercise's benefits are thought to involve the kynurenine pathway and the activation of PGC-1 $\alpha$ 1 in muscles, which may bolster resistance to chronic stress and CNS inflammation.

### Medications

Medications profoundly affect the gut microbiota, which encompasses the diverse microorganisms in our digestive system. This impact extends beyond antibiotics to non-antibiotic drugs, influencing behaviour and how drugs work in the body [67,68]. Common medications, including antibiotics, laxatives, IBD treatments, female hormones, benzodiazepines, antidepressants, and antihistamines, significantly alter the gut's microbial composition [69]. Advanced sequencing studies have linked 44 drug categories to changes in the gut microbiota. This relationship spans various drugs, including proton pump inhibitors (ppis), metformin, statins, and laxatives, each altering the microbiota in distinct ways [70]. Polypharmacy, the use of multiple medications simultaneously, correlates with reduced microbial diversity in the gut. Specific microbes are especially affected by proton pump inhibitors, antidepressants, and antipsychotics. Meta transcriptomic research, which analyses gene expression in microbes, shows that short-term exposure to non-antibiotic drugs alters genes involved in drug processing. This suggests these drugs can also affect microbial function and potentially influence brain function [71-73]. Antidepressants, such as SSRI's and TCA's, demonstrate antimicrobial properties against certain bacteria, influencing gut microbiota composition [74,75]. Moreover, phenothiazines, a group of antipsychotic drugs, offer dual benefits: combating bacterial infections and modifying the gut microbiota. This is particularly relevant to the microbiota-gut-brain axis, the complex interaction network between the gut microbiota and the brain [76-79].

### Stress

Stress disrupts an organism's equilibrium, initiating cortisol release via the HPA axis to prepare for threat response [80]. Chronic stress can lead to HPA axis dysregulation, increasing the risk of health issues like anxiety and depression, which impose significant economic impacts. Research spanning over four decades and encompassing various species, including rodents and non-human primates, consistently shows that stress alters gut microbiota composition [81-86]. This alteration extends to maternal stress during pregnancy, which shapes the microbiota and HPA axis reactivity in offspring. Notably, transferring vaginal microbiota from stressed dams to nonstressed offspring can modify adult stress responses in these offspring [87]. Human studies corroborate these findings, indicating that infants born to mothers with high cumulative stress during pregnancy exhibit microbial composition changes. The microbiota-gut-brain axis is influenced by daily factors, from food cravings to inherited traits and birth delivery methods, highlighting the need for further research into how microbiota influences behaviour and disease development.

### Fear

The regulation of fear, a complex cognitive process, is significantly influenced by both the stress response and the gut-brain axis, with notable implications for clinical anxiety. Key brain regions such as the amygdala, hippocampus,







Vinod Kumar Mugada *et al.*,

and prefrontal cortex (PFC) are integral to this process. Recent studies highlight the microbiota's role in modulating these brain regions' functions [88-91]. Functional MRI (fmri) studies in humans reveal fascinating links between gut microbiota and brain activity during fear stimulus processing [92,93]. For instance, healthy women who consumed a fermented milk product with probiotics showed reduced brain responses to negatively emotional faces, particularly in areas involving the PFC.

Parallel research in animal models sheds light on the microbiota's role in fear response, especially in memory and extinction. Experiments with Germ-Free (GF) mice reveal that lacking microbiota impairs short-term fear recall, leading to diminished fear responses and altered amygdala gene expression [94]. Additionally, studies on humans and rodents show that acute antibiotic exposure disrupts fear memory and enhances extinction capabilities [95]. Probiotic examinations reveal strain-specific impacts on fear learning and memory. For example, *B. Longum* 1714 boosts fear learning and short-term memory, while *L. Rhamnosus* (JB-1) decelerates extinction. Certain probiotic strains, like *L. Rhamnosus* R0011 and *L. Helveticus* R0052, may mitigate early-life stress effects on fear behaviour and related neural networks during development [96,97].

### Circadian rhythm

Circadian rhythms, fundamental 24-hour cycles in bodily functions, are disrupted by phenomena like jet lag and shift work, leading to metabolic and psychiatric disorders [98]. Research is uncovering the complex relationship between these rhythms and the microbiome, especially in obesity, cardiovascular disease (CVD), diabetes, and neurodegenerative disorders. This work sheds light on the microbiota-gut-brain axis, a key player in these conditions [99-101]. Importantly, the microbiota can modulate the circadian clock, influencing both peripheral and central timing systems. Circadian disruptions disturb the balance of intestinal microbiota, but timed feeding shows promise in countering these effects [100]. Studies using Germ-free (GF) mice highlight the microbiota's role in regulating liver clock oscillations, crucial for maintaining liver function and metabolic gene expression [102]. Shift work and jet lag can lead to an arrhythmic microbiome, marked by significant changes in its composition. These changes, linked to metabolic imbalances, can be transferred to GF mice through faecal microbiota transplantation (FMT). As such, targeting the microbiota could be an effective strategy for managing conditions associated with circadian rhythm disturbances, particularly when combined with unhealthy diets. This interplay between circadian rhythms, microbiota, and brain health is of significant physiological and potential clinical importance [101,103].

### Food intake

**Microbiota's Role in Regulating Food Intake:** The gut microbiota plays a pivotal role in controlling food intake through hormones that regulate appetite [104, 105]. Disturbances in this microbiota are linked to conditions like anorexia nervosa and obesity [106, 107]. Notably, bariatric surgeries, including Roux-en-Y gastric bypass, effectively treat obesity by altering gut microbes. This suggests that these microbes may evolve to manipulate eating behaviour, possibly by inducing cravings or dysphoria until the host consumes nutrients beneficial to them. Gut microbes produce proteins, like caseinolytic protease B (clpb), that mimic appetite-regulating peptides, thereby influencing food intake [109]. This mimicry potentially disrupts hormone degradation. The microbiota may also affect nutrient sensing and taste perception, especially in conditions like obesity and anorexia nervosa where taste is often altered [110, 111]. The immune system's role in maintaining taste receptors further complicates this interaction.

### Social behaviour

**Exploring Microbiota's Role in Animal Social Behaviour:** Studies reveal a significant link between the microbiota and social behaviour in animals. Notably, germ-free (GF) mice, which are devoid of microbiota, display reduced social interactions and face challenges in recognizing new individuals of their species, highlighting the microbiota's critical role [112-115]. Furthermore, antibiotic treatments in rodents that diminish microbial diversity have been linked to deteriorated social behaviours [116]. The mechanisms by which microbiota influence social behaviour, though not fully unravelled, involve complex biological interactions. Key findings suggest that components from gut bacteria, such as peptidoglycan, can influence brain regions like the amygdala, essential for social interactions [115, 117]. Altering the microbiota through diet or probiotics also shows promising results in modulating social behaviour. The



**Vinod Kumar Mugada et al.,**

administration of *L. Reuteri* to mice enhances hormone levels associated with sociability, and the use of probiotics like VSL#3 alleviates social withdrawal symptoms while decreasing inflammation markers in the blood [112].

## THERAPEUTIC APPROACHES

### Prebiotics - Efficacy in Treating Gut Microbiome-Related Depression

Prebiotics, increasingly recognized in mental health, offer an innovative approach to managing cognitive and mood disorders through gut health enhancement. Unlike probiotics, they promote beneficial bacterial growth, notably *Lactobacillus* species, crucial for maintaining the intestinal barrier and reducing pro-inflammatory stimuli, thereby addressing dysbiosis and associated inflammation [120]. As immune modulators, prebiotics decrease pro-inflammatory cytokines and oxidative stress markers. They also produce short-chain fatty acids (SCFAs) like acetate, propionate, and butyrate during fermentation by gut microbiota, playing a vital role in immune regulation and potentially mitigating inflammation in central nervous system diseases. [121] In mood disorders such as major depressive disorder (MDD) and anxiety, prebiotics like fructo-oligosaccharides (FOS) and galacto-oligosaccharides (GOS) have shown promise. Animal studies indicate that these prebiotics can lessen depressive behaviours and exert anxiolytic effects, correlating with reduced plasma corticosterone and altered gene expression in brain regions involved in key neurotransmitters [122]. Moreover, they alleviate symptoms like anhedonia in stressed animals, increasing beneficial gut bacteria like *Bifidobacterium* and *Lactobacillus*.

Despite these findings, the application of prebiotics in clinical settings for mood disorders remains challenging. Clinical studies present mixed results; for instance, Bimuno-galacto-oligosaccharides (B-GOS) were found to reduce salivary cortisol and affect emotional processing, whereas the impacts of other prebiotics like FOS were less evident. Some trials reported no significant mood or inflammation improvement compared to probiotics [123]. This inconsistency highlights the necessity for further research to fully understand prebiotics' therapeutic potential in treating depression and anxiety [124].

### Probiotics - Efficacy in Treating Gut Microbiome-Related Depression

In the realm of precision psychiatry, an approach that personalizes treatment based on individual genetic, environmental, and lifestyle factors, probiotics—specifically *Lactobacillus* and *Bifidobacterium* strains—have shown promise [125-132]. These live microorganisms are gaining attention for their potential to correct imbalances in the gut microbiota, a condition often linked with depression. Such imbalances are marked by a lack of microbial diversity and the depletion of specific bacterial genera. This understanding underscores the role of probiotics in reinstating gut equilibrium, thereby contributing to improved mental health outcomes. Central to this concept is the microbiota-gut-brain axis (MGBA), a bidirectional communication system that highlights the impact of probiotics on neurobehavioral health. Through intricate interactions involving the nervous and endocrine systems, probiotics exert a positive influence on this axis [133-135]. Their ability to effectively reach and act within the gastrointestinal tract makes them viable candidates for targeted psychiatric interventions, aligning well with the principles of precision psychiatry.

### Dietary Changes - Impact on Depression

Diet significantly influences gut bacteria, surpassing genetic factors. Beneficial elements like plant proteins, unsaturated fats, and dietary fibre promote a healthy gut microbiota. Conversely, diets high in animal proteins, saturated fats, and simple sugars correlate with less favourable gut bacteria [136]. The Western diet, rich in saturated fats, processed foods, and refined sugars, leads to a gut microbiota profile characterized by reduced diversity and increased gut permeability. Such changes are linked to metabolic syndrome and chronic diseases [137]. Dietary fibre is crucial for immune health, aiding in producing short-chain fatty acids (SCFAs) by gut bacteria. This process is essential for maintaining robust immune function [138]. Digestive disorders, which affect a significant American population segment, pose a \$100 billion annual economic impact. Medications like proton pump inhibitors (PPIs), such as omeprazole, can disrupt gut microbiota diversity, increasing gastrointestinal infection risks. This impact is more significant than that of antibiotics [139].



**Vinod Kumar Mugada et al.,**

Equilibrium in gut bacteria is vital for health, preventing dominance by any single species. Imbalances can lead to irregular eating habits [140]. Gut bacteria influence food choices by mimicking or interfering with human appetite-regulating hormones, affecting reward pathways and potentially taste receptors [141]. They also impact mood through neurotransmitters like serotonin, influencing eating behaviours [142]. Dietary choices affect stress and depression. Sugar consumption may reduce stress responses, suggesting a potential preference for sweets under stress [143,144].

## CONCLUSION

In conclusion, the gut microbiome is a dynamic and intricate ecosystem with significant impacts on human health. Understanding its relationship with the gut-brain axis, neurotransmitters, and dietary factors opens new avenues for treating mental health issues, particularly depression. Continued research into probiotics, prebiotics, and dietary changes holds promise for unlocking their full therapeutic potential.

## REFERENCES

1. Goma EZ. Human gut microbiota/microbiome in health and diseases: a review. *Antonie Van Leeuwenhoek*. 2020;113(12):2019-40.
2. Maria A, Joaquim S. Intestinal microbiota in digestive diseases. *Arq Gastroenterol*. 2017;54(3):255-62.
3. Jethwani P, Grover K. Gut microbiota in health and diseases – a review. *Int J Curr Microbiol App Sci*. 2019;8(8):1586-99.
4. Odamaki T, Kato K, Sugahara H, Hashikura N, Takahashi S, Xiao J, et al. Age-related changes in gut microbiota composition from newborn to centenarian: a cross-sectional study. *BMC Microbiol*. 2016;16(1):90.
5. Mills S, Stanton C, Lane JA, Smith GJ, Ross RP. Precision nutrition and the microbiome, Part I: current state of the science. *Nutrients*. 2019;11(4):923.
6. Rothschild D, Weissbrod O, Barkan E, Kurilshikov A, Korem T, Zeevi D, et al. Environment dominates over host genetics in shaping human gut microbiota. *Nature*. 2018;555(7695):210-5.
7. Wiley N, Dinan TG, Ross RP, Stanton C, Clarke G, Cryan JF. The microbiota-gut-brain axis as a key regulator of neural function and the stress response: implications for human and animal health. *J Anim Sci*. 2017;95(7):3225-46.
8. The gut microbiome from patients with schizophrenia modulates the glutamate-glutamine-GABA cycle and schizophrenia-relevant behaviors in mice. *Sci Adv*. 2019 Jun 21;5(6):eaau0135.
9. Schachter J, Martel J, Lin CF, Chang CJ, Wu TR, Lu C, et al. Effects of obesity on depression: a role for inflammation and the gut microbiota. *Brain Behav Immun*. 2018;69:1-8.
10. Pleis JR, Lethbridge-Cejku M. Summary health statistics for U.S. adults: National Health Interview Survey, 2006. *Vital Health Stat*. 2023;10(235).
11. Limbana T, Khan F, Eskander N. Gut microbiome and depression: how microbes affect the way we think. *Cureus*. 2020;12(11):e11653.
12. Koopman MB, El Aidy S. Depressed gut? The microbiota-diet-inflammation triologue in depression. *Curr Opin Psychiatry*. 2017;30(5):369-77.
13. Sherwin E, Rea K, Dinan TG, Cryan JF. A gut (microbiome) feeling about the brain. *Curr Opin Gastroenterol*. 2016;32(2):96-102.
14. Van Ameringen M, Turna J, Patterson B, Pipe A, Mao RQ, Anglin R, et al. The gut microbiome in psychiatry: a primer for clinicians. *Depress Anxiety*. 2019;36(11):1004-25.
15. Mohajeri MH, La Fata G, Steinert RE, Weber P. Relationship between the gut microbiome and brain function. *Nutr Rev*. 2018;76(7):481-96.
16. Kelly JR, Borre Y, O'Brien C, Patterson E, El Aidy S, Deane J, et al. Transferring the blues: depression-associated gut microbiota induces neurobehavioural changes in the rat. *J Psychiatr Res*. 2016;82:109-18.





## Vinod Kumar Mugada et al.,

17. Zheng P, Zeng B, Zhou C, Liu M, Fang Z, Xu X, et al. Gut microbiome remodeling induces depressive-like behaviors through a pathway mediated by the host's metabolism. *Mol Psychiatry*. 2016;21(6):786-96.
18. Bonaz B, Sinniger V, Pellissier S. Therapeutic potential of vagus nerve stimulation for inflammatory bowel diseases. *Front Neurosci*. 2021;15:640.
19. Bonaz B, Bazin T, Pellissier S. The vagus nerve at the interface of the microbiota-gut-brain axis. *Front Neurosci*. 2018;12:49.
20. Tan C, Yan Q, Ma Y, Fang J, Yang Y. Recognizing the role of the vagus nerve in depression from microbiota-gut-brain axis. *Front Neurol*. 2022;13:931906.
21. Kaelberer MM, Rupprecht LE, Liu W, Weng P, Bohórquez DV. Neuropod cells: the emerging biology of gut-brain sensory transduction. *Annu Rev Neurosci*. 2020;43:337-53.
22. Rao M, Gershon MD. Enteric nervous system development: what could possibly go wrong? *Nat Rev Neurosci*. 2018;19(9):552-65.
23. Golubeva AV, Joyce SA, Moloney GM, Burokas A, Sherwin E, Arboleya S, et al. Microbiota-related changes in bile acid & tryptophan metabolism are associated with gastrointestinal dysfunction in a mouse model of autism. *Ebiomedicine*. 2017;24:166-78.
24. Dubois T, Reynaert C, Jacques D, Zdanowicz N. Role of gut microbiota in the interaction between immunity and psychiatry: a literature review. *Psychiatr Danub*. 2019;31(4):381-5.
25. Huo R, Zeng B, Zeng L, Cheng K, Li B, Luo Y, et al. Microbiota modulate anxiety-like behavior and endocrine abnormalities in hypothalamic-pituitary-adrenal axis. *Front Cell Infect Microbiol*. 2017;7:206.
26. Brzozowski B, Mazur-Bialy A, Pajdo R, Kwiecien S, Bilski J, Zwolinska-Wcislo M, et al. Mechanisms by which stress affects the experimental and clinical outcomes: Ingenta Connect. *Ingentaconnect.com*. 2016.
27. A gut-brain neural circuit for nutrient sensory transduction. *Science*. 2018;361(6408):eaat5027.
28. Neuropod Cells: The Emerging Biology of Gut-Brain Sensory Transduction. *Annu Rev Neurosci*. 2020;43:337-53.
29. Karakan T, Özkul C, Küpeli Akkol E, Bilici S, Sobarzo-Sánchez E, Capasso R. Gut-brain-microbiota axis: antibiotics and functional gastrointestinal disorders. *Nutrients*. 2021;13(2):389.
30. Bonder MJ, Kurilshikov A, Tigchelaar EF, Mujagic Z, Imhann F, Vich Vila A, et al. The effect of host genetics on the gut microbiome. *Nat Genet*. 2016;48(11):1407-12.
31. Stilling RM, Moloney GM, Ryan FJ, Hoban AE, Bastiaanssen TFS, Shanahan F, et al. Social interaction-induced activation of RNA splicing in the amygdala of microbiome-deficient mice. *Elife*. 2018;7:e31350.
32. O'Connor RM, Gururajan A, Dinan TG, Kenny PJ, Cryan JF. All roads lead to the mirnome: miRNAs have a central role in the molecular pathophysiology of psychiatric disorders. *Trends Pharmacol Sci*. 2016;37(12):1029-44.
33. Hoban AE, Stilling RM, Moloney G, Moloney RD, Shanahan F, Dinan TG, et al. Microbial regulation of microRNA expression in the amygdala and prefrontal cortex. *Microbiome*. 2017;5(1):1-14.
34. Sandhu K, Sherwin E, Schellekens H, Stanton C, Dinan TG, Cryan JF. Feeding the microbiota-gut-brain axis: diet, microbiome, and neuropsychiatry. *Transl Res*. 2017;179:223-44.
35. Taylor AM, Thompson SV, Edwards CG, MUSAAD S, Khan NA, Holscher HD. Associations among diet, the gastrointestinal microbiota, and negative emotional states in adults. *Nutr Neurosci*. 2019;23(12):983-92.
36. Basso N, Soricelli E, Castagneto-Gissey L, Casella G, Albanese D, Fava F, et al. Insulin resistance, microbiota, and fat distribution changes by a new model of vertical sleeve gastrectomy in obese rats. *Diabetes*. 2016;65(10):2990-3001.
37. Aslam H, Green J, Jacka FN, Collier F, Berk M, Pasco JA, et al. Fermented foods, the gut and mental health: a mechanistic overview with implications for depression and anxiety. *Nutr Neurosci*. 2018;23(9):659-71.
38. Dinan TG, Stanton C, Long-Smith CM, Kennedy P, Cryan JF, Cénit MC, et al. Feeding melancholic microbes: MyNewGut recommendations on diet and mood. *Clin Nutr*. 2019;38(5):1995-2001.
39. Morell Miranda P, Serkis V, De Palma G, Pigrau M, Lü J, Collins SM, et al. High salt diet increases susceptibility to experimental colitis: a putative role of gut microbiota. *Gastroenterology*. 2016;150(4):S583.
40. Moya-Pérez Á, Luczynski P, Renes IB, Wang S, Borre Y, Ryan CA, et al. Intervention strategies for cesarean section-induced alterations in the microbiota-gut-brain axis. *Nutr Rev*. 2017;75(4):225-40.





## Vinod Kumar Mugada et al.,

41. Reichelt AC, Loughman A, Bernard A, Raipuria M, Abbott KN, Dachtler J, Thu T, Moore RJ. An intermittent hypercaloric diet alters gut microbiota, prefrontal cortical gene expression and social behaviours in rats. *Nutr Neurosci.* 2018;23(8):613-627.
42. Sanchez KK, Chen GY, Palaferri AM, Redford SE, Shokhirev MN, Leblanc M, Lee YM, Ayres JS. Cooperative metabolic adaptations in the host can favor asymptomatic infection and select for attenuated virulence in an enteric pathogen. *Cell.* 2018;175(1):146-158.e15.
43. Karstens AJ, Tussing-Humphreys L, Zhan L, Rajendran N, Cohen J, Dion C, Zhou XJ, Lamar M. Associations of the Mediterranean diet with cognitive and neuroimaging phenotypes of dementia in healthy older adults. *Am J Clin Nutr.* 2019;109(2):361-368.
44. Romagnolo DF, Selmin OI. Mediterranean diet and prevention of chronic diseases. *Nutr Today.* 2017;52(5):208-222.
45. Schwingshackl L, Schwedhelm C, Galbete C, Hoffmann G. Adherence to Mediterranean diet and risk of cancer: An updated systematic review and meta-analysis. *Nutrients.* 2017;9(10):1063.
46. Wu L, Sun D. Adherence to Mediterranean diet and risk of developing cognitive disorders: An updated systematic review and meta-analysis of prospective cohort studies. *Sci Rep.* 2017;7(1).
47. Martínez-González MA, Ros E, Estruch R. Primary prevention of cardiovascular disease with a Mediterranean diet supplemented with extra-virgin olive oil or nuts. *N Engl J Med.* 2018;378(25):e34.
48. Lassale C, Batty GD, Baghdadli A, Jacka FN, Sánchez-Villegas A, Kivimäki M, Akbaraly T. Healthy dietary indices and risk of depressive outcomes: A systematic review and meta-analysis of observational studies. *Mol Psychiatry.* 2018;24(7):965-986.
49. Bostock S, Kirkby KC, Taylor B. The current status of the ketogenic diet in psychiatry. *Front Psychiatry.* 2017;8.
50. Lange KW, Lange K, Makulska-Gertruda E, Nakamura Y, Reißmann A, Kanaya S, Hauser J. Ketogenic diets and Alzheimer's disease. *Food Sci Hum Wellness.* 2017;6(1):1-9.
51. Olson CA, Vuong HE, Yano JM, Liang QY, Nusbaum DJ, Hsiao EY. The gut microbiota mediates the anti-seizure effects of the ketogenic diet. *Cell.* 2018;173(7):1728-1741.e13.
52. Singh R, Chang HH, Yan D, Lee KM, Uçmak D, Wong K, Abrouk M, Farahnik B, Nakamura M, Zhu TH, Bhutani T, Liao W. Influence of diet on the gut microbiome and implications for human health. *J Transl Med.* 2017;15(1).
53. Madsen L, Myrmet LS, Fjære E, Liaset B, Kristiansen K. Links between dietary protein sources, the gut microbiota, and obesity. *Front Physiol.* 2017;8.
54. Kaliannan K, Wang B, Li X, Bhan AK, Kang JX. Omega-3 fatty acids prevent early-life antibiotic exposure-induced gut microbiota dysbiosis and later-life obesity. *Int J Obes.* 2016;40(6):1039-1042.
55. Robertson RC, Oriach CS, Murphy K, Moloney GM, Cryan JF, Dinan TG, Ross RP, Stanton C. Omega-3 polyunsaturated fatty acids critically regulate behaviour and gut microbiota development in adolescence and adulthood. *Brain Behav Immun.* 2017;59:21-37.
56. Menni C, Zierer J, Pallister T, Jackson MA, Long T, Mohny RP, Steves CJ, Spector TD, Valdes AM. Omega-3 fatty acids correlate with gut microbiome diversity and production of N-carbamylglutamate in middle aged and elderly women. *Sci Rep.* 2017;7(1).
57. Claus SP, Guillou H, Ellero-Simatos S. The gut microbiota: A major player in the toxicity of environmental pollutants? *Npj Biofilms Microbiomes.* 2016;2(1).
58. Lai KP, Chung YT, Li R, Wan H, Wong CKC. Bisphenol A alters gut microbiome: Comparative metagenomics analysis. *Environ Pollut.* 2016;218:923-930.
59. Jin Y, Wu S, Zeng Z, Fu Z. Effects of environmental pollutants on gut microbiota. *Environ Pollut.* 2017;222:1-9.
60. Dong H, Yuan X, Wang W, Qiang Z. Occurrence and removal of antibiotics in ecological and conventional wastewater treatment processes: A field study. *J Environ Manag.* 2016;178:11-19.
61. Ferro G, Guarino F, Castiglione S, Rizzo L. Antibiotic resistance spread potential in urban wastewater effluents disinfected by UV/H2O2 process. *Sci Total Environ.* 2016;560-561:29-35.
62. Qian M, Wu H, Wang J, Zhang H, Zhang Z, Zhang Y, Lin H, Ma J. Occurrence of trace elements and antibiotics in manure-based fertilizers from the Zhejiang Province of China. *Sci Total Environ.* 2016;559:174-181.





**Vinod Kumar Mugada et al.,**

63. Prescott SL, Logan AC. Planetary health: From the wellspring of holistic medicine to personal and public health imperative. *Explore (NY)*. 2019;15(2):98-106. doi:10.1016/j.explore.2018.09.002
64. Mach N, Fuster-Botella D. Endurance exercise and gut microbiota: A review. *J Sport Health Sci*. 2017;6(2):179-197.
65. Changes in intestinal microbiota composition and metabolism coincide with increased intestinal permeability in young adults under prolonged physiological stress. *Am J Physiol Gastrointest Liver Physiol*. 2020.
66. Effect of antibiotic treatment on the intestinal metabolome. *Antimicrob Agents Chemother*. 2023.
67. Clarke G, Sandhu K, Griffin BT, Dinan TG, Cryan JF, Hyland NP. Gut reactions: Breaking down xenobiotic-microbiome interactions. *Pharmacol Rev*. 2019;71(2):198-224.
68. Population-level analysis of gut microbiome variation. *Science*. 2016.
69. Population-based metagenomics analysis reveals markers for gut microbiome composition and diversity. *Science*. 2016.
70. Gunics G, Motohashi N, Molnár J, Farkas S, Kawase M, Saito S, Shah A. Enhanced antibacterial effect of erythromycin in the presence of 3,5-dibenzoyl-1,4-dihydropyridines. *Anticancer Res*. 2022;21(1A).
71. Kruszevska H, Zareba T, Tyski S. Antimicrobial activity of selected non-antibiotics—activity of methotrexate against *Staphylococcus aureus* strains. *Acta Pol Pharm*. 2022;57 Suppl.
72. Kruszevska H, Zareba T, Tyski S. Search of antimicrobial activity of selected non-antibiotic drugs. *Acta Pol Pharm*. 2022;59(6).
73. Csiszar K, Molnar J. Mechanism of action of tricyclic drugs on *Escherichia coli* and *Yersinia enterocolitica* plasmid maintenance and replication. *Anticancer Res*. 2023;12(6B).
74. Molnár J. Antiplasmid activity of tricyclic compounds. *Methods Find Exp Clin Pharmacol*. 2023;10(7).
75. Europe PMC. Europe PMC. EuropePMC.org. 2016.
76. Maier L, Pruteanu M, Kuhn M, Zeller G, Telzerow A, Anderson EE, Brochado AR, Fernandez KC, Dose H, Mori H, Patil KR, Bork P, Typas A. Extensive impact of non-antibiotic drugs on human gut bacteria. *Nature*. 2018;555(7698):623-628.
77. Kao ACC, Spitzer S, Anthony DC, Lennox B, Burnet PWJ. Probiotic attenuation of olanzapine-induced weight gain in rats: analysis of central and peripheral biomarkers and gut microbiota. *Transl Psychiatry*. 2018;8(1).
78. Flowers SA, Evans SJ, Ward KM, McInnis MG, Ellingrod VL. Interaction between atypical antipsychotics and the gut microbiome in a bipolar disease cohort. *Pharmacotherapy*. 2017;37(3):261-267.
79. Dickerson SS, Kemeny ME. Acute stressors and cortisol responses: A theoretical integration and synthesis of laboratory research. *Psychol Bull*. 2004;130(3):355-391.
80. Bailey MT, Coe CL. Maternal separation disrupts the integrity of the intestinal microflora in infant rhesus monkeys. *Dev Psychobiol*. 2023;35(2).
81. Prenatal stress alters bacterial colonization of the gut in infants. *J Pediatr Gastroenterol Nutr*. 2023;LWW.
82. Bharwani A, Mian MF, Foster JA, Surette MG, Bienenstock J, Forsythe P. Structural and functional consequences of chronic psychosocial stress on the microbiome and host. *Psychoneuroendocrinology*. 2016;63:217-227.
83. Partrick KA, Chassaing B, Beach LQ, McCann KE, Gewirtz AT, Huhman KL. Acute and repeated exposure to social stress reduces gut microbiota diversity in Syrian hamsters. *Behav Brain Res*. 2018;345:39-48.
84. Mudd AT, Alexander LS, Berding K, Waworuntu R, Berg BM, Donovan SM, Dilger RN. Dietary prebiotics, milk fat globule membrane, and lactoferrin affect structural neurodevelopment in the young piglet. *Front Pediatr*. 2016;4.
85. Mach N, Fuster-Botella D. Endurance exercise and gut microbiota: A review. *J Sport Health Sci*. 2017;6(2):179-197.
86. Jašarević E, Howard CD, Morrison KE, Misić AM, Weinkopff T, Scott P, Hunter CA, Beiting DP, Bale TL. The maternal vaginal microbiome partially mediates the effects of prenatal stress on offspring gut and hypothalamus. *Nat Neurosci*. 2018;21(8):1061-1071.
87. Hoban CA, Ventura-Silva AP, Dinan TG, Clarke G, Cryan JF. Gutsy moves: The amygdala as a critical node in microbiota-to-brain signaling. *Bioessays*. 2017;40(1).







## Vinod Kumar Mugada et al.,

88. Gacias M, Gaspari S, Santos PMG, Tamburini S, Andrade M, Zhang F, Shen N, Tolstikov V, Kiebish MA, Dupree JL, Zachariou V, Clemente JC, Casaccia P. Microbiota-driven transcriptional changes in prefrontal cortex override genetic differences in social behavior. *Elife*. 2016;April 20.
89. Hoban AE, Stilling RM, Ryan FJ, Shanahan F, Dinan TG, Claesson MJ, Clarke G, Cryan JF. Regulation of prefrontal cortex myelination by the microbiota. *Transl Psychiatry*. 2016;6(4):e774.
90. Luczynski P, Whelan S, O'Sullivan CTD, Clarke G, Shanahan F, Dinan TG, Cryan JF. Adult microbiota-deficient mice have distinct dendritic morphological changes: Differential effects in the amygdala and hippocampus. *Eur J Neurosci*. 2016;44(9):2654-2666.
91. Tillisch K, Mayer EA, Gupta AR, Gill Z, Brazeilles R, Le Nevé B, van Hylckama, Guyonnet D, Derrien M, Labus JS. Brain structure and response to emotional stimuli as related to gut microbial profiles in healthy women. *Psychosom Med*. 2017;79(8):905-913.
92. Callaghan B, Fields A, Gee DG, Gabard-Durnam L, Caldera C, Humphreys KL, Goff B, Flannery J, Telzer EH, Shapiro M, Tottenham N. Mind and gut: Associations between mood and gastrointestinal distress in children exposed to adversity. *Dev Psychopathol*. 2019;32(1):309-328.
93. Hoban AE, Stilling RM, Moloney GM, Shanahan F, Dinan TG, Clarke G, Cryan JF. The microbiome regulates amygdala-dependent fear recall. *Mol Psychiatry*. 2017;23(5):1134-1144.
94. Bach DR, Tzovara A, Vunder J. Blocking human fear memory with the matrix metalloproteinase inhibitor doxycycline. *Mol Psychiatry*. 2017;23(7):1584-1589.
95. Callaghan BL. Treating generational stress: Effect of paternal stress on development of memory and extinction in offspring is reversed by probiotic treatment. *Psychol Sci*. 2016.
96. Callaghan BL, Richardson R. The effects of a probiotic formulation (*Lactobacillus rhamnosus* and *L. Helveticus*) on developmental trajectories of emotional learning in stressed infant rats. *Transl Psychiatry*. 2016;6(5):e823.
97. Pantazopoulos H, Gamble KL, Stork O, Amir S. Circadian rhythms in regulation of brain processes and role in psychiatric disorders. *Neural Plast*. 2018;2018:1-3.
98. Dyar KA, Lutter D, Artati A, Ceglia N, Liu Y, Armenta D, Jastroch M, Schneider S, de Mateo S, Cervantes M, Abbondante S, Tognini P, Orozco-Sólis R, Kinouchi K, Wang C, Swerdloff RS, Nadeef S, Masri S, Magistretti PJ, Orlando V. Atlas of circadian metabolism reveals system-wide coordination and communication between clocks. *Cell*. 2018;174(6):1571-1585.e11.
99. Fitzgerald GA. Timing the microbes: The circadian rhythm of the gut microbiome. *J Biol Rhythms*. 2017.
100. Voigt RM, Forsyth CB, Green SJ, Engen PA, Keshavarzian A. Circadian rhythm and the gut microbiome. *Int Rev Neurobiol*. 2016:193-205.
101. Montagner A, Korecka A, Polizzi A, Lippi Y, Blum Y, Canlet C, Tremblay-Franco M, Gautier-Stein A, Burcelin R, Je HS, Al-Asmakh M, Mithieux G, Arulampalam V, Lagarrigue S, Wahli W. Hepatic circadian clock oscillators and nuclear receptors integrate microbiome-derived signals. *Sci Rep*. 2016;6(1).
102. Thaiss CA, Levy M, Korem T, Dohnalová L, Shapiro H, Jaitin DA, Winter DR, Gury-Benari M, Tatirovsky E, Tuganbaev T, Federici S, Zmora N, Zeevi D, Dori-Bachash M, Pevsner-Fischer M, Harmelin A, Shibolet O. Microbiota diurnal rhythmicity programs host transcriptome oscillations. *Cell*. 2016;167(6):1495-1510.e12.
103. Fetissov SO. Role of the gut microbiota in host appetite control: Bacterial growth to animal feeding behavior. *Nat Rev Endocrinol*. 2016;13(1):11-25.
104. The Journal of Nutrition [Internet]. 2023. Nutrition.org.
105. Mack I, Cuntz U, Grämer C, Niedermaier S, Pohl C, Schwiertz A, Zimmermann K, Zipfel S, Enck P, Penders J. Weight gain in anorexia nervosa does not ameliorate the faecal microbiota, branched chain fatty acid profiles and gastrointestinal complaints. *Sci Rep*. 2016;6(1).
106. The effect of diet on the human gut microbiome: A metagenomic analysis in humanized gnotobiotic mice. *Sci Transl Med*. 2023.
107. Fetissov SO, Sinno H, Coëffier M, Bole-Feysot C, Ducrotté P, Hökfelt T, Déchelotte P. Autoantibodies against appetite-regulating peptide hormones and neuropeptides: Putative modulation by gut microflora. *Nutrition*. 2008;24(4):348-359.
108. Aschenbrenner K, Scholze N, Joraschky P, Hummel T. Gustatory and olfactory sensitivity in patients with anorexia and bulimia in the course of treatment. *J Psychiatr Res*. 2008;43(2):129-137.



**Vinod Kumar Mugada et al.,**

109. Berthoud HR, Zheng H. Modulation of taste responsiveness and food preference by obesity and weight loss. *Physiol Behav.* 2012;107(4):527-532.
110. Buffington SA, Viana G, Auchtung T, Ajami NJ, Petrosino JF, Costa-Mattioli M. Microbial reconstitution reverses maternal diet-induced social and synaptic deficits in offspring. *Cell.* 2016;165(7):1762-1775.
111. Sgritta M, Dooling SW, Buffington SA, Momin EN, Francis M, Britton RA, Costa-Mattioli M. Mechanisms underlying microbial-mediated changes in social behavior in mouse models of autism spectrum disorder. *Neuron.* 2019;101(2):246-259.e6.
112. Stilling RM, Moloney GM, Ryan FJ, Hoban AE, Bastiaanssen TFS, Shanahan F, Clarke G, Claesson MJ, Dinan TG, Cryan JF. Social interaction-induced activation of RNA splicing in the amygdala of microbiome-deficient mice. *Elife.* 2018;7: e34386.
113. Arentsen T, Yu Q, Gkatzis SG, Femenía T, Wang T, Udekwu KI, Forsberg H, Diaz Heijtz R. The bacterial peptidoglycan-sensing molecule Pglyrp2 modulates brain development and behavior. *Mol Psychiatry.* 2016;22(2):257-66.
114. Degroote S, Hunting DJ, Baccarelli AA, Takser L. Maternal gut and fetal brain connection: Increased anxiety and reduced social interactions in Wistar rat offspring following peri-conceptual antibiotic exposure. *Prog Neuropsychopharmacol Biol Psychiatry.* 2016;71:76-82.
115. Luczynski P, McVey Neufeld KA, Oriach CS, Clarke G, Dinan TG, Cryan JF. Growing up in a bubble: Using germ-free animals to assess the influence of the gut microbiota on brain and behavior. *Int J Neuropsychopharmacol.* 2016;19(8):pyw020.
116. Robertson RC, Oriach CS, Murphy K, Moloney GM, Cryan JF, Dinan TG, Ross RP, Stanton C. Omega-3 polyunsaturated fatty acids critically regulate behaviour and gut microbiota development in adolescence and adulthood. *Brain Behav Immun.* 2017;59:21-37.
117. Robertson RC, Oriach CS, Murphy K, Moloney GM, Cryan JF, Dinan TG, Ross RP, Stanton C. Deficiency of essential dietary n-3 PUFA disrupts the caecal microbiome and metabolome in mice. *Br J Nutr.* 2017;118(11):959-70.
118. Onarman Umu ÖC, Rudi K, Diep DB. Modulation of the gut microbiota by prebiotic fibres and bacteriocins. *Microb Ecol Health Dis.* 2017;28(1):1348886.
119. Park JH, Wang Q, Wu Q, Mao-Draayer Y, Kim CH. Bidirectional regulatory potentials of short-chain fatty acids and their G-protein-coupled receptors in autoimmune neuroinflammation. *Sci Rep.* 2019;9(1):12574.
120. Burokas A, Arboleya S, Moloney RD, Peterson VL, Murphy K, Clarke G, Stanton C, Dinan TG, Cryan JF. Targeting the microbiota-gut-brain axis: Prebiotics have anxiolytic and antidepressant-like effects and reverse the impact of chronic stress in mice. *Biol Psychiatry.* 2017;82(7):472-87.
121. Kazemi A, Noorbala AA, Azam K, Eskandari MH, Djafarian K. Effect of probiotic and prebiotic vs placebo on psychological outcomes in patients with major depressive disorder: A randomized clinical trial. *Clin Nutr.* 2019;38(2):522-8.
122. Liu RT, Walsh RFL, Sheehan AE. Prebiotics and probiotics for depression and anxiety: A systematic review and meta-analysis of controlled clinical trials. *Neurosci Biobehav Rev.* 2019;102:13-23.
123. Johnson D, Thurairajasingam S, Letchumanan V, Chan KG, Lee LH. Exploring the role and potential of probiotics in the field of mental health: Major depressive disorder. *Nutrients.* 2021;13(5):1728.
124. Autointoxication and historical precursors of the microbiome-gut-brain axis. *Microb Ecol Health Dis.* 2018.
125. Anukam K, Reid G. Probiotics: 100 years (1907-2007) after Elie Metchnikoff's observation. Retrieved September 2, 2023, from [URL].
126. Cammarota G, Ianiro G, Ahern AM, Carbone C, Temko A, Claesson MJ, Gasbarrini A, Tortora G. Gut microbiome, big data and machine learning to promote precision medicine for cancer. *Nat Rev Gastroenterol Hepatol.* 2020;17(10):635-48.
127. Ballester P. Precision psychiatry: The future is now. Passos IC, Rabelo-da-Ponte FD, Kapczinski F, editors. *Can J Psychiatry.* 2022;67(11):848-52.
128. Radjabzadeh DJ, Bosch JA, Uitterlinden AG, Zwinderman AH, Ikram MA, Joyce J, Luik AI, Nieuwdorp M, Lok A, Kraaij C, Amin N. Gut microbiome-wide association study of depressive symptoms. *Nat Commun.* 2022;13(1):718.
129. Bzdok D, Meyer-Lindenberg A. Machine learning for precision psychiatry: Opportunities and challenges. *Biol Psychiatry Cogn Neurosci Neuroimaging.* 2018;3(3):223-30.
130. Namkung J. Machine learning methods for microbiome studies. *J Microbiol.* 2020;58(3):206-16.



Vinod Kumar Mugada *et al.*,

131. Zhao L, Xiong Q, Sary CM, Mahgoub OK, Ye Y, Gu L, Xiong XQ, Zhu S. Bidirectional gut-brain-microbiota axis as a potential link between inflammatory bowel disease and ischemic stroke. *J Neuroinflammation*. 2018;15(1):53.
132. Zhu F, Tu H, Chen T. The microbiota-gut-brain axis in depression: The potential pathophysiological mechanisms and microbiota combined antidepressant effect. *Nutrients*. 2022;14(10):2081.
133. Méndel-Del Barrio C, Sánchez SA, Martín-Monzón I. The gut microbiota-brain axis, psychobiotics and its influence on brain and behaviour: A systematic review. *Psychoneuroendocrinology*. 2022;137:105640.
134. Wilson K, Situ C. Systematic review on effects of diet on gut microbiota in relation to metabolic syndromes. *J Clin Nutr Metab*. 2017;1(2):42–53.
135. Corrêa-Oliveira R, Fachi JA, Vieira AA, Sato FT, M. Regulation of immune cell function by short-chain fatty acids. *Clin Transl Immunol*. 2016;5(4):e73.
136. Ma N, Yan T, Wu Y, Ma X. Contributions of the interaction between dietary protein and gut microbiota to intestinal health. *Curr Protein Pept Sci*. 2017;18(8):725–34.
137. Sender R, Fuchs S, Milo R. Revised estimates for the number of human and bacteria cells in the body. *PLoS Biol*. 2016;14(8):e1002533.
138. Breton J, Tennoune N, Lucas N, François M, Legrand R, Jacquemot J, Goichon A, Guérin C, Peltier J, Pestel-Caron M, Chan P, Vaudry D, Rego JC, Liénard F, Pénicaud L, Fioramonti X, Ebenezzer IS, Hökfelt T, Déchelotte P, Fetissov SO. Gut commensal *E. coli* proteins activate host satiety pathways following nutrient-induced bacterial growth. *Cell Metab*. 2016;23(2):324–34.
139. Aarts E, Naaijen J, Zwieters MP, Boekhorst J, Timmerman HM, Smeekens SP, Netea MG, Buitelaar JK, Franke B, Vasquez AA. Gut microbiome in ADHD and its relation to neural reward anticipation. *PLoS One*. 2017;12(9):e0183509.
140. Kaczmarek J, Musaad S, Holscher HD. Time of day and eating behaviors are associated with the composition and function of the human gastrointestinal microbiota. *Am J Clin Nutr*. 2017;106(5):1220–31.
141. Tosti V, Bertozzi B, Fontana L. Health benefits of the Mediterranean diet: Metabolic and molecular mechanisms. *J Gerontol A Biol Sci Med Sci*. 2017;73(3):318–26.
142. Tillisch K, Mayer EA, Gupta AR, Gill Z, Brazeilles R, Le Nevé B, van Hylckama, Guyonnet D, Derrien M, Labus JS. Brain structure and response to emotional stimuli as related to gut microbial profiles in healthy women. *Psychosom Med*. 2017;79(8):905–13.
143. Molendijk ML, Molero P, Sánchez-Pedreño FE, Martínez-González MA. Diet quality and depression risk: A systematic review and dose-response meta-analysis of prospective studies. *J Affect Disord*. 2018;226:346–54.
144. Bailey MA, Holscher HD. Microbiome-mediated effects of the Mediterranean diet on inflammation. *Adv Nutr*. 2018;9(3):193–206.

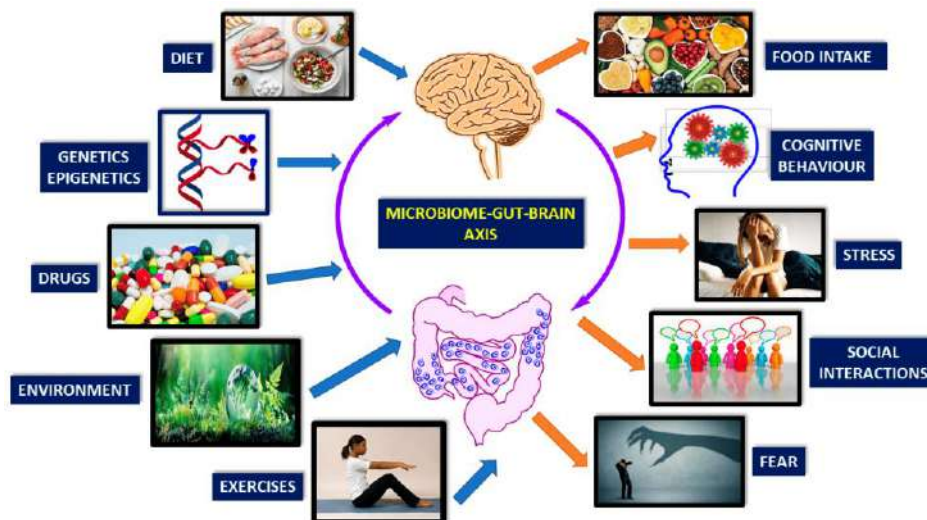


Figure 1: Factors affecting microbiome gut brain axis [29]





## M/D/1 Queuing Model with Picture Fuzzy Set

V.Chitra<sup>1</sup> and B. Maheswari<sup>2\*</sup>

<sup>1</sup>Associate Professor, Department of Mathematics, Nallamuthu Gounder Mahalingam College, Pollachi, (Affiliated to Bharathiar University), Coimbatore, Tamil Nadu, India.

<sup>2</sup>Assistant Professor, Department of Mathematics, Dr. Mahalingam College of Engineering and Technology, Pollachi, Coimbatore, (Affiliated to Anna University, Chennai), Tamil Nadu, India.

Received: 19 July 2024

Revised: 12 Sep 2024

Accepted: 13 Nov 2024

### \*Address for Correspondence

#### B. Maheswari

Assistant Professor, Department of Mathematics,  
Dr. Mahalingam College of Engineering and Technology,  
Pollachi, Coimbatore, (Affiliated to Anna University, Chennai),  
Tamil Nadu, India.  
E.Mail: mahes.sint@gmail.com



This is an Open Access Journal / article distributed under the terms of the **Creative Commons Attribution License** (CC BY-NC-ND 3.0) which permits unrestricted use, distribution, and reproduction in any medium, provided the original work is properly cited. All rights reserved.

### ABSTRACT

This paper introduces the integration of Picture Fuzzy Sets (PFS) into the M/D/1 queuing model with an infinite queue capacity. To capture the uncertainties inherent in both arrival and service processes, we model the entry and utility rates using Single Valued Trapezoidal Picture Fuzzy Numbers (SVTPN). The DSW algorithm and the  $(\alpha, \beta, \gamma)$  cut method are utilized to develop our proposed model. Our analysis employs a hierarchical approach, evaluating the system based on varying  $(\alpha, \beta, \gamma)$  cuts. This multi-level approach effectively illustrates how membership values are represented and managed within the SVTPN framework. Through a detailed numerical example, we demonstrate the implementation and benefits of our fuzzy-based method in queuing system analysis. Future research will extend these findings to more complex and varied queuing scenarios and exploring the potential of picture fuzzy set theory in operational analysis.

**Keywords:** Picture Fuzzy Set, single valued trapezoidal picture fuzzy number, DSW algorithm,  $(\alpha, \beta, \gamma)$  cut

## INTRODUCTION

Queuing theory has evolved since the early 1900's in three main phases. It was born with the work of A.K. Erlang, who published in 1917 the important formulas which now bear his name. Erlang's motivation was to develop tools for the analysis and design of telephone systems, an application that continues to the present day to motivate research in queueing theory. Renewed interest in queueing theory and its potential applications outside of telecommunications came with the codification of the field of operations research in the early 1950's. The use of





**Chitra and Maheswari**

queueing theory as a tool for the performance evaluation of computer systems and components of computer systems is now well established, with the result that most undergraduate computer science majors receive at least some exposure to its models and methodology. The present trend combining computing and telecommunications promises an acceleration in the development of queueing theory and its importance to computer scientists and engineers.

Queueing models are fundamental tools in the study of systems where entities wait for service. They provide insights into system performance, guiding the design and optimization of various operational processes. Traditional queueing models, like the M/D/1 queue, rely on precise numerical inputs for arrival and service rates. However, real-world systems often exhibit uncertainties that challenge the precision of these parameters. To address these uncertainties, fuzzy set theory has been widely applied to queueing models, providing a more flexible approach to modeling and analysis. Fuzzy sets, introduced by Zadeh (1965) (22), allow for a gradual assessment of membership rather than a binary classification. This concept was further expanded by Atanassov (1986) (2) into intuitionistic fuzzy sets, which account for degrees of membership, non-membership, and hesitation. These advancements paved the way for more nuanced fuzzy models, such as the trapezoidal fuzzy numbers used by Sumathi and Antony Crispin Sweety (2019) (16) and the single valued neutrosophic sets discussed by Wang et al. (2010) (26). The integration of fuzzy sets into queueing models has been extensively studied. Li and Lee (1989) (8) explored the analysis of fuzzy queues, demonstrating how fuzzy logic can enhance the understanding of queueing dynamics. Similarly, Kalpana and Anusheela (2018) (4) analyzed a single-server non-preemptive fuzzy priority queue, showcasing the utility of fuzzy sets in prioritizing service. The work of Rashad and Mohamed (2021) (9) on neutrosophic theory in queueing models further illustrates the application of advanced fuzzy concepts to capture even more complex uncertainties.

Kumuthavalli and Sangeetha (2017) (7) introduced neutrosophic fuzzy sets to queueing theory, emphasizing their role in modeling ambiguous and conflicting information. This approach aligns with the developments in neutrosophic sets by Smarandache (2010)(13), (2020)(14), who explored their applications in various operational scenarios. The neutrosophic extension of fuzzy sets allows for a more comprehensive representation of uncertainty, which is particularly useful in the context of queueing models with variable parameters. In the realm of performance evaluation of fuzzy queueing systems, the DSW algorithm has been a prominent tool. Srinivasan (2014) (15) and Shanmugasundaram and Venkatesh (2015) (10) employed the DSW algorithm to analyze fuzzy queueing models, demonstrating its effectiveness in handling fuzzy data. The algorithm's ability to process fuzzy numbers into crisp values makes it a valuable asset in operational research and system analysis. A picture fuzzy set (PFS) is a mathematical technique in queueing theory that is used to analyse and characterize complicated systems with uncertainty. A PFS is made up of several fuzzy sets that work together to describe inaccurate or hazy information about a system, including how consumers or servers behave. When modelling and assessing the performance of queueing systems, where inaccurate data or presumptions could result in wrong results, this approach is helpful. Because PFS-based models take into account the uncertainty inherent in real-world systems, they can yield forecasts and judgements that are more accurate.

The picture fuzzy set, introduced by Bui Cong Cung (2014) (3), extends the intuitionistic fuzzy set by adding a fourth parameter, capturing the degree of neutrality. This additional parameter allows for a richer representation of uncertainty, making picture fuzzy sets a powerful tool for modeling complex systems. This extended model is particularly useful in situations where decisions or classifications cannot be strictly binary or even dualistic but require an intermediate or neutral state. For instance, in sentiment analysis of social media posts, picture fuzzy sets allow for a more nuanced understanding of public sentiment, capturing not just positive and negative sentiments but also neutral or ambivalent feelings (Thakkar et al., 2021) (17). Moreover, the picture fuzzy sets have found applications in medical diagnosis, where patients' conditions can be classified not just as positive or negative for a particular disease but can also consider indeterminate states or varying degrees of symptom severity (Thao et al., 2019). This (18) granularity improves decision-making processes by providing a richer set of information. The picture fuzzy set's application to queueing models offers a new dimension in analyzing systems with ambiguous and imprecise data. Building on these foundational works, our paper introduces the use of Picture Fuzzy Sets (PFS) in the M/D/1 queueing model with an infinite queue capacity. We represent both the arrival rate and service time using





### Chitra and Maheswari

Single Valued Trapezoidal Picture Fuzzy Numbers (SVTPN), following the approach of Varadharajan and Susmitha (2018) (21) who evaluated performance measures of priority queues with fuzzy parameters using the  $\alpha$ -cut method. The DSW algorithm and the  $(\alpha, \beta, \gamma)$  cut method are utilized to compute the system's performance metrics, aligning with the methodologies proposed by Usha Prameela and Pavan Kumar (2019) (19) (20) in their study of fuzzy multi-server queuing models. Building on these concepts, Shi, Kosari, and Khan (2023) (12) introduce interval-valued picture fuzzy graphs, which combine the strengths of interval-valued fuzzy graphs and PFSs. This new model enhances the ability to manage and analyze data characterized by multiple degrees of membership, non-membership, and hesitancy. Our analysis is structured across primary, secondary and tertiary levels, each corresponding to different  $(\alpha, \beta, \gamma)$  cuts, to capture the varying degrees of uncertainty within the system. This multi-level approach provides a comprehensive view of the system's performance under different fuzzy scenarios. The practical implications of our model are demonstrated through a numerical example, highlighting the benefits of using picture fuzzy sets in queuing analysis. This approach not only captures traditional uncertainties but also accommodates the degrees of membership, non-membership, and hesitation inherent in real-world systems.

Future research will extend our findings to more advanced fuzzy set models, such as Type-II fuzzy sets and Pythagorean fuzzy sets, as explored by Kanufmann (1975) (5) and Smarandache (2020). These models can capture even higher levels of uncertainty and complexity, providing deeper insights into the dynamics of queuing systems. Our study contributes to the ongoing development of fuzzy set theory and its application in queuing models, offering a novel approach to understanding and managing uncertainty in operational processes. The purpose of this research is to look at a single server queuing model with fixed utility period that uses single valued picture fuzzy set (SVPS). The suppositions and calculations are explained in part three. The fourth part has the proposed queuing miniature. The fifth part addresses the present model's result strategy and sixth part contains the conclusion and results.

#### Basic definitions

**Definition 2.1 [3].** A picture fuzzy set  $A$  on a universe  $X$  is an object in the form of

$$A = \{x, (\mu_A(x), \eta_A(x), \gamma_A(x))\}; (x \in X)$$

Where  $\mu_A(x) \in [0,1]$  is called the degree of positive membership of  $x$  in  $A$ ,  $\eta_A(x) \in [0,1]$  is called the degree of neutral membership of  $x$  in  $A$  and  $\gamma_A(x) \in [0,1]$  is called the degree of negative membership of  $x$  in  $A$ , and where  $\mu_A$ ,  $\eta_A$ , and  $\gamma_A$  satisfy the following condition:

$$(\forall x \in X) (\mu_A(x) + \eta_A(x) + \gamma_A(x) \leq 1)$$

Now  $\theta_A(x) = (1 - (\mu_A(x) + \eta_A(x) + \gamma_A(x)))$  could be called the degree of refusal membership of  $x$  in  $A$ .

Let PFS( $X$ ) denote the set of all the picture fuzzy sets on universe  $X$ .

**Definition 2.2 [3]:** A intuitionistic fuzzy set  $A$  on a universe  $X$  is an object of the form

$$A = \{ (x, (\mu_A(x), \gamma_A(x))) \mid x \in X \}$$

Where  $\mu_A(x) \in [0,1]$  is called the degree membership of  $x$  in  $A$ ,  $\gamma_A(x) \in [0,1]$  is called the degree of non-membership of  $x$  in  $A$ , and where  $\mu_A$  and  $\gamma_A$  satisfy the following condition:

$$(\forall x \in X) (\mu_A(x) + \gamma_A(x) \leq 1).$$

**Definition 2.3 [3]:** For every two PFSs  $A$  and  $B$ , the union, intersection and complement are defined as follows:

- $A \subseteq B$  iff  $(\forall x \in X, \mu_A(x) \leq \mu_B(x) \text{ and } \eta_A(x) \leq \eta_B(x) \text{ and } \gamma_A(x) \geq \gamma_B(x))$
- $A = B$  iff  $(A \subseteq B \text{ and } B \subseteq A)$
- $A \cup B = \{(x, \max(\mu_A(x), \mu_B(x)), \min(\eta_A(x), \eta_B(x)), \min(\gamma_A(x), \gamma_B(x))) \mid x \in X\}$
- $A \cap B = \{(x, \min(\mu_A(x), \mu_B(x)), \min(\eta_A(x), \eta_B(x)), \max(\gamma_A(x), \gamma_B(x))) \mid x \in X\}$
- $\text{co}(A) = \bar{A} = \{(\gamma_A(x), \eta_A(x), \mu_A(x)) \mid x \in X\}$

#### Definition 2.5 [16]

The representation of a single-valued picture fuzzy set (SVPFS)  $N$  that exists within the set  $X$  is articulated as follows:







Chitra and Maheswari

$$\gamma_A(x) = \begin{cases} \frac{p^\gamma - q_1^\gamma}{q_2^\gamma - q_1^\gamma} & \text{for } q_1^\gamma \leq p^\gamma \leq q_2^\gamma \\ 1 & \text{for } q_2^\gamma \leq p^\gamma \leq q_3^\gamma \\ \frac{q_4^\gamma - p^\gamma}{q_4^\gamma - q_3^\gamma} & \text{for } q_3^\gamma \leq p^\gamma \leq q_4^\gamma \\ 0 & \text{for otherwise} \end{cases}$$

Where  $q_1^\gamma \leq q_2^\gamma \leq q_3^\gamma \leq q_4^\gamma$

$$\eta_A(x) = \begin{cases} \frac{p^\eta - q_1^\eta}{q_2^\eta - q_1^\eta} & \text{for } q_1^\eta \leq p^\eta \leq q_2^\eta \\ 1 & \text{for } q_2^\eta \leq p^\eta \leq q_3^\eta \\ \frac{q_4^\eta - p^\eta}{q_4^\eta - q_3^\eta} & \text{for } q_3^\eta \leq p^\eta \leq q_4^\eta \\ 1 & \text{for otherwise} \end{cases}$$

Where  $q_1^\eta \leq q_2^\eta \leq q_3^\eta \leq q_4^\eta$

$$\mu_A(x) = \begin{cases} \frac{p^\mu - q_1^\mu}{q_2^\mu - q_1^\mu} & \text{for } q_1^\mu \leq p^\mu \leq q_2^\mu \\ 1 & \text{for } q_2^\mu \leq p^\mu \leq q_3^\mu \\ \frac{q_4^\mu - p^\mu}{q_4^\mu - q_3^\mu} & \text{for } q_3^\mu \leq p^\mu \leq q_4^\mu \\ 1 & \text{for otherwise} \end{cases}$$

Where  $q_1^\mu \leq q_2^\mu \leq q_3^\mu \leq q_4^\mu$

**Definition 2.6** [16]

The definition of the  $(\alpha, \beta, \gamma)$ -cut approach for SVTPN is articulated as follows:

$$A_{\alpha,\beta,\gamma} = [\tilde{A}_1(\alpha), \tilde{A}_2(\alpha)]; [\tilde{A}_1(\beta), \tilde{A}_2(\beta)], [\tilde{A}_1(\gamma), \tilde{A}_2(\gamma)], 0 \leq \alpha + \beta + \gamma \leq 3, \text{ where}$$

$$[\tilde{A}_1(\alpha), \tilde{A}_2(\alpha)] = [(q_1^T + \alpha(q_2^T - q_1^T)), (q_3^T - \alpha(q_4^T - q_3^T))]$$

$$[\tilde{A}_1(\beta), \tilde{A}_2(\beta)] = [(q_1^I - \beta(q_2^I - q_1^I)), (q_3^I + \beta(q_4^I - q_3^I))]$$

$$[\tilde{A}_1(\gamma), \tilde{A}_2(\gamma)] = [(q_1^F - \gamma(q_2^F - q_1^F)), (q_3^F + \gamma(q_4^F - q_3^F))]$$

**Definition 2.7**[6]

Let us consider the two interval values denoted by ordered pairs of actual numbers with the lower and upper bounds  $beF = [m_1, m_2], m_1 \leq m_2$  and  $H = [n_1, n_2], n_1 \leq n_2$ , with following properties:

$$[m_1, m_2] + [n_1, n_2] = [m_1 + n_1, m_2 + n_2]$$

$$[m_1, m_2] - [n_1, n_2] = [m_1 - n_1, m_2 - n_2]$$

$$[m_1, m_2] \times [n_1, n_2] = [\min(m_1 n_1, m_1 n_2, m_2 n_1, m_2 n_2), \max(m_1 n_1, m_1 n_2, m_2 n_1, m_2 n_2)]$$

$$[m_1, m_2] \div [n_1, n_2] = [m_1, m_2] \times [1/n_1, 1/n_2], \text{ provided that } 0 \text{ does not belong to } [n_1, n_2]$$

$$\alpha \times [m_1, m_2] = [\alpha m_1, \alpha m_2] \text{ for } \alpha > 0 \text{ and } [\alpha m_2, \alpha m_1] \text{ for } \alpha < 0$$

**The Picture Fuzzy Queuing Model(M/D/1)**

In this section, we are going to introduce a single server queue with deterministic service time in a picture fuzzy environment.

**Presumptions and Notations**

Corresponding as sumptions are used in the current model

- i) M/D/1/∞/FCF Squeuing system with single server has an unbounded limit.
- ii) Entry period that are distributed exponentially
- iii) Deterministic utility period, i.e. fixed





**Chitra and Maheswari**

iv) Entry and utility period are picture trapezoidal fuzzy numbers and symbols are represented as:

$\mu$  = utility period

$\lambda$  = entry period

$N_s$  = Expected no of consumer count in the system

$N_q$  = Expected no of consumers waiting in line

$W_s$  = System's average client hold time

$W_q$  = Expected time of an average consumer waits in queue

$W$  = Customer Entry level

$Z$  = Utility period of Customer

$A$  = entry level

$S$  = utility level

**Suggested queuing miniature**

In this paper, we prefer (FCFS) first come first serve single server queuing model. In Kendall's notation, it is denoted as (M/D/1): ( $\infty$ /FCFS). Here, D denotes picture fuzzy steady (constant) distribution with utility rate and M denotes picture fuzzy exponential distribution with entry rate. This stochastic process, which includes any entity currently engaged in administration, has a sequence with the values 0, 1, 2, 3... where the numbers denotes how many peoples currently utilizing the server. Its size is infinite, therefore there is no limitation to the no of clients it can accommodate.

Expected no of consumer count in the system:

$$N_{L_s} = \frac{\lambda}{\mu} + \frac{\lambda^2}{2\mu(\mu - \lambda)}$$

Expected no of consumers waiting in line:

$$N_{L_q} = \frac{\lambda^2}{2\mu(\mu - \lambda)}$$

Expected time of an average consumer waits in queue:

$$N_{W_q} = \frac{\lambda}{2\mu(\mu - \lambda)}$$

System's average client hold time:

$$N_{W_s} = \frac{1}{\mu} + \frac{\lambda}{2\mu(\mu - \lambda)}$$

**Solution procedure**

A simple method called DSW (Dong, Shah, and Wong) uses intervals at different  $\alpha, \beta, \gamma$ -cut dimensions to describe execution proportions. The segregation extending on the picture fuzzy variable area prevents variance from the output membership function. Each ongoing involvement capacity can be addressed by an endless range of cuts with terms ranging from 0 to 1. Let  $\mu_A(\tilde{a})$  &  $\mu_S(\tilde{s})$  be the membership performs of the utility period and the inter entry period. Intervals between entry period and utility period are shown as picture fuzzy sets as follows:

$$A' = \{\tilde{a}, \mu_A(\tilde{a}), \eta_A(\tilde{a}), \gamma_A(\tilde{a}), \tilde{a} \in W\} \text{ and } S' = \{\tilde{s}, \mu_S(\tilde{s}), \eta_S(\tilde{s}), \gamma_S(\tilde{s}), \tilde{s} \in Z\}$$

The  $\alpha, \beta, \gamma$ -cuts of entry period, utility period are represented as:

$$A'(\alpha) = \{\mu_A(\tilde{a}), \eta_A(\tilde{a}), \gamma_A(\tilde{a}) / \tilde{a} \in W\} \text{ and}$$

$$S'(\alpha) = \{\mu_S(\tilde{s}), \eta_S(\tilde{s}), \gamma_S(\tilde{s}) / \tilde{s} \in Z\}$$

The DSW calculation contains the following steps:

Step 1: Define  $(\alpha, \beta, \gamma)$ -cut value where  $0 \leq \alpha, \beta, \gamma \leq 1$

Step 2: Next to compare with this  $\alpha, \beta, \gamma$  find the membership performs intervals.

Step 3: The interval for the output membership perform is processed for the selected  $(\alpha, \beta, \gamma)$  - cut measurements using common binary interval operation

Step 4: Repeat steps 1-3 for various estimates of  $\alpha, \beta, \gamma$ .





**Chitra and Maheswari**

**Formulation of M/D/1 queuing model**

Let's contemplate a queuing model featuring a solitary server M/D/1 configuration and deterministic service time. The picture fuzzy entry period  $\bar{A}$ , the approximate knowledge of picture fuzzy utility periods  $\bar{S}$  is elucidated as follows:

$$\bar{A} = \{a, \mu_{\bar{A}}(a), \eta_{\bar{A}}(a), \gamma_{\bar{A}}(a) / a \in W\}$$

$$\bar{S} = \{s, \mu_{\bar{S}}(s), \eta_{\bar{S}}(s), \gamma_{\bar{S}}(s) / s \in Z\}$$

where  $W$  and  $Z$  represents crisp sets of the picture fuzzy entry period and picture fuzzy utility period and  $\mu_{\bar{A}}(a), \mu_{\bar{S}}(s)$  are the corresponding membership performs. The  $(\alpha, \beta, \gamma)$ -cut of  $\bar{A}$  and  $\bar{S}$  are

$$A(\alpha, \beta, \gamma) = \{a \in X / T_{\bar{A}}(a) \geq \alpha, I_{\bar{A}}(a) \leq \beta, F_{\bar{A}}(a) \leq \gamma\}$$

$$S(\alpha, \beta, \gamma) = \{s \in X / T_{\bar{S}}(s) \geq \alpha, I_{\bar{S}}(s) \leq \beta, F_{\bar{S}}(s) \leq \gamma\}$$

where  $A(\alpha, \beta, \gamma)$  and  $S(\alpha, \beta, \gamma)$  are the subsets of  $W$  and  $Z$  respectively. Here we can represent picture fuzzy inter entry time and picture fuzzy overhauled time by the different levels of intervals using  $(\alpha, \beta, \gamma)$ -cuts. As a result, a picture fuzzy queue can be transformed into a collection of crisp queues, each characterized by distinct  $(\alpha, \beta, \gamma)$ -cuts.

$$\{A(\alpha, \beta, \gamma): 0 < \alpha \leq 1, 0 \leq \beta < 1, 0 \leq \gamma < 1\}$$

$$\{S(\alpha, \beta, \gamma): 0 < \alpha \leq 1, 0 \leq \beta < 1, 0 \leq \gamma < 1\}.$$

In this paper, we proposed a queuing model with both inter entry time  $\bar{A}$  and overhauled time  $\bar{S}$  are defined as SVTPN and the intervals of  $\bar{A}$  and  $\bar{S}$  are denoted by  $[l_{\bar{A}}(\alpha, \beta, \gamma), u_{\bar{A}}(\alpha, \beta, \gamma)]$  and  $[l_{\bar{S}}(\alpha, \beta, \gamma), u_{\bar{S}}(\alpha, \beta, \gamma)]$ . Following the application of Zadeh's extension principle, we can define the positive(truth) membership function, neutral membership function and negative(false) membership function of the performance measure  $P$  as follows.

$$T_{P(\bar{A}, \bar{S})}(w) = \sup \left\{ \min_{a \in W, a' \in Z} (\mu_{\bar{A}}(a), \mu_{\bar{S}}(a')) : w = p(a, a') \right\}$$

$$I_{P(\bar{A}, \bar{S})}(w) = \inf \left\{ \min_{a \in W, a' \in Z} (\mu_{\bar{A}}(a), \mu_{\bar{S}}(a')) : w = p(a, a') \right\}$$

$$F_{P(\bar{A}, \bar{S})}(w) = \inf \left\{ \min_{a \in W, a' \in Z} (\mu_{\bar{A}}(a), \mu_{\bar{S}}(a')) : w = p(a, a') \right\}$$

We determine the lower and upper bounds of the  $(\alpha, \beta, \gamma)$  cuts of  $(\bar{A}, \bar{S})$  as follows;

$$l_{P(\alpha, \beta, \gamma)} = \min p(a, a') \ni l_{\bar{A}}(\alpha, \beta, \gamma) \leq a \leq u_{\bar{A}}(\alpha, \beta, \gamma), l_{\bar{S}}(\alpha, \beta, \gamma) \leq a' \leq u_{\bar{S}}(\alpha, \beta, \gamma) \tag{1}$$

$$u_{P(\alpha, \beta, \gamma)} = \max p(a, a') \ni l_{\bar{A}}(\alpha, \beta, \gamma) \leq a \leq u_{\bar{A}}(\alpha, \beta, \gamma), l_{\bar{S}}(\alpha, \beta, \gamma) \leq a' \leq u_{\bar{S}}(\alpha, \beta, \gamma) \tag{2}$$

Provided  $a \in \bar{A}(\alpha, \beta, \gamma)$  and  $a' \in \bar{S}(\alpha, \beta, \gamma)$ . If both  $l_{P(\alpha, \beta, \gamma)}$  and  $u_{P(\alpha, \beta, \gamma)}$  are invertible with respect to  $(\alpha, \beta, \gamma)$  then the left shape function  $L_T(w) = (l_{P(\alpha, \beta, \gamma)})^{-1}$  and right shape functions  $R_T(w) = (u_{P(\alpha, \beta, \gamma)})^{-1}$  may be constructed and the truth membership function  $T_{P(\bar{A}, \bar{S})}(w)$  is obtained by

$$T_{P(\bar{A}, \bar{S})}(w) = \begin{cases} L_T(w); w_1^T \leq w \leq w_2^T \\ R_T(w); w_3^T \leq w \leq w_4^T \\ 0; otherwise \end{cases}$$

where  $w_1^T \leq w \leq w_4^T$  and  $L_T(w_1^T) = R_T(w_4^T) = 0$  for the SVTPN.

Similarly, the neutral membership function  $I_{P(\bar{A}, \bar{S})}(w)$  and the falsity membership function  $F_{P(\bar{A}, \bar{S})}(w)$ , are derived in the same way,

$$I_{P(\bar{A}, \bar{S})}(w) = \begin{cases} L_T(w); w_1^T \leq w \leq w_2^T \\ R_T(w); w_3^T \leq w \leq w_4^T \\ 0; otherwise \end{cases}$$





**Chitra and Maheswari**

where  $w_1^I \leq w \leq w_4^I$  and  $L_I(w_1^I) = R_I(w_4^I) = 0$  for the SVTPN.

$$F_{P(\bar{A}, \bar{S})}(w) = \begin{cases} L_F(w); w_1^F \leq w \leq w_2^F \\ R_F(w); w_3^F \leq w \leq w_4^F \\ 0; \text{otherwise} \end{cases}$$

where  $w_1^F \leq w \leq w_4^F$  and  $L_F(w_1^F) = R_F(w_4^F) = 0$  for the SVTPN.

By applying  $(\alpha, \beta, \gamma)$  - cut approach, the proposed M/D/1 queue with deterministic service time can be streamlined into a conventional M/D/1 queue

**Numerical demonstration**

Let's examine an M/D/1:∞/FCFS model where both the entry rate and utility rate are represented by single valued trapezoidal picture fuzzy number and from equations (1) & (2) the membership functions of  $\bar{N}_{L_q}$ ,  $\bar{N}_{L_s}$  and  $\bar{N}_{w_q}$ ,  $\bar{N}_{w_s}$  are listed below.

Let the arrival and service rates are represented by

$$\bar{A} = \{(x_1, 0.2, 0.0, 0.2, 0.6), (x_2, 0.7, 0.0, 0.1, 0.2), (x_3, 0.5, 0.0, 0.4, 0.1)\}$$

$$\bar{S} = \{(x_1, 0.3, 0.0, 0.0, 0.7), (x_2, 0.7, 0.0, 0.3, 0.0), (x_3, 0.5, 0.0, 0.5, 0.0)\}$$

The  $(\alpha, \beta, \gamma)$ -cut of  $\bar{A}$  and  $\bar{S}$  are

$$\bar{A} = [0.2 + \alpha, 0.6 - \alpha], [0 - \beta, 0.1 + \beta], [0 - \gamma, 0.4 + \gamma]$$

$$\bar{S} = [0.3 + \alpha, 0.7 - \alpha], [0 - \beta, 0.3 + \beta], [0 - \gamma, 0.5 + \gamma]$$

Now,

$$l_{L_q}(\alpha) = \min \left\{ \frac{e_1^2}{2e_2(e_2 - e_1)} \right\} \tag{3}$$

and

$$u_{L_q}(\alpha) = \max \left\{ \frac{e_1^2}{2e_2(e_2 - e_1)} \right\} \tag{4}$$

Such that  $0.2 + \alpha < e_1 < 0.6 - \alpha$   
 $0.3 + \alpha < e_2 < 0.7 - \alpha$

where  $0 < \alpha \leq 1$ ,  $l_{L_q}(\alpha)$  is discovered while  $e_1$  approaching their lower bound (l.b) and  $e_2$  approaching its upper bound (u.b) and as well as  $u_{L_q}(\alpha)$  is discovered while  $e_1$  approaching their u.b and  $e_2$  approaching its l.b. As a result the best solution for (3) and (4) is

$$l_{L_q}(\alpha) = \frac{\alpha^2 + 0.4\alpha + 0.04}{4\alpha^2 - 3.8\alpha + 0.7}, \quad u_{L_q}(\alpha) = \frac{\alpha^2 - 1.2\alpha + 0.36}{4\alpha^2 + 0.6\alpha - 0.18};$$

The truth membership function is

$$T_{\bar{N}_{L_q}}(w) = \begin{cases} L_T(w); & -4.57 \leq w \leq 4.54 \\ R_T(w); & -3.125 \leq w \leq 1.6 \\ 0; & \text{otherwise} \end{cases}$$

$$l_{L_q}(\beta) = \min \left\{ \frac{e_1^2}{2e_2(e_2 - e_1)} \right\} \tag{5}$$

and

$$u_{L_q}(\beta) = \max \left\{ \frac{e_1^2}{2e_2(e_2 - e_1)} \right\} \tag{6}$$

Such that  $0 - \beta < e_1 < 0.1 + \beta$   
 $0 - \beta < e_2 < 0.3 + \beta$

where  $0 < \alpha \leq 1$ ,  $l_{L_q}(\beta)$  is discovered while  $e_1$  approaching their lower bound (l.b) and  $e_2$  approaching its upper bound (u.b) and as well as  $u_{L_q}(\beta)$  is discovered while  $e_1$  approaching their u.b and  $e_2$  approaching its l.b. As a result the best solution for (5) and (6) is

$$l_{L_q}(\beta) = \frac{\beta^2}{4\beta^2 + 1.8\beta + 0.18}; \quad u_{L_q}(\beta) = \frac{\beta^2 + 0.2\beta + 0.01}{4\beta^2 + 0.2\beta};$$





Chitra and Maheswari

$$I_{\tilde{N}_{L_q}}(w) = \begin{cases} L_I(w); & 0 \leq w \leq 0.1672 \\ R_I(w); & 0 \leq w \leq 0.67 \\ 0; & \text{otherwise} \end{cases} \tag{7}$$

$$l_{L_q}(\gamma) = \min \left\{ \frac{e_1^2}{2e_2(e_2 - e_1)} \right\} \tag{7}$$

and

$$u_{L_q}(\gamma) = \max \left\{ \frac{e_1^2}{2e_2(e_2 - e_1)} \right\} \tag{8}$$

Such that  $0 - \gamma < e_1 < 0.4 + \gamma$

$0 - \gamma < e_2 < 0.5 + \gamma$

where  $0 < \alpha \leq 1$ ,  $l_{L_q}(\gamma)$  is discovered while  $e_1$  approaching their lower bound (l.b) and  $e_2$  approaching its upper bound (u.b) and as well as  $u_{L_q}(\gamma)$  is discovered while  $e_1$  approaching their u.b and  $e_2$  approaching its l.b. As a result the best solution for (7) and (8) is

$$l_{L_q}(\gamma) = \frac{\gamma^2}{4\gamma^2 + 3\gamma + 0.5}; \quad u_{L_q}(\gamma) = \frac{\gamma^2 + 0.2\gamma + 1.6}{4\gamma^2 + 0.8\gamma};$$

The falsity membership function is

$$F_{\tilde{N}_{L_q}}(w) = \begin{cases} L_F(w); & 0 \leq w \leq 0.13 \\ R_F(w); & 0 \leq w \leq 2.91 \\ 0; & \text{otherwise} \end{cases}$$

We have calculated the expected number of consumers waiting in line for various values of  $\alpha$ ,  $\beta$ , and  $\gamma$ , and the results are presented in Table 1.

Additionally, we have provided graphical representations of truth, indeterminacy and falsity of  $\tilde{N}_{L_q}$  is shown in figures. 1, 2 and 3.

Similarly the performance measure of  $\tilde{N}_{L_S}$  for  $\alpha$ -cut is given below,

$$l_{L_S}(\alpha) = \min \left\{ \frac{e_1}{e_2} + \frac{e_1^2}{2e_2(e_2 - e_1)} \right\} \tag{9}$$

and

$$u_{L_S}(\alpha) = \max \left\{ \frac{e_1}{e_2} + \frac{e_1^2}{2e_2(e_2 - e_1)} \right\} \tag{10}$$

The objective functions for  $\tilde{N}_{L_S}$  is given through the equations (9) and (10)

$$l_{L_S}(\alpha) = \frac{3\alpha^3 - 2.7\alpha^2 + 0.18\alpha + 0.168}{-4\alpha^3 + 6.6\alpha^2 - 3.36\alpha + 0.49}; \quad u_{L_S}(\alpha) = \frac{-3\alpha^3 + 0.9\alpha^2 + 0.54\alpha - 0.108}{4\alpha^3 + 1.8\alpha^2 - 0.054};$$

$$T_{\tilde{N}_{L_S}}(w) = \begin{cases} L_T(w); & -5.445 \leq w \leq 2.4 \\ R_T(w); & -0.25 \leq w \leq 2 \\ 0; & \text{otherwise} \end{cases}$$

Similarly the performance measure of  $\tilde{N}_{L_S}$  for  $\beta$ -cut is given below,

$$l_{L_S}(\beta) = \min \left\{ \frac{e_1}{e_2} + \frac{e_1^2}{2e_2(e_2 - e_1)} \right\} \tag{11}$$

and

$$u_{L_S}(\beta) = \max \left\{ \frac{e_1}{e_2} + \frac{e_1^2}{2e_2(e_2 - e_1)} \right\} \tag{12}$$

The objective functions for  $\tilde{N}_{L_S}$  is given through the equations (11) and (12)

$$l_{L_S}(\beta) = \frac{-3\beta^3 - 1.5\beta^2 - 0.18\beta}{4\beta^3 + 3\beta^2 + 0.72\beta + 0.054}; \quad u_{L_S}(\beta) = \frac{3\beta^2 + 0.4\beta + 0.01}{-4\beta^2 - 0.2\beta};$$

$$I_{\tilde{N}_{L_S}}(w) = \begin{cases} L_I(w); & -0.602 \leq w \leq 0 \\ R_I(w); & -0.81 \leq w \leq 0 \\ 0; & \text{otherwise} \end{cases}$$

Similarly the performance measure of  $\tilde{N}_{L_S}$  for  $\gamma$ -cut is given below,

$$l_{L_S}(\gamma) = \max \left\{ \frac{e_1}{e_2} + \frac{e_1^2}{2e_2(e_2 - e_1)} \right\} \tag{13}$$

and

$$u_{L_S}(\gamma) = \max \left\{ \frac{e_1}{e_2} + \frac{e_1^2}{2e_2(e_2 - e_1)} \right\} \tag{14}$$

The objective functions for  $\tilde{N}_{L_S}$  is given through the equations (13) and (14)





**Chitra and Maheswari**

$$l_{L_s}(\gamma) = \frac{-3\gamma^3 - 2.5\gamma^2 - 0.5\gamma}{4\gamma^3 + 5\gamma^2 + 2\gamma + 0.25}; \quad u_{L_s}(\gamma) = \frac{-3\gamma^2 - 2.2\gamma + 1.28}{4\gamma^2 + 0.8\gamma};$$

$$F_{\bar{N}_{L_s}}(w) = \begin{cases} L_F(w); & -0.53 \leq w \leq 0 \\ R_F(w); & -0.8 \leq w \leq 8.5 \\ 0; & \text{otherwise} \end{cases}$$

We have computed the expected number of consumers in the system for varying values of  $\alpha, \beta, \gamma \in [0,1]$  and these results are presented in Table 2.

Additionally, Figures 4, 5, and 6 present a graphical representation of the truth, indeterminacy, and falsity of  $\bar{N}_{L_s}$  is being discussed.

Similarly the performance measure of  $\bar{N}_{W_q}$  for  $\alpha$ -cut is given below,

$$l_{W_q}(\alpha) = \min \left\{ \frac{e_1}{2e_2(e_2 - e_1)} \right\} \tag{15}$$

and

$$u_{W_q}(\alpha) = \max \left\{ \frac{e_1}{2e_2(e_2 - e_1)} \right\} \tag{16}$$

The objective functions for  $\bar{N}_{W_q}$  is given through the equations (15) and (16)

$$l_{w_q}(\alpha) = \frac{0.2 + \alpha}{4\alpha^2 - 3.8\alpha + 0.7}; \quad u_{w_q}(\alpha) = \frac{0.6 - \alpha}{4\alpha^2 + 0.6\alpha - 0.18};$$

$$T_{\bar{N}_{L_{w_q}}}(w) = \begin{cases} L_T(w); & -6.25 \leq w \leq 4.5454 \\ R_T(w); & -3.333 \leq w \leq 0.8333 \\ 0; & \text{otherwise} \end{cases}$$

similarly the performance measure of  $\bar{N}_{W_q}$  for  $\beta$ -cut is given below,

$$l_{W_q}(\beta) = \min \left\{ \frac{e_1}{2e_2(e_2 - e_1)} \right\} \tag{17}$$

and

$$u_{W_q}(\beta) = \max \left\{ \frac{e_1}{2e_2(e_2 - e_1)} \right\} \tag{18}$$

The objective functions for  $\bar{N}_{W_q}$  is given through the equations (17) and (18)

$$l_{w_q}(\beta) = \frac{-\beta}{4\beta^2 + 1.8\beta + 0.18}; \quad u_{w_q}(\beta) = \frac{0.1 + \beta}{4\beta^2 + 0.2\beta};$$

$$I_{\bar{N}_{L_{w_q}}}(w) = \begin{cases} L_I(w); & -0.2857 \leq w \leq 0 \\ R_I(w); & 0.1467 \leq w \leq 0.2381 \\ 0; & \text{otherwise} \end{cases}$$

similarly the performance measure of  $\bar{N}_{W_q}$  for  $\gamma$ -cut is given below,

$$l_{W_q}(\gamma) = \min \left\{ \frac{e_1}{2e_2(e_2 - e_1)} \right\} \tag{19}$$

and

$$u_{W_q}(\gamma) = \max \left\{ \frac{e_1}{2e_2(e_2 - e_1)} \right\} \tag{20}$$

The objective functions for  $\bar{N}_{W_q}$  is given through the equations (19) and (20)

$$l_{w_q}(\gamma) = \frac{-\gamma}{4\gamma^2 + 3\gamma + 0.5}; \quad u_{w_q}(\gamma) = \frac{0.4 + \gamma}{4\gamma^2 + 0.8\gamma};$$

$$F_{\bar{N}_{L_{w_q}}}(w) = \begin{cases} L_F(w); & -0.2 \leq w \leq 0 \\ R_F(w); & 0 \leq w \leq 4.17 \\ 0; & \text{otherwise} \end{cases}$$

We have performed calculations for the expected time an average customer waits in the queue, considering different values of  $\alpha, \beta,$  and  $\gamma,$  and the results are documented in Table 3. Furthermore, Figures 7, 8, and 9 depict a graphical examination of the truth, indeterminacy, and falsity aspects of  $\bar{N}_{W_q}$  is discussed.

Similarly the performance measure of  $\bar{N}_{W_s}$  for  $\alpha$ -cut is given below,

$$l_{W_s}(\alpha) = \min \left\{ \frac{1}{e_2} + \frac{e_1}{2e_2(e_2 - e_1)} \right\} \tag{21}$$

and







**Chitra and Maheswari**

$$u_{W_s}(\alpha) = \max \left\{ \frac{1}{e_2} + \frac{e_1}{2e_2(e_2 - e_1)} \right\} \tag{22}$$

The objective functions for  $\tilde{N}_{W_s}$  is given through the equations (21) and (22)

$$l_{W_s}(\alpha) = \frac{3\alpha^2 - 3.3\alpha + 0.84}{-4\alpha^3 + 6.6\alpha^2 - 3.36\alpha + 0.49}; \quad u_{W_s}(\alpha) = \frac{3\alpha^2 + 0.9\alpha}{4\alpha^3 + 1.8\alpha^2 - 0.054};$$

$$T_{\tilde{N}_{W_s}}(w) = \begin{cases} L_T(w); & -5.4545 \leq w \leq 6 \\ R_T(w); & -3.75 \leq w \leq 2.75 \\ 0; & \text{otherwise} \end{cases}$$

similarly the performance measure of  $\tilde{N}_{W_s}$  for  $\beta$ -cut is given below,

$$l_{W_s}(\beta) = \min \left\{ \frac{1}{e_2} + \frac{e_1}{2e_2(e_2 - e_1)} \right\} \tag{23}$$

and

$$u_{W_s}(\beta) = \max \left\{ \frac{1}{e_2} + \frac{e_1}{2e_2(e_2 - e_1)} \right\} \tag{24}$$

The objective functions for  $\tilde{N}_{W_s}$  is given through the equations (23) and (24)

$$l_{W_s}(\beta) = \frac{3\beta^2 + 1.5\beta + 0.18}{4\beta^3 + 3\beta^2 + 0.72\beta + 0.054}; \quad u_{W_s}(\beta) = \frac{3\beta + 0.1}{-4\beta^2 - 0.2\beta};$$

$$I_{\tilde{N}_{W_s}}(w) = \begin{cases} L_I(w); & 0.6020 \leq w \leq 3.333 \\ R_I(w); & -6.667 \leq w \leq 0 \\ 0; & \text{otherwise} \end{cases}$$

similarly the performance measure of  $\tilde{N}_{W_s}$  for  $\gamma$ -cut is given below,

$$l_{W_s}(\gamma) = \min \left\{ \frac{1}{e_2} + \frac{e_1}{2e_2(e_2 - e_1)} \right\} \tag{25}$$

and

$$u_{W_s}(\gamma) = \max \left\{ \frac{1}{e_2} + \frac{e_1}{2e_2(e_2 - e_1)} \right\} \tag{26}$$

The objective functions for  $\tilde{N}_{W_s}$  is given through the equations (25) and (26)

$$l_{W_s}(\gamma) = \frac{3\gamma^2 + 2.5\gamma + 0.5}{4\gamma^3 + 5\gamma^2 + 2\gamma + 0.25}; \quad u_{W_s}(\gamma) = \frac{3\gamma + 0.4}{-4\gamma^2 - 0.8\gamma};$$

$$F_{\tilde{N}_{W_s}}(w) = \begin{cases} L_F(w); & 0.533 \leq w \leq 1.5476 \\ R_F(w); & -5.833 \leq w \leq -0.708 \\ 0; & \text{otherwise} \end{cases}$$

The system's average client hold time has been computed for various values of  $\alpha$ ,  $\beta$ , and  $\gamma$ , and the outcomes are presented in Table 4. Also a graphical analysis of truth, indeterminacy and falsity of  $\tilde{N}_{W_s}$  is shown in figures. 10, 11 and 12.

## CONCLUSION

In this paper, we have successfully introduced and applied Picture Fuzzy Sets (PFS) to the M/D/1 queuing model, providing a novel approach to capturing and analyzing the uncertainties in queuing systems. Our hypothesis suggested that integrating PFS into the queuing model offers a more nuanced understanding of the relationships between the arrival process, service process, and customer behavior in the queue. This hypothesis was validated through the derivation of performance measures within a picture fuzzy environment. Both the entry level (arrival rate) and the utility period (service time) were expressed using Single Valued Trapezoidal Picture Fuzzy Numbers (SVTPN). This representation allowed us to effectively manage and analyze the inherent uncertainties in these parameters. We demonstrated our model with a numerical example.

Our analysis revealed that using PFS in queuing models not only captures the traditional uncertainties but also provides a richer framework to represent and evaluate the degrees of membership, non-membership, and hesitation that are typical in such systems. This leads to a more comprehensive understanding of the system dynamics and performance. Looking ahead, our study opens the door to further research and development in the field of fuzzy set theory applied to queuing systems. Future work could explore the extension of this approach to more advanced fuzzy set models, such as Type-II fuzzy sets and Pythagorean fuzzy sets, which can capture even higher levels of uncertainty and complexity. These advanced models could provide deeper insights and more precise performance





### Chitra and Maheswari

metrics in queuing theory and other operational research areas. In summary, the integration of Picture Fuzzy Sets into the M/D/1 queuing model represents a significant advancement in the modeling and analysis of queuing systems. This work lays a foundation for future explorations into more sophisticated fuzzy set applications, promising to broaden the scope and impact of fuzzy logic in both theoretical and practical domains.

## REFERENCES

1. Al-Kridi, Khudr; Anan, Mohammed Taher; Zeina, Mohammed Bisher. Journal of King Abdulaziz University: Science; Jeddah Vol. 30(1), (2018): 71-75. DOI:10.4197/Sci.30-1.7
2. Atanassov, K. Intuitionistic fuzzy sets. Fuzzy Sets and Systems 1986, 20(1), 87-96.
3. Cuong, B. C. Picture fuzzy sets. *Journal of Computer Science and Cybernetics*, 2014, 30(4), 409-420.
4. Kalpana, B.; Anusheela, N. Analysis of a Single Server Non-Preemptive Fuzzy Priority Queue using LR Method. *ARNP Journal of Engineering and Applied Sciences* (2018), 13(23), 9306-9310
5. Kanufmann, A. Introduction to the theory of fuzzy subsets, 1975, Vol.I. Academic Press, New York.
6. Klir, G.J.; Yuan, B., Fuzzy Sets and Fuzzy Logic: Theory and Applications, 2009, Prentice Hall of India Private Limited.
7. Kumuthavalli, P.; Sangeetha, An introduction to the neutrosophic fuzzy in queue. *International journal of innovative research in technology*, 2017,3(11),122-126.
8. Li, R. J and Lee, E. S., Analysis of fuzzy queues. *Computers and Mathematics with Applications*, 1989, 17(7), 1143–1147.
9. Rashad, H.; Mohamed, M. Neutrosophic Theory and its Application in Various Queuing Models: Case Studies. *Neutrosophic Sets and Systems*, 2021, 45
10. Shanmugasundaram, S. and Venkatesh, B. B. Study of fuzzy multi server queuing model through DSW algorithm *International Journal of Latest Trends in Engineering and Technology*, 2015, 5(3), 452–457.
11. Shortle, J. F., Thompson, J. M., Gross, D. and Harris, C. M., *Fundamentals of queuing theory* (Wiley Series in Probability and Statistics), 2018, New York: John Wiley & Sons, Inc.
12. Shi, X., Kosari, S., & Khan, W. A. Some novel concepts of interval-valued picture fuzzy graphs with applications toward the Transmission Control Protocol and social networks. *Frontiers in Physics*, 2023, 11.
13. Smarandache, F. Introduction to neutrosophic measure, neutrosophic integral, and neutrosophic probability, 2013, <http://dx.doi.org/10.5281/zenodo.8843>.
14. Smarandache, F. Neutrosophy: neutrosophic probability, set, and logic: analytic synthesis & synthetic analysis, 2000, <http://dx.doi.org/10.5281/zenodo.57726>.
15. Srinivasan, R. Fuzzy queuing model using DSW algorithm. *International Journal of Advanced Research in Mathematics and Applications*, 2014, 1(1), 57–62.
16. Sumathi, I.R.; Antony Crispin Sweety, C. New approach on differential equation via trapezoidal neutrosophic number. *Complex & Intelligent Systems*, 2019, 5(4), 417-424.
17. Thakkar, H. K., Patel, K. N., & Patel, R. C. Sentiment analysis using picture fuzzy sets. *International Journal of Advanced Computer Science and Applications*, 2021, 12(1), 279-287.
18. Thao, N. H., Cuong, B. C., & Tuan, N. H. Medical diagnosis with picture fuzzy sets. *IEEE Access*, 2019, 7, 17360-17370.
19. Usha Prameela, K. and Pavan Kumar, FM/F Ek/1 queuing model with Erlang service under various types of fuzzy numbers. *International Journal of Recent Technology and Engineering*, 2019, 8(1), 942–946.
20. Usha Prameela, K. and Pavan Kumar, Execution proportions of multiserver queuing model with pentagonal fuzzy number: DSW algorithm approach. *International Journal of Innovative Technology and Exploring Engineering*, 2019, 8(7), 1047–1051.
21. Varadharajan, R.; Susmitha, R. Evaluation of performance measures of priority queues with fuzzy parameters using  $\alpha$  cut approach. *ARNP Journal of Engineering and Applied Sciences*, 2018, 13, 2636-2641.
22. Zadeh, L.A. Fuzzy sets, *Information and Control*, 1965, 8, 338-353





**Chitra and Maheswari**

- 23. Zeina, M. B. Erlang Service Queuing Model with Neutrosophic Parameters, International Journal of Neutrosophic Science,6(2), 106-112.
- 24. Zeina, M.B. Neutrosophic M/M/1, M/M/c, M/M/1/b Queuing Systems, Infinite Study, 2020.
- 25. Zhang,F,Wang, H.Smarandache, Y.Q.Sunderraman, Single valued neutrosophic sets. Multispace Multistructure, 2010, 4, 410–413.

**Table 1.  $\alpha, \beta, \gamma$  cuts for expected no of consumers in the queue**

$\alpha$	$l_q(\alpha)$	$u_l q(\alpha)$	$\beta$	$l_q(\beta)$	$u_l q(\beta)$	$\gamma$	$l_q(\gamma)$	$u_l q(\gamma)$
0	0.057142857	-2	0	0	0	0	0	0
0.1	0.25	-3.125	0.1	0.025	0.666666667	0.1	0.01	13.58333333
0.2	1.6	1.6	0.2	0.057142857	0.45	0.2	0.03	5.25
0.3	-3.125	0.25	0.3	0.083333333	0.380952381	0.3	0.05	2.916666667
0.4	-2	0.057142857	0.4	0.103896104	0.347222222	0.4	0.07	1.916666667
0.5	-2.45	0.008928571	0.5	0.120192308	0.327272727	0.5	0.08	1.392857143
0.6	-4.57142857	0	0.6	0.133333333	0.314102564	0.6	0.1	1.083333333
0.7	0	0.004545455	0.7	0.144117647	0.304761905	0.7	0.11	0.884920635
0.8	4.545454545	0.013986014	0.8	0.153110048	0.297794118	0.8	0.12	0.75
0.9	2.326923077	0.025	0.9	0.160714286	0.292397661	0.9	0.13	0.654040404
1	1.6	0.036199095	1	0.16722408	0.288095238	1	0.13	0.583333333

**Table .2.  $\alpha, \beta, \gamma$  cuts for expected no of consumers in the system**

$\alpha$	$l_q(\alpha)$	$u_l q(\alpha)$	$\beta$	$l_q(\beta)$	$u_l q(\beta)$	$\gamma$	$l_q(\gamma)$	$u_l q(\gamma)$
0	0.34285714	2	0	0	0	0	0	0
0.1	0.75	1.5	0.1	-0.225	-0.73333333	0.1	-0.1547619	8.58333333
0.2	2.4	0.24	0.2	-0.34285714	-0.73	0.2	-0.2539682	2.25
0.3	-1.875	0.25	0.3	-0.41666667	-0.7523809	0.3	-0.3238636	0.58333333
0.4	5.1399E-16	0.12244898	0.4	-0.46753246	-0.7694444	0.4	-0.3760683	-0.08333333
0.5	1.05	0.01339285	0.5	-0.50480769	-0.7818181	0.5	-0.4166666	-0.40714285
0.6	3.42857142	-0.07407407	0.6	-0.53333333	-0.7910256	0.6	-0.4491978	-0.58333333
0.7	0	-0.14454545	0.7	-0.55588235	-0.7980952	0.7	-0.4758771	-0.68650793
0.8	-5.45454545	-0.20216147	0.8	-0.57416267	-0.8036764	0.8	-0.4981685	-0.75
0.9	-3.17307692	-0.25	0.9	-0.58928571	-0.8081871	0.9	-0.5170807	-0.79040404
1	-2.4	-0.29028889	1	-0.60200668	-0.8119047	1	-0.5333333	-0.81666666

**Table.3.  $\alpha, \beta, \gamma$  cuts for expected no of consumers waiting in queue**

$\alpha$	$l_q(\alpha)$	$u_l q(\alpha)$	$\beta$	$l_q(\beta)$	$u_l q(\beta)$	$\gamma$	$l_q(\gamma)$	$u_l q(\gamma)$
0	0.28571428	-3.33333333	0	0	0.2	0	0	0
0.1	0.83333333	-6.25	0.1	-0.25	0.238095238	0.1	-0.1	4.17
0.2	4	4	0.2	-0.2857142	0.238095238	0.2	-0.2	1.88
0.3	-6.25	0.83333333	0.3	-0.2777777	0.227272727	0.3	-0.2	1.17
0.4	-3.33333333	0.285714286	0.4	-0.2597402	0.213675214	0.4	-0.2	0.83
0.5	-3.5	0.089285714	0.5	-0.2403846	0.2	0.5	-0.2	0.64
0.6	-5.71428571	0	0.6	-0.2222222	0.187165775	0.6	-0.2	0.52
0.7	0	-0.04545454	0.7	-0.2058823	0.175438596	0.7	-0.2	0.44
0.8	4.545454545	-0.06993007	0.8	-0.1913875	0.164835165	0.8	-0.1	0.38
0.9	2.115384615	-0.08333333	0.9	-0.1785714	0.155279503	0.9	-0.1	0.33
1	1.33333333	-0.09049773	1	-0.1672240	0.146666667	1	-0.1	0.29

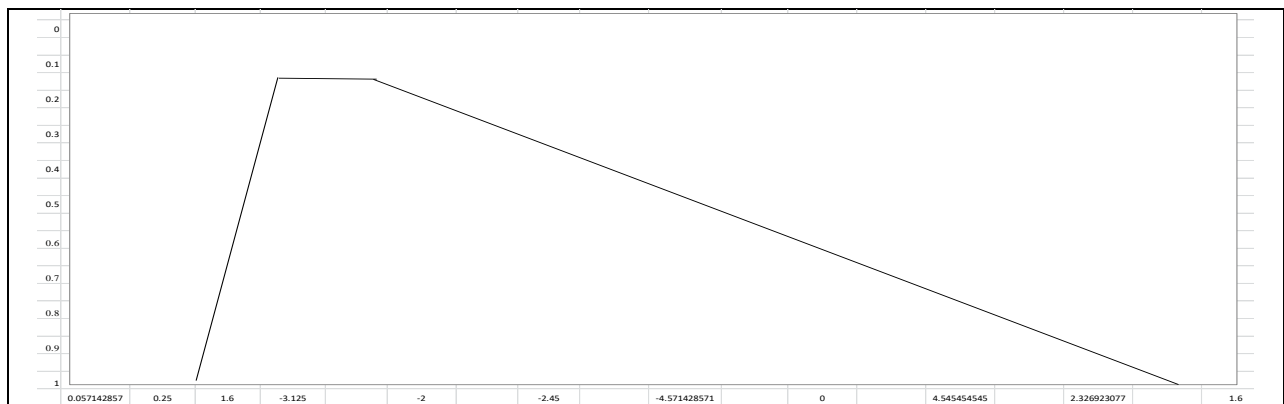




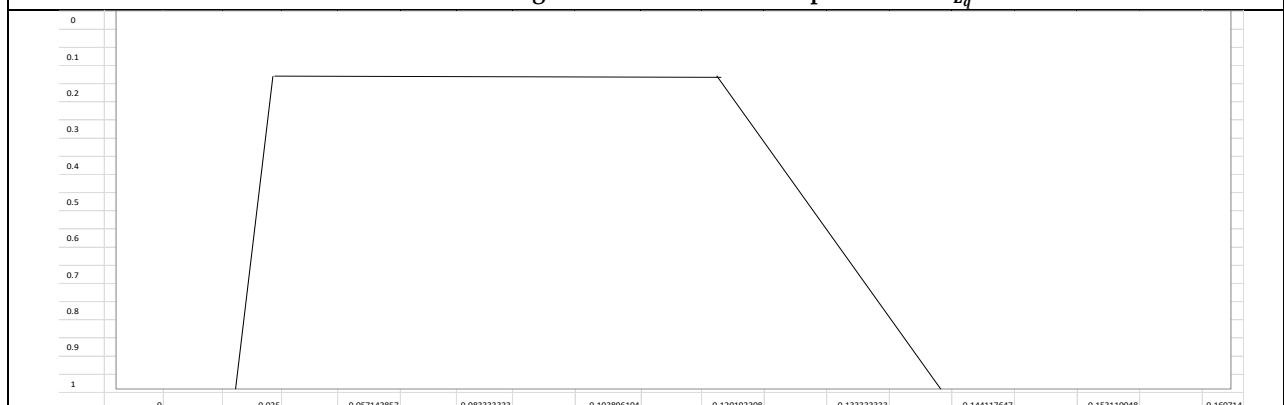
**Chitra and Maheswari**

**Table.4  $\alpha, \beta, \gamma$  cuts system's average client hold time**

$\alpha$	$l_{Lq}(\alpha)$	$u_{Lq}(\alpha)$	$\beta$	$l_{Lq}(\beta)$	$u_{Lq}(\beta)$	$\gamma$	$l_{Lq}(\gamma)$	$w_{Lq}(\gamma)$
0	1.714285714	0	0	3.333333333	0	0	2	0
0.1	2.5	-3.75	0.1	2.25	-6.66666666	0.1	1.547619048	-5.833333
0.2	6	6	0.2	1.714285714	-3.5	0.2	1.26984127	-3.125
0.3	-3.75	2.5	0.3	1.388888889	-2.3809523	0.3	1.079545455	-2.166666
0.4	0	1.714285714	0.4	1.168831169	-1.8055555	0.4	0.94017094	-1.666666
0.5	1.5	1.339285714	0.5	1.009615385	-1.4545454	0.5	0.833333333	-1.357142
0.6	4.285714286	1.111111111	0.6	0.888888888	-1.2179487	0.6	0.748663102	-1.145833
0.7	0	0.954545455	0.7	0.794117647	-1.0476190	0.7	0.679824561	-0.992063
0.8	-5.45454545	0.839160839	0.8	0.717703349	-0.9191176	0.8	0.622710623	-0.875
0.9	-2.88461538	0.75	0.9	0.654761905	-0.8187134	0.9	0.574534161	-0.782828
1	-2	0.678733032	1	0.602006689	-0.7380952	1	0.533333333	-0.708333



**Figure .1 Truth me mbership value for  $\tilde{N}_{Lq}$**



**Figure .2Neutral membership value for  $\tilde{N}_{Lq}$**





**Chitra and Maheswari**

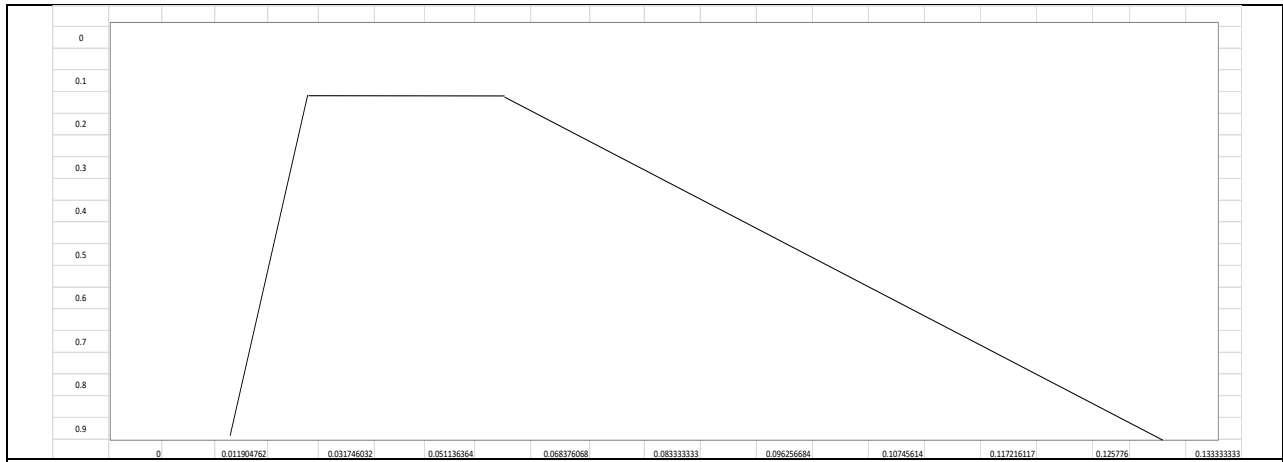


Figure .3 Falsity membership value for  $\bar{N}_{Lq}$

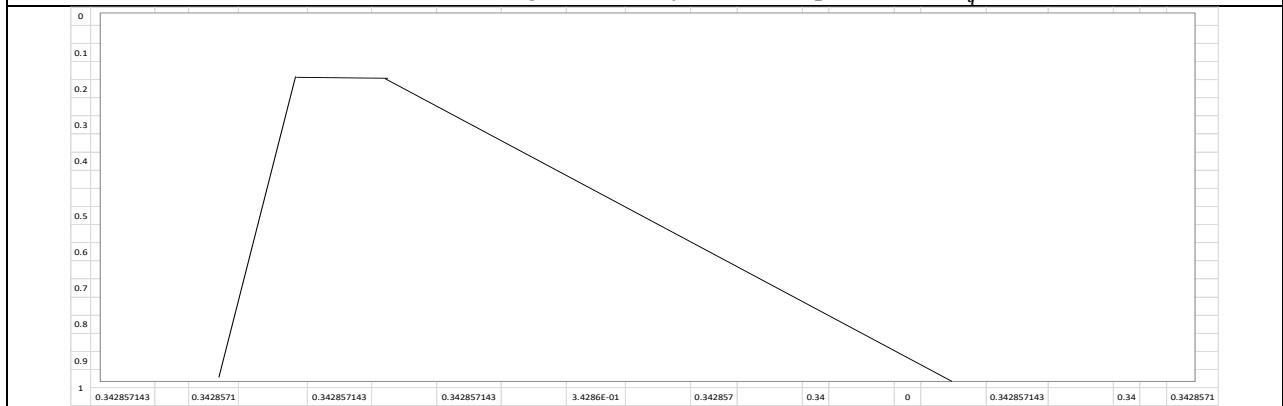


Figure .4 Truth membership value for  $\bar{N}_{Ls}$

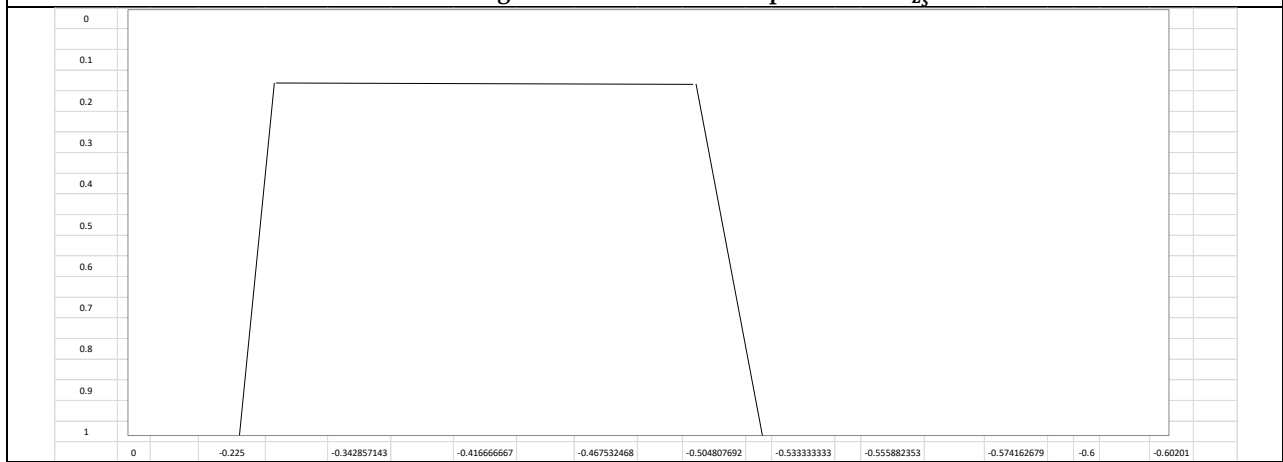
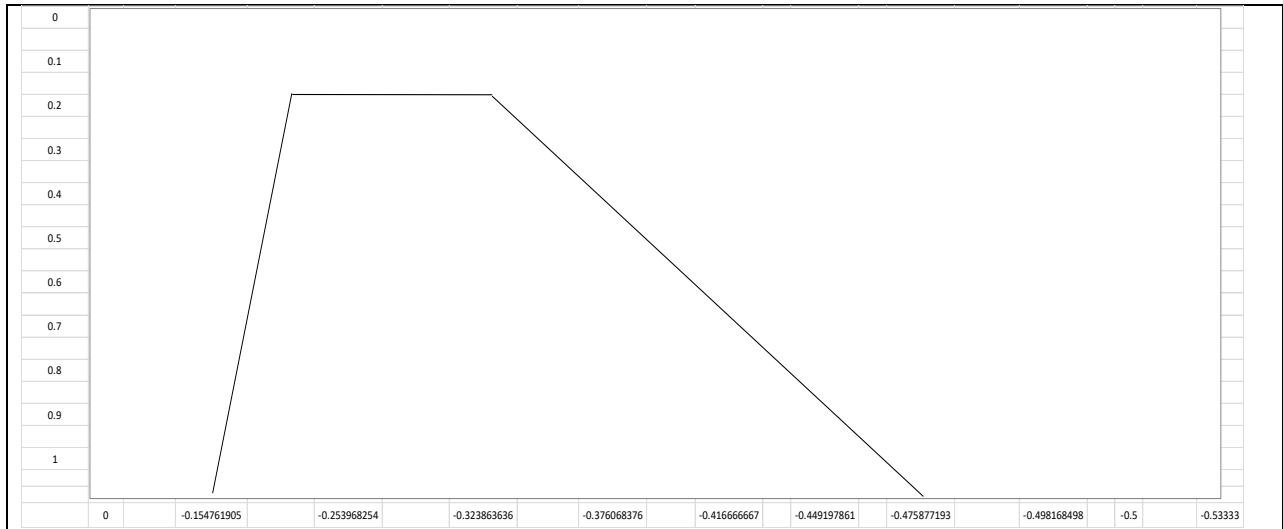


Figure .5 Neutral membership value for  $\bar{N}_{Ls}$

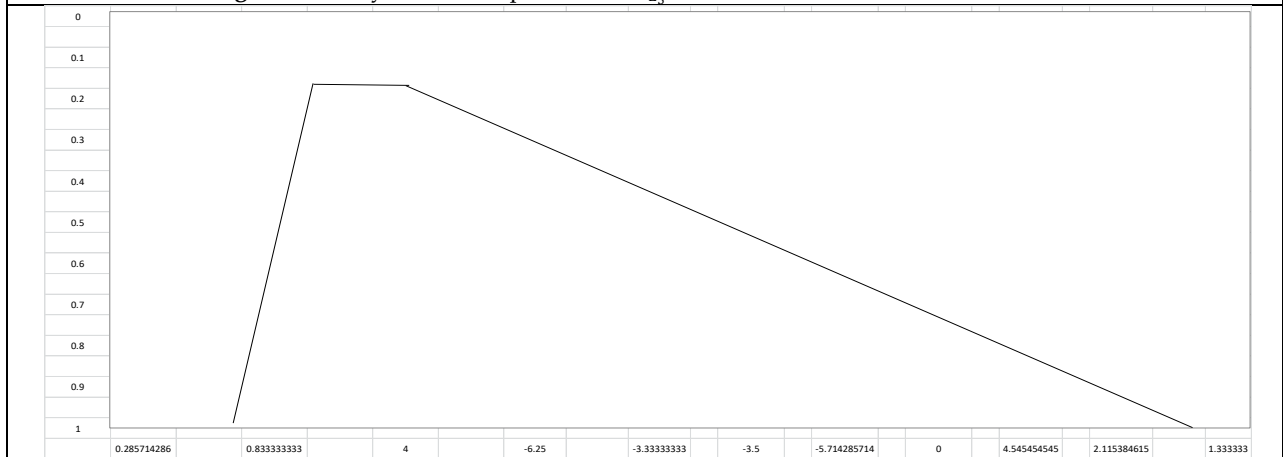




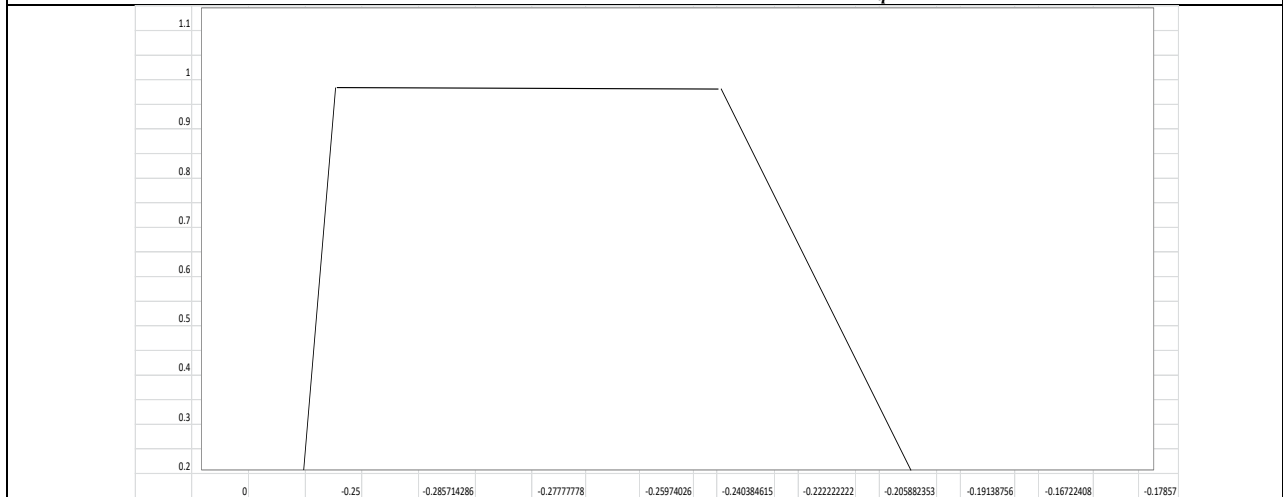
**Chitra and Maheswari**



**Figure .6 Falsity membership value for  $\bar{N}_{L_s}$**



**Figure .7 Truth membership value for  $\bar{N}_{W_q}$**



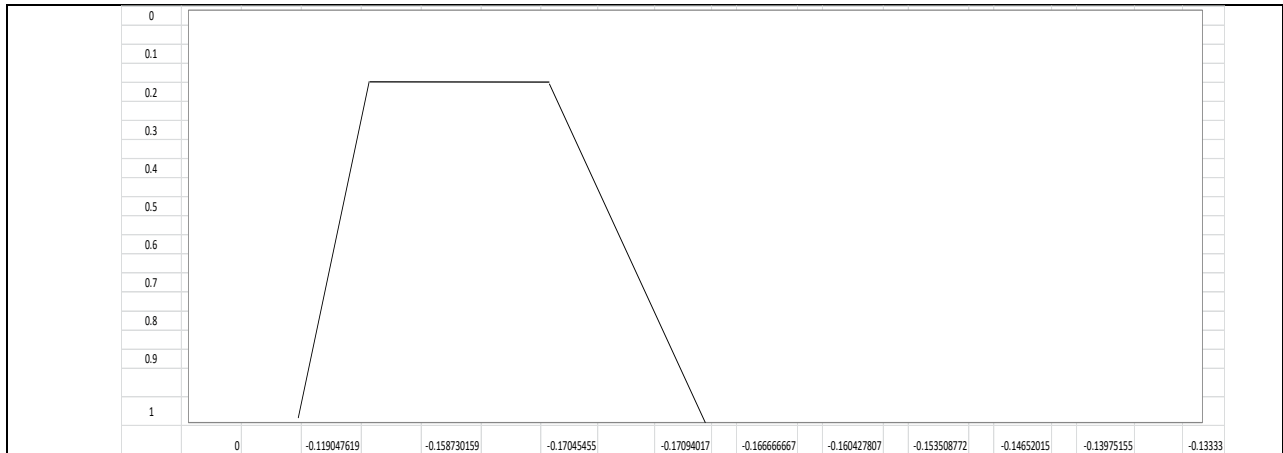
**Figure .8 Neutral membership value for  $\bar{N}_{W_q}$**



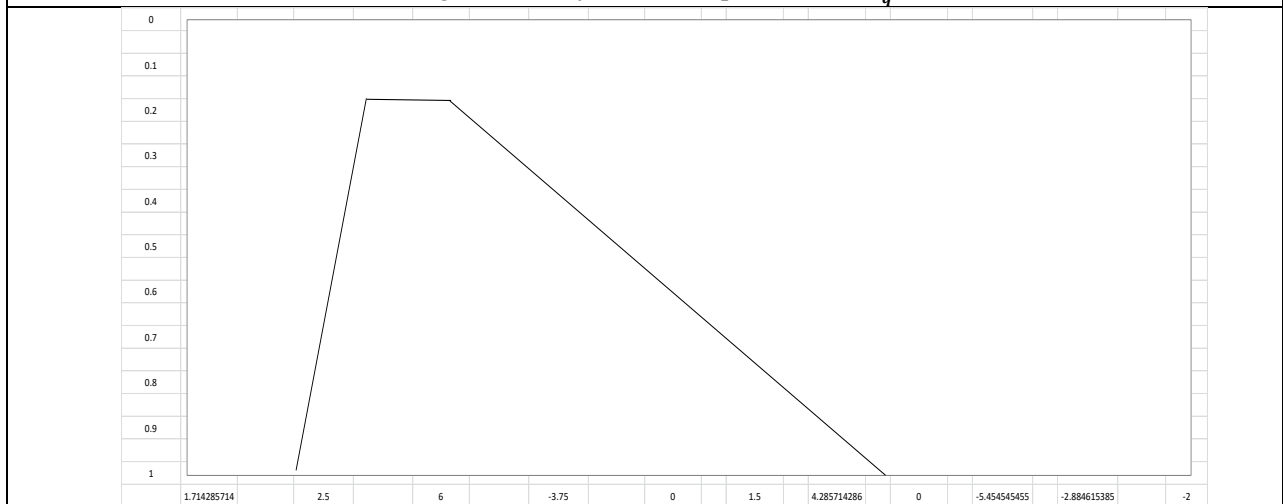




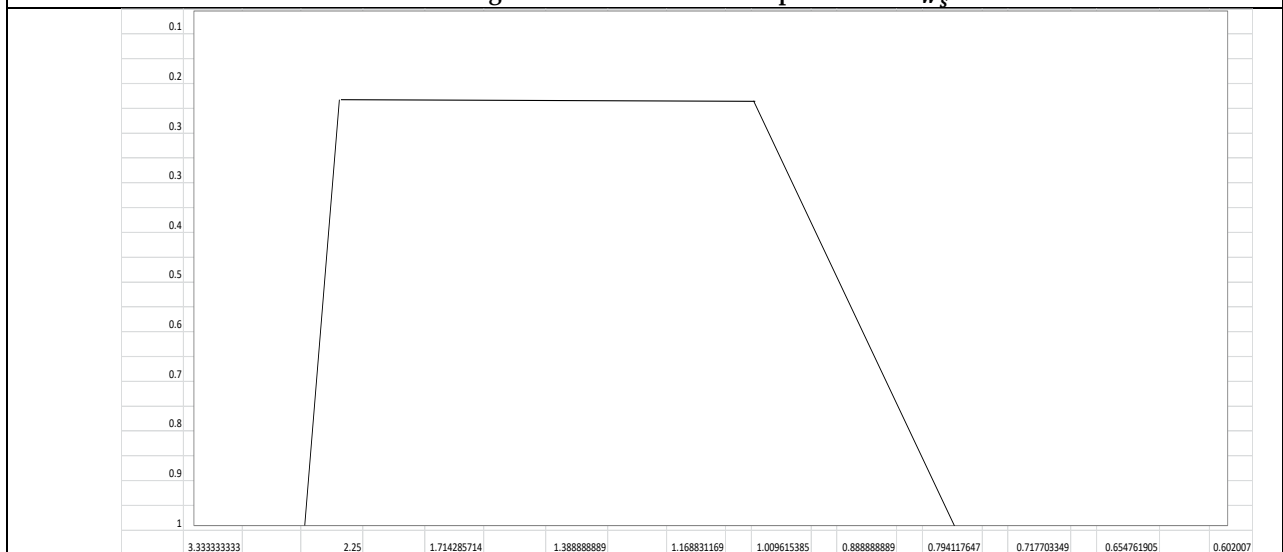
**Chitra and Maheswari**



**Figure .9 Falsity membership value for  $\bar{N}_{W_q}$**



**Figure .10 Truth membership value for  $\bar{N}_{W_s}$**

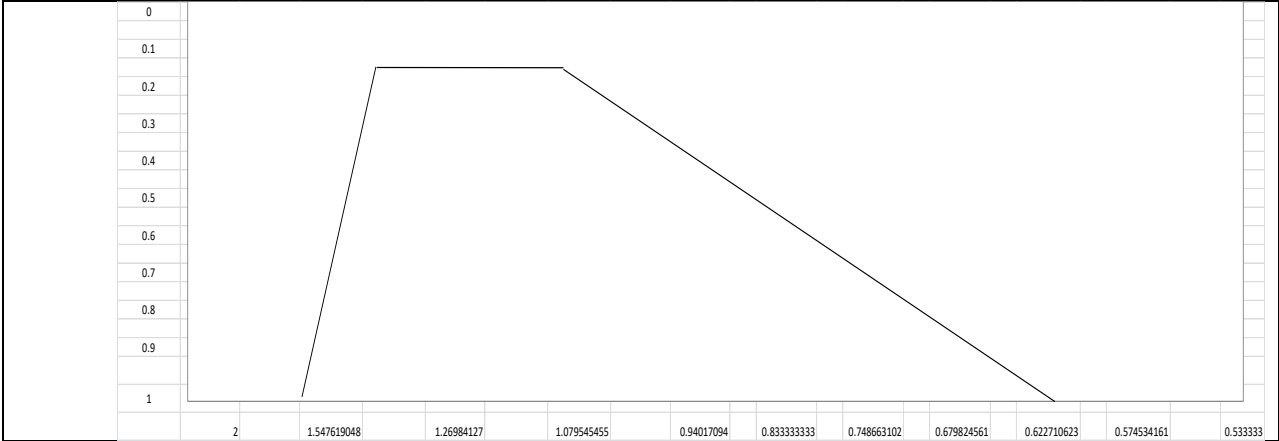


**Figure .11 Neutral membership value for  $\bar{N}_{W_s}$**





**Chitra and Maheswari**



**Figure.12 Falsity membership value for  $\bar{N}_{W_s}$**





## Preparation and Evaluation of Polyherbal Tea Bags with Anti-Oxidant Activity for Management of Oxidative Stress

Ch.Nooka Raju<sup>1</sup>, S Bala Chandrika<sup>2</sup>, J Ramya<sup>2</sup> and Ponnam Chiranjeevi<sup>3\*</sup>

<sup>1</sup>Department of Radiology, Centurion University of Technology and Management, Vizianagaram, Andhra Pradesh, India.

<sup>2</sup> Students, Department of Pharmaceutical Chemistry, Vignan Institute of Pharmaceutical Technology, (Affiliated to Jawaharlal Nehru Technological University), Visakhapatnam, Andhra Pradesh, India.

<sup>3</sup>Professor, Department of Pharmaceutical Chemistry, Vignan Institute of Pharmaceutical Technology, (Affiliated to Jawaharlal Nehru Technological University), Visakhapatnam, Andhra Pradesh, India.

Received: 06 Oct 2024

Revised: 10 Nov 2024

Accepted: 12 Dec 2024

### \*Address for Correspondence

**Ponnam Chiranjeevi**

<sup>3</sup>Professor, Department of Pharmaceutical Chemistry,  
Vignan Institute of Pharmaceutical Technology,  
(Affiliated to Jawaharlal Nehru Technological University),  
Visakhapatnam, Andhra Pradesh, India.

E.Mail: ponnam107@gmail.com



This is an Open Access Journal / article distributed under the terms of the **Creative Commons Attribution License** (CC BY-NC-ND 3.0) which permits unrestricted use, distribution, and reproduction in any medium, provided the original work is properly cited. All rights reserved.

### ABSTRACT

Tea in general and herbal tea in particular, are gaining increasing consumer attention due to a growing awareness of health benefits derived from their consumption. Even though several underutilized plants exist with potential for processing into herb tea, research in product development of herb teas is limited. This research was conducted to formulate herbal tea which is efficacious to scavenge the free radicals. The objectives of the study are to select plants possessing antioxidant and antidiabetic properties, evaluate and compare the individual plants for their antioxidant properties with marketed formulation of green tea and to develop a polyherbal formulation with composition of herbs that has potential antioxidant activity. Free radical scavenging ability of the extracts was tested by DPPH radical scavenging assay as described by Blois[1] and Desmarchelier et al.[2] in comparison to green tea. *Aegle marmelos*, *Momordica charantia*, *Azadirachta indica*, *Cissus quadrangularis*, *Trigonella foenum graecum* were tested for antioxidant activity. *Aegle marmelos*, *Momordica charantia*, *Azadirachta indica* have shown significant Antioxidant activities. Two polyherbal tea formulations were done with compositions *Aegle marmelos* : *Azadirachta indica* : *Momordica charantia* in ratio 3:2:1(PHF1) and *Aegle marmelos* : *Momordica charantia* : *Azadirachta indica* in ratio 3:2:1(PHF2) respectively. Polyherbal formulations in fixed ratio i.e 3:2:1 of *Aegle marmelos*, *Momordica charantia*, and *Azadirachta indica* respectively showed 78% more inhibition of DPPH free radical at 20ug /ml in comparison to marketed green tea formulation. A poly herbal tea bag was prepared on weighing accurately 0.956gms *Aegle marmelos*, 0.636gms *Momordica*



**Nooka Raju et al.,**

*charantia* and 0.311gms *Azadirachta indica* herb powders and mixed properly and packed in a sachet. This can be used as a herbal tea for a cup containing a volume of 240ml water.

**Keywords:** DPPH, water, powders, formulations, product.

## INTRODUCTION

Tea, especially herbal tea, is attracting more consumer interest as awareness of its health benefits continues to rise. Despite the presence of numerous underutilized plants that could be processed into herbal tea, there is a scarcity of research focused on the development of such products. This study was undertaken to create an herbal tea that effectively scavenges free radicals. Oxidative stress plays a significant role in the development of numerous common health issues, affecting individuals of all age groups. Among the various diseases and conditions associated with oxidative stress are: cardiovascular diseases[3], cancer, neurodegenerative disorders[4], diabetes, liver diseases[5], and inflammatory conditions[6]. Given the extensive influence of oxidative stress, it is essential to comprehend its underlying mechanisms, contributing factors, and strategies for mitigating its detrimental effects in order to prevent and manage a variety of chronic illnesses. The health complications of oxidative stress are illustrated in Figure1. Oxidative stress is a key factor in the onset of insulin resistance, dysfunction of  $\beta$ -cells, and the advancement of complications associated with diabetes. The persistent presence of reactive oxygen species (ROS) in diabetic patients exacerbates blood glucose regulation and is linked to severe complications such as cardiovascular disease, neuropathy, and retinopathy. Mitigating oxidative stress through antioxidant treatments, dietary changes, and lifestyle adjustments presents considerable promise for the prevention and management of diabetes and its associated complications [8-13].

The increasing incidence of diabetes and related health conditions has sparked a heightened interest in herbal teas due to their potential preventive and therapeutic properties. Herbal teas are primarily composed of the leaves, buds, flowers, and fruits of medicinal plants, and they are recognized for their diverse biological activities, which include antioxidant, anti-inflammatory, antibacterial, anti-diabetic, and anti-cancer effects. Unlike traditional teas, which are derived from the *Camellia sinensis* plant, herbal teas consist of a variety of dried herbs, seeds, flowers, fruits, barks, and other plant components. Furthermore, tisanes are naturally free of caffeine and are often enjoyed for their appealing flavor and health benefits. Each herbal blend is typically designed to fulfill a specific function, such as promoting relaxation or mitigating the adverse effects of oxidative stress, which is crucial for the prevention and management of numerous chronic diseases. [14]. Herbal remedies have been increasingly studied for their ability to mitigate oxidative stress through their antioxidant, anti-inflammatory, and cellular-protective properties. Numerous plants contain compounds that can help neutralize reactive oxygen species (ROS), protect cellular structures, and support the body's natural detoxification and repair mechanisms. Below is a review of several commonly used herbs, supported by scientific evidence, and their role in managing oxidative stress.

Herbal teas represent a flexible and readily available means to promote health and well-being. Although scientific research validating their effectiveness is still evolving, it has been established that numerous herbs traditionally utilized in infusions possess significant medicinal qualities. Both tea in general and herbal tea specifically are attracting heightened consumer interest, driven by an increasing recognition of the health advantages associated with their consumption. Despite the existence of several underutilized plants that could be processed into herbal teas, research focused on the development of these products remains limited.

### Role of anti-oxidants

Antioxidants can decrease the oxidative damage directly via reacting with free radicals or indirectly by inhibiting the activity or expression of free radical generating enzymes or enhancing the activity or expression of intracellular antioxidant enzymes. Antioxidants may decrease the cellular level of free radicals either by inhibiting the activities or



**Nooka Raju et al.,**

expressions of free radical generating enzymes such as NAD(P)H oxidase and xanthine oxidase (XO) or by enhancing the activities and expressions of antioxidant enzymes such as superoxide dismutase (SOD), catalase (CAT) and glutathione peroxidase (GPX). The mechanism of action for antioxidation is represented in Figure 2.

## HERBS IN PRESENT STUDY

### *Aegle marmelos*

*Aegle marmelos* Commonly known as bael, is a tropical tree native to the Indian subcontinent. It belongs to the Rutaceae family and is widely recognized for its medicinal properties. The plant is traditionally used in Ayurvedic and folk medicine for a variety of health conditions. Reported to have anti diarrhoea, peptic ulcers healing, diuretic, analgesic, antioxidant, and antidiabetic activities, with chief chemical constituents Coumarin, Xanthotoxol, Imperatorin, Aegeline, Marmeline. [15-18].

### *Azadirachta indica*

*Azadirachta indica*, commonly known as neem, is a tropical evergreen tree native to the Indian subcontinent and widely distributed throughout Asia and Africa. Neem is a member of the Meliaceae family and is renowned for its numerous medicinal properties. Often referred to as the "village pharmacy" in India, neem has been used for thousands of years in traditional medicine. Reported to have Antioxidant Activity, anticancer, anti inflammatory, wound healing effect, antidiabetic, antifungal, antimalarial, antibacterial and antiviral activities, with chief chemical constituents quercetin, nimbosterol, nimbin, kaempferol, nimbidin, Azadirachtin, Azadiradione, vepinin [19-23]

### *Cissus quadrangularis*

*Cissus quadrangularis*, commonly known as Veldt Grape or Devil's Backbone, is a perennial plant belonging to the Vitaceae family. Native to tropical and subtropical regions of Africa and Asia, particularly India, this plant has been widely used in traditional medicine, especially in Ayurvedic and African healing practices. Reported to be beneficial in treatment of Diabetes, obesity, high cholesterol, bone fractures, allergies, cancer, stomach upset, painful menstrual periods, asthma, malaria, wound healing, peptic ulcer disease, weak bones, weak bones (osteoporosis) , with chief chemical constituents quercetin, Daidzein, genistein, friedelin, Vitamin 'C, quadrangularin-A, Resveratrol and piceatannol, 6-o-meta-methoxy-benzoyl catapol, Picoside and pallidol and Phytosterols. [24-27]

### *Momordica charantia*

*Momordica charantia*, commonly known as bitter melon or bitter gourd, is a tropical and subtropical vine belonging to the Cucurbitaceae family. Native to Africa, Asia, and the Caribbean, this plant is widely consumed for its edible fruit, which is known for its sharp, bitter taste. Bitter melon has been used for centuries in traditional medicine systems, such as Ayurveda, Traditional Chinese Medicine (TCM), and African medicine, due to its numerous health benefits. Reported to have antidiabetic, anticancer, antioxidants, anti-inflammation, antiviral activities, and cholesterol lowering effects, with chief chemical constituents Triterpenoids, Saponins, Polypeptides, Flavonoids, Alkaloids, sterols [28-30]

### *Trigonella foenum graecum*

*Trigonella foenum-graecum*, commonly known as fenugreek, is an annual herb in the Fabaceae (legume) family. Native to the Mediterranean region, the Middle East, and Asia, fenugreek is widely used as both a culinary spice and in traditional medicine for its numerous health benefits. Fenugreek seeds, in particular, have been the subject of significant interest due to their medicinal properties, which include anti-inflammatory, antioxidant, and antidiabetic effects. Reported to have carminative, gastric stimulant, antidiabetic, galactagogue (lactation-inducer) effects, hypocholesterolemic, antilipidemic, antioxidant, hepatoprotective, anti-inflammatory, antibacterial, antifungal, antiulcer, antilithogenic activities, with chief chemical constituents Diosgenin, Trigogenin, Yamogenin, Gitogenin, Trigocoumarin, Trigoforin, Trigonelline [31-33]





Nooka Raju et al.,

### *Camellia sinensis*

*Camellia sinensis* is the botanical name for the tea plant, the source of all traditional teas, including green tea, black tea, white tea, oolong tea, and pu-erh tea. Native to East Asia, particularly China and India, it has been cultivated for thousands of years for its leaves, which are processed in different ways to produce various types of tea. The plant is also valued for its rich chemical composition, particularly its high content of catechins and caffeine, which contribute to its numerous health benefits. Used to Treat metabolic syndrome, such as obesity, type II diabetes, and cardiovascular risk factors, with chief chemical constituents Catechins, Gallocatechins, Caffeine, Theophylline, Theobromine, Gallic acid [34-36].

### ANTIOXIDANT ACTIVITY

Antioxidant activity can be defined as a limitation or inhibition of nutrient oxidation (especially lipids and proteins) by restraining oxidative chain reactions. Oxidation is essential for many living organisms for the production of energy to fuel biological processes however, the uncontrolled production of oxygen derived free radicals is involved in triggering many diseases such as cancer, rheumatoid arthritis, cirrhosis and atherosclerosis as well as in degenerative processes associated with ageing. The aim of this work is to conduct evaluation of antioxidant properties of selected polyherbal formulation extracts.

#### Principle

##### DPPH Radical Reducing Activity:

DPPH is a cell membrane stable free radical that acts as a hydrogen radical scavenger. The DPPH radicals are widely used to investigate the scavenging activity of natural compounds. In DPPH assay it involves reduction of alcoholic DPPH by using a free radical of DPPH (1,1-Diphenyl-1-picrylhydrazyl). The odd electron in the DPPH free radical gives a strong absorption at 517 nm and is purple in colour. The colour turns from purple to yellow when an odd electron of DPPH radical becomes paired with hydrogen from a free radical scavenging antioxidant to form the reduced (Diphenyl-picrylhydrazine) DPPH-H. The resulting decolourisation is stoichiometric with respect to the number of electrons captured Figure 3.

##### Preparation of hot infusion:

*Aegle marmelos*, *Azardirecta indica*, *Momordica charantia*, *Cissus quardangularis*, *Trigonella foenum graecum* plant fresh leaves are collected, washed properly, shade dried and are pulverised. These powdered leaves are taken and weighed 0.1g each and added to 100ml of the hot boiling water separately and infused for 1 minutes. In the same way the marketed *Camellia sinensis* is infused for comparison of the marketed antioxidant activity with these selected *Aegle marmelos*, *Azardirecta indica*, *Momordica charantia*, *Cissus quardangularis*, *Trigonella foenum graecum* plants. Plan of work is showed in figure 4.

##### Preparation of 0.004% of methanolic DPPH Solution:

6 mg of 1,1-Diphenyl-1-picrylhydrazyl is accurately weighted and dissolved in 150 ml of methanol to make methanolic DPPH solution.

##### Preparation of dilutions

The hot infusions are filtered with Whatman filter paper and from the filtrate 10 ml is taken and the volume is made up to 100 ml with distilled water which makes it 100µg/ml. From these hot infusions various concentrations like 20, 40, 60, 80 and 100 µg/ml are taken i.e. by taking in various concentrations as in Table 1.

Now 1 ml of each plant extract is taken and 3 ml of Methanolic DPPH solution is added to the test tube and covered with aluminium foil and kept in a dark place (as DPPH is light sensitive) to react for **1 hour**.







Nooka Raju et al.,

## RESULTS

The reacted plant extract with Methanolic DPPH solution is checked for the absorbance at 517nm in UV-visible spectrophotometer of make Elico double beam SL.210 using ethanol as blank and ethanolic DPPH solution as control

### Calculation of Percentage inhibition:

The percentage inhibition of DPPH radical production by the extract was calculated using the formula:

$$\text{Inhibitory Ration} = \frac{(A_0 - A_1) \times 100}{A_0}$$

Where,  $A_0$  is the absorbance of control;

$A_1$  is the absorbance with addition of plant extract

The absorbance, transmission and percentage inhibition of DPPH radical for various plant extracts is tabulated in Tables 2-7. The absorbance were measured at 517nm using ethanol as blank and ethanolic DPPH solution as control. The comparison of anti-oxidant activities were done in Figure 5.

- Ethanol:- 0.0882 absorbance
- Ethanoic DPPH solution: 1.4227 absorbance

### Preparing polyherbal mixture in ratios based on % inhibition values:

Based on the % inhibition values of individual plants in comparison to green tea, 3 plant samples were selected they are

1. *Aegle marmelos*
2. *Azadirachta indica*
3. *Momordica charantia*

They were weighed in two different ratios which are

1. *Aegle marmelos*:*Azadirachta indica*:*Momordica charantia* (3:2:1) as 300mg ,200mg and 100mg respectively they are mixed well and 100mg of the mixture is weighed and infused with 100ml boiled water for 10minutes.
2. *Aegle marmelos*: *Momordica charantia*: *Azadirachta indica* (3:2:1) as 300mg ,200mg and 100mg respectively are mixed well and 100mg of mixture is weighed and infused with 100ml boiled water for 10minutes.

Later both the combinations are filtered and from the filtrate and 10 ml of filtrate is diluted to 100ml with distilled water to make it 100µg/ml. From the above Concentration 10ml, 8ml, 6ml, 4ml, 2ml are taken and diluted to 10ml with distilled water making the 100µg , 80µg ,60µg , 40µg , 20µg per ml concentrations. These were measured for absorbance at 517 nm in UV-Visible spectrophotometer. Green tea hot infusion is also prepared for 1mg/ml concentration and series dilutions of 100µg, 80µg, 60µg, 40µg, 20µg per ml concentrations and absorbance is measured at 517 nm in UV visible spectrophotometer taking Ethanol as blank and Ethanolic DPPH as control.

### Sachets preparation

0.956gms *Aegle marmelos*, 0.636gms *Momordica charantia* and 0.311gms *Azadirachta indica* powders are weighed accurately and mixed properly and packed in a sachet. This can be used as a herbal tea for a cup containing a volume of 200ml

### Comparison of green tea with Polyherbal Formulations

The prepared poly herbal formulations were compared with commercial Green tea sachet, hot infusions were prepared and made to react with Ethanolic DPPH solution is checked for the absorbance at 517nm in UV-visible spectrophotometer of make Elico double beam SL.210 using ethanol as blank and ethanolic DPPH solution as control





Nooka Raju et al.,

The absorbance, transmission and percentage inhibition of DPPH radical for poly herbal formulation 1(PHF1) and poly herbal formulation 2(PHF2) in comparison with marketed green tea formulation is tabulated in **Tables 8-10**. The absorbance were measured at 517nm using ethanol as blank and ethanolic DPPH solution as control. The comparison of anti-oxidant activities for PHF1, PHF2 and green tea were done in **Figure 6**.

- Ethanol 0.0001 absorbance and 99.98 transmittance
- Ethanolic DPPH solution 0.4884 absorbance and 32.48 Transmittance

## SUMMARY AND CONCLUSION

All the five plants *Aegle marmelos*, *Momordica charantia*, *Azadirachta indica*, *Cissus quadrangularis*, *Trigonella foenum graecum* have shown Antioxidant properties in comparison to marketed formulation Green tea. The concentrations at which individually plants showed highest activity at 100ug/ml concentration *Aegle marmelos* showed 53.18%, *Azadirachta indica* showed 60.63%, at 80ug/ml concentration *Momordica charantia* showed 40.78%, at 60 ug /ml concentration *cissus quadrangularis* showed 38.28 %, 20ug/ml *Trigonella foenum graecum* showed 35.23% and at 100ug/ml green tea showed 55.37%. Wherein polyherbal formulations in fixed ratio i.e 3:2:1 of *Aegle marmelos*, *Momordica charantia*, and *Azadirachta indica* respectively showed 78% more inhibition of DPPH free radical at 20ug /ml in comparison to marketed green tea formulation.

### Future Scope

The future scope of the project is development of a polyherbal antidiabetic formulation based on the results obtained in the In-vitro antioxidant tests performed on the plants *Aegle marmelos*, *Azadirachta indica*, *Cissus quadrangularis*, *Momordica charantia*, *Trigonella foenum graecum* in comparison to marketed *Camelia sinensis* individually and in combination of *Aegle marmelos*, *Azadirachta indica* and *Momordica charantia* performed for the plants selected as these plants show the antioxidant properties are said to have the antidiabetic property as per the literature so this formulation can further be screened for the antidiabetic property.

## REFERENCES

1. Blois MS. Antioxidant determinations by the use of a stable free radical. *Nature*. 1958;181:1199–1200. doi: 10.1038/1811199a0.
2. Desmarchelier C, Bermudez MJN, Coussio J, Ciccio G, Boveris A. Antioxidant and prooxidant activities in aqueous extract of Argentine plants. *Int J Pharmacogn*. 1997;35:116–120. doi: 10.1076/phbi.35.2.116.13282.
3. Basu, A., Rhone, M., & Rhone, A. (2014). "Green tea catechins and cardiovascular risk factors: An overview of the clinical evidence." *The Journal of Nutrition*, 144(5), 1156-1164. doi: 10.3945/jn.114.191515
4. Vellas, B., et al. (2013). "Ginkgo biloba extract in the treatment of Alzheimer's disease." *Current Neuropharmacology*, 11(1), 11-17. doi: 10.2174/1570159X11311010005
5. Baptista, L. C., (2016). "Silymarin reduces oxidative stress and improves liver function in patients with chronic liver disease." *Free Radical Biology and Medicine*, 101, 229-236. doi: 10.1016/j.freeradbiomed.2016.02.035
6. Ghosh, D., (2014). "Curcumin and rheumatoid arthritis: Biological mechanisms and future perspectives." *Free Radical Biology and Medicine*, 69, 385-395. doi: 10.1016/j.freeradbiomed.2014.02.013
7. Pham-Huy LA, He H, Pham-Huy C., et al. "Free radicals, antioxidants in disease and health". *Int J Biomed Sci*. 2008 Jun;4(2):89-96. PMID: 23675073;
8. Ceriello, A., (2008). "Oxidative stress and diabetic complications." *Current Opinion in Clinical Nutrition & Metabolic Care*, 11(3), 255-259. DOI: 10.1097/MCO.0b013e3282f57b0a
9. Fujita, T., (2010). "Oxidative stress and diabetic nephropathy." *Current Diabetes Reviews*, 6(4), 304-314. DOI: 10.2174/157339910793602888
10. Hotamisligil, G. S., (1999). "Oxidative stress and inflammation in diabetes." *Current Opinion in Immunology*, 11(1), 278-283. DOI: 10.1016/S0952-7915(99)80042-8



**Nooka Raju et al.,**

11. Masiello, P., (2006). "Insulin resistance and oxidative stress in diabetes: role of mitochondrial dysfunction." *Diabetes & Metabolism*, 32(3), 188-196. DOI: 10.1016/j.diabet.2006.03.004
12. Ramasamy, R., (2012). "The role of oxidative stress in diabetic complications." *Free Radical Biology and Medicine*, 53(3), 557-570. DOI: 10.1016/j.freeradbiomed.2012.06.034
13. Knight JA., (1995) Diseases related to oxygen-derived free radicals. *Ann Clin Lab Sci*. Mar-Apr;25(2):111-21. PMID: 7785961.
14. O. Lasekan, A. Lasekan, (2012) "Flavour chemistry of mate and some common herbal teas" *Trends in Food Science & Technology*, 27(1), 37-46. <https://doi.org/10.1016/j.tifs.2012.05.004>.
15. Mazumder R, Bhattacharya S, Mazumder A, Pattnaik AK, Tiwary PM, Chaudhary S. Antidiarrhoeal evaluation of *Aegle marmelos* (Correa) Linn. root extract. *Phytother Res* 2006; 20(1):82-84
16. Madhu C, Hindu K, Sudeepthi C, Maneela P, Reddy KV, Sree BB. Anti ulcer activity of aqueous extract of *Aegle marmelos* leaves on rats.
17. Singh S, Singh SK, Srivastava S, Singh P, Trivedi M, Shanker P, et al. Experimental evaluation of diuretic activity of *Aegle marmelos* in rats. *Int J Pharm Biol Sci* 2013; 3(1):98-102.
18. Sharmila S, Devi PAV. A review on: *Aegle marmelos*. *Journal of Pharmacy Research*. 2011; 4:720-2.
19. Nunes P. X., Silva S. F., Guedes R. J., Almeida S. Phytochemicals as Nutraceuticals—Global Approaches to Their Role in Nutrition and Health. InTech; 2012. Biological oxidations and antioxidant activity of natural products.
20. Rahmani A. H., Alzohairy M. A., Khan M. A., Aly S. M. Therapeutic implications of black seed and its constituent thymoquinone in the prevention of cancer through inactivation and activation of molecular pathways. *Evidence-Based Complementary and Alternative Medicine*. 2014;2014:13.
21. Chattopadhyay R. R. Possible biochemical mode of anti-inflammatory action of *Azadirachta indica* A. Juss. in rats. *Indian Journal of Experimental Biology*.
22. Baligar N. S., Aladakatti R. H., Ahmed M., Hiremath M. B. Hepatoprotective activity of the neem-based constituent azadirachtin-A in carbon tetrachloride intoxicated Wistar rats. *Canadian Journal of Physiology and Pharmacology*. 2014;92(4):267–277. doi: 10.1139/cjpp-2013-0449
23. Ofusori D. A., Falana B. A., Ofusori A. E., Abayomi T. A., Ajayi S. A., Ojo G. B. Gastroprotective effect of aqueous extract of neem *Azadirachta indica* on induced gastric lesion in rats. *International Journal of Biological and Medical Research*. 2010;1:219–222
24. Irvine F.R., "Woody plants of Ghana, with special reference to their uses". Oxford university press London: 1961.
25. Savithramma N, Linga Rao M and Suhrulatha D. "Screening of Medicinal Plants for Secondary Metabolites". *Middle-East Journal of Scientific Research*. 2011; 8(3): 579.
26. eigler, David S. "Plant Secondary Metabolism". Springer Publications: 1998.
27. Donald.T.Sawyer. "Superoxide chemistry". McGraw Hill: 2014.
28. Alam M. A., Uddin R., Subhan N., Rahman M. M., Jain P., Reza H. M. (2015). Beneficial role of bitter melon supplementation in obesity and related complications in metabolic syndrome. *J. Lipids* 2015:496169. 10.1155/2015/496169
29. Chao C. Y., Sung P. J., Wang W. H., Kuo Y. H. (2014). Anti-inflammatory effect of *Momordica charantia* in sepsis mice. *Molecules* 19 12777–12788. 10.3390/molecules190812777
30. Fachinan R., Yessoufou A., Nekoua M. P., Moutairou K. (2017b). Effectiveness of antihyperglycemic effect of *Momordica charantia*: implication of t-cell cytokines. *Evid. Based Complement. Alternat. Med.* 2017:3707046. 10.1155/2017/3707046.
31. Benzie IFF. Evolution of dietary antioxidants. *Comp Biochem Physiol Part A* 2003; 136: 113-126.
32. Fang Y, Yang S, Wu G., Free radicals, antioxidants and nutrition. *Nutrition* 2002; 18: 872-879. 3. Manavalan K, Ramasamy C. *Physical pharmaceuticals*. 2nd ed. Chennai: Vignesh publishers. p. 286 (2001)
33. Nagendrappa CG. An appreciation of free radical chemistry- 3. Free radicals in diseases and health. *Resonance* 2005; 10(2): 65-73.
34. Sueoka N, Sukanuma M, Sueoka E, Okabe S, Matsuyama S, Imai K, Nakachi K, Fujiki H. A new function of green tea: prevention of lifestyle-related diseases. *Ann N Y Acad Sci*. 2001;928:274–280





**Nooka Raju et al.,**

35. Tsuneki H, Ishizuka M, Terasawa M, Wu JB, Sasaoka T, Kimura I. Effect of green tea on blood glucose levels and serum proteomic patterns in diabetic (db/db) mice and on glucose metabolism in healthy humans. *BMC Pharmacol.* 2004;4:18–21. doi: 10.1186/1471-2210-4-18
36. Yokozawa T, Nakagawa T, Kitani K. Antioxidative activity of green tea polyphenol in cholesterol-fed rats. *J Agric Food Chem.* 2002;50:3549–3552.

**Table 1: preparation of infusions with different concentration**

Concentration in micrograms	Plant exact taken (ml)	Water (ml)
20 µg /ml	2	8
40 µg /ml	4	6
60 µg /ml	6	4
80 µg /ml	8	2
100 µg /ml	10	-

**Table 2: Antioxidant activity of Green tea in Ethanolic DPPH solution**

Green tea			
Concentration µg/ml	Absorbance	Transmittance	% inhibition
20	1.114	7.69	21.69
40	1.0615	8.67	25.38
60	0.923	11.94	35.12
80	0.824	15.09	42.28
100	0.6349	23.18	55.37

**Table 3: Antioxidant activity of *Aegle marmelos***

<i>Aegle marmelos</i>			
Concentration µg/ml	Absorbance	Transmittance	%inhibition
20	0.7821	16.13	45.02
40	0.7576	17.47	46.74
60	0.7167	19.2	49.62
80	0.699	21.42	52.97
100	0.666	21.58	53.18

**Table 4: Antioxidant activity of *Azardirachta indica***

<i>Azardirachta indica</i>			
Concentration µg/ml	Absorbance	Transmittance	%inhibition
20	0.6197	24	56.44
40	0.6585	21.94	53.69
60	0.6975	20.07	50.97
80	0.6101	25.54	57.116
100	0.5601	27.54	60.63

**Table 5: Antioxidant activity of *Momordica charantia***

<i>Momordica charantia</i>			
Concentration µg/ml	Absorbance	Transmittance	%inhibition
20	0.8642	13.14	39.25
40	0.8544	13.96	39.94
60	0.8448	14.52	40.619
80	0.8425	14.82	40.78
100	0.8585	13.84	39.656





Nooka Raju et al.,

Table 6: Antioxidant activity of *Cissus quadrangularis*

<i>Cissus quadrangularis</i>			
Concentration µg/ml	Absorbance	Transmittance	%inhibition
20	0.9032	12.5	36.51
40	0.896	12.7	37.02
60	0.9207	12	38.28
80	0.8943	12.75	37.14
100	0.8891	12.9	37.15

Table 7: Antioxidant activity of *Trigonella foenum graecum*

<i>Trigonella foenum graecum</i>			
Concentration µg/ml	Absorbance	Transmittance	%inhibition
20	0.9214	11.98	35.23
40	0.9314	11.71	34.53
60	0.9832	10.39	30.891
80	0.9359	10.59	34.216
100	0.9916	10.19	30.301

Table 8: Antioxidant activity of Green tea in Ethanolic DPPH solution

<i>Green tea</i>			
Concentration µg/ml	Absorbance	Transmittance	%inhibition
20	0.3220	47.75	34.07
40	0.2839	51.93	41.87
60	0.2234	59.79	54.25
80	0.2203	60.21	54.89
100	0.1812	65.89	62.89

Table 9: Antioxidant activity of PHF1 in Ethanolic DPPH solution

<i>Aegle marmelos:Azadirachta indica:Momordica charantia(3:2:1)</i>			
Concentration µg/ml	Absorbance	Transmittance	%inhibition
20	0.2940	50.82	39.80
40	0.2575	55.27	47.27
60	0.2305	58.82	52.80
80	0.2579	55.22	47.19
100	0.2766	52.89	43.36

Table 10: Antioxidant activity of PHF2 in Ethanolic DPPH solution

<i>Aegle marmelos : Momordica charantia: Azadirachta indica (3:2:1)</i>			
Concentration µg/ml	Absorbance	Transmittance	%inhibition
20	0.1916	64.33	60.76
40	0.2259	59.44	53.74
60	0.1767	66.57	63.82
80	0.1576	69.57	67.73
100	0.2954	50.65	39.516





Nooka Raju et al.,

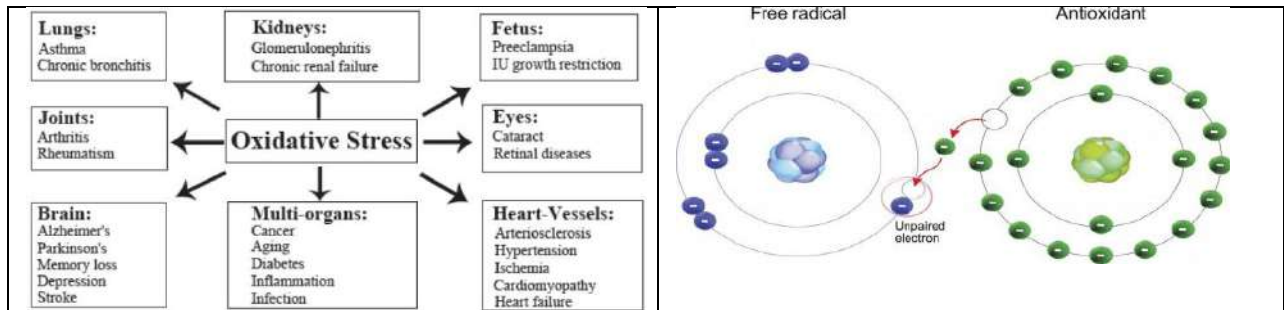


Figure 1: Health Complications of oxidative stress  
Pham-Huy LA, et al. He H, Pham-Huy C., et al [7]

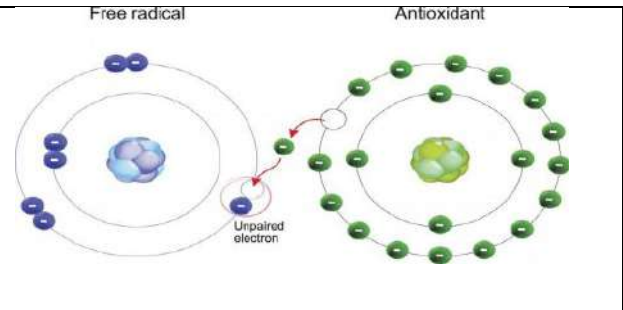


Figure 2: Antioxidants Mechanism of action Zawn Villines et al.

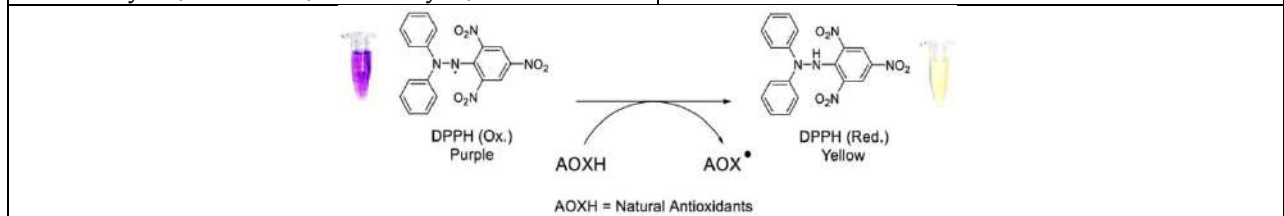


Figure 3: Principle involved in DPPH Radical Reducing Activity

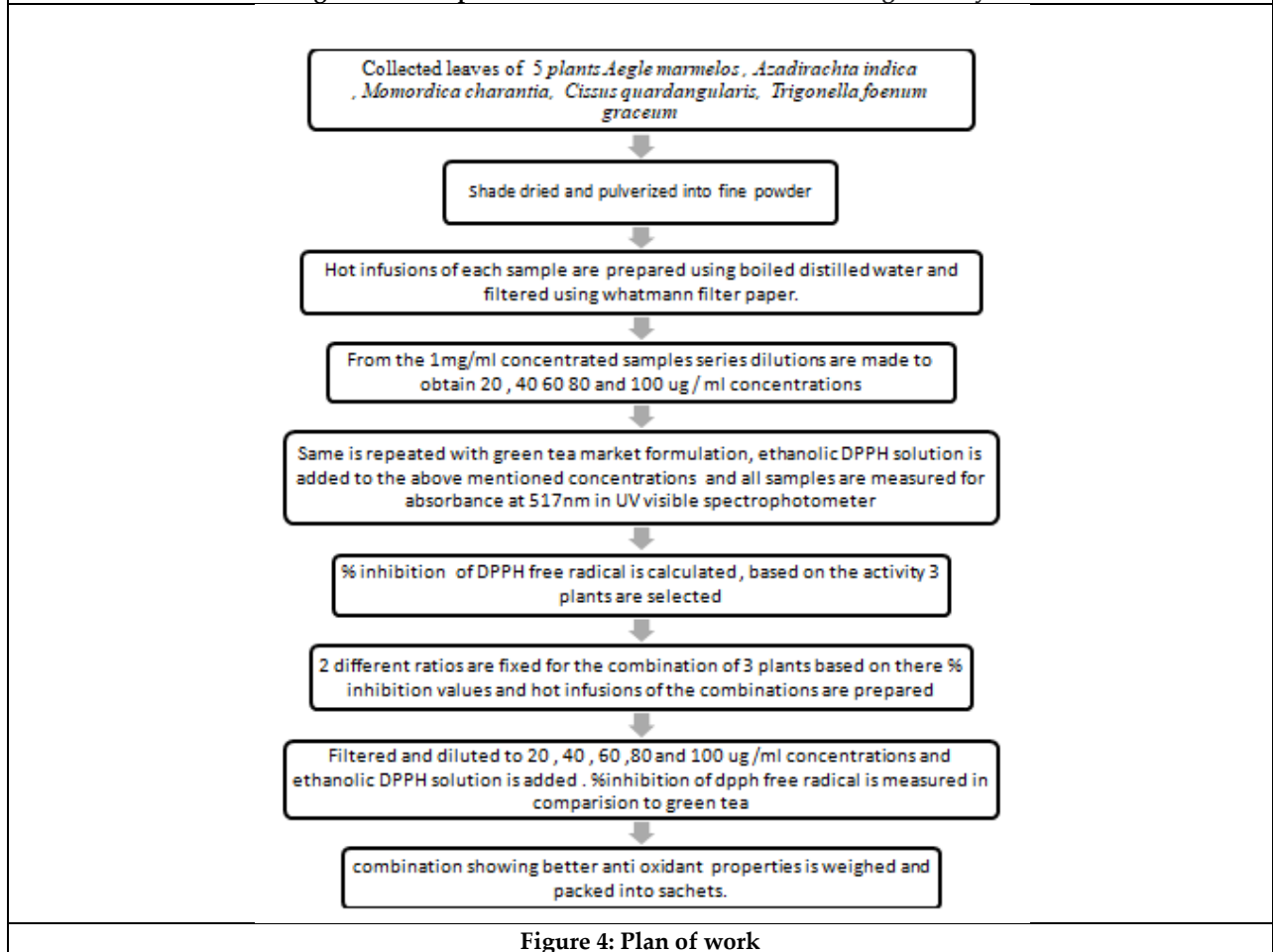


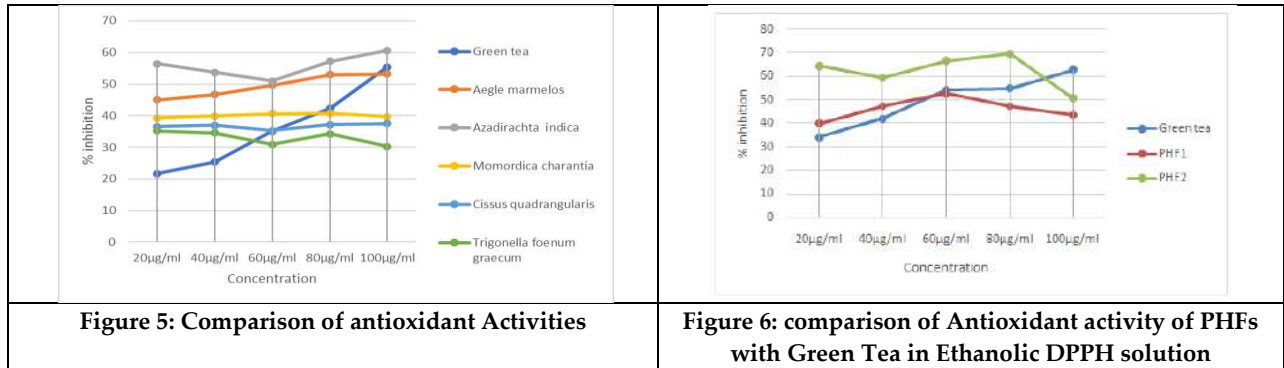
Figure 4: Plan of work







Nooka Raju et al.,





## Molecular Docking Investigation into the Hepatic Effects of Cyclooxygenase and CYP2E1 by the Methanol Extract of *Padina gymnospora* in Male Albino Wistar Rats

Tanima Debnath Sarkar<sup>1</sup>, John Anbumani Ganesan<sup>2</sup>, A. Therasa Alphonsa<sup>3</sup> and M. Muthulingam<sup>4\*</sup>

<sup>1</sup>Ph.D. Research Scholar, Department of Zoology of Annamalai University, Annamalai Nagar, Tamil Nadu, India.

<sup>2</sup>Ph.D. Research Scholar, Department of Biochemistry and Biotechnology of Annamalai University, Annamalai Nagar, Tamil Nadu, India.

<sup>3</sup>Assistant Professor, Department of Chemistry, Faculty of Science, Annamalai University, Annamalai Nagar, Tamil Nadu, India.

<sup>4</sup>Associate Professor, Department of Zoology, Faculty of Science, Annamalai University, Annamalai Nagar, Tamil Nadu, India.

Received: 21 Jun 2024

Revised: 12 Oct 2024

Accepted: 18 Nov 2024

### \*Address for Correspondence

#### M. Muthulingam

Associate Professor, Department of Zoology,

Faculty of Science, Annamalai University,

Annamalai Nagar, Tamil Nadu, India.

E.Mail: muthuau@rediffmail.com



This is an Open Access Journal / article distributed under the terms of the **Creative Commons Attribution License** (CC BY-NC-ND 3.0) which permits unrestricted use, distribution, and reproduction in any medium, provided the original work is properly cited. All rights reserved.

### ABSTRACT

Abstract: Proteins are vital macronutrients essential numerous functions for sustaining all living organisms, as they possess the unique ability to bind various molecules. This study kingpin on the methanolic extract of the *Padina gymnospora* is a brown seaweed, which yields several important fatty acids including Stearidonic acid, 9-Oxo-10,12-octadecadienoic acid, Nonadecanoic acid, Oleic acid, Linoleic acid, Eicosanolic acid, Arachidonic acid, Eicosapentaenoic acid, Linolenic acid, and Palmitoleic acid. Among these components, Nonadecanoic acid stands out with a negative charge (-0.07). Paracetamol, a widely used analgesic and antipyretic drug, undergoes oxidation primarily through the enzyme CYP2E1 (Cytochrome P450 2E1). Besides CYP2E1enzyme, its subclasses CYP1, CYP2, and CYP3, facilitates the breakdown of foreign compounds in mammals. Although Paracetamol does not belong to the NSAIDs family, it acts on cyclooxygenase (COX) isoenzymes COX-1 and COX-2, by inhibiting prostaglandin H (PGHS) production. PGHS, with its dual functionality as cyclooxygenase and peroxidase, plays a crucial role in inflammation. Paracetamol exerts its pain-relieving effects by modulating tissue receptors in the spinal cord, thalamus, and cerebral cortex, where pain sensations are processed. Additionally, it induces the production of fatty acid amide N-arachidonoylphenolamine (AM404) through the L-arginine/NO pathway and descending serotonergic routes within the brain. Molecular modeling techniques analysis shows that both the 4th position phenolic OH group of silymarine and Paracetamol bind to the carboxylic acid of Nonadecanoic acid in *Padina gymnospora*. This interaction highlights a potential mechanism for the therapeutic action of Paracetamol in association





Tanima Debnath Sarkar et al.,

with fatty acids from seaweed extracts. Graphical abstract the hepatoprotective of *Padina gymnospora* is shown in Figure:1.

**Keywords:** Protein, paracetamol, silymarine, nonadecanoic acid, cyclooxygenase, Cytochrome P450, L-arginine pathway, serotonergic pathway.

## INTRODUCTION

*Padina gymnospora* was collected from Gulf of Mannar area, Tuticorin located (8.76°42" N; 78.13° 48" E) at Rameswaram, district Ramanathapuram in Tamil Nadu. Phaeophyta (brown algae) are more abundant in a shallow rocky, low tide area. The plant was identified and authenticated at the herbarium (AU Bota#609) of Botany, Professor Dr.L.Mullainathan, Academic affairs Director, Faculty of Science, Annamalai University, Tamilnadu, India. *Padina gymnospora* [(Kützting) Sonder 1871] thallus (Figure 2B) of *Padina gymnospora* is medium brown on the upper surface and dark brown below, with a relatively robust structure. It is often lightly calcified on the upper surface and measures 5–15 cm in length and 5–20 cm in spread. When young, it has a flabellate shape, becoming shallowly to deeply divided with cuneate to flabellate segments that are mostly 1–5 cm wide at the top, featuring acute to rounded axils. The thallus is attached to substrates by a rhizoidal holdfast measuring 0.5–2 cm in length and 0.2–1 cm in width, making it epilithic [Figure:2(A)] Paracetamol, Silymarin and Nonadecanoic acid from *Padina gymnospora* are three ligands and COX-2 and p450 are two proteins who are binding with them.

**Paracetamol:** (Molecular formula  $C_8H_9NO_2$ ) is a dependence, tolerance, safe antipyretic or analgesia drug without risk factoring when it is used alone. Using of large quantity of paracetamol is dangerous harmful of hepatotoxicity. Paracetamol undergoes metabolic changes, resulting in the creation of two main compounds: N-(4-hydroxyphenyl)-arachidonamide (AM404) catalyzed by fatty acid amide hydrolase (FAAH) and N-acetyl-p-benzoquinone imine (NAPQI) facilitated by cytochrome P450 (CYP) enzymes. Despite these known metabolic pathways, the fundamental mechanism underlying the actions of paracetamol remains unclear. Additionally, paracetamol exhibits interactions with drugs involving the CYP family enzymes, such as inducers, inhibitors, and substrates, including illicit drugs. In contrast to ibuprofen, a non-steroidal anti-inflammatory drug (NSAID), The uncertainty persists about whether analgesic effect of paracetamol stems from the inhibition of cyclooxygenases (COXs). [1]. A crucial metabolic pathway of significance involves the hepatic cytochrome P450-dependent mixed-function oxidase system converting paracetamol to a reactive metabolite [2,3]. This active metabolite is hypothesized to be either N-acetyl-para-benzoquinoneimine [4] or its related semiquinone free radical form [5,6]. Paracetamol induced hepatotoxicity are balanced both 'toxic' and 'detoxification' pathway. A similar relationship was observed in rats, where the covalent binding of radiolabel to liver proteins 48 hours after administering [ring-14C]-paracetamol was directly proportional to the extent of liver damage [7]. It showed the evidence of covalent binding of radiolabel to liver plasma membranes and microsomes 2.5 hours after oral administering 2.5 g/kg body weight of  $^3H$ -paracetamol to rats [8].

**Silymarin:** (Molecular formula  $C_{25}H_{22}O_{10}$ ) is categorized as a hepatoprotective medication, designed to safeguard the liver. For centuries, milk thistle extracts are recognized as beneficial for the liver, often referred to as "liver tonics." These extracts are reported to possess protective properties that enhance liver function. Milk thistle is frequently used to address ailments like liver cirrhosis, chronic hepatitis (liver inflammation), toxin-induced liver damage (including protection against severe effects from *Amanita phalloides*, the 'death cap' mushroom poisoning), and disorders related to the gallbladder. In a specific study, individuals with Type II Diabetes experienced noteworthy reductions in Hemoglobin A1C levels, and fasting blood sugar, insulin, liver enzymes SGOT or AST and SGPT or ALT, LDH after the administration of silymarin at a dosage of 200 mg thrice daily. Additionally, supplementation with silymarin showed notable improvements in specific antioxidant indicators (total antioxidant capacity and thiol levels) and a reduction in liver enzyme levels in patients suffering from trauma-induced liver injury. It is noteworthy that the two species naturally interbreed, giving rise to a hybrid known as *Silybum × gonzaloi* Cantó, Sánchez Mata & Rivas Mart. (a cross between *S. eburneum* var. *hispanicum* and *S. marianum*) [9]. Different constituents of milk thistle





Tanima Debnath Sarkar et al.,

(such as silymarin, silybin, etc.) possess diverse mechanisms of action that could potentially safeguard the liver, including anti-inflammatory properties, antioxidant effects, blocking toxins, promoting protein synthesis, and anti-fibrotic effects [10,11].

Silymarin facilitates the transport of bile acid molecules from the liver to the small intestine and back to the liver. The term "enterohepatic circulation" (EHC) describes the complex process wherein bile acid molecules travel from the liver to the small intestine and then return to the liver. This cyclical movement entails the active secretion of bile acids into canalicular bile within hepatocytes, thus completing the enterohepatic cycle. During this circulation, bile salts interact with facultative and anaerobic bacterial populations, which, though relatively sparse in number, display substantial diversity in the small bowel.

**Nonadecanoic acid:** Nonadecanoic acid (Molecular formula  $C_{19}H_{38}O_2$  /  $CH_3(CH_2)_{17}COOH$ ) is an odd chain (19 carbon) saturated fatty acid which is primarily produced by initiating the synthetic series with the three-carbon compound, propionic acid. Propionate must be converted to succinate in order for the primary energy pathway to be oxidized, and this requires vitamin B<sub>12</sub>. *Padina gymnospora*, a type of dark brown algae from the Dictyotaceae family, exhibits a distinctive morphology with its base and fan-shaped lobes dividing into wedge-shaped pieces. This algae is well recognized for playing a significant role in the healing of wounds naturally [12]. Moreover, it demonstrates notable medicinal properties, serving as an agent against cancer, bacteria, inflammation, and oxidative stress [14], while also showing larvicidal activity [13]. To detect the molecules within the methyl alcohol extract of *P. gymnospora* being investigated, a solution was prepared by dissolving 10  $\mu$ L of the methyl alcohol extract in a 1000  $\mu$ L mixture of methanol and water (50% v/v). The electrospray ionization (ESI-) negative ion mode of the mass spectrometer employed for the analysis covered a mass range of m/z 150 to 1500 [14]. FTIR (Fourier Transform Infrared Spectroscopy) utilizes infrared absorption spectra to discern the chemical bonding within molecules, facilitating the screening and scanning of samples for various components. On the other hand, SEM (Scanning Electron Microscopy) generates high-resolution images for the detailed analysis of a sample's chemical characteristics.

**COX-2 (Cyclooxygenase-2):** Prostaglandin-endoperoxide synthase (PTGS), commonly referred to as cyclooxygenase, is essential for the synthesis of prostaglandins such prostacyclin and prostanoids like thromboxane which come from arachidonic acid, a polyunsaturated omega-6 fatty acid characterized by a 20-carbon chain and four cis-double bonds, with the first double bond positioned at the sixth carbon from the omega end. Phospholipids, specifically phosphatidylethanolamine, phosphatidylcholine, and phosphatidylinositides, are composed of polyunsaturated fatty acids and are responsible for the membranes of body cells. They are notably abundant in the brain, muscles, and liver. Inhibition of COX through pharmaceutical means can alleviate symptoms of inflammation and pain [15]. Nonsteroidal anti-inflammatory drugs (NSAIDs) like aspirin and ibuprofen work by inhibiting COX. Drugs that target specifically the COX-2 isozyme are referred to as COX-2 inhibitors. Paracetamol's active metabolite (AM404) also acts as a COX inhibitor, a characteristic that contributes to its therapeutic effects, potentially involving G-protein coupled membrane receptors [16]. Paracetamol's mechanism of action includes the inhibition of cyclooxygenases (COX-1, COX-2, and COX-3) and involvement in the endocannabinoid system and serotonergic pathways. Additionally, it impacts transient receptor potential (TRP) channels and voltage-gated Kv7 potassium channels, while also inhibiting T-type Cav3.2 calcium channels. Paracetamol additionally modulates the L-arginine pathway in nitric oxide (NO) synthesis. Cyclooxygenase activity was assessed using an oxygen electrode with 100 $\mu$ M arachidonic acid as the substrate [17], while inhibition studies involving IBP were conducted [18]. The thermal stability of protein in different chemical environments (Thermal shift assays) were performed using apo muCOX-2 and a Stratagene Mx3005P real-time PCR instrument [19]. Coordinates and the fundamental quantities on which the function of electron density depends on the Protein Data Bank (PDB ID: 4PH9) [20].

**Cytochrome P450:** Cytochrome P450 (CYP) enzymes, membrane-bound hemoproteins, are pivotal in detoxifying xenobiotics, regulating cellular metabolism, and upholding homeostasis. The induction or inhibition of these enzymes stands as a significant mechanism driving drug-drug interactions. Different xenobiotics and endogenous





Tanima Debnath Sarkar et al.,

substrates have the potential to activate CYP enzymes transcriptionally via receptor-dependent mechanisms. Inhibition of these enzymes serves as a fundamental mechanism for metabolism-related drug-drug interactions. Chemotherapeutic medications, in particular, can precipitate such interactions by either inhibiting or inducing the CYP enzyme system. Through in silico analyses, followed by validation, many short RNA molecules have been found in eukaryotic cell as key regulators of CYPs. Furthermore, genetic polymorphisms and epigenetic alterations in CYP genes may subscribe to variances in disease susceptibility and the remedial efficacy of drugs among individuals and across different ethnicities. The super family of hemoproteins known as cytochromes P450 (CYP P450s) in the liver of humans is in charge of catalyzing the oxidative metabolism of medications and foreign substances when they enter the body. Adverse events and treatment failures are frequently caused by interactions between medicines or xenobiotics. When inducers are used at the same time with other CYP450-metabolizing medications, changes in their metabolism may occur in the liver or gastrointestinal tract. The therapeutic intention of these interactions is related to autoinduction, which has the potential to cause a certain result therapy outcomes that are not ideal or successful. Pharmaceutical corporations have worry about the situation of matter when developing new medications.

Non-CYP-mediated oxidative processes are equally important for xenobiotic metabolism, even though the CYP is a group of homologous enzymes that share a common mechanistic attribute but catalyze different overall reactions, mainly mediates oxidative metabolic reactions. Together with CYPs, these non-CYP oxidase include lipoxygenases, prostaglandin H synthase, flavin-containing monooxygenases, alcohol and aldehyde dehydrogenases, molybdenum hydroxylases (like aldehyde oxidase and xanthine oxidase), amine oxidases (like monoamine, polyamine, diamine, and semicarbazide-sensitive amine oxidases), and lipoxygenases. Like CYPs, these catalyze oxidation reduction reactions can produce reactive/toxic metabolites in addition therapeutically active metabolites, which can affect the effectiveness of remedial agent medications or aid in detoxification. Numerous them are important players in the metabolism of endobiotics, which may result in interactions between medications and endogenous molecules when pharmaceuticals are being metabolized. Within the enzyme CYP2E1 (Cytochrome P450 2E1), there are five proteins: 3GPH, 3KOH, 3T3Z, 3LC4, and 3E4E. [ Figure:2(B)]

## MATERIALS AND METHODS

*Padina gymnospora* extracts both Soxhlet and filtration process:- The choice of solvent for soxhlet extraction is crucial and typically based on polarity and the phytoconstituent isolation process. It's important for the solvent to be easily removable and inert. Methanol, being a semi-polar solvent, is often preferred as it can effectively extract many phytoconstituents

### Experimental Design

Albino rats were segregated into seven groups, each consisting of six individuals:

**Group 1 (Control):** Administered physiological saline solution at a dosage of 10ml/kg body weight.

**Group 2:** Received a single dose of paracetamol at 3 g/kg weight of the body via oral gavage (Size 16 Gauge, Length 3 inches, Ball diameter 3mm).

**Group 3:** Given paracetamol along with *Padina gymnospora* at a dosage of 50 mg/kg weight of the body daily one time for 28 days, administered orally using the same oral gavage method as Group 2.

**Group 4:** Given paracetamol along with *Padina gymnospora* at a dosage of 100 mg/kg weight of the body daily one time for 28 days, administered orally using the same oral gavage method as Group 2.

**Group 5:** Given paracetamol along with *Padina gymnospora* at a dosage of 200 mg/kg weight of the body daily one time for 28 days, administered orally using the same oral gavage method as Group 2.

**Group 6:** Given paracetamol along with silymarin at a dosage of 25 mg/kg weight of the body daily one time for 28 days, administered orally using the same oral gavage method as Group 2.

**Group 7:** Administered *Padina gymnospora* alone at a dosage of 200 mg/kg weight of the body daily one time for 28 days, using the same oral gavage method as Group 2.







Tanima Debnath Sarkar *et al.*,

The animals were euthanized by cervical dislocation 24 hours after the final dose, marking the end of the tentative test. Blood specimens were obtained without the use of an anticoagulant to separate serum and measure serum marker enzymes such as AST, ALT, ALP, LDH, GGT, bilirubin, cholesterol, and protein levels. The liver tissue was instead of taken away, washed with cold physiological saline, and preserved in 10% formalin for subsequent histological analyses.

**UniProt Database:** The UniProt Knowledgebase (UniProtKB) acts as the principal repository for extensive protein data, providing accurate, standardized, and detailed annotations. The FASTA sequence was retrieved from the UniProt database, with the UniProt ID assigned as Q99497. Additionally, the corresponding PDB ID was sourced from the UniProt database. Protein-ligand binding denotes the interaction wherein a small molecule, frequently a drug (ligand), attaches to a receptor or protein within the body, triggering a biological response such as inflammation reduction or pain relief. The hurdle in drug discovery lies in pinpointing the precise bioactive pose of the protein-ligand complex, which may adopt a restricted number of poses or configurations.

Determining the bioactive pose is complex since there isn't always a sole lowest energy pose for either the protein or the ligand. The complex might stabilize a higher energy conformation of the ligand. Both the protein and ligand are three-dimensional and flexible, constantly altering their shape. This presents a multi-step challenge, beginning with identifying the bioactive 3D conformation of the ligand. As we shift to the protein, this always daunting due to its larger size and expanded possibilities.

Successfully pinpointing both the bioactive conformation of the ligand and the protein presents the additional hurdle of accurately positioning the ligand within the protein to attain the desired activity. Various methods are available to generate these poses, differing in computational expense. One approach entails employing a cost-effective method to produce a vast array of potential poses, succeeded by a more resource-intensive calculation to prioritize them based on the probability of being the bioactive pose. This process aims to generate promising binding configurations for further study. The Protein Data Bank (PDB) serves as an official experimental repository housing three-dimensional structures of proteins, nucleic acids, and other biological macromolecules. The PDB format, denoted by the .pdb extension, comprises a file format containing a four-character alphanumeric identifier (e.g., 3T3Z), which aids in the description and annotation of protein and nucleic acid structures, including atomic coordinates and connectivity. Additionally, the PDB format encompasses information relevant to structural biology, such as gene expression, in-silico methodologies, and studies on protein-nucleic acid interactions. This standard format is used for structures deposited in the Protein Data Bank (PDB) at the Research Collaboratory for Structural Bioinformatics (RCSB) [21].

**Molecular docking studies:** The Lamarckian genetic algorithm was utilized in conducting investigations on flexible ligand docking [22]. CB-Dock2 stands as an improved iteration of the CB-Dock server, specifically designed for protein-ligand blind docking. This upgraded version seamlessly integrates features for cavity detection, docking, and homologous template fitting. Through the utilization of the protein and ligand's three-dimensional (3D) structures, CB-Dock2 facilitates the prediction of binding sites and assesses affinity, contributing and the power to produce a desired result. of computer-aided drug discovery endeavors. ChemBioDraw Ultra 12.0 was used to create the ligand molecules initially, and ChemBio3D Ultra 12.0 was used to transform them into their three-dimensional structures. After that, energy conservation was done with the MOPAC Ultra 2009 program utilizing the PM3 technique [23]. The resultant ligands, post-preparation, were utilized as input files for the CB Dock 2 online software (see figure-3). CB-Dock 2 performs an initial retrieval from our server's protein-ligand complexes database. This retrieval seeks template ligands with high topology similarity ( $FP2 \geq 0.4$ ). If such templates are found, CB-Dock2 calculates the similarity between the user's protein and proteins complexed with the selected template ligands. Retained are complexes with over 40% sequence identity and a pocket RMSD of  $\leq 4\text{\AA}$  in the template ligand binding site. These selected complexes then undergo template-based cavity detection followed by molecular docking. The docking process utilizes FitDock, an internally developed technique that employs a hierarchical multi-feature alignment approach to align the initial conformation with the specified template. It then explores potential conformations and produces refined docking poses. Upon file submission, an automated Perl script will handle the processing of the required files. The script utilizes the most recent release (version 1.2.0) of AutoDock Vina, specifically designed for







Tanima Debnath Sarkar et al.,

template-independent blind docking. The blind docking pipeline follows a template-based approach and incorporates the BioLip database (as of September 15, 2021) as the template repository for guiding the docking process.

The default worth for all other parameters were maintained. After docking, hydrogen bonding and  $\pi$ - $\pi$  interactions were examined in the top poses, and the root mean square deviation (RMSD) was computed using Discovery Studio Visualizer 2.5. Each ligand's inhibition constant ( $K_i$ ) was calculated using the predicted free energy of its binding ( $\Delta G_{\text{binding}}$ , kcal/mol). The model with the lowest Discrete Optimized Protein Energy (DOPE) score was selected, refined, and evaluated using structural characteristics such as the Ramachandran plot with PROCHECK [24], the ERRAT plot [25], and the ProSA [26] web servers. Additionally, the model underwent energy minimization before being used in docking and molecular dynamics (MD) simulation studies.

**Physicochemical parameters Calculation:** Absorption (%ABS) was calculated using the formula:  $\%ABS = 109 - [0.345 \times \text{topological polar surface area (TPSA)}]$ , as described by Zhao et al [27]. TPSA [28], miLogP, the number of rotatable bonds, and adherence to Lipinski's "Rule of Five" [29] were determined using the Molinspiration online property calculation toolkit [30]. The molecular binding are shown in the below Table-A.

## RESULTS AND DISCUSSION

Bold and under line docking works (binding energy and related amino acids) which are shown the Table-A and Table:1 to Table:6 with binding images are provided in below (Results and Discussion). Also Graphical represented of molecular binding (protein ligand bond).

Milk thistle, particularly silymarin, exhibits hepatoprotective effects against liver cirrhosis, viral hepatitis, and alcoholic liver disorders. In an experiment involving Paracetamol combined with *Padina gymnospora* (200mg/body weight), liver enzyme levels of AST, ALT, and LDH were measured at 165mg/dL, 145.5mg/dL, and 131mg/dL respectively. When *Padina gymnospora* was combined with silymarin at 25mg/Kg body weight, these enzyme levels decreased to 123mg/dL, 137.9mg/dL, and 146mg/dL respectively, indicating a reduction in AST, ALT, and LDH levels with silymarin use. It has observed that Paracetamol, silymarin, and nonadecanoic acid from *Padina gymnospora* inhibit cytochrome P-450 and Cyclooxygenase 2 (COX-2). When *Padina gymnospora* was administered alone at 200mg/Kg body weight, AST, ALT, and LDH values were 170mg/dL, 479mg/dL, and 128mg/dL respectively. This suggests a weaker interaction (loose binding of -3.62) with COX-2. However, when Paracetamol and silymarin were combined, the binding energy improved significantly (-5.5) (See Graphical represented molecular binding (protein ligand bond)).

The binding affinities of these compounds with specific proteins were also examined. COX-2 (PDB id-4PH9) exhibited binding with nonadecanoic acid (-6.1), paracetamol (-6.3), and silymarin (-10.2). In comparison, CYP2E1 (Cytochrome P4502E1) displayed different protein binding characteristics, with nonadecanoic acid showing good binding to protein 3GPH (-8.1), paracetamol to 3LC4 protein (-7), and silymarin to 3T3Z (-10.8). Overall, the research indicates that P-450 binding is more significant than COX-2 binding. The presence of nonadecanoic acid with paracetamol appears to strongly bind and potentially treat liver diseases induced by paracetamol toxicity. The study explores the potential therapeutic effects of *Padina gymnospora*, a type of brown seaweed, focusing on its methanolic extract rich in various fatty acids, notably Nonadecanoic acid. Paracetamol, a commonly used analgesic, is metabolized by the enzyme CYP2E1 and affects cyclooxygenase isoenzymes, modulating pain sensation and inducing the production of AM404. Molecular docking analysis suggests a potential interaction between Paracetamol and silymarin with Nonadecanoic acid, shedding light on a possible mechanism underlying the therapeutic action of Paracetamol in conjunction with fatty acids from seaweed extracts.





Tanima Debnath Sarkar *et al.*,

## CONCLUSION

The investigation focused on the binding pockets of COX-2 and Cytochrome P450 2E1 as part of the quest for small molecules with potential in combating liver disease. Through a comparative analysis, it was determined that the silymarin ligand exhibited a higher docking score compared to remdesivir and displayed superior binding affinity compared to remdesivir in these contexts. Nonadecanoic acid is better binding with cytochrome P450 than Cyclooxygenase-2 due to its' ability of high binding .

## ACKNOWLEDGMENT

The author wishes to thank her friends Karthiga AR, Reshwen Shalo R, Akila S, Surya U, John Anbumani Ganesan, and guide Dr. M. Muthulingam Associate Professor, Department of Zoology Annamalai University, and Dr. A. Therasa Alphonso Assistant Professor, Department of Chemistry, Annamalai University.

### Conflict of interest

Regarding the content of this article, the writers declare that they have no conflicts of interest.

### Funding

None

### Author's contribution

In addition to producing the initial draft of the manuscript, the author also assisted with its conceptualization, data curation, formal analysis, funding procurement, research, methodology, resource management, software development, supervision, validation, and visualization.

## REFERENCES

1. Hylands-White N, Duarte RV, Raphael JH (2017) An overview of treatment approaches for chronic pain management. *Rheumatol Int* 37(1):29–42.
2. Mitchell J.R., Jollow D.J., Potter W.Z., Davis D.C., Gillette J.R., Brodie B.B. Acetaminophen-induced hepatic necrosis. I. Role of drug metabolism. *J. Pharmacol. exp. Ther.* 1973;187:185–194.
3. Potter W.Z., Davis D.C., Mitchell H.R., Jollow D.G., Gillette J.R., Brodie B.B. Acetaminophen-induced hepatic necrosis. III. Cytochrome P-450-mediated covalent binding in vitro. *J. Pharmacol. exp. Ther.* 1973;187:203–209.
4. Corcoran G.B., Mitchell J.R., Vaishnav Y.N., Horning E.C. Evidence that acetaminophen and *N*-hydroxyacetaminophen form a common arylating intermediate, *N*-acetyl-*para*-benzoquinoneimine. *Mol. Pharmacol.* 1980;18:536–542.
5. De Vries J. Hepatotoxic metabolic activation of paracetamol and its derivatives phenacetin and benorilate: oxygenation or electron transfer? *Biochem. Pharmacol.* 1981;30:399–402.
6. Nelson S.D., Dahlin D.C., Rauckman E.J., Rosen G.M. Peroxidase-mediated formation of reactive metabolites of acetaminophen. *Mol. Pharmacol.* 1981;20:195–199.
7. Davis M., Harrison N.G., Ideo G., Portman B., Labadarios D., Williams R. Paracetamol metabolism in the rat: relationship to covalent binding and hepatic damage. *Xenobiotica.* 1976;6:249–255.
8. Tsokos-Kuhn J.O., Hughes H., Smith C.V., Mitchell J.R. Alkylation of the liver plasma membrane and inhibition of the Ca<sup>2+</sup> ATPase by acetaminophen. *Biochem. Pharmacol.* 1988;37:2125–2131.
9. Singh, Rana P.; Agarwal, Rajesh (2009). "Cosmeceuticals and silibinin". *Clinics in Dermatology.* 27 (5): 479–484.
10. Davis-Searles PR, NakanishiY, Kim N, Graf TN, Oberlies NH, Wani MC, Wall ME, Agarwal R and Kroll DJ. Milk Thistle and Prostate Cancer: Differential Effects of Pure Flavonolignans from *Silybum marianum* on Antiproliferative end Points in Human Prostate Carcinoma Cells. *Cancer Res.* 2005; 65 (10): 4448 - 57.



**Tanima Debnath Sarkar et al.,**

11. John S, Scaler F, Sonnenbichler I and Weyhenmeyerr. Stimulatory Effects of Silibinin and Silicristin from the Milk Thistle *Silybum marianum* on Kidney Cells. JPET. 1999; 290 (3): 1375 – 83.
12. Mosmann T 1983 Rapid colorimetric assay for cellular growth and survival: application to proliferation and cytotoxicity assays J. Immunol. Methods 65 55–63.
13. Rajagopal, G., Manivannan, N., Sundararajan, M., Kumar, A. G., Senthilkumar, S., Mathivanan, N., & Ilango, S. (2021). Biocompatibility assessment of silver chloride nanoparticles derived from *Padina gymnospora* and its therapeutic potential. *Nano Express*, 2(1), 010010.
14. Baliano, A. P., Pimentel, E. F., Buzin, A. R., Vieira, T. Z., Romão, W., Tose, L. V., & Endringer, D. C. (2016). Brown seaweed *Padina gymnospora* is a prominent natural wound-care product. *Revista Brasileira de Farmacognosia*, 26, 714-719.
15. Litalien, C., & Beaulieu, P. (2011). Molecular mechanisms of drug actions: from receptors to effectors. In *Pediatric critical care* (pp. 1553-1568). Mosby.
16. Högestätt, E. D., Jönsson, B. A., Ermund, A., Andersson, D. A., Björk, H., Alexander, J. P., & Zygmunt, P. M. (2005). Conversion of acetaminophen to the bioactive N-acylphenolamine AM404 via fatty acid amide hydrolase-dependent arachidonic acid conjugation in the nervous system. *Journal of Biological Chemistry*, 280(36), 31405-31412.
17. Vecchio AJ, Orlando BJ, Nandagiri R, Malkowski MG. Investigating substrate promiscuity in cyclooxygenase-2: the role of Arg-120 and residues lining the hydrophobic groove. *J Biol Chem*. 2012; 287:24619–24630.
18. Orlando BJ, McDougale DR, Lucido MJ, Eng ET, Graham LA, Schneider C, Stokes DL, Das A, Malkowski MG. Cyclooxygenase-2 catalysis and inhibition in lipid bilayer nanodiscs. *Arch Biochem Biophys*. 2014; 546:33–40
19. Koszelak-Rosenblum M, Krol AC, Simmons DM, Goulah CC, Wroblewski L, Malkowski MG. His-311 and Arg-559 are key residues involved in fatty acid oxygenation in pathogen-inducible oxygenase. *J Biol Chem*. 2008; 283:24962–24971.
20. Orlando, B. J., Lucido, M. J., & Malkowski, M. G. (2015). The structure of ibuprofen bound to cyclooxygenase-2. *Journal of structural biology*, 189(1), 62-66.
21. Vedansh Upadhyay and Dr. Dhruvo Jyoti Sen, PROTEIN DATA BANK AS A GOLDMINE IN DRUG DISCOVERY, wjpmr, ISSN 2455-3301 , Vol 10, Issue 2,2024.
22. Morris GM, Goodsell DS, Halliday RS, Huey R, Hart WE, Belew RK, et al. Automated docking using a Lamarckian genetic algorithm and an empirical binding free energy function. *J Comput Chem* 1998;19:1639-62.
23. Stewart JJ. Stewart Computational Chemistry, Version 9.03CS. MOPAC 2009. Available from: <http://OpenMOPAC.net>.
24. Šali A, Potterton L, Yuan F, van Vlijmen H, Karplus M. Evaluation of Comparative Protein Modeling By MODELLER. *Proteins*. 1995; 23: 318-326.
25. Laskowski RA, Macarthur MW, Moss DS, Thornton JM, PROCHECK: a program to check the stereochemical quality of protein structures. *J. App. Cryst*. 1993; 26(2): 283–91.
26. Colovos C, Yeates TO, Verification of protein structures: Patterns of nonbonded atomic interactions. *Protein Sci*. 1993; 2(9):1511–9.
27. Zhao Y, Abraham MH, Lee J, Hersey A, Luscombe NC, Beck G, et al. Rate-limited steps of human oral absorption and QSAR studies. *Pharm Res* 2002;19:1446-57.
28. Ertl P, Rohde B, Selzer P. Fast calculation of molecular polar surface area as a sum of fragment-based contributions and its application to the prediction of drug transport properties. *J Med Chem* 2000;43:3714-7.
29. Lipinski CA, Lombardo L, Dominy BW, Feeney PJ. Experimental and computational approaches to estimate solubility and permeability in drug discovery and development settings. *Adv Drug Deliv Rev* 2001;46:3-26.
30. Molinspiration Cheminformatics, Bratislava, Slovak Republic. Available from: <http://www.molinspiration.com/services/properties.html>. [Last Accessed on 2010 Apr 22].
31. Orlando BJ, Lucido MJ, Malkowski MG. The structure of ibuprofen bound to cyclooxygenase-2. *J Struct Biol*. 2015 Jan;189(1):62-6. doi: 10.1016/j.jsb.2014.11.005. Epub 2014 Nov 25. PMID: 25463020; PMCID: PMC4276492.
32. Porubsky PR, Battaile KP, Scott EE. Human cytochrome P450 2E1 structures with fatty acid analogs reveal a previously unobserved binding mode. *J Biol Chem*. 2010 Jul 16;285(29):22282-90. doi: 10.1074/jbc.M110.109017. Epub 2010 May 12. PMID: 20463018; PMCID: PMC2903405.





**Tanima Debnath Sarkar et al.,**

33. DeVore NM, Meneely KM, Bart AG, Stephens ES, Battaile KP, Scott EE. Structural comparison of cytochromes P450 2A6, 2A13, and 2E1 with pilocarpine. FEBS J. 2012 May;279(9):1621-31. doi: 10.1111/j.1742-4658.2011.08412.x. Epub 2011 Nov 25. PMID: 22051186; PMCID: PMC3572744.
34. Porubsky PR, Meneely KM, Scott EE. Structures of human cytochrome P-450 2E1. Insights into the binding of inhibitors and both small molecular weight and fatty acid substrates. J Biol Chem. 2008 Nov 28;283(48):33698-707. doi: 10.1074/jbc.M805999200. Epub 2008 Sep 24. PMID: 18818195; PMCID: PMC2586265.

**Table - A: Table of Molecular Binding**

PDB ID	Molecular Name Protein	Nonadecanoic acid	Paracetamol	Silymarin
4PH9	The configuration of Ibuprofen attached to cyclooxygenase-2 <sup>31</sup>	-6.1	<u>-6.3</u>	<u>-10.2</u>
3GPH	The human cytochrome P450 2E1 complexed with omega-imidazolyl-decanoic acid <sup>32</sup>	<u>-8.1</u>	-6.8	-8.6
3KOH	Cytochrome P450 2E1 in complex with omega-imidazolyl octanoic acid. <sup>32</sup>	-7.4	-6.7	-10.7
3T3Z	The human Cytochrome P450 2E1 bound with pilocarpine <sup>33</sup>	-7.1	-6.2	<u>-10.8</u>
3LC4	The complex of human Cytochrome P450 2E1 with Omega-Imidazolyl-Dodecanoic Acid <sup>32</sup>	-7.5	<u>-7</u>	-10.1
3E4E	The human cytochrome P450 2E1 bound to the inhibitor 4-methylpyrazole <sup>34</sup>	-6.6	-5.9	-9.6

**Table no-1 Nonadecanoic acid with COX-2 (4PH9 protein) binding energy and related aminoacids:-**

Ligand Name	PDB Code	Amino acid residue	Nature of Interaction	Binding Distance(Å)	Binding Energy (kcal/mol)
Nonadecanoic acid	4PH9	TYR A:386	Conventional Hydrogen Bond	2.58	-6.1
		THR A:207	Conventional Hydrogen Bond	2.71	
		ALA A:203	Alkyl	5.02	
		ALA A:200	Alkyl	4.85	
		LEU A:391	Alkyl	4.76	
		LEU A:392	Alkyl	5.29, 4.02, 4.46	
		LEU A:409	Alkyl	4.19	
		VAL A:296	Alkyl	4.06	
		LEU A:295	Alkyl	5.30	
		VAL A:445	Alkyl	5.37	
		HIS A:389	Pi-Alkyl	4.65	
PHE A:405	Pi-Alkyl	5.30			





**Tanima Debnath Sarkar et al.,**

**Table no-2 Paracetamol with COX-2 (4PH9 protein) binding energy and related aminoacids:-**

Ligand Name	PDB Code	Amino acid residue	Nature of Interaction	Binding Distance(Å)	Binding Energy (kcal/mol)
Paracetamol	4PH9	ALA A:200	Conventional Hydrogen Bond	2.82	-6.3
		TYR A:386	Conventional Hydrogen Bond	1.92	
		HIS A:387	Pi-Sigma	3.78	
		HIS A:389	Pi –Pi T Shaped	5.17	
		ALA A:203	Pi-Alkyl	5.12	

**Table no-3 Silymarin with COX-2 (4PH9 protein) binding energy and related aminoacids:-**

Ligand Name	PDB Code	Amino acid residue	Nature of Interaction	Binding Distance (Å)	Binding Energy(kcal/mol)
Silymarin	4PH9	ASN A:145	Conventional Hydrogen Bond	2.15	-10.2
		SER A:147	Conventional Hydrogen Bond	3.63	
		ARG A:377	Conventional Hydrogen Bond	3.02	
		GLN A:375	Conventional Hydrogen Bond	3.02	
		LEU A:146	Carbon Hydrogen Bond	4.02	
		ARG B:377	Unfavorable Donor-Donor	2.37	
		SER A:144	Pi -Donor Hydrogen Bond	3.71	
		LEU B:225	Alkyl	4.14	

**Table no-4 Nonadecanoic acid with P-450 (3GPH protein) binding energy and related aminoacids:-**

Ligand Name	PDB Code	Amino acid residue	Nature of Interaction	Binding Distance (Å)	Binding Energy (kcal/mol)
Nonadecanoic acid	3GPH	ASN A:206	Conventional Hydrogen Bond	3.11	-8.1
		VAL A:239	Carbon Hydrogen Bond	3.13	
		ILE A:361	Carbon Hydrogen Bond	3.44	
		PHE A:207	Pi- Sigma	3.87	
		VAL A:365	Alkyl	3.52	
		ILE A:115	Alkyl	4.06	
		LEU A:368	Alkyl	4.79	
		ALA A:299	Alkyl	4.21	
		PHE A:478	Pi-Alkyl	5.19	
				4.68	
		PHE A:298	Pi-Alkyl	4.86	
				4.06	
		PHE A:478	Pi-Alkyl	4.68	







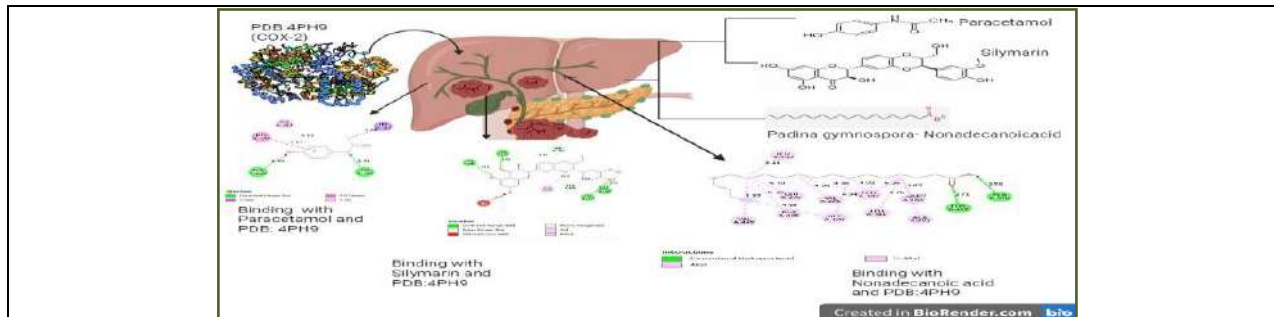
**Tanima Debnath Sarkar et al.,**

**Table no-5 Paracetamol with P-450 (3LC4 protein) binding energy and related aminoacids**

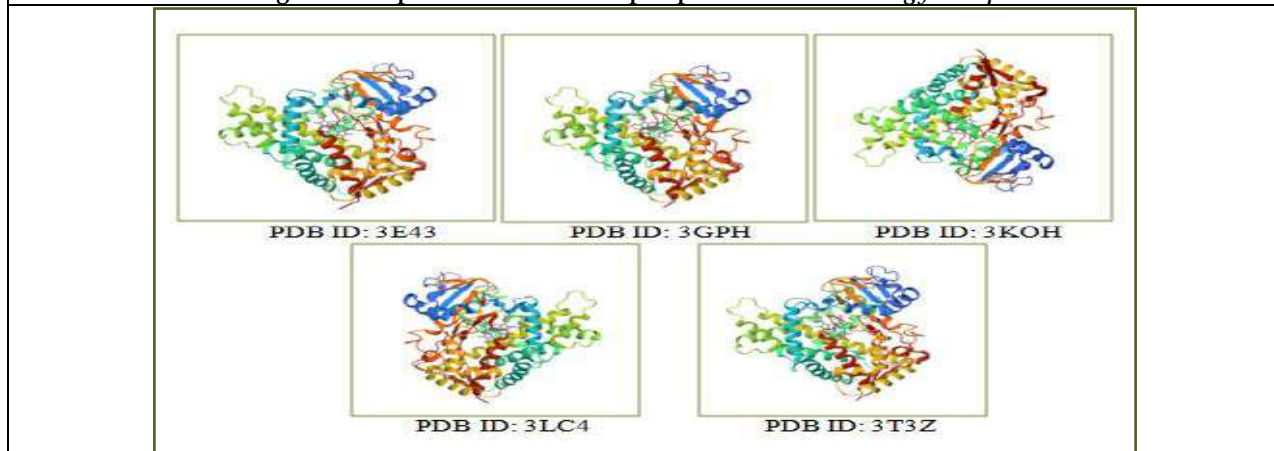
Ligand Name	PDB Code	Amino acid residue	Nature of Interaction	Binding Distance(Å)	Binding Energy (kcal/mol)
Paracetamol	3LC4	ASN A:206	Conventional Hydrogen Bond	3.29	-7
		PHE A:207	Pi-Donor Hydrogen Bond	2.91	
		PHE A:207	Pi-Sigma	3.45	
		PHE A:298	Pi-Pi Stacked	3.90	

**Table no- 6 Silymarin with P-450 (3T3Z protein) binding energy and related aminoacids:-**

Ligand Name	PDB Code	Amino acid residue	Nature of Interaction	Binding Distance (Å)	Binding Energy (kcal/mol)
Silymarin	3T3Z	THR D:307	Conventional Hydrogen Bond	2.07	-10.8
		CYS D:437	Pi-Donor Hydrogen Bond	4.09	
		VAL D:364	Alkyl	3.78	
		LEU D:363	Pi-Alkyl	4.34	
		ALA D:299	Pi-Alkyl	5.28	
		LEU D:368	Pi-Alkyl	4.72	
		ILE D:115	Pi-Alkyl	4.72	
		PHE D:207	Pi-Alkyl	4.84	
		PRO D:429	Pi-Alkyl	4.79	



**Figure :1 Graphical abstract the hepatoprotective of *Padina gymnospora***



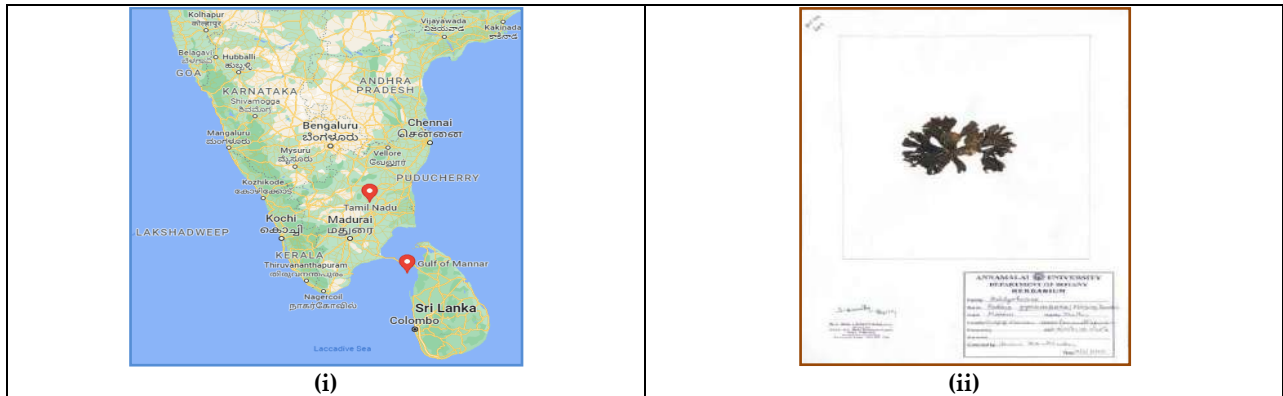
**Figure 2 Types of proteins CYP2E1**







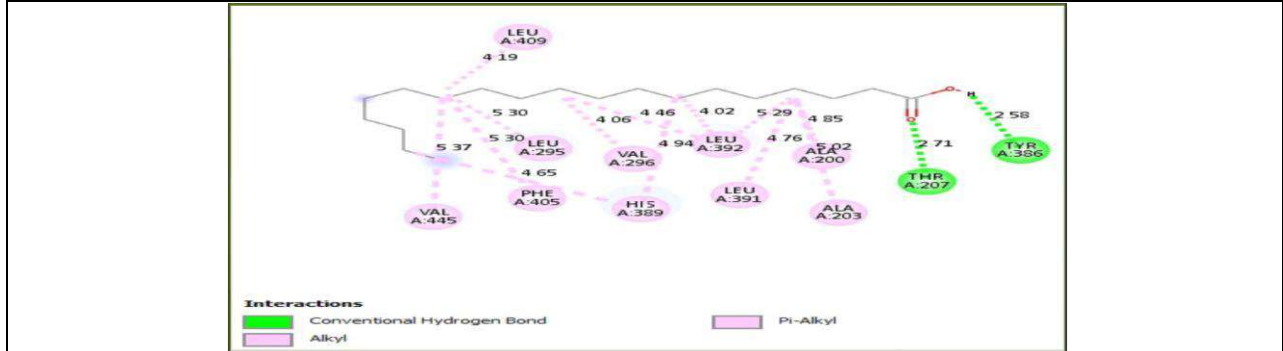
**Tanima Debnath Sarkar et al.,**



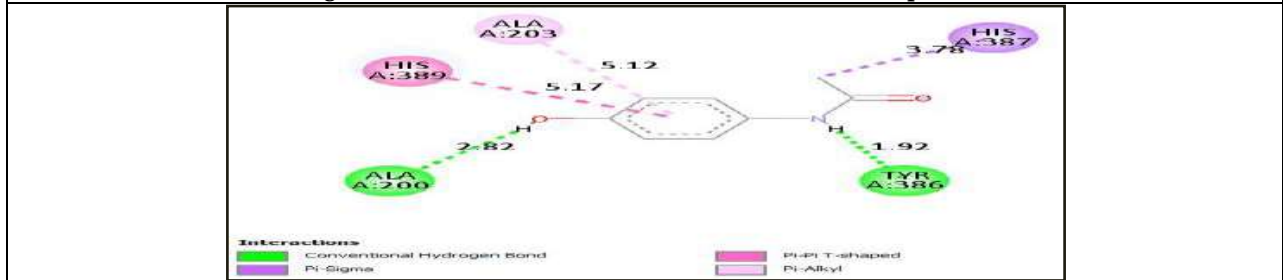
**Figure:2(A) (i) Map:- *Padina gymnospora* founds Gulf of Mannar,Tuticorin located (8.76°42" N; 78.13° 48" E) at Rameswaram in Tamil Nadu in India; (ii) Herbarium sheet-Fan shaped thallus.**



**Figure : 3 Online CB Dock-2 process is showing**



**Figure 4. 2D structure of Nonadecanoic acid with 4PH9 protein**



**Figure 5 . 2D structure of Paracetamol with 4PH9 protein**





Tanima Debnath Sarkar et al.,

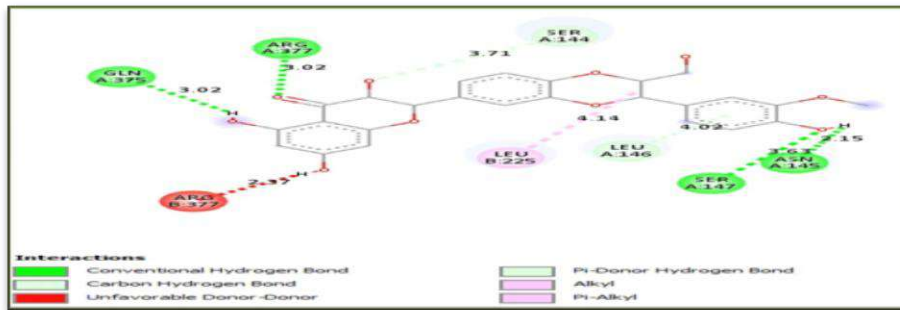


Figure 6. 2D structure of Silymarin with 4PH9 protein

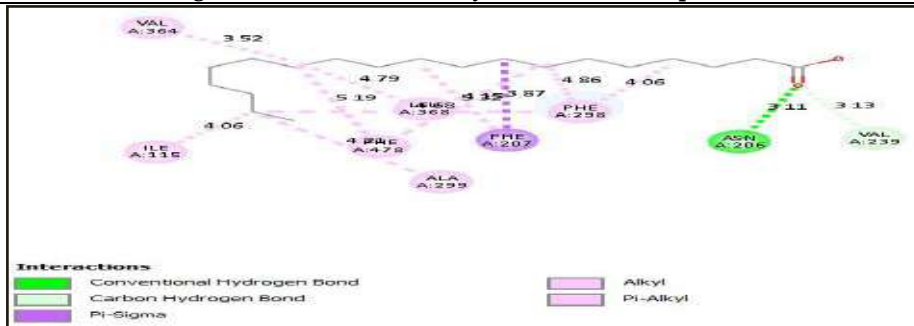


Figure 7. 2D structure of Nonadecanoic acid with 3GPH protein

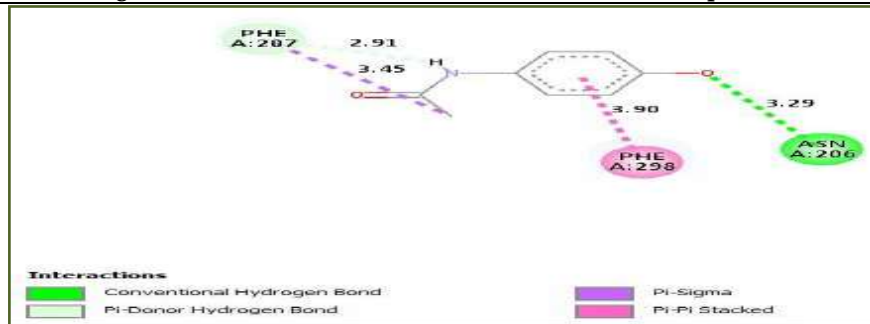


Figure 8. 2D structure of Paracetamol with 3LC4 protein

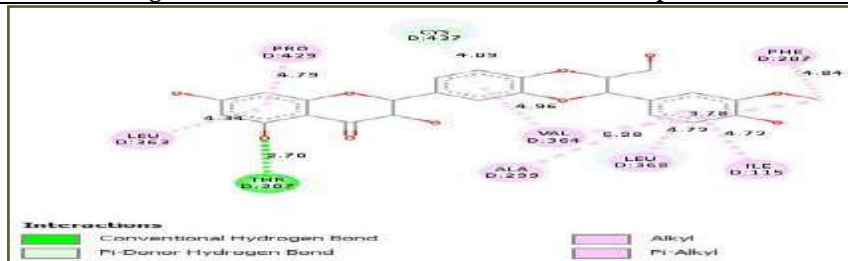


Figure 9. 2D structure of Silymarin with 3T3Z protein





Tanima Debnath Sarkar et al.,

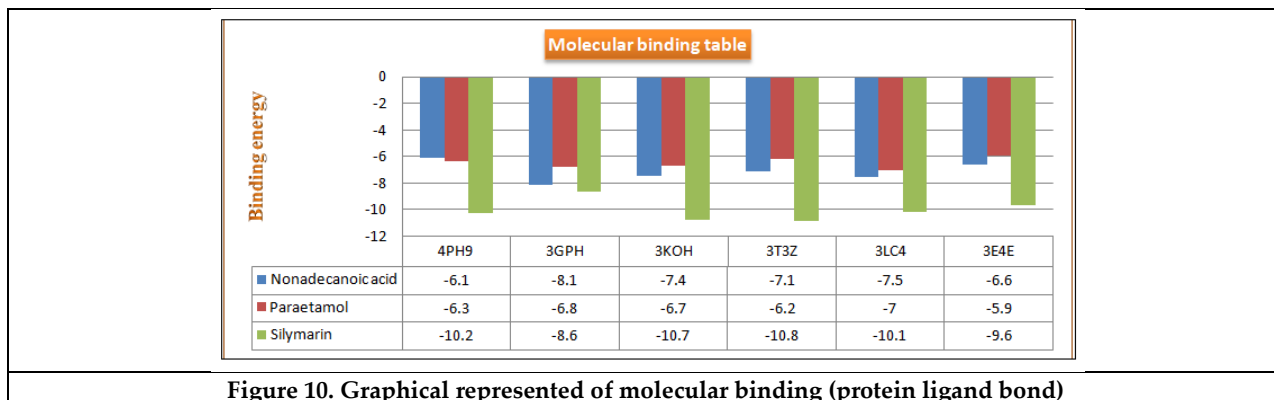


Figure 10. Graphical represented of molecular binding (protein ligand bond)





## Drug Solubility: Importance and Enhancement Strategies

Rajkiran Kolakota<sup>1\*</sup>, Chandaka Haribabu<sup>2</sup>, Pasala Priyanka<sup>2</sup> and Akasapu Sravankumar<sup>2</sup>

<sup>1</sup>Professor, Sri Sivani College of Pharmacy (Affiliated to Jawaharlal Nehru Technological University), Chilakapalem, Srikakulam, Andhra Pradesh, India.

<sup>2</sup>M.Pharm Student, Sri Sivani College of Pharmacy (Affiliated to Jawaharlal Nehru Technological University), Chilakapalem, Srikakulam, Andhra Pradesh, India.

Received: 06 Oct 2024

Revised: 12 Nov 2024

Accepted: 18 Dec 2024

### \*Address for Correspondence

#### Rajkiran Kolakota

Professor, Sri Sivani College of Pharmacy  
(Affiliated to Jawaharlal Nehru Technological University),  
Chilakapalem, Srikakulam, Andhra Pradesh, India.  
E.Mail: rajkiran.kolakota@gmail.com



This is an Open Access Journal / article distributed under the terms of the **Creative Commons Attribution License** (CC BY-NC-ND 3.0) which permits unrestricted use, distribution, and reproduction in any medium, provided the original work is properly cited. All rights reserved.

### ABSTRACT

Solubility, the process of dissolving a solute in a solvent to form a homogeneous mixture, plays a critical role in achieving the desired drug concentration in systemic circulation to elicit the anticipated pharmacological effect. Poor aqueous solubility poses a significant challenge in the formulation of both new chemical entities (NCEs) and generic drugs. Over 40% of NCEs developed by the pharmaceutical industry are practically insoluble in water. The Biopharmaceutical Classification System (BCS) categorizes compounds based on their solubility and permeability. This classification is widely adopted by regulatory authorities and health organizations to utilize dissolution testing as evidence of bioequivalence for substances that are highly soluble and highly permeable. For formulation scientists, improving solubility is a key hurdle, as drugs must exist in a dissolved state at the absorption site for effective uptake. Various approaches, including physical and chemical modifications of the drug and techniques like particle suspension, are employed to enhance the solubility of poorly soluble drugs.

**Keywords:** solubility, chemical, permeable, Classification System.

## INTRODUCTION

Solubility refers to the ability of a solid, liquid, or gaseous substance, known as the solute, to dissolve in a solid, liquid, or gaseous solvent, resulting in a homogeneous solution. The solubility of a substance is primarily influenced by the choice of solvent, as well as factors such as temperature and pressure. It is typically measured by the saturation point, where adding more solute does not increase the concentration of the solution.[1].



**Rajkiran Kolakota et al.,**

In scientific terms, solubility represents the maximum amount of a substance that can dissolve in a specified volume of solvent. It can be described both qualitatively and quantitatively. Qualitatively, solubility is the natural interaction between two or more substances to form a uniform mixture. Quantitatively, it refers to the concentration of the solute in a solvent at a particular temperature, resulting in a homogeneous solution. In pharmaceutical contexts, solubility may be expressed in various units, including percentages, parts per quantity, molarity, molality, mole fraction, or volume fraction. [2]. Solubility plays a crucial role in pharmaceuticals, especially for drugs with poor water solubility, such as those in Biopharmaceutical Classification System (BCS) classes II and IV, which often encounter challenges related to dissolution. [3]. The phenomenon of solubility occurs at dynamic equilibrium, where two opposing processes—dissolution and phase separation (e.g., precipitation)—take place at equal rates. This balance creates a state known as solubility equilibrium. Under specific conditions, the equilibrium solubility can be surpassed, leading to a metastable supersaturated solution.

IUPAC defines solubility as the analytical composition of a saturated solution expressed as a proportion of a designated solute in a designated solvent. Solubility may be stated in units of concentration, molality, mole fraction, mole ratio, and other units [4]. The concept of solubility is applied in various contexts, leading to its expression through multiple measures. Solubility is commonly quantified as a concentration, such as grams of solute per kilogram of solvent, grams per deciliter (100 mL) of solvent, molarity, molality, or mole fraction. The solubility of a substance represents the maximum amount of solute that can dissolve in a given quantity of solvent under specified conditions. This approach is straightforward but can be influenced by other components in the solvent, such as the common ion effect. [5]. For ionic compounds with limited solubility, solubility is often described using solubility constants. This equilibrium-based measure represents the balance between dissolved ions and undissolved salt. Like other equilibrium constants, the solubility constant is temperature-dependent but is generally unaffected by the presence of other species in the solvent. The Biopharmaceutics Classification System (BCS), developed by the U.S. Food and Drug Administration, predicts intestinal drug absorption based on solubility and intestinal permeability. Solubility is determined by the highest-dose strength of an immediate-release product. A drug is classified as highly soluble if its highest dose strength can dissolve in 250 mL or less of aqueous media across a pH range of 1 to 7.5. This volume is based on bioequivalence study protocols where drugs are administered with a standard glass of water to fasting volunteers. [6]

The classification of intestinal permeability is based on comparisons with intravenous administration. These factors are critical since 85% of the most widely sold drugs in the U.S. and Europe are orally administered.

Drugs are categorized into four classes under the BCS:

- **Class I:** High solubility and high permeability
- **Class II:** Low solubility and high permeability
- **Class III:** High solubility and low permeability
- **Class IV:** Low solubility and low permeability

**Significance of Solubility**

Oral drug delivery is the most widely used and convenient route for medication administration due to its ease of use, high patient compliance, cost-effectiveness, minimal sterility requirements, and flexibility in designing dosage forms. Consequently, many generic pharmaceutical companies focus on developing bioequivalent oral drug products. [7]. However, a key challenge in formulating oral dosage forms is achieving optimal bioavailability. Oral bioavailability is influenced by factors such as aqueous solubility, drug permeability, dissolution rate, first-pass metabolism, presystemic metabolism, and susceptibility to efflux mechanisms. Among these, poor solubility and low permeability are the most common causes of reduced bioavailability. [8]. Solubility is not only critical for oral dosage forms but also plays a significant role in other formulations, including parenteral preparations. It is a fundamental parameter for achieving the desired drug concentration in systemic circulation, which is essential for eliciting the intended pharmacological effect. Drugs with poor water solubility often require higher doses to achieve therapeutic plasma concentrations after oral administration. [9]



**Rajkiran Kolakota et al.,**

The development of formulations for poorly water-soluble drugs remains a significant challenge in both new chemical entity (NCE) research and generic drug development. For a drug to be absorbed, it must exist in an aqueous solution at the site of absorption. Since water is the preferred solvent for liquid pharmaceutical formulations, poor aqueous solubility becomes a major hurdle, especially as many drugs are weak acids or weak bases with limited solubility in water. [10]. Over 40% of NCEs developed by the pharmaceutical industry are practically insoluble in water. This low solubility results in slow absorption, inconsistent bioavailability, and sometimes gastrointestinal mucosal toxicity. For orally administered drugs, solubility is often the primary rate-limiting factor in achieving the desired systemic drug concentration for therapeutic action. Addressing solubility issues remains a critical focus for formulation scientists.

Enhancing drug solubility and consequently improving oral bioavailability remains one of the most significant challenges in drug development, particularly for oral delivery systems. Various strategies have been explored and documented in the literature to address the solubility issues of poorly water-soluble drugs. The choice of technique depends on factors such as the physicochemical properties of the drug, the nature of the excipients, and the intended dosage form. Poor solubility and slow dissolution rates in the aqueous gastrointestinal environment often result in inadequate bioavailability for such drugs. This issue is particularly relevant for Biopharmaceutics Classification System (BCS) Class II drugs, which are characterized by low solubility but high permeability. For these drugs, the rate-limiting factor is not absorption but rather drug release from the dosage form and solubility in gastric fluids. Therefore, enhancing solubility and dissolution rates can significantly improve the bioavailability of BCS Class II compounds. [10]. Low-solubility drugs pose several challenges, including poor absorption and bioavailability, limited solubility for intravenous administration, prolonged development timelines, increased costs, and a higher dosing burden on patients, often requiring frequent administration of large doses. Addressing these solubility challenges is crucial for the efficient development of effective and patient-friendly drug formulations.

### **Methods to Enhance Solubility**

Solubility improvement techniques can be categorized into physical modification, chemical modifications of the drug substance, and other techniques.

#### **Physical Modifications**

Particle size reduction like micronization and nanosuspension, modification of the crystal habit like polymorphs, amorphous form and cocrystallization, drug dispersion in carriers like eutectic mixtures, solid dispersions, solid solutions and cryogenic techniques.

#### **Chemical Modifications**

Change of pH, use of buffer, derivatization, complexation, and salt formation.

#### **Miscellaneous Methods**

Supercritical fluid process, use of adjuvant like surfactant, solubilizers, cosolvency, hydrotrophy, and novel excipients.

#### **Particle Size Reduction**

The solubility of a drug is closely linked to its particle size. Reducing particle size increases the surface area, which enhances the drug's dissolution properties. For poorly soluble drugs, particle size reduction often correlates with improved bioavailability. Techniques such as milling, using tools like colloid mills and jet mills, are commonly employed to reduce particle size. However, while these methods improve dissolution rates, they do not alter the drug's saturation solubility, making them unsuitable for drugs with a high dose number. Particle size reduction can also be achieved through advanced techniques like nanosuspension and micronization. [11]







Rajkiran Kolakota et al.,

### Micronization

Micronization involves reducing the particle size to enhance the dissolution rate of drugs by increasing the surface area of the particles. However, it does not increase the equilibrium solubility. By decreasing particle size, the rate of dissolution improves, leading to better absorption and bioavailability. This technique has been applied to drugs such as progesterone, fenofibrate, griseofulvin, spironolactone, and diosmin, resulting in enhanced bioavailability, improved digestive absorption, and greater clinical efficacy. [12]

### Modification of Crystal Habit

Crystal habit modification involves altering the solid-state forms of drugs, including polymorphs and pseudopolymorphs:

**Polymorphs:** These are different crystalline forms of the same drug, characterized by distinct arrangements in the crystal lattice. While chemically identical, polymorphs exhibit different physicochemical properties, such as melting point, density, solubility, stability, and texture.

**Pseudopolymorphs:** These refer to solvates or hydrates, where solvents are incorporated into the crystal lattice. Amorphous forms of drugs, which lack a well-defined crystalline structure, often exhibit better solubility and dissolution rates compared to crystalline forms. This is due to their higher surface area and greater associated energy. The solubility hierarchy for solid drug forms is typically as follows:

**Amorphous > Metastable Polymorphs > Stable Polymorphs**

### Solid Dispersion

The concept of solid dispersions was first introduced by Sekiguchi and Obi in the 1960s when they explored the dissolution and performance of eutectic mixtures of sulfonamide drugs with water-soluble carriers. Solid dispersion is a versatile pharmaceutical approach to enhance the dissolution rate, absorption, and therapeutic efficacy of poorly water-soluble drugs in dosage forms. Solid dispersions consist of at least two components: a hydrophilic matrix and a hydrophobic drug. Common hydrophilic carriers used in solid dispersions include polyvinylpyrrolidone (PVP), polyethylene glycols (PEGs), and Pladone-S630. Surfactants such as Tween-80, docusate sodium, Myrj-52, Pluronic-F68, and sodium lauryl sulfate (SLS) are also incorporated into these formulations to enhance performance. [13]. The solubility of drugs like celecoxib, halofantrine, and ritonavir has been improved using solid dispersion techniques. For instance, celecoxib with PVP and ritonavir with Gelucire have demonstrated increased aqueous solubility. Key techniques for preparing solid dispersions include:

- **Fusion Method:** In this approach, the hydrophilic carrier is heated above its melting point, and the drug is incorporated into the molten carrier with continuous stirring. The mixture is then cooled to allow the drug to be evenly dispersed throughout the matrix.
- **Solvent Evaporation Method:** The drug and carrier are dissolved in an appropriate organic solvent. The solvent is then evaporated under vacuum and elevated temperatures to yield a solid residue containing the dispersed drug.

### Nanosuspension[14]

Nanosuspension technology has emerged as a promising strategy for the effective delivery of hydrophobic drugs, especially those insoluble in both water and oils. A nanosuspension is a biphasic system composed of nanometer-sized drug particles stabilized by surfactants, and it is suitable for oral, topical, parenteral, and pulmonary administration. The solid particles in a nanosuspension typically have a particle size of less than one micron, with an average size ranging from 200 to 600 nm. Various techniques for the preparation of nanosuspensions include:

**Precipitation Technique:** Involves reducing the drug particle size by precipitation in a suitable solvent system.





Rajkiran Kolakota *et al.*,

**Media Milling:** Utilizes high-energy milling to achieve nano-sized particles.

**High-Pressure Homogenization in Water:** Drug particles are reduced to the nanoscale by applying high pressure in an aqueous medium.

**High-Pressure Homogenization in Nonaqueous Media:** The same process is applied using nonaqueous media for drugs with special stability requirements.

**Combination of Precipitation and High-Pressure Homogenization:** Combines the benefits of both techniques to achieve optimal particle size and stability.

Nanosuspension technology addresses the challenges of poor solubility and enhances the bioavailability of hydrophobic drugs, offering versatility across different routes of administration.

### Supercritical Fluid (SCF) Process[15]

The supercritical fluid (SCF) process is an innovative nanosizing and solubilization technique that has gained significant attention in recent years for particle size reduction. A supercritical fluid is defined as a substance at a temperature and pressure above its critical point, allowing it to exhibit the combined properties of gases and liquids. At near-critical temperatures, SCFs become highly compressible, enabling slight changes in pressure to significantly alter their density and mass transport characteristics, which are crucial in determining their solvent capabilities.

In SCF processes, drug particles are dissolved in a supercritical fluid, most commonly carbon dioxide, and subsequently recrystallized into much smaller sizes. This technique offers precision and flexibility, allowing for the production of drug particles with sizes in the submicron range. Current SCF technologies are capable of producing nanoparticulate suspensions with particle sizes ranging from 5 to 2,000 nm.

Several pharmaceutical companies, such as Nektar Therapeutics and Lavipharm, specialize in using SCF technologies for particle size reduction and solubility enhancement. Various SCF techniques have been developed to optimize specific aspects of the process, including:

- Precipitation with Compressed Antisolvent Process (PCA)
- Solution-Enhanced Dispersion by SCF (SEDS)
- Supercritical Antisolvent Process (SAS)
- Rapid Expansion of Supercritical Solutions (RESS)
- Gas Antisolvent Recrystallization (GAS)
- Aerosol Supercritical Extraction System (ASES)

These methods enhance solubility and dissolution rates by producing uniform particles with improved bioavailability.

### Cryogenic Techniques[16,17]

Cryogenic techniques are advanced methods aimed at improving the dissolution rate of drugs by creating nanostructured amorphous particles with high porosity under extremely low-temperature conditions. These techniques utilize various cryogenic injection devices, including capillary, rotary, pneumatic, and ultrasonic nozzles. Depending on the system design, the nozzles may be positioned above or below the liquid level, and the cryogenic liquids employed can include hydrofluoroalkanes, nitrogen (N<sub>2</sub>), argon (Ar), oxygen (O<sub>2</sub>), or organic solvents.

Following cryogenic processing, the resulting dry powders are typically obtained through drying processes such as spray freeze drying, atmospheric freeze drying, vacuum freeze drying, or lyophilization.

Key cryogenic techniques include:

1. **Spray Freezing onto Cryogenic Fluids:** A process where the drug is atomized into cryogenic fluids to create nanostructured particles.
2. **Spray Freezing into Cryogenic Liquids (SFL):** The drug solution is sprayed directly into a cryogenic liquid to rapidly solidify the particles.





Rajkiran Kolakota *et al.*,

3. **Spray Freezing into Vapor over Liquid (SFV/L):** Drug particles are formed by spraying into the vapor phase above a cryogenic liquid.
4. **Ultra-Rapid Freezing (URF):** This technique uses extremely rapid cooling rates to produce highly porous, nanostructured drug particles.

Cryogenic methods offer significant advantages for enhancing solubility and dissolution by reducing particle size and increasing surface area, making them an effective approach for poorly water-soluble drugs.

#### **Inclusion Complex Formation-Based Techniques[18]**

Inclusion complex formation is a widely utilized method for enhancing the aqueous solubility, dissolution rate, and bioavailability of poorly water-soluble drugs. This technique involves the encapsulation of a nonpolar molecule or its nonpolar region (the guest) into the cavity of another molecule or group of molecules (the host). Cyclodextrins are the most commonly used host molecules in this process. Cyclodextrins (CDs) are cyclic oligomers produced through the enzymatic degradation of starch by cyclodextrin-glycosyltransferase (CGT). The three naturally occurring types of cyclodextrins are  $\alpha$ -Cyclodextrin,  $\beta$ -Cyclodextrin, and  $\gamma$ -Cyclodextrin. While the hydrophilic exterior of cyclodextrins makes them soluble in water, their hydrophobic cavities provide an ideal microenvironment for accommodating nonpolar molecules. Several techniques have been developed to prepare inclusion complexes of poorly water-soluble drugs with cyclodextrins, including:

1. **Kneading Method:** Mixing the drug and cyclodextrin in a small amount of solvent to form a paste, followed by drying.
2. **Lyophilization/Freeze-Drying Technique:** Dissolving both the drug and cyclodextrin in a suitable solvent, freezing the solution, and removing the solvent by sublimation.
3. **Microwave Irradiation Method:** Using microwave energy to facilitate the formation of inclusion complexes by heating and mixing the drug and cyclodextrin in a solvent.

#### **Micellar Solubilization[19]**

Micellar solubilization is one of the oldest and most fundamental techniques for improving the solubility and dissolution rates of poorly soluble drugs. This method involves the use of surfactants to reduce surface tension, which enhances the dissolution of lipophilic drugs in aqueous media. Surfactants are also employed to stabilize suspensions of drugs and improve the wetting of solid drug particles. When the concentration of surfactants exceeds their critical micelle concentration (CMC), which typically ranges from 0.05% to 0.10%, micelles form. These micelles can encapsulate poorly soluble drugs within their hydrophobic cores, significantly enhancing solubility. In addition, surfactants aid in the disintegration of solid drug particles into finer particles, further improving dissolution rates.

Common nonionic surfactants used in micellar solubilization include:

- Polysorbates
- Polyoxyethylated castor oil
- Polyoxyethylated glycerides
- Lauroyl macroglycerides
- Mono- and di-fatty acid esters of low molecular weight polyethylene glycols

Surfactants are also frequently used to stabilize microemulsions and suspensions, which serve as carriers for solubilized drugs. Examples of poorly soluble drugs that have benefited from micellar solubilization include antidiabetic medications such as gliclazide, glyburide, glimepiride, glipizide, repaglinide, pioglitazone, and rosiglitazone. This technique has proven effective in improving the bioavailability and therapeutic efficacy of such compounds.





Rajkiran Kolakota et al.,

### Hydrotropy[20]

Hydrotropy is a solubilization technique in which the addition of a large quantity of a second solute, known as a hydrotropic agent, enhances the aqueous solubility of a poorly soluble substance. Hydrotropic agents are typically ionic organic salts, often composed of alkali metal salts of various organic acids. These agents either increase solubility in a solvent ("salting in") or decrease it ("salting out"). Salts with large anions or cations that are highly soluble in water can lead to the "salting in" of non-electrolytes, a phenomenon referred to as "hydrotropism." Hydrotropy thus describes the enhancement of solubility in water through the presence of a significant amount of additives. The mechanism underlying hydrotropy involves weak interactions, such as complexation, between the hydrotropic agents (e.g., sodium benzoate, sodium acetate, sodium alginate, urea) and the poorly soluble drugs. Hydrotropes are known to self-assemble in solution, contributing to their solubilization effect.

Classifying hydrotropes based on molecular structure is challenging because a wide range of compounds exhibit hydrotropic behavior. Common examples include:

- **Alcohols:** Ethanol, resorcinol, pyrogallol, catechol
- **Aromatic alcohols:**  $\alpha$ - and  $\beta$ -naphthols, salicylates
- **Alkaloids:** Caffeine, nicotine
- **Ionic surfactants:** Diacids, sodium dodecyl sulfate (SDS), dodecylated oxidibenzene

Among these, aromatic hydrotropes with anionic head groups are the most extensively studied. Their efficacy is often attributed to the interactive  $\pi$  ( $\pi$ ) orbitals available in their structure. Conversely, hydrotropes with cationic hydrophilic groups are rare, but examples include salts of aromatic amines such as procaine hydrochloride. In addition to improving solubility, hydrotropes influence surfactant behavior by enhancing micelle formation, altering the phase behavior of multicomponent systems, and affecting nanodispersions, conductance percolation, surfactant clouding, and polymer interactions. These diverse effects make hydrotropy a valuable tool in the development of solubility-enhancing formulations.

### Crystal Engineering[21,22]

The surface area of a drug available for dissolution is influenced by its particle size and its ability to be wetted by luminal fluids. The particle size, which directly affects the dissolution rate of the drug, is determined by crystallization conditions or methods such as impact milling and fluid energy milling. Comminution techniques can produce particles that are highly heterogeneous, charged, and cohesive, potentially causing issues in downstream processing and product performance. To address these challenges, crystal engineering techniques have been developed to enable the controlled crystallization of drugs, resulting in high-purity powders with well-defined particle size distribution, crystal habit, crystal form (either crystalline or amorphous), surface characteristics, and surface energy. By manipulating crystallization conditions—such as altering solvents, changing stirring rates, or adding other components to the drug solution—it is possible to prepare crystals with different packing arrangements. These different forms are called polymorphs.

Crystal engineering provides various routes to improve solubility and dissolution rates through a deep understanding of crystallization processes and the molecular properties of active pharmaceutical ingredients. The process often involves dissolving the drug in a solvent and controlling its precipitation to produce nanoparticles, typically through the addition of an antisolvent (commonly water). Pharmaceutical cocrystals represent a significant advancement in addressing the solubility issues of poorly soluble drugs. These cocrystals consist of two or more distinct molecules arranged to create a new crystal form with properties superior to those of the separate entities. Pharmaceutical cocrystals are formed between a molecular or ionic drug and a cocrystal former that remains solid under ambient conditions. Cocrystals are typically prepared through slow evaporation from a drug solution containing stoichiometric amounts of the components (cocrystal formers), although other methods such as sublimation, melt growth, or grinding in a ball mill are also viable.



**Rajkiran Kolakota et al.,**

Traditional crystallization techniques, such as sublimation, crystallization from solutions, evaporation, thermal treatment, desolvation, grinding, and milling, continue to be employed alongside other methods like salt formation, altering the dielectric constant of solvents, chemical modification, the use of hydrates or solvates, soluble prodrugs, and application of ultrasonic waves or spherical crystallization, to enhance the solubility of poorly water-soluble drugs.

## CONCLUSION

In this review paper, we emphasize that the solubility of a molecule is fundamental and plays a crucial role in pharmaceutical formulation and development. The rate of oral absorption of weakly water-soluble drugs is primarily influenced by drug dissolution, making solubility an essential factor in the formulation and development of various dosage forms. The techniques discussed can be used individually or in combination to enhance the solubility of drugs. The proper selection of a solubility enhancement method is vital to achieving key formulation goals such as improved oral bioavailability, reduced dosing frequency, enhanced patient compliance, and cost-effective production. The choice of solubility enhancement method depends on several factors, including the drug's characteristics—such as solubility, chemical nature, melting point, absorption site, and pharmacokinetic behavior. Additionally, the method must align with the dosage form requirements (e.g., tablet or capsule, immediate or modified release), and meet regulatory standards regarding excipient use, maximum daily dose, approved excipients, and analytical accuracy.

## REFERENCES

1. L. Lachman, H. Lieberman, and J. L. Kanig, *The Theory And Practise of Industrial Pharmacy*, Lea & Febiger, 3rd edition, 1986.
2. Kshirsagar S, Choudhari M, Sathyan R, Dhore S. Solubility Enhancement by Various Techniques based on Pharmaceutical and Medicinal Chemistry Approach: An Overview. *Asian Journal of Pharmacy and Technology*, 2019; 9(2): 141-146.
3. P. B. Myrdal and S. H. Yalkowsky, "Solubilization of drugs in aqueous media," in *Encyclopedia of Pharmaceutical Technology*, J. Swarbrick, Ed., p. 3311, Informa Health Care, New York, NY, USA,, 3rd edition, 2007. View at: Google Scholar
4. M. Aulton, "Dissolution and solubility," in *Pharmaceutics: The Science of Dosage form Design*, M. E. Aulton, Ed., p. 15, Churchill Livingstone, 2nd edition, 2002. View at: Google Scholar
5. The United States Pharmacopeia, USP 30-NF 25, 2007.
6. British Pharmacopoeia, 2009.
7. K. H. Edward and D. Li, "Solubility," in *Drug Like Properties: Concept, Structure, Design and Methods, from ADME to Toxicity Optimization*, p. 56, Elsevier, 2008. View at: Google Scholar
8. V. R. Vemula, V. Lagishetty, and S. Lingala, "Solubility enhancement techniques," *International Journal of Pharmaceutical Sciences Review and Research*, vol. 5, no. 1, pp. 41–51, 2010. View at: Google Scholar
9. D. Sharma, M. Soni, S. Kumar, and G. D. Gupta, "Solubility enhancement—eminent role in poorly soluble drugs," *Research Journal of Pharmacy and Technology*, vol. 2, no. 2, pp. 220–224, 2009. View at: Google Scholar
10. A. Kumar, S. K. Sahoo, K. Padhee, P. S. Kochar, A. Sathapathy, and N. Pathak, "Review on solubility enhancement techniques for hydrophobic drugs," *Pharmacie Globale*, vol. 3, no. 3, pp. 001–007, 2011. View at: Google Scholar
11. Loh ZH, Samanta AK, Heng PWS. Overview of milling techniques for improving the solubility of poorly water-soluble drugs. *Asian journal of pharmaceutical sciences*, 2015; 10(4): 255-274.
12. Kasimedu S, Thoppani SR, Pommala N, Orugonda G, Yelamanda J. A Review on Solubility Enhancement Techniques. *J. Compr. Pharma*, 2015; 2(2): 36-41.
13. Patel BB, Patel JK, Chakraborty S, Shukla D. Revealing facts behind spray dried solid dispersion technology used for solubility enhancement. *Saudi Pharmaceutical Journal*, 2015; 23(4): 352-365.



**Rajkiran Kolakota et al.,**

14. V. B. Patravale, A. A. Date, and R. M. Kulkarni, "Nanosuspensions: a promising drug delivery strategy," *Journal of Pharmacy and Pharmacology*, vol. 56, no. 7, pp. 827–840, 2004. View at: [Publisher Site](#) | [Google Scholar](#)
15. L. Manna, M. Banchero, D. Sola, A. Ferri, S. Ronchetti, and S. Sicardi, "Impregnation of PVP microparticles with ketoprofen in the presence of supercritical CO<sub>2</sub>," *Journal of Supercritical Fluids*, vol. 42, no. 3, pp. 378–384, 2007. View at: [Publisher Site](#) | [Google Scholar](#)
16. H. Leuenberger, "Spray freeze-drying—the process of choice for low water soluble drugs?" *Journal of Nanoparticle Research*, vol. 4, no. 1-2, pp. 111–119, 2002. View at: [Publisher Site](#) | [Google Scholar](#)
17. M. Mumenthaler and H. Leuenberger, "Atmospheric spray-freeze drying: a suitable alternative in freeze-drying technology," *International Journal of Pharmaceutics*, vol. 72, no. 2, pp. 97–110, 1991. View at: [Publisher Site](#) | [Google Scholar](#)
18. X. Wen, F. Tan, Z. Jing, and Z. Liu, "Preparation and study the 1:2 inclusion complex of carvedilol with  $\beta$ -cyclodextrin," *Journal of Pharmaceutical and Biomedical Analysis*, vol. 34, no. 3, pp. 517–523, 2004. View at: [Publisher Site](#) | [Google Scholar](#)
19. C. D. Rangel-Yagui, A. Pessoa, and L. C. Tavares, "Micellar solubilization of drugs," *Journal of Pharmacy and Pharmaceutical Sciences*, vol. 8, no. 2, pp. 147–163, 2005. View at: [Google Scholar](#)
20. A. A. Badwan, L. K. El Khordagui, A. M. Saleh, and S. A. Khalil, "The solubility of benzodiazepines in sodium salicylate solution and a proposed mechanism for hydrotropic solubilization," *International Journal of Pharmaceutics*, vol. 13, no. 1, pp. 67–74, 1983. View at: [Publisher Site](#) | [Google Scholar](#)
21. S. V. Patil and S. K. Sahoo, "Pharmaceutical overview of spherical crystallization," *Der Pharmacia Lettre*, vol. 2, no. 1, pp. 421–426, 2010. View at: [Google Scholar](#)
22. N. Blagden, M. de Matas, P. T. Gavan, and P. York, "Crystal engineering of active pharmaceutical ingredients to improve solubility and dissolution rates," *Advanced Drug Delivery Reviews*, vol. 59, no. 7, pp. 617–630, 2007. View at: [Publisher Site](#) | [Google Scholar](#)







## High Performance Liquid Chromatography for the Development and Validation of Meropenem and Vaborbactam

Mounik Sai Kumar N<sup>1</sup>, Chiranjeevi Ponnamm<sup>2\*</sup>, Sridevi Ranjitha Karanam<sup>3</sup> and CH.Nooka Raju<sup>4</sup>

<sup>1</sup>M.Pharm Student, Department of Pharmaceutical Analysis, Vignan Institute of Pharmaceutical Technology, (Affiliated to Jawaharlal Nehru Technological University), Visakhapatnam, Andhra Pradesh, India

<sup>2,3</sup>Associate Professor, Department of Pharmaceutical Analysis, Vignan Institute of Pharmaceutical Technology, (Affiliated to Jawaharlal Nehru Technological University), Visakhapatnam, Andhra Pradesh, India

<sup>4</sup>Department of Radiology, Centurion University of Technology and Management, Vizianagaram, Andhra Pradesh, India.

Received: 06 Oct 2024

Revised: 10 Nov 2024

Accepted: 12 Dec 2024

### \*Address for Correspondence

#### Chiranjeevi Ponnamm

M.Pharm Student, Department of Pharmaceutical Analysis,  
Vignan Institute of Pharmaceutical Technology,  
(Affiliated to Jawaharlal Nehru Technological University),  
Visakhapatnam, Andhra Pradesh, India  
E.Mail: ponnamm107@gmail.com



This is an Open Access Journal / article distributed under the terms of the **Creative Commons Attribution License** (CC BY-NC-ND 3.0) which permits unrestricted use, distribution, and reproduction in any medium, provided the original work is properly cited. All rights reserved.

### ABSTRACT

Meropenem and vaborbactam were analyzed and quantified using a reverse-phase high-performance liquid chromatography (RP-HPLC) technology that was developed and verified to be quick, sensitive, and reliable. A photodiode array (PDA) detector Waters HPLC system was used for the analysis. Using an Inertsil ODS C18 column (250 × 4.6 mm, 5 μm) at a flow rate of 1.0 mL/min, chromatography was performed. The detection was carried out at a wavelength of 252 nm, and the mobile phase was a degassed combination of methanol and buffer (80:20, v/v). Vaborbactam had a retention duration of 6.691 minutes, whilst Meropenem showed a retention time of 4.713 minutes. ICH guidelines were followed in the rigorous testing of each of these parameters: System Suitability, Specificity, LOD & LOQ, Linearity, Recovery, Precision, Ruggedness, and Robustness

**Keywords:** Meropenem, Vaborbactam, RP-HPLC, Method Development, Validation.





Mounik Sai Kumar et al.,

## INTRODUCTION

Patient safety is seriously at stake due to the alarming rate at which the overall danger of antibiotic resistance is growing. The World Health Organization (WHO) has named carbapenem-resistant Enterobacteriaceae (CRE) as one of the three most important infections that require the development of new antibiotic treatments, and the Centers for Disease Control and Prevention has designated CRE as a "urgent" danger [1–3]. In the past, patients with invasive CRE infections have had up to 70% mortality rates. This emphasizes how urgently new therapeutic alternatives must be found and developed, especially for gram-negative bacteria. The FDA recently approved Meropenem-Vaborbactam (Vabomere™), a carbapenem antibiotic and a first-in-class  $\beta$ -lactamase inhibitor based on boronic acid, to treat complex urinary tract infections, including pyelonephritis, in response to this urgent need [4]. The molecular name for meropenem is (4R,5S,6S)-3-(((3S,5S)6-((R)-1-hydroxyethyl)-5-(dimethylcarbamoyl)pyrrolidin-3-yl)thio)4-methyl-7-oxo-1-azabicyclo[3.2.0]heptane-2-sulfur-to-carbon substitution at position 1 and an unsaturated link between C2 and C3 in the penicillin core structure (Fig. 1a) are two important structural characteristics that hept-2-ene-2-carboxylic acid, a carbapenem antibiotic, shares with other medications in this family [5]. The action of Meropenem against gram-negative bacteria is increased by the dimethyl-carbamoylpyrrolidinethio side chain at position C2. Meropenem, like other carbapenems, inhibits the formation of cell walls by attaching itself to penicillin-binding proteins (PBPs). Meropenem may offer a stronger antibacterial backbone than cephalosporins when used with carbapenemase inhibitors.

The molecular name for vaborbactam is (3R,6S)-2-Hydroxy-3-[2-(thiophen-2-yl)acetamido]-6-oxo-1-azabicyclo[3.2.0]heptane-2-sulfur-to-carbon substitution at position 1 and an unsaturated link between C2 and C3 in the penicillin core structure (Fig. 1a) are two important structural characteristics that hept-2-ene-2-carboxylic acid, a carbapenem antibiotic, shares with other medications in this family [5]. When it comes to *Klebsiella pneumoniae* carbapenemase (KPC), VAB is especially effective. A conformation that preferentially increases its action against  $\beta$ -lactamases is designed into its cyclic boronate ester structure. By adding a 2-thienyl acetyl group, Vaborbactam's efficiency as a  $\beta$ -lactamase inhibitor is increased and its potency is further enhanced [6]. Vaborbactam mainly targets class A and C  $\beta$ -lactamase enzymes, such as the *Serratia marcescens* enzyme and those that cause imipenem resistance [7]. Figures 1 and 2 depict the structures of vaborbactam and meropenem.

## MATERIALS AND METHODS

### Materials and Reagents

On the day of preparation, meropenem and vaborbactam were obtained, the solutions were made, well-protected from the effects of light, and analyzed. The glassware used in the procedure was carefully cleaned using a solution of sulfuric and chromic acids, rinsed with double-distilled water, and then dried in a hot air oven. Analytical-reagent (AR) grade reagents were utilized. Acetonitrile, Methanol HPLC Grade, and Buffer (KH<sub>2</sub>PO<sub>4</sub>) HPLC Grade were purchased from Merck, India.

### Instrumentation

Reversed-phase high-performance liquid chromatography (RP-HPLC) was used for the chromatographic analysis on a Waters Model 2690/5 Series Compact System that had an Inertsil-C18 ODS column installed. A Rheodyne injector with a 20  $\mu$ L loop made up the sample injection apparatus. Empower 2.0 software was used to record and evaluate the data. An electronic scale (SARTORIUS) was utilized for the purpose of weighing, and the medication and sample solutions were sonicated using a sonicator (FAST CLEAN).

### Chromatographic Conditions

Using a mobile phase composition of 80:20 V/V with acetonitrile and methanol at a flow rate of 1.0 ml/min, the analyte separation was performed on the Inertsil-ODS C18 (250  $\times$  4.6 mm, 5) column. The eluents were detected at 252 nm with an injection volume of 20  $\mu$ L. A room temperature of 30°C was used for the chromatographic analysis.





Mounik Sai Kumar *et al.*,

#### Preparation of Buffer(KH<sub>2</sub>PO<sub>4</sub> 0.1 M)

3.8954 grams of di-sodium hydrogen phosphate and 3.4023 grams of potassium dihydrogen phosphate should dissolve completely in a beaker filled with 1000 milliliters of pure water. After that, the pH is adjusted using orthophosphoric acid and passed through a 0.45µm membrane filter.

#### Solution for Stocks Preparation

Reference solution: In two 100.0 mL volumetric flasks, 20.0 mg of Meropenem and 25.0 mg of Vaborbactam were dissolved in a mobile process, and the mixture was then sonicated for 20 minutes each. Put 10.0 mL of each of the previously indicated solutions into a 50.0 mL volumetric flask, mix with the mobile phase for 10 minutes, and then sonicate.

#### Standard Working Solution Preparation

Together with Meropenem and Vaborbactam, stock solutions ranging from 20 ppm to 80 ppm for both medications were created, sonicated, and filtered through a 0.45 membrane.

#### Method Validation

Following the ICH recommendations, the procedure was validated under optimal chromatographic conditions [17–21]. Stability, specificity, recovery, linearity, accuracy, precision, robustness, robustness LOD, and LOQ were all validated for the parameter system suitability test.

## RESULTS

#### Optimization of chromatographic condition

The UV spectra of Meropenem and Vaborbactam showed a significant absorption at 252 nm, which was chosen as the analytical wavelength. Numerous combinations were tested using varying acetonitrile and methanol compositions as the mobile phase. To resolve Meropenem and Vaborbactam and to achieve appropriate retention durations and peak symmetry, preliminary experiments were conducted using various mixtures of acetonitrile and methanol. In order to get acceptable system compatibility characteristics, a mobile phase comprising 80:20 V/V with methanol and buffer, Inertsil-ODS C18 (250 x 4.6 mm, 5) column was finally chosen. We experimented with flow rates ranging from 0.5 to 1.2 ml/min. A flow rate of 1.0 ml/min was proved to be better as with both drugs have retention time less than 10 min. The optimized chromatogram Figure. 3 The retention time of Meropenem and Vaborbactam were found to be 4.713 and 6.691 min respectively.

#### Method Validation

##### System Suitability Test

System suitability parameters for the new method were calculated from the optimized chromatographic settings and compared with suggested limits. Table 1 illustrated the method's system suitability parameters. The findings showed that the approach was appropriate for the analysis and that all of the system suitability parameters fell within the suggested ranges.

##### Linearity

A range of solutions with concentration levels ranging from 20 ppm to 80 ppm of the target concentration are created using the working standards for vaborbactam and meropenem. The device's linear fit was illustrated graphically. Table 2 presents the results (a-b). In Figure 4(a-b), the linearity curve was displayed.





**Mounik Sai Kumar et al.,**

### Repeatability(Repetition)

- a. System precision (system precision): Five injections of a standard solution were made using the test procedure.
- b. Technique precision (precision process): Each solution was injected separately, and six sample preparations were generated independently using a single test procedure.

The results of the tests show that the research technique is valid. The accuracy of the system and technique may be found in Tables 3-5.

### Intermediate accuracy (variable analyst):

Two analysts conducted a test technique analysis. Both the individual percentage assays and the percentage RSD of the assay pass the intermediate accuracy test and fall within the allowed range. Table 5(i-ii).

### Recovery

An accuracy investigation was carried out. Using the test method in triplicate, with an equivalent amount of Meropenem and Vaborbactam in each volumetric flask for each spike level, the concentration of Meropenem and Vaborbactam equal to 50%, 100%, and 150% of the labeled quantity was ascertained. Meropenem and Vaborbactam's average recovery rate was determined.

$$\% \text{ Recovery} = \frac{\text{Amount found}}{\text{Amount added}} \times 100$$

The findings of the recovery show that the test procedure has an appropriate degree of precision. Refer Table 6.

### Ruggedness

A study on system-to-system variability was conducted on many HPLC systems under comparable conditions and at different times. The test protocol called for the production and analysis of six samples. It is evident from comparing the two tests conducted on two distinct HPLC systems that the assay test process is unaffected by system variability. The RSD percentage was judged to be inside the mark. Refer to Tables 3 and 7.

### Robustness

#### The Impact of Flux Rate Variation:

An investigation of the effects of flux rate variation was carried out. At flow rates of 1.0 and 1.2 milliliters per minute, the standard solution generated in accordance with the test protocol was introduced into the HPLC network. After testing, it was discovered that the machine's suitability parameters flowed between 1.0 and 1.2 milliliters per minute. The retention durations for Vaborbactam and Meropenem were similar to those achieved using the 1.0 ml/min mobile method. Meropenem and Vaborbactam's tailing factor was found to be within acceptable bounds. In accordance with Table 8(i-ii).

### Specificity

Normal and sample solutions had to be prepared for the test technique and then injected into the chromatographic equipment. In terms of retention time, the standard and sample chromatograms ought to be almost comparable. Both the Standard and the Sample had the same retention duration and identical chromatograms. As shown in picture 4(c). Meropenem has a Retention time of 4.707 minutes and Vaborbactam has a Retention time of 6.684 minutes.

### LOD and LOQ

From linearity data, use the formula below to calculate the detection and quantitation limit.

$$\text{LOD} = \frac{3.3 \sigma}{S}$$

$\sigma$  = Normal reaction variance

S = Slope of Analyte calibration curve.

$$\text{LOQ} = \frac{10 \sigma}{S}$$



**Mounik Sai Kumar et al.,** $\sigma$  = Normal reaction variance

S = Slope of Analyte calibration curve.

**Meropenem:**

The LOD and LOQ are determined from the linearity plot.:

$$\text{LOD} = \frac{3.3 \sigma}{S} = \frac{3.3 \times 2796.31}{35296} = 0.261$$

$$\text{LOQ} = \frac{10 \sigma}{S} = \frac{10 \times 2796.31}{35296} = 0.792$$

**Vaborbactam:**

$$\text{LOD} = \frac{3.3 \sigma}{S} = \frac{3.3 \times 185.59}{5099} = 0.120$$

$$\text{LOQ} = \frac{10 \sigma}{S} = \frac{10 \times 185.59}{5099} = 0.363$$

**DISCUSSION**

Normal and sample preparation was necessary for the test technique. The analytical method was developed by the analysis of many parameters [13–16]. Meropenem's maximum absorbance was measured at 237 nm, but Vaborbactam's was at 275 nm. Peak purity was determined to be good, and the typical detection wavelength was 252 nm. The ideal peak area was obtained with an injection volume of 20  $\mu\text{L}$ . The superior peak shape of the Inertsil C18 ODS column led to its selection. It was determined that the ambient temperature was adequate to preserve the drug solution's purity. The good peak area, adequate retention time, and high resolution led to the selection of a flow rate of 1.0 mL/min. The buffer's capacity to generate symmetrical peaks and high resolution led to its selection. The 80:20 methanol-to-buffer ratio produced the best results out of all the mobile phase ratios that were examined. The suggested approach then made use of this mobile phase ratio.

The results of the new analytical technique fell within the same 98.0–101.5% range as the guidelines, indicating that it was linear, accurate, and robust. It was shown that the procedure's and the device's precision were both dependable and within an acceptable range. For Meropenem and Vaborbactam, the detection limits were found to be 0.261  $\mu\text{g/mL}$  and 0.120  $\mu\text{g/mL}$ , respectively. Both medications' linearity was validated by the curve fitting and coefficient of correlation analysis. Both Meropenem and Vaborbactam showed linearity in the analytical method within the 20–80 ppm target concentration range. In every instance, the robustness and roughness tests were passed with outstanding relative standard deviations.

**CONCLUSION**

The suggested approach, which is straightforward, precise, and cost-effective, and free from excipient interference, was successfully used for the quantification of Meropenem and Vaborbactam in the fixed dose formulation after being validated in accordance with ICH recommendations.





Mounik Sai Kumar et al.,

## ACKNOWLEDGEMENT

The authors are grateful to Dr.L.Rathaiah, Chairman of Lavu educational society and Dr. Y Srinivasa Rao, Principal, Vignan Institute of Pharmaceutical Technology for providing necessary facilities to carry out the above research work.

## REFERENCES

1. Patel TS, Pogue JM, Mills JP, Kaye KS. Meropenem vaborbactam: a new weapon in the war against gram-negative bacteria. *Future Microbiol* 2018;13:971-83.
2. Centers for Disease Control and Prevention. Carbapenem-resistant Enterobacteriaceae in Healthcare Settings. Available from: <https://www.cdc.gov/hai/organisms/cre/index.html>.
3. Tacconelli E, Magrini N. Global priority list of antibiotic-resistant bacteria to guide research, discovery, and development of new antibiotics. WHO 2017. Available from: [https://www.who.int/medicines/publications/WHO-PPLShort\\_Summary\\_25Feb-ETNMWHO.pdf?ua=1](https://www.who.int/medicines/publications/WHO-PPLShort_Summary_25Feb-ETNMWHO.pdf?ua=1).
4. VABOMERE™ (Meropenem and Vaborbactam) for injection. FDA. Available from: [https://www.accessdata.fda.gov/drugsatfda\\_docs/label/2017/209776lbl.pdf](https://www.accessdata.fda.gov/drugsatfda_docs/label/2017/209776lbl.pdf). [Last accessed on 01 Mar 2019].
5. Jorgensen SC, Rybak MJ. Meropenem and vaborbactam: stepping up the battle against carbapenem-resistant enterobacteriaceae. *Pharmacotherapy* 2018;38:444-61.
6. Hecker SJ, Reddy KR, Totrov M, Hirst GC, Lomovskaya O, Griffith DC, et al. Discovery of a cyclic boronic acid  $\beta$ -lactamase inhibitor (RPX7009) with utility vs class a serine carbapenemases. *J Med Chem* 2015;58:3682-92.
7. Bush K. A resurgence of  $\beta$ -lactamase inhibitor combinations effective against multidrug-resistant gram-negative pathogens. *Int J Antimicrob Agents* 2015;46:483-93.
8. B.K.Sharma, page 286-370 a chemical analysis procedure that uses instruments;
9. "RP-HPLC Method for Valsartan quantification in Pharmaceutical Dosage Forms," M.9. Manoranjani IJSID, et al., *Pharmacy Research Journal*(2011).
10. Meropenem and Vaborbactam are available from <http://www.en.wikipedia.org/wiki>
11. Meropenem and Vaborbactam / *Pharmacol.com*. Displayed on: <http://www.. Pubmed>.
12. Vaborbactam and Meropenem are available at <http://www.en. Rxlist.com/Vaborbactam and Meropenem>.
13. Reverse phase high-performance chromatographic liquid system for Meropenem hydrochloride analysis in pharmaceutical dose type, Bhattacharyya I, Bhattacharyya SP, and Sen S. *International Pharmacy and Technology Review*, vol. 2, no. 2, pp. 224-232, 2010.
14. Stable RT, Francies M, Khedkar SMA, A Moghe, and Patil P. Gas chromatographic determination of Meropenem hydrochloride from its pharmaceutical composition *Indian Medicines* 2003; 40: 231.
15. Vidyadhara S, Rao Y. S, Ramu A, Sasidhar R. L, Ramya A. J. Method Development and Validation for the Simultaneous Estimation of Cinitapride and Pantoprazole in Solid Dosage Forms By RP-HPLC. *Orient J Chem* 2013;29(3).
16. T.Hemant kumar, Ch.Asha, D.Gowri Sankar . Estimation of Amlodipine Besylate and Irbesartan in Pharmaceutical Formulation by RP-HPLC with forced degradation studies. *Int J App Pharm*, vol 11, issue 3, 2019, 159-167
17. Theoretical Methodological Validation: Methodology, ICH Harmonized Tripartite Recommendations, Federal Register 1996, Q2B (R1):1-8.
18. International Conference on Technical Requirement Harmonization for Pharmaceuticals for Human Use Registration. Validation of analytical techniques: text and approach 1-13 in ICH Q2 (R1) 2005.
19. Draft Guidance on Specifications: Test Procedures and Acceptance Criteria for New Drug Substances and Products: Chemicals, 17th International Harmonization Conference. The Federal Register, Volume 65, Numbers 83041-83063, 2000.
20. Analytical Techniques and Method Validation: Chemistry, Performance, and Controls, FDA. 65: 776-777 in the Federal Register of 2000.







**Mounik Sai Kumar et al.,**

21. Quality Pharmaceutical Assurance is number 19 on the list. A collection of instructional resources and publications. WHO, Geneva, 1997; 1:19-24.

**Table- 1(a): Meropenem system suitability data**

Injection	RT	Peak Area	USP Plate count	USP Tailing
1	4.712	1412455	10023.845712	1.158
2	4.707	1413987	10410.547812	1.121
3	4.705	1418948	10236.874214	1.141
4	4.706	1416555	10127.254178	1.134
5	4.707	1412589	10184.658952	1.145
Mean	4.704232	1414906	10336.825471	1.144
SD	0.00314	2796.31	-----	-----
% RSD	0.096627	0.197	-----	-----

**TABLE-1(b): Vaborbactam System Fitting Data**

Injection	RT	Peak Area	USP Plate count	USP Tailing
1	6.691	204258	8325.874512	1.036
2	6.684	204012	8384.547862	1.045
3	6.681	203902	8314.875424	1.056
4	6.680	204155	8372.784518	1.078
5	6.684	204365	8392.084512	1.033
Mean	6.686208	204138	8358.875421	1.047
SD	0.0.0507	185.59	-----	-----
% RSD	0.112138	0.090	-----	-----

**Table 2(a): Data of Linearity (Meropenem)**

Concentration (ppm)	Average Area
0	0
0	706445
30	1059486
40	1412450
50	1745687
60	2119450
70	2472451
80	2825606
Statistical Analysis	
Slope	: 35296
y-Intercept	: -1504
Correlation Coefficient	: 0.999

**Table 2 (b): Details on linearity (Vaborbactam)**

Concentration (ppm)	Average Area
0	0
20	102056
30	153287
40	204256





Mounik Sai Kumar et al.,

50	248598
60	306482
70	357589
80	408513
<b>Statistical Analysis</b>	
Slope	5099
y-Intercept	-489.1
Correlation Coefficient	0.999

**Table 3(i): Meropenem Information on Reliability (System Precise)**

	Injection	Peak Areas of Meropenem	%Assay
<b>Concentration 40ppm</b>	1	1413654	100.23
	2	1415782	100.38
	3	1412748	100.16
	4	1412320	100.13
	5	1414875	100.31
<b>Statistical Analysis</b>	Mean	1415501	100.36
	SD	1414146	100.26
	% RSD	1454.28	0.103

**Table 3(ii): Information on Vaborbactam Reliability (System Precise)**

	Injection	Peak Areas of Vaborbactam	%Assay
<b>Concentration 40ppm</b>	1	204511	100.67
	2	204687	100.76
	3	204015	100.43
	4	204194	100.52
	5	204906	100.86
<b>Statistical Analysis</b>	Mean	204735	100.78
	SD	204508	100.67
	% RSD	341.6513	0.167

**Table 4(ii): Vaborbactam repeatability data (precision technique)**

	Injection	Peak Areas of Vaborbactam	%Assay
<b>Concentration 40ppm</b>	1	204324	100.58
	2	204578	100.70
	3	204689	100.76
	4	204714	100.77
	5	204177	100.51
	6	204866	100.85
<b>Statistical Analysis</b>	Mean	204558	100.69
	SD	259.491	0.127
	% RSD	0.126	0.126





**Mounik Sai Kumar et al.,**

**Table 5(i): Data of Intermediate precision (Analyst 2) for Meropenem**

Concentration 40ppm	Injection	Peak Areas of Meropenem	%Assay
	1	1410056	99.97
	2	1405487	99.65
	3	1418789	100.59
	4	1414010	100.25
	5	1416545	100.43
	6	1415930	100.39
Statistical Analysis	Mean	1413469	100.21
	SD	4888.23	0.346
	% RSD	0.345	0.345

**Table 5(ii): Data of Intermediate precision (Analyst 2) for Vaborbactam**

Concentration 40ppm	Injection	Peak Areas of Vaborbactam	%Assay
	1	204148	100.49
	2	204025	100.43
	3	204298	100.57
	4	204151	100.49
	5	204286	100.56
	6	204568	100.70
Statistical Analysis	Mean	204246	100.54
	SD	187.32	0.091
	% RSD	0.091	0.091

**Table 6(i): Meropenem data with accuracy**

Concentration % of spiked level	Amount added (ppm)	Amount found (ppm)	% Recovery	Statistical Analysis of % Recovery	
				MEAN	%RSD
50%	Injection 1	20	20.05	100.28	100.29 0.033
	Injection 2	20	20.06	100.33	
	Injection 3	20	20.05	100.26	
100%	Injection 1	40	40.05	100.14	100.23 0.083
	Injection 2	40	40.09	100.23	
	Injection 3	40	40.12	100.31	
150%	Injection 1	60	60.09	100.01	99.98 0.025
	Injection 2	60	59.97	99.97	
	Injection 3	60	59.99	99.98	

**Table 6(ii): Vaborbactam data with accuracy**

Concentration % of spiked level	Amount added (ppm)	Amount found (ppm)	% Recovery	Statistical Analysis of % Recovery	
				MEAN	%RSD
50%	Injection 1	20	20.17	100.88	100.88 0.043
	Injection 2	20	20.16	100.83	
	Injection 3	20	20.18	100.92	





**Mounik Sai Kumar et al.,**

100%	Injection 1	40	40.24	100.62	MEAN %RSD	100.62 0.084
	Injection 2	40	40.21	100.54		
	Injection 3	40	40.28	100.71		
150%	Injection 1	60	60.28	100.47	MEAN %RSD	100.46 0.050
	Injection 2	60	60.30	100.50		
	Injection 3	60	60.24	100.40		

**Table 7(i): Data on System Variability (Meropenem) (System-2)**

S.No	Peak area	Assay % of Meropenem
1	1418465	100.57
2	1413568	100.22
3	1416875	100.46
4	1415536	100.36
5	1414750	100.31
6	1412842	100.17
<b>Mean</b>	1415339	100.35
<b>%RSD</b>	0.147	0.147

**Table 7(ii): Data on device variations (Vaborbactam) (System-2)**

S.No	Peak area	Assay % of Vaborbactam
1	204087	100.46
2	204298	100.57
3	204351	100.59
4	204624	100.73
5	204194	100.52
6	204550	100.69
<b>Mean</b>	204350	100.59
<b>%RSD</b>	0.100	0.100

**Table 8(i): There's proof that flux rate variability has an impact (Meropenem):**

	Std Area	Tailing factor		Std Area	Tailing factor		Std Area	Tailing factor
	<b>Flow 0.8 ml</b>	1408784		1.011	<b>Flow 1.0 ml</b>		1412118	1.051
1408015		1.013	1415487	1.087		1483568	1.046	
1407009		1.011	1412689	1.056		1487521	1.084	
1407752		1.007	1412594	1.039		1485654	1.050	
1408329		1.016	1418745	1.045		1486895	1.064	
1405452		1.010	1412290	1.035		1482058	1.086	
<b>Avg</b>	1407556	1.011	<b>Avg</b>	1413987	1.052	<b>Avg</b>	1485279	1.069
<b>SD</b>	1190.01	0.003	<b>SD</b>	2641.468	0.018	<b>SD</b>	2076.99	0.019
<b>%RSD</b>	0.0845		<b>%RSD</b>	1.86		<b>%RSD</b>	0.1398	

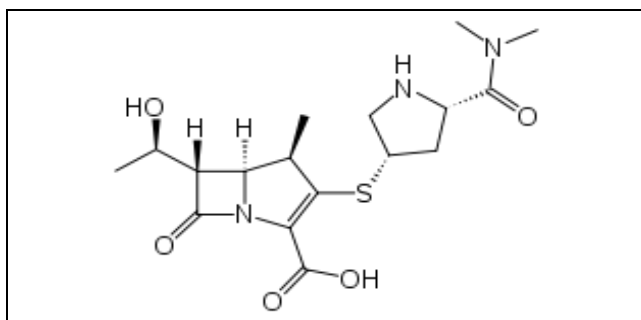




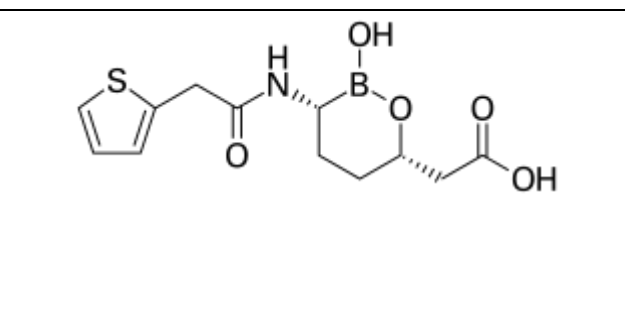
**Mounik Sai Kumar et al.,**

**Table 8(ii): Flow rate shift impact data (Vaborbactam)**

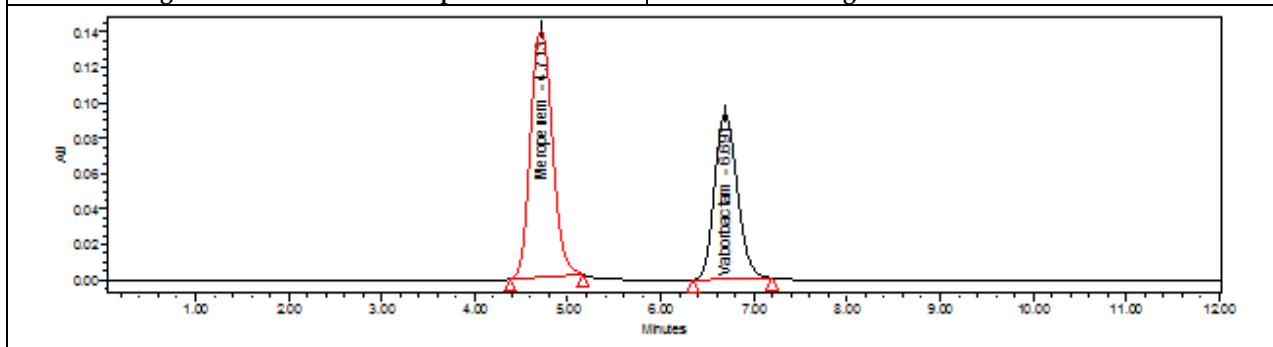
	Std Area	Tailing factor		Std Area	Tailing factor		Std Area	Tailing factor
	<b>Flow 0.8 ml</b>	203145		1.078	<b>Flow 1.0 ml</b>		204235	1.097
203084		1.068	204298	1.078		2022984	1.036	
203198		1.058	204659	1.089		2022346	1.044	
203248		1.064	204879	1.086		2022684	1.024	
203265		1.044	204098	1.080		2022485	1.012	
203942		1.048	204845	1.069		2022895	1.032	
<b>Avg</b>		203313	1.060	<b>Avg</b>		204502	1.083	<b>Avg</b>
<b>SD</b>	314.9785	0.015	<b>SD</b>	334.8275	0.009	<b>SD</b>	272.1358	0.014
<b>%RSD</b>	<b>0.154</b>		<b>%RSD</b>	<b>0.163</b>		<b>%RSD</b>	<b>0.013</b>	



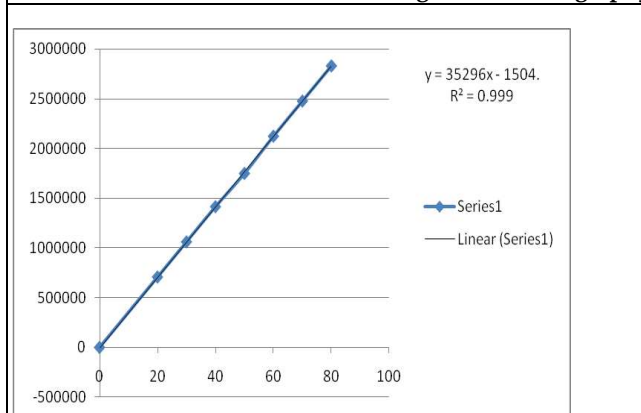
**Figure 1: Structure of Meropenem**



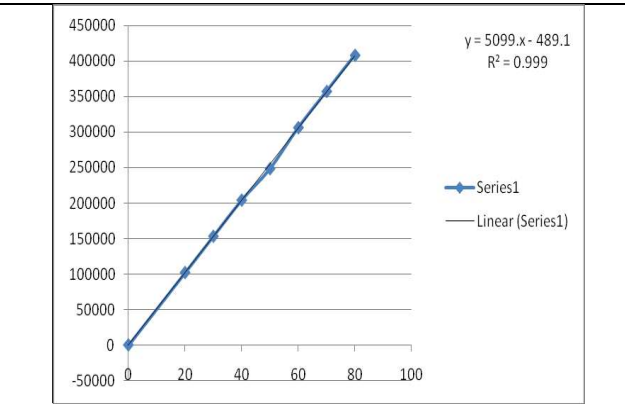
**Figure 2: Structure of Vaborbactam**



**Fig 3: Chromatography in its traditional form**



**Fig: 4(a) Meropenem's Linearity Plot**



**Fig: 4(b) Plot of Vaborbactam**





Mounik Sai Kumar et al.,

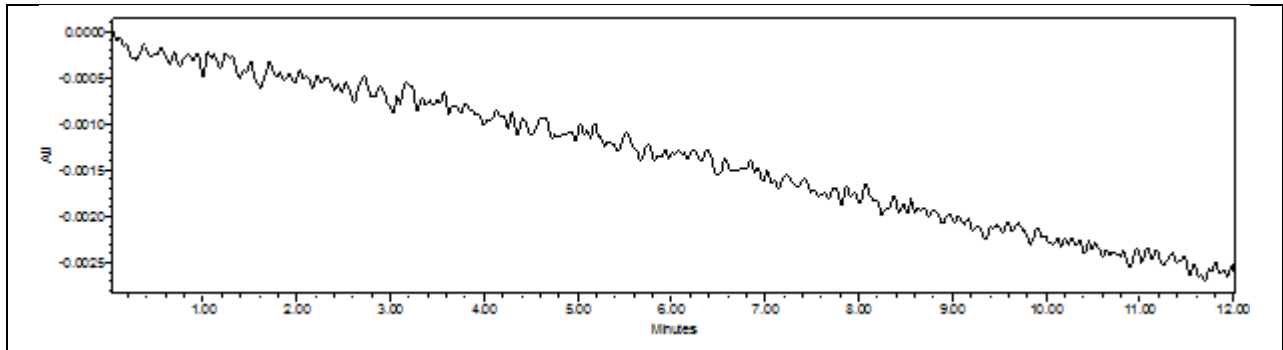


Fig 4(c): Blank Chromatograph

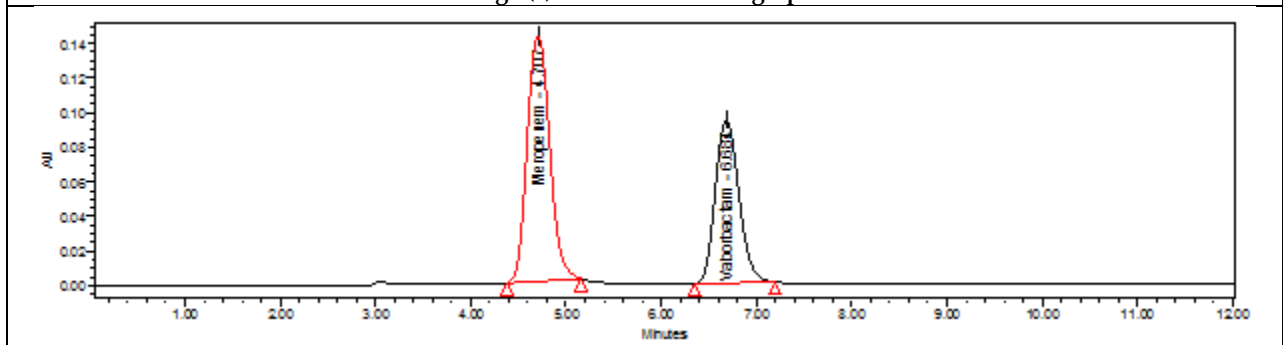


Fig 5: Chromatogram Standard

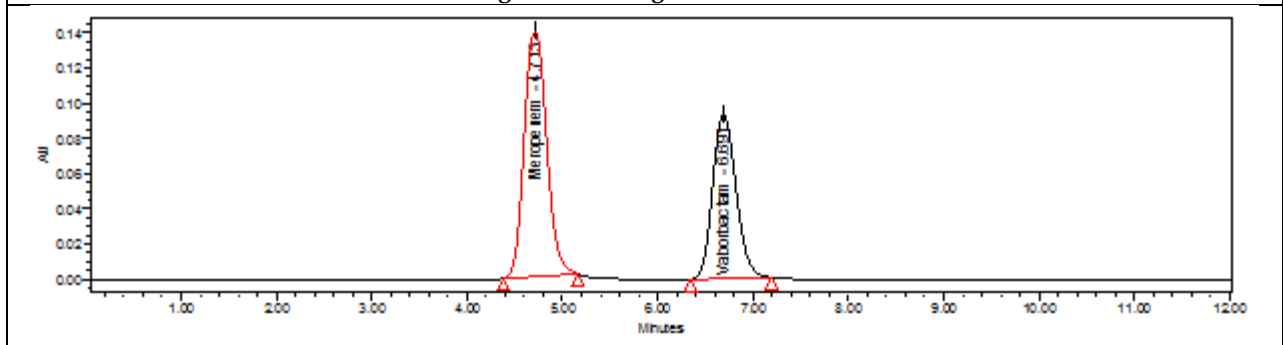


Fig 6: Chromatogram Sample







## Innovative ML Methods for Automatic Blood Cell Images Analysis and Labeling: Improving Medical Imaging Diagnostic Precision with Extracting Features and Classification Approaches

Routhu Shanmukh<sup>1</sup>, Venkateswara Reddy B, Rowthu Neelima <sup>3</sup>, Yerravarapu Durga Prasad<sup>4</sup> and CH Nooka Raju<sup>5\*</sup>

<sup>1</sup>Department of Computer Science and Engineering, KL University, Guntur, Andhra Pradesh, India.

<sup>2</sup>Assistant Professor , Department of Computer Science and Engineering-Artificial Intelligence & Machine Learning, Vasireddy Venkatadri Institute of Technology, (Affiliated to Jawaharlal Nehru Technological University), Guntur, Andhra Pradesh, India.

<sup>3</sup>Assistant Professor, Department of Computer Science and Engineering, B V Raju Institute of Technology, (Affiliated to Jawaharlal Nehru Technological University), Telangana, India.

<sup>4</sup>Assistant Professor, Department of Computer Science and Engineering, Aditya University , Surampale, Andhra Pradesh, India

<sup>5</sup>Department of Radiology, Centurion University of Technology and Management, Vizianagaram, Andhra Pradesh, India.

Received: 06 Oct 2024

Revised: 12 Nov 2024

Accepted: 18 Dec 2024

### \*Address for Correspondence

**CH Nooka Raju**

Department of Radiology,

Centurion University of Technology and Management,

Vizianagaram, Andhra Pradesh, India.

E.Mail: nookaraju@cutmap.ac.in



This is an Open Access Journal / article distributed under the terms of the **Creative Commons Attribution License** (CC BY-NC-ND 3.0) which permits unrestricted use, distribution, and reproduction in any medium, provided the original work is properly cited. All rights reserved.

### ABSTRACT

Advanced machine learning methods to automatically analyze and categorize images of blood cells with the goal of enhancing the precision of medical imaging diagnosis. The work focuses on identifying important structural characteristics in red and white blood cells by utilizing extraction of characteristics and segmentation methods. Deep learning models are among the sophisticated methods used to improve picture segmentation and classification procedures. The suggested techniques have the ability to effectively identify blood illnesses such as leukemia, anemia, and infections, resulting in quicker and more accurate diagnosis. According to experimental findings, these automated techniques perform better than conventional techniques with respect to overall precision, memory, and overall accuracy, which qualifies them for use in clinical settings.

**Keywords :** Medical Imaging, Feature Extraction, Machine Learning.



**Routhu Shanmukh et al.,**

## INTRODUCTION

Early disease diagnosis, treatment, and detection depend heavily on medical imaging. Specifically, the diagnosis of hematological illnesses such as anemia, leukemia, and infections depends heavily on the study of blood cell images[1,2]. The conventional procedure has been for pathologists to manually examine blood smears; however, this procedure is laborious, subjective, highly highly susceptible to accidental mistakes. Because imaging techniques and computerisation have made analyses faster and more precise, diagnostic procedures have been greatly enhanced[3,4,5]. But even with these advancements in technology, issues with accuracy and scalability still exist[6]. Because machine learning (ML) approaches can automate and improve the reliability of blood vessels characterisation and overall diagnostic processes, there has been an increase in interest in these techniques as a result[7]. Medical imaging diagnostic procedures can now be automated with great power thanks to machine learning, especially when it comes to picture processing[8]. Machine learning (ML) methods in blood vessel analysis can be utilized to spot complex patterns and anomalies that human observers might overlook[9]. Large datasets of labeled blood cell images are used by these mathematical models to help them learn to distinguish between diseased and normal cells without an exceptionally high level of accuracy[10,11]. Additionally, predictive models are very effective at handling large amounts of data in a short amount of time, which makes them ideal for regular diagnostic tasks[12]. By lowering error rates and enhancing patient outcomes, such abilities have the capacity to revolutionize diagnostic operations[13]. In medical image analysis, including blood cell categorisation, obtaining features is an essential first step[14]. In order to use a picture as an input for machine learning algorithms, it is necessary to recognise and isolate important features from the image. Shape, size, texture, including color are examples of traits that can be found in tissue analysis[15]. These aspects are crucial for differentiating between different blood cell types and identifying pathological abnormalities. Models created using machine learning can focus on the most important details of a picture with the help of efficient feature extraction, which increases classification accuracy[16]. The technique of feature extraction has been significantly improved by recent developments in deep learning, enabling more sophisticated analysis of complicated images with no requiring a lot of manual preliminary processing. In the computerized examination of medical images, segmentation is yet another crucial step[17]. Segmentation algorithms are employed in blood cell imaging to distinguish individual cells between background and additionally overlapping cells, an important step towards precise categorisation[18]. The presence of artifacts in the images and the variety in cell morphology can make this process difficult. Such complications are beyond the capabilities provided by conventional segmentation techniques like thresholding along with edge detection[19]. More accurate blood cell picture segmentation has been demonstrated using contemporary machine learning techniques, especially convolutional neural networks (CNNs). More precise and trustworthy detection of aberrant neurons in clinical settings is now possible because of these developments[20].

## METHODOLOGY

By incorporating modern machine learning methods within blood cell analysis, evaluation accuracy could be greatly increased. These algorithms can increase uniformity among diagnoses and lessen the inherent disparities in assessments by humans by simplifying the identification process. Furthermore, the ability to continually develop and refresh machine learning models with fresh data enables them to keep up with the rapidly advancing field of medicine. This flexibility is particularly crucial for diagnosing uncommon or unusual cases, when human experience may be scarce. Research has demonstrated that machine learning techniques can perform better for classifying blood cells than conventional techniques that are manual in regard to acceleration, awareness, and precision.

### Activity Diagram for the Blood Cell Image Processing Workflow

This illustrates the steps involved in making decisions and deciding the categorisation outcome while analyzing blood cell images. Because deep learning, a kind of machine learning, is capable of distinguishing hierarchical characteristics from unprocessed data, it has become increasingly popular in the field of medical picture analysis. Deep learning models, with the value recurrent neural networks (RNNs) and CNNs, have shown impressive results





Routhu Shanmukh et al.,

in blood cell categorisation. These models enable more precise distinction between healthy and sick cells by capturing both the regional and global characteristics of blood cells. Deep learning models are especially useful for difficult and high-dimensional tasks including blood cell analysis because they can independently retrieve pertinent features from huge datasets, in contrast to typical statistical techniques that depend on manually generated features. Partitioning an image into recognizable portions that correspond to distinct structures, like particular blood cells, is a crucial step in the analysis of blood cells. This procedure is essential for separating individual cells within their surroundings and guaranteeing that every cell gets examined separately. Precise segmentation is crucial for the later phases of features being extracted and categorized because improperly divided images can provide machine learning models with inaccurate or insufficient data. Machine learning-driven approaches to segmentation have made tremendous progress in handling noisy and elaborate medical pictures, especially when cells have irregular shapes or overlap. Machine learning approaches are additionally being used to predict how a disease would progress and how the proposed therapy will be implemented based on images of blood cells. In diseases such as leukemia for example, where early identification and surveillance are crucial, machine learning algorithms assist in detecting subtle modifications to red blood cells in existence composition that may indicate the onset or progression of the disease. By providing real-time analysis and ongoing monitoring, these innovations can assist healthcare providers in making more informed decisions regarding treatment regimens and patient care. The technique of machine learning possesses the ability to completely transform the discipline of hematology by offering faster diagnosis times along with more individualized and accurate medication options .

## RESULTS ANALYSIS

The below table represents the Predicted blood cells

Healthy vs Abnormal

Through replicating cells with white circles against a dark backdrop, the generate\_synthetic\_data utility produces artificial plasma cell images.

At random, labels are allocated as aberrant (0) or healthy (1).

## CONCLUSION

The continuous improvement of predictive algorithms and their incorporation into clinical workflows hold the key to the next generation of automation blood cell analysis. New methods that have the potential to overcome existing constraints include transfer learning, which enables models to utilize data collected from related tasks, and generative adversarial networks (GANs), and this can enhance small datasets. Furthermore, the creation of more comprehensible models will boost doctors' confidence in diagnosis based on machine learning. Those methods will probably develop into an essential tool in hematology as they get more advanced, allowing for quicker, more precise, and easier access to diagnosis for a variety of life-threatening illnesses, ultimately leading to better clinical results and care.

## REFERENCES

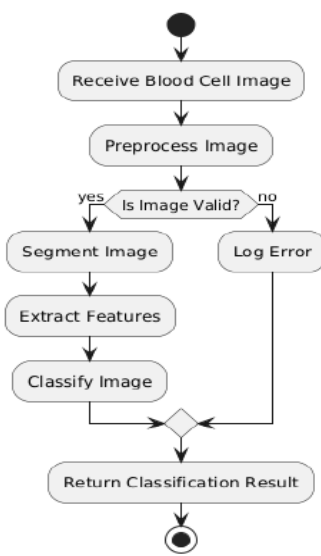
1. Routhu Shanmukh, CH Nooka Raju, Rowthu, Lakshmana Rao. Analysis of fundus images using conventional edge detection techniques. *Journal of Information and Computational Science*, 17(12), 206-217. (2022)
2. Goodfellow, I., Bengio, Y., & Courville, A. *Deep Learning*. MIT Press. (2016)
3. LeCun, Y., Bottou, L., Bengio, Y., & Haffner, P. Gradient-based learning applied to document recognition. *Proceedings of the IEEE*, 86(11), 2278-2324. (1998)
4. Ronneberger, O., Fischer, P., & Becker, A. U-net: Convolutional networks for biomedical image segmentation. *Medical Image Computing and Computer-Assisted Intervention*, 9341, 234-241. (2015)
5. Zhang, Y., & Yang, Y. A survey on deep learning techniques for medical image analysis. *Artificial Intelligence in Medicine*, 91, 12-25. (2018)





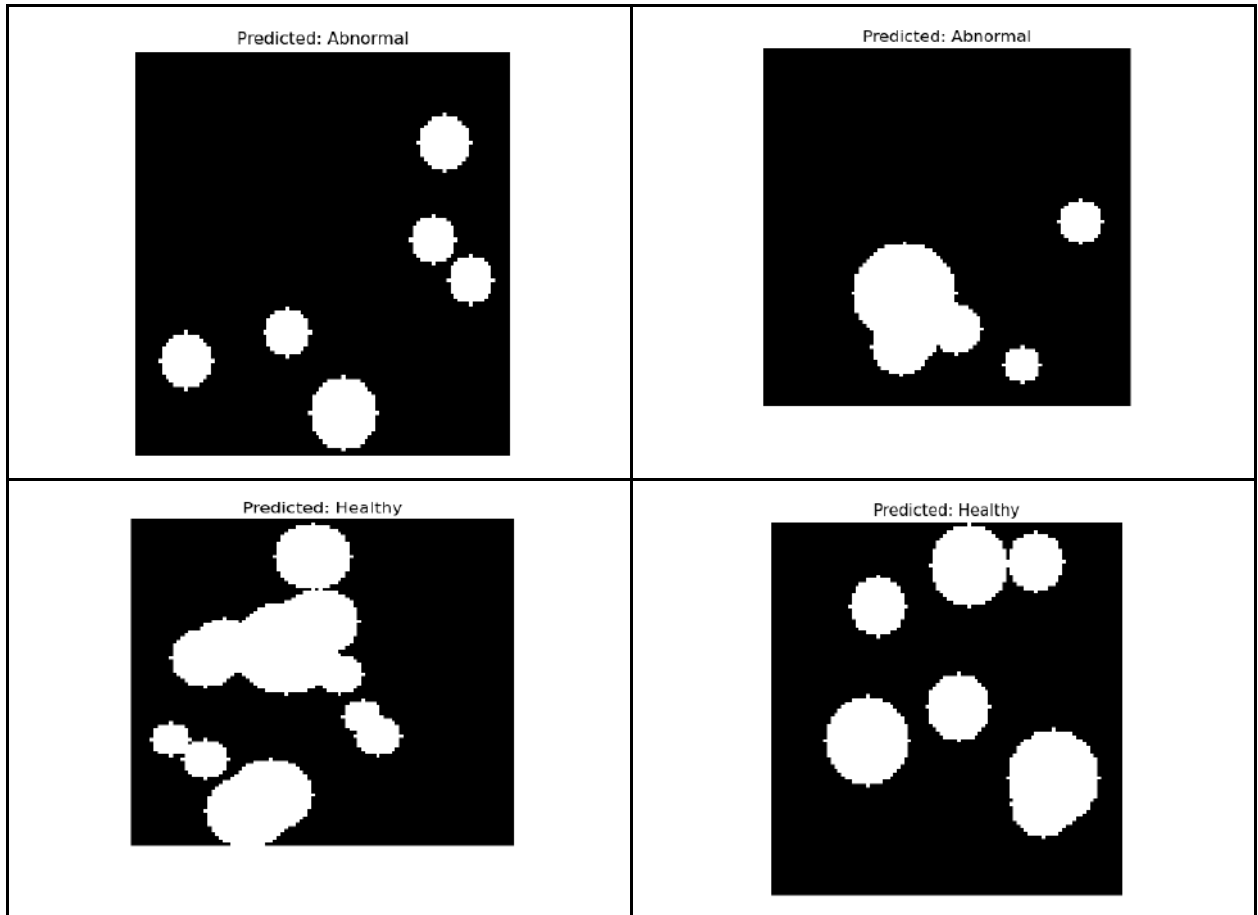
**Routhu Shanmukh et al.,**

6. Esteva, A., Kuprel, B., Blauwendraad, A., et al. Dermatologist-level classification of skin cancer with deep neural networks. *Nature*, 542(7639), 115-118. (2017)
7. Suk, H. I., & Shen, D. Deep learning in medical image analysis: A survey. *Artificial Intelligence in Medicine*, 59(3), 300-307. (2013)
8. Yadav, S. K., & Bansal, A. Image segmentation techniques in medical imaging: A review. *International Journal of Computer Applications*, 182(18), 1-7. (2019)
9. Çiçek, Ö., Abdulkadir, A., Lienkamp, S. S., et al. 3D U-Net: Learning dense volumetric segmentation from sparse annotation. *Medical Image Computing and Computer-Assisted Intervention*, 9901, 424-432. (2016)
10. Havaei, M., Davy, A., Warde-Farley, D., et al. Brain tumor segmentation with deep neural networks. *Medical Image Computing and Computer-Assisted Intervention*, 9901, 506-513. (2016)
11. Routhu Shanmukh, CH Nooka Raju, Naveen Kumar Challa, CH Mukesh. A comparative analysis of CNN techniques on application to fundus images. *Journal of Chemical Health Risks*. (2024)
12. Gulshan, V., Peng, L., Coram, M., et al. Development and validation of a deep learning algorithm for detection of diabetic retinopathy in retinal fundus photographs. *JAMA*, 316(22), 2402-2410. (2016)
13. Litjens, G., Kooi, T., Bejnordi, B. E., et al. A survey on deep learning in medical image analysis. *Medical Image Analysis*, 42, 60-88. (2017)
14. Ronneberger, O., Fischer, P., & Becker, A. U-Net: Convolutional networks for biomedical image segmentation. *Medical Image Computing and Computer-Assisted Intervention*, 9351, 234-241. (2015)
15. Makhdoom, I. S., Ali, M., & Rashid, A. A comprehensive review of machine learning in healthcare. *Journal of Healthcare Engineering*, 2020. (2020)
16. Khosravi, P., & Sadeghi, S. A comprehensive review of blood cell image classification techniques. *Journal of Healthcare Engineering*, 2020. (2020)
17. Akinyemi, O., & Adewole, M. Automated blood cell classification using deep learning. *International Journal of Computer Applications*, 182(3), 9-14. (2019)
18. Routhu Shanmukh, CH Nooka Raju, Syed Raashed Andrabi. Analysis of intensity variations on applications of edge detection techniques to fundus images. *GRADIVA REVIEW JOURNAL*. (2023)
19. Wang, J., Chen, H., Zhang, Y., et al. A review of machine learning in healthcare. *Artificial Intelligence Review*, 54, 325-352. (2021)
20. Ge, L., et al. Artificial intelligence in medical imaging: Overview and future directions. *Journal of Computer Assisted Tomography*, 44(3), 325-336. (2020)





**Routhu Shanmukh et al.,**



### Classification Report

	precision	recall	f1-score	support
0	0.4296875	0.6111111111111112	0.5045871559633027	90.0
1	0.5138888888888888	0.33636363636363636	0.40659340659340654	110.0
accuracy	0.46	0.46	0.46	0.46
macro avg	0.4717881944444444	0.4737373737373738	0.45559028127835466	200.0
weighted avg	0.4759982638888889	0.46	0.45069059380985976	200.0





## Formulation of Geomatrix Extended Release Tablets of Metformin HCl using CO Processed Gums

Ponnada Sowmya<sup>1</sup>, Konathala Rajesh<sup>2</sup>, Ch.Nooka Raju<sup>3</sup> and P.N.Mallikarjun<sup>4\*</sup>

<sup>1</sup>M.Pharm. Student, Department of Pharmaceutics, Vignan Institute of Pharmaceutical Technology, (Affiliated to Jawaharlal Nehru Technological University), Visakhapatnam, Andhra Pradesh, India.

<sup>2</sup>Professor & Principal, Bhaskara institute of Pharmacy, (Affiliated to Andhra University), Andhra Pradesh, India.

<sup>3</sup>Department of Radiology, Centurion University of Technology and Management, Vizianagaram, Andhra Pradesh, India.

<sup>4</sup>Associate Professor, Department of Pharmaceutics, Vignan Institute of Pharmaceutical Technology, (Affiliated to Jawaharlal Nehru Technological University), Visakhapatnam, Andhra Pradesh, India.

Received: 06 Oct 2024

Revised: 10 Nov 2024

Accepted: 12 Dec 2024

### \*Address for Correspondence

**P.N.Mallikarjun**

Associate Professor, Department of Pharmaceutics,  
Vignan Institute of Pharmaceutical Technology,  
(Affiliated to Jawaharlal Nehru Technological University),  
Visakhapatnam, Andhra Pradesh, India.  
E.Mail: mallik6567@gmail.com



This is an Open Access Journal / article distributed under the terms of the **Creative Commons Attribution License** (CC BY-NC-ND 3.0) which permits unrestricted use, distribution, and reproduction in any medium, provided the original work is properly cited. All rights reserved.

### ABSTRACT

Metformin is a water-soluble drug and it acts primarily by reducing hepatic glucose production by enhancing insulin sensitivity in peripheral tissues their by lowering the blood glucose levels. In this research initially co processed gums were prepared using Xanthin gum and Acacia gum. The geomatrix tablet contains active middle layer and two barrier layers to retard the drug release. The active middle layer in development of geo matrix tablets was consist of metformin and coprocessed gums. Tablets were prepared by the direct compression by sandwich active middle layer with two barrier layers. These tablets were evaluated for various pre, post compression parameters and in vitro dissolution studies for 24 hours. FTIR studies proved that there was a good compatibility between drug and excipients. All the geo matrix tablets were showed significant retardation in drug release and geo matrix tablet formulation CM5 showed maximum drug release at end of 24 hours.

**Keywords:** metformin, extended release, geo matrix tablets, coprocessed gums.







Ponnada Sowmya et al.,

## INTRODUCTION

Pharmaceutical excipients are defined as the substances other than the API which has been appropriately evaluated for safety and are intentionally included in a drug delivery system [1]. The International Pharmaceutical Excipients Council (2009) defines excipients as the substances which present in a finished pharmaceutical dosage form other than the active drug substance [2]. Excipient can be classified into four categories generally: single entity excipient, a physical blend of multiple excipients, new chemical entity excipient and co-processed excipient [3]. An excipient that has undergone co-processing is a combination of two or more 84418 possible 84418 or non-compendial excipients with the goal of physically changing their properties without altering chemical properties.[4] There is no single-component excipient 84418 possible all the requisite performance to allow an active pharmaceutical ingredient to be formulated into a specific dosage form. Co-processed excipient has received much more attention in the formulation development of various dosage forms, specially for tablet preparation by direct compression method.

The pharmaceutical industry first started to use co-processed excipients from the late 1980s, with early examples including co-processed microcrystalline cellulose and calcium carbonate, introduced in 1988, MEGGLE's co-processed cellulose and lactose (1990), and co-processed glucomannan and galactomannan (1996). The geo-matrix multilayer tablet technology was developed by conte and co-workers for constant drug release [5]. The technology includes triple – layered and bi-layered tablets. The triple-layered tablet which is exemplified consists of an active core which is a hydrophilic matrix layer and two polymeric barriers layers on either side that are hydrophobic or semi permeable [6]. The Bi-layered tablet consist of the drug layer and one barrier layer . The barrier layer modifies the swelling rate of the active core and reduces the surface area available for diffusion of drug [7,8]. Zero-order drug release can be achieved with the Geo-matrix system [9]. However release is limited to one drug. Metformin is a BCS-I drug and Soluble in water, slightly soluble in alcohol, practically insoluble in acetone and methylene chloride. It acts primarily by reducing hepatic glucose production by enhancing insulin sensitivity in peripheral tissues their by lowering the blood glucose levels[10,11].

## EXPERIMENTAL METHODOLOGY

### Preparation of co – processed gums

Xanthan gum and acacia gum, at concentrations of 3% each, were dispersed in distilled water. The xanthan gum and acacia gum were mixed at varying ratios ( 1:2, 2:1, 1:3, and 3:1) and homogenized with a rotation of 3000 rpm for 30 min to obtain a homogeneous mass. The mass was then dried with a hot air drier at  $80\pm 5^{\circ}\text{C}$ . The obtained layer or flakes were milled and sieved using a 60 mesh. Functional characterizations of the mass were then performed. The process of preparation is shown in Figure-1 .

### Drug – Excipient Compatibility Studies by FTIR:

Compatibility study was performed by making ready compatibility blends at completely ratios of various excipients with the drug, supportive tentative average weight. These blend were stored at accelerated condition of  $40^{\circ}\text{C}/75\%\text{RH}$ . Control samples were stored at  $40^{\circ}\text{C}$ . the ratio of the drug to excipient varies from 1:1 to 1:10 depending on the purpose of use, and the samples were kept in double lined poly- bags. These samples were evaluated for any change in the physical characteristics with reference to its controlled sample stored at  $40^{\circ}\text{C}$  for a period of 15 days. In the present study, the potassium bromide disc (pellet) method was employed. Chemical stability was confirmed by IR spectrometry.

### Preparation of middle active layer Using co processed gums

The middle active layer was prepared by direct compression method using co processed gums using xanthan and acacia gums. The formulation was prepared according to the formulation table given in Table-1. These materials were screened through #60 and mixed together in motor by using pestle. Final mixtures were compressed by using





Ponnada Sowmya et al.,

11mm diameter flat punches on a eight- station rotary tablet press. The prepared tablets were subjected to dissolution studies.

#### Preparation of upper and lower layers

The barrier layers were formulated employing hydrophilic swellable polymer HPMC K100M and Ethyl Cellulose. The procedure tried to make the compacts was via direct compressions. For the first procedure the both polymers were mixed in mortar and lubricated with magnesium stearate.

#### Formulation of Geo matrix (Tri-layer) tablets

The powder mixtures required for active and barrier layers were weighed accurately and thoroughly mixed using mortar and pestle for about 20 minutes. Initially, the volume of die cavity; (12mm, round) was adjusted equivalence to the weight of tri-layered matrix tablets (900mg). Then the pre-weighed amount of powder equivalent to bottom layer (25mg) was taken and placed in the die cavity and slightly compressed for uniform spreading. The upper punch was lifted and 850mg of the drug containing middle active layer was placed over the bottom layer in the die cavity and again slightly compressed. The remaining volume of the die cavity was filled with pre-weighed (25mg) amount of powder equivalent to top layer and compressed with the full force of compression on rotary tablets press to obtain tri-layered tablets. The schematic diagram of geomatrix tablet is shown in Figure-2.

#### Evaluation of Pre compression Parameters:

All the formulations precompression parameters like Bulk density, Tapped density, Compressibility index and angle of repose were determined according to the official methods.

#### Evaluation of Post compression Parameters:

All the formulations post compression parameters like hardness, Friability, average weight and drug content were determined according to the pharmacopoeial procedures.

#### In vitro dissolution studies of Extended- Release Geo-Matrix Tablets

Drug release from the of geo matrix tablets were studied using USP I basket dissolution apparatus, in 900 mL of pH 6.8 Phosphate buffer for 18 hours at  $37 \pm 0.5^\circ\text{C}$  at 75 rpm. 5 mL of dissolution medium was withdrawn using a syringe fitted with  $0.45 \mu\text{m}$  pre filter at regular time intervals and the same volume of ( $37 \pm 0.5^\circ\text{C}$ ) fresh dissolution medium maintained at  $37 \pm 0.5^\circ\text{C}$  was replaced. The samples were diluted wherever necessary and analyzed at appropriate wavelengths for Metformin spectrophotometrically. The cumulative percent of drug released at different time intervals was calculated. All the dissolution studies were performed 6 times and average values were reported.

#### Drug release kinetics and mechanism

The rate and mechanism of drug release play an important role in assessing the quality of the dosage form and also for achieving the desired time of drug action in the body for controlled release dosage forms. The drug release kinetics was evaluated by fitting the data to zero and first order. Mechanism of drug release was evaluated by fitting the data to Higuchi diffusion model, erosion model and further characterized by using Korsmeyer-Peppas equation.

## RESULTS AND DISCUSSION

#### Functional group analysis

The purpose of the functional group analysis was to ascertain whether a chemical reaction occurred between each of the functional groups of the two excipients. Xanthan gum and acacia gum only interact or mix physically. No new functional groups presented in the spectrum (Fig. 1), indicating that these interactions do not involve chemical changes. The Fourier-transform infrared spectroscopy spectrum of xanthan gum, at wavenumber  $1780.8 \text{ cm}^{-1}$  showed a sharp peak, suggesting the presence of  $\text{-C=O}$  carboxylic bonds. This is reinforced by the presence of wide peaks with strong intensities in the range of wavenumbers  $2500\text{--}3300 \text{ cm}^{-1}$ , indicating the presence of the  $\text{-OH}$  carboxylate group.



**Ponnada Sowmya et al.,**

**Drug – Excipient Compatibility Studies :**Overall there was no alteration in peaks of Metformin pure drug (Figure 3) and optimized formulation (Figure 10), suggesting that there was no interaction between drug & excipients. FTIR spectrum of pure drug and other polymers is shown in (Figure 4). There is no additional peaks appeared or disappeared hence no significant changes in peaks of optimized formulation was observed when compared to pure drug indicating absence of any interaction

**Precompression Parameters**

The bulk density (g/ml) & tapped density of powdered blend of all the formulations is found to be in the range of 0.61 to 0.66 & 0.7 to 0.75 respectively. All formulations are within the pharmacopeial limits.

The CI & angle of repose of powdered blend of all the formulations is found to be in the range of 10.81 to 13.89 & 31.16 to 34.89 respectively. All formulations are within the pharmacopeial limits.

**Post Compression Parameters**

The hardness of all formulations was measured in kg/cm<sup>2</sup>. Hardness of all formulations was in the range of 4.5±1.02 to 6.1 kg/cm<sup>2</sup> and friability values of none of the formulations exceeded 1% the results of friability indicate that the tablets were mechanically stable.

The weights & Drug content of the tablets were between 849.02 ±2.789 to 852.86±2.988 mg & 97.5±0.50 to 102.7±0.21 respectively. All the post compression parameters given in Table-2

**In vitro dissolution studies of extended release metformin tablets:**

The *In vitro* drug profile of metformin from different formulations was carried out in phosphate buffer pH 6.8, and the results are depicted in Figure-5 & 6. The geo matrix tablets extended the drug release up to 24 h. Among all the formulations AM5 & BM5 failed to retard drug release upto 24 hours because of low polymer content in coprocessed gums. Formulations CM5 & DM5 retarded drug release upto 24 hours. because of high polymer content in coprocessed gums. The highest drug release was found in the formulation CM5 i.e 99.98±0.05% within 24 h. CM5 was found to be optimized formulation based on the dissolution and other evaluation parameters. In the present study drug release mechanism is best fitting to zero order and Higuchi model because regression coefficient was seen closest to 1 in these models which conforms diffusion assisted mechanism of release. The correlation coefficient values are given in Table-3.

**CONCLUSION**

Based on the evaluation parameters, drug dissolution profile and release drug kinetics CM5 was found to be optimized formulation. The drug release from CM5 was found to fit Zero order of concentration independent and best fitted to Higuchi's model confirming to be diffusion assisted mechanism. The developed drug delivery systems showed prolonged and complete drug release rates over a period of 24 h. These results also demonstrated the suitability of geo matrix (three-layered) tablet formulation of metformin to provide controlled release for prolonged period of time and improved linearity for metformin in the effective management of diabetes with patient compliance. It was concluded that geo matrix tablets of Metformin could be successfully prepared by direct compression technique using different coprocessed excipient combination. Metformin tablets were prepared by direct compression and consist of middle active layer with different co processed gum and upper and lower layers were prepared with HPMCK100M, ethyl cellulose, Talc and Magnesium stearate.

**ACKNOWLEDGMENT**

The authors would like to our sincere thanks to Dr. L.Rathaih garu Chairmain Vignan Educational institutions and Dr.Y.Srinivasa Rao garu principal of VIPT for providing support throughout the completion of the present work





Ponnada Sowmya et al.,

## REFERENCES

1. Bin LK, Gaurav A, Mandal UK. A review on co-processed excipients: current and future trend of excipient technology. Int J Pharm Sci. 2019.
2. Pawar SB, Ahirrao SP, Kshirsagar SJ, City BK, Knowledge B. Review on novel pharmaceutical co-processed excipients. Pharm. Reson. 2019, 2:14-20
3. Adeps R, Brahmaiah B, Nama S, Desu PK. International Journal of Current Trends in Pharmaceutical Research. Pharm. Res. 2013, 1.
4. Chaudhari PD, Phatak AA, Desai U. A review: co processed excipients-an alternative to novel chemical entities. International Journal of Pharmaceutical and chemical sciences. 2012 Oct, 1(4):1480-98.
5. Conte, U.; Maggi, L.; Colombo, P.; Manna, L. Multilayered hydrophilic matrices as constant release devices. J. Control. Release 1993, 26, 39–47
6. Shionogi Pharma, Inc. Once a day Sular® (Nisoldipine) with Geomatrix® delivery system for the treatment of hypertension. 2008. Available online: <http://www.sular.com/html/geomatrix.html> (accessed on 24 August 2010)
7. Streubel, A.; Siepmann, J.; Peppas, N.A.; Bodmeier, R. Bimodal drug release achieved with multi layer matrix tablets: Transport mechanisms and device design. J. Control. Release 2000, 69, 455–468.
8. Efentakis, M.; Peponaki, C. Formulation study and evaluation of matrix and three-layer tablet sustained drug delivery systems based on carbopols with isosorbide mononitrate. AAPS PharmSci. 2008, 9, 917–923
9. Tobyn MJ, Stani forth JN, Baichwal AR, Mc Call TW. Prediction of physical properties of a novel polysaccharide controlled release system. Int J Pharm 1996;128: 113-22.
10. N. Papanas and e. Maltezos Metformin: A Review of Its Use in the Treatment of Type 2 Diabetes s 2009 : 1 1367–1381
11. K.Manga\*, K.Meghana, K.Avanthi,G.Swathi A Review on Formulation and Evaluation of Bilayered Tablets of Sustained Release Metformin Hcl and Gliclazide Volume 8, Issue 3 2023

Table-1.Formulation Table

INGREDIENTS	FORMULATION CODE			
	AM5	BM5	CM5	DM5
<b>MIDDLE LAYER</b>				
Metformin HCl	500	500	500	500
Co-XG-AG 1:2	300	-	-	-
Co-XG-AG 2:1	-	300	-	-
Co-XG-AG 3:1	-	-	300	-
Co-XG-AG 1:3	-	-	-	300
Talc	8	8	8	8
Magnesium stearate	8	8	8	8
Micro crystalline cellulose	34	34	34	34
<b>TOP LAYER</b>				
Ethyl Cellulose	10	10	10	10
HPMC K100M	10	10	10	10
Talc	1	1	1	1
Magnesium stearate	1	1	1	1





**Ponnada Sowmya et al.,**

BOTTOM LAYER				
Ethyl Cellulose	10	10	10	10
HPMC K100M	10	10	10	10
Talc	1	1	1	1
Magnesium stearate	1	1	1	1
<b>Total Weight of Tablet</b>	900	900	900	900

Table-2. Post compression parameters

Formulationcode	Hardness	Friability	Average weight	Drug contentd
	(Kg/cm2)	(%)	of tablet sc (mg)	(%)
AM5	4.5±1.02	0.48	901.26±2.268	99.5±0.60
BM5	4.1±0.98	0.32	901.02±2.789	101.7±0.67
CM5	4.2±1.23	0.29	900.86±2.186	99.±0.97
DM5	4.1±1.25	0.25	901.02±2.868	101.2±1.54

Table-3. Correlation coefficient values of different kinetic models of drug release of all formulations

Formualtion	Zero order	First order	Higuchi model	Korsmeyers model	n value
AM5	0.9924	0.9495	0.9905	0.9466	0.989
BM5	0.9939	0.9488	0.991	0.9416	0.994
CM5	0.9936	0.9304	0.9909	0.9435	0.9923
DM5	0.9939	0.8714	0.991	0.9416	0.994

<p>Figure-1. Different steps involved in preparation of co processed gums</p>	<p>Figure-2. Schematic diagram of geo matrix tablet</p>





Ponnada Sowmya et al.,

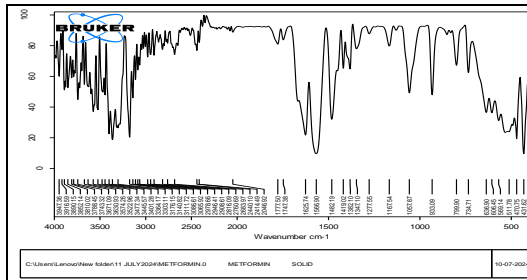


Figure-3.FT-IR spectrum of pure metformin

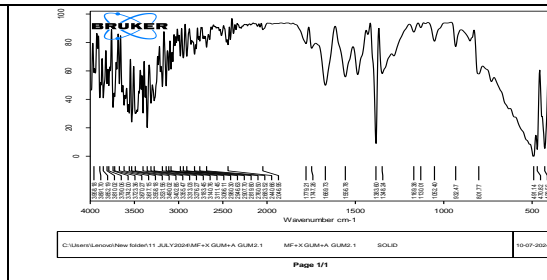


Figure-4.FT-IR spectrum of pure metformin with co-processed gum

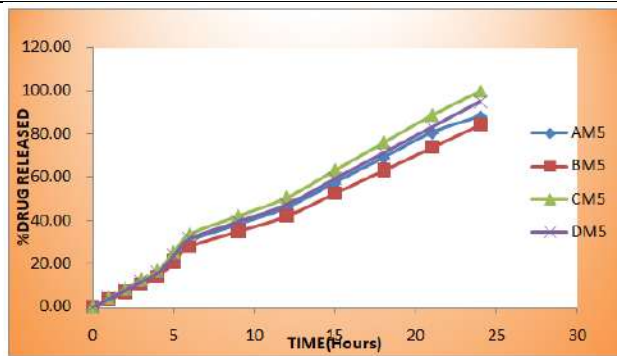


Figure 5 Dissolution Profile of Geomatrix tablets

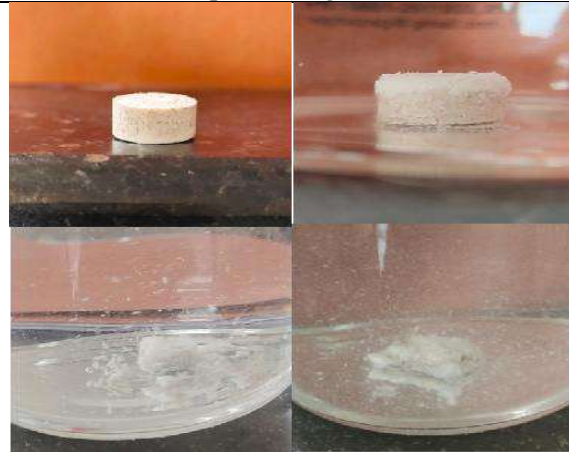


Figure 6. Dissolution study of geomatrix tablet at different time intervals

